IMPACT OF CANCER PLASTICITY ON DRUG RESISTANCE AND TREATMENT IN SOLID TUMORS

EDITED BY: Dong-Hua Yang, Pascale Cohen and Chang Zou

PUBLISHED IN: Frontiers in Oncology

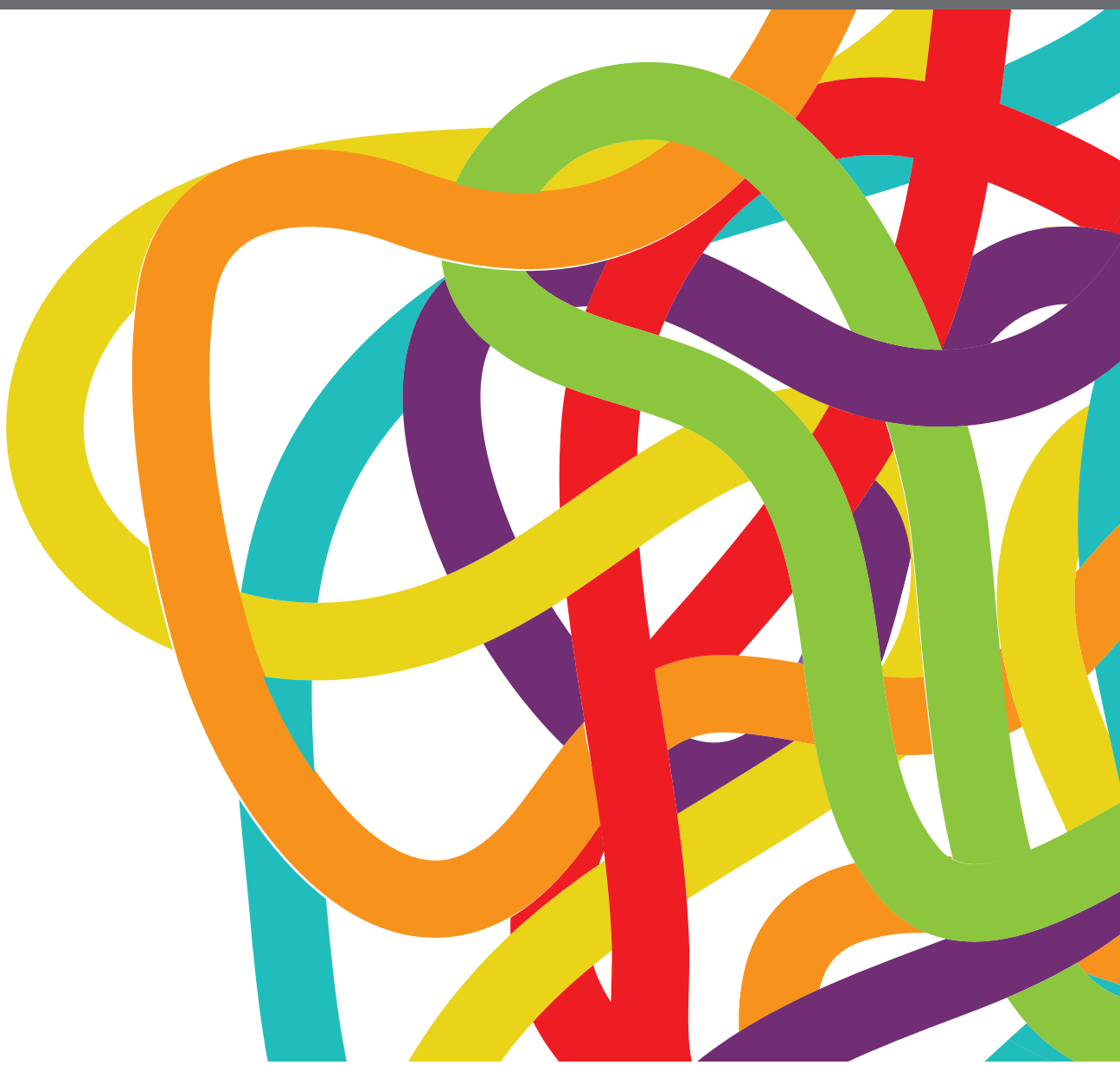

frontiers Research Topics

ISSN 1664-8714
ISBN 978-2-88966-275-3
DOI 10.3389/978-2-88966-275-3

About Frontiers

Frontiers is more than just an open-access publisher of scholarly articles: it is a pioneering approach to the world of academia, radically improving the way scholarly research is managed. The grand vision of Frontiers is a world where all people have an equal opportunity to seek, share and generate knowledge. Frontiers provides immediate and permanent online open access to all its publications, but this alone is not enough to realize our grand goals.

Frontiers Journal Series

The Frontiers Journal Series is a multi-tier and interdisciplinary set of open-access, online journals, promising a paradigm shift from the current review, selection and dissemination processes in academic publishing. All Frontiers journals are driven by researchers for researchers; therefore, they constitute a service to the scholarly community. At the same time, the Frontiers Journal Series operates on a revolutionary invention, the tiered publishing system, initially addressing specific communities of scholars, and gradually climbing up to broader public understanding, thus serving the interests of the lay society, too.

Dedication to Quality

Each Frontiers article is a landmark of the highest quality, thanks to genuinely collaborative interactions between authors and review editors, who include some of the world's best academicians. Research must be certified by peers before entering a stream of knowledge that may eventually reach the public - and shape society; therefore, Frontiers only applies the most rigorous and unbiased reviews.
Frontiers revolutionizes research publishing by freely delivering the most outstanding research, evaluated with no bias from both the academic and social point of view. By applying the most advanced information technologies, Frontiers is catapulting scholarly publishing into a new generation.

What are Frontiers Research Topics?

Frontiers Research Topics are very popular trademarks of the Frontiers Journals Series: they are collections of at least ten articles, all centered on a particular subject. With their unique mix of varied contributions from Original Research to Review Articles, Frontiers Research Topics unify the most influential researchers, the latest key findings and historical advances in a hot research area! Find out more on how to host your own Frontiers Research Topic or contribute to one as an author by contacting the Frontiers Editorial Office: researchtopics@frontiersin.org

IMPACT OF CANCER PLASTICITY ON DRUG RESISTANCE AND TREATMENT IN SOLID TUMORS

Topic Editors:
Dong-Hua Yang, St. John's University, United States
Pascale Cohen, Université Claude Bernard Lyon 1, France
Chang Zou, Jinan University, China

Citation: Yang, D.-H., Cohen, P., Zou, C., eds. (2020). Impact of Cancer Plasticity on Drug Resistance and Treatment in Solid Tumors. Lausanne: Frontiers Media SA. doi: 10.3389/978-2-88966-275-3

Table of Contents

frontiers in Oncology

EDITORIAL
published: 23 October 2020
doi: 10.3389/fonc.2020.596963

Editorial: Impact of Cancer Plasticity on Drug Resistance and Treatment in Solid Tumors

Pascale A. Cohen[1,2,3]*, *Chang Zou*[4] *and Dong-Hua Yang*[5]*

[1] Université Lyon 1, Lyon, France, [2] INSERM, UMR1033 LYOS, Lyon, France, [3] CRCL-Centre de Recherche en Cancérologie de Lyon-Inserm U1052-CNRS U5286, Lyon, France, [4] Clinical Medical Research Center, Shenzhen People's Hospital, Jinan University, Shenzhen, China, [5] Department of Pharmaceutical Sciences, College of Pharmacy and Health Sciences, St. John's University, Queens, NY, United States

Keywords: cancer plasticity, solid tumor, drug resistance, biomarker, therapeutic

Editorial on the Research Topic

Impact of Cancer Plasticity on Drug Resistance and Treatment in Solid Tumors

The Research Topic "Impact of Cancer Plasticity on Drug Resistance and Treatment in Solid Tumors" consists of 32 articles contributed by more than 270 authors in the field of oncology, pharmacology, and translational research. Our aim was to provide a collaborative discussion on molecular and cellular regulators of cancer cell plasticity contributing to tumor progression and drug resistance for the future direction of biomarker discovery and therapeutic strategies.

Cancer stem cells, tumor microenvironment, stroma/cancer cells interactions, changes in metabolism and epithelial-mesenchymal transition offer explanation for tumor plasticity. The current state of art in this era was elegantly reviewed by Fanelli et al., Yang et al., and Lin X. et al., who discussed the clinical relevance of cancer cell plasticity, the novel approaches for monitoring tumor plasticity and the current advances for therapeutic targeting. Yu et al. found that the FAP-a^{+}GOLPH3^{+} immunophenotype, combining the expression of both the fibroblast activation protein-alpha and the oncogenic Golgi phosphoprotein 3 protein predict the recurrence and progression of ductal carcinoma *in-situ* (DCIS) into invasive breast cancer. Yao et al. demonstrated in mouse experiments that the levels of MTA3 and SOX2 decreased and increased, respectively, during the progression of tongue squamous cell cancer (TSCC), and that MTA3^{low}/SOX2^{high} can serve as an independent prognostic factor for TSCC patients. Chen et al. confirmed that overexpression of PD-L1 occurred predominantly in highly aggressive glioma cells, and Akt binding/activation prevented autophagic cytoskeleton collapse, thus facilitating glioma cell invasion upon starvation stress. Sun et al. showed that SIRT5, a mitochondrial class III NAD-dependent deacetylase, contributes to cisplatin resistance in ovarian cancer by suppressing cisplatin-induced DNA damage in a reactive oxygen species (ROS)-dependent manner, via the regulation of the nuclear factor erythroid 2-related factor 2 (Nrf2)/heme oxygenase 1 (HO-1) pathway. The study from Tang et al. suggested that the Pigment epithelium-derived factor (PEDF) participates the carcinogenesis of human esophageal squamous cell carcinoma and might be a candidate therapeutic target. Finally, analyses conducted by Zhang J. et al. on single-cell sequencing datasets of several human cancers indicated a tumor suppression function of the ZNF671 transcription factor. Fahs et al. demonstrated that the PAX3-FOXO1 fusion protein modulates exosome cargo to confer a protective effect on recipient cells against oxidative stress and to promote plasticity and survival, potentially contributing to the known aggressive phenotype of the fusion gene-positive subtype of Rhabdomyosarcoma. Guo T. et al. reported a clinical case showing change of pathological type to metaplastic squamous cell carcinoma of the breast during disease recurrence.

OPEN ACCESS

Edited and reviewed by:
Paolo Pinton,
University of Ferrara, Italy

****Correspondence:***
Pascale A. Cohen
pascale.cohen@univ-lyon1.fr
Dong-Hua Yang
yangd1@stjohns.edu

Specialty section:
This article was submitted to Molecular and Cellular Oncology, a section of the journal Frontiers in Oncology

Received: *20 August 2020*
Accepted: *16 September 2020*
Published: *23 October 2020*

Citation:
Cohen PA, Zou C and Yang D-H (2020) Editorial: Impact of Cancer Plasticity on Drug Resistance and Treatment in Solid Tumors. Front. Oncol. 10:596963. doi: 10.3389/fonc.2020.596963

Epigenetic reprogramming favors cancer plasticity. The discovery of non-coding RNA such as microRNA (miR), Long non-coding RNA (LncRNA) and circular RNA (circ-RNA) is propelling the future advancement of biomarker development and offers opportunities to understand their role in the hallmarks of cancer, including signaling pathways involved in cell proliferation, cell invasion, metabolic plasticity and drug resistance. Wan et al. deciphered the functional domains of the channel-kinase transient receptor potential ion channel subfamily M, member 7 (TRPM7) involved in glioma cell growth or migration/invasion. TRPM7 was found to regulate miR-28-5p expression, which suppresses cell proliferation and invasion in glioma cells by targeting the Rap1b signaling. Guo J. et al. demonstrated that miR-204-3p, whose down-regulation was significantly associated with poor prognosis in bladder cancer patients, negatively modulated the proliferation of bladder cancer cells via targeting the lactate dehydrogenase (LDHA)-mediated glycolysis. Huang et al. elegantly provided evidence that LncRNA AFAP1-S1 up-regulates the RRM2 protein levels by sponging miR-139-5, then activating an RRM2/EGFR/Akt axis that promotes chemoresistance in non-small cell lung cancer. Supportive *in vivo* experiments further demonstrated that knockdown of AFAP1-AS1 significantly suppressed tumor growth and chemoresistance. Li W. et al. proved that miR-199a, by directly regulating K-RAS and thus the downstream AKT and ERK signaling, inhibits glioma cell proliferation *in vitro*, tumor growth *in vivo* and increases sensitivity to telozomide, a drug used in first line treatment of glioma. Lin X.-J. et al. highlighted the role of miR-936 in sensitizing laryngeal squamous cancer cells to doxorubicin and cisplatin. Liu C. et al. experiments suggested that miR-34a-5p, by directly targeting thymidine kinase 1 (TKI), may be part of the mechanisms negatively regulating TKI-driven thyroid carcinoma cell aggressiveness. Growing body of evidence indicate that circRNAs play a role in disease progression, partly by sponging miRNA, and may be used as biomarkers. Gao et al. identified a candidate circRNA associated with poor prognosis in multiple myeloma. Finally, the review by Guo Q. et al. elegantly depicted and discussed the role of exosomal miRNA as a regulators and biomarkers in cancer drug resistance.

It is of utmost importance to decipher how chronic exposure to environmental carcinogens contribute to cell plasticity and tumor progression. The identification of such molecular mechanisms may help in the discovery of human biomarkers of environmental carcinogen exposure and the development of candidate preventive strategies. Using an *in vitro* model for malignant transformation of normal lung cells upon long-term exposure to cigarette smoke, Wang et al. deciphered complex miRNA-mRNA networks associated with cancer-related signaling pathways, in particular those governing the metastasis-associated epithelial-mesenchymal transition and the PI3K/Akt/mTOR survival pathway. Donini et al. demonstrated a functional interplay between the aryl hydrocarbon receptor (AhR) and the G protein-coupled receptor 30 (GPR30) by which chronic and low-dose exposure of the genotoxic Benzo[a]pyrene and/or the endocrine disruptor Bisphenol A fosters the progression of early-transformed human mammary cells into a more aggressive stage. Zhang F. et al. proved that the chronic exposure of endometrial carcinoma cells to the polybrominated diphenyl ether endocrine disruptor BDE-47 triggers phenotypic plasticity, promotes progression and chemoresistance to cisplatin or paclitaxel, at least in part, via ERα/GPR30 and EGFR/ERK signaling pathways.

Antineoplastic drugs can induce cancer cells resistant to treatment that makes the therapeutic effect reduced. Circumventing drug resistance or delineating novel biomarkers of drug efficacy thus represent a great challenge, in particular in the era of precision medicine. To overcome multidrug resistance (MDR) mediated by overexpression of ATP binding cassette (ABC), Wang et al. provided a promising strategy, by nicely highlighting that NVP-TAE684, a novel ALK inhibitor, could reduce the chemo-resistance of MDR cells via the reversion of ABCG2-mediated efflux activity. Zhou et al. found that Erastin inhibits the drug efflux activity of ABCB1 and reverses ABCB1-mediated docetaxel resistance in ovarian cancer. Altogether, these two studies reveal that combination of NVP-TAE684 or Erastin with classical chemotherapy may offer potential effective combinations for the treatment of MDR cancers. Fan et al. explored novel methods to circumvent MDR in B cell lymphoma and demonstrated that an engineered anti-CD19(Fab)-lidamycin cytotoxic fusion protein could effectively inhibit, both *in vitro* and *in vivo,* the growth of adriamycin-resistant B cell lymphoma cells. Finally, to clarify the correlation between drug efficacy and mutations in circulating tumor DNA (ctDNA), Cao et al. monitored the mutational changes and therapeutic response of late-stage colorectal cancers following chemotherapy combined with bevacizumab and/or cetuximab, and confirmed that dynamic changes in drug resistance can be sensitively monitored by gene variation status in ctDNA.

Elucidating the mechanisms of cancer plasticity offers new opportunities for the development of therapeutic targeting. Among future candidate targets is the microbiota, demonstrated to be involved in both tumor initiation and progression. Zhang H. et al. found that Canmei formula, a classical traditional Chinese herbal formulation, reduced *in vivo* colitis-associated colorectal carcinogenesis by modulating inflammation and the composition of the gut microbiota. Huang et al. explored *in vitro* the anticancerous activity the Methyl-cantharidimide drug, originally discovered in insects, and proved that it inhibits growth of human hepatocellular carcinoma cells by inducing cell cycle arrest and promoting apoptosis. Nan et al. proposed that ROS-mediated proteasome-dependent pathway can be exploited to overcome apoptosis resistance triggered by aberrant expression of the anti-apoptotic survivin protein in cancers, by demonstrating that the alkaloid/amide Piperlongumine extracted from peppers efficiently induced the proteasome-dependent degradation of the survivin *in vitro*, downregulated survivin *in vivo* and inhibition of ovarian cancer cells xenograft tumor growth. Finally, an elegant study from Liu K. et al. identified, by proteomics investigation of breast cancer specimen, increased protein levels of Hsp90

proteins associated with poor prognosis. BJ-B11, an Hsp90 inhibitor, was shown to hamper *in vitro* the cancerous properties of triple negative breast cancer cells and to inhibit tumor growth in xenograft model. Wen et al. explored the antitumor effects of 7-methoxy-1-tetralone in hepatocellular carcinoma and found that this compound induces apoptosis, suppresses cell proliferation and migration via regulating c-Met, p-AKT, NF-κB, MMP2, and MMP9 expression. Finally, Yan and Wang nicely reviewed brain cancer-associated alterations of proteoglycans making these latter as putative biomarkers or therapeutic targets.

In conclusion, the "Impact of Cancer Plasticity on Drug Resistance and Treatment in Solid Tumors" Research Topic highlights the complex phenomenon of cancer cell plasticity. The recent insights into the role of plasticity in cancer progression implies the need to continue improving our understanding into the fundamental mechanisms governing tumor progression and drug resistance, with the aim to identify relevant new biomarkers and to develop innovative therapies.

AUTHOR CONTRIBUTIONS

All authors listed have made a substantial, direct and intellectual contribution to the work, and approved it for publication.

FUNDING

PC was funded by the Region Auvergne Rhone-Alpes, France (Pack Ambition International 2020) and the Agence Nationale de la Recherche, France (2011 ANR-CESA-018-01).

Conflict of Interest: The authors declare that the research was conducted in the absence of any commercial or financial relationships that could be construed as a potential conflict of interest.

frontiers in Oncology

ORIGINAL RESEARCH
published: 13 August 2019
doi: 10.3389/fonc.2019.00754

SIRT5 Promotes Cisplatin Resistance in Ovarian Cancer by Suppressing DNA Damage in a ROS-Dependent Manner via Regulation of the Nrf2/HO-1 Pathway

*Xiaodan Sun[1], Shouhan Wang[2], Junda Gai[1], Jingqian Guan[1], Ji Li[1], Yizhuo Li[1], Jinming Zhao[1], Chen Zhao[3], Lin Fu[1,4] and Qingchang Li[1,4]**

[1] Department of Pathology, College of Basic Medical Sciences, China Medical University, Shenyang, China, [2] Department of Hepatopancreatobiliary Surgery, Jilin Province Cancer Hospital, Changchun, China, [3] Department of Pathology, Carver College of Medicine, University of Iowa, Iowa City, IA, United States, [4] Department of Pathology, The First Affiliated Hospital, China Medical University, Shenyang, China

Sirtuin 5 (SIRT5), a mitochondrial class III NAD-dependent deacetylase, plays controversial roles in tumorigenesis and chemoresistance. Accordingly, its role in ovarian cancer development and drug resistance is not fully understood. Here, we demonstrate that SIRT5 is increased in ovarian cancer tissues compared to its expression in normal tissues and this predicts a poor response to chemotherapy. SIRT5 levels were also found to be higher in cisplatin-resistant SKOV-3 and CAOV-3 ovarian cancer cells than in cisplatin-sensitive A2780 cells. Furthermore, this protein was revealed to facilitate ovarian cancer cell growth and cisplatin-resistance *in vitro*. Mechanistically, we show that SIRT5 contributes to cisplatin resistance in ovarian cancer by suppressing cisplatin-induced DNA damage in a reactive oxygen species (ROS)-dependent manner via regulation of the nuclear factor erythroid 2-related factor 2 (Nrf2)/heme oxygenase 1 (HO-1) pathway.

Keywords: ovarian cancer, SIRT5, Nrf2/HO-1, reactive oxygen species, drug resistance

OPEN ACCESS

Edited by:
Dong-Hua Yang,
St. John's University, United States

Reviewed by:
Monica Montopoli,
University of Padova, Italy
Daniele Vergara,
University of Salento, Italy

***Correspondence:**
Qingchang Li
qcli@cmu.edu.cn

Specialty section:
This article was submitted to Molecular and Cellular Oncology, a section of the journal Frontiers in Oncology

Received: *03 June 2019*
Accepted: *26 July 2019*
Published: *13 August 2019*

Citation:
Sun X, Wang S, Gai J, Guan J, Li J, Li Y, Zhao J, Zhao C, Fu L and Li Q (2019) SIRT5 Promotes Cisplatin Resistance in Ovarian Cancer by Suppressing DNA Damage in a ROS-Dependent Manner via Regulation of the Nrf2/HO-1 Pathway. Front. Oncol. 9:754. doi: 10.3389/fonc.2019.00754

INTRODUCTION

SIRT5 is a unique member of the Sirtuin family (Sirt1–7), which possesses multiple enzymatic activities including NAD-dependent histone deacetylase (1), potent lysine demalonylase, lysine desuccinylase (2), and lysine glutarylase (3) activities. These specific enzymatic activities indicate that SIRT5 plays a crucial role in regulating multiple cellular metabolic processes such as glycolysis, the tricarboxylic acid cycle, fatty acid oxidation, nitrogen metabolism, and the pentose phosphate pathway (4, 5). In addition, certain aspects of cancer biology, such as stress responses (6, 7), apoptosis (8, 9), and autophagy (10, 11), can be regulated by SIRT5. Moreover, altered cellular metabolism has been recently identified as a hallmark of malignancy and emerging literature suggests that SIRT5 is involved in oncogenesis. For example, either the mRNA or protein expression of SIRT5 was found to be increased in non-small cell lung cancer (NSCLC) (12, 13), hepatocellular carcinoma (HCC) (14), colorectal cancer (CRC) (15), Waldenstrom macroglobulinemia (16), and breast cancer (9, 17), compared to the levels in matched normal tissues. Janus-faced roles of SIRT5 in cancer have also been described. Specifically, the downregulation of SIRT5 was observed

in head and neck squamous cell carcinoma (18), liver cancer (19), and endometrial carcinoma (20), which highlight the tumor-suppressive role of SIRT5. Furthermore, controversial roles for SIRT5 in drug resistance have been reported. SIRT5 facilitates NSCLC resistance to cisplatin, 5-fluorouracil (5-FU), and bleomycin (13). Moreover, SIRT5-positive cells in wild-type Kras CRCs were found to be resistant to either chemotherapeutic agents or cetuximab (21). However, a positive association between SIRT5 expression and complete response to neoadjuvant chemotherapy in triple-negative breast cancer patients was previously shown by analyzing data from the Gene Expression Omnibus (GEO) DataSet. In addition, by analyzing the ONCOMINE online database, SIRT5 expression levels were found to be higher in chemotherapy-responders than in non-responders (17). Considering these discrepant findings, further studies are needed to explore the functions of SIRT5 in tumorigenesis and chemoresistance.

Globally, ovarian cancer ranked eighth in incidence and seventh in mortality among all cancers in females in 2018 (WHO, http://gco.iarc.fr/today/home). Standard treatment for this disease involves surgery combined with chemotherapy. However, chemoresistance has become a major reason for poor outcomes in ovarian cancer. Although emerging targeted therapies have improved the survival of chemoresistant ovarian cancer patients, their quality of life and overall survival are still limited due to the side effects associated with such drugs, and the 5-year survival rate for advanced-stage ovarian cancer is only 28.9% (22). Therefore, better curative outcomes for ovarian cancer therapeutics are required. Considering the diverse roles of SIRT5 in cancer biology, we speculated that SIRT5 is a therapeutic target for ovarian cancer. To date, the role of this protein in ovarian cancer has not been elucidated. Therefore, in this context, we investigated the expression pattern of SIRT5 in both human ovarian cancer tissues and ovarian cancer cells. Furthermore, we reveal a potential role for SIRT5 in ovarian cancer cell growth and chemoresistance.

MATERIALS AND METHODS

Antibodies and Reagents

The following antibodies were purchased: primary antibodies to SIRT5 (Cell Signaling Technology, Danvers, MA), H2A histone family member X phosphorylated on S139 (γ-H2AX, Cell Signaling Technology), nuclear factor erythroid-2-related factor 2 (Nrf2; Proteintech, Wuhan, China), heme oxygenase 1 (HO-1; Proteintech), manganese-dependent superoxide dismutase (MnSOD)/SOD2 (Proteintech), breast cancer gene 1 (BRCA1, Cell Signaling Technology), histone H3 (Cell Signaling Technology), and β-actin (Cell Signaling Technology); and secondary antibodies, specifically goat anti-rabbit IgG (Proteintech), goat anti-mouse IgG (Proteintech), and tetramethylrhodamine (TRITC)-conjugated secondary antibody (Proteintech).

Cisplatin and ML385 (an Nrf2-specific inhibitor) were purchased from MCE, China. N-acetyl-L-cysteine (NAC), a reactive oxygen species (ROS) scavenger, was purchased from Selleck, China.

Immunohistochemical Staining

SIRT5 staining was performed on an ovarian cancer and normal tissue microarray (Biomax, USA), which contained 90 tumor tissues and 10 normal ovarian tissues. Immunostaining was performed based on the ABC immunostaining protocol (MaiXin, Fuzhou, China). Two independent investigators scored the microarray by evaluating the staining intensity and percentage of stained cells blindly and randomly. The staining intensity was scored from 0 to 3 as follows: 0 (negative), 1 (weak), 2 (moderate), and 3 (strong). The percentage of positively stained cells was scored from 0 to 4 as follows: 0 (0%), 1 (1–25%), 2 (26–50%), 3 (51–75%), and 4 (76–100%). The final multiplied scores ranged from 0 to 12 and SIRT5 expression was regarded as positive if the final score was ≥ 6.

Cell Culture and Transfection

A2780, SKOV-3, and CAOV-3 human ovarian cancer cell lines were used in this study. A2780 and CAOV-3 cells were cultured in DMEM supplemented with 10% fetal bovine serum. SKOV-3 cells were cultured in RPMI-1640 medium supplemented with 10% fetal bovine serum. These cells were grown at 37°C in a humidified atmosphere with 5% CO_2.

Transient transfection was carried out using Lipofectamine 3000 reagent (Invitrogen) according to the manufacturer's instructions. A SIRT5 expression plasmid (OriGene, Rockville, MD, USA) and the corresponding empty plasmid (OriGene) were used for SIRT5 overexpression and as a negative control, respectively. Cells were transfected with SIRT5-siRNA and negative control siRNA (GenePharma, Shanghai, China) for SIRT5 knockdown experiments.

The cells were pretreated with 5 mM NAC for 2 h to inhibit ROS generation. ML385 was added to cells at a concentration of 5 μM for 48 h in the presence of cisplatin to block the Nrf2 pathway.

Cell Proliferation and Cell Viability Assays

Cell Counting Kit-8 (CCK-8) assays were performed to assess cell proliferation and cell viability *in vitro*. For cell proliferation, the cells were seeded in 96-well plates at a density of 3,000 cells/well and incubated for 5 days. For cell viability, the cells were seeded in 96-well plates at a density of 5,000 cells/well and treated with the indicated concentration of cisplatin for 48 h or 5 days, changing the cisplatin-containing medium every 2 days. Next, 10 μl of CCK-8 reagent (Beyotime, Shanghai, China) was added to each well, and the cells were incubated for 2 h. The absorbance value (OD) of each well was measured at 450 nm and the cell viability was calculated as follows: cell viability (%) = experimental group OD value / control group OD value × 100%. IC_{50} values (50% inhibition of surviving fraction) were calculated using GraphPad Prism 7.0 software.

Colony Formation Assays

Cells were plated in six-well culture plates at 500 cells/well. After incubation for 14 days at 37°C in a humidified atmosphere at 5% CO_2, the cells were washed three times with PBS and stained with Giemsa solution. The number of colonies containing ≥ 50

cells was then counted under a microscope. Colony formation efficiency was calculated as colony numbers / 500 × 100%.

ROS Detection and Measurement of Intracellular Glutathione (GSH)

The ROS levels induced by cisplatin in ovarian cancer cells were detected using the probe 2′,7′-dichlorodihydrofluorescein diacetate (DCFH-DA, Beyotime), which can be oxidized by intracellular oxygen to dichlorofluorescein, a highly fluorescent compound. After exposure to the indicated concentration of cisplatin for 2, 6, 24, or 48 h, the cells were incubated with a final concentration of 10 μM DCFH-DA in the dark for 20 min at 37°C in a humidified atmosphere at 5% CO_2, after which the cells were washed three times with cold PBS to remove excess fluorescent probe. The cells were then resuspended in 300 μl of PBS and assessed for fluorescence intensity using a flow cytometer (LSRFortessa, BD Biosciences). The data were analyzed using FlowJo X 10.0.7 Software.

Intracellular GSH levels were measured using a Total Glutathione Assay Kit (Beyotime) according to the manufacturer's instructions. Briefly, the ovarian cancer cells were harvested and lysed in the protein removal solution S provided in the kit. After incubation for 5 min at 4°C, the samples were centrifuged at 10,000 g for 10 min at 4°C. The supernatant was treated with assay solution for 5 min at 25°C and the absorbance at 412 nm was measured using a microplate

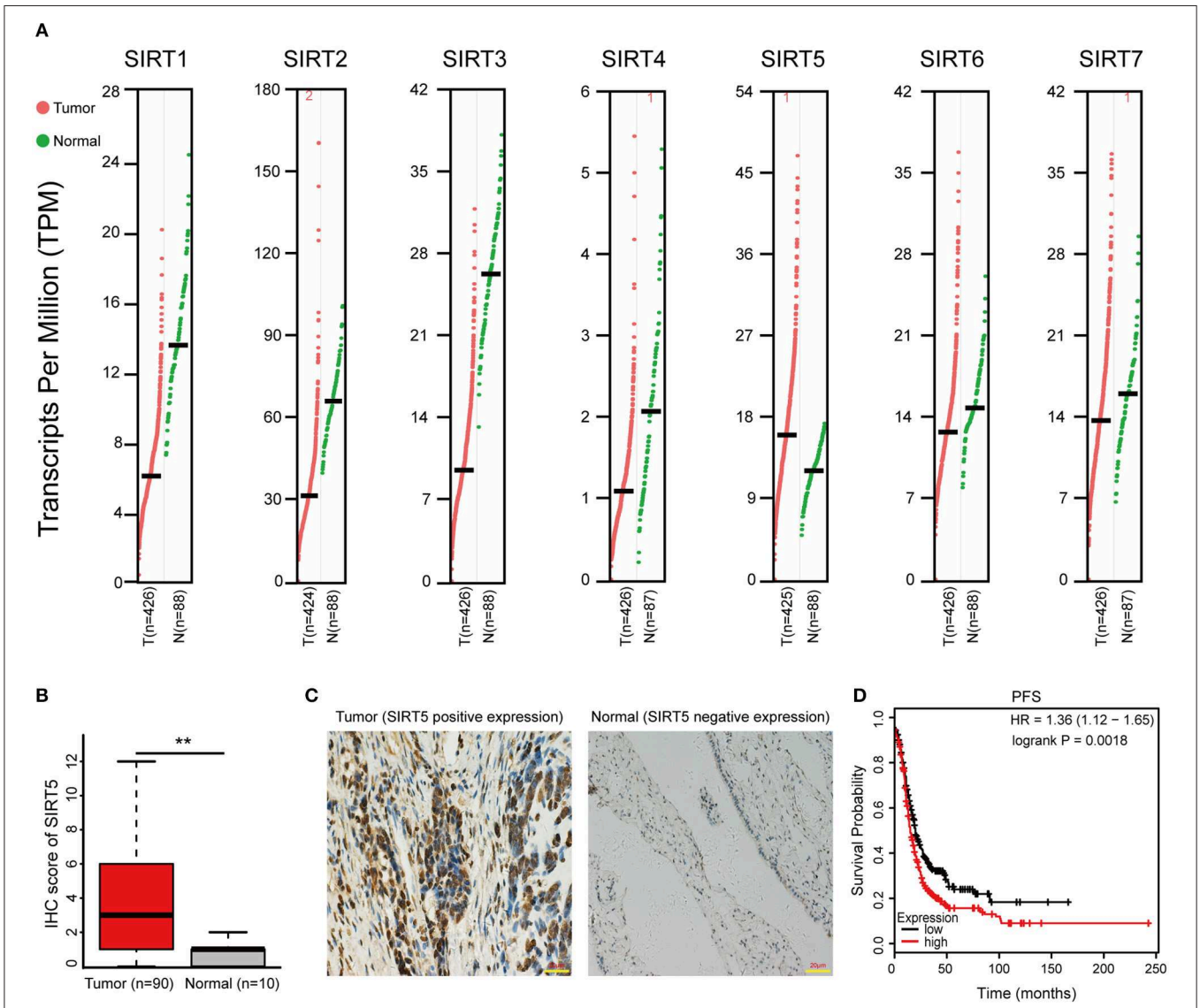

FIGURE 1 | SIRT5 expression is increased in ovarian cancer tissues and high SIRT5 level predicts poor chemo-response. **(A)** The mRNA expression of *Sirtuins* in patients with ovarian cancer (GEPIA). **(B)** Immunohistochemical staining results of SIRT5 expression in 90 cases ovarian cancer tissues and 10 cases normal tissues microarrays. **(C)** Representative immunohistochemical staining images of SIRT5 expression (positive or negative) in ovarian cancer and normal tissues. (Magnification, × 400; Scale bar = 20 μm). **(D)** High SIRT5 level predicts poor progression-free survival (PFS) by online Kaplan-Meier analysis. $^{**}P < 0.01$.

TABLE 1 | Association of SIRT5 expression with clinicopathological characteristics of ovarian cancer tissue microarrays.

Clinicopathological characteristics	Total number	SIRT5 negative or weak expression	SIRT5 positive expression	*P* value
Age				0.0786
<60	73	47 (64.38%)	7 (35.62%)	
≥60	17	7 (41.18%)	10 (58.82%)	
Histology				0.085
Serous carcinoma	72	40 (55.56%)	32 (44.44%)	
Mucinous adenocarcinoma+others	18	14 (77.78%)	4 (22.22%)	
Differentiation				**0.0179**
High grade	65	34 (52.31%)	31 (47.69%)	
Low grade	25	20 (80.00%)	5 (20.00%)	
Figo stage				**<0.0001**
I	47	44 (93.62%)	3 (6.38%)	
II-IV	43	10 (23.26%)	33 (76.74%)	
Lymph node metastasis				**0.0019**
Negative	68	47 (69.12%)	21 (30.88%)	
Positive	22	7 (31.82%)	15 (68.18%)	

The bold fonts represent the significant values.

reader (SpectraMax i3x, Molecular Devices, Sunnyvale, CA). Intracellular GSH levels were quantified by interpolation on standard curves and relative GSH levels were calculated by normalization to the values obtained from A2780 cells.

Immunofluorescence Staining

Cells were plated in 20-mm culture plates, pretreated with the indicated concentrations of cisplatin for 24 h to observe γ-H2AX foci formation, washed with PBS three times, fixed with 4% paraformaldehyde for 15 min, and permeabilized in 0.1% Triton X-100 for 5 min. After blocking with 5% bovine serum albumin for 1 h at room temperature, the cells were incubated with primary antibodies against γ-H2AX (dilution 1:200), SIRT5 (dilution 1:200), or Nrf2 (dilution 1:200) overnight at 4°C. Then, TRITC-conjugated secondary antibody (dilution 1:1,000) was incubated with the cells for 2 h in the dark at room temperature, and the cells were stained with 4′,6-diamidino-2-phenylindole (DAPI) for 5 min to visualize their nuclei. Images were captured using a fluorescence microscope or an Olympus FV1000 confocal laser-scanning microscope (Olympus, Tokyo, Japan). For quantification of γ-H2AX foci, 5 random fields of cells from each slide were quantified by ImageJ software and foci containing ≥5 cells were considered positive.

Western Blotting and Isolation of Cytosolic and Nuclear Cell Fractions

Total protein was isolated from SIRT5 overexpressing or knockdown ovarian cancer cells and their corresponding controls, with or without cisplatin treatment. The cells were washed with ice-cold PBS three times and lysed in lysis buffer supplemented with a cocktail of proteinase inhibitors (MCE). Equal amounts of protein (60 μg) from cell extracts were separated by 10% SDS-PAGE and transferred to 0.45- or 0.22-μm (the latter for γ-H2AX) polyvinylidene fluoride (PVDF) membranes (Millipore, Billerica, MA, USA). Following blocking with 5% fat-free milk for 2 h at room temperature, the membranes were incubated with primary antibodies (anti-SIRT5, anti-actin, anti-Nrf2, anti-HO-1, anti-MnSOD/SOD2, anti-BRCA1, anti-histone H3, or anti-γ-H2AX; dilution, 1:1,000) in blocking buffer overnight at 4°C. Then, the membranes were washed three times in Tris-buffered saline with Tween 20 and incubated with secondary antibodies at a dilution of 1:2,500 for 2 h at 37°C. Immunoreactivity was detected using ECL (Thermo Fisher Scientific, Waltham, MA, USA) with a BioImaging System (UVP Inc., Upland, CA, USA). ImageJ software was used to evaluate the gray value of each band.

For cytosolic and nuclear isolation, a Nuclear and Cytoplasmic Protein Extraction kit (Beyotime) was used, following the manufacturer's instructions. Briefly, the collected cells were suspended in ice-cold hypotonic buffer and incubated on ice for 20 min. The extracts were then centrifuged at 12,000 g for 5 min, and the supernatants were collected as cytosolic fractions. The pellets were washed with ice-cold PBS and resuspended in lysis buffer, followed by vortexing at the highest speed. These extracts were centrifuged at 12,000 g for 10 min, and the supernatants were collected as nuclear fractions.

Gene Expression Profiling Interactive Analysis (GEPIA) Database and Statistical Analysis

The GEPIA database (http://gepia.cancer-pku.cn/), a newly developed web-based tool, provides tumor vs. normal differential expression analysis, correlation analysis based on the Cancer Genome Atlas, and genotype-tissue expression data. It was used to analyze the expression of SIRT5, Nrf2, and HO-1 in ovarian cancer and normal tissues and the correlation between SIRT5 and Nrf2, MnSOD, and BRCA1. All experiments were repeated at least three times and the data were expressed as the means ± standard deviations. Statistical analysis was performed

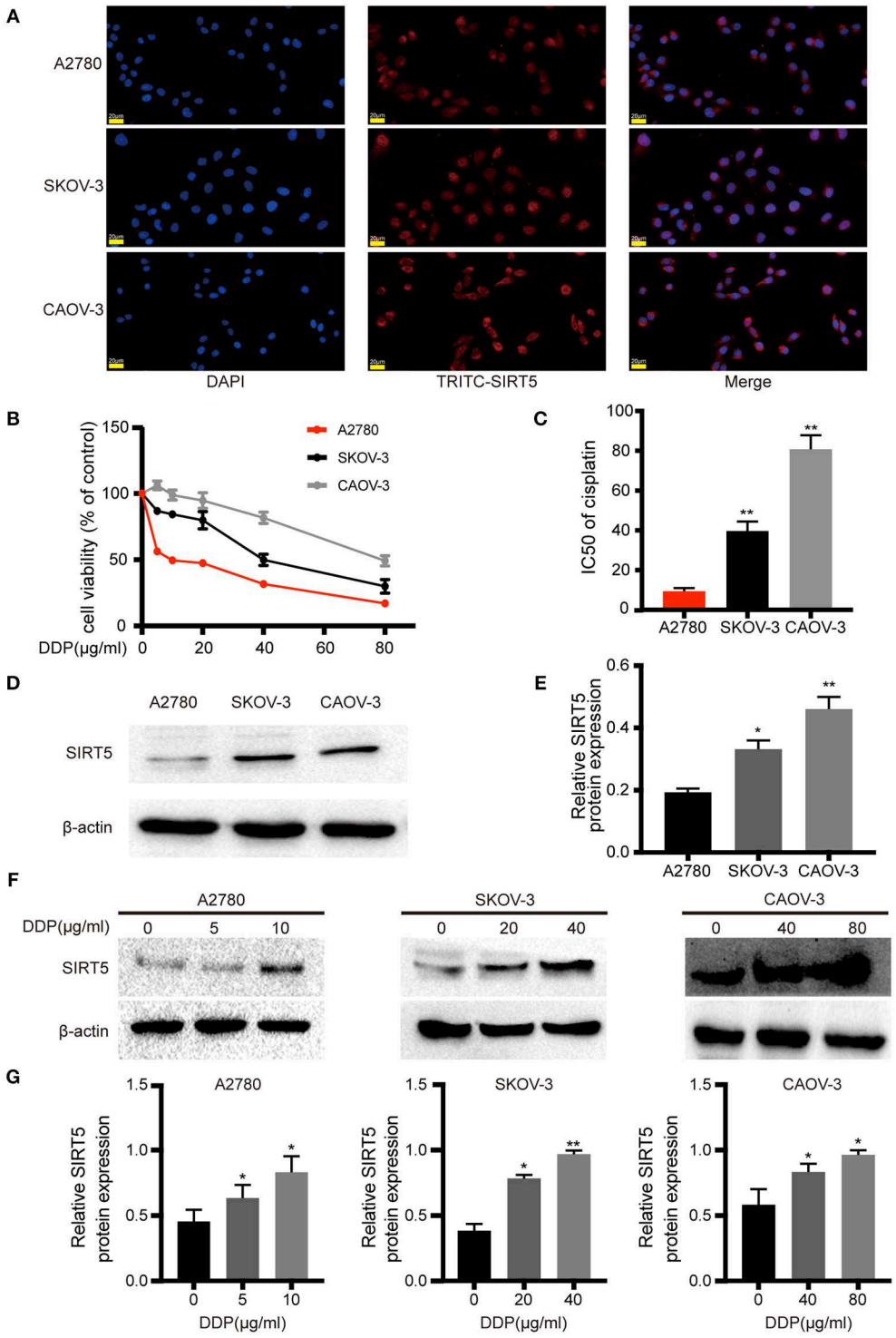

FIGURE 2 | SIRT5 expression is involved in cisplatin-resistant of ovarian cancer cells. **(A)** SIRT5 expression in three ovarian cancer cell lines analyzed by immunofluorescence staining using TRITC-labeled antibodies; nuclei were stained with DAPI. **(B)** Differences in cisplatin sensitivity of three ovarian cancer cell lines assessed by CCK-8 assay. **(C)** Calculated IC50 values after cells were exposed to the indicated dose of cisplatin for 48 h. **(D)** SIRT5 protein levels in three ovarian cancer cell lines assessed by western blot and **(E)** relative protein expression was quantified by relative gray value of bands with ImageJ software. **(F,G)** SIRT5 protein levels were upregulated during exposed to indicated dose of cisplatin in three ovarian cancer cell lines for 48 h. DDP, cisplatin. Data are presented as the mean ± SD of three independent experiments. Scale bar = 20 μm, $^{*}P < 0.05$, $^{**}P < 0.01$, compared with A2780 or control cells.

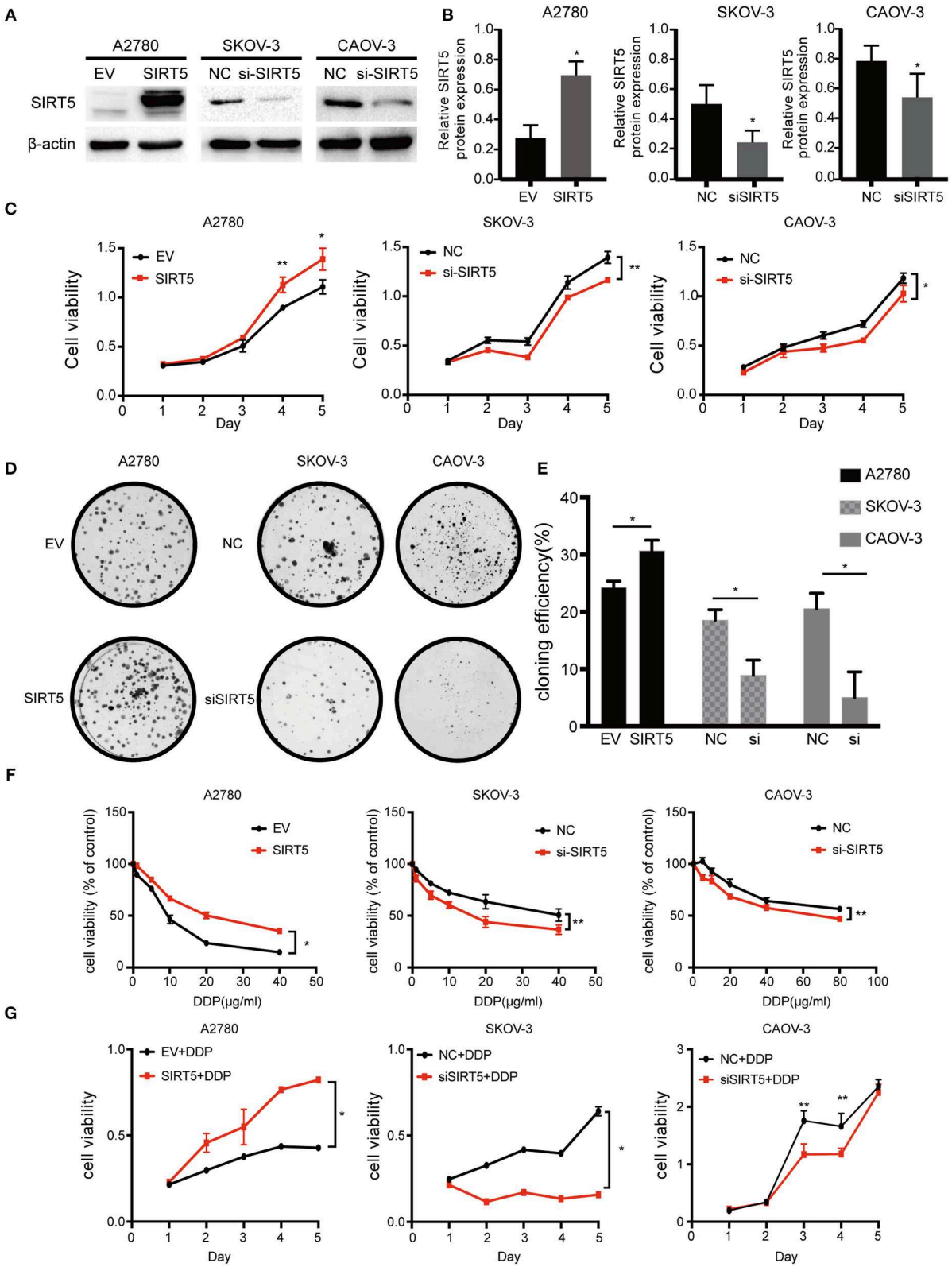

FIGURE 3 | SIRT5 promotes cell proliferation and cisplatin resistance in ovarian cancer cells. **(A)** A2780 cell lines were transfected with SIRT5 plasmid and SKOV-3 and CAOV-3 cell lines were transfected with SIRT5-siRNA. The transfection efficiency was detected by western blot and **(B)** the relative gray values were shown in histogram. **(C)** Overexpression of SIRT5 in A2780 cells promoted cell growth and knockdown of SIRT5 inhibited cell growth in SKOV-3 and CAOV-3 cells. After

(Continued)

FIGURE 3 | treated with indicated dose of cisplatin, the relative cell numbers were evaluated with CCK-8 assay at the indicated time points. **(D)** A significant increase in colony number was observed in A2780 cells with SIRT5 overexpression and an opposite trend was observed in SKOV-3 and CAOV-3 cells with knockdown of SIRT5. **(E)** Colony numbers were counted under microscope and the colony formation efficiency was calculated. **(F)** IC50 of cisplatin was increased in A2780 cells with SIRT5 overexpression and decreased in SKOV-3 and CAOV-3 cells with knockdown of SIRT5. **(G)** The transfected cells were treated with IC50 dose of cisplatin for consecutive 5 days respectively. Cell viability was assessed by CCK-8 assay. Data are presented as the mean ± SD of three independent experiments. EV, empty vector. NC, negative control. DDP, cisplatin. $^{*}P < 0.05$, $^{**}P < 0.01$, compared with the EV or NC cells.

with GraphPad Prism 7.0 software. Statistical significance was determined based on a Student's *t*-test or one-way ANOVA. The χ^2 test was used to determine the correlation between SIRT5 expression and clinicopathologic characteristics. $P < 0.05$ was considered to denote a statistically significant difference.

RESULTS

SIRT5 Expression Is Increased in Ovarian Cancer Tissues and High SIRT5 Levels Predict Poor Chemotherapy Response

First, the GEPIA database was used to compare the mRNA expression of seven *Sirtuin* members between ovarian cancer and normal tissues. Only the mRNA level of *SIRT5* was higher, while that of other isoforms was lower, in tumors than it was in normal tissues (**Figure 1A**). Then, immunohistochemistry was performed to verify this result. SIRT5 was more highly expressed in ovarian cancer tissues than in normal tissues and was mainly localized to the cytoplasm (**Figures 1B,C**). In addition, as shown in **Table 1**, higher SIRT5 levels were positively correlated with advanced International Federation of Gynecology and Obstetrics (FIGO) stage ($P < 0.0001$) and lymph node metastasis ($P = 0.0019$), but negatively correlated with a low grade of differentiation ($P = 0.0179$). The prognostic value of SIRT5 was then determined by Kaplan–Meier analysis using the KM plotter online software (http://kmplot.com/analysis/) based on 614 ovarian cancer patients who received chemotherapy. To investigate whether SIRT5 is relevant to chemoresistance, progression-free survival (PFS) was chosen as the primary endpoint, and patients with high SIRT5 expression exhibited significantly shorter PFS than those with low expression ($P = 0.0018$; **Figure 1D**). In summary, SIRT5 expression is increased in ovarian cancer tissues and high SIRT5 levels predict poor chemotherapy response.

SIRT5 Expression Is Increased in Cisplatin-Resistant Ovarian Cancer Cells and Cisplatin Upregulates SIRT5 Levels

Based on the aforementioned results, the expression pattern of SIRT5 in ovarian cancer cells was assessed. First, immunofluorescence staining indicated that this marker was localized mainly to the cytoplasm of A2780, SKOV-3, and CAOV-3 cells (**Figure 2A**), in agreement with the immunohistochemistry staining of tissues. Western blotting of cytosolic and nuclear fractions verified this result (**Figure S1A**). Then, the sensitivities to cisplatin among the three ovarian cancer cell lines were compared. The cells were treated with different concentrations of cisplatin (0–80 μg/ml) for 24 h and different degrees of sensitivity to cisplatin were noted. SKOV-3 ($IC_{50} = 39.743 \pm 4.756$ μg/ml) and CAOV-3 ($IC_{50} = 80.813 \pm 7.058$ μg/ml) cell lines were less sensitive to cisplatin than A2780 cells ($IC_{50} = 9.362 \pm 0.489$ μg/ml; **Figures 2B,C**). These results are consistent with previous descriptions of these three ovarian cancer cell lines (23–25).

SIRT5 expression was higher in SKOV-3 and CAOV-3 cisplatin-resistant cells than in A2780 cisplatin-sensitive cells (**Figures 2D,E**). Then, whether cisplatin could affect the protein levels of SIRT5 was investigated. The three ovarian cancer cell lines were incubated without cisplatin, with 50% of the IC_{50} dose, and with the IC_{50} dose of cisplatin for 24 h. SIRT5 expression was significantly upregulated in the cisplatin-treated cells in a concentration-dependent manner compared to control cells (**Figures 2F,G**). Taken together, these results reveal a causal relationship between SIRT5 expression and cisplatin resistance in ovarian cancer cells.

SIRT5 Promotes Cell Proliferation and Cisplatin Resistance in Ovarian Cancer Cells

As SIRT5 was hypothesized to play a role in ovarian cancer development and chemoresistance, its effect on the biological behaviors of the three cell lines was investigated. Based on its basal protein levels, SIRT5 was either overexpressed or silenced. A2780 cells were transfected with a SIRT5 overexpression plasmid or empty vector, while knockdown of SIRT5 in SKOV-3 and CAOV-3 cells was achieved by transfecting them with SIRT5-siRNA or negative control siRNA (**Figures 3A,B**). The results indicated that SIRT5 overexpression could significantly promote A2780 cell proliferation and colony formation, while the opposite effect was observed in SKOV-3 and CAOV-3 cells upon SIRT5 knockdown (**Figures 3C–E**).

Next, cell viability assays were performed to investigate the relationship between SIRT5 and cisplatin resistance. The transfected cell lines were treated with increasing concentrations of cisplatin for 24 h to observe the effect on cisplatin IC_{50} values. Moreover, these transfected cells were treated with their respective IC_{50} dose of cisplatin for 5 consecutive days. The results showed that the IC_{50} values and cell viability were elevated after overexpression of SIRT5 in A2780 cells, whereas both values were decreased upon SIRT5 downregulation in SKOV-3 and CAOV-3 cells (**Figures 3F,G**). These findings suggest that SIRT5 promotes proliferation and cisplatin resistance in ovarian cancer cells.

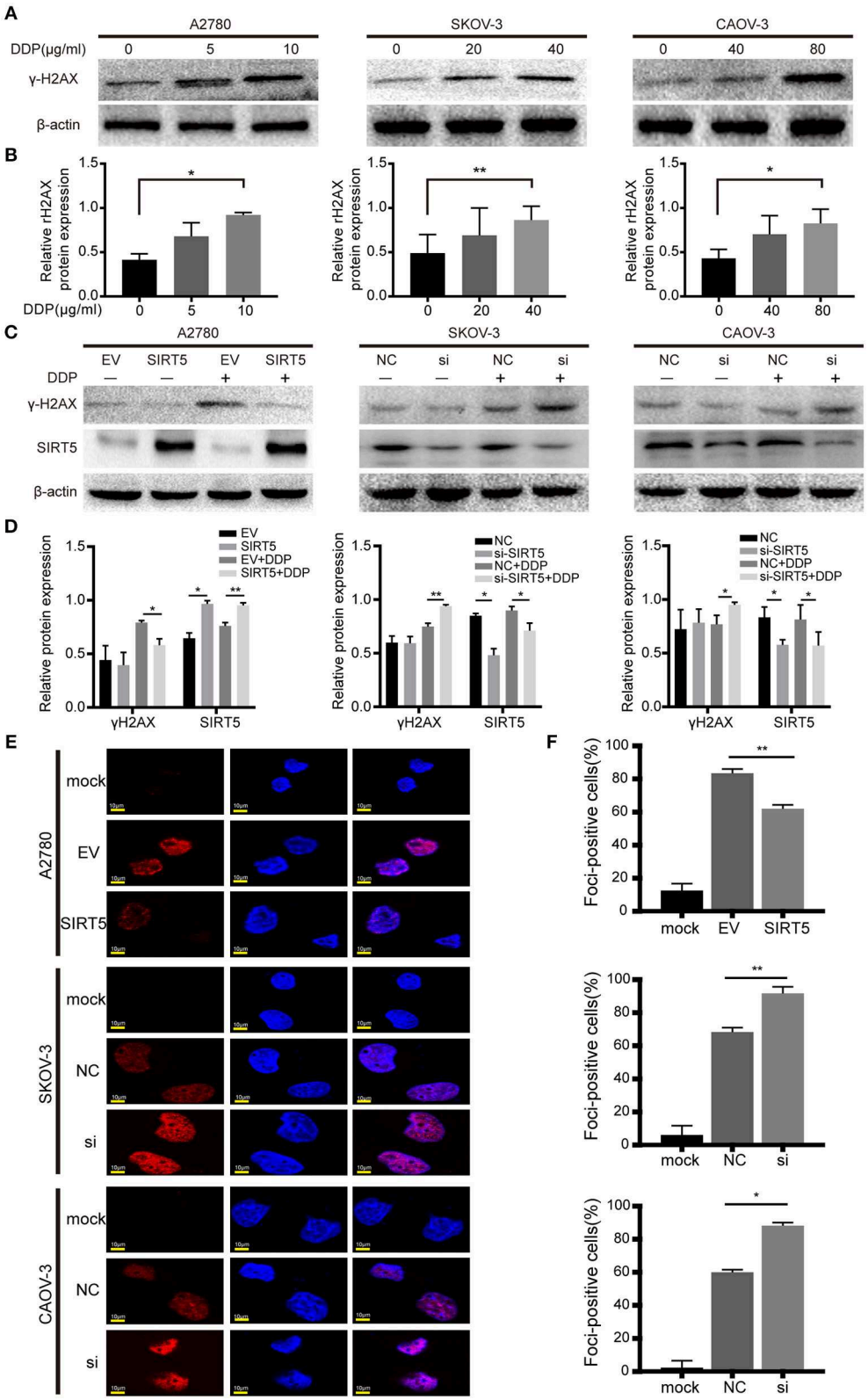

FIGURE 4 | SIRT5 suppresses cisplatin induced DNA damage. **(A)** The γ-H2AX protein levels were upregulated during exposure to cisplatin in three ovarian cancer cells assessed by western blot and **(B)** the relative gray values were shown in histogram. **(C)** The transfected cells were treated with or without IC50 dose of cisplatin for 24 h. The γ-H2AX protein levels were assessed by western blot and **(D)** the relative gray values were shown in histogram. **(E)** The γ-H2AX foci formation was

(Continued)

FIGURE 4 | observed by immunofluorescence staining. The mock cells were untreated and the transfected cells were treated with IC50 dose of cisplatin for 24 h respectively. **(F)** The quantification results of γ-H2AX foci in three ovarian cancer cells. Data are presented as the mean ± SD of three independent experiments. EV, empty vector. NC, negative control. DDP, cisplatin. Scale bar = 10 μm, $^{*}P < 0.05$, $^{**}P < 0.01$.

SIRT5 Suppresses Cisplatin-Induced DNA Damage

As mentioned above, SIRT5 was found to promote resistance to cisplatin in ovarian cancer cells, raising the question of how SIRT5 participates in the induction of chemoresistance. First, we confirmed that cisplatin can lead to the accumulation of γ-H2AX protein, which is a marker of DNA double-strand breaks, in a concentration-dependent manner (**Figures 4A,B**). Moreover, cisplatin-induced DNA damage could be suppressed by the overexpression of SIRT5 in A2780 cells, whereas γ-H2AX protein levels were increased upon SIRT5 downregulation in SKOV-3 and CAOV-3 cells (**Figures 4C,D**). In addition, immunofluorescence validated that SIRT5 overexpression could inhibit the formation of γ-H2AX foci, whereas this suppressive effect was abrogated upon SIRT5 knockdown (**Figures 4E,F**). Therefore, SIRT5 was shown to promote cisplatin resistance in ovarian cancer cells by inhibiting DNA damage.

SIRT5 Eliminates Cisplatin-Induced ROS to Reduce DNA Damage

Next, the mechanism by which SIRT5 suppresses cisplatin-induced DNA damage was investigated. As SIRT5 has been reported to regulate ROS (26) and excessive ROS induced by cisplatin can lead to DNA damage (27–29), we hypothesized that SIRT5 suppresses cisplatin-induced DNA damage by eliminating ROS. First, we confirmed that the levels of intracellular ROS induced by cisplatin were increased in both a concentration- and time-dependent manner. The levels of ROS peaked after 24 h of exposure to cisplatin and decreased by 48 h in all three ovarian cancer cell lines (**Figures 5A,B**). Therefore, we observed ROS levels in these cell lines at 24 h after cisplatin treatment for the subsequent experiments. Cisplatin-induced ROS levels were significantly inhibited upon overexpression of SIRT5 in A2780 cells, whereas the levels were increased after SIRT5 was silenced in SKOV-3 and CAOV-3 cells (**Figures 5C,D**). As expected, the inhibition of cisplatin-induced DNA damage by SIRT5 was reversed by the administration of NAC, a ROS scavenger (**Figures 5E–G**). These results indicate that SIRT5 suppresses cisplatin-induced DNA damage in a ROS-dependent manner in ovarian cancer cells.

In addition, using the GEPIA database, *SIRT5* expression was found to have a positive relationship with *BRCA1* expression, which is a well-known DNA damage repair gene ($P = 6.6e\text{-}7$, **Figure S1B**). In the present study, the levels of γ-H2AX were suppressed when BRCA1 was upregulated upon overexpression of SIRT5, and they were increased after downregulation of BRCA1 upon knockdown of SIRT5 (**Figure 5H**). These results suggest that SIRT5 also suppresses γ-H2AX expression by positively regulating BRCA1 expression, but the specific mechanism needs to be further explored.

SIRT5 Inhibits ROS by Positively Regulating the Nrf2/HO-1 Pathway

As SIRT5 is closely related to the mitochondria, the expression of MnSOD/SOD2, which is a well-known antioxidant enzyme, was measured initially. However, the level of this enzyme was not significantly changed after upregulation or downregulation of SIRT5 and the expression of *SOD2* mRNA had no significant relationship with *SIRT5* mRNA expression in ovarian cancer based on the GEPIA database (**Figures S1C,D**). Next, whether SIRT5 could inhibit ROS by regulating the Nrf2/HO-1 pathway, which is also known to eliminate ROS (30), was investigated. The mRNA expression levels of *Nrf2* and *HO-1* were lower in ovarian cancer than in normal tissues based on the GEPIA database (**Figure 6A**). Interestingly, the protein levels of Nrf2 and HO-1 were higher in SKOV-3 and CAOV-3 cells than in A2780 cells (**Figure 6B**). Moreover, a significant, positive correlation was identified between *Nrf2* and *SIRT5* mRNA expression in ovarian cancer based on the GEPIA database ($P = 1.5e\text{-}10$, $R = 0.3$) (**Figure 6C**). Further, Nrf2 and HO-1 proteins were upregulated upon SIRT5 overexpression in A2780 cells and were downregulated upon SIRT5 silencing in SKOV-3 and CAOV-3 cells (**Figure 6D**). In addition, overexpression of SIRT5 facilitated the nuclear translocation of Nrf2 by immunofluorescence staining, which was corroborated by western blotting of cytosolic and nuclear fractions (**Figures 6E,F**). These observations suggest that SIRT5 can enhance the expression of Nrf2 and its target gene HO-1 in ovarian cancer.

To provide further support, ML385, a specific inhibitor of Nrf2, was utilized to treat A2780 cells for 24 or 48 h. As shown in **Figure 6G**, Nrf2 was significantly suppressed at 48 h. ROS levels in A2780 cells overexpressing SIRT5 were then measured after pretreating the cells with or without ML385 for 48 h and cisplatin for 24 h. The results show that the inhibition of ROS by SIRT5 was reversed upon ML385 treatment (**Figures 6H,I**). Taken together, SIRT5 can inhibit ROS by positively regulating the Nrf2/HO-1 pathway.

DISCUSSION

In this study, among the *Sirtuin* family, *SIRT5* was highly expressed in ovarian cancer compared to its expression in normal tissues, based on the GEPIA database and this result was verified by immunohistochemistry. In addition, high levels of SIRT5 predicted shorter PFS and were positively associated with clinicopathologic characteristics of ovarian cancer, such as advanced FIGO stage and lymph node metastasis, but were negatively correlated with differentiation. These results reveal a potential prognostic role for SIRT5 in ovarian cancer patients. Consistent with our results, SIRT5 was shown to be overexpressed in human NSCLC (13), triple-negative breast cancer, breast cancer with BRCA1 mutation subtypes (17), CRC

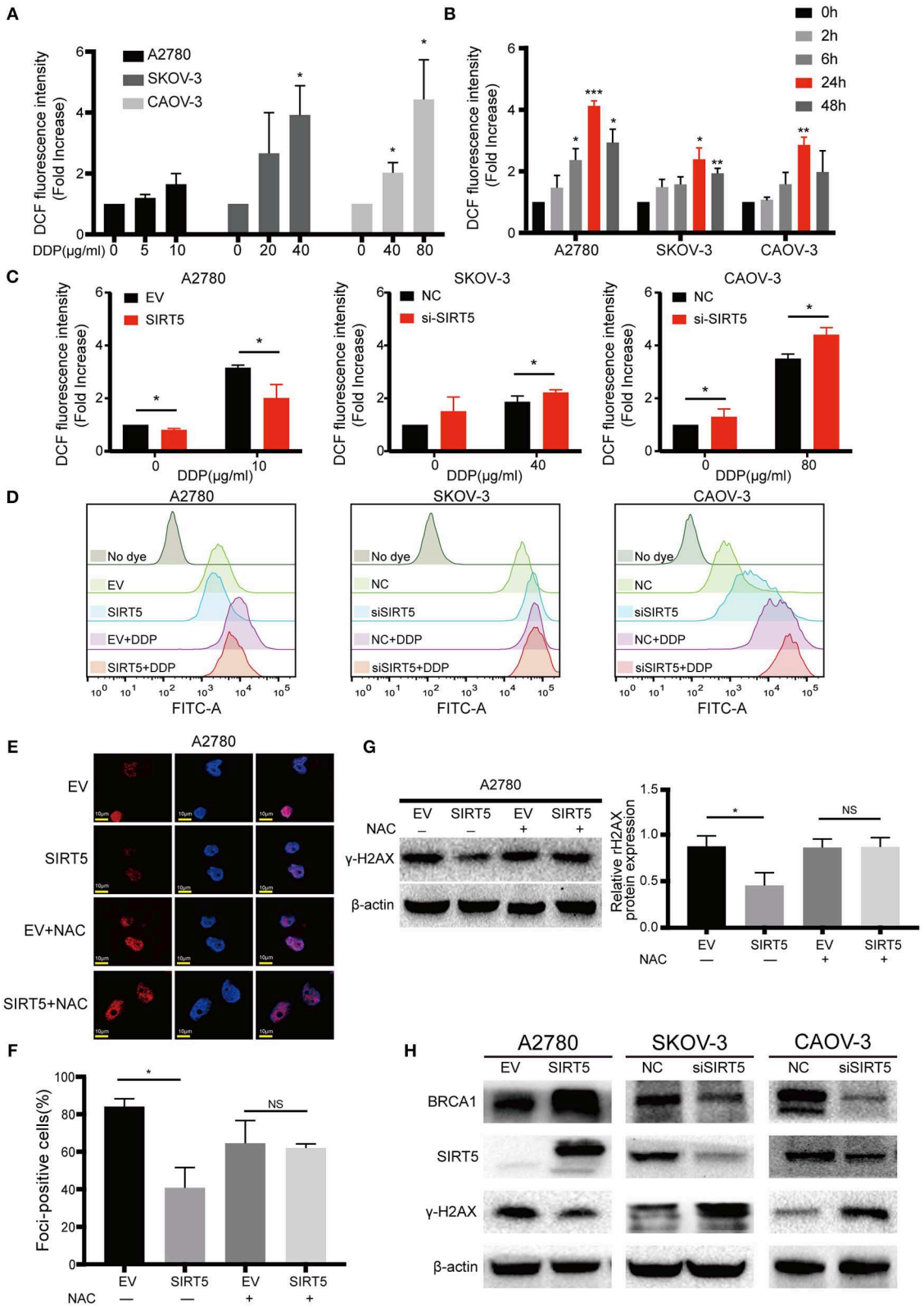

FIGURE 5 | SIRT5 eliminates cisplatin induced ROS to reduce DNA damage. **(A)** Cisplatin induced ROS generation in concentration and **(B)** time dependent manner in three ovarian cancer cells. The cells were treated with indicated dose of cisplatin and collected at indicated time points. The ROS levels were measured by flow

(Continued)

FIGURE 5 | cytometry and 0 h served as a control group. **(C)** Overexpression of SIRT5 inhibited ROS production and knockdown of SIRT5 attenuated the inhibition effect. **(D)** Representative flow cytometry results analyzed by FlowJo software. **(E,F)** NAC, a ROS scavenger, reversed the inhibition of cisplatin induced DNA damage in A2780 cells with overexpression SIRT5 by assessing γ-H2AX foci formation and **(G)** γ-H2AX protein levels. Cells were pretreated with 5 mM NAC for 2 h to inhibit ROS generation and then exposure to cisplatin for 24 h. **(H)** The levels of γ-H2AX was suppressed when BRCA1 was upregulated upon overexpression of SIRT5, and increased after downregulated of BRCA1 upon knockdown of SIRT5. Data are presented as the mean ± SD of three independent experiments. EV, empty vector; NC, negative control; DDP, cisplatin; NS, not significant. Scale bar = 10 μm, $^{*}P < 0.05$, $^{**}P < 0.01$, $^{***}P < 0.001$.

(15), and HCC (14). Further statistical analysis showed that higher SIRT5 was significantly associated with malignant tumor characteristics such as larger tumor size, lymph node metastasis, advanced TNM stage, and poor survival. Besides, a shorter time to post-therapeutic recurrence in wild-type Kras CRC patients was found to correlate with high expression of SIRT5 (21). However, upregulated SIRT5 in liver cancer tissues was found to be associated with favorable prognosis (19). Regarding mRNA or protein levels of SIRT5, Janus-faced expression has been identified. For example, SIRT5 was overexpressed in the aforementioned tumors and B cell malignancies (16), but was decreased in endometrial carcinoma (20) and head and neck squamous cell carcinoma (18).To summarize, SIRT5 might act as either a tumor promoter or suppressor, in a context-specific manner.

Although SIRT5 is predominantly a mitochondrial matrix protein, possessing a well-defined mitochondrial localization sequence (31), it was localized to both the cytoplasm and nucleus in three ovarian cancer cell lines, but the majority of SIRT5 was found in the cytoplasm in our study, which is consistent with other reports (32–34). Interestingly, nuclear and cytosolic SIRT5 in cerebellar granule neurons exerted a protective effect for cells, whereas mitochondrial SIRT5 promoted neuronal death (34). However, the mechanism by which SIRT5 localization contributes to these effects remains unknown.

Additionally, we revealed that SIRT5 expression was higher in SKOV-3 and CAOV-3 cells, which were shown to be resistant to cisplatin in our study, than in A2780 cells, which were confirmed to be sensitive to cisplatin (23–25). Moreover, SIRT5 expression was upregulated by cisplatin in a concentration-dependent manner. Similarly, the significant enrichment of endogenous SIRT5 protein after exposure to chemotherapeutic agents or cetuximab was confirmed previously in two wild-type Kras CRC cell lines (21). Consequently, we speculated that SIRT5 is involved in the progression and chemoresistance of ovarian cancer. As expected, the overexpression of SIRT5 significantly promoted cell proliferation and cisplatin resistance *in vitro*, while an inhibitory effect was observed upon SIRT5 downregulation. In agreement with our results, SIRT5 was found to drive HEK293 cancer cell proliferation via desuccinylation and activation of the serine hydroxymethyltransferase SHMT2 (35) and promote cell proliferation in HCC by targeting E2F transcription factor 1 (14). In contrast, SIRT5 was found to inhibit gastric cancer cell proliferation and tumor formation by inhibiting aerobic glycolysis (36). Interestingly, SIRT5 is not necessary for BrafV600E-mediated cutaneous melanoma initiation and growth *in vivo* (37). With respect to its function in chemoresistance, SIRT5 knockdown sensitizes NSCLC A549 cells to multiple chemotherapeutics including cisplatin (13). Moreover, SIRT5 was determined to have a partial inhibitory effect on the tumor suppressor SUN2, which was found to increase the sensitivity of lung cancer to cisplatin by inducing apoptosis (12). In wild-type Kras CRCs, SIRT5-positive cells were also shown to be resistant to either chemotherapeutic agents, such as 5-FU and oxaliplatin, or cetuximab (21). In contrast, an analysis of data from the GEO DataSet revealed high levels of *SIRT5* in triple-negative breast cancer patients who showed complete response to neoadjuvant chemotherapy. Analysis of the ONCOMINE database also suggested that SIRT5 expression levels were higher in chemotherapy responders than in non-responders (17). In conclusion, further study is needed to explore the role of SIRT5 in tumorigenesis and chemoresistance.

Cisplatin, one of the most widely applied chemotherapeutic agents for multiple solid tumors including ovarian cancer, was initially described as a DNA intrastrand cross-linker that interacts with DNA to form DNA adducts, resulting in the activation of several signal transduction pathways including those involved in DNA damage repair and apoptosis (38). Recent reports have suggested that a novel cytotoxic effect for most genotoxic drugs including cisplatin is to promote ROS-dependent apoptosis (39, 40) or DNA damage (27–29). Therefore, the activation of a ROS-scavenging mechanism in cancer cells confers resistance to chemotherapy (21). In this study, we found that SIRT5 potently inhibits cisplatin-induced DNA damage, as indicated by γ-H2AX protein levels in western blotting and foci formation in immunofluorescence staining. Similarly, after SIRT5 knockdown, the levels of γ-H2AX were previously shown to be significantly upregulated in both CRCs and HCC (15, 19). Then, we confirmed that cisplatin can induce ROS production in a concentration- and time-dependent manner, and that ROS levels peaked after exposure to an IC_{50} treatment of cisplatin for 24 h. ROS levels induced by cisplatin were significantly reduced upon SIRT5 overexpression but were increased after SIRT5 knockdown. Furthermore, the inhibitory effect of SIRT5 on DNA damage was attenuated when NAC, a ROS scavenger, was applied. These results verified our hypothesis that SIRT5 promotes cisplatin resistance in ovarian cancer by suppressing cisplatin-induced DNA damage in a ROS-dependent manner. In agreement with our results, SIRT5 was found to demalonylate and inactivate succinate dehydrogenase complex subunit A (SDHA) in CRCs, resulting in activation of the ROS-scavenging enzyme, thioredoxin reductase 2 (TrxR2) and finally leading to chemotherapy resistance (21). Likewise, other mechanisms underlying SIRT5-mediated ROS detoxification have been reported. For instance, SIRT5 was identified as a safeguard against oxidative stress-induced apoptosis in cardiomyocytes and neuroblastoma cells (6, 7). In NSCLC, SIRT5 was found to desuccinylate and activate Cu/Zn superoxide

FIGURE 6 | SIRT5 inhibits ROS via positively regulating Nrf2/HO-1 pathway. **(A)** The mRNA expression of *Nrf2* and *HO-1* in ovarian cancer and normal tissues (GEPIA). **(B)** Nrf2 and HO-1 protein levels were higher in SKOV-3 and CAOV-3 than A2780 cells assessed by western blot and the relative gray values were shown in histogram. **(C)** The correlation between *Nrf2* and *SIRT5* in ovarian cancer based on GEPIA database by Pearson correlation coefficient. **(D)** Overexpression of SIRT5

(Continued)

FIGURE 6 | upregulated Nrf2 and HO-1 protein levels and knockdown of SIRT5 reduced their expression assessed by western blot and the relative gray values were shown in histogram. **(E,F)** Overexpression of SIRT5 facilitated the nuclear translocation of Nrf2 by immunofluorescence staining and western blot after nuclear and cytoplasm isolation. **(G)** ML385, a specific inhibitor of Nrf2, was added into A2780 cells with terminal concentration of 5 μM for 24 or 48 h and the inhibition efficiency was measured by western blot. **(H)** The inhibition effect of ROS by overexpression SIRT5 in A2780 cells was reversed when ML385 was applied. **(I)** Representative flow cytometry results analyzed by FlowJo software. Data are presented as the mean ± SD of three independent experiments. EV, empty vector; NC, negative control; DDP, cisplatin; TPM, transcripts per million. Scale bar = 20 μm, $^{*}P < 0.05$, $^{**}P<0.01$, $^{***}P<0.001$, compared with A2780, the EV or NC cells.

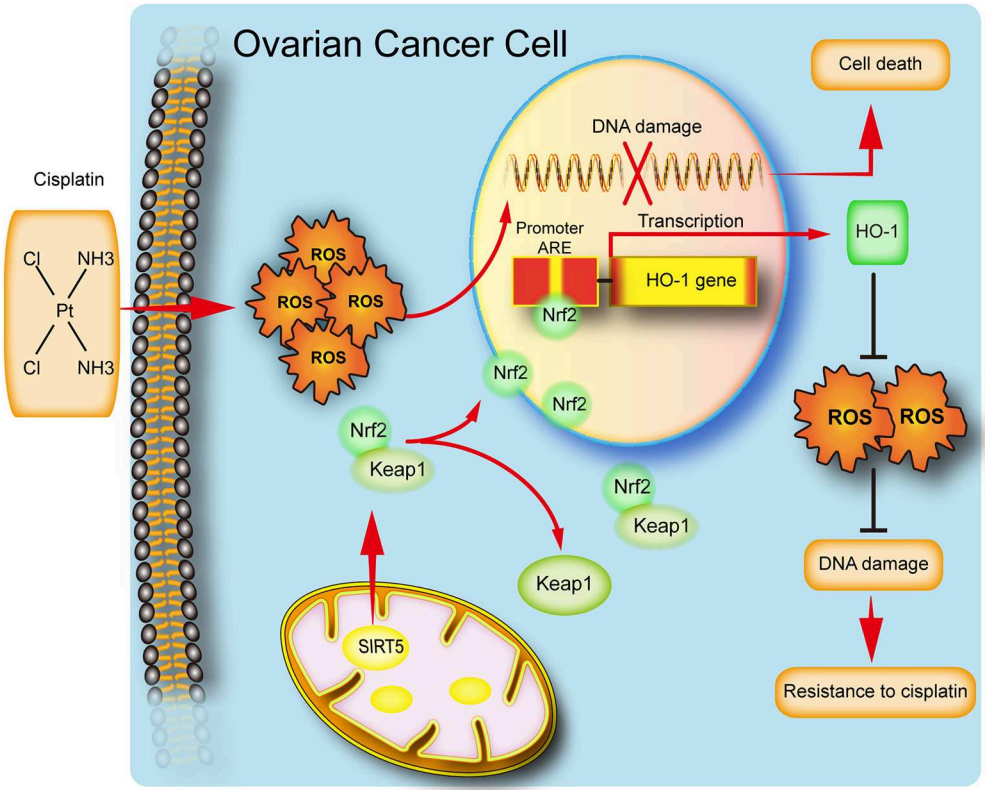

FIGURE 7 | Schematic representation of SIRT5 mediated resistance of ovarian cancer cells to cisplatin.SIRT5 positively regulates Nrf2, resulting in the nuclear translocation of Nrf2. Nuclear Nrf2 binds to antioxidant responsive elements(ARE) and activates HO-1 transcription and thus eliminates cisplatin induced ROS, leading to inhibition of DNA damage and finally cisplatin resistance.

dismutase (SOD1) to eliminate ROS when the proteins were co-expressed (41). Moreover, the desuccinylation of isocitrate dehydrogenase 2 (IDH2) or pyruvate kinase M2 (PKM2) and the deglutarylation of glucose-6-phosphate dehydrogenase (G6PD) by SIRT5 leads to the production of sufficient NADPH, a major intracellular reductant, to attenuate cellular ROS levels (42, 43). Interestingly, the expression of MnSOD/SOD2, a known antioxidant enzyme, was not significantly changed after upregulation or downregulation of SIRT5 in our study. Collectively, these studies highlight the fact that SIRT5 promotes ROS detoxification via the post-translational modification of multiple, vital antioxidant enzymes.

Another mechanism of cisplatin resistance is the enhancement of DNA damage repair. *BRCA1*, which is a key gene in the DNA damage repair pathway, was identified as having a positive correlation with *SIRT5* expression in ovarian cancer, based on the GEPIA database. Further, the levels of γ-H2AX were suppressed when BRCA1 was upregulated upon overexpression of SIRT5, and they were increased when BRCA1 was downregulated upon knockdown of SIRT5. These results suggested that SIRT5 also contributes to cisplatin resistance by positively regulating BRCA1 expression, but the exact mechanism needs to be explored further.

In addition to the abovementioned enzymes, transcription factors that promote the expression of antioxidant defense genes, such as forkhead box O3 (FOXO3), could be deacetylated at critical lysine residues by SIRT5, promoting their nuclear localization and leading to decreased ROS levels (44). In our study, another transcription factor, Nrf2, which promotes the expression of antioxidant and detoxifying genes, and HO-1, a key target gene of Nrf2, were overexpressed in cisplatin-resistant SKOV-3 and CAOV-3 cells, in agreement with reports of high levels of Nrf2 and HO-1 in drug-resistant tumor cells (45–47). Interestingly, the mRNA expressions of *Nrf2* and

HO-1 were lower in ovarian cancer than in normal tissues based on the GEPIA database, in contrast to reports of their upregulated protein levels in tumors such as ovarian cancer (48, 49). Moreover, in our study, the Nrf2/HO-1 pathway was found to be positively regulated by SIRT5 and overexpression of SIRT5 facilitated Nrf2 nuclear translocation, consistent with a report that the mRNA levels of *Nrf2* and its downstream target genes are reduced upon SIRT5 knockdown in NSCLC (13). In addition, in the present study, the downregulation of ROS by SIRT5 was reversed when a specific Nrf2 inhibitor, ML385, was utilized. These results provide evidence that SIRT5 inhibits ROS production via positive regulation of the Nrf2/HO-1 pathway. GSH, a known ROS scavenger, was identified previously as mediating resistance to cisplatin (50–53). It was reported that Nrf2 is involved in the regulation of GSH abundance and that Nrf2 activation can result in high GSH dependency of the affected cells (54). Consistent with these reports, in our study, higher levels of GSH were found in SKOV-3 and CAOV-3 cisplatin-resistant cell lines relative to the levels in A2780 sensitive cells (**Figure S1E**). To summarize, SIRT5 may also function as a ROS inhibitor by activating Nrf2, leading to increased GSH levels, but this hypothesis should be confirmed by future experiments.

The limitation of our study is that the exact mechanism by which SIRT5 functions as a mitochondrial enzyme to regulate the Nrf2/HO-1 pathway was not clarified. However, one possibility is that SIRT5 inhibits autophagic flux via the deacetylation of lactate dehydrogenase B (LDHB) (10), leading to an increase in p62, which competes with Nrf2 for Kelch-like ECH-associated protein 1 (KEAP1) binding (55). This results in Nrf2 dissociation from KEAP1 and prolonged activation of Nrf2 (56, 57). Another possibility is that SIRT5 competes with SIRT2 to interact with Nrf2, which blocks the deacetylation of Nrf2 by SIRT2, leading to an increase in nuclear Nrf2 levels (58, 59). In addition, it was also reported that BRCA1 could interact with Nrf2 and promote its stability and activation (60–62), we hypothesize that SIRT5 actives Nrf2 pathway by positively regulating BRCA1. However, these hypotheses need to be tested further.

In conclusion, our study implies that SIRT5 expression is increased in ovarian cancer tissues and its high level predicts a poor chemotherapy response. We also reveal a potential function for SIRT5 in ovarian cancer proliferation and chemoresistance. Specifically, SIRT5 contributes to cisplatin resistance by suppressing cisplatin-induced DNA damage in a ROS-dependent manner via the regulation of Nrf2/HO-1 signaling (**Figure 7**). Therefore, SIRT5 might serve as a prognostic factor for ovarian cancer and SIRT5 inhibitors combined with chemotherapy could represent a novel therapeutic strategy for ovarian cancer patients.

DATA AVAILABILITY

The raw data supporting the conclusions of this manuscript will be made available by the authors, without undue reservation, to any qualified researcher. Publicly available datasets were also analyzed in this study. This data can be found here: http://gepia.cancer-pku.cn/.

AUTHOR CONTRIBUTIONS

QL, LF, CZ, SW, and XS contributed conception and design of the study. XS, SW, JGa, JGu, JL, YL, and JZ performed experiment and the statistical analysis. XS and SW wrote the first draft of the manuscript. All authors contributed to manuscript revision, read and approved the submitted version.

FUNDING

This work was supported by the National Natural Science Foundation of China (grant numbers 81672964, 81874214, and 81702269).

ACKNOWLEDGMENTS

We would like to thank Editage [www.editage.cn] for English language editing and Mr. Yifu Song for technological support. XS would like to thank her families for helping her take care of her little daughter.

SUPPLEMENTARY MATERIAL

The Supplementary Material for this article can be found online at: https://www.frontiersin.org/articles/10.3389/fonc.2019.00754/full#supplementary-material

Figure S1 | (A) The localization of SIRT5 in three ovarian cancer cell lines was validated by western blot after nuclear and cytoplasm isolation. **(B)** *SIRT5* had a positive relationship with *BRCA1* based on GEPIA database. **(C)** MnSOD/SOD2 protein levels were not significantly changed after upregulation or downregulation of SIRT5 levels. **(D)** *SIRT5* had no significant relationship with *MnSOD/SOD2* based on GEPIA database. **(E)** The relative levels of glutathione (GSH) in three ovarian cancer cells. TPM, transcripts per million. $^{*}P < 0.05$.

REFERENCES

1. Nakagawa T, Lomb DJ, Haigis MC, Guarente L. SIRT5 Deacetylates carbamoyl phosphate synthetase 1 and regulates the urea cycle. *Cell.* (2009) 137:560–70. doi: 10.1016/j.cell.2009.02.026
2. Du J, Zhou Y, Su X, Yu JJ, Khan S, Jiang H, et al. Sirt5 is a NAD-dependent protein lysine demalonylase and desuccinylase. *Science.* (2011) 334:806–9. doi: 10.1126/science.1207861
3. Tan M, Peng C, Anderson KA, Chhoy P, Xie Z, Dai L, et al. Lysine glutarylation is a protein posttranslational modification regulated by SIRT5. *Cell Metab.* (2014) 19:605–17. doi: 10.1016/j.cmet.2014.03.014
4. Bringman-Rodenbarger LR, Guo AH, Lyssiotis CA, Lombard DB. Emerging roles for SIRT5 in metabolism and cancer. *Antioxid Redox Signal.* (2017) 28:677–90. doi: 10.1089/ars.2017.7264
5. Zou R, Shi W, Tao J, Li H, Lin X, Yang S, et al. SIRT5 and post-translational protein modifications: a potential therapeutic target for myocardial ischemia-reperfusion injury with regard to mitochondrial dynamics and oxidative metabolism. *Eur J Pharmacol.* (2018) 818:410–8. doi: 10.1016/j.ejphar.2017.11.005
6. Liang F, Wang X, Ow SH, Chen W, Ong WC. Sirtuin 5 is anti-apoptotic and anti-oxidative in cultured SH-EP neuroblastoma cells. *Neurotox Res.* (2017) 31:63–76. doi: 10.1007/s12640-016-9664-y

7. Liu B, Che W, Zheng C, Liu W, Wen J, Fu H, et al. SIRT5: a safeguard against oxidative stress-induced apoptosis in cardiomyocytes. *Cell Physiol Biochem.* (2013) 32:1050–9. doi: 10.1159/000354505
8. Wang Y, Liu Q, Huan Y, Li R, Li C, Sun S, et al. Sirtuin 5 overexpression attenuates glucolipotoxicity-induced pancreatic β cells apoptosis and dysfunction. *Exp Cell Res.* (2018) 371:205–13. doi: 10.1016/j.yexcr.2018.08.011
9. Li F, He X, Ye D, Lin Y, Yu H, Yao C, et al. NADP+-IDH mutations promote hypersuccinylation that impairs mitochondria respiration and induces apoptosis resistance. *Mol Cell.* (2015) 60:661–75. doi: 10.1016/j.molcel.2015.10.017
10. Shi L, Yan H, An S, Shen M, Jia W, Zhang R, et al. SIRT5-mediated deacetylation of LDHB promotes autophagy and tumorigenesis in colorectal cancer. *Mol Oncol.* (2019) 13:358–75. doi: 10.1002/1878-0261.12408
11. Polletta L, Vernucci E, Carnevale I, Arcangeli T, Rotili D, Palmerio S, et al. SIRT5 regulation of ammonia-induced autophagy and mitophagy. *Autophagy.* (2015) 11:253–70. doi: 10.1080/15548627.2015.1009778
12. Lv XB, Liu L, Cheng C, Yu B, Xiong L, Hu K, et al. SUN2 exerts tumor suppressor functions by suppressing the Warburg effect in lung cancer. *Sci Rep.* (2015) 5:1–12. doi: 10.1038/srep17940
13. Lu W, Zuo Y, Feng Y, Zhang M. SIRT5 facilitates cancer cell growth and drug resistance in non-small cell lung cancer. *Tumor Biol.* (2014) 35:10699–705. doi: 10.1007/s13277-014-2372-4
14. Chang L, Xi L, Liu Y, Liu R, Wu Z, Jian Z. SIRT5 promotes cell proliferation and invasion in hepatocellular carcinoma by targeting E2F1. *Mol Med Rep.* (2018) 17:342–9. doi: 10.3892/mmr.2017.7875
15. Wang YQ, Wang HL, Xu J, Tan J, Fu LN, Wang JL, et al. Sirtuin5 contributes to colorectal carcinogenesis by enhancing glutaminolysis in a deglutarylation-dependent manner. *Nat Commun.* (2018) 9:1–15. doi: 10.1038/s41467-018-02951-4
16. Sun JY, Xu L, Tseng H, Ciccarelli B, Fulciniti M, Hunter ZR, et al. Histone deacetylase inhibitors demonstrate significant preclinical activity as single agents, and in combination with bortezomib in Waldenstrom's macroglobulinemia. *Clin Lymphoma Myeloma Leuk.* (2011) 11:152–6. doi: 10.3816/CLML.2011.n.036
17. Xu L, Che X, Wu Y, Song N, Shi S, Wang S, et al. SIRT5 as a biomarker for response to anthracycline-taxane-based neoadjuvant chemotherapy in triple-negative breast cancer. *Oncol Rep.* (2018) 39:2315–23. doi: 10.3892/or.2018.6319
18. Lai CC, Lin PM, Lin SF, Hsu CH, Lin HC, Hu ML, et al. Altered expression of SIRT gene family in head and neck squamous cell carcinoma. *Tumor Biol.* (2013) 34:1847–54. doi: 10.1007/s13277-013-0726-y
19. Chen X, Tian M, Sun R, Zhang M, Zhou L, Jin L, et al. SIRT5 inhibits peroxisomal ACOX1 to prevent oxidative damage and is downregulated in liver cancer. *EMBO Rep.* (2018) 19:e45124. doi: 10.15252/embr.201745124
20. Bartosch C, Monteiro-Reis S, Almeida-Rios D, Vieira R, Castro A, Moutinho M, et al. Assessing sirtuin expression in endometrial carcinoma and non-neoplastic endometrium. *Oncotarget.* (2016) 7:1144–54. doi: 10.18632/oncotarget.6691
21. Du ZG, Liu XJ, Chen T, Gao WC, Wu ZM, Hu ZQ, et al. Targeting a Sirt5-positive subpopulation overcomes multidrug resistance in wild-type kras colorectal carcinomas. *Cell Rep.* (2018) 22:2677–89. doi: 10.1016/j.celrep.2018.02.037
22. McGuire S. World cancer report 2014. Geneva, Switzerland: world health organization, international agency for research on cancer, WHO press, 2015. *Adv Nutr.* (2016) 7:418–9. doi: 10.3945/an.116.012211
23. Chen J, Solomides C, Parekh H, Simpkins F, Simpkins H. Cisplatin resistance in human cervical, ovarian and lung cancer cells. *Cancer Chemother Pharmacol.* (2015) 75:1217–27. doi: 10.1007/s00280-015-2739-2
24. Hahne JC. Practices platinum-resistance and AKT over-expression in ovarian cancer. *Int J Gynecol Clin.* (2015) 2:110. doi: 10.15344/2394-4986/2015/110
25. Beaufort CM, Helmijr JCA, Piskorz AM, Hoogstraat M, Ruigrok-Ritstier K, Besselink N, et al. Ovarian cancer cell line panel (OCCP): clinical importance of *in vitro* morphological subtypes. *PLoS ONE.* (2014) 9:e103988. doi: 10.1371/journal.pone.0103988
26. Kumar S, Lombard DB. Functions of the sirtuin deacylase SIRT5 in normal physiology and pathobiology. *Crit Rev Biochem Mol Biol.* (2018) 53:311–34. doi: 10.1080/10409238.2018.1458071
27. Luo H, Yang A, Schulte BA, Wargovich MJ, Wang GY. Resveratrol induces premature senescence in lung cancer cells via ROS-mediated DNA damage. *PLoS ONE.* (2013) 8:e60065. doi: 10.1371/journal.pone.0060065
28. Marullo R, Werner E, Degtyareva N, Moore B, Altavilla G, Ramalingam SS, et al. Cisplatin induces a mitochondrial-ros response that contributes to cytotoxicity depending on mitochondrial redox status and bioenergetic functions. *PLoS ONE.* (2013) 8:e81162. doi: 10.1371/journal.pone.0081162
29. Srinivas US, Tan BWQ, Vellayappan BA, Jeyasekharan AD. ROS and the DNA damage response in cancer. *Redox Biol.* (2019) 21:101084. doi: 10.1016/j.redox.2018.101084
30. Furfaro AL, Traverso N, Domenicotti C, Piras S, Moretta L, Marinari UM, et al. The Nrf2/HO-1 axis in cancer cell growth and chemoresistance. *Oxid Med Cell Longev.* (2016) 2016:1958174. doi: 10.1155/2016/1958174
31. Matsushita N, Yonashiro R, Ogata Y, Sugiura A, Nagashima S, Fukuda T, et al. Distinct regulation of mitochondrial localization and stability of two human Sirt5 isoforms. *Genes Cells.* (2011) 16:190–202. doi: 10.1111/j.1365-2443.2010.01475.x
32. Du Y, Hu H, Hua C, Du K, Wei T. Tissue distribution, subcellular localization, and enzymatic activity analysis of human SIRT5 isoforms. *Biochem Biophys Res Commun.* (2018) 503:763–69. doi: 10.1016/j.bbrc.2018.06.073
33. Mahlknecht U, Ho AD, Letzel S, Voelter-Mahlknecht S. Assignment of the NAD-dependent deacetylase sirtuin 5 gene (SIRT5) to human chromosome band 6p23 by *in situ* hybridization. *Cytogenet Genome Res.* (2006) 112:208–12. doi: 10.1159/000089872
34. Pfister JA, Ma C, Morrison BE, D'Mello SR. Opposing effects of sirtuins on neuronal survival: SIRT1-mediated neuroprotection is independent of its deacetylase activity. *PLoS ONE.* (2008) 3:e4090. doi: 10.1371/journal.pone.0004090
35. Yang X, Wang Z, Li X, Liu B, Liu M, Liu L, et al. SHMT2 desuccinylation by SIRT5 drives cancer cell proliferation. *Cancer Res.* (2018) 78:372–86. doi: 10.1158/0008-5472.CAN-17-1912
36. Tang Z, Li L, Tang Y, Xie D, Wu K, Wei W, et al. CDK2 positively regulates aerobic glycolysis by suppressing SIRT5 in gastric cancer. *Cancer Sci.* (2018) 109:2590–8. doi: 10.1111/cas.13691
37. Moon H, Zhu J, White AC. Sirt5 is dispensable for BrafV600E-mediated cutaneous melanoma development and growth *in vivo*. *Exp Dermatol.* (2019) 28:83–5. doi: 10.1111/exd.13845
38. Siddik ZH. Cisplatin: mode of cytotoxic action and molecular basis of resistance. *Oncogene.* (2003) 22:7265–79. doi: 10.1038/sj.onc.1206933
39. Chen X, Wang KW, Chen YQ. Cisplatin induces apoptosis of A549 cells by downregulating peroxidase V. *Eur Rev Med Pharmacol Sci.* (2018) 22:7289–95. doi: 10.26355/eurrev_201811_16265
40. Liu Y, Li Q, Zhou L, Xie N, Nice EC, Zhang H, et al. Cancer drug resistance: redox resetting renders a way. *Oncotarget.* (2016) 7:42740–61. doi: 10.18632/oncotarget.8600
41. Lin ZF, Xu HB, Wang JY, Lin Q, Ruan Z, Liu FB, et al. SIRT5 desuccinylates and activates SOD1 to eliminate ROS. *Biochem Biophys Res Commun.* (2013) 441:191–5. doi: 10.1016/j.bbrc.2013.10.033
42. Zhou L, Wang F, Sun R, Chen X, Zhang M, Xu Q, et al. SIRT5 promotes IDH2 desuccinylation and G6PD deglutarylation to enhance cellular antioxidant defense. *EMBO Rep.* (2016) 17:811–22. doi: 10.15252/embr.201541643
43. Xiangyun Y, Xiaomin N, Linping G, Yunhua X, Ziming L, Yongfeng Y, et al. Desuccinylation of pyruvate kinase M2 by SIRT5 contributes to antioxidant response and tumor growth. *Oncotarget.* (2017) 8:6984–93. doi: 10.18632/oncotarget.14346
44. Wang Y, Zhu Y, Xing S, Ma P, Lin D. SIRT5 prevents cigarette smoke extract-induced apoptosis in lung epithelial cells via deacetylation of FOXO3. *Cell Stress Chaperones.* (2015) 20:805–10. doi: 10.1007/s12192-015-0599-7
45. Jozkowicz A, Was H, Dulak J. Heme oxygenase-1 in tumors: is it a false friend? *Antioxid Redox Signal.* (2007) 9:2099–117. doi: 10.1089/ars.2007.1659
46. Berberat PO, Dambrauskas Z, Gulbinas A, Giese T, Giese N, Künzli B, et al. Inhibition of heme oxygenase-1 increases responsiveness of pancreatic cancer cells to anticancer treatment. *Clin Cancer Res.* (2005) 11:3790–8. doi: 10.1158/1078-0432.CCR-04-2159
47. Jaramillo MC, Zhang DD. The emerging role of the Nrf2-Keap1 signaling pathway in cancer. *Genes Dev.* (2013) 27:2179–91. doi: 10.1101/gad.225680.113

48. Shim G, Manandhar S, Shin D, Kim TH, Kwak MK. Acquisition of doxorubicin resistance in ovarian carcinoma cells accompanies activation of the NRF2 pathway. *Free Radic Biol Med.* (2009) 47:1619–31. doi: 10.1016/j.freeradbiomed.2009.09.006
49. Bao LJ, Jaramillo MC, Zhang ZB, Zheng YX, Yao M, Zhang DD, et al. Nrf2 induces cisplatin resistance through activation of autophagy in ovarian carcinoma. *Int J Clin Exp Pathol.* (2014) 7:1502–13.
50. Pan H, Kim E, Rankin GO, Rojanasakul Y, Tu Y, Chen YC. Theaflavin-3,3'-digallate enhances the inhibitory effect of cisplatin by regulating the copper transporter 1 and glutathione in human ovarian cancer cells. *Int J Mol Sci.* (2018) 19:E117. doi: 10.3390/ijms19010117
51. Nunes SC, Serpa J. Glutathione in ovarian cancer: a double-edged sword. *Int J Mol Sci.* (2018) 19:E1882. doi: 10.3390/ijms19071882
52. Zheng ZG, Xu H, Suo SS, Xu XL, Ni MW, Gu LH, et al. The essential role of H19 contributing to cisplatin resistance by regulating glutathione metabolism in high-grade serous ovarian cancer. *Sci Rep.* (2016) 6:26093. doi: 10.1038/srep26093
53. Godwin AK, Meister A, O'Dwyer PJ, Huang CS, Hamilton TC, Anderson ME. High resistance to cisplatin in human ovarian cancer cell lines is associated with marked increase of glutathione synthesis. *Proc Natl Acad Sci USA.* (1992) 89:3070–4. doi: 10.1073/pnas.89.7.3070
54. Bansal A, Celeste Simon M. Glutathione metabolism in cancer progression and treatment resistance. *J Cell Biol.* (2018) 217:2291–8. doi: 10.1083/jcb.201804161
55. Ichimura Y, Waguri S, Sou Y, Kageyama S, Hasegawa J, Ishimura R, et al. Phosphorylation of p62 activates the Keap1-Nrf2 pathway during selective autophagy. *Mol Cell.* (2013) 51:618–31. doi: 10.1016/j.molcel.2013.08.003
56. Komatsu M, Kurokawa H, Waguri S, Taguchi K, Kobayashi A, Ichimura Y, et al. The selective autophagy substrate p62 activates the stress responsive transcription factor Nrf2 through inactivation of Keap1. *Nat Cell Biol.* (2010) 12:213–23. doi: 10.1038/ncb2021
57. Lau A, Zheng Y, Tao S, Wang H, Whitman SA, White E, et al. Arsenic inhibits autophagic flux, activating the Nrf2-Keap1 pathway in a p62-dependent manner. *Mol Cell Biol.* (2013) 33:2436–46. doi: 10.1128/MCB.01748-12
58. Qin K, Han C, Zhang H, Li T, Li N, Cao X. NAD^+ dependent deacetylase Sirtuin 5 rescues the innate inflammatory response of endotoxin tolerant macrophages by promoting acetylation of p65. *J Autoimmun.* (2017) 81:120–9. doi: 10.1016/j.jaut.2017.04.006
59. Gius D, Shang M, Vassilopoulos A, Knutson M, Chen C, Shapiro JS, et al. Sirtuin 2 regulates cellular iron homeostasis via deacetylation of transcription factor NRF2. *J Clin Invest.* (2017) 127:1505–16. doi: 10.1172/JCI88574
60. Gorrini C, Baniasadi PS, Harris IS, Silvester J, Inoue S, Snow B, et al. BRCA1 interacts with Nrf2 to regulate antioxidant signaling and cell survival. *J Exp Med.* (2013) 210:1529–44. doi: 10.1084/jem.20121337
61. Bae I, Fan S, Meng Q, Rih JK, Kim HJ, Kang HJ, et al. BRCA1 induces antioxidant gene expression and resistance to oxidative stress BRCA1 induces antioxidant gene expression and resistance to oxidative stress. *Cancer Res.* (2004) 7893–909. doi: 10.1158/0008-5472.CAN-04-1119
62. Labanca E, De Luca P, Gueron G, Paez A, Moiola CP, Massillo C, et al. Association of HO-1 and BRCA1 Is critical for the maintenance of cellular homeostasis in prostate cancer. *Mol Cancer Res.* (2015) 13:1455–64. doi: 10.1158/1541-7786.MCR-15-0150-T

Conflict of Interest Statement: The authors declare that the research was conducted in the absence of any commercial or financial relationships that could be construed as a potential conflict of interest.

frontiers in Oncology

ORIGINAL RESEARCH
published: 27 August 2019
doi: 10.3389/fonc.2019.00816

MTA3-SOX2 Module Regulates Cancer Stemness and Contributes to Clinical Outcomes of Tongue Carcinoma

Zhimeng Yao[1†], Liang Du[1,2†], Min Xu[3], Kai Li[1], Haipeng Guo[3], Guodong Ye[4], Dianzheng Zhang[5], Robert P. Coppes[2] and Hao Zhang[4,6]*

[1] Cancer Research Center, Shantou University Medical College, Shantou, China, [2] Department of Biomedical Sciences of Cells and Systems, Section Molecular Cell Biology and Radiation Oncology, University Medical Center Groningen, University of Groningen, Groningen, Netherlands, [3] Department of Head and Neck Surgery, Cancer Hospital of Shantou University Medical College, Shantou, China, [4] Institute of Precision Cancer Medicine and Pathology, Jinan University Medical College, Guangzhou, China, [5] Department of Bio-Medical Sciences, Philadelphia College of Osteopathic Medicine, Philadelphia, PA, United States, [6] Research Centre of Translational Medicine, The Second Affiliated Hospital of Shantou University Medical College, Shantou, China

OPEN ACCESS

Edited by:
Dong-Hua Yang,
St. John's University, United States

Reviewed by:
Anca Maria Cimpean,
Victor Babes University of Medicine and Pharmacy, Romania
Jun Yan,
Nanjing University, China

***Correspondence:**
Hao Zhang
haozhang@jnu.edu.cn

[†] These authors have contributed equally to this work

Specialty section:
This article was submitted to Molecular and Cellular Oncology, a section of the journal Frontiers in Oncology

Received: 04 June 2019
Accepted: 09 August 2019
Published: 27 August 2019

Citation:
Yao Z, Du L, Xu M, Li K, Guo H, Ye G, Zhang D, Coppes RP and Zhang H (2019) MTA3-SOX2 Module Regulates Cancer Stemness and Contributes to Clinical Outcomes of Tongue Carcinoma. Front. Oncol. 9:816. doi: 10.3389/fonc.2019.00816

Cancer cell plasticity plays critical roles in both tumorigenesis and tumor progression. Metastasis-associated protein 3 (MTA3), a component of the nucleosome remodeling and histone deacetylase (NuRD) complex and multi-effect coregulator, can serve as a tumor suppressor in many cancer types. However, the role of MTA3 in tongue squamous cell cancer (TSCC) remains unclear although it is the most prevalent head and neck cancer and often with poor prognosis. By analyzing both published datasets and clinical specimens, we found that the level of MTA3 was lower in TSCC compared to normal tongue tissues. Data from gene set enrichment analysis (GSEA) also indicated that MTA3 was inversely correlated with cancer stemness. In addition, the levels of MTA3 in both samples from TSCC patients and TSCC cell lines were negatively correlated with SOX2, a key regulator of the plasticity of cancer stem cells (CSCs). We also found that SOX2 played an indispensable role in MTA3-mediated CSC repression. Using the mouse model mimicking human TSCC we demonstrated that the levels of MTA3 and SOX2 decreased and increased, respectively, during the process of tumorigenesis and progression. Finally, we showed that the patients in the $MTA3^{low}/SOX2^{high}$ group had the worst prognosis suggesting that $MTA3^{low}/SOX2^{high}$ can serve as an independent prognostic factor for TSCC patients. Altogether, our data suggest that MTA3 is capable of repressing TSCC CSC properties and tumor growth through downregulating SOX2 and $MTA3^{low}/SOX2^{high}$ might be a potential prognostic factor for TSCC patients.

Keywords: tongue squamous cell carcinoma, MTA3, SOX2, cancer stem cell, prognosis, proliferation, progression

INTRODUCTION

More than 500,000 new cases of oral and pharyngeal cancers are diagnosed yearly worldwide (World Cancer report 2014, https://www.who.int/cancer/publications/WRC_2014/en/). Oral cancer is malignant neoplasia which arises on the lip or oral cavity. Although progress has been made in cancer treatments, the oral cancer survival rate has not been improved significantly

for decades (1, 2). Since ∼90% of these cancers are histologically shown to be originated from squamous cells (3), this subtype of cancers is traditionally defined as oral squamous cell carcinoma (OSCC). OSCC may show different levels of differentiation and has a propensity to coincide with lymph node metastasis (4). Among OSCC, tongue squamous cell cancer (TSCC) has the highest incidence and is usually associated with a poor survival rate. Therefore, TSCC is one of the most lethal types of cancers in the head and neck region (5). Thus, a better understanding of the underlying mechanisms in TSCC development will provide not only a more reliable biomarkers for diagnosis and prognosis but also potential therapeutic targets for the treatment of this cancer.

Cellular plasticity plays critical roles in tumor initiation, progression, and metastasis. It is now well-established that stem cell-like cancer cells or cancer stem cells (CSCs) are responsible for both cell plasticity and treatment (6–10). CSCs are a small subset of cancer cells and multiple lines of evidence indicate that CSCs are responsible for tumor initiation, indefinite, and progression (7, 11, 12). Accumulating data also indicate that plasticity of CSCs closely correlates with recurrences and metastasis (13–16) with poor prognosis in a wide variety of cancers, including tongue cancer (17–20).

Metastasis-associated protein 3 (MTA3) is a multi-effect coregulatory factor and plays indispensable roles in cell proliferation, tumorigenesis, and metastasis (21–26). Compelling evidence suggests that MTA3 is a tumor suppressor in many cancer types (26–28) by serving as an integral subunit of the nucleosome remodeling and histone deacetylase (NuRD) complex (21, 25, 27). As a transcriptional corepressor (29), MTA3 either directly or indirectly regulates the expression and activity of EMT-associated genes such as Snail and E-cadherin (25, 27). Dysregulation of MTA3 has been observed in many different human tumors (26–28). Reduced levels of MTA3 lead to the upregulation of Snail and subsequently enhance the process of epithelial-mesenchymal transition (EMT) (25, 27, 30). Consistently, the dysfunctional MTA3 reduces cell-cell adhesion and promotes cancer invasion and metastasis (23, 26). Moreover, reduced expression of MTA3 in tumor specimens has been associated with poor survival and therefore the expression of MTA3 has been suggested as an independent predictor of patient prognosis in uterine non-endometrioid carcinomas, gastroesophageal junction adenocarcinoma, glioma, and colorectal cancer (27, 28, 31, 32). However, the role of MTA3 and the underlying mechanism of MTA3's function in TSCC remain largely unknown.

In this study, we found that reduced levels of MTA3 in the patient specimens correlated with poorer clinical outcomes with concurrently increased cancer stemness. We also showed that MTA3 was capable of repressing cancer cell proliferation through inhibiting SOX2 expression. Using a chemical-induced mouse model of TSCC, we demonstrated that MTA3 and SOX2 decreased and increased, respectively, during the process of carcinogenesis and progression. Finally, our findings suggested that $MTA3^{low}/SOX2^{high}$ could potentially serve as an independent prognostic factor for TSCC patients.

MATERIALS AND METHODS

Patient Tissue Samples

A total of 119 patients with TSCC were recruited at the Affiliated Tumor Hospital of Shantou University Medical College from 2009 to 2011 and their TSCC were clinically diagnosed and histologically confirmed. The primary TSCC specimens and their matched non-cancerous tissues were paraffin-embedded. Samples from patients who underwent preoperative radiotherapy or chemotherapy for TSCC were excluded. Clinical research protocols of this study were reviewed and approved by the Ethics Committee of Shantou University Medical College.

Immunohistochemistry (IHC)

Tissue sections (4 μm) from the formalin-fixed paraffin-embedded clinical specimens or 4NQO-induced tongue tumor tissues were processed and immune-stained with antibodies against MTA3 (Catalog No. A300-160A, Bethyl, 1: 600), SOX2 (Catalog No. 23064, Cell Signaling, 1: 200), each with at least two cores of the primary tumor as well as two cores of normal tongue tissue. Sections immune-labeled with rabbit IgG or mouse IgG as the primary antibody were used as negative controls, known MTA3 and SOX2 positive slides were used as a positive control.

IHC Evaluation

The percentage of positively stained cells were scored using the following scales: 0, no staining in any field; 1, $\leq$ 10; 2, 11–50; 3, 51–75; 4, > 75%. The intensity of staining was scored using the following scales: 1+, weak staining; 2+, moderate staining; 3+, strong staining. Percentage (P) and intensity (I) of nuclear, cytoplasm or membrane expression were multiplied to generate a numerical score ($S = P \bullet I$).

The tissue sections were scored by two pathologists blind to the clinical outcomes. Receiver operating characteristic (ROC) curves were employed to define an optical cut-off score, which was closest to the point with maximum sensitivity and specificity. The cases with scores lower than or equal to the cut-off value were designated as low expression group and those with higher scores were categorized as high expression group.

Histological Analysis

For histological analysis, tissues were fixed in 4% neutral buffer formalin, embedded in paraffin, sectioned (4 μm) and stained with hematoxylin and eosin.

Gene Set Enrichment Analyses

Microarray data (accession no. GSE78060) were obtained from the Gene Expression Omnibus of NCBI (http://www.ncbi.nlm.nih.gov/geo/) and subjected to Gene set enrichment analysis (GSEA) using GSEA software (version 2.0.13) (http://www.broadinstitute.org/gsea/index.jsp).

Immunofluorescence Staining

FFPE tissue sections were deparaffinized and dehydrated in xylene and graded ethanol solutions in preparation for MTA3 and SOX2 double immunofluorescence (IF) staining. All slides were subjected to heat-induced epitope retrieval in Citrate

Buffer [pH = 6.0]. Endogenous tissue peroxidases were blocked by incubating the slides in 3% hydrogen peroxide solution and blocking buffer before incubation with MTA3 (Catalog A300-160A, Bethyl, 1: 600), SOX2 (Catalog No. #23064, Cell Signaling, 1: 200) as primary antibodies. And HRP-conjugated streptavidin as the secondary antibody. The signal in IF labeled slides were visualized with AlexaFluor 488 and AlexaFluor 594 Tyramide Super Boost kits (Invitrogen, Carlsbad, CA), and nuclei were visualized with Prolong Diamond Antifade Reagent with 4',6-diamidino-2-phenylindole (DAPI; Invitrogen, Carlsbad, CA). Primary and secondary antibodies were stripped using Citrate Buffer [pH = 6.0] in the microwave. Known MTA3 and SOX2 positive slides were used as a positive control. Immunofluorescence staining was analyzed using the PerkinElmer Vectra analysis platform to estimate the cell numbers. The percentage of positive cells was estimated by two pathologists.

Cell Culture

Human TSCC cell lines (SCC-25 and SCC-4) were obtained from the Cell Bank of the Chinese Academy of Sciences (Shanghai, China). The cells were cultured in Dulbecco's Modified Eagle Media (DMEM, Gibco/Invitrogen) supplemented with 10% FBS (Gibco/Invitrogen) at 37°C in a humidified atmosphere containing 5% CO_2.

Virus Production and Transduction

The full-length cDNA of MTA3 was PCR amplified from SCC-25 cells and cloned into the pCDNA3.1-flag plasmid. The shRNA targeting human MTA3 (target sequence: GAGGATACCTTCTTCTACTCA) was cloned into pBabe/U6 plasmid. The SOX2 overexpression plasmid and SOX2 short hairpin RNA (shSOX2) plasmid (shSOX2 target sequence: GGTTGACACCGTTGGTAATTT) were obtained from GeneCopoeia. Transfection of plasmid was performed using Lipofectamine 3000 (Thermo Fisher Scientific, catalog no. L3000015) according to the manufacturer's instructions. Stable cells were selected by culturing the cells in the medial with puromycin for 2 weeks.

RNA Isolation and Quantitative Real-Time PCR

Total RNA was extracted from cells using TRIzol (Invitrogen) according to the manufacturer's instruction and 2 μg RNA was reversely transcribed using High Capacity cDNA Reverse Transcription Kit (Applied Biosystems, Foster City, CA, USA). The cDNA was amplified and quantified in ABI-7500 system (Applied Biosystems) using SYBR Green Master (Roche). The cDNA was subjected to quantitative real-time PCR (qPCR) with the following primers: MTA3 forward: 5′-AAGCCTGGT GCTGTGAAT-3′ and reverse: 5′-AGGGTCCTCTGTAGTTGG-3′; SOX2 forward: 5′-CATCACCCACAGCAAATGACA-3′ and reverse: 5′-GCTCCTACCGTACCACTAGAACTT-3′; GADPH forward: 5′-TCCTCCTGTTTCATCCAAGC-3′ and reverse: 5′-TAGTAGCCGGGCCCTACTTT-3′.

Western Blot Analysis

Whole-cell lysates were prepared by lysing the cells in lysis buffer. Cell lysates with an equal amount of proteins were separated on 10% SDS-PAGE and transferred to PVDF membranes. The membranes were incubated with primary antibodies (MTA3, Catalog No. A300-160A, Bethyl, 1: 2,000; SOX2, Catalog No.23064, Cell Signaling, 1: 1,000; GAPDH, Catalog No. ab8245, Abcam, 1:3,000) followed by HRP-conjugated secondary antibodies as previously described (33). Blotted proteins were visualized by incubating in SuperSignal West Pico Chemiluminescent Substrate (Thermo Scientific) followed by exposure to X-ray film (Eastman Kodak, Rochester, NY, USA) (33).

ALDEFLUOR Assay

ALDEFLUOR assay kit (Stem Cell Technologies™, Vancouver, BC, Canada) was used to determine ALDH1 activity according to the manufacturer's protocol. Cells were suspended in ALDEFLUOR assay buffer containing 1 μM per 1×10^6 cells of the ALDH substrate, boron-dipyrromethene-aminoacetaldehyde (BAAA), and incubated for 50 min at 37°C. Each sample was treated with 50 mM of an ALDH-specific inhibitor, and diethylaminobenzaldehyde (DEAB) as a negative control. Stained cells were analyzed by BD FACSAria™ II (BD Biosciences, San Jose, CA, USA). To evaluate cell viability the cells were stained with 1 mg/ml of propidium iodide prior to analysis.

Proliferation and Survival Assays

Real-time cell analysis (RTCA) was performed to estimate cell proliferation using the xCELLigence DP device (ACEA Biosciences) as described in the supplier's instructions. In brief, 3,000 cells were seeded in E-plates, and the plates were locked into the RTCA DP device supplied with humidified air with 5% CO_2 at 37°C. The proliferative ability was monitored by the xCELLigence RTCA Analyzer (Roche Applied Science, Mannheim, Germany) (34, 35).

Animals and Carcinogen Treatment

Male and female wild-type C57BL/six mice were supplied by Beijing Vital Laboratory Animal Technology (Beijing, China). To induce tumorigenesis in the tongue, 4NQO (Sigma-Aldrich, St. Louise, MO) was added to the drinking water (100 mg/mL) for the 6-week-old young adult mice for 16 weeks. The mice were sacrificed when the bodyweight loss >1/3, otherwise they were sacrificed at the indicated time. After sacrifice, the tongue surface was photographed. The tissues were resected for histopathological examination and immunohistochemistry (IHC) analyses. Animals were housed in pathogen-free conditions at the Animal Center of Shantou University Medical College in compliance with Institutional Animal Care and Use Committee (IACUC) regulations (SUMC2014-148). All animal experiments were performed according to protocols approved by the Animal Care and Use Committee of the Medical College of Shantou University.

Gaussia Luciferase Assay

The pEZX-PG04 plasmid carrying double-expression cassette for *Gaussia* luciferase under the control of the SOX2 promoter (+270 to −1038), and secreted Alkaline Phosphatase (SeAP) under the control of the CMV promoter was obtained from GeneCopoeia (Catalog No. HPRM15202). Cells were seeded in 24-well plates, and transiently transfected with the above plasmid using Lipofectamine 3000 (Thermo Fisher Scientific, catalog no. L3000015) according to the manufacturer's instructions. After 72 h of transfection, the culture medium was collected for analysis of *Gaussia* luciferase and secreted Alkaline Phosphatase (SeAP) activities using a Secrete-PairTM Dual Luminescence Assay Kit (GeneCopoeia, SPDA-D010) according to the manufacturer's instructions. *Gaussia* luciferase activity was normalized on the basis of seAP activity.

Statistical Analyses

All statistical analyses except for microarray data were carried out using the statistical software package SPSS 17.0 (SPSS, Inc., Chicago, IL, USA). The comparisons between two groups were performed with Student's *t*-test. The correlation between MTA3 expression and clinicopathological data of patients was analyzed with Pearson $\chi 2$ test. Survival curves were plotted with the Kaplan-Meier method and compared by log-rank test. Survival data were evaluated by univariate and multivariate Cox regression analyses. The correlations of the histoscore between MTA3 and SOX2 was determined by Spearman's rank test. Two-way ANOVA followed by a Tukey–Kramer *post hoc* test was performed to compare the difference of proliferation affected by MTA3 and SOX2 among four groups. All data were presented as the mean ± SEM. The $P < 0.05$ was considered statistically significant.

RESULTS

MTA3 Is Reduced in Human TSCC

To estimate the expression MTA3, we first assessed the mRNA levels of MTA3 in OSCC from GEO database (https://www.ncbi.nlm.nih.gov/geo/) GSE30784 (36) and GSE25099 (37). We found that the MTA3 mRNA levels were significantly lower in OSCC when compared with the normal controls ($P < 0.001$ and 0.01, respectively; **Figure 1A** and **Supplementary Figure 1A**). Since TSCC is the highest incidence of all oral squamous cell cancers (5), we focused on the role of MTA3 in TSCC. Data from both datasets GSE78060 (38) and GSE34105 (39) revealed higher *MTA3* mRNA levels in normal tongue tissues than in TSCC tissues ($P = 0.014$ and 0.003, respectively; **Figure 1B** and **Supplementary Figure 1B**). Next, we examined the MTA3 expression at protein levels in TSCC of 119 patient specimens using immunohistochemistry (IHC). Representative

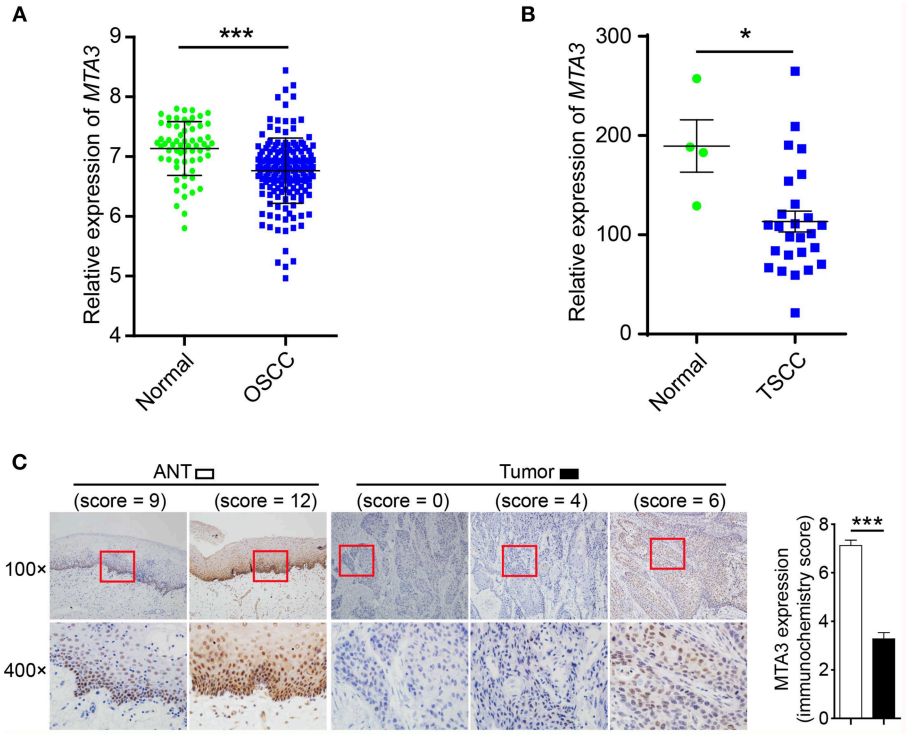

FIGURE 1 | MTA3 is downregulated in human TSCC. **(A)** Analysis of *MTA3* mRNA expression was performed in an OSCC dataset from GEO (GSE30784). **(B)** *MTA3* mRNA expression was analyzed in a TSCC dataset from GEO (GSE78060). **(C)** MTA3 expression in 119 human TSCC tissues and paired adjacent normal tissues (ANT) was monitored by immunohistochemistry (IHC) (left panel). The immunohistochemistry score of MTA3 in TSCC (filled bar) and paired normal adjacent (open bar) tissues were plotted (right panel). Shown are the mean values or representative data from at least three independent experiments. Error bars indicate SEM. $^{*}P < 0.05$, $^{***}P < 0.001$ using student's *t*-test.

photomicrographs for MTA3 IHC scores of level 0, 4, 6, 9, and 12 are shown in **Figure 1C** (left panel). TSCC showed significantly ($P < 0.001$, $n = 119$) lower levels of MTA3 protein in the primary tumors compared to the corresponding normal tissue (**Figure 1C**, Right panel). These findings demonstrate that MTA3 is downregulated in TSCC tissues compared to normal controls.

Downregulation of MTA3 Correlates With Clinical Outcomes in TSCC Patients

We next assessed the prognostic impact of MTA3 on the outcome of TSCC patients. An optimal cutoff value was identified using Receiver operator characteristic (ROC) analysis which categorized 51.3% (61/119) of the patient cohort into a high MTA3 group and the remainder into a low MTA3 group (**Figure 2A**). Then Kaplan-Meier survival analyses were performed and showed that patients with low MTA3 were associated with shorter overall survival than those with high MTA3 ($P = 0.002$, **Figure 2B**).

Univariate analyses found that MTA3 expression, pTNM stage, pN status, and tumor depth were significantly related to TSCC patient outcome (**Table 1**). However, after multivariate Cox regression analysis only MTA3 expression (HR 0.420; 95% CI 0.218–0.810; $P = 0.010$) and pTNM stage (HR 3.029; 95% CI 1.075–8.538; $P = 0.036$) were independently significant with overall survival (**Table 1**). These results reveal that reduced expression of MTA3 may be an independent prognostic factor for the overall survival of patients with TSCC.

MTA3 Inhibits Key TSCC Plasticity Regulator SOX2

The plasticity of CSC plays an important role in oncogenesis and progression (7, 11, 12, 40). Therefore, we next explored the relationship between MTA3 level and cancer cell stemness using gene set enrichment analysis (GSEA) of published human TSCC expression profiles (GSE78060) and found that a cancer stemness related gene signature (BOQUEST_STEM_CELL_UP) was significantly enriched in TSCC with low MTA3 expression ($P < 0.001$, **Figure 3A**). Interestingly, SOX2, a key regulator in the plasticity of cancer stemness, was also closely associated with poor prognosis in TSCC patients (20). To study the relation between MTA3 and SOX2, we measured the (co-)expression

TABLE 1 | Univariate and multivariate Cox proportional hazards analyses of survival in TSCC patients.

Variables	Univariate analysis	*P*-value	Multivariate analysis	*P*-value
	HR (95% CI)		HR (95% CI)	
Age (years)				
> 60 vs. ≤ 60	1.106 (0.620–1.973)	0.734	1.171 (0.633–2.167)	0.616
Gender				
Male vs. Female	1.620 (0.909–2.886)	0.102	1.630 (0.882–3.010)	0.119
Differentiation				
Poor vs. Well/Moderate	1.418 (0.684–2.936)	0.348	1.159 (0.533–2.518)	0.709
pTNM stage				
III–IV vs. I–II	4.428 (2.284–8.583)	0.000	3.029 (1.075–8.538)	0.036
MTA3 expression				
High vs. Low	0.401 (0.221–0.727)	0.003	0.420 (0.218–0.810)	0.010
pN status				
N1–N3 vs. N0	2.991 (1.672–5.349)	0.000	1.340 (0.590–3.047)	0.484
Tumor depth				
T1/T2 vs. T3/T4	2.472 (1.373–4.449)	0.003	1.064 (0.518–2.187)	0.865

HR, hazard ratio; CI, confidence interval.
High in this analysis is based on an MTA3 level > 5.5; the remaining individuals were classified as low.

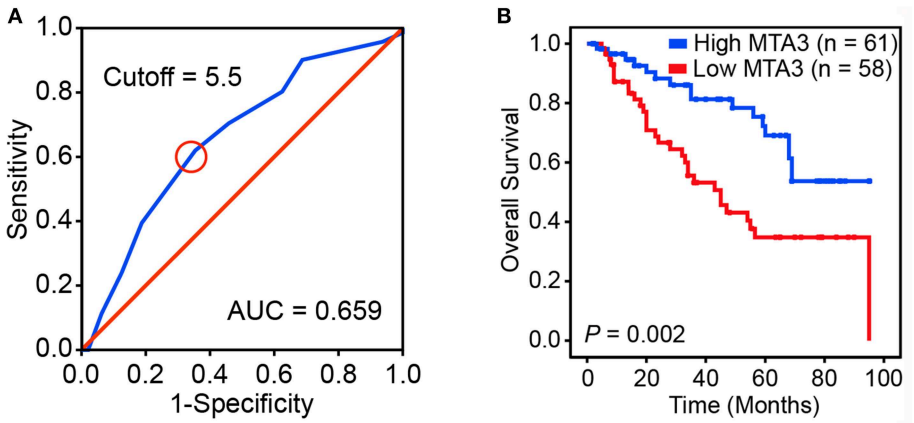

FIGURE 2 | Downregulation of MTA3 correlates with poor prognosis in human TSCC. **(A)** Receiver operating characteristic (ROC) curve analysis was performed to determine the cut-off score for the low expression of MTA3. **(B)** Kaplan–Meier curves compared the overall survival in TSCC patients with high and low protein levels of MTA3.

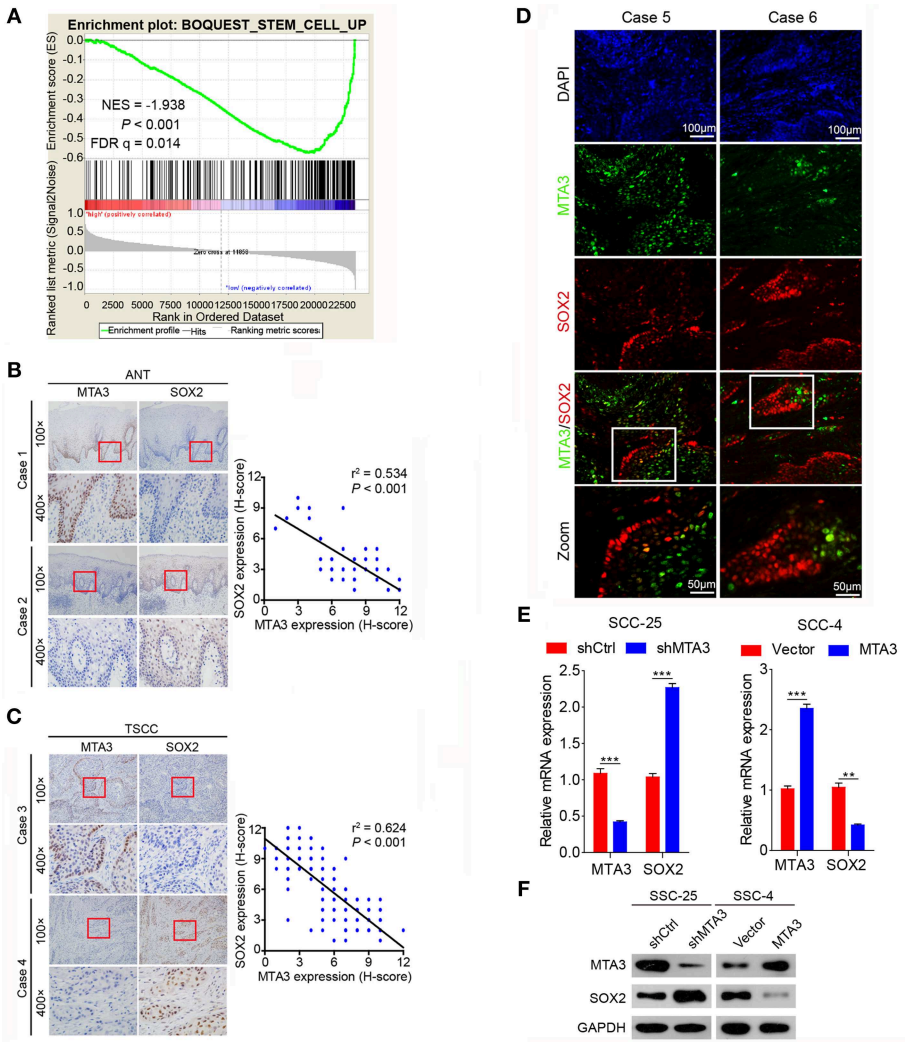

FIGURE 3 | MTA3 represses key TSCC plasticity regulator SOX2. **(A)** GSEA plots of enrichment of BOQUEST_STEM_CELL_UP signatures in MTA3^{High} tumors vs. MTA3^{Low} tumors in the GSE78060 dataset. **(B)** Representative IHC image against MTA3 and SOX2 of normal tissues (left panel), Pearson's correlation analysis of MTA3 and SOX2 IHC intensity in 119 adjacent non-tumor tissues (ANT) (right panel). **(C)** Representative IHC image against MTA3 and SOX2 of TSCC tissues (left panel), Pearson's correlation analysis of MTA3 and SOX2 IHC intensity in 119 TSCC tissues (right panel). **(D)** Representative double immunofluorescence of MTA3 and SOX2 in TSCC patient tissues. DAPI = blue, MTA3 = green, SOX2 = red. **(E)** qRT-PCR of MTA3 and SOX2 in SCC-25 cells with MTA3 depletion (Left panel) and SCC-4 cells MTA3 overexpression (Right panel), $^{**}P < 0.01$ and $^{***}P < 0.001$ using student's *t*-test. **(F)** Western blot of MTA3 and SOX2 in SCC-25 cells with MTA3 depletion (Left panel) and SCC-4 cells with MTA3 overexpression (Right panel).

of MTA3 and SOX2 in adjacent non-tumor tissues (ANT) and TSCC tissues from the 119 patients. Indeed, a highly significant inverse correlation between the MTA3 and SOX2 levels ($r^2 = 0.534$, $P < 0.001$ and $r^2 = 0.624$, $P < 0.001$, respectively; **Figures 3B,C**) was observed. Moreover, a low level of SOX2 was accompanied by high expression of MTA3, and vice versa, as indicated by double immunofluorescent staining (**Figure 3D**). In addition, two TSCC cell lines, SSC-25 and SSC-4, were transfected with shMTA3 or the plasmid overexpressing MTA3, respectively. The mRNA and protein levels of MTA3 were then assessed by qRT-PCR and western blot analysis, respectively. When compared to the controls, the expression level of MTA3 was obviously enhanced in cells transfected with pcMTA3 ($P < 0.001$), while it was significantly decreased in cells transfected with shMTA3 ($P < 0.001$) (**Figures 3E,F**). Knockdown MTA3 dramatically increased, whereas overexpression of MTA3 decreased, the expression levels of SOX2 (**Figures 3E,F**), suggesting that the MTA3 inhibits SOX2 expression in TSCC cells.

MTA3 Suppresses TSCC Cell Stemness and Proliferation Via SOX2

To determine whether SOX2 plays a key role in MTA3-mediated plasticity of CSC and cell growth, we first established TSCC cells with knockdown of MTA3 or SOX2 alone or in combination using specific shRNA (**Figure 4A**) or stably

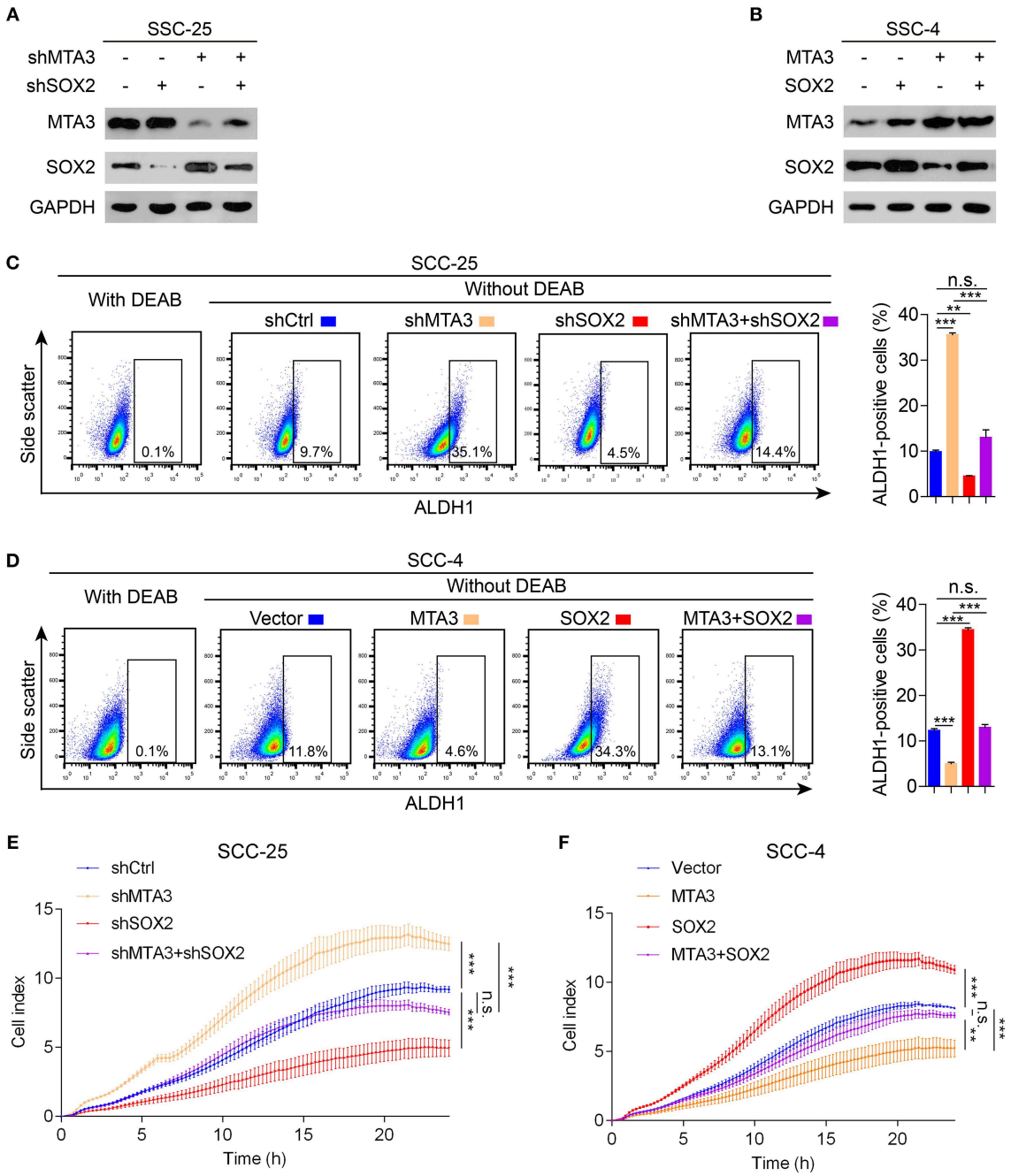

FIGURE 4 | MTA3 reduces CSC properties and cell proliferation via SOX2 in TSCC cells. **(A,B)** Western blot and qRT-PCR in TSCC cells transfected with a combination of shMTA3 and shSOX2 **(A)** or MTA3 and SOX2 expressing plasmid **(B)**. **(C,D)** Flow cytometry analysis of the ALDH1$^+$ population. Histograms showing the proportion of ALDH1$^+$ cells. **(E,F)** Cells were monitored by RTCA for 24 h. Data were shown as the means of three independent experiments or representative data. Error bars indicate SEM. n.s., not statistically significant; $^{**}P < 0.01$, $^{***}P < 0.001$ by two-way ANOVA followed by a Tukey–Kramer *post hoc* test.

overexpressing MTA3 or SOX2 alone or in combination (**Figure 4B**). As expected, knockdown MTA3 significantly promoted the percentage of cells expressing ALDH1, a major CSC marker (**Figure 4C**). MTA3-depletion-mediated increase of the number of ALDH1-positive cells were significantly reduced when SOX2 is removed suggesting SOX2 plays a crucial role in MTA3-repressed CSC properties (**Figure 4C**). Next, the effects of overexpressed MTA3 individually or in combination with SOX2 were examined. **Figure 4D** showed that overexpression of MTA3 and SOX2 reduced and increased the number of ALDH1-positive cells, respectively. However, overexpressed SOX2 counteracted MTA3-repressed the number

of ALDH1-positive cells (**Figure 4D**). In addition, real-time proliferation assays were conducted to assess changes in cell dynamics. Silencing SOX2 inhibited MTA3-depletion-induced cell proliferation (**Figure 4E**) and forced SOX2 expression was capable of counteracting MTA3-repressed cell proliferation (**Figure 4F**). These data altogether demonstrate that in TSCC cells MTA3 represses CSC property and proliferation by targeting SOX2.

Dysregulated MTA3/SOX2 Axis Is Associated With Tumor Progression

The results above indicate a role of MTA3/SOX2 in TSCC progression. Therefore, we next investigated the role of MTA3/SOX2 in a mouse model of tongue tumorigenesis induced by 4 nitroquinoline 1-oxide (4NQO). Exposure to 4NQO caused a temporal progression from hyperplasia to invasive carcinoma in the murine tongue, resembling human tongue carcinogenesis and development (41, 42). Mice were exposed to 4NQO in daily drinking water for 16 weeks followed by 4NQO-free drinking water for 12 additional weeks (**Figure 5A**), which resulted in tongue carcinogenesis and progression (**Figure 5B**) similar to what has been published previously (41, 42). Next, we studied the expression of MTA3/SOX2 in normal tongue tissue samples, hyperplasia, carcinoma *in situ*, early invasive carcinoma and invasive carcinoma by immunohistochemistry. As shown in **Figure 5C**, the expression of MTA3 gradually

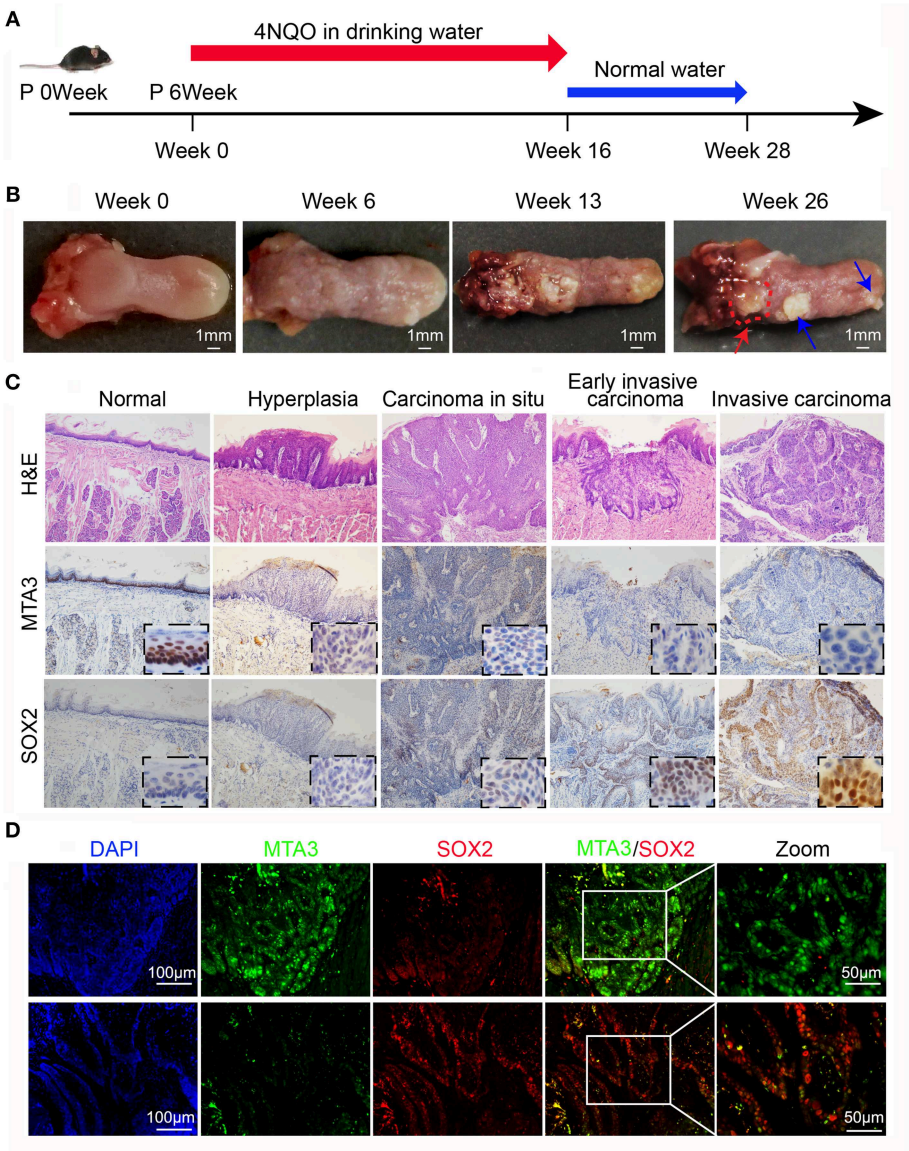

FIGURE 5 | MTA3-SOX2 axis changes dynamically in a mouse model mimicking human TSCC. **(A)** Schematic representation of 4NQO tumorigenesis protocol in wild-type C57BL/6 mice. **(B)** Representative macroscopic view of the normal tongue and tumor development. The red arrow indicates invasive carcinoma, the blue arrow indicates papilloma. **(C)** Representative H&E and IHC stain for mice tongue preneoplastic and neoplastic tissues. **(D)** Representative double immunofluorescent staining image against MTA3 and SOX2 of mice tongue neoplastic tissues. DAPI = blue, MTA3 = green, SOX2 = red.

decreased during the process of carcinogenesis and progression, in contrast to SOX2. This is indicative of an inverse relation between MTA3 and SOX2 associated with cancer occurrence and development, which was confirmed in mouse TSCC by double immunofluorescent staining (**Figure 5D**). Thus, the levels of MTA3 and SOX2 may change dynamically during tongue carcinogenesis and progression.

Dysregulated MTA3/SOX2 Axis Associated Strongly With Poor Prognosis

To validate our findings in a clinical setting, we assessed the levels of MTA3 and SOX2 in 119 TSCC samples and related this to the overall survival rate. Receiver operator characteristic (ROC) analysis identified an optimal cutoff value and categorized 39.5% (47/119) of the patients into a high SOX2 group and the remainder into a low SOX2 group (**Figure 6A**). Indeed, patients with low levels of MTA3 but high levels of SOX2 ($MTA3^{low}/SOX2^{high}$) had significantly shorter overall survival rate ($P < 0.001$; **Figure 6B**) than those with high levels of MTA3. Moreover, low levels of SOX2 ($MTA3^{high}/SOX2^{low}$), were associated with an even shorter overall survival compared to TSCC patients with any other expression pattern ($MTA3^{high}/SOX2^{high}$, $MTA3^{low}/SOX2^{high}$, $MTA3^{low}/SOX2^{low}$) ($P < 0.001$; **Figure 6C**). These data altogether suggest that combined $MTA3^{low}$-$SOX2^{high}$ expression had stronger correlation with worst patient prognosis than that of the individual components. Indeed, univariate and multivariate Cox regression analysis ($P < 0.001$ and $P < 0.001$, HR = 4.044, 95 %CI = 1.925–8.495, respectively) indicated that combined $MTA3^{low}/SOX2^{high}$ expression is an independent prognostic factor of TSCC as it was significantly associated with prognosis (**Table 2**). Overall, these data indicate that dysregulated MTA3/SOX2 axis may contribute to patient outcomes and could be of value as a predictive biomarker for TSCC prognosis.

DISCUSSION

Here we demonstrated that MTA3 was a potential independent prognosis factor for TSCC patients. Moreover, we established the negative regulation of SOX2, a key regulator in the plasticity of

TABLE 2 | Univariate and multivariate Cox proportional hazards model predicting survival in TSCC patients.

Variables	Univariate analysis	*P*-value	Multivariate analysis	*P*-value
	HR (95% CI)		HR (95% CI)	
Age (years)				
> 60 vs. ≤ 60	1.106 (0.620–1.973)	0.734	1.310 (0.714–2.404)	0.383
Gender				
Male vs. Female	1.620 (0.909–2.886)	0.102	1.623 (0.878–3.000)	0.123
Differentiation				
Poor vs. Well/Moderate	1.418 (0.684–2.936)	0.348	1.211 (0.581–2.525)	0.610
pTNM stage				
III–IV vs. I–II	4.428 (2.284–8.583)	0.000	1.642 (0.569–4.735)	0.359
Combination of MTA3 and SOX2				
MTA3 Low/SOX2 High vs. Other groups	5.209 (2.891–9.386)	0.000	4.044 (1.925–8.495)	0.000
pN status				
N1–N3 vs. N0	2.991 (1.672–5.349)	0.000	1.495 (0.673–3.318)	0.323
Tumor depth				
T1/T2 vs. T3/T4	2.472 (1.373–4.449)	0.003	1.069 (0.533–2.142)	0.852

HR, hazard ratio; CI, confidence interval.

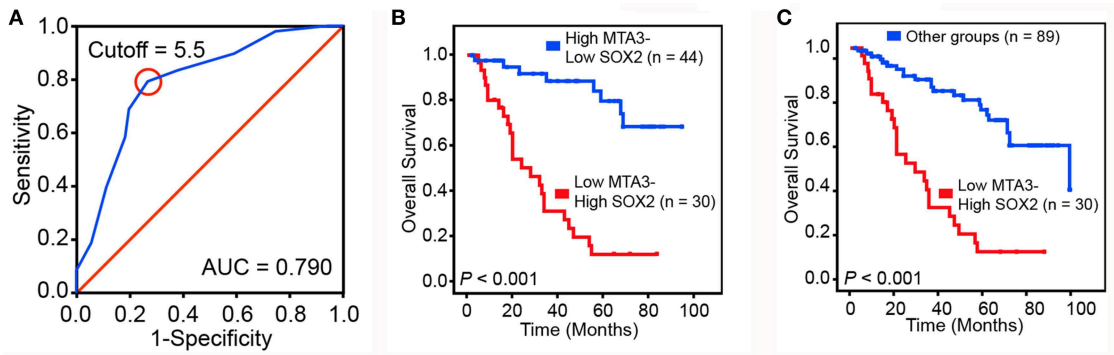

FIGURE 6 | Dysregulated MTA3-SOX2 axis is associated with poor prognosis. **(A)** Receiver operating characteristic (ROC) curve analysis was performed to determine the cut-off score for the low expression of SOX2. **(B,C)** The overall survival of TSCC patients with tumors expressing low levels of MTA3 and high levels of SOX2 and those with high levels of MTA3 and low levels of SOX2 **(B)**, as well as all other subjects **(C)**.

cancer stemness, by MTA3 repressed the number of ALDH1-positive cells and cell proliferation in TSCC cells. We identified the expression of MTA3 and SOX2 as important markers in a 4NQO-induced TSCC mouse model, human TSCC progression and clinical outcomes.

The biological and clinical significance of the MTA family members in malignancies has been well-established. The levels of these factors have even been proposed as potential diagnostic parameters and targeting each one of the family members could be potential treatments for different cancers (26, 43–45). However, unlike MTA1 and MTA2 which were mainly involved in cancer progression and metastasis, MTA3 possesses both tumor-suppressing and tumor-promoting properties depending on specific cancer types (21, 43). We found that MTA3 was negatively associated with overall survival and could act as an independent prognosis factor in TSCC. To the best of our knowledge, this is the first study to show the expression of MTA3 in TSCC.

The plasticity of CSCs is key mechanisms in oncogenesis and progression of cancers (7, 11, 12, 16) and a predictive factor of poor prognosis in a wide variety of cancers, including tongue cancer (17–20). Accumulating evidence suggests that transcription factor SOX2 is a key regulator in the plasticity of cancer stemness (46–48). Moreover, overexpression of SOX2 is often associated with increased cancer aggressiveness, resistance to chemoradiation therapy and decreased survival rate, which has been reported in various cancer types (49, 50), including TSCC (51). Previous studies revealed that SOX2 is vital in the regulation of TSCC motility, invasion, tumorigenicity, and upregulated SOX2 is significantly associated with the progression of TSCC (51). SOX2 is detectable in oral pre-invasive lesions, suggesting that SOX2 upregulation may be an early event in TSCC carcinogenesis. We found that MTA3 can inhibit CSC properties and cell proliferation via downregulating SOX2 in TSCC cells. In addition, luciferase reporter assays showed that knockdown or overexpression MTA3 had no significant effect on the luciferase activity (**Supplementary Figure 2**), suggesting that MTA3 does not regulate the expression of SOX2 by interacting with its proximal promoter. However, these results do not necessarily rule out the possibility that MTA3 is directly involved in the regulation of SOX2 expression by interacting with its enhancer region or the sequence other than the proximal promoter. Further studies will better the understanding about the mechanisms in MTA3-regulated SOX2 expression in tongue cancer.

Given the fact that alterations of MTA3 and SOX2 highly correlate with clinical outcomes and the predictability of prognosis, the levels of MTA3 and SOX2, especially $MTA3^{low}/SOX2^{high}$, could be used as diagnostic parameters. In addition, targeting MTA3 and/or SOX2 could be potential therapeutic strategies in TSCC treatment. Finally, 4NQO-induce TSCC mice model has been widely used in the study of TSCC (41, 42). And we used this model to further elaborate the dynamic changes of MTA3 and SOX2 in the occurrence and developmental progression of TSCC.

In summary, consistent with the fact that MTA3 is often silenced in the process of carcinogenesis and development, we found that MTA3 was capable of inhibiting CSC properties and cell proliferation by negatively regulating SOX2. Additionally, we found that TSCC patients in the $MTA3^{low}/SOX2^{high}$ group had a poor prognosis. Future research may involve translational research to clinically evaluate the efficacy of this therapeutic strategy using IHC evaluation of low MTA3 and high SOX2 as a companion diagnostic for patient selection.

DATA AVAILABILITY

The datasets generated for this study are available on request to the corresponding author.

AUTHOR CONTRIBUTIONS

HZ designed the experiments. ZY and LD performed the *in vivo* experiments. ZY, KL, and LD assayed and analyzed of patient samples. LD and KL performed bioinformatics analyses. LD, MX, KL, ZY, and GY performed the *in vitro* experiments. LD, MX, KL, and ZY performed the statistical analysis. MX and HG collected the clinical samples. DZ and HZ analyzed data. HZ, LD, RC, and DZ prepared the manuscript. All the authors read and approved the final manuscript.

FUNDING

This work was supported in part by funding from the National Natural Science Foundation of China (Grant Nos. 81773087, 81071736, and 81572876 to HZ and 81871977 to GY).

SUPPLEMENTARY MATERIAL

The Supplementary Material for this article can be found online at: https://www.frontiersin.org/articles/10.3389/fonc.2019.00816/full#supplementary-material

REFERENCES

1. Rivera C. Essentials of oral cancer. *Int J Clin Exp Pathol.* (2015) 8:11884–94. doi: 10.5281/zenodo.192487
2. Kademani D. Oral cancer. *Mayo Clin Proc.* (2007) 82:878–87. doi: 10.4065/82.7.878
3. Lingen MW, Kalmar JR, Karrison T, Speight PM. Critical evaluation of diagnostic aids for the detection of oral cancer. *Oral Oncol.* (2008) 44:10–22. doi: 10.1016/j.oraloncology.2007.06.011
4. Ho AS, Kim S, Tighiouart M, Gudino C, Mita A, Scher KS, et al. Metastatic lymph node burden and survival in oral cavity cancer. *J Clin Oncol.* (2017) 35:3601–9. doi: 10.1200/JCO.2016.71.1176
5. Ganly I, Patel S, Shah J. Early stage squamous cell cancer of the oral tongue–clinicopathologic features affecting outcome. *Cancer.* (2012) 118:101–11. doi: 10.1002/cncr.26229
6. Carnero A, Garcia-Mayea Y, Mir C, Lorente J, Rubio IT, Me LL. The cancer stem-cell signaling network and resistance to therapy. *Cancer Treat Rev.* (2016) 49:25–36. doi: 10.1016/j.ctrv.2016.07.001

7. Lytle NK, Barber AG, Reya T. Stem cell fate in cancer growth, progression and therapy resistance. Nature reviews. *Cancer.* (2018) 18:669–80. doi: 10.1038/s41568-018-0056-x
8. Cojoc M, Mabert K, Muders MH, Dubrovska A. A role for cancer stem cells in therapy resistance: cellular and molecular mechanisms. *Semin Cancer Biol.* (2015) 31:16–27. doi: 10.1016/j.semcancer.2014.06.004
9. Batlle E, Clevers H. Cancer stem cells revisited. *Nat Med.* (2017) 23:1124–34. doi: 10.1038/nm.4409
10. Vlashi E, Pajonk F. Cancer stem cells, cancer cell plasticity and radiation therapy. *Semin Cancer Biol.* (2015) 31:28–35. doi: 10.1016/j.semcancer.2014.07.001
11. Hayashi H, Higashi T, Yokoyama N, Kaida T, Sakamoto K, Fukushima Y, et al.. An imbalance in TAZ and YAP expression in hepatocellular carcinoma confers cancer stem Cell-like behaviors contributing to disease progression. *Cancer Res.* (2015) 75:4985–97. doi: 10.1158/0008-5472.CAN-15-0291
12. Li C, Wang J. Quantifying the landscape for development and cancer from a core cancer stem cell circuit. *Cancer Res.* (2015) 75:2607–18. doi: 10.1158/0008-5472.CAN-15-0079
13. de Sousa e Melo F, Kurtova AV, Harnoss JM, Kljavin N, Hoeck JD, Hung J, et al. A distinct role for Lgr5(+) stem cells in primary and metastatic colon cancer. *Nature.* (2017) 543:676–80. doi: 10.1038/nature21713
14. Samanta D, Park Y, Andrabi SA, Shelton LM, Gilkes DM, Semenza GL. PHGDH expression is required for mitochondrial redox homeostasis, breast cancer stem cell maintenance, and lung metastasis. *Cancer Res.* (2016) 76:4430–2. doi: 10.1158/0008-5472.CAN-16-0530
15. Lawson DA, Bhakta NR, Kessenbrock K, Prummel KD, Yu Y, Takai K, et al. Single-cell analysis reveals a stem-cell program in human metastatic breast cancer cells. *Nature.* (2015) 526:131–5. doi: 10.1038/nature15260
16. Li Y, Rogoff HA, Keates S, Gao Y, Murikipudi S, Mikule K, et al. Suppression of cancer relapse and metastasis by inhibiting cancer stemness. *Proc Natl Acad Sci USA.* (2015) 112:1839–44. doi: 10.1073/pnas.1424171112
17. de Sousa EMF, Colak S, Buikhuisen J, Koster J, Cameron K, de Jong JH, et al. Methylation of cancer-stem-cell-associated Wnt target genes predicts poor prognosis in colorectal cancer patients. *Cell Stem Cell.* (2011) 9:476–85. doi: 10.1016/j.stem.2011.10.008
18. Zheng H, Pomyen Y, Hernandez MO, Li C, Livak F, Tang W, et al. Single-cell analysis reveals cancer stem cell heterogeneity in hepatocellular carcinoma. *Hepatology.* (2018) 68:127–40. doi: 10.1002/hep.29778
19. Peng F, Wang JH, Fan WJ, Meng YT, Li MM, Li TT, et al. Glycolysis gatekeeper PDK1 reprograms breast cancer stem cells under hypoxia. *Oncogene.* (2018) 37:1062–74. doi: 10.1038/onc.2017.368
20. Du L, Yang Y, Xiao X, Wang C, Zhang X, Wang L, et al. Sox2 nuclear expression is closely associated with poor prognosis in patients with histologically node-negative oral tongue squamous cell carcinoma. *Oral Oncol.* (2011) 47:709–13. doi: 10.1016/j.oraloncology.2011.05.017
21. Ma L, Yao Z, Deng W, Zhang D, Zhang H. The many faces of MTA3 protein in normal development and cancers. *Curr Prot Peptide Sci.* (2016) 17:726–34. doi: 10.2174/1389203717666160401150122
22. Li X, Jia S, Wang S, Wang Y, Meng A. Mta3-NuRD complex is a master regulator for initiation of primitive hematopoiesis in vertebrate embryos. *Blood.* (2009) 114:5464–72. doi: 10.1182/blood-2009-06-227777
23. Si W, Huang W, Zheng Y, Yang Y, Liu X, Shan L, et al. Dysfunction of the reciprocal feedback loop between GATA3- and ZEB2-nucleated repression programs contributes to breast cancer metastasis. *Cancer Cell.* (2015) 27:822–36. doi: 10.1016/j.ccell.2015.04.011
24. Du L, Ning Z, Zhang H, Liu F. Corepressor metastasis-associated protein 3 modulates epithelial-to-mesenchymal transition and metastasis. *Chin J Cancer.* (2017) 36:28. doi: 10.1186/s40880-017-0193-8
25. Fujita N, Jaye DL, Kajita M, Geigerman C, Moreno CS, Wade PA. MTA3, a Mi-2/NuRD complex subunit, regulates an invasive growth pathway in breast cancer. *Cell.* (2003) 113:207–19. doi: 10.1016/S0092-8674(03)00234-4
26. Zhang H, Stephens LC, Kumar R. Metastasis tumor antigen family proteins during breast cancer progression and metastasis in a reliable mouse model for human breast cancer. *Clin Cancer Res.* (2006) 12:1479–86. doi: 10.1158/1078-0432.CCR-05-1519
27. Dong H, Guo H, Xie L, Wang G, Zhong X, Khoury T, et al. The metastasis-associated gene MTA3, a component of the Mi-2/NuRD transcriptional repression complex, predicts prognosis of gastroesophageal junction adenocarcinoma. *PLoS ONE.* (2013) 8:e62986. doi: 10.1371/journal.pone.0062986
28. Shan S, Hui G, Hou F, Shi H, Zhou G, Yan H, et al. Expression of metastasis-associated protein 3 in human brain glioma related to tumor prognosis. *Neurol Sci.* (2015) 36:1799–804. doi: 10.1007/s10072-015-2252-8
29. Zhang H, Singh RR, Talukder AH, Kumar R. Metastatic tumor antigen 3 is a direct corepressor of the Wnt4 pathway. *Genes Dev.* (2006) 20:2943–8. doi: 10.1101/gad.1461706
30. Singh RR, Kumar R. MTA family of transcriptional metaregulators in mammary gland morphogenesis and breast cancer. *J Mammary Gland Biol Neoplasia.* (2007) 12:115–25. doi: 10.1007/s10911-007-9043-7
31. Mylonas I, Bruning A. The metastasis-associated gene MTA3 is an independent prognostic parameter in uterine non-endometrioid carcinomas. *Histopathology.* (2012) 60:665–70. doi: 10.1111/j.1365-2559.2011.04103.x
32. Huang Y, Li Y, He F, Wang S, Li Y, Ji G, et al. Metastasis-associated protein 3 in colorectal cancer determines tumor recurrence and prognosis. *Oncotarget.* (2017) 8:37164–71. doi: 10.18632/oncotarget.16332
33. Feng Y, Ke C, Tang Q, Dong H, Zheng X, Lin W, et al. Metformin promotes autophagy and apoptosis in esophageal squamous cell carcinoma by downregulating Stat3 signaling. *Cell Death Dis.* (2014) 5:e1088. doi: 10.1038/cddis.2014.59
34. Wang L, Li K, Lin X, Yao Z, Wang S, Xiong X, et al. Metformin induces human esophageal carcinoma cell pyroptosis by targeting the miR-497/PELP1 axis. *Cancer Lett.* (2019) 450:22–31. doi: 10.1016/j.canlet.2019.02.014
35. Wang L, Li W, Li K, Guo Y, Liu D, Yao Z, et al. The oncogenic roles of nuclear receptor coactivator 1 in human esophageal carcinoma. *Cancer Med.* (2018) 7:5205–16. doi: 10.1002/cam4.1786
36. Chen C, Mendez E, Houck J, Fan W, Lohavanichbutr P, Doody D, et al. Gene expression profiling identifies genes predictive of oral squamous cell carcinoma. *Cancer Epidemiol Biomarkers Prev.* (2008) 17:2152-2162. doi: 10.1158/1055-9965.EPI-07-2893
37. Peng CH, Liao CT, Peng SC, Chen YJ, Cheng AJ, Juang JL, et al. A novel molecular signature identified by systems genetics approach predicts prognosis in oral squamous cell carcinoma. *PLoS ONE.* (2011) 6:e23452. doi: 10.1371/journal.pone.0023452
38. Enokida T, Fujii S, Takahashi M, Higuchi Y, Nomura S, Wakasugi T, et al. Gene expression profiling to predict recurrence of advanced squamous cell carcinoma of the tongue: discovery and external validation. *Oncotarget.* (2017) 8:61786–99. doi: 10.18632/oncotarget.18692
39. Rentoft M, Coates PJ, Laurell G, Nylander K. Transcriptional profiling of formalin fixed paraffin embedded tissue: pitfalls and recommendations for identifying biologically relevant changes. *PLoS ONE.* (2012) 7:e35276. doi: 10.1371/journal.pone.0035276
40. Vidal SJ, Rodriguez-Bravo V, Galsky M, Cordon-Cardo C, Domingo-Domenech J. Targeting cancer stem cells to suppress acquired chemotherapy resistance. *Oncogene.* (2014) 33:4451–63. doi: 10.1038/onc.2013.411
41. Vered M, Allon I, Buchner A, Dayan D. Stromal myofibroblasts and malignant transformation in a 4NQO rat tongue carcinogenesis model. *Oral Oncol.* (2007) 43:999–1006. doi: 10.1016/j.oraloncology.2006.11.007
42. Chen YF, Yang CC, Kao SY, Liu CJ, Lin SC, Chang KW. MicroRNA-211 enhances the oncogenicity of carcinogen-induced oral carcinoma by repressing TCF12 and increasing antioxidant activity. *Cancer Res.* (2016) 76:4872–86. doi: 10.1158/0008-5472.CAN-15-1664
43. Ning Z, Gan J, Chen C, Zhang D, Zhang H. Molecular functions and significance of the MTA family in hormone-independent cancer. *Cancer Metast. Rev.* (2014) 33:901–19. doi: 10.1007/s10555-014-9517-1
44. Kumar R. Another tie that binds the MTA family to breast cancer. *Cell.* (2003) 113:142–3. doi: 10.1016/S0092-8674(03)00274-5
45. Li DQ, Pakala SB, Nair SS, Eswaran J, Kumar R. Metastasis-associated protein 1/nucleosome remodeling and histone deacetylase complex in cancer. *Cancer Res.* (2012) 72:387–94. doi: 10.1158/0008-5472.CAN-11-2345
46. Singh SK, Chen NM, Hessmann E, Siveke J, Lahmann M, Singh G, et al. Antithetical NFATc1-Sox2 and p53-miR200 signaling networks govern pancreatic cancer cell plasticity. *EMBO J.* (2015) 34:517–30. doi: 10.15252/embj.201489574

47. Mu P, Zhang Z, Benelli M, Karthaus WR, Hoover E, Chen CC, et al. SOX2 promotes lineage plasticity and antiandrogen resistance in TP53- and RB1-deficient prostate cancer. *Science.* (2017) 355:84–8. doi: 10.1126/science.aah4307
48. Tan Y, Tajik A, Chen J, Jia Q, Chowdhury F, Wang L, et al. Matrix softness regulates plasticity of tumour-repopulating cells via H3K9 demethylation and Sox2 expression. *Nat Commun.* (2014) 5:4619. doi: 10.1038/ncomms5619
49. Maurizi G, Verma N, Gadi A, Mansukhani A, Basilico C. Sox2 is required for tumor development and cancer cell proliferation in osteosarcoma. *Oncogene.* (2018) 37:4626–32. doi: 10.1038/s41388-018-0292-2
50. Wang K, Ji W, Yu Y, Li Z, Niu X, Xia W, et al. FGFR1-ERK1/2-SOX2 axis promotes cell proliferation, epithelial-mesenchymal transition, and metastasis in FGFR1-amplified lung cancer. *Oncogene.* (2018) 37:5340–54. doi: 10.1038/s41388-018-0311-3
51. Liu X, Qiao B, Zhao T, Hu F, Lam AK, Tao Q. Sox2 promotes tumor aggressiveness and epithelialmesenchymal transition in tongue squamous cell carcinoma. *Int J Mol Med.* (2018) 42:1418–26. doi: 10.3892/ijmm.2018.3742

Conflict of Interest Statement: The authors declare that the research was conducted in the absence of any commercial or financial relationships that could be construed as a potential conflict of interest.

frontiers in Oncology

ORIGINAL RESEARCH
published: 04 September 2019
doi: 10.3389/fonc.2019.00861

An Engineered Fusion Protein Anti-CD19(Fab)-LDM Effectively Inhibits ADR-Resistant B Cell Lymphoma

Dongmei Fan[1†], Linlin Jiang[2†], Yuewen Song[1], Shiqi Bao[1], Yuanyuan Yang[1], Xiangfei Yuan[1], Yongsu Zhen[3], Ming Yang[1] and Dongsheng Xiong[1*]*

[1] State Key Laboratory of Experimental Hematology, Institute of Hematology and Hospital of Blood Diseases, Chinese Academy of Medical Sciences and Peking Union Medical College, Tianjin, China, [2] School of Life Sciences, Ludong University, Yantai, China, [3] Department of Oncology, Institute of Medicinal Biotechnology (IMB), Chinese Academy of Medical Sciences and Peking Union Medical College, Beijing, China

OPEN ACCESS

Edited by:
Dong-Hua Yang,
St. John's University, United States

Reviewed by:
Pranav Gupta,
Massachusetts General Hospital and Harvard Medical School, United States
Hamid Morjani,
Université de Reims Champagne-Ardenne, France

***Correspondence:**
Ming Yang
my1970@163.com
Dongsheng Xiong
dsxiong9070@163.com

[†] These authors have contributed equally to this work

Specialty section:
This article was submitted to Molecular and Cellular Oncology, a section of the journal Frontiers in Oncology

Received: 24 June 2019
Accepted: 20 August 2019
Published: 04 September 2019

Citation:
Fan D, Jiang L, Song Y, Bao S, Yang Y, Yuan X, Zhen Y, Yang M and Xiong D (2019) An Engineered Fusion Protein Anti-CD19(Fab)-LDM Effectively Inhibits ADR-Resistant B Cell Lymphoma. Front. Oncol. 9:861. doi: 10.3389/fonc.2019.00861

The 5-year survival rate of patients with B cell lymphoma is about 50% after initial diagnosis, mainly because of resistance to chemotherapy. Hence, it is necessary to understand the mechanism of chemo-resistance and to explore novel methods to circumvent multidrug resistance. Previously, we showed that an engineered cytotoxic fusion protein anti-CD19(Fab)-LDM (lidamycin), can induce apoptosis of B-lymphoma cells. Herein, we successfully established an adriamycin (ADR)-resistant B cell lymphoma cell line BJAB/ADR. The mRNA and protein level of ATP-binding cassette subfamily B member 1 (ABCB1) were significantly overexpressed in BJAB/ADR cells. Increased efflux function of ABCB1 was observed by analyzing intracellular accumulation and efflux of Rhodamine 123. The efflux of Rhodamine 123 could be significantly ameliorated by verapamil. Treatment with anti-CD19(Fab)-LDM at different concentrations induced cytotoxic response of BJAB/ADR cells similar to that of the sensitive cells. *In vivo* studies showed that anti-CD19(Fab)-LDM had better antitumor effect in BJAB and BJAB/ADR cell lymphoma xenografts compared with ADR or LDM treatment alone. Taken together, anti-CD19(Fab)-LDM can effectively inhibit the growth of BJAB/ADR cells both *in vitro* and *in vivo*. Anti-CD19(Fab)-LDM could be a promising molecule for the treatment of drug resistant cancers.

Keywords: adriamycin, BJAB cell line, BJAB/ADR cell line, engineered fusion protein, anti-CD19(Fab)-LDM

INTRODUCTION

Lymphomas are a common heterogeneic group of hematologic diseases, among which B cell origin lymphoma represents the largest proportion (1, 2). At present, chemotherapy or chemoimmunotherapy remains the most effective therapeutic modality in the multifaceted treatment of lymphomas (3). Most patients who experience remission for more than 5 years have benefitted from the overall improvements in the treatment of B cell lymphomas. However, a significant portion of patients still show unfavorable response toward drug treatment. Currently, the clinical approaches to relapsed B lymphomas mainly involve in administering high-dose chemotherapeutic agents, using inhibitors to reverse drug resistance toward chemotherapy (4), or

finding novel therapeutic strategies such as targeting CD20 or using Chimeric Antigen Receptor T-Cell Immunotherapy (CAR-T) (5–8). Multidrug resistance (MDR) or acquired chemo-drug resistance is a major contributor to the failure of chemotherapy as well as one of the major reasons for tumor relapse and metastasis (9–11). To investigate the mechanisms involved in the acquisition of chemotherapy resistance and subsequent poor prognosis, it is necessary to establish a proper resistant cell model derived from a drug-sensitive human lymphoma cell line. Adriamycin (ADR; generic name: doxorubicin, DOX) is a chemotherapeutic drug frequently used in multiple clinical protocols of chemotherapy and is also a critical drug in the treatment of lymphoma (12). Unfortunately, some lymphomas have shown ADR resistance with continued treatment (13, 14). Therefore, establishing an ADR-resistant lymphoma cell model is useful for studying the mechanism of resistance in B cell lymphoma and for searching solutions regarding ADR resistance.

Lidamycin (LDM), originally named C-1027, is a member of the enediyne antibiotic family with strong cytotoxic effect toward human cancer cells and its mechanism of action is related to DNA damage. Importantly, LDM molecule is composed of a highly active group enediyne chromophore (AE) and a protective group apoprotein (LDP) (15, 16). The non-covalent bond between AE and LDP can be dissociated and re-associated, leading to rebuilting a molecule that exhibits similar activity as that of natural LDM. Taking advantage of the LDP genetic reassortment and the specific targeting capability of antibody fragments, different types of engineered fusion proteins were created (17–20). In short, lidamycin can be linked with another component, such as antibodies, due to its unique structure. As a result, lidamycin can target a specific site with its cytotoxicity. CD19 is a biomarker that is expressed on virtually all neoplastic cells of the B-cell lineage (21, 22). Previous studies demonstrated that the engineered fusion protein anti-CD19(Fab)-LDM, which comprises the chemo-drug lidamycin and anti-CD19(Fab) antibody, showed targeted cytotoxicity against lymphoma cells both *in vitro* and *in vivo* (23).

In this article, to verify the anticancer activity of the engineered fusion protein anti-CD19(Fab)-LDM on multidrug-resistant cells, we established an ADR resistant lymphoma cell line BJAB/ADR. Furthermore, we showed that anti-CD19(Fab)-LDM engineered fusion proteins could target the cell surface marker CD19 and exert the same cytotoxicity effect on ADR-resistant BJAB cells as on BJAB-sensitive cells. Our study indicates that anti-CD19(Fab)-LDM has anticancer effects on ADR-resistant B cell lymphoma. This result sheds light on the therapeutic effect of this fusion protein and provides a promising solution for MDR, especially ADR-resistant B cell lymphoma.

MATERIALS AND METHODS

Chemicals and Reagents

Adriamycin (ADR), propidium iodide (PI), verapamil and RNase A were obtained from Sigma-Aldrich Trading Co, Ltd (St. Louis, MO, USA). The phospho-glycoprotein (P-gp, MDR1) mouse monoclonal antibody conjugated with Alexa Fluor 594 (sc-390883), ABCG2 mouse monoclonal antibody conjugated with Alexa Fluor 488 (sc-18841) and MRP1 mouse monoclonal antibody conjugated with Alexa Fluor 488 (sc-53130) were obtained from Santa Cruz Biotechnology, Inc (Dallas, TX, USA). LDM was provided by the Institute of Medicinal Biotechnology of the Chinese Academy of Medical Sciences (Beijing, China). Antitumor agents were prepared fresh in PBS (phosphate-buffered saline) immediately prior to use.

Cells and Cell Culture

Cell culture supplies, including Dulbecco's modified Eagle's Medium (DMEM), fetal bovine serum (FBS), penicillin/streptomycin and 0.25% trypsin, were purchased from Corning Incorporated (Corning, NY, USA). The BJAB cell line was obtained from Cell Resource Center, Institute of Hematology and Hospital of Blood Diseases, Peking Union Medical College (PUMC) (Beijing, China). The cells were cultured in RPMI 1640 medium supplemented with 10% fetal bovine serum (FBS) and 1% penicillin/streptomycin, and they are maintained in an incubator containing 37°C humidified air with 5% CO_2.

Establishment of an ADR-Resistant BJAB Cell Line

The ADR-resistant cell line was created from the BJAB parental cell line via intermittent exposure to increasing concentrations of ADR for 6 months. Briefly, BJAB/ADR cells were treated with ADR with the concentrations ranging from 37 nM to 294 nM in a stepwise increasing manner. At first, the majority of the cells died after being treated with low concentrations of ADR for 24 h. We used 0.01 mol/L PBS to wash the surviving cells and continued to culture them in ADR-free growth medium. When cells were in the logarithmic growth phase, they were exposed to a higher ADR concentration for 24 h. After this process was repeated in a stepwise manner, a single-cell-derived ADR-resistant subclone, designated as BJAB/ADR, was established. For the maintenance of MDR, BJAB/ADR cells were cultured with 147 nM ADR. Two weeks before the experiment, BJAB/ADR cells were maintained in drug-free culture medium and passaged at least 3 times.

Cell Growth Assay

To investigate cell growth in both BJAB and BJAB/ADR cells, a cell proliferation assay was performed. Briefly, we seeded cells into 24-well culture plates at a density of 5×10^3 cells per well and cultured in complete RPMI 1640 culture medium for 8 days. Trypan blue exclusion-based methods were used to determine cell counts, and cells from triplicate wells were counted every 24 h for 8 days. All experiments were independently performed three times.

Analysis of Cell Cycle Distribution

After BJAB and BJAB/ADR cells were treated with ADR, they were harvested, washed twice with ice-cold PBS (pH 7.2), centrifuged and resuspended in 500 μL ice-cold PBS, and adjusted to a density of 1×10^6 cells/mL. Then, the cells were fixed with 70% ethanol at −20°C overnight. For the next step, the cells were incubated with 100 μL RNase (100 μg/mL, Sigma) for half an hour and stained with 200 μL PI (50 μg/mL) for 1 h.

Data from 100,000 events/sample were collected via FACScan flow cytometer (Becton Dickinson, San Diego, CA) and analyzed using FlowJo software.

Cell Viability Analysis (MTT Assay)

The MTT colorimetric assay was used to determine cell viability. Briefly, BJAB or BJAB/ADR cells (approximately 6,000 cells/well) were seeded into 96-well plates one day before drug treatment. After 72 h of drug treatment, 20 μL MTT solution (5 mg/mL thiazolyl blue powder in PBS) was added into each well and further incubated for 4 h at 37°C in a humidified atmosphere with 5% CO_2. At the end of the incubation period, the supernatant, including the medium and MTT solution, was removed from each well, and the forming formazan crystals were dissolved by adding 100 μL dimethyl sulphoxide (DMSO) solution and agitating the plate for 15 min. The spectrophotometric absorbance was measured at 570 nm. The percentage of viable cells was calculated compared with the untreated control group (assumed 100% viability). After treatment with ADR at different concentrations, the resistance fold was reflected by MTT colorimetric analysis. In a separate experiment, 10 μL verapamil (2.5 mg/mL) was used to treat BJAB/ADR cells to observe whether verapamil can reverse ADR-induced MDR. The cytotoxicity of anti-CD19(Fab)-LDM on cells was evaluated in the same way. All experiments were repeated three times independently.

Primer Design

Primers were designed according to published sequences using web-based software. We used the "BLAST" program (http://www.ncbi.nlm.nih.gov/blast) to determine the specificity of the primers. The primers used in this study were as follows: GAPDH-F: GAAGGTGAAGGTCGGAGTC, GAPDH-R: GAAGATGGTGATGGGATTTC; and MDR1-F: CCCATC ATTGCAATAGCAGG, MDR1-R: GTTCAAACTTCTGCTC CTGA.

RNA Extraction

Total RNA was extracted from cells using a RNeasy Mini Kit (Qiagen) following the instructions of manufacturer. Then, cDNA was synthesized with an M-MLV Reverse Transcriptase Kit (Invitrogen™) following the manufacturer's instructions.

Quantitative Real-Time PCR (qRT-PCR)

Quantitative Real-time PCR (RT-PCR) was used to quantitatively detect mRNA of *ABCB1*, *ABCC1,* and *ABCG2* in BJAB and BJAB/ADR cells. RT-PCR was performed using a SYBR® Green PCR Master Mix kit (Applied Biosystems®) on the Applied Biosystems 7500 system. The thermal profile comprised 40 cycles as follows: 95°C for 30 s, 55°C for 60 s, and 72°C for 30 s. The expression of each gene was normalized using the mean expression of the housekeeping gene. Linearized relative expression was obtained according to the $2^{-\Delta\Delta CT}$ method (24).

Detection of MDR Protein Expression Level by Flow Cytometry

Control and ADR-resistant BJAB cells were harvested, washed twice with ice-cold PBS (pH 7.2) and placed on ice immediately after collection. Samples (50 μL) were stained at 4°C for 20 min using predetermined saturating concentrations of phycoerythrin (PE)-labeled anti-P-gp monoclonal antibody, fluorescein (FITC)-labeled anti-ABCG2 monoclonal antibody, or FITC-labeled anti-MRP1 monoclonal antibody, respectively. Cells were analyzed on a FACScan flow cytometer (Becton Dickinson, San Diego, CA). Positive and negative cell populations were determined by using unreactive isotype-matched mAbs (Coulter) as controls for background staining. Background levels of staining were delineated using gates established to include 98% of the control cells.

Assessment of the Efflux Function of ABC Transporter in BJAB/ADR Cells

Because Rhodamine 123 (Rho 123) is a reference fluorescent substrate of ABCB1, we detected the fluorescence intensity to obtain efflux function of ABCB1 (25). Briefly, BJAB and BJAB/ADR cells were suspended at a density of 5×10^5 cells/mL in serum-free RPMI 1640 medium, and 200 μL of the cell suspension was put into 1.5 mL microcentrifuge tubes. BJAB cells were divided into two groups: negative control group (PBS) and positive control group (Rho 123). BJAB/ADR cells were divided into three groups: negative control group (PBS), positive control group (Rho 123) and experimental group (verapamil plus Rho 123). In the experimental group, 50 μmol/L verapamil was added to the tubes and incubated for 30 min at 37°C. After incubation, Rho 123 (200 nmol/L) was added to each tube. The cells were incubated for 1 h and then washed twice with ice-cold PBS after the incubation period. Finally, the fluorescence intensity was determined by flow cytometry to measure intracellular accumulation and efflux of Rho 123. Data was obtained from FACScan flow cytometer (Becton Dickinson, San Diego, CA). All experiments were independently conducted three times.

In vivo Antitumor Activity in Subcutaneous Xenograft Tumor Models

All experiments on mice received humane care in compliance with the Public Health Service Policy on Humane Care and Use of Laboratory Animals. The study protocol was approved by the Institutional Animal Care and Use Committee of the State Key Laboratory of Experimental Hematology (SKLEH).

BJAB and BJAB/ADR cells were harvested, suspended in PBS, and then subcutaneously injected into 5-week-old female BALB/c nude mice (1×10^7 cells/0.2 mL/mouse) to establish the BJAB and BJAB/ADR xenograft tumor models. When tumor volumes reached 60–80 mm^3, mice were randomized into eight treatment groups (five mice per group). Group 1: animals received PBS; group 2: animals received 6 nmol/kg ADR; group 3–5: animals received 2 nmol/kg, 4 nmol/kg, and 6 nmol/kg LDM, respectively; and group 6–8: animals received 2 nmol/kg, 4 nmol/kg, and 6 nmol/kg anti-CD19(Fab)-LDM, respectively. Drugs were intravenously injected once. The body

weights of the mice and the two perpendicular diameters of the tumors were recorded every third day, and tumor volumes were calculated by the following formula: tumor volume=1/2 × length × width^2. Animals were sacrificed, and xenograft tumors were surgically dissected, weighed and measured 28 days after treatment initiation.

Statistical Analysis

All the data was shown as the mean ± SD obtaining from three independent experiments performed in triplicate. The results were analyzed with one-way analysis of variance (ANOVA). Comparisons are made between control groups and corresponding treatment groups and they were carried out via SPSS 10.0 software. A value of $P < 0.05$ was considered statistically significant.

RESULTS

Successful Establishment of the ADR Resistant BJAB/ADR Cell Line

The BJAB/ADR cell line was established after intermittent treatment with ADR at concentrations ranging from 37 to 294 nM in a stepwise increasing manner. Over 6 months, a clone of BJAB cells that resistant to ADR was successfully screened and named BJAB/ADR. BJAB/ADR cells could grow sufficiently even if cultured in RPMI 1640 medium with 294 nM ADR, and cells also maintained resistance to ADR after removal of the drug for at least 2 weeks. Normally, the ADR-resistant cells were maintained in complete culture medium with 147 nM ADR, which is the approximate IC_{50} value (concentration that reduces viability to 50%) of BJAB/ADR cells to ADR. Moreover, BJAB/ADR cells can stably grow in drug-free RPMI 1640 medium for more than 2 weeks. These results suggest that an ADR-resistant cell line was successfully established.

In addition, the morphological characteristics of the established ADR-resistant BJAB/ADR cells were distinct from those of its parental cells under optical microscope. Although both types of cells exhibited suspension growth and had relatively consistent size and shape, the BJAB parental cells grew as a monolayer (**Figure 1A**), while the BJAB/ADR resistant cells tended to grow in clusters (**Figure 1B**).

BJAB/ADR Cells Had a Slower Growth Rate Than the Parental Cells and Were Arrested in G0/G1 Phase

The growth curves of BJAB and BJAB/ADR cells are shown in **Figure 2A**. The proliferation rate of both cell lines was not significantly different when the cells were cultured at low density. However, the growth rate of BJAB cells increased much more quickly as the density increased ($P < 0.05$). Specifically, the cell population doubling times for BJAB and BJAB/ADR cells were 31.66 ± 1.2 h and 35.19 ± 2.1 h, respectively ($P < 0.05$).

To investigate the effect of ADR on cell growth, a cell cycle assay was performed via flow cytometry. The results showed that the proportion of BJAB/ADR cells in the G0/G1 phase increased ($P < 0.05$, **Table 1**) and was accompanied by a decreased proportion in the S phase and G2/M phase. These results indicated that ADR could induce G0/G1 phase arrest in BJAB/ADR cells compared with the phase distribution of BJAB cells. However, the difference of phase distribution between BJAB and BJAB/ADR was not obvious, even they were repeatable and statistically significant. Hence, BJAB/ADR cell line may involve in other mechanisms of action resulting in ADR-resistant, which is needed to be addressed further.

BJAB/ADR Cells Exhibited a 43-fold Greater ADR Resistance Level Than the Parental Cells and Showed Cross-Resistance to Other Anticancer Drugs

After cells were treated with ADR, we performed the MTT assay to determine the drug resistance factor (RF). The IC_{50} values of ADR for BJAB and BJAB/ADR cells were 57.156 ± 2.30 nM and 2,434 ± 111.476 nM (**Figure 2B**), respectively. As shown in the results, the ADR resistance level of BJAB/ADR cells was 43-fold

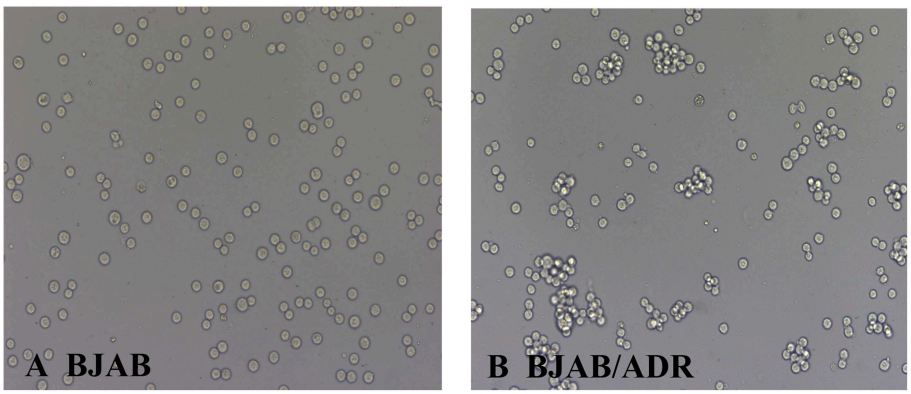

FIGURE 1 | Morphological characteristics of BJAB and BJAB/ADR cells. BJAB cells **(A)** and BJAB/ADR cells **(B)** were observed under an optical microscope (original magnification × 200). Compared with BJAB cells, BJAB/ADR cells tended to grow in clusters.

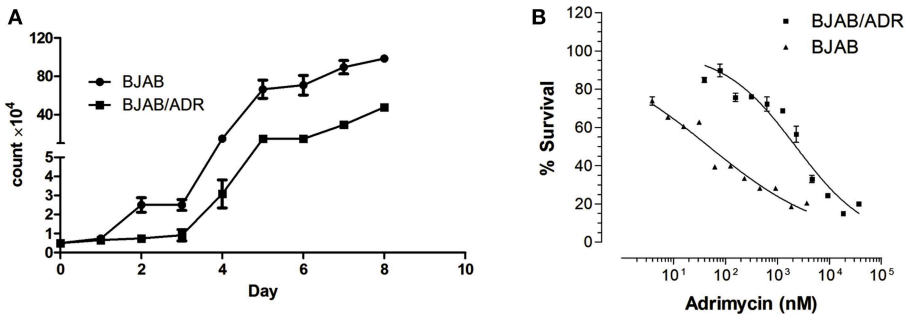

FIGURE 2 | Cell growth curve of BJAB and BJAB/ADR cells. **(A)** Growth curves of BJAB and BJAB/ADR cells. BJAB/ADR cells grew slower than BJAB cells ($P < 0.05$). **(B)** Cytotoxicity of adriamycin against BJAB and BJAB/ADR cells. Each data point was obtained from three independent experiments in triplicate. BJAB/ADR cells were resistant to adriamycin.

TABLE 1 | Cell cycle distribution of BJAB and BJAB/ADR cells.

Cell line	Cell cycle phase		
	G0/G1 (%)[b]	S (%)	G2/M (%)
BJAB	30.28 ± 0.36	5.98 ± 0.422	63.73 ± 0.537
BJAB/ADR	34.03 ± 0.068*[a]	4.16 ± 0.18*	61.81 ± 0.12

[a]*$P < 0.05$, the values are shown as the mean ± SD obtained from three independent assays.*
[b]*The increased proportion of resistant BJAB/ADR cells in G0/G1 phase was accompanied by a decreased proportion of cells in S and G2/M phases.*

TABLE 2 | Cross-resistance profile of BJAB/ADR cells to other anticancer drugs.

Treatment	IC_{50}(mean ± SD)[a]		RF[b]
	BJAB (nM)	BJAB/ADR (nM)	
Adriamycin	57.16 ± 2.30	2,434.12 ± 111.48	43
Etoposide	680.53 ± 21.11	21,200.22 ± 0.47	31
Cisplatin	6,772.20 ± 375.38	7,068.27 ± 435.44	1
Daunorubicin	277.09 ± 39.02	11,100.05 ± 0.14	40
Homoharringtonine	73.34 ± 20.11	568.23 ± 22.67	8
Mitoxantrone	75.36 ± 6.93	2,900.59 ± 410.21	38

[a]*IC_{50} values are shown as the mean ± SD calculated from the results of at least three independent MTT assays.*
[b]*RF refers to the resistance factor, which was calculated by dividing the IC_{50} values of the resistance cell line by the IC_{50} values of the respective parental cell line.*

greater than that of the parental cells. This result verified that the BJAB/ADR cell line acquired ADR resistance.

Additionally, BJAB/ADR cells showed resistance to various structurally unrelated anticancer drugs other than ADR. The cross-resistance profile of BJAB/ADR was summarized in **Table 2**. BJAB/ADR cells showed strong cross-resistance to etoposide, daunorubicin, homoharringtonine, and mitoxantrone but not cisplatin. Interestingly, the ADR-resistant subclone was 40 times more resistant to daunorubicin than the parental cell line. Hence, the established BJAB/ADR cell line can also be used for MDR study of its substrate drugs.

The Expression of Both *ABCB1* Gene and P-gp Protein Increased in BJAB/ADR Cells

Since it is reported that ADR is transported by ATP-binding cassette (ABC) transporters, especially ABCB1 and ABCG2 (4, 11), we hypothesized that the resistance mechanism of BJAB/ADR cells was associated with overexpression of ABC transporters. The *ABCB1* gene is a member of the ABC transporter superfamily that encodes a 170-kDa plasma membrane ABCB1 (P-glycoprotein, P-gp). ABC transporter functions as a drug efflux pump, thus resulting in decreased intracellular concentrations of broad drugs, such as paclitaxel, doxorubicin and others (26).

To determine the underlying resistance mechanism of BJAB/ADR cells, qRT-PCR was performed to detect the expression of the *ABCB1*, *ABCC1,* and *ABCG2* genes. We found that the *ABCB1* gene was upregulated in BJAB/ADR cells ($P < 0.05$) (**Figure 3A**). Moreover, the expression of P-gp protein was evaluated by flow cytometry analysis. Compared with the BJAB-sensitive cells, BJAB/ADR cells showed higher protein expression level of P-gp ($P < 0.05$) (**Figure 3B**). The results were consistent with those results from the qRT-PCR assay. We also examined the mRNA level of *ABCC1* and *ABCG2*, plus protein expression level of MRP1 (multidrug resistance-associated protein 1) and BCRP (breast cancer resistance protein), as shown in **Figures 3C–F**. Both transporters showed increased mRNA and protein expression, but not increased as much as *ABCB1* and P-gp expression. These results implicated that these two transporters were probably related to cross-resistance or MDR, suggesting that the mechanism of drug resistance of BJAB/ADR cells might be due to the overexpression of ABCB1.

Overexpression of ABCB1 in BJAB/ADR Cells Increased Drug Efflux, and Verapamil Reversed the Chemoresistance of the Cells to Adriamycin

As shown above, ABCB1 was overexpressed in the ADR-resistant cell line. To further understand the effects of

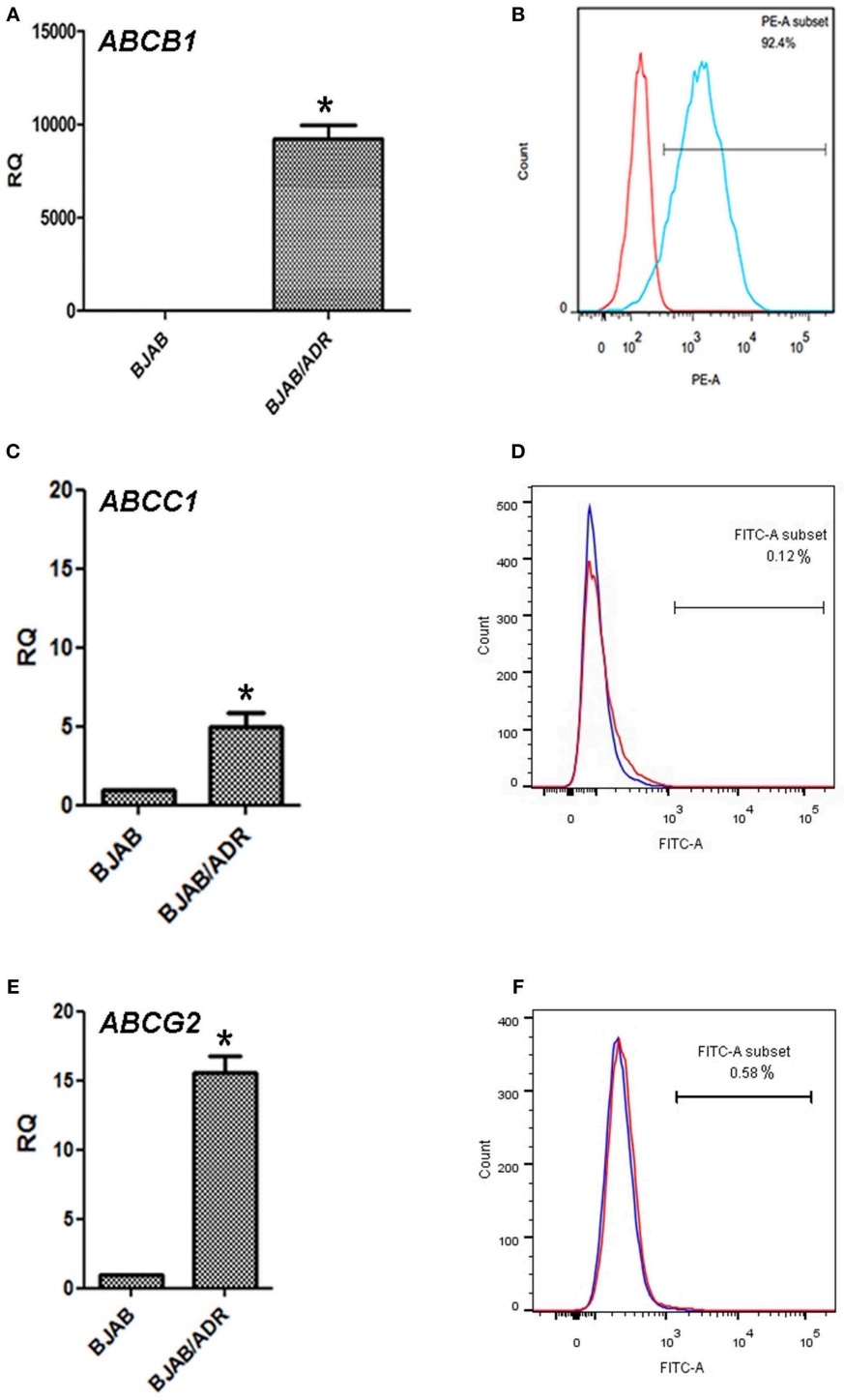

FIGURE 3 | Expression of the *ABCB1*, *ABCC1*, *ABCG2* genes and P-gp, MRP1, BCRP proteins in BJAB/ADR cells. **(A)** The expression of the *ABCB1* gene in the ADR-resistant BJAB/ADR cells. The mRNA level of MDR1 analyzed by qRT-PCR and normalized to the mRNA level of the housekeeping gene GAPDH. Compared with the sensitive cells BJAB, BJAB/ADR drug-resistant cells showed increased expression of *ABCB1* mRNA. $^*P < 0.05$, compared with control group. **(B)** The protein expression of P-gp on BJAB/ADR cells. The expression of P-gp was evaluated via flow cytometry analysis. BJAB/ADR cells showed higher expression of the membrane protein P-gp compared with the BJAB sensitive cells. **(C,E)** The qRT-PCR on the gene expression of *ABCC1* and *ABCG2*, respectively. These results showed higher expression levels of both genes, but the increased expression was not as high as that of *ABCB1*. $^*P < 0.05$, compared with control group. **(D,F)** The protein expression level of MRP1 and BCRP, separately. The results were obtained from flow cytometry analysis. These results indicated that higher expression levels of both protein, but the increased expression was not as high as that of P-gp.

ABCB1 overexpression on drug resistance, we performed an accumulation and efflux assay using Rho 123, a reference fluorescence substrate of ABCB1, via flow cytometry (27). As **Figure 4A**a,b shown, the mean values of the fluorescence intensity in BJAB and BJAB/ADR cells were 11,900 ± 312.05 and 165.67 ± 24.74, respectively, with statistical significance ($P < 0.05$). This result suggested that overexpression of ABCB1 in BJAB/ADR cells could decrease intracellular chemo-drug accumulation by increasing its efflux function.

Verapamil is a known reversal agent against drug resistance that can reverse MDR by blocking the efflux function of ABCB1 without changing its expression level (4, 11). After confirming the efflux function of ABCB1, we further treated BJAB/ADR cells with verapamil to observe the cells' sensitivity to ADR. When BJAB/ADR cells were pretreated with verapamil, the peak fluorescence intensity significantly shifted to the right, and the mean values of the fluorescence intensity increased to 4,890 ± 43.52 (**Figure 4A**c). As shown in **Figure 4B**, verapamil could sensitize the chemoresistance of BJAB/ADR cells to ADR and make BJAB/ADR cells more sensitive to ADR. These results suggested that the resistance mechanism of BJAB/ADR cells might be due to the increased efflux function of ABCB1, and verapamil could mitigate the efflux activity of ABCB1.

Anti-CD19(Fab)-LDM Had Similar Antitumor Activity in Both Resistant and Parental Cells

Previous experiments in our laboratory showed that the engineered fusion protein anti-CD19(Fab)-LDM exerted significant cytotoxic effects on BJAB cells (23). We performed the MTT assay to ascertain the cytotoxic effect of anti-CD19(Fab)-LDM toward BJAB/ADR cells. As shown in **Figure 5A**, the growth inhibition curves showed that two types of cells had similar drug sensitivity to anti-CD19(Fab)-LDM ($P > 0.05$). Additionally, the engineered fusion protein anti-CD19(Fab)-LDM showed a much stronger inhibitory effect than ADR in ADR-resistant cells ($P < 0.01$). More importantly, the fusion protein had a stronger cytotoxic effect than LDM alone (**Figure 5B**). These results suggested that anti-CD19(Fab)-LDM exerted cytotoxic effects on BJAB and BJAB/ADR cells and had a much stronger inhibitory function than either ADR or LDM alone in BJAB/ADR cells.

Anti-CD19(Fab)-LDM Inhibited Tumor Growth in Both BJAB and BJAB/ADR Xenograft Tumors in BALB/c Nude Mice

We previously demonstrated that anti-CD19(Fab)-LDM suppresses tumor growth in a human B-cell lymphoma xenograft model (23). To assess whether the observed anti-CD19(Fab)-LDM-mediated inhibition of cell growth of MDR cells *in vitro* would extend to animal models, we established BJAB and BJAB/ADR xenograft tumor mouse models to investigate the MDR phenomenon *in vivo* to investigate the therapeutic effect of anti-CD19(Fab)-LDM on the BJAB/ADR xenograft model.

We induced tumors by subcutaneously injecting BJAB or BJAB/ADR cells into the nude mice. When the tumor volume reached 60–80 mm^3, we treated the mice with PBS (as a control), ADR (6 nmol/kg), LDM (2, 4, or 6 nmol/kg), or anti-CD19(Fab)-LDM (2, 4, or 6 nmol/kg). Tumor volume was measured every 3 days following inoculation. Compared with the LDM- and ADR-treated mice, mice treated with anti-CD19(Fab)-LDM at doses of 2, 4, and 6 nmol/kg showed a significant inhibition of tumor growth in a dose-dependent manner in both the BJAB and BJAB/ADR xenograft models ($P < 0.05$) as shown in **Figure 6A**. Specifically, the ratio of tumor volume of the anti-CD19(Fab)-LDM group (6 nmol/kg) compared to the PBS control group was 92.79% on day 30, while the inhibitory effect of ADR was 53.45%.

After treatment for 28 days, the tumor tissues were excised and weighed. In the ADR-resistant xenograft model, the antitumor activity of anti-CD19(Fab)-LDM was stronger than that of LDM or ADR alone in a concentration-dependent manner ($P < 0.05$) (**Figure 6B**). More importantly, anti-CD19(Fab)-LDM was well-tolerated in both the BJAB and

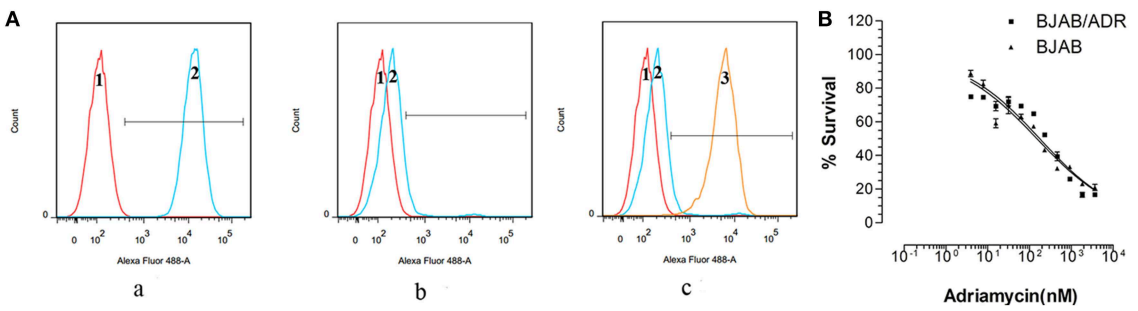

FIGURE 4 | Intercellular accumulation and efflux of Rho 123. **(A)** Flow cytometry measured intracellular accumulation and efflux of Rho 123. (a) Treatment of BJAB cells with Rho 123 resulted in Rho 123 accumulation in parental cells. (b) Decreased fluorescence intensity of Rho 123 in BJAB/ADR cells compared with that in the BJAB cells. (c) The chemo-drug accumulation significantly increased after BJAB/ADR cells treated with verapamil, an inhibitor of ABCB1 transporter, for 1 h (1 represents negative cells, 2 represents positive cells and 3 represents BJAB/ADR positive cells treated with verapamil). **(B)** Verapamil reversed the chemoresistance of BJAB/ADR cells to adriamycin, thus increasing the sensitivity of the drug-resistant cells to adriamycin.

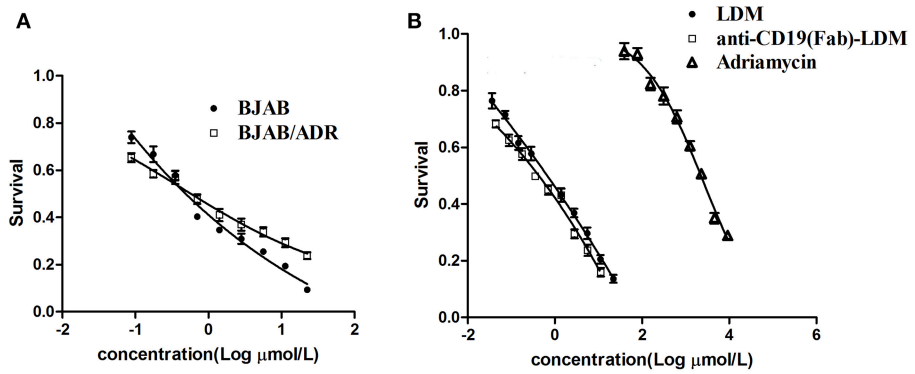

FIGURE 5 | Antitumor activity of anti-CD19(Fab)-LDM on ADR resistant cells. Antitumor activity of anti-CD19(Fab)-LDM on BJAB and BJAB/ADR cells assessed by MTT assay. **(A)** The anti-CD19(Fab)-LDM has a similar cytotoxic effect on resistant cells and their corresponding parental cells. **(B)** The anti-CD19(Fab)-LDM had a stronger inhibitory effect on BJAB/ADR cells than either adriamycin or LDM alone ($P < 0.05$).

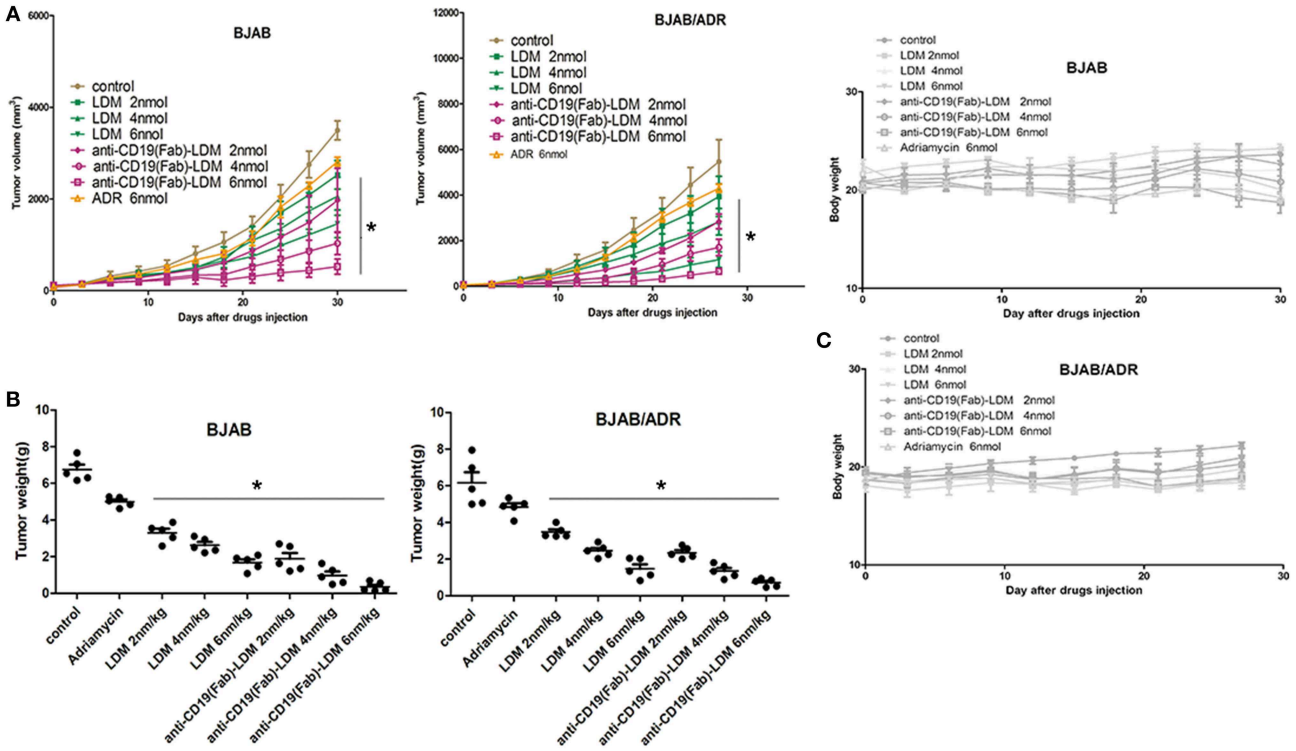

FIGURE 6 | Inhibitory effect of anti-CD19(Fab)-LDM on the growth of xenograft tumors. **(A)** Changes in tumor volume over time in BJAB and BJAB/ADR xenograft models ($n = 5$). Tumor volume was measured once every 3 days. Mice in the anti-CD19(Fab)-LDM groups showed significant inhibition of tumor growth compared with the adriamycin-treated mice in the BJAB and BJAB/ADR xenograft models (*$P < 0.05$ compared to the control). **(B)** Tumor weights of excised BJAB and BJAB/ADR tumor tissues from different mice measured on the 28th day after implantation. The anti-CD19(Fab)-LDM had a significant antitumor effect on both the BJAB and BJAB/ADR xenograft models compared to the effects of adriamycin treatment alone *in vivo*, especially in the high dose group (*$P < 0.05$ compared to the control). **(C)** Body weight of mice with BJAB or BJAB/ADR cell xenografts after treatment. Weight was measured once every 3 days. There was no significant difference in body weight among the groups ($P > 0.05$ compared with control group).

BJAB/ADR xenograft models, as indicated by the absence of significant differences in body weight compared with that in the vehicle-treated animals ($P > 0.05$) (**Figure 6C**). These results suggested that anti-CD19(Fab)-LDM was able to inhibit the growth of ADR-resistant BJAB cells and was well-tolerated. Therefore, anti-CD19(Fab)-LDM could be exploited as a potential drug used in the treatment of multidrug-resistant tumors.

DISCUSSION

B cell lymphoma is a hematopoietic malignant tumor, and its poor prognosis and short survival are mainly associated with multidrug resistance (MDR). Overcoming MDR and enhance the therapeutic effect of regimens for the treatment of B cell lymphoma is a major concern in clinical oncology (28–30). Thus, there is an immediate need to identify novel targets for the treatment of B cell leukemias and lymphomas. It was known that the poor response of lymphoma to chemotherapeutic drugs is mainly due to acquired MDR rather than innate resistance (31–33). Therefore, an appropriate experimental model is urgently needed for the study of MDR in B cell lymphoma. Since Bielder and Riehm first reported the MDR phenomenon of tumor cells in 1970, a series of multidrug-resistant cell lines have been constructed. However, there is few report on the stable MDR cell line of B cell lymphoma (34). In this article, our laboratory successfully established a B lymphoma MDR cell line, named BJAB/ADR, with the first-line chemotherapeutic drug adriamycin (ADR). The resistance factor (RF) between the parental and resistant cell lines was 43-fold. In fact, the resistance fold is highly variable between cell lines. For example, Wattanawongdon established two gemcitabine-resistant human cholangiocarcinoma cell lines with resistance indices of approximately 25- and 62-fold, respectively (35). In contrast, Iwasaki developed a cisplatin-resistant human neuroblastoma cell line with a resistance variant of approximately 1.1 (36). Generally, medium resistance is the most common type encountered in clinical practice. It is worth mentioning that BJAB/ADR cells could stably grow in drug-free medium for several weeks, and the morphological characteristics are consistent with those of parental cells, indicating a resistance-mediated improvement in survival. However, BJAB/ADR cells prefer to grow in clusters and have a slower growth rate than its parental cells (**Figures 1**, **2**). More importantly, these cells exhibited cross-resistance to a variety of structurally and functionally unrelated antineoplastic agents, such as etoposide, daunorubicin, homoharringtonine and mitoxantrone (**Table 2**). This result provides important information for further clinical evaluation.

We firstly examined the cell cycle of BJAB and BJAB/ADR. The results showed that ADR could induce G0/G1 phase arrest in BJAB/ADR cells compared with that in BJAB cells (**Table 1**). Combined the results of growth rate in **Figure 2**, we postulated that ADR could induce longer proliferation time and poorer proliferation ability. However, the difference of phase distribution between BJAB and BJAB/ADR was not obvious. Hence, it is needed more further studies to figure out the exact resistance mechanism of ADR on BJAB/ADR cell line. Also, we hypothesized that ADR resistance is probably associated with the overexpression of ABC transporters. This hypothesis is supported by the cross-resistance to other structurally unrelated chemotherapeutic drugs, most of which are substrates of ABC transporters, in resistant cells. ABCB1 (P-gp), ABCG2 (BCRP), and ABCC1 (MRP1) are three ABC transporters that are broadly expressed in multidrug-resistant cell lines (37). Thus, we examined the expression of these three ABC transporters and found that the *ABCB1* gene and P-gp protein expression was significantly upregulated in the BJAB/ADR cells. In contrast, the *ABCC1* and *ABCG2* mRNA and protein levels were only slightly increased compared to ABCB1 (**Figure 3**). This result is consistent with the previous reports that upregulated *ABCB1* gene is the main response for MDR in B-cell lymphoma (38, 39). Moreover, the Rhodamine 123 (Rho 123) exclusion assay verified that overexpression of ABCB1 participated in MDR, and verapamil, a known ABCB1 inhibitor, could reverse this drug resistance, thus increasing the sensitivity of BJAB/ADR cells to ADR (**Figure 4**). According to the present results, we could conclude that ABCB1-overexpressing is responsible for chemoresistance in BJAB/ADR cell line and poor efficacy of chemotherapeutic agents.

About 80–90% of cases of non-Hodgkin lymphoma (NHL) are of B-cell origin (40). The current therapeutic approach for B cell lymphoma involves chemotherapy, radiotherapy and the incorporation of the anti-CD20 monoclonal antibody rituximab (41, 42). Chemotherapy is the most common treatment strategy, but the outcomes of patients are often very poor, because of the development of resistance to conventional chemotherapeutic strategies. To overcome this issue, chemo-immunotherapies using rituximab in combination with CHOP (refers to cyclophosphamide, doxorubicin, vincristine, and prednisone) (R-CHOP) have markedly improved the outcome of patients with B cell lymphoma in recent decades. Currently, there are some novel treatment regimes, such as bendamustine or valproate, in combination with R-CHOP for patients with different phases of lymphoma (43–45). Unfortunately, about 10–15% of patients fail to respond to R-CHOP treatment, and 20–25% of patients develop relapse (46, 47). Therefore, novel strategies are needed to improve patients' response rate. Lidamycin is a novel antibiotic with antitumor activity emerged in recent years. Its mechanism of antineoplastic action is to inhibit DNA synthesis and break down cellular DNA in carcinoma cells (16). Due to its unique structure, lidamycin is often reconstituted with antibodies to establish engineered fusion proteins to maintain both the target property of antibodies and the cytotoxic effect. This type of biopharmaceutical drug is called antibody-drug conjugate (ADC) (48). Specifically, anti-C19(Fab)-LDM is an engineered fusion protein previously established in our laboratory and has been reported to have high antineoplastic activity toward B cell lymphoma (23). The fusion protein anti-CD19(Fab)-LDM was developed as a targeted therapy for lymphoma and induces significant tumor-specific cytotoxicity. Thus, anti-CD19(Fab)-LDM can overcome the deficiencies of traditional chemotherapy agents and significantly decrease adverse effects in patients. Additionally, this study shed light on the solution of drug resistance in tumor treatment. With all of these advantages, the use of engineered fusion proteins can circumvent the clinical issue of chemotherapy in the treatment of lymphoma. More importantly, due to the strong cytotoxic effects of LDM, the antibody-drug conjugate anti-CD19(Fab)-LDM can be administered at a lower dose to achieve therapeutic effects. Thus, it is a novel strategy worth exploring to find out its promising potential in preclinical and clinical trials.

Considering the strong antitumor activity of LDM and the B cell-targeted property of the anti-C19(Fab) antibody, we postulated that the anti-C19(Fab)-LDM could exert cytotoxic effect on the resistant cells of B cell lymphoma. As expected, anti-C19(Fab)-LDM showed similar cytotoxic effects toward BJAB/ADR and BJAB cells and showed a greater effect than either LDM or ADR alone (**Figure 5**). From the *in vivo* results, anti-C19(Fab)-LDM exhibited more potent antitumor activities than LDM and ADR in the BJAB/ADR xenograft mouse model (**Figure 6**). The *in vivo* results were in consistent with the *in vitro* results. Importantly, the therapeutic effect of anti-C19(Fab)-LDM was better than that of LDM both *in vitro* and *in vivo*. Therefore, our current results indicated that anti-C19(Fab)-LDM could be a promising targeted therapy for patients with ADR-resistant B cell lymphoma. Considering our *in vitro* results above, it is reasonable to postulate that anti-C19(Fab)-LDM may have inhibitory effect to pumped function of ABCB1, in turn probably increase the intracellular concentration of antineoplastic drugs. However, the exactly underlying re-sensitive mechanism of anti-C19(Fab)-LDM is needed to be addressed in the future.

In summary, we established an MDR B cell lymphoma cell line named BJAB/ADR, which could represent a drug-resistant cell model for lymphoma research. Additionally, our previously developed engineered fusion protein anti-C19(Fab)-LDM can be used to overcome MDR for the treatment of B cell lymphoma, especially in patients with acquired ADR resistance.

DATA AVAILABILITY

The raw data supporting the conclusions of this manuscript will be made available by the authors, without undue reservation, to any qualified researcher.

AUTHOR CONTRIBUTIONS

DF, LJ, MY, and DX designed the experiments. DF, LJ, YS, and SB performed experiments. YY, XY, and YZ provided technical and material support. DF and LJ wrote the first draft. DF, LJ, and MY revised the manuscript. All authors discussed the results and implications and developed the manuscript at all stages.

FUNDING

This work was supported by the Natural Science Foundation of China (Grant numbers 30873091, 30971291, and 81170512), the Natural Science Foundation of Tianjin (Grant number 05YFGZGX02800), and the National Science and Technology Major Project (Grant number 2012ZX09102301-015).

REFERENCES

1. Armitage JO, Gascoyne RD, Lunning MA, Cavalli F. Non-Hodgkin lymphoma. *Lancet.* (2017) 390:298–310. doi: 10.1016/S0140-6736(16)32407-2
2. Jiang M, Bennani NN, Feldman AL. Lymphoma classification update: T-cell lymphomas, Hodgkin lymphomas, and histiocytic/dendritic cell neoplasms. *Exp Rev Hematol.* (2017) 10:239–49. doi: 10.1080/17474086.2017.1281122
3. Chiappella A, Santambrogio E, Castellino A, Nicolosi M, Vitolo U. Integrating novel drugs to chemoimmunotherapy in diffuse large B-cell lymphoma. *Exp Rev Hematol.* (2017) 10:697–705. doi: 10.1080/17474086.2017.1350164
4. Ji N, Yang Y, Cai CY, Lei ZN, Wang JQ, Gupta P, et al. VS-4718 Antagonizes multidrug resistance in ABCB1- and ABCG2-overexpressing cancer cells by inhibiting the efflux function of ABC transporters. *Front Pharmacol.* (2018) 9:1236. doi: 10.3389/fphar.2018.01236
5. Flodr P, Latalova P, Tichy M, Kubova Z, Papajik T, Svachova M, et al. Diffuse large B-cell lymphoma: the history, current view and new perspectives. *Neoplasma.* (2014) 61:491–504. doi: 10.4149/neo_2014_062
6. Roesch K, Hasenclever D, Scholz M. Modelling lymphoma therapy and outcome. *Bull Math Biol.* (2014) 76:401–30. doi: 10.1007/s11538-013-9925-3
7. Crump M. Management of relapsed diffuse large B-cell lymphoma. *Hematol Oncol Clin N Am.* (2016) 30:1195–213. doi: 10.1016/j.hoc.2016.07.004
8. Camicia R, Winkler HC, Hassa PO. Novel drug targets for personalized precision medicine in relapsed/refractory diffuse large B-cell lymphoma: a comprehensive review. *Mol Cancer.* (2015) 14:207. doi: 10.1186/s12943-015-0474-2
9. Aszalos A. Drug-drug interactions affected by the transporter protein, P-glycoprotein (ABCB1, MDR1) II. Clinical aspects. *Drug Discov Today.* (2007) 12:838–43. doi: 10.1016/j.drudis.2007.07.021
10. Kartal-Yandim M, Adan-Gokbulut A, Baran Y. Molecular mechanisms of drug resistance and its reversal in cancer. *Crit Rev Biotechnol.* (2016) 36:716–26. doi: 10.3109/07388551.2015.1015957
11. Ji N, Yang Y, Lei ZN, Cai CY, Wang JQ, Gupta P, et al. Ulixertinib (BVD-523) antagonizes ABCB1- and ABCG2-mediated chemotherapeutic drug resistance. *Biochem Pharmacol.* (2018) 158:274–85. doi: 10.1016/j.bcp.2018.10.028
12. Lees C, Keane C, Gandhi MK, Gunawardana J. Biology and therapy of primary mediastinal B-cell lymphoma: current status and future directions. *Br J Haematol.* (2019) 185:25–41. doi: 10.1111/bjh.15778
13. Ogura M. [Adriamycin (doxorubicin)]. *Gan To Kagaku Ryoho.* (2001) 28:1331–8.
14. Chao CC. Lack of elevated drug efflux in adriamycin-resistant immunoblastic B lymphoma cells with mdr1 overexpression. *FEBS Lett.* (1995) 373:285–90. doi: 10.1016/0014-5793(95)01063-K
15. Liu W, Christenson SD, Standage S, Shen B. Biosynthesis of the enediyne antitumor antibiotic C-1027. *Science.* (2002) 297:1170–3. doi: 10.1126/science.1072110
16. Shao RG, Zhen YS. Enediyne anticancer antibiotic lidamycin: chemistry, biology and pharmacology. *Anticancer Agents Med Chem.* (2008) 8:123–31. doi: 10.2174/187152008783497055
17. Gao RJ, Zhao CY, Li DD, Zhen YS. [Optimization of the preparation process for fusion protein Fv-LDP that composes lidamycin apoprotein and single-chain Fv antibody directed against type IV collagenase]. *Yao Xue Xue Bao.* (2013) 48:1563–9.
18. Fang H, Miao Q, Zhang S, Cheng X, Xiong D, Zhen Y. Antitumor effects of an engineered and energized fusion protein consisting of an anti-CD20 scFv fragment and lidamycin. *Sci China Life Sci.* (2011) 54:255–62. doi: 10.1007/s11427-011-4143-4
19. Ding LL, Liu M, Zhang SH, Zhao XZ, Wu N, Chen L, et al. [Lidamycin inhibits angiogenesis of zebrafish embryo via down-regulation of VEGF]. *Yao Xue Xue Bao.* (2010) 45:456–61.
20. Miao Q, Shang B, Ouyang Z, Liu X, Zhen Y. Generation and antitumor effects of an engineered and energized fusion protein VL-LDP-AE composed of single-domain antibody and lidamycin. *Sci China C Life Sci.* (2007) 50:447–56. doi: 10.1007/s11427-007-0058-5
21. Del Nagro CJ, Otero DC, Anzelon AN, Omori SA, Kolla RV, Rickert RC. CD19 function in central and peripheral B-cell development. *Immunol Res.* (2005) 31:119–31. doi: 10.1385/IR:31:2:119
22. Pieper K, Grimbacher B, Eibel H. B-cell biology and development. *J Allergy Clin Immunol.* (2013) 131:959–71. doi: 10.1016/j.jaci.2013.01.046
23. Jiang L, Yang M, Zhang X, Bao S, Ma L, Fan D, et al. A novel antibody-drug conjugate anti-CD19(Fab)-LDM in the treatment of B-cell non-Hodgkin

lymphoma xenografts with enhanced anticancer activity. *J Drug Target.* (2015) 24:47–5. doi: 10.3109/1061186X.2015.1055568
24. Mocellin S, Rossi CR, Pilati P, Nitti D, Marincola FM. Quantitative real-time PCR: a powerful ally in cancer research. *Trends Mol Med.* (2003) 9:189–95. doi: 10.1016/S1471-4914(03)00047-9
25. Zhao W, Uehera S, Tanaka K, Tadokoro S, Kusamori K, Katsumi H, et al. Effects of polyoxyethylene alkyl ethers on the intestinal transport and absorption of Rhodamine 123: a P-glycoprotein substrate by *in vitro* and *in vivo* studies. *J Pharm Sci.* (2016) 105:1526–34. doi: 10.1016/j.xphs.2016.01.020
26. Panczyk M, Salagacka A, Mirowski M. MDR1 (ABCB1) gene encoding glycoprotein P (P-gp), a member of ABC transporter superfamily: consequences for therapy and progression of neoplastic diseases. *Postepy Biochem.* (2007) 53:361–73.
27. Nobili S, Landini I, Giglioni B, Mini E. Pharmacological strategies for overcoming multidrug resistance. *Curr Drug Targets.* (2006) 7:861–79. doi: 10.2174/138945006777709593
28. Ni Y, Xiao Z, Yin G, Fan L, Wang L, Zhu H, et al. The single nucleotide polymorphism and haplotype analysis of MDR1 in Chinese diffuse large B cell lymphoma patients. *Biomed Pharmacother.* (2015) 73:24–8. doi: 10.1016/j.biopha.2015.05.005
29. Yagi K, Yamamoto K, Umeda S, Abe S, Suzuki S, Onishi I, et al. Expression of multidrug resistance 1 gene in B-cell lymphomas: association with follicular dendritic cells. *Histopathology.* (2013) 62:414–20. doi: 10.1111/his.12035
30. Rund D. The elusive predisposing polymorphism: MDR1 and lymphoma. *Leuk Lymphoma.* (2013) 54:1129–30. doi: 10.3109/10428194.2012.749407
31. Pop I, Pop L, Vitetta ES, Ghetie MA. Generation of multidrug resistant lymphoma cell lines stably expressing P-glycoprotein. *Oncol Rep.* (2008) 19:889–95.
32. Ghetie MA, Ghetie V, Vitetta ES. Anti-CD19 antibodies inhibit the function of the P-gp pump in multidrug-resistant B lymphoma cells. *Clin Cancer Res.* (1999) 5:3920–7.
33. Stuart DD, Kao GY, Allen TM. A novel, long-circulating, and functional liposomal formulation of antisense oligodeoxynucleotides targeted against MDR1. *Cancer Gene Ther.* (2000) 7:466–75. doi: 10.1038/sj.cgt.7700145
34. Biedler JL, Riehm H. Cellular resistance to actinomycin D in Chinese hamster cells *in vitro*: cross-resistance, radioautographic, and cytogenetic studies. *Cancer Res.* (1970) 30:1174–84.
35. Wattanawongdon W, Hahnvajanawong C, Namwat N, Kanchanawat S, Boonmars T, Jearanaikoon P, et al. Establishment and characterization of gemcitabine-resistant human cholangiocarcinoma cell lines with multidrug resistance and enhanced invasiveness. *Int J Oncol.* (2015) 47:398–410. doi: 10.3892/ijo.2015.3019
36. Iwasaki I, Sugiyama H, Kanazawa S, Hemmi H. Establishment of cisplatin-resistant variants of human neuroblastoma cell lines, TGW and GOTO, and their drug cross-resistance profiles. *Cancer Chemother Pharmacol.* (2002) 49:438–44. doi: 10.1007/s00280-002-0452-4
37. Ji N, Yang Y, Cai CY, Lei ZN, Wang JQ, Gupta P, et al. Selonsertib (GS-4997), an ASK1 inhibitor, antagonizes multidrug resistance in ABCB1- and ABCG2-overexpressing cancer cells. *Cancer Lett.* (2019) 440–441:82–93. doi: 10.1016/j.canlet.2018.10.007
38. Ankathil R. ABCB1 genetic variants in leukemias: current insights into treatment outcomes. *Pharmacogenomics Pers Med.* (2017) 10:169–81. doi: 10.2147/PGPM.S105208
39. Pongstaporn W, Pakakasama S, Chaksangchaichote P, Pongtheerat T, Hongeng S, Permitr S. MDR1 C3435T and C1236T polymorphisms: association with high-risk childhood acute lymphoblastic leukemia. *Asian Pac J Cancer Prev.* (2015) 16:2839–43. doi: 10.7314/APJCP.2015.16.7.2839
40. Armitage JO. Treatment of non-Hodgkin's lymphoma. *N Engl J Med.* (1993) 328:1023–30. doi: 10.1056/NEJM199304083281409
41. Alduaij W, Ivanov A, Honeychurch J, Cheadle EJ, Potluri S, Lim SH, et al. Novel type II anti-CD20 monoclonal antibody (GA101) evokes homotypic adhesion and actin-dependent, lysosome-mediated cell death in B-cell malignancies. *Blood.* (2011) 117:4519–29. doi: 10.1182/blood-2010-07-296913
42. Aviles A, Neri N, Fernandez R, Huerta-Guzman J, Nambo MJ. Randomized clinical trial to assess the efficacy of radiotherapy in primary mediastinal large B-lymphoma. *Int J Radiat Oncol Biol Phys.* (2012) 83:1227–31. doi: 10.1016/j.ijrobp.2011.09.012
43. Rummel MJ, Niederle N, Maschmeyer G, Banat GA, von Grunhagen U, Losem C, et al. Bendamustine plus rituximab versus CHOP plus rituximab as first-line treatment for patients with indolent and mantle-cell lymphomas: an open-label, multicentre, randomised, phase 3 non-inferiority trial. *Lancet.* (2013) 381:1203–10. doi: 10.1016/S0140-6736(12)61763-2
44. Park SI, Grover NS, Olajide O, Asch AS, Wall JG, Richards KL, et al. A phase II trial of bendamustine in combination with rituximab in older patients with previously untreated diffuse large B-cell lymphoma. *Br J Haematol.* (2016) 175:281–9. doi: 10.1111/bjh.14232
45. Drott K, Hagberg H, Papworth K, Relander T, Jerkeman M. Valproate in combination with rituximab and CHOP as first-line therapy in diffuse large B-cell lymphoma (VALFRID). *Blood Adv.* (2018) 2:1386–92. doi: 10.1182/bloodadvances.2018019240
46. Kurita D, Miura K, Nakagawa M, Ohtake S, Sakagami M, Uchino Y, et al. Dose-intensified CHOP with rituximab (R-Double-CHOP) followed by consolidation high-dose chemotherapies for patients with advanced diffuse large B-cell lymphoma. *Int J Hematol.* (2015) 101:585–93. doi: 10.1007/s12185-015-1780-6
47. Gisselbrecht C. TP53 mutations and rituximab-CHOP. *Blood.* (2012) 120:3867–9. doi: 10.1182/blood-2012-09-455865
48. Wang R, Li L, Duan A, Li Y, Liu X, Miao Q, et al. Crizotinib enhances anti-CD30-LDM induced antitumor efficacy in NPM-ALK positive anaplastic large cell lymphoma. *Cancer Lett.* (2019) 448:84–93. doi: 10.1016/j.canlet.2019.02.002

Conflict of Interest Statement: The authors declare that the research was conducted in the absence of any commercial or financial relationships that could be construed as a potential conflict of interest.

frontiers in Oncology

MINI REVIEW
published: 10 September 2019
doi: 10.3389/fonc.2019.00887

Current Advance of Therapeutic Agents in Clinical Trials Potentially Targeting Tumor Plasticity

*Xiao-Guang Yang†, Lan-Cao Zhu†, Yan-Jun Wang, Yan-Yu Li and Dun Wang**

Key Laboratory of Structure-Based Drug Design & Discovery of Ministry of Education, Shenyang Pharmaceutical University, Shenyang, China

Tumor plasticity refers to tumor cell's inherent property of transforming one type of cell to different types of cells. Tumor plasticity is the main cause of tumor relapse, metastasis and drug resistance. Cancer stem cell (CSC) model embodies the trait of tumor plasticity. During carcinoma progression, epithelial-mesenchymal transition (EMT) plays crucial role in the formation of CSCs and vasculogenic mimicry (VM) based on epithelial-mesenchymal plasticity. And the unique tumor microenvironment (TME) not only provides suitable niche for CSCs but promotes the building of CSCs and VM that nourishes tumor tissue together with neoplasm metabolism by affecting tumor plasticity. Therapeutic strategies targeting tumor plasticity are promising ways to treat malignant tumor. In this article, we discuss the recent developments of potential drug targets related to CSCs, EMT, TME, VM, and metabolic pathways and summarize drugs that target these areas in clinical trials.

Keywords: tumor plasticity, cancer stem cells, vasculogenic mimicry, extracellular matrix, tumor microenvironment, targeting

OPEN ACCESS

Edited by:
Dong-Hua Yang,
St. John's University, United States

Reviewed by:
Aamir Ahmad,
Mitchell Cancer Institute,
United States
Xiaojun Yang,
Shantou University Medical
College, China

***Correspondence:**
Dun Wang
wangduncn@hotmail.com

† These authors have contributed equally to this work

Specialty section:
This article was submitted to Molecular and Cellular Oncology, a section of the journal Frontiers in Oncology

Received: *24 July 2019*
Accepted: *27 August 2019*
Published: *10 September 2019*

Citation:
Yang X-G, Zhu L-C, Wang Y-J, Li Y-Y and Wang D (2019) Current Advance of Therapeutic Agents in Clinical Trials Potentially Targeting Tumor Plasticity. Front. Oncol. 9:887. doi: 10.3389/fonc.2019.00887

INTRODUCTION

The universal methods for cancer treatment include surgery, radiotherapy, and chemotherapy. Chemotherapy is the principle modality for the treatment of malignant tumor, especially tumors in the late stages. Despite significant improvement of cancer chemotherapy in clinical practice, there are still many obstacles that chemotherapeutic drugs must overcome: (1) lack of effective treatments for metastatic tumors; (2) ineffectiveness in killing drug-resistant tumor cells; and (3) lack of new targets based on the characteristics of neoplasm, such as tumor plasticity.

Tumor plasticity prompts tumor cells to differentiate into a variety of cell types to adapt to different environment (1). Emerging evidence suggested that tumor plasticity played critical roles in the emergence of drug resistance and the promotion of tumor growth, invasion and metastasis. Therefore, there is an urgent need to develop new therapeutic agents to target tumor plasticity.

The cancer stem cells (CSCs) model offers one explanation for tumor plasticity. The CSCs model revealed that only a minority of tumorigenic cells contribute to tumor growth and progression. However, there are many other aspects closely related to tumor plasticity. For example: (1) epithelial-mesenchymal transition (EMT), which contributes to the phenotypic plasticity and promotes cancer metastasis; (2) tumor microenvironment (TME), which contains extracellular matrix (ECM) and cells such as fibroblasts, endothelial and immune cells that are the primary source of signals to and from the tumors; (3) vasculogenic mimicry (VM), which is a microcirculation that is independent of angiogenesis in aggressive primary and metastatic tumors

and comprised of non-endothelial cell generated by tumor cells and ECM; and (4) neoplastic metabolic pathways, that mainly include glycolysis and oxidative phosphorylation (OXPHOS). Changes of metabolic pathways between glycolysis and OXPHOS in cancer cells is prevalent during tumorigenesis and metastasis. Hence, targeting glycolysis and OXPHOS is essential to wipe out metabolic plasticity in cancer cells. Here, the potential targets related to tumor plasticity was summarized in **Figure 1**. In this mini review, we summarize the recent advances in anticancer compounds targeting CSCs, ETM, TEM, VM formation, and metabolic pathways, which is associated with tumor plasticity.

THERAPEUTIC TARGETING OF CSCS

The concept of CSCs was proposed several decades ago. The existence of CSCs has been confirmed by lineage tracing and cell ablation experiments in tumors (2–6). Similar to normal stem cells, a small subset of CSCs could proliferate and differentiate into a wide variety of cell types to sustain and promote tumor growth. The characteristic of tumor plasticity in CSCs is that CSCs could differentiate in different directions. The CSCs model provides a new explanation for the metastasis and recurrence of malignant tumors. CSCs have also been recognized as a major driver of tumor growth, metastasis and chemotherapeutic resistance. Therefore, CSCs has become crucial targets for cancer treatment. The ways to eliminate CSCs mainly consist of two aspects (7): (1) inhibition of key CSCs signaling pathways, including Wnt pathway, porcupine (PORCN) pathway and Hedgehog (Hh) pathway (8, 9); and (2) ablate CSCs by targeting CSC surface markers, such as CD133, CD44, (leucine-rich repeat containing G protein-coupled receptor 5) LGR5, (aldehyde dehydrogenase1) ALDH1, and breast cancer-resistant protein (BCRP; ABCG2). **Table 1** summarizes drugs that target CSCs in recent clinical trials.

Therapeutic agents targeting Wnt signaling pathway in clinical trials include porcupine (PORCN) inhibitors, β-catenin inhibitors and antibodies against Wnt signaling molecules (24). Among these, PORCN inhibitors gradually became research focus of antitumor drugs. **WNT-974**, an orally first-in-class PORCN inhibitor, is a pyridinyl acetamide derivative that target Wnt signaling to inhibit the expression of Wnt related genes and Wnt-dependent LRP6 phosphorylation. **WNT-974** showed significant growth inhibitory effect on Wnt-driven neoplasms, such as pancreatic cancer and head and neck squamous cell carcinoma. The pharmacokinetics (PK) and pharmacodynamics (PD) of **WNT974** were tested in patients with advanced cancers in phase I clinical trial, and the results showed rapid absorption (median T_{max} 1–3 h) and appropriate elimination half-life of 5–8 h. These clinical data demonstrated that **WNT-974** possesses favorable safety profile and potential antineoplastic activity in selected populations (25). Currently, **WNT-974** is being tested in a phase I study for the treatment of solid tumors including colorectal cancer and melanoma (10). In addition, PORCN inhibitor **ETC-159** is in phase I clinical trial for advanced solid

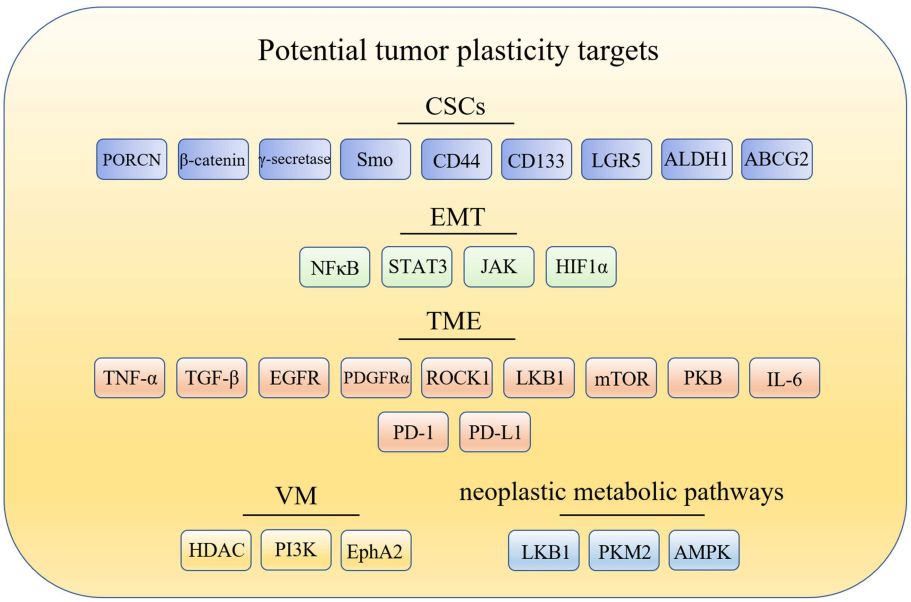

FIGURE 1 | Potential drug targets related to tumor plasticity. CSCs, cancer stem cells; EMT, epithelial-mesenchymal transition; TME, tumor microenvironment; TME, tumor microenvironment; PORCN, porcupine; Smo, smoothened; LGR5, leucine-rich repeat containing G protein-coupled receptor 5; ALDH1, aldehyde dehydrogenase1; ABCG2, breast cancer-resistant protein; NF-κB, nuclear factor-kappa B; JAK/STAT3, the Janus kinase/signal transducer and activator of tran-ions 3; HIF1α, hypoxia-inducible factor 1α; TNF-α, tumor necrosis factor alpha; TGF-β, transforming growth factor-β; EGFR, epidermal growth factor receptor; PDGFRα, platelet derived growth factor receptor alpha; ROCK1, Rho kinase1; LKB1, liver kinase B1; mTOR, mammalian target of rapamycin; PKB/Akt, protein kinase B; IL-6, interleukin-6; PD-1, programmed cell death receptor-1; PD-L1, programmed cell death-ligand 1; HDAC, histone deacetylases inhibitor; PI3K, phosphatidylinositide 3-kinases; MMPs, matrix metalloproteinases; Eck/EphA2, epithelial cell kinase; LKB1, liver kinase B1; PKM2, pyruvate kinase M2; AMPK, AMP-activated protein kinase.

TABLE 1 | Potential drugs targeting CSCs in clinical trials.

Drug	Mechanism of action	Condition or disease	Phase	References
WNT-974	PORCN inhibitors	Colorectal cancer and melanoma	I	(10)
ETC-159	PORCN inhibitors	Advanced solid tumors	I	(11, 12)
CGX-1321	PORCN inhibitors	Refractory solid tumors and advanced gastrointestinal cancers	I	(13)
RXC-004	PORCN inhibitors	Solid tumors	I/II	(14)
BC-2059	β-catenin inhibitors	Desmoid tumors	I	(15)
E-7386	CREB-binding protein (CBP)/β-catenin interaction inhibitors	Solid tumors	I	(16)
AL-101	γ-secretase inhibitors	Adenoid cystic carcinoma	II	(17)
Vismodegib	p-glycoprotein inhibitors Breast cancer-resistant protein inhibitors Smo receptor antagonists	Basal cell carcinoma, other cancers	Launched in 2012	(18)
Sonidegib phosphate	Smo receptor antagonists	Basal cell carcinoma, other cancers	Launched in 2015	(19)
Patidegib	Smo receptor antagonists	Sarcoma, basal cell carcinoma	III	(20, 21)
Taladegib	Smo receptor antagonists	Adenocarcinoma, solid tumors	I/II	(22, 23)

TABLE 2 | Potential drugs targeting CSC surface marker in clinical trials.

Drug	Mechanism of action	Condition or disease	Phase	References
P5	Anti-CD49e/CD29 (integrin α5β1)	Non-small cell lung cancer (NSCLC)	III	(32)
ALM-201	Microtubule inhibitors (binds CD44)	Advanced ovarian cancer and other solid tumors	I	(33)
RO-5429083	Anti-CD44	Acute myeloid leukemia	I	(34)
RG-7356	Anti-CD44	Acute myeloid leukemia	I	(35)
AMC-303	CD44 Antigen Exon 6 (CD44v6) inhibitors	Advanced or metastatic malignant solid tumors of epithelial origin	I/II	(36)
CX-2009	Tubulin polymerization inhibitors Anti-ALCAM (CD166)	Solid tumors	I/II	(37)
Chrysin	ABCG2 inhibitors	Chronic lymphocytic leukemia (CLL)	II	(38)

tumors, **CGX-1321** is in phase I clinical trials for advanced gastrointestinal cancers and **RXC-004** is in phase I/II clinical trials for the treatment of solid tumors (11–14). Through the inhibition of β-catenin, **Tegavivint** (BC-2059), an anthraquinone derivative and **E-7386** are both being evaluated in phase I clinical trials to treat symptomatic or progressive unresectable desmoid tumors and solid tumors (15, 16).

The small-molecule inhibitors and macromolecule monoclonal antibodies (mAbs) including γ-secretase inhibitors and mAbs to NOTCH receptors have been tested in clinical trials. A small-molecule inhibitor of γ-secretase, which is a key enzyme in NOTCH signaling pathway, **AL-101** with favorable *in vitro* potency and oxidative metabolic stability, is in phase II clinical development for the treatment of adenoid cystic carcinoma bearing NOTCH activated mutations (17). On the other hand, among the therapeutic molecules targeting Hh pathway, smoothened (Smo) receptor antagonists are the most promising molecules (26). A novel small-molecule inhibitor or antagonist of Smo, **Sonidegib phosphate** was launched in 2015 for the treatment of advanced basal cell carcinoma (BCC). **Sonidegib phosphate** exhibited excellent therapeutic effect (roughly 35–60% response rates of patients) in patients with locally advanced, unresectable and metastatic BCC, with high disease control rates and clinical benefit (19, 27). Recent advances in the development of Hh signaling inhibitors include **Vismodegib** (18), which is launched in 2012 for the treatment of patients with advanced BCC; **Patidegib**, which is in phase III clinical trial for reducing the incidence of BCC (20, 21) and **Taladegib**, which is in phase I/II clinical trial) for the treatment of patients with recurrent, advanced solid tumors (22, 23).

Because of the highly plasticity of CSCs in tumors, the identification and eradication of CSCs are difficult. Generally, their identification depends on cell surface markers. CD34, CD44, and CD133 are common examples of CSC-specific surface markers (28). CSC surface markers can mediate adhesion of the cells. A cell surface membrane protein CD133, which was first discovered in hematopoietic stem and progenitor cells, is considered to be one of the common surface markers in multiple stem cells (29). Others like ALDH1 and ABCG2 also play significant roles in the regulation of CSCs (30, 31). Because CSCs drive cancer development, a number of agents targeting the biomarkers of CSCs have been developed (**Table 2**).

A novel mAb **P5**, which targets CD49e/CD29, is currently being tested in phase III clinical trials to evaluate its anti-tumor effect, but there are only a few reports about its progress of new clinical trials (32). As a FK506 binding protein like (FKBPL) peptide derivative, **ALM-201** can bind to CD44 and inhibit cancer related pathways, such as DLL4/NOTCH signal pathway as well as inhibit cell migration, tubule formation and angiogenesis. **ALM-201** showed an excellent safety profile and acceptable PK in patients with advanced solid tumors in a phase I dose-escalation study (39). This candidate is currently in phase I clinical trials for the treatment of patients with advanced ovarian cancer and other solid tumors (33). **RO-5429083** and **RG-7356**

are both humanized monoclonal antibodies against extracellular domain of CD44 which had been used in phase I clinical studies for the treatment of acute myeloid leukemia and solid tumors (34, 35). In addition, **AMC-303**, a high specific inhibitor of CD44v6, was evaluated as monotherapy to treat patients with advanced epithelial tumors. **AMC-303** was proved to be well-tolerated with a favorable PK profile ($t_{1/2}$ of 4–7 h, CL of 40–60 mL/h/kg) (40). At present, **AMC-303** is in phase I/II clinical trials to treat patients with advanced or metastatic malignant solid tumors of epithelial origin (36). A probody drug conjugate **CX-2009** against CD166 is in phase I/II clinical development for the treatment of adult patients with metastatic or locally advanced unresectable solid tumors (37). Furthermore, a recent research reported that **chrysin**, which is an ABCG2 inhibitor, could enhance sorafenib mediated inhibition of cell viability by sustained phosphorylation of ERK1/2 (41). And **chrysin** is being used in phase II clinical trials to treat CLL (38).

THERAPEUTIC TARGETING OF EMT

The conversion of cells from epithelial phenotype into mesenchymal phenotype is a critical transformation for embryonic development and during cancer progression. Through EMT process, tumor cells can acquire the ability to disarm anti-tumor defenses in the body, resist apoptosis and antineoplastic drugs, spread through the body and expand the population of tumor cells (42). At the same time, EMT may play an important role in generating CSCs (43). Hence, EMT is an important target for inhibiting tumor metastasis and reducing drug resistance. Various approaches can be used to target the EMT process: (1) targeting the inducing signals in EMT process; (2) reversing EMT to reduce tumor cell aggressiveness; and (3) killing the cells in EMT-like state (44). As one of the key factors of tumor invasion, metastasis and drug resistance, EMT is a promising target for oncotherapy. The following summarized the progress of potential drugs targeting EMT-related signals (**Table 3**).

Modulators of transcription factors, such as nuclear factor-kappa B (NF-κB) and signaling transducer and activator of transcription 3 (STAT3) have made progress in clinical trials (59, 60). **Denosumab**, which is a macromolecule of humanized mAbs to receptor activator of NF-κB ligand (RANKL), was originally approved to treat and prevent postmenopausal osteoporosis in 2010 (45). **Denosumab** prevents RANKL binding to RANK, and blocks the development of osteoclasts, leading to restraining the resorption of bone. So far, phase III clinical studies have been ongoing for evaluating its therapeutic effect on metastatic non-small cell lung cancer (NSCLC) together with other chemotherapeutics. **TK-006** is another anti-RANKL antibody in early clinical development for the treatment of patients with bone metastases caused by breast cancer through hypodermic injection (46). In addition, **WO-1066** is a JAK/STAT3 (the Janus kinase/signal transducer and activator of tran-ions 3) signaling pathway and programmed cell death-ligand 1 (PD-L1) inhibitor, which is derived from the JAK2 inhibitor AG490. In 2019, the compound was granted an orphan drug designation in the U.S. for treating glioblastoma. Currently, the candidate is in phase I clinical trials for patients with melanoma or glioblastoma multiforme with brain metastases (47, 48). **DSP-0337**, **Danvatirsen** and **OPB-111077,** all inhibit STAT3 and are in phase I or II clinical trials to assess their therapeutic efficacy in solid tumors (49–52).

TABLE 3 | Potential drugs targeting EMT-related modulators in clinical trials.

Drug	Mechanism of action	Condition or disease	Phase	References
Denosumab	Receptor activator of NF-κB ligands (RANKL)	Tenosynovial giant cell tumor	Launched in 2013	(45)
TK-006	Anti-TNFSF11 (RANKL)	Breast cancer-related bone metastases	I	(46)
WO-1066	STAT3 inhibitors, anti-PD-L1, Janus kinase (JAK) inhibitors	Melanoma, brain cancer	I	(47, 48)
DSP-0337	STAT3 inhibitor	Solid tumors	I	(49)
Danvatirsen	STAT3 expression inhibitors	Solid tumors	II	(50, 51)
OPB-111077	STAT3 ligands	Solid tumors	II	(52)
Napabucasin	STAT3 inhibitors	Colorectal carcinoma, pancreatic cancer	III	(53, 54)
PEGPH20	HIF1α inhibitors	Metastatic breast cancer	I/II	(55, 56)
CRLX-101	HIF1α inhibitors, DNA Topoisomerase I inhibitors	peritoneum cancer	II	(57, 58)

Hypoxia-inducible factor 1α (HIF1α) and β-catenin also regulate the expression of other transcription factors related to EMT (61, 62). **PEGPH20** (PEGylated recombinant human hyaluronidase PH20), which enzymatically degrades hyaluronic acid (HA), is currently being evaluated in phase II and III trials. It shows promising efficacy in preclinical and early clinical studies in the treatment of metastatic pancreatic carcinoma and other malignant tumors (55, 56). **CRLX-101** was proved to be a potent topoisomerase 1 and HIF1α inhibitor, which is a nanoparticle composed of CPT conjugated to a biocompatible copolymer of cyclodextrin and polyethylene glycol (PEG). Currently, CRLX101 is being evaluated in phase II clinical trials for several tumor types (58).

THERAPEUTIC TARGETING OF TME

Studies have shown that epigenetic changes of tumor cells caused by TME play a prominent role in tumor progression and invasion (1, 63). Tumor cells usually adapt to the changing external environment through changing the plasticity of tumor cells to meet the demand of tumor development. The research of relationship between TME and tumor plasticity is making progress in recent years (64). TME is composed of a complex

mixture of ECM and various cells including cancer associated fibroblasts (CAFs) (65), cancer associated macrophages (CAMs) (66) and endothelial progenitor cells (EPCs) (67). Many components in ECM contribute to tumor growth. TME has become one of the key targets in tumor treatment due to its special pathophysiological characteristics and physicochemical properties (**Table 4**).

Tumor necrosis factor alpha (TNF-α) could promote tumor growth via a PKCa- and AP-1-dependent pathway (90). **Avadomide** (**CC-122**) is a small molecule drug that inhibits both TNF-α and cereblon E3 ligase. The first-in-human phase I study, which evaluated the safety and clinical therapeutic effect of **avadomide** in patients with advanced solid tumors and others, showed acceptable safety and favorable pharmacokinetics (68). A**vadomide** is currently being evaluated in advanced melanoma in combination with Nivolumab. Transforming growth factor-β (TGF-β) signaling pathway is related to EMT in cancer cells (91). Therapeutic agents modulating the expression of TGF-β that are monoclonal antibodies include: **NIS-793** (a humanized anti-TGF-β monoclonal antibody), **AVID-200** (a recombinant inhibitor of TGF-β1 and TGF-β3), **SAR-439459** (targeting transforming TGF-β) and **fresolimumab** (a pan-specific human anti-TGF-β monoclonal antibody). Among these therapeutic agents, **fresolimumab** is able to neutralize all human isoforms of transforming TGF-β and being evaluated in phase I/II trials (72, 92).

TABLE 4 | Potential drugs targeting TME in clinical trials.

Drug	Mechanism of action	Condition or disease	Phase	References
Avadomide hydrochloride	TNF-α production inhibitor and cereblon inhibitors	Solid tumors	I/II	(68)
NIS-793	Anti-TGF-β	Solid tumors	I	(69)
AVID-200	TGF-β inhibitors	Solid tumors	I	(70)
SAR-439459	Anti-TGF-β	Solid tumors	I	(71)
Fresolimumab	Anti-TGF-β	Lung cancer	I/II	(72)
Simotinib hydrochloride	EGFR inhibitors	Lung cancer	I	(73)
Amcasertib	PDGFRα inhibitors	Hepatocellular carcinoma, cholangiocarcinoma	II	(74)
Olaratumab	Anti-CD140a (PDGFRα)	Soft tissue sarcoma	Launched in 2016	(75)
Cerdulatinib	JAK and Syk kinase inhibitors	Hematologic cancers	II	(76)
AZD-8055	mTORC1/2 inhibitors	Solid tumors	I	(77)
BI-860585	mTORC1/2 inhibitors	Solid tumors	I	(78)
DCBCI-0901	mTORC1/2 inhibitors Phosphatidylinositol 3-Kinase alpha (PI3Kα) inhibitors	Solid tumors	I	(79)
LXI-15029	mTORC1/2 inhibitors	Solid tumors	I	(80)
ABI-009	mTOR inhibitors	Metastatic cancer	II	(81)
Sapanisertib	mTORC1/2 inhibitors	Endometrial cancer	II	(82)
GSK-690693	Akt kinases 1 inhibitors	Lymphoma, solid tumors	I	(83)
ARQ-751	pan-Akt inhibitors	Solid tumors	I	(84)
TAS-117	PKB/Akt inhibitors	Solid tumors	II	(85)
Ipatasertib	PKB/Akt inhibitors	Prostate cancer	III	(86)
Siltuximab	Anti-IL6	Multiple myeloma	II	(87)
Sintilimab	Anti-PD-1	Lymphoma, Hodgkin's	Launched in 2019	(88)
Avelumab	Anti-PD-L1	Bladder and kidney cancer	Launched in 2017	(89)

Epidermal growth factor receptor (EGFR) regulates ECM and promotes cancer invasion (93). A small EGFR inhibitor **Simotinib** is used in phase I study to treat NSCLC (73). Platelet derived growth factor receptor alpha (PDGFRα), which contributes to fibroblast reprograming toward CAFs, plays a significant role in colorectal carcinogenesis (94). **Amcasertib**, a PDGFRα inhibitor and cancer stemness kinase inhibitor, is used to treat hepatocellular carcinoma and cholangiocarcinoma in phase II trials (74). Different from **Amcasertib**, **Lartruvo**(**R**) (**olaratumab**) is a fully humanized monoclonal antibody to neutralize PDGFRα. It was first launched in the U.S. for front-line treatment with doxorubicin in adults with soft tissue sarcoma in 2016 (75).

Some signaling pathways are also critical in cancer development. Janus kinase 1 (JAK1)/Rho kinase1 (ROCK1) signaling could promote fibroblast-dependent carcinoma cell invasion (95). **Cerdulatinib** is a small-molecule anti-cancer drug targeting JAK and syk kinase for the treatment of hematologic cancers (76). Liver kinase B1 (LKB1)/mammalian target of rapamycin (mTOR) signaling axis regulates ECM stiffness and participates in lung adenocarcinoma progression (96). Potential drugs such as **AZD-8055**, **BI-860585**, **DCBCI-0901**, **LXI-15029,** and **ABI-009** are in early clinical stage for various cancers (77–81). **Sapanisertib** is an orally and highly selective ATP-competitive inhibitor of mTORC1/2 and demonstrates satisfactory anticancer activity. The phase II study of **sapanisertib** in metastatic castration resistant prostate cancer was not entirely satisfactory likely because of dose reductions secondary to toxicity (82). In addition, abnormal expression of protein kinase B (PKB/Akt) is related to many cancers (97). **GSK-690693** (83), **ARQ-751** (84), and **TAS-117** (85) that can effectively treat solid tumors through inhibiting PKB/Akt are being evaluated in phase I and II clinical studies. **Ipatasertib** has been combined with other antitumor drugs to treat prostate cancer and breast cancer and is undergoing an investigation in a phase III clinical trial (86).

With the exception of targets above, interleukin-6 (IL-6) showed high expression in prostate cancer (98). **Siltuximab**, a chimeric monoclonal antibody, was first launched in 2014 to treat HIV-negative and Human Herpes Virus-8 negative

multicentric Castleman's disease. Its tight binding to IL-6 inhibits IL-6 bioactivity and thus causes apoptosis of tumor cell. Recently, a phase II clinical trial of **siltuximab** was conducted for the treatment of multiple myeloma (87). Others like immunity-related programmed cell death receptor-1 (PD-1) and PD-L1 inhibitors show satisfied antitumor effects by restoring antitumor immunity. **Sintilimab** is a fully human IgG4 mAb, which blocks the interaction of PD-1 with PD-L1 and PL-L2 (88). It was firstly approved in China to treat classical Hodgkin's lymphoma. **Avelumab**, an anti-PD-L1 antibody, was approved by the FDA in 2019 for first-line treatment of advanced renal cell carcinoma together with axitinib (89).

VM RELATED TARGETS AND THERAPEUTIC AGENTS

VM refers to a tumor microcirculation pattern that tumor cells aggregate, migrate and remodel to form a vascular-like structure based on the adhesion of ECM. VM differs from traditional endothelial tumor angiogenesis and plays a crucial role in tumor invasion and spreading. It is worth noting that there is an obvious increase of EMT-related regulators and transcription factors in VM, which indicates the crucial rule of EMT in VM formation (99). VM has been observed in a broad range of tumor types such as prostate cancer, malignant glioma, and melanoma (100). Currently, certain mechanism of VM formation remains matters of frenetic investigation and the mechanism of VM formation mainly include TME, EMT, tumor plasticity, RNA, and other regulators (100). Because VM is important for tumor progression, targeted therapies related to VM could also be a promising antitumor strategy to reducing tumor plasticity.

The major signaling molecules participating in VM formation and promising drugs are summarized in **Table 5**. Histone deacetylases inhibitor (HDACi) inhibits key molecule MMP-2 in PI3K-MMPs-Ln-5γ2 signaling pathway to block VM formation (112). **Panobinostat lactate**, which is lunched in 2015, is a first-line HDAC inhibitor applied in combination with bortezomib and dexamethasone to the treatment of multiple myeloma (113). **Panobinostat lactate** is not only a HDAC inhibitor but also a pan-deacetylase inhibitor. The pharmacokinetics of **panobinostat lactate** is affected by some factors such as hepatic impairment. HDAC inhibitor **romidepsin**, which is launched in 2010, could cause cell cycle arrest, differentiation and apoptosis in various cancer cells and is used for the treatment of cutaneous T-cell lymphoma (103). **OKI-179** and **remetinostat** are HDAC inhibitors in early clinical development (101, 102).

Phosphatidylinositide 3-kinases (PI3K) participate in VM formation by activating matrix metalloproteinases (MMPs) (114). The PI3Kα/δ inhibitor **copanlisib hydrochloride** was launched in 2017 as a treatment for relapsed follicular lymphoma in patients receiving two or more prior therapy regimens (110). **Copanlisib** characterizes low risk of PK-related pharmacological interaction due to reduced oxidation metabolism and unchanged excretion of copanlisib. Other PI3K inhibitors in clinical trials include **MEN-1611** (phase I for breast cancer), **HMPL-689** (phase I for B-cell lymphoma), **Gedatolisib** (phase II for acute myeloid leukemia and solid tumors), **GDC-0980** (phase II for prostate cancer) and **Buparlisib** (phase III in patients with head and neck squamous cell carcinoma, HNSCC) (105–109).

VE-cadherin mediates the activities of epithelial cell kinase (Eck/EphA2) to affect the formation of VM (115). EphA2 interacts with cell membrane surface ligands by phosphorylation and regulates the extracellular expression of protein kinases ERK and focal adhesion kinase FAK to activate PI3K (116, 117). **SiRNA-EphA2-DOPC** is a small interfering RNA targeting EphA2 loaded in neutral 1,2-dioleoyl-sn-glycero-3-phosphocholin (DOPC) liposomes (111). **SiRNA-EphA2-DOPC** reaches to tumor site by interacting with endothelial cells of tumor vasculature. As an EphA2 inhibitor, **siRNA-EphA2-DOPC** is in early clinical investigations to treat recurrent and advanced solid tumors.

THERAPEUTIC TARGETING OF NEOPLASM METABOLIC PATHWAYS

Cancer cells reprogram metabolic pathways by oncogenic mutations, result in enhanced demand of nutrient uptake to supply anabolic metabolism. Not only must energy production and consumption processes in cancer cells be balanced to

TABLE 5 | Potential drugs targeting VM in clinical trials.

Drug	Mechanism of action	Condition or disease	Phase	References
OKI-179	HDAC inhibitors	Solid tumor	I	(101)
Remetinostat	HDAC inhibitors	Cutaneous T-cell lymphoma	II	(102)
Romidepsin	HDAC inhibitors	Cutaneous T-cell lymphoma, peripheral T-cell lymphoma	Launched in 2010	(103)
Panobinostat lactate	HDAC inhibitors	Multiple myeloma	Launched in 2015	(104)
MEN-1611	PI3K inhibitors	Breast cancer	I	(105)
HMPL-689	PI3Kδ inhibitors	B-cell lymphoma	I	(106)
Gedatolisib	PI3K/mTOR inhibitors	Acute myeloid leukemia, solid tumors	II	(107)
GDC-0980	PI3K/mTOR inhibitors	Prostate cancer	II	(108)
Buparlisib	PI3K inhibitors	HNSCC	III	(109)
Copanlisib hydrochloride	PI3K inhibitors	Lymphoma	Launched in 2017	(110)
siRNA-EphA2-DOPC	EphA2 inhibitors	Solid tumors	I	(111)

TABLE 6 | Potential drugs targeting neoplasm metabolic pathways in clinical trials.

Drug	Mechanism of action	Condition or disease	Phase	References
Dimethylamino-micheliolide	PKM2 activators	Solid tumors	I	(121)
Acadesine	AMPK activators	Multiple myeloma therapy	I/II	(122)

sustain tumor growth, but also cancer cells have to adapt to the changes in nutrition and oxygen supply caused by their rapid growth. Hence, malignant cells exhibit metabolic flexibility for them to exist and develop. Different from normal cells, cancer cells are more dependent on anaerobic glycolysis even in a sufficient oxygen supply environment, called Warburg effect (118). HIF-1α is crucial for anaerobic glycolysis under oxygen free conditions. Tumor suppressor liver kinase B1 (LKB1) regulates HIF-1α-dependent metabolic reprogramming (119). Recent studies have shown that Pyruvate kinase M2 (PKM2) plays a crucial part in the plasticity of cancer metabolism, and up regulation of PKM2 leads to oxidative metabolism (120). **Dimethylaminomicheliolide** (DMAMCL), a PKM2 activator, is a prodrug of micheliolide (MCL) that suppresses tumor growth and targets CSCs in the form of guaianolide sesquiterpene lactone. **Dimethylaminomicheliolide** could inhibit inflammation and tumor growth by releasing MCL into plasma. Early clinical trial using **Dimethylaminomicheliolide** for patients with solid tumors is being conducted (**Table 6**) (121).

In addition to this, oxidative phosphorylation plays an important role in cancer metabolism. Oxidative phosphorylation is mainly regulated by AMP-activated protein kinase (AMPK) (123). As an AMPK activator, **acadesine** increases the availability of adenosine in tissues under ischemic conditions and shows antitumor activity. **Acadesine** causes B cells apoptosis selectively in chronic lymphocytic leukemia (CLL) and phase I/II studies are being tested for sieving out the best methods for the treatment of resistant/refractory B-cell chronic lymphocytic leukemia (122). Metabolic plasticity of cancer triggers the adaptive "metabolic switch" needed for cancer development. Mechanism of metabolic switch provides insights into therapies, which could be used to target cancer development.

CONCLUSIONS

Tumor plasticity provides new explanation for the mechanisms of drug resistance, metastasis and recurrence of neoplasm. Interfering tumor plasticity is becoming strategies to treat malignant tumors. The drugs in clinical trials that targeting tumor plasticity are still on intense research. However, targeted therapy also has some limitations that most drugs could only be effective on a small part of tumors of genetic transformation and engender drug resistance after a period of time of taking drugs. How to find effective multi-targeted inhibitors or combine with traditional chemotherapeutic drugs and other therapeutics like photodynamic or photothermal therapy become particularly important. The quest for new therapeutic targets toward tumor plasticity continues to be a great impetus to promote cancer treatment.

AUTHOR CONTRIBUTIONS

DW, X-GY, and L-CZ wrote the draft. Y-JW and Y-YL edited the manuscript. All authors read and approved the final version of manuscript.

REFERENCES

1. Meacham CE, Morrison SJ. Tumour heterogeneity and cancer cell plasticity. *Nature*. (2013) 501:328–37. doi: 10.1038/nature12624
2. Al-Hajj M, Wicha MS, Benito-Hernandez A, Morrison SJ, Clarke MF. Prospective identification of tumorigenic breast cancer cells. *Proc Natl Acad Sci USA*. (2003) 100:3983–88. doi: 10.1073/pnas.0530291100
3. O'Brien CA, Pollett A, Gallinger S, Dick JE. A human colon cancer cell capable of initiating tumour growth in immunodeficient mice. *Nature*. (2007) 445:106–10. doi: 10.1038/nature05372
4. Dalerba P, Dylla SJ, Park I-K, Liu R, Wang X, Cho RW, et al. Phenotypic characterization of human colorectal cancer stem cells. *Proc Natl Acad Sci USA*. (2007) 104:10158–63. doi: 10.1073/pnas.0703478104
5. Fang D, Nguyen TK, Leishear K, Finko R, Kulp AN, Hotz S, et al. A tumorigenic subpopulation with stem cell properties in melanomas. *Cancer Res*. (2005) 65:9328–37. doi: 10.1158/0008-5472.CAN-05-1343
6. Ricci-Vitiani L, Lombardi DG, Pilozzi E, Biffoni M, Todaro M, Peschle C, et al. Identification and expansion of human colon-cancer-initiating cells. *Nature*. (2007) 445:111–15. doi: 10.1038/nature05384
7. Batlle E, Clevers H. Cancer stem cells revisited. *Nat Med*. (2017) 23:1124–34. doi: 10.1038/nm.4409
8. Bariwal J, Kumar V, Dong Y, Mahato RI. Design of Hedgehog pathway inhibitors for cancer treatment. *Med Res Rev*. (2019) 39:1137–204. doi: 10.1002/med.21555
9. Zeng X, Ju D. Hedgehog signaling pathway and autophagy in cancer. *Int J Mol Sci*. (2018) 19:2279. doi: 10.3390/ijms19082279
10. Liu J, Pan S, Hsieh MH, Ng N, Sun F, Wang T, et al. Targeting Wnt-driven cancer through the inhibition of Porcupine by LGK974. *Proc Natl Acad Sci USA*. (2013) 110:20224–29. doi: 10.1073/pnas.1314239110
11. *A Study to Evaluate the Safety and Tolerability of ETC-1922159 in Advanced Solid Tumors* (NCT02521844) (2015). Available online at: http://clinicaltrials.gov/show/NCT02521844
12. Madan B, Ke Z, Harmston N, Ho SY, Frois AO, Alam J, et al. Wnt addiction of genetically defined cancers reversed by PORCN inhibition. *Oncogene*. (2016) 35:2197–207. doi: 10.1038/onc.2015.280
13. *Phase I, Dose-Escalation Study of CGX-1321 in Subjects With Advanced Gastrointestinal Tumors* (NCT03507998) (2018). Available online at: http://clinicaltrials.gov/show/NCT03507998
14. *Study to Evaluate the Safety and Tolerability of RXC-004 in Advanced Malignancies* (NCT03447470) (2018). Available online at: https://clinicaltrials.gov/show/NCT03447470
15. Savvidou I, Khong T, Cuddihy A, McLean C, Horrigan S, Spencer A. beta-Catenin inhibitor BC2059 is efficacious as monotherapy or in combination with proteasome inhibitor bortezomib in multiple myeloma. *Mol Cancer Ther*. (2017) 16:1765–78. doi: 10.1158/1535-7163.MCT-16-0624
16. *A Study of E-7386 in Participants With Advanced Solid Tumor Including Colorectal Cancer (CRC)* (NCT03833700) (2019). Available online at: https://clinicaltrials.gov/show/NCT03833700
17. Morgan KM, Fischer BS, Lee FY, Shah JJ, Bertino JR, Rosenfeld J, et al. Gamma secretase inhibition by BMS-906024 enhances efficacy of paclitaxel in lung adenocarcinoma. *Mol Cancer Ther*. (2017) 16:2759–69. doi: 10.1158/1535-7163.MCT-17-0439
18. Dlugosz A, Agrawal S, Kirkpatrick P. Vismodegib. *Nat Rev Drug Discov*. (2012) 11:437–38. doi: 10.1038/nrd3753
19. Burness CB. Sonidegib: first global approval. *Drugs*. (2015) 75:1559–66. doi: 10.1007/s40265-015-0458-y
20. Campbell VT, Nadesan P, Ali SA, Wang CY, Whetstone H, Poon R, et al. Hedgehog pathway inhibition in chondrosarcoma using the smoothened inhibitor IPI-926 directly inhibits sarcoma cell growth. *Mol Cancer Ther*. (2014) 13:1259–69. doi: 10.1158/1535-7163.MCT-13-0731

21. Sasaki K, Gotlib JR, Mesa RA, Newberry KJ, Ravandi F, Cortes JE, et al. Phase II evaluation of IPI-926, an oral Hedgehog inhibitor, in patients with myelofibrosis. *Leuk Lymphoma*. (2015) 56:2092–97. doi: 10.3109/10428194.2014.984703
22. Jin G, Sivaraman A, Lee K. Development of taladegib as a sonic hedgehog signaling pathway inhibitor. *Arch Pharmacal Res*. (2017) 40:1390–93. doi: 10.1007/s12272-017-0987-x
23. Ueno H, Kondo S, Yoshikawa S, Inoue K, Andre V, Tajimi M, et al. A phase I and pharmacokinetic study of taladegib, a Smoothened inhibitor, in Japanese patients with advanced solid tumors. *Invest New Drugs*. (2018) 36:647–56. doi: 10.1007/s10637-017-0544-y
24. Harb J, Lin PJ, Hao J. Recent development of wnt signaling pathway inhibitors for cancer therapeutics. *Curr Oncol Rep*. (2019) 21:12. doi: 10.1007/s11912-019-0763-9
25. Janku F, Connolly R, LoRusso P, de Jonge M, Vaishampayan U, Rodon J, et al. Abstract C45: phase I study of WNT974, a first-in-class Porcupine inhibitor, in advanced solid tumors. *Mol Cancer Ther*. (2015) 14. doi: 10.1158/1535-7163.TARG-15-C45
26. Xin M, Ji X, De La Cruz LK, Thareja S, Wang B. Strategies to target the Hedgehog signaling pathway for cancer therapy. *Med Res Rev*. (2018) 38:870–913. doi: 10.1002/med.21482
27. Salati M, Stathis A. Sonidegib Phosphate Smoothened (SMO) receptor antagonist. *Drugs Future*. (2014) 39:677–84. doi: 10.1358/dof.2014.039.010.2207247
28. Dianat-Moghadam H, Heydarifard M, Jahanban-Esfahlan R. Cancer stem cells-emanated therapy resistance: implications for liposomal drug delivery systems. *J Control Release*. (2018) 288:62–83. doi: 10.1016/j.jconrel.2018.08.043
29. Miraglia S, Godfrey W, Yin AH, Atkins K, Warnke R, Holden JT, et al. A novel five-transmembrane hematopoietic stem cell antigen: isolation, characterization, and molecular cloning. *Blood*. (1997) 90:5013–21.
30. Ginestier C, Hur MH, Charafe-Jauffret E, Monville F, Dutcher J, Brown M, et al. ALDH1 is a marker of normal and malignant human mammary stem cells and a predictor of poor clinical outcome. *Cell Stem Cell*. (2007) 1:555–67. doi: 10.1016/j.stem.2007.08.014
31. Ding X, Wu J, Jiang C. ABCG2: a potential marker of stem cells and novel target in stern cell and cancer therapy. *Life Sci*. (2010) 86:631–37. doi: 10.1016/j.lfs.2010.02.012
32. Kim MY, Cho WD, Hong KP, Choi da B, Hong JW, Kim S, et al. Novel monoclonal antibody against beta 1 integrin enhances cisplatin efficacy in human lung adenocarcinoma cells. *J Biomed Res*. (2016) 30:217–24. doi: 10.7555/JBR.30.2016K0005
33. McClements L, Annett S, Yakkundi A, O'Rourke M, Valentine A, Moustafa N, et al. FKBPL and its peptide derivatives inhibit endocrine therapy resistant cancer stem cells and breast cancer metastasis by downregulating DLL4 and Notch4. *BMC Cancer*. (2019) 19:351. doi: 10.1186/s12885-019-5500-0
34. *Open-Label, Multicenter, Dose-Escalation Phase Ia/b Study of RO-5429083, Administered as Intravenous Infusion Alone or in Combination With Cytarabine in Patients With Acute Myelogenous Leukemia (AML)* (NCT01641250) (2012). Available online at: https://clinicaltrials.gov/show/NCT01641250
35. Vey N, Delaunay J, Martinelli G, Fiedler W, Raffoux E, Prebet T, et al. Phase I clinical study of RG7356, an anti-CD44 humanized antibody, in patients with acute myeloid leukemia. *Oncotarget*. (2016) 7:32532–42. doi: 10.18632/oncotarget.8687
36. *A Safety and Pharmacokinetic Phase I/Ib Study of AMC-303 in Patients With Solid Tumors* (NCT03009214) (2017). Available online at: https://clinicaltrials.gov/show/NCT03009214
37. *A Trial to Find Safe and Active Doses of an Investigational Drug CX-2009 for Patients With Selected Solid Tumors* (NCT03149549) (2017). Available online at: https://clinicaltrials.gov/show/NCT03149549
38. Salimi A, Roudkenar MH, Seydi E, Sadeghi L, Mohseni A, Pirahmadi N, et al. Chrysin as an anti-cancer agent exerts selective toxicity by directly inhibiting mitochondrial complex II and v in CLL b-lymphocytes. *Cancer Invest*. (2017) 35:174–86. doi: 10.1080/07357907.2016.1276187
39. El-Helali A, Plummer R, Jayson G, Coyle V, Drew Y, Mescallado N, et al. 383PA phase I dose-escalation study of the novel peptide ALM201 in patients (pts) with advanced solid tumours. *Ann Oncol*. (2017) 28:128. doi: 10.1093/annonc/mdx367.017
40. Calvo E, Aftimos P, Azaro A, de Miguel M, Jungels C, Zeron-Medina Cuairan J, et al. 410O First-in-human, first-in-class study of the CD44v6 inhibitor AMC303 as monotherapy in patients with advanced epithelial tumors. *Ann Oncol*. (2018) 29:viii134. doi: 10.1093/annonc/mdy279.398
41. Wei C-T, Chen L-C, Hsiang Y-P, Hung Y-J, Chien P-H, Pan H-L, et al. Chrysin-induced ERK1/2 phosphorylation enhances the sensitivity of human hepatocellular carcinoma cells to sorafenib. *Anticancer Res*. (2019) 39:695–701. doi: 10.21873/anticanres.13165
42. Marcucci F, Stassi G, De Maria R. Epithelial-mesenchymal transition: a new target in anticancer drug discovery. *Nat Rev Drug Discov*. (2016) 15:311–25. doi: 10.1038/nrd.2015.13
43. Ye X, Weinberg RA. Epithelial-mesenchymal plasticity: a central regulator of cancer progression. *Trends Cell Biol*. (2015) 25:675–86. doi: 10.1016/j.tcb.2015.07.012
44. Vanneste M, Henry MD. Targeting phenotypic plasticity in prostate cancer. *Curr Mol Biol Rep*. (2017) 3:183–96. doi: 10.1007/s40610-017-0070-x
45. By:Drooger J, van der Padt A, Sleijfer S, Jager A. Denosumab in breast cancer treatment. *Eur J Pharmacol*. (2013) 717:12–9. doi: 10.1016/j.ejphar.2013.03.034
46. *Assessment of TK006 in Patients With Breast Cancer-Related Bone Metastases* (NCT03239756) (2017). Available online at: https://clinicaltrials.gov/show/NCT03239756
47. Geng L, Li X, Zhou X, Fang X, Yuan D, Wang X. WP1066 exhibits antitumor efficacy in nasal-type natural killer/T-cell lymphoma cells through downregulation of the STAT3 signaling pathway. *Oncol Rep*. (2016) 36:2868–74. doi: 10.3892/or.2016.5091
48. Tsurumaki H, Katano H, Sato K, Imai R, Niino S, Hirabayashi Y, et al. WP1066, a small molecule inhibitor of the JAK/STAT3 pathway, inhibits ceramide glucosyltransferase activity. *Biochem Biophys Res Commun*. (2017) 491:265–70. doi: 10.1016/j.bbrc.2017.07.115
49. *A Study of DSP-0337 in Patients With Advanced Solid Tumors to Determine the Safety and the Pharmacokinetic Profile* (NCT03416816) (2018). Available online at: https://clinicaltrials.gov/show/NCT03416816
50. *Neoadjuvant Durvalumab Alone or in Combination With Novel Agents in Resectable Non-small Cell Lung Cancer* (NCT03794544) (2019). Available online at: https://clinicaltrials.gov/show/NCT03794544
51. Reilley MJ, McCoon P, Cook C, Lyne P, Kurzrock R, Kim Y, et al. STAT3 antisense oligonucleotide AZD9150 in a subset of patients with heavily pretreated lymphoma: results of a phase 1b trial. *J Immunother Cancer*. (2018) 6:119. doi: 10.1186/s40425-018-0436-5
52. Tolcher A, Flaherty K, Shapiro GI, Berlin J, Witzig T, Habermann T, et al. A first-in-human phase i study of OPB-111077, a small-molecule STAT3 and oxidative phosphorylation inhibitor, in patients with advanced cancers. *Oncologist*. (2018) 23:658–e72. doi: 10.1634/theoncologist.2017-0325
53. Loecken H, Clamor C, Mueller K. Napabucasin and related heterocycle-fused naphthoquinones as STAT3 inhibitors with antiproliferative activity against cancer cells. *J Nat Prod*. (2018) 81:1636–44. doi: 10.1021/acs.jnatprod.8b00247
54. *A Study of Napabucasin (GB-201) in Combination With Paclitaxel and Low-Dose Gemcitabine in Patients With Pancreatic Cancer* (NCT03721744) (2018). Available online at: https://clinicaltrials.gov/show/NCT03721744
55. Doherty GJ, Tempero M, Corrie PG. HALO-109–301: a Phase III trial of PEGPH20 (with gemcitabine and nab-paclitaxel) in hyaluronic acid-high stage IV pancreatic cancer. *Future Oncol*. (2018) 14:13–22. doi: 10.2217/fon-2017-0338
56. Wong KM, Horton KJ, Coveler AL, Hingorani SR, Harris WP. Targeting the tumor stroma: the biology and clinical development of pegylated recombinant human hyaluronidase (PEGPH20). *Curr Onco Rep*. (2017) 19:47. doi: 10.1007/s11912-017-0608-3
57. *Combining CRLX-101, A Nanoparticle Camptothecin, With Enzalutamide in People With Progressive Metastatic Castration Resistant Prostate Cancer Following Prior Enzalutamide Treatment* (NCT03531827) (2018). Available online at: https://clinicaltrials.gov/show/NCT03531827
58. Tian X, Nguyen M, Foote HP, Caster JM, Roche KC, Peters CG, et al. CRLX101, a nanoparticle–drug conjugate containing camptothecin,

improves rectal cancer chemoradiotherapy by inhibiting DNA repair and HIF1α. *Cancer Res*. (2017) 77:112–22. doi: 10.1158/0008-5472.CAN-15-2951
59. Erstad DJ, Cusack JC. Targeting the NF-κB path way in cancer therapy. *Surg Oncol Clin N Am*. (2013) 22:705–46. doi: 10.1016/j.soc.2013.06.011
60. Sikka S, Surana R, Dai X, Zhang J, Kumar AP, Tan BKH, et al. Targeting the STAT3 signaling pathway in cancer: Role of synthetic and natural inhibitors (review). *Biochim Biophys Acta*. (2014) 1845:136–54. doi: 10.1016/j.bbcan.2013.12.005
61. Wong CC-L, Zhang H, Gilkes DM, Chen J, Wei H, Chaturvedi P, et al. Inhibitors of hypoxia-inducible factor 1 block breast cancer metastatic niche formation and lung metastasis(Article). *J Mol Med*. (2012) 90:803–15. doi: 10.1007/s00109-011-0855-y
62. Onder TT, Gupta PB, Mani SA, Yang J, Lander ES, Weinberg RA. Loss of E-cadherin promotes metastasis via multiple downstream transcriptional pathways. *Cancer Res*. (2008) 68:3645–54. doi: 10.1158/0008-5472.CAN-07-2938
63. McCullough KD, Coleman WB. Plasticity of the neoplastic phenotype *in vivo* is regulated by epigenetic factors. *Proc Natl Acad Sci USA*. (1998) 95:15333–33. doi: 10.1073/pnas.95.26.15333
64. Bhat R, Bissell MJ. Of plasticity and specificity: dialectics of the microenvironment and macroenvironment and the organ phenotype. *Wires Dev Biol*. (2014) 3:147–63. doi: 10.1002/wdev.130
65. Chu T, Yang J, Huang T, Liu H. Crosstalk with cancer-associated fibroblasts increases the growth and radiation survival of cervical cancer cells. *Radiat Res*. (2014) 181:540–47. doi: 10.1667/RR13583.1
66. Ziebart T, Ziebart J, Gauss L, Pabst A, Ackermann M, Smeets R, et al. Investigation of inhibitory effects on EPC-mediated neovascularization by different bisphosphonates for cancer therapy. *Biomed Rep*. (2013) 1:719–22. doi: 10.3892/br.2013.145
67. Yang T, Zhang X, Wang M, Zhang J, Huang F, Cai J, et al. Activation of mesenchymal stem cells by macrophages prompts human gastric cancer growth through NF-κB pathway. *PLoS ONE*. (2014) 9:e97569. doi: 10.1371/journal.pone.0097569
68. Rasco DW, Papadopoulos KP, Pourdehnad M, Gandhi AK, Hagner P, Li Y, et al. A first-in-human study of novel cereblon modulator avadomide (CC-122) in advanced malignancies. *Clin Cancer Res*. (2018) 25:90–8. doi: 10.1158/1078-0432.CCR-18-1203
69. *Phase I/Ib Study of NIS-793 in Combination With PDR-001 in Patients With Advanced Malignancies* (NCT02947165) (2016). Available online at: https://clinicaltrials.gov/show/NCT02947165
70. *A Trial of AVID-200, A Transforming Growth Factor Beta (TGFbeta) Inhibitor, in Patients Malignancies* (NCT03834662) (2019). Available online at: https://clinicaltrials.gov/show/NCT03834662
71. *A First-in-Human Study of the Safety, Pharmacokinetics, Pharmacodynamics and Anti-tumor Activity of SAR-439459 Monotherapy and Combination of SAR-439459 and REGN-2810 in Patients With Advanced Solid Tumors* (NCT03192345) (2017). Available online at: https://clinicaltrials.gov/show/NCT03192345
72. Lacouture ME, Morris JC, Lawrence DP, Tan AR, Olencki TE, Shapiro GI, et al. Cutaneous keratoacanthomas/squamous cell carcinomas associated with neutralization of transforming growth factor beta by the monoclonal antibody fresolimumab (GC1008). *Cancer Immunol Immunother*. (2015) 64:437–46. doi: 10.1007/s00262-015-1653-0
73. He L, Li S, Xie F, Cheng Z, Ran L, Liu X, et al. LC-ESI-MS/MS determination of simotinib, a novel epidermal growth factor receptor tyrosine kinase inhibitor: application to a pharmacokinetic study. *J Chromatogr B Anal Technol Biomed Life Sci*. (2014) 947–8:168–72. doi: 10.1016/j.jchromb.2013.12.021
74. *A Study of BBI-503 in Combination With Selected Anti-cancer Therapeutics in Adult Patients With Advanced Cancer* (NCT02483247) (2015). Available online at: https://clinicaltrials.gov/show/NCT02483247
75. Deshpande HA, Cecchini M, Ni Choileain S, Jones R. Olaratumab for the treatment of soft tissue sarcoma. *Drugs Today*. (2017) 53:247–55. doi: 10.1358/dot.2017.53.4.2560077
76. Coffey GP, Feng J, Betz A, Pandey A, Birrell M, Leeds JM, et al. Cerdulatinib pharmacodynamics and relationships to tumor response following oral dosing in patients with Relapsed/Refractory b-cell malignancies. *Clin Cancer Res*. (2019) 25:1174–84. doi: 10.1158/1078-0432.CCR-18-1047
77. Phyu SM, Smith TAD. Combination treatment of cancer cells with pan-Akt and pan-mTOR inhibitors: effects on cell cycle distribution, p-Akt expression level and radiolabelled-choline incorporation. *Invest New Drugs*. (2019) 37:424–30. doi: 10.1007/s10637-018-0642-5
78. *BI-860585 Dose Escalation Single Agent and in Combination With Exemestane or With Paclitaxel in Patients With Various Advanced and/or Metastatic Solid Tumors* (NCT01938846) (2013). Available online at: https://clinicaltrials.gov/show/NCT01938846
79. *Safety, Tolerability and Pharmacokinetics of DCBCI-0901 in Patients With Advanced Solid Tumor* (NCT02151357) (2014). Available online at: https://clinicaltrials.gov/show/NCT02151357
80. *A Study of LXI-15029 in Patients With Advanced Malignant Solid Tumors* (NCT03125746) (2017). Available online at: https://clinicaltrials.gov/show/NCT03125746
81. Gonzalez-Angulo AM, Meric-Bernstam F, Chawla S, Falchook G, Hong D, Akcakanat A, et al. Weekly nab-rapamycin in patients with advanced nonhematologic malignancies: final results of a phase I trial. *Clin Cancer Res*. (2013) 19:5474–84. doi: 10.1158/1078-0432.CCR-12-3110
82. Graham L, Banda K, Torres A, Carver BS, Chen Y, Pisano K, et al. A phase II study of the dual mTOR inhibitor MLN0128 in patients with metastatic castration resistant prostate cancer. *Invest New Drugs*. (2018) 36:458–67. doi: 10.1007/s10637-018-0578-9
83. Pandey V, Wang BC, Mohan CD, Raquib AR, Rangappa S, Srinivasa V, et al. Discovery of a small-molecule inhibitor of specific serine residue BAD phosphorylation. *Proc Natl Acad Sci USA*. (2018) 115:E10505–14. doi: 10.1073/pnas.1804897115
84. Yu Y, Savage RE, Eathiraj S, Meade J, Wick MJ, Hall T, et al. Targeting AKT1-E17K and the PI3K/AKT pathway with an allosteric AKT inhibitor, ARQ 092. *PLoS ONE*. (2015) 10:e0140479. doi: 10.1371/journal.pone.0140479
85. Mimura N, Hideshima T, Shimomura T, Suzuki R, Ohguchi H, Rizq O, et al. Selective and potent akt inhibition triggers anti-myeloma activities and enhances fatal endoplasmic reticulum stress induced by proteasome inhibition. *Cancer Res*. (2014) 74:4458–69. doi: 10.1158/0008-5472.CAN-13-3652
86. de Bono J, Bracarda S, Chi K, Massard C, Hidalgo D, Sandhu S, et al. Randomized phase III trial of ipatasertib vs. placebo, plus abiraterone and prednisone/prednisolone, in men with asymptomatic or mildly symptomatic previously untreated metastatic castrate-resistant prostate cancer (mCRPC). *Ann Oncol*. (2017) 28:290. doi: 10.1093/annonc/mdx370.051
87. San-Miguel J, Blade J, Shpilberg O, Grosicki S, Maloisel F, Min CK, et al. Phase 2 randomized study of bortezomib-melphalan-prednisone with or without siltuximab (anti-IL-6) in multiple myeloma. *Blood*. (2014) 123:4136–42. doi: 10.1182/blood-2013-12-546374
88. Hoy SM. Sintilimab: first global approval. *Drugs*. (2019) 79:341–46. doi: 10.1007/s40265-019-1066-z
89. Motzer RJ, Penkov K, Haanen J, Rini B, Albiges L, Campbell MT, et al. Avelumab plus Axitinib versus Sunitinib for advanced renal-cell carcinoma. *N Engl J Med*. (2019) 380:1103–15. doi: 10.1056/NEJMoa1816047
90. Arnott CH, Scott KA, Moore RJ, Hewer A, Phillips DH, Parker P, et al. Tumour necrosis factor-alpha mediates tumour promotion via a PKCalpha- and AP-1-dependent pathway. *Oncogene*. (2002) 21:4728–38. doi: 10.1038/sj.onc.1205588
91. Leight JL, Wozniak MA, Chen S, Lynch ML, Chen CS, Wang Y-L. Matrix rigidity regulates a switch between TGF-β1-induced apoptosis and epithelial–mesenchymal transition. *Mol Biol Cell*. (2012) 23:781–91. doi: 10.1091/mbc.e11-06-0537
92. Morris JC, Tan AR, Olencki TE, Shapiro GI, Dezube BJ, Reiss M, et al. Phase I study of GC1008 (fresolimumab): a human anti-transforming growth factor-beta (TGFbeta) monoclonal antibody in patients with advanced malignant melanoma or renal cell carcinoma. *PLoS ONE*. (2014) 9:e90353. doi: 10.1371/journal.pone.0090353
93. Grasset EM, Bertero T, Bozec A. Matrix stiffening and EGFR cooperate to promote the collective invasion of cancer cells. *Cancer Res*. (2018) 78:5229–42. doi: 10.1158/0008-5472.CAN-18-0601

94. Saplacan RMM, Balacescu L, Gherman C, Chira RI, Craiu A, Mircea PA, et al. The role of PDGFs and PDGFRs in colorectal cancer. *Mediat Inflamm*. (2017) 2017:1–9. doi: 10.1155/2017/4708076
95. Albrengues J, Bourget I, Pons C, Butet V, Hofman P, Tartare-Deckert S, et al. LIF mediates proinvasive activation of stromal fibroblasts in cancer. *Cell Rep*. (2014) 7:1664–78. doi: 10.1016/j.celrep.2014.04.036
96. Gao Y, Xiao Q, Ma HM, Li L, Liu J, Feng Y, et al. LKB1 inhibits lung cancer progression through lysyl oxidase and extracellular matrix remodeling. *Proc Natl Acad Sci USA*. (2010) 107:18892–97. doi: 10.1073/pnas.1004952107
97. Chen Q, Zhang X-F, Massagué J. Macrophage binding to receptor VCAM-1 transmits survival signals in breast cancer cells that invade the lungs. *Cancer Cell*. (2011) 20:538–49. doi: 10.1016/j.ccr.2011.08.025
98. Yu SH, Maynard JP, Vaghasia AM, Marzo AMD, Drake CG, Sfanos KS. A role for paracrine interleukin-6 signaling in the tumor microenvironment in prostate tumor growth. *Prostate*. (2019) 79:215–22. doi: 10.1002/pros.23726
99. Liu Q, Qiao L, Liang N, Xie J, Zhang J, Deng G, et al. The relationship between vasculogenic mimicry and epithelial-mesenchymal transitions. *J Cell Mol Med*. (2016) 20:1761–69. doi: 10.1111/jcmm.12851
100. Qiao L, Liang N, Zhang J, Xie J, Liu F, Xu D, et al. Advanced research on vasculogenic mimicry in cancer. *J Cell Mol Med*. (2015) 19:315–26. doi: 10.1111/jcmm.12496
101. *A Study of OKI-179 in Patients With Solid Tumors* (NCT03931681) (2019). Available online at: https://clinicaltrials.gov/show/NCT03931681
102. *Efficacy, Safety and Tolerability Study of SHAPE in IA, IB or IIA Cutaneous T-Cell Lymphoma* (NCT02213861) (2014). Available online at: https://clinicaltrials.gov/show/NCT02213861
103. O'Connor OA, Oezcan M, Jacobsen ED, Roncero JM, Trotman J, Demeter J, et al. Randomized phase III study of alisertib or investigator's choice (selected single agent) in patients with relapsed or refractory peripheral t-cell lymphoma. *J Clin Oncol*. (2019) 37:613–23. doi: 10.1200/JCO.18.00899
104. Surati M, Valla K, Shah KS, Panjic EH, Lonial S. Panobinostat for the treatment of multiple myeloma. *Expert Opin Orphan D*. (2015) 229–38. doi: 10.1517/21678707.2015.999665
105. Blagden S, Olmin A, Josephs D, Stavraka C, Zivi A, Pinato DJ, et al. First-in-human study of CH5132799, an oral class I PI3K inhibitor, studying toxicity, pharmacokinetics, and pharmacodynamics, in patients with metastatic cancer. *Clin Cancer Res*. (2015) 21:660–60. doi: 10.1158/1078-0432.CCR-14-3188
106. *Trial to Evaluate the Safety and Pharmacokinetics of HMPL-689 in Patients With Lymphomas* (NCT03786926) (2018). Available online at: https://clinicaltrials.gov/show/NCT03786926
107. Gazi M, Moharram SA, Marhaell A, Kazi JU. The dual specificity PI3K/mTOR inhibitor PKI-587 displays efficacy against T-cell acute lymphoblastic leukemia (T-ALL). *Cancer Lett*. (2017) 392:9–16. doi: 10.1016/j.canlet.2017.01.035
108. Makker V, Recio FO, Ma L, Matulonis UA, Lauchle JO, Parmar H, et al. A multicenter, single-arm, open-label, phase 2 study of apitolisib (GDC-0980) for the treatment of recurrent or persistent endometrial carcinoma (MAGGIE study). *Cancer*. (2016) 122:3519–28. doi: 10.1002/cncr.30286
109. de Gooijer MC, Zhang P, Buil LCM, Citirikkaya CH, Thota N, Beijnen JH, et al. Buparlisib is a brain penetrable pan-PI3K inhibitor. *Sci Rep*. (2018) 8:10784–92. doi: 10.1038/s41598-018-29062-w
110. Markham A. Copanlisib: first global approval. *Drugs*. (2017) 77:2057–62. doi: 10.1007/s40265-017-0838-6
111. Shen H, Rodriguez-Aguayo C, Xu R, Gonzalez-Villasana V, Mai J, Huang Y, et al. Enhancing chemotherapy response with sustained EphA2 silencing using multistage vector delivery. *Clin Cancer Res*. (2013) 19:1806–15. doi: 10.1158/1078-0432.CCR-12-2764
112. Liu X, Wang JH, Li S, Li LL, Huang M, Zhang YH, et al. Histone deacetylase 3 expression correlates with vasculogenic mimicry through the phosphoinositide3-kinase/ERK-MMP-laminin5gamma2 signaling pathway. *Cancer Sci*. (2015) 106:857–66. doi: 10.1111/cas.12684
113. Van Veggel M, Westerman E, Hamberg P. Clinical pharmacokinetics and pharmacodynamics of panobinostat. *Clin Pharmacokinet*. (2018) 57:21–9. doi: 10.1007/s40262-017-0565-x
114. Hess AR, Seftor EA, Seftor REB, Hendrix MJC. Phosphoinositide 3-kinase regulates membrane Type 1-matrix metalloproteinase (MMP) and MMP-2 activity during melanoma cell vasculogenic mimicry. *Cancer Res*. (2003) 63:4757–62. Available online at: https://cancerres.aacrjournals.org/content/63/16/4757
115. Hess AR, Seftor EA, Gardner LMG, Carles-Kinch K, Schneider GB, Seftor REB, et al. Molecular regulation of tumor cell vasculogenic mimicry by tyrosine phosphorylation: role of epithelial cell kinase (Eck/EphA2). *Cancer Res*. (2001) 61:3250–55. Available online at: https://cancerres.aacrjournals.org/content/61/8/3250
116. Hess AR, Hendrix MJ. Focal adhesion kinase signaling and the aggressive melanoma phenotype. *Cell Cycle*. (2006) 478–80. doi: 10.4161/cc.5.5.2518
117. Li Y, Wu Z, Yuan J, Sun L, Lin L, Huang N, et al. Long non-coding RNA MALAT1 promotes gastric cancer tumorigenicity and metastasis by regulating vasculogenic mimicry and angiogenesis. *Cancer Lett*. (2017) 31–44. doi: 10.1016/j.canlet.2017.02.035
118. Warburg O. On the origin of cancer cells. *Science*. (1956) 123:309–14. doi: 10.1126/science.123.3191.309
119. Faubert B, Vincent EE, Griss T, Samborska B, Izreig S, Svensson RU, et al. Loss of the tumor suppressor LKB1 promotes metabolic reprogramming of cancer cells via HIF-1α. *Proc Natl Acad Sci USA*. (2014) 111:2554–59. doi: 10.1073/pnas.1312570111
120. Wong N, De Melo J, Tang D. PKM2, a central point of regulation in cancer metabolism. *Int J Cell Biol*. (2013) 2013:1–11. doi: 10.1155/2013/242513
121. Xu N, Hua ZY, Ba G, Zhang SM, Liu ZH, Thiele CJ, et al. The anti-tumor growth effect of a novel agent DMAMCL in rhabdomyosarcoma *in vitro* and *in vivo*. *J Exp Clin Cancer Res*. (2019) 38:118. doi: 10.1186/s13046-019-1107-1
122. Du L, Yang F, Fang H, Sun H, Chen Y, Xu Y, et al. AICAr suppresses cell proliferation by inducing NTP and dNTP pool imbalances in acute lymphoblastic leukemia cells. *FASEB J*. (2019) 33:4525–37. doi: 10.1096/fj.201801559RR
123. Yu L, Lu M, Jia D, Ma J, Ben-Jacob E, Levine H, et al. Modeling the genetic regulation of cancer metabolism: Interplay between glycolysis and oxidative phosphorylation. *Cancer Res*. (2017) 1564–74. doi: 10.1158/0008-5472.CAN-16-2074

Conflict of Interest Statement: The authors declare that the research was conducted in the absence of any commercial or financial relationships that could be construed as a potential conflict of interest.

frontiers in Oncology

ORIGINAL RESEARCH
published: 09 October 2019
doi: 10.3389/fonc.2019.01029

MicroRNA and mRNA Interaction Network Regulates the Malignant Transformation of Human Bronchial Epithelial Cells Induced by Cigarette Smoke

*Jin Wang, Xiao-fan Yu, Nan Ouyang, Shiyu Zhao, Haiping Yao, Xifei Guan, Jian Tong, Tao Chen and Jian-xiang Li**

Department of Toxicology, School of Public Health, Medical College of Soochow University, Suzhou, China

This study analyzes the correlation and interaction of miRNAs and mRNAs and their biological function in the malignant transformation of BEAS-2B cells induced by cigarette smoke (CS). Normal human bronchial epithelial cells (BEAS-2B) were continuously exposed to CS for 30 passages (S30) to establish an *in vitro* cell model of malignant transformation. The transformed cells were validated by scratch wound healing assay, transwell migration assay, colony formation and tumorigenicity assay. The miRNA and mRNA sequencing analysis were performed to identify differentially expressed miRNAs (DEMs) and differentially expressed genes (DEGs) between normal BEAS-2B and S30 cells. The miRNA-seq data of lung cancer with corresponding clinical data obtained from TCGA was used to further identify lung cancer-related DEMs and their correlations with smoking history. The target genes of these DEMs were predicted using the miRDB database, and their functions were analyzed using the online tool "Metascape." It was found that the migration ability, colony formation rate and tumorigenicity of S30 cells enhanced. A total of 42 miRNAs and 753 mRNAs were dysregulated in S30 cells. The change of expression of top five DEGs and DEMs were consistent with our sequencing results. Among these DEMs, eight miRNAs were found dysregulated in lung cancer tissues based on TCGA data. In these eight miRNAs, six of them including miR-96-5p, miR-93-5p, miR-106-5p, miR-190a-5p, miR-195-5p, and miR-1-3p, were found to be associated with smoking history. Several DEGs, including *THBS1*, *FN1*, *PIK3R1*, *CSF1*, *CORO2B*, and *PREX1*, were involved in many biological processes by enrichment analysis of miRNA and mRNA interaction. We identified the negatively regulated miRNA-mRNA pairs in the CS-induced lung cancer, which were implicated in several cancer-related (especially EMT-related) biological process and KEGG pathways in the malignant transformation progress of lung cells induced by CS. Our result demonstrated the dysregulation of miRNA-mRNA profiles in cigarette smoke-induced malignant transformed cells, suggesting that these miRNAs might contribute to cigarette smoke-induced lung cancer. These genes may serve as biomarkers for predicting lung cancer pathogenesis and progression. They can also be targets of novel anticancer drug development.

Keywords: cigarette smoke, BEAS-2B, miRNA-mRNA network, lung cancer, The Cancer Genome Atlas

OPEN ACCESS

Edited by:
Dong-Hua Yang,
St. John's University, United States

Reviewed by:
Chun Wu,
Bristol Myers Squibb, United States
Yi-Chao Zheng,
Zhengzhou University, China

***Correspondence:**
Jian-xiang Li
aljxcr@suda.edu.cn

Specialty section:
This article was submitted to Molecular and Cellular Oncology, a section of the journal Frontiers in Oncology

Received: *25 July 2019*
Accepted: *23 September 2019*
Published: *09 October 2019*

Citation:
Wang J, Yu X, Ouyang N, Zhao S, Yao H, Guan X, Tong J, Chen T and Li J (2019) MicroRNA and mRNA Interaction Network Regulates the Malignant Transformation of Human Bronchial Epithelial Cells Induced by Cigarette Smoke. Front. Oncol. 9:1029. doi: 10.3389/fonc.2019.01029

INTRODUCTION

Lung cancer is one of the most common carcinomas in men and women around the world. It is the first and second leading cause of cancer-related deaths in men and women, respectively (1, 2). There were 2.09 million new lung cancer cases and 1.76 million lung cancer deaths, which accounts for about 18.4% of all cancer deaths around the world in 2018 (3). The incidence of lung cancer is closely associated with cigarette smoking (2, 4). The risk of developing lung cancer in smokers is nearly ten times higher than that in non-smokers (5, 6). However, it is still not clear how normal lung epithelial cells become cancerous change in cigarette smokers.

It is well-known that the initiation and development of lung cancer are associated with abnormal expression of oncogenes and tumor suppressor genes. Numerous evidence suggested that the change in gene expression, which affects the occurrence and progression of tumors is closely related to epigenetic modification (7). Epigenetic modification could be DNA methylation, microRNAs (miRNAs), histone modifications, and nucleosome remodeling. These modifications are independent but could interact with each other to regulate gene expression (8). Epigenetic disruptions could promote the acquisition of a cancerous phenotype and aggressive behavior in lung cancer cells as well as primary or acquired resistance to treatment (9).

MiRNAs are highly conserved non-coding RNAs and consist of 18–24 nucleotides (nt) that are involved in the post-transcriptional regulation of gene (10). An individual miRNA is able to regulate many different transcripts. It is also believed that miRNAs can regulate more than one in three coding RNAs in the genome (11). MiRNAs participate in many vital biological processes through pairing with target mRNAs and regulating their expression (12, 13). The imbalance of miRNAs is usually associated with the progression and suppression of cancer, suggesting that miRNAs may play important roles as oncogenes or tumor suppressors (14).

The rapid development of high-throughput next-generation sequencing technology made it possible to identify changes in single bases in coding sequences of specific genes during lung tumorigenesis. A meticulous and thorough analysis of these data identified various vital genes and signaling pathways related to the tumor resulting in a better understanding of the mechanism of occurrence, development, and prognosis of lung cancer. Using novel technology and bioinformatics analysis, The Cancer Genome Atlas (TCGA, http://cancergenome.nih.gov/) project has previously identified panels of genetic mutations contributed to or were associated with the cause of a variety of cancers (15). Recently, the TCGA had shown studies on lung adenocarcinoma (LUAD) and squamous cell carcinomas (LUSC) at the molecular level (16, 17).

The aim of this study is to analyze the correlation and regulating mechanism of the regulatory network of miRNAs and mRNAs during carcinogenesis. An *in vitro* cell model of malignant transformation was established by exposing normal lung epithelial cells BEAS-2B to cigarette smoke (CS). Using high-throughput sequencing analysis, we analyzed the miRNA and mRNA expression profile in BEAS-2B cells with or without CS exposure. The differential expression miRNAs (DEMs) and differentially expressed genes (DEGs) were selected, and the integrative miRNA-mRNA network was analyzed. We identified some critical genes involved in carcinogenesis. This study will provide potential target candidates for novel drug development.

METHODS

Preparation of Malignantly Transformed Cells

The CS-exposed malignant transformed cell model was established as described previously. Briefly, exponentially growing BEAS-2B cells were plated onto transwell membrane (Corning, USA) with 1×10^5 in a single well (18). CS was produced using an automatic smoking machine, and the CS was pumped into an inhalation exposure chamber. Cells were directly exposed to CS for 10 min every day at a smoke concentration of 20%. This procedure was continued until the cells reached 30 passages and named S30 cells (18).

Scratch Wound Healing Assay

The normal BEAS-2B cells and S30 cells (2×10^5) were seeded into 6 well plates and cultured at 37 °C. Cells were allowed to grow up to 100% confluence and a scratch was made in the plate using a P10 pipette. The cells were cultured in fresh serum-free DMEM medium. Images were collected at 0 and 24 h under an inverted microscope (Olympus, Germany) and quantitatively analyzed with NIH ImageJ software.

Transwell Migration Assay

The normal BEAS-2B cells and S30 cells (2×10^5) were seeded in the upper chambers (pore size, 8 μm) of the 6 well plate (Corning, USA) in 1 ml serum-free medium. The lower chambers were filled with 2 ml complete medium with 10% FBS, and the plate was incubated under standard conditions for 24 h. At the end of incubation, after removing the cells in the upper surface of the membrane with a cotton swab, cells in the lower chamber were fixed with methanol and stained with 0.5% crystal violet solution. The images were taken with an inverted microscope (Olympus, Germany) and analyzed using NIH ImageJ software.

Colony Formation Assay

1×10^3 normal BEAS-2B cells and S30 cells were plated in 0.35% agarose on top of a 0.7% agarose base supplemented with complete medium. The medium was renewed every 2–3 days. The colonies were stained with 0.5% crystal violet (Sigma, USA) for 20 min at room temperature. The colony formation rate was calculated by the following equation: colony formation rate = the number of colonies/number of seeded cells × 100%.

Tumorigenicity Assay

Five-week-old male BALB/c-nude mice of SPF grade were purchased from Beijing Vital River Laboratory Animal Technology Company Limited (Beijing, China). All nude mice were housed in the Laboratory Animal Center Soochow University. The animal experiment protocol was approved by the Laboratory Animal Ethics Committee of Experiment

Animal Center of the Soochow University (Suzhou, China). Approximately 5×10^6 normal BEAS-2B cells or S30 cells were injected subcutaneously into the right flank of male BALB/c-nude mice (5 mice were used for BEAS-2B cells injection and 10 mice for S30 cells injection). Animals were euthanized 45 days after injection, and tumors were collected and photographed.

RNA Extraction and Sequencing

Total cellular RNA was extracted from S30 and normal BEAS-2B cells using TRIzol reagent (Invitrogen, USA) according to the manufacturer's protocol. Small RNA sequencing was performed on the Illumina Hiseq 2500 platform (Illumina, San Diego, CA). NEBNext® Multiplex Small RNA Library Prep Set for Illumina® (NEB, USA.) was used to prepare the small RNA sequencing library. To determine the known and novel miRNAs, unique clustered reads were aligned with the reference genome and database obtained from miRBase 20.0 (http://www.mirbase.org/). The miRDeep2 algorithm was used to predict novel miRNA precursors. The expression levels were estimated by transcript per million (TPM) and mRNA sequencing was performed on the Illumina HiSeq 4000 platform. The Illumina TruSeq RNA kit was used for preparing the mRNA sequencing library. The mRNAs with expression profiles that differed between the samples were normalized as fragments per kilobase of transcript per million mapped reads (FKPM). The DEGSeq package was used to analyze the differential expressed miRNAs (DEMs) or mRNAs (DEGs). P-value < 0.05 and $|\log2\ (\text{foldchange})| \geq 1$ were regarded as the threshold of significantly differential expression.

Data Source and Processing

The NSCLC (LUAD and LUSC) miRNA-Seq datasets and related clinicopathology information were obtained from the Xena (https://xena.ucsc.edu). The LUAD miRNA expression data included a total of 493 samples consisting of 448 LUAD samples and 45 normal adjacent samples. The LUSC miRNA expression data included a total of 380 samples comprising 336 LUSC samples and 44 normal adjacent samples. The limma package was used to identify the differential expressed miRNAs in LUAD and LUSC when compared with corresponding normal adjacent samples. The differentially expressed miRNAs were defined by a threshold of p-value < 0.05 and $|\log2\ (\text{foldchange})| \geq 1$.

TABLE 1 | Primers used in this study.

Symbol		Sequence
miR-106b-5p	Forward	5′-TAAAGTGCTGACAGTGCAGAT-′3
miR-589-5p	Forward	5′-TGAGAACCACGTCTGCTCTGAG-′3
miR-96-5p	Forward	5′-TTTGGCACTAGCACATTTTTGCT-′3
miR-181a-5p	Forward	5′-AACATTCAACGCTGTCGGTGAGT-′3
miR-361-3p	Forward	5′-TCCCCCAGGTGTGATTCTGATTT-′3
IGFBP3	Forward	5′-AGAGCACAGATACCCAGAACT-′3
	Reverse	5′-GGTGATTCAGTGTGTCTTCCATT-′3
KRT17	Forward	5′-GCCGCATCCTCAACGAGAT-′3
	Reverse	5′-CGCGGTTCAGTTCCTCTGTC-′3
FAM129A	Forward	5′-GCCTGGAAGGAACGATCCG-′3
	Reverse	5′-GGCCACCATCGCTTTGATCTT-′3
FLNC	Forward	5′-GCTCGTGTCCATAGACAGCAA-′3
	Reverse	5′-CTGGGGCACCTTGTTCTGG-′3
TIE1	Forward	5′-ACGACCATGACGGCGAATG-′3

Reverse primers of miRNAs and U6 primers are provided by Mir-X™ miRNA First-Strand Synthesis Kit.

Real-Time Quantitative PCR

A total of 1.5 μg RNA isolated from each sample was reversely transcribed into complementary DNA (cDNA) using Revert Aid First Strand Complementary DNA Synthesis Kit (for mRNA detecting, Thermo, USA) or Mir-X™ miRNA First-Strand Synthesis Kit (for miRNA detecting, Clontech Laboratories, USA) according to the manufacturer's instructions. Quantitative PCR (qPCR) was performed using NovoScript® SYBR Two-Step qRT-PCR Kit (novoprotein, China) with a QuantStudioTM 6 Flex qRT-PCR system (USA). The internal control for the quantitive analysis of miRNA and mRNA were U6 and GAPDH, respectively. The primer used for qPCR were listed in **Table 1**.

Analysis of Gene Expression and Smoking History

To validate the correlation between expression of miRNAs and patients' smoking history, all valid LUAD samples in the TCGA database were divided into four groups according to smoking history, including (1) lifelong non-smoker ($n = 66$); (2) current smokers ($n = 104$); (3) Current reformed smoker for >15 years ($n = 116$); (4) current reformed smoker for ≤15 years ($n = 144$). The expression of miRNAs in lung adenocarcinoma tissues of each group was compared.

miRNA-mRNA Integrative Network

For identification of the candidate miRNA-mRNA network in smoking-induced malignant transformed cells, two separate steps were carried out. First, the target mRNAs of interest miRNAs were predicted through the miRDB database (http://mirdb.org/miRDB/). Second, the intersection of differently expressed genes and target genes was taken to screen the potential target genes of miRNAs in smoking-induced malignant transformed cells. These different expression target genes and miRNAs were used to construct the miRNA-mRNA regulation network through the Cytoscape software (V3.7.1, https://cytoscape.org).

Enrichment Analyses

Metascape (http://metascape.org/gp/index.html) is an effective and efficient tool for experimental biologists to comprehensively analyze and interpret OMICs-based studies in the big data era (19). The database was used to perform the Gene Ontology (GO) and Kyoto Encyclopedia of Genes and Genomes (KEGG) pathway enrichment analysis, which is used to predict the potential biological functions of the overlapping genes of the DEGs and target genes.

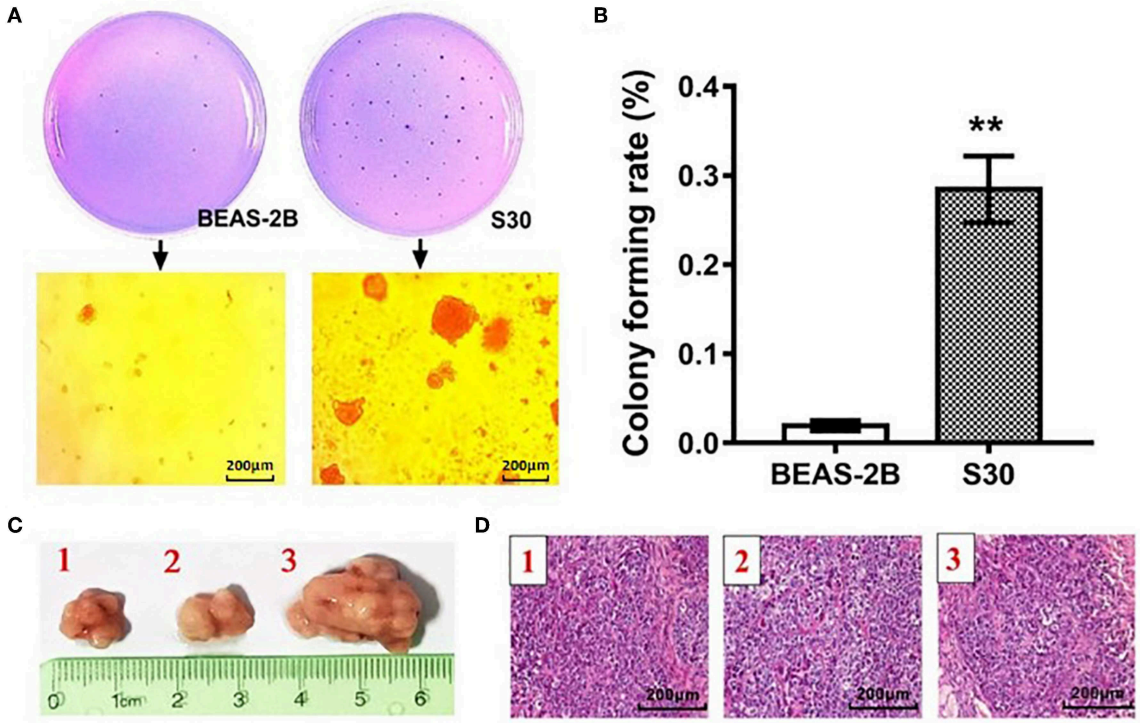

FIGURE 1 | CS-induced malignant transformation in BEAS-2B cells *in vitro* and *in vivo*. **(A)** Representative photographs of the colony formation assay of the normal BEAS-2B cells and S30 cells. **(B)** Graph of soft agar colony forming rate of normal BEAS-2B cells and S30 cells. $^{**}p < 0.01$ vs. BEAS-2B. **(C)** Photographs of tumors excised 45 days after injection of normal BEAS-2B cells and S30 cells into nude mice. **(D)** Representative HE staining histopathologic image of tumor tissues excised 45 days after injection of S30 cells into nude mice.

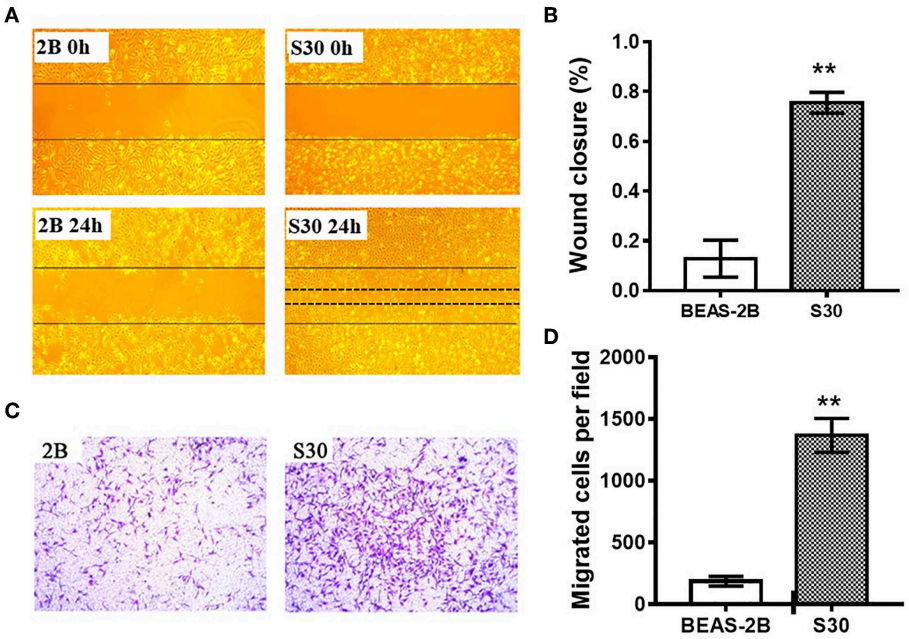

FIGURE 2 | CS promoted the migratory ability of BEAS-2B cells. **(A)** Representative images of scratch wound healing assay of normal BEAS-2B cells and CS-induced malignant transformed cells (S30). **(B)** Graph of wound closure rate in scratch wound healing assay of normal BEAS-2B cells and S30 cells. $^{**}p < 0.01$ vs. BEAS-2B. **(C)** Representative images of transwell assay of normal BEAS-2B cells and S30 cells. **(D)** Graph of migrated cells in transwell assay of normal BEAS-2B cells and S30 cells. $^{**}p < 0.01$ vs. BEAS-2B.

Statistical Analysis

SPSS 22.0 was used for statistical analysis. Values were presented as mean ± standard deviation (SD). Difference analysis between two groups was performed by using student *t*-test. A $p < 0.05$ was considered statistically significant. Correlation between differentially expressed miRNAs and predicted target mRNAs were calculated by Pearson's correlation. A $p < 0.05$ was regarded as statistically significant.

RESULTS

CS-Induced Malignant Transformation in BEAS-2B Cells

To validate the malignant change of S30 cells, the normal BEAS-2B cells and S30 cells were seeded in soft agar. As shown in **Figure 1A**, cells formed significantly more and bigger colonies in S30 cells compared to the normal BEAS-2B cells. Besides, colony formation rate in S30 cells was remarkably higher than in the normal BEAS-2B cells (**Figure 1B**). Moreover, the normal BEAS-2B cells and S30 cells were used to generate xenograft tumors in nude mice. Among the ten mice injected with S30 cells, 3 developed tumor tissue (**Figures 1C,D**). While no tumor was found in the five mice injected with normal BEAS-2B cells.

CS Promoted the Migratory Ability of BEAS-2B Cells

To investigate the effect of CS in cell migration, we performed scratch wound healing and transwell cell migration assays. Scratch wound healing assay indicated that the migratory ability was significantly increased in S30 cells compared to the normal BEAS-2B cells (**Figures 2A,B**). As shown in **Figures 2C,D**, further transwell migratory assay demonstrated that the migrated cells were significantly increased in S30 cells compared to the normal BEAS-2B cells. These results suggested that long-term exposure to CS could promote the migratory ability of BEAS-2B cells.

Differentially Expressed miRNAs Between S30 Cells and Normal BEAS-2B Cells

To test whether CS affects the miRNA-mRNA regulatory network in BEAS-2B cells, the miRNAs in normal BEAS-2B cells and S30 cells were quantitatively analyzed using small RNA sequencing. Compared with the normal BEAS-2B cells, the S30 cells showed dysregulation of 42 miRNAs that had significantly different expression levels with 2-fold change as a cut off (**Figures 3A,B**, **Supplementary Table 1**). Of these 42 miRNAs, 28 were upregulated (67%), and 14 were downregulated

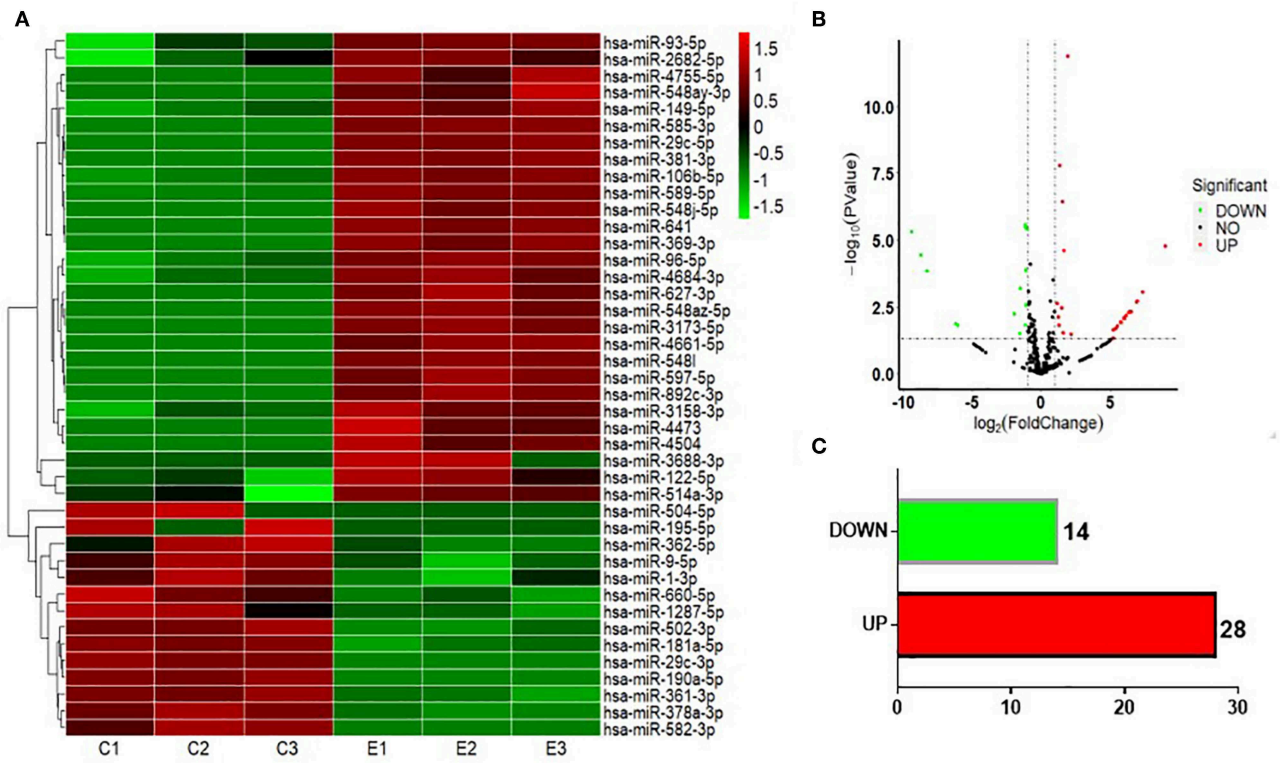

FIGURE 3 | Graphical representation of the 42 miRNAs differentially expressed between S30 cells and normal BEAS-2B cells. **(A)** Heatmap of the 42 differentially expressed miRNAs (DEMs) between the CS-induced malignant transformed cells (S30) and normal BEAS-2B cells. The colors in the heatmap represent the normalized expression values, with low expression values being colored in shades of green and high expression values in shades of red. **(B)** Volcano plots were generated to visualize the distribution of DEMs between normal BEAS-2B and S30 cells. The top five most significantly dysregulated miRNAs are marked. **(C)** Counts of miRNAs upregulated or downregulated in S30 cells.

(33%) in the S30 cells (**Figure 3C**). The top five most significantly aberrant expression miRNAs are marked in the scatter plot; miR-106b-5p, miR-589-5p, and miR-96-5p were upregulated, and miR-181a-5p and miR-361-3p were downregulated (**Figure 3B**). The qPCR results of the top five miRNAs showed the increased miR-106b-5p, miR-589-5p, and miR-96-5p and decreased miR-181a-5p and miR-361-3p expression in S30 cells compared to normal BEAS-2B cells (**Figure 4**).

Differentially Expressed mRNAs Between S30 Cells and Normal BEAS-2B Cells

Next, we investigated the expression patterns of mRNAs using transcriptome resequencing. Compared with the normal BEAS-2B cells, the S30 cells showed dysregulation of 753 mRNAs that had significantly different expression levels with 2-fold change as a cut off (**Figures 5A,B**). Of these 753 mRNAs, 273 were upregulated (36%), and 480 were downregulated (64%) in the S30 cells (**Figure 5C**). The top five most significantly dysregulated mRNAs are marked in the scatter plot; *IGFBP3* and *KRT17* were upregulated, and *FAM129A*, *FLNC*, and *TIE1* were downregulated (**Figure 5B**). The qPCR results of the top five mRNAs validated the increased *IGFBP3* and *KRT17* and decreased *FAM129A*, *FLNC*, and *TIE1* expression in S30 cells compared to normal BEAS-2B cells (**Figure 6**).

Integrated Analysis of the DEMs in S30 Cells and Lung Cancer Samples

To explore whether the DEMs' expression is altered in lung cancer tissues, we analyzed the miRNAs sequencing data of lung cancer, including lung adenocarcinomas (LUAD) and squamous cell lung carcinomas (LUSC), in the TCGA database. A total of 8 miRNAs were found dysregulation in S30 cells, LUAD and LUSC samples with a similar tendency of change. Among these 8 miRNAs, 5 were upregulated (miR-96-5p, miR-93-5p, miR-589-5p, miR-4661-5p, and miR-106b-5p) and 3 were downregulated (miR-190a-5p, miR-195-5p, and miR-1-3p) in the three datasets (**Figure 7**).

Association of miRNA Expression With Smoking History

Among the five up-regulated miRNAs, three miRNAs, including miR-96-5p, miR-93-5p, and miR-106-5p, showed a higher

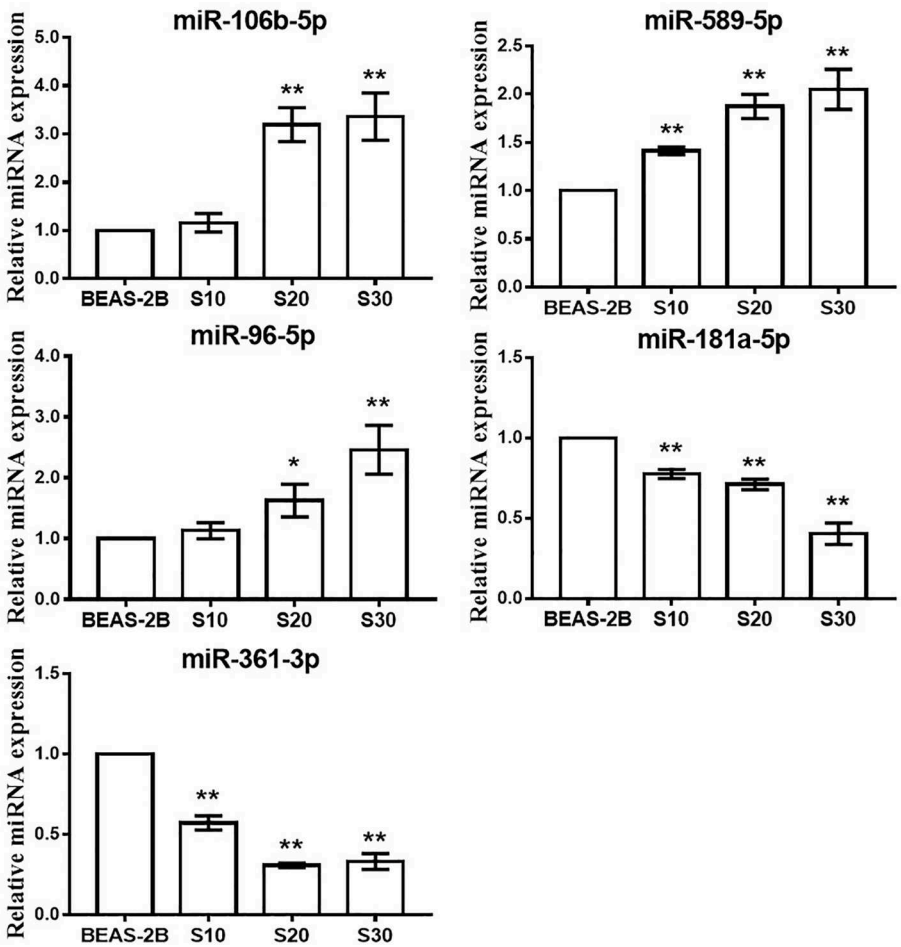

FIGURE 4 | qPCR analysis of the top five most significantly dysregulated miRNAs in CS-exposed cells. Data are presented as relative fold induction compared with normal BEAS-2B cells. $^{*}p < 0.05$, $^{**}p < 0.01$ vs. BEAS-2B.

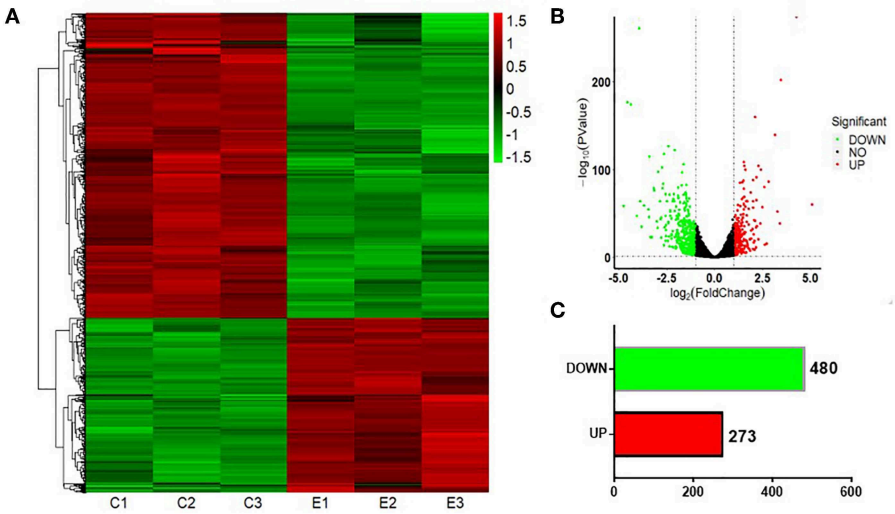

FIGURE 5 | Graphical representation of the 753 mRNAs differentially expressed between S30 cells and normal BEAS-2B cells. **(A)** Heatmap of the 753 differentially expressed genes (DEGs) between the CS-induced malignant transformed cells (S30) and normal BEAS-2B cells. The colors in the heatmap represent the normalized expression values, with low expression values being colored in green and high expression values in red. **(B)** Volcano plots were generated to visualize the distribution of DEGs between normal BEAS-2B and S30 cells. The top five most significantly dysregulated genes are marked. **(C)** Counts of genes upregulated or downregulated in S30 cells.

expression in current smoking LUAD patients when compared with the lifelong non-smokers (**Table 2**). Three of the screened down-regulated miRNAs, including miR-190a-5p, miR-195-5p, and miR-1-3p, showed lower expression in current smoking LUAD patients when compared with the lifelong non-smokers (**Table 2**). Moreover, miR-96-5p and miR-106b-5p are overexpressed in the current reformed smoker for >15 years, while miR-190a-5p has lower expression in the current reformed smoker for >15 years when compared with the lifelong non-smoker (**Table 2**).

Integrative Analysis of Correlation of miRNA and mRNA in S30 Cells

To understand the potential functions of the smoking-related differentially expressed miRNAs, and to explore miRNA-mRNA interaction in S30 cells, we predicted the target genes of miRNAs and performed an intersection analysis with the gene expression data to identify genes that were inversely co-expressed with miRNAs. A total of 2,477 target genes of low-expressed miRNAs and 2,295 target genes of high-expressed miRNAs were screened by searching miRDB database. Consequently, 25 up-regulated genes and 70 down-regulated genes were found to have at least one negatively regulated miRNA-mRNA pair for smoking-related differentially expressed miRNAs (**Figure 8A**, **Supplementary Table 2**). The miRNAs-DEGs network was generated by Cytoscape software, as showed in **Figure 8B**.

Enrichment Analysis of Correlation of miRNA and mRNA in S30 Cells

To further explore the function of the negatively correlated miRNA-mRNA pairs, 95 up-regulated or down-regulated target genes in S30 cells were selected for mapping into the Metascape database and subjected to functional enrichment analysis. As shown in **Figure 9A**, GO analysis demonstrated that these target genes are associated with several cancer-related, especially tumor migration related GO terms, including "positive regulation of cell motility," "regulation of cell adhesion," "mononuclear cell migration," "cell junction organization," "extracellular structure organization" and so on. Among these enriched DEGs, several DEGs, including *THBS1*, *FN1*, *PIK3R1*, *CSF1*, *CORO2B*, and *PREX1*, were involved in many biologic processes which derived from enrichment analysis of negative miRNA-mRNA correlations (**Figure 9B**). Moreover, the KEGG pathway enrichment analysis suggested that these target genes were significantly correlated with "TNF signaling pathway," "Small cell lung cancer," "Rap1 signaling pathway," "PI3K-Akt signaling pathway," "mTOR signaling pathway," "FoxO signaling pathway," "Focal adhesion," "ECM-receptor interaction," and some other cancer-related pathways (**Figure 10A**). In particular, "Focal adhesion" and "ECM-receptor interaction" are closely related to cell migration. In addition, *THBS1*, *FN1*, *PIK3R1*, and *IRS1*, were involved in many KEGG pathways which derived from enrichment analysis of negative miRNA-mRNA correlations (**Figure 10B**).

DISCUSSION

There are nearly 1.3 billion cigarette smokers in the world, which leads to 5 million cancer related deaths every year (20). Cigarette-smoking is a notable risk factor for multiple pathologies (21–23), among them lung cancer takes the lead with smokers having a much higher risk than non-smokers. Our previous studies have

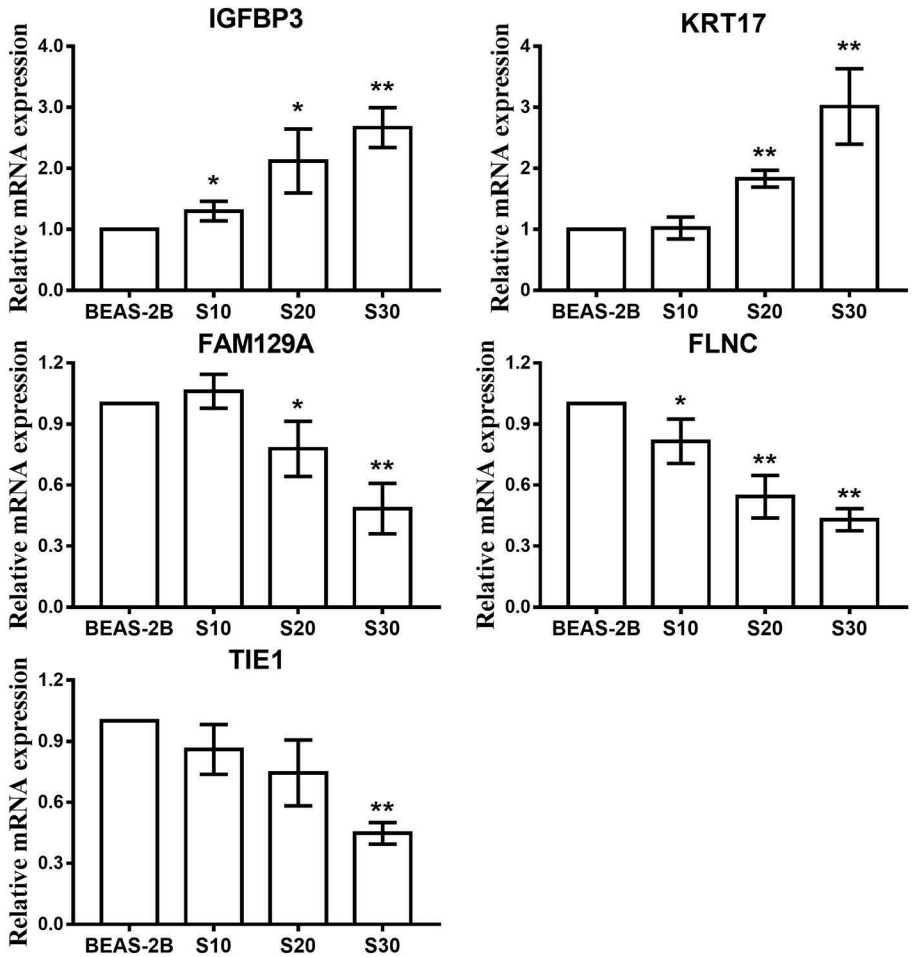

FIGURE 6 | qPCR analysis of the top five most significantly dysregulated genes in CS-exposed cells. Data are presented as relative fold induction compared with normal BEAS-2B cells. $^{*}p < 0.05$, $^{**}p < 0.01$ vs. BEAS-2B.

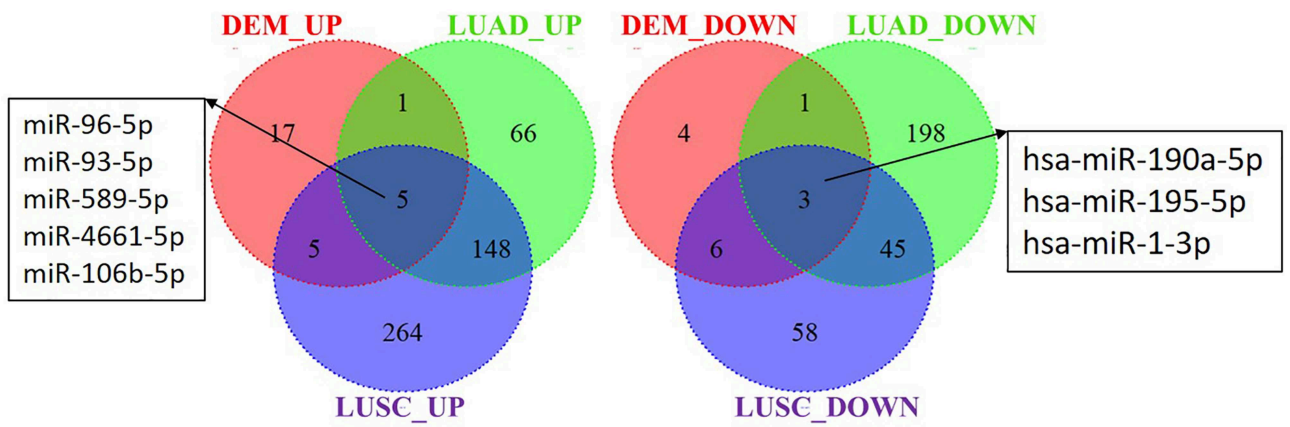

FIGURE 7 | Identification of differential expressed miRNAs in S30 cells and lung cancer samples. DEM_UP/DEM_DOWN: up-regulated/ down-regulated miRNAs in S30 cells; LUAD_UP/LUAD_DOWN: up-regulated/ down-regulated miRNAs in LUAD samples; LUSC_UP/LUSC_DOWN: up-regulated/ down-regulated miRNAs in LUSC samples.

TABLE 2 | The expression of miRNAs in the LUAD patients with different smoking history.

miRNAs	Significant	1 (n = 66)	2 (n = 104)	3 (n = 116)	4 (n = 144)
miR-96-5p	UP	4.25 ± 0.74	4.58 ± 1.07*	4.39 ± 1.12	4.55 ± 1.04*
miR-93-5p	UP	11.70 ± 0.87	12.09 ± 0.87**	11.65 ± 0.86	11.79 ± 0.97
miR-589-5p	UP	6.66 ± 0.65	6.72 ± 0.79	6.26 ± 0.71**	6.49 ± 0.77
miR-4661-5p	UP	2.03 ± 0.71	2.14 ± 1.05	1.94 ± 0.84	2.10 ± 1.02
miR-106b-5p	UP	7.72 ± 0.65	8.21 ± 0.72**	7.75 ± 0.68	8.03 ± 0.72**
miR-190a-5p	DOWN	1.87 ± 0.77	1.52 ± 0.74**	1.74 ± 0.65	1.57 ± 0.56**
miR-195-5p	DOWN	5.15 ± 0.98	4.73 ± 0.84**	5.11 ± 0.82	5.02 ± 0.87
miR-1-3p	DOWN	3.37 ± 1.41	2.44 ± 1.25**	3.41 ± 1.34	3.04 ± 1.28

*Lifelong non-smoker (<100 cigarettes smoked in Lifetime) = 1; Current smoker (includes daily smokers and non-daily smokers or occasional smokers) = 2; Current reformed smoker for > 15 years (>15 years) = 3; Current reformed smoker for ≤15 years (≤15 years) = 4 (*p < 0.05 vs. non-smoker; **p < 0.01 vs. non-smoker).*

suggested that chronic exposure to CS could induce malignant transformation of the human bronchial epithelial cell line (BEAS-2B) and tumorigenesis (18, 24). In recent years, studies have indicated that miRNAs play an essential role in tumor initiation, development, and metastasis as well as the cellular response to stress by modulating the expression of their target genes (25–27). In this study, we investigate the effect of chronic exposure to CS on the expression of miRNA and mRNA in BEAS-2B cells and further examined the interaction of miRNA and mRNAs.

Based on our high throughput sequencing data and the TCGA database analysis, we found significant dysregulation of 6 smoking-related miRNAs in S30 cells compared with normal BEAS-2B cells. Among these miRNAs, miR-190a is found downregulated in aggressive neuroblastoma (NBL). Overexpression of miR-190a contributed to the inhibition of tumor growth and prolonged the dormancy period of fast-growing tumors (28). A recent study showed that miR-190a could inhibit the metastasis of breast tumor by involving in estrogen receptor (ERα) signaling (29). miR-195 usually serves as a tumor suppressor in several cancer types, such as gastric cancer (30), renal cancer (31), cervical cancer (32), liver cancer (33), and osteosarcoma (34), and its downregulation was related to lymph node metastasis and advanced clinical stage (32). Similarly, miR-1 can regulate multiple behavior of the tumor cells, such as proliferation (35, 36), migration (37), apoptosis (38, 39), and metabolism (40). In addition, miR-106b and miR-93 are both the members of miR-106b∼25 cluster, which have regarded as significant oncogenic drivers as well as potential biomarkers and therapeutic targets in various tumors (41–44). Moreover, Several studies have demonstrated that miR-96 could act as an oncogene (45–47) or tumor suppressor (48, 49) depending on the different types of cancer. Although these miRNAs have extensively been reported to be associated with many other kinds of cancer, their roles in lung cancer has yet been demonstrated.

Numerous studies have established the regulatory relationships between miRNA and mRNA expression (50, 51). CS-induced DEMs can bind to 3′UTR regions of several genes and down-regulate their expression, indicating that these miRNAs may contribute to the pathogenesis of smoking-related diseases. It has been reported that negatively regulated miRNA-mRNA pairs are significantly contributed to the initialization and development of different kinds of cancer (52–54). In order to further comprehend the roles of the miRNA-mRNA pairs in CS-induced lung cancer, we selected 95 dysregulated target mRNAs of the 6 CS-related miRNAs and found that they are involved in several cancer-related signaling pathways including TNF signaling pathway, Rap1 signaling pathway, PI3K-Akt signaling pathway, mTOR signaling pathway, FoxO signaling pathway, ECM-receptor interaction, and so on. Meanwhile, the GO enrichment analysis results indicated that these target genes were participated in a series of cell adhesion and migration biological processes, suggesting these miRNA-mRNA pairs related to the process of epithelial-mesenchymal transformation (EMT). EMT is considered to be an important regulator of metastasis by promoting the invasion and spread of tumor cells to distant organs (55). Among these enriched DEGs, *IRS1*, *PIK3R1*, *THBS1*, and *FN1* are related to more than 4 KEGG pathways. As an adaptor of the insulin growth factor-1 receptor, *IRS1* plays an essential role in cell growth and proliferation, primarily via the Akt pathway, and it was reported to be regulated by several miRNAs through direct or indirect action (56–59). Moreover, studies have demonstrated that *PIK3R1* was directly targeted by miR-127 (60), miR-21 (61), miR-155 (62), and some other miRNAs in different kinds of cancers. It's reported that the activity of phosphoinositide 3- kinase (PI3K) is activated by many oncogenes and the PI3K family members are involved in a serious of biological processes and the genesis and progression of various tumors (63). Thrombospondin 1 (*THBS1*) is a secreted protein with multiple biological functions (64), including a potent anti-angiogenic activity and activation of latent transforming growth factor beta (TGF-β) (65, 66). A recent study suggested that the expression of *THBS1* was modulated by multiple miRNAs (67). Moreover, it's reported that fibronectin 1 (*FN1*) is crucial to many cellular processes, including cell proliferation, adhesion, migration and differentiation (68, 69), and the expression of *FN1* was regulated by miR-1271 (70), miR-9 (71), and miR-206 (72). Similar to previous studies, we identified the negatively regulated miRNA-mRNA pairs in the CS-induced lung cancer, which were implicated in several cancer-related (especially EMT-related) biological process and KEGG pathways in the malignant transformation progress of lung cells induced by CS. Further study will be needed to explore

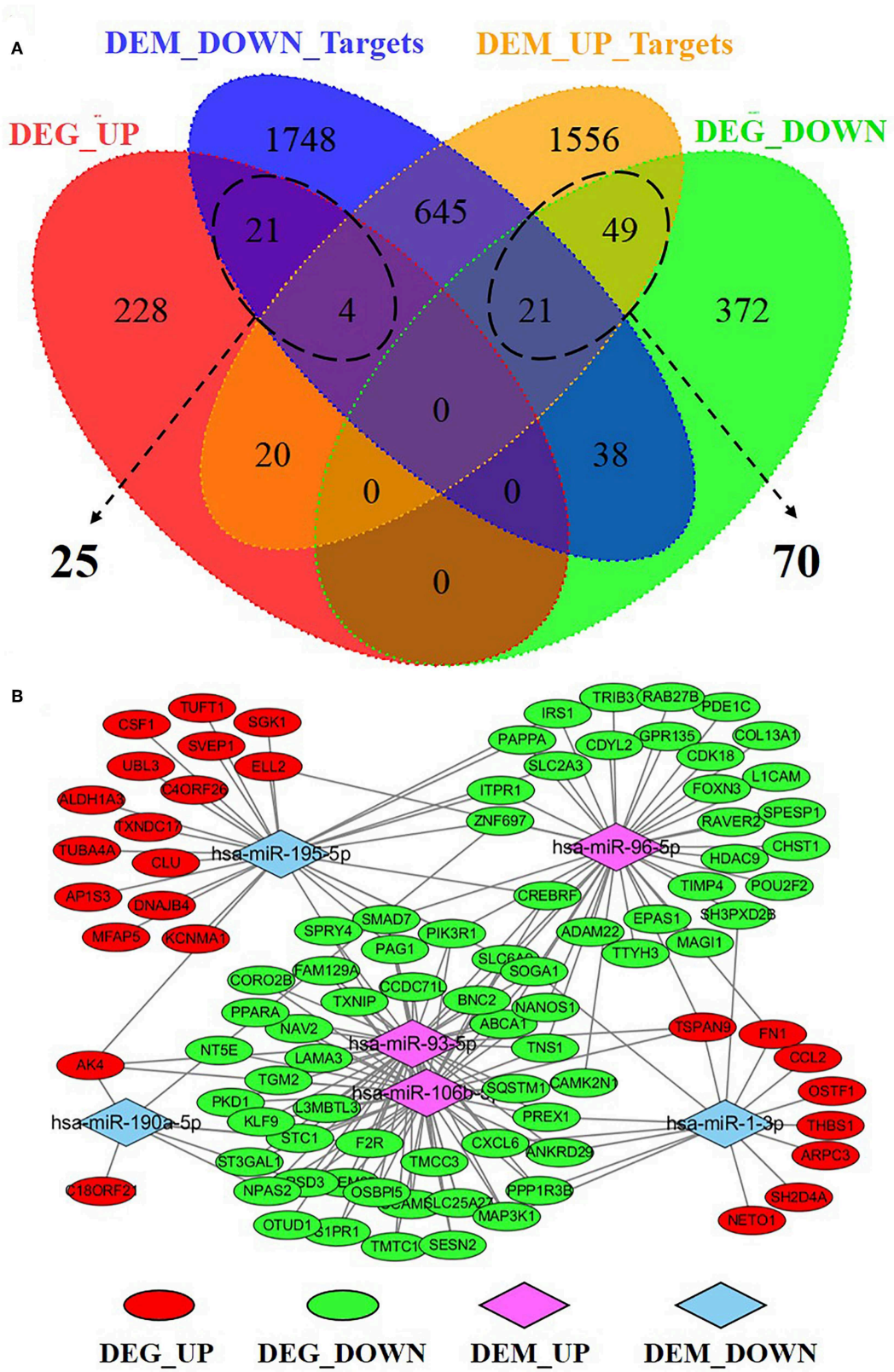

FIGURE 8 | Integrative analysis of miRNA-mRNA regulatory network in S30 cells. **(A)** Venn Diagram depicting the distribution of negatively correlated miRNA-mRNA pairs within the four datasets. **(B)** Regulatory network for 95 negatively correlated miRNA-mRNA, including 25 DEG_UP/DEM_DOWN_Targets pairs and 70 DEG_DOWN/DEM_UP_Targets pairs. DEG_UP/DEG_DOWN: up-regulated/down-regulated genes in S30 cells; DEM_UP/DEM_DOWN: up-regulated/down-regulated miRNAs in S30 cells.

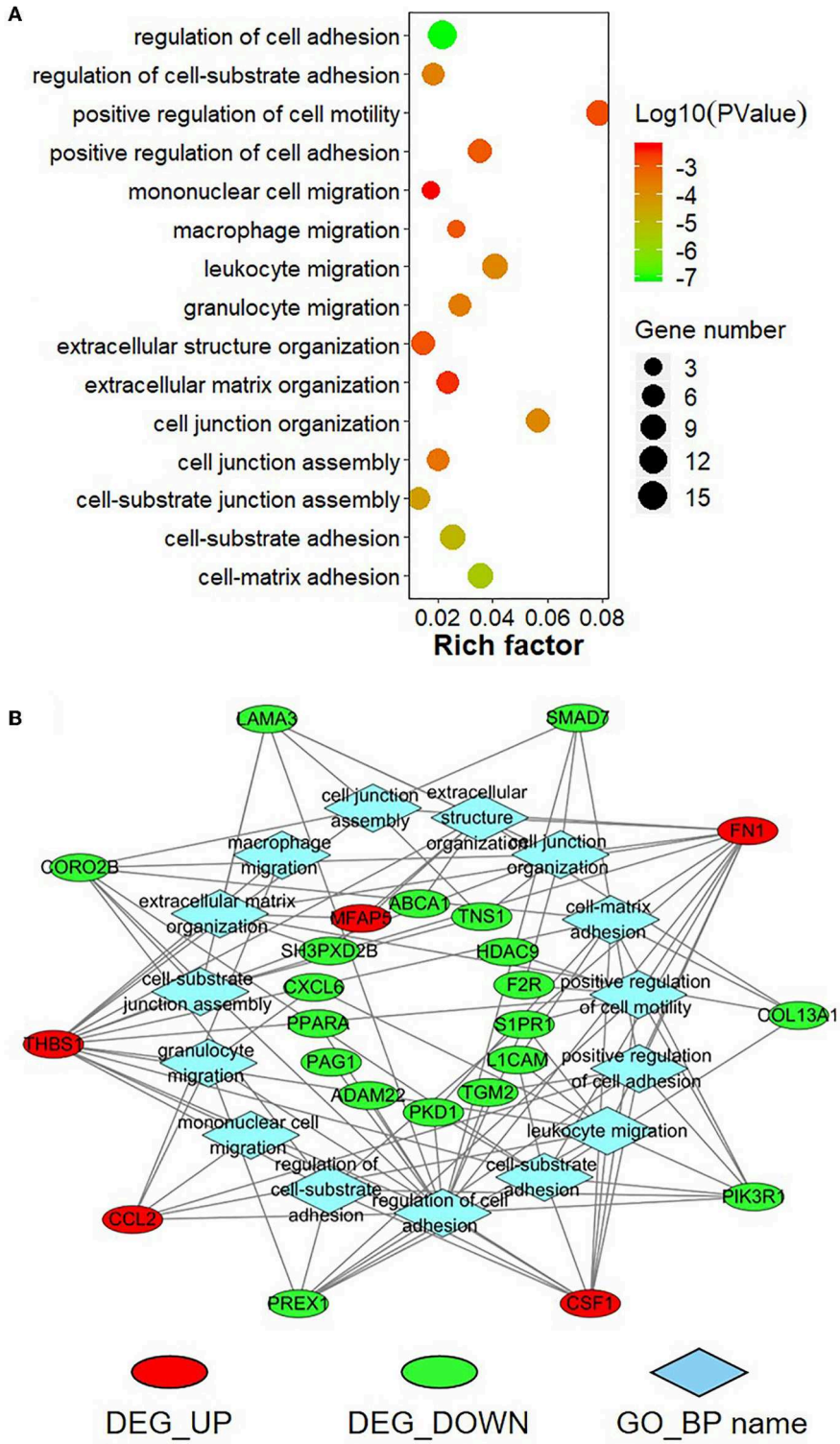

FIGURE 9 | Gene Ontology (GO) enrichment analysis for negatively correlated miRNA-mRNA. **(A)** The top enriched GO terms are shown in the bubble chart. The Y-axis represents the biologic process GO terms, and the X-axis represents the rich factor (rich factor = amount of differentially expressed genes enriched in the GO term/amount of all genes in background gene set). The color and size of the bubble represent enrichment significance and the number of genes enriched in the GO term, respectively. **(B)** Network diagram of top enriched GO terms for the negatively correlated miRNA-mRNA. DEG_UP: up-regulated differentially expressed genes; DEG_Down: down-regulated differential expression genes; GO_BP: Gene Ontology of biological process.

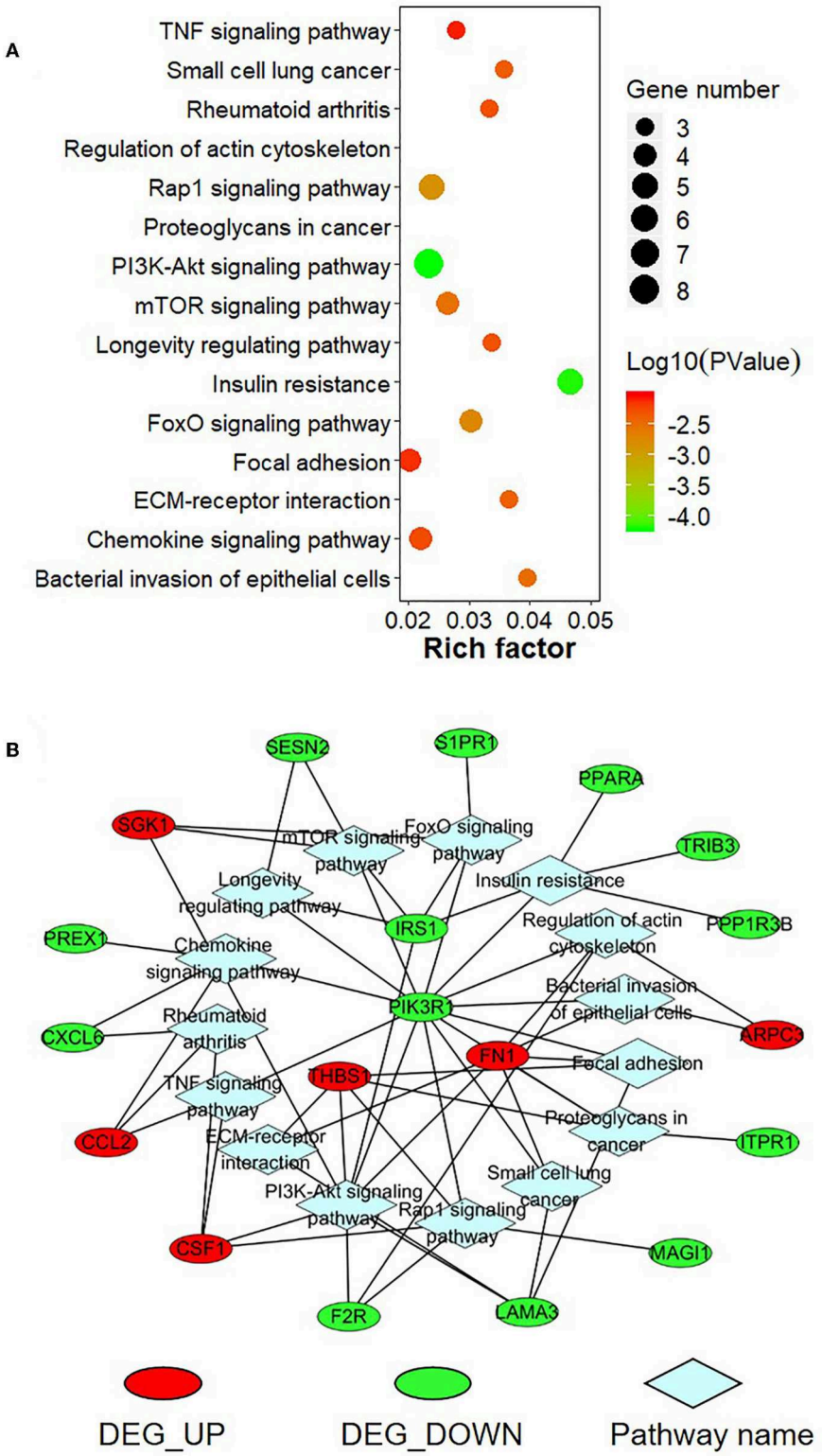

FIGURE 10 | KEGG pathway enrichment analysis for negatively correlated miRNA-mRNA. **(A)** The top enriched KEGG pathways are shown in the bubble chart. The Y-axis represents the KEGG pathways, and the X-axis represents the rich factor (rich factor = amount of differential expressed genes enriched in the pathway/amount of all genes in the background gene set). The color and size of the bubble represent enrichment significance and the number of genes enriched in the pathway, respectively. **(B)** Network diagram of top enriched KEGG pathways for the negatively correlated miRNA-mRNA. DEG_UP: up-regulated differential expressed genes; DEG_Down: down-regulated differential expression genes.

the targeting relationships of these miRNAs and their target mRNAs and their possible roles on cancer-related molecular mechanisms for the development of novel targeted therapy for CS-induced lung cancer.

In conclusion, our study demonstrated that the expression profiles of miRNA and mRNA were significantly dysregulated in BEAS-2B cells with long-term exposure to CS. Smoking induced miRNAs are associated with EMT and carcinogenesis.

DATA AVAILABILITY STATEMENT

The datasets generated for this study can be found in the Sequence Read Archive (SRA) database (https://trace.ncbi.nlm.nih.gov/Traces/sra/) with identifier SRP182926 and SRP181756. The LUAD and LUSC datasets analyzed for this study can be obtained from UCSC Xena (https://xenabrowser.net/datapages/).

ETHICS STATEMENT

The animal study was reviewed and approved by The Laboratory Animal Ethics Committee of Experiment Animal Center of the Soochow University. Written informed consent was obtained from the owners for the participation of their animals in this study.

AUTHOR CONTRIBUTIONS

JL conceived and designed the study. JW performed and analyzed the experiments. XY, NO, SZ, HY, and XG assisted to collect and analyze the data. JW wrote the manuscript. JT and TC were of immense help in the modification of the manuscript. All authors read and approved the final manuscript.

FUNDING

This study was supported by the National Natural Science Foundation of China (81573178 and 81172707) and the Suzhou Science and Technology Project (SS201832). The study was also supported by Jiangsu Key Laboratory of Preventive and Translational Medicine for Geriatric Diseases as well as the Priority Academic Program Development of Jiangsu Higher Education Institutions (PAPD).

SUPPLEMENTARY MATERIAL

The Supplementary Material for this article can be found online at: https://www.frontiersin.org/articles/10.3389/fonc.2019.01029/full#supplementary-material

REFERENCES

1. Ferlay J, Soerjomataram I, Dikshit R, Eser S, Mathers C, Rebelo M, et al. Cancer incidence and mortality worldwide: sources, methods and major patterns in GLOBOCAN 2012. *Int J Cancer.* (2015) 136:E359–386. doi: 10.1002/ijc.29210
2. Torre LA, Bray F, Siegel RL, Ferlay J, Lortet-Tieulent J, Jemal A. Global cancer statistics, 2012. *CA Cancer J Clin.* (2015) 65:87–108. doi: 10.3322/caac.21262
3. Bray F, Ferlay J, Soerjomataram I, Siegel RL, Torre LA, Jemal A. Global cancer statistics 2018: GLOBOCAN estimates of incidence and mortality worldwide for 36 cancers in 185 countries. *CA Cancer J Clin.* (2018) 68:394–424. doi: 10.3322/caac.21492
4. Thun M, Peto R, Boreham J, Lopez AD. Stages of the cigarette epidemic on entering its second century. *Tob Control.* (2012) 21:96–101. doi: 10.1136/tobaccocontrol-2011-050294
5. Hecht SS. Tobacco smoke carcinogens and lung cancer. *J Natl Cancer Inst.* (1999) 91:1194–210. doi: 10.1093/jnci/91.14.1194
6. Shields PG. Molecular epidemiology of smoking and lung cancer. *Oncogene.* (2002) 21:6870–6. doi: 10.1038/sj.onc.1205832
7. Nebbioso A, Tambaro FP, Dell'Aversana C, Altucci L. Cancer epigenetics: moving forward. *PLoS Genet.* (2018) 14:e1007362. doi: 10.1371/journal.pgen.1007362
8. Portela A, Esteller M. Epigenetic modifications and human disease. *Nat Biotechnol.* (2010) 28:1057–68. doi: 10.1038/nbt.1685
9. Duruisseaux M, Esteller M. Lung cancer epigenetics: from knowledge to applications. *Semin Cancer Biol.* (2018) 51:116–28. doi: 10.1016/j.semcancer.2017.09.005
10. Kang SM, Lee HJ. MicroRNAs in human lung cancer. *Exp Biol Med.* (2014) 239:1505–13. doi: 10.1177/1535370214533887
11. Bartel DP. MicroRNAs: target recognition and regulatory functions. *Cell.* (2009) 136:215–33. doi: 10.1016/j.cell.2009.01.002
12. Lim LP, Lau NC, Garrett-Engele P, Grimson A, Schelter JM, Castle J, et al. Microarray analysis shows that some microRNAs downregulate large numbers of target mRNAs. *Nature.* (2005) 433:769–73. doi: 10.1038/nature03315
13. Valencia-Sanchez MA, Liu J, Hannon GJ, Parker R. Control of translation and mRNA degradation by miRNAs and siRNAs. *Genes Dev.* (2006) 20:515–24. doi: 10.1101/gad.1399806
14. Esquela-Kerscher A, Slack FJ. Oncomirs—microRNAs with a role in cancer. *Nat Rev Cancer.* (2006) 6:259–69. doi: 10.1038/nrc1840
15. Kandoth C, McLellan MD, Vandin F, Ye K, Niu B, Lu C, et al. Mutational landscape and significance across 12 major cancer types. *Nature.* (2013) 502:333–9. doi: 10.1038/nature12634
16. Cancer Genome Atlas Research Network. Comprehensive genomic characterization of squamous cell lung cancers. *Nature.* (2012) 489:519–25. doi: 10.1038/nature11404
17. Cancer Genome Atlas Research Network. Comprehensive molecular profiling of lung adenocarcinoma. *Nature.* (2014) 511:543–50. doi: 10.1038/nature13385
18. Du H, Sun J, Chen Z, Nie J, Tong J, Li J. Cigarette smoke-induced failure of apoptosis resulting in enhanced neoplastic transformation in human bronchial epithelial cells. *J Toxicol Environ Health A.* (2012) 75:707–20. doi: 10.1080/15287394.2012.690088
19. Zhou Y, Zhou B, Pache L, Chang M, Khodabakhshi AH, Tanaseichuk O, et al. Metascape provides a biologist-oriented resource for the analysis of systems-level datasets. *Nat Commun.* (2019) 10:1523. doi: 10.1038/s41467-019-09234-6
20. Schembri F, Sridhar S, Perdomo C, Gustafson AM, Zhang XL, Ergun A, et al. MicroRNAs as modulators of smoking-induced gene expression changes in human airway epithelium. *Proc Natl Acad Sci USA.* (2009) 106:2319–24. doi: 10.1073/pnas.0806383106
21. Blakely T, Barendregt JJ, Foster RH, Hill S, Atkinson J, Sarfati D, et al. The association of active smoking with multiple cancers: national census-cancer registry cohorts with quantitative bias analysis. *Cancer Causes Control.* (2013) 24:1243–55. doi: 10.1007/s10552-013-0204-2
22. Momi N, Kaur S, Rachagani S, Ganti AK, Batra SK. Smoking and microRNA dysregulation: a cancerous combination. *Trends Mol Med.* (2014) 20:36–47. doi: 10.1016/j.molmed.2013.10.005
23. Krishnan AR, Zheng H, Kwok JG, Qu Y, Zou AE, Korrapati A, et al. A comprehensive study of smoking-specific microRNA alterations in head and neck squamous cell carcinoma. *Oral Oncol.* (2017) 72:56–64. doi: 10.1016/j.oraloncology.2017.07.009

24. Huang H, Ji Y, Zhang J, Su Z, Liu M, Tong J, et al. Aberrant DNA methylation in radon and/or cigarette smoke-induced malignant transformation in BEAS-2B human lung cell line. *J Toxicol Environ Health A.* (2017) 80:1321–30. doi: 10.1080/15287394.2017.1384156
25. Cheng AM, Byrom MW, Shelton J, Ford LP. Antisense inhibition of human miRNAs and indications for an involvement of miRNA in cell growth and apoptosis. *Nucleic Acids Res.* (2005) 33:1290–7. doi: 10.1093/nar/gki200
26. Chen B, Li H, Zeng X, Yang P, Liu X, Zhao X, et al. Roles of microRNA on cancer cell metabolism. *J Transl Med.* (2012) 10:228. doi: 10.1186/1479-5876-10-228
27. Plaisier CL, Pan M, Baliga NS. A miRNA-regulatory network explains how dysregulated miRNAs perturb oncogenic processes across diverse cancers. *Genome Res.* (2012) 22:2302–14. doi: 10.1101/gr.133991.111
28. Almog N, Briggs C, Beheshti A, Ma L, Wilkie KP, Rietman E, et al. *Transcription*al changes induced by the tumor dormancy-associated microRNA-190. *Transcription.* (2013) 4:177–91. doi: 10.4161/trns.25558
29. Chu HW, Cheng CW, Chou WC, Hu LY, Wang HW, Hsiung CN, et al. A novel estrogen receptor-microRNA 190a-PAR-1-pathway regulates breast cancer progression, a finding initially suggested by genome-wide analysis of loci associated with lymph-node metastasis. *Hum Mol Genet.* (2014) 23:355–67. doi: 10.1093/hmg/ddt426
30. Wang J, Li L, Jiang M, Li Y. MicroRNA-195 inhibits human gastric cancer by directly targeting basic fibroblast growth factor. *Clin Transl Oncol.* (2017) 19:1320–8. doi: 10.1007/s12094-017-1668-4
31. Wang K, Sun Y, Tao W, Fei X, Chang C. Androgen receptor (AR) promotes clear cell renal cell carcinoma (ccRCC) migration and invasion via altering the circHIAT1/miR-195-5p/29a-3p/29c-3p/CDC42 signals. *Cancer Lett.* (2017) 394:1–12. doi: 10.1016/j.canlet.2016.12.036
32. Zhong JY, Yuan H, Xu XQ, Kong SF. MicroRNA-195 inhibits cell proliferation, migration and invasion by targeting defective in cullin neddylation 1 domain containing 1 in cervical cancer. *Int J Mol Med.* (2018) 42:779–88. doi: 10.3892/ijmm.2018.3660
33. Zhang H, Zhou D, Ying M, Chen M, Chen P, Chen Z, et al. Expression of long non-coding RNA (lncRNA) small nucleolar RNA host gene 1 (SNHG1) exacerbates hepatocellular carcinoma through suppressing miR-195. *Med Sci Monit.* (2016) 22:4820–9. doi: 10.12659/msm.898574
34. Qu Q, Chu X, Wang P. MicroRNA-195-5p suppresses osteosarcoma cell proliferation and invasion by suppressing naked cuticle homolog 1. *Cell Biol Int.* (2017) 41:287–95. doi: 10.1002/cbin.10723
35. Reid JF, Sokolova V, Zoni E, Lampis A, Pizzamiglio S, Bertan C, et al. miRNA profiling in colorectal cancer highlights miR-1 involvement in MET-dependent proliferation. *Mol Cancer Res.* (2012) 10:504–15. doi: 10.1158/1541-7786.MCR-11-0342
36. Stope MB, Stender C, Schubert T, Peters S, Weiss M, Ziegler P, et al. Heat-shock protein HSPB1 attenuates microRNA miR-1 expression thereby restoring oncogenic pathways in prostate cancer cells. *Anticancer Res.* (2014) 34:3475–80.
37. Xu L, Zhang Y, Wang H, Zhang G, Ding Y, Zhao L. Tumor suppressor miR-1 restrains epithelial-mesenchymal transition and metastasis of colorectal carcinoma via the MAPK and PI3K/AKT pathway. *J Transl Med.* (2014) 12:244. doi: 10.1186/s12967-014-0244-8
38. Nohata N, Hanazawa T, Kikkawa N, Sakurai D, Sasaki K, Chiyomaru T, et al. Identification of novel molecular targets regulated by tumor suppressive miR-1/miR-133a in maxillary sinus squamous cell carcinoma. *Int J Oncol.* (2011) 39:1099–107. doi: 10.3892/ijo.2011.1096
39. Yamasaki T, Yoshino H, Enokida H, Hidaka H, Chiyomaru T, Nohata N, et al. Novel molecular targets regulated by tumor suppressors microRNA-1 and microRNA-133a in bladder cancer. *Int J Oncol.* (2012) 40:1821–30. doi: 10.3892/ijo.2012.1391
40. Singh A, Happel C, Manna SK, Acquaah-Mensah G, Carrerero J, Kumar S, et al. Transcription factor NRF2 regulates miR-1 and miR-206 to drive tumorigenesis. *J Clin Invest.* (2013) 123:2921–34. doi: 10.1172/JCI66353
41. Fang L, Deng Z, Shatseva T, Yang J, Peng C, Du WW, et al. MicroRNA miR-93 promotes tumor growth and angiogenesis by targeting integrin-beta8. *Oncogene.* (2011) 30:806–21. doi: 10.1038/onc.2010.465
42. Li F, Liu J, Li S. MicorRNA 106b approximately 25 cluster and gastric cancer. *Surg Oncol.* (2013) 22:e7–10. doi: 10.1016/j.suronc.2013.01.003
43. Li N, Miao Y, Shan Y, Liu B, Li Y, Zhao L, et al. MiR-106b and miR-93 regulate cell progression by suppression of PTEN via PI3K/Akt pathway in breast cancer. *Cell Death Dis.* (2017) 8:e2796. doi: 10.1038/cddis.2017.119
44. Mehlich D, Garbicz F, Wlodarski PK. The emerging roles of the polycistronic miR-106b approximately 25 cluster in cancer—A comprehensive review. *Biomed Pharmacother.* (2018) 107:1183–95. doi: 10.1016/j.biopha.2018.08.097
45. Song HM, Luo Y, Li DF, Wei CK, Hua KY, Song JL, et al. MicroRNA-96 plays an oncogenic role by targeting FOXO1 and regulating AKT/FOXO1/Bim pathway in papillary thyroid carcinoma cells. *Int J Clin Exp Pathol.* (2015) 8:9889–900.
46. Hong Y, Liang H, Uzair Ur R, Wang Y, Zhang W, Zhou Y, et al. miR-96 promotes cell proliferation, migration and invasion by targeting PTPN9 in breast cancer. *Sci Rep.* (2016) 6:37421. doi: 10.1038/srep37421
47. Song CL, Zhang LJ, Wang J, Huang ZY, Li X, Wu MQ, et al. High expression of microRNA-183/182/96 cluster as a prognostic biomarker for breast cancer. *Sci Rep.* (2016) 6. doi: 10.1038/srep24502
48. Huang X, Lv W, Zhang JH, Lu DL. miR-96 functions as a tumor suppressor gene by targeting NUAK1 in pancreatic cancer. *Int J Mol Med.* (2014) 34:1599–605. doi: 10.3892/ijmm.2014.1940
49. Ress AL, Stiegelbauer V, Winter E, Schwarzenbacher D, Kiesslich T, Lax S, et al. MiR-96-5p influences cellular growth and is associated with poor survival in colorectal cancer patients. *Mol Carcinogenesis.* (2015) 54:1442–50. doi: 10.1002/mc.22218
50. Boren T, Xiong Y, Hakam A, Wenham R, Apte S, Wei ZZ, et al. MicroRNAs and their target messenger RNAs associated with endometrial carcinogenesis. *Gynecol Oncol.* (2008) 110:206–15. doi: 10.1016/j.ygyno.2008.03.023
51. Prado MM, Frampton AE, Giovannetti E, Stebbing J, Castellano L, Krell J. Investigating miRNA-mRNA regulatory networks using crosslinking immunoprecipitation methods for biomarker and target discovery in cancer. *Expert Rev Mol Diagnostics.* (2016) 16:1155–62. doi: 10.1080/14737159.2016.1239532
52. Luo D, Wilson JM, Harvel N, Liu J, Pei L, Huang S, et al. A systematic evaluation of miRNA:mRNA interactions involved in the migration and invasion of breast cancer cells. *J Transl Med.* (2013) 11:57. doi: 10.1186/1479-5876-11-57
53. Zhou X, Xu X, Wang J, Lin J, Chen W. Identifying miRNA/mRNA negative regulation pairs in colorectal cancer. *Sci Rep.* (2015) 5:12995. doi: 10.1038/srep12995
54. Andres-Leon E, Cases I, Alonso S, Rojas AM. Novel miRNA-mRNA interactions conserved in essential cancer pathways. *Sci Rep.* (2017) 7:46101. doi: 10.1038/srep46101
55. Santamaria PG, Moreno-Bueno G, Portillo F, Cano A. EMT: present and future in clinical oncology. *Mol Oncol.* (2017) 11:718–38. doi: 10.1002/1878-0261.12091
56. Baserga R. The contradictions of the insulin-like growth factor 1 receptor. *Oncogene.* (2000) 19:5574–81. doi: 10.1038/sj.onc.1203854
57. Tomasetti M, Nocchi L, Staffolani S, Manzella N, Amati M, Goodwin J, et al. MicroRNA-126 suppresses mesothelioma malignancy by targeting IRS1 and interfering with the mitochondrial function. *Antioxid Redox Signal.* (2014) 21:2109–25. doi: 10.1089/ars.2013.5215
58. Ye JJ, Cao J. MicroRNAs in colorectal cancer as markers and targets: recent advances. *World J Gastroenterol.* (2014) 20:4288–99. doi: 10.3748/wjg.v20.i15.4288
59. Yu Y, Li X, Liu L, Chai J, Haijun Z, Chu W, et al. miR-628 promotes burn-induced skeletal muscle atrophy via targeting IRS1. *Int J Biol Sci.* (2016) 12:1213–24. doi: 10.7150/ijbs.15496
60. Xu Y, Luo S, Liu Y, Li J, Lu Y, Jia Z, et al. Integrated gene network analysis and text mining revealing PIK3R1 regulated by miR-127 in human bladder cancer. *Eur J Med Res.* (2013) 18:29. doi: 10.1186/2047-783X-18-29
61. Yan LX, Liu YH, Xiang JW, Wu QN, Xu LB, Luo XL, et al. PIK3R1 targeting by miR-21 suppresses tumor cell migration and invasion by reducing PI3K/AKT signaling and reversing EMT, and predicts clinical outcome of breast cancer. *Int J Oncol.* (2016) 48:471–84. doi: 10.3892/ijo.2015.3287
62. Kim S, Lee E, Jung J, Lee JW, Kim HJ, Kim J, et al. microRNA-155 positively regulates glucose metabolism via PIK3R1-FOXO3a-cMYC axis in breast cancer. *Oncogene.* (2018) 37:2982–91. doi: 10.1038/s41388-018-0124-4

63. Fruman DA, Chiu H, Hopkins BD, Bagrodia S, Cantley LC, Abraham RT. The PI3K pathway in human disease. *Cell.* (2017) 170:605–35. doi: 10.1016/j.cell.2017.07.029
64. Murphy-Ullrich JE, Mosher DF. Localization of thrombospondin in clots formed *in situ*. *Blood.* (1985) 66:1098–104.
65. Schultzcherry S, Ribeiro S, Gentry L, Murphyullrich JE. Thrombospondin binds and activates the small and large forms of latent transforming growth-factor-beta in a chemically-defined system. *J Biol Chem.* (1994) 269:26775–82.
66. Bornstein P. Thrombospondins function as regulators of angiogenesis. *J Cell Commun Signal.* (2009) 3:189–200. doi: 10.1007/s12079-009-0060-8
67. Dogar AM, Semplicio G, Guennewig B, Hall J. Multiple microRNAs derived from chemically synthesized precursors regulate thrombospondin 1 expression. *Nucleic Acid Ther.* (2014) 24:149–59. doi: 10.1089/nat.2013.0467
68. Williams CM, Engler AJ, Slone RD, Galante LL, Schwarzbauer JE. Fibronectin expression modulates mammary epithelial cell proliferation during acinar differentiation. *Cancer Res.* (2008) 68:3185–92. doi: 10.1158/0008-5472.CAN-07-2673
69. Yen CY, Huang CY, Hou MF, Yang YH, Chang CH, Huang HW, et al. Evaluating the performance of fibronectin 1 (FN1), integrin alpha4beta1 (ITGA4), syndecan-2 (SDC2), and glycoprotein CD44 as the potential biomarkers of oral squamous cell carcinoma (OSCC). *Biomarkers.* (2013) 18:63–72. doi: 10.3109/1354750x.2012.737025
70. Gong J, Wang ZX, Liu ZY. miRNA-1271 inhibits cell proliferation in neuroglioma by targeting fibronectin 1. *Mol Med Rep.* (2017) 16:143–50. doi: 10.3892/mmr.2017.6610
71. Ding Y, Pan YH, Liu S, Jiang F, Jiao JB. Elevation of MiR-9-3p suppresses the epithelial-mesenchymal transition of nasopharyngeal carcinoma cells via down-regulating FN1, ITGB1 and ITGAV. *Cancer Biol Ther.* (2017) 18:414–24. doi: 10.1080/15384047.2017.1323585
72. Gunadi B, Budi NYP, Kalim AS, Santiko W, Musthofa FD, Iskandar K, et al. Aberrant expressions of miRNA-206 target, FN1, in multifactorial Hirschsprung disease. *Orphanet J Rare Dis.* (2019) 14:5. doi: 10.1186/s13023-018-0973-5

Conflict of Interest: The authors declare that the research was conducted in the absence of any commercial or financial relationships that could be construed as a potential conflict of interest.

frontiers in Oncology

ORIGINAL RESEARCH
published: 15 October 2019
doi: 10.3389/fonc.2019.01071

MiR-199a Inhibits Tumor Growth and Attenuates Chemoresistance by Targeting K-RAS via AKT and ERK Signalings

Wei Li[1†], Lin Wang[2†], Xiang-Bo Ji[2], Li-Hong Wang[2], Xin Ge[3], Wei-Tao Liu[3], Ling Chen[1], Zhong Zheng[1], Zhu-Mei Shi[3], Ling-Zhi Liu[4], Marie C. Lin[2], Jie-Yu Chen[1] and Bing-Hua Jiang[2,3,4*]*

[1] Department of Pathology, Affiliated Drum Tower Hospital of Nanjing University Medical School, Nanjing, China, [2] Institute of Medical and Pharmaceutical Sciences, The Academy of Medical Sciences, Zhengzhou University, Zhengzhou, China, [3] Key Laboratory of Human Functional Genomics of Jiangsu Province, Department of Pathology, Nanjing Medical University, Nanjing, China, [4] Department of Pathology, Carver College of Medicine, The University of Iowa, Iowa, IA, United States

OPEN ACCESS

Edited by:
Pascale Cohen,
Université Claude Bernard
Lyon 1, France

Reviewed by:
Jessica Dal Col,
University of Salerno, Italy
Vishwa Jeet Amatya,
Hiroshima University, Japan

***Correspondence:**
Jie-Yu Chen
crucianfish@hotmail.com
Bing-Hua Jiang
binghjiang@yahoo.com

[†] These authors have contributed equally to this work

Specialty section:
This article was submitted to Molecular and Cellular Oncology, a section of the journal Frontiers in Oncology

Received: 09 July 2019
Accepted: 30 September 2019
Published: 15 October 2019

Citation:
Li W, Wang L, Ji X-B, Wang L-H, Ge X, Liu W-T, Chen L, Zheng Z, Shi Z-M, Liu L-Z, Lin MC, Chen J-Y and Jiang B-H (2019) MiR-199a Inhibits Tumor Growth and Attenuates Chemoresistance by Targeting K-RAS via AKT and ERK Signalings. Front. Oncol. 9:1071. doi: 10.3389/fonc.2019.01071

Glioma is the most malignant brain tumors in the world, the function and molecular mechanism of microRNA-199a (miR-199a) in glioma is not fully understood. Our research aims to investigate miR-199a/K-RAS axis in regulation of glioma tumor growth and chemoresistance. The function of miR-199a in glioma was investigated through *in vitro* and *in vivo* assays. We found that miR-199a in tumor tissues of glioma patients was significantly downregulated in this study. Kinase suppressor of ras 1 (K-RAS), was indicated as a direct target of miR-199a, as well as expression levels of K-RAS were inversely correlated with expression levels of miR-199a in human glioma specimens. Forced expression of miR-199a suppressed AKT and ERK activation, decreased HIF-1α and VEGF expression, inhibited cell proliferation and cell migration, forced expression of K-RAS restored the inhibitory effect of miR-199a on cell proliferation and cell migration. Moreover, miR-199a renders tumor cells more sensitive to temozolomide (TMZ) via targeting K-RAS. *In vivo* experiment validated that miR-199a functioned as a tumor suppressor, inhibited tumor growth by targeting K-RAS and suppressed activation of AKT, ERK and HIF-1α expression. Taken together, these findings indicated that miR-199a inhibits tumor growth and chemoresistance by regulating K-RAS, and the miR-199a/K-RAS axis is a potential therapeutic target for clinical intervention in glioma.

Keywords: miR-199a, glioma, K-RAS, chemoresistance, tumorigenesis

INTRODUCTION

Malignant gliomas, as most common brain tumors around the world (1, 2), are classified according to their degree of malignancy as Grades I to IV (3, 4). Glioma clinical treatment includes surgery, chemotherapy and radiotherapy (5, 6). The most malignant grade IV glioma, glioblastomamultiforme (GBM), has an average life expectancy of only 15 months (7). Investigation of glioma carcinogenesis mechanisms would improve clinical diagnosis, drug therapy and prevention of glioma.

MicroRNAs (miRNAs) are a class of endogenous 18–22 nucleotides RNA molecules (8, 9), which always bind to the 3′-untranslated region (UTR) of specific target mRNAs, and then regulate

expression of several genes at the post-transcriptional level (10–14). Accumulated evidence has clearly demonstrated that aberrant miRNA expression profiles (15) and dysregulations of specific miRNAs and their target genes, are closely associated with tumor initiation and promotion in glioma (16, 17). In particular, the miR-199a has demonstrated to suppress tumor growth in a variety of cancers including esophageal, liver, and colorectal cancers. So far, the reported miR-199a downstream target genes include oncogenes PHLPP1, E2F3, FZD6/7, HK2, and MAP3K11 (18–23), which are functioned in pathogenesis of various cancers.

K-RAS, which is reported as a family member of Ras oncogene, has involved in regulation of some cellular signal transductions (24). K-RAS is implicated in the pathogenesis of various tumors, such as GBM and pilocytic astrocytoma (25, 26). Activation of K-RAS could promote the activations of several downstream molecules, such as MAPK and ERK to regulate biological processes (27, 28).

In this study for the first time in glioma, we demonstrated the loss of miR-199a, and that K-RAS is an important direct target gene of miR-199a. Results from *in vitro* studies in human glioma U87 and U251 cells indicated that forced expression of miR-199a downregulated K-RAS signaling and suppressed cancer development and Temozolomide (TMZ) chemoresistance. The forced miR-199a overexpression also inhibited AKT and ERK1/2 pathways, through K-RAS signaling. The *in vivo* studies further demonstrated that over-express of miR-199a exhibited reduced tumor growth with down-regulated K-RAS/AKT/ERK/HIF-1α signalings. These results suggested that the loss of miR-199a/K-RAS signaling in glioma plays a pivotal role in glioma progression, and it is a potential novel targets for future clinical treatment.

MATERIALS AND METHODS

Specimen Collection

Human glioma specimens ($n = 24$) and normal brain tissues ($n = 9$) were collected from patients in Nanjing University Medical School, China. Samples were obtained from patients with informed consents and were histologically classified by clinical pathologist.

Cell Culture and Reagents

Human glioma cells (U87, U251) were cultured in DMEM medium. Antibodies against anti-GAPDH and anti-HIF-1α were purchased from Bioworld Technology (Atlanta, USA). Antibodies against anti-p-AKT (Ser473), anti-AKT, anti-p-ERK1/2 and anti-ERK1/2 were purchased from Cell Signaling Technology (Danvers, USA), and antibody against K-RAS was purchased from Santa Cruz (Santa Cruz, USA). TMZ (Sigma-Aldrich, USA) was used for *in vitro* chemosensitivity assay.

Real-Time PCR

RNAs were isolated from human specimens and cells using Trizol (Invitrogen, USA). To measure expression levels of miR-199a (U6 as internal control) and mRNA levels of K-RAS(GAPDH as internal control), the cDNAs were amplified by Real-time PCR with SYBR Green reagents (Vazyme, China) on a 7900HT system(Applied Biosystems), and fold changes were analyzed by relative quantification ($2^{-\Delta\Delta Ct}$).

Primers for K-RAS and GAPDH as below:

K-RAS: Forward Primer: ACAGAGAGTGGAGGATGCTTT, Reverse Primer: TTTCACACAGCCAGGAGTCTT; GAPDH: Forward Primer: ACAACTTTGGTATCGTGGAAGG, Reverse Primer: GCCATCACGCCACAGTTTC.

Immunoblotting

According to the manufacturer's instruction, cell lysates in this study were prepared using RIPA buffer and indicated protease inhibitors. Aliquots of protein lysates from treated cells were fractionated by SDS-PAGE, after electrophoresis, transferred to a PVDF membrane (Roche, Switzerland), and then subjected to immunoblotting analysis.

Cell Proliferation Assay

Indicated miR-NC and miR-199a stable cell lines were plated for 2×10^3 cells per well. To evaluate the proliferation activity

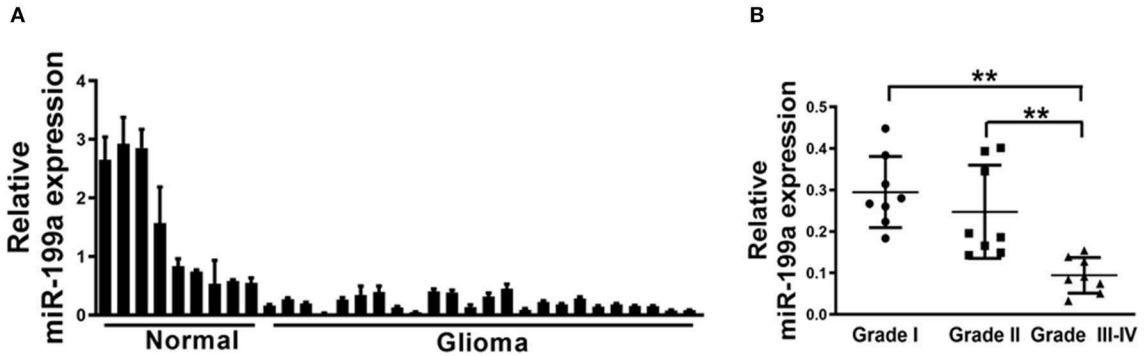

FIGURE 1 | Loss of MiR-199a in human glioma specimens. **(A)** Relative miR-199a expression levels were analyzed by Real-time RT-PCR in glioma specimens ($n = 24$) and adjacent normal tissues ($n = 9$). U6 RNA levels were used as an internal control; **(B)** Relative expression levels of miR-199a in cancer tissues at Grades I, II and III-IV (for each grade, $n = 8$). Data represent mean ± SD. from three replicates. **Indicates significant difference at $p < 0.01$ when compared Grade I or Grade II group with Grade III–IV group.

of miR-199a in glioma cells, according to the manufacturer's instruction, cell proliferation rate was analyzed with CCK-8 kit (Dojindo Laboratories, Japan).

Migration Assay

Migration assay was conducted with migration chambers (BD Biosciences, UK). 5×10^4 cells were plated per well in the upper chamber without serum, and the lower chamber was filled with DMEM medium with 10% FBS. 18–20 h later, the bottom cells were fixed and stained, while non-invading cells were removed. Finally, cells were extracted by 33% acetic acid and quantitatively detected (OD at 570 nm).

Luciferase Reporter Assay

3′-UTR region of K-RAS containing software predicted miR-199a-matching seed sites (WT) and corresponding mutant sites (mut) were amplified by High fidelity PCR, and inserted into pMIR-REPORTER vector (Ambion, USA). Dual-luciferase activities were analyzed in U87 cells by the Reporter Assay (Promega, USA).

Apoptosis Assay

Apoptosis assay (BD Pharmingen) in indicated cells were conducted according to the manufacturer's instruction with AnnexinV staining. Then samples were analyzed by flow cytometry (FACS Canto II, BD Biosciences). These data were analyzed by FlowJo software.

In vivo Tumor Growth Assay

Nude mice (4-weeks-old) were purchased from Animal Center (Shanghai, China), and then bred in special pathogen-free condition. Cells (5×10^6) were then injected subcutaneously into the posterior flanks of each nude mouse. Tumor sizes were measured by vernier caliper using the formula, that is volume

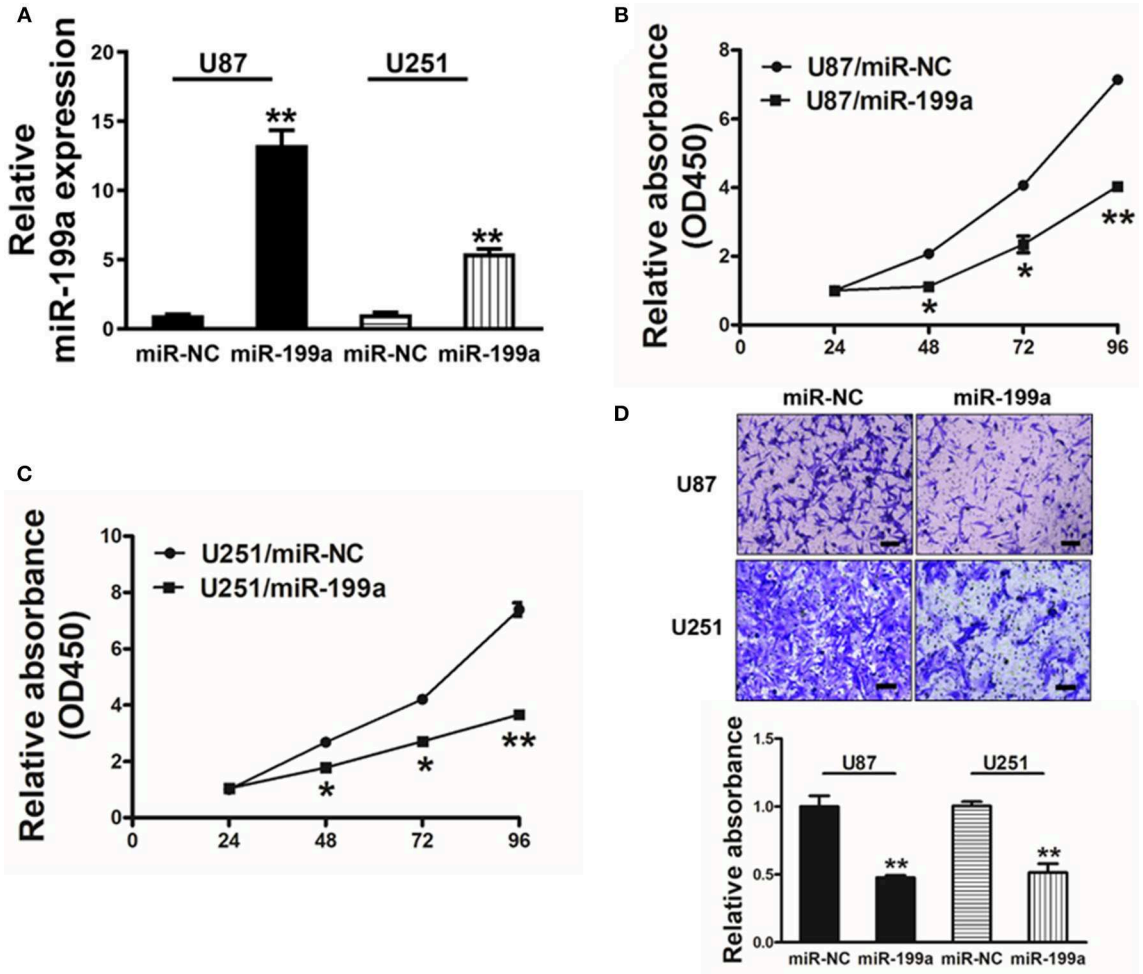

FIGURE 2 | Forced overexpression of miR-199a inhibited cell proliferation and migration in human glioma U87 and U251 cells. **(A)** Relative expression levels of miR-199a in U87 and U251 stable cell lines were determined by real-time RT-PCR; **(B,C)** Cells were plated with 2,000 cells per well in 96-well plates, and cell proliferation was determined using Cell Counting Kit-8 (CCK-8) by detecting the absorbance at 450 nm at indicated time points; **(D)** Migration assay of cells were performed as previously described. Data represent mean ± SD. from three replicates. *Indicates significant difference at $p < 0.05$ when compared to miR-NC group; **Indicates significant difference at $p < 0.01$ when compared to miR-NC group.

$= 0.5 \times (\text{Length} \times \text{Width}^2)$. Twenty-four days later, mice were sacrificed as well as tumors were dissected. All mice used in this study were sacrificed according to the institutional guidelines and regulations.

Statistical Analysis

All cellular experiments were performed three times. Data were analyzed with GraphPad Prism 5 software. The correlations between miR-199a and K-RAS in human glioma tissues were analyzed by Pearson's test. The differences were considered as statistically significant at $P < 0.05$ by t-test.

RESULTS

Loss of MiR-199a in Human Glioma Specimens

Since mechanism of miR-199a is not fully understood in glioma, qRT-PCR analysis was then performed to determine indicated

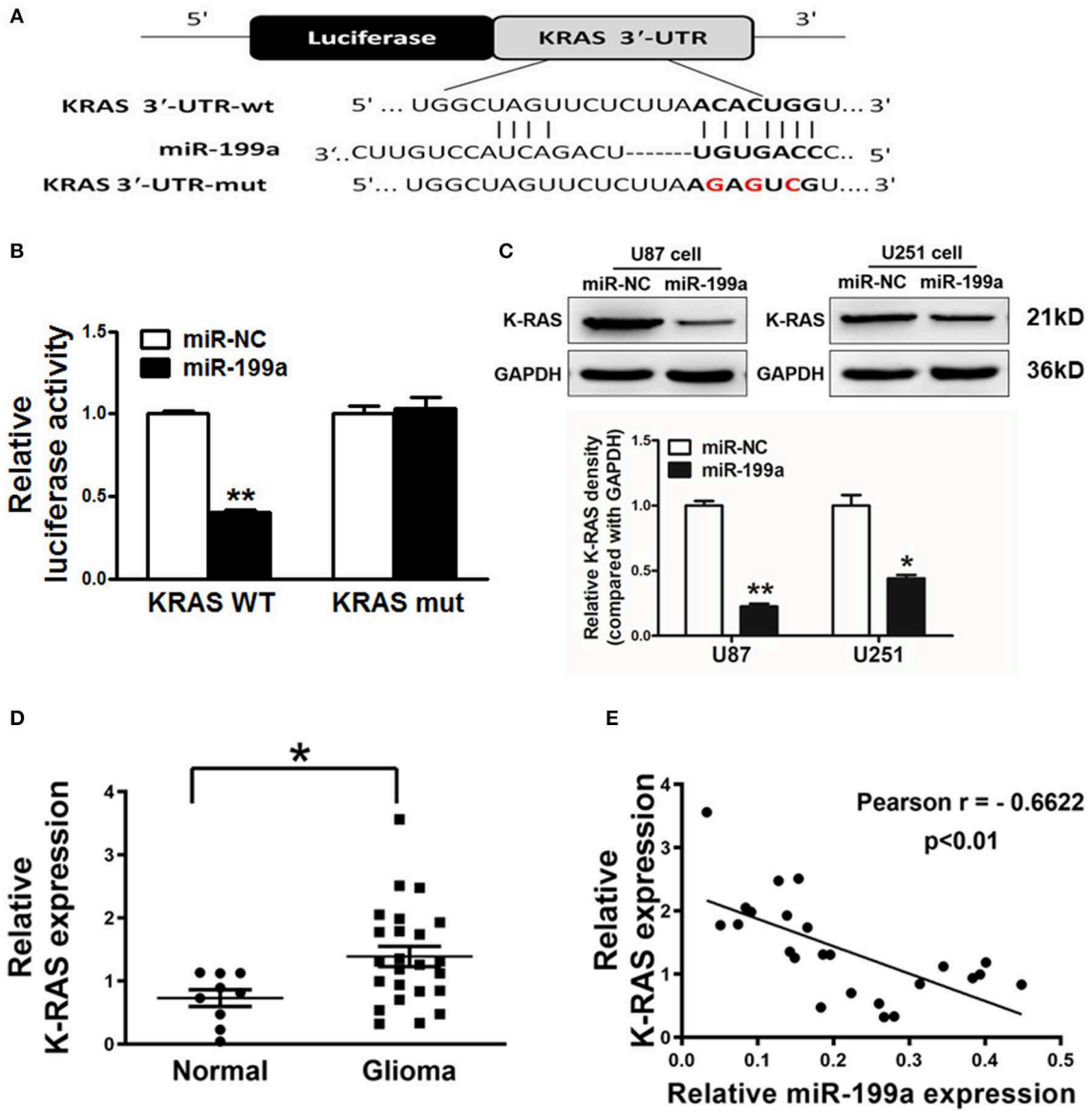

FIGURE 3 | K-RAS is a direct target of miR-199a, and there is a inverse correlation between the expression levels of K-RAS and miR-199a in tumor tissues. **(A)** The complementary pairings of miR-199a with K-RAS wild-type (WT) and mutant (mut) 3′-UTR reporter constructs are shown. The mutant nucleotides of the K-RAS 3′-UTR region were labeled in red; **(B)** U87 cells were co-transfected with the reporter constructs containing the WT or mut K-RAS 3′-UTR, miR-NC or miR-199a and pRL-TK plasmids. The luciferase activities were analyzed 24 h after the transfection; **(C)** U87 cells were transfected with miR-199a or miR-NC as above. After 72 h, the expression levels of K-RAS and GAPDH in the cells were determined using immunoblotting assay; **(D)** The expression levels of K-RAS in normal tissues and human glioma specimens were determined by RT-qPCR analysis, and fold changes were obtained by the ratios of K-RAS to GAPDH levels; **(E)** Pearson's correlation analysis was used to determine the correlation between expression levels of K-RAS and miR-199a in human glioma specimens. These data are means ± SD. from separate experiments. *Indicates significant difference at $p < 0.05$; **Indicates significant difference at $p < 0.01$.

expression levels of miR-199a in human glioma specimens. The results clarified that miR-199a expression in tumor ($n = 24$) tissues were significantly lower, as compared to normal ($n = 9$) tissues (**Figure 1A**). Furthermore, in tumor tissues of glioma patients, we showed that miR-199a expression were correlated with the clinical stages, which indicated that miR-199a in high grade tumors ($n = 8$, WHO Grades III-IV) were significantly lower when compared to those in low grade tumors ($n = 8$, WHO Grade I and $n = 8$, WHO Grade II) (**Figure 1B**). Thus, our results indicated that miR-199a may be a potential novel biomarker for glioma staging.

Forced Overexpression of miR-199a Inhibited Cell Proliferation and Migration Activity in Human Glioma U87 and U251 Cells

To overexpress miR-199a, human glioma cells U87 and U251 were infected with lentivirus expressing miR-199a, and lentivirus expressing miR-NC was used as control. Stable cell lines which termed as U87/miR-NC, U87/miR-199a, U251/miR-NC, and U251/miR-199a were established after puromycin selection, and higher miR-199a expression in U87/miR-199a and U251/miR-199a were demonstrated by qRT-PCR (**Figure 2A**). Overexpression of miR-199a markedly attenuated cell proliferation activity in U87/miR-199a (**Figure 2B**) and U251/miR-199a cells (**Figure 2C**). In addition, forced expression of miR-199a markedly reduced cell migration activity (**Figure 2D**). These results are consistent with the tumor suppressor activities of miR-199a in glioma cells.

K-RAS Is a Direct Target of miR-199a

TargetScan software was used to predict the direct targets of miR-199a, and K-RAS was found to be a potential target (**Figure 3A**). We constructed luciferase reporter plasmids with either the putative K-RAS wild-type binding sites (WT) or seed sequence mutant sites (mut). Luciferase assay were used to investigate whether the K-RAS is a candidate target of miR-199a. Our results clarified that overexpressing miR-199a in U87 cells reduced the luciferase activity of WT K-RAS reporter by 65%, whereas it did not change the mutant luciferase activities (**Figure 3B**). Furthermore, forced overexpression of miR-199a significantly attenuated protein expression of K-RAS in U87 and U251 cells (**Figure 3C**), suggesting that in human glioma cells, miR-199a targets K-RAS directly by binding with its 3′-UTR.

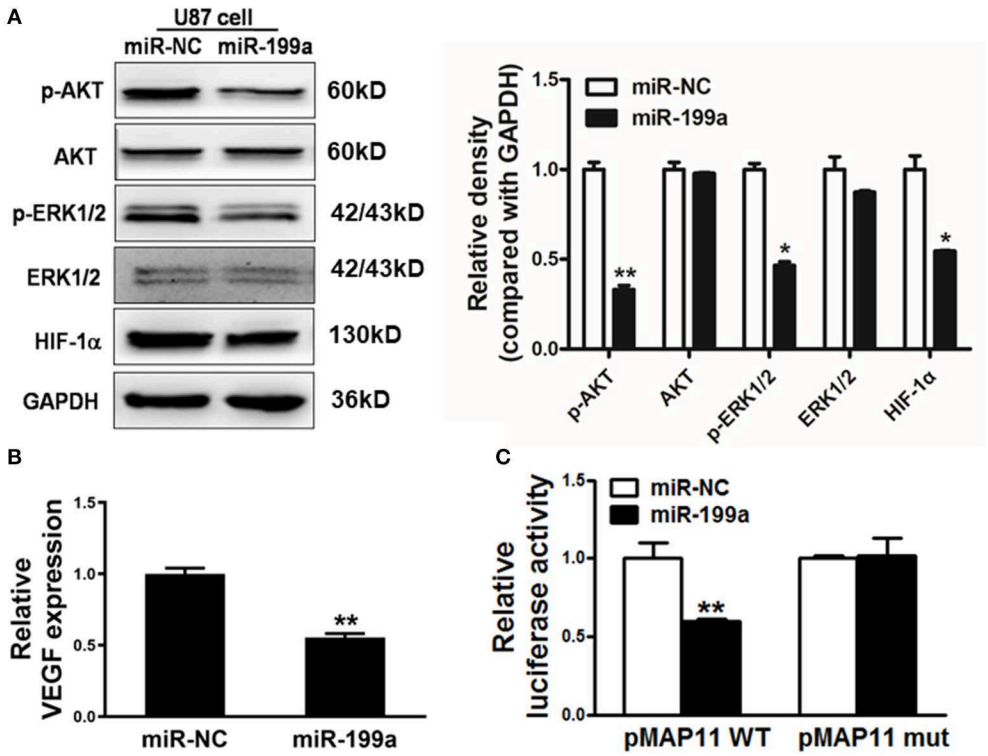

FIGURE 4 | MiR-199a inhibited AKT and ERK1/2 pathways as well as the expression of HIF-1α and VEGF. **(A)** The expression levels of phosphorylated AKT (p-AKT), phosphorylated ERK1/2 (p-ERK1/2), total AKT, total ERK1/2 and HIF-1α in cells were detected by immunoblotting assay; **(B)** VEGF levels were measured by RT-qPCR in stable cell lines overexpressing miR-NC or miR-199a and normalized to level of GAPDH. *Indicates significant difference at $p < 0.05$ when compared to miR-NC group; **(C)** The wild type VEGF reporter plasmid pMAP11-WT or mutant reporter plasmid pMAP11-mut was co-transfected with pRL-TK plasmid and miR-NC or miR-199a. Firefly and Renilla luciferase activities were measured 24 h later. Data represent mean ± SD. of three replicates. **Indicates significant difference at $p < 0.01$ when compared to miR-NC group.

Inverse Correlations of Lower miRNA-199a and Higher K-RAS Levels in Human Glioma Patient Tissues

To further support the notion that K-RAS oncogene is a direct target, we tested expression levels of K-RAS in human glioma specimens. Our results clarified that K-RAS expression levels were significantly higher in tumor tissues compared with normal tissues (**Figure 3D**). Furthermore, we determined the correlation between miR-199a and K-RAS oncogene levels in human glioma specimens using Pearson's correlation analysis. Inverse correlation in **Figure 3E** was found between K-RAS and miR-199a in the human glioma specimens (Pearson's correlation, $r = -0.6622$).

Forced Expression of miR-199a Reduced Activation of K-RAS Downstream Molecules AKT and ERK1/2 as Well as HIF-1α and VEGF Expression Levels in U87 Cells

The downstream molecules of RAS signaling are AKT and ERK1/2, which are linked to effectors, such as hypoxia-inducible factor 1α (HIF-1α) as well as vascular endothelial growth factor (VEGF). We found that overexpression of miR-199a in U87 cells dramatically suppressed AKT and ERK1/2 activation as indicated by significantly reduced phosphorylated AKT and ERK1/2 levels and a reduction of HIF-1α protein level without change of total protein levels (**Figure 4A**).

Accumulated research have shown the importance role of HIF-1α/VEGF in the regulation of glioma angiogenesis (29, 30). Our previous study has reported that HIF-1α promotes VEGF gene expression through binding to the hypoxia response element (HRE) in the promoter region of VEGF. In addition to decreased HIF-1α, we also detected a significant reduction of VEGF mRNA levels in miR-199a-expressing U87 cells (**Figure 4B**). To test whether miR-199a inhibited VEGF expression through HIF-1α, we analyzed and compared effects of miR-199a on (1) a VEGF promoter reporter plasmid (pMAP11WT) containing the HIF-1α binding site, and (2) a mutant (pMAP11 mut) plasmid with mutation, overexpression of miR-199a inhibited the luciferase activities of the VEGF promoter reporter plasmid as shown in **Figure 4C**. Thus, our results indicated that miR-199a suppressed the gene expression of VEGF through HIF-1α.

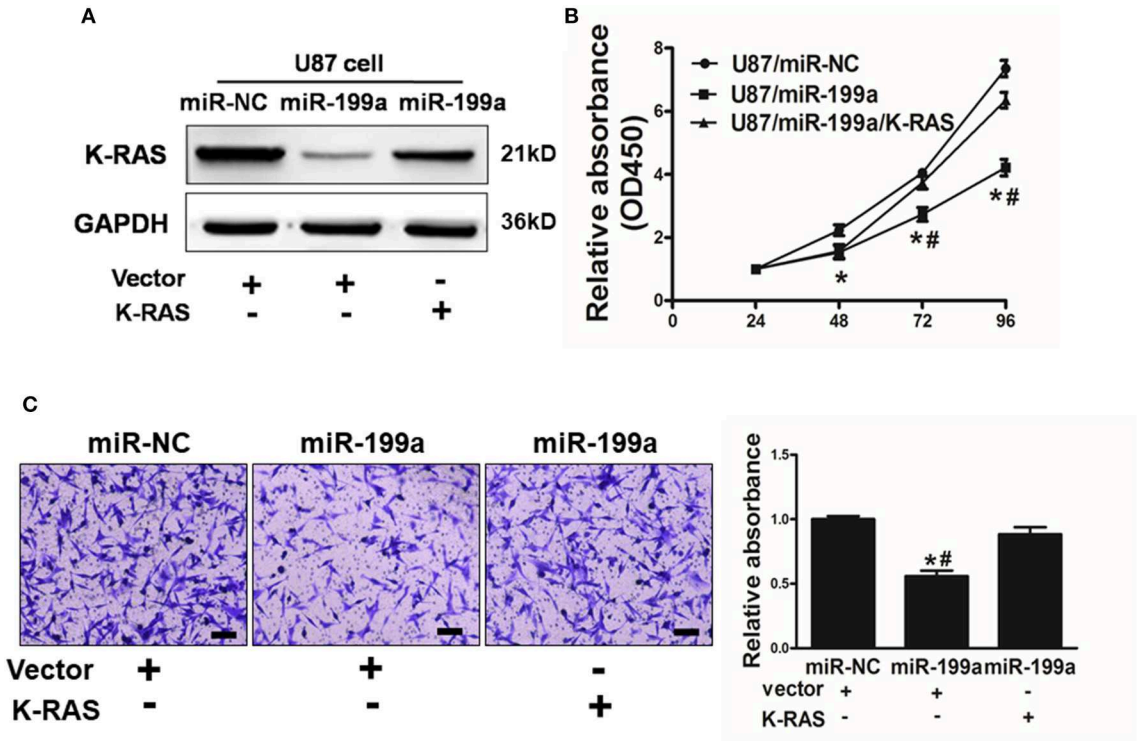

FIGURE 5 | Overexpression of K-RAS cDNA reversed miR-199a-suppressed cell proliferation and cell migration. **(A)** U87 cells were co-transfected with miR-199a precursor or miR-NC, and empty vector or K-RAS cDNA without 3′-UTR. After 72 h, immunoblotting assay was performed as described above; **(B)** Cells were treated as above, and cell proliferation assay was determined using CCK-8 kit; **(C)** U87 cells overexpressing miR-NC or miR-199a were treated as described above, cell migration was determined using 24-well BD migration chambers and quantified using a standard microplate reader (OD at 570 nm). Data represent mean ± SD. of three replicates. *Indicates significant difference at $p < 0.05$ compared to miR-NC control; #Indicates significant difference at $p < 0.05$ compared to miR-199a and K-RAS overexpression group.

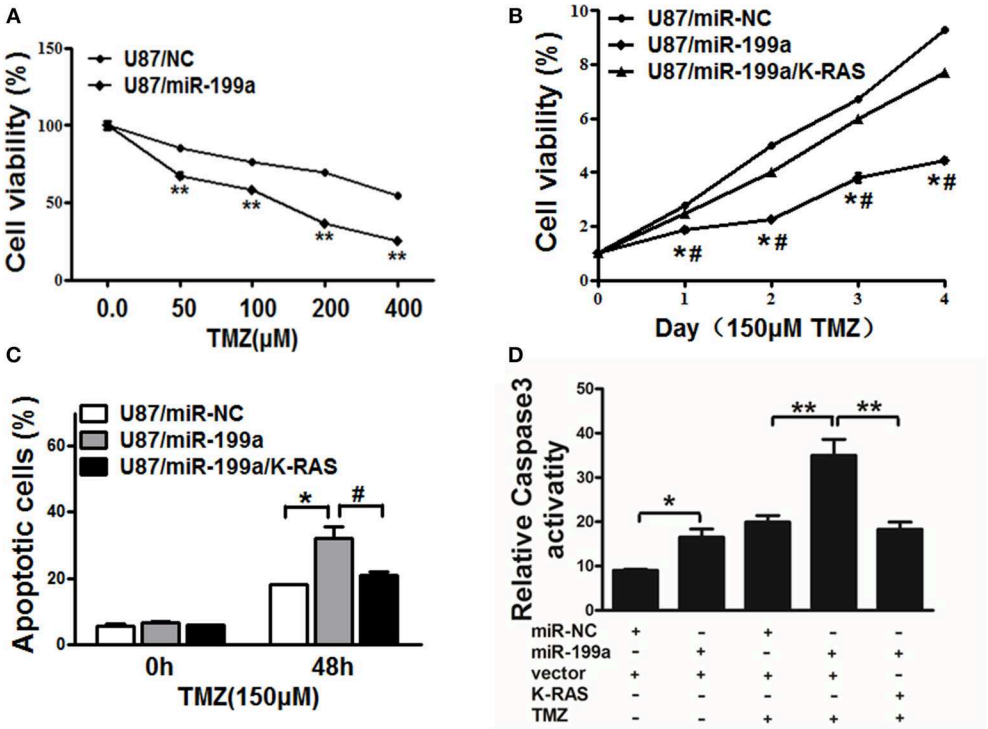

FIGURE 6 | MiR-199a increased TMZ chemosensitivity by targeting K-RAS in glioma cells. **(A)** U87 cells stably expressing miR-NC or miR-199a were treated with different concentrations of TMZ for 48 h, and cell viability was analyzed using CCK-8 assay; **(B)** U87 cells stably expressing miR-NC, miR-199a, or miR-199a in combination with K-RAS overexpression were treated with 150 μM of TMZ for indicated time points. Cell viability was analyzed by CCK-8 assay; **(C,D)** Cell apoptosis was analyzed by flow cytometry and by caspase-3 assay. Data represent mean ± SD. from three replicates. *Indicates significant difference at $p < 0.05$ compared to miR-NC control; **Indicates significant difference at $p < 0.01$ compared to miR-NC control; #Indicates significant difference at $p < 0.05$ compared to miR-199a and K-RAS overexpression group.

Restoration of K-RAS Reversed miR-199a Mediated Suppression on Cell Proliferation and Migration

To further demonstrate the role of K-RAS in miR-199a mediated effects on cell proliferation and migration, U87/miR-NC cells or U87/miR-199a cells were co-transfected with control vector (Vector) or K-RAS without 3′-UTR. miR-199a reduced K-RAS expression significantly, and forced expression of K-RAS restored K-RAS expression as shown in **Figure 5A**. We also determined the effect on cell proliferation activity. As shown in **Figure 5B**, U87/miR-199a cells has significantly reduced cell proliferation rate, while overexpressing K-RAS in U87/miR-199a cells (U87/miR-199a/K-RAS), restored the cell proliferation rate. The cell migration was determined and quantified by a microplate reader using migration chambers (OD at 570 nm). As we expected, overexpression of K-RAS (U87/miR-199a/K-RAS) restored miR-199a-inhibited cell migration activity (**Figure 5C**). To sum up, these results suggested that miR-199a suppresses human glioma cell proliferation and migration, and forced expression of K-RAS reversed miR-199a effects.

Overexpression of miR-199a Rendered Cells More Sensitive to TMZ Through Targeting K-RAS

TMZ chemoresistance is the major obstacle in process of glioma chemotherapy. In this study, U87/miR-NC cells or U87/miR-199a were treated with TMZ at different concentrations for 2 days, as shown in **Figure 6A**, U87/miR-199a cells were significantly more sensitive to TMZ treatment. Furthermore, overexpressing K-RAS in U87/miR-199a cells (U87/miR-199a/K-RAS) nearly completely reversed the chemosensitivity to TMZ treatment (**Figure 6B**). We further investigated the role of miR-199a/K-RAS axis in TMZ mediated apoptosis by apoptosis analysis and caspase-3 activity assay. As shown in **Figure 6C**, TMZ treatment produced significantly higher apoptotic cell population in U87/miR-199a cells as compare to the control U87/miR-NC cells. Forced expression of K-RAS in U87/miR-199a cells (U87/miR-199a/K-RAS) nearly completely reversed the effect. Moreover, activities of caspase-3 were determined. As shown in **Figure 6D**, compared to the negative control (Bar 1, U87/miR-NC), overexpression of miR-199a (Bar 2, U87/miR-199a) significantly increased caspase 3 activity. TMZ treatmentof

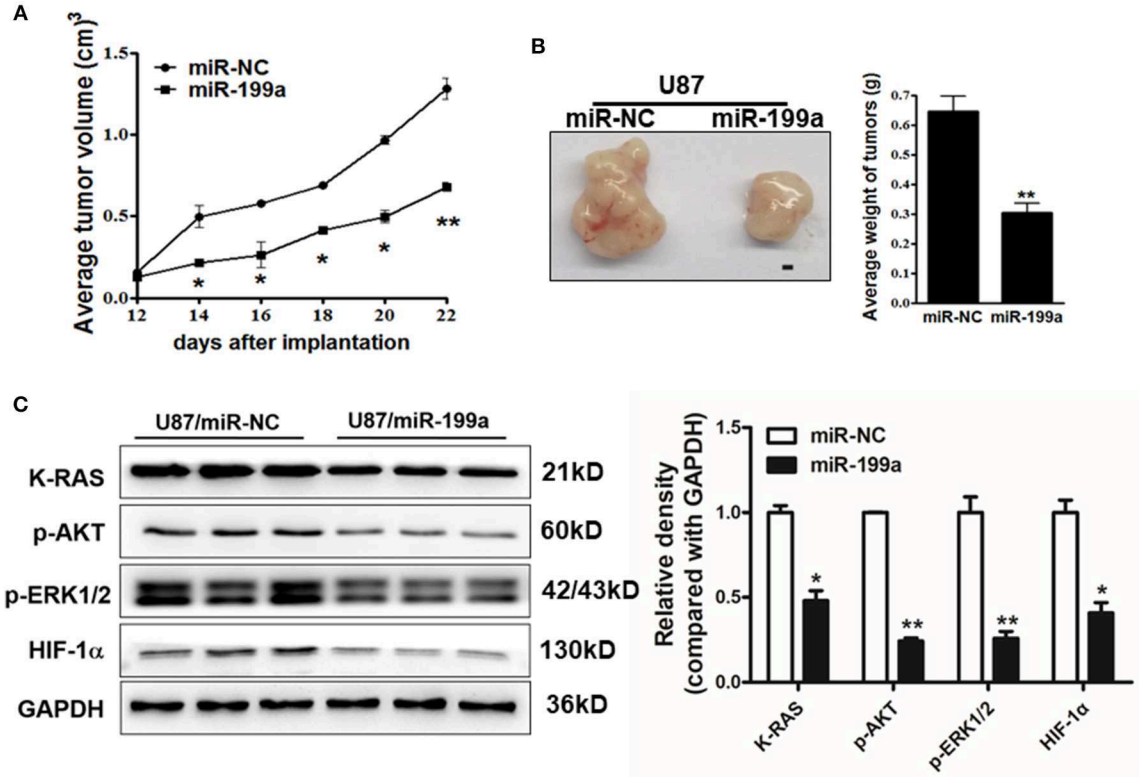

FIGURE 7 | MiR-199a overexpression suppressed tumor growth and decreased expression levels of K-RAS and its downstream molecules in tumor tissues. **(A)** U87/miR-199a or U87/miR-NC cells (5×10^6 cells) were dispersed in 100 μl of serum-free DMEM medium, and subcutaneously injected into posterior flanks of the nude mice ($n = 5$). Tumors were measured every 2 days after they were apparently detectable on Day 12. Tumor volumes were calculated using the following formula: volume = 0.5 × (length × width^2); **(B)** Mice were sacrificed 24 days after implantation, tumors were harvested and photographed. Representative pictures from each group were shown (Bar = 1 mm) and tumors were weighted; **(C)** Total proteins were extracted from xenografts and subjected to immunoblotting assay to test K-RAS, p-AKT, p-ERK1/2, HIF-1α, and GAPDH expression levels. Data were presented mean ± SD. *Indicates significant difference at $p < 0.05$ when compared to miR-NC group; **Indicates significant difference at $p < 0.01$ when compared to miR-NC group.

control U87/miR-NC cells increased caspase3 activity (Bar 3, U87/miR-NC + TMZ), and TMZ treatment of U87/miR-199a cells strongly and significantly increased caspase3 activity (Bar 4, U87/miR-199a + TMZ). In addition, overexpression of K-RAS in U87/miR-199a cells attenuated the activation of caspase-3 (Bar 5, U87/miR-199a/K-RAS + TMZ). To sum up, our results showed that miR-199a rendered glioma cells more sensitive to TMZ through targeting K-RAS.

MiR-199a Suppressed Tumor Growth *in vivo*

To determine whether over-expression of miR-199a inhibited tumor growth *in vivo*, U87/miR-NC cells and U87/miR-199a cells were injected into immunodeficient nude mice. After cell injection, tumor sizes were measured. Compared to control mice injected with U87/miR-NC cells, mice injected with U87/miR-199a cells developed significantly smaller tumors from Day 14 (**Figure 7A**). Twenty-four days later, Mice were sacrificed after implantation, tumors were harvested, photographed, and weighed. A pair of representative tumors trimmed out from U87/miR-199a and U87/miR-NC groups, and the average tumor weight were shown in **Figure 7B**. Forced expression of miR-199a produced tumors with significantly lower tumor weight. We also determined the protein levels of K-RAS, p-AKT, p-ERK1/2 and HIF-1α in tumor tissues, and found that these proteins from U87/miR-199a group were significantly lower than that of U87/miR-NC group, which is consistent with *in vitro* data (**Figure 7C**). Our results suggested that miR-199a inhibited tumor growth by inhibiting K-RAS expression and its downstream molecules.

DISCUSSION

MicroRNAs (miRNAs) in diverse human cancers have been frequently indicated to be dysregulated (31, 32). The miR-199a have reported to be downregulated in multiple malignancies (33–35). We first demonstrated that expression levels of miR-199a was downregulated in clinical glioma samples, and function as a tumor suppressor to increase sensitivity to treatment.

The reported miR-199a targets include GRP78, GSK-3β, Discoidin domain receptor 1 (DDR1), mTOR, CD44, and IκB kinase-beta. It works through targeting GRP78, a major

endoplasmic reticulum chaperone, in prostate cancer cells to induce apoptosis and increase sensitivity to trichostatin A, the histone deacetylase inhibitor (36); through GSK-3β in renal cell cancer cells to decreases cell proliferation (37); through a receptor tyrosine kinase DDR1, to suppress invasiveness and migratory ability of colorectal cancer cells (38); through the mTOR and CD44 to increase sensitivity to cisplatin treatment and to reduce the number of ovarian cancer stem cells (39, 40). Finally, it works through targeting IκB kinase-beta to increase TNF-α-induced ovarian cancer cell apoptosis (41). Here, we first identified K-RAS as a novel target of miR-199a. We also confirm the inverse correlation between miR-199a and K-RAS levels in glioma specimens.

Temozolomide (TMZ) is a first-line drug for glioma treatment. A recent study has shown that miR-29c contributed to sensitize cells to temozolomide treatment by targeting O^6-methylguanine-DNA methyltransferases in glioma (42). On the other hand, miR-423-5p was reported to function as a oncogene and promoted chemoresistance to temozolomide in glioblastomas (43). Here we found that overexpression of miR-199a rendered cells more sensitive to TMZ through its target K-RAS. Thus, miR-199a/K-RAS signaling may be a potential new target to overcome chemoresistance to TMZ in glioma.

CONCLUSIONS

To sum up, we have clarified that K-RAS is a novel direct target of miR-199a. MiR-199a inhibit activity of cell proliferation, cell migration, drug chemoresistance and tumor growth by regulating K-RAS via AKT and ERK signalings. These results elucidated that miR-199a/K-RAS in the future may be used as a target for glioma treatment.

DATA AVAILABILITY STATEMENT

The datasets generated for this study are available on request to the corresponding author.

ETHICS STATEMENT

The studies involving human participants were reviewed and approved by Ethics Committee of Nanjing University. The patients/participants provided their written informed consent to participate in this study. The animal study was reviewed and approved by Ethics Committee of Nanjing University.

AUTHOR CONTRIBUTIONS

WL, LW, and XG carried out the samples collection and performed the experiments. X-BJ and L-HW revised the manuscript. W-TL, LC, ZZ, Z-MS, L-ZL, and ML designed the studies. WL, LW, J-YC, and B-HJ wrote the manuscript.

FUNDING

This work was supported in part by National Natural Science Foundation of China (81502170, 81772951, 81803197).

REFERENCES

1. Chen J, Li Y, Yu TS, McKay RM, Burns DK, Kernie SG, et al. A restricted cell population propagates glioblastoma growth after chemotherapy. *Nature.* (2012) 488:522–6. doi: 10.1038/nature11287
2. Del Vecchio CA, Li G, Wong AJ. Targeting EGF receptor variant III: tumor-specific peptide vaccination for malignant gliomas. *Expert Rev Vaccines.* (2012) 11:133–44. doi: 10.1586/erv.11.177
3. Fuller GN, Scheithauer BW. The 2007 Revised World Health Organization (WHO) classification of tumours of the central nervous system: newly codified entities. *Brain Pathol.* (2007) 17:304–7. doi: 10.1111/j.1750-3639.2007.00084.x
4. Louis DN, Ohgaki H, Wiestler OD, Cavenee WK, Burger PC, Jouvet A, et al. The 2007 WHO classification of tumours of the central nervous system. *Acta Neuropathol.* (2007) 114:97–109. doi: 10.1007/s00401-007-0243-4
5. Zhang L, Wu X, Xu T, Luo C, Qian J, Lu Y. Chemotherapy plus radiotherapy versus radiotherapy alone in patients with anaplastic glioma: a systematic review and meta-analysis. *J Cancer Res Clin Oncol.* (2013) 139:719–26. doi: 10.1007/s00432-013-1387-3
6. Van Meir EG, Hadjipanayis CG, Norden AD, Shu HK, Wen PY, Olson JJ. Exciting new advances in neuro-oncology: the avenue to a cure for malignant glioma. *CA Cancer J Clin.* (2010) 60:166–93. doi: 10.3322/caac.20069
7. Wen PY, Kesari S. Malignant gliomas in adults. *N Engl J Med.* (2008) 359:492–507. doi: 10.1056/NEJMra0708126
8. Jiang CF, Shi ZM, Li DM, Qian YC, Ren Y, Bai XM, et al. Estrogen-induced miR-196a elevation promotes tumor growth and metastasis via targeting SPRED1 in breast cancer. *Mol Cancer.* (2018) 17:83. doi: 10.1186/s12943-018-0830-0
9. Niu XB, Fu GB, Wang L, Ge X, Liu WT, Wen YY, et al. Insulin-like growth factor-I induces chemoresistence to docetaxel by inhibiting miR-143 in human prostate cancer. *Oncotarget.* (2017) 8:107157–66. doi: 10.18632/oncotarget.22362
10. Ambros V, Lee RC. Identification of microRNAs and other tiny noncoding RNAs by cDNA cloning. *Methods Mol Biol.* (2004) 265:131–58. doi: 10.1385/1-59259-775-0:131
11. Pillai RS, Bhattacharyya SN, Filipowicz W. Repression of protein synthesis by miRNAs: how many mechanisms? *Trends Cell Biol.* (2007) 17:118–26. doi: 10.1016/j.tcb.2006.12.007
12. Thai TH, Christiansen PA, Tsokos GC. Is there a link between dysregulated miRNA expression and disease? *Discov Med.* (2010) 10:184–94.
13. German MA, Pillay M, Jeong DH, Hetawal A, Luo S, Janardhanan P, et al. Global identification of microRNA-target RNA pairs by parallel analysis of RNA ends. *Nat Biotechnol.* (2008) 26:941–6. doi: 10.1038/nbt1417
14. Bartel DP. MicroRNAs: genomics, biogenesis, mechanism, and function. *Cell.* (2004) 116:281–97. doi: 10.1016/s0092-8674(04)00045-5
15. Gibson NW. Engineered microRNA therapeutics. *J R Coll Physicians Edinb.* (2014) 44:196–200. doi: 10.4997/JRCPE.2014.302
16. Wang L, Shi ZM, Jiang CF, Liu X, Chen QD, Qian X, et al. MiR-143 acts as a tumor suppressor by targeting N-RAS and enhances temozolomide-induced apoptosis in glioma. *Oncotarget.* (2014) 5:5416–27. doi: 10.18632/oncotarget.2116
17. Shi Z, Chen Q, Li C, Wang L, Qian X, Jiang C, et al. MiR-124 governs glioma growth and angiogenesis and enhances chemosensitivity by targeting R-Ras and N-Ras. *Neuro Oncol.* (2014) 16:1341–53. doi: 10.1093/neuonc/nou084
18. Byrnes KA, Phatak P, Mansour D, Xiao L, Zou T, Rao JN, et al. Overexpression of miR-199a-5p decreases esophageal cancer cell proliferation through repression of mitogen-activated protein kinase kinase kinase-11 (MAP3K11). *Oncotarget.* (2016) 7:8756–70. doi: 10.18632/oncotarget.6752
19. Guo W, Qiu Z, Wang Z, Wang Q, Tan N, Chen T, et al. MiR-199a-5p is negatively associated with malignancies and regulates glycolysis and lactate

production by targeting hexokinase 2 in liver cancer. *Hepatology*. (2015) 62:1132–44. doi: 10.1002/hep.27929
20. Kim BK, Yoo HI, Kim I, Park J, Kim Yoon S. FZD6 expression is negatively regulated by miR-199a-5p in human colorectal cancer. *BMB Rep*. (2015) 48:360–6. doi: 10.5483/bmbrep.2015.48.6.031
21. Lee JM, Heo MJ, Lee CG, Yang YM, Kim SG. Increase of miR-199a-5p by protoporphyrin IX, a photocatalyzer, directly inhibits E2F3, sensitizing mesenchymal tumor cells to anti-cancer agents. *Oncotarget*. (2015) 6:3918–31. doi: 10.18632/oncotarget.2928
22. Mussnich P, Rosa R, Bianco R, Fusco A, D'Angelo D. MiR-199a-5p and miR-375 affect colon cancer cell sensitivity to cetuximab by targeting PHLPP1. *Expert Opin Ther Targets*. (2015) 19:1017–26. doi: 10.1517/14728222.2015.1057569
23. Song J, Gao L, Yang G, Tang S, Xie H, Wang Y, et al. MiR-199a regulates cell proliferation and survival by targeting FZD7. *PLoS ONE*. (2014) 9:e110074. doi: 10.1371/journal.pone.0110074
24. Hall A. The cellular functions of small GTP-binding proteins. *Science*. (1990) 249:635–40.
25. Milinkovic VP, Skender Gazibara MK, Manojlovic Gacic EM, Gazibara TM, Tanic NT. The impact of TP53 and RAS mutations on cerebellar glioblastomas. *Exp Mol Pathol*. (2014) 97:202–7. doi: 10.1016/j.yexmp.2014.07.009
26. Ryu MJ, Liu Y, Zhong X, Du J, Peterson N, Kong G, et al. Oncogenic Kras expression in postmitotic neurons leads to S100A8-S100A9 protein overexpression and gliosis. *J Biol Chem*. (2012) 287:22948–58. doi: 10.1074/jbc.M112.357772
27. Bodemann BO, White MA. Ral GTPases and cancer: linchpin support of the tumorigenic platform. *Nat Rev Cancer*. (2008) 8:133–40. doi: 10.1038/nrc2296
28. Schubbert S, Shannon K, Bollag G. Hyperactive Ras in developmental disorders and cancer. *Nat Rev Cancer*. (2007) 7:295–308. doi: 10.1038/nrc2109
29. Gillespie DL, Whang K, Ragel BT, Flynn JR, Kelly DA, Jensen RL. Silencing of hypoxia inducible factor-1alpha by RNA interference attenuates human glioma cell growth *in vivo*. *Clin Cancer Res*. (2007) 13:2441–8. doi: 10.1158/1078-0432.CCR-06-2692
30. Zagzag D, Lukyanov Y, Lan L, Ali MA, Esencay M, Mendez O, et al. Hypoxia-inducible factor 1 and VEGF upregulate CXCR4 in glioblastoma: implications for angiogenesis and glioma cell invasion. *Lab Invest*. (2006) 86:1221–32. doi: 10.1038/labinvest.3700482
31. Liu LZ, Li C, Chen Q, Jing Y, Carpenter R, Jiang Y, et al. MiR-21 induced angiogenesis through AKT and ERK activation and HIF-1alpha expression. *PLoS ONE*. (2011) 6:e19139. doi: 10.1371/journal.pone.0019139
32. Xu Q, Liu LZ, Qian X, Chen Q, Jiang Y, Li D, et al. MiR-145 directly targets p70S6K1 in cancer cells to inhibit tumor growth and angiogenesis. *Nucleic Acids Res*. (2012) 40:761–74. doi: 10.1093/nar/gkr730
33. He XJ, Ma YY, Yu S, Jiang XT, Lu YD, Tao L, et al. Up-regulated miR-199a-5p in gastric cancer functions as an oncogene and targets klotho. *BMC Cancer*. (2014) 14:218. doi: 10.1186/1471-2407-14-218
34. Song G, Zeng H, Li J, Xiao L, He Y, Tang Y, et al. miR-199a regulates the tumor suppressor mitogen-activated protein kinase kinase kinase 11 in gastric cancer. *Biol Pharm Bull*. (2010) 33:1822–7. doi: 10.1248/bpb.33.1822
35. Zhang Y, Fan KJ, Sun Q, Chen AZ, Shen WL, Zhao ZH, et al. Functional screening for miRNAs targeting Smad4 identified miR-199a as a negative regulator of TGF-beta signalling pathway. *Nucleic Acids Res*. (2012) 40:9286–97. doi: 10.1093/nar/gks667
36. Su SF, Chang YW, Andreu-Vieyra C, Fang JY, Yang Z, Han B, et al. miR-30d, miR-181a and miR-199a-5p cooperatively suppress the endoplasmic reticulum chaperone and signaling regulator GRP78 in cancer. *Oncogene*. (2013) 32:4694–701. doi: 10.1038/onc.2012.483
37. Tsukigi M, Bilim V, Yuuki K, Ugolkov A, Naito S, Nagaoka A, et al. Re-expression of miR-199a suppresses renal cancer cell proliferation and survival by targeting GSK-3beta. *Cancer Lett*. (2012) 315:189–97. doi: 10.1016/j.canlet.2011.10.008
38. Hu Y, Liu J, Jiang B, Chen J, Fu Z, Bai F, et al. MiR-199a-5p loss up-regulated DDR1 aggravated colorectal cancer by activating epithelial-to-mesenchymal transition related signaling. *Dig Dis Sci*. (2014) 59:2163–72. doi: 10.1007/s10620-014-3136-0
39. Cheng W, Liu T, Wan X, Gao Y, Wang H. MicroRNA-199a targets CD44 to suppress the tumorigenicity and multidrug resistance of ovarian cancer-initiating cells. *FEBS J*. (2012) 279:2047–59. doi: 10.1111/j.1742-4658.2012.08589.x
40. Wang Z, Ting Z, Li Y, Chen G, Lu Y, Hao X. microRNA-199a is able to reverse cisplatin resistance in human ovarian cancer cells through the inhibition of mammalian target of rapamycin. *Oncol Lett*. (2013) 6:789–94. doi: 10.3892/ol.2013.1448
41. Chen R, Alvero AB, Silasi DA, Kelly MG, Fest S, Visintin I, et al. Regulation of IKKbeta by miR-199a affects NF-kappaB activity in ovarian cancer cells. *Oncogene*. (2008) 27:4712–23. doi: 10.1038/onc.2008.112
42. Xiao S, Yang Z, Qiu X, Lv R, Liu J, Wu M, et al. miR-29c contribute to glioma cells temozolomide sensitivity by targeting O6-methylguanine-DNA methyltransferases indirectly. *Oncotarget*. (2016) 7:50229–38. doi: 10.18632/oncotarget.10357
43. Li S, Zeng A, Hu Q, Yan W, Liu Y, You Y. miR-423-5p contributes to a malignant phenotype and temozolomide chemoresistance in glioblastomas. *Neuro Oncol*. (2016) 19:55–65. doi: 10.1093/neuonc/now129

Conflict of Interest: The authors declare that the research was conducted in the absence of any commercial or financial relationships that could be construed as a potential conflict of interest.

frontiers in Oncology

ORIGINAL RESEARCH
published: 22 October 2019
doi: 10.3389/fonc.2019.01103

LncRNA AFAP1-AS1 Supresses miR-139-5p and Promotes Cell Proliferation and Chemotherapy Resistance of Non-small Cell Lung Cancer by Competitively Upregulating RRM2

Na Huang[1†], Wei Guo[2†], Ke Ren[2†], Wancheng Li[1†], Yi Jiang[1], Jian Sun[1], Wenjing Dai[1] and Wei Zhao[1,2]*

[1] Department of Respiratory Medicine, The First Affiliated Hospital of Chengdu Medical College, Chengdu, China, [2] School of Laboratory Medicine/Sichuan Provincial Engineering Laboratory for Prevention and Control Technology of Veterinary Drug Residue in Animal-origin Food, Chengdu Medical College, Chengdu, China

OPEN ACCESS

Edited by:
Dong-Hua Yang,
St. John's University, United States

Reviewed by:
Shuaishuai Liu,
University of Maryland, Baltimore County, United States
Yunkai Zhang,
Vanderbilt University Medical Center, United States

***Correspondence:**
Wei Zhao
zw198626520@126.com

[†] These authors have contributed equally to this work

Specialty section:
This article was submitted to Molecular and Cellular Oncology, a section of the journal Frontiers in Oncology

Received: 05 August 2019
Accepted: 07 October 2019
Published: 22 October 2019

Citation:
Huang N, Guo W, Ren K, Li W, Jiang Y, Sun J, Dai W and Zhao W (2019) LncRNA AFAP1-AS1 Supresses miR-139-5p and Promotes Cell Proliferation and Chemotherapy Resistance of Non-small Cell Lung Cancer by Competitively Upregulating RRM2. Front. Oncol. 9:1103. doi: 10.3389/fonc.2019.01103

Non-small cell lung cancer (NSCLC) is the leading cause of cancer-related death worldwide. This study aims to understand the underlying mechanism of lncRNA, actin filament-associated protein 1 antisense RNA 1(AFAP1-AS1) in mediating chemotherapeutic resistance in NSCLC. The levels of AFAP1-AS1 in NSCLC tissues and cells were determined using RT-PCR. The protein levels of RRM2, EGFR, and p-AKT were analyzed using Western blotting. Binding between AFAP1-AS1 and miR-139-5p was confirmed using dual luciferase reporter and RNA immunoprecipitation (RIP) assays, and binding between miR-139-5p and RRM2 was confirmed by a dual luciferase reporter assay. NSCLC cell proliferation, apoptosis, and colony formation were examined using MTT, flow cytometry, and colony formation assays, respectively. It was found that AFAP1-AS1 expression was upregulated in NSCLC tissues and cells. In addition, AFAP1-AS1 bound to and downregulated the expression of miR-139-5p, which was reduced in NSCLC tissues. Knockdown of AFAP1-AS1 and overexpression of miR-139-5p inhibited NSCLC cell proliferation, colony formation and chemotherapy resistance and increased cell apoptosis. Additionally, AFAP1-AS1 upregulates RRM2 expression via sponging miR-139-5p. Furthermore, AFAP1-AS1 enhanced NSCLC cell proliferation and chemotherapy resistance through upregulation of RRM2 by inhibiting miR-139-5p expression. Moreover, RRM2 promoted cellular chemotherapy resistance by activating EGFR/AKT. Finally, knockdown of AFAP1-AS1 significantly suppressed tumor growth and chemoresistance in nude mice. In conclusion, AFAP1-AS1 promoted chemotherapy resistance by supressing miR-139-5p expression and promoting RRM2/EGFR/AKT signaling pathway in NSCLC cells.

Keywords: AFAP1-AS1, miR-139-5p, RRM2, non-small cell lung cancer, EGFR/AKT

INTRODUCTION

Lung cancer is the leading cause of cancer-related death worldwide (1–3). Non-small cell lung cancer (NSCLC) accounts for approximately 80% of all lung cancer cases and comprises two histological subtypes, adenocarcinoma (AD) and squamous cell cancer (SCC) (4, 5). The current overall 5-year survival rate for NSCLC is <15% due to both limited therapeutic options and recurrence (4). The prognosis of NSCLC is affected by chemotherapy resistance (6, 7). Thus, a better understanding of carcinogenesis and chemotherapy resistance is critical for developing novel therapies to treat NSCLC patients.

Long non-coding RNAs (lncRNAs) are a family of non-coding RNAs with lengths of >200 nucleotides. Accumulating evidence suggests that lncRNAs contribute to cancer initiation and progression and chemotherapy resistance (8–11). For example, the highly conserved lncRNA MALAT1 is a predictive biomarker for metastasis of lung cancer (12). Elevated LINC00473 expression often correlates with poor prognosis and is a robust biomarker for LKB1-inactivated NSCLC (13). HOTAIR is involved in the invasion and motility of lung cancer cells (14). However, MEG3 serves as a tumor suppressor in NSCLC, inhibiting cell proliferation and inducing p53-mediated cancer cell apoptosis (15).

TABLE 1 | Association between lncRNA AFAP1-AS1 expression to clinical factors in the NSCLC tissues.

Factor	AFAP1-AS1 level (High)	AFAP1-AS1 level (Low)	*P*-value (High vs. low)
Sex			0.409
Male	15	13	
Female	9	7	
Age			0.556
≤60	13	16	
>60	8	7	
Smoker?			
Yes	17	15	0.622
No	16	16	
Histology			0.437
SSC	17	16	
AC	5	6	
Others	0	0	
Tissue differentiation			0.024
Middle and high	18	7	
Low	14	5	
TNM stage			0.017
I/II	18	10	
III/IV	11	5	
Lymph node metastasis			0.041
Present	15	9	
Absent	13	7	

SCC, lung squamous cell carcinoma; AC, lung adenocarcinoma; P value < 0.05 was statistically significant.

LncRNA actin filament-associated protein 1 antisense RNA 1 (AFAP1-AS1) is a 6.8-kb lncRNA located on chromosome 4p16.1. AFAP1-AS1 participates in the development of various cancers, including pancreatic ductal adenocarcinoma (16), esophageal adenocarcinoma (17), hepatocellular carcinoma (18), nasopharyngeal carcinoma (19), gallbladder cancer (20), and colorectal cancer (21). In addition, AFAP1-AS1 plays roles in NSCLC tumourigenesis by epigenetically repressing p21 expression (22, 23). However, the molecular mechanisms and global gene regulation mediated by AFAP1-AS1 and the role of AFAP1-AS1 in chemotherapy resistance in human NSCLC has not been explored.

Ribonucleoside-diphosphate reductase subunit M2 (RRM2) is the catalytic subunit of ribonucleotide reductase and modulates the enzymatic activity, which is essential for DNA replication and repair (24). RRM2 has been reported to be involved in the progression of various cancers, including gliomas (25), colorectal cancer (26), bladder cancer (27) and NSCLC (28–31). In addition, RRM2 is a prognostic biomarker for NSCLC (28–31). Interestingly, AKT-induced tamoxifen resistance is reversed by RRM2 inhibition in breast cancer (32), suggesting that RRM2 may participate in the chemotherapy resistance of cancer cells. The abnormal overexpression or activation of AKT has been observed in cancers including lung, ovarian and pancreatic cancers (33), and AKT could be activated by epidermal growth factor receptor (EGFR) (34), implying that targeting EGFR or AKT could offer important approaches for cancer prevention and therapy. Subsequently, we investigated the effect of RRM2 on EGFR/AKT signaling.

In this study, we investigate the role of AFAP1-AS1 in NSCLC cell proliferation and chemotherapy resistance to DDP (Cisplatin) and 5-FU (fluorouracil), which are commonly used for countering progression of cancers in clinic. We also explore the function of RRM2 in the chemotherapy resistance of NSCLC cells. Our data indicate that AFAP1-AS1 expression was elevated in patients with NSCLC and that AFAP1-AS1 acts as a competing endogenous RNA for miR-139-5p, which is an important suppressor in several tumors (35–39). Knockdown of AFAP1-AS1 or overexpression of miR-139-5p inhibited the proliferation, increased the apoptosis, and attenuated the chemotherapy resistance of lung cancer cells by upregulating RRM2. In addition, knockdown of AFAP1-AS1 reduced tumor volume and weight *in vivo*. Taken together, AFAP1-AS1 supresses miR-139-5p and promotes cell proliferation and chemotherapy resistance of NSCLC cells by competitively upregulating RRM2 expression.

MATERIALS AND METHODS

Tissue Collection

This study was approved by the ethics committee of first affiliated hospital of Chengdu Medical College. From Feb. 2018 to Apr. 2019, a total of 44 NSCLC patients were recruited from Department of Respiratory Medicine, the First Affiliated Hospital of Chengdu Medical College Chengdu. All participants signed an informed consent form. NSCLC tissues and adjacent normal lung tissues were collected and stored at −80 °C until used. The drugs cisplatin (DDP), 5-fluorouracil (5-FU),

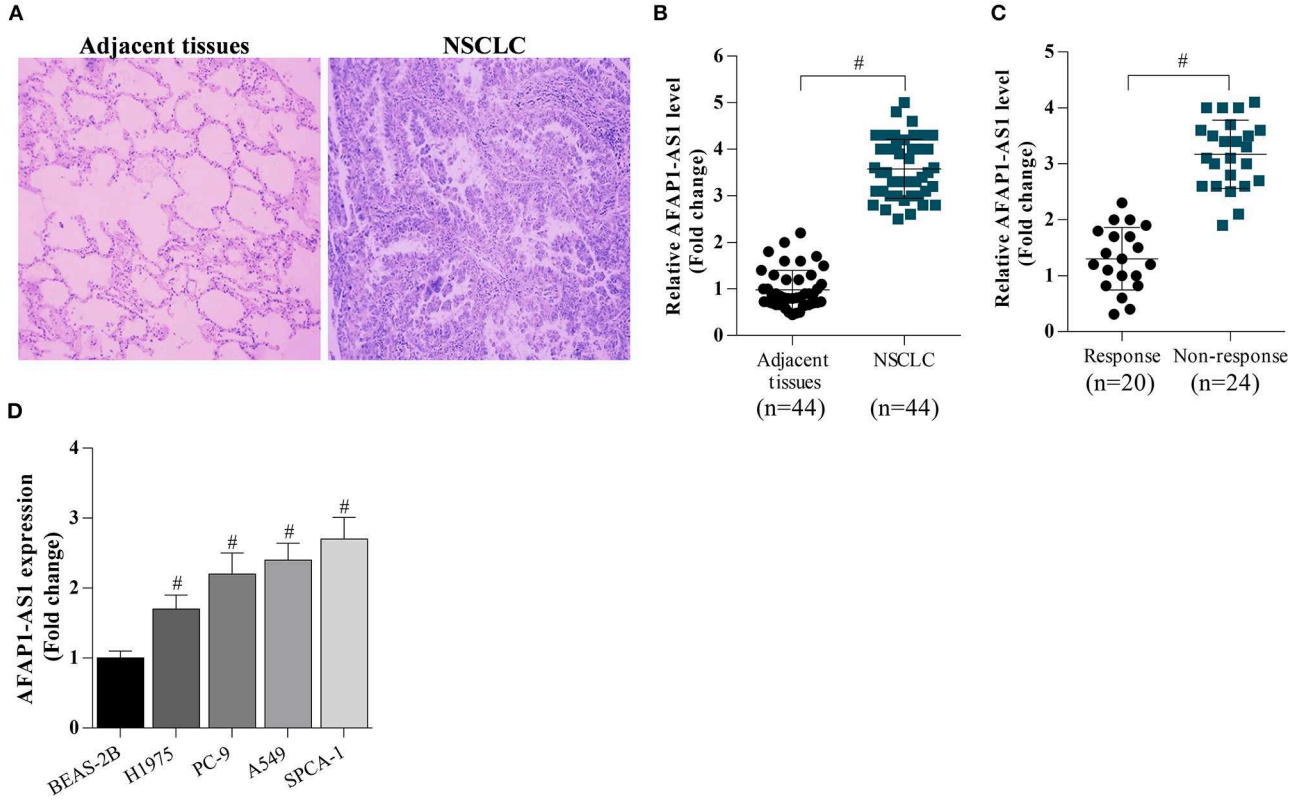

FIGURE 1 | AFAP1-AS1 expression in NSCLC tissues and cells. **(A)** H&E staining of lung clinic tissues. **(B)** RT-PCR on the expression of AFAP1-AS1 in the 44 NSCLC tissues and in 20 adjacent normal tissues. **(C)** RT-PCR on the expression of AFAP1-AS1 in NSCLC tissues of patients in chemotherapy response group ($n = 20$) and the chemotherapy non-response group ($n = 24$). **(D)** AFAP1-AS1 expression in lung cancer cells analyzed by RT- PCR. The results shown as means ± S.D. $^{\#}P < 0.05$ compared with BEAS-2B cells.

adriamycin, and paclitaxel were used for NSCLC treatment in all patients. In accordance with the Response Evaluation Criteria in Solid Tumors, we grouped the patients with a complete or partial response as responders and defined those with stable or progressive disease as non-responders. The clinicopathological characteristics of the patients with NSCLC are summarized in **Table 1**.

Cell Culture

The NSCLC cell lines H1975, PC-9, A549, and SPCA-1, and a human normal lung epithelial cell line BEAS-2B were purchased from the Institute of Biochemistry and Cell Biology of the Chinese Academy of Sciences (Shanghai, China). The H1975 and SPCA-1 cells were maintained in RPMI 1640 basic medium (GIBCO, Carlsbad, CA), and the PC-9 and A549 cells were cultured in DMEM (GIBCO) in a humidified incubator at 37°C with 5% CO_2. All media were supplemented with heat-inactivated 10% fetal bovine serum (FBS) and antibiotics (100 U/mL penicillin and 100 mg/mL streptomycin) (GIBCO).

Cell Transfection

The cells were plated in dishes or plates and grown to 70% confluence for the transfection of small interfering RNA (siRNA) or plasmids using Lipofectamine 2000 (Thermo Fisher Scientific, Shanghai, China). The siAFAP1-AS1#1 and siAFAP1-AS1#2 sequences, the miR-139-5p mimic or inhibitor, the pcDNA-RRM2 plasmid, and the Lv-AFAP1-AS1 knockdown (KD) (Lv-siAFAP1-AS1#1) construct and their paired controls were synthesized by GenePharma (Shanghai, China). The pcDNA-RRM2 plasmid contained the full-length RRM2 coding mRNA sequence (NM_001165931.1), the pcDNA-AFAP1-AS1 plasmid contained the full-length AFAP1-AS1 sequence (ENST00000608442.1), and the Lv-AFAP1-AS1 KD lentivirus expressed siRNA targeting AFAP1-AS1. The siRNA sequences targeting AFAP1-AS1 were designed as follows: siAFAP1-AS1, 5′-GCA TTA TTT TGC TAA TTC AAC-3′ and the scrambled negative control siRNA was the sequence: 5′-CCT AAC CAC AAA CTC TAC GGC-3′ (abbreviated as scramble). The inhibitor sequences targeting miR-139-5p were designed as follows: 5′-CUG GAG ACU GCG ACU GUA GAC UGG AGA CUG CGA CUG UAG ACU GGA GAC UGC GAC UGU AGA CUG GAG ACU GCG ACU GUA GAC UGG AGA CUG CGA CUG UAG A-3′, and the miR-139-5p mimic sequences were designed as follows: 5′-UCU ACA GUG CAC GUG UCU CCA G-3′, and the negative control sequences were 5′-UCU CCG AAC GUG UCA CGU-3′ (abbreviated as pre-NC, or NC). Then, both the full length and mutant of AFAP1-AS1 (or RRM2 3′UTR) were constructed into pmirGLO plasmid for luciferase assay.

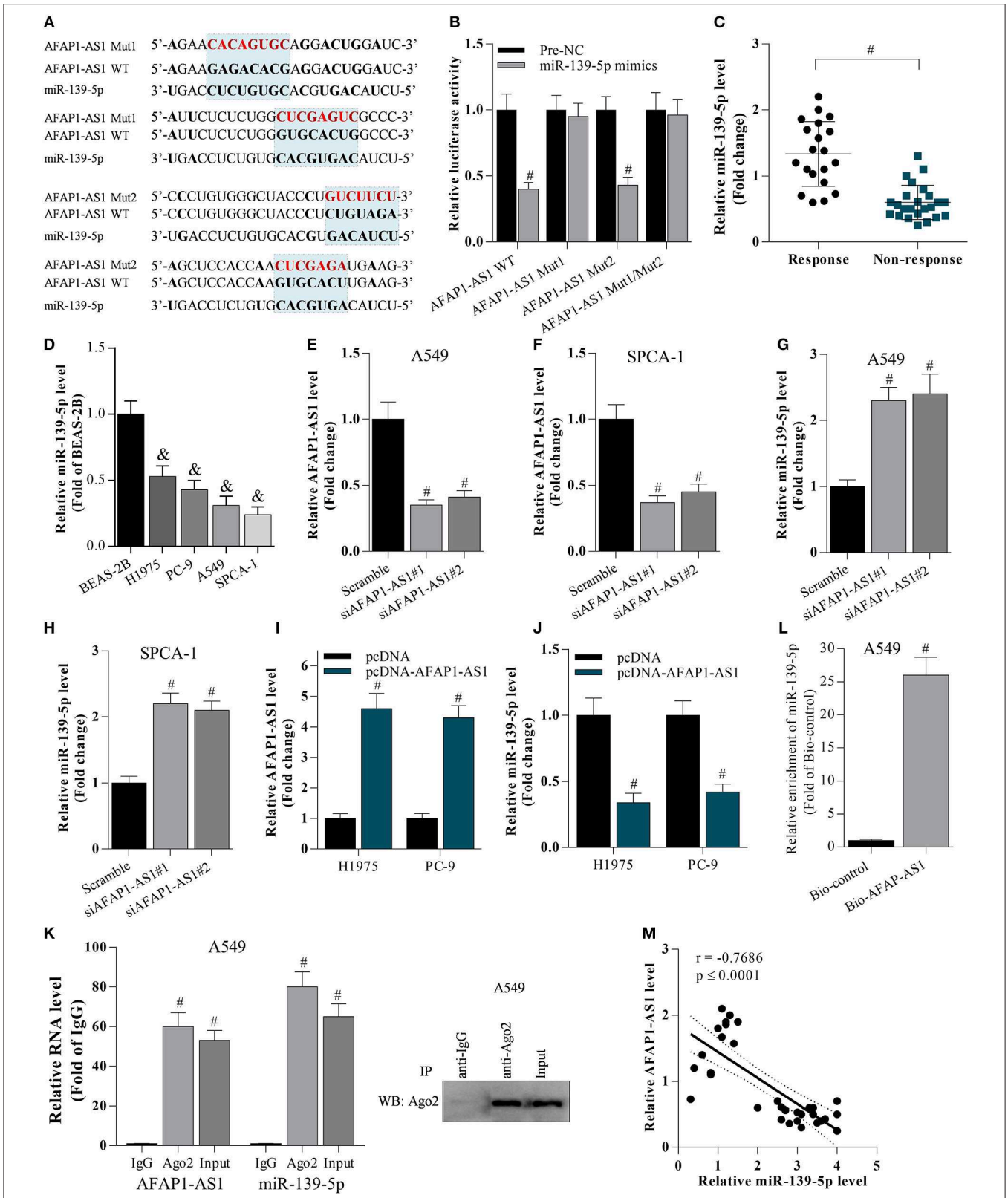

FIGURE 2 | AFAP1-AS1 supresses miR-139-5p expression. **(A)** The potential binding sites between AFAP1-AS1 and miR-139-5p predicted by bioinformatics. "AFAP1-AS1 Mut1" represents the mutation of the first two binding sites, and "AFAP1-AS1 Mut2" represents the mutation of the latter two binding sites. **(B)** A dual

(Continued)

FIGURE 2 | luciferase reporter assay on cells transfected with AFAP1-AS1 WT, AFAP1-AS1 Mut1, and AFAP1-AS1 Mut2. Data shown as means ± S.D. $^{\#}P < 0.05$ compared with the pre-NC-transfected samples. **(C)** RT-PCR on the miR-139-5p expression in chemoresistant tissues. Data shown as means ± S.D. $^{\#}P < 0.05$ compared with chemoresponsive tissues. **(D)** RT-PCR on the miR-139-5p expression in cancer cells. Data shown as means ± S.D. $^{\&}P < 0.05$ compared with BEAS-2B cells. **(E–H)** RT-PCR on the effect of AFAP1-AS1 knockdown on miR-139-5p mRNA expression. Data shown as means ± S.D. $^{\#}P < 0.05$ compared with the scramble-transfected group. **(I,J)** The effect of AFAP1-AS1 overexpression on miR-139-5p mRNA expression analyzed by RT- PCR. Data shown as means ± S.D. $^{\#}P < 0.05$ compared with the pcDNA-transfected group. **(K)** Cell lysate incubated with an anti-Ago2 antibody for RIP, and the AFAP1-AS1 content detected by RT-PCR. Data shown as means ± S.D. $^{\#}P < 0.05$ compared with the IgG control group. **(L)** Cell lysate incubated with Bio-AFAP1-AS1 for RIP, and the enrichment of miR-139-5p detected by RT- PCR. Data shown as means ± S.D. $^{\#}P < 0.05$ compared with Bio-control group. **(M)** The expression of AFAP1-AS1 and miR-139-5p negatively correlated in NSCLC tissues. $r = -0.7686$ and $p \leq 0.0001$.

RNA Extraction and Real-Time Polymerase Chain Reaction (PCR) Analyses

Total RNA was extracted from NSCLC tissues or cells with TRIzol reagent (Thermo Fisher Scientific) following the manufacturer's instructions. The expression of AFAP1-AS1, miR-139-5p, and RRM2 was analyzed with SYBR Green Master Mix (Takara, Beijing, China). Complementary DNA (cDNA) was synthesized using a PrimeScript RT Reagent Kit and gDNA Eraser (Takara). Real-time PCR was carried out on an ABI 7500 Real-Time PCR System (Applied Biosystems, Foster City, CA, USA). The primers used were as follows: AFAP1-AS1, 5′-TCG CTC AAT GGA GTG ACG GCA-3′ (forward) and 5′-CGG CTG AGA CCG CTG AGA ACT-3′ (reverse); miR-139-5p, 5′-TCT ACA GTG CAC GTG TCT CCA G-3′ (forward) and 5′-GTG CAG GGT CCG AGG T-3′ (reverse); U6, 5′-TGC GGG TGC TCG CTT CGG CAG C-3′ (forward) and 5′-GTG CAG GGT CCG AGG T-3′ (reverse); and GAPDH, 5′-CAC CCA CTC CTC CAC CTT TG-3′ (forward) and 5′-CCA CCA CCC TGT TGC TGT AG-3′ (reverse); RRM2, 5′-GGC GCG GGA GAT TTA AAG GC-3′ (forward) and 5′-CGG AGG GAG AGC ATA GTG GA-3′ (reverse). The relative expression levels of AFAP1-AS1, miR-139-5p, and RRM2 were calculated using the $2^{-\Delta\Delta Ct}$ method with U6 or GAPDH as the internal control.

Luciferase Reporter Assay

The luciferase reporter vector pGLO-basic (Promega, Beijing, China) containing the wild-type (WT) or mutant AFAP1-AS1 sequences 1/2 (Mut 1/2) were transfected into A549 cells. The pGLO plasmids containing the full-length RRM2 3′ UTR or its corresponding mutant were co-transfected with an miR-139-5p mimic or inhibitor into A549 cells. After 48 h of incubation, the cells were harvested and luciferase activity was determined using a dual luciferase assay kit (Promega).

MTT Assay and CCK-8 Assay

Cell proliferation was measured by a 3-(4,5-dimethylthiazol-2-yl)-2,5-diphenyl-tetrazolium bromide (MTT) assay. Lung cancer cells were plated in a 96-well plate (2×10^3 cells/well). After cells were incubated with MTT (Sigma, Shanghai, China), the optical density (OD) value was determined at 450 nm. Additionally, we used a Cell Counting Kit-8 (CCK-8, Sigma) to analyse NSCLC cell viability. In the MTT and CCK-8 assays, the inhibition rate (%) = 100% × (1–OD value of the treated sample/OD value of the control sample).

Colony Formation Assay

NSCLC cells were seeded in fresh six-well plates in a 5% CO_2 incubator at 37°C and were then transfected with the indicated siRNAs. Following incubation for 2 weeks, NSCLC cells would grow into colonies, and they were fixed with methanol and stained with 0.1% crystal violet. Visible colonies were manually counted and recorded.

Apoptosis Analyses

Treated cells were collected, centrifuged at 2,000 rpm for 5 min and washed with PBS three times. The cells were resuspended in 100 μL of PBS, and annexin V/FITC (5 μL) and propidium iodide (PI) (1 μL) were added to each sample. After 15 min incubation at room temperature in the dark, the apoptosis of the cancer cells was analyzed on an S3e flow cytometer (Bio-Rad, Shanghai, China). Cells stained with either annexin V or PI were counted as apoptotic cells.

Caspase-3 activity was also checked in cancer cells by Caspase-3 Activity Assay Kit (Beyotime, Shanghai, China) followed the instruction.

RNA Immunoprecipitation (RIP) Assays

Rip experiments were performed using a Magna RIP RNA-Binding Protein Immunoprecipitation Kit (Millipore, USA) according to the manufacturer's instructions. Antibodies against EZH2 and AGO-2 were obtained from Sigma. The AGO2 expression level was determined by immunoprecipitation and Western blotting, and the AFAP1-AS1 expression level was determined by real-time PCR.

Chemical Treatment in Cells

In this study, transfected NSCLC cells were incubated with DDP (solute in PBS) at concentrations of 0, 1, 2, 4, 8, and 12 μM or with 5-FU (solute in PBS) at concentrations of 0, 1, 4, 8, 16, and 32 μM for 36 h. DDP and 5-FU were purchased from Sigma.

A549 and SPCA-1 cells were treated with AST1306 (Selleck, Shanghai, China) at 1 μM for 24 h.

Generation of Drug-Resistant Cell Lines

The DDP- or 5-FU-resistant cell lines were generated by incubating NSCLC cells with increasing concentration of the indicated drugs. NSCLC cells were plated into plates and maintained in medium containing 0.2 μM DDP. After 48 h incubation, the 0.2 μM DDP-containing medium was discarded, and medium containing gradually increasing concentrations of DDP was added. Finally, cells resistant to 10 μM DDP were obtained and named A549/DDP or SPCA-1/DDP cells.

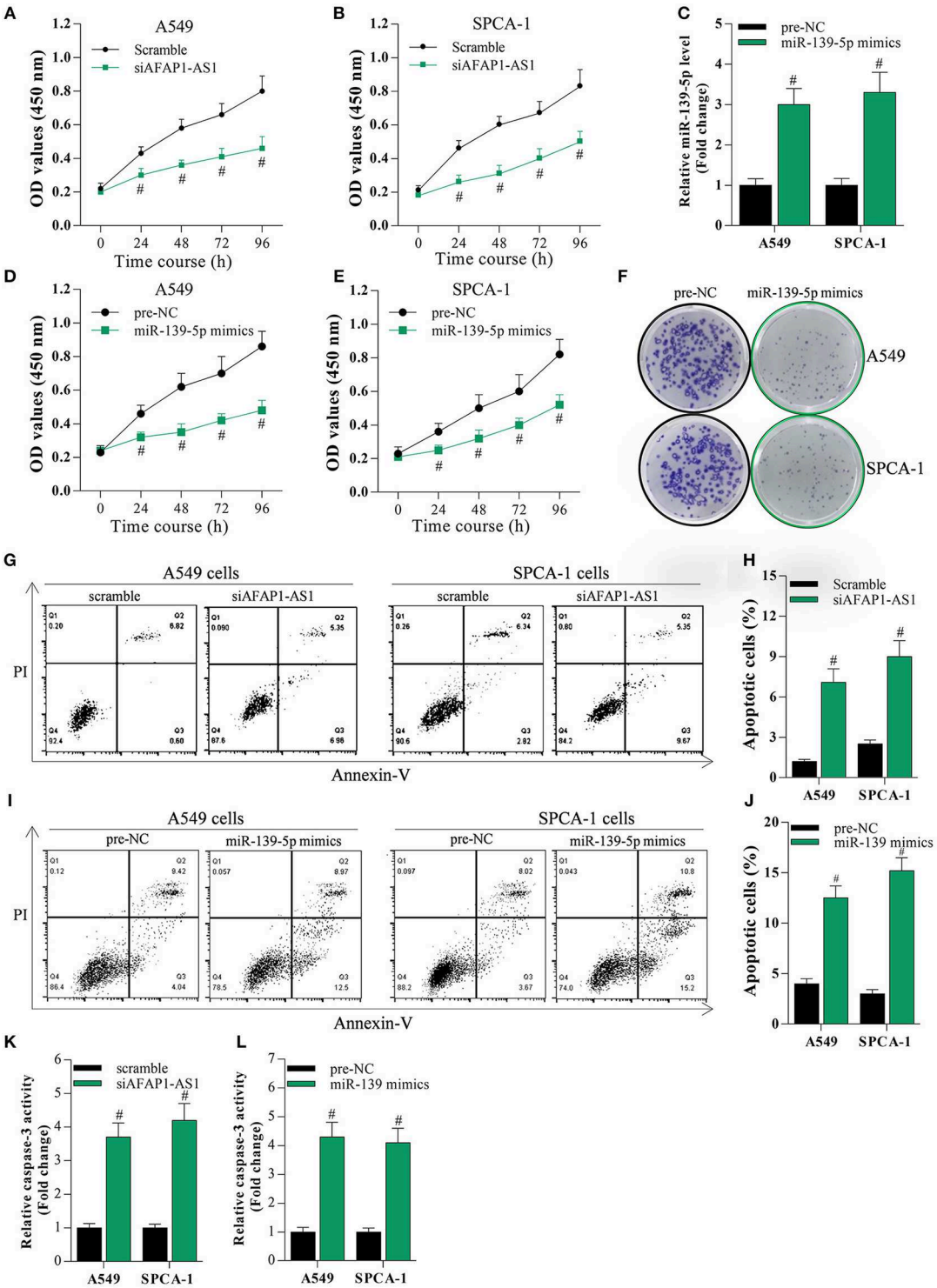

FIGURE 3 | Suppression of AFAP1-AS1 or overexpression of miR-139-5p inhibits the proliferation and increases cell apoptosis of NSCLC cells. **(A,B)** MTT assay on the proliferation of A549 and SPCA-1 cells with AFAP1-AS1 knockdown. Data shown as means ± S.D. $^{\#}P < 0.05$ compared with the scramble-transfected cells. **(C)** MiR-139-5p overexpressed in A549 and SPCA-1 cells. Data shown as means ± S.D. $^{\#}P < 0.05$ compared with the pre-NC-transfected group. **(D,E)** MTT assay on the proliferation of A549 and SPCA-1 cells with miR-139-5p overexpression. Data shown as means ± S.D. $^{\#}P < 0.05$ compared with the pre-NC-transfected group. **(F)** A colony formation assay on the effect of miR-139-5p overexpression on cell proliferation. **(G,H)** Annexin V/PI staining to assess the effect of AFAP1-AS1 knockdown on the apoptosis of A549 and SPCA-1 cells. The cell apoptosis data shown as means ± S.D. $^{\#}P < 0.05$ compared with the scramble-transfected cells. **(I,J)** Annexin V/PI staining to assess the effect of miR-139-5p overexpression on the apoptosis of A549 and SPCA-1 cells. **(K,L)** Caspase-3 activity was identified in A549 and SPCA-1 cells, which were treated as indicated. The cell apoptosis data shown as means ± S.D. $^{\#}P < 0.05$ compared with the pre-NC-transfected cells.

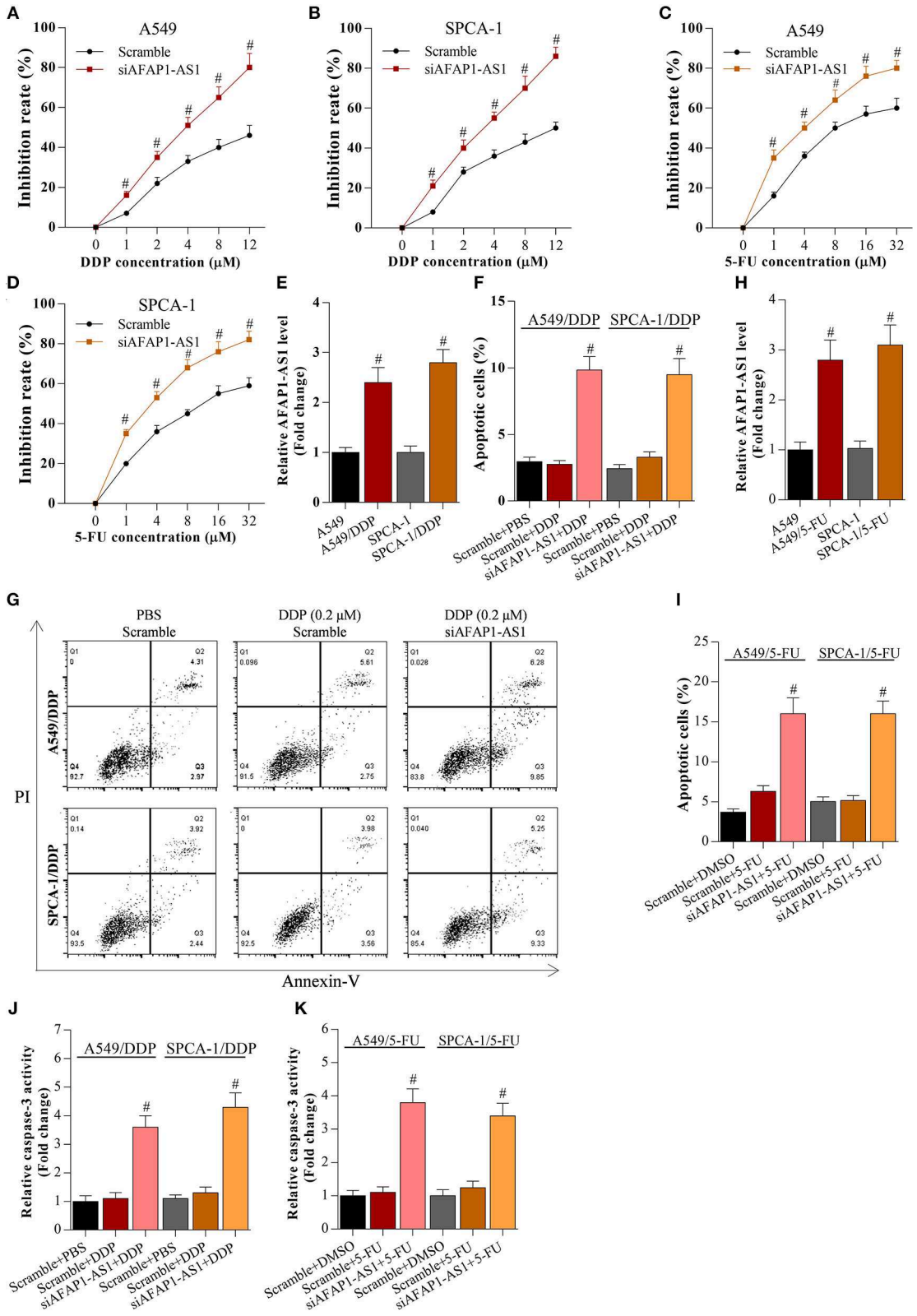

FIGURE 4 | Knockdown of AFAP1-AS1 decreases the chemotherapy resistance of NSCLC cells. **(A,B)** CCK-8 assay on A549 or SPCA-1 cells transfected with scramble or siAFAP1-AS1 and incubated with DDP for 36 h at the indicated concentrations. Data shown as means ± S.D. $^{\#}P < 0.05$ compared with the

(Continued)

FIGURE 4 | scramble-transfected cells. **(C,D)** CCK-8 assay on A549 or SPCA-1 cells transfected with scramble or siAFAP1-AS1 and incubated with 5-FU for 36 h at the indicated concentrations. Data shown as means ± S.D. $^{\#}P < 0.05$ compared with the scramble-transfected cells. **(E)** AFAP1-AS1 levels determined by RT-PCR in A549 and drug-resistant A549/DDP cells as well as in SPCA-1 and SPCA-1/DDP cells. Data shown as means ± S.D. $^{\#}P < 0.05$ compared with parental A549 cells. **(F,G)** Knockdown of AFAP1-AS1 increased the DDP-induced apoptosis of drug-resistant NSCLC cells. Data presented as means ± S.D. $^{\#}P < 0.05$ compared with the scramble-transfected DDP-resistant cancer cells. **(H)** AFAP1-AS1 levels determined by RT-PCR in A549 and drug-resistant A549/5-FU cells as well as in SPCA-1 and SPCA-1/5-FU cells. Data shown as means ± S.D. $^{\#}P < 0.05$ compared with parental A549 cells. **(I)** Knockdown of AFAP1-AS1 increased the 5-FU-induced apoptosis of drug-resistant NSCLC cells. Data presented as means ± S.D. $^{\#}P < 0.05$ compared with the scramble-transfected 5-FU-resistant cancer cells. **(J,K)** Caspase-3 activity was identified in A549 and SPCA-1 cells, which were treated as indicated. $^{\#}P < 0.05$ compared with the scramble+PBS group.

Western Blot Analysis

Tissues and cancer cells were lysed using RIPA lysis buffer (Beyotime, Haimen, China) containing protease inhibitor cocktail (Roche). Approximately 20 μg of extracted protein was separated by 10% sodium dodecyl sulfate-polyacrylamide gel electrophoresis (SDS-PAGE) and transferred to 0.22 mm polyvinylidene difluoride (PVDF) membranes (Millipore, Shanghai, China). We blocked the PVDF membranes in 2% bovine serum albumin (BSA) and incubated them with primary antibodies against RRM2 (catalog No. #65939), EGFR (catalog No. #2085), p-AKT (catalog No. #4060), AKT (catalog No. #9272), and GAPDH (catalog No. #5174) (Cell Signaling Technology, Shanghai, China). Then, these immunoblots were incubated with horseradish peroxidase-conjugated secondary antibodies for 60 min at room temperature. GAPDH was used as the internal control.

Pull Down Assay With Biotinylated AFAP1-AS1 DNA Probe

The biotin-labeled ABHD11-AS1 DNA probe was designed (Thermo), dissolved in binding and washing buffer and mixed with M-280 streptavidin magnetic beads (Thermo) to generate probe-coated beads according to the manufacturer's instruction. The A549 cell lysates were incubated with the probe-coated beads. Then, we used real-time PCR analysis to determine the beads-binding RNAs. The AFAP1-AS1 pull-down probe sequence was 5′-Bio-AGT AAA CAC GCA GTT GCA CAT GGC TGG GGA GGC CTC AGA ATC ATG GCG GGA GGC GAA AGA CAC TTC TTA CGT GGC AGC AGC-3′; and random pull-down probe sequence used as negative control was 5′-Bio-TGC ATC CAA GCC GAT TGC GGT AAC GTG CAT CCA AGC CGA TTG CGG TAA CG-3′.

Xenograft Tumor Assay

Male athymic nude BALB/c mice were purchased from the Model Animal Research Center of Nanjing University (Nanjing, China). At 5 weeks of age, the mice were randomly divided into four groups. The animal procedure was approved by the Ethics Committee of Animal Experiments of Chengdu Medical College (Chengdu, China). A549 cells were transfected with Lv-scramble or Lv-AFAP1-AS1 KD. 2×10^6 cells were inoculated subcutaneously into the mice. After 10 days, the mice were administered 3 mg/kg (body weight) DDP or PBS every 4 days for 28 days. During this period, the tumor lengths and widths were measured, and tumor volumes were calculated as follows: tumor volume = (length × width^2)/2. Finally, the tumors were harvested and weighed.

Bioinformatic Analyses

In this study, LNCipedia version 5.2, lncBase version 2, and starBase were used to predict the potential binding sites between AFAP1-AS1 and miR-139-5p. miRBase and miRDB were applied to analyse the binding sites between miR-139-5p and the RRM2 3′ UTR. In addition, we predicted the RNA-binding activity by examining previous studies (40).

Statistical Analysis

Statistical analyses were performed using SPSS software (version 19.0). The data are expressed as means ± standard deviations (S.D.). A two-tailed Student's t-test was used to analyse difference between two groups. For multi-group comparisons, we used one-way analysis of variance (ANOVA) with a *post-hoc* Tukey's honestly significant difference (HSD) test. P-value of < 0.05 were considered statistically significant.

RESULTS

AFAP1-AS1 Is Overexpressed in NSCLC Tissues and Cells

Firstly, NSCLC tissues and adjacent tissues were collected from hospital. The tissues were analyzed by H&E staining, and the results showed that abnormal cell over-growth appeared in tumors (**Figure 1A**). RT-PCR was performed to determine the expression of AFAP1-AS1 in NSCLC tissues and cells. It was found that the expression of AFAP1-AS1 was significantly higher in NSCLC tissues than in normal tissues (**Figure 1B**). In addition, AFAP1-AS1 was overexpressed in NSCLC tissues of patients in the chemotherapy non-response group compared to the chemotherapy response group (**Figure 1C**). Moreover, Additionally, the expression of AFAP1-AS1 was higher in NSCLC cells than in BEAS-2B cells and was highest in SPCA-1 cells and lowest in H1975 cells (**Figure 1D**).

AFAP1-AS1 Inhibits miR-139-5p Expression

The potential binding sites between AFAP1-AS1 and miR-139-5p were predicted based on bioinformatic analysis (**Figure 2A**). The dual luciferase reporter assay demonstrated that the miR-139-5p mimic significantly reduced the luciferase activity of cells transfected with AFAP1-AS1 WT as well as that of cells transfected with the AFAP1-AS1 mutated type AFAP1-AS1 Mut2 (**Figure 2B**). However, the miR-139-5p mimic failed to suppress the luciferase activity of cells transfected with the other AFAP1-AS1 mutated type Mut1, suggesting that miR-139-5p may bind to more than one site on the AFAP1-AS1 Mut1 construct (**Figure 2B**). We found that the level of miR-139-5p was lower

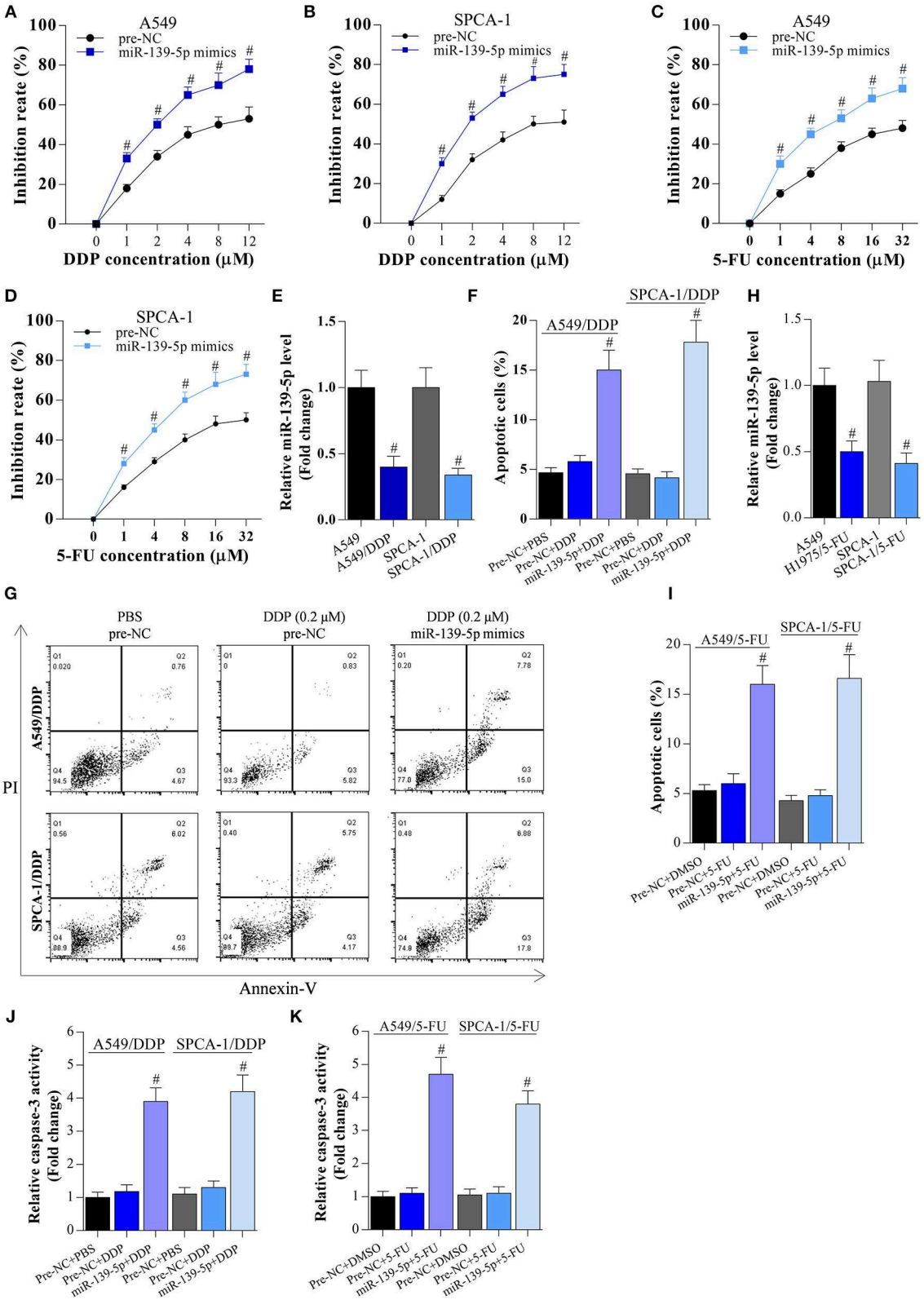

FIGURE 5 | Overexpression of miR-139-5p decreases the chemotherapy resistance of NSCLC cells. **(A,B)** CCK-8 assay on A549 or SPCA-1 cells transfected with pre-NC or miR-139-5p mimic and incubated with DDP for 36 h at the indicated concentrations. Data shown as means ± S.D. $^{\#}P < 0.05$ compared with the

(Continued)

FIGURE 5 | pre-NC-transfected cells. **(C,D)** CCK-8 assay on A549 or SPCA-1 cells transfected with pre-NC or the miR-139-5p mimic and incubated with 5-FU for 36 h at the indicated concentrations. Data shown as means ± S.D. $^{\#}P < 0.05$ compared with the pre-NC-transfected cells. **(E)** RT-PCR on the expression of miR-139-5p in A549 and drug-resistant A549/DDP cells, as well as in SPCA-1 and SPCA-1/DDP cells. Data presented as means ± S.D. $^{\#}P < 0.05$ compared with parental A549 cells. **(F,G)** Overexpression of miR-139-5p increased DDP-induced apoptosis in drug-resistant NSCLC cells. Data shown as means ± S.D. $^{\#}P < 0.05$ compared with the pre-NC-transfected DDP-resistant cancer cells. **(H)** RT-PCR on the expression of miR-139-5p in A549 and drug-resistant A549/5-FU cells, as well as in SPCA-1 and SPCA-1/5-FU cells. Data presented as means ± S.D. $^{\#}P < 0.05$ compared with parental A549 cells. **(I)** Overexpression of miR-139-5p increased 5-FU-induced apoptosis in drug-resistant NSCLC cells. Data shown as means ± S.D. $^{\#}P < 0.05$ compared with the pre-NC-transfected 5-FU-resistant cancer cells. **(J,K)** Caspase-3 activity was identified in A549 and SPCA-1 cells, which were treated as indicated. $^{\#}P < 0.05$ compared with the scramble+PBS group.

in patients in the chemotherapy non-response group than in the chemotherapy response group (**Figure 2C**), and miR-139-5p was decreased in lung cancer cell lines compared with BEAS-2B cells (**Figure 2D**). Furthermore, transfection with siRNA targeting AFAP1-AS1 reduced AFAP1-AS1 expression (**Figures 2E,F**) and upregulated miR-139-5p expression (**Figures 2G,H**) in A549 and SPCA-1 cells. In contrast, pcDNA-AFAP1-AS1-mediated overexpression of AFAP1-AS1 reduced the miR-139-5p level in H1975 and PC-9 cells (**Figures 2I,J**). AFAP1-AS1 expression was significantly elevated in anti-Ago2 (Protein argonaute-2)-incubated A549 cells (**Figure 2K**), and AFAP1-AS1 could directly bind to miR-139-5p (**Figure 2L**). There was a negative correlation between AFAP1-AS1 and miR-139-5p expression in NSCLC cells (**Figure 2M**). These findings indicated that AFAP-AS1 was a sponge of miR-139-5p.

Suppression of AFAP1-AS1 or Overexpression of miR-139-5p Inhibits the Proliferation and Increases Cell Apoptosis of NSCLC Cells

To investigate the effect of AFAP1-AS1 and miR-139-5p on the proliferation and apoptosis of NSCLC cells, A549 and SPCA-1 cells were transfected with scramble, siAFAP1-AS1, pre-NC, or the miR-139-5p mimic. Knockdown of AFAP1-AS1 suppressed cancer cell proliferation, as evidenced by the MTT assay results (**Figures 3A,B**). Similarly, overexpression of miR-139-5p decreased cell proliferation (**Figures 3C–E**) and inhibited colony formation (**Figure 3F**). As expected, suppression of AFAP1-AS1 or overexpression of miR-139-5p significantly increased the apoptosis of A549 and SPCA-1 cells (**Figures 3G–L**).

Knockdown of AFAP1-AS1 or Overexpression of miR-139-5p Decreases the Chemotherapy Resistance of NSCLC Cells

To analyse the effect of AFAP1-AS1 and miR-139-5p on the chemoresistance of NSCLC cells, scramble- or siAFAP1-AS1-transfected A549 and SPCA-1 cells were incubated with DDP or 5-FU. It was found that the drug-induced growth inhibition increased in a dose-dependent manner, and AFAP1-AS1 knockdown increased the inhibitory activity of DDP and 5-FU in NSCLC cells (**Figures 4A–D**), implying that suppression of AFAP1-AS1 alleviated the chemotherapy resistance of NSCLC cells. In addition, we also observed that AFAP1-AS1 was significantly overexpressed in DDP-resistant A549 and SPCA-1 cells compared with canonical A549 and SPCA-1 cells (**Figure 4E**). Furthermore, interfering with AFAP1-AS1 expression significantly increased the DDP-induced apoptosis in the drug-resistant cancer cells (**Figures 4F,G**). Similarly, AFAP1-AS1 was obviously increased in 5-FU-resistant A549 and SPCA-1 cells, and knockdown of AFAP1-AS1 also promoted 5-FU-triggered cell apoptosis (**Figures 4H–K**).

Meanwhile, miR-139-5p mimic enhanced the inhibitory activity of DDP and 5-FU on these cancer cells (**Figures 5A–D**), indicating that overexpression of miR-139-5p decreased the chemotherapy resistance of NSCLC cells to DDP and 5-FU. Although miR-139-5p expression was reduced in DDP- or 5-FU-resistant NSCLC cells (**Figures 5E–H**), overexpression of miR-139-5p significantly enhanced the apoptosis of DDP- or 5-FU-resistant cancer cells (**Figures 5F–K**).

Cooperation of miR-139-5p and AFAP1-AS1 Regulates RRM2 Expression by Targeting Its 3′ UTR

To investigate the interaction between miR-139-5p and RRM2, a luciferase reporter gene assay was performed. The binding sites between miR-139-5p and the RRM2 3′ UTR were predicted by bioinformatics (**Figure 6A**). The RRM2 3′ UTR sequences were sub-cloned into the pGLO plasmid, and A549 and SPCA-1 cells were co-transfected with the RRM2 3′ UTR plasmid and the miR-139-5p mimic or inhibitor. The results showed that the miR-139-5p mimic or inhibitor significantly decreased or increased, respectively, the luciferase activity driven by RRM2 WT; however, the miR-139-5p mimic or inhibitor did not affect the luciferase activity driven by the mutated RRM2 3′ UTR (termed RRM2 MUT) (**Figures 6B,C**). The miR-139-5p mimic or inhibitor noticeably decreased or increased RRM2 mRNA expression (**Figure 6D**) and protein expression (**Figures 6E,F**), respectively. Interestingly, the miR-139-5p mimic or inhibitor also modulated the protein levels of EGFR and p-AKT (**Figures 6E,F**). RRM2 was found to be overexpressed in NSCLC tissues (**Figure 6F**) and multi-drug resistant NSCLC cells (**Figures 6G,H**). RRM2 was also found has higher mRNA level in NSCLC cells than normal. To determine the cooperation of miR-139-5p and AFAP1-AS1 on regulation of RRM2 expression, the data showed that AFAP1-AS1 significantly increased luciferase activity of RRM2 3′UTR, and elevated RRM2 protein level (**Figures 6J–M**). However, AFAP1-AS1-induced elevation of RRM2 could be reversed by overexpression of miR-139-5p in A549 and SPCA-1 cells (**Figures 6J–M**).

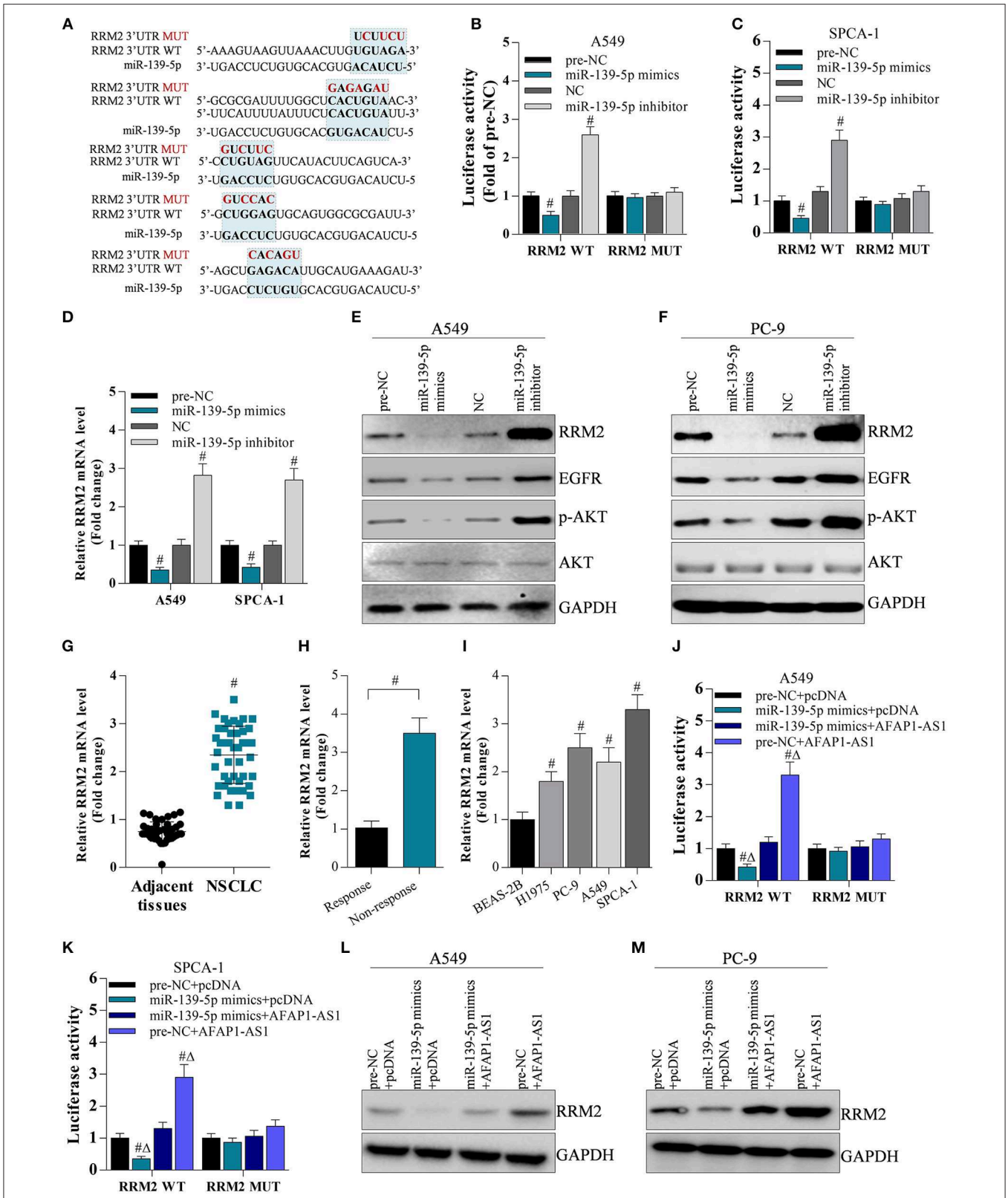

FIGURE 6 | AFAP1-AS1 upregulates RRM2 expression by sponging miR-139-5p. **(A)** The potential binding sites between RRM2 and miR-139-5p predicted by bioinformatics. All binding sites in the RRM2 3′ UTR were mutated and named "RRM2 MUT". **(B,C)** A dual luciferase reporter assay on A549 cells and SPCA-1 cells

(Continued)

FIGURE 6 | with WT RRM2 3′ UTR or mutated 3′ UTR. Data shown as means ± S.D. $^{\#}P < 0.05$ compared with the pre-NC-transfected or NC-transfected cancer cells. **(D)** RT-PCR on the cDNA from A549 cells to determine the effect of miR-139-5p on RRM2 mRNA expression. Data shown as means ± S.D. $^{\#}P < 0.05$ compared with the pre-NC-transfected or NC-transfected A549 cells. **(E,F)** Western blot on the effect of miR-139-5p on protein expression of RRM2, EGFR, AKT, and p-AKT in A549 and SPCA-1 cells. **(G)** RT-PCR on the expression of RRM2 mRNA in NSCLC tissues ($n = 44$) and in adjacent normal tissues ($n = 20$). Data shown as means ± S.D. $^{\#}P < 0.05$ compared with the normal tissues. **(H)** The mRNA level of RRM2 in chemotherapy response ($n = 4$) and resistance ($n = 7$) NSCLC tumors by RT-PCR. The results shown as means ± S.D. $^{\#}P < 0.05$ compared with the response group. **(I)** RRM2 mRNA expression in lung cancer cells analyzed by RT-PCR. The results shown as means ± S.D. $^{\#}P < 0.05$ compared with BEAS-2B cells. **(J,K)** A dual luciferase reporter assay on A549 cells and SPCA-1 cells with WT RRM2 3′ UTR or mutated 3′ UTR. Data shown as means ± S.D. $^{\#}P < 0.05$ compared with the pre-NC-transfected or NC-transfected cancer cells. **(L,M)** Western blot on the effect of miR-139-5p and AFAP1-AS1 on protein expression of RRM2in A549 and SPCA-1 cells.

Knockdown of AFAP1-AS1 Inhibits Cell Proliferation and Alleviates Chemotherapy Resistance Via the miR-139-5p/RRM2 Axis

To determine the role of the miR-139-5p/RRM2 axis in AFAP1-AS1-mediated cell proliferation and chemotherapy resistance, NSCLC cells were transfected with scramble, siAFAP1-AS1, siAFAP1-AS1+NC, and siAFAP1-AS1+miR-139-5p inhibitor. The miR-139-5p inhibitor reversed the suppressive effect of siAFAP1-AS1 on cell proliferation (**Figures 7A,B**) and colony formation (**Figures 7C,D**) and reversed the increased cancer cell apoptosis (**Figures 7E,F**). In addition, the miR-139-5p inhibitor reversed the suppressive effect of siAFAP1-AS1 on DDP resistance (**Figures 7G,H**) and 5-FU resistance (**Figures 7I,J**). Additionally, AFAP1-AS1 knockdown downregulated the protein expression of RRM2 and decreased the protein levels of EGFR and p-AKT. However, the miR-139-5p inhibitor reversed these effects (**Figures 7K,L**).

EGFR/AKT Signaling Is Involved in RRM2-Mediated Chemotherapy Resistance

To investigate the role of EGFR/AKT in RRM2-mediated chemotherapy resistance, A549 and SPCA-1 cells were transfected with the pcDNA vector, pcDNA-RRM2, pcDNA-RRM2+DMSO, and pcDNA-RRM2+AST1306 (inhibitor of EGFR). AST1306 reversed the RRM2-mediated promotion of chemotherapy resistance (**Figures 8A–D**). Additionally, AST1306 reversed the RRM2-induced upregulation of EGFR expression and p-AKT levels in A549 and SPCA-1 cells (**Figures 8E,F**). These results indicated that RRM2 enhanced the chemotherapy resistance of NSCLC cells via EGFR/AKT signaling pathway.

Moreover, the *in vivo* experiments show that knockdown of AFAP1-AS1 suppresses tumorigenicity and chemo-resistance of NSCLC cells in the nude mice (**Figures 9A–D**). These results indicated that AFAP1-AS1/miR-139-5p/RRM2/EGFR/AKT signaling pathway was involved in the progression of NSCLC (**Figure 9D**).

DISCUSSION

LncRNAs are involved in many aspects of cancer development and chemotherapy resistance (8–11). To investigate whether there is an abnormal expression of lncRNA AFAP1-AS1 in NSCLC tissues and cancer cells, real-time PCR was performed. We assessed the effect of AFAP1-AS1 on the proliferation, apoptosis and chemotherapy resistance of lung cancer cells. AFAP1-AS1 could perform as a sponge of miR-139-5p in cancer progression. Suppression of AFAP1-AS1 or overexpression of miR-139-5p significantly repressed the proliferation, increased the apoptosis, and ameliorated the chemotherapy resistance of NSCLC cells by downregulating RRM2. Furthermore, downregulation of AFAP1-AS1 decreased xenograft tumor volume and weight. These findings suggested that AFAP1-AS1 could be an oncogene and induce chemotherapy resistance by modulating miR-139-5p/RRM2 signaling in NSCLC.

Accumulating evidence demonstrated that dysregulated lncRNAs are major contributors to tumourigenesis and cancer development. For example, HOTAIR plays an important role in cellular proliferation, invasion, and clinical relapse in small cell lung cancer (41). HOTAIR also mediates chemoresistance in NSCLC by regulating HOXA1 methylation and could be a potential target for new adjuvant therapy against chemoresistance (42). In addition, the p53-regulated lncRNA TUG1 affects NSCLC cell proliferation in part by epigenetically controlling HOXB7 expression (43). MEG3 acts as a tumor suppressor in NSCLC cell proliferation and induces p53-mediated cancer cell apoptosis (15). Moreover, downregulation of AFAP1-AS1 results in growth inhibition and apoptosis promotion in lung adenocarcinoma cells, indicating that this lncRNA participates in tumourigenesis (44). In NSCLC, AFAP1-AS1 increases tumourigenesis by epigenetically repressing p21 expression. AFAP1-AS1 recruits EZH2 to the p21 promoter region, resulting in downregulation of p21, which is a tumor suppressor (22, 23). Consistent with these previous findings, we found that AFAP1-AS1 was upregulated in NSCLC tissues and cells, and it was overexpressed in chemotherapy-resistant tissues, indicating that AFAP1-AS1 is a positive regulator of NSCLC development and chemoresistance. Previous studies have shown that lncRNAs can act as competing endogenous RNAs of miRNAs (45). Thus, in the present study, we predicted binding sites between AFAP1-AS1 and miR-139-5p, which is a tumor suppressor in colorectal cancer and endometrial cancer (38, 46). However, the role of miR-139-5p in NSCLC has not been explored. Luciferase reporter assays, RIP assays, and real-time PCR were performed, and the data showed that AFAP1-AS1, as a sponge, directly bound to miR-139-5p, leading to downregulation of miR-139-5p expression, and that miR-139-5p expression was

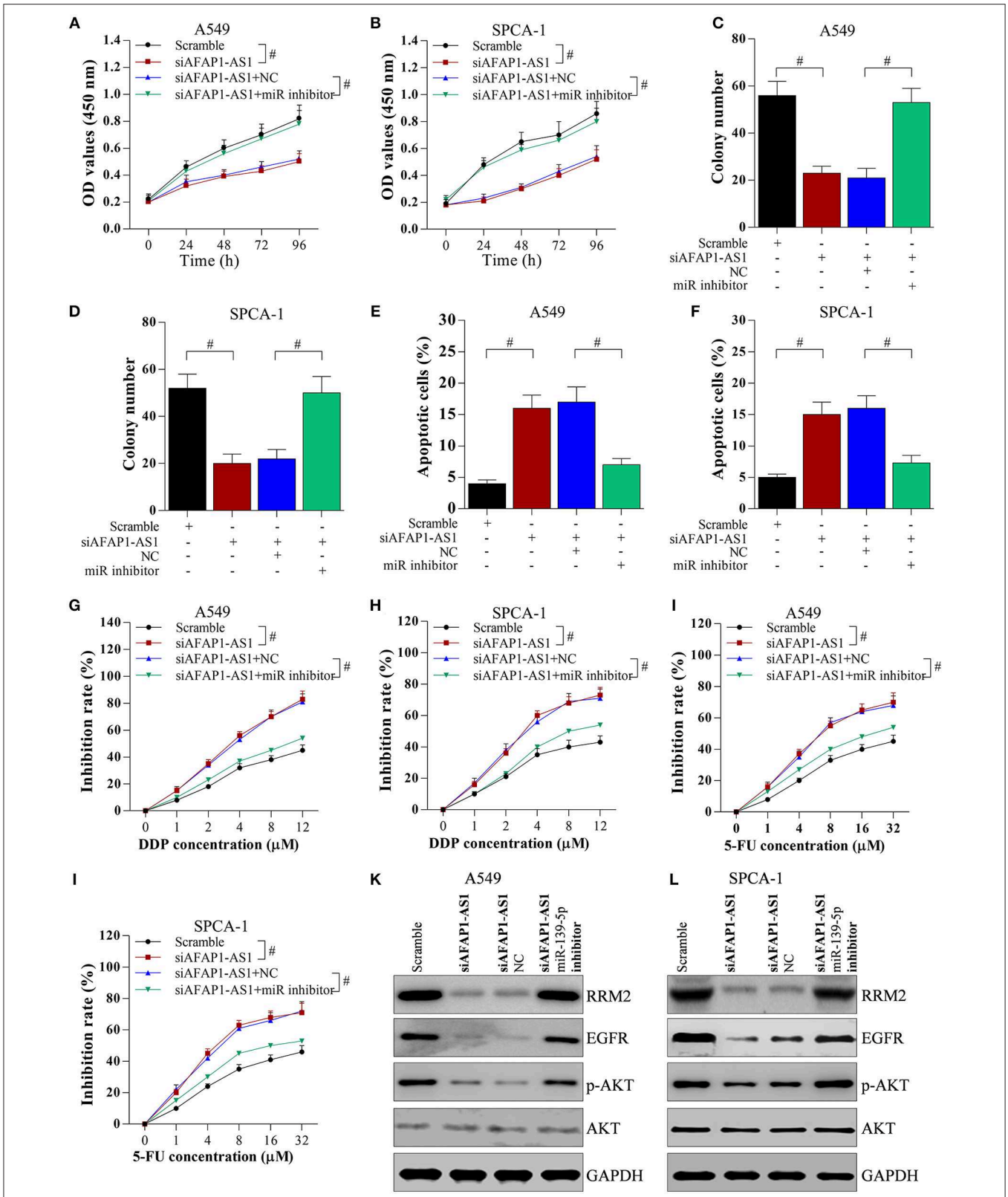

FIGURE 7 | AFAP1-AS1 promotes cell proliferation and chemotherapy resistance through the miR-139-5p/RRM2 axis. A549 or SPCA-1 cells were transfected with scramble, siAFAP1-AS1, siAFAP1-AS1+NC, and siAFAP1-AS1+miR-139-5p inhibitor. **(A,B)** MTT assay showed miR-139-5p inhibitor reversed the inhibitory effect of

(Continued)

FIGURE 7 | AFAP1-AS1 knockdown on lung cancer cell proliferation. **(C)** and **(D)** The miR-139-5p inhibitor reversed the inhibitory effect of AFAP1-AS1 knockdown on colony formation. **(E,F)** The miR-139-5p inhibitor reversed the inhibitory effect of AFAP1-AS1 knockdown on apoptosis of NSCLC cells. **(G,H)** In A549 and SPCA-1 cells incubated with DDP for 36 h, the miR-139-5p inhibitor reversed the inhibitory effect of siAFAP1-AS1 on chemotherapy resistance (DDP). **(I,J)** the miR-139-5p inhibitor reversed the inhibitory effect of siAFAP1-AS1 on chemotherapy resistance in cells incubated with 5-FU. **(K,L)**Knockdown of AFAP1-AS1 downregulated RRM2 protein expression and reduced the protein levels of EGFR and p-AKT, while miR-139-5p reversed these effects in A549, and SPCA-1 cells. All data shown as means ± S.D. $^{\#}P < 0.05$ indicates a significant difference between the two indicated groups.

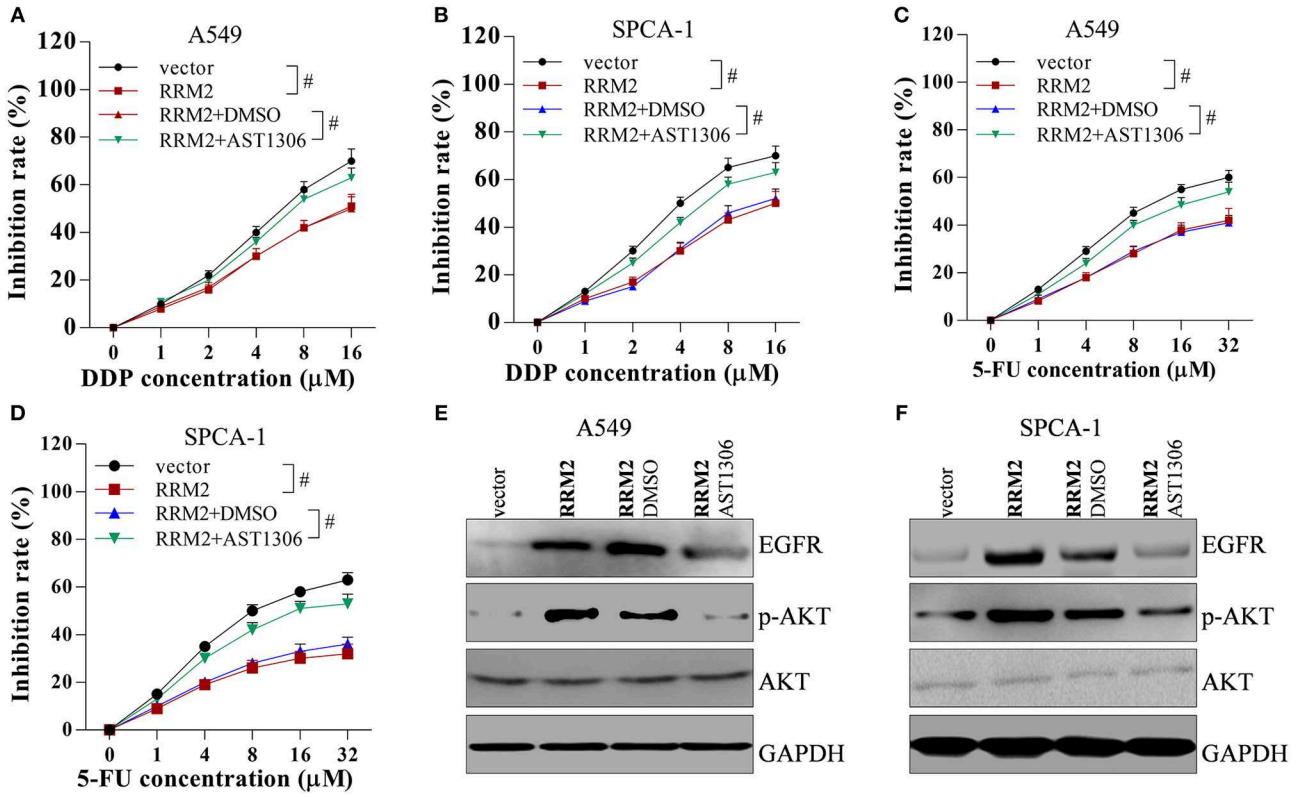

FIGURE 8 | RRM2 increases the chemotherapy resistance of NSCLC cells via EGFR/AKT signaling pathway. Cancer cells were transfected with empty vector, RRM2, RRM2+DMSO and RRM2+AST1306, and then incubated with the EGFR inhibitor AST1306 at 1 μM for 24 h. **(A,B)** In NSCLC cells incubated with DDP for 36 h, overexpression of RRM2 enhanced chemotherapy resistance, and AST1306 reversed this effect. **(C,D)** In NSCLC cells incubated with 5-FU for 36 h, overexpression of RRM2 enhanced chemotherapy resistance and AST1306 reversed this effect. **(E,F)** In A549 and SPCA-1 cells, overexpression of RRM2 elevated the protein expression of EGFR and the level of p-AKT, and AST1306 reversed this effect. All data shown as means ± S.D. $^{\#}P < 0.05$ indicates a significant difference between the two indicated groups.

decreased in chemotherapy-resistant tissues. We also found that the miR-139-5p inhibitor reversed AFAP1-AS1-induced biological effects, indicating that the interaction of AFAP1-AS1 and miR-139-5p is involved in NSCLC progression and chemotherapy resistance.

In addition, we found that AFAP1-AS1 participated in positively modulating luciferase activity of RRM2 3′ UTR and RRM2 level by acting as a sponge of miR-139-5p in cancer cells, suggesting that RRM2, as AFAP1-AS1, is a oncogenic regulator. This finding is in consistent with previous reports that RRM2 is an oncogene in certain cancers (25–32). It was reported that silencing RRM2 suppresses glioblastoma cell invasion and migration by reducing the expression of metalloproteinase-2 (MMP-2) and MMP-9 (25). The abnormal overexpression or activation of AKT has been observed in many cancers, including lung, ovarian, and pancreatic cancers, and is associated with increased cancer cell proliferation and survival (33). AKT could be activated by epidermal growth factor receptor (EGFR) (34). Consequently, targeting EGFR or AKT could offer important approaches for cancer prevention and therapy. More importantly, overexpression of RRM2 in gastric cancer cells promotes their invasiveness by regulating the AKT/NF-κB signaling pathway (47), and RRM2 increases tumor angiogenesis and growth by modulating the expression of thrombospondin-1 (TSP-1) and vascular endothelial growth factor (VEGF) (48). Subsequently, we investigated the effect of AFAP1-AS1/miR-139-5p/RRM2 signaling on EGFR expression and phosphorylation of AKT. Expectedly, our data showed

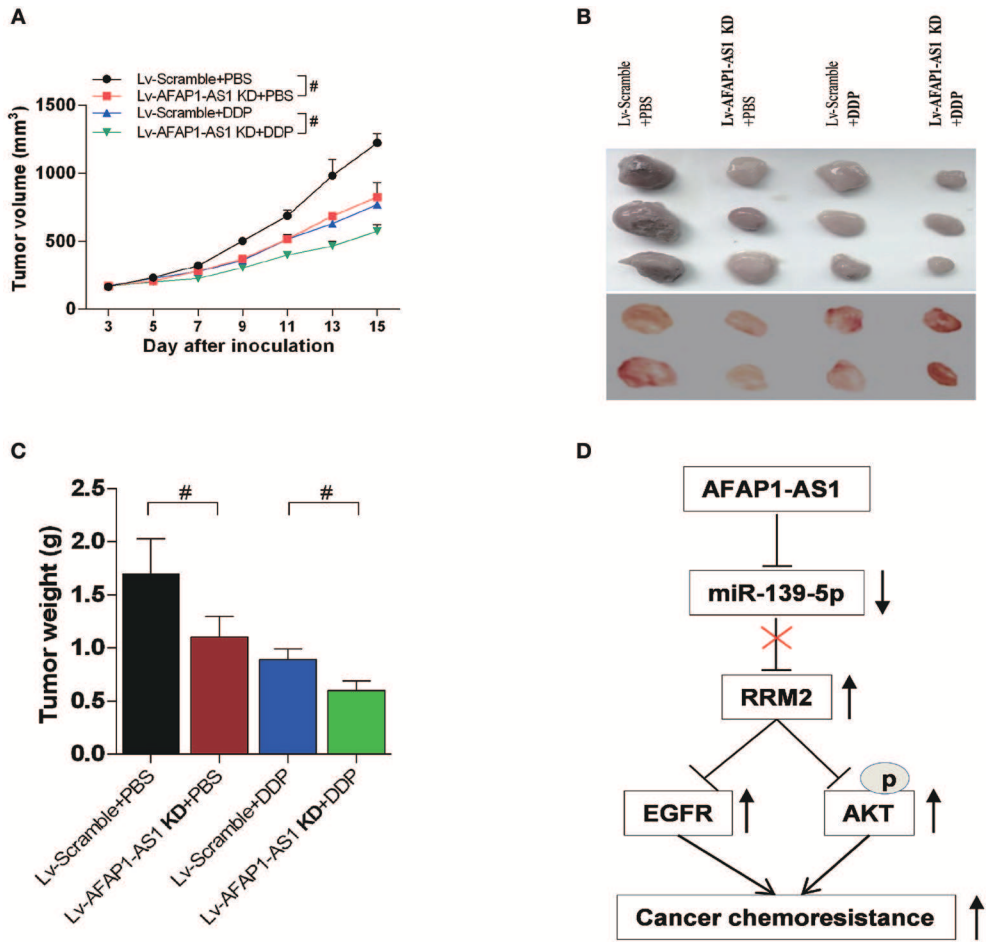

FIGURE 9 | Knockdown of AFAP1-AS1 decreases the tumourigenicity and chemoresistance of NSCLC cells in nude mice. Male BALB/c nude mice injected with A549 cells and treated for 4 weeks as follows: Lv-Scramble+PBS, Lv-AFAP1-AS1 KD+PBS, Lv-Scramble+DDP, and Lv-AFAP1-AS1 KD+DDP. **(A–C)** Tumor volumes, sizes and weights of 2 independent repeats. Data shown as means ± S.D. $n = 5$. $^{\#}P < 0.05$ indicates a significant difference between the two indicated groups. **(D)** Schema of the signaling pathways involved in AFAP1-AS1/miR-139-5p/RRM2-mediated chemotherapy resistance in NSCLC cells.

that overexpression of RRM2 promoted the proliferation, inhibited the apoptosis, and increased the chemotherapy resistance of NSCLC cells through upregulating EGFR expression and AKT phosphorylation. The EGFR inhibitor AST1306 reversed the RRM2-induced effects on cancer cells, indicating that the function of RRM2 is associated with EGFR/AKT signaling pathway. These findings suggested that miR-139-5p inhibited the proliferation and promoted the apoptosis of NSCLC cells by upregulating RRM2/EGFR/AKT signaling pathway. The mutation of EGFR was thought main driver in NSCLC (49, 50), our data shown the mutation of EGFR in H1975 (L858R+T790M) and PC-9 (del19) has little affect on AFAP1-AS1. The underlying mechanism needs more research to lighten.

Taken together, our study demonstrates that AFAP1-AS1 expression is upregulated and miR-139-5p expression downregulated in NSCLC tissues and cells. AFAP1-AS1 promotes NSCLC development and increased chemotherapy resistance by modulating miR-139-5p/RRM2/EGFR/AKT pathway. Suppression of AFAP1-AS1 expression reduced tumor growth and attenuated chemotherapy resistance *in vivo*. Therefore, AFAP1-AS1 could be a promising and therapeutic target of NSCLC.

DATA AVAILABILITY STATEMENT

All datasets generated for this study are included in the manuscript/supplementary files.

ETHICS STATEMENT

The studies involving human participants were reviewed and approved by the ethics committee of first affiliated hospital of Chengdu Medical College. The patients/participants provided their written informed consent to participate in this study. The animal study was reviewed and approved by the Ethics Committee of Animal Experiments of Chengdu Medical College.

AUTHOR CONTRIBUTIONS

WG, KR, and NH performed the experiments, analyzed the data, and prepared the manuscript draft. YJ provided the human specimens. YJ, JS, and WD set up the experiments and repeated the key experiments. WZ and WL conceived the work, analyzed the data, and prepared the manuscript. All authors critically revised the manuscript, approved the final version, and agreed to be accountable for all aspects of the manuscript.

FUNDING

This work was supported by the National Natural Science Foundation of China (81602636 and 31800154), the Fundamental Research Funds for the Central Universities (2242015K40034), Nanjing medical science and technology development project (ZKX15049), Jiangsu postdoctoral research grant (1601182B), Key project of science of Sichuan Education Department (18ZA0163 and 18ZA0164), and Natural Science Foundation of Chengdu Medical College (CYZ18-04).

REFERENCES

1. Siegel RL, Miller KD, Fedewa SA, Ahnen DJ, Meester RGS, Barzi A, et al. Colorectal cancer statistics, 2017. *CA Cancer J Clin.* (2017) 67:177–93. doi: 10.3322/caac.21395
2. Siegel RL, Miller KD, Jemal A. Cancer Statistics, 2017. *CA Cancer J Clin.* (2017) 67:7–30. doi: 10.3322/caac.21387
3. Chen W, Zheng R, Baade PD, Zhang S, Zeng H, Bray F, et al. Cancer statistics in China, 2015. *CA Cancer J Clin.* (2016) 66:115–32. doi: 10.3322/caac.21338
4. Wood SL, Pernemalm M, Crosbie PA, Whetton AD. Molecular histology of lung cancer: from targets to treatments. *Cancer Treat Rev.* (2015) 41:361–75. doi: 10.1016/j.ctrv.2015.02.008
5. Boolell V, Alamgeer M, Watkins DN, Ganju V. The evolution of therapies in non-small cell lung cancer. *Cancers.* (2015) 7:1815–46. doi: 10.3390/cancers7030864
6. Xu W, Ying Y, Shan L, Feng J, Zhang S, Gao Y, et al. Enhanced expression of cohesin loading factor NIPBL confers poor prognosis and chemotherapy resistance in non-small cell lung cancer. *J Transl Med.* (2015) 13:153. doi: 10.1186/s12967-015-0503-3
7. Chatterjee S, Crozet L, Damotte D, Iribarren K, Schramm C, Alifano M, et al. TLR7 promotes tumor progression, chemotherapy resistance, and poor clinical outcomes in non-small cell lung cancer. *Cancer Res.* (2014) 74:5008–18. doi: 10.1158/0008-5472.CAN-13-2698
8. Chang ZW, Jia YX, Zhang WJ, Song LJ, Gao M, Li MJ, et al. LncRNA-TUSC7/miR-224 affected chemotherapy resistance of esophageal squamous cell carcinoma by competitively regulating DESC1. *J. Exp. Clin. Cancer Res.* (2018) 37:56. doi: 10.1186/s13046-018-0724-4
9. Gong Z, Zhang S, Zeng Z, Wu H, Yang Q, Xiong F, et al. LOC401317, a p53-regulated long non-coding RNA, inhibits cell proliferation and induces apoptosis in the nasopharyngeal carcinoma cell line HNE2. *PLoS ONE.* (2014) 9:e110674. doi: 10.1371/journal.pone.0110674
10. Bautista RR, Gomez AO, Miranda AH, Dehesa AZ, Villarreal-Garza C, Avila-Moreno F, et al. Correction to: long non-coding RNAs: implications in targeted diagnoses, prognosis, and improved therapeutic strategies in human non- and triple-negative breast cancer. *Clin Epigenetics.* (2018) 10:106. doi: 10.1186/s13148-018-0537-5
11. Fatica A, Bozzoni I. Long non-coding RNAs: new players in cell differentiation and development. *Nat Rev Genet.* (2014) 15:7–21. doi: 10.1038/nrg3606
12. Gutschner T, Hammerle M, Eissmann M, Hsu J, Kim Y, Hung G, et al. The noncoding RNA MALAT1 is a critical regulator of the metastasis phenotype of lung cancer cells. *Cancer Res.* (2013) 73:1180–9. doi: 10.1158/0008-5472.CAN-12-2850
13. Chen Z, Li JL, Lin S, Cao C, Gimbrone NT, Yang R, et al. cAMP/CREB-regulated LINC00473 marks LKB1-inactivated lung cancer and mediates tumor growth. *J Clin Invest.* (2016) 126:2267–79. doi: 10.1172/JCI85250
14. Zhao W, An Y, Liang Y, Xie XW. Role of HOTAIR long noncoding RNA in metastatic progression of lung cancer. *Eur Rev Med Pharmacol Sci.* (2014) 18:1930–6.
15. Lu KH, Li W, Liu XH, Sun M, Zhang ML, Wu WQ, et al. Long non-coding RNA MEG3 inhibits NSCLC cells proliferation and induces apoptosis by affecting p53 expression. *BMC Cancer.* (2013) 13:461. doi: 10.1186/1471-2407-13-461
16. Ye Y, Chen J, Zhou Y, Fu Z, Zhou Q, Wang Y, et al. High expression of AFAP1-AS1 is associated with poor survival and short-term recurrence in pancreatic ductal adenocarcinoma. *J Transl Med.* (2015) 13:137. doi: 10.1186/s12967-015-0490-4
17. Wu W, Bhagat TD, Yang X, Song JH, Cheng Y, Agarwal R, et al. Hypomethylation of noncoding DNA regions and overexpression of the long noncoding RNA, AFAP1-AS1, in Barrett's esophagus and esophageal adenocarcinoma. *Gastroenterology.* (2013) 144:956–66.e4. doi: 10.1053/j.gastro.2013.01.019
18. Zhang JY, Weng MZ, Song FB, Xu YG, Liu Q, Wu JY, et al. Long noncoding RNA AFAP1-AS1 indicates a poor prognosis of hepatocellular carcinoma and promotes cell proliferation and invasion via upregulation of the RhoA/Rac2 signaling. *Int J Oncol.* (2016) 48:1590–8. doi: 10.3892/ijo.2016.3385
19. Tang Y, He Y, Shi L, Yang L, Wang J, Lian Y, et al. Co-expression of AFAP1-AS1 and PD-1 predicts poor prognosis in nasopharyngeal carcinoma. *Oncotarget.* (2017) 8:39001–11. doi: 10.18632/oncotarget.16545
20. Ma F, Wang SH, Cai Q, Zhang MD, Yang Y, Ding J. Overexpression of LncRNA AFAP1-AS1 predicts poor prognosis and promotes cells proliferation and invasion in gallbladder cancer. *Biomed Pharmacother.* (2016) 84:1249–55. doi: 10.1016/j.biopha.2016.10.064
21. Tang J, Zhong G, Wu J, Chen H, Jia Y. Long noncoding RNA AFAP1-AS1 facilitates tumor growth through enhancer of zeste homolog 2 in colorectal cancer. *Am J Cancer Res.* (2018) 8:892–902.
22. Yin D, Lu X, Su J, He X, De W, Yang J, et al. Long noncoding RNA AFAP1-AS1 predicts a poor prognosis and regulates non-small cell lung cancer cell proliferation by epigenetically repressing p21 expression. *Mol Cancer.* (2018) 17:92. doi: 10.1186/s12943-018-0836-7
23. Deng J, Liang Y, Liu C, He S, Wang S. The up-regulation of long non-coding RNA AFAP1-AS1 is associated with the poor prognosis of NSCLC patients. *Biomed Pharmacother.* (2015) 75:8–11. doi: 10.1016/j.biopha.2015.07.003
24. Nordlund P, Reichard P. Ribonucleotide reductases. *Annu Rev Biochem.* (2006) 75:681–706. doi: 10.1146/annurev.biochem.75.103004.142443
25. Li C, Zheng J, Chen S, Huang B, Li G, Feng Z, et al. RRM2 promotes the progression of human glioblastoma. *J Cell Physiol.* (2018) 233:6759–67. doi: 10.1002/jcp.26529
26. Yoshida Y, Tsunoda T, Doi K, Tanaka Y, Fujimoto T, Machida T, et al. KRAS-mediated up-regulation of RRM2 expression is essential for the proliferation of colorectal cancer cell lines. *Anticancer Res.* (2011) 31:2535–9.
27. Morikawa T, Maeda D, Kume H, Homma Y, Fukayama M. Ribonucleotide reductase M2 subunit is a novel diagnostic marker and a potential therapeutic target in bladder cancer. *Histopathology.* (2010) 57:885–92. doi: 10.1111/j.1365-2559.2010.03725.x
28. Rahman MA, Amin AR, Wang D, Koenig L, Nannapaneni S, Chen Z, et al. RRM2 regulates Bcl-2 in head and neck and lung cancers: a potential target for cancer therapy. *Clin Cancer Res.* (2013) 19:3416–28. doi: 10.1158/1078-0432.CCR-13-0073
29. Mah V, Alavi M, Marquez-Garban DC, Maresh EL, Kim SR, Horvath S, et al. Ribonucleotide reductase subunit M2 predicts survival in subgroups of patients with non-small cell lung carcinoma: effects of gender and smoking status. *PLoS ONE.* (2015) 10:e0127600. doi: 10.1371/journal.pone.0127600
30. Wang L, Meng L, Wang XW, Ma GY, Chen JH. Expression of RRM1 and RRM2 as a novel prognostic marker in advanced non-small cell

lung cancer receiving chemotherapy. *Tumour Biol.* (2014) 35:1899–906. doi: 10.1007/s13277-013-1255-4
31. Zhao H, Zhang H, Du Y, Gu X. Prognostic significance of BRCA1, ERCC1, RRM1, and RRM2 in patients with advanced non-small cell lung cancer receiving chemotherapy. *Tumour Biol.* (2014) 35:12679–88. doi: 10.1007/s13277-014-2592-7
32. Tang H, Xiao G, Behrens C, Schiller J, Allen J, Chow CW, et al. A 12-gene set predicts survival benefits from adjuvant chemotherapy in non-small cell lung cancer patients. *Clin Cancer Res.* (2013) 19:1577–86. doi: 10.1158/1078-0432.CCR-12-2321
33. Song M, Bode AM, Dong Z, Lee MH. AKT as a therapeutic target for cancer. *Cancer Res.* (2019) 79:1019–31. doi: 10.1158/0008-5472.CAN-18-2738
34. Liu Q, Yu S, Zhao W, Qin S, Chu Q, Wu K. EGFR-TKIs resistance via EGFR-independent signaling pathways. *Mol Cancer.* (2018) 17:53. doi: 10.1186/s12943-018-0793-1
35. Zhang L, Dong Y, Zhu N, Tsoi H, Zhao Z, Wu CW, et al. microRNA-139–5p exerts tumor suppressor function by targeting NOTCH1 in colorectal cancer. *Mol Cancer.* (2014) 13:124. doi: 10.1186/1476-4598-13-124
36. Li Q, Liang X, Wang Y, Meng X, Xu Y, Cai S, et al. miR-139–5p inhibits the epithelial-mesenchymal transition and enhances the chemotherapeutic sensitivity of colorectal cancer cells by downregulating BCL2. *Sci Rep.* (2016) 6:27157. doi: 10.1038/srep27157
37. Zou F, Mao R, Yang L, Lin S, Lei K, Zheng Y, et al. Targeted deletion of miR-139–5p activates MAPK, NF-kappaB and STAT3 signaling and promotes intestinal inflammation and colorectal cancer. *FEBS J.* (2016) 283:1438–52. doi: 10.1111/febs.13678
38. Liu J, Li C, Jiang Y, Wan Y, Zhou S, Cheng W. Tumor-suppressor role of miR-139–5p in endometrial cancer. *Cancer Cell Int.* (2018) 18:51. doi: 10.1186/s12935-018-0545-8
39. Catanzaro G, Besharat ZM, Miele E, Chiacchiarini M, Po A, Carai A, et al. The miR-139–5p regulates proliferation of supratentorial paediatric low-grade gliomas by targeting the PI3K/AKT/mTORC1 signalling. *Neuropathol Appl Neurobiol.* (2018) 44:687–706. doi: 10.1111/nan.12479
40. Zhao W, Li W, Dai W, Huang N, Qiu J. LINK-A promotes cell proliferation through the regulation of aerobic glycolysis in non-small-cell lung cancer. *Onco Targets Therapy.* (2018) 11:6071–80. doi: 10.2147/OTT.S171216
41. Liu XH, Liu ZL, Sun M, Liu J, Wang ZX, De W. The long non-coding RNA HOTAIR indicates a poor prognosis and promotes metastasis in non-small cell lung cancer. *BMC Cancer.* (2013) 13:464. doi: 10.1186/1471-2407-13-464
42. Fang S, Gao H, Tong Y, Yang J, Tang R, Niu Y, et al. Long noncoding RNA-HOTAIR affects chemoresistance by regulating HOXA1 methylation in small cell lung cancer cells. *Lab Invest.* (2016) 96:60–8. doi: 10.1038/labinvest.2015.123
43. Zhang EB, Yin DD, Sun M, Kong R, Liu XH, You LH, et al. P53-regulated long non-coding RNA TUG1 affects cell proliferation in human non-small cell lung cancer, partly through epigenetically regulating HOXB7 expression. *Cell Death Dis.* (2014) 5:e1243. doi: 10.1038/cddis.2014.201
44. Zhuang Y, Jiang H, Li H, Dai J, Liu Y, Li Y, et al. Down-regulation of long non-coding RNA AFAP1-AS1 inhibits tumor cell growth and invasion in lung adenocarcinoma. *Am J Transl Res.* (2017) 9:2997–3005.
45. Huang YA, Chan KCC, You ZH. Constructing prediction models from expression profiles for large scale lncRNA-miRNA interaction profiling. *Bioinformatics.* (2018) 34:812–9. doi: 10.1093/bioinformatics/btx672
46. Bian Z, Zhang J, Li M, Feng Y, Yao S, Song M, et al. Long non-coding RNA LINC00152 promotes cell proliferation, metastasis, and confers 5-FU resistance in colorectal cancer by inhibiting miR-139–5p. *Oncogenesis.* (2017) 6:395. doi: 10.1038/s41389-017-0008-4
47. Zhong Z, Cao Y, Yang S, Zhang S. Overexpression of RRM2 in gastric cancer cell promotes their invasiveness via AKT/NF-kappaB signaling pathway. *Pharmazie.* (2016) 71:280–4.
48. Zhang K, Hu S, Wu J, Chen L, Lu J, Wang X, et al. Overexpression of RRM2 decreases thrombspondin-1 and increases VEGF production in human cancer cells *in vitro* and *in vivo*: implication of RRM2 in angiogenesis. *Mol Cancer.* (2009) 8:11. doi: 10.1186/1476-4598-8-11
49. Buonerba C, Iaccarino S, Dolce P, Pagliuca M, Izzo M, Scafuri L, et al. Predictors of outcomes in patients with EGFR-mutated non-small cell lung cancer receiving EGFR tyrosine kinase inhibitors: a systematic review and meta-analysis. *Cancers.* (2019) 11:E1259. doi: 10.3390/cancers11091259
50. Tay RY, Ackermann CJ, Califano R. Immunotherapy in tyrosine kinase inhibitor-naive advanced epidermal growth factor receptor-mutant non-small cell lung cancer-driving down a precarious road in driver-mutated lung cancer. *Transl Lung Cancer Res.* (2018) 7 (Suppl. 4):S377–80. doi: 10.21037/tlcr.2018.09.16

Conflict of Interest: The authors declare that the research was conducted in the absence of any commercial or financial relationships that could be construed as a potential conflict of interest.

frontiers in Oncology

ORIGINAL RESEARCH
published: 31 October 2019
doi: 10.3389/fonc.2019.01079

Chronic BDE-47 Exposure Aggravates Malignant Phenotypes and Chemoresistance by Activating ERK Through ERα and GPR30 in Endometrial Carcinoma

Fan Zhang[1,2†], *Lin Peng*[3†], *Yiteng Huang*[4†], *Xueqiong Lin*[3], *Li Zhou*[5*] *and Jiongyu Chen*[1,2*]

[1] Oncology Research Laboratory, Cancer Hospital of Shantou University Medical College, Shantou, China, [2] Guangdong Provincial Key Laboratory for Breast Cancer Diagnosis and Treatment, Cancer Hospital of Shantou University Medical College, Shantou, China, [3] Department of Laboratory Medicine, Cancer Hospital of Shantou University Medical College, Shantou, China, [4] Health Care Center, The First Affiliated Hospital of Shantou University Medical College, Shantou, China, [5] Department of Gynecologic Oncology, Cancer Hospital of Shantou University Medical College, Shantou, China

OPEN ACCESS

Edited by:
Dong-Hua Yang,
St. John's University, United States

Reviewed by:
Nicoletta Filigheddu,
University of Eastern Piedmont, Italy
Ryszard Maciejewski,
Medical University of Lublin, Poland

***Correspondence:**
Li Zhou
zlyyzl@126.com
Jiongyu Chen
513980484@qq.com

[†] These authors have contributed equally to this work

Specialty section:
This article was submitted to Molecular and Cellular Oncology, a section of the journal Frontiers in Oncology

Received: 25 August 2019
Accepted: 30 September 2019
Published: 31 October 2019

Citation:
Zhang F, Peng L, Huang Y, Lin X, Zhou L and Chen J (2019) Chronic BDE-47 Exposure Aggravates Malignant Phenotypes and Chemoresistance by Activating ERK Through ERα and GPR30 in Endometrial Carcinoma. Front. Oncol. 9:1079. doi: 10.3389/fonc.2019.01079

Environmental exposure to certain compounds contribute to cell plasticity, tumor progression and even chemoresistance. 2,2′,4,4′-tetrabromo diphenyl ether (BDE-47), one of the most frequently detected polybrominated diphenyl ethers (PBDEs) in environmental and biological samples, is a known estrogen disruptor closely associated with the development of hormone-dependent cancers. However, the effect of BDE-47 on endometrial carcinoma (EC), an estrogen-dependent cancer, remains to be elucidated. Mechanisms of estrogen receptor α (ERα) and G-protein-coupled receptor-30 (GPR30) involved in BDE-47 carcinogenesis are yet to be identified. This study aims to investigate the effect of BDE-47 on the invasive phenotype of estrogen-dependent EC cells. BDE-47-treated cells, such as Ishikawa-BDE-47 and HEC-1B-BDE-47 cells, exhibited increased cell viability and enhanced metastatic ability. *In vivo* studies showed larger tumor volumes and more metastasis in mice injected with Ishikawa-BDE-47 cells compared with parental Ishikawa cells. MTT assay showed that BDE-47 exposure could attenuate sensitivity of EC cells to cisplatin or paclitaxel treatment *in vitro*. Western blotting revealed overexpression of ERα, GPR30, pEGFR (phosphorylated epidermal growth factor receptor), and pERK (phosphorylated extracellular-regulated protein kinase) in Ishikawa-BDE-47 and HEC-1B-BDE-47 cells. Knockdown of ERα or GPR30 by small interfering RNA reversed the stimulating effect of BDE-47 on cell growth, migration and invasion of EC cells. Additionally, treatment with pEGFR or pERK inhibitor impaired cell viability, migration and invasion in Ishikawa-BDE-47 and HEC-1B-BDE-47 cells. Overall, our results indicate that chronic BDE-47 exposure triggers phenotypic plasticity, promotes progression and even chemoresistance in EC cells, at least in part, via ERα/GPR30 and EGFR/ERK signaling pathways.

Keywords: 2,2′,4,4′-tetrabromo diphenyl ether, endometrial carcinoma, estrogen receptor α, G-protein-coupled receptor-30, cisplatin, paclitaxel, phosphorylated epidermal growth factor receptor, phosphorylated extracellular-regulated protein kinase

INTRODUCTION

Endometrial carcinoma (EC) is a major malignant tumor of the female reproductive system (1). The incidence of EC has been increasing in recent decades because of lifestyle change and environmental contamination (2). In China, EC was diagnosed in 63,400 patients and accounted for more than 21,800 deaths in 2016 (3). EC has been proposed to be classified into two pathogenetic groups, of which type I mostly occurs in pre- and peri-menopausal women with a history of unopposed estrogen exposure (4). However, studies found no difference in the positivity of estrogen receptor (ER) or progesterone receptor (PR) as well as the level of sex hormones between these two types of EC. Thus, type II is not completely estrogen-independent (5). Previous studies supported the role of ERα in the development of EC (4, 6). Additionally, G-protein-coupled receptor-30 (GPR30), which encodes a multi-pass membrane protein mediating the estrogen action of intracellular estrogen receptor (7, 8), has been suggested to be an indicator of EC progression (9). However, the etiology and pathogenesis of EC remain poorly defined.

Environmental exposure to certain compounds contributes to cell plasticity and tumor progression (10, 11); an example of these compounds is a group of flame retardants. These synthetic chemical additives are found in consumer products such as building materials, electronics and electrical goods, textiles, and furnishings. Polybrominated diphenyl ethers (PBDEs) are a class of flame retardants most commonly used in a variety of polymers and plastics, as well as in a broad range of consumer products. PBDEs have been produced in notable quantities (12), and consequently, their adverse health effects, environmental persistence and toxicity have raised concerns. Certain kinds of PBDEs (penta-, octa-, and deca-BDE) have been listed as prevalent organic pollutants, and have been banned or voluntarily phased out by manufacturers (13). However, consumer products containing large amounts of PBDEs are still in use and continue to release toxic chemicals into the environment (14). 2,2′,4,4′-tetrabromodiphenyl ether (BDE-47), one of the most predominant PBDE congeners, is characterized by its lipophilic, bio-accumulative, degradation-resistant, and toxic properties. BDE-47 may enter the environment through volatilization and is ultimately found in dust, air, and seafood. It was reported that many products contain BDE-47 and landfill waste containing BDE-47 will persist for many years (15). BDE-47 enters the human body through oral ingestion and inhalation, and can become detectable in various types of human samples including blood, adipose tissue, and human milk (16).

Previous studies about the impact of BDE-47 mostly focused on neurological development, endocrine disruption and tumor initiation. Several studies have revealed that BDE-47 could impair neuronal differentiation (17). BDE-47 could cause DNA damage mediated by oxidative stress, and increase the *in vitro* migration and invasion of human neuroblastoma cells (18–21). Because of the association between PBDEs and hormone levels in humans (22), the impact of PBDEs on hormone-dependent cancers has become a topic of interest. BDE-47 was thought to be an estrogen disruptor with adverse effects on sexual behavior and reproductive function in zebra fish (23). Furthermore, BDE-47 could induce oxidative stress in MCF-7 cells by inhibiting the pentose phosphate pathway (16). An epidemiological survey reported that the serum concentration of BDE-47 in breast cancer women was significantly higher than that of controls (24). However, this pattern was not consistent across all cancers, for instance, BDE-47 could stimulate cell proliferation in human ovarian carcinoma cells OVCAR-3 but not in MCF-7 breast cancer cells (25), reflecting the complicated and inconsistent mechanisms underlying the effect of BDE-47 on different types of cancers.

Chemotherapy is commonly used to treat disseminated or recurrent EC, often after the failure of hormonal therapy. Although the management of EC has undergone a dramatic shift in recent years, and that early-stage EC has a favorable prognosis, the advanced or recurrent EC still has a poor prognosis partially because of chemoresistance. The underlying causes of drug resistance in EC are multi-factorial. Resistance to anti-microtubule agents such as paclitaxel and cisplatin (DDP) is particularly challenging given the importance of these agents in first-line treatment of EC (26). A recent study revealed that cadmium prevented the 5-fluorouracil cytotoxic effect by modifying cell cycle and apoptotic profiles in MCF-7 cells (27). Nonetheless, the potential antagonist effect of BDE-47 against chemotherapy sensitivity of EC has not been well-clarified.

Since EC is an estrogen-dependent cancer and BDE-47 could cause endocrine disruption, we hypothesized that BDE-47 might affect the progression and drug resistance of EC. In this study, the impact of BDE-47 on two human EC cell lines, Ishikawa and HEC-1B cells, was investigated. It has been found that chronic BDE-47 exposure could trigger phenotypic plasticity, promote progression, and even chemoresistance in EC cells, at least in part, via ERα/GPR30 and EGFR (epidermal growth factor receptor)/ERK (extracellular-regulated protein kinase) signaling pathways.

MATERIALS AND METHODS

Cell Lines and Cell Culture

Two endometrial cancer cell lines, Ishikawa (ERα-positive/EGFR-positive), and HEC-1B (ERα-negative/EGFR-positive), were generously provided by Dr. Xiaolong Wei (Cancer Hospital of Shantou University Medical College, Shantou, China) and Dr. Bo Qiu (Southern Medical University, Guangzhou, China). Both these two cell lines have been authenticated. These cells were maintained in complete RPMI 1640 medium (Gibco, ThermoFisher Scientific Inc., California, US), supplemented with 10% fetal bovine serum (FBS, Biological Industry, Kibbutz BeitHaemek, Israel) at 37°C in a 5% CO_2 incubator. To develop a chronically poisoned cell model, both Ishikawa and HEC-1B cells were exposed to 10 μM BDE-47 (Lot No. 3798900, Chemservice Inc., Worms, Germany) for up to 45 days before the experiments, and were designated as Ishikawa-BDE-47 and HEC-1B-BDE-47, respectively.

Cell Treatment

To investigate the effect of BDE-47 on paclitaxel- and DDP-induced cytotoxicity in EC cells, Ishikawa-BDE-47 (10 μM),

HEC-1B-BDE-47 (10 μM), and their parental cells (1×10^4) were treated with 0, 0.1, 1, 1.25, 5 μM of paclitaxel (Bristol-Myers Squibb Company, New York, USA) and 0, 1.25, 2.5, 5, 10, 20, 50, 100 μM of DDP (Hansoh pharma co. LTD, Jiangsu, China) for 48 h, respectively. After that cell viability was evaluated by MTT assays.

To further identify the cross-talk between ERα/GPR30 and EGFR/ERK signal pathway, 10 μM erlotinib (No. #5083, Cell Signaling Technology Inc., Danvers, Massachusetts, US) and 20 μM PD98059 (No. #9900, Cell Signaling Technology Inc., Danvers, Massachusetts, US) were used to inhibit EGFR autophosphorylation and ERK kinases for 48 h before MTT and Western blotting assay.

Transfection With siRNA

Twenty-four hours prior to transfection, approximately 8×10^4 cells (Ishikawa-BDE-47 or HEC-1B-BDE-47) were seeded into 6-well plates and grew to 70–80% confluence. These EC cells were then separately transfected with siERα (sc-29305, Santa Cruz Biotechnology, Inc., Dallas, Texas, US) to silence ERα expression, or with siGPR30 (sc-60743, Santa Cruz Biotechnology, Inc., Dallas, Texas, US) to silence GPR30 expression. Control siRNAs (sc-44230, Santa Cruz Biotechnology, Inc., Dallas, Texas, US) was used as the negative control for the parallel experiments. The EC cells were transfected with siRNA oligonucleotides (20 μM) using lipofectamine 3000 (ThermoFisher Scientific Inc., California, US) following manufacturer's protocols, and then collected after 72 h for MTT and Western blotting assay.

MTT Assay

Cells were separately seeded into 96-well plates at a concentration of 4,000 cells/well, and then subjected to MTT assay. Briefly, MTT assay was performed as follows: cells were first incubated with 5 mg/ml of the sterile filtered MTT solution (Santa Cruz Biotechnology, Inc., Dallas, Texas, US) in phosphate-buffered saline (PBS) and incubated for 4 h in a moist chamber at 37°C, followed by washing with PBS and incubation with DMSO for 10 min with shaking. Solubilized formazan product was detected at OD 490 nm using a microplate reader (Multiskan MK3, ThermoFisher Scientific Inc., California, US). The relative cell viability was calculated using the formula: $(OD_{treatment} - OD_{blank})/(OD_{control} - OD_{blank})$, and the cell inhibition rate was assessed through the formula: 1 − the relative cell viability. Results were summarized by four technical replicates, and each experiment was repeated for triple times.

Cell Migration and Invasion Assay

The transwell chamber (Lot #5011036, Falcon® Cell Culture Inserts, Krackeler Scientific lnc. Albany, New York, US) was used to detect cell migration and invasion. The bottom of the transwell chamber was made of a polycarbonate membrane with 8 μm membrane pores. For invasion assays, an additional matrigel (50 μl: 50 mg/l, BD biosciences, Franklin Lakes, New Jersey, US) was used to cover the surface of the polycarbonate membrane. Each group of cells (1×10^5 cells suspended in 200 μl serum-free RPMI-1640 medium with 1% BSA) was seeded into the upper chamber, and 600 μl 10% FBS-supplemented RPMI-1640 medium was added to the lower chamber. After 24 h (migration assay) or 48 h (invasion assay), the upper chamber and cells on the upper surface of the membrane were removed. Cells transferred to the lower surface of the membrane were stained with 0.1% crystal violet, and the number of cells was counted under a Leica microscope (Model: DM3000, Wetzlar, Germany). Five fields from each sample were randomly selected for calculating stained cells (28). Results were summarized by three technical replicates, and each experiment was repeated for three times.

EC Xenografts

Twenty nude mice were purchased from Vital River Laboratory Animal Technology Co. Ltd (Beijing, China). The animal protocol was reviewed and approved by the Medical Animal Care and Welfare Committee at Shantou University Medical College. The body weights of the mice ranged from 20 to 25 g. The mice were randomly allocated into two groups. The right axilla of ten mice was subcutaneously injected with 4×10^6 Ishikawa or Ishikawa-BDE-47 (10 μM) cells. The growth of xenograft tumors was measured every 3 days using a digital caliper, and tumor volume was calculated using the formula: Length × Width^2 × 0.5. After 31 days, mice were euthanized, and the xenograft tumors were dissected. Additionally, other ten mice were used to detect effect of BDE-47 on the migration ability of EC cells. In that case, 5×10^6 Ishikawa or Ishikawa-BDE-47 (10 μM) cells were given intravenously through the tail. After 14 days, mice were euthanized, and potential metastasis were found and counted in the cervical, axillary, and abdominal lymph nodes, lung and liver. Lymph nodes were fixed and embedded in paraffin for histology and immunohistochemistry (IHC) staining analyses.

Hematoxylin-Eosin Staining and Immunohistochemistry

Lymph nodes of mice were collected, fixed in 10% phosphate-buffered formalin for 24 h, and embedded in paraffin wax. Sections of tumors (4 μm in thickness) were stained with hematoxylin-eosin and pictured under a light microscope (DX45, Olympus Microsystems Ltd., Japan). IHC for Pan Cytokeratin (Kit-0009, MXB Biotechnologies, Fuzhou, China) was carried out on sections using a standard EnVision complex method. After deparaffinization and rehydration, endogenous peroxidase activity was blocked with 0.3% hydrogen peroxide for 30 min. Then tissue sections were autoclaved at 121°C in citrate buffer (pH 6.0) for 10 min, and incubated with mouse anti-Cytokeratin monoclonal antibody. IHC staining was carried out with the anti-Mouse/Rabbit (Kit-5030, MXB Biotechnologies, Fuzhou, China) and 3,3′-diaminobenzidine as the chromogen substrate. Negative control was obtained by replacing the primary antibody with normal rabbit IgG.

Western Blotting (WB)

For WB analysis, cells were first lysed with a cell lysis buffer containing PMSF (Phenylmethanesulfonyl fluoride, both from Beyotime, Shanghai, China) on ice for 30 min and centrifuged at 12,000 rpm for 15 min at 4°C to remove cell debris. Proteins

(50 μg) of each cell lysate were then separated by SDS-PAGE and transferred onto a PVDF membrane followed by blocking with Tris-buffered saline containing 0.05% Tween 20 (TBST) and 5% non-fat milk for 1 h at room temperature, washed 3 times for 5 min each in TBST, and incubated at 4°C overnight with either mouse anti-GAPDH monoclonal antibody (1:3,000, ZSGB-BIO, Beijing, China), rabbit anti-phospho-EGF receptor (Tyr1148) polyclonal antibody (EGFR antibody, 1:1,000, #4404, Cell Signaling Technology Inc., Danvers, Massachusetts, US), rabbit anti-GPR30 polyclonal antibody (1:1,000, sc-48525-R, Santa Cruz Biotechnology Inc., Dallas, Texas, US), rabbit ERα monoclonal antibody (1:1,000, #2294327, Millipore Inc., Darmstadt, Germany), rabbit P-EGFR antibody (Y1148) (pEGFR antibody, 1:1,000, #4404S, Cell Signaling Technology Inc., Danvers, Massachusetts, US), rabbit P-p44/42 MAPK antibody (T202/Y204) (pERK antibody, 1:1,000, #4370S, Cell Signaling Technology Inc., Danvers, Massachusetts, US), or rabbit p44/42 MAPK antibody (ERK antibody, 1:1,000, #4695S, Cell Signaling Technology Inc., Danvers, Massachusetts, US) in blocking buffer. Following washes with TBST (3 times for 5 min each), the blots were incubated with horseradish peroxidase-labeled anti-rabbit (1:5,000, Novus Biologicals, Littleton, Massachusetts, US) or anti-mouse (1:3,000, Santa Cruz Biotechnology Inc., Dallas, Texas, US) IgG at room temperature for 2 h, washed with TBST, and observed through chemiluminescence (ChemiDoc™ XRS+, Bio-Rad Laboratories, Inc., Hercules, California, US).

Statistical Analysis

Statistical analyses were performed using the SPSS 13.0 software package (SPSS Inc., Chicago, IL). The comparisons of cell viability, cell numbers representing the capacity of cell migration and invasion, and xenograft tumor size between different treatment groups were conducted using *t*-tests. For all tests, a *P*-value of <0.05 was considered significant.

RESULTS

BDE-47 Boosted Viability and Metastatic Capacity of EC Cells

Ishikawa and HEC-1B cells were incubated with different concentrations (0.1, 1, 2.5, 5, 10, 20, 40, and 80 μM) of BDE-47. The positive effect of BDE-47 on cell viability was observed at concentrations of 10 μM (relative cell viability at 48 and 72 h after BDE-47 treatment: 1.246, $P = 0.005$; 1.416, $P < 0.001$) and 20 μM (1.218, $P = 0.014$; 1.319, $P < 0.001$) in Ishikawa cells, as well as in HEC-1B cells at concentrations of 10 μM (1.282, $P < 0.001$; 1.416, $P < 0.001$) and 20 μM (1.179, $P < 0.001$; 1.265, $P = 0.001$) in contrast to that in their parental cells (**Figure 1A**). Based on these data, 10 μM was selected as the chronic BDE-47 treatment concentration in Ishikawa and HEC-1B cells. MTT assays showed that the cell viability of Ishikawa-BDE-47 cells was slightly increased in contrast to Ishikawa cells after 24 h (OD values: 0.42 vs. 0.35, $P = 0.045$) and 48 h (0.63 vs. 0.55, $P = 0.031$), and the increase was more obvious after 72 h (1.23 vs. 0.90, $P = 0.008$) and 96 h (1.55 vs. 1.23, $P = 0.001$). A similar trend was observed in HEC-1B-BDE-47 cells and their parental cell line, of which OD values were 0.36 and 0.27 at 24 h ($P = 0.010$), 0.51 and 0.36 at 48 h ($P = 0.001$), 1.16 and 0.84 at 72 h ($P = 0.019$), and 1.32 and 0.93 at 96 h ($P = 0.013$; **Figure 1B**).

To examine whether BDE-47 could promote metastasis in EC cells, transwell chamber assays were performed. As shown in **Figure 1C**, the average number of Ishikawa-BDE-47 cells migrating across the membrane was significantly higher than that of the parental cells (89.6 ± 8.0 vs. 44.0 ± 8.1, $P < 0.001$). Similarly, the average number of migrated HEC-1B-BDE-47 cells was evidently higher than that of HEC-1B cells (75.0 ± 13.7 vs. 18.4 ± 5.8, $P < 0.001$). Moreover, both Ishikawa-BDE-47 (number of invaded cells: 49.8 ± 8.8 vs. 11.2 ± 0.45, $P < 0.001$) and HEC-1B-BDE-47 (19.6 ± 2.5 vs. 6.0 ± 1.3, $P < 0.001$) showed more invasive ability as compared to their parental cells. These results indicated that Ishikawa-BDE-47 and HEC-1B-BDE-47 cells have increased the cell viability and metastatic capacity.

BDE-47 Enhanced the Growth and Metastasis of EC *in vivo*

In order to understand the effect of BDE-47 on EC cell growth *in vivo*, Ishikawa cells were subcutaneously injected into mice. As shown in **Figure 1D**, tumor volumes of Ishikawa xenografts on days 10, 22, and 31 reached 11.08 mm^3 (±4.38), 167.11 mm^3 (±37.46), and 296.78 (±65.71) mm^3, respectively, while larger tumor sizes were observed in Ishikawa-BDE-47 xenografts: 39.85 mm^3 (±14.83, $P = 0.010$), 261.76 mm^3 (±61.91, $P = 0.040$), and 408.95 mm^3 (±54.83, $P = 0.040$). Additionally, potential metastasis were found and quantified. In the mice inoculated with Ishikawa-BDE-47 cells, there were 22, 10, and 4 metastatic tumors confirmed by cytokeratin IHC staining (**Figures 1E,F**, **Table 1**) in the lymph nodes of the neck, axilla and enterocoele of these mice, respectively. However, only one metastasis in the lymph nodes of the neck was found in the mice with Ishikawa xenografts (**Figures 1E,F**, **Table 1**). The cellular morphology of metastasis was assessed by HE staining (**Figure 1F**).

BDE-47 Lessened the Paclitaxel and DDP Cytotoxic Effects on EC Cells

We next explored whether BDE-47 exposure could attenuate sensitivity of EC cells to DDP or paclitaxel. As shown in **Figures 2A,B**, both of Ishikawa-BDE-47 and HEC-1B-BDE-47 cells consistently exhibited lower DDP sensitivity compared to their parental non-treated cells at different concentrations. The cell inhibition rates of Ishikawa-BDE-47 at the concentration of 2.5 and 5 μg/l were 0.275 and 0.436, while these numbers of Ishikawa cells were 0.555 and 0.711 ($P = 0.007$; $P < 0.001$). Similarly, the cell inhibition rates in HEC-1B at the concentrations of 2.5, 5, and 10 μg/l were 0.517, 0.609, and 0.679, but separately reduced to 0.234, 0.337, and 0.573 in HEC-1B-BDE47 cells ($P = 0.002$; $P = 0.003$; $P = 0.014$). Regarding paclitaxel, BDE-47 treatment also reduced its cytotoxicity to Ishikawa and HEC-1B cells. As seen in **Figure 2C**, Ishikawa-BDE-47 had significantly lower cell inhibition rates than that in Ishikawa cells, when exposed to paclitaxel (at 0.1 μg/l: 0.088 vs. 0.341, $P = 0.029$; 1 μg/l: 0.158 vs. 0.339, $P < 0.001$; 2.5 μg/l: 0.332 vs. 0.688, $P < 0.001$; 5 μg/l: 0.689 vs. 1.018, $P < 0.001$). Likewise, HEC-1B-BDE-47 displayed an

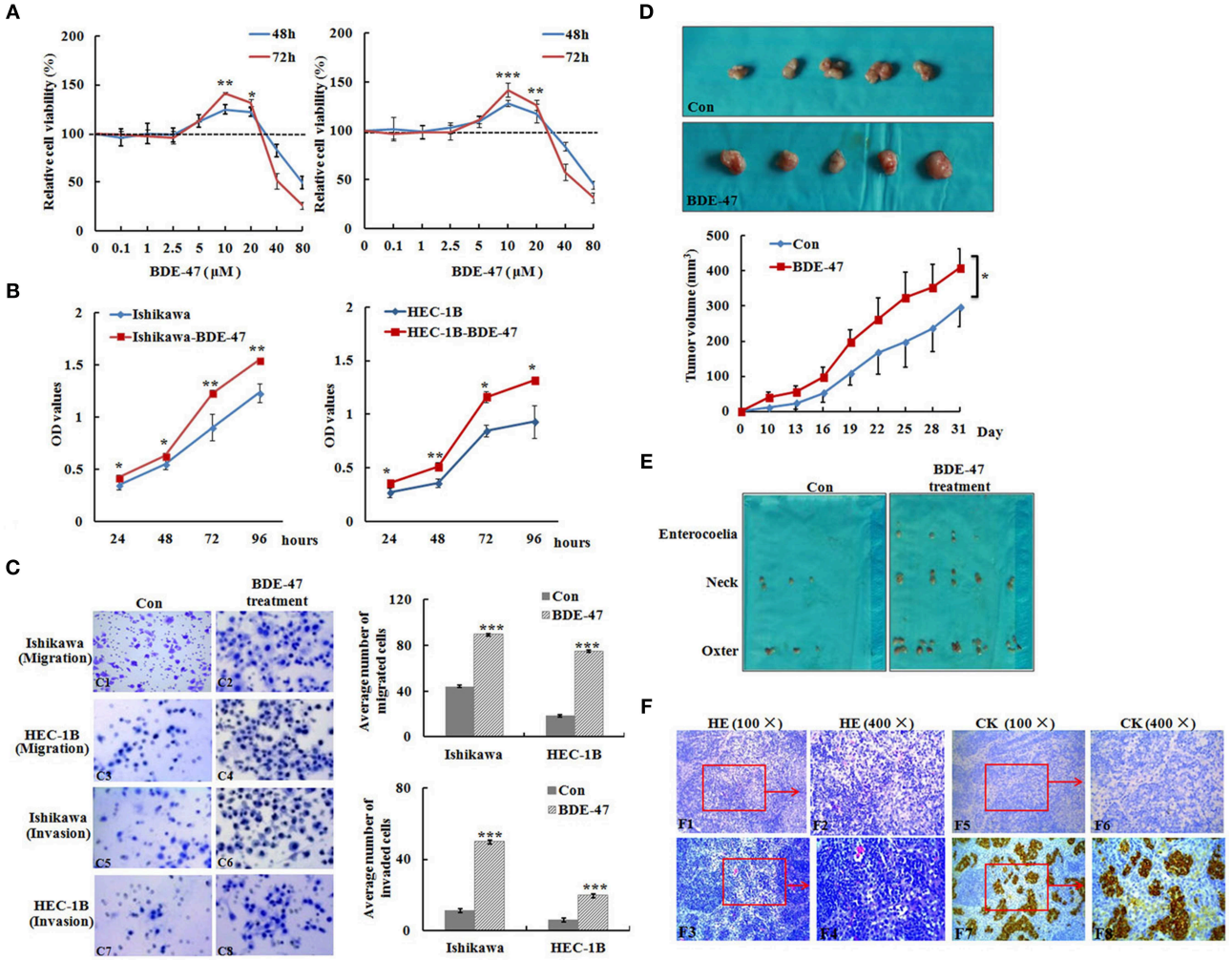

FIGURE 1 | Effect of BDE-47 on the viability and metastasis of EC cells. **(A)** MTT assay on Ishikawa (Left panel) and HEC-1B (Right panel) cells treated with BDE-47 at the concentrations of 0.1, 1, 2.5, 5, 10, 20, 40, and 80 μM for 48 and 72 h. **(B)** OD values reflecting the viability capacity of Ishikawa (Left panel) and HEC-1B cells (Right panel) recorded at 24, 48, 72, and 96 h after cells were exposed to BDE-47 at 10 μM for 45 days. **(C)** Cell migration (C1–C4) and invasion (C5–C8) assay on Ishikawa/Ishikawa-BDE-47 and HEC-1B/HEC-1B-BDE-47 cells. Representative images (400×) of cell migration (C1–C4) and invasion (C5–C8) are shown on the left side. **(D)** Primary xenograft tumors of Ishikawa cells and tumor volumes. **(E)** Lymph nodes containing potential metastasis from mice were found and shown. **(F)** Upper panel: HE staining assessed cellular morphology of lymph nodes with or without metastatic tumors. F1: 100×, F2: 400×, F3: 100×, F4: 400×). Lower panel: IHC staining of cytokeratin negative in F5 (100×) and F6 (400×), and positive in F7 (100×) and F8 (400×). CK, Cytokeratin; Con, Ishikawa cells without BDE-47 treatment. *$P < 0.05$; **$P < 0.01$; ***$P < 0.001$.

inferior cell inhibition rate with the treatment of paclitaxel at the concentration of 5 μg/l compared to its parental cells (0.809 vs. 0.993, $P = 0.002$, **Figure 2D**).

BDE-47 Increased Viability and Metastatic Capacity of EC Cells Through the ERα/GPR30 and ERFR/ERK Signaling Pathways

Estrogens are steroid hormones that regulate a plethora of physiological processes in mammals. Activation of ERα by estrogens is a well-known mechanism underlying EC development. Expression of GPR30 has been suggested to be a novel indicator of EC progression (9). As shown in **Figure 3A**, levels of both ERα and GPR30 proteins were elevated in ERα-positive Ishikawa-BDE-47 cells when compared to that in their parental cell line. In ERα-negative HEC-1B cells, BDE-47 treatment significantly up-regulated GPR30 expression. Since activation of EGFR/ERK signaling pathway through ERα/GPR30 was present in other cancer cells (29), we detected proteins of EGFR, pEGFR, ERK, and pERK by Western blotting. Significant up-regulation of pEGFR and pERK, but not total EGFR and ERK expression, was seen in Ishikawa-BDE-47 cells compared to that in Ishikawa cells. A similar phenomenon was observed in HEC-1B-BDE-47 and its parental cells. These results indicated a cross talk between ERα/GPR30 and ERFR/ERK signaling pathways potentially underlying the increased proliferative and metastatic effect of BDE-47.

TABLE 1 | Summary of the numbers of lymph nodes with or without metastatic tumors by Cytokeratin IHC staining.

Characteristics	Control	BDE-47
Number of mice	5	5
Total lymph nodes[a]	8	37
Without met[b]	7	1
With met[c]	1	36
Proportion (%)[d]	12.5	97.3
NECK		
Total lymph nodes[e]	4	22
Without met[f]	3	0
With met[g]	1	22
Proportion (%)[h]	25	100
AXILLA		
Total lymph nodes[e]	4	10
Without met[f]	4	0
With met[g]	0	10
Proportion (%)[h]	0	100
ENTEROCOELE		
Total lymph nodes[e]	0	5
Without met[f]	0	1
With met[g]	0	4
Proportion (%)[h]	0	80

[a] *Total number of extracted lymph nodes.*
[b] *Lymph nodes without metastasis.*
[c] *Lymph nodes with metastasis.*
[d] *The proportion of lymph nodes with metastasis to all extracted lymph nodes.*
[e] *Total number of extracted lymph nodes from neck, axilla, or enterocoele.*
[f] *Lymph nodes without metastasis from neck, axilla, or enterocoele.*
[g] *Lymph nodes with metastasis from neck, axilla, or enterocoele.*
[h] *The proportion of lymph nodes with metastasis to all extracted lymph nodes from neck, axilla, or enterocoele.*

Down-Regulation of ERα/GPR30 Attenuated Viability and Metastatic Capacity of EC Cells Induced by BDE-47

To investigate the role of ERα/GPR30 in BDE-47 induced EC cell viability, Ishikawa-BDE-47 (ERα+/GPR30+) cells were treated with siERα and siGPR30. Because of its ER-negativity, HEC-1B-BDE-47 cells were only treated with siGPR30. As shown in **Figure 3B**, significant reductions in ERα and GPR30 expression were observed in Ishikawa-BDE-47-siER and Ishikawa-BDE-47-siGPR30 cells in contrast to that in Ishikawa-BDE-47 cells. Similarly, GPR30 expression was reduced in HEC-1B-BDE-47-siGPR30 compared to that in HEC-1B-BDE-47 cells. MTT assay also revealed significant inhibition of cell viability in Ishikawa-BDE-47-siER cells (OD values at 24, 48, 72 h: 0.42 vs. 0.40, $P = 0.500$; 0.63 vs. 0.48, $P = 0.005$; 1.17 vs. 0.66, $P < 0.001$) and Ishikawa-BDE-47-siGPR30 cells (OD values at 24, 48, 72 h: 0.46 vs. 0.39, $P = 0.296$; 0.65 vs. 0.46, $P = 0.008$; 1.17 vs. 0.67, $P < 0.001$) when compared to their parental cells. Similarly, a significant reduction in cell viability was seen in HEC-1B-BDE-47-siGPR30 in contrast to HEC-1B-BDE-47 (OD values at 24, 48, 72 h: 0.44 vs. 0.39, $P = 0.367$; 0.63 vs. 0.48, $P = 0.012$; 1.11 vs. 0.62, $P < 0.001$). **Figure 4A** illustrates the MTT results of siRNA at 72 h. Additionally, the transwell assay revealed an impaired capacity of metastasis in Ishikawa-BDE-47-siER (number of migrated cells: 44.0 vs. 81.4, $P < 0.001$; number of invaded cells: 37.0 vs. 48.2, $P = 0.003$, **Figures 4B–D**) and Ishikawa-BDE-47-siGPR30 (number of migrated cells: 47.8 vs. 76.4, $P < 0.001$; number of invaded cells: 39.8 vs. 57.6, $P = 0.003$, **Figures 4B–D**) compared to the corresponding parental cells. A similar trend was seen in HEC-1B-BDE-47-siGPR30 and its parental cells (number of migrated cells: 51.6 vs. 64.4, $P = 0.010$; number of invaded cells: 17.6 vs. 26.2, $P = 0.009$, **Figures 4B–D**).

Inhibition of pEGFR or pERK Weakened Viability and Metastatic Capacity in BDE-47-Treated EC Cells

As shown in **Figure 3B**, gene knock-down using siGPR30 or siER down-regulated the expression of pERK and pEGFR but not total ERK and EGFR. To further demonstrate the role of EGFR/ERK signaling pathway in EC cell viability induced by BDE-47, a pEGFR inhibitor or a pERK inhibitor was applied to Ishikawa-BDE-47 and HEC-1B-BDE-47 cells (**Figure 3C**). As shown in **Figure 4A**, the pEGFR inhibitor significantly down-regulated the extent of cell viability and metastasis stimulated by BDE-47 in both Ishikawa-BDE-47 and HEC-1B-BDE-47 cells. OD values at 48 h of Ishikawa-BDE-47 treated with and without the pEGFR inhibitor at 10 μM were 0.36 and 0.68 ($P < 0.001$), indicating significant inhibition. Similarly, notable suppression was seen in HEC-1B-BDE-47 cells treated with the pEGFR inhibitor at a concentration of 10 μM (OD values at 48 h: 0.34 vs. 0.64, $P < 0.001$). The EGFR/ERK signaling pathway is the classical MAPK pathway. The pERK inhibitor seemed to block the effect of BDE-47 on Ishikawa and HEC-1B cells. As shown in **Figure 4A**, OD values at 48 h of Ishikawa-BDE-47 was 0.68, but this was reduced to 0.38 ($P < 0.001$) after the pERK inhibitor treatment at a concentration of 20 μM. Similarly, OD value of HEC-1B was reduced from 0.64 to 0.34 ($P < 0.001$) after the pERK inhibitor treatment. These results suggested that the EGFR/ERK signaling pathway might be at the downstream of ER/GPR30 and be involved in BDE-47-induced EC cell viability.

The transwell assay was used to examine the metastatic capacity of Ishikawa-BDE-47 and HEC-1B-BDE-47 cells treated with a pEGFR inhibitor at 10 μM or a pERK inhibitor at 20 μM for 48 h. After the addition of a pEGFR inhibitor, the number of migrated and invaded cells was reduced from 78.0 ± 8.8 to 38.8 ± 13.7 ($P < 0.001$), and from 63.0 ± 2.7 to 38.8 ± 5.2 ($P < 0.001$, **Figures 4B–D**), respectively. The same trend of cell invasion and migration was also seen in HEC-1B-BDE47 cells after the pEGFR inhibitor treatment. The number of migrated cells was reduced from 49.8 ± 6.5 to 19.2 ± 2.2 ($P < 0.001$), and the number of invaded cells was reduced from 25.0 ± 3.6 to 19.2 ± 2.2 ($P = 0.015$). Likewise, as shown in **Figures 4B–D**, treatment with a pERK inhibitor for 48 h impaired the metastatic ability of Ishikawa-BDE-47 and HEC-1B-BDE-47 cells, accompanied with reductions in the numbers of migrated and invaded cells from 77.0 ± 5.43 to 24.2 ± 3.77 ($P < 0.001$, **Figure 4D** left panel for Ishikawa-BDE-47), from 48.2 ± 4.92 to 20.4 ± 5.86 ($P < 0.001$, **Figure 4D** right panel for Ishikawa-BDE-47), from 75.0 ± 13.69

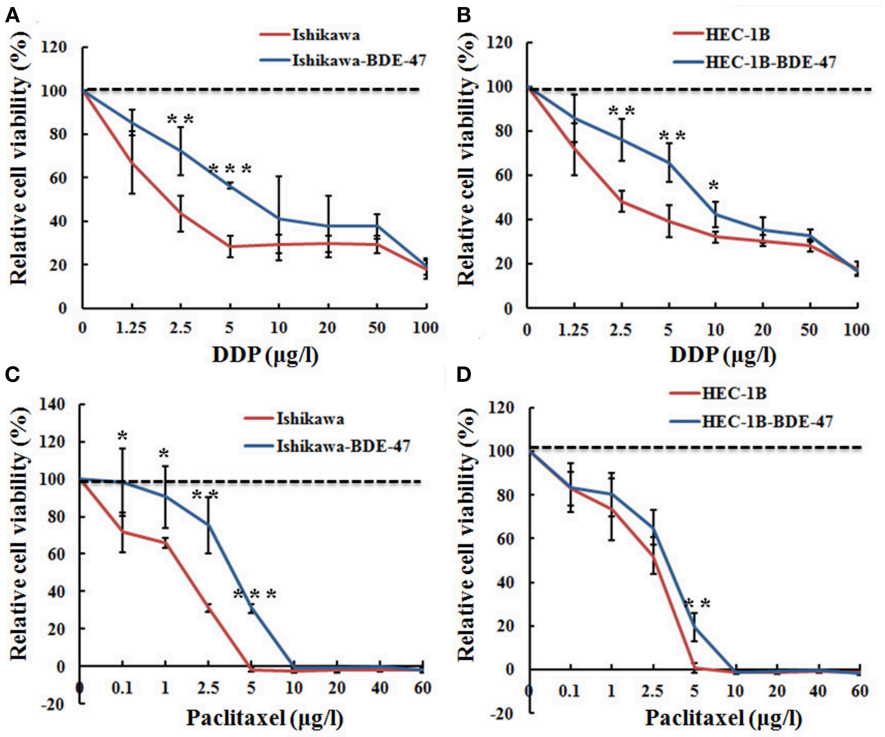

FIGURE 2 | Relative cell viability of Ishikawa-BDE-47, HEC-1B-BDE-47 and their parental cells before and after treatment with DDP or paclitaxel. MTT assays were performed before and after retreatment with different concentrations of DDP for 48 h in Ishikawa-BDE-47 **(A)**, or in HEC-1B-BDE-47 cells **(B)**, as well as their parental cells. Different concentrations of paclitaxel were also used to treat Ishikawa and Ishikawa-BDE-47 **(C)**, as well as HEC-1B and HEC-1B-BDE-47 **(D)**, and then after 48 h, relative cell viability was assessed. $^{*}P < 0.05$; $^{**}P < 0.01$; $^{***}P < 0.001$.

to 25.2 ± 3.49 ($P < 0.001$, **Figure 4D** left panel for HEC-1B-BDE-47), and from 19.6 ± 2.88 to 12.2 ± 2.05 ($P = 0.001$, **Figure 4D** right panel for HEC-1B-BDE-47).

DISCUSSION

PBDEs are considered as endocrine-disrupting chemicals with thyroxine- and estrogen-like effects (30). One publication by Li et al. revealed that PBDE-209 increased the viability and proliferation of cells in several types of cancer, including breast cancer, cervical cancer, and ovarian cancer. Interestingly, PBDE-209-up-regulated phosphorylation of ERK was also observed (31). In colon cancer HCT-116 cells, BDE-99 was found to increase the cell migration and invasion as well as to trigger EMT (epithelial–mesenchymal transition), most likely via the PI3K/AKT/Snail signaling pathway (11).

Interestingly, BDE-47 could exert a differential effect on different types of cancer cells. In human neuroblastoma SH-SY5Y cells, BDE-47 had limited cytotoxicity but significantly increased the *in vitro* cell migration and invasion by up-regulating MMP-9 through the GPR30/PI3K/Akt signaling pathway (21). In OVCAR-3cells, BDE-47 was found to stimulate cell proliferation by activating CDK1, CDK7, E2F1, and E2F2; however, this effect was not observed in MCF-7 cells. Notably, BDE-47 had no effect on ERα protein expression in OVCAR-3 cells, while decreased ERα protein expression in MCF-7 cells. Additionally, BDE-47 had no effect on ERK phosphorylation in the two cell lines (25). In contrast, Kanaya et al. recently reported that BDE-47 stimulated proliferation of an estrogen-dependent breast cancer cell line MCF-7aroERE and induced ER-regulated genes expression, which suggested that BDE-47 acted as a weak agonist of both ERα and estrogen-related receptor α (ERRα) (32). One previous case-control study from our laboratory demonstrated that BDE-47 level was positively with breast-cancer risk regardless of ER stratification (33). Similarly in this study, BDE-47 treatment enhanced the cell growth, invasion and migration in both Ishikawa and HEC-1B cells.

The differences between the above studies may attribute to cell specificity, exposure time, and moreover, a different effect for the parent compound and its metabolites. We noticed that the exposure model in Karpeta's research was short-term treatment for 72 h, while that in Kanaya's paper and the present study were longer for 5 days and up to 45 days, respectively. Furthermore, hydroxylated metabolites of PBDE were found to be more potent agonists of estrogen receptors than the parent compounds (34). For instance, BDE-47 had no effect on ERα and ERβ protein expression in OVCAR-3 cells, whereas 5-OHBDE-47 upregulated ERα only and 6-OH-BDE-47 increased both ERα and ERβ protein expression (25). Previous studies have indicated that CYP2B6, a predominant cytochrome P450s, was involved in the

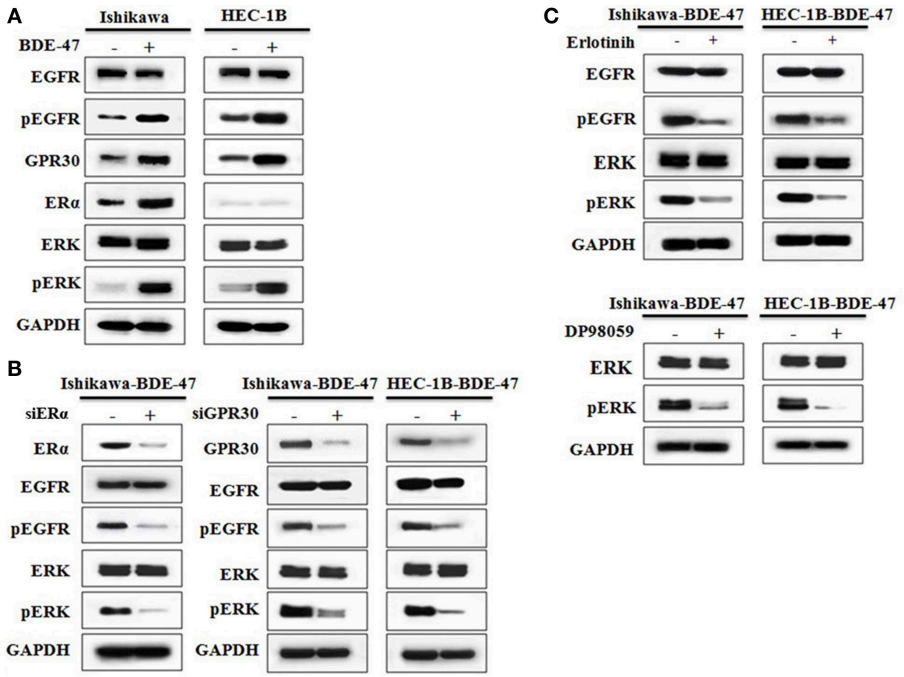

FIGURE 3 | Western blotting on protein expressions of ERα, GPR30, EGFR, pEGFR, ERK, and pERK. **(A)** Protein expression in Ishikawa and HEC-1B cells with or without exposure to 10 μM BDE-47. **(B)** Protein expression in Ishikawa-BDE-47 and HEC-1B-BDE-47 cells treated with or without siERα, and siGPR30. **(C)** Expression of pEGFR and EGFR in Ishikawa-BDE-47 and HEC-1B-BDE-47 after pEGFR inhibitor (erlotinib) treatment (left). Expression of pERK and total ERK in Ishikawa-BDE-47 and HEC-1B-BDE-47 after pERK inhibitor (DP98059) treatment (right).

formation of hydroxylated PBDEs (OH-PBDEs) (35). Although no evidence has been established for the expression of this enzyme in EC cells, detecting hydroxylated BDE-47 in the culture medium of Ishikawa-BDE-47 and HEC-1B-BDE-47 cells will help to exclude the potential effect of hydroxylated metabolites of BDE-47 on EC cell biology in the present study.

ERα, a ligand-activated transcription factor localizing in the nucleus, is expressed in approximately 80–90% of endometrioid tumors. The estrogen-ERα signaling pathway is implicated in increased uterine growth (36). The newly discovered membrane estrogen receptor GPR30, expressed in ∼80% of endometrioid tumors (5), is a specific receptor for 17β-estradiol involved in the non-genomic effect of estrogen. GPR30 was also addressed to mediate the proliferative and invasive effects of estrogen and tumorigenesis in EC cell line (37) and suggested to be an indicator of clinical outcomes of EC (9). It is well-known that the classical mechanism of estrogen action involves binding to the ERα and ERβ, which regulates transcription through direct binding at estrogen-responsive elements in the promoter region of target genes or through tethering to other well-known transcription factors such as AP1, SP1, and nuclear factor κB (38). Emerging evidence has indicated that GPR30 mediated invasion and carcinogenesis induced by 17-β estradiol in an EC cell line (37). To highlight a possible estrogen receptors involvement in the effect of BDE-47 on EC cells, we detected the status of ERα and GPR30 in these two cell lines. The upregulation of ERα and GPR30 in Ishikawa-BDE-47 cells and increased GPR30 expression in HEC-1B-BDE-47 suggest that both ERα and GPR30 are the main targets of BDE-47. Furthermore, siRNA for ERα or GPR30 in BDE-47-treated Ishikawa and HEC-1B cells attenuated the catalytic role of BDE-47 on malignant phenotypes. Since the upregulation of ERα and GPR30 in BDE-47-treated EC cells, we speculate BDE-47 carried out its cancer-promoting effect on EC cells via estrogen molecular pathways. Mitogen-activated protein kinase (MAPK) cascades are key signaling pathways involved in various cellular functions, including cell proliferation, differentiation, survival, and metastasis. EGFR/ERK is the classical MAPK signaling pathway. Recently, a link between environmental chemicals such as Bisphenol A and cancer progression has been suggested in ER-negative in flammatory breast cancer cells, in which EGFR/ERK signaling was involved (39). It is believed that the cross-talk between EGFR and ERα plays a critical role in the regulation of breast cancer development (40). Polychlorinated biphenyl 104 was found to promote migration and invasion of endometrial stromal cells by inducing the expression of MMP-3 and MMP-10, which may involve in the EGFR signaling pathway (41). The cross talk between GPR30 and EGFR/ERK signaling pathways is supported by other studies. GPR30-EGFR signaling pathway was reported to be involved in Bisphenol A promoting the proliferation of leiomyoma cells (42). One study from Zhang et al. (43) revealed that tamoxifen, known for its agonist activity on GPR30, could up-regulate the phosphorylated protein expression of both EGFR and ERK in EC cells, without altering total EGFR/ERK protein expression, indicating that the growth stimulation of EC cells in response to 4-OH tamoxifen

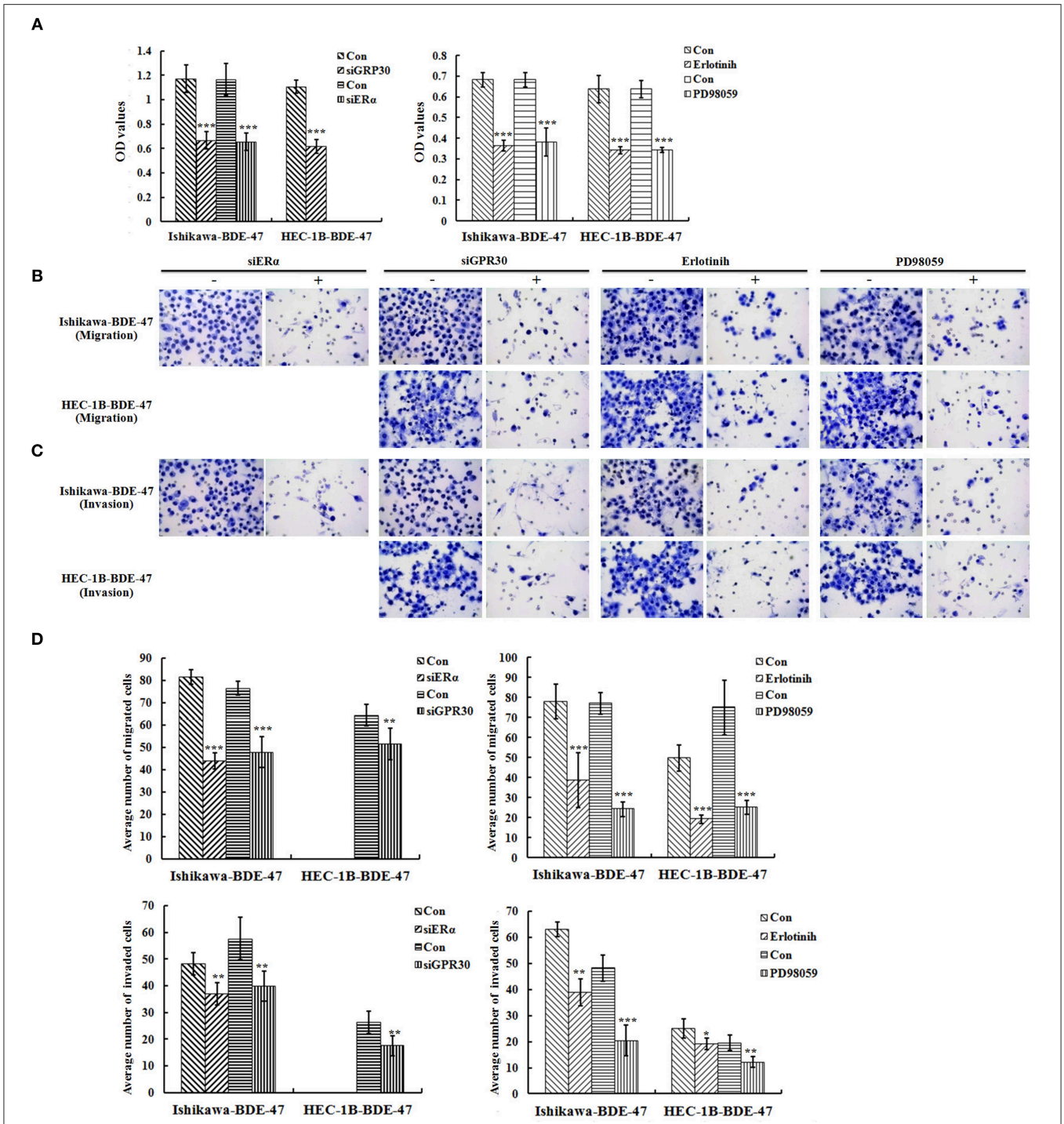

FIGURE 4 | Role of ERα/GPR30 and EGFR/ERK signaling pathway underlying the viability and metastatic effect induced by BDE-47. **(A)** Cell viability of Ishikawa-BDE-47 and HEC-1B-BDE-47 cells at 72 h after transfection with siERα or siGPR30, or the treatment with pEGFR inhibitor (erlotinib) or pERK inhibitor (PD98059) for 48 h. **(B–D)** The migration and invasive capacity of Ishikawa-BDE-47 and HEC-1B-BDE-47 cells after transfection with siERα or siGPR30, and treatment with pEGFR inhibitor (erlotinib) or pERK inhibitor (PD98059). Representative images (400×) of cell migration **(B)** and invasion **(C)** are shown. Con: refer to Ishikawa-BDE-47 or HEC-1B-BDE-47 without any other treatment. *$P < 0.05$; **$P < 0.01$; ***$P < 0.001$.

was via the GPR30/EGFR pathway. Another publication noted that both estradiol and tamoxifen could induce cell migration through GPR30 in EC cells with or without ERα expression, accompanied by elevated ratios of pEGFR/Total-EGFR and pERK/Total-ERK. ERα could only be partially involved in this progress (44). Unlike in either the OVCAR-3 cells or MCF-7 cells

mentioned above, increased phosphorylation of EGFR and ERK were observed in the BDE-47-treated EC cells. Simultaneously, siRNA for ERα and GPR30 reduced phosphorylated EGFR and ERK expression levels. Moreover, BDE-47-induced estrogen-like effect was partially impaired in cells treated with either an EGFR inhibitor (erlotinib) or an ERK inhibitor (PD98059). The present study is the first to investigate the cross talk between EGFR/ERK and ERα/GPR30 underlined the stimulation of EC cells by BDE-47. GPR30/ERα and EGFR/ERK seem to be the general pathways mediating the impact of BDE-47 on the development of EC.

Previous studies indicated that cadmium, a metalloestrogen, influenced the 5-Fluorouracil cytotoxic effects on breast cancer cells (27, 45). Both clinical observations and experimental studies have suggested that steroid hormones and their receptors affect the therapeutic efficacy of antineoplastic drugs (46). It was demonstrated that ERα/17β-estradiol attenuates therapeutic efficacy of paclitaxel on breast xenograft tumors (47). Another *in vitro* study showed that the increase in ERα expression in ERα-negative Bcap37 breast cancer cells significantly increased their chemoresistance, whereas ERα activation by 17β-estradiol increased the sensitivity of natural ERα-positive T47D breast cancer cells to chemotherapeutic agents (48). Considering the upregulation of ERα and/or GPR30 in BDE-47-treated EC cell lines, we speculate that estrogen signaling pathway is involved in the chemoresistance mechanism. In the present study, the resistance to paclitaxel and DDP induced by BDE-47 was enhanced in both Ishikawa and HEC-1B cells, which suggests that not only the ER alpha status but also other molecular mechanism influence on observed results. Interestingly, up-regulating GPR30 was also found in high-risk endometrial cancer patients with lower survival rates (9) and in tamoxifen-resistant breast cancer cells through the EGFR/ERK transduction pathway (49). More exhaustive and systematic studies are essential to reach deeper understandings on the cross talk between ERα/GPR30 and EGFR/ERK signaling pathway involved in BDE-47 induced chemoresistance as well as the chemoresistance differences in HEC-1-B-DBE-47 and Ishikawa-BDE-47 cells. It suggests that considering the influence of BDE-47 exposure on chemosensitivity, determining the body BDE-47 burden in EC patients might be taken into account when using chemotherapeutic drugs.

The concentration used in this BDE-47 exposure model is based on the dose-response experiment and the data shown previously in other *in vitro* systems (34, 50–52). Recently, Kanaya compared with *in vitro* breast cancer cell culture treatment at dosage of 10 μM to the published human serum/tissue concentrations of PBDEs (BDE-47 included), and concluded that the maximum concentrations observed in human serum and tissue concentrations were ∼1,300 and 350 times lower than 10 μM, respectively (32). Therefore, future study will be needed to advance understanding the effect of environmentally relevant low-dose PBDEs on the progression and chemoresistance of EC cells *in vitro* and *in vivo*, which will help to answer the critical question whether real-life BDE-47 exposure could be a risk of human EC and resistance factor for chemotherapy.

In summary, this preliminary study shows BDE-47 promotes cell growth, migration and even chemoresistance of EC cells both *in vivo* and *in vitro*. We speculate that this progress, at least in part, mimicks the effects of estrogen. The cross talk between ERα/GPR30 and the EGFR/ERK signaling pathway might be a crucial mechanism underlying the impact of BDE-47 on EC cell plasticity and chemoresistance.

DATA AVAILABILITY STATEMENT

The raw data supporting the conclusions of this manuscript will be made available by the authors, without undue reservation, to any qualified researcher.

ETHICS STATEMENT

The animal study was reviewed and approved by Medical Animal Care & Welfare Committee of Shantou University Medical College.

AUTHOR CONTRIBUTIONS

FZ performed the statistical analyses and drafted the manuscript. JC designed and performed the experiments. YH and LP helped to draft and revise the manuscript. XL helped to revise this manuscript. LP and LZ conceived of the study and supervised the work. All authors read and approved the final manuscript.

FUNDING

This work was supported by the Science and Technology Planning Project of Guangdong Province, China (No. 2014A020212287), Science and Technology Planning Project of Shantou City, China (No. [2018]121-12), and Shantou University Medical College Clinical Research Enhancement Initiative (No. [2014]29-13).

REFERENCES

1. Ferlay J, Soerjomataram I, Dikshit R, Eser S, Mathers C, Rebelo M, et al. Cancer incidence and mortality worldwide: sources, methods and major patterns in GLOBOCAN 2012. *Int J Cancer.* (2015) 136:E359–86. doi: 10.1002/ijc.29210
2. Zhao H, Yao Y, Yang H, Ma D, Chen A. Hormone therapy as a management strategy for lung metastasis after 5 years of endometrial cancer: a case report and literature review. *Medicine.* (2017) 96:e9223. doi: 10.1097/MD.0000000000009223
3. Chen W, Zheng R, Baade PD, Zhang S, Zeng H, Bray F, et al. Cancer statistics in China, 2015. *Cancer J Clin.* (2016) 66:115–32. doi: 10.3322/caac.21338
4. Srijaipracharoen S, Tangjitgamol S, Tanvanich S, Manusirivithaya S, Khunnarong J, Thavaramara T, et al. Expression of ER, PR, and Her-2/neu in endometrial cancer: a clinicopathological study. *Asian Pac J Cancer Prev.* (2010) 11:215–20. doi: 10.4172/2155-9929.1000056

5. Wan J, Yin Y, Zhao M, Shen F, Chen M, Chen Q. The positivity of G-protein-coupled receptor-30 (GPR 30), an alternative estrogen receptor is not different between type 1 and type 2 endometrial cancer. *Oncotarget.* (2017) 8:90897–904. doi: 10.18632/oncotarget.18545
6. Di Donato V, Iacobelli V, Schiavi MC, Colagiovanni V, Pecorella I, Palaia I, et al. Impact of hormone receptor status and Ki-67 expression on disease-free survival in patients affected by high-risk endometrial cancer. *Int J Gynecol Cancer.* (2018) 28:505–13. doi: 10.1097/IGC.0000000000001191
7. Revankar CM, Cimino DF, Sklar LA, Arterburn JB, Prossnitz ER. A transmembrane intracellular estrogen receptor mediates rapid cell signaling. *Science.* (2005) 307:1625–30. doi: 10.1126/science.1106943
8. Thomas P, Pang Y, Filardo EJ, Dong J. Identity of an estrogen membrane receptor coupled to a G protein in human breast cancer cells. *Endocrinology.* (2005) 146:624–32. doi: 10.1210/en.2004-1064
9. Smith HO, Leslie KK, Singh M, Qualls CR, Revankar CM, Joste NE, et al. GPR30: a novel indicator of poor survival for endometrial carcinoma. *Am J Obstet Gynecol.* (2007) 196:386.e1–9; discussion: 386.e9–11. doi: 10.1016/j.ajog.2007.01.004
10. Parsa N. Environmental factors inducing human cancers. *Iran J Public Health.* (2012) 41:1–9.
11. Wang F, Ruan XJ, Zhang HY. BDE-99 (2,2′,4,4′,5-pentabromodiphenyl ether) triggers epithelial-mesenchymal transition in colorectal cancer cells via PI3K/Akt/Snail signaling pathway. *Tumori.* (2015) 101:238–45. doi: 10.5301/tj.5000229
12. Linares V, Belles M, Domingo JL. Human exposure to PBDE and critical evaluation of health hazards. *Arch Toxicol.* (2015) 89:335–56. doi: 10.1007/s00204-015-1457-1
13. Roscales JL, Munoz-Arnanz J, Ros M, Vicente A, Barrios L, Jimenez B. Assessment of POPs in air from Spain using passive sampling from 2008 to 2015. Part I: Spatial and temporal observations of PBDEs. *Sci Total Environ.* (2018) 634:1657–68. doi: 10.1016/j.scitotenv.2018.03.043
14. Hurley S, Goldberg D, Nelson DO, Guo W, Wang Y, Baek HG, et al. Temporal evaluation of polybrominated diphenyl ether (PBDE) serum levels in middle-aged and older California women, 2011-2015. *Environ Sci Technol.* (2017) 51:4697–704. doi: 10.1021/acs.est.7b00565
15. Danon-Schaffer MN, Mahecha-Botero A, Grace JR, Ikonomou M. Transfer of PBDEs from e-waste to aqueous media. *Sci Total Environ.* (2013) 447:458–71. doi: 10.1016/j.scitotenv.2012.11.015
16. Wei J, Xiang L, Yuan Z, Li S, Yang C, Liu H, et al. Metabolic profiling on the effect of 2,2′,4,4′-tetrabromodiphenyl ether (BDE-47) in MCF-7 cells. *Chemosphere.* (2018) 192:297–304. doi: 10.1016/j.chemosphere.2017.10.170
17. Slotkin TA, Skavicus S, Stapleton HM, Seidler FJ. Brominated and organophosphate flame retardants target different neurodevelopmental stages, characterized with embryonic neural stem cells and neuronotypic PC12 cells. *Toxicology.* (2017) 390:32–42. doi: 10.1016/j.tox.2017.08.009
18. Gao P, He P, Wang A, Xia T, Xu B, Xu Z, et al. Influence of PCB153 on oxidative DNA damage and DNA repair-related gene expression induced by PBDE-47 in human neuroblastoma cells *in vitro*. *Toxicol Sci.* (2009) 107:165–70. doi: 10.1093/toxsci/kfn224
19. Pellacani C, Buschini A, Galati S, Mussi F, Franzoni S, Costa LG. Evaluation of DNA damage induced by 2 polybrominated diphenyl ether flame retardants (BDE-47 and BDE-209) in SK-N-MC cells. *Int J Toxicol.* (2012) 31:372–9. doi: 10.1177/1091581812449663
20. Zhang S, Kuang G, Zhao G, Wu X, Zhang C, Lei R, et al. Involvement of the mitochondrial p53 pathway in PBDE-47-induced SH-SY5Y cells apoptosis and its underlying activation mechanism. *Food Chem Toxicol.* (2013) 62:699–706. doi: 10.1016/j.fct.2013.10.008
21. Tian PC, Wang HL, Chen GH, Luo Q, Chen Z, Wang Y, et al. 2,2′,4,4′-Tetrabromodiphenyl ether promotes human neuroblastoma SH-SY5Y cells migration via the GPER/PI3K/Akt signal pathway. *Hum Exp Toxicol.* (2016) 35:124–34. doi: 10.1177/0960327115578974
22. Liu S, Zhao G, Li J, Zhao H, Wang Y, Chen J. Association of polybrominated diphenylethers (PBDEs) and hydroxylated metabolites (OH-PBDEs) serum levels with thyroid function in thyroid cancer patients. *Environ Res.* (2017) 159:1–8. doi: 10.1016/j.envres.2017.07.042
23. Huang Y, Zhu G, Peng L, Ni W, Wang X, Zhang J, et al. Effect of 2,2′,4,4′-tetrabromodiphenyl ether (BDE-47) on sexual behaviors and reproductive function in male zebrafish (*Danio rerio*). *Ecotoxicol Environ Saf.* (2015) 111:102–8. doi: 10.1016/j.ecoenv.2014.09.037
24. Holmes AK, Koller KR, Kieszak SM, Sjodin A, Calafat AM, Sacco FD, et al. Case-control study of breast cancer and exposure to synthetic environmental chemicals among Alaska Native women. *Int J Circumpolar Health.* (2014) 73:25760. doi: 10.3402/ijch.v73.25760
25. Karpeta A, Maniecka A, Gregoraszczuk EL. Different mechanisms of action of 2,2′, 4,4′-tetrabromodiphenyl ether (BDE-47) and its metabolites (5-OH-BDE-47 and 6-OH-BDE-47) on cell proliferation in OVCAR-3 ovarian cancer cells and MCF-7 breast cancer cells. *J Appl Toxicol.* (2016) 36:1558–67. doi: 10.1002/jat.3316
26. Brasseur K, Gevry N, Asselin E. Chemoresistance and targeted therapies in ovarian and endometrial cancers. *Oncotarget.* (2017) 8:4008–42. doi: 10.18632/oncotarget.14021
27. Asara Y, Marchal JA, Carrasco E, Boulaiz H, Solinas G, Bandiera P, et al. Cadmium modifies the cell cycle and apoptotic profiles of human breast cancer cells treated with 5-fluorouracil. *Int J Mol Sci.* (2013) 14:16600–16. doi: 10.3390/ijms140816600
28. Jiang F, Zhao H, Wang L, Guo X, Wang X, Yin G, et al. Role of HLA-G1 in trophoblast cell proliferation, adhesion and invasion. *Biochem Biophys Res Commun.* (2015) 458:154–60. doi: 10.1016/j.bbrc.2015.01.085
29. Ge LC, Chen ZJ, Liu HY, Zhang KS, Liu H, Huang HB, et al. Involvement of activating ERK1/2 through G protein coupled receptor 30 and estrogen receptor α/β in low doses of bisphenol A promoting growth of Sertoli TM4 cells. *Toxicol Lett.* (2014) 226:81–9. doi: 10.1016/j.toxlet.2014.01.035
30. Kodavanti PR, Coburn CG, Moser VC, MacPhail RC, Fenton SE, Stoker TE, et al. Developmental exposure to a commercial PBDE mixture, DE-71: neurobehavioral, hormonal, and reproductive effects. *Toxicol Sci.* (2010) 116:297–312. doi: 10.1093/toxsci/kfq105
31. Li ZH, Liu XY, Wang N, Chen JS, Chen YH, Huang JT, et al. Effects of decabrominated diphenyl ether (PBDE-209) in regulation of growth and apoptosis of breast, ovarian, and cervical cancer cells. *Environ Health Perspect.* (2012) 120:541–6. doi: 10.1289/ehp.1104051
32. Kanaya N, Bernal L, Chang G, Yamamoto T, Nguyen D, Wang YZ, et al. Molecular mechanisms of polybrominated diphenyl ethers (BDE-47, BDE-100, and BDE-153) in human breast cancer cells and patient-derived xenografts. *Toxicol Sci.* (2019) 169:380–98. doi: 10.1093/toxsci/kfz054
33. He Y, Peng L, Zhang W, Liu C, Yang Q, Zheng S, et al. Adipose tissue levels of polybrominated diphenyl ethers and breast cancer risk in Chinese women: a case-control study. *Environ Res.* (2018) 167:160–8. doi: 10.1016/j.envres.2018.07.009
34. Kojima H, Takeuchi S, Uramaru N, Sugihara K, Yoshida T, Kitamura S. Nuclear hormone receptor activity of polybrominated diphenyl ethers and their hydroxylated and methoxylated metabolites in transactivation assays using Chinese hamster ovary cells. *Environ Health Perspect.* (2009) 117:1210–8. doi: 10.1289/ehp.0900753
35. Feo ML, Gross MS, McGarrigle BP, Eljarrat E, Barcelo D, Aga DS, et al. Biotransformation of BDE-47 to potentially toxic metabolites is predominantly mediated by human CYP2B6. *Environ Health Perspect.* (2013) 121:440–6. doi: 10.1289/ehp.1205446
36. Vahrenkamp JM, Yang CH, Rodriguez AC, Almomen A, Berrett KC, Trujillo AN, et al. Clinical and genomic crosstalk between glucocorticoid receptor and estrogen receptor α in endometrial cancer. *Cell Rep.* (2018) 22:2995–3005. doi: 10.1016/j.celrep.2018.02.076
37. He YY, Du GQ, Cai B, Yan Q, Zhou L, Chen XY, et al. Estrogenic transmembrane receptor of GPR30 mediates invasion and carcinogenesis by endometrial cancer cell line RL95-2. *J Cancer Res Clin Oncol.* (2012) 138:775–83. doi: 10.1007/s00432-011-1133-7
38. Edwards DP. Regulation of signal transduction pathways by estrogen and progesterone. *Annu Rev Physiol.* (2005) 67:335–76. doi: 10.1146/annurev.physiol.67.040403.120151
39. Sauer SJ, Tarpley M, Shah I, Save AV, Lyerly HK, Patierno SR, et al. Bisphenol A activates EGFR and ERK promoting proliferation, tumor spheroid formation and resistance to EGFR pathway inhibition in estrogen receptor-negative inflammatory breast cancer cells. *Carcinogenesis.* (2017) 38:252–60. doi: 10.1093/carcin/bgx003
40. Song X, Wei Z, Shaikh ZA. Requirement of ERα and basal activities of EGFR and Src kinase in Cd-induced activation of MAPK/ERK pathway in

human breast cancer MCF-7 cells. *Toxicol Appl Pharmacol.* (2015) 287:26–34. doi: 10.1016/j.taap.2015.05.010
41. Hu T, Yao M, Fu X, Chen C, Wu R. Polychlorinated biphenyl 104 promotes migration of endometrial stromal cells in endometriosis. *Toxicol Lett.* (2018) 290:19–28. doi: 10.1016/j.toxlet.2018.03.009
42. Li Z, Lu Q, Ding B, Xu J, Shen Y. Bisphenol A promotes the proliferation of leiomyoma cells by GPR30-EGFR signaling pathway. *J Obstet Gynaecol Res.* (2019) 45:1277–85. doi: 10.1111/jog.13972
43. Zhang L, Li Y, Lan L, Liu R, Wu Y, Qu Q, et al. Tamoxifen has a proliferative effect in endometrial carcinoma mediated via the GPER/EGFR/ERK/cyclin D1 pathway: a retrospective study and an *in vitro* study. *Mol Cell Endocrinol.* (2016) 437:51–61. doi: 10.1016/j.mce.2016.08.011
44. Tsai CL, Wu HM, Lin CY, Lin YJ, Chao A, Wang TH, et al. Estradiol and tamoxifen induce cell migration through GPR30 and activation of focal adhesion kinase (FAK) in endometrial cancers with low or without nuclear estrogen receptor α (ERα). *PLoS ONE.* (2013) 8:e72999. doi: 10.1371/journal.pone.0072999
45. Asara Y, Marchal JA, Bandiera P, Mazzarello V, Delogu LG, Sotgiu MA, et al. Cadmium influences the 5-Fluorouracil cytotoxic effects on breast cancer cells. *Eur J Histochem.* (2012) 56:e1. doi: 10.4081/ejh.2012.e1
46. Sui M, Zhang H, Fan W. The role of estrogen and estrogen receptors in chemoresistance. *Curr Med Chem.* (2011) 18:4674–83. doi: 10.2174/092986711797379348
47. Chang J, Sui M, Fan W. Estrogen receptor α attenuates therapeutic efficacy of paclitaxel on breast xenograft tumors. *Breast Cancer Res Treat.* (2012) 134:969–80. doi: 10.1007/s10549-012-1994-8
48. Jiang Z, Guo J, Shen J, Jin M, Xie S, Wang L. The role of estrogen receptor alpha in mediating chemoresistance in breast cancer cells. *J Exp Clin Cancer Res.* (2012) 31:42. doi: 10.1186/1756-9966-31-42
49. Vivacqua A, Lappano R, De Marco P, Sisci D, Aquila S, De Amicis F, et al. G protein-coupled receptor 30 expression is up-regulated by EGF and TGF alpha in estrogen receptor alpha-positive cancer cells. *Mol Endocrinol.* (2009) 23:1815–26. doi: 10.1210/me.2009-0120
50. Hamers T, Kamstra JH, Sonneveld E, Murk AJ, Kester MH, Andersson PL, et al. *In vitro* profiling of the endocrine-disrupting potency of brominated flame retardants. *Toxicol Sci.* (2006) 92:157–73. doi: 10.1093/toxsci/kfj187
51. He Y, Murphy MB, Yu RM, Lam MH, Hecker M, Giesy JP, et al. Effects of 20 PBDE metabolites on steroidogenesis in the H295R cell line. *Toxicol Lett.* (2008) 176:230–8. doi: 10.1016/j.toxlet.2007.12.001
52. Lefevre PL, Wade M, Goodyer C, Hales BF, Robaire B. A mixture reflecting polybrominated diphenyl ether (PBDE) profiles detected in human follicular fluid significantly affects steroidogenesis and induces oxidative stress in a female human granulosa cell line. *Endocrinology.* (2016) 157:2698–711. doi: 10.1210/en.2016-1106

Conflict of Interest: The authors declare that the research was conducted in the absence of any commercial or financial relationships that could be construed as a potential conflict of interest.

frontiers in Oncology

ORIGINAL RESEARCH
published: 08 November 2019
doi: 10.3389/fonc.2019.01214

The Tumor Suppressor Role of Zinc Finger Protein 671 (*ZNF671*) in Multiple Tumors Based on Cancer Single-Cell Sequencing

*Jian Zhang[1,2†], Jianli Luo[3†], Huali Jiang[4†], Tao Xie[1,2†], Jieling Zheng[5], Yunhong Tian[1,2], Rong Li[1,2], Baiyao Wang[1,2], Jie Lin[1,2], Anan Xu[1,2], Xiaoting Huang[1,2] and Yawei Yuan[1,2]**

[1] Department of Radiation Oncology, Affiliated Cancer Hospital & Institute of Guangzhou Medical University, Guangzhou, China, [2] State Key Laboratory of Respiratory Diseases, Guangzhou Institute of Respiratory Disease, Affiliated Cancer Hospital & Institute of Guangzhou Medical University, Guangzhou, China, [3] Department of General Disease, Health Center of Shuichun Town, Shanwei, China, [4] Department of Cardiovascularology, Tungwah Hospital of Sun Yat-sen University, Dongguan, China, [5] Department of Radiation Oncology, Nanfang Hospital, Southern Medical University, Guangzhou, China

In humans, zinc finger protein 671 (*ZNF671*) is a type of transcription factor. However, the contribution of tumor heterogeneity to the functional role of *ZNF671* remains unknown. The present study aimed to determine the functional states of *ZNF671* in cancer single cells based on single-cell sequencing datasets (scRNA-seq). We collected cancer-related *ZNF671* scRNA-seq datasets and analyzed *ZNF671* in the datasets. We evaluated 14 functional states of *ZNF671* in cancers and performed *ZNF671* expression and function state correlation analysis. We further applied t-distributed stochastic neighbor embedding to describe the distribution of cancer cells and to explore the functional state of *ZNF671* in cancer subgroups. We found that *ZNF671* was downregulated in eight cancer-related *ZNF671* scRNA-seq datasets. Functional analysis identified that *ZNF671* might play a tumor suppressor role in cancer. The heterogeneous functional states of cell subgroups and correlation analysis showed that *ZNF671* played tumor suppressor roles in heterogeneous cancer cell populations. Western blot and transwell assays identified that *ZNF671* inhibited EMT, migration, and invasion of CNS cancers, lung cancer, melanoma, and breast carcinoma *in vitro*. These results from cancer single-cell sequencing indicated that *ZNF671* played a tumor suppressor role in multiple tumors and may provide us with new insights into the role of *ZNF671* for cancer treatment.

Keywords: *ZNF671*, tumor suppressor, solid tumor, single-cell sequencing, data mining

OPEN ACCESS

Edited by:
Chang Zou,
Shenzhen People's Hospital, China

Reviewed by:
Fahd Al-Mulla,
Genatak, Kuwait
Zi-Qi Zheng,
Sun Yat-sen University Cancer Center (SYSUCC), China

***Correspondence:**
Yawei Yuan
yuanyawei@gzhmu.edu.cn

† These authors have contributed equally to this work

Specialty section:
This article was submitted to Molecular and Cellular Oncology, a section of the journal Frontiers in Oncology

Received: *10 June 2019*
Accepted: *23 October 2019*
Published: *08 November 2019*

Citation:
Zhang J, Luo J, Jiang H, Xie T, Zheng J, Tian Y, Li R, Wang B, Lin J, Xu A, Huang X and Yuan Y (2019) The Tumor Suppressor Role of Zinc Finger Protein 671 (ZNF671) in Multiple Tumors Based on Cancer Single-Cell Sequencing. Front. Oncol. 9:1214. doi: 10.3389/fonc.2019.01214

INTRODUCTION

Cancer is a complex ecosystem composed of cells with heterogeneous functional states, leading to both therapeutic resistance, and frequent cancer recurrence or metastasis, which poses a major obstacle to cancer diagnosis and treatment (1–3). Some tumor cells have high proliferative or apoptotic capacity, some have invasion and metastasis activities, some show stem-like properties, and some exhibit a quiescent state (4, 5). These functionally heterogeneous cancer cells act cooperatively or competitively during tumor progression or metastasis, leading to distinct tumor phenotypes (6–8). Therefore, it is essential to systematically and comprehensively identify the functional states of cancer cells.

Single-cell mRNA-sequencing (scRNA-seq) provides a powerful tool for characterizing the omic-scale features of heterogeneous cell populations (9, 10). ScRNA-seq technologies permit the dissection of primary tumor cells, metastatic tumor cells, cancer stem cells (CSC), circulating tumor cells (CTC), and disseminated tumor cells in a comprehensive and unbiased manner, with no need of any prior knowledge of the cell population. ScRNA-seq has become a reference tool for analyzing the composition of cancer tissues and for establishing the characteristics of the cellular microenvironment (11). Thus, understanding single cancer cells will advance our understanding of not only therapeutic resistance but all facets of cell biology. Furthermore, the application of scRNA-seq in the clinic has the potential to change our approach to cancer management fundamentally (12).

Zinc finger protein 671 (*ZNF671*) is a member of the KRAB-ZF (KRAB-ZFP) family of mammalian transcriptional repressors (13–15). KRAB-ZFPs can regulate tumor cell differentiation, proliferation, apoptosis, invasion, metastasis, and transformation (16–21). Previous studies showed that *ZNF671* could act as a tumor suppressor in several solid tumors (22–26). Our studies identified that *ZNF671* played a tumor suppressor role in breast invasive carcinoma (BRCA), cervical squamous cell carcinoma, and endocervical adenocarcinoma (CESC), head and neck squamous cell carcinoma (HNSC), kidney renal papillary cell carcinoma (KIRP), lung adenocarcinoma (LUAD), pancreatic adenocarcinoma (PAAD), and uterine corpus endometrial carcinoma (UCEC) (26, 27). However, the roles of *ZNF671* in the functional heterogeneity of cancer single cells remain unclear.

In this study, we analyzed the expression of *ZNF671* in cancer scRNA-seq datasets systematically. We explored the functional role of *ZNF671* in solid tumors and analyzed its expression and functional correlation in tumors. We further described the distribution of cancer single cells and explored their functional relevance in different tumor cell subgroups. Our results provide important insights into tumor heterogeneity and enhance knowledge of the tumor suppressor role of *ZNF671* in solid tumors.

MATERIALS AND METHODS

Data Collection

Data were collected based on the following keywords: ("single cells" OR "single cell" OR "single-cell" OR "single-cells") AND ("transcriptome" OR "transcriptomics" OR "scRNA-seq" OR "scRNA seq" OR "RNA-sequencing" OR "RNA-seq" OR"RNA sequencing") AND ("carcinoma" OR "tumor" OR "tumor" OR "cancer" OR "neoplasm" OR "neoplastic"). According to the method used by Yuan et al. (28), three human data sets from Array Express, Sequence Read Archive (SRA), and Gene Expression Omnibus (GEO) datasets were collected and all single-cell data in these datasets were analyzed via expression quantification, quality control, and characterization of functional states.

Data Processing

Transcript expression quantification was performed using Salmon (version 0.9.1) with the optional parameter k ($k = 31$ for long reads and $k = 15$ for short reads). The GENCODE (Release 28, GRCh38) reference transcriptome was used to detect gcBias, seqBias, and other default parameters in the quasi-mapping-based mode. For scRNA-seq datasets with only an expression matrix, we directly converted the expression values to transcripts per million (TPM)/counts per million (CPM) values using a custom script. Expression values were log2 transformed with an offset of 1.

Characterizing Functional States of Cancer Single Cells

After reviewing cancer single-cell sequencing studies, 14 crucial functional states of cancer cells were selected, including angiogenesis, apoptosis, cell cycle, differentiation, DNA damage, DNA repair, epithelial–mesenchyme transition (EMT), hypoxia, inflammation, invasion, metastasis, proliferation, quiescence, and stemness using Gene Ontology, MSigDB, Cyclebase, HCMDB, and StemMapper (29–33). According to the method used by Yuan et al. (28), the activities of the 14 functional states across cancer single cells in the datasets were assessed using the Gene Set Variation Analysis (GSVA) package downloaded from http://www.bioconductor.org (34).

Dimensionality Reduction Using t-distributed Stochastic Neighbor Embedding (t-SNE) Analysis

According to the method used by Li et al. (35), donor files were imported into R, and expression matrices containing measured intensities at the single-cell level were extracted from the flowCore package. A subset of cells was selected for each donor at random and merged into a single expression matrix before t-SNE analysis. The beads, viability, center, offset, residual, event length, intercalator, and time channels were removed from the expression matrix. The *ZNF671* protein marker was the only factor included in the t-SNE analysis, and *ZNF671* intensities were transformed using the inverse hyperbolic sine (arcsinh) function.

T-SNE calculations were performed with 1,000 iterations, a perplexity parameter of 30, and a trade-off θ of 0.5, which was used to visualize similarities and the proximity of cells in a two-dimensional plot. T-SNE maps were generated by plotting each event of the t-SNE dimensions in a dot-plot. *ZNF671* intensities were overlaid on the dot-plot to show the expression in different cell islands and to facilitate the assignment of cell subsets to these islands. The t-SNE dimensions were characterized by t-SNE1 and t-SNE2 in the given graphs. The software is available at https://github.com/KlugerLab/FIt-SNE.

ZNF671 Expression and Functional State Correlation Analysis

The expression level statistics of *ZNF671* in each cell were converted to normalized ranks and Next, the Kolmogorov–Smirnov liker random walk statistic, similar to the GSEA

method, was used to summarize the *ZNF671* expression-level rank statistics of a given signature gene set into a final enrichment score, which was used to characterize the signature activity. The enrichments of 14 signatures across cells in the scRNA-seq data were calculated, and only cells with detectable expression of *ZNF671* were used. Correlations between *ZNF671* expression and functional state activities were assessed using correlation analysis with false discovery rate (FDR) corrections for multiple comparisons (FDR < 0.05 and $P < 0.05$).

Cell Culture

Human GBM cell lines (U87 and U251), the A375 melanoma cell line, and triple-negative breast cancer cell lines (MDA-MB-231 and BT-549) were obtained from the American Type Culture Collection (ATCC, Manassas, VA, USA). Cells were maintained at 37°, 5% CO_2 in 10% DMEM (Invitrogen, Carlsbad, CA, USA) supplemented with 10% fetal bovine serum.

Western Blot Analysis

After cells were transfected with the pEnter-*ZNF671* or pEnter-*vector* plasmids (Vigene Biosciences, Shandong, China) for 48 h, RIPA lysis buffer (Beyotime, Shanghai, China) was used to isolate proteins. Proteins were separated by sodium dodecyl sulfate (SDS)-polyacrylamide gel electrophoresis (SDS-PAGE, Beyotime), transferred onto polyvinylidene fluoride (PVDF) membranes (Millipore, Billerica, MA, USA), and incubated with primary anti-ZNF671 (1:500; Proteintech, Chicago, IL, USA), E-cadherin (1:500, BD Biosciences), Vimtenin (1:500, BD Biosciences), and anti-GAPDH (1:1,000, Proteintech, Chicago, IL, USA).

Migration and Invasion Assays

Transwell plates (8-μm pores) (Costar/Corning, Lowell, MA) were used for Transwell migration or invasion assays. 5×10^4 (migration assay) or 1×10^5 (invasion assay) cells resuspended in serum-free medium were placed in the upper chamber of each insert, either uncoated or coated with Matrigel (BD Biosciences). The lower chamber contained culture medium with 10% FBS to act as a chemoattractant. The cells were incubated for 12 or 24 h and were then fixed and stained. Cells on the undersides of the filters were observed and counted under 200× magnification.

Statistical Analysis

Statistical analysis was performed using SPSS version 17.0 (SPSS Inc., Chicago, IL, USA). Differences between two groups were analyzed using the two-tailed unpaired Student's *t*-test; $P < 0.05$ was considered statistically significant.

RESULTS

scRNA-seq Dataset Features

As shown in **Table 1**, a total of eight cancer-related *ZNF671* scRNA-seq datasets were included in the study. They contained 14 functional states of 13941 cancer single cells from glioblastoma (GBM; $n = 623$), glioma (brain; $n = 2259$), glioma (PDX; $n = 167$), astrocytoma (AST; $n = 5097$), oligodendroglioma (ODG; $n = 4043$), lung adenocarcinoma (LUAD; $n = 126$), melanoma (MEL; $n = 1257$), and breast cancer (BRCA; $n = 369$).

TABLE 1 | Features of the scRNA-seq datasets searched with *ZNF671*.

ExpID	Name	Cancer	No. Cells
0058	Patel AP. Science. 2014 (Brain)	Glioblastoma	623
0059	Filbin MG.Science. 2018 (Brain)	Glioma	2259
0060	Filbin MG.Science. 2018 (PDX)	Glioma	167
0056	Venteicher AS. Science. 2017 (Brain)	Astrocytoma	5097
0062	Tirosh I. Nature. 2016 (Brain)	Oligodendroglioma	4043
0066	Kim KT. Genome Biol. 2015 (PDX)	Lung adenocarcinoma	126
0071	Tirosh I. Science. 2016 (Skin)	Melanoma	1257
0052	Braune EB. Stem Cell Reports. 2016 (PDX)	Breast cancer	369

ZNF671 Functional States in the scRNA-seq Datasets

Expression analysis showed that *ZNF671* was obviously downregulated in GBM, glioma, AST, ODG, LUAD, MEL, and BRCA (**Figure 1**), which indicated that *ZNF671* might play an important role in tumor progression. To further explore the functional role of *ZNF671* in different cancers, 14 crucial functional states of cancer cells, including angiogenesis, apoptosis, cell cycle, differentiation, DNA damage, DNA repair, EMT, hypoxia, inflammation, invasion, metastasis, proliferation, quiescence, and stemness were summarized and analyzed. As shown in **Figure 2**, the expression of *ZNF671* and the activity of each functional state across single-cell datasets in different cancers were explored using an interactive bubble chart. The upper bar plot shows a summary of the association between the functional state and the number of single-cell datasets. We found that the expression of *ZNF671* had a significant negative regulation for angiogenesis, apoptosis, EMT, hypoxia, invasion, and quiescence, which was consistent with our previous research (26, 27). These results indicate that *ZNF671* might play a suppressor role in tumor development.

The Different Roles of *ZNF671* in Cancers

We next explored the functional roles of *ZNF671* in cancers, and analyzed the correlation between *ZNF671* expression and functional state. We found that *ZNF671* was positively associated with DNA damage ($R = 0.18$; $^{***}P < 0.001$), apoptosis ($R = 0.13$; $^{*}P < 0.05$), DNA repair ($R = 0.10$; $^{*}P < 0.05$) in GBM; with stemness ($R = 0.11$; $^{*}P < 0.05$) and inflammation ($R = 0.06$; $^{*}P < 0.05$) in AST; with proliferation ($R = 0.29$; $^{**}P < 0.01$), quiescence ($R = 0.23$; $^{*}P < 0.05$), and differentiation ($R = 0.21$; $^{*}P < 0.05$) in MEL; with inflammation ($R = 0.17$; $^{***}P < 0.001$), metastasis ($R = 0.16$; $^{***}P < 0.001$), stemness ($R = 0.15$;

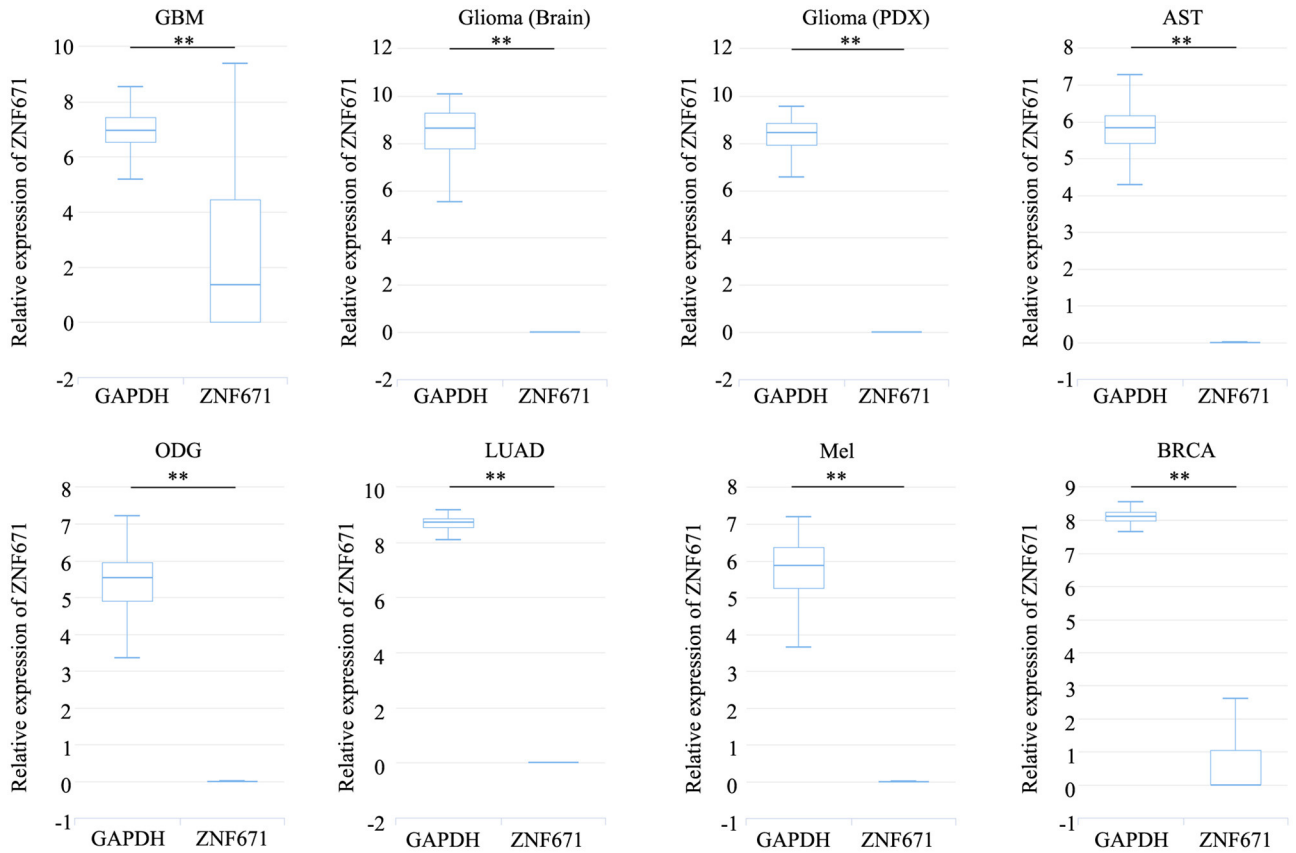

FIGURE 1 | *ZNF671* is downregulated in primary solid tumors. Box diagram indicates the expression distribution of *ZNF671* in cells in the scRNA-seq datasets. Glioblastoma (GBM), Glioma (Brain), Glioma (PDX), Astrocytoma (AST), Oligodendroglioma (ODG), Lung adenocarcinoma (LUAD), Melanoma (MEL), and Breast cancer (BRCA). $^{**}p \leq 0.01$ compared with the control using Student's *t*-test.

$^{**}P < 0.01$), hypoxia ($R = 0.13$; $^{**}P < 0.01$), EMT ($R = 0.13$; $^{*}P < 0.05$), and differentiation ($R = 0.08$; $^{*}P < 0.05$) in ODG; with EMT ($R = 0.12$; $^{*}P < 0.05$) and hypoxia ($R = 0.12$; $^{*}P < 0.05$) in glioma (brain); and with stemness ($R = 0.18$; $^{*}P < 0.05$), and hypoxia ($R = 0.18$; $^{*}P < 0.05$) in BRCA (**Figures 3**, **4**).

However, *ZNF671* was negatively associated with DNA damage in ODG ($R = -0.11$; $^{**}P < 0.01$); with hypoxia ($R = -0.55$; $^{*}P < 0.05$), EMT ($R = -0.50$; $^{*}P < 0.05$), apoptosis ($R = -0.49$; $^{*}P < 0.05$), angiogenesis ($R = -0.48$; $^{*}P < 0.05$), and quiescence ($R = -0.43$; $^{*}P < 0.05$) in glioma (PDX), and with inflammation ($R = -0.20$; $^{*}P < 0.05$) and differentiation ($R = -0.18$; $^{*}P < 0.05$) in BRCA (**Figures 3**, **4**). These results indicated that *ZNF671* plays a different functional role in cancers and that the functional difference could be associated with the functional populations of cancer cells.

The Different Roles of *ZNF671* in Different Cell Groups

To determine the functionally heterogeneous roles of *ZNF671* in cancer cells, we inferred that single cells exhibited widespread heterogeneity in terms of their functional states in cancer. We applied t-SNE to reduce the non-linear dimensionality of the cancer cell data and placed different cell clusters on a t-SNE map (**Figure 5**), which indicated that the cell groups might be associated with the functional heterogeneity of cancer.

To reveal the roles of *ZNF671* in different cell groups, we further the explored functional roles and correlations of *ZNF671* in different cancer subgroups. As shown in **Figure 6**, *ZNF671* expression was positively associated with DNA repair, DNA damage, and apoptosis but negatively associated with angiogenesis, differentiation, and proliferation in MGH30 cell groups of GBM, while *ZNF671* expression was positively associated with proliferation in MGH31 cell groups of GBM. In glioma (brain), *ZNF671* expression was negatively correlated with angiogenesis in MUV1, with DNA repair, DNA damage, and cell cycle in MUV5, with DNA repair in BCH836, and with apoptosis in BCH869. *ZNF671* expression was positively correlated with hypoxia in MUV10, BCH836, and BCH869 in glioma (brain). In glioma (PDX), *ZNF671* expression in BCH869 correlated negatively not only with hypoxia but also with EMT, apoptosis, angiogenesis, and quiescence. In AST, *ZNF671* expression was positively correlated with stemness in MGH45 and MGH56, with invasion in MGH61, and with inflammation in MGH64, and it was negatively correlated with cell cycle and invasion in MGH45, with angiogenesis in MGH57, and with invasion in MGH64. In ODG, *ZNF671* expression was positively

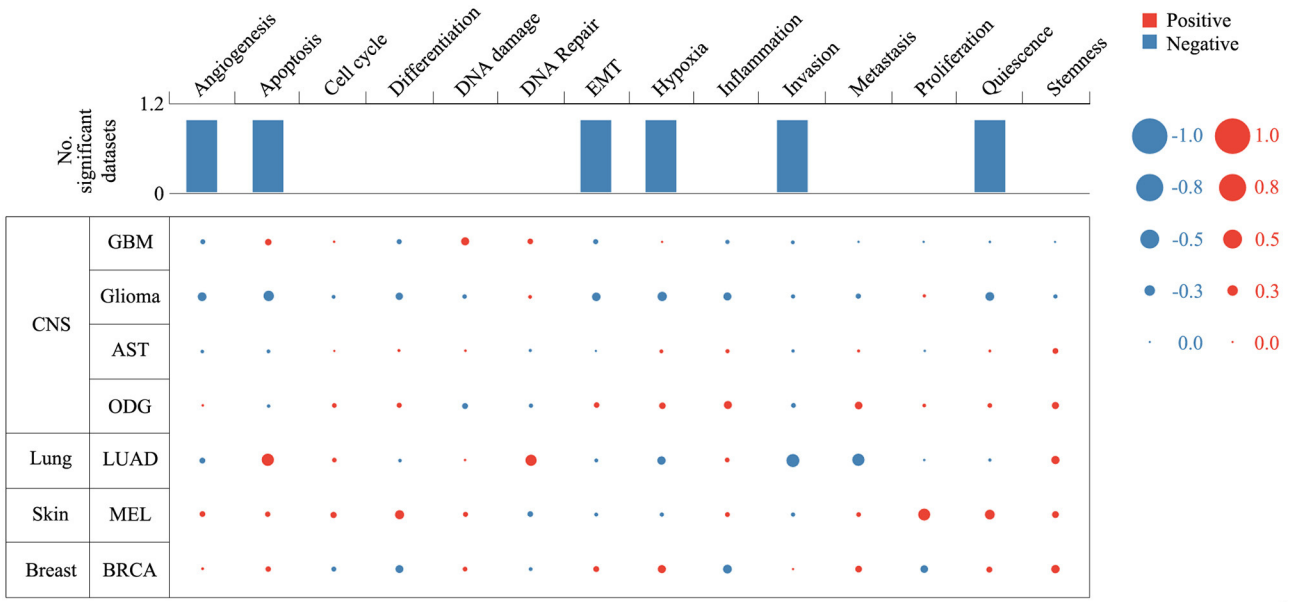

FIGURE 2 | Relevance of *ZNF671* across 14 functional states in distinct cancers. The upper bar chart shows the number of datasets in which *ZNF671* is significantly related to the corresponding state. In the bubble chart in the second section, a results table is used to display the basic information of all single-cell datasets in the selected cancer type and the corresponding correlations with the 14 functional states. Glioblastoma (GBM), Glioma (Brain), Glioma (PDX), Astrocytoma (AST), Oligodendroglioma (ODG), Lung adenocarcinoma (LUAD), Melanoma (MEL), and Breast cancer (BRCA).

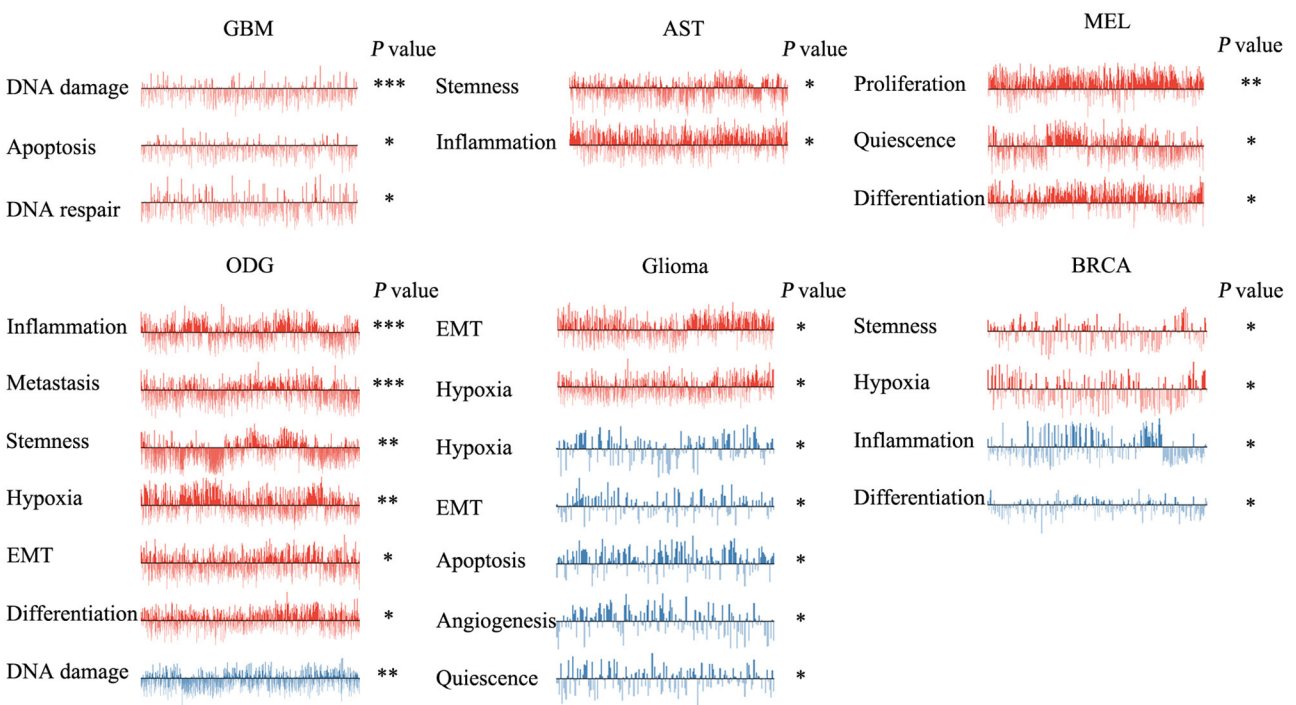

FIGURE 3 | Functional relevance of *ZNF671* in primary solid tumors. *ZNF671* plays different functional states in different single-cell datasets. Glioblastoma (GBM), Glioma (Brain), Glioma (PDX), Astrocytoma (AST), Oligodendroglioma (ODG), Lung adenocarcinoma (LUAD), Melanoma (MEL), and Breast cancer (BRCA). ***$p \leq 0.001$; **$p \leq 0.01$; *$p \leq 0.05$ compared with the control using Student's *t*-test.

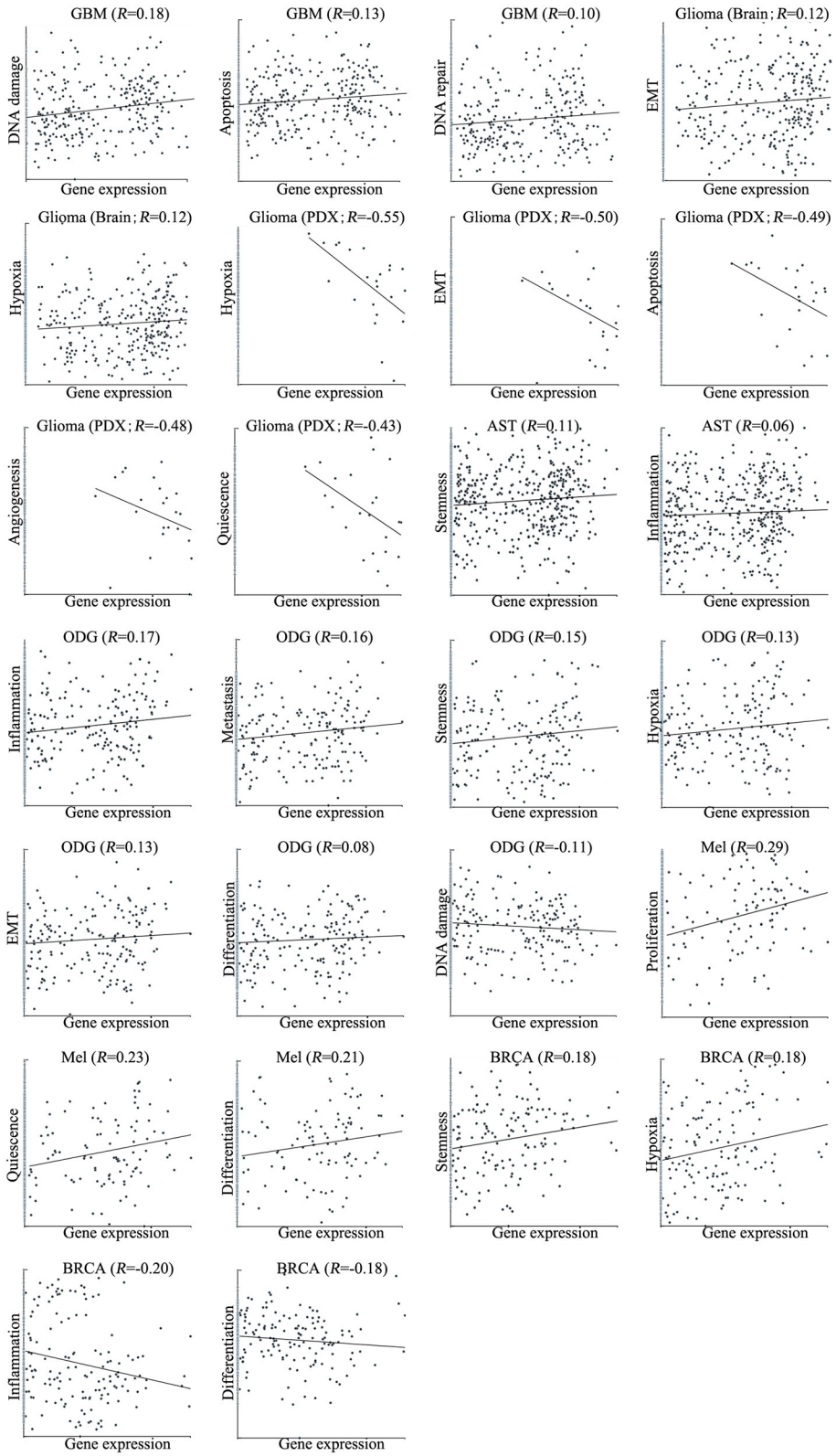

FIGURE 4 | Correlations between *ZNF671* mRNA expression and functional states in primary solid tumors. The detailed functional relevance in each specific cell group of a specific scRNA-seq dataset is shown. Glioblastoma (GBM), Glioma (Brain), Glioma (PDX), Astrocytoma (AST), Oligodendroglioma (ODG), Lung adenocarcinoma (LUAD), Melanoma (MEL), and Breast cancer (BRCA).

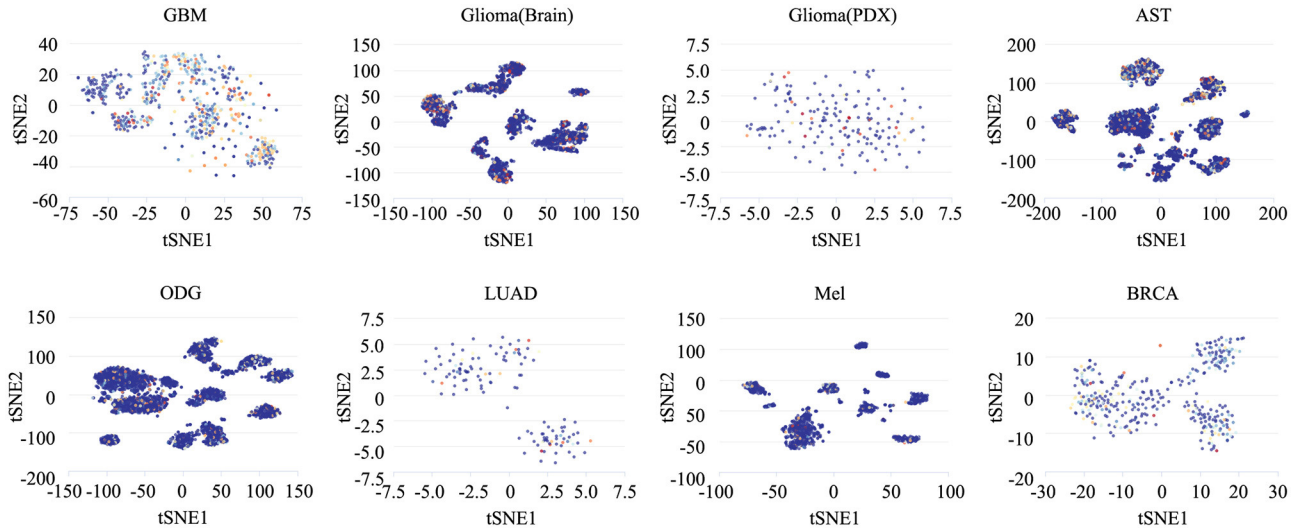

FIGURE 5 | The distribution of heterogeneous cell groups. Tridimensional t-SNE representation of cell clusters in primary tumors after classic multidimensional scaling and dimensionality reduction. Every point represents a single cell, and the color of the point represents the expression level of the gene (gene list) in the cell. Glioblastoma (GBM), Glioma (Brain), Glioma (PDX), Astrocytoma (AST), Oligodendroglioma (ODG), Lung adenocarcinoma (LUAD), Melanoma (MEL), and Breast cancer (BRCA).

correlated with metastasis, hypoxia, inflammation, and apoptosis in MGH36 and with inflammation in MGH60 but negatively correlated with apoptosis in MGH54 and with quiescence in MGH93. Similarly, in MEL, *ZNF671* expression was positively correlated with stemness in tumor78, with proliferation and stemness in tumor79, with proliferation and differentiation in tumor88, and with inflammation in tumor89. However, *ZNF671* expression was negatively correlated with DNA repair in tumor78, DNA damage and angiogenesis in tumor80, and cell cycle in tumor89. In LUAD, *ZNF671* expression was positively correlated with DNA repair in MBT15 but negatively correlated with metastasis and invasion in PT45. In BRCA, *ZNF671* expression was only positively correlated with DNA damage in CSL KO xenograft tumor (**Figure 6**, all $^{*}P < 0.05$; $^{**}P < 0.01$).

ZNF671 Inhibits Cell EMT, Migration, and Invasion *in vitro*

To determine the functional roles of ZNF671 in cancer cells, we performed Western blot assay and migration and invasion assays using U87, U251, A375, MDA-MB-231, and BT-549 cell lines transfected with *ZNF671* or vector plasmids. As shown in **Figure 7A**, Western blot analysis validated that ZNF671 protein was obviously upregulated after transfection of *ZNF671* plasmid. Furthermore, the overexpression of ZNF671 was associated with increased expression of the epithelial marker E-cadherin and decreased expression of the mesenchymal marker Vimentin. Transwell assays showed that overexpression of ZNF671 inhibited cancer cell migration and invasion *in vitro* (**Figures 7B–D**). These findings indicate that ZNF671 inhibits the EMT, migration, and invasion of U87, U251, A375, MDA-MB-231, and BT-549 cells *in vitro*.

DISCUSSION

ZNF671, which contains C2H2-type zinc fingers (ZFs) and a Krüppel-associated box (KRAB) domain, is a member of the KRAB-ZF (KRAB-ZFP) transcriptional family. KRAB-ZFPs are involved in regulating angiogenesis (36), apoptosis (37–39), the cell cycle (40, 41), inflammation (42), invasion and metastasis (43, 44), and stemness (45). Our previous studies demonstrated that *ZNF671* is a tumor suppressor that is epigenetically silenced by DNA methylation in nasopharyngeal carcinoma, BRCA, CESC, HNSC, KIRP, LUAD, PAAD, and UCEC (26, 27). However, there is limited information regarding the role of *ZNF671* in cancer progression and development, and there have been no systematic studies of the role of *ZNF671* in cancer's heterogeneous functional states.

In this study, we found a total of eight solid tumor-related *ZNF671* scRNA-seq datasets, including GBM, glioma, AST, ODG, LUAD, MEL, and BRCA. ScRNA-seq functional state analysis showed that *ZNF671* played a tumor suppressor role and/or an oncogenic role in angiogenesis, apoptosis, cell cycle, differentiation, DNA damage, DNA repair, EMT, hypoxia, inflammation, invasion, metastasis, proliferation, quiescence, and stemness. The different functional states in tumors may be associated with the inherent heterogeneity of the tumor. However, the synthetic analysis of eight solid tumors showed that *ZNF671* was negatively associated with angiogenesis, apoptosis, EMT, hypoxia, invasion, and quiescence. Western blot and transwell assays showed that *ZNF671* inhibited EMT, migration, and invasion of CNS cancers, lung cancer, melanoma, and breast carcinoma *in vitro*. These results suggested a crucial tumor suppressor role for *ZNF671* in the progression of these cancers, which was consistent with our previous studies (26, 27).

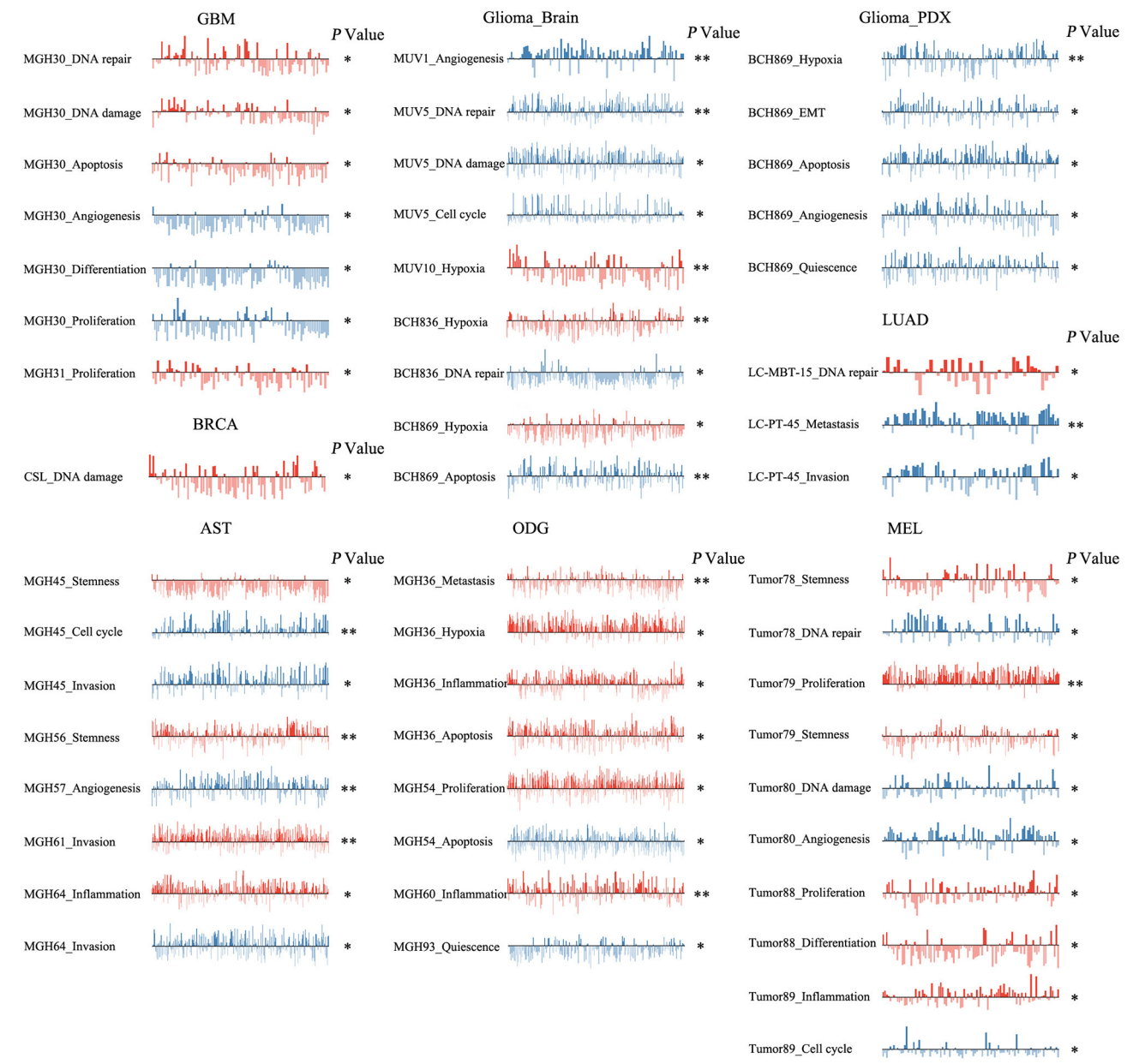

FIGURE 6 | Detailed functional relevance of *ZNF671* in different specific cell groups. The detailed functional relevance of *ZNF671* in each specific cell group of a specific dataset. Glioblastoma (GBM), Glioma (Brain), Glioma (PDX), Astrocytoma (AST), Oligodendroglioma (ODG), Lung adenocarcinoma (LUAD), Melanoma (MEL), and Breast cancer (BRCA). $^{**}p \leq 0.01$; $^{*}p \leq 0.05$ compared with the control using Student's *t*-test.

To further explore the heterogeneous functional state of *ZNF671* in cancers, we applied t-SNE to describe the distribution of cells. We found different cell clusters on a t-SNE map and proposed that these cell subgroups might lead to cancer functional heterogeneity. Functional analysis of the cancer cell subgroups validated that the heterogeneous cell populations had different roles in cancer progression and development, which provided us with a fine level of resolution for cancer treatment. However, there were still several limitations. First, this study was based on current scRNA datasets, and several scRNA datasets only contain data for hundreds of single cells, so more cells should be considered for analysis. Second, we found the *ZNF671* inhibits angiogenesis, apoptosis, EMT, hypoxia, invasion, and quiescence in CNS cancers, lung cancer, melanoma, and breast carcinoma. Moreover, we only identified that *ZNF671* suppresses cell EMT, migration, and invasion in *vitro*. The angiogenesis, apoptosis, hypoxia, and quiescence functional states need be identified further, and the suppressor role of *ZNF671 in vivo* needs to be explored further.

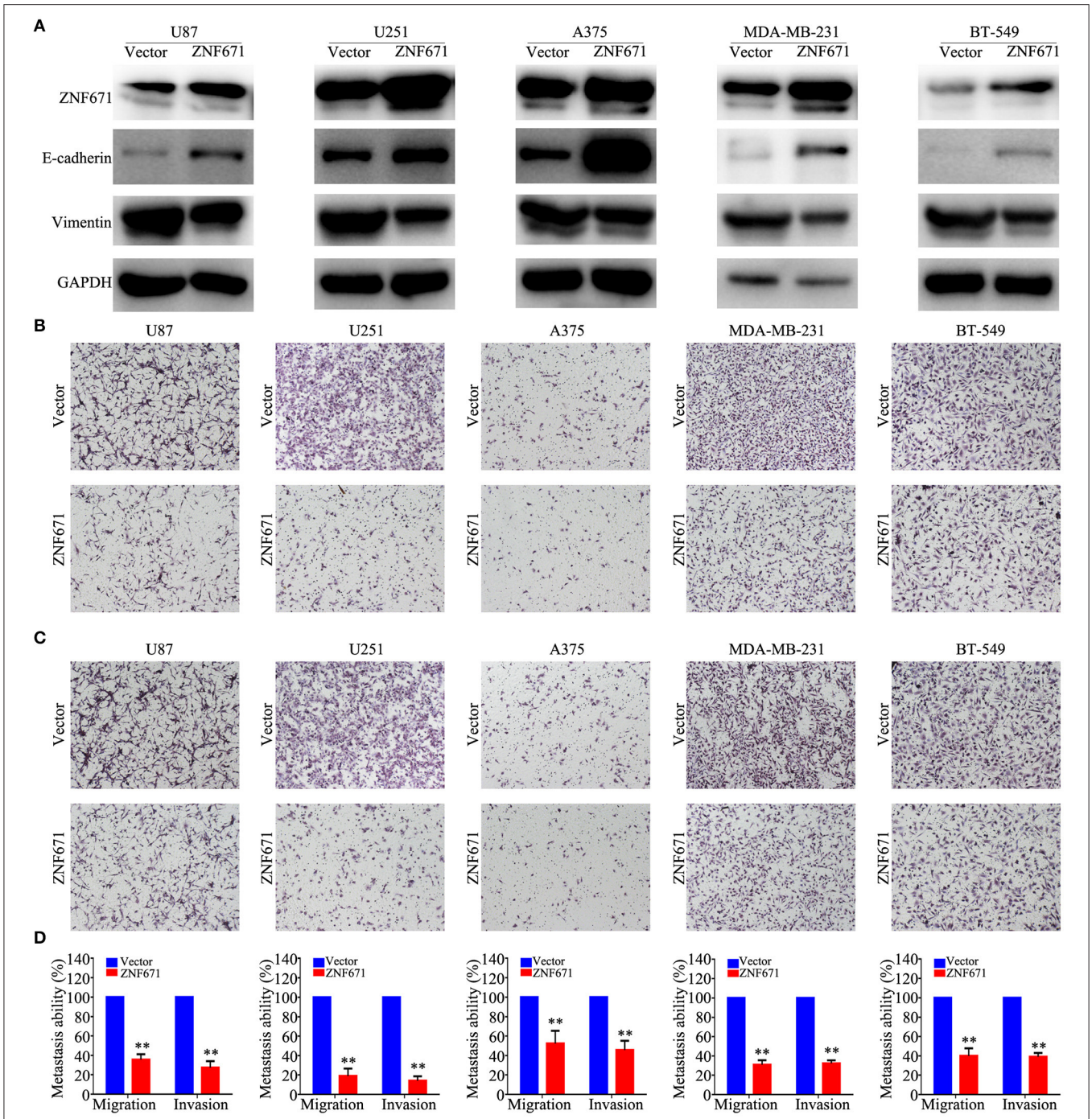

FIGURE 7 | Effects of ZNF671 overexpression on EMT, migration, and invasion *in vitro*. **(A)** Representative western blot analysis of ZNF671 overexpression in U87, U251, A375, MDA-MB-231, and BT-549 cell lines. **(B,C)** Representative images of the effects of ZNF671 overexpression on the migratory and invasive abilities of cells as determined by Transwell migration **(B)** and invasion **(C)** assays. **(D)** Quantification of the effects of ZNF671 overexpression on migratory and invasive abilities. All of the experiments were performed at least three times. Data presented are the mean ± SD; $^{**}P < 0.01$. All of the experiments were performed at least three test.

In conclusion, this study systematically evaluated the tumor suppressor role of *ZNF671* based on scRNA-seq datasets. Our findings revealed that *ZNF671* is a tumor suppressor in LUAD, BRCA, GBM, glioma, AST, ODG, and MEL. However, the mechanism of *ZNF671*'s tumor suppressor role remains unknown, and further studies are needed to clarify this issue. Our results provide new insights into the role of *ZNF671* in multiple tumors and identifies *ZNF671* as a novel target for cancer treatment.

DATA AVAILABILITY STATEMENT

Publicly available datasets were analyzed in this study. This data can be found here: http://www.bioconductor.org.

AUTHOR CONTRIBUTIONS

JZha, JLu, and HJ designed the research. TX, JZhe, YT, RL, BW, JLi, AX, and XH acquired and analyzed the data. JZha, HJ, and YY wrote the manuscript.

FUNDING

This work was supported by grants from the Social Science and Technology Development Key Project of Dongguan (201750715046462); Guangzhou Key Medical Discipline Construction Project Fund (B195002004042); Open Funds of State Key Laboratory of Oncology in South China (KY013711).

ACKNOWLEDGMENTS

We thank professors Ying Sun, Jun Ma, and Na Liu (State Key Laboratory of Oncology in South China, Collaborative Innovation Center of Cancer Medicine; Guangdong Key Laboratory of Nasopharyngeal Carcinoma Diagnosis and Therapy; Sun Yat-sen University Cancer Center, Guangzhou 510060, P.R. China) for supporting this work. We would like to thank the native English-speaking scientists of Elixigen Company (Huntington Beach, California) for editing our manuscript.

REFERENCES

1. Burrell RA, McGranahan N, Bartek J, Swanton C. The causes and consequences of genetic heterogeneity in cancer evolution. *Nature.* (2013) 501:338–45. doi: 10.1038/nature12625
2. Meacham CE, Morrison SJ. Tumour heterogeneity and cancer cell plasticity. *Nature.* (2013) 501:328–37. doi: 10.1038/nature12624
3. Kreso A, Dick JE. Evolution of the cancer stem cell model. *Cell Stem Cell.* (2014) 14:275–91. doi: 10.1016/j.stem.2014.02.006
4. Lawson DA, Bhakta NR, Kessenbrock K, Prummel KD, Yu Y, Takai K, et al. Single-cell analysis reveals a stem-cell program in human metastatic breast cancer cells. *Nature.* (2015) 526:131–5. doi: 10.1038/nature15260
5. Sancho P, Barneda D, Heeschen C. Hallmarks of cancer stem cell metabolism. *Br J Cancer.* (2016) 114:1305–12. doi: 10.1038/bjc.2016.152
6. Visvader JE, Lindeman GJ. Cancer stem cells in solid tumours: accumulating evidence and unresolved questions. *Nat Rev Cancer.* (2008) 8:755–68. doi: 10.1038/nrc2499
7. Bao S, Wu Q, McLendon RE, Hao Y, Shi Q, Hjelmeland AB, et al. Glioma stem cells promote radioresistance by preferential activation of the DNA damage response. *Nature.* (2006) 444:756–60. doi: 10.1038/nature05236
8. Hanahan D, Weinberg RA. Hallmarks of cancer: the next generation. *Cell.* (2011) 144:646–74. doi: 10.1016/j.cell.2011.02.013
9. Wen L, Tang F. Single-cell sequencing in stem cell biology. *Genome Biol.* (2016) 17:71. doi: 10.1186/s13059-016-0941-0
10. Zhang X, Marjani SL, Hu Z, Weissman SM, Pan X, Wu S. Single-cell sequencing for precise cancer research: progress and prospects. *Cancer Res.* (2016) 76:1305–12. doi: 10.1158/0008-5472.CAN-15-1907
11. Regev A, Teichmann SA, Lander ES, Amit I, Benoist C, Birney E, et al. The human cell atlas. *eLife.* (2017) 6:e27041. doi: 10.7554/eLife.27041
12. Pizzolato G, Kaminski H, Tosolini M, Franchini DM, Pont F, Martins F, et al. Single-cell RNA sequencing unveils the shared and the distinct cytotoxic hallmarks of human TCRVdelta1 and TCRVdelta2 gammadelta T lymphocytes. *Proc Natl Acad Sci USA.* (2019) 116:11906–15. doi: 10.1073/pnas.1818488116
13. Margolin JF, Friedman JR, Meyer WK, Vissing H, Thiesen HJ, Rauscher FJ III. Kruppel-associated boxes are potent transcriptional repression domains. *Proc Natl Acad Sci USA.* (1994) 91:4509–13. doi: 10.1073/pnas.91.10.4509
14. Witzgall R, O'Leary E, Leaf A, Onaldi D, Bonventre JV. The Kruppel-associated box-A (KRAB-A) domain of zinc finger proteins mediates transcriptional repression. *Pro Natl Acad Sci USA.* (1994) 91:4514–8. doi: 10.1073/pnas.91.10.4514
15. Urrutia R. KRAB-containing zinc-finger repressor proteins. *Genome Biol.* (2003) 4:231. doi: 10.1186/gb-2003-4-10-231
16. Friedman JR, Fredericks WJ, Jensen DE, Speicher DW, Huang XP, Neilson EG, et al. KAP-1, a novel corepressor for the highly conserved KRAB repression domain. *Genes Dev.* (1996) 10:2067–78. doi: 10.1101/gad.10.16.2067
17. Moosmann P, Georgiev O, Le Douarin B, Bourquin JP, Schaffner W. Transcriptional repression by RING finger protein TIF1 beta that interacts with the KRAB repressor domain of KOX1. *Nucleic Acids Res.* (1996) 24:4859–67. doi: 10.1093/nar/24.24.4859
18. Cheng Y, Geng H, Cheng SH, Liang P, Bai Y, Li J, et al. KRAB zinc finger protein ZNF382 is a proapoptotic tumor suppressor that represses multiple oncogenes and is commonly silenced in multiple carcinomas. *Cancer Res.* (2010) 70:6516–26. doi: 10.1158/0008-5472.CAN-09-4566
19. Zheng L, Pan H, Li S, Flesken-Nikitin A, Chen PL, Boyer TG, et al. Sequence-specific transcriptional corepressor function for BRCA1 through a novel zinc finger protein, ZBRK1. *Mol Cell.* (2000) 6:757–68. doi: 10.1016/S1097-2765(00)00075-7
20. White DE, Negorev D, Peng H, Ivanov AV, Maul GG, Rauscher FJ III. KAP1, a novel substrate for PIKK family members, colocalizes with numerous damage response factors at DNA lesions. *Cancer Res.* (2006) 66:11594–9. doi: 10.1158/0008-5472.CAN-06-4138
21. Peng H, Zheng L, Lee WH, Rux JJ, Rauscher FJ III. A common DNA-binding site for SZF1 and the BRCA1-associated zinc finger protein, ZBRK1. *Cancer Res.* (2002) 62:3773–81.
22. Mase S, Shinjo K, Totani H, Katsushima K, Arakawa A, Takahashi S, et al. ZNF671 DNA methylation as a molecular predictor for the early recurrence of serous ovarian cancer. *Cancer Sci.* (2019) 110:1105–16. doi: 10.1111/cas.13936
23. Schmitz M, Eichelkraut K, Schmidt D, Zeiser I, Hilal Z, Tettenborn Z, et al. Performance of a DNA methylation marker panel using liquid-based cervical scrapes to detect cervical cancer and its precancerous stages. *BMC Cancer.* (2018) 18:1197. doi: 10.1186/s12885-018-5125-8
24. Yeh CM, Chen PC, Hsieh HY, Jou YC, Lin CT, Tsai MH, et al. Methylomics analysis identifies ZNF671 as an epigenetically repressed novel tumor suppressor and a potential non-invasive biomarker for the detection of urothelial carcinoma. *Oncotarget.* (2015) 6:29555–72. doi: 10.18632/oncotarget.4986
25. Tian Y, Arai E, Gotoh M, Komiyama M, Fujimoto H, Kanai Y. Prognostication of patients with clear cell renal cell carcinomas based on quantification of DNA methylation levels of CpG island methylator phenotype marker genes. *BMC Cancer.* (2014) 14:772. doi: 10.1186/1471-2407-14-772
26. Zhang J, Wen X, Liu N, Li YQ, Tang XR, Wang YQ, et al. Epigenetic mediated zinc finger protein 671 downregulation promotes cell proliferation and tumorigenicity in nasopharyngeal carcinoma by inhibiting cell cycle arrest. *J Exp Clin Cancer Res.* (2017) 36:147. doi: 10.1186/s13046-017-0621-2
27. Zhang J, Zheng Z, Zheng J, Xie T, Tian Y, Li R, et al. Epigenetic-mediated downregulation of Zinc finger protein 671 (ZNF671) predicts poor prognosis in multiple solid tumors. *Front Oncol.* (2019) 9:342. doi: 10.3389/fonc.2019.00342
28. Yuan H, Yan M, Zhang G, Liu W, Deng C, Liao G, et al. CancerSEA: a cancer single-cell state atlas. *Nucleic Acids Res.* (2019) 47:D900–8. doi: 10.1093/nar/gky939

29. The Gene Ontology C. Expansion of the Gene Ontology knowledgebase and resources. *Nucleic Acids Res.* (2017) 45:D331–8. doi: 10.1093/nar/gkw1108
30. Liberzon A, Birger C, Thorvaldsdottir H, Ghandi M, Mesirov JP, Tamayo P. The molecular signatures database (MSigDB) hallmark gene set collection. *Cell Syst*. (2015) 1:417–25. doi: 10.1016/j.cels.2015.12.004
31. Santos A, Wernersson R, Jensen LJ. Cyclebase 3.0: a multi-organism database on cell-cycle regulation and phenotypes. *Nucleic Acids Res.* (2015) 43:D1140–4. doi: 10.1093/nar/gku1092
32. Zheng G, Ma Y, Zou Y, Yin A, Li W, Dong D. HCMDB: the human cancer metastasis database. *Nucleic Acids Res.* (2018) 46:D950–5. doi: 10.1093/nar/gkx1008
33. Pinto JP, Machado RSR, Magno R, Oliveira DV, Machado S, Andrade RP, et al. StemMapper: a curated gene expression database for stem cell lineage analysis. *Nucleic Acids Res.* (2018) 46:D788–93. doi: 10.1093/nar/gkx921
34. Hanzelmann S, Castelo R, Guinney J. GSVA: gene set variation analysis for microarray and RNA-seq data. *BMC Bioinform.* (2013) 14:7. doi: 10.1186/1471-2105-14-7
35. Li W, Cerise JE, Yang Y, Han H. Application of t-SNE to human genetic data. *J Bioinform Comput Biol.* (2017) 15:1750017. doi: 10.1142/S0219720017500172
36. Sun HY, Wei SP, Xu RC, Xu PX, Zhang WC. Sphingosine-1-phosphate induces human endothelial VEGF and MMP-2 production via transcription factor ZNF580: novel insights into angiogenesis. *Biochem Biophys Res Commun.* (2010) 395:361–6. doi: 10.1016/j.bbrc.2010.04.019
37. Li K, Gao B, Li J, Chen H, Li Y, Wei Y, et al. ZNF32 protects against oxidative stress-induced apoptosis by modulating C1QBP transcription. *Oncotarget.* (2015) 6:38107–26. doi: 10.18632/oncotarget.5646
38. Huang J, Teng L, Li L, Liu T, Li L, Chen D, et al. ZNF216 Is an A20-like and IkappaB kinase gamma-interacting inhibitor of NFkappaB activation. *J Biol Chem*. (2004) 279:16847–53. doi: 10.1074/jbc.M309491200
39. Kuramoto K, Uesaka T, Kimura A, Kobayashi M, Watanabe H, Katoh O. ZK7, a novel zinc finger gene, is induced by vascular endothelial growth factor and inhibits apoptotic death in hematopoietic cells. *Cancer Res.* (2000) 60:425–30.
40. Pozner A, Terooatea TW, Buck-Koehntop BA. Cell-specific Kaiso (ZBTB33) Regulation of cell cycle through Cyclin D1 and Cyclin E1. *J Biol Chem.* (2016) 291:24538–50. doi: 10.1074/jbc.M116.746370
41. Huang C, Jia Y, Yang S, Chen B, Sun H, Shen F, et al. Characterization of ZNF23, a KRAB-containing protein that is downregulated in human cancers and inhibits cell cycle progression. *Exp Cell Res.* (2007) 313:254–63. doi: 10.1016/j.yexcr.2006.10.009
42. Kim GD, Das R, Goduni L, McClellan S, Hazlett LD, Mahabeleshwar GH. Kruppel-like factor 6 promotes macrophage-mediated inflammation by suppressing B cell leukemia/lymphoma 6 expression. *J Biol Chem.* (2016) 291:21271–82. doi: 10.1074/jbc.M116.738617
43. Wang T, Wang XG, Xu JH, Wu XP, Qiu HL, Yi H, et al. Overexpression of the human ZNF300 gene enhances growth and metastasis of cancer cells through activating NF-kB pathway. *J Cell Mol Med.* (2012) 16:1134–45. doi: 10.1111/j.1582-4934.2011.01388.x
44. Liu Y, Huang W, Gao X, Kuang F. Regulation between two alternative splicing isoforms ZNF148(FL) and ZNF148(DeltaN), and their roles in the apoptosis and invasion of colorectal cancer. *Pathol Res Pract.* (2019) 215:272–7. doi: 10.1016/j.prp.2018.10.036
45. Oleksiewicz U, Gladych M, Raman AT, Heyn H, Mereu E, Chlebanowska P, et al. TRIM28 and interacting KRAB-ZNFs control self-renewal of human pluripotent stem cells through epigenetic repression of pro-differentiation genes. *Stem Cell Rep.* (2017) 9:2065–80. doi: 10.1016/j.stemcr.2017.10.031

Conflict of Interest: The authors declare that the research was conducted in the absence of any commercial or financial relationships that could be construed as a potential conflict of interest.

frontiers in Oncology

ORIGINAL RESEARCH
published: 15 November 2019
doi: 10.3389/fonc.2019.01234

Methyl-Cantharidimide Inhibits Growth of Human Hepatocellular Carcinoma Cells by Inducing Cell Cycle Arrest and Promoting Apoptosis

Xiangzhong Huang[1†], Wen Xie[2†], Xiaofan Yu[2], Caiyun Fan[2], Jin Wang[2], Yi Cao[2] and Jianxiang Li[2]*

[1] Department of Interventional Therapy, Affiliated Jiangyin Hospital, Medical College of Southeast University, Jiangyin, China,
[2] School of Public Health, Medical College of Soochow University, Suzhou, China

Methyl-Cantharidimide (MCA) is a derivative of cantharidin which has potential anticancer activity. This study investigates the effect of MCA on the growth and metastasis of human hepatocellular carcinoma (HCC) cells. Human HCC HepG2 and Hep3B2.1-7 cells, and normal hepatocytes (L02) were treated with a series of concentrations of MCA. The inhibition ability of these cells was examined by CCK-8 assay. Cell cycle and cell apoptosis were determined using Flow Cytometry. The effect of MCA on cell migration and invasion was evaluated through scratch wound healing and transwell migration assays. Furthermore, Western blot was used to evaluate biomarkers associated with cell cycle and apoptosis. It was found that: (i) MCA inhibited cell proliferation in HCC cells in a dose- and time-dependent manner, especially in HepG2 cells; (ii) MCA arrested HCC cells in G-1 phase cell cycle; (iii) MCA induced HCC cells apoptosis; (iv) MCA inhibited the migration ability of HCC cells; and (v) MCA treatment significantly increased cleaved-caspase3 and decreased NF-κB protein in HCC cells. These results suggest that MCA has cytotoxic effect on HCC cells by inducing cell cycle arrest and promoting apoptosis. MCA could be developed as an previous anticancer drug for the treatment of human hepatocellular carcinoma.

Keywords: methyl-cantharidimide (MCA), cantharidin (CTD), hepatocellular carcinoma, cell growth, invasion

OPEN ACCESS

Edited by:
Dong-Hua Yang,
St. John's University, United States

Reviewed by:
Haichang Li,
The Ohio State University,
United States
Xiaozhuo Liu,
University at Buffalo, United States

****Correspondence:***
Jianxiang Li
aljxcr@suda.edu.cn

† These authors have contributed equally to this work

Specialty section:
This article was submitted to Molecular and Cellular Oncology, a section of the journal Frontiers in Oncology

Received: *22 August 2019*
Accepted: *28 October 2019*
Published: *15 November 2019*

Citation:
Huang X, Xie W, Yu X, Fan C, Wang J, Cao Y and Li J (2019) Methyl-Cantharidimide Inhibits Growth of Human Hepatocellular Carcinoma Cells by Inducing Cell Cycle Arrest and Promoting Apoptosis. Front. Oncol. 9:1234. doi: 10.3389/fonc.2019.01234

INTRODUCTION

Hepatocellular carcinoma (HCC) is a primary malignant tumor in the liver. It is the third leading cause of cancer deaths worldwide. The annual incidence of HCC in North America and Western Europe ranges from 10 to 15 cases per 100,000 people, while in parts of Africa and Asia, the incidence is much higher and range from 50 to 150 cases per 100,000 people (1). The median survival following diagnosis ranges from ∼6 to 20 months. Currently, tumor resection is an option of choice for the treatment of HCC. However, since most of the diagnosis is made in late stages of the disease, HCC patients have few opportunity to undergo surgery. Thus, there is an urgent need for early diagnosis and effective therapeutic medication (2, 3). In recent years, there were several reports suggest that some traditional Chinese medicines showed remarkable

anti-cancer activity (4–7). Cantharidin (CTD) is a biologically active ingredient isolated from Chinese blister Beetle, *Mylabris phalerata*. It is used in traditional Chinese medicine for more than 2000 years to treat various diseases including cancers (8–14). Several recent reports have identified potential mechanisms of action of cantharidin in different types of human cancer cells, including hepatocellular carcinoma cells (15–21). Although CTD is a natural toxin possessing potent anti-tumor properties, its use in cancer treatment has been limited because of severe side effects due to its highly toxic nature. Analogs of chemically modified CTD have been synthesized to achieve a comparable anti-tumor property with less toxic effect (22).

Methyl-cantharidimide (MCA, 2,3a,7a-Trimethyl-hexahydro -4,7-epoxido-isoindol-1,3-dion, C11H15NO3, molecular weight 209.242) is one such derivative of CTD. MCA is chemically synthesized and developed as a powerful anticancer drug with less toxicity (23). However, the anticancer effect of MCA and its mechanism of action has not been evaluated. This study investigates the anticancer effect of MCA using hepatocellular carcinoma cell models. Human hepatocellular carcinoma cell lines, HepG2 and Hep3B2.1-7 and normal hepatocyte LO_2 cells were used. Various concentrations of MCA were tested in these cells to determine its tumor growth inhibitory effect. The mechanism of anticancer activity of MCA was explored by determining the change of cell cycle, cell apoptosis and cell migration ability. The activity of key-players that regulate cell apoptosis, caspase-3 and Nuclear Factor kappa-light-chain-enhancer of activated B cells (NF-κB), were evaluated.

MATERIALS AND METHODS

Cell Culture

Human hepatocellular carcinoma cell lines, HepG2 and Hep3B2.1-7, were purchased from Chinese Type Culture Collection, Chinese Academy of Sciences, Shanghai, China. Normal human hepatic cell L02, was a gift from the Department of Toxicology, School of Public Health, Soochow University, Suzhou, China. Cells were cultured in complete Dulbecco's modified Eagle's medium (DMEM) containing 10% fetal bovine serum, 100 μg/ml streptomycin and penicillin (all obtained from Hyclone, Suzhou, China) in an incubator maintaining at 37 ± 0.5°C in a humidified atmosphere with 5% CO_2. Cells were trypsinized after reaching confluence and aliquots were kept frozen at −80°C. Cells were sub-cultured and those in 3–4 passages were used in experiments described below. All experiments were repeated three times.

Methyl-Cantharidimide (MCA)

Methyl-Cantharidimide (MCA) was a gift of Sihuan Bioengineering Co., Ltd., Jiangsu, China. A stock solution (20 mM) was freshly prepared by dissolving MCA in dimethyl sulfoxide (DMSO, PanReac Applichem, Germany) and diluted in desired concentrations in complete DMEM. HepG2, Hep3B2.1-7, and LO_2 cells were treated *in vitro* with a series of final concentrations of MCA or with the solvent DMEM as control.

Cytotoxicity Essay (IC50)

Two-hundred μl aliquots of HepG2, Hep3B2.1-7 and L02 cells in DMEM complete medium (∼3000 cells each) were distributed into 96-well plate and cultured for 24 h at 37 ± 0.5°C. Then, 200 μl MCA solution was added to give a final concentration of 50, 100, 200, 400, and 800 μM. The cells were cultured for 24, 48, and 72 h. The proliferation ability of the cells in each well was assessed using a CCK-8 assay kit (Dojindo, China) according to manufacturer's instructions. Briefly, 20 μl of CCK-8 solution was added to each well and the cells were incubated for 4 h at 37 ± 0.5°C. The plates were then read in the standard plate reader (FilterMax F5, Molecular Devices, USA) at a reference wavelength of 450 nm. The percent inhibition of growth in cells treated with MCA was calculated as follows: % Inhibition = [A450(drug) – A450(blank)]/[A450(control) – A450(blank)] × 100%. The IC30 that was obtained for HepG2 cells was 137.56 μM MCA. This dose was used in subsequent experiments.

Cell Cycle Evaluation

Two-hundred μl aliquots of HepG2 and Hep3B2.1-7 cells in complete DMEM medium (∼1 × 10^5 cells each) were distributed in 6-well plates and cultured for 24 h at 37 ±−0.5°C. Then, the cells were treated with 137.56 μM MCA (IC30 concentration obtained for HepG2 cells) for 48 h, collected by trypsinization, washed twice with cold phosphate buffered saline (PBS), suspended in cold 70% methanol and left at −20°C overnight. The cells were then washed twice with cold PBS and stained with PBS solution containing 20 μg/ml PI and 50 μg/ml of RNaseA for 30 min. The cell cycle analysis was carried out using a flow cytometer (Beckman coulter, Shanghai, China) (24).

Cell Apoptosis Detection

Annexin V-FITC apoptosis detection kit (KeyGEN Biotech, Shanghai, China) was used to evaluate cell apoptosis. Two-hundred μl aliquots of HepG2 and Hep3B2.1-7 in complete DMEM medium (∼1 × 10^5 cells each) were distributed in 6-well plates and cultured for 24 h. Then, the cells were treated with 137.56 μM MCA (IC30 concentration obtained for HepG2 cells) for 48 h. The cells were collected by trypsinization, incubated with Annexin V in a buffer containing propidium iodide for 15 min. The percent cells in apoptosis were then determined using a flow cytometer (Beckman coulter, Shanghai, China) (25).

Scratch Wound Healing Assay

Two hundred microliters aliquots of HepG2 and Hep3B2.1-7 cells in complete DMEM medium (∼2 × 10^5 cells each) were distributed in 6-well plates and cultured for 24 h at 37°C. Then, the cells were treated with 137.56 μM MCA (IC30 concentration obtained for HepG2 cells) for 48 h. Cells were allowed to grow up to 100% confluence and a scratch was made in the plate using with a P10 pipette tip. The cells were cultured in fresh serum-free DMEM medium. images were collected at 0 and 24 h under an inverted microscope (Olympus, Germany) and quantitatively analyzed using the NIH Image J software.

Transwell Migration Assay

HepG2 and Hep3B2.1-7 cancer cells and MCA treated cells (2×10^5) were seeded in the upper chambers (pore size, 8 μm) of the 6-well plate (Corning, USA) in 1 ml serum-free medium. The lower chambers were filled with 2 ml complete medium with 10% FBS, and the plate was incubated under standard conditions for 24 h. After removing the cells in the upper surface of the membrane with a cotton swab, cells in the lower chamber were fixed with methanol and stained with 0.5% crystal violet solution. The images were taken using an inverted microscope (Olympus, Germany and analyzed using NIH Image J software.

Western Blot Analysis

Approximated 2×10^5 HepG2 cells were treated with 137.56 μM MCA (IC30 concentration obtained for HepG2 cells) for 48 h. Protein extracts were prepared by lysing the cells in lysis buffer containing 50 mM Tris (pH 7.4), 150 mM sodium chloride, 1% Triton X-100, 1% sodium deoxycholate, 0.1% sodium dodecyl sulfate and 1 mM phenyl-methyl-sulfonyl fluoride (all obtained from Beyotime, Shanghai, China). The cell lysates were centrifuged at 14,000 × *g* for 5 min at 4°C and the supernatant containing solubilized proteins was collected. The protein concentration in all samples was determined by using the BCA protein assay kit (Beyotime, Shanghai, China). From each sample, equal amount of protein (40 μg per lane) was loaded, separated by 10% sodium dodecyl sulfate polyacrylamide gel (SDS–PAGE) and then transferred to polyvinylidene difluoride (PVDF) membranes (Millipore Corporation, Billerica, MA, USA). The membranes were blocked for 2 h in 5% fat-free dry milk (Yili Industrial, Inner Mongolia, China) containing Tween 20-Tris-buffered saline (TTBS). The membranes were then incubated with primary antibodies (rabbit monoclonal anti-NF-κB antibody, rabbit monoclonal anti-cleaved caspase 3 antibody and rabbit monoclonal anti-GADPH, Abcam, Cambridge, USA) overnight at 4°C. They were washed three times in TTBS and incubated further with horseradish peroxidase-conjugated antibodies (Beyotime, Shanghai, China) for 1.5 h at room temperature. This was followed by washing the membranes three times with TTBS. The immunoreactive proteins on the membranes were detected using enhanced chemiluminescence reagents (Millipore Corporation) and G-BOX Chemi XRQ (Syngene, UK). The blots were quantified and normalized with the level of GADPH to correct the differences in loading of the proteins in MCA-treated cells.

TABLE 1 | IC50 of MCA in HCC cells and normal hepatic cells.

Cell type	Treatment duration		
	24 h	48 h	72 h
HepG2	301.49 ± 21.48*	227.00 ± 6.11*#	157.00 ± 3.98*#
Hep3B2.1-7	295.63 ± 25.61*	273.44 ± 18.52*	238.10 ± 7.43*#
L02	583.92 ± 63.17	363.56 ± 44.46#	347.40 ± 31.53#

*All experiments were repeated three times. Data are mean ± Standard Deviation. *p < 0.05: Compared to L02 cells; #p < 0.05: Compared to 24 h.*

TABLE 2 | Alteration of cell cycle in HepG2 and Hep3B2.1-7 HCC cells treated with MCA.

Cell type	Treatment	G1	S	G2
HeoG2	Solvent	54.58 ± 1.67	26.02 ± 2.27	19.39 ± 2.33
	MCA	60.23 ± 0.70*	22.04 ± 0.65*	17.73 ± 0.22
Hep3B2.1-7	Solvent	47.48 ± 0.62	29.92 ± 1.62	22.60 ± 2.22
	MCA	50.81 ± 0.76*	28.31 ± 0.09	20.88 ± 0.83

*All experiments were repeated three times. MCA treatment with IC30 concentration (137.56 μM) for 48 h. Data are mean ± Standard Deviation. *p < 0.05.*

TABLE 3 | Apoptosis of HepG2 and Hep3B2.1-7 cells after treatment with MCA (mM).

Cell type	Treatment	Early apoptosis	Late apoptosis	Total apoptosis
HepG2	Solvent	1.29 ± 0.42	1.53 ± 0.62	2.83 ± 1.04
	MCA	9.26 ± 2.27*	3.08 ± 0.65*	12.34 ± 2.81*
Hep3B2.1-7	Solvent	2.56 ± 0.88	1.14 ± 0.62	3.70 ± 1.48
	MCA	5.44 ± 0.38*	2.04 ± 0.38	7.49 ± 0.42*

*All experiments were repeated three times. MCA treatment with IC30 concentration (137.56 μM) for 48 h. Data are mean ± Standard Deviation. *p < 0.05.*

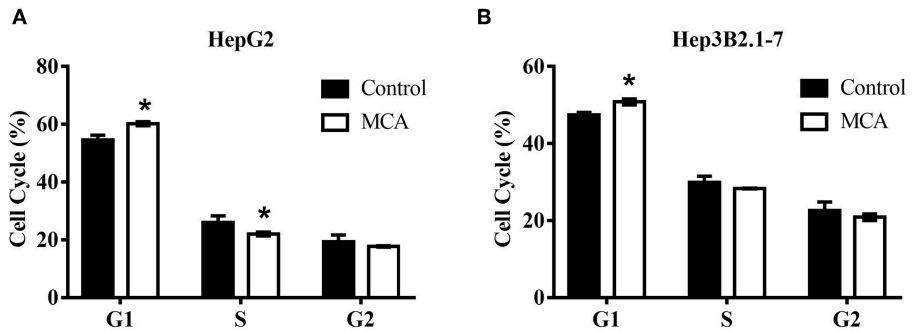

FIGURE 1 | Flow cytometry on cell cycle analysis in HepG2 and Hep3B2.1-7 cells following treatment with MCA for 48 h. **(A)** Effect of MCA on cell cycle of HepG2 cells. **(B)** Effect of MCA on cell cycle of Hep3B2.1-7 cells. *p <0.05 via control.

Statistical Analysis

The results from three independent experiments were pooled and analyzed using GraphPad Prism 5.0 (GraphPad Software, San Diego, CA, USA). The data were presented as mean ± SD. Statistical significances of differences were analyzed by one way analysis of variance (ANOVA) test followed by Sidak's multiple comparison post-test. A p-value of <0.05 was considered as significant difference between MCA treated and untreated cells.

RESULTS

MCA Inhibits the Proliferation of HCC Cells With Little Effect on the Proliferation of Normal Hepatic Cells

The effect of MCA on the proliferation of HCC and normal hepatic cells was evaluated using CCK 8 assay. The inhibition rate of growth in L02, HepG2 and Hep3B2.1-7 cells treated with 50, 100, 200, 400 and, 800 μM MCA were presented. In all three types of cells, there was a decrease in growth which was positively correlated with not only the increased concentration of MCA but also the duration of treatment from 24 to 72 h. The IC50 observed in HepG2 and Hep3B2.17 HCC cells and normal LO_2 hepatic cells treated with MCA for 24, 48, and 72 h were presented in **Table 1**. The IC50 observed in LO_2, HepG2 and Hep3B2.1-7 cells, after 48 h treatment with MCA were at concentrations of 363.56 ± 44.46, 227.00 ± 6.11, and 273.44 ± 18.52 μM, respectively. This result indicated that MCA inhibits the proliferation of HepG2 and Hep3B2.1-7 cells with little effect on the proliferation of normal hepatocyte LO_2 cells.

MCA Induces Cell Cycle Arrest at G1/S of HCC Cells

Since MCA inhibits HCC cell proliferation, we next examine whether MCA affects cell cycle progression in HCC cells by flow cytometry. HepG2 and Hep3B2.1-7 cells were treated with and without MCA for 48 hrs. The IC30 concentration of MCA obtained from HepG2 cells in the above experiment 137.56 μM was used. It was found that MCA treatment blocks the progression of cell cycle from G1- to S-phase in both HepG2 and Hep3B2.1-7 HCC cells, resulting in increased cell

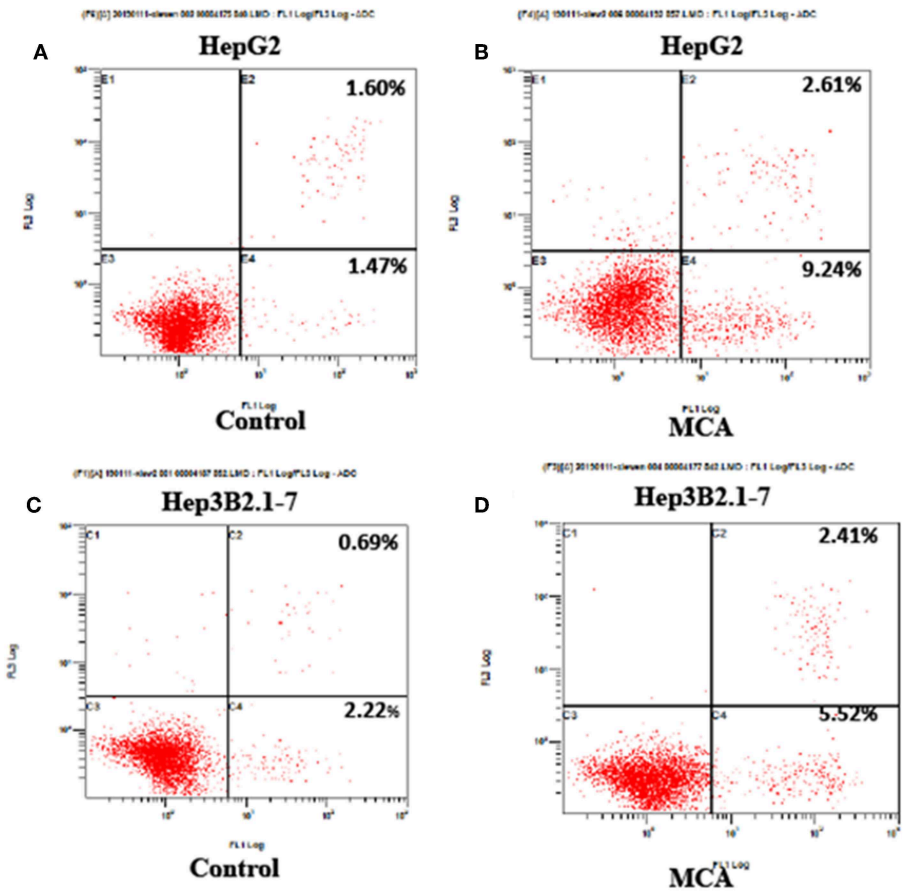

FIGURE 2 | Flow cytometry on cell apoptosis analysis in HepG2 and Hep3B2.1-7 cells following treatment with MCA for 48 h. **(A)** Apoptosis of untreated HepG2 cells for 48 h. **(B)** Apoptosis of HepG2 cell treated with MCA for 48 h. **(C)** Apoptosis of untreated Hep3B2.1-7 cells for 48 h. **(D)** Apoptosis of Hep3B2.1-7 cell treated with MCA for 48 h.

number in G1-phase. The percent of HepG2 cells at G1-phase was 60.23 ± 0.70 which was significantly higher than in solvent-treated cells, which was 54.58 ± 1.67 ($p < 0.05$). Similarly, the percent of Hep3B2.1-7 cells at G1-phase was 50.81 ± 0.76, which was significantly higher than that in solvent-treated cells, 47.48 ± 0.62 ($p < 0.05$). There was no significant difference in percent cells in S- and G2-phase in both cell types ($p > 0.05$). This result indicates that

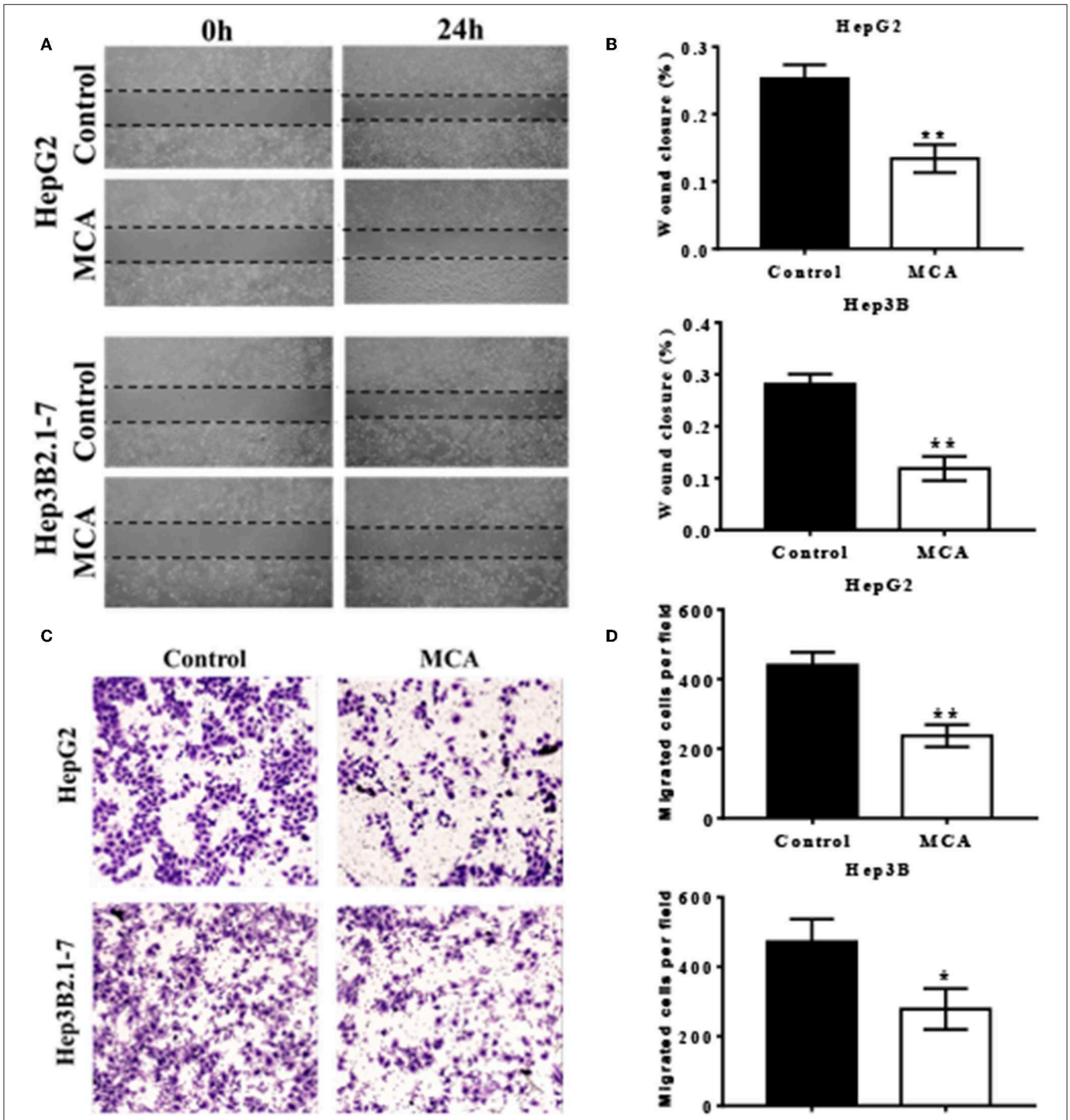

FIGURE 3 | Scratch wound healing assays performed in HepG2 and Hep3B2.1-7 cells treated with conditioned medium containing MCA or vehicle control for 48 h **(A)**. Quantitative analysis of wound closure **(B)**. HepG2 and Hep3B2.1-7 cells were treated with the indicated conditioned medium containing MCA or vehicle control for 48 h in a transwell assay **(C)**. Cells that migrated through transwells were stained with crystal violet and photomicrographed. Quantitative analysis of migrated cells perfield **(D)**. *$p < 0.05$, **$p < 0.01$ via Control.

MCA induces cell cycle arrest at G1/S phase (**Table 2** and **Figures 1A,B**).

MCA Promotes Apoptosis of HCC Cells

The effect of MCA on cell apoptosis of HCC cells was evaluated by flow cytometry. The early, late and total cell apoptosis in HepG2 and Hep3B2.1-7 cells, treated with or without 137.56 μM MCA for 48 h were presented in **Table 3** and **Figure 2**. The data showed a significant increase in total percent of cells of apoptosis in both HepG2 and Hep3B2.1-7 cells: 12.34 ± 2.81 and 7.49 ± 0.42% in HepG2 and Hep3B2.1-7 cells, respectively compared with solvent-treated cells, 2.83 ± 1.04 and 3.70 ± 1.48%, respectively. This result indicates that MCA treatment promotes apoptosis of HCC cells.

MCA Inhibits Cell Migration

To investigate the effect of MCA in the migratory ability of HCC cells, we performed scratch wound healing and transwell cell migration assays. Scratch wound healing assay indicated that MCA significantly inhibited the migration ability of HepG2 and Hep3B2.1-7 cells (**Figures 3A,B**). As shown in **Figures 3C,D**, further transwell migration assay demonstrated that the migrated cells were significantly decreased in MCA treated HepG2 and Hep3B2.1-7 cells compared to the untreated cells.

MCA Up-Regulates the Expression of Cleaved Caspase-3 and Down-Regulates the Expression of NF-κB Proteins

Because MCA induces apoptosis of HCC cells, we explored whether the molecules that regulate cell apoptosis were involved. Western blot analysis on the protein expression of cleaved caspase-3 and NF-κB was performed and the results were presented in **Figure 4**. The data showed significantly increased level of caspase-3 protein ($p < 0.05$) and significantly decreased level of NF-κB protein ($p < 0.05$) in HepG2 cells treated with 137.56 μM MCA for 48 hrs. This result suggested that MCA up-regulates the expression of Cleaved Caspase-3 and down-regulates the expression of NF-κB proteins.

DISCUSSION

Hepatocellular carcinoma is the primary malignant tumor in liver. It is usually associated with liver cirrhosis, viral hepatitis, aflatoxin exposure, and alcohol abuse. Typically, HCC is diagnosed in late stages and thus, patients have few opportunity for surgical resection or transplantation (2, 3). Currently, there is no ideal treatment option for the cure of the disease. In recent years, there have been increasing efforts to develop drugs for the treatment and prevention of HCC. Cantharidin (CTD) is a biologically active ingredient isolated from the Chinese blister beetle (*Mylabris phalerata*) and has been used in traditional Chinese medicine for over 2000 years to treat various diseases including cancers (8–14). However, the dose of CTD used for cancer treatment is very close to its toxic dose and its use had been

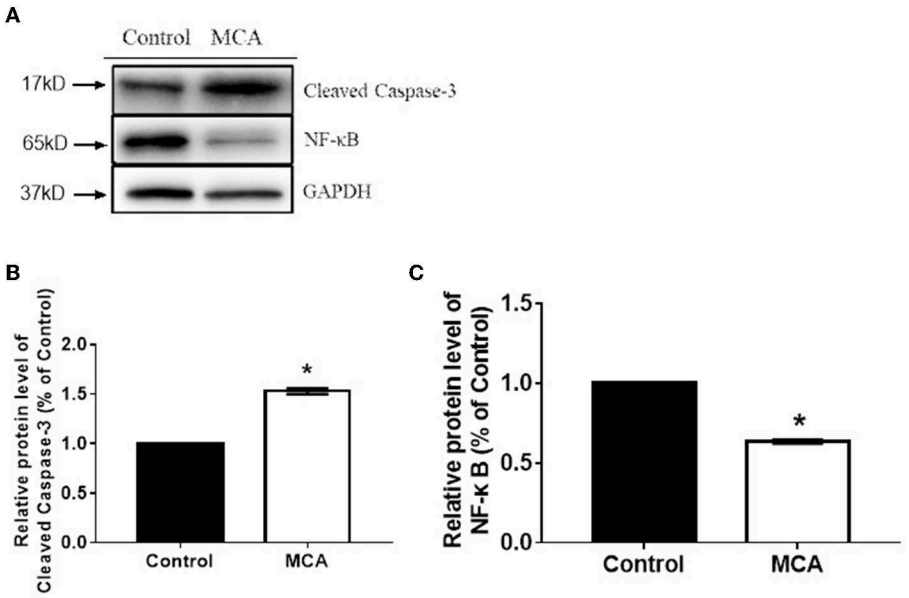

FIGURE 4 | Western blot analysis on the expression of cleaved caspase-3 and NF-κB protein in HCC cells (HepG2 and Hep3B2.1-7) following treatment with MCA for 48 h. **(A)** the bar graph illustrates data normalized to house-keeping genes (GAPDH) and expressed as % control. Cleaved-Caspase3 and NF-κB protein expression levels in the control and MCA groups. **(B)** The bar graph of Cleaved-Caspase3 proteins extracted from HepG2 cell. **(C)** The Bar graph of BF-κB protein extracted from HepG2 cell. *$p < 0.05$ via Control.

hampered in clinics. Nonetheless, researchers have identified the pharmacological and toxicological properties of CTD (26–30), and started to synthesize and develop bioactive derivatives that have anti-cancer potential with low toxicological profile (31).

MCA is one of such synthetic derivatives of CTD (23). Its anti-cancer effect and the mechanism of action particularly in hepatocellular carcinoma cells has not been delineated. In this study, MCA was tested in a series of concentrations to determine its growth inhibitory effect in different human HCC cells, HepG2, and Hep3B2.1-7 cells, and compared with the normal LO_2 hepatic cells. The 50% growth inhibitory effect of MCA in HepG2 and Hep3B2.1-7 cells was observed at a concentration of 226.82 and 273.18 μM, respectively, while that in normal hepatic LO_2 cells was at 379.41 μM. This result suggests that normal hepatic cells required a higher concentration of MCA to elicit 50% growth inhibitory effect. In other words, MCA was selectively toxic to HCC cells compared with that in normal hepatic cells. We also found that treatment of HepG2 and Hep3B2.1-7 HCC cells with IC30 dose of MCA induces cell cycle G1/S arrest, resulting in accumulation of cells in G1 phase of the cell cycle. Flow cytometric analysis showed that the IC30 dose of MCA induced significantly higher percent of cell apoptosis in HepG2 and Hep3B2.1-7 cells compared with normal hepatic cells. These observations suggested that MCA exert growth inhibitory effect and induce cell apoptosis in HCC cells. Transwell migration assay demonstrated that the migrated cells were significantly decreased in MCA treated HepG2 and Hep3B2.1-7 cells compared to the untreated cells. Caspases are crucial mediators of cell apoptosis, among them, caspase-3 is a frequently activated protease, catalyzing the specific cleavage of key cellular proteins. Caspase-3 is indispensable for apoptotic chromatin condensation and DNA fragmentation. Thus, caspase-3 is essential for certain processes associated with the formation of apoptotic bodies, but it may also function before or at the stage when commitment to loss of cell viability is made (32, 33). NF-κB is a primary transcription factor which plays a key role in several cellular processes including cell proliferation and survival (34–36). In this study, 48 h after treatment of HepG2 cells with MCA, the protein level of cleaved-caspase3 was significantly increased while that of NF-κB was significantly decreased. These results suggested that both cleaved caspase-3 and NF-κB played important roles in MCA-induced cell apoptosis in HCC cells. Our results are in consistent with other study which showed that MCA can inhibit the proliferation of HCC cells and prolong the survival of mice with hepatocellular carcinoma (37). Studies on sodium cantharidate, another derivative of cantharidin, have also shown that sodium cantharidate can inhibit the growth of liver cancer cells and induce cell apoptosis (38). Therefore, the inhibitory effect of CTD derivatives on HCC cells is most likely associated with inhibiting cancer cell growth and inducing cancer cell apoptosis by activating caspace-3 and inhibiting NF-κB. The mechanism of action of MCA *in vivo* warrants further investigation.

CONCLUSIONS

Our results suggest that MCA can inhibit cell proliferation and migration of cancer cells. This study provides a rational for developing MCA as a therapeutic agent for the treatment of hepatocellular carcinoma.

DATA AVAILABILITY STATEMENT

Data will be available upon request by writing to the corresponding author.

AUTHOR CONTRIBUTIONS

XH performed MTT assay and write the first draft. XH, WX, CF, and XY performed flow cytometry, cell migration, and invasion assays. CF and JW performed Western blotting, YC performed statistics. JL conceived the study, supervise experiments and results analysis. All authors edited the manuscript and approved the final version.

ACKNOWLEDGMENTS

We are grateful to Dr. Vijayalaxmi, Department of Radiology, University of Texas Health Science Center, San Antonio, TX, USA for her helpful comments on the manuscript.

REFERENCES

1. Blum HE, Moradpour D. Hepatocellular carcinoma. *N Engl J Med*. (2011) 365:1118–314. doi: 10.1056/NEJMra1001683
2. Sakaguchi T, Suzuki S, Morita Y, Oishi A, Fukumoto K, Inaba K, et al. Impact of the preoperative des-gamma-carboxy prothrombin level on prognosis after hepatectomy for hepatocellular carcinoma meeting the Milan criteria. *Surg Today*. (2010) 40:638–45. doi: 10.1007/s00595-009-4109-3
3. Yamashita Y, Morita K, Iguchi T, Tsujita E, Soejima Y, Taketomi A, et al. Surgical impacts of an en bloc resection of the diaphragm for hepatocellular carcinoma with gross diaphragmatic involvement. *Surg Today*. (2011) 41:101–6. doi: 10.1007/s00595-010-4289-x
4. Hsu YL, Yen MH, Kuo PL, Cho CY, Huang YT, Tseng CJ, et al. San-Zhong-Kui-Jian-Tang, a traditional Chinese medicine prescription, inhibits the proliferation of human breast cancer cell by blocking cell cycle progression and inducing apoptosis. *Biol Pharm Bull*. (2006) 29:2388–94. doi: 10.1248/bpb.29.2388
5. Chen Z-F, Liang H. Progresses in TCM metal-based antitumour agents. *Anticancer Agents Med Chem*. (2010) 10:412–23. doi: 10.2174/1871520611009050412
6. Lee S, Lee Y, Choi YJ, Han KS, Chung HW. Cyto-/genotoxic effects of the ethanol extract of Chan Su, a traditional Chinese medicine, in human cancer cell lines. *J Ethnopharmacol*. (2014) 152:372–6. doi: 10.1016/j.jep.2014.01.023
7. Jiang Y, Liu LS, Shen LP, Han ZF, Jian H, Liu JX, et al. Traditional Chinese Medicine treatment as maintenance therapy in advanced non-small-cell lung cancer: a randomized controlled trial. *Complement Ther Med*. (2016) 24:55–62. doi: 10.1016/j.ctim.2015.12.006
8. Nakatani T, Konishi T, Miyahara K, Noda N. Three novel cantharidin-related compounds from the Chinese blister beetle, *Mylabris phalerata* Pall. *Chem Pharm Bull*. (2004) 52:807–9. doi: 10.1248/cpb.52.807

9. Liu D, Zhiwei C. The effects of cantharidin and cantharidin derivatives on tumor cells. *Anticancer Agents Med Chem*. (2009) 9:392–6. doi: 10.2174/1871520610909040392
10. Yeh CB, Su CJ, Hwang JM, Chou MC. Therapeutic effects of cantharidin analogues without bridging ether oxygen on human hepatocellular carcinoma cells. *Eur J Med Chem*. (2010) 45:3981–5. doi: 10.1016/j.ejmech.2010.05.053
11. Kizaki M, Sagawa M. *Mylabris phalerata* (Chinese blister beetle) on hematological malignancies. In: Cho CS, editor. *Evidence-Based Anticancer Materia Medica*. Dordrecht: Springer (2011), p. 376–88. doi: 10.1007/978-94-007-0526-5_17
12. Liang F, Wang M-Y, Huang W-B, Li AJ. Effect of sodium cantharidinate on the angiogenesis of nude mice with human gastric cancer. *Zong Yao Cai*. (2011) 34:343–6.
13. Shao H, Hong G, Luo X. Evaluation of sodium cantharidinate/vitamin B6 in the treatment of primary hepatoma. *J Cancer Res Ther*. (2014) 1:75–8. doi: 10.4103/0973-1482.139770
14. Deng YY, Zhang W, Li NP, Lei XP, Gong XY, Zhang DM, et al. Cantharidin derivatives from the medicinal insect *Mylabris phalerata*. *Tetrahedron*. (2017) 73:5932–9. doi: 10.1016/j.tet.2017.08.034
15. Hsia TC, Lin JH, Hsu SC, Tang NY, Lu HF, Wu SH, et al. Cantharidin induces DNA damage and inhibits DNA repair-associated protein levels in NCI-H460 human lung cancer cells. *Environ Toxicol*. (2015) 30:1135–43. doi: 10.1002/tox.21986
16. Kuo JH, Shih TY, Lin JP, Lai KC, Lin ML, Yang MD, et al. Cantharidin induces DNA damage and inhibits DNA repair-associated protein expressions in TSGH8301 human bladder cancer cell. *Anticancer Res*. (2015) 35:795–804.
17. Su CC, Liu SH, Lee KI, Huang KT, Lu TH, Fang KM, et al. Cantharidin induces apoptosis through the calcium/PKC-regulated endoplasmic reticulum stress pathway in Human Bladder Cancer Cells. *Am J Chin Med*. (2015) 43:581–600. doi: 10.1142/S0192415X15500366
18. Tian X, Zeng G, Li X, Wu Z, Wang L. Cantharidin inhibits cell proliferation and promotes apoptosis in tongue squamous cell carcinoma through suppression of miR-214 and regulation of p53 and Bcl-2/Bax. *Oncol Rep*. (2015) 33:3061–8. doi: 10.3892/or.2015.3942
19. Le AP, Zhang LL, Liu W, Shi YF. Cantharidin inhibits cell proliferation and induces apoptosis through G2/M phase cell cycle arrest in hepatocellular carcinoma stem cells. *Oncol Rep*. (2016) 35:2970–6. doi: 10.3892/or.2016.4684
20. Ren Y, Zhang SW, Xie ZH, Xu XM, Chen LL, Lou ZG, et al. Cantharidin induces G2/M arrest and triggers apoptosis in renal cell carcinoma. *Mol Med Rep*. (2016) 14:5614–8. doi: 10.3892/mmr.2016.5963
21. Li CC, Yu FS, Fan MJ, Chen YY, Lien JC, Chou YC, et al. Anticancer effects of cantharidin in A431 human skin cancer (epidermoid carcinoma) cells *in vitro* and *in vivo*. *Environ Toxicol*. (2017) 32:723–38. doi: 10.1002/tox.22273
22. Wang G, Dong J, Deng L. Overview of cantharidin and its analogues. *Curr Med Chem*. (2018) 25:2034–44. doi: 10.2174/0929867324666170414165253
23. Wei FC, Du J, Wei N-N, Wang Y, Li S-W. Progress and application of cantharidin and its derivatives. *Prog Modern Biomed*. (2012) 12:1586–9.
24. Hashem MA, Bhandari DP, Kang SK, Lee BC. Cell cycle analysis and interspecies nuclear transfer of *in vitro* cultured skin fibroblasts of the Siberian tiger (*Panthera tigris altaica*). *Mol Reprod Dev*. (2007) 74:403–11. doi: 10.1002/mrd.20528
25. Rieger AM, Nelson KL, Konowalchuk JD, Barreda DR. Modified annexin V/propidium iodide apoptosis assay for accurate assessment of cell death. *J Vis Exp*. (2011) 50:e2597. doi: 10.3791/2597
26. Honkanen RF. Cantharidin, another natural toxin that inhibits the activity of serine/threonine protein phosphatases type 1 and 2A. *FEBS Lett*. (1993) 330:283–6. doi: 10.1016/0014-5793(93)80889-3
27. Li W, Xie L, Chen Z, Zhu Y, Sun Y, Miao Y, et al. Cantharidin, a potent and selective PP2A inhibitor, induces an oxidative stress-independent growth inhibition of pancreatic cancer cells through G2/M cell-cycle arrest and apoptosis. *Cancer Sci*. (2010) 101:1226–33. doi: 10.1111/j.1349-7006.2010.01523.x
28. Moed BA, Shwayder TA, Chang MW. Cantharidin revisited. *Arch Dermatol*. (2001) 137:1357–60. doi: 10.1001/archderm.137.10.1357
29. Lu S, Gao Y, Huang X, Wang X. Cantharidin exerts anti-hepatocellular carcinoma by Mir-214 modulating macrophage polarization. *Int J Biol Sci*. (2014) 10:415–25. doi: 10.7150/ijbs.8002
30. Xu MD, Liu SL, Zheng BB, Wu J, Wu MY, Zhang Y, et al. The radiotherapy-sensitizing effect of cantharidin: mechanisms involving cell cycle regulation, enhanced DNA damage, and inhibited DNA damage repair. *Pancreatology*. (2018) 18:822–32. doi: 10.1016/j.pan.2018.08.007
31. Galvis CEP, Mendez LYV, Kouznetsov VV. Cantharidin-based small molecules as potential therapeutic targets. *Chem Biol Drug Des*. (2013) 82:477–99. doi: 10.1111/cbdd.12180
32. Salvesen GS. Caspases: opening the boxes and interpreting the arrows. *Cell Death Diff*. (2002) 9:3–5. doi: 10.1038/sj.cdd.4400963
33. Porter AG, Jänicke RU. Emerging roles of caspase-3 in apoptosis. *Cell Death Diff*. (1999) 6:99–104. doi: 10.1038/sj.cdd.4400476
34. Wu M, Lee H, Bellas RE, Schauer SL, Arsura M, Katz D, et al. Inhibition of NF-κB/Rel induces apoptosis of murine B cells. *EMBO J*. (1996) 15:4682–90. doi: 10.1002/j.1460-2075.1996.tb00845.x
35. Fan Y, Dutta J, Gupta N, Fan G, Gélinas C. Regulation of programmed cell death by NF-kappaB and its role in tumorigenesis and therapy. *Adv Exp Med Biol*. (2008) 615:223–50. doi: 10.1007/978-1-4020-6554-5_11
36. Finkin S, Pikarsky E. NF-κB in hepatoma: the plot thickens. *Curr Top Microbiol Immunol*. (2011) 349:185–96. doi: 10.1007/82_2010_104
37. Zeng Y. Study on the treatment of primary liver cancer with methyl scutella. *Chin J Integr Trad West Med*. (1985) 1985:121–421.
38. Gui Y, Cao X, Chen J. Experimental study of human hepatocellular carcinoma cells apoptosis induced with sodium cantharidate *in vitro*. *J Hubei Med Univ*. (2004) 25:493–6.

Conflict of Interest: The authors declare that the research was conducted in the absence of any commercial or financial relationships that could be construed as a potential conflict of interest.

frontiers in Oncology

ORIGINAL RESEARCH
published: 19 November 2019
doi: 10.3389/fonc.2019.01261

hsa_circ_0007841: A Novel Potential Biomarker and Drug Resistance for Multiple Myeloma

Meng Gao†, Chengyuan Li†, Han Xiao, Hang Dong, Siyi Jiang, Yunfeng Fu and Liying Gong**

The Third Xiangya Hospital of Central South University, Changsha, China

Purpose: Circular RNA (circRNA) is a key regulatory factor in the development and progression of human tumors. However, the working mechanism and clinical significance of most circRNAs remain unknown in human cancers, including multiple myeloma (MM).

Patients and Methods: This study employs high-throughput circRNA microarray with bioinformatics to identify differentially expressed circRNAs in patients with MM. The hsa_circ_0007841 expressions were observed in the MM tissues of 86 patients. Drug-resistant cell lines and pathological features were also detected. In addition, the relationship between hsa_circ_0007841 expressions in the MM tissues and the pathological features of patients with MM were evaluated and role of hsa_circ_0007841 as a potential biomarker and therapeutic target was assessed.

Results: The results show that in the MM cell lines and drug-resistant cell lines, hsa_circ_0007841 expression was significantly upregulated, which was closely associated with disease prognosis. Specifically, hsa_circ_0007841 upregulation was correlated with chromosomal aberrations such as gain 1q21, *t* (4:14) and mutations in ATR and IRF4 genes. This finding was corroborated in large samples. Finally, bioinformatics analysis showed that eight differentially expressed miRNAs and 10 candidate mRNAs interacted with hsa_circ_0007841, shedding some new light on the basic functional research.

Conclusion: This study may be the first to report that hsa_circ_0007841 is significantly upregulated in MM. It also suggests that hsa_circ_0007841 may be a novel biomarker for MM and its involvement in the progression of MM.

Keywords: circular RNAs, biomarker, diagnosis, prognosis, multiple myeloma

OPEN ACCESS

Edited by:
Pascale Cohen,
Université Claude Bernard Lyon 1, France

Reviewed by:
Mingli Liu,
Morehouse School of Medicine, United States
Qing Xu,
Tongji University, China
Fengxia Wu,
Capital Medical University, China

****Correspondence:***
Yunfeng Fu
fuyfeng427@163.com
Liying Gong
gongliying1987@163.com

†These authors have contributed equally to this work

Specialty section:
This article was submitted to Molecular and Cellular Oncology, a section of the journal Frontiers in Oncology

Received: *02 June 2019*
Accepted: *31 October 2019*
Published: *19 November 2019*

Citation:
Gao M, Li C, Xiao H, Dong H, Jiang S, Fu Y and Gong L (2019) hsa_circ_0007841: A Novel Potential Biomarker and Drug Resistance for Multiple Myeloma. Front. Oncol. 9:1261. doi: 10.3389/fonc.2019.01261

INTRODUCTION

Non-coding RNA (ncRNA) consists of long non-coding RNA (lncRNA), short microRNA (miRNA/miRs), and circular RNA (circRNA), the latter being the most common in the eukaryotic transcriptome. Unlike the conventional linear RNA (including 5′ and 3′ terminals), circRNA has a closed loop structure generated by back-splicing of RNA introns and/or exons. After the discovery of circRNA in viral RNAs in 1970 (1), it was later found in eukaryocytes (2). In recent years, high-throughput sequencing combined with transcriptome analysis has indicated the large abundance of circRNA in eukaryocytes (3).

Circular RNAs, repleted with miRNA binding sites, serve as sponge molecules for miRNAs and inhibit the binding of miRNAs to their target genes (4, 5). They bind competitively to miRNAs

through the sponging action, thereby abolishing the inhibitory effect on the transcription of downstream target genes (6). Besides sponging action, circRNAs can also regulate gene expressions in parents and influence gene transcription or even protein translation by interacting with the proteins. Moreover, circRNAs are large RNA molecules with closed loop structures. Most ncRNAs and circRNAs are involved in the regulation of transcription and posttranscriptional gene expression. They play important roles in cancer progression, metastasis, and therapeutic response (7). Given the specificity of circRNAs in the disease state and their stability in the body fluid, circRNAs may be used in the diagnosis of cancer (8, 9).

Multiple myeloma (MM) is a hematologic malignancy caused by an abnormal proliferation of bone marrow plasma cells. In the clinical setting, MM is the second most common hematologic malignancy and accounts for 10% of all hematologic malignancies. Its incidence rate reaches 2–3 per 100,000. The ratio of affected male to female patients is 1.6:1. The features of MM are diverse but include anemia, bone pain, renal insufficiency, infection, hemorrhage, neurological symptoms, hypercalcemia, and amyloidosis (10). The development of MM is usually accompanied by a series of genetic variations, such as cytogenetic abnormalities, primary or secondary chromosomal translocation, and some oncogenes activations (11). Identifying these alterations is highly valuable for understanding the pathogenesis of tumors and predicting prognosis and therapeutic response. Some genetic mutations are correlated with the poor outcome of MM, including chromosomal variations *t* (11:14), *t* (14:16), and *t* (14:20) (12). The identified mutations include CCND1 and DNA repair pathway-related genes (TP53, ATM, ATR, and ZFHX4) (13). In contrast, some mutations predict positive outcomes such as mutations in the IRF4 and EGR1 genes (14). Individualized therapy for MM based on biomarkers can increase therapeutic efficacy while reducing toxicity (15). Therefore, some biomarkers for MM can be used as predictive and prognostic indicators to guide diagnosis and treatment.

In the present study, the bioinformatics method was combined with high-throughput sequencing in small samples. By using the circRNA database, circRNAs that might influence the treatment and prognosis of patients with MM were preliminarily screened. Next, real-time quantitative polymerase chain reaction (qRT-PCR) was applied for sample amplification. It was found that hsa_circ_0007841 was significantly upregulated in patients with MM and MM cell lines. The correlation between hsa_circ_0007841 expressions and clinicopathological features of such patients with MM was determined. It was determined whether the hsa_circ_0007841 expression could be used as a diagnostic and prognostic indicator for MM. The results provide the basis for identifying novel prognostic markers and therapeutic targets for MM.

MATERIALS AND METHODS

Clinical Data

From January 2012 to January 2018, 86 MM patients and 30 IDA patients treated at the Third Xiangya Hospital of Central South University were included as the case group. Their bone marrow samples and clinical data were collected. There were 53 males and 33 females in the case group, and the median age of onset was 55 years (range, 44–78 years). The diagnosis, staging, and risk stratification of MM were performed according to the National Comprehensive Cancer Network (NCCN). All of the cases had complete clinical and pathological data (**Table S1**). Due to a lack of normal bone marrow donors, 30 patients with iron deficiency anemia (IDA) were chosen as controls, and their bone marrow samples were collected to avoid sample variation. The bone marrow samples were cryopreserved at −80°C. The collection of all samples was approved by the ethics committee of Xiangya third hospital (Approval number: 2016121), and the consent acquired was both written and informed consent.

The microarray data has been deposited in public, community-supported repositories (GEO, GSE133058).

Cell Culture

Normal human mononuclear cell line THP-1 and MM cell lines KM3, U266, and RPMI-8226 were provided by the basic laboratory of Central South University Xiangya School of Medicine. Drug-resistant cell lines KM3/BTZ, U266/BTZ, and RPMI-8226/BTZ were acquired by inducing tolerance through stepwise increase of drug concentrations. The cells were cultured in the 1,640 culture medium (HyClone, Logan, UT, USA) supplemented with 10% fetal bovine serum (ExCell Biology, Shanghai, China), 50 U/ml penicillin, and 50 g/ml streptomycin (HyClone). The cells were incubated in a 37°C, 5% CO_2 incubator and harvested in the log phase of growth.

RNA Extraction

Firstly, the bone marrow samples from 3 MM patients were sorted by magnetic activated cell sorting (MACS) using anti-CD138 MicroBeads (Miltenyi, Germany), and the plasma cells were enriched. According to the instruction manual of TRIzol reagent (Invitrogen, USA), total RNA extraction was performed from the enriched plasma cells and plasma cells in the normal human bone marrows. The extracted products were preserved at −80°C. The RNA concentration and activity were first detected by NanoDrop ND-1000 (NanoDrop, USA). Then RNA purity and integrity were detected by denaturing formaldehyde agarose gel electrophoresis.

High-Throughput Sequencing of circRNAs and Identification of Differentially Expressed circRNAs

Sample preparation and microarray hybridization were performed according to Arraystar's standard protocols. First, linear RNAs in the extracted total RNA were removed by using RNaseR (Epicentre, USA), and the circRNAs were enriched. Then, using random primers, the enriched circRNAs were amplified and transcribed into fluorescent cRNAs. Alignment and hybridization were performed between the labeled circRNAs and Arraystar Human circRNA Array V2 (8x15K, Arraystar), followed by washes with the cleaning solution kit (Agilent, USA). The microarrays were scanned with the Agilent Scanner G2505C. The microarray images were analyzed with Agilent Feature Extraction software (version 11.0.1.1). The quantiles

TABLE 1 | Primers designed for qRT-PCR validation of candidate circRNAs.

	Primer	Tm (°C)
β-actin (human)	F: 5′ GTGGCCGAGGACTTTGATTG 3′	60
	R: 5′ CCTGTAACAACGCATCTCATATT 3′	
hsa_circ_0010402	F: 5′ ACAAATCTGGCTCTGGCACC 3′	60
	R: 5′ GAGGTAGACAGATGAGACGCCA 3′	
hsa_circ_0004777	F: 5′ CTGGACTTCAACCGAAATTTGA 3′	60
	R: 5′ GCTCCTCATGGACATCCTTTG 3′	
hsa_circ_0007841	F: 5′ CTAACATCTGTGAAACCATCGT 3′	60
	R: 5′ TCATCACATACACGATAGACTGG 3′	
hsa_circ_0080212	F: 5′ CTACCTGAGCCAGTTCTCCTAA 3′	60
	R: 5′ GGGTTCCTCATCGGTGTAAT 3′	

were normalized and subsequent data processing was performed using limma package in R. Differentially expressed circRNAs were identified based on the fold change and *P* value. Significantly upregulated and downregulated genes were those with fold change > 2.0 and $P < 0.05$.

Verification of Quantitative RT-PCR

Sample RNA was reversely transcribed into cDNA using SuperScript III Reverse Transcriptase (Invitrogen, Grand Island, NY, USA). Real-time qRT-PCR (Arraystar) was implemented by using ViiA 7 Real-time PCR System (Applied Biosystems) and 2 × PCR Master Mix. Each mix (10 μL) contains 2 × Master Mix 5 μL, specific primer F 0.5 μL, specific primer R 0.5 μL, and 2 μL cDNA. The mix was added into each well of the 384-Well PCR Plate, which was then placed in the real-time PCR instrument for PCR reaction. The reaction conditions were as follows: incubation at 95°C for 10 min, then 40 cycles of 10 s at 95°C and 1 min at 60°C. GAPDH was used as internal reference and its expression was normalized. ΔCt value reflected the circRNA expression level. The expression levels of each target gene were calculated and normalized by that of the internal reference. The primers used for each target gene are shown in **Table 1**.

Functional Analysis of circRNA

The circRNA/microRNA interaction was predicted using Arraystar's home-made miRNA target prediction software based on miRanda and TargetScan. To establish circRNA-miRNA network, we searched MREs on circRNAs using the software, then selected the miRNAs according to seed match sequences. The graph of the circRNA/miRNA network was drawn with the help of Cytoscape 3.01 (16, 17). GO analysis was conducted using Kyoto Encyclopedia of Genes and Genomes GO analysis was also used to determine the biological functions of the adjacent protein-coding genes of the target circRNAs (18).

Statistical Analysis

SPSS 20.0 software was used for statistical analysis. The data were described as mean ± standard deviation. Mann-Whitney test was used for pair wise comparison, and Kruskal-Wallis *H*-test for multiple comparison. For the analysis of clinical data, Kaplan-Meier survival curve was plotted, and log-rank test was used for statistical hypothesis test. The correlation between circRNA expressions and chromosomal variation and genetic mutations was analyzed by the chi-squared test. $P < 0.05$ indicated significant difference.

RESULTS

Analysis of circRNA Profiles

To identify the differentially expressed circRNAs in MM patients, high-throughput circRNA microarray was applied to 3 MM patients and 3 IDA patients. Thousands of circRNAs were detected, including 4,727 upregulated circRNAs and 5,283 downregulated circRNAs (**Figure 1A**). There were 147 differentially expressed circRNAs (fold change > 2), including 131 upregulated and 16 downregulated circRNAs. The block diagram represents the normalized intensity of the two groups (**Figure 1B**), and the volcano plot indicates the differential expressions of circRNAs (**Figure 1C**).

hsa_circ_0007841 Was Upregulated in MM Cells

Four significantly upregulated circRNAs were then verified by qRT-PCR in 20 MM patients and 10 IDA patients. As shown in **Figure 2B**, the expression of hsa_circ_0007841 was upregulated to the highest degree. hsa_circ_0007841 is localized to chr3:127778944-127779504 and generated by back-splicing of exons 6 and 7 in the sec61a1 gene (**Figure 2A**). We further detected expressions of hsa_circ_0007841 in the bone marrow of 66 MM patients and 20 IDA patients (**Figure 2C**). The results showed that hsa_circ_0007841 may be a potential biomarker for MM. Moreover, hsa_circ_0007841 expression was also detected in THP-1 mononuclear cells, MM cell lines (KM3, U266, 8226), drug-resistant cell lines (KM3/BTZ, U266/BTZ, 8226/BTZ) (**Figure 2E**) and patients with MM with BTZ resistance (**Figure 2D**). hsa_circ_0007841 was selectively expressed in the MM cell lines but lowly expressed in the THP-1 mononuclear cells, and the difference was of statistical significance ($P < 0.05$). In bortezomib-resistant cell lines (KM3/BTZ, U266/BTZ), the expression of hsa_circ_0007841 was significantly higher than that in KM3 and U266 cells. And also significantly increased in patients with MM with bortezomib (BTZ) resistant ($N = 21$) than bortezomib (BTZ) sensitive ($N = 36$). The above results indicated that the upregulation of hsa_circ_0007841 may be involved in the bortezomib tolerance of MM patients.

Correlation Between hsa_circ_0007841 Expressions and Clinicopathological Parameters of MM Patients

According to the 2018 NCCN Guidelines, the correlation between hsa_circ_0007841 expressions and age, gender, type, staging, and risk stratification (IMWG) of MM patients was analyzed. The clinical correlation between hsa_circ_0007841 and MM was established. The results showed (**Table 2**) that hsa_circ_0007841 was correlated with typing ($P = 0.002$), cytogenetic mutation ($P = 0.025$), bone destruction ($P = 0.014$), R-ISS staging ($P < 0.001$), but not correlated with gender, age, percentage of plasma cells in the bone marrow and kidney injury.

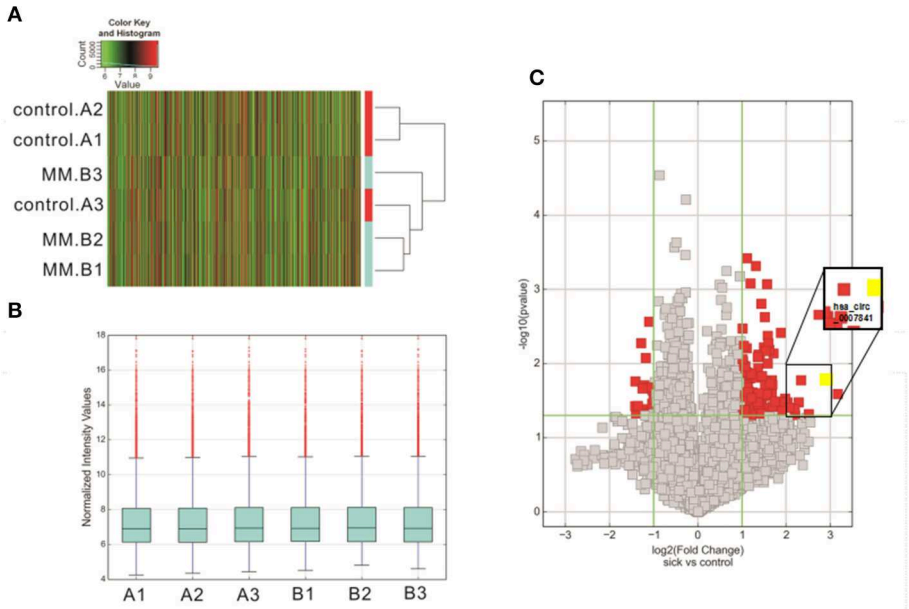

FIGURE 1 | Overview of the microarray signatures. **(A)** Cluster analysis diagram of differentially expressed circRNAs. **(B)** The block diagram represents the normalized intensity of the two groups. **(C)** Volcano plot showing the significantly deregulated genes in MM samples. MM, multiple myeloma.

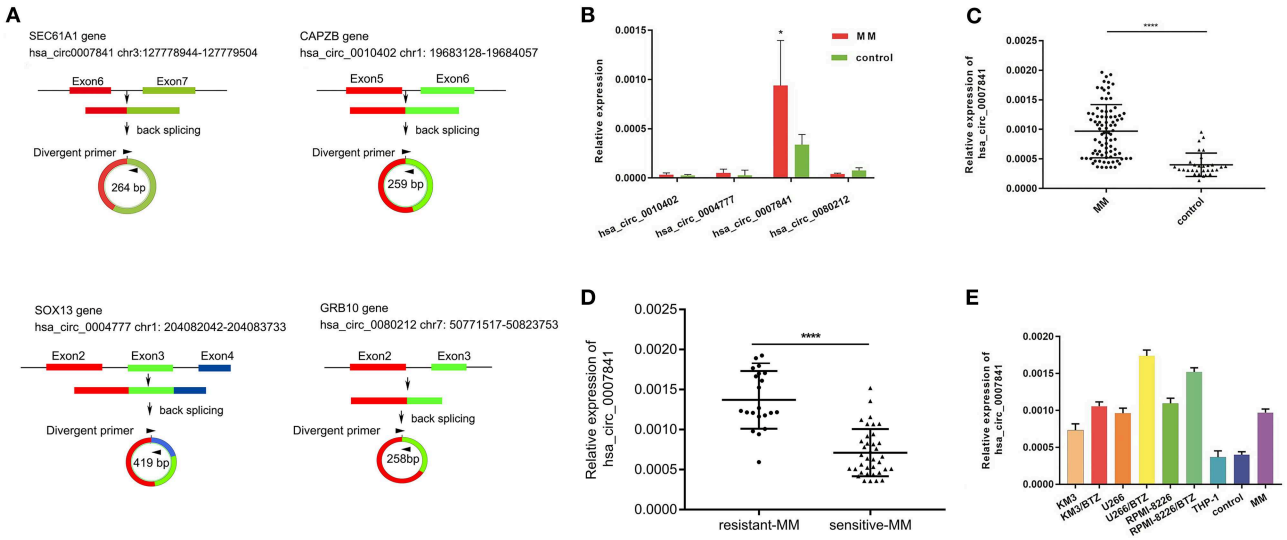

FIGURE 2 | Differentially expressed circRNAs. **(A)** Key circRNAs are circulated by exons. **(B)** qRT-PCR verification of four circRNAs in MM patients and controls. **(C)** Expression of hsa_circ_0007841 in the bone marrow of 86 MM patients and 30 controls. **(D)** Expression of hsa_circ_0007841 in bortezomib (BTZ) sensitive ($N = 36$) and bortezomib (BTZ) resistant ($N = 21$) patients. **(E)** Expression of hsa_circ_0007841 in MM patients, cell lines, and controls. MM, multiple myeloma; qRT-PCR, Real-time quantitative polymerase chain reaction. $^{*}P < 0.05$, $^{****}P < 0.01$.

The Role of hsa_circ_0007841 in the Diagnosis of MM

ROC curves can reflect the specificity and sensitivity of continuous variables comprehensively. ROC curves were plotted for the MM group and control group to assess the diagnostic potential of hsa_circ_0007841 in MM patients (**Figure 3A**). The sensitivity and specificity of hsa_circ_0007841 were verified by this method, and the AUC value was calculated as 0.907 (95% CI 0.8476–0.9663). Therefore, hsa_circ_0007841 may be used as a diagnostic marker for MM.

Prognostic Value of hsa_circ_0007841 in MM

The survival curve was constructed to analyze the correlation between hsa_circ_0007841 and the prognosis of MM patients (**Figure 3B**). All 86 patients adhered to the follow-ups. Using

TABLE 2 | Correlations between the relative expression of hsa_circ_0007841 and clinicopathologic features in 86 MM patients.

Clinicopathologic features	Cases	hsa_circ_000784 relative expression $(x \pm s) \times 10^{-4}$	*P*-value
Age (year)			0.524
<60	48	9.895 ± 4.713	
≥60	38	9.453 ± 4.259	
Sex			0.289
M	53	10.118 ± 4.615	
F	33	9.060 ± 4.300	
Isotype			0.002*
IgG	43	9.995 ± 4.763	
IgA	22	11.972 ± 4.047	
Light chain	12	7.147 ± 2.801	
Unclassified	9	6.144 ± 1.840	
Cytogenetic abnormality			0.025*
Yes	57	10.428 ± 4.520	
No	29	8.269 ± 4.166	
Percentage of myeloma cells in BM			0.655
≥40%	29	9.521 ± 4.460	
<40%	57	10.052 ± 4.630	
Bone lesion			0.014*
Yes	79	10.043 ± 4.516	
No	7	5.826 ± 1.553	
Renal inadequacy			0.583
Yes	19	5.582 ± 4.564	
No	67	10.113 ± 4.348	
Revised International Staging System			0.000*
Stage 1	10	5.569 ± 1.457	
Stage 2	37	8.087 ± 3.719	
Stage 3	39	12.290 ± 4.211	

*MM, multiple myeloma; SD, standard deviation; *P < 0.05.*

the median hsa_circ_0007841 expression in the bone marrow of MM patients as threshold, all 86 patients were divided into low and high hsa_circ_0007841 expression groups. The prognostic value of hsa_circ_0007841 in MM patients was assessed based on progression-free survival (PFS). The survival analysis showed that the upregulation of hsa_circ_0007841 was significantly correlated with poor prognosis of MM patients (log-rank $P = 0.0206$).

Prognostic biomarkers can be used to predict the possibility of recurrence and patient survival. As the prognosis of MM patients is closely related to genetic mutations, the correlation between hsa_circ_0007841 expressions in bone marrow and cytogenetic mutation was analyzed. It was found that the upregulation of hsa_circ_0007841 was correlated with chromosomal variations gain 1q21 ($P = 0.039$) and *t* (4;14) ($P = 0.025$) and mutations in ATR and IRF4 genes, but not correlated with del (17p) or mutations in TP53 (**Table 3**).

Prediction and Annotation of Target miRNA and mRNA Networks of hsa_circ_0007841

miRNA target prediction software TargetScan and miRanda from Arraystar was used to predict the circRNA—miRNA—mRNA network. The miRNAs and candidate mRNAs binding to hsa_circ_220 were identified. The circRNA-miRNA interaction network was predicted on the CircInteractome database (**Figure 4A**). A total of 8 differentially expressed miRNAs and 10 candidate mRNAs were predicted to interact with hsa_circ_0007841. As shown in **Figure 4B**, the predicted mRNAs might be involved in multiple pathways. Therefore, it was necessary to further investigate the role of hsa_circ_0007841 in the progression of MM.

DISCUSSION

The incidence of MM has been rising yearly due, in part, to the aging population. Although new therapies have greatly improved the prognosis of MM, it remains incurable. One of the major contributing factors to this is the high heterogeneity of MM cells that leads to disease recurrence and drug resistance in patients (19). Individualized therapy based on biomarkers can maximize the efficacy and reduce disease recurrence as well as drug resistance. Some of the biomarkers already identified for MM may be useful in the selection of the most suitable therapy to alter the clinical outcome (20).

circRNA is the sponge molecule for miRNA that indirectly regulates the expression of miRNA target genes; thus, playing an important role in the onset and development of human diseases. As biomarkers, circRNAs are now widely used for disease diagnosis. Recently, circRNAs have received an increasing amount of attention in the biomedical literature. Vo et al. analyzed over 2,000 human tumor specimens derived from different tissues by exome capture and studied the circRNA profiles (21). Boutros and He systematically analyzed the expression characteristics of circRNAs in localized prostate cancer and designed the shRNA library for high-throughput sequencing. They reported that circCSNK1G3 competitively bind to miR-181b/d and exhibit fundamental function on four prostate cancer cells (22). Shen et al. reported the upregulation of circFAT1, formed by exon 2 in the FAT1 gene, in human osteosarcoma (OS). Their study demonstrated the oncogenicity of circFAT1 in OS and its potential value as a therapeutic target in OS (23). In addition, specifically expressed circRNAs have been identified in hepatocellular carcinoma (24), colorectal cancer (25), and lung cancer (26). These observations suggest the idea that circRNAs may be used as potential diagnostic and prognostic biomarkers. However, the clinical value of circRNAs in MM remains unclear.

We screen carefully the key circRNA based on the following considerations: (1) the significant difference in FC (fold change) value will be considered priority; (2) each sample has the original signal value, the tendency to select the original signal value is relatively large, and the average within the group is stable; (3) small *P* value and combined with the original signal value average within the group; (4) the appropriate length is

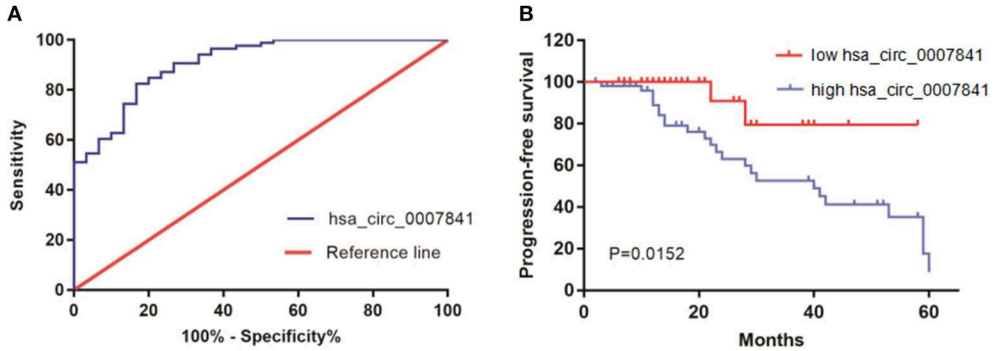

FIGURE 3 | The role of hsa_circ_0007841. **(A)** ROC curve for hsa_circ_0007841. **(B)** Kaplan-Meier survival curve for low and high expression of hsa_circ_0007841 in MM patients. MM, multiple myeloma; ROC curve, receiver operating characteristic curve.

TABLE 3 | Cytogenetic aberration status distribution between low/high hsa_circ_0007841 expression groups of MM patients.

Group	Low hsa_circ_0007841	High hsa_circ_0007841	*P*-value
	del (17p)		0.721
Positive	30.2% (4/32)	53.5% (5/54)	
Negative	69.8% (28/32)	46.5% (49/54)	
	gain 1q21		0.039*
Positive	34.4% (11/32)	57.4% (31/54)	
Negative	65.6% (21/32)	32.6% (23/54)	
	t (4;14)		0.025*
Positive	6.3% (2/32)	25.9% (14/54)	
Negative	93.7% (30/32)	74.1% (40/54)	
	TP53 variants		0.147
Positive	41.9% (1/32)	32.6% (8/54)	
Negative	58.1% (31/32)	67.4% (46/54)	
	ATR abnormalities		0.048*
Positive	3.1% (1/32)	18.5% (10/54)	
Negative	96.9% (31/32)	81.5% (44/54)	
	IRF4 variants		0.042*
Positive	6.3% (2/32)	24.1% (13/54)	
Negative	93.7% (30/32)	75.9% (41/54)	

*MM, multiple myeloma; *P < 0.05.*

recommended within 200–2,500 bp, in order to facilitate the later functional test; (5) try to choose the exonic type. In the present study, high-throughput sequencing was used to identify differentially expressed circRNAs in the bone marrow tissues of patients with MM. Several circRNAs were found to be upregulated, four significantly upregulated circRNAs were then verified by qRT-PCR in small clinical sample and MM cell lines, include hsa_circ_0010402, hsa_circ_0004777, hsa_circ_0080212, hsa_circ_0007841, and the hsa_circ_0007841 expression showed the most significant increase. This result was later verified by qRT-PCR in large samples ($n = 86$). To the best of our knowledge, this finding is the first confirmation of the expression, diagnostic, and prognostic value of hsa_circ_0007841 in MM. By combining these parameters with the clinicopathological indicators of patients with MM, we found a significant difference in hsa_circ_0007841 expressions among patients with different typing and staging. We further analyzed disease progression during the survival period between 1 and 4 years. We found that hsa_circ_0007841 overexpression was correlated with poor prognosis in patients with MM. Moreover, since the circ-miRNA axis has a considerable impact on the onset and development of human diseases, it has been speculated that hsa_circ_0007841 might influence the occurrence of MM by mediating the expression of oncogenes through its miRNA target. Annotation and functional prediction have shown that hsa_circ_0007841 interacted with eight miRNAs and 10 target mRNAs. Among these, hsa_circ_0007841 is the sponge molecule of hsa-miR-29b-2-5p. Rossi et al. found that miR29b overexpression inhibited osteoclast differentiation and reversed the MM cells-triggered osteoclast activation, which delayed the progression of MM. Furthermore, miR-29b caused the apoptosis of the BTZ-induced MM cells through activation of the feedback loop of transcription factor Sp1 (27). In the present study, hsa_circ_0007841 overexpression was found to be correlated with osteolytic bone destruction in MM and it was overexpressed in BTZ-resistance cell lines in MM. These results agree with previous studies, further showing the close connection between hsa_circ_0007841 and its diagnostic and prognostic value in patients with MM.

Drug resistance is the one that causes the most trouble during the therapy of MM in clinic settings and need urgent solution (28, 29). In our study, hsa_circ_0007841 expression was also detected in drug-resistant cell lines (KM3/BTZ, U266/BTZ, 8226/BTZ) and MM patients. hsa_circ_0007841 also is the sponge molecule of hsa-miR-199a-3p. Fornari et al. found that miR-199a-3p regulated mTOR and c-Met to influence the doxorubicin sensitivity of human hepatocarcinoma cells (30). Lei et al. found that miR-199a-3p affected the multi-chemoresistance of osteosarcoma through targeting AK4 (31). Although, a large biological signal pathways of circRNAs involved in drug resistance are still unknown. More mechanisms and functions of chemoresistance-related circRNAs need to be further mined for advance of MM therapy, which may offer new approaches to reverse drug resistance.

Prognostic biomarkers can be used to assess the probability of disease recurrence and the prediction of clinical outcomes. Since prognostic indicators are not formulated by considering

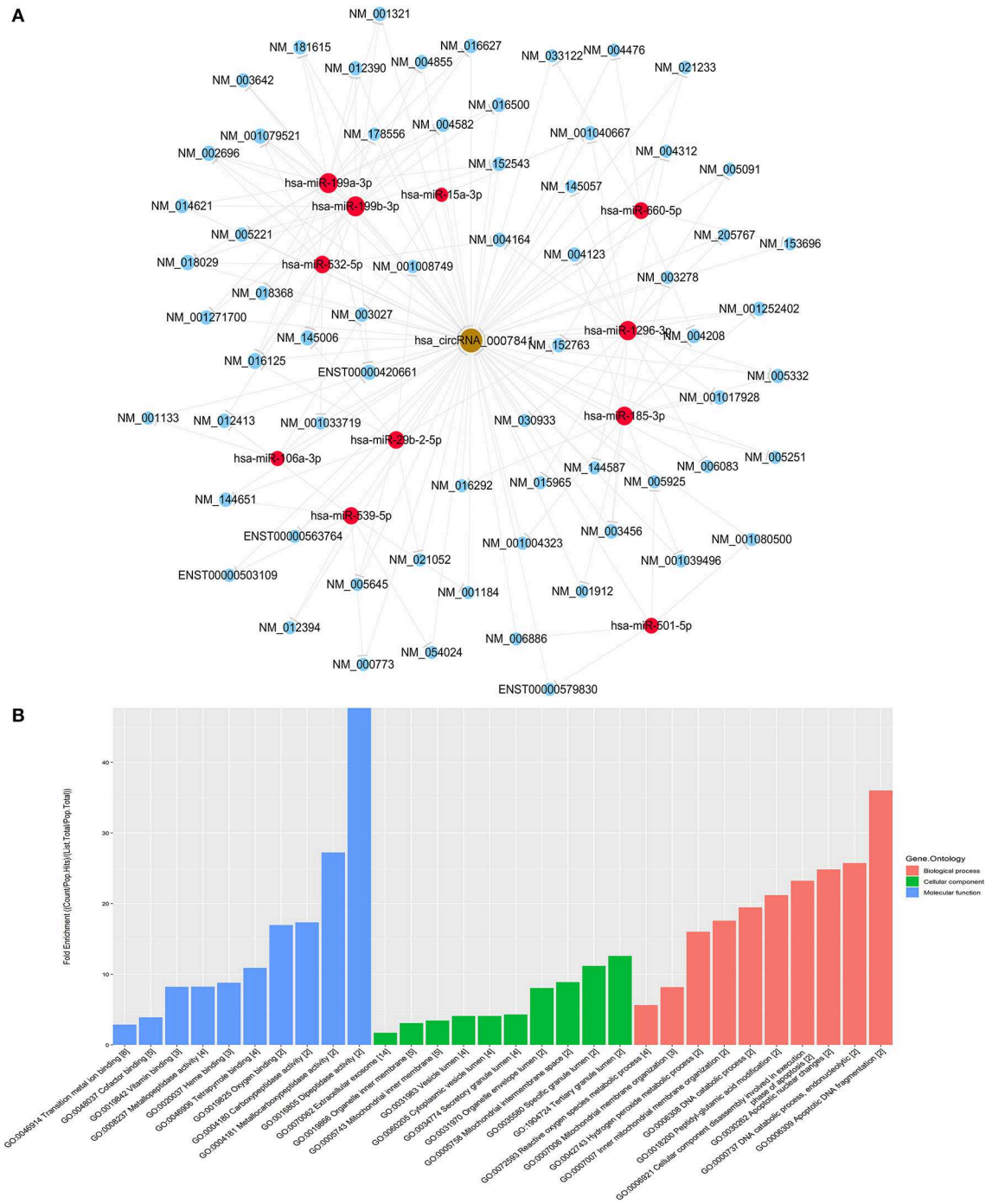

FIGURE 4 | Functional analysis of circRNA. **(A)** hsa_circ_0007841-miRNA-mRNA co-expression network established using hsa_circ_0007841. **(B)** The GeneOntology_Fold Enrichment.

the factor of treatment, they can be used to guide individualized therapy. It has been shown that some genetic mutations are closely related to the poor outcome of MM, including chromosomal alterations *t* (4; 14), *t* (14; 16), and *t* (14; 20). Due to chromosomal translocation, oncogenes such as MMSET/FGFR3, CCND3, CCND1, MAF, and MAFB are still regulated by the IgH gene enhancer and their expressions increase (11, 32). As a result, the cyclin D family members are upregulated, leading to the dysregulation of the G1/S checkpoint. In the present study, hsa_circ_0007841 was closely related to chromosomal variations and genetic mutations in patients with MM. However, the present study is a single-center small-sample-size experiment, from which the results had limitations in guiding clinical treatment. In the future, the sample size should be enlarged.

Further detection of its expression changes at different stages of disease progression is needed. Cell and animal experiments are needed to further explore its biological functions. Based on this fact, hsa_circ_0007841 may be used to predict the prognosis, recurrence, and drug resistance in patients with MM.

This study has evaluated the diagnostic and prognostic value of hsa_circ_0007841 as a circRNA in MM and the results provide the basis for preclinical research. Currently, the factors of age and complications are mainly considered for individualized therapy of MM, However, to further improve treatment outcome, molecular information will be needed to guide treatment. The endogenous competitive mechanism of circRNAs provides the theoretical basis for research on the replacement of antinucleotide chemotherapy. However, studies on circRNAs are still at the preliminary stage and very little has been hitherto understood about their functions and working mechanisms. But there is a high potential for clinical translational research with the advancement of research and development of RNA-targeted drugs based on circRNAs.

DATA AVAILABILITY STATEMENT

This manuscript contains previously unpublished data. The name of the repository and accession number(s) are not available.

ETHICS STATEMENT

The studies involving human participants were reviewed and approved by 2016121. The patients/participants provided their written informed consent to participate in this study.

AUTHOR CONTRIBUTIONS

MG and CL designed and performed the study. HD and LG wrote the manuscript with inputs from all authors. YF and SJ performed the analytic calculations and statistical analysis. All authors provided critical feedback and helped to shape the research, analysis, and manuscript. We thank HX for her contribution to the collection of data.

FUNDING

This study was supported by Hunan Provincial Natural Science Foundation of China (Grant No. 2017JJ3463).

SUPPLEMENTARY MATERIAL

The Supplementary Material for this article can be found online at: https://www.frontiersin.org/articles/10.3389/fonc.2019.01261/full#supplementary-material

REFERENCES

1. Sanger HL, Klotz G, Riesner D, Gross HJ, Kleinschmidt AK. Viroids are single-stranded covalently closed circular RNA molecules existing as highly base-paired rod-like structures. *Proc Natl Acad Sci USA.* (1976) 73:3852–6. doi: 10.1073/pnas.73.11.3852
2. Chiou CS, Wu CM, Dubey NK, Lo WC, Tsai FC, Tung TDX, et al. Mechanistic insight into hyaluronic acid and platelet-rich plasma-mediated anti-inflammatory and anti-apoptotic activities in osteoarthritic mice. *Aging.* (2018) 10:4152–65. doi: 10.18632/aging.101713
3. Kristensen LS, Andersen MS, Stagsted LVW, Ebbesen KK, Hansen TB, Kjems J. The biogenesis, biology and characterization of circular RNAs. *Nat Rev Genet.* (2019) 20:675–91. doi: 10.1038/s41576-019-0158-7
4. Yu T, Wang Y, Fan Y, Fang N, Wang T, Xu T, et al. CircRNAs in cancer metabolism: a review. *J Hematol Oncol.* (2019) 12:90. doi: 10.1186/s13045-019-0776-8
5. Patop IL, Wüst S, Kadener S. Past, present, and future of circRNAs. *EMBO J.* (2019) 38:e100836. doi: 10.15252/embj.2018100836
6. Zheng Q, Bao C, Guo W, Li S, Chen J, Chen B, et al. Circular RNA profiling reveals an abundant circHIPK3 that regulates cell growth by sponging multiple miRNAs. *Nat Commun.* (2016) 7:11215. doi: 10.1038/ncomms11215
7. Kristensen LS, Hansen TB, Venø MT, Kjems J. Circular RNAs in cancer: opportunities and challenges in the field. *Oncogene.* (2018) 37:555–65. doi: 10.1038/onc.2017.361
8. Arnaiz E, Sole C, Manterola L, Iparraguirre L, Otaegui D, Lawrie CH. CircRNAs and cancer: biomarkers and master regulators. *Semin Cancer Biol.* (2018) 58:90–9. doi: 10.1016/j.semcancer.2018.12.002
9. Han B, Chao J, Yao H. Circular RNA and its mechanisms in disease: from the bench to the clinic. *Pharmacol Ther.* (2018) 187:31–44. doi: 10.1016/j.pharmthera.2018.01.010
10. Rajkumar SV. Multiple myeloma: 2016 update on diagnosis, risk-stratification, and management. *Am J Hematol.* (2016) 91:719–34. doi: 10.1002/ajh.24402
11. Shah V, Sherborne AL, Walker BA, Johnson DC, Boyle EM, Ellis S, et al. Prediction of outcome in newly diagnosed myeloma: a meta-analysis of the molecular profiles of 1905 trial patients. *Leukemia.* (2018) 32:102–10. doi: 10.1038/leu.2017.179
12. Lakshman A, Alhaj Moustafa M, Rajkumar SV, Dispenzieri A, Gertz MA, Buadi FK, et al. Natural history of t(11;14) multiple myeloma. *Leukemia.* (2018) 32:131–8. doi: 10.1038/leu.2017.204
13. Walker BA, Boyle EM, Wardell CP, Murison A, Begum DB, Dahir NM, et al. Mutational spectrum, copy number changes, and outcome: results of a sequencing study of patients with newly diagnosed myeloma. *J Clin Oncol.* (2015) 33:3911–20. doi: 10.1200/JCO.2014.59.1503
14. Ohguchi H, Hideshima T, Bhasin MK, Gorgun GT, Santo L, Cea M, et al. The KDM3A-KLF2-IRF4 axis maintains myeloma cell survival. *Nat Commun.* (2016) 7:10258. doi: 10.1038/ncomms10258
15. Chim CS, Kumar SK, Orlowski RZ, Cook G, Richardson PG, Gertz MA, et al. Management of relapsed and refractory multiple myeloma: novel agents, antibodies, immunotherapies and beyond. *Leukemia.* (2018) 32:252–62. doi: 10.1038/leu.2017.329
16. Pasquinelli AE. MicroRNAs and their targets: recognition, regulation and an emerging reciprocal relationship. *Nat Rev Genet.* (2012) 13:271–82. doi: 10.1038/nrg3162
17. Enright AJ, John B, Gaul U, Tuschl T, Sander C, Marks DS. MicroRNA targets in Drosophila. *Genome Biol.* (2003) 5:R1. doi: 10.1186/gb-2003-5-1-r1
18. Zhao Z, Bai J, Wu A, Wang Y, Zhang J, Wang Z, et al. Co-LncRNA: investigating the lncRNA combinatorial effects in GO annotations and KEGG pathways based on human RNA-Seq data. *Database.* (2015) 2015:bav082. doi: 10.1093/database/bav082
19. Robak P, Drozdz I, Szemraj J, Robak T. Drug resistance in multiple myeloma. *Cancer Treat Rev.* (2018) 70:199–208. doi: 10.1016/j.ctrv.2018.09.001
20. Landgren O, Morgan GJ. Biologic frontiers in multiple myeloma: from biomarker identification to clinical practice. *Clin Cancer Res.* (2014) 20:804–13. doi: 10.1158/1078-0432.CCR-13-2159
21. Vo JN, Cieslik M, Zhang Y, Shukla S, Xiao L, Zhang Y, et al. The landscape of circular RNA in cancer. *Cell.* (2019) 176:869–81.e13. doi: 10.1016/j.cell.2018.12.021

22. Chen S, Huang V, Xu X, Livingstone J, Soares F, Jeon J, et al. Widespread and functional RNA circularization in localized prostate cancer. *Cell.* (2019) 176:831–43.e22. doi: 10.1016/j.cell.2019.01.025
23. Liu G, Huang K, Jie Z, Wu Y, Chen J, Chen Z, et al. CircFAT1 sponges miR-375 to promote the expression of Yes-associated protein 1 in osteosarcoma cells. *Mol Cancer.* (2018) 17:170. doi: 10.1186/s12943-018-0917-7
24. Chen D, Zhang C, Lin J, Song X, Wang H. Screening differential circular RNA expression profiles reveal that hsa_circ_0128298 is a biomarker in the diagnosis and prognosis of hepatocellular carcinoma. *Cancer Manag Res.* (2018) 10:1275–83. doi: 10.2147/CMAR.S166740
25. Li J, Ni S, Zhou C, Ye M. The expression profile and clinical application potential of hsa_circ_0000711 in colorectal cancer. *Cancer Manag Res.* (2018) 10:2777–84. doi: 10.2147/CMAR.S172388
26. Tian X, Zhang L, Jiao Y, Chen J, Shan Y, Yang W. CircABCB10 promotes nonsmall cell lung cancer cell proliferation and migration by regulating the miR-1252/FOXR2 axis. *J Cell Biochem.* (2019) 120:3765–72. doi: 10.1002/jcb.27657
27. Amodio N, Di Martino MT, Foresta U, Leone E, Lionetti M, Leotta M, et al. miR-29b sensitizes multiple myeloma cells to bortezomib-induced apoptosis through the activation of a feedback loop with the transcription factor Sp1. *Cell Death Dis.* (2012) 3:e436. doi: 10.1038/cddis.2012.175
28. Harding T, Baughn L, Kumar S, Van Ness B. The future of myeloma precision medicine: integrating the compendium of known drug resistance mechanisms with emerging tumor profiling technologies. *Leukemia.* (2019) 33:863–83. doi: 10.1038/s41375-018-0362-z
29. Uckun FM, Qazi S, Demirer T, Champlin RE. Contemporary patient-tailored treatment strategies against high risk and relapsed or refractory multiple myeloma. *EBioMedicine.* (2019) 39:612–20. doi: 10.1016/j.ebiom.2018.12.004
30. Fornari F, Milazzo M, Chieco P, Negrini M, Calin GA, Grazi GL, et al. MiR-199a-3p regulates mTOR and c-Met to influence the doxorubicin sensitivity of human hepatocarcinoma cells. *Cancer Res.* (2010) 70:5184–93. doi: 10.1158/0008-5472.CAN-10-0145
31. Lei W, Yan C, Ya J, Yong D, Yujun B, Kai L. MiR-199a-3p affects the multi-chemoresistance of osteosarcoma through targeting AK4. *BMC Cancer.* (2018) 18:631. doi: 10.1186/s12885-018-4460-0
32. Murase T, Ri M, Narita T, Fujii K, Masaki A, Iida S, et al. Immunohistochemistry for identification of CCND1, NSD2, and MAF gene rearrangements in plasma cell myeloma. *Cancer Sci.* (2019) 110:2600–6. doi: 10.1111/cas.14109

Conflict of Interest: The authors declare that the research was conducted in the absence of any commercial or financial relationships that could be construed as a potential conflict of interest.

frontiers in Oncology

ORIGINAL RESEARCH
published: 19 November 2019
doi: 10.3389/fonc.2019.01149

Canmei Formula Reduces Colitis-Associated Colorectal Carcinogenesis in Mice by Modulating the Composition of Gut Microbiota

Huayue Zhang[1†], Dengcheng Hui[2†], Yuan Li[1], Guangsu Xiong[3] and Xiaoling Fu[1*]*

[1] Department of Medical Oncology, Yueyang Hospital of Integrated Traditional Chinese and Western Medicine, Shanghai University of Traditional Chinese Medicine, Shanghai, China, [2] Department of Cirrhosis, Shuguang Hospital, Shanghai University of Traditional Chinese Medicine, Shanghai, China, [3] Endoscopic Center, Yueyang Hospital of Integrated Traditional Chinese and Western Medicine, Shanghai University of Traditional Chinese Medicine, Shanghai, China

OPEN ACCESS

Edited by:
Dong-Hua Yang,
St. John's University, United States

Reviewed by:
Jianfeng Cai,
University of South Florida,
United States
Guoxiang Cai,
Fudan University Shanghai Cancer
Center, China

***Correspondence:**
Xiaoling Fu
fuxiaoling111@163.com
Guangsu Xiong
xiongguangsu@
shyueyanghospital.com

[†] These authors have contributed
equally to this work

Specialty section:
This article was submitted to
Molecular and Cellular Oncology,
a section of the journal
Frontiers in Oncology

Received: 09 August 2019
Accepted: 16 October 2019
Published: 19 November 2019

Citation:
Zhang H, Hui D, Li Y, Xiong G and
Fu X (2019) Canmei Formula Reduces
Colitis-Associated Colorectal
Carcinogenesis in Mice by Modulating
the Composition of Gut Microbiota.
Front. Oncol. 9:1149.
doi: 10.3389/fonc.2019.01149

The gut microbiota, including pathogenic microorganisms and probiotics, has been involved in tumor initiation and progression by regulating the components of intestinal flora. Canmei formula (CMF), a traditional Chinese medicine, chronicled in the Chuang Yang Jing Yan Quan Shu, has been clinically used as an adjuvant therapy to treat patients with colorectal carcinoma (CRC) in China. In this study, we investigate the treatment effect of CMF in the azoxymethane (AOM) and dextran sodium sulfate (DSS) induced and high-fat diet augmented colitis-associated colorectal cancer *in vivo*, and explore its mechanism of action. We found that CMF treatment relieved the inflammation and alteration of the gut microbiota and significantly inhibited the development of intestinal adenoma. Linear discriminant analysis showed that the flora diversity in the normal mice, model mice and CMF treatment mice was different. At the family level, the relative abundance of Desulfovibrionaceae decreased in CMF groups. The relative abundance of Desulfovibrionaceae were lower in the CMF groups than in model group, whereas Rikenellaceae and Alistipes were increased. Altogether our results indicate that CMF treatment ameliorate colitis-associated colorectal carcinogenesis by modulating the composition of the gut microbiota *in vivo*.

Keywords: Canmei formula (CMF), traditional Chinese medicine, gut microbiota, AOM/DSS, colorectal carcinogenesis

INTRODUCTION

Colorectal carcinoma (CRC) is the second leading cause of cancer-related death worldwide (1). There are about 1.4 million new CRC patients and 700,000 deaths each year (2). Colorectal adenoma (CRA) refers to any lesion that originates from the surface of colorectal mucosa and protrudes into the intestinal cavity. It is a precancerous lesion of CRC and has the characteristics of high recurrence and high incidence of cancerous change (3). Microscopic removal is currently the main treatment for CRA, which can effectively reduce the incidence of CRC and reduce mortality

by 67% (4). However, microscopic resection did not reduce the recurrence rate of CRA. Aspirin, celecoxib, and cyclooxygenase-2 inhibitors are used clinically to treat inflammatory bowel disease, but the efficacy is limited according to the large sample clinical data (5). To date, there is no therapeutic agent specific for this disease. It is critical to explore drugs that can safely and effectively prevent and treat the recurrence of CRA.

In China, traditional Chinese medicine (TCM) has a long history dating back several thousands of years ago. Results from both pre-clinical laboratory and human studies have indicated that TCM has been widely used in anticancer therapy. Previous studies have indicated that PHY906, a modified formulation derived from Huang-Qin-Tang, could ameliorate chemotherapy-induced GI tract toxicity (6, 7). Qingjie Fuzheng granules (QFGs) has been proven to be able to inhibit proliferation and induce apoptosis of CRC cells (8). These studies indicate that TCM play important roles in cancer treatment and could be expected to become a promising therapeutic candidate for tumor.

Over the past decade, CRC have emerged as one of the most studied human conditions link to gut microbiota. Studies indicate that changes in the composition of gut microbiota, one of the most important internal environmental factors, are closely associated with the progression of CRC (9, 10). At present, the study on the secretion of toxin-activated inflammation by the intestinal flora is the most in-depth study of CRA carcinogenesis (3). The changes of intestinal flora are positively correlated with colorectal cancer. The secretion of toxins by the bacteria is a key factor for activating inflammation and oxidative stress pathways (11, 12). A number of studies have confirmed that *Enterococcus faecalis*, *Escherichia coli*, Enterotoxin-producing *Bacteroides fragilis* (ETBF), *Streptococcus bovis*, *Fusobacterium nucleatum*, and *Helicobacter pylori* are the main species that can induce cancer (3, 12, 13). Among them, *Fusarium nucleatum* induces uncontrolled intestinal epithelial cell growth by activating β-catenin; *E. coli* produces colibactin with genotoxicity (3).

Canmei formula (CMF), a classical traditional Chinese herbal formulation with Titanium and Marci Hieronymi, is widely used to treat colorectal diseases. The active constituents in CMF, including Citric acid, DL-TYROSINE, L(-)-Carnitine, L-Tyrosine, Ambrosic acid and others, have been reported (14, 15). However, there is no study on the effect of CMF in modulating gut microbiota. In our previous studies, 16sDNA sequencing technique was used to compare the change of gut microbiota induced by CMF treatment in AOM/DSS and high-fat diet-induced CRC mice (16, 17). This study provides evidence of the modulations of gut microbiota through CMF treatment, which will help understanding the host-microbe interactions during the treatment of CRC.

MATERIALS AND METHODS

Preparation of the Extracts for CMF

Mume Sieb and Marci Hieronymi were purchased from Yueyang Hospital of Integrated Traditional Chinese and Western Medicine, Shanghai University of Traditional Chinese Medicine. Mume Sieb was the fruit of *Prunus mume*. The Marci Hieronymi is a dry body of the larvae of the camphor family, *Bombyx mori* linnaeus, 4 ∼ 5 years old, infected with *Beauveria bassiana*. They were formally identified by the department of pharmacy, Yueyang Hospital of Integrated Traditional Chinese and Western Medicine, Shanghai University of Traditional Chinese Medicine, Shanghai, China.

CMF was formulated with Titanium and Marci Hieronymi in a ratio of 1:1. All the herbs were purchased from Yueyang hospital herbal pharmacy. Formulation was performed as described below. Briefly, 980 g mixture was extracted twice for 1.5 and 1 h for each time. The filtrates were concentrated in a vacuum at 60°C and dried to obtain the CMF extract powder of 335.2 g, the rate of the extract was 32.1%.The extract obtained in this part is CMF-L/H. The same process was repeated twice for the CMF extract. Then the liquid was poured through the column of the macroporous resin, and then the resin column was rinsed with pure water, 20% ethanol and 90% ethanol. After alcohol precipitation, the filtrateswere concentrated in a vacuum at 60°C and dried to obtain the CMF extract powder of 60.3 g, the rate of the purified product was 18%. The extract obtained in this part is used as CMF-A. The quality of preparations was controlled according to the guidelines from Chinese food and drug administration (CFDA).

Liquid Chromatograph and Mass Spectrometry

The solution obtained by the above preparation method was stored at 4°C. For HPLC analysis, the solution was centrifuged at 12,000 rpm for 10 min, then the supernatant was filtered through a 0.22 μm membrane before injection into the HPLC system. Analysis were performed by using Dionex UltiMate 3000 HPLC system (ThermoFisherScientific, USA) with a diode array detector. The C18 column (150 × 2.1 mm, 2.5 μm) was used with a flow rate of 0.3 ml·min^{-1}. The injection volume was 5 μl, and the column temperature was maintained at 40°C. The mobile phase was composed of (A) aqueous formic acid (0.1%, v/v) and (B) acetonitrile (0.1%, v/v) under following gradient elution: 95% A from 0 to 0.5 min, 95-2% A from 0.5 to 15 min, 2% A from 15 to 17 min, 2-95% A from 17 to 17.5 min, 95% A from 17.5 to 25 min. Mass spectrometry was performed on a Q Exactive high-resolution benchtop quadrupole Orbitrap mass spectrometer (Thermo Fisher Scientific, USA) using a heated electrospray ionization (HESI) source for ionization of the target compounds in positive and negative ion modes. The key parameters were as follows: ionization voltage, +3.5 kV/−3.2 Kv; sheath gas pressure, 40 arbitrary units; auxiliary gas, 10 arbitrary units; heat temperature, 350°C. For the compounds of interest, a scan range of m/z 120–1,500 was chosen. Resolution for higher energy collisional dissociation cell (HCD) spectra was set to 17,500 at m/z 120 on the QExactive.

Animal Experiments and Grouping

The animal procedures and care in this study was approved by the IRB of Yueyang Hospital of Integrated Traditional Chinese and Western Medicine, Shanghai University of Traditional Chinese Medicine. Seven-week-old female C57/BL6 mice were purchased from Shanghai Jihui Experimental Animal Breeding Co., Ltd. After arrival, the animals were quarantined for the

first 7 days. Under controlled conditions: humidity 50 + 10%, 12/12 h light/dark cycle, and temperature ∼23°C, all animals were housed in plastic cages (6 mice/cage)and provided with free drinking water and basic diet. AOM, the colonic carcinogen, was purchased from Sigma-Aldrich, USA. DSS with a molecular weight of 36,000–50,000 (No.216011080) was purchased from MPBIO Company, USA. For the induction of tumorigenesis, mice were injected with AOM (12 mg/kg body weight) intraperitoneally. Starting 5 day after the injection, animals received 2.5% DSS in the drinking water for 5 days. At the same time, the mice were given a high-fat diet. Then mice were given normal drinking water and normal diet for 2 weeks and subjected to two more DSS treatment cycles. Subsequently, mice were randomized into experimental and control groups. Group 1, NC, $n = 8$. Experimental groups included 5 groups: group 2: treatment with AOM and DSS (MC, $n = 8$); group 3: treatment with AOM, DSS, and Aspirin (Aspirin, $n = 8$); group 4: treatment with AOM, DSS, and CMF ethanol extract (CMF-A, $n = 8$); group 5: treatment with AOM, DSS, and CMF aqueous extract (CMF-L, $n = 8$); group 6: treatment with AOM, DSS, and CMF water extract high dose group(CMF-H, $n = 8$). Aspirin was given every day at the dose of 1.4 mg/kg/d. CMF-L and CMF-H were given at the doses of 3.65 and 7.3 g/kg/d, respectively. CMF-A was given at the doses of 0.657 g/kg/d. In the clinical practice of Chinese herbal medicine, the prescription dose of CMF is usually 60 g of herbal materials per day. When this human dose was converted into an animal dose (a person of 60 kg, and a conversion factor of 9.1 between human and mouse), it was equivalent to the low dose (3.65 g/kg/d) used in this study. All animals were sacrificed at the 18th week after the corresponding drug was administrated.

Colon Tissue Collection and Processing

After mice were sacrificed, the colorectal adenoma tissues were rapidly isolated, freed of adherent tissues and rinsed with phosphate buffer saline. Subsequently, tumor biopsy specimens of 1 cm-length were fixed with 4% paraformaldehyde for 24 h, embedded in paraffin and sectioned into 4-μm-thick slices. Slices were hydrated and stained with hematoxylin and eosin (H&E) followed by microscopic examination. Then portions of adenoma tissues were homogenized (10% W/V) in (20 mM Tris-HCI containing 1 mM EDTA, PH 7.4) by a glass homogenizer. The homogenates were centrifuged at 3,000 × g for 20 min at 4°C and supernatants were stored at −80°C.

Real Time Quantitative Reverse Transcription PCR

According to the modified methods as described, the RNA extracts of the colorectal tissues were prepared (8). By normalizing target mRNA *Ct* values to those for GAPDH (Ct), the relative amount of target mRNA was determined by the comparative threshold (Ct) method. The primer sequences used were as follows:

MUS-NF-κB-F (bp1297): (ATGCACCGTAACAGCAGGAC);
MUS-NF-κB-R (bp1405C): (TGTCATCCGTGCTTCCAGTG);
MUS-IL-17C-F (bp269) (AGGAGGTGCTGGAAGCTGAC);
MUS-IL-17C-R (bp391C) (TGCATCCACGACACAAGCAT);
GAPDH-F (5′-GTGAGGCCGGTGCTGAGTAT-3′);
GAPDH-R (5′-GTGCAGGATGCATTGCTGAC-3′);

ELISA Assay

Concentration of IL-17C in serum and NF-κB in supernatants of colonic tissues were quantified by IL-17C assay kit and NF-κB assay kit (Shanghai Pusheng Biological Technology Co., Ltd. China) according to manufacturer's instruction.

Fecal DNA Extraction and Illumina Miseq Sequencing

Genomic DNA was extracted from every stool sample using the FastDNA Spin Kit for Soil (MP Biomedical, LLC, catalog 116560-200) following the manufacturer's instructions.V3 and V4 region of the 16s rDNA sequencing was amplified by Primer F (5′-AAC GGGAAGACAACGTACGG-3′) and Primer R (5′-CAGATG CAGGAGGACATGTC-3′) with barcode sequence. Library was constructed following the manufacturer's instructions of the Ion Plus Fragment Library Kit and sequenced by Ion S5 Sequencer.

Bioinformatics Analysis

Reads was filtered and chimera sequence was removed.

The read pairs were de-multiplexed based on their unique molecular barcodes and overlapping reads were merged using USEARCH v7.0.1001 software. Operational taxonomic unit (OTU) picking was conducted using the QIIME (Quantitative Insights Into Microbial Ecology) software package. By using UCLUST, 16S rRNA gene sequences were clustered at a similarity cutoff value of 97%. By the SILVA reference database (https://www.arb-silva.de/download/), matching of OTUs to bacteria was conducted. By mapping the de-multiplexed reads to the identified OTUs, abundances were recovered. Alpha andbeta diversity plots were also generated using QIIME. The non-weighted UniFrac approach was used to measure the beta diversity between five bacterial cave communities. The relative abundance of transporter genes was predicted and performed by picrust analysis. Independent of the taxonomic analysis, aclosed-reference OTU picking protocol (QIIME) and the Greengenes database (http://greengenes.lbl.gov) were used to pre-cluster at 97% identity, and 97% of the OTUs were picked. The obtained OTU table was normalized by 16S rRNA copy number, and the functional genes were predicted according to the Kyoto Encyclopedia ofGenes and Genomes (KEGG) catalog. By using SPSS version 15.0 statistical software (IBM, Armonk, NY, USA), Fisher's test and the Mann-Whitney U testwere used to analyze, respectively, the gender distribution of subjects and intergroup differences at the genus level in each subcluster. The linear discriminant analysis (LDA) effectsize (LEfSe) method with default settings was used to analyze the differences among groups in phyla, class, order, family, and genera levels.

Statistical Analysis

SPSS software version 15.0 was used for statistical analysis. The data were presented as mean ± SD. Unpaired students' *t*-test was used to compare the means of the two groups. One-way

analysis of variance and Adonis were used to compare the means of more than two groups. A level of $P < 0.05$ was considered as statistically significant.

RESULTS

Identification of the Main Components in the Extract of CMF

To identify the components of Mume Sieb and Marci Hieronymi extract, Q Exactive high-performance benchtop quadrupole-Orbitrap LC-MS/MS was performed. The main components in the extract of CMF were identified according to the elemental composition data determined from accurate mass measurements and comparison with the literature data. Forty-one compounds were identified in the CMF extract and demonstrated in **Table 1**. In addition, to exclude the possibility of manufacturing problems relating to procession, extraction, handling, and storage, two batches of CMF were evaluated by HPLC. We found that the magnitude, number, and retention time of the peaks were similar between the two batches (**Figure 1**). These results confirmed the stability of the CMF extraction process.

TABLE 1 | Major chemical constituents identified in CMF.

No.	Name	RT (min)	Formula	Molecular weight	Area (max.)
1	DL-Arginine	1.28	C6 H14 N4 O2	174.1117	1300061.86
2	L(-)-Carnitine	1.37	C7 H15 N O3	161.10527	9750518.42
3	DL-Stachydrine	1.40	C7 H13 N O2	143.09471	1508022.19
4	Adenine	1.42	C5 H5 N5	135.05457	12469462.57
5	Guanine	1.43	C5 H5 N5 O	151.04946	7435505.89
6	Hypoxanthine	1.57	C5 H4 N4 O	136.03858	12616671.18
7	Nicotinic acid	1.58	C6 H5 N O2	123.03221	1086991.17
8	L-Tyrosine	1.64	C9 H11 N O3	181.07401	6502680.25
9	Adenosine	1.69	C10 H13 N5 O4	267.09676	26955456.82
10	Adenine	1.69	C5 H5 N5	135.05457	3750819.71
11	2-Hydroxycinnamic acid	1.72	C9 H8 O3	164.04745	37877896.83
12	Hypoxanthine	1.76	C5 H4 N4 O	136.03858	2774356.88
13	L-Norleucine	2.07	C6 H13 N O2	131.09474	55189905.01
14	Alanyltyrosine	2.81	C12 H16 N2 O4	230.12691	433071.84
15	Nornicotine	2.88	C9 H12 N2	148.10023	477190.87
16	2-Oxindole	3.52	C8 H7 N O	151.06347	420066.93
17	2′-Deoxyadenosine	3.54	C10 H13 N5 O3	251.10184	148660.32
18	Glycyl-L-leucine	4.17	C8 H16 N2 O3	188.11627	4092286.76
19	Chlorogenic acid	4.80	C16 H18 O9	354.09487	36388021.14
20	tert-Butyl N-[1-(aminocarbonyl)-3-methylbutyl]carbamate	5.41	C11 H22 N2 O3	230.16338	2831504.35
21	D-(+)-Tryptophan	5.45	C11 H12 N2 O2	204.08996	21112273.16
22	3,4-Dihydroxybenzaldehyde	5.90	C7 H6 O3	138.03188	196915.08
23	Leucylproline	5.94	C11 H20 N2 O3	228.14765	2951420.35
24	7-Hydroxycoumarine	6.51	C9 H6 O3	162.03159	3160911.99
25	6-Methylquinoline	6.93	C10 H9 N	143.07372	1669486.73
26	3-Phenylpropanoic acid	7.18	C9 H10 O2	150.06808	50678.13
27	3-O-feruloyl-D-quinic acid	7.63	C17 H20 O9	368.11073	285397.82
28	4-Coumaric acid	7.90	C9 H8 O3	164.04747	616864.76
29	Rutin	7.92	C27 H30 O16	610.15385	383860.64
30	N-Acetyl-L-leucine	7.95	C8 H15 N O3	173.10535	172744.27
31	Quercetin-3β-D-glucoside	8.13	C21 H20 O12	464.09641	532784.34
32	3,5-Dimethoxybenzoic acid	8.22	C9 H10 O4	182.05817	712514.01
33	Quercetin	8.52	C15 H10 O7	302.0428	150731.57
34	Kaempferol-7-O-glucoside	8.53	C21 H20 O11	448.10099	407020.68
35	(3R,4S)-4,6,8-Trihydroxy-7-methoxy-3-methyl-3,4-dihydro-1H-isochromen-1-one	8.89	C11 H12 O6	222.05297	117315.38
36	(2E)-3-(3,4-Dimethoxyphenyl)acrylic acid	9.07	C11 H12 O4	208.07356	2293865.83
37	Ambrosic acid	10.00	C15 H20 O4	264.13609	678788.38
38	Andrographolide	10.34	C20 H30 O5	350.20662	1261013.91
39	Ipratropium	11.70	C20 H29 N O3	331.21202	224430.08
40	Pinolenic acid	13.35	C18 H30 O2	278.22456	293978.53
41	α-Eleostearic acid	14.23	C18 H30 O2	278.22457	1744840.46

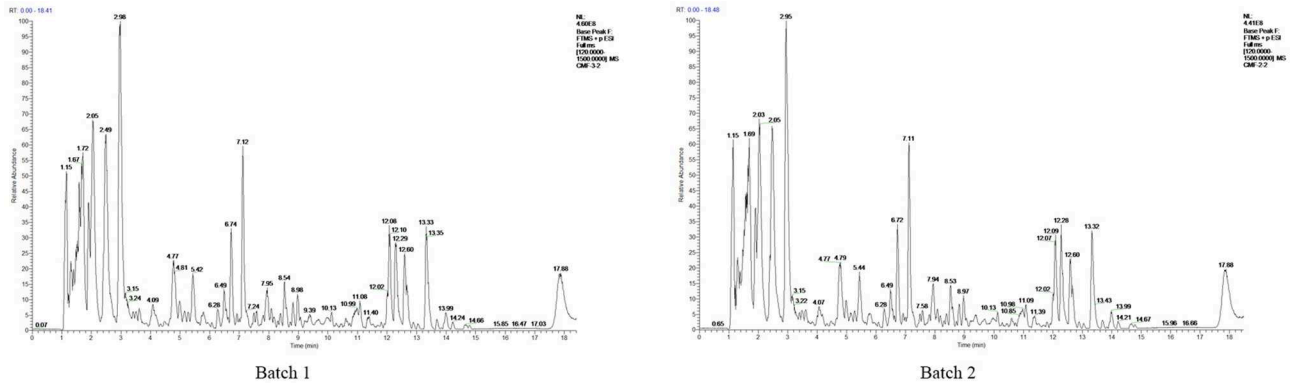

FIGURE 1 | HPLCprofile of two batches of CMF. The chemical fingerprint of CMF batch #1 and batch #2 was measured by HPLC analysis.

CMF Attenuated AOM/DSS-Induced Colitis-Associated Tumorigenesis

To evaluate the protective effect of CMF on the development of colitis-associated cancer, the well-established AOM/DSS and high-fat diet-induced colitis-associated colorectal tumor model in C57BL/6 mice were used (**Figure 2A**). Initially, the toxicity of CMF was tested *in vivo*. We did not find weight loss or behavioral changes in all mice. These results indicate that each of those extracts of CMF were well-tolerated (**Figure 2B**). AOM/DSS colorectal cancer mice were induced as described. All mice were treated with CMF once a day. After CMF treatment, tumor development and growth was inhibited in AOM/DSS colorectal cancer mice (**Figures 2C–F**). As a control, aspirin treatment effectively inhibited the occurrence of intestinal adenomas of 3 mm and above, but had no inhibitory effect on the occurrence of adenomas smaller than 3 mm (**Figure 2C**). Different extracts of CMF can significantly inhibit the growth of intestinal glands. **Figures 2D–F** shows that the ethanol extract of CMF significantly inhibited the occurrence of intestinal adenoma, and there is no difference in the occurrence of adenoma in the colon and small intestine. Histological examination revealed that mucosal inflammation, aberrant crypt foci adenoma, ulcer, or dysplasia in the colon tissues of the model group. Histological studies indicated that there was a large adenocarcinoma inside mucosa with several abnormal cells exhibiting cylindrical shape, large nuclei, increasing nuclear/cytoplasmic (N/C) ratio and cellular cleavagein AOM/DSS group (**Figure 2G**). CMF remarkably relieved the condition. These results suggest that CMF treatment inhibits inflammation-associated carcinogenesis in the AOM/DSS and high-fat diet mice.

CMF Treatment Repressed NF-κB and IL-17C Signaling in AOM/DSS Induced Mice

As NF-κB and IL-17C play important roles in the development of CRC, the mRNA expression of IL-17C and NF-κB collected from CRC mice were detected by Quantitative real-time PCR (**Figures 3A,B**). IL-17C was upregulated in the colorectal tissues of AOM/DSS mice. However, treatment with different extracts of CMF, including water extract and alcohol extract, effectively suppressed the mRNA expression of IL-17C. Drugs treatment, including aspirin, induced the mRNA expression of NF-κB. ELISA assay was performed to detect the protein expressions of inflammatory factors. As it is illustrated in **Figure 3C**, the protein levels of IL-17C in the serum of AOM/DSS-induced mice were significantly highest among mice with other drug intervention. The level of NF-κB significantly reduced in the tumor tissues of CMF-A, CMF-H, CMF-L, and Aspirin groups when compared to MC group (**Figure 3D**). All these results indicate that CMF treatment represses the expression of NF-κB and IL-17C.

CMF Treatment Regulated Gut Microbiota

To examine the effect of CMF on the regulation of components of gut microbiota, high-throughput pyrosequencing was performed with an Illumine MiSeq platform to generate 39584 high quality and valid sequences from 16 samples from different groups. We conducted a bar-coded pyrosequencing run to analyze the changes of gut microbiota in the five studied groups. In total, 39,584 available reads and 1461 OUTs were obtained. Shannon diversity and rarefaction curves are shown in **Figures 4A,B**. The rarefaction curves were consistent with the current sequencing, demonstrating that most of the flora diversity has been captured in all samples. What's more, the overlap of OUTs between groups revealed that 482 OUTs coexisted in both the MC group and CMF-A group, 496 OUTs coexisted in both the NC group and CMF-A group, 514 OUTs coexisted in both the NC group and MC group and 467 OUTs coexisted in both the MC group and Aspirin group (**Figures 4C,D**). In addition, we examined the flora community richness and diversity in mice. No statistical difference was observed for the ACE, Chao, Shannon, and Simpson indices among these groups (**Figures 4E–H**), although Simpson index were lower, but other indices are higher in NC group and the different CMF extract groups compared with MC group. Nonmetric multidimensional scaling (NMDS) analysis indicated the changes of overall structure of gut microbiota among different groups (**Figure 4I**). These results showed that the

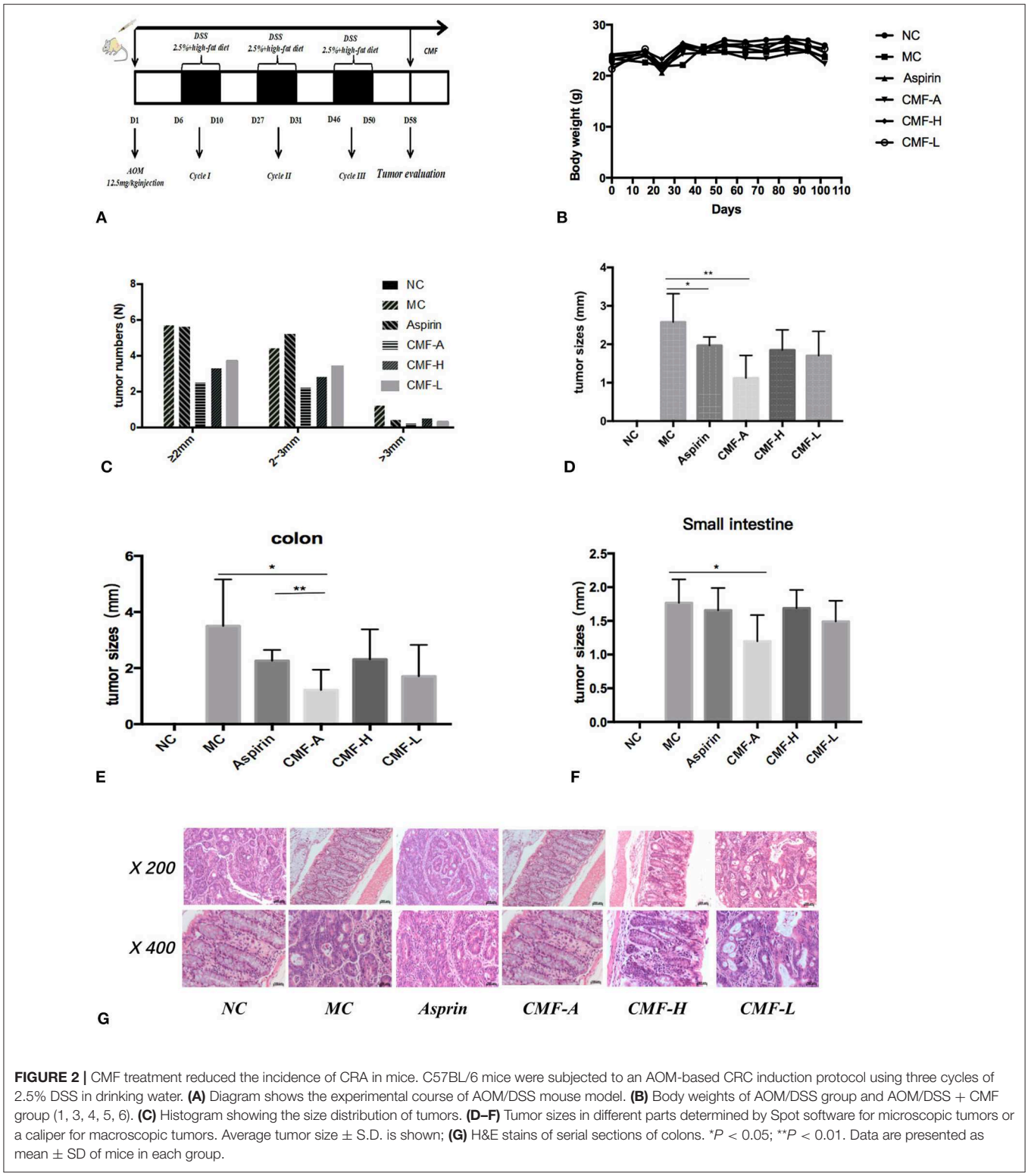

FIGURE 2 | CMF treatment reduced the incidence of CRA in mice. C57BL/6 mice were subjected to an AOM-based CRC induction protocol using three cycles of 2.5% DSS in drinking water. **(A)** Diagram shows the experimental course of AOM/DSS mouse model. **(B)** Body weights of AOM/DSS group and AOM/DSS + CMF group (1, 3, 4, 5, 6). **(C)** Histogram showing the size distribution of tumors. **(D–F)** Tumor sizes in different parts determined by Spot software for microscopic tumors or a caliper for macroscopic tumors. Average tumor size ± S.D. is shown; **(G)** H&E stains of serial sections of colons. $^{*}P < 0.05$; $^{**}P < 0.01$. Data are presented as mean ± SD of mice in each group.

diversity of bacterial population of the NC group was higher than that of the MC group. There was a statistical difference between the CMF-H group and the MC group. These results suggested that CMF treatment increases the diversity of the intestinal flora.

Analysis of the Relative Abundance of Microbiota at the Family Level and Genus Level

The family muribaculaceae, bacteroidales, and prevotellaceae were the most prevalent taxa in these groups (**Figure 5A**).

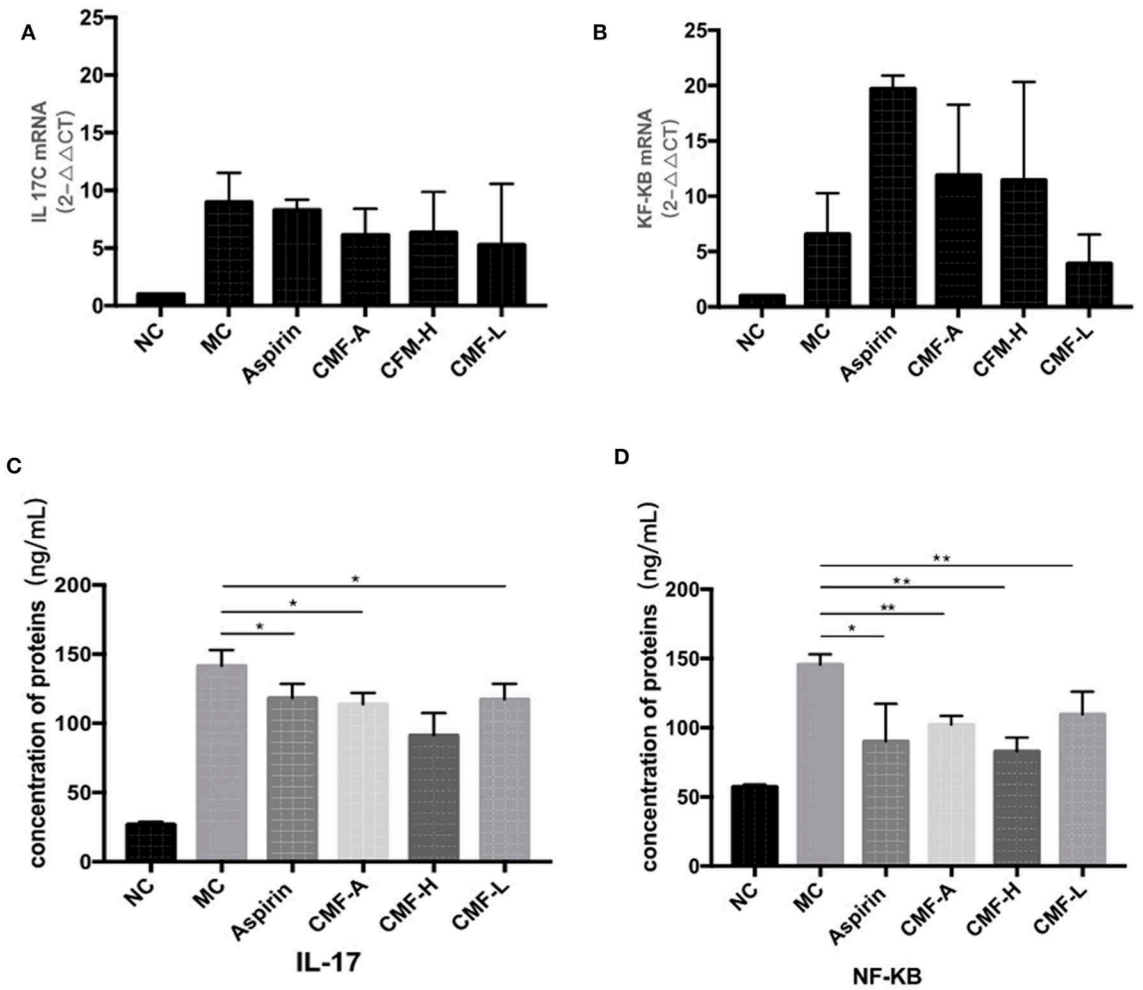

FIGURE 3 | CMF changed the inflammatory microenvironment and regulated the expression of IL-17C and NF-κB *in vivo*. mRNA level of IL-17C **(A)** and NF-κB **(B)** in the colonic tissues were measured by real-time RT-PCR. All data are expressed as the mean ± S.D, $^{*}P < 0.05$, $^{**}P < 0.01$ compared with AOM/DSS group. The level of IL-17C in serum **(C)** and the level of NF-κB in tumor tissue homogenate **(D)** were measured using ELISA kits. All data are expression as the mean ± S.D, $^{*}P < 0.05$, $^{**}P < 0.01$ compared with AOM/DSS group.

It was found that these bacteria are dominant bacteria at the genus level (**Figure 5B**). Intraindividual changes were detected in these groups. Compared with the model group, the abundance of a small number of bacteria increased or decreased to varying degrees, and most of the bacteria remain unchanged. At the family level, abundance of Desulfovibrionaceae decreased in groups that were treated with CMF. Conversely, a transient CMF-treatment increase several family microbiota, including Rikenellaceae, Erysipelotrichaceae, Lactobacillaceae, Streptococcaceae, and Tannerellaceae. At the genus level, the abundance of genus *Alistipes*, *Faecalibaculum*, *Lactobacillus*, and *Parabacterioides*, were up-regulated after the treatment of CMF. The genus *Parasutterella* was found down-regulated in CMF treatment groups. It is worth mentioning that genus Desulfovibrionaceae_uncultured acted to AOM/DSS-mediated gut microbiota dysbiosis had statistical difference (**Figure 5F**). There arechanges in the gut microbiota but there is no statistical difference in these changes (**Figures 5C–E**).

To systematically examine the alteration of taxa abundance according to CMF treatment, we conducted LEfSe (LDA Effect Size). The microbial cladogram indicates that the gut microbiome significantly altered in Bacteroidaceae and Staphylococcaceae, ranging from family to genus level (**Figures 6A,C**). At the genus level, the relative abundance of *Turicibacter*, *Bacteroides*, *Bacteroidaceae*, *Faecalibaculum*, *Erysipelatoclostridium*, and *Staphylococcus* were enriched in mice treated with the CMF-A diet (**Figures 6B,D**).

DISCUSSION

Traditional Chinese medicine (TCM) have been used for the treatment of diseases and health conditions for several thousands of years. In the treatment of CRC, the application of TCM has

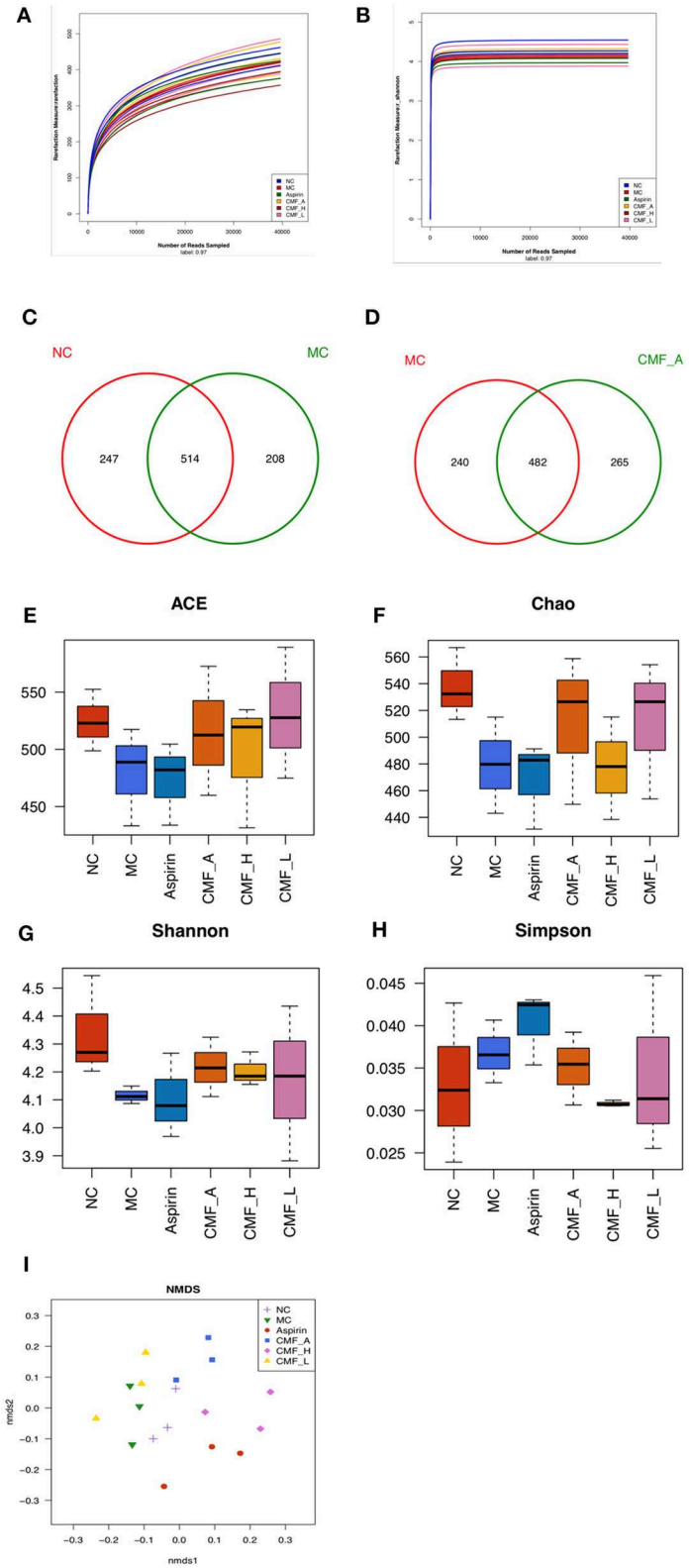

FIGURE 4 | Illumina Miseq sequencing data showed CMF modulates the overall component of gut microbiota. **(A)** Rarefaction curves determined at the 97% similarity level. **(B)** Shannon-Wiener curves of samples, calculated using mothur. **(C–F)** Venn diagram of OUTs in the different groups. **(G–I)** Community richness and diversity index of the model control group (MC), normal control group (NC), aspirin group, and CMF intervention groups (CMF-A/H/L) on ACE, Chao, Shannon, Simpson analysis.

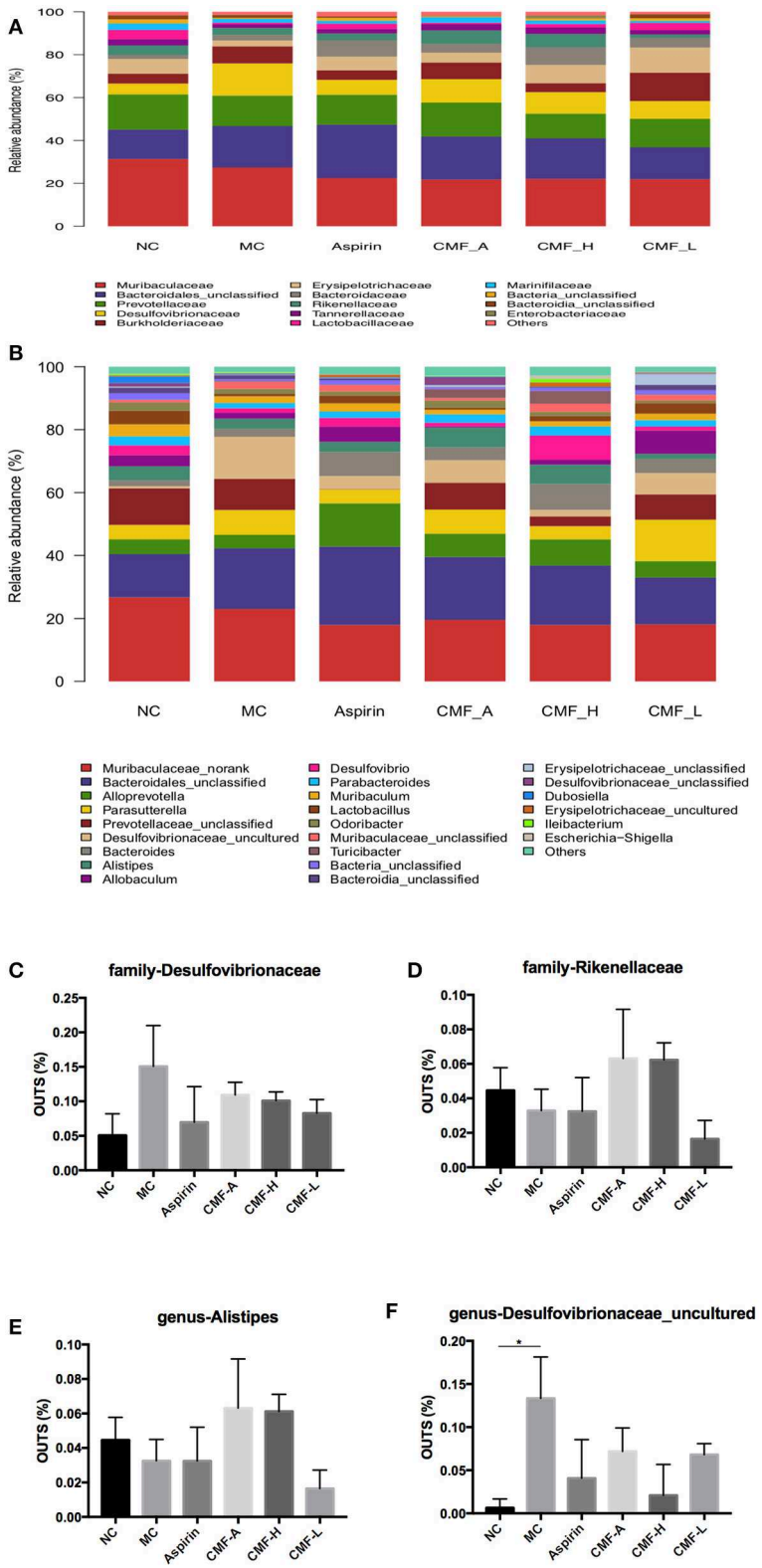

FIGURE 5 | Comparison of gut microbiota among groups. Microbiota distribution at the family level **(A)** and the genus level **(B)**. Relative abundance measured with qPCR for family-Desulfovibrionaceae, family- Rikenellaceae, and genus-Alistipes, genus- Desulfovibrionaceae_uncultured **(C–F)**. Superscript letters indicate statistical differences (*$P < 0.05$).

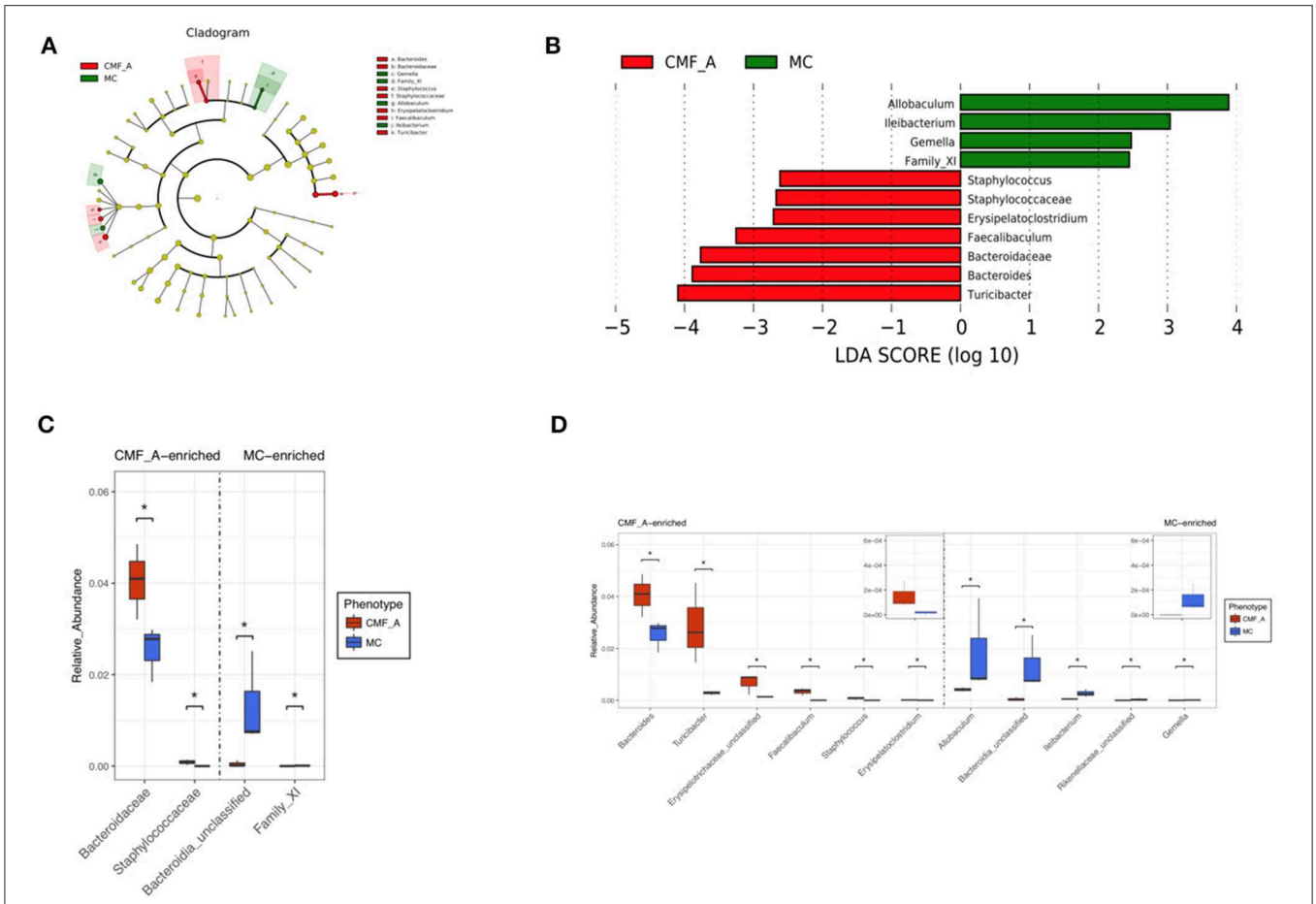

FIGURE 6 | Comparison of gut microbiota between CMF-A group and MC group. Cladogram of linear discriminant analysis (LDA) coupled with effective size measurement showing differentially abundant genera **(A)**. Histogram of LDA scores for differentially abundant genera **(B)**. qPCR identified the difference in CMF-A group and MC group of mice and *t*-test for significance testing at family level **(C)** and genus level **(D)**. Superscript letters indicate statistical differences (*$P < 0.05$).

received worldwide attention. Many studies have demonstrated the anti-tumor effect of TCM in CRC therapy. For example, Wei et al. showed that JianPi JieDu decoction (JPJD) is able to inhibit tumorigenesis, metastasis, as well as angiogenesis of tumors through the mTOR/HIF-1α/VEGF pathway (18). Wu et al. demonstrated that Gegen Qinlian decoction (GGT) can ameliorate gut-toxicity through anti-inflammatory pathways, inhibition of neutrophil migration, anti-oxidative stress via the Nrf2/Keap-1 pathway in the colon (19). Wing lam et al. reported that PHY906 reduced the CPT-11-induced gastrointestinal toxicity by inhibiting multiple steps of inflammation and the promotion of intestinal progenitor cell repopulation (20). Extensive studies have revealed that TCM antitumor drugs work by inhibiting tumor proliferation, promoting tumor apoptosis, and affecting diverse molecular targets (21–23).

The alterations of cancer genetic and molecular targets in CRC treatment have been extensively reported. Recent studies have reported that the regulation of gut microbiota may affect carcinogenesis (24–28). Intestinal flora is a direct factor of intestinal cancer. In this study, we found that CMF can ameliorate colitis-associated colorectal carcinogenesis in mice by modulating the fecal microbiota. The gut microbiota, including *Fusobacterium* (F.) *nucleatum* (29) and Firmicutes, Bacteroidetes Ley et al. (30), plays an important role in human health. In addition, many factors will affect and destroy the balance of intestinal microbiota, including the invasion of antigens, activation of immune cells, and production of cytokines. Therefore, investigating the relationship between CMF and the gut microbiota in AOM/DSS-induced colitis in miceis critical.

In our study, the anti-inflammatory role of CMF in the *in vivo* model of colitis-associated colorectal carcinogenesis induced by AOM/DSS and high-fat diet in C57BL/6 micewere investigated. Two different solvent extraction components of CMF were used to treat these mice to evaluate its therapeutic effect. The results showed that each of these extracts of CMF were well-tolerated. Histopathology findings were consistent with previous experimental results (31). The CRC mice treated with AOM/DSS and high-fat diet presented more severe condition than CMF-treated mice. In contrast, administration of CMF decreased tumor number and tumor size. Especially the ethanol extract of

CMF can effectively inhibit the occurrence of colitis-associated colorectal carcinogenesis in the colon and small intestine.

Previous studies showed that tumor-prone mice colonized with *E. coli* and *B. fragilis* and increased IL-17 expression that promotes colon tumorigenesis in AOM mice (3, 32). It was reported that spontaneous activation of NF-κB was detected in tissues of human colorectal cancer (31, 33).We found that CMF could decrease the expression level of IL-17C and inhibit the activity of NF-κB.

High-throughput sequencing determined microbiological composition in mice. Most of the diversity of microorganisms was captured in all samples. The ACE, Chao, Simpson, and Shannon indices reveal that the microbial diversity in control mice and CMF treated mice were greater than in the model mice (16). The microflora analysis show that there are significant differences between the control mice and the model mice. There was a statistical difference between the ethanol extract of CMF treated mice and the model mice. This result indicated that the ethanol extract of CMF could increase the diversity of the intestinal flora. We evaluated phylum, class, order, family, and genus, the gut microbiota community in all samples. From the experiment, Muribaculaceae, Bacteroidales, and Prevotellaceae were the dominant family found in the gut. In accordance with family criteria, these flora occupied a main tier in the genus level. Focus on certain bacteria, statistical results reveal that CMF reversed the gut microbiota dysbiosis in CRC mice, including inhibiting the growth of Desulfovibrionaceae and promoting the Rikenellaceae. Desulfovibrionaceae, a kind of sulfate-reducing and endotoxin-producing bacteria, were mostly enriched in mice with long term high-fat feeding. Previous studies found that the family Desulfovibrionacea is positively associated with obesity (9, 34–36). This phenomenon was also found in our study. Wu et al. found that relative abundances of Rikenellaceae increased in the AOM/DSS mice (32). This result was in consistent with our study. We speculate that Rikenellaceae might be a bacterium that could cause cancer.

Because the results of our study showed that the alcohol extract of CMF is more effective than that of the water extract, we analyzed the difference of flora of the mice treated with the alcohol extract of CMF and the model mice. The results showed that the gut microbiome significantly altered in Bacteroidaceae and Staphylococcaceae, ranging from family to genus level. As shown in our results, at genus level, the relative abundance of *Turicibacter*, *Bacteroides*, *Faecalibaculum*, *Erysipelatoclostridium,* and *Staphylococcus* were enriched in mice treated with the CMF-A diet. In a previous study, the abundance of Bacteroidaceae had an important influence in the active progression of colitis in DSS-treated mice (16), which was in contrast to our study. Liu et al. found that the abundance of *Turicibacter* decreased in obesity mice (37, 38). Similarly, the *Turicibacter* was also reduced in AOM/DSS and high-fat diet mice in this study. Therefore, we suspect that *Turicibacter*, *Bacteroides*, *Faecalibaculum*, *Erysipelatoclostridium,* and *Staphylococcus* were the beneficial bacteria in the gut. But the specific role of these gut microbiota needs to be further investigated.

In summary, we report that CMF, a two-herb formulation, has reduced the incidence of CRC by inhibiting inflammatory factors and regulating gut microbiota. In addition, the mechanism of action of CMF is through the direct action on inflammatory factors or the indirect effect on regulating gut flora. Understanding the role of gut microbiota would be helpful for the prevention of CRC development.

DATA AVAILABILITY STATEMENT

All datasets generated for this study are included in the article/supplementary material.

ETHICS STATEMENT

The animal study was reviewed and approved by IRB of Yueyang Hospital Affiliated with Shanghai University of Traditional Chinese Medicine. Written informed consent was obtained from the owners for the participation of their animals in this study.

AUTHOR CONTRIBUTIONS

XF, HZ, and GX contributed to study design, data interpretation, and manuscript preparation. YL contributed to animal rearing. DH contributed to data acquisition and analysis.

FUNDING

This work was supported by the National Natural Science Foundation of China (81403360). The funders play no role in data collection and analysis, design, decision to publish, or preparation of the manuscript.

REFERENCES

1. Siegel RL, Miller KD, Jemal, A. Cancer statistics. *CA Cancer J Clin.* (2016) 66:7–30. doi: 10.3322/caac.21332
2. McGuire S. World cancer report 2014. Geneva, Switzerland: World Health Organization, International Agency for Research on Cancer, WHO Press, 2015. *Adv. Nutr.* (2015) 418–9. doi: 10.3945/an.116.012211
3. Dejea CM, Fathi P, Craig JM, Boleij A, Taddese R, Geis AL, et al. Patients with familial adenomatous polyposis harbor colonic biofilms containing tumorigenic bacteria. *Science.* (2018) 359:592–7. doi: 10.1126/science.aah3648
4. Nishihara R, Wu K, Lochhead P, Morikawa T, Liao X, Qian ZR, et al. Long-term colorectal-cancer incidence and mortality after lower endoscopy. *N Engl J Med.* (2013) 369:1095–105. doi: 10.1056/NEJMoa1301969
5. Logan RF, Grainge MJ, Shepherd VC, Armitage NC, Muir KR, ukCAP Trial Group. Aspirin and folic acid for the prevention of recurrent colorectal adenomas. *Gastroenterology.* (2008) 134:29–38. doi: 10.1053/j.gastro.2007.10.014
6. Kummar S, Copur MS, Rose M, Wadler S, Stephenson J, O'Rourke M, et al. A phase I study of the chinese herbal medicine PHY906 as a modulator of irinotecan-based chemotherapy in patients with advanced colorectal cancer. *Clin Colorectal Cancer.* (2011) 10:85–96. doi: 10.1016/j.clcc.2011.03.003

7. Lam W, Jiang Z, Guan F, Hu R, Liu SH, Chu E, et al. The number of intestinal bacteria is not critical for the enhancement of antitumor activity and reduction of intestinal toxicity of irinotecan by the Chinese herbal medicine PHY906 (KD018). *BMC Complement Altern Med*. (2014) 14:490. doi: 10.1186/1472-6882-14-490
8. Yang H, Liu JX, Shang HX, Lin S, Zhao JY, Lin JM. Qingjie Fuzheng granules inhibit colorectal cancer cell growth by the PI3K/AKT and ERK pathways. *World J Gastrointest Oncol.* (2019) 11:377–92. doi: 10.4251/wjgo.v11.i5.377
9. Zhao J, Li Y, Sun M, Xin L, Wang T, Wei L. The Chinese herbal formula Shenzhu Tiaopi Granule results in metabolic improvement in type 2 diabetic rats by modulating the gut microbiota. *Evid Based Complement Alternat Med*. (2019) 2019:6976394. doi: 10.1155/2019/6976394
10. Wei Z, Cao S, Liu S, Yao Z, Sun T, Li Y, Li J, et al. Could gut microbiota serve as prognostic biomarker associated with colorectal cancer patients' survival? A pilot study on relevant mechanism. *Oncotarget.* (2016) 7:46158–72. doi: 10.18632/oncotarget.10064
11. Siegel RL, Jemal A, Wender RC, Gansler T, Ma J, Brawley OW. An assessment of progress in cancer control. *CA Cancer J Clin*. (2018) 68:329–39. doi: 10.3322/caac.21460
12. Wong SH, Zhao L, Zhang X, Nakatsu G, Han J, Xu W, et al. Gavage of fecal samples from patients with colorectal cancer promotes intestinal carcinogenesis in germ-free and conventional mice. *Gastroenterology.* (2017) 153:1621–33. doi: 10.1053/j.gastro.2017.08.022
13. Song X, Zhu S, Chen P, Hou W, Wen Q, Liu J, et al. AMPK-mediated BECN1 phosphorylation promotes ferroptosis by directly blocking system X(c)(-) activity. *Curr Biol*. (2018) 28:2388–99. doi: 10.1016/j.cub.2018.05.094
14. Zhang H, Li Q, Fu X. Research progress in chemical constituents and pharmacological effects of Wumei. *Shanghai J. Tradit. Chin. Med.* (2017) 296–300. doi: 10.16305/j.1007-1334.2017.S1.078
15. Xu C, Shang S, Liu M, Yang M. Research progress on chemical constituents and pharmacological activities of silkworm, Bombyx mori. *Chinese Pharm.* (2014) 3732–4. doi: 10.6039/j.issn.1001-0408.2014.39.29
16. Yang Y, Chen G, Yang Q, Ye J, Cai X, Tsering P, et al. Gut microbiota drives the attenuation of dextran sulphate sodium-induced colitis by Huangqin decoction. *Oncotarget.* (2017) 8:48863–74. doi: 10.18632/oncotarget.16458
17. Kim DH, Hossain MA, Kang YJ, Jang JY, Lee YJ, Im E. Baicalein, an active component of *Scutellaria baicalensis.* Georgi, induces apoptosis in human colon cancer cells and prevents AOM/DSS-induced colon cancer in mice. *Int J Oncol.* (2013) 43:1652–8. doi: 10.3892/ijo.2013.2086
18. Peng W, Zhang S, Zhang Z, Xu P, Mao D, Huang S, et al. Jianpi Jiedu decoction, a traditional Chinese medicine formula, inhibits tumorigenesis, metastasis, and angiogenesis through the mTOR/HIF-1α/VEGF pathway. *J Ethnopharmacol.* (2018) 224:140–8. doi: 10.1016/j.jep.2018.05.039
19. Wu Y, Wang D, Yang X, Fu C, Zou L, Zhang J. Traditional Chinese medicine Gegen Qinlian decoction ameliorates irinotecan chemotherapy-induced gut toxicity in mice. *Biomed Pharmacother.* (2019) 109:2252–61. doi: 10.1016/j.biopha.2018.11.095
20. Lam W, Bussom S, Guan F, Jiang Z, Zhang W, Gullen EA, et al. The four-herb Chinese medicine PHY906 reduces chemotherapy-induced gastrointestinal toxicity. *Sci Trans Med.* (2010) 2:45. doi: 10.1126/scitranslmed.3001270
21. Liu H, Liu H, Zhou Z, Parise RA, Chu E, Schmitz JC. Herbal formula Huang Qin Ge Gen Tang enhances 5-fluorouracil antitumor activity through modulation of the E2F1/TS pathway. *Cell Commun Signal.* (2018) 16:7. doi: 10.1186/s12964-018-0218-1
22. Yuan L, Zhou M, Wasan HS, Zhang K, Li Z, Guo K, et al. Jiedu Sangen decoction inhibits the invasion and metastasis of colorectal cancer cells by regulating EMT through the Hippo signaling pathway. *Evid Based Complement Alternat Med.* (2019) 2019:1431726. doi: 10.1155/2019/1431726
23. Ma Q, Ouyang Y, Meng F, Noolvi MN, Avvaru SP, More UA, et al. A review of pharmacological and clinical studies on the application of Shenling Baizhu San in treatment of Ulcerative colitis. *J Ethnopharmacol*. (2019):112105. doi: 10.1016/j.jep.2019.112105
24. Iida N, Dzutsev A, Stewart CA, Smith L, Bouladoux N, Weingarten RA, et al. Commensal bacteria control cancer response to therapy by modulating the tumor microenvironment. *Science.* (2013) 342:967–70. doi: 10.1126/science.1240527
25. Viaud S, Saccheri F, Mignot G, Yamazaki T, Daillère R, Hannani D, et al. The intestinal microbiota modulates the anticancer immune effects of cyclophosphamide. *Science.* (2013) 342:971–6. doi: 10.1126/science.1240537
26. Sivan A, Corrales L, Hubert N, Williams JB, Aquino-Michaels K, Earley ZM, et al. Commensal *Bifidobacterium* promotes antitumor immunity and facilitates anti-PD-L1 efficacy. *Science.* (2015) 350:1084–9. doi: 10.1126/science.aac4255
27. Vètizou M, Pitt JM, Daillè re R, Lepage P, Waldschmitt N, Flament C, et al. Anticancer immunotherapy by CTLA-4 blockade relies on the gut microbiota. *Science.* (2015) 350:1079–84. doi: 10.1126/science.aad1329
28. Schirmer M, Smeekens SP, Vlamakis H, Jaeger M, Oosting M, Franzosa EA, et al. Linking the human gut microbiome to inflammatory cytokine production capacity. *Cell.* (2016) 167:1125–36.e8. doi: 10.1016/j.cell.2016.10.020
29. Yu T, Guo F, Yu Y, Sun T, Ma D, Han J, et al. Fusobacterium nucleatum promotes chemoresistance to colorectal cancer by modulating autophagy. *Cell.* (2017) 170:548–63.e16. doi: 10.1016/j.cell.2017.07.008
30. Ley RE, Turnbaugh PJ, Klein S, Gordon JI. Microbial ecology: human gut microbes associated with obesity. *Nature.* (2006) 444:1022–3. doi: 10.1038/4441022a
31. Lv Z, Wang Z, Luo L, Chen Y, Han G, Wang R, et al. Spliceosome protein Eftud2 promotes colitis-associated tumorigenesis by modulating inflammatory response of macrophage. *Mucosal Immunol.* (2019) 12:1164–73. doi: 10.1038/s41385-019-0184-y
32. Chan JL, Wu S, Geis AL, Chan GV, Gomes TAM, Beck SE, et al. Non-toxigenic *Bacteroides fragilis* (NTBF) administration reduces bacteria-driven chronic colitis and tumor development independent of polysaccharide A. *Mucosal Immunol.* (2019) 12:164–77. doi: 10.1038/s41385-018-0085-5
33. Guo M, Li Z, Huang Y, Shi M. Polysaccharides from Nostoc commune Vaucher activate macrophages via NF-κB and AKT/JNK1/2 pathways to suppress colorectal cancer growth *in vivo*. *Food Funct.* (2019) 10:4269–79. doi: 10.1039/C9FO00595A
34. Sun J, Qi C, Zhu H, Zhou Q, Xiao H, Le G, et al. IgA-targeted *Lactobacillus jensenii* modulated gut barrier and microbiota in high-fat diet-fed mice. *Front Microbiol.* (2019) 10:1179. doi: 10.3389/fmicb.2019.01179
35. Wang Z, Lam KL, Hu J, Ge S, Zhou A, Zheng B, et al. Chlorogenic acid alleviates obesity and modulates gut microbiota in high-fat-fed mice. *Food Sci Nutr*. (2019) 7:579–88. doi: 10.1002/fsn3.868
36. Wu C, Ouyang M, Guo Q, Jia J, Liu R, Jiang Y, et al. Changes in the intestinal microecology induced by bacillus subtilis inhibit the occurrence of ulcerative colitis and associated cancers: a study on the mechanisms. *Am J Cancer Res.* (2019) 9:872–86.
37. Liu W, Crott JW, Lyu L, Pfalzer AC, Li J, Choi SW, et al. Diet- and genetically-induced obesity produces alterations in the microbiome, inflammation and Wnt pathway in the intestine of Apc(+/1638N) mice: comparisons and contrasts. *J Cancer.* (2016) 7:1780–90. doi: 10.7150/jca.15792
38. Wu M, Wu Y, Li J, Bao Y, Guo Y, Yang W. The dynamic changes of gut microbiota in Muc2 deficient mice. *Int J Mol Sci*. (2018) 19:E2809. doi: 10.3390/ijms19092809

Conflict of Interest: The authors declare that the research was conducted in the absence of any commercial or financial relationships that could be construed as a potential conflict of interest.

frontiers in Oncology

ORIGINAL RESEARCH
published: 29 November 2019
doi: 10.3389/fonc.2019.01345

Survivin Promotes Piperlongumine Resistance in Ovarian Cancer

Xing-Wei Nan[1†], Li-Hua Gong[1†], Xu Chen[1†], Hai-Hong Zhou[1], Piao-Piao Ye[1], Yang Yang[2], Zi-Hao Xing[2], Meng-Ning Wei[2], Yao Li[2], Sheng-Te Wang[2], Kun Liu[2], Zhi Shi[2] and Xiao-Jian Yan[1,3*]*

[1] Department of Gynecology, The First Affiliated Hospital of Wenzhou Medical University, Wenzhou, China, [2] Guangdong Provincial Key Laboratory of Bioengineering Medicine, Department of Cell Biology and Institute of Biomedicine, National Engineering Research Center of Genetic Medicine, College of Life Science and Technology, Jinan University, Guangzhou, China, [3] Center for Uterine Cancer Diagnosis & Therapy Research of Zhejiang Province, Women's Hospital and Institute of Translational Medicine, Zhejiang University School of Medicine, Hangzhou, China

Ovarian cancer is one of the most fatal female malignancies while targeting apoptosis is critical for improving ovarian cancer patients' lives. Survivin is regarded as the most robust anti-apoptosis protein, and its overexpression in ovarian cancer is related to poor survival and apoptosis resistance. Piperlongumine (PL) extracted from peppers is defined as an active alkaloid/amide and exhibits a broad spectrum of antitumor effects. Here, we demonstrate that PL induces the rapid depletion of survivin protein levels via reactive oxygen species (ROS)-mediated proteasome-dependent pathway *in vitro*, while exerting a remarkable inhibitory influence on the proliferation of ovarian cancer cells. Overexpression of survivin raises the survival rate of ovarian cancer cells to PL. Moreover, PL inhibits ovarian cancer cells xenograft tumor growth and downregulates survivin *in vivo*. Our findings reveal a previously unrecognized mechanism of PL in suppressing survivin expression as well as survivin promotes piperlongumine resistance in ovarian cancer and suggest that ROS-mediated proteasome-dependent pathway can be exploited to overcome apoptosis resistance triggered by aberrant expression of survivin.

Keywords: piperlongumine, survivin, ovarian cancer, ROS, proteasome

OPEN ACCESS

Edited by:
Chang Zou,
Shenzhen People's Hospital, China

Reviewed by:
Qing Wang,
Sun Yat-sen University, China
Shuangping Liu,
Dalian University, China

***Correspondence:**
Zhi Shi
tshizhi@jnu.edu.cn
Xiao-Jian Yan
yxjbetter@126.com

† These authors have contributed equally to this work

Specialty section:
This article was submitted to Molecular and Cellular Oncology, a section of the journal Frontiers in Oncology

Received: *27 September 2019*
Accepted: *15 November 2019*
Published: *29 November 2019*

Citation:
Nan X-W, Gong L-H, Chen X, Zhou H-H, Ye P-P, Yang Y, Xing Z-H, Wei M-N, Li Y, Wang S-T, Liu K, Shi Z and Yan X-J (2019) Survivin Promotes Piperlongumine Resistance in Ovarian Cancer. Front. Oncol. 9:1345. doi: 10.3389/fonc.2019.01345

INTRODUCTION

Ovarian cancer is the most fatal female reproductive tract cancer and the seventh most common cancer among women all over the world (1). It was evaluated that 22,240 ovarian cancer cases would be diagnosed while concurrently 14,070 women would succumb to the disease in 2018 (2). Between 1976 and 2015, owing to effective approaches to the clinical treatment, including aggressive cytoreductive surgery followed by system chemotherapy, the mortality rate of ovarian cancer declined by 33% (2). However, despite the markable achievement of ovarian cancer during the last decade, the prognosis for women with advanced disease remains poor and chemoresistance appears to be a significant obstacle constraining the clinical application (3). Progress in curbing the incidence and mortality of human ovarian cancer can be propelled by the development of novel agents.

Survivin, one of the inhibitor of apoptosis proteins family (IAP) firstly found in 1997, may accelerate the progress of cancer via promoting the insurgence of mutations as well as inducing resistance to chemotherapy (4). While undetectable in terminally differentiated adult tissues, the

survivin gene has been proved to be overexpressed in lots of cancers including ovarian cancer (5) in which survivin overexpression is detected in 74% of case and is related to the advanced clinical stage (6). Furthermore, our previous studies showed that the cytoplasmic protein expression level of survivin was an independent prognosis marker for ovarian cancer, downregulating survivin expression could enhance apoptosis (7, 8). Thus, survivin could be a promising target for apoptosis-based treatment in ovarian cancer therapy (9).

Piperlongumine (PL) extracted from the long pepper (*Piperlongum L.*) belongs to a biological alkaloid, embodying potential selective cytotoxic and antitumor properties over cancer cells of several histo-types including ovarian cancer (10). Our previous studies firstly demonstrated that PL facilitated G2/M cell cycle arrest, impeded the proliferation of human ovarian cancer cells, and induced reactive oxygen species (ROS) mediated apoptosis (11). Our previous cell-based experiments (11) and data published (12) indicated that the effect of PL to suppress the growth of tumors without general toxicity and to perturb redox and ROS homeostasis verify the PL treatment as a potential therapeutic opportunity against ovarian cancer.

However, the detailed molecular mechanism of the PL-mediated antitumor effect is not well-understood and still requires further investigation. Here, we firstly demonstrate that PL depleted the expression of survivin protein via a ROS-mediated proteasome-dependent pathway in ovarian cancer cells. We further evaluate the efficacy of PL to inhibit tumor growth *in vivo* as a potentially effective therapy for ovarian cancer treatment.

MATERIALS AND METHODS

Cell Culture

The cancer cell lines A2780, OVCAR-3, and HEK293T were cultured in DMEM (Gibco, NY, USA). Ten percent fetal bovine serum (Gibco, NY, USA) and antibiotics (10 mg/mL streptomycin and 10,000 U/mL penicillin) were additionally supplemented. The aforementioned cell lines were cultivated in a 37°C incubator at 5% CO_2.

Chemicals and Antibodies

PL, N-Acetyl-cysteine (NAC) and Chloroquine (CQ) were obtained from Sigma Chemical Co (St. Louis, MO, USA). MG132 was from ApexBio. The HRP secondary antibodies, anti-survivin (#2808), and anti-PARP (#9542) were obtained from Cell Signaling Technologies (Danvers, MA, USA). Anti-Vinculin (BM1611) antibody was obtained from Boster, China. Anti-β-actin (KM9001), and anti-GAPDH (KM9002) antibodies were obtained from Tianjin Sungene Biotech Co., China. MG132, CQ, and NAC were added 1 h before PL treatment in all co-treated experimented.

Western Blot

Cells were lysed in RIRA buffer at 4°C for around 30 min followed by centrifugation at 13,200 × rpm for 10 min to remove nuclei and other cell debris. Total protein concentration was detected by the Micro BCA Protein Assay Kit (Sangon Biotech, C503061) and the lysates were either used immediately or stored at −80°C. 10–12% SDS-PAGE gels were used to separate the proteins extracted before and thereby separated proteins were completely transferred to polyvinylidene difluoride (PVDF) membranes. Five percent BSA was used to block the membranes for 1 h and the indicated primary antibodies were added and incubated overnight. Membranes were probed with the chemiluminescent detection reagents, and reactive bands were visualized using UVP ChemStudio PLUS (Analytikjena) (13, 14).

RT-PCR

Total RNA was extracted from 5×10^6 to 5×10^7 cells using the RaPure Total RNA Mini Kit (Magen, #R4011-02), treated with DNAseI to eliminate genomic DNA, and quantitated using the Epoch spectrophotometer. Reverse transcription (RT) followed instructions provided by StarScript II First-strand cDNA Synthesis Kit-II (GenStar, #A214-05). The resulting cDNA was used as a template for the amplification of target gene transcripts by RT-PCR, using Hieff™ qPCR SYBR® Green Master Mix (YEASEN, #11201ES08) on the Hema9600 PCR machine. After 35 amplification cycles, reaction products were analyzed and β-actin RNA was used as a loading control. The primer sequences were as follows: survivin forward: CCGAC GTTGCCCCCTGC; survivin reverse: TCGATGGCACGGC GCAC; β-actin forward: AAATCGTGCGTGACATTAAGC; β-actin reverse: CCGATCCACACGGAGTACTT (15, 16).

Lentivirus Production and Infection

pDONR201-survivin was inserted into pCDH-Neo-Venus/DEST via LR clonase (Invitrogen, #11791) to form pCDH-Neo-Venus-survivin plasmid. At a 4:3:1 ratio, the lentiviral transfer vector, packaging plasmids psPAX2 and pMD.2G were transferred to the HEK293T cells to produced lentivirus. The PEI reagent was performed for transfection. Then, the viral supernatant was, respectively, collected 24, 48, 72, 96 h following transfection, filtered through a 0.20 μm filter, and concentrated. Using the polybrene (Solarbio, H8761), A2780, OVCAR-3 cells were transfected with pCDH-Neo-Venus-survivin or pCDH-Neo-Venus/DEST, followed by incubation with 48 h for the subsequent trials (17, 18).

Cell Viability Assay

It was assessed using a 3-(4,5-dimethylthiazol-2-yl)-2,5-diphenyltetrazolium bromide (MTT) assay. Briefly, ovarian cancer cells were seeded in 96-well plates, 4,500 cells per well, supplementing with 100 μL of medium and exposed to PL at different concentrations for 72 h, followed by the addition of 10 μL of MTT solution (5 mg/mL) per well to the medium and incubation 4 h at 37°C. After we discarded the medium, 50 μL of DMSO per well was used to elute the blue MTT-formazan product, and absorbance of the solution was read at 570 nm (19, 20).

Nude Mice Xenograft Assay

Balb/c nude female mice with 4–5 weeks of age and 20–22 g weight were purchased from the Guangdong Medical Laboratory Animal Center. For *in vivo* experiments, 4×10^6 A2780 cells in 100 μL of medium were injected subcutaneously into the left and right shoulders of each mouse. After the subcutaneous tumors reached a size of 0.3×0.3 cm^2, mice were randomized to treatment with PL (20 mg/kg) intraperitoneally or 0.5% methylcellulose alone every day. In the end, the tumors were got rid of mice and weighed after they were sacrificed. The bodyweight and the tumor volume (V) of mice were recorded every day. Formula: $V = \pi/6\ (1/2\ (A + B))^3$, the rate of inhibition (IR) = 1 – Mean tumor weight of experiment group/Mean tumor weight of control group × 100% (21, 22).

Statistical Analysis

Statistical significance of differences was determined by student's *t*-test. Differences were defined as significant at $P < 0.05$.

RESULTS

PL Downregulates the Expression of Survivin in Ovarian Cancer Cells

Our previous study firstly demonstrated that PL facilitated G2/M cell cycle arrest, impeded the proliferation of human ovarian cancer cells, and induced ROS dependent apoptosis in ovarian cancer (11). Due to the ability to inhibit the cell apoptosis, survivin may take part in various processes associated with the tumor development and progression, facilitated metastasis and angiogenesis, as well as favor cell cycle progression (9). Because

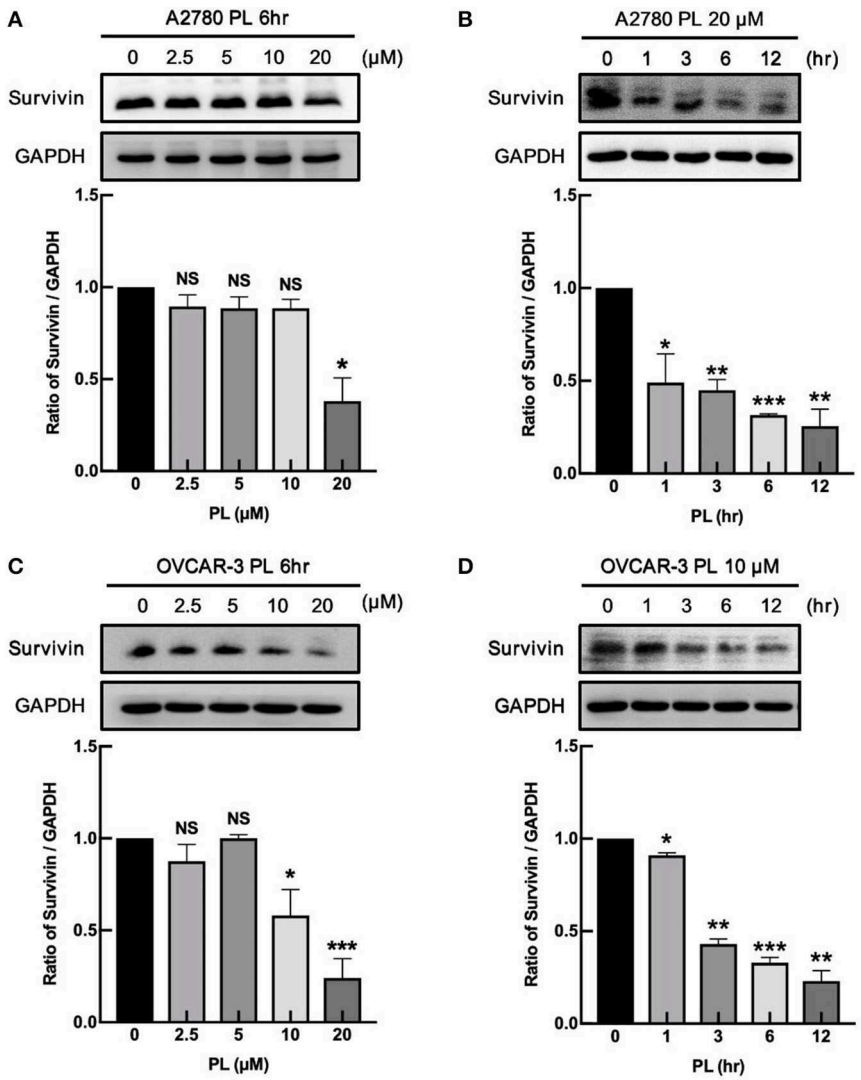

FIGURE 1 | PL downregulates the expression of survivin in ovarian cancer cells. A2780 **(A)** and OVCAR-3 **(C)** cells were treated with PL for indicated periods with different concentrations (0, 2.5, 5, 10, 20 μM), respectively. A2780 **(B)** and OVCAR-3 **(D)** cells were treated with 20 or 10 μM PL for 0, 1, 3, 6, 12 h. The expression of survivin was assayed by immunoblotting. GAPDH was used as a loading control. The band quantification was performed using ImageJ software. The representative of three experiments. $^*P < 0.05$, $^{**}P < 0.01$, and $^{***}P < 0.001$, Student's *t*-test. NS, not significant.

of the apoptotic effect of PL induced in ovarian cancer cells, we explored the negative regulation of PL on survivin expression. As shown in **Figures 2A,C**, A2780 and OVCAR-3 cells were exposed to increasing concentrations of PL (up to 20 μM) for 6 h, and the survivin protein was detected by western blot assay. PL effectively depleted the survivin expression in both A2780 and OVCAR-3 cells at the low micromolar concentration (10 or 20 μM) in contrast to the control cells. Furthermore, as demonstrated in **Figures 1B,D**, downregulation of survivin was significant as soon as 6 h following PL treatment. Together, these evidences manifested that PL induces the reduction of survivin ovarian cancer cells *in vitro*, which may contribute to its apoptotic effect.

PL Does Not Alter mRNA Expression of Survivin

To deliberate the discipline of PL-mediated survivin reduction, our group detected whether PL regulates the survivin mRNA expression in ovarian cancer cells. A2780 and OVCAR-3 cells were exposed to increasing concentrations of PL for 6 h or treated for different time scales at the same concentration of PL (10 or 20 μM), and the expression levels of survivin mRNA were examined by RT-PCR. In **Figures 2A–D**, the survivin mRNA expression levels were not altered both on concentration and time scales, which were not similar to the depletion of survivin protein levels. These findings strongly supported the notion

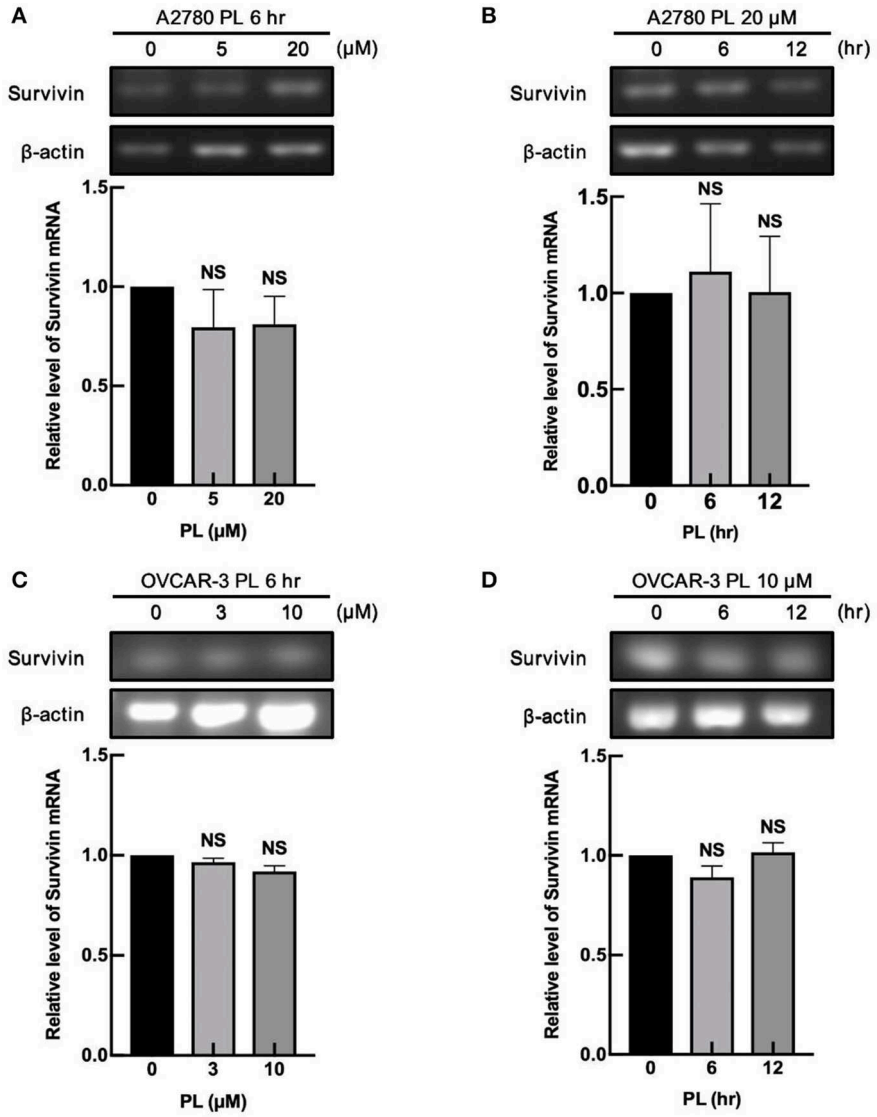

FIGURE 2 | PL does not alter mRNA expression of survivin. A2780 **(A)** and OVCAR-3 **(C)** cells were treated with indicated concentrations of PL for 6 h. Moreover, A2780 **(B)** and OVCAR-3 **(D)** cells were treated with 20 or 10 μM PL for the indicated periods. Survivin mRNA levels were detected by RT-PCR using specific primers. β-actin served as a loading control. The band quantification was performed using ImageJ software. The representative of three experiments. Student's *t*-test. NS, not significant.

that the PL regulates survivin gene expression at the non-transcriptional level.

PL Induces Proteasome-Dependently Degradation of Survivin

The aforementioned findings indicated that PL might induce depletion of survivin at the post-transcription level. The possible discipline expounding PL-induced decrease of survivin protein expression may associate with its rapidly increased ubiquitin-proteasome degradation. In order to verify this supposition, our group preincubated A2780 and OVCAR-3 cells with proteasome inhibitors MG132 (1 μM). The results presented in **Figures 3A,C** demonstrated that MG132 reversed PL-mediated survivin depletion compared with control cells, hinting that PL-mediated degradation of survivin occurs via ubiquitin-proteasome mechanism.

Otherwise, the autophagy-lysosome system and the ubiquitin-proteasome system are the essential intracellular proteolytic pathways in eukaryotes (23). To clarify whether the degradation of survivin protein was related to the induction of autophagy, CQ, a potent inhibitor of autophagy, was used to verify this hypothesis. However, in contrast to the result of the MG132, the expression levels of survivin stayed unchanged in response to autophagy inhibition **(Figures 3B,D)**, indicating that the cellular autophagic flux is not involved in the PL-mediated degradation of survivin expression. Collectively, these results showed that PL induces the depletion of survivin via the proteasome-dependent pathway.

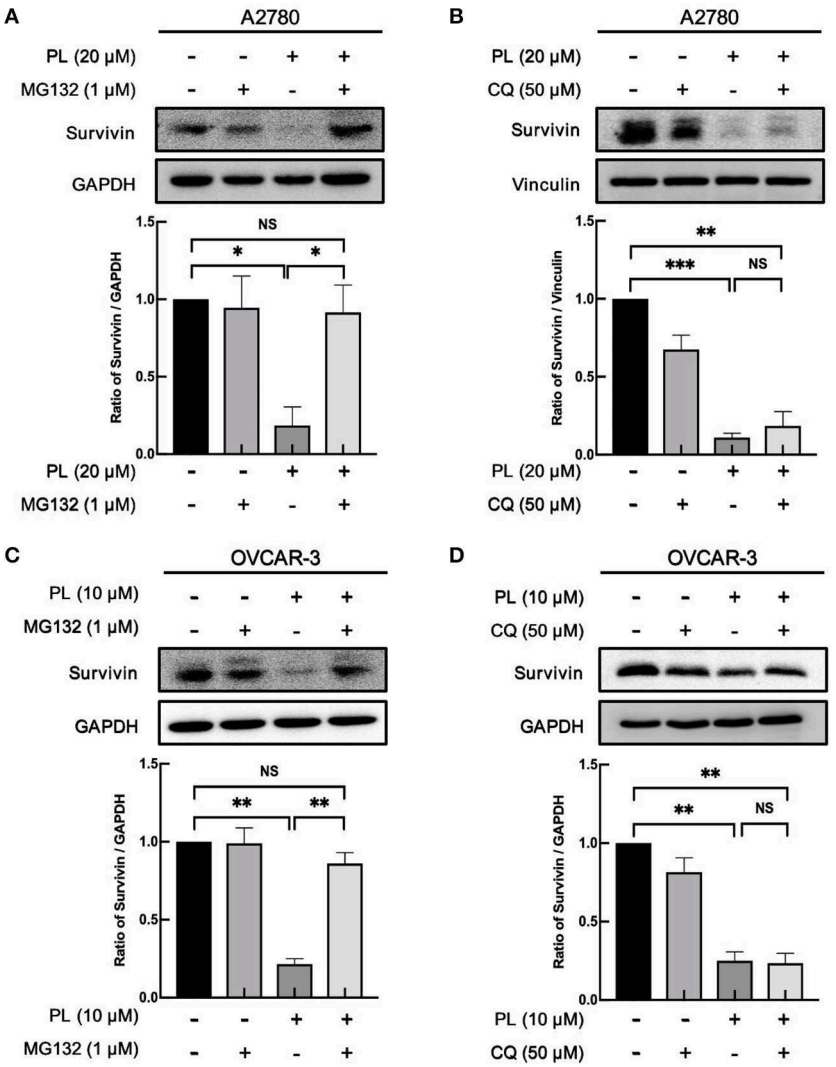

FIGURE 3 | PL induces proteasome-dependently degradation of survivin. A2780 **(A)** and OVCAR-3 **(C)** cells were pre-treated with 1 μM MG132 for 1 h and cultured with the indicated concentration of PL for 24 h. A2780 **(B)** and OVCAR-3 **(D)** cells were pre-treated with 50 μM CQ for 1 h and cultured with the indicated concentration of PL for 24 h. The expression of survivin was detected by immunoblotting. GAPDH and Vinculin were used as loading controls. The band quantification was performed using ImageJ software. Results were obtained based on three separate experiments. $^{*}P < 0.05$, $^{**}P < 0.01$, and $^{***}P < 0.001$, Student's *t*-test. NS, not significant.

PL Induces ROS-Dependently Apoptosis and Survivin Depletion

Lots of anticancer agents perform the antitumor property by the activation of intracellular ROS. Indeed, it has been elucidated that PL-induced apoptotic cell death in mammary tumors and sarcoma are closely related to the increased elevation of the intracellular ROS level (24). Of note, our previous study found that PL caused a prominent rise in ROS levels and induced significant apoptosis in ovarian cancer cells (11). Meanwhile, co-administration of PL and NAC fully restored the PL-mediated increase in ROS and inhibited the depletion of survivin **(Figures 4A,B)**. Taken together, these data offered additional support to our hypothesis that ROS generation is significant for PL-mediated ovarian cancer cells apoptosis and survivin degradation.

Overexpression of Survivin Raises the Survival Rate of Ovarian Cancer Cells to PL

To explore the role of survivin involved in PL-induced ovarian cancer apoptosis, we performed survivin infection taking advantage of pCDH-Neo-Venus-survivin lentivirus, while pCDH-Neo-Venus/DEST was adopted as the control. The Western blotting analysis was used to confirm the result of infection. As shown in **Figures 5A,C**, A2780 and OVCAR-3 cells infected with pCDH-Neo-Venus-survivin exhibited a much higher survivin expression. To detect the role of survivin in the apoptosis effect of PL, stable cells overexpressing survivin were treated with the increasing concentrations of PL and assayed to examine the survival rate **(Figures 5B,D)**. In the presence of PL, the IC_{50} value of OVCAR-3 cells was 4.59 μM. However, in survivin overexpression cells, the IC_{50} value was 9.65 μM, which was 2.10-fold higher than the control group. Consistently, similar results were also demonstrated in A2780 cells. Collectively, these results suggested that survivin overexpression raises the survival rate of ovarian cancer cells.

PL Inhibits A2780 Xenograft Tumor Growth and Downregulates Survivin *in vivo*

To evaluate the antitumor effects of PL *in vivo*, a xenografts model of A2780 cells in BALB/c mice was conducted.

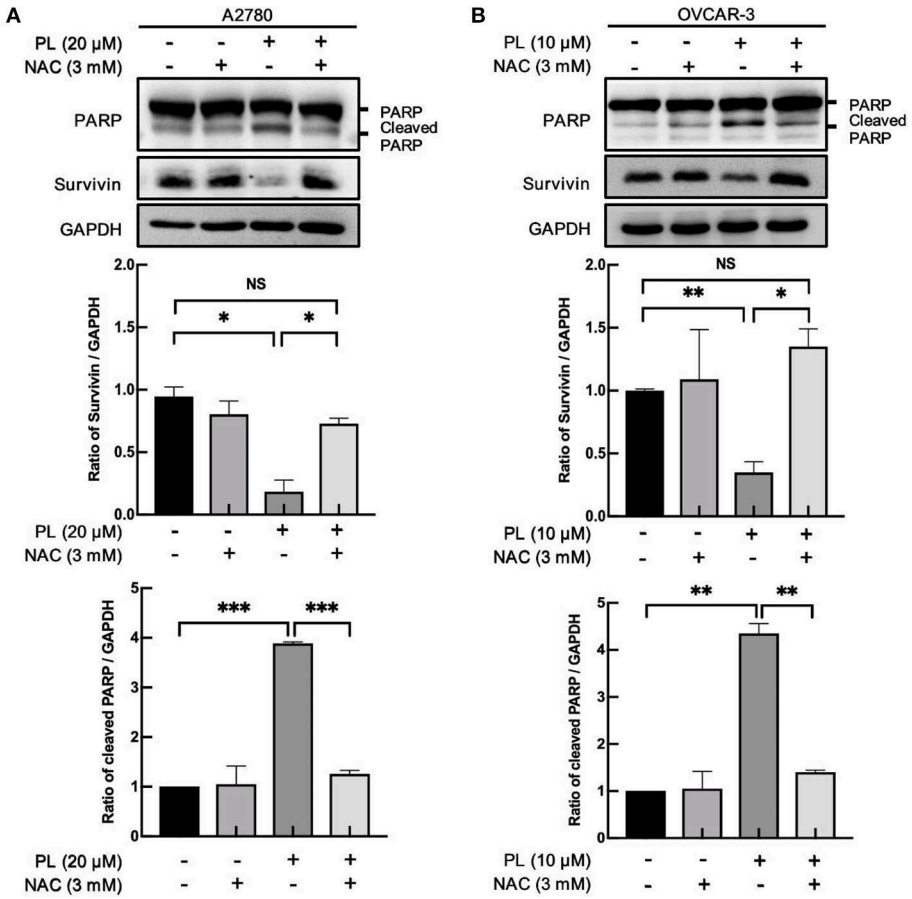

FIGURE 4 | PL induces ROS-dependently apoptosis and survivin depletion. A2780 **(A)** and OVCAR-3 **(B)** cells were treated with the indicated concentration of PL for 24 h in the present or absent of 3 mM NAC pretreatment for 1 h. Western blotting was taken to detect PARP, cleaved PARP, and survivin protein levels. GAPDH served as a loading control. The band quantification was performed using ImageJ software. Results were obtained based on three separate experiments. $^{*}P < 0.05$, $^{**}P < 0.01$, and $^{***}P < 0.001$, Student's *t*-test. NS, not significant.

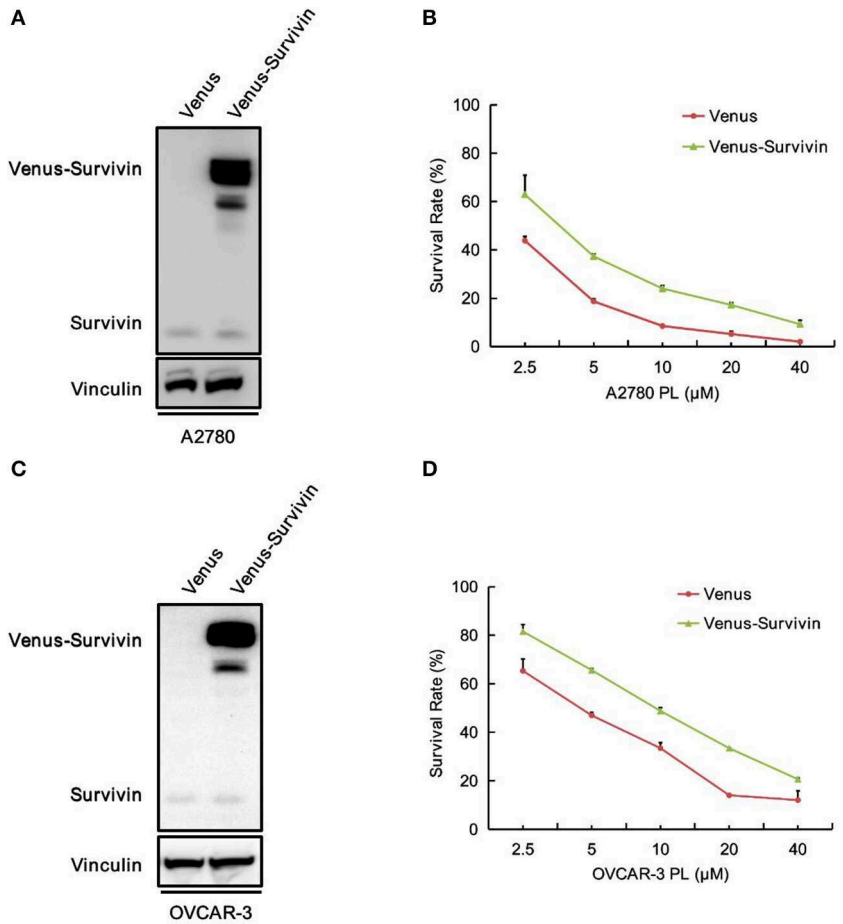

FIGURE 5 | Overexpression of survivin raises the survival rate of ovarian cancer cells to PL.A2780 **(A)** and OVCAR-3 **(C)** cells were infected with lentivirus for overexpressing survivin. Protein levels were examined by Western blot. Vinculin was used as a loading control. The viability of A2780 **(B)** and OVCAR-3 **(D)** cells were measured by MTT assay.

Intraperitoneal injection of PL at doses of 20 mg/kg for 15 days decreased A2780 tumors weight as well as the tumor volume vs. vehicle control **(Figures 6A,B,E)**. Notably, PL administration was endurable without severe weight loss **(Figures 6C,D)**. Additionally, immunoblotting analyses of the tumor tissues showed that survivin was significantly downregulated after PL exposure for 15 days **(Figure 6F)**, which was in accordance with the results *in vitro*. In short, these data indicated that PL suppresses the xenograft tumor growth *in vivo* accompanied by a decreased survivin level.

DISCUSSION

Because of the advanced stage at the time of diagnosis (80%) and a high recurrence rate (70–80%), human ovarian cancer surpassing other gynecological cancers lies in the fifth-leading cause of cancer-related deaths. The first-line treatment for it is the tumor cytoreductive surgery combined with platinum-taxane chemotherapy (25, 26) or neoadjuvant chemotherapy followed by debulking surgery (27). Although ∼80% of patients will have a response to the frontline therapies, 25% of women within 6 months will experience resistant cancer recurrence, and the overall 5-year survival rate ranges between 30 and 40% on a global scale (1). Thus, the explore of applicable treatment drugs remains a crucial goal for carrying out a better outcome.

Owing to the abnormal expression of anti-apoptotic proteins resulting in antitumor treatments less effective or ineffective, the reactivation of cell apoptosis becomes a potential therapy to conquer antitumor drug resistance. Survivin, the smallest member of IAP proteins, participates in the inhibition of apoptosis, affects the proper process of mitosis and promotes angiogenesis or even DNA repair (28). Generally, abnormal expression of survivin is associated with decreased apoptosis, increased tumor recurrence, poor prognosis, and high chemoresistance in human ovarian cancer (29, 30). Downregulating the expression of survivin elevated the sensitivity of ovarian cancer to chemotherapy and promoted apoptosis (7, 31). Thus, elucidating the regulatory mechanisms of survivin protein expression in cancers may propose mechanistic clues to future therapeutic strategies (32, 33). In general, survivin

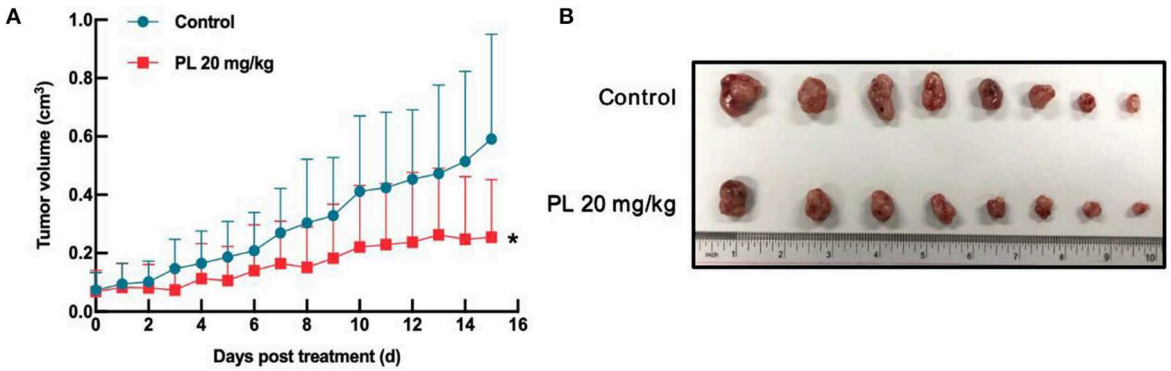

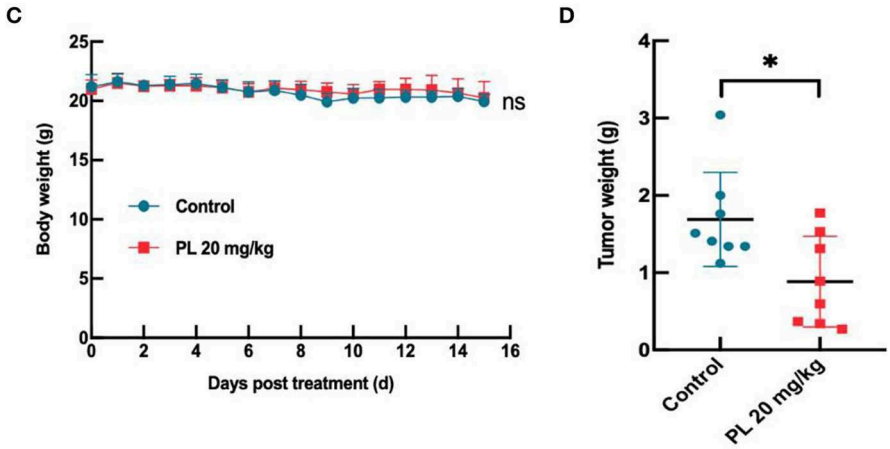

E

Cell	Group	Before Experiment		After Experiment		Weight of	Inhibition
		Mice	Weight (g)	Mice	Weight (g)	Tumors (g)	(%)
A2780	Control	4	21.19 ± 1.03	4	19.95 ± 0.60	1.44 ± 0.88	
	Piperlongumine	4	21.01 ± 0.75	4	20.26 ± 1.38	0.89 ± 0.57	38.50% *

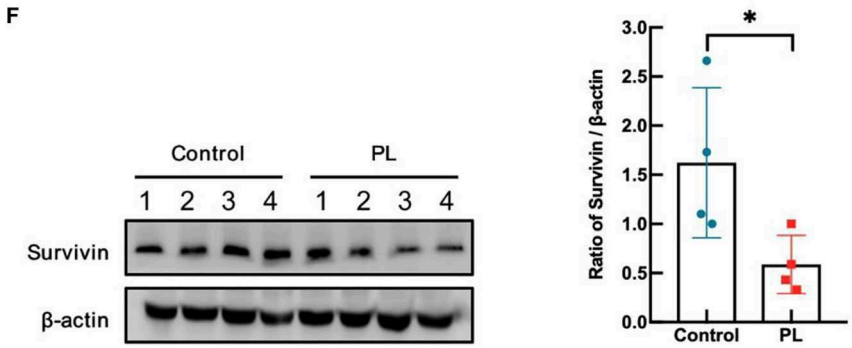

FIGURE 6 | PL inhibits A2780 xenograft tumor growth and downregulates survivin *in vivo*. Each mouse was injected subcutaneously with A2780 cells (4×10^6 in 100 μL of medium) under the left and right shoulders. When the subcutaneous tumors were ~0.3 cm × 0.3 cm^2 in size, mice were randomized into two groups and received an intraperitoneal injection of the vehicle alone (0.5% methylcellulose) or PL (20 mg/kg) every day. The body weight and tumor volume were recorded. After the experiment, the mice were anesthetized, and tumor tissue was excised from the mice and weighed. The tumor volume **(A)**, original tumors **(B)**, body weight **(C)**, tumor weight **(D)**, summary data **(E)**, and Western blot analysis of survivin **(F)** were shown. β-actin served as a loading control. The band quantification was performed using ImageJ software. *$P < 0.05$ vs. corresponding control.

combines with XIAP to indirectly suppress the function of caspases. XAF1 binds to XIAP resulting in the activation of ubiquitin-protein isopeptide ligase (E3) activity of XIAP, then promotes survivin ubiquitination and degradation (34). Conversely, the activation of ERK leads to the combination obstruction between survivin and the XIAP-XAF1 E3 ligase complex, which exactly stabilizes survivin proteins (35). The proapoptotic F-box protein FBXL7 acting as a ubiquitin E3 ligase interacts with Glu-126 to modulate the polyubiquitylation of survivin and thereby enhance its proteasomal degradation (36). Nonetheless, aurora kinase A (AURKA) restricts survivin to combine with FBXL7 E3 ubiquitin ligase through the negative regulation on FOXP1-FBXL7 axis, which upregulates the survivin expression (37). lncRNA LINC00473 (LNC473) remarkably suppresses the ubiquitination of survivin through recruiting deubiquitinase USP9X and then enhanced the stability of survivin (38). The Culling 9 (CUL9) is a putative E3 ligase and deplete the protein abundance of survivin via enhancing its ubiquitylation (39). Additionally, it has been reported that the ubiquitin-like-modifier proteins FAT10 (40), the heat shock protein (HSP90) (41) and CSN5/JAB1 (42) directly bind to survivin and therefore are resistant to ubiquitin-proteasome degradation. Therefore, the therapeutic regiment targeting the survivin axis is pushing the door of ovarian cancer. Such treatments include regiments that target transcription or post-translational level, vaccines based on cytotoxic activities of immune-cells and gene therapy methods that suppress survivin's function (43).

Piperlongumine, a biologically active alkaloid/amide isolated from peppers, has selectively excellent ability to inhibit tumor cells via the induction of oxidative stress and genotoxicity, as well as the significant oral bioavailability in mice burden tumor without unbearable systemic toxicity (44). We have previously reported that exposure of ovarian cancer cells to PL selectively suppressed cell viability in a concentration- and time-dependent manner (11). We deeply take an insight into the underlying mechanism of PL-induced apoptosis in ovarian cancer and find that survivin plays a vital role in the regulation of PL-mediated apoptosis in this study. Here, we firstly elucidated that PL induced apoptosis as well as the rapid depletion of survivin in ovarian cancer *in vitro* and *vivo*. Furthermore, overexpression of survivin raised the survival rate of ovarian cancer cells, implying that PL induced apoptosis of ovarian cancer via inhibiting survivin expression. In addition, our data suggested that the levels of survivin mRNA stayed unchanged under PL administration, indicating that PL induced depletion of survivin at the non-transcriptional level. This notion may lead to a rational concern about the strategy modulating either ubiquitin-proteasome or autophagy because both of them are the two primary proteolytic mechanisms. Then, a blockage of proteasome activity reversed the reduction of survivin by PL, as compared with keeping stable under autophagy inhibition. Otherwise, the previous studies also observed that the elevated levels of intracellular ROS induced by PL involved in the process of apoptosis in ovarian cancer. Considering that ROS-mediated signaling in cancer cells has long been thought to participate in malignant transformation, carcinogenesis initiation, and the survival of cancer cells, it is reasonable that the ROS-dependent pathway may take part in the regulation of survivin (45). In agreement with this notion, we observed that the apoptosis and the depletion of survivin under PL were reversed by NAC.

As all the data we assembled suggest, it is reasonable to regard the ROS-mediated proteasome-dependent mechanism as the major system responsible for the depletion of survivin under PL treatment. PL is on the way to transform ovarian cancer patients' outcomes and looking for finding its place in ovarian cancer therapeutic strategies.

DATA AVAILABILITY STATEMENT

All datasets generated for this study are included in the article/supplementary material.

ETHICS STATEMENT

The animal study was reviewed and approved by the ethics committee of Jinan University.

AUTHOR CONTRIBUTIONS

X-WN, L-HG, XC, ZS, and X-JY designed the experiments, performed the experiments, analyzed the data, and wrote the paper. H-HZ, P-PY, YY, Z-HX, M-NW, YL, S-TW, and KL conducted the experiments. All authors read and approved the final manuscript.

FUNDING

This study was supported by funds from the National Key Research and Development Program of China No. 2017YFA0505104 (ZS), the National Natural Science Foundation of China Nos. 81772540 (ZS), 81503293 (X-JY), the Science and Technology Foundation of Wenzhou City, Zhejiang Province, China No. 2015Y0304 (L-HG), the Technology Development Funds of Wenzhou City No. Y20190014 (X-JY), and the Traditional Chinese Medicine Science and Technology Foundation of Zhejiang Province, China No. 2020ZB144 (X-JY).

REFERENCES

1. Reid BM, Permuth JB, Sellers TA. Epidemiology of ovarian cancer: a review. *Cancer Biol Med.* (2017) 14:9–32. doi: 10.20892/j.issn.2095-3941.2016.0084
2. Torre LA, Trabert B, DeSantis CE, Miller KD, Samimi G, Runowicz CD, et al. Ovarian cancer statistics, 2018. *CA Cancer J Clin.* (2018) 68:284–96. doi: 10.3322/caac.21456
3. Herzog TJ, Monk BJ. Bringing new medicines to women with epithelial ovarian cancer: what is the unmet medical need? *Gynecol Oncol Res Pract.* (2017) 4:13. doi: 10.1186/s40661-017-0050-0

4. Ambrosini G, Adida C, Altieri DC. A novel anti-apoptosis gene, survivin, expressed in cancer and lymphoma. *Nat Med.* (1997) 3:917–21. doi: 10.1038/nm0897-917
5. Stauber RH, Mann W, Knauer SK. Nuclear and cytoplasmic survivin: molecular mechanism, prognostic, and therapeutic potential. *Cancer Res.* (2007) 67:5999–6002. doi: 10.1158/0008-5472.CAN-07-0494
6. Cohen C, Lohmann CM, Cotsonis G, Lawson D, Santoianni R. Survivin expression in ovarian carcinoma: correlation with apoptotic markers and prognosis. *Mod Pathol.* (2003) 16:574–83. doi: 10.1097/01.MP.0000073868.31297.B0
7. Chen L, Liang L, Yan X, Liu N, Gong L, Pan S, et al. Survivin status affects prognosis and chemosensitivity in epithelial ovarian cancer. *Int J Gynecol Cancer.* (2013) 23:256–63. doi: 10.1097/IGC.0b013e31827ad2b8
8. Zaffaroni N, Daidone MG. Survivin expression and resistance to anticancer treatments: perspectives for new therapeutic interventions. *Drug Resist Updat.* (2002) 5:65–72. doi: 10.1016/S1368-7646(02)00049-3
9. Altieri DC. Survivin, cancer networks and pathway-directed drug discovery. *Nat Rev Cancer.* (2008) 8:61–70. doi: 10.1038/nrc2293
10. Piska K, Gunia-Krzyzak A, Koczurkiewicz P, Wojcik-Pszczola K, Pekala E. Piperlongumine (piplartine) as a lead compound for anticancer agents - synthesis and properties of analogues: a mini-review. *Eur J Med Chem.* (2018) 156:13–20. doi: 10.1016/j.ejmech.2018.06.057
11. Gong LH, Chen XX, Wang H, Jiang QW, Pan SS, Qiu JG, et al. Piperlongumine induces apoptosis and synergizes with cisplatin or paclitaxel in human ovarian cancer cells. *Oxid Med Cell Longev.* (2014) 2014:906804. doi: 10.1155/2014/906804
12. Fruehauf JP, Meyskens FL Jr. Reactive oxygen species: a breath of life or death? *Clin Cancer Res.* (2007) 13:789–94. doi: 10.1158/1078-0432.CCR-06-2082
13. Lv M, Qiu JG, Zhang WJ, Jiang QW, Qin WM, Yang Y, et al. Wallichinine reverses ABCB1-mediated cancer multidrug resistance. *Am J Transl Res.* (2016) 8:2969–80.
14. Chen X, Gong L, Ou R, Zheng Z, Chen J, Xie F, et al. Sequential combination therapy of ovarian cancer with cisplatin and gamma-secretase inhibitor MK-0752. *Gynecol Oncol.* (2016) 140:537–44. doi: 10.1016/j.ygyno.2015.12.011
15. Li P, Yang Y, Liu H, Yang AK, Di JM, Tan GM, et al. MiR-194 functions as a tumor suppressor in laryngeal squamous cell carcinoma by targeting Wee1. *J Hematol Oncol.* (2017) 10:32. doi: 10.1186/s13045-017-0402-6
16. Yang Y, Guan D, Lei L, Lu J, Liu JQ, Yang G, et al. H6, a novel hederagenin derivative, reverses multidrug resistance *in vitro* and *in vivo*. *Toxicol Appl Pharmacol.* (2018) 341:98–105. doi: 10.1016/j.taap.2018.01.015
17. Huang SZ, Wei MN, Huang JR, Zhang ZJ, Zhang WJ, Jiang QW, et al. Targeting TF-AKT/ERK-EGFR pathway suppresses the growth of hepatocellular carcinoma. *Front Oncol.* (2019) 9:150. doi: 10.3389/fonc.2019.00150
18. Wang K, Xing ZH, Jiang QW, Yang Y, Huang JR, Yuan ML, et al. Targeting uPAR by CRISPR/Cas9 system attenuates cancer malignancy and multidrug resistance. *Front Oncol.* (2019) 9:80. doi: 10.3389/fonc.2019.00080
19. Lv G, Sun D, Zhang J, Xie X, Wu X, Fang W, et al. Lx2-32c, a novel semi-synthetic taxane, exerts antitumor activity against prostate cancer cells *in vitro* and *in vivo*. *Acta Pharm Sin B.* (2017) 7:52–8. doi: 10.1016/j.apsb.2016.06.005
20. Xu LN, Zhao N, Chen JY, Ye PP, Nan XW, Zhou HH, et al. Celastrol inhibits the growth of ovarian cancer cells *in vitro* and *in vivo*. *Front Oncol.* (2019) 9:2. doi: 10.3389/fonc.2019.00002
21. Zheng DW, Xue YQ, Li Y, Di JM, Qiu JG, Zhang WJ, et al. Volasertib suppresses the growth of human hepatocellular carcinoma *in vitro* and *in vivo*. *Am J Cancer Res.* (2016) 6:2476–88.
22. Mei XL, Yang Y, Zhang YJ, Li Y, Zhao JM, Qiu JG, et al. Sildenafil inhibits the growth of human colorectal cancer *in vitro* and *in vivo*. *Am J Cancer Res.* (2015) 5:3311–24.
23. Kim E, Park S, Lee JH, Mun JY, Choi WH, Yun Y, et al. Dual function of USP14 deubiquitinase in cellular proteasomal activity and autophagic flux. *Cell Rep.* (2018) 24:732–43. doi: 10.1016/j.celrep.2018.06.058
24. Raj L, Ide T, Gurkar AU, Foley M, Schenone M, Li X, et al. Selective killing of cancer cells by a small molecule targeting the stress response to ROS. *Nature.* (2011) 475:231–4. doi: 10.1038/nature10167
25. Marth C, Reimer D, Zeimet AG. Front-line therapy of advanced epithelial ovarian cancer: standard treatment. *Ann Oncol.* (2017) 28:viii36–9. doi: 10.1093/annonc/mdx450
26. Armbruster S, Coleman RL, Rauh-Hain JA. Management and treatment of recurrent epithelial ovarian cancer. *Hematol Oncol Clin North Am.* (2018) 32:965–82. doi: 10.1016/j.hoc.2018.07.005
27. Vergote I, Trope CG, Amant F, Kristensen GB, Ehlen T, Johnson N, et al. Neoadjuvant chemotherapy or primary surgery in stage IIIC or IV ovarian cancer. *N Engl J Med.* (2010) 363:943–53. doi: 10.1056/NEJMoa0908806
28. Brany D, Dvorska D, Slavik P, Skolka R, Adamkov M. Survivin and gynaecological tumours. *Pathol Res Pract.* (2017) 213:295–300. doi: 10.1016/j.prp.2017.02.009
29. Du J, Li B, Fang Y, Liu Y, Wang Y, Li J, et al. Overexpression of Class III beta-tubulin, Sox2, and nuclear Survivin is predictive of taxane resistance in patients with stage III ovarian epithelial cancer. *BMC Cancer.* (2015) 15:536. doi: 10.1186/s12885-015-1553-x
30. Zaffaroni N, Pennati M, Colella G, Perego P, Supino R, Gatti L, et al. Expression of the anti-apoptotic gene survivin correlates with taxol resistance in human ovarian cancer. *Cell Mol Life Sci.* (2002) 59:1406–12. doi: 10.1007/s00018-002-8518-3
31. Kar R, Palanichamy JK, Banerjee A, Chattopadhyay P, Jain SK, Singh N. Survivin siRNA increases sensitivity of primary cultures of ovarian cancer cells to paclitaxel. *Clin Transl Oncol.* (2015) 17:737–42. doi: 10.1007/s12094-015-1302-2
32. Jaiswal PK, Goel A, Mittal RD. Survivin: a molecular biomarker in cancer. *Indian J Med Res.* (2015) 141:389–97. doi: 10.4103/0971-5916.159250
33. Li F, Aljahdali I, Ling X. Cancer therapeutics using survivin BIRC5 as a target: what can we do after over two decades of study? *J Exp Clin Cancer Res.* (2019) 38:368. doi: 10.1186/s13046-019-1362-1
34. Arora V, Cheung HH, Plenchette S, Micali OC, Liston P, Korneluk RG. Degradation of survivin by the X-linked inhibitor of apoptosis (XIAP)-XAF1 complex. *J Biol Chem.* (2007) 282:26202–9. doi: 10.1074/jbc.M700776200
35. Ju JH, Yang W, Oh S, Nam K, Lee KM, Noh DY, et al. HER2 stabilizes survivin while concomitantly down-regulating survivin gene transcription by suppressing Notch cleavage. *Biochem J.* (2013) 451:123–34. doi: 10.1042/BJ20121716
36. Liu Y, Lear T, Iannone O, Shiva S, Corey C, Rajbhandari S, et al. The proapoptotic F-box protein Fbxl7 regulates mitochondrial function by mediating the ubiquitylation and proteasomal degradation of survivin. *J Biol Chem.* (2015) 290:11843–52. doi: 10.1074/jbc.M114.629931
37. Kamran M, Long ZJ, Xu D, Lv SS, Liu B, Wang CL, et al. Aurora kinase A regulates Survivin stability through targeting FBXL7 in gastric cancer drug resistance and prognosis. *Oncogenesis.* (2017) 6:e298. doi: 10.1038/oncsis.2016.80
38. Chen H, Yang F, Li X, Gong ZJ, Wang LW. Long noncoding RNA LNC473 inhibits the ubiquitination of survivin via association with USP9X and enhances cell proliferation and invasion in hepatocellular carcinoma cells. *Biochem Biophys Res Commun.* (2018) 499:702–10. doi: 10.1016/j.bbrc.2018.03.215
39. Li Z, Pei XH, Yan J, Yan F, Cappell KM, Whitehurst AW, et al. CUL9 mediates the functions of the 3M complex and ubiquitylates survivin to maintain genome integrity. *Mol Cell.* (2014) 54:805–19. doi: 10.1016/j.molcel.2014.03.046
40. Dong D, Jiang W, Lei J, Chen L, Liu X, Ge J, et al. Ubiquitin-like protein FAT10 promotes bladder cancer progression by stabilizing survivin. *Oncotarget.* (2016) 7:81463–73. doi: 10.18632/oncotarget.12976
41. de Souza HS, West GA, Rebert N, de la Motte C, Drazba J, Fiocchi C. Increased levels of survivin, via association with heat shock protein 90, in mucosal T cells from patients with Crohn's disease. *Gastroenterology.* (2012) 143:1017–26.e9. doi: 10.1053/j.gastro.2012.06.039

42. Li J, Li Y, Wang B, Ma Y, Chen P. CSN5/Jab1 facilitates non-small cell lung cancer cell growth through stabilizing survivin. *Biochem Biophys Res Commun.* (2018) 500:132–38. doi: 10.1016/j.bbrc.2018.03.183
43. Khan Z, Khan AA, Yadav H, Prasad G, Bisen PS. Survivin, a molecular target for therapeutic interventions in squamous cell carcinoma. *Cell Mol Biol Lett.* (2017) 22:8. doi: 10.1186/s11658-017-0038-0
44. Bezerra DP, Pessoa C, de Moraes MO, Saker-Neto N, Silveira ER, Costa-Lotufo LV. Overview of the therapeutic potential of piplartine (piperlongumine). *Eur J Pharm Sci.* (2013) 48:453–63. doi: 10.1016/j.ejps.2012.12.003
45. Karki K, Hedrick E, Kasiappan R, Jin UH, Safe S. Piperlongumine induces reactive oxygen species (ROS)-dependentdownregulation of specificity protein transcription factors. *Cancer Prev Res.* (2017) 10:467–77. doi: 10.1158/1940-6207.CAPR-17-0053

Conflict of Interest: The authors declare that the research was conducted in the absence of any commercial or financial relationships that could be construed as a potential conflict of interest.

frontiers in Oncology

ORIGINAL RESEARCH
published: 29 November 2019
doi: 10.3389/fonc.2019.01242

MiR-204-3p Inhibited the Proliferation of Bladder Cancer Cells via Modulating Lactate Dehydrogenase-Mediated Glycolysis

Jinan Guo[1,2], Pan Zhao[2,3], Zengqin Liu[2,3], Zaishang Li[1,2], Yeqing Yuan[1,2], Xueqi Zhang[1,2], Zhou Yu[1,2], Jiequn Fang[1,2] and Kefeng Xiao[1,2]**

[1] Department of Urology, Shenzhen Urology Minimally Invasive Engineering Center, The Second Clinical Medical College of Jinan University, Shenzhen People's Hospital, The First Affiliated Hospital of South University of Science and Technology of China, Shenzhen, China, [2] Shenzhen Public Service Platform on Tumor Precision Medicine and Molecular Diagnosis, Shenzhen Urology Minimally Invasive Engineering Center, The Second Clinical Medical College of Jinan University, Shenzhen People's Hospital, The First Affiliated Hospital of South University of Science and Technology of China, Shenzhen, China, [3] Clinical Medical Research Center, Shenzhen Urology Minimally Invasive Engineering Center, The Second Clinical Medical School of Jinan University, Shenzhen People's Hospital, The First Affiliated Hospital of South University of Science and Technology of China, Shenzhen, China

OPEN ACCESS

Edited by:
Chang Zou,
Shenzhen People's Hospital, China

Reviewed by:
Jianqing Ruan,
Soochow University Medical College, China
Yan Deng,
The Chinese University of Hong Kong, China
Jigang Wang,
China Academy of Chinese Medical Sciences, China

***Correspondence:**
Jiequn Fang
sz2011@sohu.com
Kefeng Xiao
xiao.kefeng@szhospital.com

Specialty section:
This article was submitted to Molecular and Cellular Oncology, a section of the journal Frontiers in Oncology

Received: 16 August 2019
Accepted: 29 October 2019
Published: 29 November 2019

Citation:
Guo J, Zhao P, Liu Z, Li Z, Yuan Y, Zhang X, Yu Z, Fang J and Xiao K (2019) MiR-204-3p Inhibited the Proliferation of Bladder Cancer Cells via Modulating Lactate Dehydrogenase-Mediated Glycolysis. Front. Oncol. 9:1242. doi: 10.3389/fonc.2019.01242

MicroRNAs (miRNAs) are endogenous non-coding RNAs that negatively regulate the expression of downstream targeted mRNAs. Increasing evidence has suggested that miRNAs act as tumor suppressors or oncogenes to interfere the progression of cancers. Here, we showed that miR-204-3p was decreased in bladder cancer tissues and cell lines. Down-regulation of miR-204-3p was significantly associated with a poor prognosis in bladder cancer patients. Overexpression of miR-204-3p inhibited proliferation and induced apoptosis in bladder cancer cells. Furthermore, miR-204-3p was found to bind to the 3′-untranslated region (UTR) of the lactate dehydrogenase (LDHA), which consequently reduced the expression of both mRNA and protein of LDHA. Interestingly, overexpression of miR-204-3p decreased glucose consumption and lactate production of bladder cancer cells. Overexpression of LDHA relieved the growth inhibition and cell apoptosis enhancement by miR-204-3p in bladder cancer cells. These results demonstrated that miR-204-3p negatively modulated the proliferation of bladder cancer cells via targeting LDHA-mediated glycolysis. MiR-204-3p might be a promising candidate for designing anticancer medication.

Keywords: bladder cancer, miR-204-3p, lactate dehydrogenase, glycolysis, proliferation

INTRODUCTION

Bladder cancer (BC) is one of the most common malignancies in the urological system (1). There are approximately 356,000 new cases and 145,000 deaths annually around the world (1–3). The high occurrence and mortality of BC make it a big threat to the health of patients. Although remarkable progress has been made in the treatment of BC including surgical resection and chemotherapy, the 5-year overall survival of BC remains poor (4, 5). Therefore, it is urgent to identify novel biomarkers and targets of BC.

MicroRNAs (miRNAs) are a class of single-stranded non-coding RNAs with the length of 22–24 nucleotides (6, 7). MiRNAs negatively regulate the gene expression via binding with the 3′-untranslated region (UTR) of targets, which leads to the degradation or translation inhibition of mRNAs (8). MiRNAs are reported to be involved in both physiological and pathological conditions including cell proliferation, differentiation, and apoptosis (9, 10). Recent research found that aberrant expression of miRNAs was associated with the tumorigenesis of BCs (9–12). Therefore, detecting the abundance of miRNA might provide novel evidence for the diagnosis of BC and benefit the outcome of cancer patients. To get a whole picture about the expression of miRNAs in BC, we reviewed the previous publications relevant to the altered miRNAs in BC and performed a meta-analysis. The data showed that miR-204-3p was significantly down-regulated in the urine supernatant of BC patients (13). Interestingly, miR-204-3p was frequently found to be down-regulated in cancers, which acted as a tumor suppressor in tumorigenesis (14). Abnormal expression of miR-204-3p was observed in gastrointestinal stromal tumors, breast cancer, and hepatocellular carcinoma (HCC) (15, 16). However, the expression and function of miR-204-3p in BC remain largely unknown.

Aerobic glycolysis has been considered as a distinct hallmark of cancer cells, which represents that cancer cells addictively depend on glycolysis to metabolize glucose even in oxygen-rich condition (17–19). Therefore, understanding the mechanisms that contribute to the glycolysis process will provide novel cues for therapeutic strategies for cancer treatment. The lactate dehydrogenase (LDHA) is a critical enzyme of the glycolysis, which catalyzes the production of lactate (20). Up-regulation of LDHA has been found in a variety of human cancers, which is associated with cell growth, metastasis, and poor prognosis of cancer patients (21–24). Notably, miRNAs are reported to target LDHA and negatively regulate the expression of LDHA. For example, repression of LDHA by miR-34a inhibited the glycolysis and suppressed the growth of breast cancer cells (20). Recent study showed that miR-142-3p targeted LDHA, which reduced the glycolysis and growth of HCC cells (25). These reports suggest that the negative modulation of LDHA by miRNA is an important strategy to regulate the progression of cancers.

In this study, we investigated the function of miR-204-3p in BC. The data showed that miR-204-3p was down-regulated in BC tissues and cell lines. Overexpression of miR-204-3p decreased the proliferation of BC cells via modulating LDHA-mediated glycolysis.

MATERIALS AND METHODS

Meta-Analysis

The studies that reported the alternation of miRNAs in BCs was searched using the National Center for Biotechnology Information (NCBI) Gene Expression Omnibus (GEO) and EBI ArrayExpress databases with the keywords "human" and "bladder" and "miRNA." For a meta-analysis, priority was given to the peer-reviewed publications that investigated the expression of miRNAs in both the BC and corresponding normal controls. For the studies without data of control group, only cell-culture-based results were excluded. Data extraction from the selected publications contained the first author's name, publication time, sample size, patient's age, type of case, origin of the studied population, tumor stage, detection method, and cutoff values for down-regulation or up-regulation. The quality of the publications was evaluated by the Newcastle-Ottawa scale, which was generally used for assessing the quality of non-randomized studies in meta-analyses. Each article was subjected to assessment with eight methodology items with the score ranging from 0 to 9. The higher score indicated better quality of the publication. The articles with score of 7 or more were recruited for the meta-analysis.

Clinical Samples and Cell Lines

A total of 60 paired BC and adjacent normal tissues were obtained from the BC patients who underwent surgery in the Shenzhen People's Hospital. The tissues were confirmed by three pathologists independently. None of the patients received radiotherapy or chemotherapy before the surgical resection. All the tissues were maintained in liquid nitrogen until use. All the experimental procedures were approved by the Research Ethics Committee of Shenzhen People's Hospital, and each patient signed the written informed consent.

The normal human urothelial SV-HUC-1 cells were purchased from the Institute of Cell Research, Chinese Academy of Sciences (Shanghai, China). BC cell lines including SW780, J82, UMUC3, 5637, and T24 were purchased from the American Type Culture Collection (ATCC, Rockville, MD, USA). Cells were cultured in Roswell Park Memorial Institute (RPMI)-1640 medium (Gibco, Thermo Fisher Scientific, Carlsbad, CA, USA) supplemented with 10% fetal bovine serum (FBS; Sigma-Aldrich, St. Louis, MO, USA), 100 U/ml of penicillin and 100 mg/ml of streptomycin (Invitrogen, Carlsbad, CA, USA) at 37°C with 5% CO_2.

Reverse Transcriptase Quantitative PCR Analysis

MiRNAs were extracted from the cell lines or bladder tissues using the miRNeasy Mini Kit (QIAGEN, Hilden, Germany) according to the manufacturer's instruction; 0.5 μg of RNA was reversely transcripted into cDNA with the PrimeScript RT Master Mix (Takara, Dalian, China). Real-time PCR analysis was performed with the SYBR Select Master Mix (Takara, Dalian, China) on the ABI7500 platform (Applied Biosystems, Foster City, CA, USA). The expression of U6 RNA and GAPDH was detected as the respective endogenous control. The expression level of miR-204-3p and LDHA was normalized to U6 and GAPDH and calculated using the $2^{-\Delta\Delta CT}$ method. The primers were as follows: miR-204-3p, F, 5′-ACACTCCAGCTG GGGCTGGGAAGGCAAAGGG-3′ and R, 5′-CTCAACTGG TGTCGTGGA-3′; LDHA, F, 5′-AGCCCGATTCCGTTACCT-3′ and R, 5′-CACCAGCAACATTCATTCCA-3′; U6, F, 5′-CTC GCTTCGGCAGCACA-3′ and R, 5′-AACGCTTCACGAATT TGCGT-3′; and GAPDH, F, 5′-TGACGCTGGGGCTGGCAT TG-3′ and R, 5′-GCTCTTGCTGGGGCTGGTGG-3′.

Cell Viability

The proliferation of BC cells with the transfection of control miRNA or miR-204-3p mimics was evaluated by the Cell Counting Kit-8 assay (CCK-8, Beyotime, Shanghai, China). Briefly, 10 μl of CCK-8 reagent was added into the medium at the indicated time points of 1, 2, 3, 4, and 5 days and incubated for 4 h at 37°C. The absorbance value (optical density [OD]) of each well at 450 nm was detected with a microplate reader (Bio-Rad, CA, USA). The results were obtained from three independent experiments.

Cell Colony Formation

The BC cells expressing the indicated miRNA were seeded in a 6-well plate with the density of 1,000 cells per well. Cells were cultured with the RPMI-1640 medium for 2 weeks. And then the medium was discarded, and the cells were washed twice with phosphate-buffered saline (PBS). Cells were fixed with methanol for 15 min at room temperature (RT). After being washed with PBS, the colonies were stained with 1% crystal violet, and the number of colonies was counted with light microscopy.

Western Blot

Protein was extracted from the BC cells with the NP-40 lysis buffer (150 mM of NaCl, 1% NP-40, 50 mM of Tris–HCl (pH 8.0), and 1 mM of EDTA) in the presence of proteinase inhibitor (Millipore, Braunschweig, Germany). The protein concentration was evaluated using the bicinchoninic acid (BCA) assay kit (Beyotime, Shanghai, China); 15 μg of proteins was loaded and separated by the 15% sodium dodecyl sulfate–polyacrylamide gel electrophoresis (SDS-PAGE) and then transferred onto the polyvinylidene difluoride (PVDF) membrane (Millipore, Braunschweig, Germany). The membrane was firstly blocked with 5% non-fat milk at RT for 1 h, followed by incubation with primary antibodies at RT for 2 h and by incubation of the membrane with goat anti-mouse IgG secondary antibody (1:3,000, Bio-Rad, CA, USA), and then analyzed using the chemiluminescent horseradish peroxidase (HRP) conjugated substrate (Millipore, Braunschweig, Germany). GAPDH was used as the loading control. Antibodies including anti-LDHA (#2012, 1:3,000, Cell Signaling Technology, Inc., Danvers, MA, USA) and anti-GAPDH (#5174, 1:3,000, Cell Signaling Technology, Inc., Danvers, MA, USA) were commercially obtained.

Luciferase Reporter Assay

The wild-type (WT) or mutant (MUT) 3′-UTR of LDHA containing the putative binding sites of miR-204-3p was inserted into the pmiR-GLO vector. BC cells were transfected with the control miRNA or miR-204-3p mimics in the presence of luciferase reporter vector. After transfection for 48 h, cells were harvested, and the luciferase activity was determined with the dual-luciferase reporter system (Promega, Madison, WI, USA). The experiment was performed in triplicate.

Measurement of the Glucose Consumption and Lactate Production

BC cells transfected with the corresponding miRNAs were cultured in RPMI-1640 medium without phenol red (Gibco, New York, NY, USA) for 24 h, and then the medium was collected. The glucose consumption and lactate production were determined using the Glucose Assay Kit (GAHK20-1KT; Sigma-Aldrich, USA) and Lactate Assay Kit (BioVision, CA, USA) according to manufacturers' instructions, respectively. The protein level in each group was measured using the BCA assay kit (Beyotime, Shanghai, China) for the normalization.

Statistical Analysis

Results were presented as mean ± standard deviation from three independent experiments. The data were analyzed with the SPSS 19.0 software (SPSS Inc., Chicago, IL, USA). Significant differences between/among treatment groups were analyzed using unpaired Student's *t*-test or one-way ANOVA followed by Dunnett's *post hoc* test. $P < 0.05$ was considered to be statistically significant.

RESULTS

MiR-204-3p Was Down-Regulated in Bladder Cancer Tissues and Cell Lines

To obtain a whole picture of miRNA expression in BC, a miRNA meta-analysis was performed using previous publications. The data found that miR-204-3p was significantly aberrantly expressed in the urine supernatant of the BC patients (**Figure 1A**). To confirm this result, the expression of miR-204-3p was detected by reverse transcriptase quantitative PCR (RT-qPCR) with paired BC tissues and corresponding normal tissues. The result showed that the level of miR-204-3p was significantly decreased in BC tissues in comparison with that of the normal counterparts (**Figure 1B**). To further confirm the aberrant expression of miR-204-3p in BC, the abundance of miR-204-3p in several BC cell lines was examined. As indicated in **Figure 1C**, miR-204-3p was remarkably decreased in BC cells, compared with the normal cells, including SW780, J82, UMUC3, 5637, and T24. These results suggested the down-regulation of miR-204-3p in BC. To further characterize the association between miR-204-3p expression and the clinicopathological features, the abundance of miR-204-3p in BC patients with or without lymph node metastasis was compared. The data revealed that lower expression of miR-204-3p was correlated with positive lymph node metastasis (**Figure 1D**). Consistently, decreased expression of miR-204-3p was also observed in BC patients with larger tumor size (**Figure 1E**). These results demonstrated that miR-204-3p was down-regulated in BC and associated with a poor prognosis of cancer patients.

Overexpression of MiR-204-3p Inhibited the Proliferation and Induced Apoptosis of Bladder Cancer Cells

As miR-204-3p was decreased in BC, to investigate the effect of aberrant expression of miR-204-3p on the growth

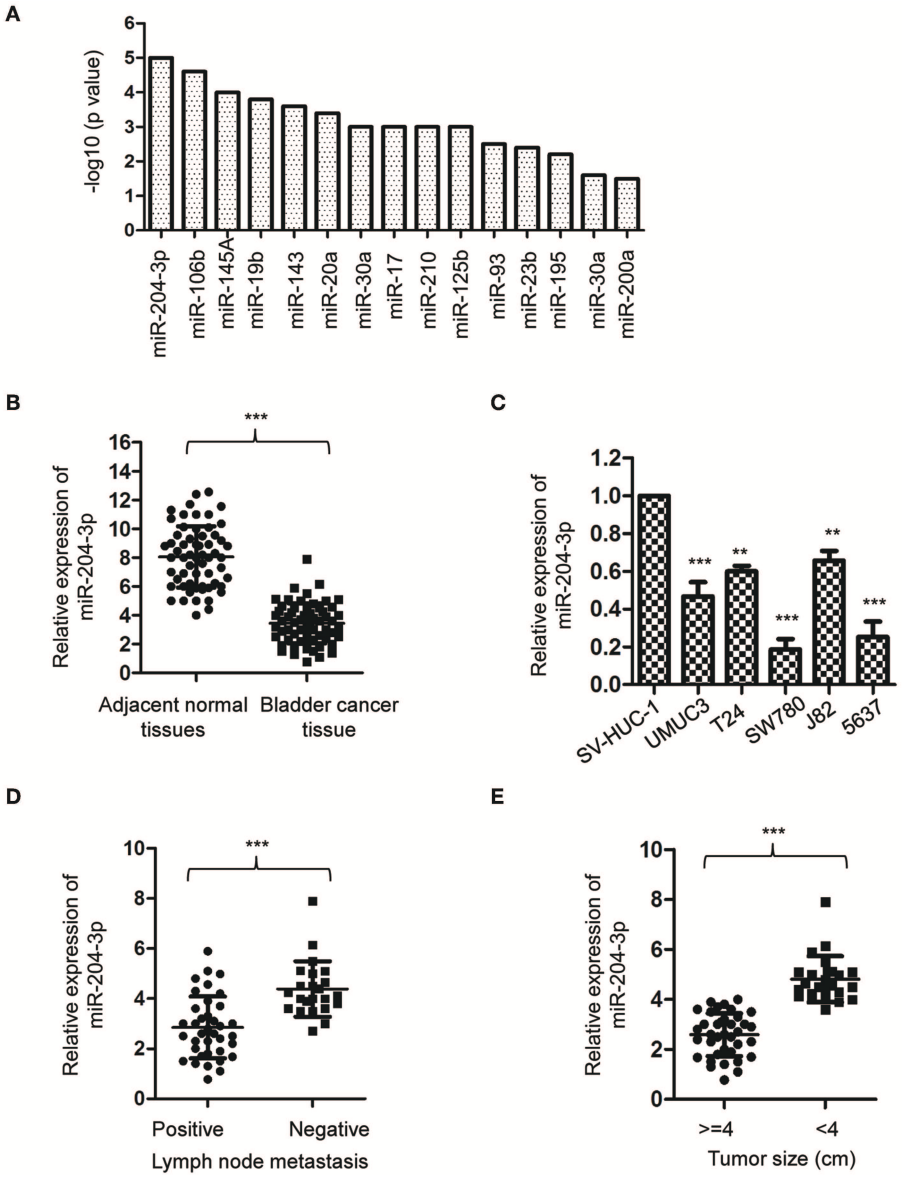

FIGURE 1 | MiR-204-3p was decreased in bladder cancer. **(A)** Meta-analysis on the aberrantly expressed miRNAs in bladder cancer patients. **(B)** The expression of miR-204-3p in 60 paired bladder cancer tissues and the corresponding adjacent normal tissues was determined by RT-qPCR. **(C)** The expression of miR-204-3p in bladder cancer cells and normal bladder epithelial cell SV-HUC-1 was determined by the RT-qPCR analysis. **(D)** The expression of miR-204-3p in the bladder cancer patients with or without lymph node metastasis was determined by RT-qPCR. **(E)** The expression of miR-204-3p in bladder cancer tissues stratified by tumor size was determined by RT-qPCR. $^{**}P < 0.01$ and $^{***}P < 0.001$. RT-qPCR, reverse transcriptase quantitative PCR.

of BC cells, SW780 and 5637, which harbored the lowest expression of miR-204-3p among all the cell lines we tested (**Figure 1C**), were transfected with miR-204-3p mimics to up-regulate the expression of miR-204-3p. The overexpression of miR-204-3p in both SW780 and 5637 cells was detected by RT-qPCR (**Figure 2A**). The influence of miR-204-3p on the proliferation of BC cells was determined by CCK-8 assay. As showed in **Figures 2B,C**, the growth of both SW780 and 5637 cells was significantly inhibited with overexpressed miR-204-3p. Consistently, the colony formation assay indicated that overexpression of miR-204-3p dramatically decreased the number of colonies compared with those of the control cells (**Figure 2D**). In addition, to further confirm the negative regulation of overexpressed miR-204-3p on the growth of BC cells, the apoptosis rate of both SW780 and 5637 cells was examined with the fluorescence-activated cell sorting (FACS) analysis. The result suggested that ectopic expression of miR-204-3p significantly enhanced the apoptosis of BC cells (**Figure 2E**). These data demonstrated that overexpression of miR-204-3p inhibited the growth of BC cells, which

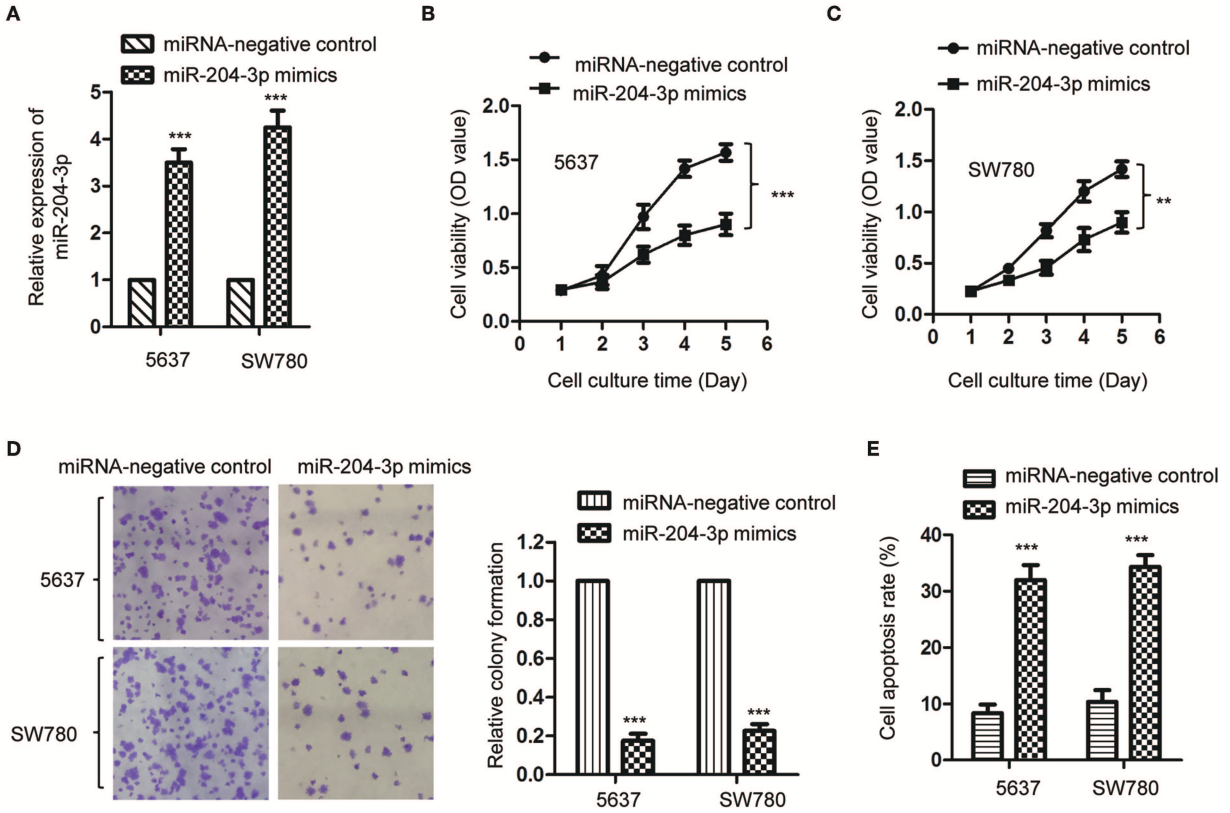

FIGURE 2 | Overexpression of miR-204-3p inhibited the proliferation of bladder cancer cells. **(A)** The expression of miR-204-3p in both SW780 and 5637 cells with the transfection of miR-204-3p mimics or control miRNA was validated by RT-qPCR. **(B,C)** The proliferation of cells with miR-204-3p mimics or control miRNA transfection was determined by CCK-8 assay. **(D)** Colony formation assay was performed in both SW780 and 5637 cells with the transfection of miR-204-3p mimics or control miRNA. **(E)** Flow cytometry was performed in both SW780 and 5637 cells with the transfection of miR-204-3p or control miRNA. $N = 3$; $^{**}P < 0.01$ and $^{***}P < 0.001$. RT-qPCR, reverse transcriptase quantitative PCR; CCK-8, Cell Counting Kit-8.

suggested the potential tumor suppressive function of miR-204-3p in BC.

Lactate Dehydrogenase Was a Target of MiR-204-3p in Bladder Cancer Cells

To further explore the underlying molecular mechanism by which miR-204-3p modulated the growth of BC cells, the targets of miR-204-3p were predicted using the miRDB database (http://mirdb.org). Among the candidates, LDHA was found as a possible target of miR-204-3p (**Figure 3A**). To confirm the potential binding between miR-204-3p with the LDHA 3′-UTR (position 515-521), the WT or MUT 3′-UTR of LDHA containing the putative binding sites of miR-204-3p was inserted into the pmiR-GLO vector. Luciferase reporter assay was performed by co-transfecting negative control miRNA or miR-204-3p mimics with WT or MUT 3′-UTR of LDHA. The results showed that overexpression of miR-204-3p significantly reduced the luciferase activity of the WT 3′-UTR of LDHA; however, no remarkable decrease was observed when cells were transfected with MUT 3′-UTR of LDHA (**Figures 3B,C**). This result indicated that miR-204-3p bound the 3′-UTR of LDHA.

To detect whether the binding of miR-204-3p at the 3′-UTR affected the mRNA stability of LDHA, both SW780 and 5637 cells were transfected with control miRNA or miR-204-3p mimics, and the mRNA level of LDHA was examined with the RT-qPCR assay. As shown in **Figure 3D**, overexpression of miR-204-3p significantly reduced the mRNA level of LDHA in BC cells. Additionally, the protein level of LDHA in SW780 and 5637 cells expressing miR-204-3p was also investigated by Western blot using the anti-LDHA antibody. The data showed that the level of LDHA was down-regulated with the transfection of miR-204-3p in SW780 and 5637 cells (**Figure 3E**). These results demonstrated that LDHA was a target of miR-204-3p and negatively regulated by miR-204-3p in BC cells.

MiR-204-3p Suppressed the Glycolysis of Bladder Cancer Cells by Modulating Lactate Dehydrogenase

LDHA was critical for the glucose metabolism of cancer cells. Considering the negative regulation of miR-204-3p on the expression of LDHA, the influence of miR-204-3p on the glycolysis of BC cells was determined by measuring the glucose consumption and lactate production. The results showed that overexpression of miR-204-3p significantly decreased the glucose uptake of SW780 and 5637 cells (**Figure 4A**). Consistently, the generation of lactate of BC cells was also dramatically reduced

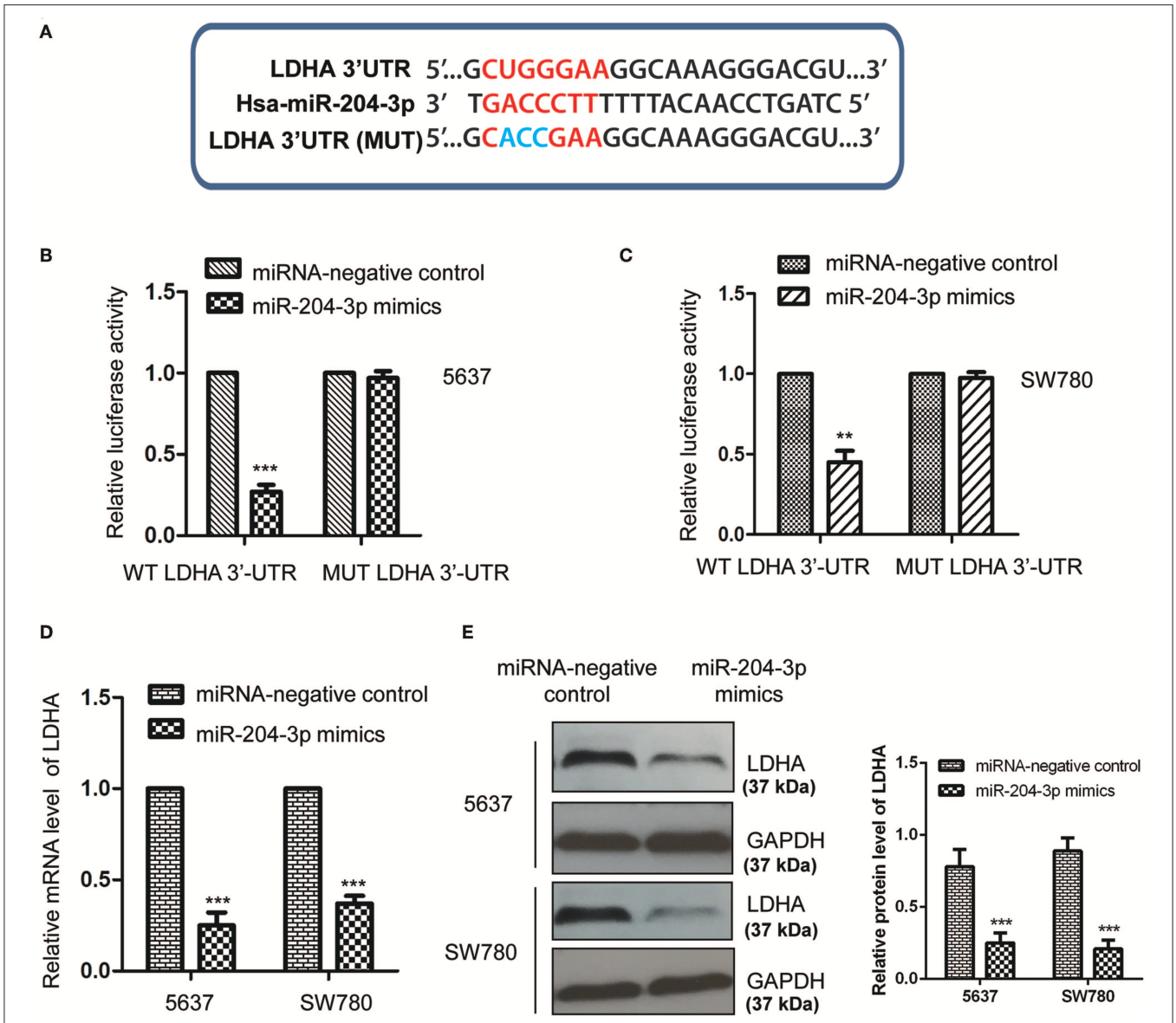

FIGURE 3 | MiR-204-3p targeted LDHA in bladder cancer cells. **(A)** The complementary sequences in the 3′-UTR of LDHA and miR-204-3p. **(B,C)** The effects of miR-204-3p on the luciferase activity of wild-type or mutant LDHA 3′-UTR were determined by luciferase reporter assay. **(D,E)** The effects of miR-204-3p overexpression on the mRNA and protein levels of LDHA in both SW780 and 5637 cells were validated by RT-qPCR and western blot assay, respectively. $N = 3$; $^{**}P < 0.01$ and $^{***}P < 0.001$. LDHA, lactate dehydrogenase; UTR, untranslated region; RT-qPCR, reverse transcriptase quantitative PCR.

in the presence of high level of miR-204-3p (**Figure 4B**). To further confirm these results, miR-204-3p was knocked down in SW780 and 5637 cells by transfecting miR-204-3p antagomir. The reduction of miR-204-3p was verified by RT-qPCR assay (**Figure 4C**). The glycolysis of BC cells harboring depleted miR-204-3p was explored. As shown in **Figure 4D**, down-regulation of miR-204-3p remarkably elevated the glucose consumption of both SW780 and 5637 cells. Increased lactate production was also obtained with the decreased expression of miR-204-3p (**Figure 4E**). These results indicated that miR-204-3p was a negative regulator of the glycolysis of BC cells.

To further investigate whether the inhibitory effect of miR-204-3p on the proliferation of BC cells was achieved via LDHA, CCK-8 assay was performed by transfecting LDHA in miR-204-3p overexpressed cells. The results showed that highly expressed miR-204-3p suppressed the proliferation and growth and induced cell apoptosis of both SW780 and 5637 cells, while rescue the expression of LDHA attenuated the inhibitory effect of miR-204-3p on the proliferation growth of BC cells and the enhanced effect of miR-204-3p on the cell apoptosis of BC cells (**Figures 4F–I**). These data demonstrated that miR-204-3p decreased the expression of LDHA, inhibited the glycolysis, and suppressed the growth of BC cells.

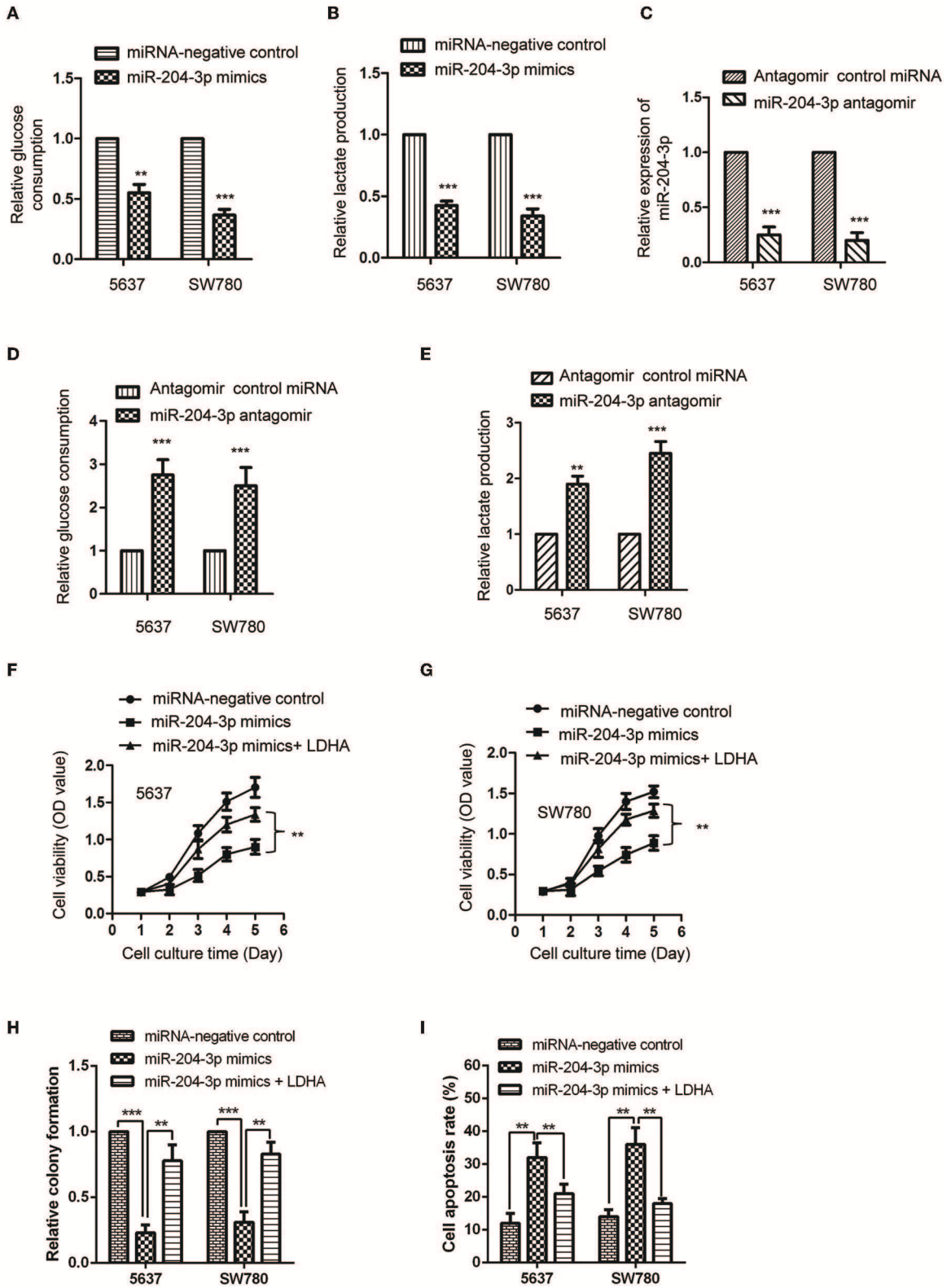

FIGURE 4 | MiR-204-3p modulated the glycolysis of bladder cancer cells. **(A,B)** SW780 and 5637 cells were transfected with control miRNA or miR-204-3p mimics, and the glucose consumption and lactate production were measured. **(C)** The expression of miR-204-3p in SW780 and 5637 cells with antagomir control miRNA or

(Continued)

FIGURE 4 | miR-204-3p antagomir transfection was determined by the RT-qPCR. **(D,E)** The effects of miR-204-3p knockdown on the glucose uptake and lactate generation ofthe SW780 and 5637 cells were determined by Glucose Assay Kit and Lactate Assay Kit, respectively. **(F,G)** The cell viability of SW780 and 5637 with co-transfection with miRNAs and plasmid vectors was determined by CCK-8 assay. **(H)** The cell growth of SW780 and 5637 with co-transfection with miRNAs and plasmid vectors was determined by colony formation assay. **(I)** The cell apoptosis of SW780 and 5637 cells with co-transfection with miRNA and plasmid vectors was evaluated by flow cytometry. $N = 3$; $^{**}P < 0.01$ and $^{***}P < 0.001$. RT-qPCR, reverse transcriptase quantitative PCR; CCK-8, Cell Counting Kit-8.

DISCUSSION

Although remarkable progression has been made in the treatment of BC with the application of surgery and chemotherapy, the prognosis of BC is still poor. Moreover, most patients are diagnosed at the advanced stage and showed unsatisfactory response to treatments. Notably, increasing evidence has suggested the critical roles of miRNAs in the initiation and progression of cancers (9–11). Here, we showed that miR-204-3p was decreased in both BC tissues and cell lines, which was associated with the poor prognosis of BC patients. Further gain-of-function analysis demonstrated that overexpression of miR-204-3p suppressed the growth of BC cells, which suggested the potential suppressive function of miR-204-3p in modulating the progression of BC.

The involvement of miR-204-3p in cancer has been highlighted by the studies that aberrant expression of miR-204-3p can be used to distinguish the malignant progression in gastric cancer (16) and breast cancer (26). Significant decrease of miR-204-3p was observed in HCC, which suppressed the growth of HCC via targeting fibronectin 1 (15). Recent study by Chen et al. showed that xanthohumol, a prenylated chalcone potential for anticancer therapy, up-regulated the expression of miR-204-3p in glioma cells and induced the cell apoptosis through modulating the insulin-like growth factor (IGF)-binding protein (27). In clear cell renal cell carcinoma (ccRCC), miR-204-3p was found to be down-regulated by the ERβ-suppressed circular RNA ATP2B1, which increased the expression of fibronectin 1 and promoted the invasion of ccRCC cells (28). These findings suggested the potential tumor suppressive function of miR-204-3p in cancers. In the present study, our data revealed that miR-204-3p was decreased in BC tissues compared with the normal tissue. Down-regulation of miR-204-3p was correlated with lymph node metastasis and larger tumor size. Further investigation might be of interest to explore the relationship between the expression of miR-204-3p with the 5-year overall survival of BC patients. Consistent with the decreased level of miR-204-3p in BC, overexpression of miR-204-3p significantly suppressed the proliferation and induced apoptosis of BC cells. *In vivo* tumorigenesis assay might be necessary to further confirm the modulating of miR-204-3p on the growth of BC cells in the future study.

The function of miRNAs was achieved via regulating the expression of downstream targets. In this study, the possible targets of miR-204-3p were predicted with the bioinformatics, and LDHA was identified as one of the binding partners of miR-204-3p. Overexpression of miR-204-3p significantly decreased both the mRNA and protein levels of LDHA in BC cells. Consistently, overexpression of miR-204-3p reduced the glucose consumption and lactate production of BC cells. LDHA deficiency results in a decrease in lactate production accompanied by inhibition of cell migration and invasion. Therefore, LDHA has been the target of different miRNAs in cancer cells to regulate the tumorigenesis. Among them, miR-142-3p was reported to target LDHA and inhibited the aerobic glycolysis of HCC (25). In breast cancer, miR-30-5p inhibited the cell growth and metastasis through suppression of LDHA-mediated glucose metabolism (29). These results collectively demonstrated that reprograming the glycolysis via targeting LDHA has been a promising way to modulate the progression of cancers.

Our study still presented several limitations. Firstly, the relationship between miR-204-3p and the overall survival of the BC patients has not been determined in the study, which needs further examination. Secondly, the present study lacks the *in vivo* animal studies, and the effects of miR-203-3p on the *in vivo* BC growth should be considered in future studies. Thirdly, the targets of miR-204-3p were not limited to LDHA, and other potential targets may be explored in future studies.

In conclusions, our results demonstrated that miR-204-3p was down-regulated in BC and correlated with the progression of the BC patients. Overexpression of miR-204-3p decreased the growth of BC cells via down-regulating LDHA, which consequently suppressed the glucose metabolism of BC cells. These data indicated that targeting the miR-204-3p-LDHA pathway might interfere with the tumorigenesis of cancer cells.

DATA AVAILABILITY STATEMENT

All datasets for this study are included in the article/supplementary material.

ETHICS STATEMENT

The studies involving human participants were reviewed and approved by the Institutional Review Board of Shenzhen people's Hospital. The patients/participants provided their written informed consent to participate in this study.

AUTHOR CONTRIBUTIONS

JG and KX designed the whole study. JG, PZ, ZLiu, and ZLi performed the experiments. YY, XZ, and ZY performed the statistical analysis. JF and KX drafted the manuscript.

FUNDING

This study was supported by the grants from Sanming Project of Medicine in Shenzhen (SZSM201412014),

the Science and Technology Foundation of Shenzhen (JCYJ20170307095620828 and JCYJ20160422145718224), and the Shenzhen Urology Minimally Invasive Engineering Center (GCZX2015043016165448). All sources of funding received for the research being submitted.

REFERENCES

1. Parkin DM, Bray F, Ferlay J, Pisani P. Global cancer statistics, 2002. *CA Cancer J Clin*. (2005) 55:74–108. doi: 10.3322/canjclin.55.2.74
2. Kim WJ, Bae SC. Molecular biomarkers in urothelial bladder cancer. *Cancer Sci*. (2008) 99:646–52. doi: 10.1111/j.1349-7006.2008.00735.x
3. Mcconkey DJ, Choi W, Ochoa A, Dinney CPN. Intrinsic subtypes and bladder cancer metastasis. *Asian J Urol*. (2016) 3:260–7. doi: 10.1016/j.ajur.2016.09.009
4. Kolodziej A, Krajewski W, Matuszewski M, Tupikowski K. Review of current optical diagnostic techniques for non-muscle-invasive bladder cancer. *Cent European J Urol*. (2016) 69:150–6. doi: 10.5173/ceju.2016.780
5. Uhlman MA, Bevill MD, Goodheart MJ, Brown JA, O'donnell MA. Bladder cancer will grow anywhere: report of a urothelial carcinoma drop metastasis to the vagina and literature review. *Can J Urol*. (2016) 23:8379–81.
6. Ambros V. The functions of animal microRNAs. *Nature*. (2004) 431:350–5. doi: 10.1038/nature02871
7. Bartel DP. MicroRNAs: genomics, biogenesis, mechanism, and function. *Cell*. (2004) 116:281–97. doi: 10.1016/S0092-8674(04)00045-5
8. Mohr AM, Mott JL. Overview of microRNA biology. *Semin Liver Dis*. (2015) 35:3–11. doi: 10.1055/s-0034-1397344
9. Kwak PB, Iwasaki S, Tomari Y. The microRNA pathway and cancer. *Cancer Sci*. (2010) 101:2309–15. doi: 10.1111/j.1349-7006.2010.01683.x
10. Farazi TA, Spitzer JI, Morozov P, Tuschl T. miRNAs in human cancer. *J Pathol*. (2011) 223:102–15. doi: 10.1002/path.2806
11. Qu H, Xu W, Huang Y, Yang S. Circulating miRNAs: promising biomarkers of human cancer. *Asian Pac J Cancer Prev*. (2011) 12:1117–25.
12. Gentilin E, Degli Uberti E, Zatelli MC. Strategies to use microRNAs as therapeutic targets. *Best Pract Res Clin Endocrinol Metab*. (2016) 30:629–39. doi: 10.1016/j.beem.2016.10.002
13. Pospisilova S, Pazourkova E, Horinek A, Brisuda A, Svobodova I, Soukup V, et al. MicroRNAs in urine supernatant as potential non-invasive markers for bladder cancer detection. *Neoplasma*. (2016) 63:799–808. doi: 10.4149/neo_2016_518
14. Imam JS, Plyler JR, Bansal H, Prajapati S, Bansal S, Rebeles J, et al. Genomic loss of tumor suppressor miRNA-204 promotes cancer cell migration and invasion by activating AKT/mTOR/Rac1 signaling and actin reorganization. *PLoS ONE*. (2012) 7:e52397. doi: 10.1371/journal.pone.0052397
15. Cui ZH, Shen SQ, Chen ZB, Hu C. Growth inhibition of hepatocellular carcinoma tumor endothelial cells by miR-204-3p and underlying mechanism. *World J Gastroenterol*. (2014) 20:5493–504. doi: 10.3748/wjg.v20.i18.5493
16. Tong HX, Zhou YH, Hou YY, Zhang Y, Huang Y, Xie B, et al. Expression profile of microRNAs in gastrointestinal stromal tumors revealed by high throughput quantitative RT-PCR microarray. *World J Gastroenterol*. (2015) 21:5843–55. doi: 10.3748/wjg.v21.i19.5843
17. Zheng J. Energy metabolism of cancer: glycolysis versus oxidative phosphorylation (Review). *Oncol Lett*. (2012) 4:1151–7. doi: 10.3892/ol.2012.928
18. Akram M. Mini-review on glycolysis and cancer. *J Cancer Educ*. (2013) 28:454–7. doi: 10.1007/s13187-013-0486-9
19. Li XB, Gu JD, Zhou QH. Review of aerobic glycolysis and its key enzymes - new targets for lung cancer therapy. *Thorac Cancer*. (2015) 6:17–24. doi: 10.1111/1759-7714.12148
20. Xiao X, Huang X, Ye F, Chen B, Song C, Wen J, et al. The miR-34a-LDHA axis regulates glucose metabolism and tumor growth in breast cancer. *Sci Rep*. (2016) 6:21735. doi: 10.1038/srep21735
21. Rong Y, Wu W, Ni X, Kuang T, Jin D, Wang D, et al. Lactate dehydrogenase A is overexpressed in pancreatic cancer and promotes the growth of pancreatic cancer cells. *Tumour Biol*. (2013) 34:1523–30. doi: 10.1007/s13277-013-0679-1
22. Yao F, Zhao T, Zhong C, Zhu J, Zhao H. LDHA is necessary for the tumorigenicity of esophageal squamous cell carcinoma. *Tumour Biol*. (2013) 34:25–31. doi: 10.1007/s13277-012-0506-0
23. Cui J, Shi M, Xie D, Wei D, Jia Z, Zheng S, et al. FOXM1 promotes the warburg effect and pancreatic cancer progression via transactivation of LDHA expression. *Clin Cancer Res*. (2014) 20:2595–606. doi: 10.1158/1078-0432.CCR-13-2407
24. Shi M, Cui J, Du J, Wei D, Jia Z, Zhang J, et al. A novel KLF4/LDHA signaling pathway regulates aerobic glycolysis in and progression of pancreatic cancer. *Clin Cancer Res*. (2014) 20:4370–80. doi: 10.1158/1078-0432.CCR-14-0186
25. Hua S, Liu C, Liu L, Wu D. miR-142-3p inhibits aerobic glycolysis and cell proliferation in hepatocellular carcinoma via targeting LDHA. *Biochem Biophys Res Commun*. (2018) 496:947–54. doi: 10.1016/j.bbrc.2018.01.112
26. Li JY, Jia S, Zhang WH, Zhang Y, Kang Y, Li PS. Differential distribution of microRNAs in breast cancer grouped by clinicopathological subtypes. *Asian Pac J Cancer Prev*. (2013) 14:3197–203. doi: 10.7314/APJCP.2013.14.5.3197
27. Chen PH, Chang CK, Shih CM, Cheng CH, Lin CW, Lee CC, et al. The miR-204-3p-targeted IGFBP2 pathway is involved in xanthohumol-induced glioma cell apoptotic death. *Neuropharmacology*. (2016) 110:362–75. doi: 10.1016/j.neuropharm.2016.07.038
28. Han Z, Zhang Y, Sun Y, Chen J, Chang C, Wang X, et al. ERbeta-Mediated Alteration of circATP2B1 and miR-204-3p signaling promotes invasion of clear cell renal cell carcinoma. *Cancer Res*. (2018) 78:2550–63. doi: 10.1158/0008-5472.CAN-17-1575
29. Li L, Kang L, Zhao W, Feng Y, Liu W, Wang T, et al. miR-30a-5p suppresses breast tumor growth and metastasis through inhibition of LDHA-mediated Warburg effect. *Cancer Lett*. (2017) 400:89–98. doi: 10.1016/j.canlet.2017.04.034

Conflict of Interest: The authors declare that the research was conducted in the absence of any commercial or financial relationships that could be construed as a potential conflict of interest.

frontiers in Oncology

ORIGINAL RESEARCH
published: 03 December 2019
doi: 10.3389/fonc.2019.01347

The Binding of PD-L1 and Akt Facilitates Glioma Cell Invasion Upon Starvation via Akt/Autophagy/F-Actin Signaling

Ruo Qiao Chen[1†], Xiao Hong Xu[2†], Feng Liu[2], Chun Yang Li[2], Yuan Jun Li[2], Xiang Rui Li[1], Guo Yong Jiang[1], Feng Hu[3], Di Liu[4], Feng Pan[4], Xin Yao Qiu[2*] and Xiao Qian Chen[2*]*

[1] School of Basic Medicine, Tongji Medical College, Huazhong University of Science and Technology, Wuhan, China, [2] Department of Pathophysiology, School of Basic Medicine, Tongji Medical College, Huazhong University of Science and Technology, Wuhan, China, [3] Department of Neurosurgery, Tongji Hospital, Tongji Medical College, Huazhong University of Science and Technology, Wuhan, China, [4] Department of Urology, Union Hospital, Tongji Medical College, Huazhong University of Science and Technology, Wuhan, China

OPEN ACCESS

Edited by:
Pascale Cohen,
Université Claude Bernard
Lyon 1, France

Reviewed by:
Anupam Mitra,
University of California, Davis,
United States
Jiajun Fan,
Fudan University, China

***Correspondence:**
Feng Pan
panfeng@hust.edu.cn
Xin Yao Qiu
qiu.xinyao1991@outlook.com
Xiao Qian Chen
chenxq@mails.tjmu.edu.cn

[†] These authors have contributed equally to this work

Specialty section:
This article was submitted to Molecular and Cellular Oncology, a section of the journal Frontiers in Oncology

Received: 06 August 2019
Accepted: 15 November 2019
Published: 03 December 2019

Citation:
Chen RQ, Xu XH, Liu F, Li CY, Li YJ, Li XR, Jiang GY, Hu F, Liu D, Pan F, Qiu XY and Chen XQ (2019) The Binding of PD-L1 and Akt Facilitates Glioma Cell Invasion Upon Starvation via Akt/Autophagy/F-Actin Signaling. Front. Oncol. 9:1347. doi: 10.3389/fonc.2019.01347

Glioma, especially glioblastoma, is pathologically characterized by high aggressiveness, which largely contributed to the ineffectiveness of current therapies. It has been recently reported that intrinsic PD-L1 can regulate tumor malignancy, whereas underlying mechanisms remain mostly unclear. Here, we report a novel mechanism by which PD-L1 promotes glioma cell infiltration. In orthotopic glioma models, PD-L1 expression was up-regulated predominantly in glioma cells in the infiltrating front. For PD-L1-overexpressed glioma cells, PI3K/Akt and actin regulations were among the top six most altered signaling pathways as detected by RNA-sequencing. PD-L1 significantly activated Akt/F-actin signaling while suppressed autophagic signaling upon cell starvation. Mechanistically, PD-L1 preferentially bound to Akt among various PI3K/Akt signaling proteins. Serial truncation identified the interaction between the 128-237aa fragment of PD-L1 and the 112-480aa fragment of Akt, which facilitates the membrane translocation/activation of Akt, and was unaffected by Perifosin (specific p-Akt inhibitor targeting Akt PH-domain). Taken together, our data indicate that in glioma cells, PD-L1 is induced to prevent autophagic cytoskeleton collapse via Akt binding/activation, facilitating glioma cell invasion upon starvation stress.

Keywords: glioblastoma multiforme, CD274, p62, autophagic influx, ischemia

INTRODUCTION

Glioma, the most common primary intracranial tumor, originates from various types of cells. The most malignant glioma is glioblastoma, or glioblastoma multiforme (GBM), which accounts for around 21% of glioma and can be primary or secondary from grade II-III glioma. Recently, glioma is also classified into three types based on its molecular markers: 1p/19q deletion, IDH mutation and TERT promoter mutation. Among them, grade IV glioma mainly has the TERT promoter mutation accompanied by EGFR/PTEN mutation. Current treatments for glioma remain conventional surgery, radiotherapy and chemotherapy. However, glioma is extremely easy to relapse after treatment, with an average survival time of only 14 months for GBM patients after treatment (1). It is urgent to find new and effective therapies in order to prolong the survival time of GBM patients.

The pathological features of GBM are necrosis, high invasiveness and microvascular hyperplasia (2), which are closely related to abnormal energy metabolism. It is generally considered that solid malignant tumors including glioma suffer ischemia/hypoxia throughout their growth. For example, it is estimated that glioma tissues have wide but heterogeneous hypoxia with oxygen concentrations ranging from 0.1 to 2.5% (3). Clinical data reveal that severer GBM necrosis closely correlates to faster GBM progress and shorter patient survival time (1, 2). Upon energy stress such as ischemia, autophagy is a major mechanism to maintain cellular energy homeostasis, which is highly regulated by conserved autophagic influx signaling involving PI3K/Akt/mTOR, p62, Beclin-1 and LC3 (4–6). Higher activity levels of autophagy are widely detected in glioma tissues, particularly around necrotic tissues (7). It is reported that inducing autophagy can either improve the efficacy of chemotherapy (8) or induce chemotherapy-resistance in glioma (9). Large-scale gene knockout screening shows that mitochondrial energy-metabolism genes are necessary for anoxic adaptive growth of a variety of tumors, including GBM (10). Specifically, Kim et al. (11) reported in recent research an increase of mitochondrial SHMT2 (serine hydroxymethyltransferase) in ischemic necrosis tissues of GBM patients, this enhances the anaerobic energy metabolism of GBM cells and promotes survival of GBM cells under ischemic environment. The mechanisms by which ischemia stimulates GBM development are extremely complicated and far from clear.

Programmed cell death ligand-1 (PD-L1, i.e., CD274 or B7H1) is a key negative regulator for immune inhibitory axis signaling controlling T-lymphocyte infiltration inside solid tumors. Previous studies reported that PD-L1 is widely expressed in glioma cell lines (12, 13) and most human glioma specimens (14). However, data of PD-L1 levels and subcellular distributions in human glioma tissues vary greatly (15). Most studies reported that higher PD-L1 expression was correlated with higher glioma grades (16–18) and worse prognosis (17, 19–22), while opposite results were also reported (14, 17, 23). PTEN mutation/deletion (in 36% of glioma) is closely associated with higher PD-L1 expression in glioma (24). Present evidence suggests that PI3K/Akt is a major pathway controlling PD-L1 expression in cancer cells. For mTOR, a key downstream signaling molecule in PI3K/Akt pathway, mTOR complex 1 (mTORC1) mainly mediates PI3K/Akt-induced cell autophagy (25) and mTORC2 mediates Akt-induced cell survival (26).

PD-L1 is recently considered to be oncogenic. PD-L1 knockdown significantly decreases tumor volume in murine ovarian cancer, melanoma (27), murine medulloblastoma (28), and U87 glioma in nude mice (29), while PD-L1 overexpression promotes glioma development (29). Mechanistically, PD-L1 regulates cell growth, proliferation, apoptosis, autophagy, migration and invasion in various cancers via modulating PI3K/Akt/mTOR and Ras/Erk/EMT signalings (27, 29–31). Further exploration of biological roles and mechanisms of PD-L1 in glioma will provide therapeutic cues including targeted immunotherapies for glioma.

In the present study, we first reported that PD-L1 was mostly prominent in those highly aggressive infiltrating glioma cells *in vivo*. Our data revealed that PD-L1 promoted glioma cell infiltration via starvation-induced Akt/autophagy/F-actin signaling. Particularly, we dissected PD-L1-Akt binding fragments and elucidated how PD-L1/Akt interactions activated its downstream cascades.

MATERIALS AND METHODS

Drugs and Antibodies

Cloroquine (CQ, Selleck Chemicals, Shanghai, China) was used at a final concentration of 25 μM. LY294002 (PI3K inhibitor, Cell Signaling Technology, MA, USA) was used at a final concentration of 0–50 μM. Perifosine (inhibitor of Akt PH-domain, Selleck Chemicals, Shanghai, China) was used at a final concentration of 0–25 μM. Primary antibodies against phospho-Akt (Ser473, #D9E), total Akt (#9272), phospho-mTOR, total mTOR,pP62, phospho-P70S6K, LC3B were purchased from Cell Signaling Technology (MA, USA). Antibodies against PD-L1/CD274 (PA5-28115, Thermo Fisher, IL, USA), PD-L1 (ABM4E54, Abcam, Cambridge, UK), GST (Z-5, Santa Cruz Biotechnology, TX, USA), Beclin1 (Santa Cruz Biotechnology, TX, USA), N-terminal GFP (Sigma), β-actin (20536–1-AP, Proteintech, Wuhan, China), Na^+/K^+ ATPase α1 (Proteintech, Wuhan, China), β-tubulin (Proteintech, Wuhan, China) were commercially purchased.

Plasmids and Transfection

GFP-LC3 plasmid was a gift from Dr. He Li (Huazhong University of Science and Technology). GST-kRas/PTEN/Akt1/Akt2/Akt3/EGFR VIII/PKA plasmids were gifts from Dr. Haian Fu (Emory University). PD-L1-EGFP expressing-plasmid was purchased from GeneChem (Shanghai, China). Full-length and truncated human PD-L1 coding cDNA was PCR amplified from PD-L1-EGFP plasmids and cloned into NV (N-terminal Venus 1-157aa) vector including NV-PD-L1 FL (full length 1-290 aa), NV-PD-L1-T1-259 (truncate 1-259aa), T128-259, T128-239, T1-178. PD-L1 cloned into pDEST-26 or p-FU-Venus vector was used to express GST-PD-L1 and Venus-PD-L1 FL1-290 or T19-290. Full-length and truncated human Akt1 cDNA was PCR amplified from GST-Akt1 plasmid and cloned into p-FU-Venus vector for Venus-Akt1, Akt1-T1-111, and Akt1-T122-480. Akt1-Y176A and Akt1-K14R mutants were constructed by using overlapping-PCR from p-FU-Venus-Akt1 plasmid. Transfection of plasmids was performed by using Lipofectamine 2000 (11668, Life Technologies, CA, USA) according to the manufacturer's instructions.

RNA-Sequencing and Enrichment Analysis

Three 100-mm dishes of U251/PD-L1 and U251/Vec stable cell lines were subjected to total mRNA isolation, cDNA libraries construction and sequencing at Illumina HiSeq sequence platform (PE150) with 6G clean data by Novogene Bioinformatics Institute (Shanghai, China). Differential gene expression analysis between U251/PD-L1 and U251/Vec groups was performed using the DESeq2 R package (1.10.1). The resulting *P*-values were adjusted using the Benjamini and Hochberg's approach for controlling the false discovery rate.

Differently expressed genes (DEGs) with $P < 0.005$, adjusted $P < 0.05$ (Padj) and absolute changing fold ≥ 1.2 were subjected to Kyoto Encyclopedia of Genes and Genomes (KEGG) pathway and Gene Ontology (GO) enrichment analysis. KEGG pathways and GO terms with Padj < 0.05 were considered significantly enriched by DEGs. We have submitted our data to NCBI (https://www.ncbi.nlm.nih.gov/geo/query/acc.cgi?acc=GSE107581).

Orthotopic Mouse Glioma Model

All animal handling and experiments were performed in accordance with NIH guidelines and approved by the Ethics Committees of Huazhong University of Science and Technology. The mice were group housed in the Animal Core Facility of Tongji Medical College under a 12 h light/dark cycle with *ad libitum* access to food and water. Briefly, adult Kunming male mice (18–20 g) were anesthetized with chloral hydrate (350 mg/kg) and a burr hole was drilled in the skull 0.5 mm posterior to the bregma and 2.0 mm lateral to the midline. A 10-μl Hamilton syringe (26 gauge, Reno, NV) containing 20,000 G422 cells (mouse GBM cell line) in 1 μl of PBS was advanced to a depth of 3.5 mm from the skull surface and then withdrawal 0.3 mm. Cell suspension was delivered at the rate of 1 μl/min. After cell implantation, the needle was left in place for 6 min before withdrawal. After 6–14 d of cell inoculation, the mice were perfused with 4% paraformaldehyde (PFA) and the brains were paraffin-embedded.

Hematoxylin-Eosin (HE) Staining and Immunohistochemistry (IHC)

IHC was performed as previously reported (29). Paraffin-embedded mouse brain tissues (bearing tumor) were cut into 4 μm-thick slices for H&E staining and IHC analysis. Briefly, the slices were deparaffinized in xylene and antigen-retrieved by microwave processing. After 1 h of blocking with 5% bovine serum albumin in PBS, the slices were incubated with primary antibodies (PD-L1, Abcam, UK) overnight at 4°C, followed by corresponding secondary antibody incubation (Polink-1 HRP DAB Detection System, ZSGB-BIO, China). The immunoreaction was visualized with diaminobenzidine tetrachloride. The brain images were scanned with an automatic slice scanning system-SV120 (Olympus, Tokyo, Japan). The tumor parenchyma rim was delineated with black dashed ellipse circle, while the infiltration frontiers was delineated with blue or white dashed irregular circle.

Cell Culture and Starvation

Human glioblastoma cell lines U251, LN229, and human embryonic kidney 293T cell line were purchased from American Tissue Culture Collection (MA, USA) or China Center for Type Culture Collection (Wuhan, China). U251, LN228, U87MG with stable PD-L1 overexpression (U251/vec or PD-L1, LN229/vec or PD-L1) or knockout (U251/sgGFP or sgPD-L1) were generated as previously described (29). All cell lines were cultured in Dulbecco's modified Eagle's medium (DMEM, Gibco, CA, USA) supplemented with 10% FBS (Gemini, CA, USA) and 1% Penicillin-Streptomycin Solution (Hyclone, Thermo, Beijing, China). Fresh Earle's balanced salt solution (EBSS, GIBCO BRL, USA) media was used to induce cell starvation at 24 h after transient transfection or initial seeding. Cells were washed with EBSS media for three times and then incubated with EBSS media for various time points.

Western Blotting Analysis

Western blotting analysis was performed as previously reported (29). Briefly, the cell lysates were collected and dispersed in radio-immunoprecipitation assay lysis buffer containing phenylmethane-sulfonyl fluoride. Equal amounts of total proteins were subjected to sodium dodecyl sulfate polyacrylamide gel electrophoresis and electro-transferred onto nitrocellulose filter membranes (Merck Mil- lipore, Cork, Ireland). The blots were incubated with corresponding primary and secondary IRDye 800 or IRDye 680 CW-conjugated goat anti-rabbit or anti-mouse IgG antibodies (LI-COR Biosciences, Lincoln, USA). The labeled bands were visualized and quantified by Odyssey Infrared Imaging System (LI-COR Biosciences, MA, USA).

Palloidin Staining and Immunofluorescence

Immunofluorescence staining was performed as previously reported (29). Cells in 35-mm culture dishes were fixed, permeabilized, blocked, and then incubated with primary and corresponding Dylight 488-labeled secondary antibodies (Abbkine, CA, USA). F-actin was stained with rhodamine-phalloidin (Yisheng Bioengineering Institute, China) according to the manufacturer's instructions. Hoechst 33342 was used to stain the nucleus. For paraffin-embedded tissues, rat brain slices were deparaffinized, rehydrated, antigen unmasked, blocked with 5% bovine serum albumin (BSA) and then incubated with primary antibodies and corresponding Dylight 488/594-labeled secondary antibodies. Micrographs were taken under the same conditions with a conventional fluorescent microscope (Olympus, Tokyo, Japan).

GFP-LC3 Punctate Quantification

U251/sgGFP or U251/sgPD-L1 cells were transiently transfected with pGFP-LC3 plasmids for 24 h. Then, the cultures were subjected to EBSS treatment for 12 h and fixed. U251 cells expressing GFP-LC3 were randomly photographed under 400×-magnifications under the same conditions. Cells with five or more GFP-LC3 vacuole dots (puncta) were considered autophagy-positive. An average percentage of puncta-positive cells from nine fields/culture (total cells > 500) was calculated and used for statistical analysis.

Glutathione S-Transferase (GST)-Pull Down Assay

GST-pull down assay was performed as previously described (29). 293 cells were transfected with indicated plasmid at 1:1 for 2 d. Cell lysates were extracted with GST-lysis buffer and 400 μg of total soluble proteins from each sample were incubated with 30 μl of glutathione sepharose bead slurry (GE Healthcare Life Sciences, Piscat-away, USA) overnight at 4°C. After extensive washing, the immunoprecipitates were subjected

to Western blotting analysis. Anti-GST, anti-N-GFP or anti-PD-L1 antibodies were used to probe corresponding proteins.

Membrane and Cytosol Protein Detection

U251 cells were transfected with p-FU-Venus or p-FU-Venus-PD-L1 plasmid for 24–36 h. Membrane and cytosol proteins were extracted using Membrane and Cytosol Protein Extraction Kit (Beyotime Biotechnology, Shanghai, China) according to manufature's instructions. Membrane and cytosol proteins were then subjected to Western blotting with Na^+/K^+ ATPase α1 and β-tubulin as internal control of membrane and cytosol proteins respectively.

Statistical Analysis

All experiments were repeated independently for at least three times. The values were expressed as means ± SEM. Unpaired Student's test was used to compare between two groups of *in vitro* experiments. Paired Student's test was used to compare between two groups of animal experiments. Comparisons among multiple groups were performed through one-way ANOVA with Student–Newman–Keuls post-test. $P < 0.05$ was considered statistically significant.

RESULTS

PD-L1 Is Prominently Elevated in Invasive Frontier GBM Cells *in vivo*

To ascertain the relationships between intrinsic PD-L1 and glioma cell invasive behavior during GBM development, we examined PD-L1 expression in the whole brain at various stages of GBM development in a highly aggressive orthotopic

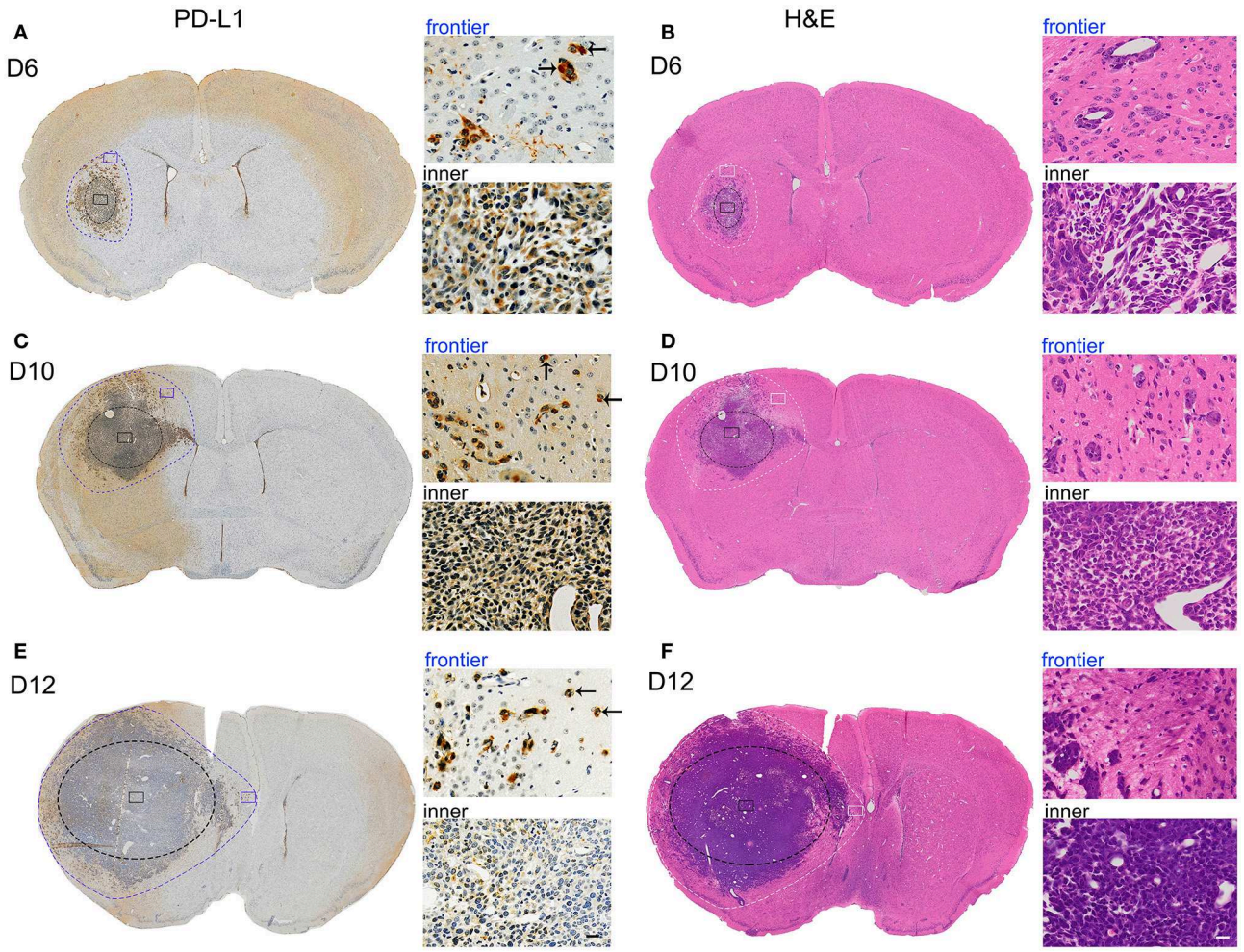

FIGURE 1 | PD-L1 is preferentially elevated in invasive frontier GBM cells *in vivo*. Mouse G422 glioma cells (20,000 cells) were inoculated into right striatum of Kunming mice. 6, 10, and 12 days after initial cell implantation, the mice were perfused with PFA and paraffin-embedded (3 mice/group). Serial mouse brain slices were cut and the slices with maximal tumor-load were used for PD-L1 (3 slice/brain) or H&E staining (3 slice/brain). **(A)** Representative PD-L1 staining of glioma on day 6. Inner black-dot ellipse delineated the boundary of tumor parenchyma while the outer irregular dot circle delineated the infiltration boundary. Left panels showed the whole brain and right panels showed enlarged square images. Arrows indicated the invasive frontier glioma cells. **(B)** Representative H&E staining of glioma at day 6. **(C,E)** Representative PD-L1 staining of glioma at day 10 and 12. **(D,F)** Representative H&E staining of glioma at day 10 and 12.

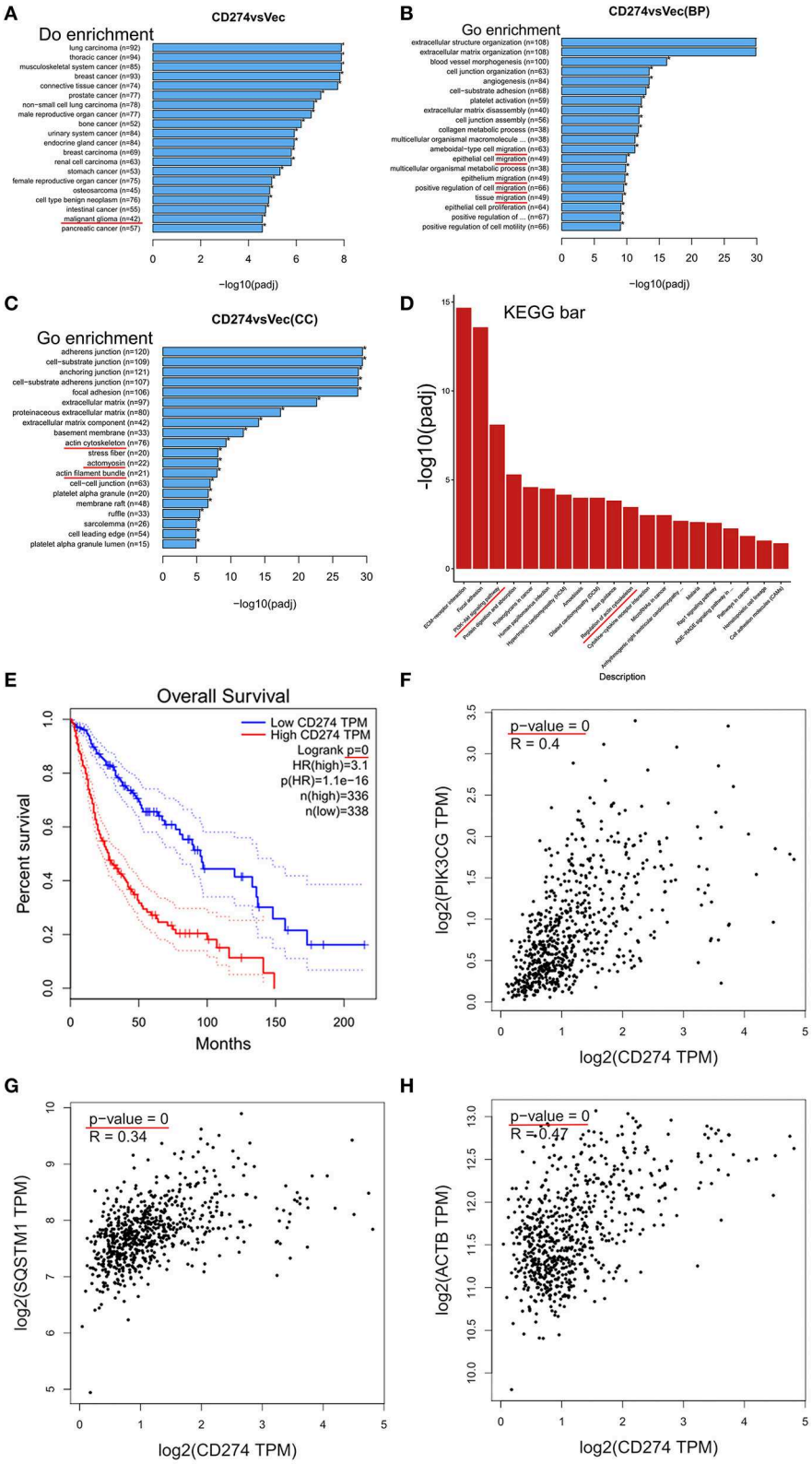

FIGURE 2 | Transcriptomic analysis in PD-L1-overexpressed GBM cells. PD-L1 (CD274) was stably overexpressed in human U251 glioma cells. Total RNA was extracted from U251/PD-L1 or its control (U251/Vec) cells and subjected to mRNA-sequencing. Significant DEGs between U251/PD-L1 and U251/Vec groups with

(Continued)

FIGURE 2 | the following creteria: $P < 0.005$, Padj < 0.05 and absolute fold change ≥ 1.2 ($n = 3$). **(A)** DO (Disease Ontology) enrichment analysis results showed that 42 of significantly altered-genes upon PD-L1 overexpression were associated with malignant glioma (indicated by red line). **(B)** BP (biological process) from GO enrichment analysis results showed that PD-L1 overexpression was closely associated with various cell migration pathways (indicated by red lines). **(C)** CC (cellular component) from GO enrichment analysis results showed that PD-L1 overexpression was closely associated with several actin signaling pathways (indicated by red lines). **(D)** KEGG (Kyoto Encyclopedia of Genes and Genomes) pathway enrichment analysis results showed that PI3K-Akt and actin regulations are among the top altered pathways by PD-L1 overexpression (indicated by red lines). **(E)** Overall survival of glioma patients with PD-L1 expression from database http://gepia.cancer-pku.cn. Survival significant longer for patients with low PD-L1($p = 0$). **(F–H)** Correlation analysis of PD-L1 with PIK3CG, SQSTM1 (p62), and ACTB (β-actin) showed that mRNA levels of PD-L1 were positively associated with those of PIK3CG, p62, and β-actin ($p = 0$) in glioma patient tissues (http://gepia.cancer-pku.cn).

mouse G422 model (**Figure 1**). PD-L1 as well as H&E staining clearly showed that the glioma tissue grew rapidly from day 6 to 12 (D6, D10, D12) after initial G422 cell-implantation. The tumor parenchyma in the left hemisphere was delineated with black-dot ellipse, and the tumor frontiers was delineated with blue (PD-L1, **Figures 1A,C,E**) or white-dot irregular circle (H&E, **Figures 1B,D,F**). Clearly, invasive GMB cells could migrate far away from its parenchyma mass at the early stage (D6) during GBM development. Along with the growth of glioma parenchyma, infiltration frontiers were also enlarged correspondingly. The frontier (blue) and inner (black) square micrographs in brain coronal sections were enlarged in right panels. It is clear that PD-L1 was prominently elevated in invasive G422 cells (indicated by arrows) in GBM infiltration frontier (**Figures 1A,C,E**). Such evidence establishes a strong positive correlation between PD-L1 and the aggressiveness of GBM cells.

PD-L1-Altered Gene Expression Are Highly Enriched in Migration and PI3K/Akt-Actin Signaling

To explore the underlying mechanisms of PD-L1$^+$-GBM cells in the infiltration frontier, mRNA sequencing was conducted in PD-L1-overexpressed U251 glioma cells. Differential expressed genes (DEGs) between U251/PD-L1 and U251/Vec cells (i.e., CD274 vs. Vec) were selected by three criteria (i.e., $P < 0.005$, Padj < 0.05 and absolute fold change ≥ 1.2) and the selected DEGs were subjected to various systemic analysis. DO (Disease Ontology) enrichment showed that PD-L1-altered gene expression was significantly associated with malignant glioma (**Figure 2A**, indicated by red line). Gene ontology (GO) enrichment analysis showed that PD-L1-altered gene expression was largely associated with cell migration (BP: biological process, **Figure 2B**, indicated by red lines), actin-structure functions (CC: cellular component, **Figure 2C**, indicated by red lines), PI3K-Akt signaling pathway and Regulation of actin cytoskeleton (KEGG: Kyoto Encyclopedia of Genes and Genomes, **Figure 2D**, indicated by red lines). Further analysis of human glioma database (http://gepia.cancer-pku.cn) revealed that PD-L1 (CD274) was negatively associated with the prognosis of glioma patients ($p = 0$, **Figure 2E**). In addition, PD-L1 expression was significantly positively correlated with PI3K ($p = 0$, **Figure 2F**), SQSTM1 (p62, a negative marker of autophagic influx signaling) (32) ($p = 0$, **Figure 2G**) and ACTB (β-actin) ($p = 0$, **Figure 2H**) in human glioma tissues. The evidence together indicates that PD-L1 greatly affects glioma cell invasion and PI3K/Akt-actin signaling.

PD-L1 Regulates Akt-p62-Autophagic Influx Signaling Upon Starvation

It is well known that GBM tissues suffer severe ischemia that causes necrosis and promotes GBM cell aggressiveness (1–3), suggesting that energy-deprivation stress is a major driving force for glioma cell invasion. Since PI3K/Akt signaling is pivotal in promoting cell survival and suppressing autophagy (6, 33), we further investigated the role of PD-L1 in regulating Akt-autophagic influx signaling in glioma cells with a EBSS-induced starvation model. Western blot results showed that PD-L1 overexpression did not evidently alter p-Akt/mTOR/p70S6K signaling under normal culture conditions (**Figure 3A**, EBSS-0 h and **Figure S1**). Upon EBSS incubation, p-Akt and p62 (a negative maker for autophagy influx) was prominently reduced in U251/Vec cells (**Figures 3A,B**), while LC3II was evidently increased (–CQ2, **Figure 3C**) as detected by Western blot. Cells with PD-L1 overexpression significantly reversed EBSS-induced p-Akt reduction, p62 reduction as well as LC3II elevation compared to their corresponding Vec controls (indicated by red boxes, **Figures 3A–C**). Consistently, fluorescent immunostaining showed that PD-L1 evidently reduced LC3B and Beclin-1 while increased p62 in starved LN229 glioma cells at EBSS-6 h (**Figure 3D**).

We further examined the effects of endogenous PD-L1 on autophagy influx signaling in glioma cells by knocking-out PD-L1 using CRISPR/Cas9 technique. Western blot results demonstrated that endogenous PD-L1 was prominently decreased in stable U251/sg-PD-L1 cell lines (single colnes #2 and #3, **Figure 4A**). Under normal culture conditions, PD-L1 knockout did not evidently affected p-Akt (**Figure 4B**) or p-mTOR (**Figure S2**) in U251 cells. Upon EBSS incubation (6 and 12 h), LC3II was significantly elevated in U251/sgPD-L1 cells as compared to its corresponding U251/sgGFP controls (**Figure 4C**). Consistently, fluorescent images of GPF-LC3-puncta clearly showed that the average number of GFP-LC3-puncta (representing autophagosome) per cell was significantly increased in U251/sgPD-L1 cells compared to its U251/sgGFP control at EBSS-12h (**Figure 4D**).

PD-L1 128-237aa Fragment Interacts With Akt 112-480aa Fragment

In order to dissect the mechanism of PD-L1 action, we screened the binding partners of PD-L1 with various key upstream signaling proteins in PI3K/Akt pathway by GST-pull down experiment. The results clearly showed that PD-L1 preferentially bound to AKT1 and AKT2 compared to KiRAS, PTEN-1, PTEN-2, AKT3, EGFRVIII and PKA under normal

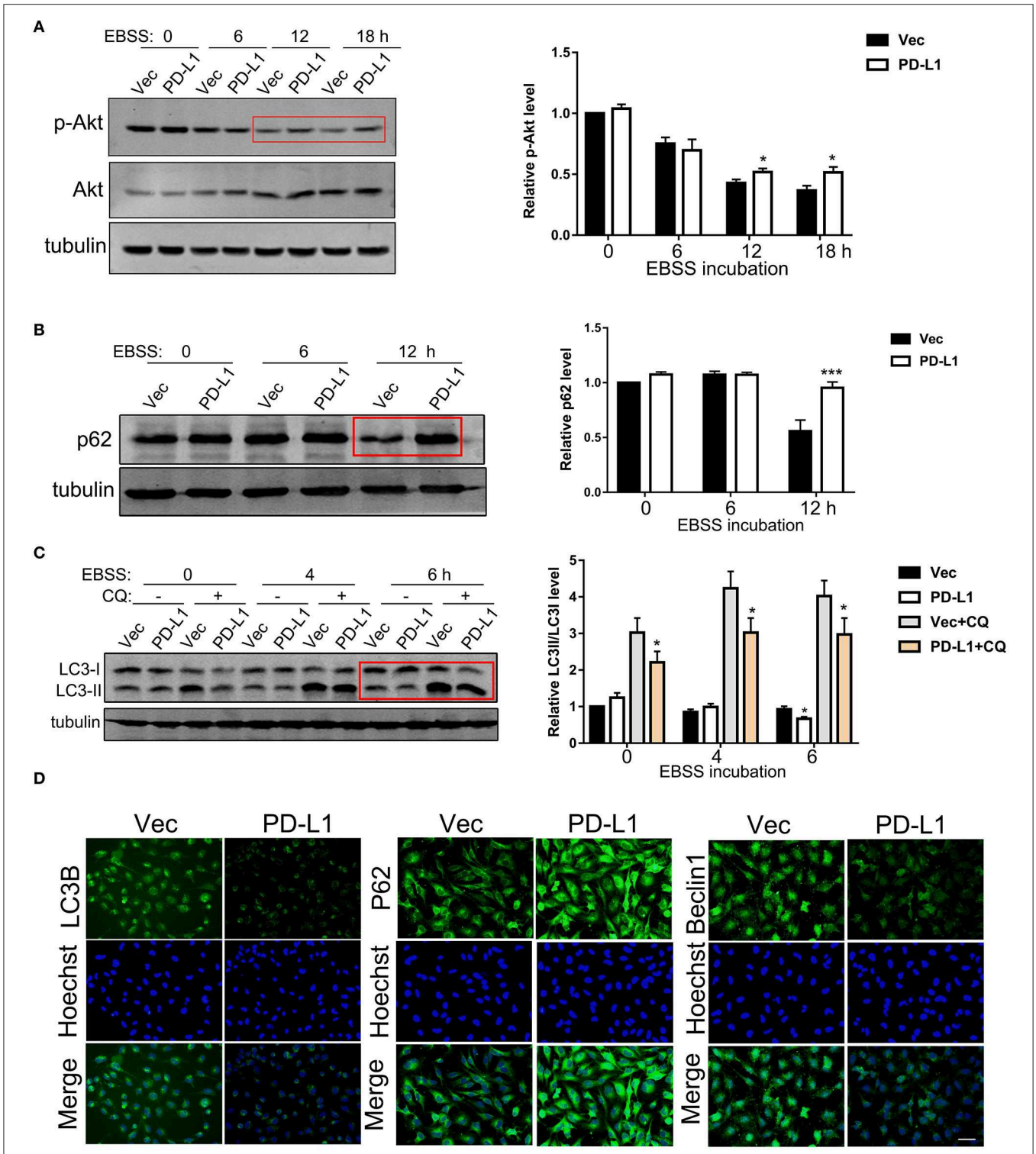

FIGURE 3 | Effects of PD-L1 overexpression on Akt-p62-autophagic influx signaling upon starvation. **(A)** Western blot analysis of p-Akt, Akt and tubulin in U251/Vec and U251/PD-L1 cells subjected to various time of EBSS incubation. $^{*}P < 0.05$ vs. corresponding Vec, $n = 3$. **(B)** Western blot analysis of p62 and tubulin in U251/Vec and U251/PD-L1 cells subjected to various time of EBSS incubation. $^{***}P < 0.001$ vs. corresponding Vec, $n = 3$. **(C)** Western blot analysis of LC3 and tubulin in U251/Vec and U251/PD-L1 cells subjected to various time of EBSS incubation with or without Chloroquine (CQ, 50 μM). $^{***}P < 0.001$ vs. corresponding Vec, $n = 3$. **(D)** Representative fluorescent immunostaining of LC3B, p62, and Beclin-1 in U251/Vec and U251/PD-L1 cells at EBSS-6 h. Bar, 20 μm. All experiments were repeated three times independently.

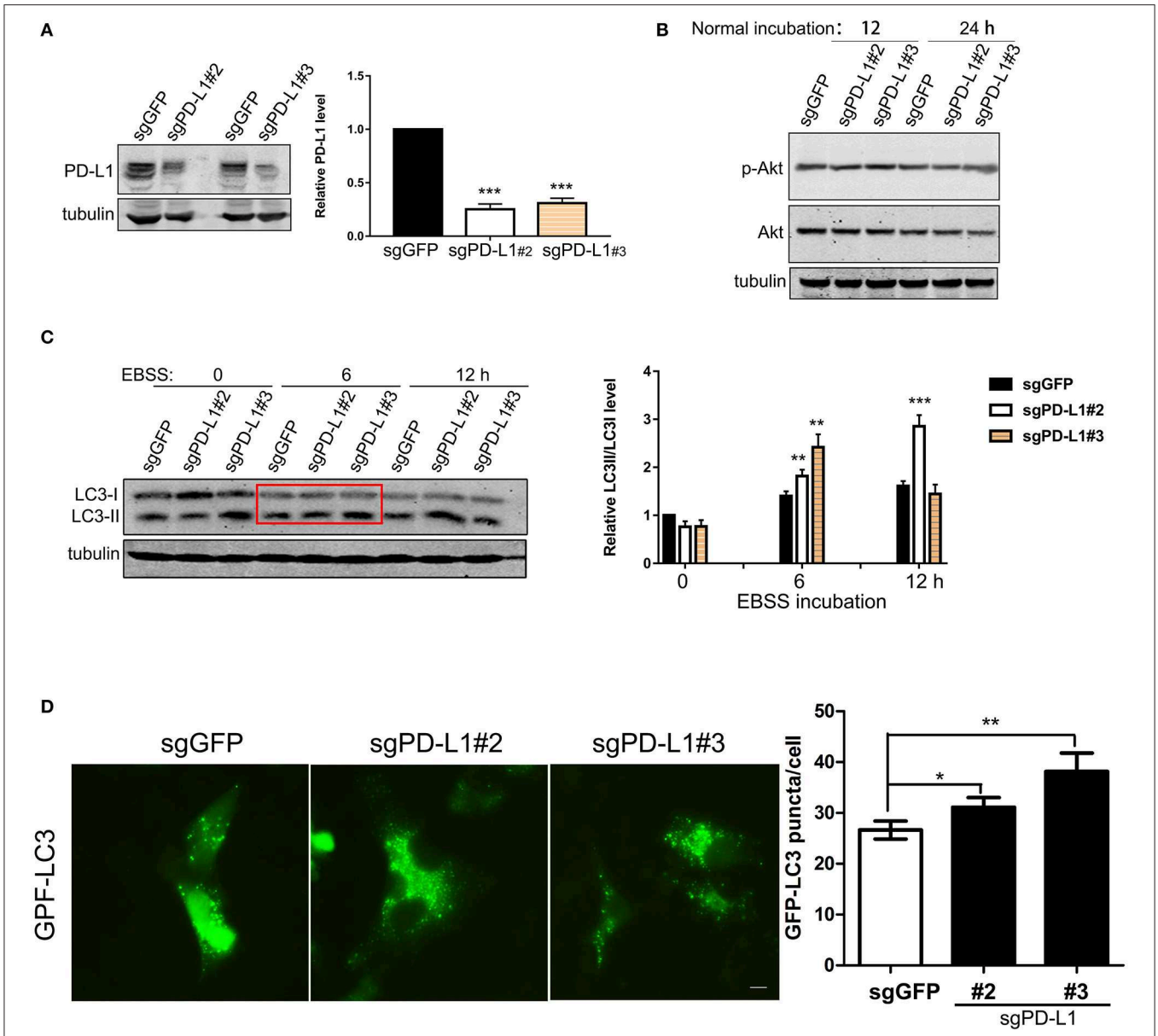

FIGURE 4 | Effects of PD-L1 knockout on Akt, LC3 and autophagy puncta upon starvation. U251 cells were transfected with lentiviral sgGFP or PD-L1 and stable cell lines were selected. **(A)** Effects of PD-L1 knockout in U251/sgGFP, U251/sgPD-L1#2 and U251/sgPD-L1#3. ***$P < 0.001$ vs. sgGFP, $n = 3$. **(B)** Effects of PD-L1 knockout on p-Akt and Akt. Representative results showed that PD-L1 knockout did not alter p-Akt in U251 cells under normal incubation ($n = 3$). **(C)** Effects of PD-L1 knockout on LC3I and CL3II upon EBSS incubation. **$P < 0.01$ and ***$P < 0.001$ vs. corresponding sgGFP, $n = 3$. **(D)** Effects of PD-L1 knockout on LC3 puncta formation upon EBSS-12 h. 100–200 cells from each culture were counted. *$P < 0.05$ and **$P < 0.01$ vs. sgGFP, $n = 3$.

culture conditions (**Figure 5A**) as well as EBSS-4h incubation (**Figure 5B**). Then, we further dissected the exact binding domain of PD-L1 for its AKT binding. We made a series of PD-L1 (full length 290 aa, FL) truncates by deleting 260–290 aa (PD-L1 T1-259), 179-290 aa (PD-L1 T1-178) from its C-terminal and 1-127 aa (PD-L1 T128-259), 1-127/238-290 (PD-L1 T128-259) (**Figure 5C**), 1-18 aa (PD-L1 T19-259) (**Figure 5D**) based on PD-L1 structure (upper panel, **Figure 5E**). GST-pull down results showed that PD-L1 FL1-290, T19-290, and T128-237 were the major truncates binding to AKT1 (indicated by red rectangles, **Figures 5B,C**). These results identified that PD-L1 128-237 fragment was required for its Akt binding.

We then seeked to identify the binding domain or key amino acid (aa) of Akt based on its structure (lower panel, **Figure 5E**). GST-pull down clearly showed that AKT1-FL (1-480 aa), T112-480 but not T1-111 bound to PD-L1 (**Figure 5F**). Single amino acid mutant of AKT Y176A (loss of TNK2 binding and membrane localization) (34) and K14R (substantial reduction of

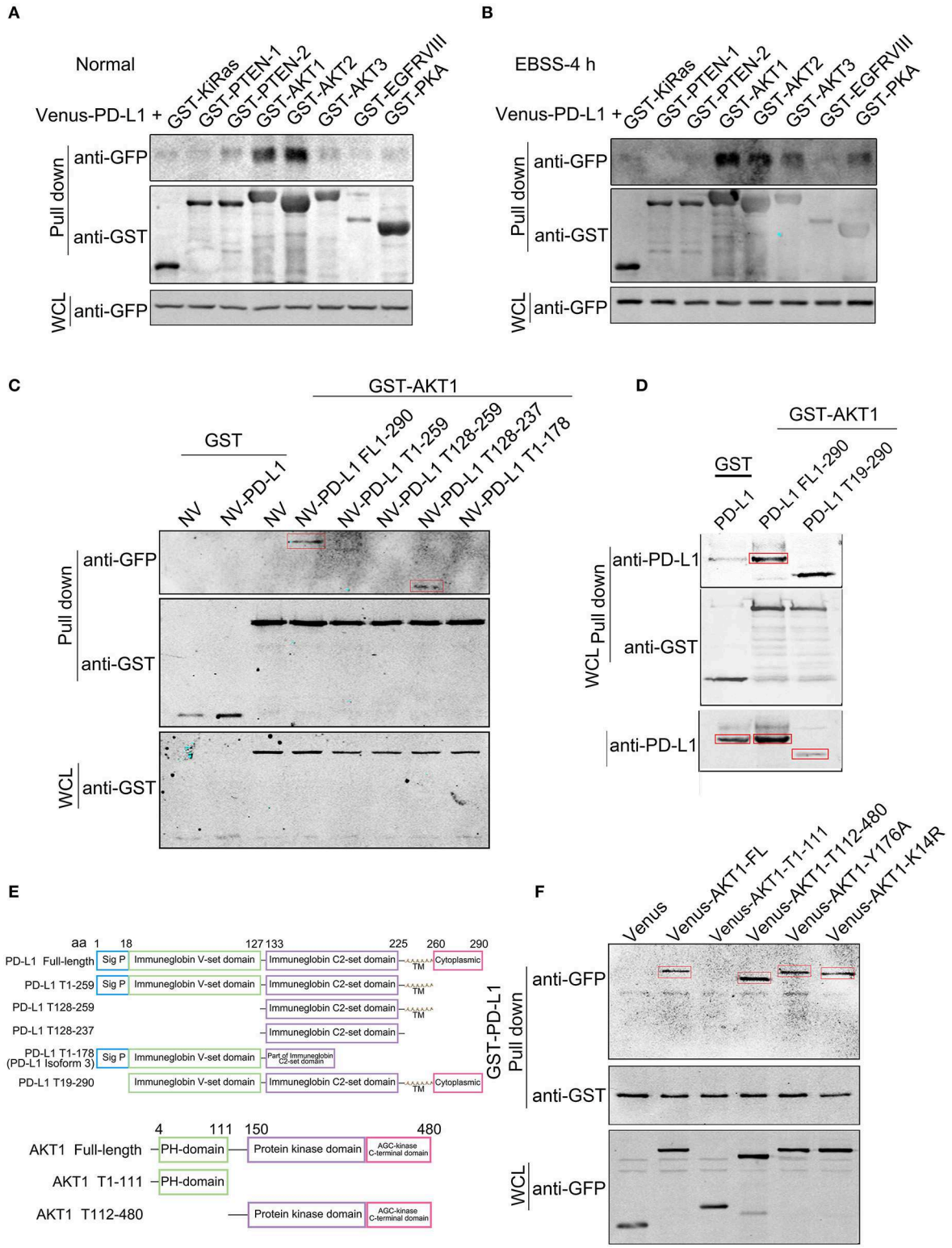

FIGURE 5 | Identification of PD-L1-Akt binding domains. Venus (or N-terminal Venus)-tagged plasmids were co-transfected with GST-tagged plasmids in 293T cells. Equal amount of total soluble proteins were subjected to GST-pull down analysis. **(A,B)** Western blot analysis of the binding between Venus-PD-L1 and GST-KiRas, PTEN-1, PTEN-2, AKT1, AKT2, AKT3, EGFRVIII, and PKA under normal culture conditions **(A)** and EBSS-4 h **(B)**. WCL, whole cell lysate. **(C,D)** Western blot analysis of the binding between GST-AKT1 and NV-PD-L1 truncates. FL, full length; T, truncate. **(E)** Schematic diagram of PD-L1 and AKT truncates. **(F)** Western blot analysis of the binding between GST-PD-L1 and Venus-AKT truncates. All experiments were repeated at least three times independently.

ubiquitination and loss of PIP3 binding) (35) did not evidently affect its interaction with PD-L1 (**Figure 5F**), suggesting that PD-L1/Akt interaction occurred in the cytosol via independent AKT K14 and Y176 sites.

PD-L1 Facilitates Akt Membrane-Translocation and F-Actin Formation in Starved Glioma Cells

Since PD-L1 selectively interacted with Akt 112–480 fragment but not its PH domain (1–111 aa) (**Figure 5F**), it is interesting to further figure out how PD-L1 promoted Akt activation upon starvation (**Figure 3A**). Full activation of Akt depends on Akt translocation from cytoplasm to cell membrane (via its PH domain) and PIP3/PDK action on cell membrane (36, 37), which can be pharmacologically inhibited by specific inhibitor Perifosin (37) and LY294002, respectively. Administration of LY294002 (GFP, **Figure 6A**) and Perifosine (GFP, **Figure 6B**; Vec, **Figure 6C**) evidently reduced p-Akt in U251/GFP cells. In PD-L1-overexpressed U251 cells, however, LY294002 but not Perifosin could reduce p-Akt level (PD-L1, **Figures 6A–C**). Such evidence suggests that PD-L1 protects the membrane-translocation of Akt. Western blot results demonstrated that membrane-bound Akt was evidently increased upon PD-L1 overexpression compared to Vec control (**Figure 6D**). Consistently, fluorescent immunostaining of Akt showed that membranous Akt (indicated by arrows) was more evident in PD-L1-overexpressed U251 cells, which was well co-localized with F-actin (Palloidin staining) (**Figure 6E**).

Finally, we examined the effects of PD-L1 on F-actin structure in starved glioma cells. Fluorescent images of Palloidin staining clearly showed that F-actin formation was evidently increased in PD-L1-overexpressed U251 cells under normal culture conditions as well as EBBS-12 h incubation (**Figure 7A**). Taken together, the evidence suggested that PD-L1 facilitated Akt translocation to cell membrane and Akt activation to modify cellular morphology via F-actin cytoskeleton during energy-deprivation stress.

DISCUSSION

In our present study, we discovered that PD-L1 elevation occurred predominantly in highly aggressive glioma cells. RNA sequencing revealed that high levels of PD-L1 in glioma cells mainly mediated cell migration and PI3K/Akt/actin signaling. PD-L1 reduced starvation-induced Akt inhibition, autophagic influx and F-actin collapse in glioma cells. Mechanistically, PD-L1 directly interacted with Akt, and this process involved PD-L1 128-237aa and Akt 112-480aa. The binding of PD-L1 to Akt facilitated membrane-translocation of Akt and thus elicited downstream biological effects in frontier glioma cells. These findings reveal a novel invasive mechanism in GBM.

PD-L1 is a pivotal negative regulatory molecule at the immune checkpoint axis and has complicated biological functions besides immune regulation (38). Detection of PD-L1 level in cancer cells is of primary importance for predicting its biological functions as well as prognosis of immune therapy in various cancers such as melanoma. Previous studies have reported that PD-L1 is widely expressed in most glioma cell lines including U251 (12, 29) and human glioma tissues (14), indicating important biological functions of PD-L1 in glioma. Here, we clearly demonstrated that PD-L1$^+$-glioma cells were highly aggressive (**Figure 1**). Compared to rat/C6 and nude mouse/U87 glioma models, in which 1,000,000 or 250,000 glioma cells were implanted in the striatum and only a few glioma cells migrated outside from the tumor rim at day 14 or 24 later (29), in our orthotopic glioma model, only 20,000 G422 cells were microinjected into the striatum of mouse brain. In very short time (6 d) after initial glioma cell injection, PD-L1$^+$-glioma cells had already migrated far from the glioma center (**Figures 1A,B**). Afterwards, invasive PD-L1$^+$-glioma cells quickly reached the outer surface of cerebral cortex at day 10 (**Figures 1C,D**) and middle line of two hemispheres at day 12 (**Figures 1E,F**) after the initial glioma cell implantation. Obviously, the G422 glioma model mimics well the invasive pathological process of GBM. Since PD-L1 in cell membrane (39), exosome (40), and cytoplasm (29) are all pivotal for cancer development and progress, we can infer that the elevation of PD-L1 levels in those infiltrating glioma cells heavily contribute to their invasiveness.

To systematically reveal the role of PD-L1 in glioma cells, we conducted RNA sequencing in PD-L1-overexpressed human glioma U251 cells, which might mimic the status of higher PD-L1 levels in those infiltrating glioma cells. Bioinformatics analysis of DEGs clearly pointed out that increased PD-L1 in glioma was closely associated with glioma malignancy (**Figure 2A**), as well as distinct signaling pathways in invasive malignant glioma, such as cell migration, PI3K/Akt and actin organization (**Figures 2B–D** and **Figures S1, S3**). In a database of 674 glioma human samples, mRNA levels of PD-L1(i.e., CD274) were significantly positively correlated to those of PI3K (i.e., PI3KCG) and β-actin (i.e., ACTB) (**Figures 2F,H**), supporting our RNA-sequencing data. Also, bioinformatics analysis of glioma patient samples in opensource database showed that higher PD-L1 expression indicates poorer patient survival (**Figure 2E**), supporting that PD-L1's increase in infiltrating glioma cells is of clinical importance.

It is well known that GBM tissues suffer severe ischemic starvation, which is an important pathological factor driving aggressiveness (1, 2). PI3K/Akt is a pivotal signaling pathway promoting cell survival and suppressing autophagy under normal and ischemic conditions, while ischemic starvation is a major pathological stimulus for autophagy and actin cytoskeleton collapse (41, 42). It is conceivable that boundary GBM cells encounter energy-deprivation and higher PD-L1 expression may prevent GBM cell death and promote invasion via Akt-autophagy-actin signaling. Indeed, bioinformatics analysis of our RNA-sequencing data showed that PD-L1 affected autophagic signaling (**Figure S2**). By applying the glioma patient database, we found that mRNA levels of PD-L1 were significantly positively correlated to those of p62 (i.e., SQSTM1) (**Figure 2G**). Consistently, our experimental results demonstrated that PD-L1 significantly resumed EBSS starvation-induced Akt-autophagy signaling in glioma cells *in vitro* (**Figure 3**) but had minor effects under normal culture conditions (**Figure 4B** and **Figure S4**).

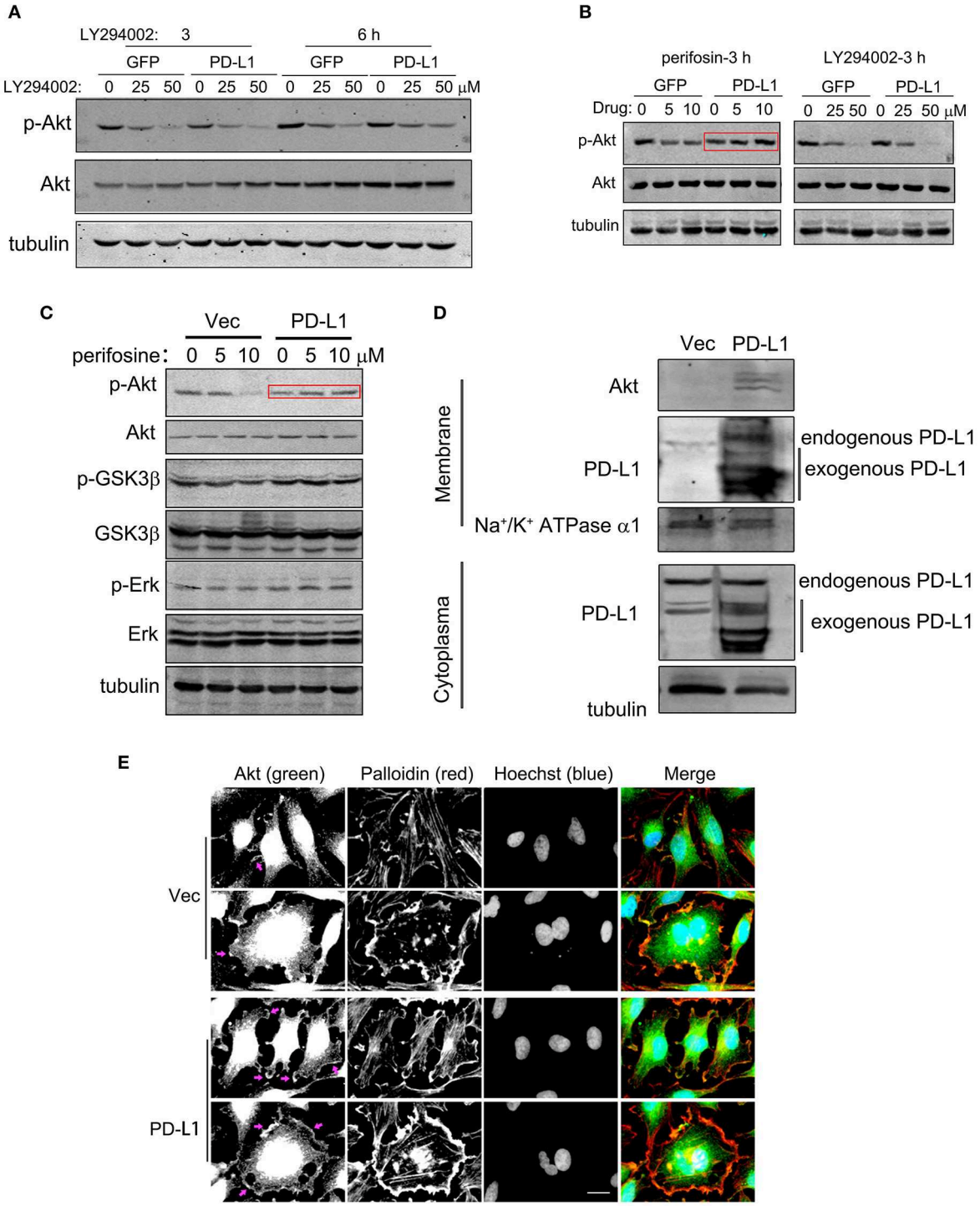

FIGURE 6 | PD-L1 facilitates membrane-translocation of Akt. **(A)** Inhibitory effects of LY294002 on Akt activation. U251/GFP and U251/PD-L1 cells were treated with PI3K inhibitor LY294002 and subjected to Western blot analysis. **(B)** Differential inhibitory effects of Perifosin (inhibiting Akt PH domain function) and LY294002 on Akt activation in U251/GFP and U251/PD-L1 cells. **(C)** Effects of Perifosin-3 h on pAkt/Akt, p-GSK3β/GSK3β, and p-Erk/Erk in U251/PD-L1 cells. **(D)** Effect of PD-L1 on membrane Akt. Total proteins from cytoplasm and membranes of U251/PD-L1 or U251/Vec cells were isolated and equal amount of proteins were subjected to Western blot analysis. **(E)** Representative fluorescent microscopy showed membrane distribution of Akt and its co-localization with F-actin. Bar, 20 μm. All experiments were repeated three times independently.

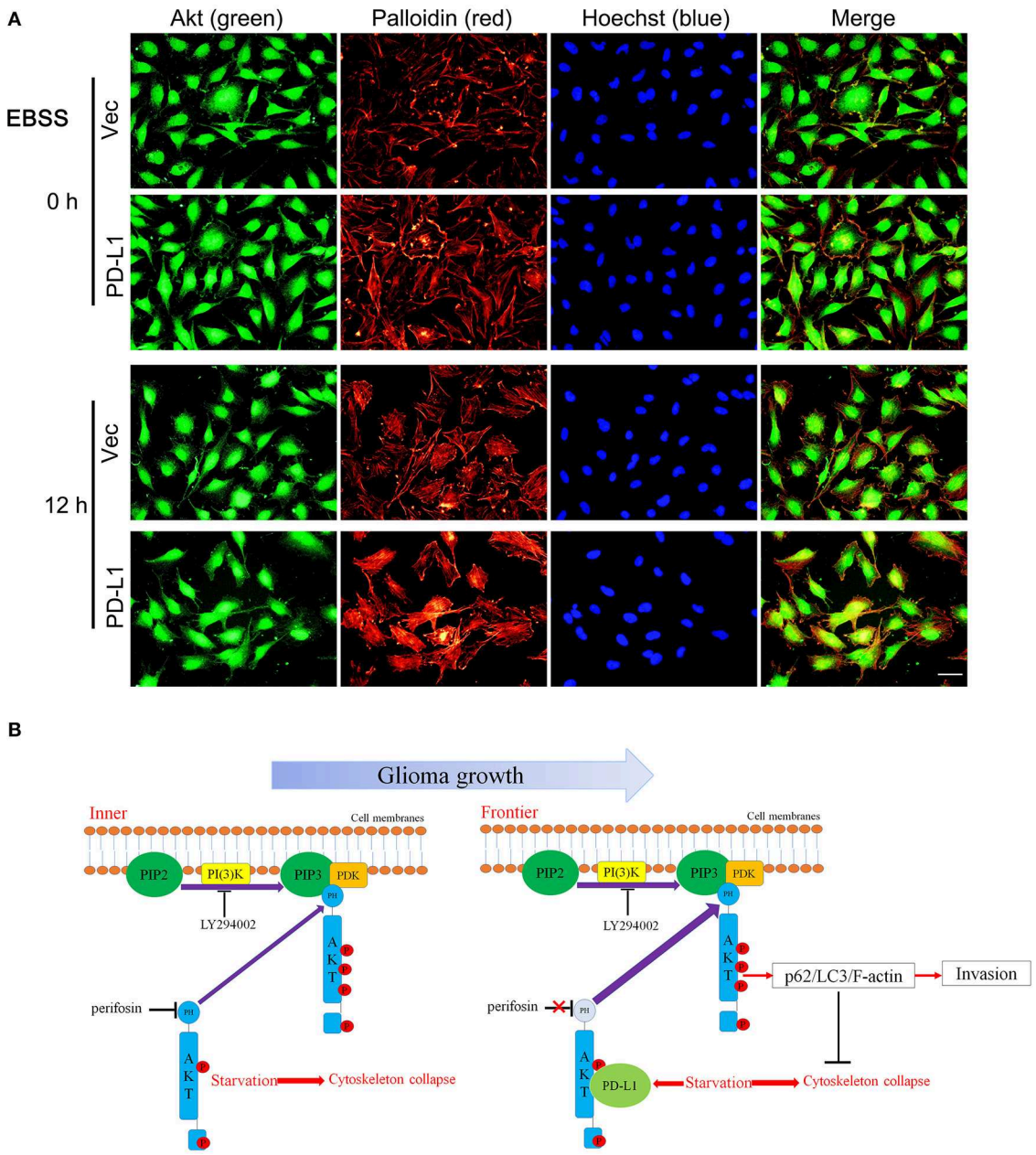

FIGURE 7 | PD-L1 facilitates F-actin formation in glioma cells upon starvation. **(A)** Representative fluorescent microscopy showed elevated F-actin in U251/PD-L1 cells upon EBBS-12 h incubation. Bar, 20 μm. The experiments were repeated at least three times independently. **(B)** Proposed mechanism of PD-L1 action in invasive frontier glioma cells.

The effects of PD-L1 overexpression on Akt increase and LC3 decrease were verified *in vivo* in a orthotopic rat/C6 glioma model (**Figure S5**). Further, via double-fluorescent immunostaining, we verified that higher PD-L1 levels in individual GBM cells were associated with lower Beclin1 and LC3 levels in GBM patient tissues (**Figure S6**). Such evidence consistently supported that PD-L1 suppressed autophagy via Akt induction/activation. In addition, PD-L1 increased F-actin formation and Akt/F-actin co-localization beneath cell membrane in glioma cells upon starvation (**Figures 6E**, **7A**). In other cancer cells such as sarcoma cells, melanoma and ovarian cancer cells, PD-L1 also regulates Akt-mediated autophagic signaling (27, 31). This data largely supported our proposed PD-L1-Akt-p62-autophagy-actin-invasion mechanism in frontier GBM cells. Further collection of evidence is helpful to elucidate the exact invasive mechanism of GBM *in vivo*.

Importantly, we identified a novel mechanism by which PD-L1 regulate PI3K/Akt signaling. Among various upstream

signaling proteins in PI3K/Akt pathway, we found that PD-L1 preferentially bound to Akt isoforms, and this became more evident upon EBSS incubation (**Figure 5** and **Figure S7**). Moreover, we dissected the binding element of PD-L1 and Akt. Our data revealed that the 128-237aa fragment of PD-L1 and the 112-480aa fragment of Akt were responsible for PD-L1/Akt interaction (**Figure 5**). Mutation of K14 and Y176, two active sites for the membrane-translocation of Akt, did not alter PD-L1/Akt interactions (**Figure 5F**), suggesting that PD-L1/Akt interaction occurred mostly in the cytoplasm. Upon PD-L1 overexpression, membrane-bound Akt was prominently increased (**Figure 6D**), supporting that cytoplasmic PD-L1/Akt interactions facilitated Akt translocation from cytoplasm to cell membrane, which is required for full activation of Akt (36). Interestingly, LY294002 (inhibiting p-Akt via PI3K) but not Perifosin (inhibitor of membrane-translocation of Akt and p-Akt via PH domain) (37) could abolished Akt phosphorylation in the presence of PD-L1 overexpression (**Figures 6A–C**). Such evidence suggested that the binding of PD-L1 to non-PH domain of Akt may prevented Perifosin action via some unknown mechanism, thus strengthened the attachment of Akt PH-domain to cell membrane and facilitated its full phosphorylation (**Figure 7B**). Further study on the mechanisms of PD-L1/Akt interactions requires more experimental data in the future.

In summary, our findings indicate the following model for PD-L1 actions in GBM (**Figure 7B**): Along with the rapid GBM growth, inner GBM cells suffer severe starvation, which causes cytoskeleton collase; while frontier GBM cells suffer less severe starvation, which induces PD-L1 expression and its binding to Akt non-PH domain. This reinforces Akt's membrane-binding and leads to increased full activation of Akt as well as its downstream p62/LC3/F-actin signaling, preventing starvation-induced Akt inhibition and facilitating GBM cell invasion. By combining our previous findings that PD-L1 promotes EMT of glioma cells, we speculate that PD-L1/Akt/autophagy/F-actin is a key driving force for GBM aggressiveness, which serves as a potential therapeutic target for GBM.

DATA AVAILABILITY STATEMENT

The datasets generated for this study can be found in the NCBI (https://www.ncbi.nlm.nih.gov/geo/query/acc.cgi?acc=GSE107581).

ETHICS STATEMENT

The animal study was reviewed and approved by Experimental Animal Ethics Committee, Tongji Medical College, Huazhong University of Science and Technology.

AUTHOR CONTRIBUTIONS

RC, XX, XQ, FL, CL, YL, XL, and GJ performed the experiment. RC, FP, XQ, and XC data analysis, wrote the manuscript, and contributed to discussion. FH and DL contributed to discussion. RC, FP, XQ, and XC designed and wrote the manuscript.

FUNDING

This work was supported by grants from the National Nature Science Foundation of China (Grant Nos. 81471386, 81672504 to XC, Grant No. 81873854 to FP, Grant No. 81602202 to FH). The Fundamental Research Funds for the Central Universities, HUST (Grant No. 2017KFYXJJ048 to XC). Natural Science Foundation of Hubei Province (No. 2017 CFB639), Hubei Province Health and Family Planning Scientific Research Project (No. WJ2015Q002) and Science and Technology Planning Project of Wuhan (No. 2017060201010202) to FP. We declare all sources of funding received for the research being submitted.

SUPPLEMENTARY MATERIAL

The Supplementary Material for this article can be found online at: https://www.frontiersin.org/articles/10.3389/fonc.2019.01347/full#supplementary-material

REFERENCES

1. Stupp R, Mason WP, van den Bent MJ, Weller M, Fisher B, Taphoorn MJ, et al. Radiotherapy plus concomitant and adjuvant temozolomide for glioblastoma. *N Engl J Med*. (2005) 352:987–96. doi: 10.1056/NEJMoa043330
2. Wen PY, Kesari S. Malignant gliomas in adults. *N Engl J Med*. (2008) 359:492–507. doi: 10.1056/NEJMra0708126
3. Evans SM, Judy KD, Dunphy I, Jenkins WT, Nelson PT, Collins R, et al. Comparative measurements of hypoxia in human brain tumors using needle electrodes and EF5 binding. *Cancer Res*. (2004) 64:1886–92. doi: 10.1158/0008-5472.CAN-03-2424
4. Mizushima N, Levine B, Cuervo AM, Klionsky DJ. Autophagy fights disease through cellular self-digestion. *Nature*. (2008) 451:1069–75. doi: 10.1038/nature06639
5. Qu X, Zou Z, Sun Q, Luby-Phelps K, Cheng P, Hogan RN, et al. Autophagy gene-dependent clearance of apoptotic cells during embryonic development. *Cell*. (2007) 128:931–46. doi: 10.1016/j.cell.2006.12.044
6. Laplante M, Sabatini DM. mTOR signaling in growth control and disease. *Cell*. (2012) 149:274–93. doi: 10.1016/j.cell.2012.03.017
7. Jennewein L, Ronellenfitsch MW, Antonietti P, Ilina EI, Jung J, Stadel D, et al. Diagnostic and clinical relevance of the autophago-lysosomal network in human gliomas. *Oncotarget*. (2016) 7:20016–32. doi: 10.18632/oncotarget.7910
8. Zhang ZS, Wang J, Shen YB, Guo CC, Sai KE, Chen FR, et al. Dihydroartemisinin increases temozolomide efficacy in glioma cells by inducing autophagy. *Oncol Lett*. (2015) 10:379–83. doi: 10.3892/ol.2015.3183
9. Yan Y, Xu Z, Dai S, Qian L, Sun L, Gong Z. Targeting autophagy to sensitive glioma to temozolomide treatment. *J Exp Clin Cancer Res*. (2016) 35:23. doi: 10.1186/s13046-016-0303-5
10. Hart T, Chandrashekhar M, Aregger M, Steinhart Z, Brown KR, MacLeod G, et al. High-resolution CRISPR screens reveal fitness genes and genotype-specific cancer liabilities. *Cell*. (2015) 163:1515–26. doi: 10.1016/j.cell.2015.11.015
11. Kim D, Fiske BP, Birsoy K, Freinkman E, Kami K, Possemato RL, et al. SHMT2 drives glioma cell survival in ischaemia but imposes a dependence on glycine clearance. *Nature*. (2015) 520:363–7. doi: 10.1038/nature14363
12. Wintterle S, Schreiner B, Mitsdoerffer M, Schneider D, Chen L, Meyermann R, et al. Expression of the B7-related molecule B7-H1 by glioma cells: a potential mechanism of immune paralysis. *Cancer Res*. (2003) 63:7462–7.

13. Wilmotte R, Burkhardt K, Kindler V, Belkouch MC, Dussex G, Tribolet N, et al. B7-homolog 1 expression by human glioma: a new mechanism of immune evasion. *Neuroreport*. (2005) 16:1081–5. doi: 10.1097/00001756-200507130-00010
14. Berghoff AS, Kiesel B, Widhalm G, Rajky O, Ricken G, Wohrer A, et al. Programmed death ligand 1 expression and tumor-infiltrating lymphocytes in glioblastoma. *Neuro Oncol*. (2015) 17:1064–75. doi: 10.1093/neuonc/nou307
15. Chen RQ, Liu F, Qiu XY, Chen XQ. The prognostic and therapeutic value of PD-L1 in glioma. *Front Pharmacol*. (2018) 9:1503. doi: 10.3389/fphar.2018.01503
16. Garber ST, Hashimoto Y, Weathers SP, Xiu J, Gatalica Z, Verhaak RG, et al. Immune checkpoint blockade as a potential therapeutic target: surveying CNS malignancies. *Neuro Oncol*. (2016) 18:1357–66. doi: 10.1093/neuonc/now132
17. Wang Z, Zhang C, Liu X, Wang Z, Sun L, Li G, et al. Molecular and clinical characterization of PD-L1 expression at transcriptional level via 976 samples of brain glioma. *Oncoimmunology*. (2016) 5:e1196310. doi: 10.1080/2162402X.2016.1196310
18. Xue S, Hu M, Li P, Ma J, Xie L, Teng F, et al. Relationship between expression of PD-L1 and tumor angiogenesis, proliferation, and invasion in glioma. *Oncotarget*. (2017) 8:49702–12. doi: 10.18632/oncotarget.17922
19. Liu Y, Carlsson R, Ambjorn M, Hasan M, Badn W, Darabi A, et al. PD-L1 expression by neurons nearby tumors indicates better prognosis in glioblastoma patients. *J Neurosci*. (2013) 33:14231–45. doi: 10.1523/JNEUROSCI.5812-12.2013
20. Nduom EK, Wei J, Yaghi NK, Huang N, Kong LY, Gabrusiewicz K, et al. PD-L1 expression and prognostic impact in glioblastoma. *Neuro Oncol*. (2016) 18:195–205. doi: 10.1093/neuonc/nov172
21. Han J, Hong Y, Lee YS. PD-L1 Expression and combined status of PD-L1/PD-1-positive tumor infiltrating mononuclear cell density predict prognosis in glioblastoma patients. *J Pathol Transl Med*. (2017) 51:40–8. doi: 10.4132/jptm.2016.08.31
22. Lee KS, Lee K, Yun S, Moon S, Park Y, Han JH, et al. Prognostic relevance of programmed cell death ligand 1 expression in glioblastoma. *J Neuro Oncol*. (2018) 136:453–61. doi: 10.1007/s11060-017-2675-6
23. Miyazaki T, Ishikawa E, Matsuda M, Akutsu H, Osuka S, Sakamoto N, et al. Assessment of PD-1 positive cells on initial and secondary resected tumor specimens of newly diagnosed glioblastoma and its implications on patient outcome. *J Neuro Oncol*. (2017) 133:277–85. doi: 10.1007/s11060-017-2451-7
24. D'Arrigo P, Russo M, Rea A, Tufano M, Guadagno E, Del Basso De Caro ML, et al. A regulatory role for the co-chaperone FKBP51s in PD-L1 expression in glioma. *Oncotarget*. (2017) 8:68291–304. doi: 10.18632/oncotarget.19309
25. Dossou AS, Basu A. The emerging roles of mTORC1 in macromanaging autophagy. *Cancers*. (2019) 11:e1422. doi: 10.3390/cancers11101422
26. Jhanwar-Uniyal M, Wainwright JV, Mohan AL, Tobias ME, Murali R, Gandhi CD, et al. Diverse signaling mechanisms of mTOR complexes: mTORC1 and mTORC2 in forming a formidable relationship. *Adv Biol Regul*. (2019) 72:51–62. doi: 10.1016/j.jbior.2019.03.003
27. Clark CA, Gupta HB, Sareddy G, Pandeswara S, Lao S, Yuan B, et al. Tumor-intrinsic PD-L1 signals regulate cell growth, pathogenesis, and autophagy in ovarian cancer and melanoma. *Cancer Res*. (2016) 76:6964–74. doi: 10.1158/0008-5472.CAN-16-0258
28. Dorand RD, Nthale J, Myers JT, Barkauskas DS, Avril S, Chirieleison SM, et al. Cdk5 disruption attenuates tumor PD-L1 expression and promotes antitumor immunity. *Science*. (2016) 353:399–403. doi: 10.1126/science.aae0477
29. Qiu XY, Hu DX, Chen WQ, Chen RQ, Qian SR, Li CY, et al. PD-L1 confers glioblastoma multiforme malignancy via Ras binding and Ras/Erk/EMT activation. *Biochim Biophys Acta Mol Basis Dis*. (2018) 1864:1754–69. doi: 10.1016/j.bbadis.2018.03.002
30. Zhao L, Li C, Liu F, Zhao Y, Liu J, Hua Y, et al. A blockade of PD-L1 produced antitumor and antimetastatic effects in an orthotopic mouse pancreatic cancer model via the PI3K/Akt/mTOR signaling pathway. *OncoTargets Ther*. (2017) 10:2115–26. doi: 10.2147/OTT.S130481
31. Chang CH, Qiu J, O'Sullivan D, Buck MD, Noguchi T, Curtis JD, et al. Metabolic competition in the tumor microenvironment is a driver of cancer progression. *Cell*. (2015) 162:1229–41. doi: 10.1016/j.cell.2015.08.016
32. Ichimura Y, Komatsu M. Activation of p62/SQSTM1-Keap1-nuclear factor erythroid 2-related factor 2 pathway in cancer. *Front Oncol*. (2018) 8:210. doi: 10.3389/fonc.2018.00210
33. Liu X, Zhao P, Wang X, Wang L, Zhu Y, Gao W. Triptolide induces glioma cell autophagy and apoptosis via upregulating the ROS/JNK and downregulating the Akt/mTOR signaling pathways. *Front Oncol*. (2019) 9:387. doi: 10.3389/fonc.2019.00387
34. Mahajan K, Coppola D, Challa S, Fang B, Chen YA, Zhu W, et al. Ack1 mediated AKT/PKB tyrosine 176 phosphorylation regulates its activation. *PLoS ONE*. (2010) 5:e9646. doi: 10.1371/journal.pone.0009646
35. Yang WL, Wang J, Chan CH, Lee SW, Campos AD, Lamothe B, et al. The E3 ligase TRAF6 regulates Akt ubiquitination and activation. *Science*. (2009) 325:1134–8. doi: 10.1126/science.1175065
36. Bellacosa A, Chan TO, Ahmed NN, Datta K, Malstrom S, Stokoe D, et al. Akt activation by growth factors is a multiple-step process: the role of the PH domain. *Oncogene*. (1998) 17:313–25. doi: 10.1038/sj.onc.1201947
37. Kondapaka SB, Singh SS, Dasmahapatra GP, Sausville EA, Roy KK. Perifosine, a novel alkylphospholipid, inhibits protein kinase B activation. *Mol Cancer Therapeut*. (2003) 2:1093–103.
38. Alsaab HO, Sau S, Alzhrani R, Tatiparti K, Bhise K, Kashaw SK, et al. PD-1 and PD-L1 Checkpoint signaling inhibition for cancer immunotherapy: mechanism, combinations, and clinical outcome. *Front Pharmacol*. (2017) 8:561. doi: 10.3389/fphar.2017.00561
39. Wolchok JD. PD-1 Blockers. *Cell*. (2015) 162:937. doi: 10.1016/j.cell.2015.07.045
40. Chen G, Huang AC, Zhang W, Zhang G, Wu M, Xu W, et al. Exosomal PD-L1 contributes to immunosuppression and is associated with anti-PD-1 response. *Nature*. (2018) 560:382–6. doi: 10.1038/s41586-018-0392-8
41. Porta C, Paglino C, Mosca A. Targeting PI3K/Akt/mTOR signaling in cancer. *Front Oncol*. (2014) 4:64. doi: 10.3389/fonc.2014.00064
42. Weyerhauser P, Kantelhardt SR, Kim EL. Re-purposing chloroquine for glioblastoma: potential merits and confounding variables. *Front Oncol*. (2018) 8:335. doi: 10.3389/fonc.2018.00335

Conflict of Interest: The authors declare that the research was conducted in the absence of any commercial or financial relationships that could be construed as a potential conflict of interest.

frontiers in Oncology

ORIGINAL RESEARCH
published: 17 December 2019
doi: 10.3389/fonc.2019.01424

FAP-a and GOLPH3 Are Hallmarks of DCIS Progression to Invasive Breast Cancer

Li-Na Yu[1,2,3], *Zhen Liu*[4], *Yan Tian*[1,2,3], *Pei-Pei Zhao*[1,2,3] *and Xing Hua*[5]*

[1] Department of Pathology, Nanfang Hospital, Guangzhou, China, [2] Department of Pathology, School of Basic Medical Sciences, Southern Medical University, Guangzhou, China, [3] Guangdong Provincial Key Laboratory of Molecular Tumor Pathology, Guangzhou, China, [4] Department of Pathology, School of Clinical Medicine, Guizhou Medical University, Guiyang, China, [5] Department of Pathology, Guangzhou Red Cross Hospital, Medical College, Jinan University, Guangzhou, China

Biological markers that could predict the progression of ductal carcinoma *in-situ* (DCIS) to invasive breast cancer (IDC) are required urgently for personalized therapy for patients diagnosed with DCIS. As stroma was invaded by malignant cells, perturbed stromal-epithelial interactions would bring about tissue remodeling. With the specific expression of the fibroblast activation protein-alpha (FAP-a), Carcinoma-associated fibroblasts (CAFs) are the main cell populations in the remodeled tumor stroma. Golgi phosphoprotein 3 (GOLPH3), a documented oncogene possessing potent transforming capacity, is not only up-regulated in many tumors but also an efficient indicator of poor prognosis and more malignant tumors. The present study aimed to retrospectively evaluate the pathological value of FAP-a and GOLPH3 in predicting the recurrence or progression of DCIS to invasive breast cancer. Immunohistochemical techniques were applied to investigate the expression of FAP-a GOLPH3 in 449 cases of DCIS patients received extensive resection and with close follow-up, but not being treated with any form of chemo- or radio-therapy. The combination of FAP-a and GOLPH3 in predicating the recurrence or progression of DCIS into invasive breast cancer was specifically examined. The study demonstrated that the overexpression of FAP-a in stromal fibroblasts and GOLPH3 in carcinoma cells are highly predictive of DCIS recurrence and progression into invasive breast cancer. Both FAP-a and GOLPH3 have high specificity and sensitivity to predict the recurrence of DCIS. Moreover, the combination of FAP-a and GOLPH3 tends to further improve the specificity and sensitivity of DCIS recurrence by 9.72–10.31 and 2.72–3.63%, respectively. FAP-a and GOLPH3 serve as novel markers in predicting the recurrence or progression of DCIS into invasive breast cancer.

Keywords: FAP-a, GOLPH3, DCIS, recurrence, breast cancer

OPEN ACCESS

Edited by:
Dong-Hua Yang,
St. John's University, United States

Reviewed by:
Hamid Morjani,
Université de Reims Champagne-Ardenne, France
Shanchun Guo,
Xavier University of Louisiana, United States

****Correspondence:***
Xing Hua
nana1800@smu.edu.cn

Specialty section:
This article was submitted to Molecular and Cellular Oncology, a section of the journal Frontiers in Oncology

Received: *25 July 2019*
Accepted: *29 November 2019*
Published: *17 December 2019*

Citation:
Yu L-N, Liu Z, Tian Y, Zhao P-P and Hua X (2019) FAP-a and GOLPH3 Are Hallmarks of DCIS Progression to Invasive Breast Cancer. Front. Oncol. 9:1424. doi: 10.3389/fonc.2019.01424

INTRODUCTION

With the development and aid of high quality screening mammography, the probability of detected ductal carcinoma *in situ* (DCIS) has raised rapidly (1). DCIS declares roughly 20% of all screening-detected breast cancer recently (2). Breast conserving therapy combined with or without radiotherapy has been generally accepted as the standard and efficient method to treat DCIS (3). Although DCIS is a type of non-invasive breast cancer, in which carcinoma cells are

controlled by the basement membrane of breast duct, in reality, DCIS remains a heterogeneous cluster of pre-invasive breast cancers with various types of morphology, expansion, and malignant capacities (4).

DCIS remains the status of the carcinoma precursor lesion of invasive ductal carcinoma (IDC), but mechanisms under the conversion are largely unknown (5–7). In order to predict the fate of DCIS more accurately, to develop invasive cancer or remain at DCIS status, efforts must be made continuously to investigate the molecular aspects of the disease. In the last few years, several prognostic factors have emerged as possible contenders to help stratify risk (8). For example, a study by Martins et al. (9) demonstrated that monocarboxylate transporter 4 (MCT4) and stromal caveolin 1 (Cav-1) were differentially expressed in IDC and DCIS. Suppression of Cav-1 and activation of MCT4 in the stroma were indicators of overproduction of oxidative stress and glycolysis, indicating the progression from DCIS status into IDC.

The prolyl-specific serine proteinase fibroblast activation protein alpha (FAP-a), a type II integral membrane protein (10), is a M(r) 95,000 cell surface antigen brought about instantaneously by induced stromal fibroblasts during embryogenesis (11), which is the latter stages of wound healing (12), in some pathologic status where fibrous tissue growth is a conspicuous feature (13), and is occasionally present in normal fibroblast or pancreatic a-cells (14, 15). As shown in our previous studies, immunohistochemical analyses were applied to evaluate the expression of FAP-a in normal mammary tissues and usual ductal hyperplasia (UDH), DCIS, DCIS with microinvasive (DCIS-MI) and IDC. We further hypothesized the participation of FAP-a in designating the microemboli's formation, facilitating the pathological process of breast cancer (16). Cremasco et al. (17) showed that breast tumors contain a variety of FAP expressing stromal cells with dichotomy function, phenotype, and location. Busek et al. (18) also found that FAP is a promising therapeutic target. In this study, we found that FAP-a is specifically expressed in the stromal fibroblasts of IDC and the tumor-host interface of the invasive front of DCIS-MI. However, FAP-a is negatively expressed in stromal fibroblasts of normal mammary tissues and UDH. We are the first study that proposed and demonstrated FAP-a's potential as a novel biomarker for pathological diagnosis of DCIS with microinvasion. Although high FAP-a expression was detected in stromal fibroblasts of IDC and tumor-host interface at the invasive front of DCIS-MI, its correlation with the chemo- or radio-therapy treatment has not been studied because of the limited sample size.

Previous investigations have demonstrated that overexpression of human chromosome 5p13 contributed to tumor formation, progression, and metastasis. The expression of Golgi phosphoprotein 3(GOLPH3) was found to be correlated with copy number of 5p13 in human lung cancer, and gain or loss of function studies have proved that GOLPH3 was a genuine oncogene possessing strong transforming activity, which was induced in cancers with 5p amplification (19). Further researches on the clinical importance of GOLPH3 revealed that GOLPH3 expression was not only increased in oral tongue cancer and glioma, but also was indicating poor prediction and more malignant tumors (20–22). These results further indicated GOLPH3's significant role in the progression of various types of tumors. In our previous works, it was revealed that overexpression of GOLPH3 promoted the progression of prostate cancer from hormone sensitive stage to hormone stage, and GOLPH3's potential as a novel biomarker and potential target for antagonizing castration resistant prostate cancer (23). Zeng et al. showed that high expression of GOLPH3 was associated with low overall survival rate of breast cancer patients, and overexpression of GOLPH3 increased the proliferation and tumorigenicity of human breast cancer cells (24).

In the present study, immunohistochemical techniques were applied to evaluate the role of GOLPH3 in carcinoma cells and FAP-a in the stroma in recruited DCIS patients received combined treatment of wide-excision and close follow-up, but haven't received any type of chemo- or radio-therapy; which further explored the potentials of FAP-a and GOLPH3 as indicative marker during the natural progression of DCIS. To this end, we specifically examined the correlation between FAP-a and GOLPH3 expression, their clinico-pathological values in predicting the recurrence or progression of DCIS into invasive breast cancer.

MATERIALS AND METHODS

Case Selection

We retrospectively recruited 449 patients who had received treatment of mastectomy between May 1994 and May 2013 using the surgical oncology breast cancer database. Archives were acquired from the documentation of the Department of Pathology and Medical Records Room, the Fourth Affiliated Hospital of Jinan University and Nan Fang Hospital of Southern Medical University in Guangzhou, China. This study was approved by the Ethics Committee of Guangzhou Red Cross Hospital.

Formalin-fixed and further paraffin-embedded (FFPE) tissue sections were prepared from 449 patients with DCIS. All patients undergoing surgical excision were treated by the same surgeon, and all had negative margins (= or > 10 mm) at the end of surgical excision or re-excision. None of the patients received radiation treatment or tamoxifen therapy. The time of diagnosis and recurrence was recorded as the time of surgery that initiated the pathologic diagnosis. Data analysis indicated the endpoint of treatment based on the appearance of local recurrence of DCIS, invasive breast carcinoma and without pathological symptoms at the last time of follow-up. As to each subject, histologic patterns (comedo, cribriform, micropapillary, papillary, or solid), presence of necrosis, inflammation and nuclear grade were kept on record. Routine morphological analysis of hematoxylin and eosin stained tissue sections were blindly reviewed by five pathologists together and a diagnostic agreement was finalized.

Immunohistochemistry

The expression of GOLPH3 in tumor cells and FAP-a in tumor stroma were evaluated by immunohistochemical staining. Firstly, sections were deparaffinized by reduced xylene and then conducted antigen retrieval in Tris-EDTA retrieval buffer

(PH 9.0) (Dako, Carpinteria, CA) before immunohistochemical staining with a Dako autostainer. Immunohistochemical staining for GOLPH3 and FAP-a was completed as described previously. The GOLPH3 primary antibodies (clone 19112-1-AP, 1:100 dilution) were obtained from the ProteinTech Group, and the FAP-a primary antibodies (clone 427819, 1:50 dilution) were obtained from R & D systems. Positive and negative staining were carried out for each staining. The degrees of staining were graded based on the following criteria. Grade 1 was taken as semi-quantitative and negative staining; Grade 2 was taken when either diffuse weak staining or <30% strong staining appeared; Graded 3 was awarded when 30% or more of the cells have been stained.

Statistics

The time from surgery to recurrence (TTR) was recorded and evaluated by using Kaplan-Meier survival curves. The comparison of stratified survival curves used log-rank tests. Cox proportional hazards regression was applied to analyze the correlation among FAP-a, GOLPH3 expressions, and TTR with other potential diagnostic markers of TTR. All hypotheses testing was conducted using the Fisher exact test or the Kruskal-Wallis test, based on the discrete or continuous essence of any other factor. Correlation analysis among FAP-a, GOLPH3 staining intensity, and DCIS recurrence rate was determined using the Spearman test.

P-values were all two-sided, and $p < 0.05$ was considered as statistical significance. Statistical analysis was accomplished using the SPSS statistical analysis software version 19.0, and tables and graphs were generated.

RESULTS

Informative Analysis of the DCIS Patient Cohort

As shown in **Table 1**, 449 women were with a median age of 52 years (range 22–87 years) when diagnosed with DCIS. The median of follow-up time was 169.84 months (14.15 years). Pathological variables including grade, histologic pattern and necrosis were recorded accordingly. Meanwhile, follow-up on DCIS recurrence pattern and DCIS deterioration into invasive breast cancer were also recorded. The immunophenotype of GOLPH3 and FAP-a is correlated with each clinicopathological parameter listed in **Table 1**. As shown in **Figure 1**, the FAP-a protein expression was mainly detected in the cytoplasmic fractions of stromal fibroblasts, while GOLPH3 in was detected the cytoplasm of breast carcinoma cells. In these 449 DCIS patients, 110 of which appeared certain degree of recurrence (49 progression into DCIS, while the other 61 progression into invasive breast cancer), resulting in an final recurrence rate of 24.50%. Therefore, the progressive rate of DCIS into invasive breast cancer at the present cohort study was 13.59 percent (61/449), which is relevant to the expected rate of 12–15%. The median time of recurrence turned out to be 83.25 months (DCIS with 33.45 months, invasive breast cancer with 115.36 months).

TABLE 1 | Levels of FAP-a and GOLPH3 expression in relation to clinicopathologic variables.

Characteristics	FAP-a expression		GOLPH3 expression	
	Negative	Positive	Negative	Positive
Number	316	133	321	128
Age, year				
≤50	137	58	145	49
>50	179	75	176	79
Grade				
Low	88	29	47	21
Moderate	107	33	176	69
High	121	71	98	38
Histological pattern				
Solid	58	28	62	27
Cribriform	121	32	116	23
Papillary	11	8	15	11
Micropapillary	29	7	27	18
Comedo	97	58	101	49
Necrosis				
Yes	135	51	145	77
No	181	82	176	51

Stromal FAP-a Is Associated With DCIS Recurrence

As shown in **Table 2**, immunostaining of stromal FAP-a was scored semiquantitative as 3 (high), 2 (low), and 1 (absent of staining) based on the staining intensity. In 49 DCIS recurrence cases, the percentages of grade 3, 2, and 1 of stromal FAP-a immunostaining were 65.31% (32/49), 18.37% (9/49), and 16.33% (8/49), respectively. In 61 DCIS patients who recurred to IDC, percentages of grade 3, 2, and 1 of FAP-a immunostaining were 65.57% (40/61), 19.67% (12/61), and 14.75% (9/61), respectively. In 339 DCIS patients without recurrence, the incidence of high, low, and absent stromal FAP-a immunostaining was 7.96% (27/339), 3.54% (12/339), and 88.50% (300/339), respectively. Spearman test showed no significant correlation between FAP-a staining intensity and DCIS recurrence in DCIS recurrence patients. Among 132 FAP-a positive DCIS patients, 41 recurred to DCIS, 52 recurred, and progressed into invasive breast cancer, while the remaining 39 cases experienced no recurrence. FAP-a (high/low) is expressed in 84.55% (93/110) of the DCIS recurrence patients, while only 11.50% (39/339) in DCIS patients without recurrence. This difference was statistically significant ($P < 0.001$). By contrast, no statistical difference was detected of FAP-a expression between DCIS recurrence and invasive progression. Kaplan-Meier curves for overall recurrent rate, rate of recurrent to DCIS, and progression into invasive breast cancer data were revealed in **Figure 2**. The left panel suggested that for the patients with higher expression of FAP-a, the overall recurrent rate will be higher. The middle panel suggested that the higher expression of FAP-a may be correlate with the higher rate of recurrent to DCIS. The right panel suggested that the patients with

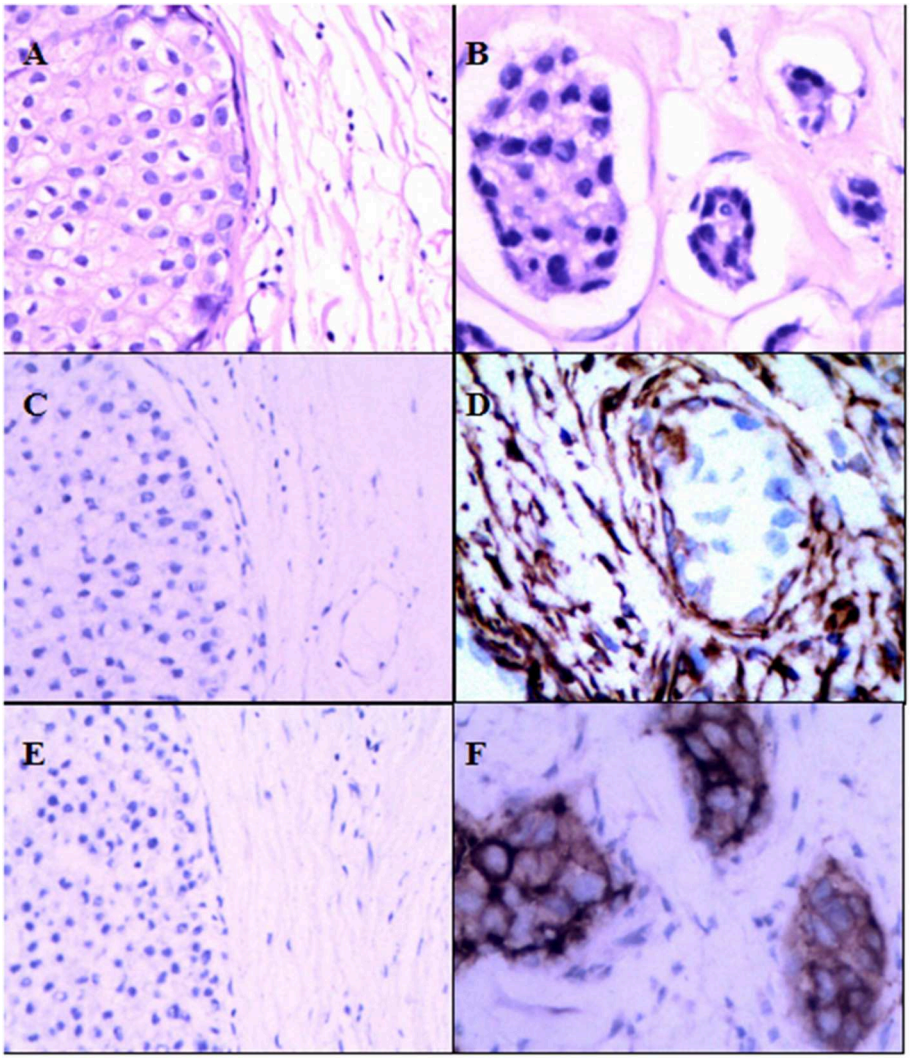

FIGURE 1 | Expression of FAP-a and GOLPH3 in DCIS and IDC. **(A)** Hematoxylin and eosin (H & E) staining of DCIS. **(B)** Hematoxylin and eosin (H & E) staining of IDC. **(C)** IHC staining of FAP-a in DCIS. **(D)** IHC staining of FAP-a in IDC. **(E)** IHC staining of GOLPH3 in DCIS. **(F)** IHC staining of GOLPH3 in IDC.

higher expression of FAP-a may have the higher possibility of progression to invasive breast cancer. It was worth noting that the presence of stromal FAP-a was positively correlated with DCIS recurrence.

GOLPH3 Expression Is Associated With DCIS Recurrence

As shown in **Table 3**, immunostaining of stromal GOLPH3 was scored semiquantitative as 3 (high), 2 (low), and 1 (absent of staining) based on the staining intensity. In 49 DCIS recurrence cases, the incidence of high, low, and absent GOLPH3 immunostaining was 69.39% (34/49), 20.41% (10/49), and 10.20% (5/49), respectively. In 61 DCIS patients who recurred to IDC, the incidence of high, low, and absent GOLPH3 immunostaining was 62.30% (38/61), 16.39% (10/61), and 21.31% (13/61), respectively. In the 339 DCIS cases without recurrence, the percentages of grades 3 (high), 2 (low), and 1 of GOLPH3 immunostaining were 6.78% (23/339), 4.13% (14/339), and 89.09% (302/339), respectively. Spearman test showed no significant correlation between the GOLPH3 staining intensity and DCIS recurrence in DCIS recurrence patients. Among the 132 GOLPH3 positive DCIS patients, 44 of them underwent a recurrence to DCIS, 48 recurred and progressed into invasive breast cancer, while the remaining 37 cases did not experienced no recurrence. GOLPH3 (high/low) is expressed in 83.64% (92/110) of the DCIS recurrence patients while in 10.91% (37/339) of the DCIS without recurrence. This difference was statistically significant ($P < 0.0001$). By contrast, no statistical difference was detected regard of GOLPH3 expression between DCIS recurrence and the invasive progression of DCIS. Kaplan-Meier curves for overall recurrence, DCIS recurrence, and progression into invasive breast cancer were shown in **Figure 3**. Note that the presence of GOLPH3 is specifically associated with DCIS recurrence.

The Combination of FAP-a and GOLPH3 Expression Is Associated With DCIS Recurrence

The immunostaining of FAP-a in stromal fibroblasts and GOLPH3 in carcinoma cells was scored semiquantitatively as 3 (high), 2 (low), and 1 (absent of staining) based on the staining intensity, respectively. The staining intensity 2 and 3 were considered as positive and the staining intensity 1 was considered as negative. As shown in **Table 4**, 41 of the 49 DCIS recurrence patients showed both FAP-a positive in stromal fibroblasts and GOLPH3 positive in carcinoma cells (FAP-a$^+$GOLPH3$^+$), three of them showed FAP-a$^-$GOLPH3$^+$, five showed FAP-a$^-$GOLPH3$^-$, while none of them showed FAP-a$^+$GOLPH3$^-$. Among the 61 DCIS patients who recurred to IDC, 48 showed FAP-a$^+$GOLPH3$^+$, four showed FAP-a$^+$GOLPH3$^-$, nine showed FAP-a$^-$GOLPH3$^-$, while none of them showed FAP-a$^-$GOLPH3$^+$. Moreover, FAP-a$^+$GOLPH3$^-$ existed in 80.91% (89/110) of DCIS recurrence patients, while only 1.18% (4/339) of DCIS patients without recurrence (4/339) showed FAP-a$^+$GOLPH3$^+$ with statistically significant difference ($P < 0.0001$). Pearson test demonstrated a positively correlative relationship among FAP-a, GOLPH3 co-expression and DCIS recurrence. As shown **Figure 4**, Kaplan-Meier curves were revealed for overall recurrence, DCIS recurrence, and invasive recurrence progressing into invasive breast cancer. Note that the co-expression of FAP-a and GOLPH3 are specifically associated with DCIS recurrence.

Specificity and Sensitivity of FAP-a and GOLPH3 in Diagnosis of DCIS Recurrence

The immunostaining of FAP-a in stromal fibroblasts and GOLPH3 in carcinoma cells was scored semiquantitatively as 3 (high), 2 (low), and 1 (absent of staining) based on the staining intensity, respectively. The staining intensity 2 and 3 were considered as positive and the staining intensity 1 was considered as negative. As shown in **Table 5**, the specificity and sensitivity of FAP-a in the diagnosis of DCIS recurrence is 88.50 and 84.55%, respectively. The specificity and sensitivity of GOLPH3 in the diagnosis of DCIS recurrence is 89.09 and 83.64%, respectively. When combined FAP-a and GOLPH3, the specificity and sensitivity in diagnosis of DCIS recurrence increased to 98.82 and 87.27%, respectively.

TABLE 2 | The expression of stromal FAP-a is associated with DCIS recurrence.

Recurrence type	Total cases	Stromal FAP-a status					
		Score = 3		Score = 2		Score = 1	
		N	%	*N*	%	*N*	%
None	339	27	7.96	12	3.54	300	88.50
DCIS	49	32	65.31	9	18.37	8	16.33
IDC	61	40	65.57	12	19.67	9	14.75
Overall (DCIS + IDC)	110	72	65.45	21	19.09	17	15.45

TABLE 3 | GOLPH3 expression is associated with DCIS recurrence.

Recurrence type	Total cases	GOLPH3 status					
		Score = 3		Score = 2		Score = 1	
		N	%	*N*	%	*N*	%
None	339	23	6.78	14	4.13	302	89.09
DCIS	49	34	69.39	10	20.41	5	10.20
IDC	61	38	62.30	10	16.39	13	21.31
Overall (DCIS + IDC)	110	72	65.46	20	18.18	18	16.36

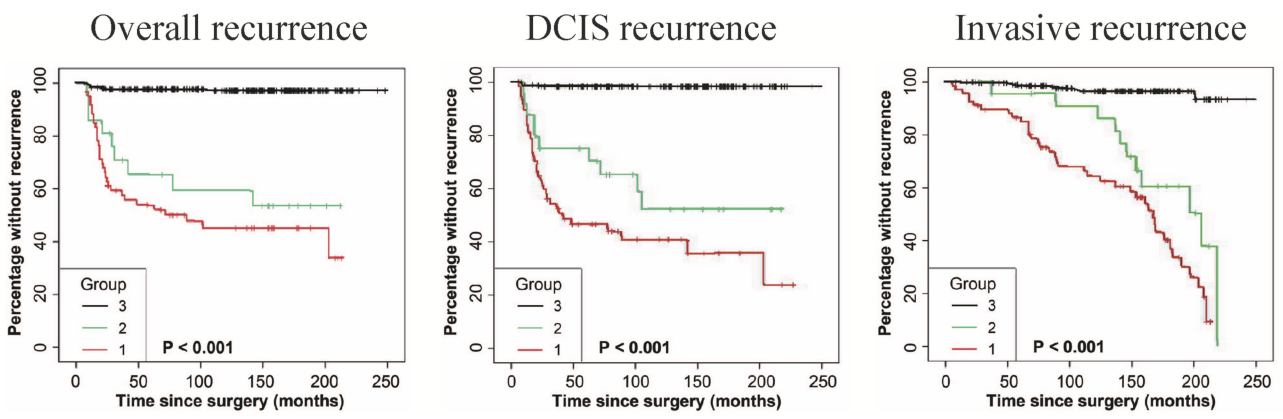

FIGURE 2 | Kaplan-Meier curves for stromal FAP-a state and duration to recurrence among DCIS patients. **(Left panel)** The expression or overexpression of stromal FAP-a is correlated with the elevation of overall recurrence. **(Middle panel)** The expression or overexpression of stromal FAP-a is correlated with the elevation of DCIS recurrence. **(Right panel)** The expression or overexpression of stromal FAP-a is positively correlated with the increase of DCIS progression to IDC. *p*-values (log rank test) are as shown.

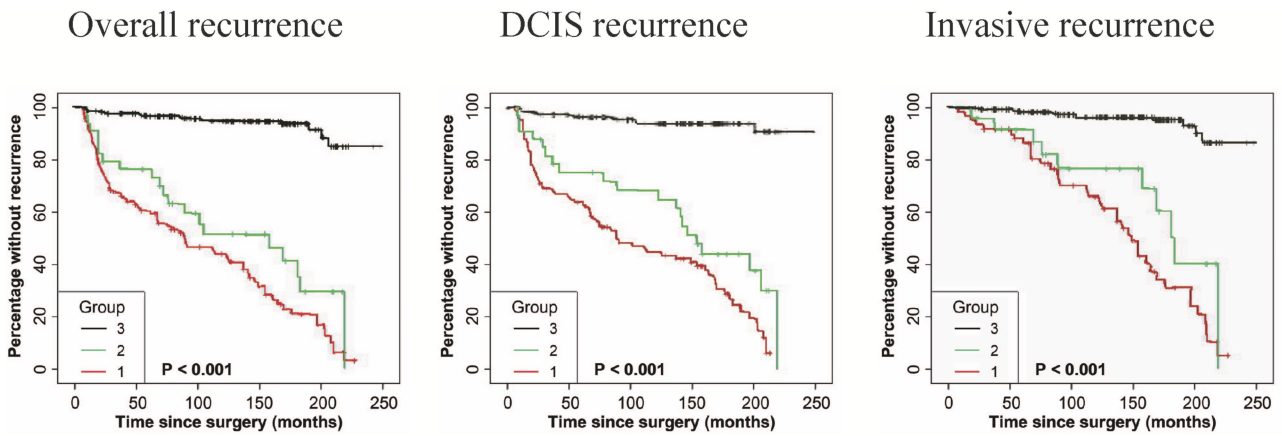

FIGURE 3 | Kaplan-Meier curves for GOLPH3 state and duration of recurrence among DCIS patients. **(Left panel)** The expression of GOLPH3 is positively associated with the induction of overall recurrence. **(Middle panel)** The expression of GOLPH3 is correlated with the increase of DCIS recurrence. **(Right panel)** The expression of GOLPH3 is associated with the induction in DCIS progression to IDC. High (score = 3), low (score = 2), and absent (score=1). *p*-values (log rank test) are as shown.

TABLE 4 | Specificity and sensitivity of FAP-a and GOLPH3 in diagnosis of DCIS recurrence.

Recurrence type	Cases	FAP-a and GOLPH3 status							
		FAP-a$^+$GOLPH3$^+$		FAP-a$^-$GOLPH3$^+$		FAP-a$^+$GOLPH3$^-$		FAP-a$^-$GOLPH3$^-$	
		N	%	*N*	%	*N*	%	*N*	%
None	339	4	1.18	20	5.90	38	11.21	277	81.71
DCIS	49	41	83.67	3	6.12	0	0	5	10.21
IDC	61	48	78.69	0	0	4	6.56	9	14.75
Overall (DCIS+IDC)	110	89	80.91	3	2.73	4	3.64	14	12.73

DISCUSSION

DCIS is considered as a precursor to invasive breast cancer. In this study, we demonstrated that 24.50% of DCIS patients undergo an ipsilateral local recurrence, and 13.59% of these recurrences are invasive in a sample of 449 DCIS patients. The risk of DCIS patients of local recurrence appearance or progression into invasive breast cancer after their treatment was still unpredicted at the present stage (25). The ability to develop a predictive model would present to be an enormous clinical advance to identify a molecular marker that would have predictive potential of DCIS's prognosis, either DCIS develops invasive cancer or stays DCIS.

Although several molecular factors have emerged as predictive marker of DCIS in the last few years, it remains challenging to clarify the prognostic significance of those bio-markers. In most studies, sample sizes were limited, and patients had undergone either endocrine treatment or radiotherapy (8, 9). In this study, all of the patients undergone only surgical excision and were treated by the same surgeon, and all of them are with negative margins to the end of surgical excision. None of the patients received radiation therapy or tamoxifen treatments, which potentiates us to evaluate the predictive potential of FAP-a and GOLPH3 during the natural history of DCIS disease progression.

Tissue remodeling stimulated by the interactions of perturbed stromal-epithelial cells is brought about during the carcinogenesis of DCIS recurrence (16). Although these interactions turns to of great importance in tumorigenesis, their underlying molecular mechanisms in tumorigenic processes are not fully understood. Most studies demonstrated that carcinoma-associated fibroblasts (CAFs) remain the major stromal cell population participating in the epithelial-stromal interaction in the remodeled micro environment, which were mainly responsible for production of FAP-a (5, 26, 27). In this study, 84.55% of the DCIS recurrence showed high/low expression of FAP-a expression in stromal fibroblasts, while only 11.50% of the DCIS without recurrence showed high/low FAP-a expression. Significant difference in the protein expression of FAP-a was detected between the DCIS recurrence group and without recurrence group. We have previously demonstrated that 82.72% (67/81) stromal fibroblasts in the invasive front of DCIS with microinvasion at the tumor-host interface showed significant FAP-a positivity, and all of the 67 cases of IDC exhibited strongly positive FAP-a staining in stromal fibroblasts. Thus, FAP-a was potentiated in the promotion of the formation of microemboli, which promotes the invasion of breast cancer. Hence, the micro environmental reprogramming of cancer revealed as a key step in DCIS recurrence, and it may of

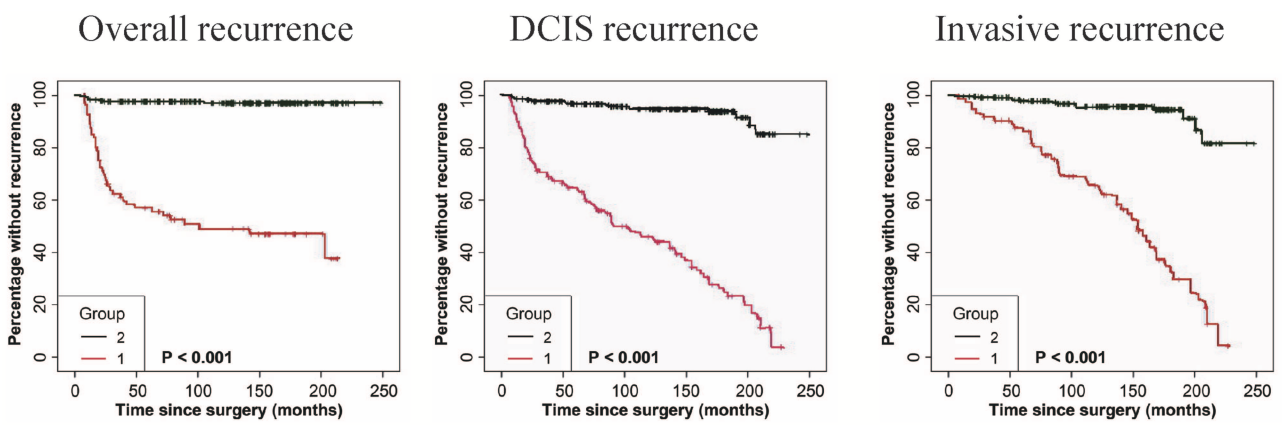

FIGURE 4 | Kaplan-Meier curves for FAP-a and GOLPH3 state and duration for recurrence among DCIS patients. **(Left panel)** The FAP-a$^+$GOLPH3$^+$ immunophenotype is correlated with the induction of overall recurrence. **(Middle panel)** The FAP-a$^+$GOLPH3$^+$ immunophenotype is associated with the increase of DCIS recurrence. **(Right panel)** The FAP-a$^+$GOLPH3$^+$ immunophenotype is correlated with the induction of DCIS progression to IDC. (FAP-a$^+$GOLPH3$^+$ immunophenotype, score=1; FAP-a$^-$GOLPH3$^-$, score = 2). *p*-values (log rank test) are as shown.

TABLE 5 | Association of the FAP-a and GOLPH3 with DCIS recurrence.

	Specificity		Sensitivity	
	N	%	*N*	%
FAP-a	300/339	88.50	93/110	84.55
GOLPH3	302/339	89.09	92/110	83.64
FAP-a + GOLPH3	335/339	98.82	96/110	87.27

greater importance to elucidate stromal metabolism other than characteristic of carcinoma cells to predict the prognosis of DCIS patients by characterizing.

Interestingly, our study elucidated that the presence of GOLPH3 in carcinoma cells is also specifically associated with DCIS recurrence. In this study, 83.64% of the DCIS recurrences demonstrated high/low GOLPH3 expression in carcinoma cells, while only 10.91% of the DCIS without recurrence showed high/low GOLPH3 expression. In addition, a significant difference was found in the expression of GOLPH3 protein between the DCIS recurrence group and without recurrence group. Several studies have shown that GOLPH3 is related to the prognosis of cancer. It has been reported that high GOLPH3 expression is associated with poor overall survival in patients with breast cancer and that GOLPH3 overexpression increases the proliferation and tumorigenicity of human breast cancer cells (24). In prostate cancer, patients with high levels of GOLPH3 will have shorter survival time (28). Zhang et al. (29) has found that GOLPH3, which is up-regulated in prostate cancer tissues, can be useful for predicting biochemical recurrence-free survival and overall survival in patients with prostate cancer. Moreover, GOLPH3 may be of significant potential as predictive marker of DFS and OS in subjects with diagnosed prostate cancer (23). Not only prostate cancer, but also GOLPH3 has been proved to be highly expressed in NSCLC tissues, indicating that GOLPH3 may be a useful diagnostic factor for NSCLC (30). Tang et al. found that high expression of GOLPH3 usually indicates poor survival of breast cancer and weak resistance to chemotherapy (31). GOLPH3L is an accessory homolog of GOLPH3. It had been found that the prognosis of ovarian cancer patients with high expression of GOLPH3L was lower than that of patients with low or no expression of GOLPH3L (32).

Meanwhile, the detection of GOLPH3 expression might serve as a reliable predictive marker. Same is reasonable that to determine the changes of GOLPH3 expression may also facilitate to comprehensively understand the incidence of progression in patients with prostate cancer.

To our understanding, a group of proteins constitutes in the trans-Golgi matrix were tightly regulated in the trans-Golgi and demonstrated to be responsible for anterograde and retrograde Golgi trafficking, as well as collaborating with the cytoskeleton and supporting the Golgi structure (33). GOLPH3 would transiently be transported to the surface of cytoplasm in the trans-Golgi and represented a first-in-class Golgi oncoprotein. Holly C. Dippold indicated that trafficking out of the Golgi relied on the interaction of GOLPH3, MYO18A, F-actin, and PtdIns (4) P. This process is controlled by MYO18A and F-actin and their transmission to the Golgi regulated by GOLPH3 and PtdIns (4) P. This evidence suggests that GOLPH3 traffics the tensile force responsible for successful tubule and vesicle formation (20). Kenneth L. Scott raised the hypothesis that GOLPH3 interacted with VPS35 and the tetramer to recycle receptor for key molecules, thus regulating downstream mTOR signaling (19). Tenorio et al. found that the cytosolic and membrane components of the three breast cell lines had biochemical differences in GOLPH3, that was that, in cancer cells, part of the overexpressed GOLPH3 was modified by differentiation (34).

We have shown here that the presence of FAP-a in stromal fibroblasts and GOLPH3 in carcinoma cells are reliable biomarker of DCIS recurrence and progression into

invasive breast cancer. Both FAP-a and GOLPH3 have high specificity and sensitivity in predicting the recurrence of DCIS. The specificity and sensitivity of FAP-a in diagnosis of DCIS recurrence was 88.50 and 84.55%, respectively. The specificity and sensitivity of GOLPH3 in the diagnosis of DCIS recurrence was 89.09 and 83.64%, respectively. However, the combination of FAP-a and GOLPH3 had higher specificity and sensitivity that the specificity and sensitivity was 98.82 and 87.27%, respectively. Compared with FAP-a and GOLPH3, the combination of FAP-a and GOLPH3 refined the specificity and sensitivity of potent prediction of DCIS recurrence by 9.72–10.31 and 2.72–3.63%, respectively. Thus, we identified that FAP-a and GOLPH3 might potentiate as a reliable biomarker for predicting the DCIS recurrence and progression of DCIS into invasive breast cancer. Though FAP-a and GOLPH3 showed significant correlation both in DCIS recurrence and in DCIS without recurrence patients, the complex interplay between FAP-a and GOLPH3 in DCIS recurrence remains poorly understood.

DATA AVAILABILITY STATEMENT

The datasets generated for this study are available on request to the corresponding author.

AUTHOR CONTRIBUTIONS

XH and L-NY: study concepts. L-NY, ZL, YT, and P-PZ: study design and statistical analysis. YT, P-PZ, and ZL: data acquisition. L-NY: quality control of data and algorithms. L-NY and ZL: data analysis and interpretation. XH: manuscript preparation. ZL and L-NY: manuscript editing. XH, L-NY, ZL, and P-PZ: manuscript review.

REFERENCES

1. Patani N, Cutuli B, Mokbel K. Current management of DCIS: a review. *Breast Cancer Res Treat.* (2008) 111:1–10. doi: 10.1007/s10549-007-9760-z
2. Ozanne EM, Shieh Y, Barnes J, Bouzan C, Hwang ES, Esserman LJ. Characterizing the impact of 25 years of DCIS treatment. *Breast Cancer Res Treat.* (2011) 129:165–73. doi: 10.1007/s10549-011-1430-5
3. Westenberg AH, Rutgers EJ, Peterse JL, Hendriks JH, Beex LV, van Tienhoven G. The treatment of ductal carcinoma *in situ* (DCIS) of the breast. *Ned Tijdschr Geneeskd*. (2003) 147:2157–61.
4. Shehata M, Grimm L, Ballantyne N, Lourenco A, Demello LR, Kilgore MR, et al. Ductal carcinoma *in situ*: current concepts in biology, imaging, and treatment. *J Breast Imaging.* (2019) 1:166–76. doi: 10.1093/jbi/wbz039.
5. Shimoda M, Mellody KT, Orimo A. Carcinoma-associated fibroblasts are a rate-limiting determinant for tumour progression. *Semin Cell Dev Biol.* (2010) 21:19–25. doi: 10.1016/j.semcdb.2009.10.002
6. Schmale I, Liu S, Rayhanabad J, Russell CA, Sener SF. Ductal carcinoma *in situ* (DCIS) of the breast: perspectives on biology and controversies in current management. *J Surg Oncol.* (2012) 105:212–20. doi: 10.1002/jso.22020.
7. Guo Q, Li VZ, Nichol JN, Huang F, Yang W, Preston S, et al. MNK1/NODAL signaling promotes invasive progression of breast ductal carcinoma *in situ*. *Cancer Res.* (2019) 79:1646–57. doi: 10.1158/0008-5472.CAN-18-1602
8. Nistor-Ciurba CC. Patient, tumor and therapeutic features related to recurrence of ductal carcinoma *in situ* (DCIS). *Rom J Morphol Embryol.* (2013) 54(3 Suppl):769–73.
9. Martins D, Beca FF, Sousa B, Baltazar F, Paredes J, Schmitt F. Loss of caveolin-1 and gain of MCT4 expression in the tumor stroma: key events in the progression from an *in situ* to an invasive breast carcinoma. *Cell Cycle.* (2013) 12:2684–90. doi: 10.4161/cc.25794
10. Kraman M, Bambrough PJ, Arnold JN, Roberts EW, Magiera L, Jones JO, et al. Suppression of antitumor immunity by stromal cells expressing fibroblast activation protein-alpha. *Science.* (2010) 330:827–30. doi: 10.1126/science.1195300
11. Bae S, Park CW, Son HK, Ju HK, Paik D, Jeon CJ, et al. Fibroblast activation protein alpha identifies mesenchymal stromal cells from human bone marrow. *Br J Haematol.* (2008) 142:827–30. doi: 10.1111/j.1365-2141.2008.07241.x
12. Yang L, Ma L, Lai D. Over-expression of fibroblast activation protein alpha increases tumor growth in xenografts of ovarian cancer cells. *Acta Biochim Biophys Sin.* (2013) 45:928–37. doi: 10.1093/abbs/gmt095
13. Kelly T, Huang Y, Simms AE, Mazur A. Fibroblast activation protein-alpha: a key modulator of the microenvironment in multiple pathologies. *Int Rev Cell Mol Biol.* (2012) 297:83–116. doi: 10.1016/B978-0-12-394308-8.00003-0
14. Aggarwal S, Brennen WN, Kole TP, Schneider E, Topaloglu O, Yates M, et al. Fibroblast activation protein peptide substrates identified from human collagen I derived gelatin cleavage sites. *Biochemistry.* (2008) 47:1076–86. doi: 10.1021/bi701921b
15. Huang Y, Simms AE, Mazur A, Wang S, Leon NR, Jones B, et al. Fibroblast activation protein-alpha promotes tumor growth and invasion of breast cancer cells through non-enzymatic functions. *Clin Exp Metastasis.* (2011) 28:567–79. doi: 10.1007/s10585-011-9392-x
16. Hua X, Yu L, Huang X, Liao Z, Xian Q. Expression and role of fibroblast activation protein-alpha in microinvasive breast carcinoma. *Diagn Pathol.* (2011) 6:111. doi: 10.1186/1746-1596-6-111
17. Cremasco V, Astarita JL, Grauel AL, Keerthivasan S, MacIsaac K, Woodruff MC, et al. FAP delineates heterogeneous and functionally divergent stromal cells in immune-excluded breast tumors. *Cancer Immunol Res.* (2018) 6:1472–85. doi: 10.1158/2326-6066.CIR-18-0098
18. Busek P, Mateu R, Zubal M, Kotackova L, Sedo A. Targeting fibroblast activation protein in cancer - prospects and caveats. *Front Biosci.* (2018) 23:1933—68.
19. Ng MM, Dippold HC, Buschman MD, Noakes CJ, Field SJ. GOLPH3L antagonizes GOLPH3 to determine Golgi morphology. *Mol Biol Cell.* (2013) 24:796–808. doi: 10.1091/mbc.E12-07-0525
20. Scott KL, Kabbarah O, Liang MC, Ivanova E, Anagnostou V, Wu J, et al. GOLPH3 modulates mTOR signalling and rapamycin sensitivity in cancer. *Nature.* (2009) 459:1085–90. doi: 10.1038/nature08109
21. Wood CS, Schmitz KR, Bessman NJ, Setty TG, Ferguson KM, Burd CG. PtdIns4P recognition by Vps74/GOLPH3 links PtdIns 4-kinase signaling to retrograde Golgi trafficking. *J Cell Biol.* (2009) 187:967–75. doi: 10.1083/jcb.200909063
22. Kunigou O, Nagao H, Kawabata N, Ishidou Y, Nagano S, Maeda S, et al. Role of GOLPH3 and GOLPH3L in the proliferation of human rhabdomyosarcoma. *Oncol Rep.* (2011) 26:1337–42. doi: 10.3892/or.2011.1413
23. Hua X, Yu L, Pan W, Huang X, Liao Z, Xian Q, et al. Increased expression of Golgi phosphoprotein-3 is associated with tumor aggressiveness and poor prognosis of prostate cancer. *Diagn Pathol.* (2012) 7:127. doi: 10.1186/1746-1596-7-127
24. Zeng Z, Lin H, Zhao X, Liu G, Wang X, Xu R, et al. Overexpression of GOLPH3 promotes proliferation and tumorigenicity in breast cancer via suppression of the FOXO1 transcription factor. *Clin Cancer Res.* (2012) 18:4059–69. doi: 10.1158/1078-0432.CCR-11-3156
25. Buonomo O, Orsaria P, Contino G, Varvaras D, Gioia A, Bonanno E, et al. Pathological classification of DCIS and planning of therapeutic management. *Anticancer Res.* (2009) 29:1499–506.
26. Haviv I, Polyak K, Qiu W, Hu M, Campbell I. Origin of carcinoma associated fibroblasts. *Cell Cycle.* (2009) 8:589–95. doi: 10.4161/cc.8.4.7669

27. Giaccia AJ, Schipani E. Role of carcinoma-associated fibroblasts and hypoxia in tumor progression. *Curr Top Microbiol Immunol.* (2010) 345:31–45. doi: 10.1007/82_2010_73
28. El-Maqsoud N, Osman N, El-Hamid A, El-Bab T, Galal EM. GOLPH3 and YB-1 are novel markers correlating with poor prognosis in prostate cancer. *World J Oncol.* (2015) 6:473–84. doi: 10.14740/wjon952w
29. Zhang L, Guo F, Gao X, Wu Y. Golgi phosphoprotein 3 expression predicts poor prognosis in patients with prostate cancer undergoing radical prostatectomy. *Mol Med Rep.* (2015) 12:1298–304. doi: 10.3892/mmr.2015.3455
30. Tang S, Yang R, Zhou X, Pan H, Liu J. Expression of GOLPH3 in patients with non-small cell lung cancer and xenografts models. *Oncol Lett.* (2018) 15:7555–62. doi: 10.3892/ol.2018.8340
31. Tang S, Pan H, Wei W, Yang H, Liu J, Yang R. GOLPH3: a novel biomarker that correlates with poor survival and resistance to chemotherapy in breast cancer. *Oncotarget.* (2017) 8:105155–69. doi: 10.18632/oncotarget.21927
32. Feng Y, He F, Wu H, Huang H, Zhang L, Han X, et al. GOLPH3L is a novel prognostic biomarker for epithelial ovarian cancer. *J Cancer.* (2015) 6:893–900. doi: 10.7150/jca.11865
33. Snyder CM, Mardones GA, Ladinsky MS, Howell KE. GMx33 associates with the trans-Golgi matrix in a dynamic manner and sorts within tubules exiting the Golgi. *Mol Biol Cell.* (2006) 17:511–24. doi: 10.1091/mbc.e05-07-0682
34. Tenorio MJ, Ross BH, Luchsinger C, Rivera-Dictter A, Arriagada C, Acuna D, et al. Distinct biochemical pools of Golgi phosphoprotein 3 in the human breast cancer cell lines MCF7 and MDA-MB-231. *PLoS ONE.* (2016) 11:e154719. doi: 10.1371/journal.pone.0154719

Conflict of Interest: The authors declare that the research was conducted in the absence of any commercial or financial relationships that could be construed as a potential conflict of interest.

frontiers in Oncology

ORIGINAL RESEARCH
published: 17 December 2019
doi: 10.3389/fonc.2019.01413

TRPM7 Induces Mechanistic Target of Rap1b Through the Downregulation of miR-28-5p in Glioma Proliferation and Invasion

*Jingwei Wan[1,2], Alyssa Aihui Guo[3,4], Indrajit Chowdhury[3], Shanchun Guo[5], Jacqueline Hibbert[1], Guangdi Wang[5] and Mingli Liu[1]**

[1] Department of Microbiology, Biochemistry and Immunology, Morehouse School of Medicine, Atlanta, GA, United States, [2] Department of Neurosurgery, The Second Xiangya Hospital, Central South University, Changsha, China, [3] Department of Obstetrics and Gynecology, Morehouse School of Medicine, Atlanta, GA, United States, [4] University of South Carolina SOM Greenville, Greenville, SC, United States, [5] Department of Chemistry, Xavier University, New Orleans, LA, United States

Objectives: Our previous findings demonstrate that channel-kinase transient receptor potential (TRP) ion channel subfamily M, member 7 (TRPM7) is critical in regulating human glioma cell migration and invasion. Since microRNAs (miRNAs) participate in complex regulatory networks that may affect almost every cellular and molecular process during glioma formation and progression, we explored the role of miRNAs in human glioma progression by comparing miRNA expression profiles due to differentially expressed TRPM7.

Methods: First, we performed miRNA microarray analysis to determine TRPM7's miRNA targets upon TRPM7 silencing in A172 cells and validated the miRNA microarray data using A172, U87MG, U373MG, and SNB19 cell lines by stem-loop RT-qPCRs. We next determined whether TRPM7 regulates glioma cell proliferation and migration/invasion through different functional domains by overexpressing wild-type human TRPM7 (wtTRPM7), two mutants with TRPM7's α-kinase domain deleted (Δkinase-DK), or a point mutation in the ATP binding site of the α-kinase domain (K1648R-KR). In addition, we determined the roles of miR-28-5p in glioma cell proliferation and invasion by overexpressing or under expressing miR-28-5p *in vitro*. Lastly, we determined whether a Ras-related small GTP-binding protein (Rap1b) is a target of miR-28-5p in glioma tumorigenesis.

Results: The miRNA microarray data revealed a list of 16 downregulated and 10 upregulated miRNAs whose transcripts are significantly changed by TRPM7 knock-down. Cell invasion was significantly reduced in two TRPM7 mutants with inactive kinase domain, Δkinase, and K1648R transfected glioma cells. miR-28-5p overexpression suppressed glioma cells' proliferation and invasion, and miR-28-5p under expression led to a significant increase in glioma cell proliferation and migration/invasion compared to that of the controls. miR-28-5p suppressed glioma cell proliferation and migration by targeting Rap1b. Co-transfection of siRap1b with miR28-5p inhibitor reduced the glioma cell proliferation and invasion, caused by the latter.

OPEN ACCESS

Edited by:
Chang Zou,
Shenzhen People's Hospital, China

Reviewed by:
Priyanka Gupta,
University of Alabama at Birmingham, United States
Prasanna Ekambaram,
University of Pittsburgh, United States

***Correspondence:**
Mingli Liu
mliu@msm.edu

Specialty section:
This article was submitted to Molecular and Cellular Oncology, a section of the journal Frontiers in Oncology

Received: *20 August 2019*
Accepted: *28 November 2019*
Published: *17 December 2019*

Citation:
Wan J, Guo AA, Chowdhury I, Guo S, Hibbert J, Wang G and Liu M (2019) TRPM7 Induces Mechanistic Target of Rap1b Through the Downregulation of miR-28-5p in Glioma Proliferation and Invasion. Front. Oncol. 9:1413. doi: 10.3389/fonc.2019.01413

Conclusions: These results indicate that TRPM7's channel activity is required for glioma cell growth while the kinase domain is required for cell migration/invasion. TRPM7 regulates miR-28-5p expression, which suppresses cell proliferation and invasion in glioma cells by targeting Rap1b signaling.

Keywords: TRPM7, Rap1b, miR-28-5p, glioma, proliferation, invasion, prognosis

INTRODUCTION

High grade malignant gliomas, also called glioblastoma multiforme (GBM), the most common and aggressive primary brain tumor, are devastating, uniformly fatal tumors for which no effective therapies currently exist. We have reported that TRPM7 channels, a subfamily member of the transient receptor potential (TRP), regulate glioma stem cell (GSC) growth/proliferation through STAT3 and Notch signaling pathways (1). Because of traditional treatments' limited success in prolonging the overall survival of GBM patients, treatments that target genomic abnormalities, epigenetics, and epigenetic modulators have been attracting an increasing amount of attention for their influence in many tumors including glioma. miRNAs, one of the epigenetic effectors, reversibly regulate transcription through binding to complementary sequences of mRNA and silencing its translation into proteins. miRNAs are small noncoding RNAs, generally 19–22 nucleotides in length, that modulate protein-coding genes by binding to the 3'-untraslated region (UTR) of the target mRNA, therefore disrupting transcription (2–4). Many studies have shown that miRNA are expressed in a variety of human tumors and exert dramatic functions in human tumorigenesis and metastasis (5). miRNAs can function as either tumor suppressor by inhibiting the expression of oncogene or tumor promoter by reducing the expression of tumor suppressor gene (6, 7). While a specific miRNA may simultaneously regulate different targets, namely a given miRNA's upstream regulation can involve different regulators at different steps of mRNA biogenesis, a single protein target can be regulated by different miRNAs. Therefore, miRNAs participate in complex regulatory networks that affect almost every cellular and molecular processes in tumor initiation and progression (6). Since miRNAs have significant roles in human tumorigenesis and metastasis (5), identification of aberrantly expressed miRNAs is a crucial initial step in illustrating miRNA-mediated tumorigenic pathways.

Our in-depth data analysis from miRNA microarray data revealed a list of 16 downregulated and 10 upregulated miRNAs whose transcripts are statistically significant with fold changes >2 by TRPM7 knock-down in A172 glioma cells. Among these, the miRNA of hsa-miR-28-5p (miR-28-5p) has been shown to exert crucial influence on tumor growth and migration by modulating AKT (8), ERK (9), and IGF-1 (10) signaling pathways. Although oncogenic and invasive roles of TRPM7 (11, 12) and tumor-inhibitory role of miR-28-5p (13) have been reported in multiple studies, how TRPM7 regulates miRNA and downstream target genes are unclear. To seal the gap between TRPM7 and miRNA in the existing literature, we determined the changes in miRNA in response to reduced TRPM7 expression in glioma cells. The aim of the present study was to investigate the functional roles of miR-28-5p to elucidate the molecular mechanism of TRPM7's regulation of miR-28-5p in multiple glioma cell lines with different genomic mutational status. Our data revealed that miR-28-5p was inversely regulated by TRPM7 expression in glioma cells; overexpression of miR-28-5p significantly inhibited glioma cell growth, migration, and invasion; the gene encoding Ras-related protein Rap1b, positively correlated with TRPM7, is a promising candidate target gene of miR-28-5p and may serve as a predictive marker for the poor survival of glioma patients (14, 15). Our study elucidated the crucial roles of TRPM7/miR-28-5p/Rap1b axis in gliomagenesis.

MATERIALS AND METHODS

Antibody and reagents: Primary antibodies used included anti-TRPM7 (Abcam, Cat no. ab232455, Cambridge, MA) and anti-β-actin (Sigma-Aldrich, St. Louis, MO, Cat no. A3854). Rabbit polyclonal Rap1b (36E1, Cat no. 2326) and mouse HA (Cat no. 2367) antibodies were purchased from Cell Signaling Technology (Danvers, MA). All secondary antibodies used for Western blot were purchased from Calbiochem (La Jolla, CA).

Plasmid, siRNA, and miRNAs

The wild-type human TRPM7 (wtTRPM7) or constructs in which the α-kinase domain was deleted (Δkinase) or rendered inactive with a point mutation in the ATP binding site of the α-kinase domain (K1648R) were provided by Dr. Carsten Schmitz, University of Colorado, Denver, CO. All constructs (wtTRPM7, Δkinase, K1648R) were tagged with a hemagglutinin (HA) at the N-terminal. Control scrambled siRNA (On-TARGETplus Non-targeting siRNA, Cat no. D-001810-01-05) and ON-TARGETplus SMARTpool siRNA (Cat no. L-005393-000005) targeting TRPM7 were purchased from Dharmacon (Lafayette, CO). Control scramble siRNA (Cat no. sc-37007) and siRNA targeting Rap1b (Cat no. sc-41854) were purchased from Santa Cruz Biotechnology (Santa Cruz, CA). The scrambled siRNAs, with no homology to any known sequence were used as controls. miR-28-5p mimic (Cat no. 4464066), miR-28-5p inhibitor (Cat no. 4464084), and control were purchased from Life Technology (Carlsbad, CA).

Cell Culture

Human glioblastoma cell line, A172, was obtained from ATCC (Manassas, VA, USA). Other glioma cell lines, U87MG, U373MG, and SNB19, were kindly provided by Dr. Yancey G. Gillespie at the University of Alabama at Birmingham (UAB), Birmingham, AL. Human glioblastoma cell line SF767 was kindly provided

by Dr. Hui-Kuo Shu at Emory University, Atlanta, Georgia. All cells were cultured in Dulbecco's Modified Eagle's Medium (DMEM, Sigma-Aldrich, St. Louis, MO) plus 10% fetal bovine serum (FBS), 50 units/ml penicillin, and 50 μg/ml streptomycin at 37°C.

Transfection of siRNA and Expression of Wild-Type Human TRPM7 and Mutant Constructs in Glioma Cells

When the glioblastoma cells reached about 50–75% confluency, the appropriate amount of siRNAs specific to TRPM7, Rap1b, and control scramble siRNA with the final concentration of 100 nM, and miR-28-5p mimics, inhibitor, and controls with final concentration of 30 nM were transfected using Lipofectamine RNAiMAX reagent in serum free OptiMEM-1 medium (Invitrogen, Carlsbad, CA) according to the manufacture's instruction. After six hours of transfection, cells were grown in Dulbecco's Modified Eagle Medium (DMEM) containing 10% fetal bovine serum (FBS) (16, 17) further for 24–72 h as indicated in each experiment. 48 or 72 h post transfection, targets knockdown were assessed by RT-PCR or Western blot, respectively. Various glioma cells at 50–75% confluency were transfected with a pcDNA4/TO plasmid that allowed protein expression of wt hTRPM7 and hTRPM7 mutants for the α-kinase deletion or lacking of phosphotransferase activity by lipofectamine 3000 transfection reagent (Invitrogen, Carlsbad, CA) according to the manufacture's instruction. The transiently transfected glioma cells expressing wt hTRPM7, Δkinase, and K1648R hTRPM7 constructs were maintained in DMEM containing 10% FBS (16, 17) for further growth for 24–72 h. The overexpression of TRPM7 and its mutants were assessed by HA expression. All studies were done in triplicates.

MTT Assay

All glioma cells were seeded at 1×10^4 cells in 100 μl of medium per well into 96-well plates and were transfected with 100 nM specific siRNA or control using Lipofectamine reagent for indicated times. Ten micorliter of 3-(4,5-dimethylthiazol-2-yl)-2,5-diphenyltetrazolium bromide (MTT) reagent (Sigma-Aldrich, St. Louis, MO, the ratio of MTT reagent to medium is 1:10) was added into each well and incubated in the dark at 37°C for 2–4 h. Absorbance at 570 nm was measured using 690 nm as the reference using a CytoFluorTM 2300 plate reader.

Cell Migration and Invasion Assay

The migration and invasion potential were assessed as previously described (1, 18). Briefly, cell culture chambers with 8 μm pore size of polycarbonate membrane filters (Corning, USA) were used for cell invasion assays with the filters pre-coated with matrigel (50 μl, 1.25 mg/ml). Each of the glioma cell lines were transfected with or without 100 nM siRNA for 48 h, harvested and seeded with 1% FBS medium in the upper chambers that were soaked in bottom chambers filled with 500 μl whole medium (DMEM and 10% FBS). After another 24 h of incubation at 37°C, matrigel and cells on the upper surface of the filter were wiped off thoroughly with a Q-tip. Cells attached on the lower surface of the membrane filters were fixed with 4% paraformaldehyde/PBS for 10 min and stained with 0.5% crystal violet/methanol for 10 min. The cells were then counted under light microscopy with 10x magnification in 3–4 random fields. Cell numbers under different treatments were normalized to the appropriate controls. Assays were done in triplicate of samples and were performed in two independent experiments.

miRNA Microarray

TRPM7-siRNA was employed to selectively suppress the expression of TRPM7 channels in A172 cells. Then, total RNA was extracted using the miRNeasy Mini Kit (Qiagen, Valencia, CA) and was subjected to the human miRNA array assay by LC Sciences (Houston, TX, www.LCsciences.com) using MRA-1001B2 version miRHuman 22, containing 2,632 standard mature miRNA unique probes with 3 repeats, 50 controls (8–32 repeats) based on Sanger miRBase Release 22 (http://www.mirbase.org/). PUC2PM-20B and PUC2MM-20B are the control probes for quality controls of chip production, sample labeling, and assay conditions. Fold changes and *P*-values were calculated using Student's *t*-test. A $P < 0.05$ with a fold change >2.0 was considered to be a significant dysregulation. In-depth data analysis from miRNA microarray data showed a list of 16 downregulated and 10 upregulated miRNAs whose transcripts are statistically significant with fold changes >2 by TRPM7 knock-down.

Real-Time RT-PCR Analysis

Total RNA isolation, cDNA synthesis, and PCR amplification were performed as previously described (19). Cell pellets were stored in Trizol reagent and homogenized in fresh Trizol. Total RNA was isolated from cells using a miRNeasy Kit (Qiagen, Valencia, CA) and quantified using the Nanodrop N-1000 by Agilent Biosystems (Santa Clara, CA). Purified total RNA (0.75 μg) was reverse transcribed using iScript cDNA Synthesis Kit according to the manufacture's protocol (Bio-Rad Laboratories, Inc., Hercules, CA). Reverse transcription was performed by using random hexamers at 25°C for 5 min, 42°C for 30 min, and 85°C for 5 min. After diluting 10 times, the cDNA was then amplified using iQ SYBR Green Supermix (Bio-Rad Laboratories, Inc.) according to the manufacture's protocol under the following conditions: activation of the Taq DNA polymerase at 95°C for 3 min, 40 cycles at 95°C for 10 s (denaturation), and 61°C for 45 s (combined annealing and extension). The quantitative gene analysis utilized the CFX Connect Real Time PCR Detection System. Each condition was conducted in biological triplicates, and each individual biological replicate was amplified in technical triplicates. Relative expression for each gene was evaluated using the $2^{-\Delta\Delta Ct}$ Livak method, and GAPDH was used as the reference gene (20). We used the melting curve analysis to assess whether or not the intercalating dye qPCR assays have produced single, specific product. The single peak was observed for each specific gene, which represented as a pure single amplicon, indicating the specificity of each primer for each specific gene.

Stem-Loop Pulsed Reverse Transcription: A Highly Sensitive RT-PCR Method for the Detection and Quantification of miRNAs

The miRNA validation was performed using stem-loop pulsed RT-PCR with some modifications as described before (21). The RT primer for miR-28-5p reverse transcription, forward and reverse primers for RT product amplification were designed based on miR-28-5p's sequence: AAGGAGCUCACAGUCUAUUGAG (http://www.mirbase.org/). For each reaction, "no RNA" master mix comprised of 10 mM dNTP, 5 μM RT primer (see **Table 1**), and appropriate water, was heated at 65°C for 5 min and incubated on ice for 2 min. Then, the "no RNA" master mix was combined with RT master mix containing first-strand buffer, 0.1M DTT, 4 units RNaseOUT, and 50 units of SuperScript III reverse transcriptase. Then the pulsed RT was performed under the following conditions: load thermal cycler and incubate for 30 min at 16°C, pulsed RT of 60 cycles at 30°C for 30 s, 42°C for 30 s and 50°C for 1 s, and incubate at 85°C for 5 min to inactivate the reverse transcriptase. Finally, the RT product was amplified using iQ SYBR Green Supermix (Bio-Rad) as described above.

Western Blotting

Cells were lysed with lysis buffer (50 mM HEPES, 150 mM NaCl, 1.5 mM MgCl2, 1 mM EGTA, 10% glycerol, 1% Nonidet P-40, 100 mM NaF, 10 mM sodium pyrophosphate, 0.2 mM sodium orthovanadate, 1 mM phenylmethylsulfonyl fluoride, 10 μg/ml aprotinin, and 10 μg/ml leupeptin). Samples were separated by SDS/PAGE, and separated proteins were transferred to nitrocellulose membranes and identified by immunoblotting. Primary antibodies were obtained from commercial sources and were diluted at the ratio of 1:1,000 according to manufacturer's instruction. Blots were developed with Supersignal Pico or Femto substrate (Pierce). A densitometric analysis of the bands was performed with the ImageQuant program (Bio-Rad).

Bioinformatics Analysis

Kaplan-Meier analysis of overall survival according to the TRPM7, Rap1b mRNA expression and Pearson correlation between TRPM7 and Rap1b were obtained from microarray analysis on 454 glioma patients in the TCGA data set (http://www.betastasis.com/glioma/tcga_gbm/). *P*-value is based on log rank test.

Statistical Analysis

The results obtained in this work were expressed as mean ± SD of at least 2 independent experiments done in triplicate. Paired Student *t*-test or one-way ANOVA tests were performed for data analysis, and significant difference was defined as $p < 0.05$.

RESULTS

TRPM7 Regulates Glioma Cell Proliferation and Migration/Invasion Through Different Functional Domains

We have reported that the activation of TRPM7 channels plays an important role in the growth and proliferation of human glioma cells (1). In the current study, we further investigated whether or not changes in glioma cell proliferation and migration might be caused by channel domain-mediated and/or kinase domain-mediated TRPM7 activation. To this end, A172 cells were transfected with (a) 5 μg of wild-type human TRPM7 (wtTRPM7 or M7-WT); (b) constructs in which the α-kinase domain was deleted (Δkinase or M7-DK) or rendered inactive with a point mutation in the ATP binding site of the α-kinase domain (K1648R, or M7-KR); all the cells were allowed to grow from 24 to 72 h as indicated. Note that *in vitro* autophosphorylation assays have been done to confirm that the phosphotransferase activity of the M7-WT channels are easily detectable and much reduced in the absence of mutant channel activities under standard conditions by Dr. Carsten Schmitz's group who provided us the constructs (17). The effects of TRPM7 on glioma cell proliferation and invasion were determined using MTT assays and transwell invasion assays, respectively. As shown in **Figure 1A**, A172 cells with Δkinase (M7-DK) and K1648R (M7-KR) mutants expressed the TRPM7 protein, as demonstrated by Western blot, in which TRPM7 expression at the lysate level was similar to that of wtTRPM7 expression (**Figure 1A**). The cells overexpressing wt TRPM7 (M7-WT), M7-KR, or M7-DK grew significantly more ($P < 0.05$) than the cells transfected with control (**Figure 1B**) in a time-dependent manner from 24 to 72 h. Cell proliferation was not significantly changed when cells were transfected with Δkinase or K1648R compared to those transfected with wt TRPM7, which indicates that TRPM7 channel, rather than kinase activity, is required for A172 cell growth (**Figure 1B**). Cell invasion was increased up to 3 times in A172 cells transfected with wt TRPM7 compared to

TABLE 1 | List of primers used in the study.

Primer set	Forward 5′-3′	Reverse 5′-3′
TRPM7	CTTTGACCAAGAGGGAATGTG	GACCAAGCGACCACAAAAAC
Rap1b	TGCTTGAAATCTTGGATACTGC	GTGGACTGTGCTGTGATGGA
GAPDH	GAAGGTGAAGGTCGGAGTC	GAAGATGGTGATGGGATTTC
SNOD48	AGTGATGATGACCCCAGGTAA	AGAGCGCTGCGGTGAT
SNOD44	CCTGGATGATGATAAGCAAATG	TTAGAGCTAATTAAGACCTTCATGTTC
SNOD47	ATGATGTAATGATTCTGCCAAA	CCTCAGAATCAAAATGGAACG
U6	CAAGGATGACACGCAAATTC	AAAAATGGAACGCTTCACGA
miR28-5p RT primer	GTCGTATCCAGTGCAGGGTCCGAGGTATTCGCACTGGATACGACCTCAAT	
miR28-5p	GTATACAAGGAGCTCACAGTC	GTGCAGGGTCCGAGGT

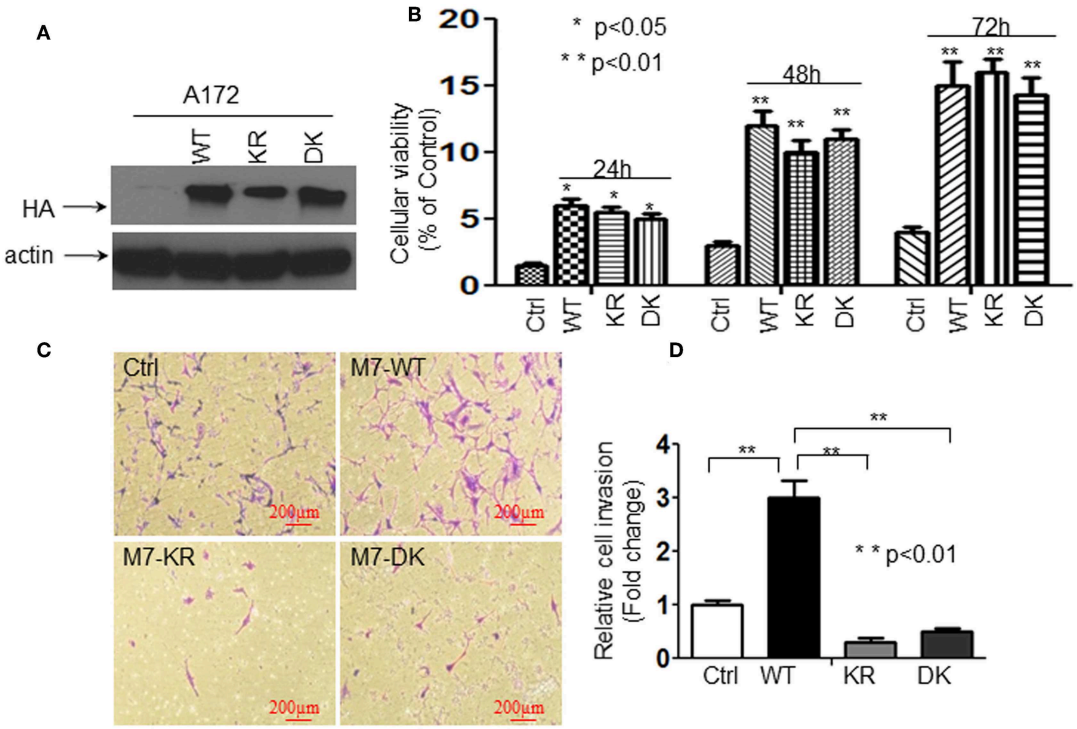

FIGURE 1 | The channel activity of TRPM7 is required for cell growth while the kinase domain is required for cell migration/invasion in A172 cells. A172 cells were transfected with (a) 5 μg of wild-type human TRPM7 (wtTRPM7 or M7-WT or WT); (b) constructs in which the α-kinase domain was deleted (Δkinase or M7-DK or DK); (c) rendered inactive with a point mutation in the ATP binding site of the α-kinase domain (K1648R, or M7-KR or KR) along with control vector (Ctrl); all the cells were allowed to grow from 24 to 72 h as indicated. **(A)** The transfection efficiency was assessed by detecting HA-TRPM7 with an anti-HA antibody by Western blot. A172 cells with Δkinase (M7-DK) and K1648R (M7-KR) mutants expressed HA-TRPM7 protein, the mutants expressed the equivalent levels of HA-TRPM7 expression as that of wt TRPM7 expression; while there is undetectable HA-TRPM7 in control. **(B)** The effects of TRPM7 on glioma cell proliferation were determined using MTT assays. Cell numbers were counted every 24 h for 3 days post-transfection with wtTRPM7, M7-DK, or M7-KR as well as the control. The values represent a fold change relative to controls and are mean ± SD of triplicated samples performed in three independent experiments. **(C)** For transwell invasion assays, each transfected A172 cells were grown for 48 h, then cells were harvested and seeded with 1% FBS medium in the upper chambers which were soaked in bottom chambers filled with 500 μl whole medium containing 10% FBS. The cells were then subjected to grow for 24 h during the invasion assay. A representative experiment of microscopy images (x10) shown the invasive cells on Transwell assay. Photomicrographs were taken at the magnification of 10x. **(D)** The cell numbers were counted on the bottom of Matrigel-coated transwell chamber at 72 h post-transfection. The data were represented as fold changes relative to controls and are the mean ± SD of triplicate samples performed in two independent samples (**$P < 0.01$, Student *t*-test).

that of the control; by contrast, the cell numbers that penetrated the Matrigel-coated transwell were significantly reduced in cells transfected with Δkinase (M7-DK) to 30% or with K1648R (M7-KR) to 50% at 72 h compared to control, indicating that TRPM7 kinase activity is required for changes in cell migration and invasion (**Figures 1C,D**). These results suggest that the channel activity of TRPM7 is required for cell growth while the kinase domain is required for cell migration/invasion.

TRPM7 Negatively Regulates miR-28-5p in Glioma Cells

The Expression Levels of hsa-miR-26b-5p, hsa-miR4530, and hsa-miR-28-5p Were Significantly Changed by TRPM7 Knock-Down

To test whether or not miRNAs are regulated by TRPM7 expression, 100 nM of siRNAs specific to TRPM7 (siTRPM7) or control scramble siRNA (siCtrl) were transfected into A172 cells for 72 h for specifically selective suppression of TRPM7 channel expression. Total RNA from triplicate biological samples, either with scramble control (siCtrl, A423, A424, and A425) or siTRPM7 (A427, A428, and A434) (**Figure 2A**), were extracted and parallelly subjected to human miRNA array assay by LC Sciences (Houston, TX, www.lcsciences.com). In-depth data analysis from miRNA microarray data revealed 16 downregulated and 10 upregulated miRNAs whose transcripts are statistically significant with fold changes >2 by TRPM7 knock-down (**Figure 2A**). Among them, microRNAs hsa-miR-26b-5p (miR-26b-5p), hsa-miR-4530 (miR-4530), and hsa-miR-28-5p (miR-28-5p) have been shown to exert crucial influence on tumor growth and migration by modulating AKT (8), ERK (9), and IGF-1 (10) signaling pathways. In our case, hsa-miR-26b-5p, hsa-miR-4530, and hsa-miR-28-5p were significantly changed by TRPM7 knock-down.

Validation of miRNA Array Results by siTRPM7

Next, miR-26b-5p, miR-4530, and miR-28-5p were further validated by real-time miRNA quantification using stem-loop

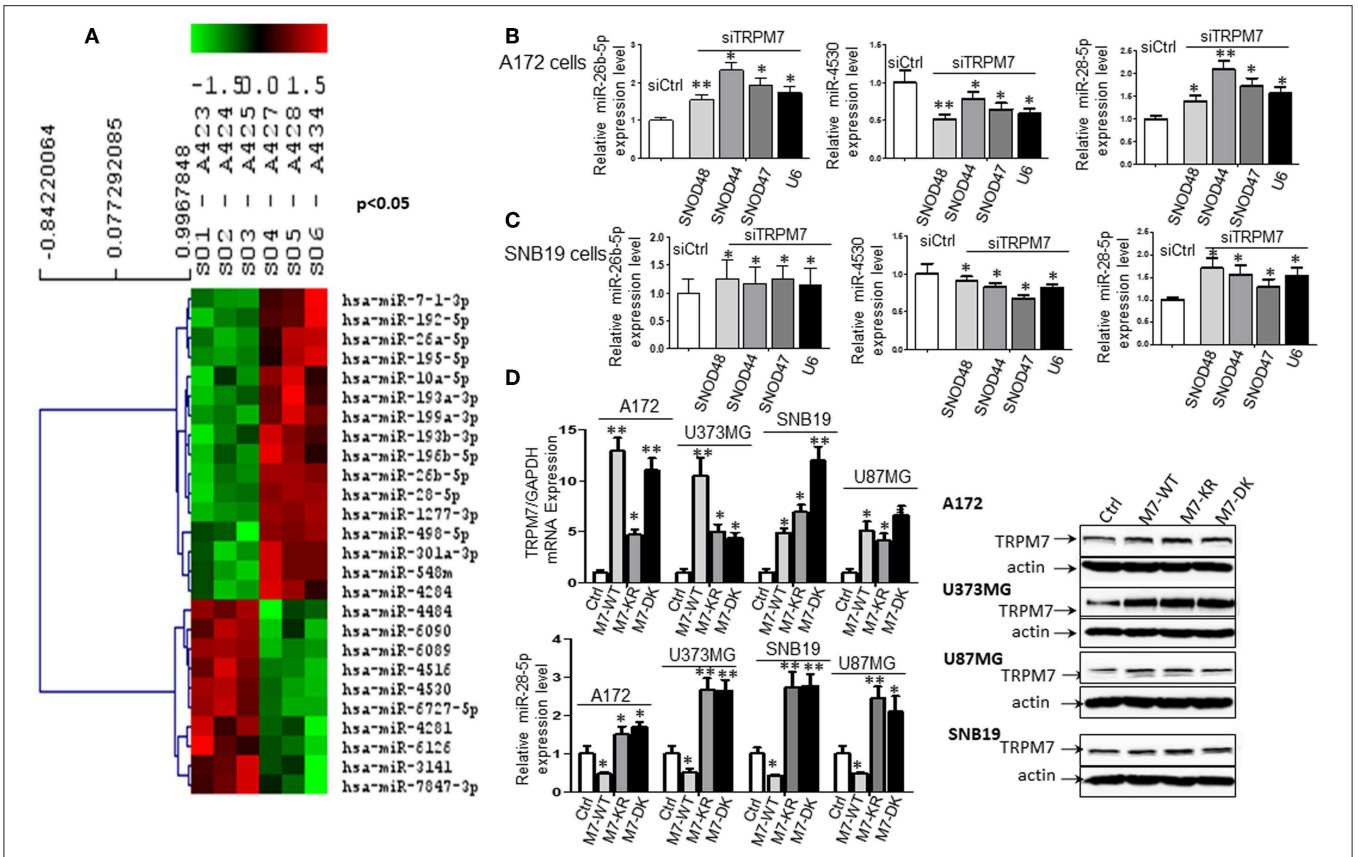

FIGURE 2 | TRPM7 negatively regulates miR-28-5p in glioma cells. **(A)** Total RNA from biological triplicate samples, either with scramble control (siCtrl, A423, A424, and A425) or siTRPM7 (A427, A428, and A434), were extracted and then parallelly subjected to human miRNA array assay. In-depth data analysis from miRNA microarray data resulted in a list of 16 downregulated and 10 upregulated miRNAs whose transcripts are statistically significant with fold changes greater than 2 by TRPM7 knock-down. **(B,C)** Validation of miRNA array by siTRPM7 by qPCR. miR-26b-5p, miR-4530, and miR-28-5p were validated by real-time miRNA quantification using stem-loop RT-PCR in glioma cell lines A172 **(B)** and SNB19 **(C)**. A set of endogenous RNAs SNOD48, SNOD44, SNOD47, and U6 served as endogenous controls in real-time miRNA quantification to normalize miRNA gene expression. **(D)** Validation of miRNA array by overexpressing TRPM7. The constructs of wt hTRPM7 (M7-WT), Δ kinase (M7-DK), K1648R (MT-KR), and control (Ctrl) were introduced into and expressed in glioma cell lines A172, U373MG, SNB19, and U87MG for 48 h. Transfection efficiency was determined by TRPM7 mRNA expression detected by qRT-PCR. GAPDH was used as an internal control to monitor the presence of amplified cDNA in samples (upper left). Western blots by overexpression of individual TRPM7 constructs confirmed the data from qRT-PCR, which showed significantly increased TRPM7 in M7-WT, M7-KR, and M7-DK compared to the control (**D**, right). The levels of miR-28-5p were determined by stem-loop RT-PCR (lower left). All the data were represented as fold changes relative to the appropriate controls and are the mean ± SD of triplicated samples performed in three independent experiments. (*$P < 0.05$, **$P < 0.01$).

RT-PCR (21–27) in glioma cell lines A172 and SNB19 (**Figures 2B,C**). A set of endogenous RNAs SNOD48, SNOD44, SNOD47, and U6 served as endogenous controls in real-time miRNA quantification to normalize miRNA gene expression. miR-26b-5p and miR-28-5p were significantly upregulated while miR-4530 was significantly downregulated upon TRPM7 silencing by siTRPM7 in both A172 and SNB19 cells as compared to each of their miRNA endogenous controls (*$P < 0.05$, **$P < 0.01$, Student *t*-test). The data indicated that the expressions of hsa-miR-26b-5p, hsa-miR-4530, and hsa-miR-28-5p in the two cell lines are consistent with those of miRNA microarray data. Since miRNA's discovery decades ago, miR-26-5p, together with miR-21-5p and miR-30-5p was only detected in breast cancer and may not have significant roles in glioma; while miR-28-5p was found to be important in multiple malignancies including glioma. Therefore, we chose miR-28-5p to further elucidate the TRPM7-mediated pathways in glioma.

Validation of miRNA Array Results by Overexpressing TRPM7

The constructs of wt hTRPM7, Δ kinase, and K1648R were introduced into and expressed in glioma cell lines A172, U373MG, SNB19, and U87MG for 48 h. Total RNA and protein lysate were isolated, and TRPM7 levels were detected by qRT-PCR. GAPDH was used as an internal control to monitor the presence of amplified cDNA in samples. Optimum mRNA expression of wt hTRPM7 and the mutants, Δkinase and K1648R, was observed after 48 h. Overexpression of TRPM7 by M7-WT, M7-KR, and M7-DK dramatically increased TRPM7 mRNA as compared to that of the pcDNA4.2 control (**Figure 2D**, upper

left, $^{*}P < 0.05$, $^{**}P < 0.01$, Student t-test) in each of four cell lines, indicating the system's high transfection efficiency. Western blots by overexpression of individual TRPM7 constructs for 72 h confirmed the data from qRT-PCR, which showed significantly increased TRPM7 in M7-WT, M7-KR, and M7-DK compared to the control (**Figure 2D**, right). Unlike proteins that showed consistent expression of M7-KR and M7-DK as M7-WT across the cell lines, there are varying expression at mRNA levels of M7-WT and M7-KR and M7-DK. This indicates that transcription levels are frequently not reflected at the protein level due to protein instability and lower rate of mRNA transcription compared to protein translation in mammalian cells (28). The levels of miR-28-5p were determined by stem-loop RT-PCR. The results showed that the overexpression of wt hTRPM7 decreased miR-28-5p expression by 53, 50, 57, and 51% in A172, U373MG, SNB19, and U87MG, respectively; on the other hand, K1648R mutants increased miR-28-5p expression by 1.5, 2.67, 2.74, and 2.45 times. Δ kinase mutants exhibited similarly increased miR-28-5p expression pattern as K1648R mutants did by 1.7, 2.64, 2.78 and 2.1 times, respectively (**Figure 2D**, lower left). These results suggest that wild type TRPM7 may have different functions from its mutants.

miR-28-5p Inhibits Glioma Cell Proliferation and Invasion

To understand the biological effect of miR-28-5p on the proliferation of glioma cells, miR-28-5p expression was manipulated by transfecting A172, U87MG, U373MG, and SNB19 cells with either miR-28-5p mimics, inhibitors, or controls (ctrl or miR-NC) for 72 h to increase or decrease miR-28-5p expression levels. The stem-loop RT-PCR assay confirmed that miR-28-5p was significantly increased in A172, U87MG, U373MG, and SNB19 cells that were transfected with miR-28-5p mimics as compared to the expression levels in cells transfected with miR-NC (**Figure 3A**, left). Similarly, miR-28-5p was significantly decreased in the above four glioma cell lines that were transfected with miR-28-5p inhibitors as compared to the expression levels in cells transfected with miR-NC (**Figure 3A**, left). We assessed TRPM7 protein expression levels simultaneously when overexpressing miR-28-5p mimics and inhibitors by Western blot, and we confirmed the negative correlation between TRPM7 and miR-28-5p (**Figure 3A**, right).

We then examined the effects of miR-28-5p on glioma cell growth using MTT assay. As shown in **Figures 3B–E**, the overexpression of miR-28-5p by transient transfection of miR-28-5p mimics dramatically inhibited the growth rate of A172, U87MG, U373MG, and SNB19 glioma cell lines, where cell proliferation decreased in A172 (**Figure 3B**), U87MG (**Figure 3C**), U373MG (**Figure 3D**), and SNB19 (**Figure 3E**) by a maximum of 51.7, 52.5, 48.9, and 53.3% on day 4, respectively. In contrast, reduced miR-28-5p expression by miR-28-5p inhibitor augmented the growth of the four glioma cell lines above, where cell proliferation increased in A172 (**Figure 3B**), U87MG (**Figure 3C**), U373MG (**Figure 3D**), and SNB19 (**Figure 3E**) by a maximum of 32.0, 83.8, 31.1, and 45% on day 4, respectively. Next, we evaluated the possible roles of miR-28-5p in glioma cells invasion. Matrigel transwell invasion assays were performed on U87MG, U373MG, and SNB19 cell lines that were transiently transfected with miR-NC, miR-28-5mimics, and miR-28-5p inhibitors, and the results showed that the ectopic expression of miR-28-5p inhibited the number of invaded cells by 50, 60, and 40%, respectively as compared with that of the controls; on the other hand, miR-28-5p inhibitors enhanced the number of invaded cells by 50, 200, and 80%, respectively (**Figure 3F**).

TRPM7 Positively Regulated Rap1b Expression in Glioma Cells

The biological roles of miRNAs in human tumors depend on their specific targets; therefore, we searched the literature for potential targets of miR-28-5p. We found 52 publications that related miR-28-5p with human tumors, with most of them serving as a tumor suppressor. Several important tumor-related genes were defined as the direct target for miR-28-5p, such as AKT in gastric cancer (8), N4BP1 in ovarian cancer (29), IL-34 (30) and IGF-1 (10) in hepatocellular carcinoma, and Rap1b in renal cell carcinoma (31). Among these, Rap1b has drawn our attention for the following reasons. First, Rap1b has been found to play a role in the glioma cell proliferation and migration (15, 32). Second, the bioinformatics analysis from TCGA (http://www.betastasis.com/glioma/tcga_gbm/) indicated both TRPM7 (**Figure 4A**, upper panel) and Rap1b (**Figure 4A**, lower panel) predict glioma patients' poor prognosis. Third, TRPM7 and Rap1b mRNA expression levels are correlated by Pearson's correlation analysis ($r = 0.515$) (**Figure 4B**). To confirm this correlation, we transfected A172, U87MG, U373MG, and SNB19 cells either with synthesized specific small interfering RNAs (siTRPM7) targeting TRPM7 mRNA to decreasing TRPM7 expression or with TRPM7 expression vector along with its mutants K1648R and Δ kinase to increase the TRPM7 expression. The transfection efficiency of TRPM7 knock-down and overexpression were examined by qPCR (**Figure 2D**, upper left and **Figure 4D**, upper right) and Western blot (**Figure 4D**, left and lower right). The results indicated that the inhibition of TRPM7 expression by siTRPM7 markedly reduced Rap1b expression at both mRNA (**Figures 4C,D**, upper right) and protein levels (**Figure 4D**, left and lower right); while the overexpression of TRPM7 dramatically enhanced the expression of Rap1b at both mRNA (**Figure 4E**) and protein levels (**Figure 4F**) in all four glioma cell lines. Again, the mutants K1648R and Δ kinase exhibited a noticeable difference in Rap1b expression pattern at the protein levels compared to that of wt TRPM7, which reflect differences in their functional roles (**Figure 4F**).

Rap1b Elevates Glioma Cell Proliferation and Invasion

We first determined whether or not Rap1b protein, a Ras-related small GTP-binding protein that acts as GTPase in several signaling cascades, is expressed in glioma cells. As shown by Western blot, all of the glioma cell lines A172, SF767, SNB19, U373MG, and U87MG expressed the Rap1b protein (**Figure 5A**, upper panel). To confirm whether or not Rap1b functions as an oncogene in glioma, we assessed the effects of Rap1b

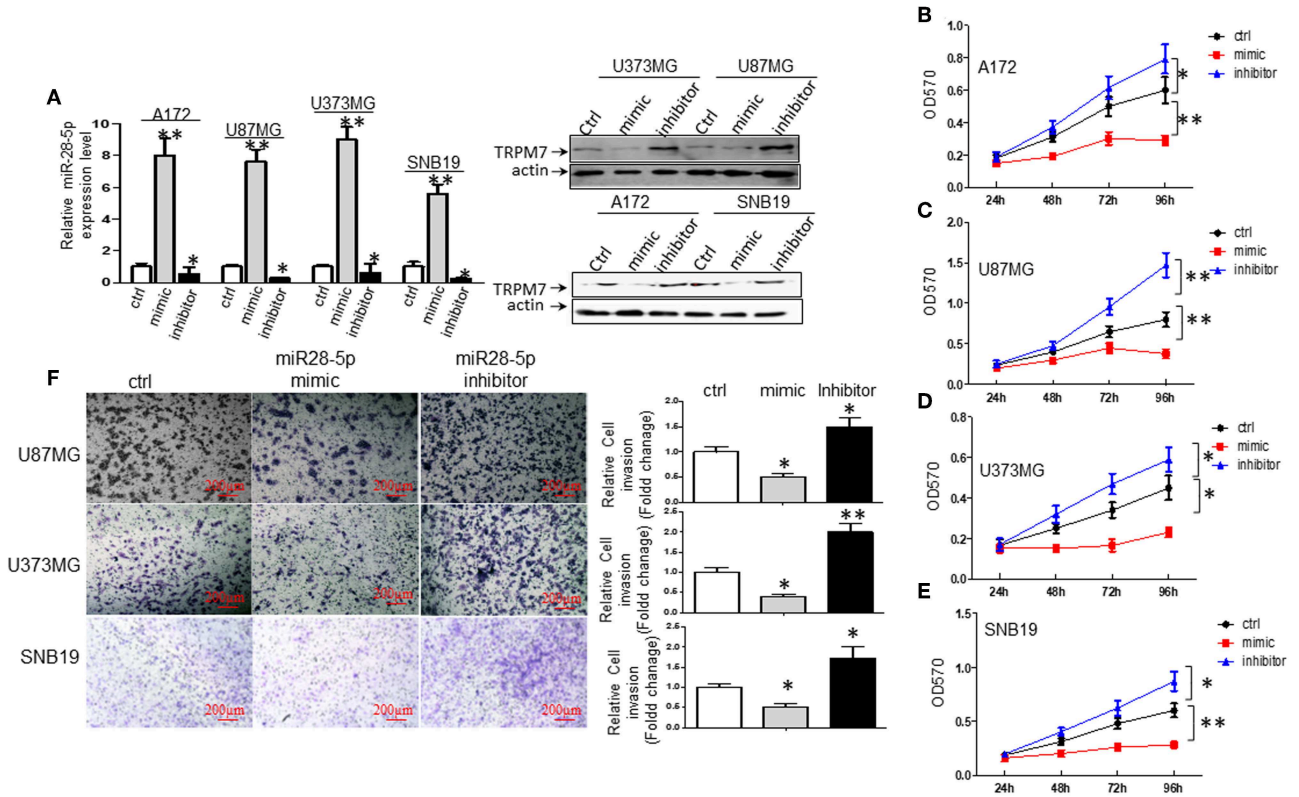

FIGURE 3 | miR-28-5p inhibits glioma cell line proliferation and invasion. **(A)** miR-28-5p mimics, miR-28-5p inhibitors and miR-NC (or ctrl) were transfected into A172, U87MG, U373MG, and SNB19 glioma cells, and stem-loop RT-PCR was conducted to examine the levels of miR-28-5p expression 72 h post-transfection with miR-28-5p mimics, miR-28-5p inhibitors and miR-NC. Left: miR-28-5p expression was significantly increased in A172, U87MG, U373MG, and SNB19 transfected with miR-28-5p mimics compared to the expression levels in cells transfected with miR-NC, miR-28-5p was significantly decreased in the above four glioma cell lines transfected with miR-28-5p inhibitors compared to the expression levels in cells transfected with miR-NC (*$P < 0.05$, **$P < 0.01$, Student *t*-test). The data were presented as the fold changes relative to the corresponding controls and are mean ± SD of triplicate samples performed in three independent experiments. Right: TRPM7 protein expression levels were checked simultaneously when overexpressing miR-28-5p mimics and inhibitors, and the negative correlation between TRPM7 and miR-28-5p was confirmed. **(B–E)** Representative experiment of the proliferation effect of miR-28-5p in A172, U87MG, U373MG, and SNB19 glioma cell lines assayed by MTT. Absorbance was measured every 24 h for 4 days post-transfection with miR-NC, miR-28-5p mimics and miR-28-5p inhibitors. miR28-5p mimics significantly decreased cell proliferation in glioma cell lines; while miR-28-5p inhibitors significantly increased cell proliferation in glioma cell lines (*$P < 0.05$, **$P < 0.01$, Student *t*-test). The data were presented as the fold changes relative to the corresponding controls and are mean ± SD of triplicate samples performed in three independent experiments. **(F)** A Matrigel transwell invasion assay, using U373MG, SNB19, and U87MG cell lines that were transiently transfected with miR-NC, miR-28-5p mimics, and miR-28-5p inhibitors were conducted exactly same as described in **Figures 1C,D**. The cell numbers were counted on the bottom of Matrigel-coated transwell chamber at 72 h post-transfection. A representative experiment was shown. The ectopic expression of miR-28-5p inhibited the number of invaded cells while inhibition of miR-28-5p expression increased the invasion compared to the controls. The data were represented as fold changes relative to controls are the mean ± SD of triplicate samples performed in two independent samples (*$P < 0.05$, **$P < 0.01$, Student *t*-test). Photomicrographs were taken at 10x magnification.

on glioma cell proliferation and invasion *in vitro* using MTT assay or Matrigel transwell invasion assay after transfecting A172, U87MG, U373MG, and SNB19 with synthesized specific small interfering RNAs (siRap1b) targeting Rap1b mRNA. The efficiency of the transfection was detected by the expression of total Rap1b protein, as examined by Western blot. As shown in **Figure 5A**, Rap1b siRNA markedly exhibited the inhibition of Rap1b expression (**Figure 5A**, lower panel). Next, MTT and cell invasion assay were conducted to examine the effects of Rap1b downregulation on the proliferation and invasion in A172, U87MG, U373MG, and SNB19, respectively. The results showed that transfection with siRap1b resulted in a significant decrease in proliferation in an approximate time-dependent manner when compared with the respective siRNA control groups in the four glioma cell lines; the cell growth viability was reduced by a maximum of 44.4% at 96 h in A172 cells, 37.4% at 96 h in U87MG cells, 46.5% at 72 h in U373MG cells, and 54.3% at 72 h in SNB19 cells (**Figure 5B**). The number of invasive cells crossed the Matrigel transwell was dramatically reduced by 40, 50, 80, and 55% in A172, U87MG, U373MG, and SNB19 cells at 72 h post-transfection, respectively (**Figure 5C**). Taken together, these results suggest that Rap1b increases glioma cell line proliferation and invasion, and promotes glioma tumorigenesis and metastasis.

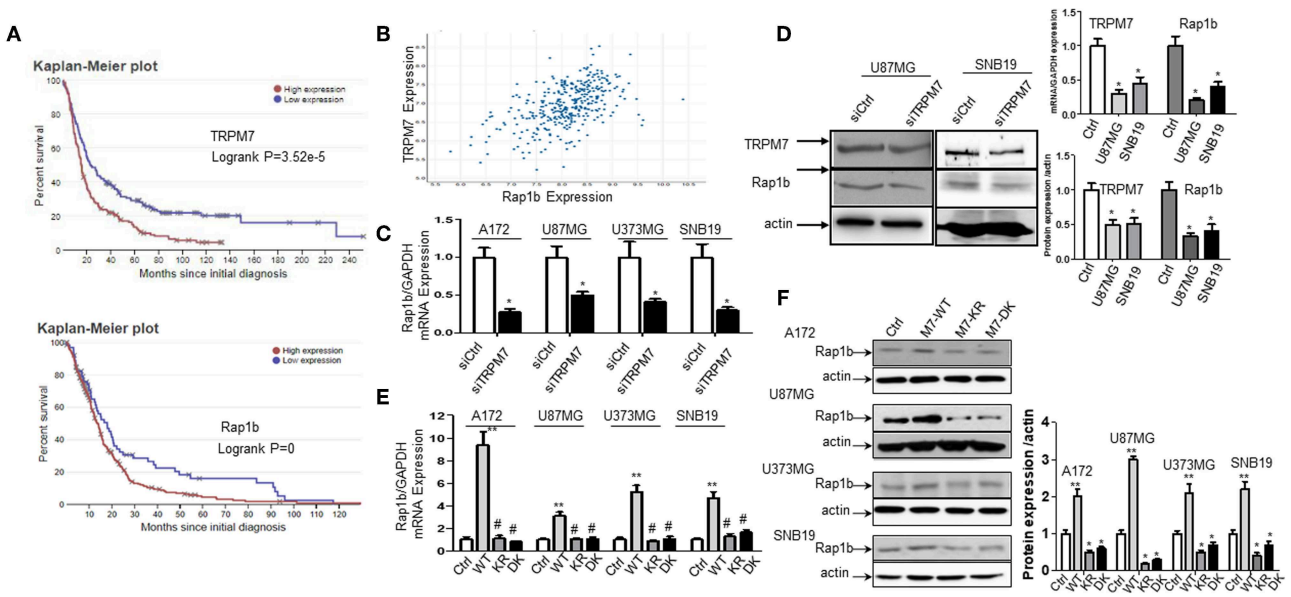

FIGURE 4 | TRPM7 positively regulated Rap1b mRNA and protein expression in glioma cells. **(A)** Kaplan-Meier survival curve for the overall survival of glioma patients. The bioinformatics analysis from Rembrandt showed a high expression level of TRPM7 and Rap1b are unfavorable prognostic biomarkers of overall survival ($p = 3.52e{-}5$ for the former, $p = 0$ for the latter, logrank tests). The data in upper panel of **(A)** showed that glioma patients with high TRPM7 expression ($n = 165$) have short overall survival compared to those with low TRPM7 expression ($n = 164$). The glioma patients with high Rap1b (lower panel) predict the poor prognosis of glioma patients as well (**A**, lower panel). **(B)** By Pearson correlation analysis via TCGA (http://www.betastasis.com/glioma/tcga_gbm/), a clearly direct correlation was observed between TRPM7 and Rap1b expression levels in 356 glioma patients with both genes are detectable ($r = 0.515$). **(C–F)** To confirm this correlation, we transfected A172, U87MG, U373MG, and SNB19 cells either with synthesized specific small interfering RNAs (siTRPM7) targeting TRPM7 mRNA to decreasing TRPM7 expression or with TRPM7 expression vector along with its mutants Δ kinase and K1648R to increase the TRPM7 expression. The transfection efficiency of TRPM7 knock-down and overexpression were examined by qPCR [see **Figure 2D** and **(D)**, upper right] and Western blot (**D** left and lower right). The lower right panel of **(D)** is the densitometry analysis of the bands performed using the ImageQuant program. The results showed that the inhibition of TRPM7 expression by siTRPM7 markedly reduced Rap1b expression at both mRNA in all four cell lines (**C**, $^{*}P < 0.05$, Student *t*-test) and protein levels in U87MG and SNB19 cells **(D)**. While overexpression of TRPM7 dramatically enhanced the expression of Rap1b at both mRNA (**E**, $^{**}P < 0.05$ compared to control-Ctrl, $^{\#}P < 0.05$ compared to wild type-WT, one-way ANOVA) and protein levels **(F)** in all four glioma cell lines. The right panel of **(F)** is the densitometry analysis of the bands performed using the ImageQuant program. Again, the mutants Δ kinase and K1648R exhibited a noticeable difference in Rap1b expression pattern at both mRNA and protein levels compared to that of wt TRPM7, which reflect differences in their functional roles. The data are expressed as the fold changes relative to the corresponding controls and are the mean ± SD of triplicated samples preformed in three independent experiments **(C–D)**. All the data represent one of the three independent experiments with similar results **(D–F)**.

miR-28-5p Directly Targets and Downregulates Rap1b Expression in Glioma Cells

miR-28-5p Expression Is Inversely Correlated With Rap1b mRNA and Protein Expression in Glioma Cells

To further explore the association between miR-28-5p and Rap1b in glioma cells, we analyzed the expression of the endogenous Rap1b after transiently transfecting cells with either (a) miR-28-5p mimics, (b) miR-28-5p inhibitor, or (c) control miR-28-5p-NC in A172, U87MG, U373MG, and SNB19 cells. The transient transfection efficiency was determined by qRT-PCR and Western blot. As shown in **Figure 6A**, Rap1b mRNA expression levels were significantly reduced by miR-28-5p mimics and significantly enhanced by miR-28-5p inhibitor in each of the four glioma cell lines. Similarly, the Rap1b protein expressions displayed the same patterns as those of mRNA expressions in U87MG, U373MG, and SNB19 cells (**Figure 6B**). These results confirm that miR-28-5p regulates both the expression levels of Rap1b mRNA and protein.

miR-28-5p Inhibits Glioma Cell Proliferation and Invasion by Directly Targeting Rap1b

To further clarify whether or not tumor suppressive roles of miR-28-5p were dependent on Rap1b expression, 100 nM of siRap1b was co-transfected with 30 nM of miR-28-5p inhibitor in A172, U87MG, U373MG, and SNB19 glioma cell lines to assess glioma cells' proliferation by MTT assay and glioma cell invasion by Matrigel transwell invasion assay. As expected, the reduction of Rap1b expression by siRap1b effectively reduced glioma cell proliferation induced by miR-28-5p inhibitor during 24 to 96 h post-transfection by a maximum of 52, 41.8, and 69.2% for A172, U87MG, and U373MG at 96 h, 60% for SNB19 at 48 h (**Figure 6C**). Similarly, siRap1b markedly reduced miR-28-5p inhibitor-induced invasion by 35.6, 42.1, and 39.0% in U87MG, U373MG, and SNB19 cells at 72 h, respectively (**Figure 6D**, $^{*}p < 0.05$, $^{**}p < 0.01$, one-way ANOVA). These results suggest that Rap1b is able to at least partially restore the function of miR-28-5p, and these functional restoration assays support that miR-28-5p functions upstream of Rap1b and is dependent on Rap1b.

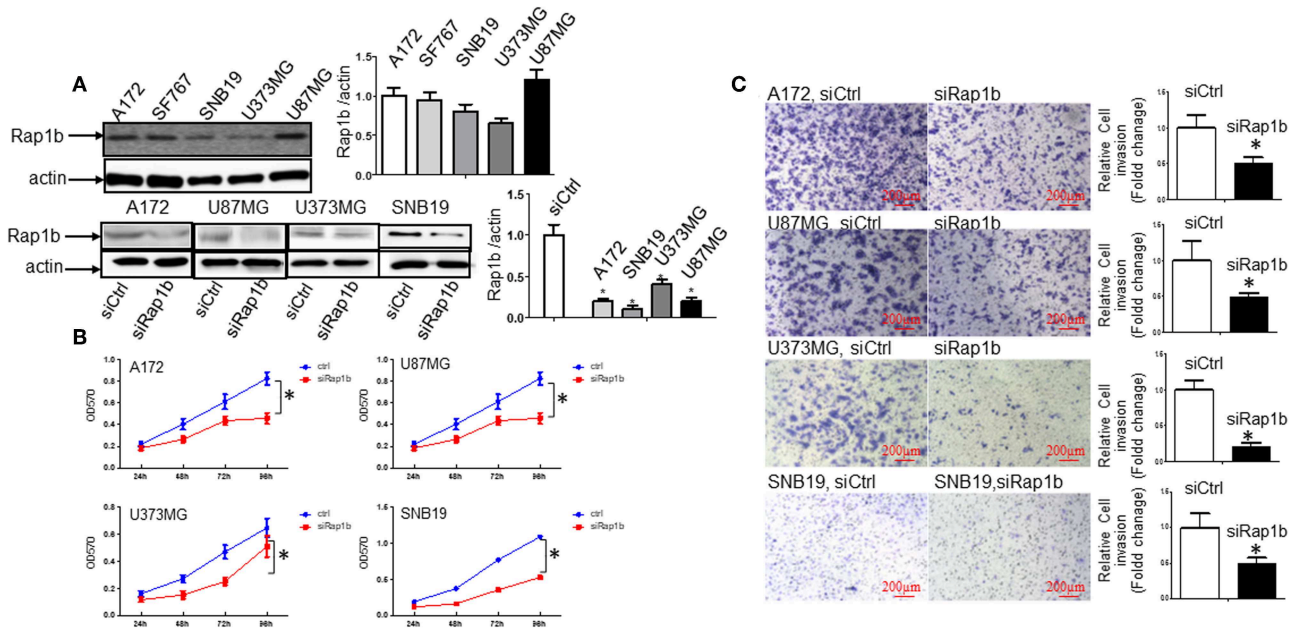

FIGURE 5 | Rap1b elevates glioma cell proliferation and invasion. **(A)** All the glioma cell lines A172, SF767, SNB19, U373MG, and U87MG expressed the Rap1b protein (upper panel). We then transfected siRap1b along with the control into the in A172, U87MG, U373MG, and SNB19 cells, the efficiency of the transfection was detected by the expression of total Rap1b protein, as examined by Western blot. Rap1b siRNA markedly inhibited Rap1b expression (lower panel). The corresponding densitometry analysis for each Western blot performed using the ImageQuant program are on the right sides correspondingly. **(B,C)** Rap1b elevates glioma cell proliferation and invasion. MTT and cell invasion assay were conducted to examine the effects of Rap1b on the proliferation and invasion after transfecting A172, U87MG, U373MG, and SNB19 with synthesized specific small interfering RNAs (siRap1b) targeting Rap1b mRNA. The results showed that transfection with siRap1b resulted in a significant decrease in proliferation **(B)** and invasion (**C**, Photomicrographs were taken at 10x magnification) compared with the respective siRNA control groups in the four glioma cell lines. These results suggested that Rap1b increases glioma cell line proliferation and invasion, and Rap1b may perform tumor promoting roles in glioma growth and metastasis [$^*P < 0.05$, one-way ANOVA for proliferation assay in **(B)**, Student *t*-test for invasion assay in **C**]. All data are from triplicate samples performed in two different independent experiments.

DISCUSSION

In the current study, we utilized four glioma cell lines, A172, U87MG, U373MG, and SNB19, based on their different molecular characteristics. U373MG has a p53 gene mutation (33), while A172, U87MG (33), and SNB19 are PTEN-mutant cell lines (34, 35). In addition to harboring PTEN and CDKN2A ($p16^{INK4a}$) mutation as in A172, U87MG has another CDKN2C ($p18^{INK4c}$) mutation (36). Although U373MG cells may share common origins with SNB19, these two cell lines appear to have evolved to exhibit distinct karyotypes and drug sensitivities (37); thus, they serve as culture models with different molecular background for comparison in this study.

TRPM7 channel is nonselectively permeable to many divalent cations such as Ca^{2+}, Mg^{2+}, and Zn^{2+}, which comprises the TRPM7-mediated inward current. In addition, it has the unique characteristic of α-kinase domain at its carboxyl-terminal (17). The kinase domain of TRPM7 is not essential for the activation of its channel, but structural changes in the kinase domain could alter the sensitivity of channel activation to divalent cation (17). TRPM7-dependent divalent cations, growth factors (GFs), hypoxia and/or other signals can open TRPM7 channel and increase cell proliferation. In this regard, the major activated signaling pathways activated include PI3K/AKT/mTOR (38–40), Src/MAPKs/JNK, p38, and ERK (41–45). Depleted TRPM7 resulted in the inactivation of STAT3 and the disruption of proliferation of thymocytes (46). On the other hand, the opening of TRPM7 channels causes a local increases in Ca^{2+}/Mg^{2+} concentration, which affects the recruitment/targeting of TRPM7 kinase substrates (16). TRPM7-kinase phosphorylates downstream eEF2-k on Ser78 in human (Ser77 in mouse eEF2-k), causing increased stability of eEF2-k, strengthening inhibitory eEF2 at Thr56 phosphorylation and resulting in an increased translational efficiency when Mg^{2+} is available (16). The channel kinase of TRPM7 participates in the regulation of cell migration by modulating phosphorylation of annexin 1 (47–50), myosin IIA (51–53) and calpain (54) in response to various stimuli in tumor cells. In the present study, we evaluated TRPM7 channels' properties using a deletion mutant of human TRPM7 in which the entire kinase domain was removed following amino acid 1569 (TRPM7 Δkinase or M7-DK) and a mutant with a point mutation in the ATP binding site of the α-kinase domain (K1648R, or M7-KR). We found that the channel activity of TRPM7 is required for cell growth while the kinase domain is required for cell migration/invasion. This finding is important for designing and developing drugs targeting TRPM7 in human malignancies.

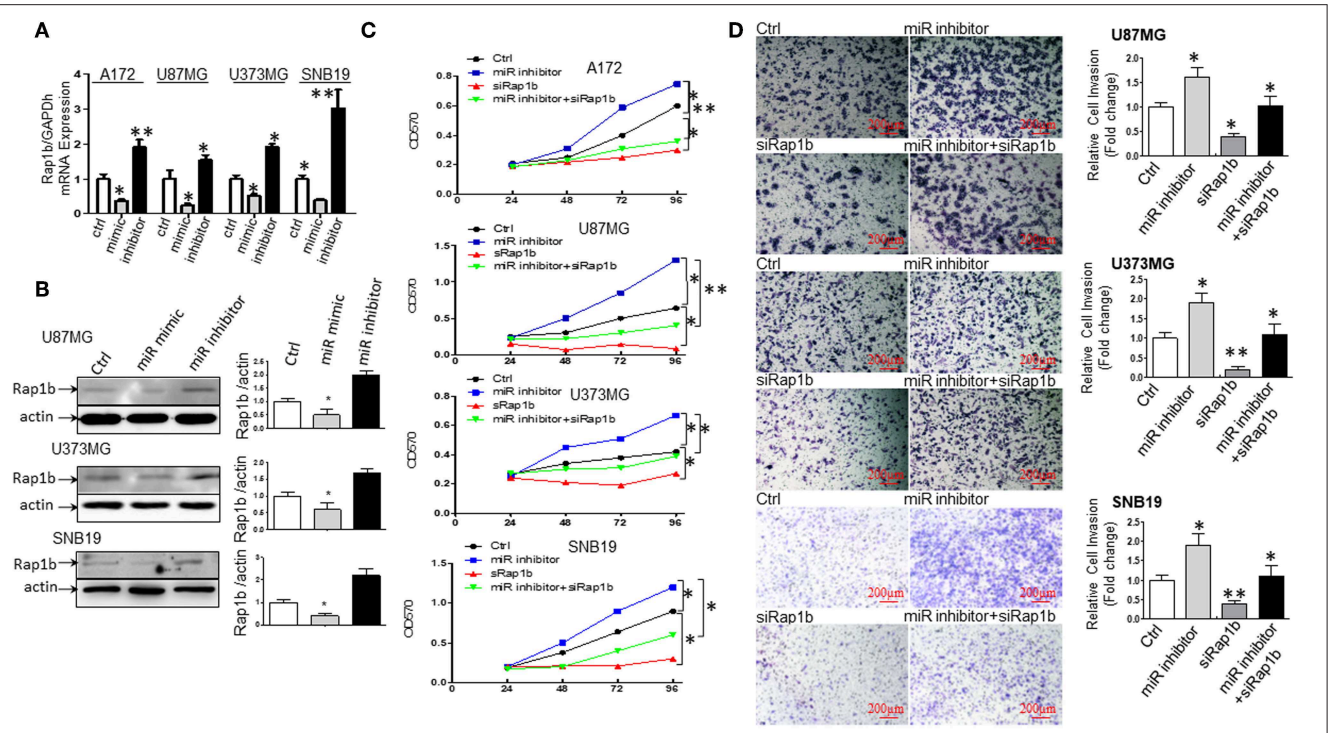

FIGURE 6 | miR-28-5p directly targets and downregulates Rap1b expression in glioma cells. **(A,B)** miR-28-5p expression is inversely correlated with Rap1b mRNA and protein expression in glioma cells. We analyzed the expression of the endogenous Rap1b after transiently transfecting cells with either (a) miR-28-5p mimics; (b) miR-28-5p inhibitor; (c) control miR-28-5p-NC (ctrl) in A172, U87MG, U373MG, and SNB19 cells. The transient transfection efficiency was determined by qRT-PCR and Western blot. As expected, Rap1b mRNA expression levels were significantly reduced by miR-28-5p mimics and significantly enhanced by miR-28-5p inhibitor in each of the four glioma cell lines **(A)**. Similar, the Rap1b protein expressions displayed the same patterns as those of mRNA expressions in U87MG, U373MG, and SNB19 cells **(B)**. The densitometry analysis performed using the ImageQuant program are on the right side of each Western blot gel. **(C,D)** miR-28-5p inhibits glioma cell proliferation and invasion by directly targeting Rap1b. To further clarify whether or not tumor suppressive roles of miR-28-5p were dependent on Rap1b expression, 100 nM of siRap1b was co-transfected with 30 nM of miR28-5p inhibitor in A172, U87MG, U373MG, and SNB19 glioma cell lines to assess glioma cells' proliferation by MTT assay and evaluate glioma cell invasion by Matrigel transwell invasion assay. The reduction of Rap1b expression by siRap1b effectively reduced the miR-28-5p inhibitor-induced glioma cell proliferation **(C)**, and the miR-28-5p inhibitor-induced invasion (**D**, Photomicrographs were taken at 10x magnification) in each of the four glioma cell lines above. All data are from triplicate samples performed in two different independent experiments. (*$P < 0.05$, **$P < 0.01$).

Among 2,588 mature and 1,881 precursor human miRNA sequences in 12 miRNA databases, 365 miRNAs were found to be deregulated in glioblastoma (55). The genes targeted by the deregulated miRNAs in glioblastoma include many pathways such as cell growth/proliferation, apoptosis, invasion and metastasis, angiogenesis, autophagy, and drug resistance (56). miR-28-5p was found to interfere with genes involved in cell replication and cell cycle checkpoints (57). In glioblastoma, the role of miR-28-5p has not yet been fully explored, but its structurally related miR-708 was demonstrated to inhibit glioblastoma cell proliferation by targeting EZH2, AKT1, MMP2, CCND1, Parp-1, and Bcl-2 (58). Our results suggest that miRNA changes demonstrate different glioma tumorigenicity, and miR-26b-5p, miR-4530, and miR-28-5p are regulated by TRPM7 and participate in glioma progression. In the present study, we further elucidated the TRPM7/miR-28-5p/Rap1b axis in gliomagenesis using multiple cell lines with different mutational status. Our results showed that miR-28-5p inhibits glioma cell proliferation and invasion by targeting its downstream Rap1b gene, and miR-28-5p is regulated by TRPM7.

Functional analyses of miR-28-5p revealed tumor suppressive properties caused by the inhibition of Rap1b, E2F6, IGF-1, IL-34, and AKT. A study reported that miR-28-5p inhibited cell proliferation and migration by directly suppressing Rap1b gene in renal cell carcinoma (31). In prostate cancer, the miR-28-5p targeted E2F6 and induced apoptosis in DU-145 cells (7). The ectopic miR-28-5p expression downregulates insulin-like growth factor 1 (IGF1) protein and the expression of miR-28-5p correlates negatively with IGF1 protein level in hepatocellular carcinoma (HCC) cells, which indicate that miR-28-5p-IGF1-PI3K/AKT pathway may play an important role in the development of HCC (10). IL-34 is a direct downstream target of miR-28-5p whose expression is inversely correlated with IL-34 expression (30). Lastly, miR-28-5p may act as a tumor suppressor gene, which inhibited the invasion and metastasis of gastric cancer by inhibiting the activation of the AKT signaling pathway (8). By contrast, miR-28 also served as a tumor promoting factor in some specific tumors. For instance, it is a thrombopoietin receptor (TpoR, MPL) targeting miRNA, which is overexpressed in the platelets of patients

with myeloproliferative neoplasms (MPNs) and its negative role in megakaryocyte differentiation leads to MPNs through the downregulation of MPL (59). In the process of ovarian cancer development and progression, miR-28-5p downregulates N4BP1, forces cancer cells to enter S phase, and promotes ovarian cancer cell proliferation and invasion (29). Taken together, miR-28-5p can function as either tumor suppressor genes or oncogenes, reflecting cell type-specific and tissue-specific roles of this miRNA.

miRNAs are involved in diverse biological processes by binding to different regions of the target mRNA sequences, such as the 3′-untranslated regions, coding sequences, or 5′-untranslated regions. The same hairpin RNA structure can produce mature miRNAs from each strand, named 5p and 3p, that can bind to different mRNAs (60). Almeida et al. (60) found that strand-specific 5p and 3p of miR-28-5 have distinct functions in colorectal cancer cells, where miR-28-5p suppressed cell proliferation, resulting in apoptosis and G1 arrest in the cell cycle, while miR-28-3p had no influence on proliferation *in vitro*. In addition, miR-28-5p and miR-28-3p had opposite effects on migration and invasion *in vitro*, with miR-28-5p decreasing cell migration and miR-28-3p increasing cell migration, which appears to be independent of cell growth. Overall, miR-28-3p overrides miR-28-5p to promote colorectal cancer cell metastases *in vivo*. The contrasting biological effects caused by miR-28-5p and miR-28-3p might be partly due to their binding to different targets where miR-28-5p targets CCND1 and HoxB3 while miR-28-3p targets Nm23-H1. In HCC, Kaplan-Meier's analysis showed that HCC patients with miR-28-5p overexpression, but not with miR-28-3p overexpression, had better overall survival rate. Girardot et al. (59) identified two miRNAs that are closely related to miR-28. miR-151 and miR-28 share 80% sequence identity, while miR-708 share 68% sequence identity with miR-28 and 71% with miR-151. All three miRNAs targeted the MPL 3′ UTR for translational inhibition. However, the combination of miR-28 with miR-151 and miR-708 did not produce synergic inhibition due to all targeting the same sequence in the 3′UTR of MPL.

The normal physiological role of the small GTP-binding protein Rap1 is to antagonize Ras mitogenic signals. However, in 1998, Altschuler et al. first revealed that Rap1 is a conditional oncoprotein (61). Later, Rap1 was demonstrated to be required for pancreatic and prostate cancer cell metastasis and angiogenesis but not for the proliferation properties of these cancer cells (62). In 2014, Sayyah's group published the first study showing that this small G-protein is required for glioblastoma cell growth *in vitro* by activating downstream signaling of G-protein-coupled receptor and RhoA utilizing Rap1 knockdown techniques. However, they stated that this critical role was caused by the isoform Rap1a, not Rap1b (32). Rap1a and Rap1b are 95% homologous, but differences in subcellular localization of two isoforms and their mechanisms of activation resulted in their distinctive functions and roles in glioblastoma cell proliferation (63, 64). In this study, we found Rap1b demonstrated the mitogenic roles in both glioma cell proliferation and invasion.

A positive correlation has been shown between TRPM7 and Rap1b in **Figure 4A**. There are several possible mechanistic links between the two proteins. First, they may connect to each other by miR-28-5p. In this study, we showed that TRPM7 downregulated miR-28-5p, while miR-28-5p downregulated Rap1b; this is likely one mechanism of a positive correlation between TRPM7 and miR-28-5p. Second, TRPM7 and Rap1b may be connected by Notch signaling. In hematopoietic stem cell development, Integrin-mediated cell adhesion was promoted by Notch-regulated Rap1b signaling (65); while our published data also demonstrated that TRPM7 regulated the Notch pathway in gliomagenesis (1).

Taken together, the discovery of cellular and molecular targets modulated by the tumor suppressor miR-28-5p and its upstream regulator TRPM7 molecule provides key insights into the potential mechanisms of glioma tumorigenesis and suggests novel therapeutic targets for glioma treatments.

DATA AVAILABILITY STATEMENT

The datasets generated for this study are available on request to the corresponding author.

AUTHOR CONTRIBUTIONS

SG, GW, and ML designed the study protocol. JW and AG performed experiments based on glioma cell cultures and evaluated the data with the help of ML. ML performed the biostatistical evaluation of the data. AG and ML wrote the manuscript with contributions and final approval by all authors. IC, SG, JH, and GW contributed to the critical reading and revision of the manuscript.

FUNDING

This study was supported by NIH NIGMS GM121230 to ML. GW was supported by NIMHD grant U54MD007595. This study was partly supported by NIH/NINHD MD007589. The funding body had no role in the design, collection, analysis and interpretation of the study's data, and in writing the manuscript.

ACKNOWLEDGMENTS

We thank Dr. Carsten Schmitz (University of Colorado, Denver, CO) for providing us with all constructs (wtTRPM7, Δkinase, K1648R) that were tagged with a HA at N-terminal. We are grateful to Dr. Yancey G. Gillespie at the University of Alabama at Birmingham (UAB) for providing us U87MG, U373MG, and SNB19 cell lines, to Dr. Hui-Kuo Shu at Emory University for providing SF767 cell line.

REFERENCES

1. Liu M, Inoue K, Leng T, Guo S, Xiong ZG. TRPM7 channels regulate glioma stem cell through STAT3 and Notch signaling pathways. *Cell Signal.* (2014) 26:2773–81. doi: 10.1016/j.cellsig.2014.08.020
2. Miyamoto K, Seki N, Matsushita R, Yonemori M, Yoshino H, Nakagawa M, et al. Tumour-suppressive miRNA-26a-5p and miR-26b-5p inhibit cell aggressiveness by regulating PLOD2 in bladder cancer. *Br J Cancer.* (2016) 115:354–63. doi: 10.1038/bjc.2016.179
3. Bartel DP. MicroRNAs: genomics, biogenesis, mechanism, and function. *Cell.* (2004) 116:281–97. doi: 10.1016/S0092-8674(04)00045-5
4. Carthew RW, Sontheimer EJ. Origins and mechanisms of miRNAs and siRNAs. *Cell.* (2009) 136:642–55. doi: 10.1016/j.cell.2009.01.035
5. Di Leva G, Croce CM. Roles of small RNAs in tumor formation. *Trends Mol Med.* (2010) 16:257–67. doi: 10.1016/j.molmed.2010.04.001
6. Malzkorn B, Wolter M, Liesenberg F, Grzendowski M, Stuhler K, Meyer HE, et al. Identification and functional characterization of microRNAs involved in the malignant progression of gliomas. *Brain Pathol.* (2010) 20:539–50. doi: 10.1111/j.1750-3639.2009.00328.x
7. Rizzo M, Berti G, Russo F, Evangelista M, Pellegrini M, Rainaldi G. The miRNA pull out assay as a method to validate the miR-28–5p targets identified in other tumor contexts in prostate cancer. *Int J Genomics.* (2017) 2017:5214806. doi: 10.1155/2017/5214806
8. Xiao F, Cheng Z, Wang P, Gong B, Huang H, Xing Y, et al. MicroRNA-28–5p inhibits the migration and invasion of gastric cancer cells by suppressing AKT phosphorylation. *Oncol Lett.* (2018) 15:9777–85. doi: 10.3892/ol.2018.8603
9. Liu J, Liu XQ, Liu Y, Sun YN, Li S, Li CM, et al. MicroRNA 28–5p regulates ATP-binding cassette transporter A1 via inhibiting extracellular signal-regulated kinase 2. *Mol Med Rep.* (2016) 13:433–40. doi: 10.3892/mmr.2015.4563
10. Shi X, Teng F. Down-regulated miR-28–5p in human hepatocellular carcinoma correlated with tumor proliferation and migration by targeting insulin-like growth factor-1 (IGF-1). *Mol Cell Biochem.* (2015) 408:283–93. doi: 10.1007/s11010-015-2506-z
11. Thuringer D, Chanteloup G, Winckler P, Garrido C. The vesicular transfer of CLIC1 from glioblastoma to microvascular endothelial cells requires TRPM7. *Oncotarget.* (2018) 9:33302–11. doi: 10.18632/oncotarget.26048
12. Sander P, Mostafa H, Soboh A, Schneider JM, Pala A, Baron AK, et al. Vacquinol-1 inducible cell death in glioblastoma multiforme is counter regulated by TRPM7 activity induced by exogenous ATP. *Oncotarget.* (2017) 8:35124–37. doi: 10.18632/oncotarget.16703
13. Chen HS, Lu AQ, Yang PY, Liang J, Wei Y, Shang YW, et al. MicroRNA-28–5p regulates glioma cell proliferation, invasion and migration by targeting SphK1. *Eur Rev Med Pharmacol Sci.* (2019) 23:6621–8. doi: 10.26355/eurrev_201908_18551
14. She X, Yu Z, Cui Y, Lei Q, Wang Z, Xu G, et al. miR-128 and miR-149 enhance the chemosensitivity of temozolomide by Rap1B-mediated cytoskeletal remodeling in glioblastoma. *Oncol Rep.* (2014) 32:957–64. doi: 10.3892/or.2014.3318
15. Malchinkhuu E, Sato K, Maehama T, Ishiuchi S, Yoshimoto Y, Mogi C, et al. Role of Rap1B and tumor suppressor PTEN in the negative regulation of lysophosphatidic acid–induced migration by isoproterenol in glioma cells. *Mol Biol Cell.* (2009) 20:5156–65. doi: 10.1091/mbc.e09-08-0692
16. Perraud AL, Zhao X, Ryazanov AG, Schmitz C. The channel-kinase TRPM7 regulates phosphorylation of the translational factor eEF2 via eEF2-k. *Cell Signal.* (2011) 23:586–93. doi: 10.1016/j.cellsig.2010.11.011
17. Schmitz C, Perraud AL, Johnson CO, Inabe K, Smith MK, Penner R, et al. Regulation of vertebrate cellular Mg2+ homeostasis by TRPM7. *Cell.* (2003) 114:191–200. doi: 10.1016/S0092-8674(03)00556-7
18. Larco DO, Semsarzadeh NN, Cho-Clark M, Mani SK, Wu TJ. β-Arrestin 2 Is a mediator of GnRH-(1–5) signaling in immortalized GnRH neurons. *Endocrinology.* (2013) 154:4726–36. doi: 10.1210/en.2013-1286
19. Liu M, Wilson NO, Hibbert JM, Stiles JK. STAT3 regulates MMP3 in heme-induced endothelial cell apoptosis. *PLoS ONE.* (2013) 8:e71366. doi: 10.1371/journal.pone.0071366
20. Haddock AN, Labuzan SA, Haynes AE, Hayes CS, Kakareka KM, Waddell DS. Dual-specificity phosphatase 4 is upregulated during skeletal muscle atrophy and modulates extracellular signal-regulated kinase activity. *AJP Cell Physiology*. (2019) 316:C567–81. doi: 10.1152/ajpcell.00234.2018
21. Varkonyi-Gasic E, Wu R, Wood M, Walton EF, Hellens RP. Protocol: a highly sensitive RT-PCR method for detection and quantification of microRNAs. *Plant Methods.* (2007) 3:12. doi: 10.1186/1746-4811-3-12
22. Chen C, Ridzon DA, Broomer AJ, Zhou Z, Lee DH, Nguyen JT, et al. Real-time quantification of microRNAs by stem-loop RT-PCR. *Nucleic Acids Res.* (2005) 33:e179. doi: 10.1093/nar/gni178
23. Balcells I, Cirera S, Busk PK. Specific and sensitive quantitative RT-PCR of miRNAs with DNA primers. *BMC Biotechnol.* (2011) 11:70. doi: 10.1186/1472-6750-11-70
24. Busk PK. A tool for design of primers for microRNA-specific quantitative RT-qPCR. *BMC Bioinformatics.* (2014) 15:29. doi: 10.1186/1471-2105-15-29
25. Czimmerer Z, Hulvely J, Simandi Z, Varallyay E, Havelda Z, Szabo E, et al. A versatile method to design stem-loop primer-based quantitative PCR assays for detecting small regulatory RNA molecules. *PLoS ONE.* (2013) 8:e55168. doi: 10.1371/journal.pone.0055168
26. Kang ST, Hsieh YS, Feng CT, Chen YT, Yang PE, Chen WM. miPrimer: an empirical-based qPCR primer design method for small noncoding microRNA. *RNA.* (2018) 24:304–12. doi: 10.1261/rna.061150.117
27. Marcial-Quino J, Gomez-Manzo S, Fierro F, Vanoye-Carlo A, Rufino-Gonzalez Y, Sierra-Palacios E, et al. Stem-loop RT-qPCR as an efficient tool for the detection and quantification of small RNAs in giardia lamblia. *Genes.* (2016) 7:131. doi: 10.3390/genes7120131
28. Liu Y, Beyer A, Aebersold R. On the dependency of cellular protein levels on mRNA abundance. *Cell.* (2016) 165:535–50. doi: 10.1016/j.cell.2016.03.014
29. Xu J, Jiang N, Shi H, Zhao S, Yao S, Shen H. miR-28–5p promotes the development and progression of ovarian cancer through inhibition of N4BP1. *Int J Oncol.* (2017) 50:2236. doi: 10.3892/ijo.2017.3977
30. Zhou SL, Hu ZQ, Zhou ZJ, Dai Z, Wang Z, Cao Y, et al. miR-28–5p-IL-34-macrophage feedback loop modulates hepatocellular carcinoma metastasis. *Hepatology.* (2016) 63:1560–75. doi: 10.1002/hep.28445
31. Wang C, Wu C, Yang Q, Ding M, Zhong J, Zhang CY, et al. miR-28–5p acts as a tumor suppressor in renal cell carcinoma for multiple antitumor effects by targeting RAP1B. *Oncotarget.* (2016) 7:73888–902. doi: 10.18632/oncotarget.12516
32. Sayyah J, Bartakova A, Nogal N, Quilliam LA, Stupack DG, Brown JH. The Ras-related protein, Rap1A, mediates thrombin-stimulated, integrin-dependent glioblastoma cell proliferation and tumor growth. *J Biol Chem.* (2014) 289:17689–98. doi: 10.1074/jbc.M113.536227
33. Ishii N, Maier D, Merlo A, Tada M, Sawamura Y, Diserens AC, et al. Frequent co-alterations of TP53, p16/CDKN2A, p14ARF, PTEN tumor suppressor genes in human glioma cell lines. *Brain Pathol.* (1999) 9:469–79. doi: 10.1111/j.1750-3639.1999.tb00536.x
34. Chakrabarti M, Ray SK. Synergistic anti-tumor actions of luteolin and silibinin prevented cell migration and invasion and induced apoptosis in glioblastoma SNB19 cells and glioblastoma stem cells. *Brain Res.* (2015) 1629:85–93. doi: 10.1016/j.brainres.2015.10.010
35. Memmel S, Sukhorukov VL, Horing M, Westerling K, Fiedler V, Katzer A, et al. Cell surface area and membrane folding in glioblastoma cell lines differing in PTEN and p53 status. *PLoS ONE.* (2014) 9:e87052. doi: 10.1371/journal.pone.0087052
36. Allen M, Bjerke M, Edlund H, Nelander S, Westermark B. Origin of the U87MG glioma cell line: good news and bad news. *Sci Transl Med.* (2016) 8:354re3. doi: 10.1126/scitranslmed.aaf6853
37. Stepanenko AA, Kavsan VM. Karyotypically distinct U251, U373, and SNB19 glioma cell lines are of the same origin but have different drug treatment sensitivities. *Gene.* (2014) 540:263–5. doi: 10.1016/j.gene.2014.02.053
38. Sahni J, Scharenberg AM. TRPM7 ion channels are required for sustained phosphoinositide 3-kinase signaling in lymphocytes. *Cell Metab.* (2008) 8:84–93. doi: 10.1016/j.cmet.2008.06.002
39. Sahni J, Tamura R, Sweet IR, Scharenberg AM. TRPM7 regulates quiescent/proliferative metabolic transitions in lymphocytes. *Cell Cycle.* (2010) 9:3565–74. doi: 10.4161/cc.9.17.12798
40. Zhan F, Barlogie B, Arzoumanian V, Huang Y, Williams DR, Hollmig K, et al. Gene-expression signature of benign monoclonal gammopathy evident in multiple myeloma is linked to good prognosis. *Blood.* (2007) 109:1692–700. doi: 10.1182/blood-2006-07-037077

41. Davis FM, Azimi I, Faville RA, Peters AA, Jalink K, Putney JW Jr, et al. Induction of epithelial-mesenchymal transition (EMT) in breast cancer cells is calcium signal dependent. *Oncogene.* (2013) 33:2307–16. doi: 10.1038/onc.2013.187
42. Desai BN, Krapivinsky G, Navarro B, Krapivinsky L, Carter BC, Febvay S, et al. Cleavage of TRPM7 releases the kinase domain from the ion channel and regulates its participation in Fas-induced apoptosis. *Dev Cell.* (2012) 22:1149–62. doi: 10.1016/j.devcel.2012.04.006
43. Inoue K, Xiong ZG. Silencing TRPM7 promotes growth/proliferation and nitric oxide production of vascular endothelial cells via the ERK pathway. *Cardiovasc Res.* (2009) 83:547–57. doi: 10.1093/cvr/cvp153
44. Meng X, Cai C, Wu J, Cai S, Ye C, Chen H, et al. TRPM7 mediates breast cancer cell migration and invasion through the MAPK pathway. *Cancer Lett.* (2013) 333:96–102. doi: 10.1016/j.canlet.2013.01.031
45. Su LT, Chen HC, Gonzalez-Pagan O, Overton JD, Xie J, Yue L, et al. TRPM7 activates m-calpain by stress-dependent stimulation of p38 MAPK and c-Jun N-terminal kinase. *J Mol Biol.* (2010) 396:858–69. doi: 10.1016/j.jmb.2010.01.014
46. Jin J, Desai BN, Navarro B, Donovan A, Andrews NC, Clapham DE. Deletion of Trpm7 disrupts embryonic development and thymopoiesis without altering Mg2+ homeostasis. *Science.* (2008) 322:756–60. doi: 10.1126/science.1163493
47. Dorovkov MV, Kostyukova AS, Ryazanov AG. Phosphorylation of annexin A1 by TRPM7 kinase: a switch regulating the induction of an alpha-helix. *Biochemistry.* (2011) 50:2187–93. doi: 10.1021/bi101963h
48. Gerke V, Moss SE. Annexins: from structure to function. *Physiol Rev.* (2002) 82:331–71. doi: 10.1152/physrev.00030.2001
49. Rescher U, Gerke V. Annexins–unique membrane binding proteins with diverse functions. *J Cell Sci.* (2004) 117:2631–9. doi: 10.1242/jcs.01245
50. Rothhut B. Participation of annexins in protein phosphorylation. *Cell Mol Life Sci.* (1997) 53:522–6. doi: 10.1007/s000180050066
51. Clark K, Langeslag M, van Leeuwen B, Ran L, Ryazanov AG, Figdor CG, et al. TRPM7, a novel regulator of actomyosin contractility and cell adhesion. *EMBO J.* (2006) 25:290–301. doi: 10.1038/sj.emboj.7600931
52. Langeslag M, Clark K, Moolenaar WH, van Leeuwen FN, Jalink K. Activation of TRPM7 channels by phospholipase C-coupled receptor agonists. *J Biol Chem.* (2007) 282:232–9. doi: 10.1074/jbc.M605300200
53. Nakasawa T, Takahashi M, Matsuzawa F, Aikawa S, Togashi Y, Saitoh T, et al. Critical regions for assembly of vertebrate nonmuscle myosin II. *Biochemistry.* (2005) 44:174–83. doi: 10.1021/bi048807h
54. Su LT, Agapito MA, Li M, Simonson WT, Huttenlocher A, Habas R, et al. TRPM7 regulates cell adhesion by controlling the calcium-dependent protease calpain. *J Biol Chem.* (2006) 281:11260–70. doi: 10.1074/jbc.M512885200
55. Moller HG, Rasmussen AP, Andersen HH, Johnsen KB, Henriksen M, Duroux M. A systematic review of microRNA in glioblastoma multiforme: micro-modulators in the mesenchymal mode of migration and invasion. *Mol Neurobiol.* (2013) 47:131–44. doi: 10.1007/s12035-012-8349-7
56. Banelli B, Forlani A, Allemanni G, Morabito A, Pistillo MP, Romani M. MicroRNA in glioblastoma: an overview. *Int J Genomics.* (2017) 2017:7639084. doi: 10.1155/2017/7639084
57. Hell MP, Thoma CR, Fankhauser N, Christinat Y, Weber TC, Krek W. miR-28–5p promotes chromosomal instability in VHL-associated cancers by inhibiting Mad2 translation. *Cancer Res.* (2014) 74:2432–43. doi: 10.1158/0008-5472.CAN-13-2041
58. Guo P, Lan J, Ge J, Nie Q, Mao Q, Qiu Y. miR-708 acts as a tumor suppressor in human glioblastoma cells. *Oncol Rep.* (2013) 30:870–6. doi: 10.3892/or.2013.2526
59. Girardot M, Pecquet C, Boukour S, Knoops L, Ferrant A, Vainchenker W, et al. miR-28 is a thrombopoietin receptor targeting microRNA detected in a fraction of myeloproliferative neoplasm patient platelets. *Blood.* (2010) 116:437–45. doi: 10.1182/blood-2008-06-165985
60. Almeida MI, Nicoloso MS, Zeng L, Ivan C, Spizzo R, Gafa R, et al. Strand-specific miR-28–5p and miR-28–3p have distinct effects in colorectal cancer cells. *Gastroenterology.* (2012) 142:886–96.e9. doi: 10.1053/j.gastro.2011.12.047
61. Altschuler DL, Ribeiro-Neto F. Mitogenic and oncogenic properties of the small G protein Rap1b. *Proc Natl Acad Sci USA.* (1998) 95:7475–9. doi: 10.1073/pnas.95.13.7475
62. Huang M, Anand S, Murphy EA, Desgrosellier JS, Stupack DG, Shattil SJ, et al. EGFR-dependent pancreatic carcinoma cell metastasis through Rap1 activation. *Oncogene.* (2012) 31:2783–93. doi: 10.1038/onc.2011.450
63. Severson EA, Lee WY, Capaldo CT, Nusrat A, Parkos CA. Junctional adhesion molecule A interacts with Afadin and PDZ-GEF2 to activate Rap1A, regulate beta1 integrin levels, and enhance cell migration. *Mol Biol Cell.* (2009) 20:1916–25. doi: 10.1091/mbc.e08-10-1014
64. Wittchen ES, Aghajanian A, Burridge K. Isoform-specific differences between Rap1A and Rap1B GTPases in the formation of endothelial cell junctions. *Small GTPases.* (2011) 2:65–76. doi: 10.4161/sgtp.2.2.15735
65. Rho SS, Kobayashi I, Oguri-Nakamura E, Ando K, Fujiwara M, Kamimura N, et al. Rap1b promotes notch-signal-mediated hematopoietic stem cell development by enhancing integrin-mediated cell adhesion. *Dev Cell.* (2019) 49:681–96.e6. doi: 10.1016/j.devcel.2019.03.023

Conflict of Interest: The authors declare that the research was conducted in the absence of any commercial or financial relationships that could be construed as a potential conflict of interest.

frontiers in Oncology

ORIGINAL RESEARCH
published: 18 December 2019
doi: 10.3389/fonc.2019.01447

BJ-B11, an Hsp90 Inhibitor, Constrains the Proliferation and Invasion of Breast Cancer Cells

Kaisheng Liu[1], Juan Chen[2], Fang Yang[1], Zhifan Zhou[1], Ying Liu[1], Yaomin Guo[1], Hong Hu[1], Hengyuan Gao[1], Haili Li[1], Wenbin Zhou[1], Bo Qin[2]* and Yifei Wang[3]**

[1] Shenzhen People's Hospital, The First Affiliated Hospital of Southern University of Science and Technology, The Second Clinical Medical College of Jinan University, Shenzhen, China, [2] Shenzhen Nanshan District Shekou People's Hospital, Shenzhen, China, [3] Institute of Biomedicine, College of Life Science and Technology, Jinan University, Guangzhou, China

Breast cancer is the leading cause of cancer-related deaths in women; however, its underlying etiology remains largely unknown. In this study, we systematically analyzed breast cancer tissues using comprehensive iTRAQ labeled quantitative proteomics, identifying 841 differentially expressed proteins (474 and 367 significantly over- and under-expressed, respectively), which were annotated by protein domain analysis. All the heat shock proteins identified were upregulated in breast cancer tissues; Hsp90 upregulation was also validated by RT-qPCR and immunohistochemistry, and high Hsp90 protein levels correlated with poorer survival. Hsp90AA1 overexpression promoted MDA-MB-231 cell proliferation, whilst BJ-B11, an Hsp90 inhibitor, hampered their invasion, migration, and proliferation in a time and dose-dependent manner and induced cell cycle arrest and apoptosis. BJ-B11 inhibited the expression of epithelial-mesenchymal transition (EMT) marker in MDA-MB-231 cells, whereas Hsp90AA1 promoted its expression. Moreover, BJ-B11 inhibited tumor growth in xenograft model. Altogether, Hsp90 activation is a risk factor in breast cancer patients, and BJ-B11 could be used to treat breast cancer.

Keywords: breast cancer, Hsp90, BJ-B11, proliferation, invasion, migration, EMT

OPEN ACCESS

Edited by:
Dong-Hua Yang,
St. John's University, United States

Reviewed by:
Haitao Mao,
UT Southwestern Medical Center, United States
Tao Hu,
University of Maryland, Baltimore, United States

***Correspondence:**
Wenbin Zhou
zhouwb1016@163.com
Bo Qin
qinbozf@163.com
Yifei Wang
twang-yf@163.com

Specialty section:
This article was submitted to Molecular and Cellular Oncology, a section of the journal Frontiers in Oncology

Received: *03 September 2019*
Accepted: *03 December 2019*
Published: *18 December 2019*

Citation:
Liu K, Chen J, Yang F, Zhou Z, Liu Y, Guo Y, Hu H, Gao H, Li H, Zhou W, Qin B and Wang Y (2019) BJ-B11, an Hsp90 Inhibitor, Constrains the Proliferation and Invasion of Breast Cancer Cells. Front. Oncol. 9:1447. doi: 10.3389/fonc.2019.01447

INTRODUCTION

Breast cancer is the most frequently diagnosed cancer in women (1), and its incidence has increased in most developing countries over the past few decades (1, 2). Although patients with breast cancer have a high 5-year survival rate following treatment, the survival rate decreases rapidly for patients with more advanced disease (3–5). Triple-negative breast cancers (TNBCs) account for 15% of all breast cancers and lack estrogen, progesterone, and ERBB2 receptor expression (6). TNBCs are poorly differentiated, and there are no specific treatment guidelines for this breast cancer subgroup (7, 8); therefore, biomarkers and more effective medical therapies are urgently required.

Breast cancer is coordinately controlled by regulatory networks; thus, understanding these networks could help identify candidates for the diagnosis, prediction, and therapy of breast cancer. Proteomics approaches are often used to acquire a comprehensive and quantitative profile of protein expression. Isobaric tags for relative and absolute quantitation (iTRAQ) is a novel and unbiased approach to simultaneously quantify relative protein abundance (9); in particular, the method enables protein quantification during various developmental stages (10).

Hsp90 is highly expressed in various cancers (11). It is responsible for the stability and function of client proteins, including Akt, IKKα, B-Raf, and GSK3β, which are critical for cell survival and proliferation (12). Therefore, Hsp90 is a potential therapeutic target and diagnostic marker for cancer (13, 14). BJ-B11 is a novel Hsp90 inhibitor that reportedly exhibits antitumor activity in myeloid leukemia and esophageal carcinoma (15, 16); however, its antitumor activity in breast cancer has not yet been investigated.

In this study, we investigated whether Hsp90 was associated with breast cancer and whether BJ-B11 affected the functions of breast cancer cells. Our findings suggested that Hsp90 could be a candidate for the early diagnosis, prognosis, and therapy of breast cancer and that BJ-B11 could be used to treat breast cancer.

MATERIALS AND METHODS

Primary Breast Cancer Samples

Tumor tissue and adjacent normal tissue samples were collected at the Department of Thyroid and Breast Surgery, Shenzhen People's Hospital, with the informed consent of the patients. The study (LL-KT-2015002) was approved by the Ethics Committee of the hospital. The clinicopathological information regarding the samples is detailed in the **Table S1**. Tumor tissues and normal tissues (10 mg) were homogenized for proteomics and iTRAQ labeling followed by LC-MS/MS analysis. The protein with iTRAQ ratio (tumor tissue/normal tissue) < 0.83 or > 1.2 ($P < 0.05$) was considered to be significantly differentially expressed.

Cell Culture and Reagents

The human breast cancer cell line MDA-MB-231 was obtained from the American Type Culture Collection (Manassas, VA, USA) and cultured in DMEM/F12 supplemented with 10% FBS, 100 μg/mL streptomycin, and 100 unit/mL penicillin in a humidified incubator in a 5% CO_2 atmosphere at 37°C.

BJ-B11 was prepared in our lab, as previously described (17), and the 10 mmol/L BJ-B11 stock solution in DMSO was stored at 4°C. Plasmids expressing wild-type Hsp90AA1 were provided by SAGENE (Guangzhou, Guangdong, China). Mouse anti-E-cadherin (cat: 14472), rabbit anti-vimentin (cat: 3932), and mouse anti-β-actin (cat: 3700) antibodies were purchased from CST (MA, USA).

Cell Viability and Apoptosis Assay

CCK-8 (Dojindo, Japan) was used to detect cell viability. Cell apoptosis induced by BJ-B11 was determined using AnnexinV/PI (KeyGEN, Nanjing, China) staining, followed by flow cytometry (Beckman Coulter, CA, USA) according to the manufacturer's instructions.

Abbreviations: Hsp90, heat shock protein 90; TNBC, triple-negative breast cancer; iTRAQ, isobaric tags for relative and absolute quantitation; GO, Gene Ontology; RT-qPCR, real-time quantitative polymerase chain reaction; GAPDH, glyceraldehyde-3-phosphate dehydrogenase; EMT, epithelial-mesenchymal transition.

Cell Cycle Analysis

Cells were treated with BJ-B11 for 48 h, harvested in cold PBS, fixed in 70% ethanol, and stored overnight at 4°C. The cells were then washed twice with cold PBS, resuspended in 50 μg/mL PI staining reagent containing 100 μg/mL RNase and 0.1% Triton X-100 for 30 min in the dark, and analyzed by flow cytometry (Becton-Dickinson, CA, USA).

Real-Time Quantitative Polymerase Chain Reaction (RT-qPCR)

Total RNA was extracted using TRIZOL (Thermo Fisher Scientific) and subjected to qRT-PCR using the primers shown in **Table S2**). Gene expression was normalized against GAPDH using the relative $^{\Delta\Delta}$CT method and is reported as relative expression compared to the control.

Cell Invasion Assay

A total of 2×10^4 MDA-MB-231 cells treated with or without BJ-B11 were added to Transwell inserts and cultured in an incubator for 16 h. Cells inside the insert were cleaned thoroughly with a cotton swab, while those on the underside were fixed in 4% paraformaldehyde for 5 min and stained with 0.5% crystal violet solution. At least five random fields were counted per insert, and each group consisted of three replicates.

Tissue Microarray

Human breast tissue (HBreD077Su01, Shanhai Xinchao, China) and breast cancer tissue (HBreD140Su05, Shanhai Xinchao, China) microarrays consisting of 77 adjacent non-malignant tissue samples and 140 breast cancer tissue samples, were stained with rabbit anti Hsp90 (4874, CST, USA). Immunohistochemical staining was carried out according to the manufacturer's instructions. Slides were evaluated for their positive staining rate (0, negative; 1, 1–25%; 2, 26–50%; 3, 51–75%; and 4, 76–100%) and the staining intensity of the positively stained cells (0, none; 1, weak; 2, moderate; and 3, strong). Samples were grouped according to the H score, which was the product of the "staining intensity" and "staining positive rate" scores: low expression group, < 8; and high expression group, ≥ 8. Two investigators evaluated each tissue section independently.

The Cancer Genome Atlas (TCGA) Data Analysis

The expression level and survival of Hsp90AA1 and Hsp90AB1 in breast cancer were analyzed using the UALCAN platform.

Xenograft Model

Female BALB/c Nude Mice (6-week-old) were obtained from the Guangdong Medical Laboratory Animal Center. They were maintained in an air-conditioned room with controlled temperature of 21 ± 2°C, and humidity of 30–70% in a 12 h light/darkness cycle regulation and were fed laboratory chow and water *ad libitum*. All animal experiments were approved by the Animal Ethics Committee of Shenzhen People's Hospital (No. LL-KY-2019512). The athymic female nude mice were injected with about 5×10^6 MDA-MB-231 cells subcutaneously. When the tumors were measurable, the mice were randomly assigned

into treatment group receiving oral BJ-B11 (20 mg/kg, daily for a total of 27 days) or the control group receiving oral vehicle alone. All mice were euthanized at day 28, and the tumors were excised and weighed to evaluate tumor growth inhibition.

Statistical Analysis

Data are presented as the mean ± SD, and Student's unpaired *t*-tests were used for the statistical analysis of differences between two groups. Differences between groups were analyzed using Prism 6 (GraphPad, Inc., San Diego, CA). $P < 0.05$ were considered statistically significant.

RESULTS

Identification of Hsp90 as a Diagnostic Marker

We screened proteins that were differentially expressed between tumor tissues and adjacent normal tissues using iTRAQ with ratio (tumor:adjacent normal tissue) thresholds of >1.2 or <0.83, which indicated higher or lower protein expression in tumor tissue than in adjacent normal tissue, respectively. A total of 841 differentially expressed proteins were identified, among which 474 and 367 were up- and down-regulated in breast cancer tissues (**Figure 1A**).

To understand the functions of these differentially expressed proteins, they were classified according to their protein domains ($P < 0.001$; **Figure 1B**). Heat shock proteins showed the most significant change of all the upregulated domains, with Hsp90AA1, Hsp90AB1, TRAP1, HspA5, HspB1, HspE1, HspD1, HspA1B, HspA8, HspA9, and HspA4 identified in breast cancer tissue (**Table S3**). RT-qPCR revealed that Hsp90AA1 and Hsp90AB1 mRNA levels increased in breast cancer (**Figure 1C**), consistent with TCGA data (**Figure 1D**). These results suggest that the highly expressed Hsp90 could act as a diagnostic marker for breast cancer.

Identification of Hsp90 as a Prognostic Marker

We then performed tissue microarray analysis, finding that Hsp90 protein levels increased in breast cancer tissue ($P = 0.014$; **Figure 2A** and **Table S4**). Moreover, Hsp90 expression was significantly correlated with clinical tumor grade (**Table S5**); therefore, we analyzed the survival rate of patients with breast cancer. High Hsp90 levels predicted poor survival (**Figure 2B**), consistent with TCGA data (**Figure S1**). Thus, the univariate and multivariate analyses suggested that Hsp90 could serve as a prognostic indicator for breast cancer (**Table S6**).

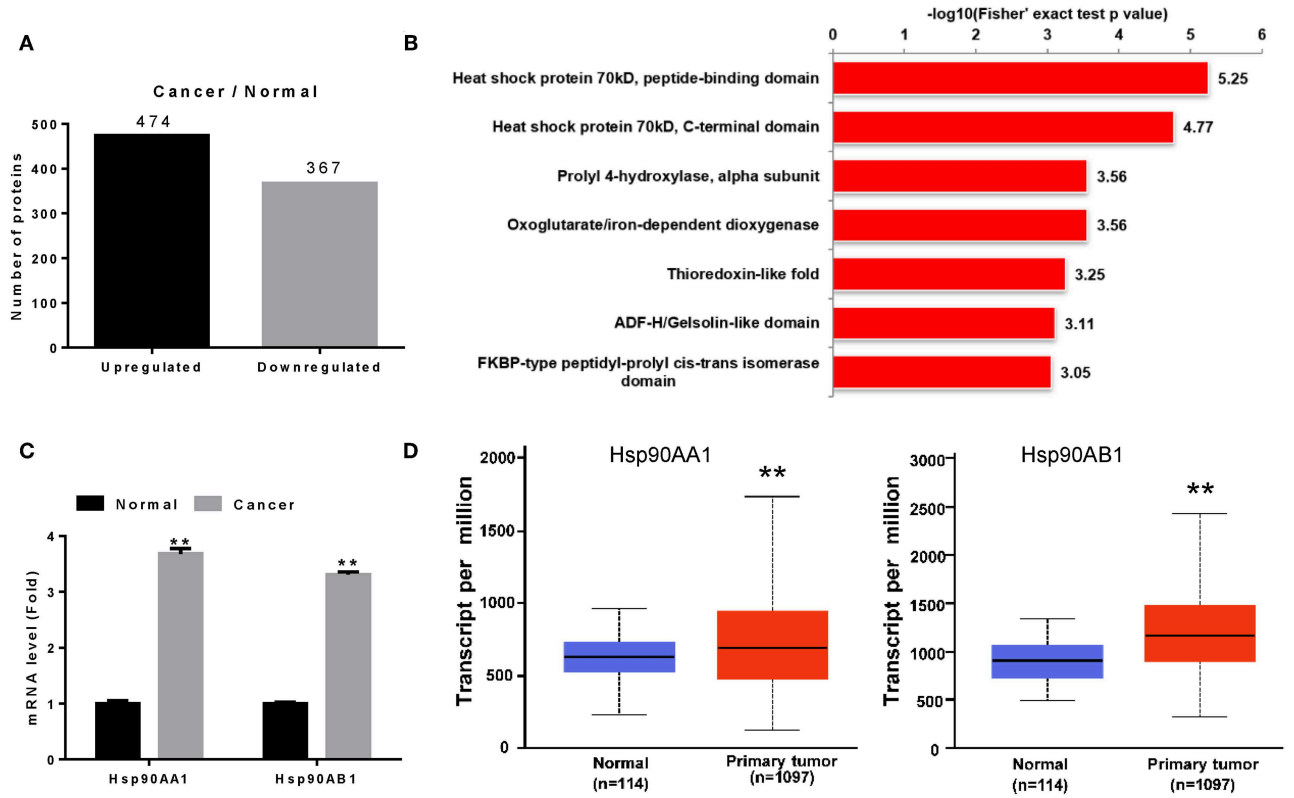

FIGURE 1 | Identification of Hsp90 as a diagnostic marker. **(A)** Differentially expressed proteins in breast cancer. **(B)** Differentially expressed proteins were classified according to their protein domains ($P < 0.001$). **(C)** Validation of Hsp90AA1 and Hsp90AB1 mRNA levels in healthy and breast cancer tissues by RT-qPCR. **(D)** Hsp90AA1 and Hsp90AB1 mRNA levels in healthy and breast cancer tissues from TCGA database ($^{**}P < 0.01$).

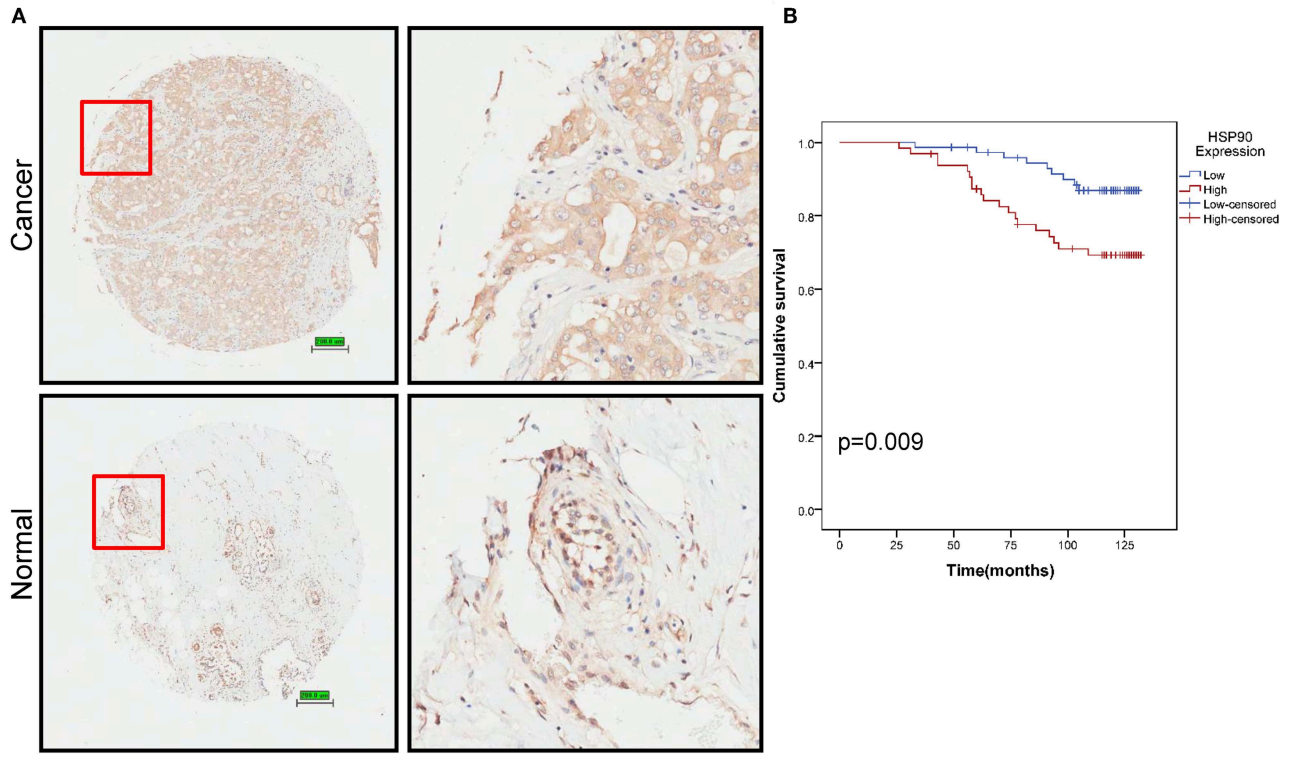

FIGURE 2 | Identification of Hsp90 as a prognostic marker. **(A)** Immunohistochemical staining of Hsp90 in normal ($n = 77$) and breast cancer ($n = 140$) tissues. Representative images are shown. Scale bar, 200 μm. **(B)** Cumulative survival of breast cancer patients with low or high Hsp90 expression.

BJ-B11 Induces Apoptosis and Cell Cycle Arrest in Breast Cancer Cells

Since our findings suggested that Hsp90 was involved in breast cancer, we examined whether manipulating the Hsp90 gene affected the proliferation of breast cancer cells. Hsp90AA1 overexpression increased MDA-MB-231 cell proliferation (**Figure 3A**), whereas treating the cells with BJ-B11, an Hsp90 inhibitor, for 24, 48, or 72 h inhibited their growth in a time- and dose-dependent manner (**Figure 3B**) and induced dose-dependent apoptosis (**Figure 3C**) and G2/M cell cycle arrest (**Figure 3D**). Taken together, Hsp90AA1 promoted the proliferation of breast cancer cells, whilst BJ-B11 could be used to treat breast cancer.

BJ-B11 Inhibited Invasion and Migration of Breast Cancer Cells

MDA-MB-231 cells were cultured with or without BJ-B11 in Transwell inserts for 16 h. BJ-B11 inhibited the invasion of the MDA-MB-231 cells (**Figure 4A**) and inhibited Hsp90, thus significantly suppressing MDA-MB-231 cell migration (**Figure 4B**). We also analyzed epithelial-mesenchymal transition (EMT) markers related to invasion and migration, finding that BJ-B11 upregulated E-cadherin and downregulated vimentin (**Figure 4C**). Conversely, Hsp90AA1 overexpression upregulated vimentin and downregulated E-cadherin and occludin (**Figure 4D**), suggesting that Hsp90 plays a vital role in EMT in breast cancer. Taken together, these data strongly suggest that BJ-B11 inhibits cell invasion and migration by affecting EMT in breast cancer.

BJ-B11 Inhibited Tumor Growth *in vivo*

We further tested whether BJ-B11 could suppress cell growth of breast cancer *in vivo*. First, we established xenograft models by subcutaneous injection of MDA-MB-231 cells into the right flanks of mice. We then tested the anti-tumor effects of BJ-B11 on MDA-MB-231 cancer cells. Nude mice bearing MDA-MB-231 tumor xenografts were treated with 20 mg/kg BJ-B11 ($n = 7$) or physiological saline ($n = 7$) for 27 days. Bodyweight was measured each day before the administration of BJ-B11. Results showed that BJ-B11 inhibited tumor growth significantly *in vivo* (**Figures 5A,B**).

DISCUSSION

This study investigated breast cancer proteome using iTRAQ to obtain a global view and identify therapeutic targets for breast cancer. We identified 841 differentially expressed proteins and showed that heat shock proteins could be candidate biomarkers for the early diagnosis and therapy of breast cancer. Moreover, this is the first study to investigate the antitumor activity of BJ-B11 in TNBCs, showing that BJ-B11 could be used to treat breast cancer.

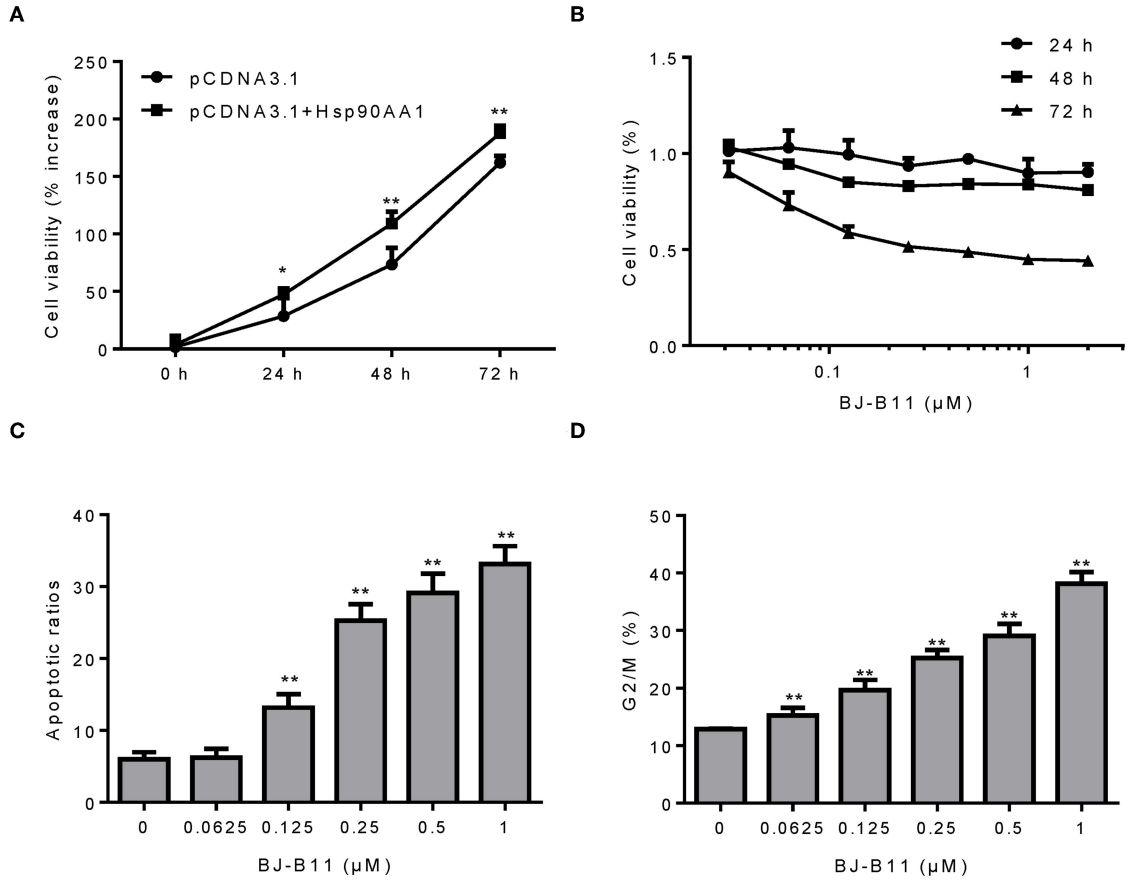

FIGURE 3 | BJ-B11 induces apoptosis and cell cycle arrest in breast cancer cells. **(A)** The viability of MDA-MB-231 cells overexpressing Hsp90AA1 was tested by CCK8 after 24, 48, and 72 h (*$P < 0.05$, **$P < 0.01$). **(B)** The viability of cells treated with the indicated concentrations of BJ-B11 for 24, 48, or 72 h was tested by CCK8. **(C)** Cells were treated with BJ-B11 for 48 h, collected, and stained with AnnexinV/PI. Apoptotic cells were analyzed by flow cytometry (**$P < 0.01$). **(D)** Cells were treated with BJ-B11 for 48 h, collected, fixed, and stained with PI. The cell cycle stage was analyzed by flow cytometry (**$P < 0.01$).

Multiple heat shock proteins, including Hsp90AA1, Hsp90AB1, TRAP1, HspA5, HspB1, HspE1, HspD1, HspA1B, HspA8, HspA9, and HspA4, were significantly upregulated in breast cancer tissue. Hsp70, HspA8, HspA9, HspA5, and Hsp110s may constitute up to 3% of the total protein in unstressed human cells (18). Moreover, Hsp70 is upregulated in various human cancers and associated with tumorigenesis (19, 20). HspA8 is overexpressed in cancer cells and it belongs to the Hsp70 family (21). Its depletion in RL-95-2 and HEC-1B cells was shown to suppress cell growth and promote apoptosis, suggesting that HspA8 could be a candidate biomarker for endometrial carcinoma (22).

Hsp90 is an ATP-dependent molecular chaperone (23). Reportedly, Hsp90 expression levels are associated with disease progression and survival in melanoma, gastrointestinal stromal tumors and non-small cell lung cancer (24, 25). Moreover, high Hsp90 expression has been associated with decreased survival in breast cancer (26) whilst its inhibition can suppress growth and promote apoptosis in breast cancer cells, suggesting that Hsp90 could act as both a biomarker and a therapeutic target for breast cancer (27). A phase II study of 17-AAG in breast cancer showed that Hsp90 inhibitors exhibit significant anticancer activity (28). Previously, we demonstrated that the Hsp90 inhibitor SNX-2112 suppressed MCF-7 cell proliferation and induced apoptosis (27), whilst the Hsp90 inhibitor PU-H71 has been shown to induce a complete response in TNBC models (29). BJ-B11 is a novel Hsp90 inhibitor that can inhibit cancer cell proliferation and exhibits anti-HSV activity (15, 16). To the best of our knowledge, this is the first study to investigate the antitumor activity of this molecule in TNBCs; BJ-B11 inhibited the proliferation, invasion, and migration of breast cancer cells, which may be associated with EMT. In addition, BJ-B11 showed significant antitumor activity *in vivo*. However, the underlying mechanism requires further clarification.

In summary, our study provides new insights into the molecular changes that occur in breast cancer. Hsp90AA1, Hsp90AB1, TRAP1, HspA5, HspB1, HspE1, HspD1, HspA1B, HspA8, HspA9, and HspA4 were validated as potential biomarkers for breast cancer tissue. In particular, Hsp90 plays important roles in breast cancer development and could be a

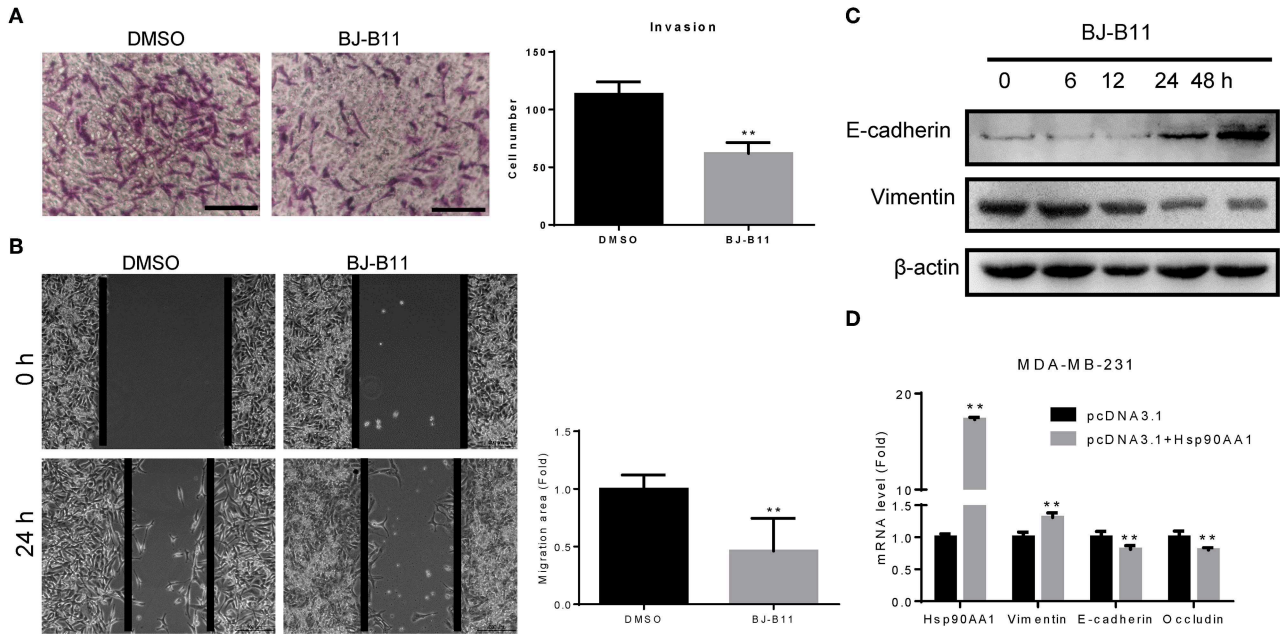

FIGURE 4 | BJ-B11 inhibited the invasion and migration of breast cancer cells. **(A)** Cells were cultured in Transwell inserts for 16 h with or without 0.0625 μM BJ-B11 and then stained with crystal violet. Cell number was calculated and analyzed (**$P < 0.01$). Scale bar, 100 μm. **(B)** Wound healing assay of MDA-MB-231 cell treated with or without 0.0625 μM BJ-B11 for 24 h (**$P < 0.01$). Scale bar, 200 μm. **(C)** Western blot assay of MDA-MB-231 cells treated with 0.0625 μM BJ-B11 for the indicated length of time. **(D)** MDA-MB-231 cells overexpressing Hsp90AA1 were cultured for 48 h. Hsp90AA1, E-cadherin, vimentin, and occludin mRNA levels were tested by RT-qPCR (**$P < 0.01$).

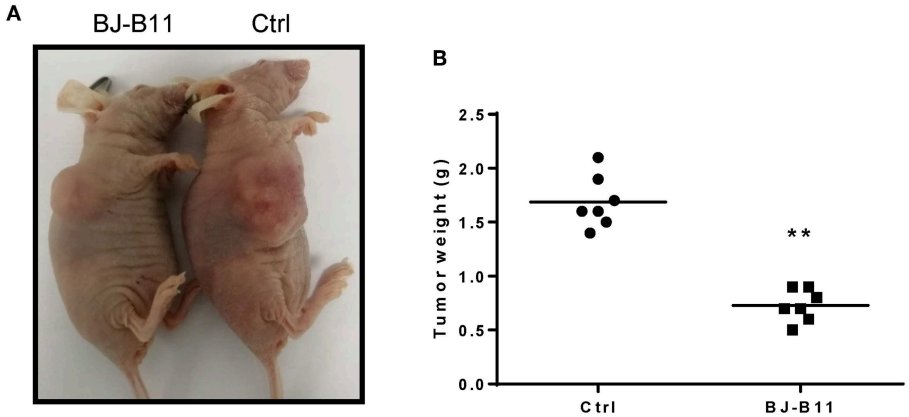

FIGURE 5 | BJ-B11 inhibited tumor growth *in vivo*. **(A)** Representative picture of the xenograft model. **(B)** Analysis of tumor weight of BJ-B11 treated group and control group ($n = 7$, **$P < 0.01$).

candidate biomarker for the early diagnosis and therapy of breast cancer. Moreover, BJ-B11 could open new, potential therapeutic alternatives for breast cancer.

DATA AVAILABILITY STATEMENT

The datasets generated for this study are available on request to the corresponding author.

ETHICS STATEMENT

The studies involving human participants were reviewed and approved by Ethics Committee of Shenzhen People's Hospital. The patients/participants provided their written informed consent to participate in this study. The animal study was reviewed and approved by Ethics Committee of Shenzhen People's Hospital.

AUTHOR CONTRIBUTIONS

KL conceived, designed the experiments, and wrote the manuscript. KL, YL, and YG performed the experiments and analyzed the data. KL, JC, FY, ZZ, HH, HG, HL, WZ, BQ, and YW contributed reagents, materials, and analysis tools.

FUNDING

This research was supported by the National Natural Science Foundation of China (81802749), the Science and Technology Foundation of Shenzhen (JCYJ20180301170047864, JCYJ20180228164300106), and the Cultivating Fund Project of Shenzhen People's Hospital (No. SYLY201704).

SUPPLEMENTARY MATERIAL

The Supplementary Material for this article can be found online at: https://www.frontiersin.org/articles/10.3389/fonc.2019.01447/full#supplementary-material

Figure S1 | Cumulative survival analysis of breast cancer patients with low or high Hsp90AA1 **(A)** or Hsp90AB1 **(B)** expression.

Table S1 | Sample information.

Table S2 | Primers used in this study.

Table S3 | Hsp family members upregulated in breast cancer tissue.

Table S4 | Differential Hsp90 expression in healthy and breast cancer tissues.

Table S5 | Correlation between Hsp90 expression and clinicopathological characteristics.

Table S6 | Univariate and multivariate analyses of factors correlated with the overall survival of breast cancer patients.

REFERENCES

1. Bray F, Ferlay J, Soerjomataram I, Siegel RL, Torre LA, Jemal A. Global cancer statistics 2018: GLOBOCAN estimates of incidence and mortality worldwide for 36 cancers in 185 countries. *CA Cancer J Clin*. (2018) 68:394–424. doi: 10.3322/caac.21492
2. DeSantis CE, Ma J, Goding Sauer A, Newman LA, Jemal A. Breast cancer statistics, 2017, racial disparity in mortality by state. *CA Cancer J Clin*. (2017) 67:439–48. doi: 10.3322/caac.21412
3. DeSantis CE, Miller KD, Goding Sauer A, Jemal A, Siegel RL. Cancer statistics for African Americans, 2019. *CA Cancer J Clin*. (2019) 69:211–33. doi: 10.3322/caac.21555
4. Miller KD, Nogueira L, Mariotto AB, Rowland JH, Yabroff KR, Alfano CM, et al. Cancer treatment and survivorship statistics, 2019. *CA Cancer J Clin*. (2019) 69:363–85. doi: 10.3322/caac.21565
5. Siegel RL, Miller KD, Jemal A. Cancer statistics, 2019. *CA Cancer J Clin*. (2019) 69:7–34. doi: 10.3322/caac.21551
6. Foulkes WD, Smith IE, Reis-Filho JS. Triple-negative breast cancer. *N Engl J Med*. (2010) 363:1938–48. doi: 10.1056/NEJMra1001389
7. Cleator S, Heller W, Coombes RC. Triple-negative breast cancer: therapeutic options. *Lancet Oncol*. (2007) 8:235–44. doi: 10.1016/S1470-2045(07)70074-8
8. Dent R, Trudeau M, Pritchard KI, Hanna WM, Kahn HK, Sawka CA, et al. Triple-negative breast cancer: clinical features and patterns of recurrence. *Clin Cancer Res*. (2007) 13(15 Pt 1):4429–34. doi: 10.1158/1078-0432.CCR-06-3045
9. Chong PK, Gan CS, Pham TK, Wright PC. Isobaric tags for relative and absolute quantitation (iTRAQ) reproducibility: Implication of multiple injections. *J Proteome Res*. (2006) 5:1232–40. doi: 10.1021/pr060018u
10. Palma JM, Corpas FJ, del Rio LA. Proteomics as an approach to the understanding of the molecular physiology of fruit development and ripening. *J Proteomics*. (2011) 74:1230–43. doi: 10.1016/j.jprot.2011.04.010
11. Liu KS, Liu H, Qi JH, Liu QY, Liu Z, Xia M, et al. SNX-2112, an Hsp90 inhibitor, induces apoptosis and autophagy via degradation of Hsp90 client proteins in human melanoma A-375 cells. *Cancer Lett*. (2012) 318:180–8. doi: 10.1016/j.canlet.2011.12.015
12. Liu KS, Ding WC, Wang SX, Liu Z, Xing GW, Wang Y, et al. The heat shock protein 90 inhibitor SNX-2112 inhibits B16 melanoma cell growth *in vitro* and *in vivo*. *Oncol Rep*. (2012) 27:1904–10. doi: 10.3892/or.2012.1738
13. Jin L, Xiao CL, Lu CH, Xia M, Xing GW, Xiong S, et al. Transcriptomic and proteomic approach to studying SNX-2112-induced K562 cells apoptosis and anti-leukemia activity in K562-NOD/SCID mice. *FEBS Lett*. (2009) 583:1859–66. doi: 10.1016/j.febslet.2009.04.046
14. Wang R, Shao F, Liu Z, Zhang J, Wang S, Liu J, et al. The Hsp90 inhibitor SNX-2112, induces apoptosis in multidrug resistant K562/ADR cells through suppression of Akt/NF-kappaB and disruption of mitochondria-dependent pathways. *Chem Biol Interact*. (2013) 205:1–10. doi: 10.1016/j.cbi.2013.06.007
15. Ju HQ, Wang SX, Xiang YF, Liu Z, Liu JY, Chen ZP, et al. BJ-B11, a novel Hsp90 inhibitor, induces apoptosis in human chronic myeloid leukemia K562 cells through the mitochondria-dependent pathway. *Eur J Pharmacol*. (2011) 666:26–34. doi: 10.1016/j.ejphar.2011.05.020
16. Liu KS, Zhang Y, Ding WC, Wang SX, Xiang YF, Yang P, et al. The selective Hsp90 inhibitor BJ-B11 exhibits potent antitumor activity via induction of cell cycle arrest, apoptosis and autophagy in Eca-109 human esophageal squamous carcinoma cells. *Int J Oncol*. (2012) 41:2276–84. doi: 10.3892/ijo.2012.1670
17. Ju HQ, Xiang YF, Xin BJ, Pei Y, Lu JX, Wang QL, et al. Synthesis and *in vitro* anti-HSV-1 activity of a novel Hsp90 inhibitor BJ-B11. *Bioorg Med Chem Lett*. (2011) 21:1675–7. doi: 10.1016/j.bmcl.2011.01.098
18. Finka A, Sharma SK, Goloubinoff P. Multi-layered molecular mechanisms of polypeptide holding, unfolding and disaggregation by HSP70/HSP110 chaperones. *Front Mol Biosci*. (2015) 2:29. doi: 10.3389/fmolb.2015.00029
19. Calderwood SK, Khaleque MA, Sawyer DB, Ciocca DR. Heat shock proteins in cancer: chaperones of tumorigenesis. *Trends Biochem Sci*. (2006) 31:164–72. doi: 10.1016/j.tibs.2006.01.006
20. Radons J. The human HSP70 family of chaperones: where do we stand? *Cell Stress Chaperones*. (2016) 21:379–404. doi: 10.1007/s12192-016-0676-6
21. Stricher F, Macri C, Ruff M, Muller S. HSPA8/HSC70 chaperone protein: structure, function, and chemical targeting. *Autophagy*. (2013) 9:1937–54. doi: 10.4161/auto.26448
22. Shan N, Zhou W, Zhang S, Zhang Y. Identification of HSPA8 as a candidate biomarker for endometrial carcinoma by using iTRAQ-based proteomic analysis. *Onco Targets Ther*. (2016) 9:2169–79. doi: 10.2147/OTT.S97983
23. Whitesell L, Lindquist SL. HSP90 and the chaperoning of cancer. *Nat Rev Cancer*. (2005) 5:761–72. doi: 10.1038/nrc1716
24. Workman P, Powers MV. Chaperoning cell death: a critical dual role for Hsp90 in small-cell lung cancer. *Nat Chem Biol*. (2007) 3:455–7. doi: 10.1038/nchembio0807-455
25. McCarthy MM, Pick E, Kluger Y, Gould-Rothberg B, Lazova R, Camp RL, et al. HSP90 as a marker of progression in melanoma. *Ann Oncol*. (2008) 19:590–4. doi: 10.1093/annonc/mdm545
26. Pick E, Kluger Y, Giltnane JM, Moeder C, Camp RL, Rimm DL, et al. High HSP90 expression is associated with decreased survival in breast cancer. *Cancer Res*. (2007) 67:2932–7. doi: 10.1158/0008-5472.CAN-06-4511
27. Wang SX, Ju HQ, Liu KS, Zhang JX, Wang X, Xiang YF, et al. SNX-2112, a novel Hsp90 inhibitor, induces G2/M cell cycle arrest and apoptosis in MCF-7 cells. *Biosci Biotechnol Biochem*. (2011) 75:1540–5. doi: 10.1271/bbb.110225

28. Modi S, Stopeck A, Linden H, Solit D, Chandarlapaty S, Rosen N, et al. HSP90 inhibition is effective in breast cancer: a phase II trial of tanespimycin (17-AAG) plus trastuzumab in patients with HER2-positive metastatic breast cancer progressing on trastuzumab. *Clin Cancer Res*. (2011) 17:5132–9. doi: 10.1158/1078-0432.CCR-11-0072
29. Caldas-Lopes E, Cerchietti L, Ahn JH, Clement CC, Robles AI, Rodina A, et al. Hsp90 inhibitor PU-H71, a multimodal inhibitor of malignancy, induces complete responses in triple-negative breast cancer models. *Proc Natl Acad Sci USA*. (2009) 106:8368–73. doi: 10.1073/pnas.0903392106

Conflict of Interest: The authors declare that the research was conducted in the absence of any commercial or financial relationships that could be construed as a potential conflict of interest.

frontiers in Oncology

ORIGINAL RESEARCH
published: 19 December 2019
doi: 10.3389/fonc.2019.01398

Erastin Reverses ABCB1-Mediated Docetaxel Resistance in Ovarian Cancer

Hai-Hong Zhou[1†], Xu Chen[1†], Lu-Ya Cai[1†], Xing-Wei Nan[1], Jia-Hua Chen[1], Xiu-Xiu Chen[1], Yang Yang[2], Zi-Hao Xing[2], Meng-Ning Wei[2], Yao Li[2], Sheng-Te Wang[2], Kun Liu[2], Zhi Shi[2] and Xiao-Jian Yan[1,3*]*

[1] Department of Gynecology, The First Affiliated Hospital of Wenzhou Medical University, Wenzhou, China, [2] Guangdong Provincial Key Laboratory of Bioengineering Medicine, Department of Cell Biology & Institute of Biomedicine, National Engineering Research Center of Genetic Medicine, College of Life Science and Technology, Jinan University, Guangzhou, China, [3] Center for Uterine Cancer Diagnosis & Therapy Research of Zhejiang Province, Women's Hospital and Institute of Translation Medicine, Zhejiang University School of Medicine, Hangzhou, China

Overexpression of drug efflux transport ABCB1 is correlated with multidrug resistance (MDR) among cancer cells. Upregulation of ABCB1 accounts for the recurrence of resistance to docetaxel therapy in ovarian cancer with poor survival. Erastin is a novel and specific small molecule that targets SLC7A11 to induce ferroptosis. In the present research, we explored the synergistic effect of erastin and docetaxel in ovarian cancer. We confirmed that the co-delivery of erastin with docetaxel significantly decreased cell viability, promoted cell apoptosis, and induced cell cycle arrest at G2/M in ovarian cancer cells with ABCB1 overexpression. Mechanistically, erastin dominantly elevated the intracellular ABCB1 substrate levels by restricting the drug-efflux activity of ABCB1 without alteration of the expression of ABCB1. Consequently, erastin can reverse ABCB1-mediated docetaxel resistance in ovarian cancer, revealing that the combination of erastin and docetaxel may potentially offer an effective administration for chemo-resistant patients suffering from ovarian cancers.

Keywords: erastin, docetaxel, ABCB1, ovarian cancer, ferroptosis

OPEN ACCESS

Edited by:
Chang Zou,
Shenzhen People's Hospital, China

Reviewed by:
Junjian Wang,
Sun Yat-sen University, China
Chaochu Cui,
Xinxiang Medical University, China

***Correspondence:**
Zhi Shi
tshizhi@jnu.edu.cn
Xiao-Jian Yan
yxjbetter@126.com

† These authors have contributed equally to this work

Specialty section:
This article was submitted to Molecular and Cellular Oncology, a section of the journal Frontiers in Oncology

Received: *01 November 2019*
Accepted: *26 November 2019*
Published: *19 December 2019*

Citation:
Zhou H-H, Chen X, Cai L-Y, Nan X-W, Chen J-H, Chen X-X, Yang Y, Xing Z-H, Wei M-N, Li Y, Wang S-T, Liu K, Shi Z and Yan X-J (2019) Erastin Reverses ABCB1-Mediated Docetaxel Resistance in Ovarian Cancer. Front. Oncol. 9:1398. doi: 10.3389/fonc.2019.01398

INTRODUCTION

Ovarian cancer threatens women's health with high morbidity and mortality and is the leading cause of death in gynecological malignancies (1). The combination of aggressive cytoreductive surgery followed by system chemotherapy is an effective way of treatment (2, 3). Despite how ∼80% of patients respond well to such therapies, ∼25% of women faced resistant cancer recurrence within 6 months (4). Multidrug resistance (MDR) in ovarian cancer is recognized as the primary cause of failing chemotherapeutic treatments and low survival rates in humans (5). ABCB1 (P-glycoprotein/MDR1), a glycosylated 170-kDa transmembrane protein encoded by the MDR1 gene (6), has emerged as a central drug transport and the best-studied drug transporter in MDR (7). ABCB1 overexpression in cancers contributes to reduced intracellular chemotherapeutics accumulation and brings about resistance against a wide variety of the recently available antineoplastic agents like taxanes (docetaxel), vinca alkaloids (vinblastine), and anthracyclines (doxorubicin) (8–11). Upregulated ABCB1 has been confirmed as the primary protein resulting in MDR in ovarian cancer treated with paclitaxel and related taxane drugs (12–15). Inhibition of ABCB1, therefore, will restore the sensitivity of ABCB1-substrate chemotherapeutic agents, such as

docetaxel and doxorubicin. However, drugs under tests that are aimed at ABCB1 to reserve MDR are far from satisfactory for clinical use.

Docetaxel, a new member of the taxane family, has been widely applied in ovarian cancer treatment, especially during first-line chemotherapy in replacement of paclitaxel. It can be delivered alone or together with other chemotherapy drugs, such as carboplatin, to inhibit the microtubule, thus inducing cell cycle arrest (16, 17). Despite the promising anti-cancer effect of docetaxel, nowadays, ovarian cancer has emerged a growing risk of resistance to it. Upregulation of ABCB1 explains part of the resistance mechanism.

Erastin is a small molecule that induces ferroptosis which is a non-apoptotic iron-dependent mode of cell death with smaller mitochondria and increasing membrane density (18). It is the most efficient inhibitor of SLC7A11 at low micromolar concentrations (19). It specifically targets SLC7A11 to prevent cystine import and cause GSH depletion (18, 20). The anticancer property of erastin has been proved to be incredibly effective in a variety of cancers, such as liver cancer, lung cancer, gastric cancer, breast cancer, osteosarcoma, etc. (21–24). Combination therapy of erastin with other chemotherapeutic agents like cisplatin shows a significant synergistic effect in a number of cancers. Nevertheless, whether erastin can enhance the anti-ovarian cancer effect of docetaxel remains unknown. In this study, we revealed that erastin can overcome docetaxel resistance and present as a magical molecule to augment docetaxel efficacy in ovarian cancer by inhibition of ABCB1. This finding may serve as a potential strategy to transform a traditional ferroptosis inducer to elevate therapeutic efficiency for human cancers in the future.

MATERIALS AND METHODS

Cell Culture and Reagents

Human ovarian cancer cells—A2780/Taxol cells—were created by continuous incremental taxol selection in A2780 cells. Cells were grown at 37°C/5% CO_2 in DMEM. Then, 10% fetal bovine serum (FBS) and antibiotics (100 U/ml penicillin and 100 ng/ml streptomycin) were added. Erastin and ferrostatin-1 were obtained from ApexBio. Deferiprone was purchased from MCE. Docetaxel was bought from Hengrui Medicine. Rhodamine 123 and verapamil were from Sigma-Aldrich. The anti-β-tublin (KM9003T) antibody was purchased from Tianjin Sungene; the Anti-vinculin (bm1611) antibody was obtained from Boster; the anti-PARP (9542) antibody was purchased from Cell Signaling Technologies; the anti-Mcl-1(RLT2679) antibody was from Ruiying; and the Anti-ABCB1 (SC-13131) antibody was purchased from Santa Cruz Biotechnology.

Cell Viability Assay

Cells were seeded in a 96-well plate, including 6,000 cells, where each well-presented in 100 μl of medium with indicated drugs for 72 h. At the end of the reaction period, 10 μl

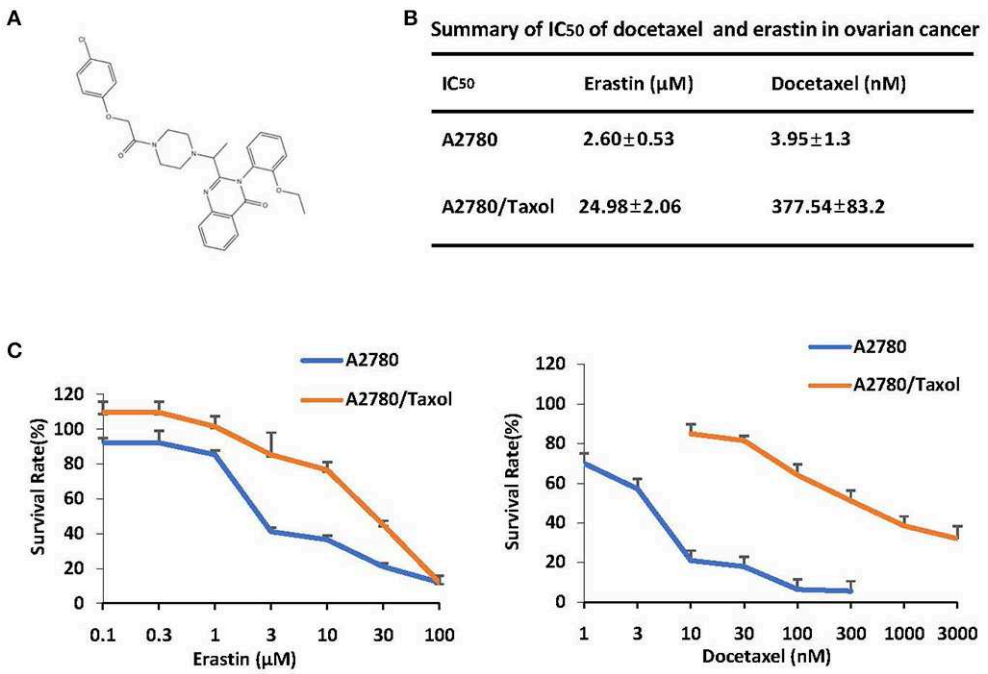

FIGURE 1 | ABCB1-overexpressing ovarian cancer cells are resistant to docetaxel and erastin. **(A)** Chemical structure of erastin download from pubchem. **(B)** Summary of IC_{50} of erastin and docetaxel in the indicated ovarian cancer cells. Cells were grown in 96-well plates for 24 h and treated with the indicated concentrations of erastin or docetaxel for 72 h; cell survival was then determined by an MTT assay. **(C)** The representative growth curves of cells treated with erastin and docetaxel are shown. Data are mean ± SD of three independent experiments.

of 5 mg/ml 3-(4,5-dimethylthiazolyl-2)-2,5-diphenyltetrazolium bromide MTT solution per well was added to the medium for another 4 h. After discarding the whole medium carefully, 100 μl of dimethyl sulfoxide (DMSO) was added to dissolve formazan grains. The absorbance value was read at 570 nm. A Bliss method was used to calculate the IC_{50} (25, 26).

Apoptosis Assay

Cell apoptosis was detected by a flow cytometry (FCM) assay. In short, cells were washed in cold PBS twice, stained with the binding buffer mixed with Annexin V-FITC and propidium iodide (PI) for more than 15 min in the dark, and then detected by FCM. Fluorescence was valued at an excitation wavelength of 480 nm by 530 and 585 nm filters. The early and late apoptosis rates were measured by FlowJo software (27, 28).

Cell Cycle Assay

Cells were collected after 48 h of drug incubation and set on cold 70% ethanol for more than 30 min. The ethanol was then discarded and cleaned with cold PBS before staining with PI (50 μg/ml) for 15 min before being measured by FCM with an excitation wavelength of 480 nm through an FL-2 filter (585 nm). ModFit LT 3.0 software (Becton Dickinson) was used to quantify the date (29, 30).

Western Blot Analysis

Cells were collected and lysed in a RIPA buffer for about 30 min at 4°C. The lysates were then centrifuged at 13,200 × rpm for 10 min to obtain supernatants without cell debris and nuclei. A total of 10% SDS-PAGE gels were used to separate the total proteins and thereby transferred proteins to polyvinylidene difluoride membranes, and 5% BSA was applied to block the membranes for 1 h and then incubated with the indicated primary antibodies overnight. Finally, the proteins were detected by the chemiluminescent detection reagents and a chemstudio plus imaging system (31, 32).

Rhodamine 123 Accumulation Assay

Cells were treated with or without inhibitors for 1 h before incubation with rhodamine 123 at a dose of 10 μM for an extra 2 h. Verapamil is used as a positive inhibitor of ABCB1. Fluorescent images were taken under fluorescence microscopy. Following that, cells were harvested and cleaned with PBS three times and analyzed with FCM as previously described to measure the fluorescence intensity (33, 34).

Docking Protocol

Firstly, we obtained the 3D chemical structure of erastin through an online search on PubChem (a national library of medicine).

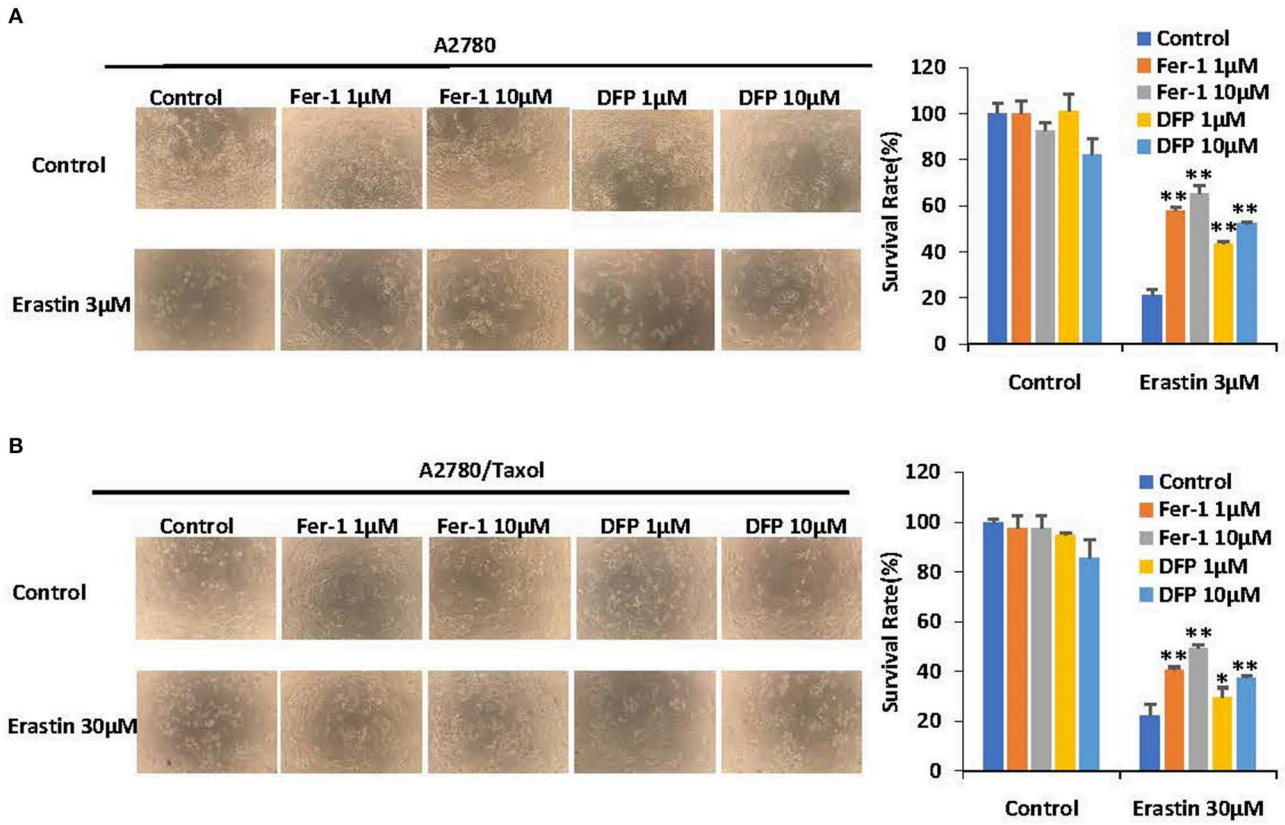

FIGURE 2 | Erastin induces ferroptosis in ovarian cells. A2780 **(A)** and A2780/Taxol **(B)** cells exposed to erastin (3 and 30 μM, respectively) with or without a pretreatment of deferiprone (DFP) or ferrostatin-1 (Fer-1) with the indicated concentrations for 72 h. The morphological changes of cells were observed by microscope as shown. Cell viabilities were analyzed by MTT assay. Data are mean ± SD of three independent experiments. $^{*}p < 0.05$, $^{**}p < 0.01$ vs. corresponding control.

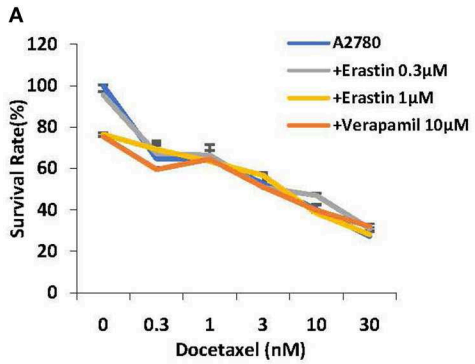

IC_{50}	A2780 (nM)
Docetaxel	4.55±0.89
+Erastin 0.3μM	4.56±0.89
+Erastin 1μM	5.53±0.15
+Verapamil 10μM	3.7±1.09

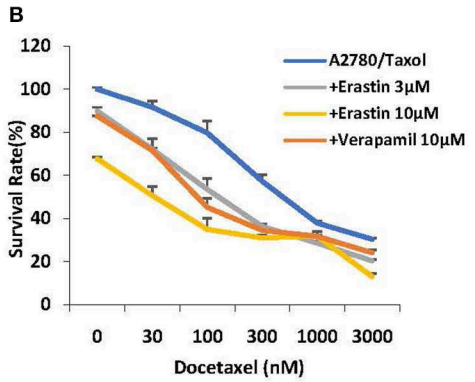

IC_{50}	A2780/Taxol (nM)
Docetaxel	355.97±66.89
+Erastin 3μM	140.31±12.73
+Erastin 10μM	32.94±6.01
+Verapamil 10μM	87.2±10.89

FIGURE 3 | Erastin enhances the sensitivity of docetaxel in the ABCB1-overexpressing ovarian cancer cells. A2780 **(A)** and A2780/Taxol **(B)** cells were treated with the indicated concentrations of docetaxel in combination of erastin or verapamil, respectively, for 72 h. Cell viabilities were analyzed by MTT assay. Data are mean ± SD of three independent experiments. The dose-effect curves and IC_{50} values are shown.

Secondly, we searched the RCSB Protein Data Bank to acquire the human ABCB1 structure, which has been reported to have an active binding site (PDB ID: 6QEX). Then, a docking experiment was executed with Discovery Studio 2.5. The most stable pose with a top-scoring of the ABCB1 complex was selected (35, 36).

Statistical Analysis

A student's *t*-test was done for date comparison among every group. A *P*-value of <0.05 was considered to indicate statistical significance.

RESULTS

ABCB1-Overexpressing Ovarian Cancer Cells Are Resistant to Docetaxel and Erastin

The structure of erastin was listed in **Figure 1A**. As shown in **Figures 1B,C**, the growth rate of ovarian cancer cells is suppressed by docetaxel in a dose-dependent manner. A2780/Taxol, overexpressing the ABCB1 gene, was resistant to docetaxel with the IC_{50} value of 377.54 nM, which was nearly 100-fold higher than A2780 cells. To examine whether erastin induced cytotoxicity in A2780 and A2780/Taxol cells, we exposed cells to increasing concentrations of erastin for 72 h. Consistent with the tolerance toward docetaxel, A2780/Taxol cells possessed more resistance to erastin with the IC_{50} value of 24.98 μM, while A2780 cells were more sensitive to erastin with a lower IC_{50} value of 2.60 nM. Such an interesting co-resistance phenomenon indicated that erastin and docetaxel may share a similar drug-resistance mechanism.

Erastin Induces Ferroptosis in Ovarian Cancer Cells

To investigate whether erastin induces ferroptosis in ovarian cancer cells, two ferroptosis inhibitors, ferrostatin-1 and deferiprone, were applied to reverse its cytotoxicity. As presented in **Figures 2A,B**, erastin-induced cell death could be partially reversed by both ferrostatin-1 and deferiprone in both A2780 and A2780/Taxol cells, indicating that erastin can induce ferroptosis in ovarian cancer cells and that there might also be other forms of cell death that can be induced by erastin.

Erastin Enhances the Sensitivity of Docetaxel in the ABCB1-Overexpressing Ovarian Cancer Cells

Cancer chemotherapy usually combines drugs for treatment. To explore the combinational effect of erastin and docetaxel in ovarian cancer cells, we co-administrated erastin and docetaxel in both A2780 cells and A2780/Taxol cells. As presented in **Figures 3A,B**, erastin dose-dependently decreased the IC_{50} values of docetaxel in A2780/Taxol cells, while there was nearly no change in A2780 cells, indicating that erastin can enhance

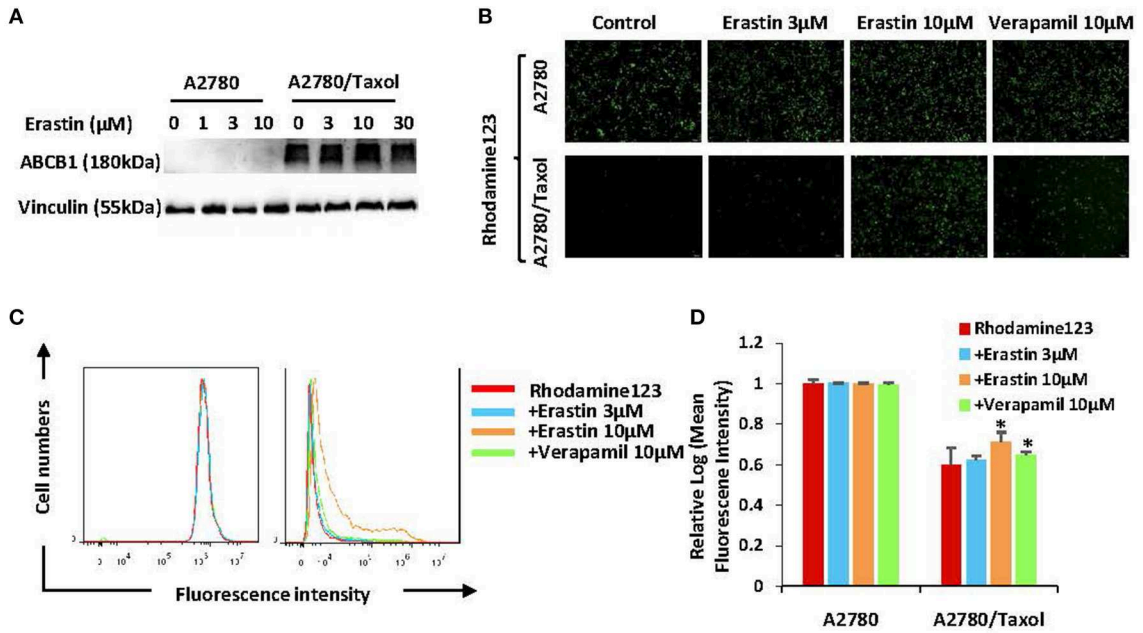

FIGURE 4 | Erastin inhibits the drug efflux activity of ABCB1. A2780 and A2780/Taxol cells were treated with the increasing concentration of erastin for 48 h (0, 1, 3, and 10 as well as 0, 3, 10, and 30 μM, respectively), and the protein expression of ABCB1 was detected by Western blot **(A)**. Cells were incubated with 10 μM rhodamine 123 for another 2 h at 37°C after being pre-treated with the indicated concentrations of erastin and verapamil for 0.5 h at 37°C, as measured by FCM and photographed by fluorescent microscope. The representative graphs **(B)**, charts **(C)**, and quantified data **(D)** are shown. Data are mean ± SD of three independent experiments. *$p < 0.05$ vs. corresponding control.

the sensitivity of docetaxel only in the ABCB1-overexpressing ovarian cancer cells.

Erastin Inhibits the Drug Efflux Activity of ABCB1

To find out whether erastin enhances the sensitivity of docetaxel in the ABCB1-overexpressing ovarian cancer cells is due to downregulation of the expression of ABCB1 or the inhibition of ABCB1 activity, we valued the protein expression of ABCB1 as well as the intracellular aggregation level of rhodamine 123 (ABCB1 substrate) in the pre-incubation of erastin or absence of erastin. The protein expression level of ABCB1 was obviously higher in A2780/Taxol cells than that in A2780 cells (**Figure 4A**), and erastin did not alter the protein expression of ABCB1 in A2780/Taxol cells. Furthermore, the intracellular rhodamine 123 accumulated in A2780/Taxol cells was at a dramatically lower level compared with A2780 cells, and erastin dose-dependently increased the intracellular rhodamine 123 levels only in A2780/Taxol cells but not in A2780 cells (**Figures 4B–D**), indicating that erastin can inhibit the drug efflux activity of ABCB1.

Erastin Enhances Docetaxel-Induced Apoptosis in the ABCB1-Overexpressing Ovarian Cancer Cells

To further examine the sufficiency of erastin in combination with docetaxel in ovarian cancer cells, cells were incubated under different conditions for 48 h, and the apoptosis rate was detected by FCM. Besides, the related proteins were measured by Western blot. Co-administration of erastin and docetaxel significantly increased the apoptosis rate (both early and late apoptosis) in A2780/Taxol cells but not in A2780 cells (**Figures 5A,B**). Additionally, as shown in **Figure 5C**, the co-treatment group showed more increase of cleaved PARP (C-PARP) protein and a higher decrease of Mcl-1 protein than those in either docetaxel or erastin alone group only in A2780/Taxol cells. There was nearly no alteration in A2780 cells, suggesting that erastin can enhance docetaxel-induced apoptosis in the ABCB1-overexpressing ovarian cancer cells.

Erastin Enhances Docetaxel-Induced Cell Cycle Arrest in the ABCB1-Overexpressing Ovarian Cancer Cells

To examine the merging effect of erastin and docetaxel in ovarian cancer cells, the distribution change of cell cycle was measured by FCM with PI staining. As demonstrated in **Figures 6A,B**, the co-treatment group of erastin and docetaxel dramatically induced more accumulation in the sub-G1 and G2/M phase in comparison with erastin or docetaxel alone treatment only in A2780/Taxol cell but not in A2780 cells, suggesting that erastin can enhance the docetaxel-induced cell cycle arrest in the ABCB1-overexpressing ovarian cancer cells.

Model for Binding of Erastin to ABCB1

Docking studies were carried out to demonstrate the binding mechanism of erastin to ABCB1. Firstly, the human ABCB1 crystal structure downloaded online was initially bound with

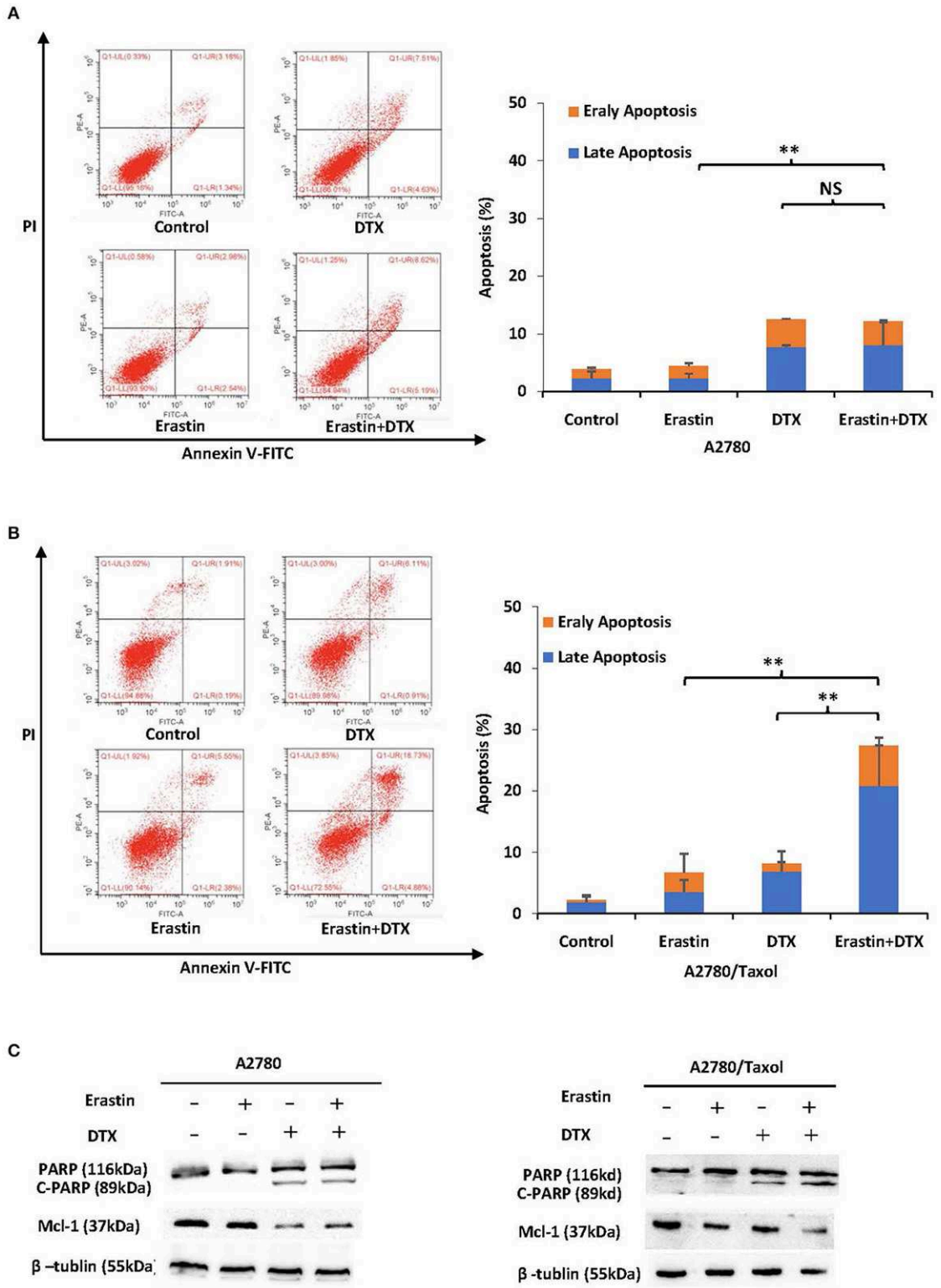

FIGURE 5 | Erastin enhances docetaxel-induced apoptosis in the ABCB1-overexpressing ovarian cancer cells. A2780 **(A)** cells were treated with 1 μM erastin, 10 nM docetaxel alone or in combination for 48 h. A2780/Taxol **(B)** cells were treated with 10 μM erastin and 300 nM docetaxel alone or in combination for 48 h. The apoptosis was detected by FCM with Annexin V/PI staining. The proportions of Annexin V+/PI– and Annexin V+/PI+ cells indicated the early and late stages of apoptosis. The protein expression was examined by Western blot after lysing cells, and β-tublin was used as loading control. The representative charts, quantified results, and Western blot results **(C)** of three independent experiments are shown. DTX, Docetaxel. $^{**}p < 0.01$ vs. corresponding control.

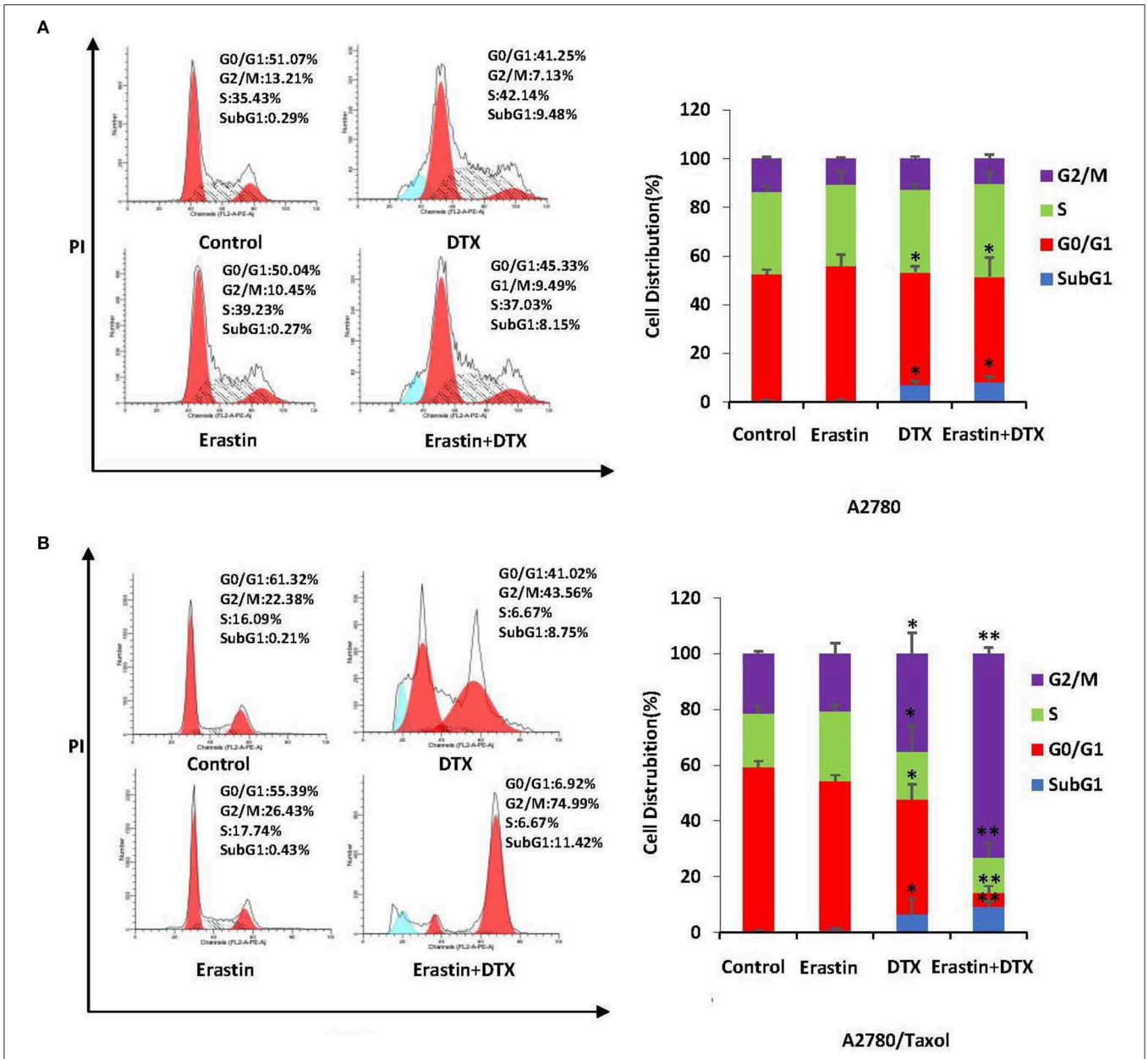

FIGURE 6 | Erastin enhances docetaxel-induced cell cycle arrest in the ABCB1-overexpressing ovarian cancer cells. A2780 **(A)** cells were treated with 1 μM erastin, and 10 nM docetaxel alone or in combination for 48 h. A2780/Taxol **(B)** cells were treated with 10 μM erastin and 300 nM docetaxel alone or in combination for 48 h. The distribution of cell cycle was detected by FCM with PI staining. The representative charts and quantified results of three independent experiments are shown. DTX, Docetaxel. $^{*}p < 0.05$ and $^{**}p < 0.01$ vs. corresponding control.

taxol (PDB ID: 6qex). As demonstrated in **Figures 7A,B**, there existed special interactions between erastin and human ABCB1 (for example, hydrogen bonding), accounting for the stable affinity. The pyridine ring and pyrimidine ring of erastin connected with Phe983 via π-π stacking. The ethyl of erastin interacted with Phe336 through π-σ stacking. The hydron bonds exist between Phe343, Leu339, Met69, Ile340, Gln946, Gly62, Gln195, Leu65, Met949, Met986, Ala987, Phe728, Gln725, Tyr953, and erastin. Meanwhile, the hydrophobic pocket was formed by His61, Gly64, Thr199, Ser344, and TYR310 (**Figure 7C**), which stabilized the other part of erastin. In short, erastin directly binds to ABCB1 by a special chemical structure connection to suppress the pump activity of ABCB1.

DISCUSSION

Overexpression of ABCB1 is identified as one of the chief components of cancer chemotherapy failure (13, 37). A recent study declaimed that ABCB1 overexpression is guilty of olaparib resistance (38). Olaparib is a PARP inhibitor that is currently emerging as a promising treatment for ovarian cancer patients with BRCA mutation. Patients with a high expression of

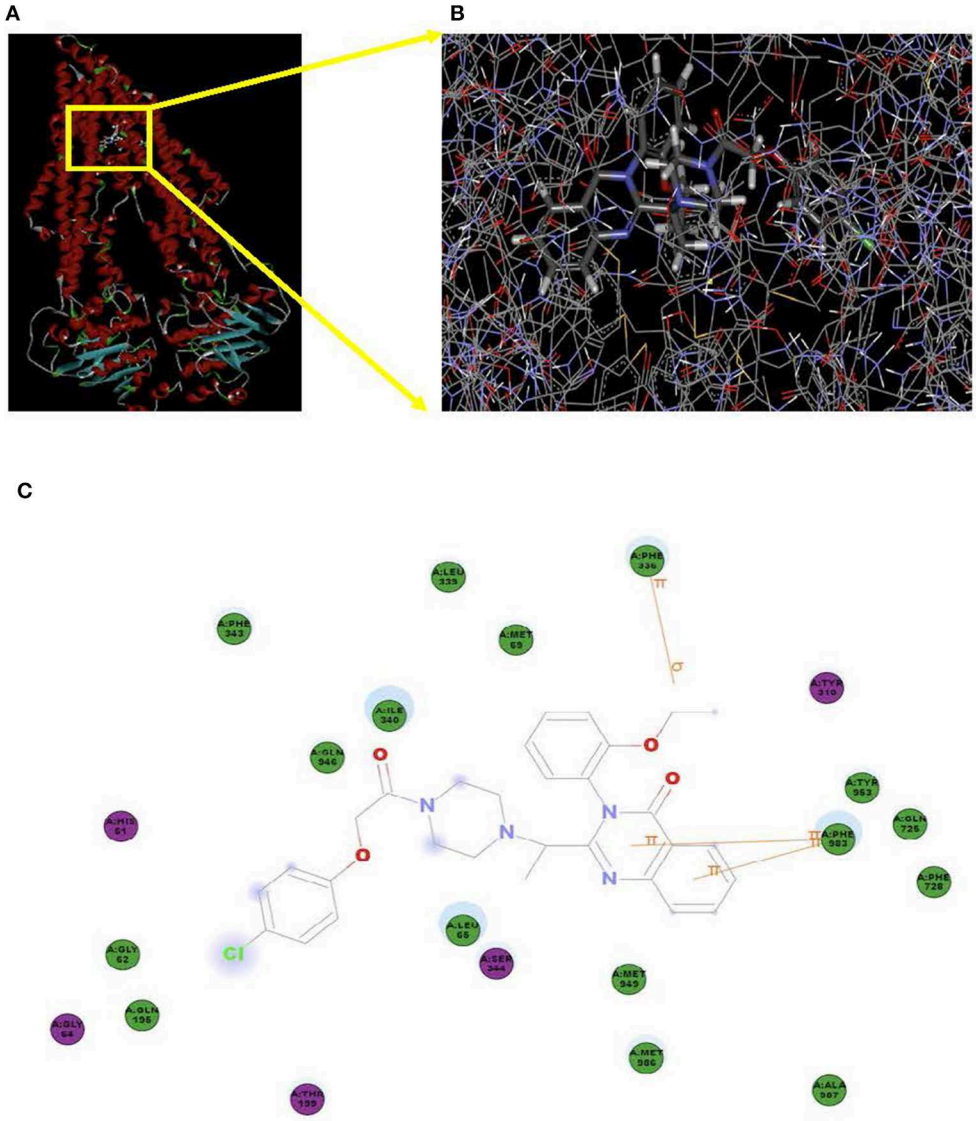

FIGURE 7 | Model for the binding of erastin to ABCB1. The ribbon diagram of 3D structure conformation **(A)** and the optimal predicted binding mode **(B)** of erastin within the human ABCB1 (PDB ID:6qex) binding site are shown. Important amino acids are depicted as lines with the atoms colored (carbon, gray; hydrogen, white; nitrogen, blue; and oxygen, red), and erastin is shown as a ball and stick model with the atoms colored (carbon, gray; hydrogen, white; nitrogen, blue; oxygen, red; and chlorine, green). Yellow lines indicate π-π and π-σ stacking. The dotted green line indicates a hydrogen bonding interaction. The dotted blue line represents the interaction site of erastin and ABCB1 **(C)**.

ABCB1 may not prospectively benefit from olaparib according to the single BRCA expression context. Therefore, strategies to inhibit ABC transporter proteins are identified as a potentially promising approach to suppress drug efflux in order to overcome drug tolerance. However, we have failed to figure out approved drugs suitable for clinical use for the inhibition of ABCB1, inducing delighted outcomes. A series of trials carried out with third-generation drugs have not been confirmed to have favorable outcomes yet (39). Therefore, developing more effective inhibitors of ABCB1 is urgently required.

Ferroptosis, a newly discovered cell death mode, is characterized by the aberrant accumulation of lipid peroxides in an iron-dependent way (40). Inhibitors of either SLC7A11 or glutathione peroxidase 4 (GPX4) can trigger ferroptosis. Some of the corresponding drugs are erastin and RSL3. Cancer cells often exhibit an increased iron demand to facilitate cell growth (41, 42), indicating that cancer cells may be more vulnerable to ferroptosis. Our work offers data to support the anti-ovarian cancer effect of erastin. Ferroptosis also plays a significant role in the drug resistance of cancer therapy. Firstly, ferroptosis is a non-apoptosis cell death pattern. Faced with the resistance caused by apoptosis-inducing chemotherapy drugs, ferroptotic reagents can serve as a promising strategy in reversing such therapeutic inefficiency. Secondly, persistent

drug-tolerant cancer cells are sensitive to ferroptosis (9). In our study, we verified a decrease in the IC_{50} value of docetaxel in the presence of erastin in the ABCB1-overexpressing ovarian cancer cells. The accumulation of rhodamine 123 confirmed that erastin significantly antagonized the drug-efflux function of ABCB1. Moreover, it has been reported that the safety of erastin in xenograft modes is acceptable (43, 44). Inhibition of SLC7A11 by erastin also increased the sensitivity of cisplatin in cancer cells (19, 45), suggesting the combination of erastin and chemotherapeutical reagents can be sufficient for cancer therapy.

In summary, our results demonstrated that erastin could reverse ABCB1-mediated docetaxel resistance in ovarian cancer, suggesting that the combination of erastin and docetaxel may expand the limited options for chemo-resistant ovarian cancers.

DATA AVAILABILITY STATEMENT

The raw data supporting the conclusions of this article will be made available by the authors, without undue reservation, to any qualified researcher.

AUTHOR CONTRIBUTIONS

H-HZ, XC, L-YC, ZS, and X-JY designed the experiments, performed the experiments, analyzed the data, and wrote the paper. X-WN, J-HC, X-XC, YY, Z-HX, M-NW, YL, S-TW, and KL performed the experiments. All authors read and approved the final manuscript.

FUNDING

This work was supported by funds from the National Key Research and Development Program of China No. 2017YFA0505104 (to ZS), the National Natural Science Foundation of China Nos. 81772540 (to ZS), and 81503293 (to X-JY), the Science and Technology Program of Guangdong No. 2019A050510023 (to ZS), the Technology Development Funds of Wenzhou City No. Y20190014 (to X-JY), and the Traditional Chinese Medicine Science and Technology Foundation of Zhejiang Province, China No. 2020ZB144 (to X-JY).

REFERENCES

1. Siegel RL, Miller KD, Jemal A. Cancer statistics, 2019. *CA Cancer J Clin.* (2019) 69:7–34. doi: 10.3322/caac.21551
2. Matulonis U, Abrahm JL. Cancer of the ovary. *N Engl J Med.* (2005) 352:1268–9; author reply 68–9. doi: 10.1056/NEJM200503243521222
3. Ledermann JA, Raja FA, Fotopoulou C, Gonzalez-Martin A, Colombo N, Sessa C, et al. Newly diagnosed and relapsed epithelial ovarian carcinoma: ESMO Clinical Practice Guidelines for diagnosis, treatment and follow-up. *Ann Oncol.* (2018) 29:iv259. doi: 10.1093/annonc/mdy157
4. Reid BM, Permuth JB, Sellers TA. Epidemiology of ovarian cancer: a review. *Cancer Biol Med.* (2017) 14:9–32. doi: 10.20892/j.issn.2095-3941.2016.0084
5. Zahedi P, De Souza R, Huynh L, Piquette-Miller M, Allen C. Combination drug delivery strategy for the treatment of multidrug resistant ovarian cancer. *Mol Pharm.* (2011) 8:260–9. doi: 10.1021/mp100323z
6. Gottesman MM, Pastan I. Biochemistry of multidrug resistance mediated by the multidrug transporter. *Annu Rev Biochem.* (1993) 62:385–427. doi: 10.1146/annurev.bi.62.070193.002125
7. Nanayakkara AK, Follit CA, Chen G, Williams NS, Vogel PD, Wise JG. Targeted inhibitors of P-glycoprotein increase chemotherapeutic-induced mortality of multidrug resistant tumor cells. *Sci Rep.* (2018) 8:967. doi: 10.1038/s41598-018-19325-x
8. Ambudkar SV, Dey S, Hrycyna CA, Ramachandra M, Pastan I, Gottesman MM. Biochemical, cellular, and pharmacological aspects of the multidrug transporter. *Annu Rev Pharmacol Toxicol.* (1999) 39:361–98. doi: 10.1146/annurev.pharmtox.39.1.361
9. Viswanathan VS, Ryan MJ, Dhruv HD, Gill S, Eichhoff OM, Seashore-Ludlow B, et al. Dependency of a therapy-resistant state of cancer cells on a lipid peroxidase pathway. *Nature.* (2017) 547:453–57. doi: 10.1038/nature23007
10. Schinkel AH, Jonker JW. Mammalian drug efflux transporters of the ATP binding cassette (ABC) family: an overview. *Adv Drug Deliv Rev.* (2003) 55:3–29. doi: 10.1016/S0169-409X(02)00169-2
11. Gottesman MM, Ling V. The molecular basis of multidrug resistance in cancer: the early years of P-glycoprotein research. *FEBS Lett.* (2006) 580:998–1009. doi: 10.1016/j.febslet.2005.12.060
12. Christie EL, Pattnaik S, Beach J, Copeland A, Rashoo N, Fereday S, et al. Multiple ABCB1 transcriptional fusions in drug resistant high-grade serous ovarian and breast cancer. *Nat Commun.* (2019) 10:1295. doi: 10.1038/s41467-019-09312-9
13. Seborova K, Vaclavikova R, Soucek P, Elsnerova K, Bartakova A, Cernaj P, et al. Association of ABC gene profiles with time to progression and resistance in ovarian cancer revealed by bioinformatics analyses. *Cancer Med.* (2019) 8:606–16. doi: 10.1002/cam4.1964
14. Hamidovic A, Hahn K, Kolesar J. Clinical significance of ABCB1 genotyping in oncology. *J Oncol Pharm Pract.* (2010) 16:39–44. doi: 10.1177/1078155209104380
15. Parekh H, Wiesen K, Simpkins H. Acquisition of taxol resistance via P-glycoprotein- and non-P-glycoprotein-mediated mechanisms in human ovarian carcinoma cells. *Biochem Pharmacol.* (1997) 53:461–70. doi: 10.1016/S0006-2952(97)83383-7
16. Li H, Lv M, Qiao B, Li X. Blockade pf CD73/adenosine axis improves the therapeutic efficacy of docetaxel in epithelial ovarian cancer. *Arch Gynecol Obstet.* (2019) 299:1737–46. doi: 10.1007/s00404-019-05139-3
17. Lu X, Meng T. Depletion of tumor-associated macrophages enhances the anti-tumor effect of docetaxel in a murine epithelial ovarian cancer. *Immunobiology.* (2019) 224:355–61. doi: 10.1016/j.imbio.2019.03.002
18. Dixon SJ, Lemberg KM, Lamprecht MR, Skouta R, Zaitsev EM, Gleason CE, et al. Ferroptosis: an iron-dependent form of nonapoptotic cell death. *Cell.* (2012) 149:1060–72. doi: 10.1016/j.cell.2012.03.042
19. Sato M, Kusumi R, Hamashima S, Kobayashi S, Sasaki S, Komiyama Y, et al. The ferroptosis inducer erastin irreversibly inhibits system xc- and synergizes with cisplatin to increase cisplatin's cytotoxicity in cancer cells. *Sci Rep.* (2018) 8:968. doi: 10.1038/s41598-018-19213-4
20. Yu Y, Nangia-Makker P, Farhana L, Majumdar APN. A novel mechanism of lncRNA and miRNA interaction: CCAT2 regulates miR-145 expression by suppressing its maturation process in colon cancer cells. *Mol Cancer.* (2017) 16:155. doi: 10.1186/s12943-017-0725-5
21. Hou LJ, Huang XX, Xu LN, Zhang YY, Zhao N, Ou RY, et al. YM155 enhances docetaxel efficacy in ovarian cancer. *Am J Transl Res.* (2018) 10:696–708.
22. Liu Q, Wang K. The induction of ferroptosis by impairing STAT3/Nrf2/GPx4 signaling enhances the sensitivity of osteosarcoma cells to cisplatin. *Cell Biol Int.* (2019) 43:1245–56. doi: 10.1002/cbin.11121
23. Nie J, Lin B, Zhou M, Wu L, Zheng T. Role of ferroptosis in hepatocellular carcinoma. *J Cancer Res Clin Oncol.* (2018) 144:2329–37. doi: 10.1007/s00432-018-2740-3
24. Roh JL, Kim EH, Jang HJ, Park JY, Shin D. Induction of ferroptotic cell death for overcoming cisplatin resistance of head and neck cancer. *Cancer Lett.* (2016) 381:96–103. doi: 10.1016/j.canlet.2016.07.035
25. Zhang WJ, Li Y, Wei MN, Chen Y, Qiu JG, Jiang QW, et al. Synergistic antitumor activity of regorafenib and lapatinib in preclinical models of human colorectal cancer. *Cancer Lett.* (2017) 386:100–9. doi: 10.1016/j.canlet.2016.11.011

26. Chen X, Gong L, Ou R, Zheng Z, Chen J, Xie F, et al. Sequential combination therapy of ovarian cancer with cisplatin and gamma-secretase inhibitor MK-0752. *Gynecol Oncol.* (2016) 140:537–44. doi: 10.1016/j.ygyno.2015.12.011
27. Zheng DW, Xue YQ, Li Y, Di JM, Qiu JG, Zhang WJ, et al. Volasertib suppresses the growth of human hepatocellular carcinoma *in vitro* and *in vivo*. *Am J Cancer Res.* (2016) 6:2476–88.
28. Huang JR, Qin WM, Wang K, Fu DR, Zhang WJ, Jiang QW, et al. Cyclin-dependent kinase 7 inhibitor THZ2 inhibits the growth of human gastric cancer *in vitro* and *in vivo*. *Am J Transl Res.* (2018) 10:3664–76.
29. Yuan ML, Li P, Xing ZH, Di JM, Liu H, Yang AK, et al. Inhibition of WEE1 suppresses the tumor growth in laryngeal squamous cell carcinoma. *Front Pharmacol.* (2018) 9:1041. doi: 10.3389/fphar.2018.01041
30. Xu LN, Zhao N, Chen JY, Ye PP, Nan XW, Zhou HH, et al. Celastrol inhibits the growth of ovarian cancer cells *in vitro* and *in vivo*. *Front Oncol.* (2019) 9:2. doi: 10.3389/fonc.2019.00002
31. Xie F-F, Pan S-S, Ou R-Y, Zheng Z-Z, Huang X-X, Jian M-T. Volasertib suppresses tumor growth and potentiates the activity of cisplatin in cervical cancer. *Am J Cancer Res.* (2015) 5:3548–59.
32. Mei XL, Yang Y, Zhang YJ, Li Y, Zhao JM, Qiu JG, et al. Sildenafil inhibits the growth of human colorectal cancer *in vitro* and *in vivo*. *Am J Cancer Res.* (2015) 5:3311–24.
33. Yang Y, Qiu JG, Li Y, Di JM, Zhang WJ, Jiang QW, et al. Targeting ABCB1-mediated tumor multidrug resistance by CRISPR/Cas9-based genome editing. *Am J Transl Res.* (2016) 8:3986–94.
34. Wang YJ, Zhang YK, Zhang GN, Al Rihani SB, Wei MN, Gupta P, et al. Regorafenib overcomes chemotherapeutic multidrug resistance mediated by ABCB1 transporter in colorectal cancer: *In vitro* and *in vivo* study. *Cancer Lett.* (2017) 396:145–54. doi: 10.1016/j.canlet.2017.03.011
35. Lv M, Qiu J-G, Zhang W-J, Jiang Q-W. Wallichinine reverses ABCB1-mediated cancer multidrug resistance. *Am J Transl Res.* (2016) 8:2969–80.
36. Qiu JG, Zhang YJ, Li Y, Zhao JM, Zhang WJ, Jiang QW, et al. Trametinib modulates cancer multidrug resistance by targeting ABCB1 transporter. *Oncotarget.* (2015) 6:15494–509. doi: 10.18632/oncotarget.3820
37. Auner V, Sehouli J, Oskay-Oezcelik G, Horvat R, Speiser P, Zeillinger R. ABC transporter gene expression in benign and malignant ovarian tissue. *Gynecol Oncol.* (2010) 117:198–201. doi: 10.1016/j.ygyno.2009.10.077
38. Vaidyanathan A, Sawers L, Gannon AL, Chakravarty P, Scott AL, Bray SE, et al. ABCB1 (MDR1) induction defines a common resistance mechanism in paclitaxel- and olaparib-resistant ovarian cancer cells. *Br J Cancer.* (2016) 115:431–41. doi: 10.1038/bjc.2016.203
39. Shi Z, Tiwari AK, Shukla S, Robey RW, Singh S, Kim IW, et al. Sildenafil reverses ABCB1- and ABCG2-mediated chemotherapeutic drug resistance. *Cancer Res.* (2011) 71:3029–41. doi: 10.1158/0008-5472.CAN-10-3820
40. Stockwell BR, Friedmann Angeli JP, Bayir H, Bush AI, Conrad M, Dixon SJ, et al. Ferroptosis: a regulated cell death nexus linking metabolism, redox biology, and disease. *Cell.* (2017) 171:273–85. doi: 10.1016/j.cell.2017.09.021
41. Kouba S, Ouldamer L, Garcia C, Fontaine D, Chantome A, Vandier C, et al. Lipid metabolism and Calcium signaling in epithelial ovarian cancer. *Cell Calcium.* (2019) 81:38–50. doi: 10.1016/j.ceca.2019.06.002
42. Basuli D, Tesfay L, Deng Z, Paul B, Yamamoto Y, Ning G, et al. Iron addiction: a novel therapeutic target in ovarian cancer. *Oncogene.* (2017) 36:4089–99. doi: 10.1038/onc.2017.11
43. Fang D, Maldonado EN. VDAC regulation: a mitochondrial target to stop cell proliferation. *Adv Cancer Res.* (2018) 138:41–69. doi: 10.1016/bs.acr.2018.02.002
44. Luo M, Wu L, Zhang K, Wang H, Zhang T, Gutierrez L, et al. miR-137 regulates ferroptosis by targeting glutamine transporter SLC1A5 in melanoma. *Cell Death Differ.* (2018) 25:1457–72. doi: 10.1038/s41418-017-0053-8
45. Guo J, Xu B, Han Q, Zhou H, Xia Y, Gong C, et al. Ferroptosis: a novel anti-tumor action for cisplatin. *Cancer Res Treat.* (2018) 50:445–60. doi: 10.4143/crt.2016.572

Conflict of Interest: The authors declare that the research was conducted in the absence of any commercial or financial relationships that could be construed as a potential conflict of interest.

frontiers in Oncology

ORIGINAL RESEARCH
published: 17 January 2020
doi: 10.3389/fonc.2019.01520

Pigment Epithelium-Derived Factor Promotes the Growth and Migration of Human Esophageal Squamous Cell Carcinoma

*De-Rong Tang, Cheng-Lin Li, Ke-Ping Xu, Qing-Quan Wu, Qi-You Chen, Jun-Jie Lv, Jian Ji, Bao Zang, Chen Chen, Biao Gu and Jian-Qiang Zhao**

Department of Thoracic Surgery, The Affiliated Huaian No.1 People's Hospital of Nanjing Medical University, Huai'an, China

Pigment epithelium-derived factor (PEDF) is an oncogene found in various types of cancers. However, how PEDF affects the development of human esophageal squamous cell carcinoma (ESCC) is unknown. This study investigates the role of PEDF in ESCC cell proliferation, migration, and cell cycle both *in vitro* and *in vivo.* The PEDF expression was examined in patient tumor samples and ESCC cell lines. Short hairpin RNA technology was used to inhibit the PEDF expression in ESCC EC9706 and KYSE150 cells. *In vitro* cell proliferation and migration assays were performed. The effects of PEDF on tumor growth and progression were examined *in vivo* in murine subcutaneous xenograft tumor models. It was found that PEDF was overexpressed in esophageal cancer cells and patient tumor tissues compared to normal control samples. PEDF enhanced cell cycle progression and inhibited cell apoptosis. Knock down of PEDF inhibited esophageal cell proliferation and migration *in vitro*. Moreover, Inhibition of PEDF significantly reduced tumor growth and tumor size *in vivo*. These results indicate that PEDF induce tumorigenesis in ESCC and can be a potential therapeutic target for cancer treatment.

Keywords: pigment epithelium-derived factor (PEDF), esophageal carcinoma, tumorigenesis, proliferation, migration

OPEN ACCESS

Edited by:
Dong-Hua Yang,
St. John's University, United States

Reviewed by:
Shuaishuai Liu,
University of Maryland, Baltimore County, United States
Wei Zhao,
Chengdu Medical College, China
Chang Zou,
Shenzhen People's Hospital, China

****Correspondence:***
Jian-Qiang Zhao
shenglee6871@sina.com

Specialty section:
This article was submitted to Molecular and Cellular Oncology, a section of the journal Frontiers in Oncology

Received: *20 August 2019*
Accepted: *17 December 2019*
Published: *17 January 2020*

Citation:
Tang D-R, Li C-L, Xu K-P, Wu Q-Q, Chen Q-Y, Lv J-J, Ji J, Zang B, Chen C, Gu B and Zhao J-Q (2020) Pigment Epithelium-Derived Factor Promotes the Growth and Migration of Human Esophageal Squamous Cell Carcinoma. Front. Oncol. 9:1520. doi: 10.3389/fonc.2019.01520

INTRODUCTION

Esophageal carcinoma is a common gastrointestinal cancer that has two major subtypes: adenocarcinoma and squamous cell carcinoma (1). It is the sixth cancer-related deaths worldwide. There were about 16,940 newly diagnosed cases of esophageal carcinoma in the United States (accounting for 1% of all new-onset cancer cases) and 15,690 deaths (accounting for 2.6% of all cancer-related deaths) In 2016 (2). The incidence of esophageal squamous cell carcinoma (ESCC) is very high in some areas of China. There are ∼5,500 confirmed cases of disease in 5 million people each year in Huai'an city, the northern part of Jiangsu Province, China. Although progress has been made in the diagnosis and treatment of esophageal carcinoma, its 5-year survival rate is still dismal (1). Therefore, it is imperative to further explore the molecular basis of esophageal carcinoma and develop more effective treatment strategy.

Pigment epithelium-derived factor (PEDF), a member of the serine protease inhibitor superfamily, was initially isolated from the retinal pigment epithelial cells of human fetus (3). PEDF has neuroprotective and anti-angiogenic activity (4). PEDF is highly expressed in adipose tissue, liver, eye, heart, skeletal muscle, spleen, brain, and bone (5–10). PEDF plays significant biological

roles in many physiological and pathophysiological processes, including neuroprotection, fibrosis and inflammation (11). Previous studies have shown that PEDF plays important roles in cancer angiogenesis, tumor growth and metastasis (12, 13). Therefore, the potential use of PEDF as a target in the treatment of cancer has attracted much attention. However, the mechanisms of PEDF in cancer development remain controversial. PEDF shows antitumour effect in some tumors, including pancreatic, melanoma, and ovarian cancers (14–16). On the other hand, the level of PEDF is higher than that of normal tissues in some other cancers. For example, PEDF can promote stem cell growth and self-renewal of glioma stem cells (17, 18). PEDF was also found in hepatocellular carcinoma cells where PEDF levels were higher in HCC cases than in normal paracancerous tissues. The secretion of PEDF was higher in HCC patients than in normal controls, suggesting the potential of using serum PEDF as a biomarker for hepatocellular carcinoma (19). Therefore, the function of PEDF and its mechanism of action in various cancers need to be further investigated before it can be used as a biomarker for diagnosis and prognosis, or for cancer treatment.

In this study, we found that PEDF is overexpressed in tissues and cells of esophageal carcinoma. In addition, we observed that PEDF promotes esophageal cancer cell growth both *in vivo* and *in vitro*. This study will provide a rational for using PEDF as a prognostic biomarker and a potential therapeutic target for esophageal carcinoma.

MATERIALS AND METHODS

Tissue Samples

A total of 40 cases of esophageal cancer patients admitted to the Affiliated Huaian No.1 People's Hospital of Nanjing Medical University were enrolled in this study. Tumor and corresponding normal tissues were obtained. None of the patients received any radiation or chemotherapy before surgery. Surgical specimens were immediately frozen in liquid nitrogen and stored at −80° C for proteins assays. This study was carried out with the approval of the Ethics Committee of the Affiliated Huaian No.1 People's Hospital of Nanjing Medical University. A written informed consent was obtained from each patient.

Cell Lines and Cell Culture

Human esophageal cancer cell lines (EC9706, KYSE150) were purchased from Shanghai Cell Bank of Chinese Academy of Sciences. The cells were cultured in RPMI-1640 medium (Invitrogen, USA) containing 10% heat inactivated fetal bovine serum (FBS; Invitrogen, Carlsbad, CA, USA) and 1% penicillin / streptomycin in an incubator with 5% CO_2 at 37°C.

Cell Transfection

The short hairpin RNA was used to knockdown PEDF (shPEDF, 5′-AGCGAACAGAATCCATCAT−3′, shPEDF1, 5′-GAAGCATGAGTATCATCTT−3′, shPEDF2, 5′-TGTTT GATTCACCAGACTT-3′), (Invitrogen, USA). Cells were transfected with pLL3.7-shPEDF, and 5 ug of packaging viral plasmid using Lipofectamine 2000 (Invitrogen).

Reverse Transcription-Quantitative Polymerase Chain Reaction (RT-PCR) Assay

Total RNA was extracted from tissues and cells using Trizol reagent (Invitrogen) according to the manufacturer's instructions. One microgram of RNA was then reversely transcribed into cDNA using M-MLV reverse transcriptase (Invitrogen). PEDF mRNA expression was detected using an Applied Biosystems 7500 Fast Real-Time PCR System (Applied Biosystems) using a fast SYBR Green Master Mix (Applied Biosystems, Foster City, CA, USA), with β-actin as an endogenous control. The primer sequences for PEDF and β-actin are as follows: PEDF, 5′-ACT GAG TAA GAT GGC GGG TCG-3′ (forward) and 5′-TTC TGG CGA AAG CGG GTA G-3′ β-actin, 5′-AAA TCG TGC GTG ACA TCA AAG A-3′ (forward) and 5′-GGC CAT CTC CTG CTC GAA-3′ (reverse).

Western Blot Analysis

Total protein was extracted from cells and patients' tissues using RIPA buffer (Beyotime, Shanghai, China) containing a protease inhibitor cocktail (Roche Diagnostics, Basel, Switzerland) and quantified using the Pierce™ BCA Protein Assay Kit (Invitrogen; Thermo Scientific). The same amount of protein (50 μg) was then separated on 10% sodium dodecyl sulfate-polyacrylamide gel electrophoresis (SDS-PAGE) and transferred to a nitrocellulose filter (NC membrane; Millipore, Billerica, MA, USA). Membranes were then blocked in 5% skim milk for 1 h at room temperature and blocked with primary antibodies against PEDF(ab10389), caspase 3(ab197202), caspase 9(ab219590) (Abcam, Cambridge, Mass., USA), overnight at 4°C followed by incubation with horseradish peroxidase (HRP) conjugated goat anti-rabbit secondary antibody (ab6721, 1: 1,000, Abcam) for 1 h at room temperature. Finally, specific protein signals were visualized using ECL Western blotting substrates (Promega, Madison, WI, USA) and quantified by Image J software (National Institutes of Health, Bethesda, Maryland, USA).

Transwell Invasion Assay

Invasion chambers (BD Bioscience, San Diego, Calif., USA) were used to assess cell invasiveness using a membrane with a pore size of 8 μm (BD Bioscience). Briefly, EC9076 and EC109 cells infected with shRNA were resuspended in serum-free RPMI-1640 medium (100 μl) and inoculated in 40 μl of Matrigel (BD Biosciences) with 700 μl RPMI-1640 medium and 10% FBS. After incubation at 37°C for 48 h, cells on the upper side of the membrane were removed with a sterile swab. The cells on the lower side of the membrane were fixed with methanol for 30 min, stained with 0.1% crystal violet for 20 min, and counted in six randomly selected fields at 200 X magnification using an inverted microscope (Nikon Eclipse TE300, Tokyo, Japan).

Flow Cytometry for Cell Cycle and Apoptosis Analysis

Cell cycle was determined according to the manufacturer's protocol with propidium iodide (PI) staining (Nanjing Kaiji Biotechnology Development Co. Ltd., Nanjing, China). Briefly,

EC9076 and EC109 cells were transfected with shRNA. The cells were then harvested and resuspended in 500 μl 1X binding buffer at a concentration of 1×10^6 cells / ml, followed by the addition of 5 μl of PI. The treated cells were then incubated for 5 min at room temperature in the dark. Finally, the cell cycle and apoptotic rate of the cells was analyzed using a FACS Calibur flow cytometer (Beckman Coulter, Atlanta, GA, USA).

In vivo Experiments

BALB/c nude mice (6–7 weeks old, male) were obtained from Chinese Academy of Sciences (Shanghai, China) and grown under specific pathogen-free conditions. All animal studies are conducted in accordance with the University Laboratory Animal Management, and approved by the Ethics Committee of The Affiliated Huaian No.1 People's Hospital of Nanjing Medical University. To investigate the knock down effect of PEDF on tumor growth *in vivo*, stably transfected EC9706 cells were subcutaneously injected into the ventral region of nude mice at a concentration of 1×10^7 cells / ml. According to the formula of $0.5 \times L \times W^2$, the tumor volume was measured every 3 days with a caliper. On day 24 after injection, tumors from all mice were obtained, weighed, and fixed in formalin.

Statistical Analysis

All data from three independent experiments were obtained and expressed as mean ± SD. Student's *t*-test or one-way ANOVA was used to analyze differences between different groups. The difference was considered statistically significant when $P < 0.05$.

RESULTS

PEDF Is Overexpressed in Esophageal Squamous Cell Carcinoma

To investigate the role of PEDF in ESCC, we compared the expression of PEDF in ESCC and adjacent normal tissues in 40 patients. Our results showed that the protein expression of PEDF in tumor samples is significantly higher than that in their corresponding normal tissues in those 40 patients (**Figure 1A**). These results indicated that PEDF is associated with the development of ESCC.

PEDF Enhances Cell Proliferation and Migration in Esophageal Squamous Cell Carcinoma

Because PEDF is overexpressed in esophageal carcinoma, we explored the role of PEDF in esophageal carcinoma by knocking down the expression of PEDF in two esophageal carcinoma cell lines EC9706 and KYSE150. In order to determine the best knock-down efficiency, we synthesized three shRNA. The results showed that shRNA-PEDF markedly suppressed the expression of PEDF proteins and mRNA (**Figure 1B**). Therefore, shRNA-PEDF was used in the following assays. Colony formation assay was used to determine the cell growth after knocking down

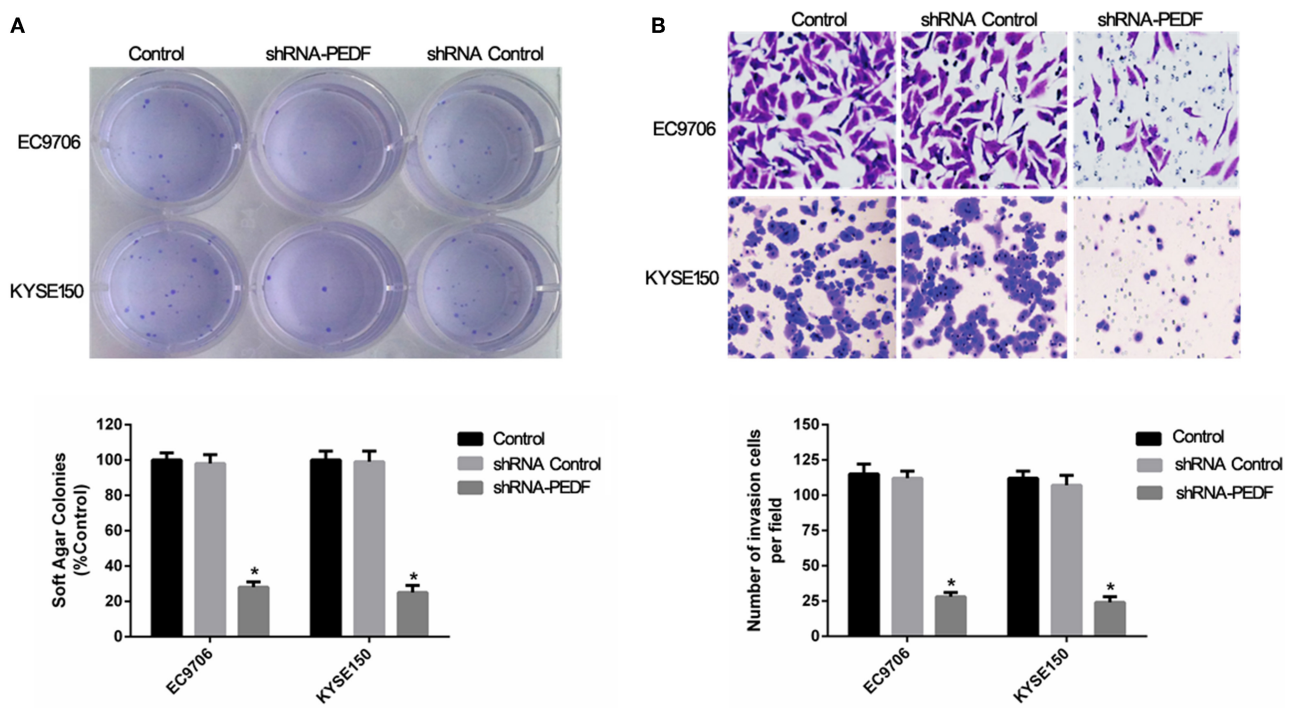

FIGURE 1 | PEDF expression in esophageal squamous cell carcinoma (ESCC). **(A)** Densitometric analysis was used to quantify the PEDF protein-related bands in Western blotting performed on ESCC and corresponding normal tissues in 40 patients **(B)** the expression of PEDF in EC9706 and KYSE150 cells after shRNA -PEDF treatment. Left, Western blot result; right, qRT-PCR on mRNA expression of PEDF, as normalized to actin. * < 0.05.

PEDF. The result showed significant reduction of the colony numbers of esophageal carcinoma cells at 7 days after transfection of shRNA (**Figure 2A**).

The effect of cell migration after knocking down PEDF in esophageal carcinoma cells was also investigated. The transwell assay revealed that shRNA-PEDF significantly attenuated cell

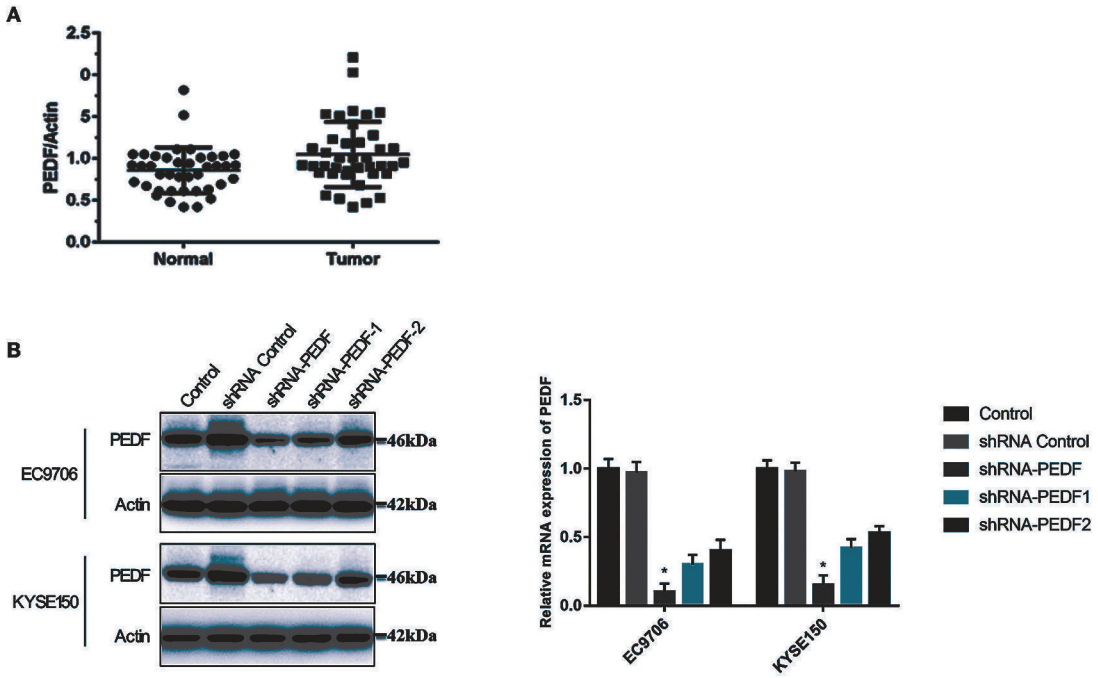

FIGURE 2 | Effect of PEDF knockdown on anchorage-independent growth of esophageal cancer cells. **(A)** Colony formation assay, and **(B)** invasion assay, of esophageal cancer cells after knocking down PEDF. * < 0.05.

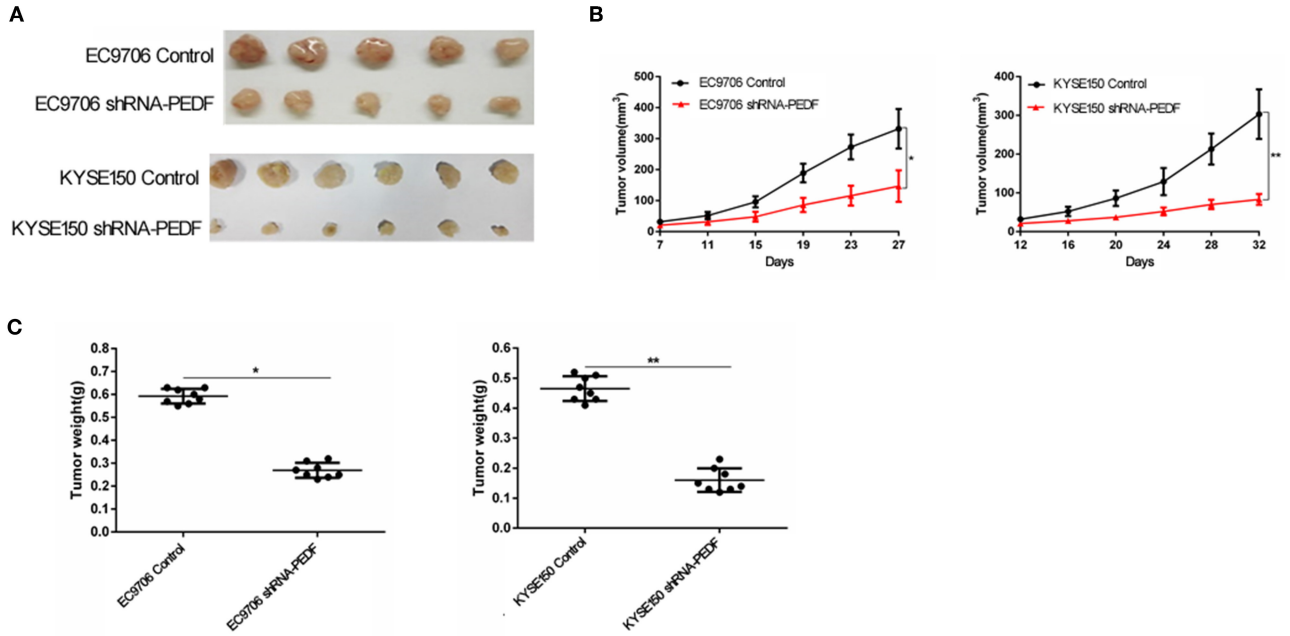

FIGURE 3 | Effect of PEDF knockdown on cell cycle and apoptosis of esophageal cancer cells. **(A)** Cell cycle change of esophageal cancer cells after knocking down PEDF. **(B)** Apoptosis assay of esophageal cancer cells after knocking down PEDF. **(C)** Western blot analysis of apoptosis-related proteins after knocking down PEDF in esophageal cancer cells. * < 0.05, ** < 0.01.

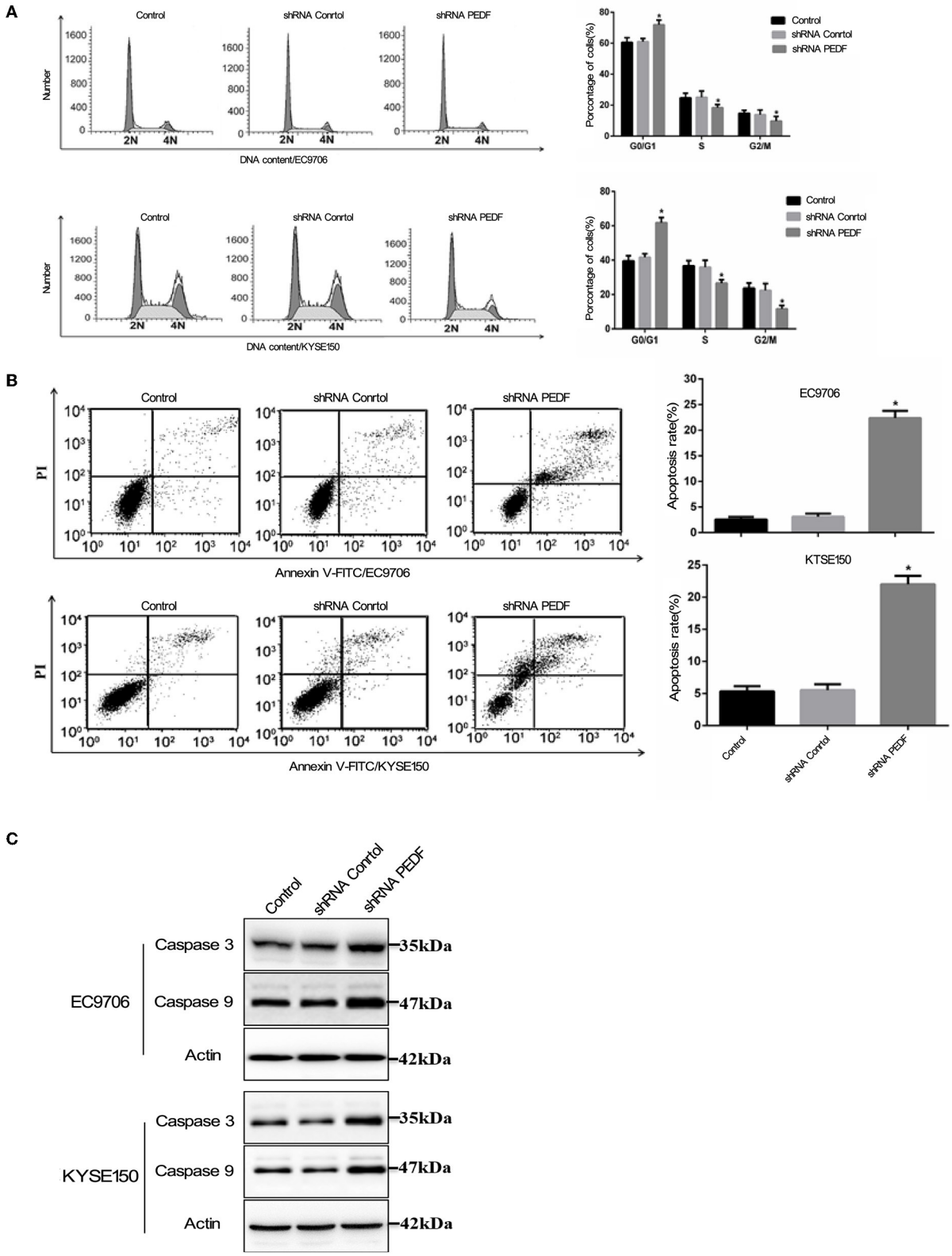

FIGURE 4 | Xenografts with or without PEDF knock down in nude mice. **(A)** Tumor size at the end time point. **(B)** Tumor volume over all time points. **(C)** Tumor weight at the end time point. * < 0.05.

migration compared to control group. There were less esophageal carcinoma cells migrated in shRNA-PEDF transfection group than those in control group. This result indicated that PEDF promote esophageal carcinoma cell migration (**Figure 2B**). The above results suggested that suppression of PEDF could reduce proliferation and migration of esophageal carcinoma cells.

PEDF Promotes Cell Cycle and Reduces Cell Apoptosis in Esophageal Squamous Cell Carcinoma

Because PEDF enhances esophageal carcinoma cell growth, we further investigated whether PEDF affects cell cycle and cell apoptosis. To explore the cell cycle change after shRNA transfection, esophageal carcinoma cells were stained with propidium iodide (PI) and analyzed by Flow cytometry. As expected, knocking down PEDF increased cells in G0/G1 phase and decreased cells in S phase and G2/M phase compared to shRNA scramble group (**Figure 3A**).

Flow cytometry was used to determine cell apoptosis after shRNA transfection and Annexin-V/PI staining. The result demonstrated that knocking down PEDF increased early apoptotic cells, late apoptotic cells, and necrotic cells (**Figure 3B**), suggesting that knocking down PEDF increased apoptosis of esophageal carcinoma cells. Furthermore, Western blot shows that the levels of caspase 3 and caspase 9 in the shRNA-PEDF group were higher than in control group (**Figure 3C**).

PEDF Promotes Tumourigenesis of Esophageal Squamous Cell Carcinoma *in vivo*

To further test the effect of PEDF in esophageal carcinoma cell growth *in vivo*, we establish xenograft mouse models. Nude mice were injected with EC9706 cells transfected with shRNA control or shRNA-PEDF. Similar to *in vitro* results, the tumor volume and tumor weight of xenografts in mice inoculated with shRNA-PEDF cells were smaller than that with shRNA control cells, suggesting that PEDF promotes esophageal carcinoma growth *in vivo* (**Figures 4A–C**).

DISCUSSION

PEDF is a 50 kDa secreted protein which is a versatile member of the widely expressed serpin family, also denoted as SERPINF1 (1). It plays important roles in angiogenesis, fibrogenesis, neuroprotection, bone matrix mineralization, and inflammation (4). Although PEDF was firstly identified as being produced by retinal pigment epithelial cells, it is now known to express in a variety of tissues and cell types, including chondrocytes, and synovial cells. PEDF is naturally present in serum (20, 21). In addition to the many beneficial effects that PEDF possesses, it is involved in the pathogenesis of diseases, such as chronic inflammatory diseases, atherosclerosis, type 2 diabetes, and some types of brain tumors (22, 23). Moreover, PEDF protects osteoblasts from glucocorticoid-induced apoptosis, and increases vascular permeability of triglycerides by ATGL degradation (24). Anti-inflammatory and antithrombotic effects of PEDF have been reported, and PEDF can also prevent the adhesion and invasion of liver cancer cells (25).

PEDF is associated with signaling pathways related to cancer development. PEDF can directly bind to PEDF receptor (PEDFR) and stimulate the activity of phospholipase (26). PEDFR is strongly linked to cell proliferation in cancers (27). Moreover, PEDF has an effect on cancer cell migration by activating MKK3 and MKK6. Tumor cell apoptosis is also regulated by PEDF acting on PPAR and NF-kB (28, 29). On the other hand, PEDF is a key regulatory factor in endothelial cells. Angiogenesis is inhibited by PEDF via cleaving VEGFR1 and VEGFR2 at the transmembrane region and VEGF-induced phosphorylation (30).

In this study, we demonstrate that PEDF is overexpressed in esophageal cancer tissues and cells compared to normal human counterparts. These results are consistent with studies of other cancers, such as prostate cancer (31). Previous studies have shown that the abnormal expression of PEDF is closely related to the pathological process of tumor development, including proliferation, migration, invasion, and apoptosis (32). shRNA-mediated knockdown of PEDF was reported to be effective in inhibiting the growth of melanoma (33). We investigated the impact of knockdown of PEDF on the progression of esophageal cancer *in vitro* and i*n vivo*. The results showed that shRNA-mediated reduction of PEDF significantly inhibited the proliferation and invasion of esophageal cancer cells and induced apoptosis. *In vivo* experiments further confirmed that shRNA-mediated PEDF knockdown significantly blocked xenograft esophageal tumor growth. Our results demonstrated that PEDF plays a role in the development of esophageal cancer. However, there was a report shown that PEDF may have potent antiangiogenic and antitumor effects in ESCC cells naturally not secreting endogenous PEDF, in the cell line secreting endogenous PEDF, there is no inhibition of angiogenesis and no subsequent antitumor properties (34).

Taken together, our study showed that PEDF expression is significantly increased in esophageal cancer tissues and cells. Knockdown of PEDF significantly inhibited esophageal cancer cell proliferation and tumourigenesis both *in vitro* and *in vivo*. Therefore, PEDF may serve as a prognostic biomarker and potential therapeutic target for esophageal cancer.

DATA AVAILABILITY STATEMENT

All datasets generated for this study are included in the article/supplementary material.

ETHICS STATEMENT

The studies involving human participants were reviewed and approved by the Ethics Committee of the Affiliated Huaian No.1 People's Hospital of Nanjing Medical University. The patients/participants provided their written informed consent to participate in this study. The animal study was reviewed and approved by Ethics committee of The Affiliated Huaian No.1 People's Hospital of Nanjing Medical University.

AUTHOR CONTRIBUTIONS

D-RT performed experiments and drafted the manuscript. CL-L carried out the cell culture. K-PX participated in the design. Q-QW, Q-YC, and J-JL collected tissue specimens. JJ carried out the Western blot analysis. BZ participated in Transwell invasion study. BG processed specimens. J-QZ conceived the study, coordination, and edited the manuscript. All authors read and approved the study.

REFERENCES

1. Zhu L, Zhang X, Fu X, Li Z, Sun Z, Wu J, et al. TIPE2 suppresses progression and tumourigenesis of esophageal carcinoma via inhibition of the Wnt/β-catenin pathway. *J Transl Med. (2018)* 16:7. doi: 10.1186/s12967-018-1383-0
2. Chen S, Zhou K, Yang L, Ding G, Li H. Racial differences in esophageal squamous cell carcinoma: incidence and molecular features. *Biomed Res Int*. (2017) 2017:1204082. doi: 10.1155/2017/1204082
3. Ohno-Matsui K, Yoshida T, Uetama T, Mochizuki M, Morita I. Vascular endothelial growth factor upregulates pigment epithelium-derived factor expression via VEGFR-1 in human retinal pigment epithelial cells. *Biochem Biophys Res Commun*. (2003) 303:962–7. doi: 10.1016/S0006-291X(03)00446-7
4. Bouck N. PEDF:anti-angiogenic guardian of ocular function. *Trends Mol Med*. (2002) 8:330–4. doi: 10.1016/S1471-4914(02)02362-6
5. Zhou Y, Xu F, Deng H, Bi Y, Sun W, Zhao Y, et al. PEDF expression is inhibited by insulin treatment in adipose tissue via suppressing 11β-HSD1. *PLoS ONE. (2013)* 8:e84016. doi: 10.1371/journal.pone.0084016
6. Moreno-Navarrete JM, Touskova V, Sabater M, Mraz M, Drapalova J, Ortega F, et al. Liver, but not adipose tissue PEDF gene expression is associated with insulin resistance. *Int J Obes.* (2013) 37:1230–7. doi: 10.1038/ijo.2012.223
7. Yang S, Luo T, Zhou H, Lv Q, Liu L, Zhang W, et al. Rosiglitazone inhibits expression and secretion of PEDF in adipose tissue and liver of male SD rats via a PPAR-γ independent mechanism. *Endocrinology*. (2014) 155:941–50. doi: 10.1210/en.2013-1813
8. Zhang W, Feng H, Gao Y, Sun L, Wang J, Li Y, et al. Role of pigment epithelium-derived factor. (PEDF) in arsenic-induced cell apoptosis of liver and brain in a rat model. *Biol Trace Elem Res*. (2013) 151:269–76. doi: 10.1007/s12011-012-9558-7
9. Jinnouchi Y, Yamagishi S, Matsui T, Takenaka K, Yoshida Y, Nakamura K, et al. Administration of pigment epithelium-derived factor. (PEDF) inhibits cold injury-induced brain edema in mice. *Brain Res*. (2007) 1167:92–100. doi: 10.1016/j.brainres.2007.04.088
10. Sanagi T, Yabe T, Yamada H. Gene transfer of PEDF attenuates ischemic brain damage in the rat middle cerebral artery occlusion model. *J Neurochem*. (2008) 106:1841–54. doi: 10.1111/j.1471-4159.2008.05529.x
11. Yoshida T, Akiba J, Matsui T, Nakamura K, Hisamoto T, Abe M, et al. Pigment epithelium-derived factor. (PEDF) Prevents hepatic fat storage, inflammation, and fibrosis in dietary steatohepatitis of mice. *Dig Dis Sci*. (2017) 62:1527–36. doi: 10.1007/s10620-017-4550-x
12. Feng C, Wu Z, Guo T, Jiang H, Guan M, Zhang Y, et al. BLCA-4 expression is related to MMP-9, VEGF, IL-1α and IL-8 in bladder cancer but not to PEDF, TNF-α or angiogenesis. *Pathol Biol*. (2012) 60:e36–40. doi: 10.1016/j.patbio.2011.11.009
13. Zhang L, Chen J, Ke Y, Mansel RE, Jiang WG. Down-regulation of PEDF expression by ribozyme transgene in endothelial and lung cancer cells and its impact on angiogenesis *in vitro*. *Oncol Rep*. (2005) 14:1615–9. doi: 10.3892/or.14.6.1615
14. Chen Y, Carlessi R, Walz N, Cruzat VF, Keane K, John AN, et al. Pigment epithelium-derived factor. (PEDF) regulates metabolism and insulin secretion from a clonal rat pancreatic beta cell line BRIN-BD11 and mouse islets. *Mol Cell Endocrinol*. (2016) 426:50–60. doi: 10.1016/j.mce.2016.02.004
15. Fernandez-Barral A, Orgaz JL, Gomez V, del Peso L, Calzada MJ, Jiménez B, et al. Hypoxia negatively regulates antimetastatic PEDF in melanoma cells by a hypoxia inducible factor-independent, autophagy dependent mechanism. *PLoS ONE.* (2012) 7:e32989. doi: 10.1371/journal.pone.0032989
16. Sahin N, Apaydin N, Töz E, Sivrikoz ON, Genç M, Turan GA, et al. Comparison of the effects of letrozole and cabergoline on vascular permeability, ovarian diameter, ovarian tissue VEGF levels, and blood PEDF levels, in a rat model of ovarian hyperstimulation syndrome. *Arch Gynecol Obstet*. (2016) 293:1101–6. doi: 10.1007/s00404-015-3987-4
17. Yin J, Park G, Kim TH, Hong JH, Kim YJ, Jin X, et al. Correction: pigment epithelium-derived factor. (PEDF) expression induced by EGFRvIII promotes self-renewal and tumour progression of glioma stem cells. *PLoS Biol.* (2016) 14:e1002367. doi: 10.1371/journal.pbio.1002367
18. Yin J, Park G, Kim TH, Hong JH, Kim YJ, Jin X, et al. Pigment epithelium-derived factor. (PEDF) expression induced by EGFRvIII promotes self-renewal and tumour progression of glioma stem cells. *PLoS Biol. (2015)* 13:e1002152. doi: 10.1371/journal.pbio.1002152
19. Jeng KS, Sheen IS, Jeng WJ, Su JC. PEDF effectively decreases VEGF to PEDF messenger RNA ratio of the inner edge of rat hepatocellular carcinoma induced by diethyl nitrosamine - an "in vivo" study. *Hepatogastroenterology*. (2012) 59:1484–90. doi: 10.5754/hge11543
20. Tahara N, Matsui T, Yamagishi S. Change in serum PEDF level after pioglitazone treatment is independently correlated with that in HOMA-IR. *Int J Cardiol*. (2014) 172:244–6. doi: 10.1016/j.ijcard.2013.12.289
21. Ji D, Li M, Zhan T, Yao Y, Shen J, Tian H, et al. Prognostic role of serum AZGP1, PEDF and PRDX2 in colorectal cancer patients. *Carcinogenesis*. (2013) 34:1265–72. doi: 10.1093/carcin/bgt056
22. Nakamura K, Yamagishi S, Adachi H, Kurita-Nakamura Y, Matsui T, Inoue H. Serum levels of pigment epithelium-derived factor. (PEDF) are positively associated with visceral adiposity in Japanese patients with type 2 diabetes. *Diabetes Metab Res Rev*. (2009) 25:52–6. doi: 10.1002/dmrr.820
23. Yamagishi S, Matsui T, Nakamura K, Takeuchi M, Imaizumi T. Pigment epithelium-derived factor. (PEDF) prevents diabetes- or advanced glycation end products. (AGE)-elicited retinal leukostasis. *Microvasc Res*. (2006) 72:86–90. doi: 10.1016/j.mvr.2006.04.002
24. Tombran-Tink J, Barnstable CJ. Osteoblasts and osteoclasts express PEDF, VEGF-A isoforms, and VEGF receptors:possible mediators of angiogenesis and matrix remodeling in the bone. *Biochem Biophys Res Commun*. (2004) 316:573–9. doi: 10.1016/j.bbrc.2004.02.076
25. Yoshida T, Yamagishi S, Nakamura K, Matsui T, Imaizumi T, Takeuchi M, et al. Pigment epithelium-derived factor. (PEDF) inhibits advanced glycation end product. (AGE)-induced C-reactive protein expression in hepatoma cells by suppressing Rac-1 activation. *FEBS Lett*. (2006) 580:2788–96. doi: 10.1016/j.febslet.2006.04.050
26. Zhao Q, Liu Z, Huang B, Yuan Y, Liu X, Zhang H, et al. PEDF improves cardiac function in rats subjected to myocardial ischemia/reperfusion injury by inhibiting ROS generation via PEDFR. *Int J Mol Med*. (2018) 41:3243–52. doi: 10.3892/ijmm.2018.3552
27. Hirsch J, Johnson CL, Nelius T, Kennedy R, Riese Wd, Filleur S. PEDF inhibits IL8 production in prostate cancer cells through PEDF receptor/phospholipase A2 and regulation of NFkappaB and PPARγ. *Cytokine*. (2011) 55:202–10. doi: 10.1016/j.cyto.2011.04.010
28. Ishibashi Y, Matsui T, Ohta K, Tanoue R, Takeuchi M, Asanuma K, et al. PEDF inhibits AGE-induced podocyte apoptosis via PPAR-gamma activation. *Microvasc Res*. (2013) 85:54–8. doi: 10.1016/j.mvr.2012.10.007
29. Gaetano C, Colussi C, Capogrossi MC. PEDF, PPAR-gamma, p53:deadly circuits arise when worlds collide. *Cardiovasc Res*. (2007) 76:195–6. doi: 10.1016/j.cardiores.2007.08.011
30. Zhu L, Xie J, Liu Z, Huang Z, Huang M, Yin H, et al. Pigment epithelium-derived factor/vascular endothelial growth factor ratio plays a crucial role in the spontaneous regression of infant hemangioma and in the therapeutic effect of propranolol. *Cancer Sci*. (2018) 109:1981–94. doi: 10.1111/cas.13611
31. Martinez-Marin D, Jarvis C, Nelius T, de Riese W, Volpert OV, Filleur S. PEDF increases the tumouricidal activity of macrophages towards prostate cancer cells *in vitro*. *PLoS ONE. (2017)* 12:e0174968. doi: 10.1371/journal.pone.0174968

32. Chen X, Li C, He T, Mao J, Li C, Lyu J, et al. Metformin inhibits prostate cancer cell proliferation, migration, and tumour growth through upregulation of PEDF expression. *Cancer Biol Ther*. (2016) 17:507–14. doi: 10.1080/15384047.2016.1156273
33. Zand S, Buzney E, Duncan LM, Dadras SS. Heterogeneity of metastatic melanoma: correlation of MITF with its transcriptional targets MLSN1, PEDF, HMB-45, and MART-1. *Am J Clin Pathol*. (2016) 146:353–60. doi: 10.1093/ajcp/aqw115
34. Kadoya M, Tamoto E, Shichinohe T, Hirano S. Pigment epithelium-derived factor inhibits the growth of human esophageal squamous cell carcinoma by suppressing neovascularization. *Hokkaido J Med Sci*. (2015) 90:17–29.

Conflict of Interest: The authors declare that the research was conducted in the absence of any commercial or financial relationships that could be construed as a potential conflict of interest.

frontiers in Oncology

ORIGINAL RESEARCH
published: 29 January 2020
doi: 10.3389/fonc.2019.01475

Knockdown of Thymidine Kinase 1 Suppresses Cell Proliferation, Invasion, Migration, and Epithelial–Mesenchymal Transition in Thyroid Carcinoma Cells

Chang Liu[1,2†], Jian Wang[3†], Li Zhao[4†], Hui He[4], Pan Zhao[1], Zheng Peng[1], Feiyuan Liu[1], Juan Chen[5], Weiqing Wu[4], Guangsuo Wang[3*] and Fajin Dong[6*]*

[1] Clinical Medical Research Center, First Affiliated Hospital of Southern University of Science and Technology, Second Clinical College of Jinan University, Shenzhen, China, [2] Central Lab, Dalian Municipal Central Hospital, Dalian, China, [3] Department of Thoracic Surgery, First Affiliated Hospital of Southern University of Science and Technology, Second Clinical College of Jinan University, Shenzhen, China, [4] Department of Health Management, First Affiliated Hospital of Southern University of Science and Technology, Second Clinical College of Jinan University, Shenzhen, China, [5] Department of Medical Research, Shenzhen Shekou People's Hospital, Shenzhen, China, [6] Department of Ultrasound, First Affiliated Hospital of Southern University of Science and Technology, Second Clinical College of Jinan University, Shenzhen, China

OPEN ACCESS

Edited by:
Chang Zou,
Shenzhen People's Hospital, Jinan University, China

Reviewed by:
Zhe-Sheng Chen,
St. John's University, United States
Yan Deng,
The Chinese University of Hong Kong, China

***Correspondence:**
Weiqing Wu
wweiqing007@sina.com
Guangsuo Wang
edward20111111@qq.com
Fajin Dong
dongfajin@szhospital.com

[†] These authors have contributed equally to this work

Specialty section:
This article was submitted to Molecular and Cellular Oncology, a section of the journal Frontiers in Oncology

Received: 10 October 2019
Accepted: 09 December 2019
Published: 29 January 2020

Citation:
Liu C, Wang J, Zhao L, He H, Zhao P, Peng Z, Liu F, Chen J, Wu W, Wang G and Dong F (2020) Knockdown of Thymidine Kinase 1 Suppresses Cell Proliferation, Invasion, Migration, and Epithelial–Mesenchymal Transition in Thyroid Carcinoma Cells. Front. Oncol. 9:1475. doi: 10.3389/fonc.2019.01475

Patients with advanced thyroid carcinoma have poor prognosis with low overall survival. Unfortunately, the underlying mechanisms of thyroid carcinoma progression remain unclear. The elevated expression of thymidine kinase 1 (TK1) has been implicated in the progression of thyroid carcinoma, while the role of TK1 in thyroid carcinoma progression has not been explored. The present study aimed to determine the role TK1 in the progression of thyroid cancer and to explore the underlying molecular mechanisms. In this study, it was found that serum TK1 levels were markedly increased in the patients with thyroid nodules. Further online data mining showed that TK1 expression was upregulated in thyroid carcinoma tissues, and higher expression of TK1 was correlated with shorter disease-free survival of patients with thyroid carcinoma. Silencing of TK1 suppressed cell proliferation, invasion, migration, and epithelial–mesenchymal transition, and also induced cell apoptosis in the thyroid carcinoma cell lines. Animal studies showed that TK1 knockdown inhibited *in vivo* tumor growth of thyroid carcinoma cells. Importantly, miR-34a-5p was found to be downregulated in the thyroid carcinoma cells. Furthermore, miR-34a-5p targeted the 3′ untranslated region of TK1 and suppressed the expression of TK1 in thyroid carcinoma cell lines. In summary, first, these results demonstrated the upregulation of TK1 in thyroid nodules and thyroid carcinoma tissues; second, TK1 promoted thyroid carcinoma cell proliferation, invasion, and migration; lastly, TK1 was negatively regulated by miR-34a-5p. Our study may provide novel insights into the role of TK1 in regulating thyroid carcinoma progression.

Keywords: thyroid carcinoma, thymidine kinase 1, thyroid nodules, progression, miR-34a-5p

INTRODUCTION

Thyroid carcinoma is one of the most common human malignancies, and the incidence rate of thyroid carcinoma is expected to gradually increase (1). Based on the characteristics of histology, thyroid carcinoma can be divided into four types including anaplastic, follicular, medullary, and papillary thyroid carcinoma (2). Papillary thyroid cancer is the main type of this malignancy and accounts for more than 80% of all cases (2). The thyroid carcinoma at the early stage is commonly curable; however, patients with advanced thyroid carcinoma have poor prognosis with relatively low 5-years survival rates (3, 4). In this regard, it is important to elucidate the molecular mechanisms of thyroid carcinoma development and to develop novel diagnostic and therapeutic strategies for thyroid carcinoma.

Thymidine kinase 1 (TK1) is an important regulatory factor in modulating cell cycle. During different stages of cell cycle, the activities of TK1 are increased at the late G1 phase and reached maximum levels at the late S phase (5, 6). Dysregulation of TK1 has been shown to be associated with the progression of human malignancies. Yu et al. screened a total of 56,178 human subjects in the southeast of China and proposed that serum TK1 was a potential biomarker for the early discovery of human subjects having the risk to process into malignancy (7). Wei et al. showed that TK1 overexpression was correlated with the poor prognosis of patients with lung cancer (8). Wang et al. demonstrated that determination of TK1 expression using immunohistology could improve the overall prediction of prognosis of ovarian cancer patients (9). Knockdown of TK1 inhibited the progression of pancreatic cancer cell via targeting E2F1-TK1-P21 axis (10). In the thyroid cancer, high levels of TK1 were correlated with the advanced clinical stage of patients with thyroid carcinoma (11). Unfortunately, the molecular mechanisms of TK1 in regulating thyroid carcinoma progression have not been explored yet.

MicroRNAs (miRNAs) are an abundant class of short (18–24 nt), endogenous non-coding RNAs that act as regulators at the transcriptional or post-transcriptional level of gene expression. MiRNAs can affect essential cellular processes including cell growth, cell differentiation, and apoptosis, which are closely correlated to carcinogenesis. Aberrant expression of miRNAs has been reported in various types of cancers including thyroid carcinoma. For example, plasma miR-346, miR-10a-5p, and miR-34a-5p were elevated in papillary thyroid carcinoma, which could be used as important biomarkers for the progression of thyroid carcinoma (12).

In this study, we identified the upregulation of TK1 in the serum of patients with thyroid nodules. The *in vitro* functional studies showed that TK1 silencing suppressed thyroid cancer cell proliferation, invasion, migration, epithelial–mesenchymal transition (EMT) and induced cell apoptosis. Furthermore, the upregulation of TK1 in the thyroid cancer may be related to the downregulation the tumor-suppressive miR-34a-5p.

MATERIALS AND METHODS

Clinical Samples

The serum samples were collected from 1,112 subjects who underwent the physical examination at First Affiliated Hospital of Southern University of Science and Technology, Second Clinical College of Jinan University between 2015 and 2018. Among the subjects, 431 patients were positive for thyroid nodules by ultrasound examination, and 681 patients were negative for thyroid nodules. The protein levels of TK1 in the serum were detected using the enzyme-linked immunosorbent assay (ELISA) assay kit (#ab223595, Abcam, Cambridge, USA). All the experimental protocols were approved by the Ethics Committee of the First Affiliated Hospital of Southern University of Science and Technology, and all the patients signed the written informed consent.

Cell Lines and Cell Culture

The normal human primary thyroid follicular epithelial cells (Nthy-ori 3-1, #90011609) and thyroid carcinoma cell line (TPC-1, #SCC147) were obtained from Merck (Darmstadt, USA). The thyroid carcinoma cell lines (BC-PAP, #ACC273) were obtained from the German Collection of Microorganisms and Cell Cultures (Braunschweig, Germany). The cells were cultured in RMPI-1640 medium (Sigma-Aldrich, St. Louis, USA) supplemented with 10% fetal bovine serum (FBS; #10100154, Life Technologies, Waltham, USA) and were kept in a humid atmosphere of 5% (*v*/*v*) CO_2 and 95% (*v*/*v*) air at 37°C.

Synthesis of Small Interfering RNAs and miRNAs, Cell Transfections

The small interfering RNAs (siRNAs) that silencing TK1 (TK1 siRNA#1 and #2) or the scrambled negative control (si-NC) were designed and synthesized by Ribobio (Guangzhou, China). The miRNA mimics for miR-34a-5p and the respective mimics NC were purchased from Thermo Fisher Scientific (Waltham, USA). The thyroid carcinoma cell transfections with these siRNAs or miRNAs were performed using Lipofectamine 2000 reagent (#11668030, Invitrogen, Carlsbad, USA) according to the manufacturer's protocol, and the transfected cells were collected after 24 h of transfection for further study.

Quantitative Real-Time PCR

Extraction of total RNAs from tissues or cells was performed using Trizol reagent (#15596018, Invitrogen) according to the manufacturer's protocol. For TK1 messenger RNA (mRNA) detection, RNAs were reversely transcribed into complementary DNA (cDNA) using the first-strand cDNA synthesis kit (#K1621, Thermo Fisher Scientific); for miR-34a-5p detection, RNAs were reversely transcribed into cDNA using the NCode miRNA first-strand cDNA synthesis kit (#MIRC10, Invitrogen). Real-time PCR was performed on an ABI7900 PCR system (Applied Biosystems, Foster City, USA) using SYBR Green PCR Master Mix (#RR820A, Takara, Dalian, China). GAPDH and U6 were used as internal control for TK1 and miR-34a-5p expression, respectively. The fold change between different groups was determined using comparative Ct method.

Western Blot

Extraction of proteins from tissues or cells was performed using radio-immunoprecipitation assay buffer (#P0013B, Beyotime, Beijing, China) supplied with the protease inhibitor cocktail (ST506, Beyotime). The protein concentrations were

determined using the bicinchoninic acid method (#23252, Thermo Fisher Scientific). Equal amount of 30 μg proteins was separated by sodium dodecyl sulfate–polyacrylamide gel electrophoresis followed by transferring to polyvinylidene fluoride membranes (#IPVH08100, Sigma-Aldrich). After incubating with 1.5% non-fat milk in the Tris-buffered saline Tween, the membranes were incubated with corresponding primary antibodies including TK1 (1:1,000; #8960, Cell Signaling Technology, Danvers, USA), active caspase-3 (1:1,000; #9661, Cell Signaling Technology), active caspase-9 (1:1,000; #7237, Cell Signaling Technology), vimentin (1:1,000) (5,741, Cell Signaling Technology), N-cadherin (1:1,000; #14215, Cell Signaling Technology), E-cadherin (1:1,000; #14472, Cell Signaling Technology), and β-actin (1:1,000; #3700, Cell Signaling Technology). After incubating with above primary antibodies overnight at 4°C, membranes were then further probed against the respective horseradish-conjugated secondary antibodies (1:2,000; #7074, #7076, Cell Signaling Technology) at room temperature for 2 h. Protein detection was performed using the enhanced chemiluminescence kit (#15159, Thermo Fisher Scientific) according to the manufacturer's protocol. β-Actin served as the loading control.

Cell Counting Kit-8 and Colony Formation Assays

Cell proliferation was measured by cell counting kit-8 (CCK-8) assay (#C0039, Beyotime) in thyroid carcinoma cells at 0, 24, 48, and 72 h after transfection. Briefly, the transfected thyroid cells were incubated with 10 μl CCK-8 reagent for 1 h at 37°C. The cell proliferation values were determined by measuring optical density values at 450 nm.

Cell growth was measured by colony formation assay. Briefly, the transfected thyroid carcinoma cells were seeded into a six-well plate at a density of 500 cells per well, after growing for 10 days, the cells were fixed with methanol for 10 min and stained with 0.1% crystal violet (#C0121, Beyotime) for 10 min. The number of colonies was counted under a light microscope (TE2000, Nikon, Tokyo, Japan).

Transwell Invasion Assay

Thyroid carcinoma cell invasion was measured by Transwell invasion assay. Briefly, the Matri-gel (#E6909, Sigma-Aldrich) was coated on the 8-μm pore size membrane Transwell inserts (#140629, Thermo Fisher Scientific), and the coated inserted were placed into the wells of a 24-well plate (#142475, Thermo Fisher Scientific). The transfected thyroid carcinoma cells were seeded onto the upper chamber filled with FBS-free RMPI-1640 medium, while the bottom chamber was filled with RMPI-1640 medium supplied with 10% FBS. After incubation for 24 h, the non-invaded carcinoma cells were removed from the upper surface of the membrane, and cells in the lower surface of the membrane were fixed with methanol for 20 min and stained with 0.5% crystal violet for 15 min. The number of invaded cells was counted under a microscope by randomly selecting five fields.

Wound Healing Assay

Thyroid carcinoma cell migration was determined by wounding healing assay. Briefly, the transfected thyroid carcinoma cells were seeded onto the six-well plates (#140675, Thermo Fisher Scientific) and cultured for 24 h. The wound was created on the monolayer cells using a sterile 200-μl tip (#94410313, Thermo Fisher Scientific), and the cells were further cultured for 24 h. The wound width was measured at 0 and 24 h, respectively. The percentage of wound closure was calculated by (wound width at 24 h—wound width at 0 h)/wound width at 0 h.

Flow Cytometry

The cell apoptosis of thyroid carcinoma cells was detected using Annexin V-fluorescein isothiocyanate/propidium iodide

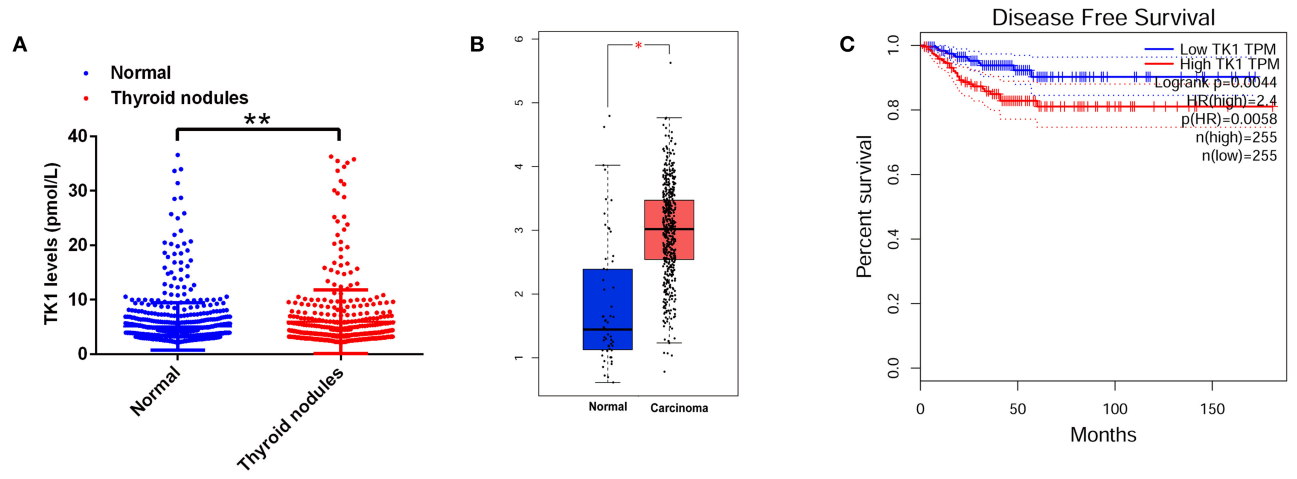

FIGURE 1 | Thymidine kinase 1 (TK1) was upregulated in patients with thyroid nodules and thyroid carcinoma. **(A)** The serum TK1 levels of normal subjects and subjects with thyroid nodules were detected by ELISA assay. **(B)** Online database [The Cancer Genome Atlas (TCGA)] analysis of the TK1 expression levels in the thyroid tissues from normal subjects and thyroid carcinoma patients. **(C)** The disease-free survival of the thyroid carcinoma patients as stratified by TK1 expression levels. $^{*}P < 0.05$ and $^{**}P < 0.01$.

(PI) apoptosis detection kit (#V13241, Thermo Fisher Scientific). Briefly, the transfected thyroid carcinoma cells were trypsinized and collected, and the cells were incubated with Annexin V-fluorescein isothiocyanate and PI in binding buffer for 10 min. The stained cells were then analyzed using a BD FACSCanto II flow cytometer (BD Biosciences, San Jose, USA).

Caspase-3 Activity Assay

The caspase-3 activity of the transfected thyroid carcinoma cells was determined using a caspase-3 activity assay kit (#5723, Cell Signaling Technology) according to the manufacturer's protocol.

In vivo Tumor Growth Assay

A total of 12 male BALB/nude mice (6–8 weeks old) were obtained from Guangzhou Laboratory Animal Center (Guangzhou, China). All animal experiments were approved by the Animal Ethics Committee of First Affiliated Hospital of Southern University of Science and Technology. TPC-1 cells (5×10^6 cells) with stably expressing TK1 shRNA (sh_TK1) or scrambled negative control shRNA (sh_NC) were subcutaneously injected into the right flank of the nude mice and six animals in each group. After injection of carcinoma cells, the tumor volume of the nude mice was measured every 7 days for 42 days. At the end of the experiments, the mice were killed, and the tumor tissues were collected for further analysis.

Dual-Luciferase Reporter Assay

To construct the reporter vectors, the 3′ untranslated region (UTR) of TK1 containing the putative binding sites of miR-34a-5p was amplified by PCR and cloned into downstream of the luciferase gene of the pGL3 vector (#E1751, Promega,

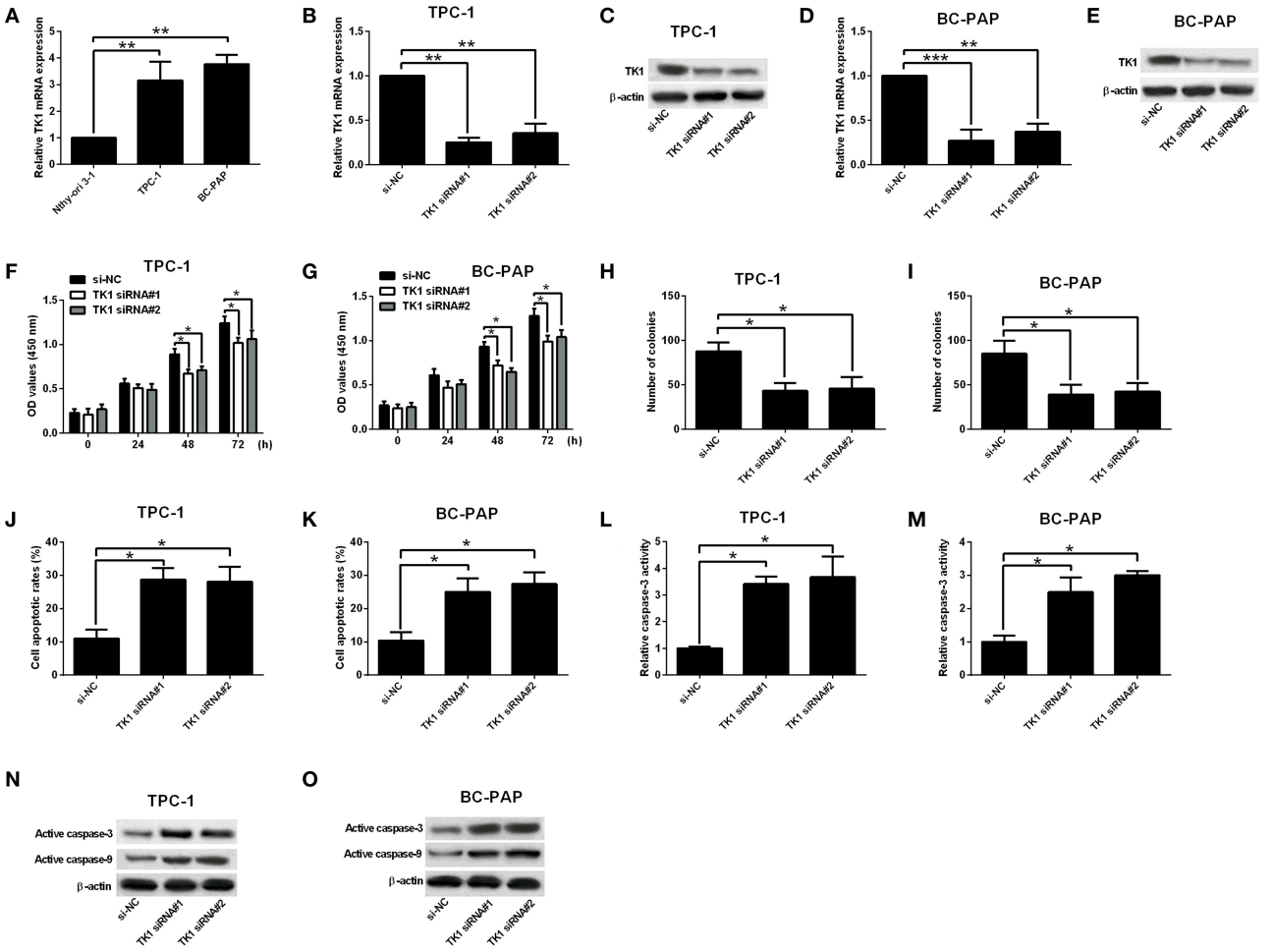

FIGURE 2 | Thymidine kinase 1 (TK1) knockdown suppressed thyroid carcinoma cell proliferation and induced cell apoptosis. **(A)** Quantitative real-time PCR (qRT-PCR) analysis of TK1 messenger RNA (mRNA) expression level in normal thyroid follicular epithelial cells and thyroid carcinoma cells (TPC-1 and BC-PAP). **(B–E)** qRT-PCR and Western blot analysis of TK1 mRNA and protein expression levels in TPC-1 and BC-PAP cells after scrambled siRNA (si-NC) or TK1 siRNAs (TK1 siRNA#1 or #2) transfections. **(F,G)** Cells proliferation by CCK-8 assay was determined in TPC-1 and BC-PAP cells, respectively. **(H,I)** Colony formation ability was assessed in TPC-1 and BC-PAP cells, respectively. **(J,K)** Flow cytometry analysis was used to detect the cell apoptotic rates in TPC-1 and BC-PAP cells, respectively. **(L,M)** Caspase-3 activity assay was used to determine the capsase-3 activity of TPC-1 and BC-PAP cells, respectively. **(N,O)** Protein expression levels of active caspase-3 and caspase-9 in TPC-1 and BC-PAP cells were detected by Western blot, respectively. $N = 3$; $^*P < 0.05$, $^{**}P < 0.01$, and $^{***}P < 0.001$.

Madison, USA). The mutant reporter vectors were generated by mutating three nucleotides in the binding region. Thyroid carcinoma cells were cotransfected with reporter vectors and miRNAs using Lipofectamine 2000 reagent (Invitrogen). At 24 h after transfection, luciferase activity in the thyroid carcinoma cells was determined using the Dual-Luciferase Reporter Assay System (#E1910, Promega).

Statistical Analysis

All data analysis was performed using GraphPad Prism (Version 5.0; GraphPad Software, La Jolla, USA). Summary data are presented as the mean ± standard deviation. Significant differences between different groups were evaluated using Student's *t* test or one-way ANOVA followed by Bonferroni's *post hoc* test. Statistical significance was set at $P < 0.05$.

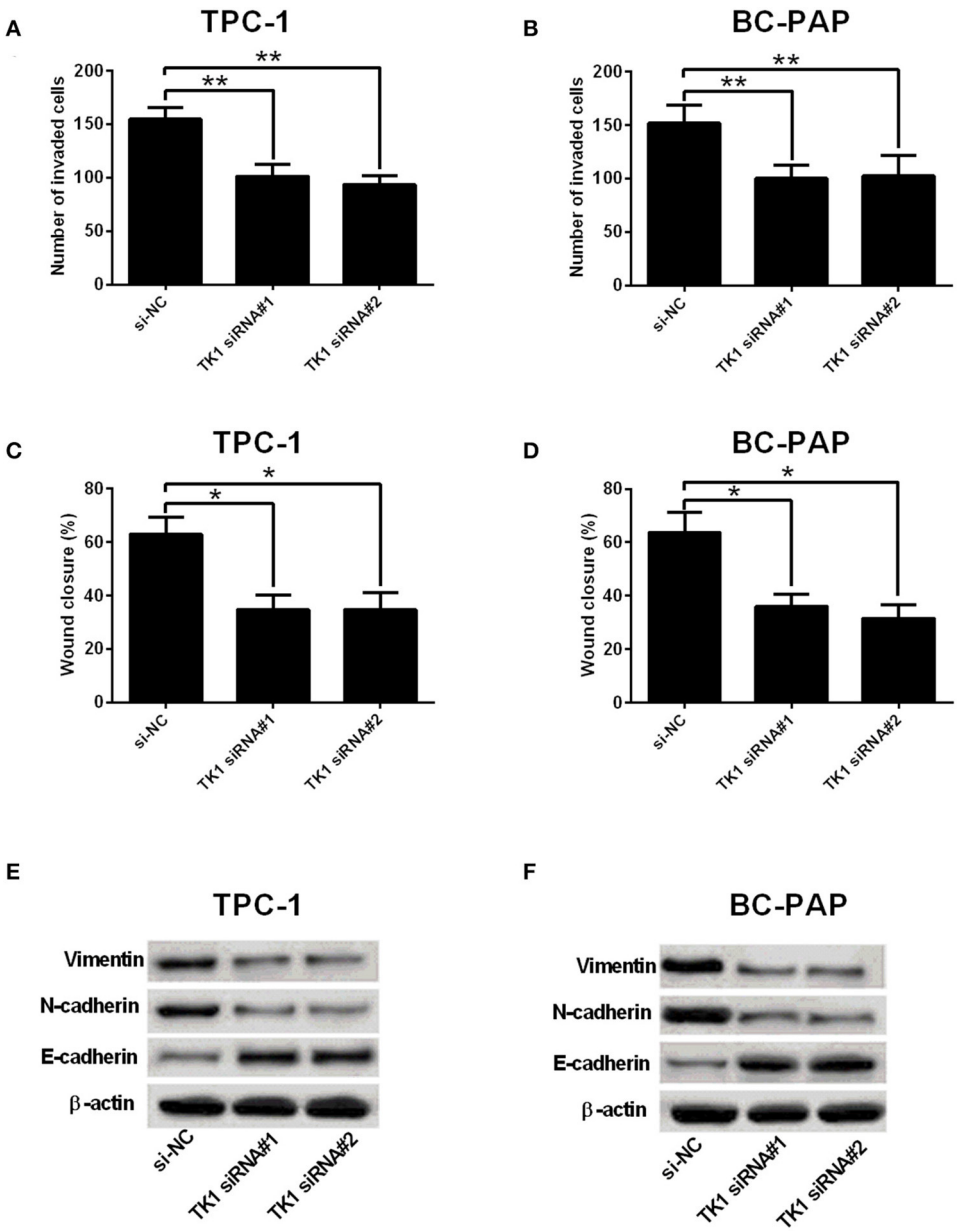

FIGURE 3 | Thymidine kinase 1 (TK1) knockdown suppressed thyroid carcinoma cell invasion, migration, and EMT. **(A,B)** Transwell invasion assay was used to investigate the invasion ability of TPC-1 and BC-PAP cells transfected with scrambled siRNA (si-NC) or TK1 siRNAs (TK1 siRNA#1 or #2), respectively. **(C,D)** The migration ability of TPC-1 and BC-PAP cells transfected with scrambled siRNA (si-NC) or TK1 siRNAs (TK1 siRNA#1 or #2) was assessed by wound healing assay, respectively. **(E,F)** Protein expression levels of epithelial–mesenchymal transition (EMT)-related markers vimentin, N-cadherin, and E-cadherin in TPC-1 and BC-PAP cells transfected with scrambled siRNA (si-NC) or TK1 siRNAs (TK1 siRNA#1 or #2) were detected by Western blot. $N = 3$; $^{*}P < 0.05$ and $^{**}P < 0.01$.

RESULTS

TK1 Was Upregulated in Serum From Patients With Thyroid Nodules and Was Upregulated in the Thyroid Carcinoma Tissues

We first analyzed the serum TK1 protein levels from the subjects who underwent physical examination in our hospital and found that serum TK1 levels were significantly higher in the subjects with thyroid nodules compared to the normal subjects (**Figure 1A**). A further analysis using data mining tool (http://gepia.cancer-pku.cn/) showed that TK1 was markedly upregulated in the thyroid carcinoma tissues when compared to normal thyroid tissues (**Figure 1B**). In addition, patients with higher expression of TK1 had poorer disease-free survival when compared to patients with lower expression of TK1 (**Figure 1C**).

TK1 Knockdown Suppressed Thyroid Carcinoma Cell Proliferation and Induced Cell Apoptosis

The mRNA expression of TK1 in carcinoma cells as well as in normal thyroid follicular epithelial cells was investigated. TK1 was upregulated in carcinoma cells when compared to normal thyroid follicular epithelial cells (**Figure 2A**). To determine whether the knockdown of TK1 could reserve the aggressiveness of carcinoma cells, TPC-1 and BC-PAP cells were transfected with scrambled siRNA or TK1 siRNAs. TK1 siRNA transfection significantly repressed mRNA and protein expression levels of TK1 in TPC-1 and BC-PAP cells when compared to scrambled siRNA transfection (**Figures 2B–E**). CCK-8 and colony formation assays showed that TK1 knockdown suppressed the TPC-1 and BC-PAP cell proliferation (**Figures 2F,G**) and colony formation ability (**Figures 2H,I**). Flow cytometry and caspase-3 activity analysis showed that TK1 knockdown increased cell apoptotic rates (**Figures 2J,K**) and caspase-3 activity of TPC-1 and BC-PAP cells (**Figures 2L,M**). The Western blot assay showed that TK1 knockdown increased the protein levels of active caspase-3 and caspase-9 in TPC-1 and BC-PAP cells (**Figures 2N,O**).

TK1 Knockdown Suppressed Thyroid Carcinoma Cell Invasion, Migration, and Epithelial–Mesenchymal Transition

A further analysis of cell invasion and migration using Transwell invasion assay and wound healing assay, respectively, showed that TK1 knockdown markedly suppressed TPC-1 and BC-PAP cell invasion (**Figures 3A,B**) and migration (**Figures 3C,D**). In addition, it was found that TK1 knockdown suppressed the protein levels of EMT-related markers vimentin and N-cadherin but increased the protein levels of E-cadherin (**Figures 3E,F**).

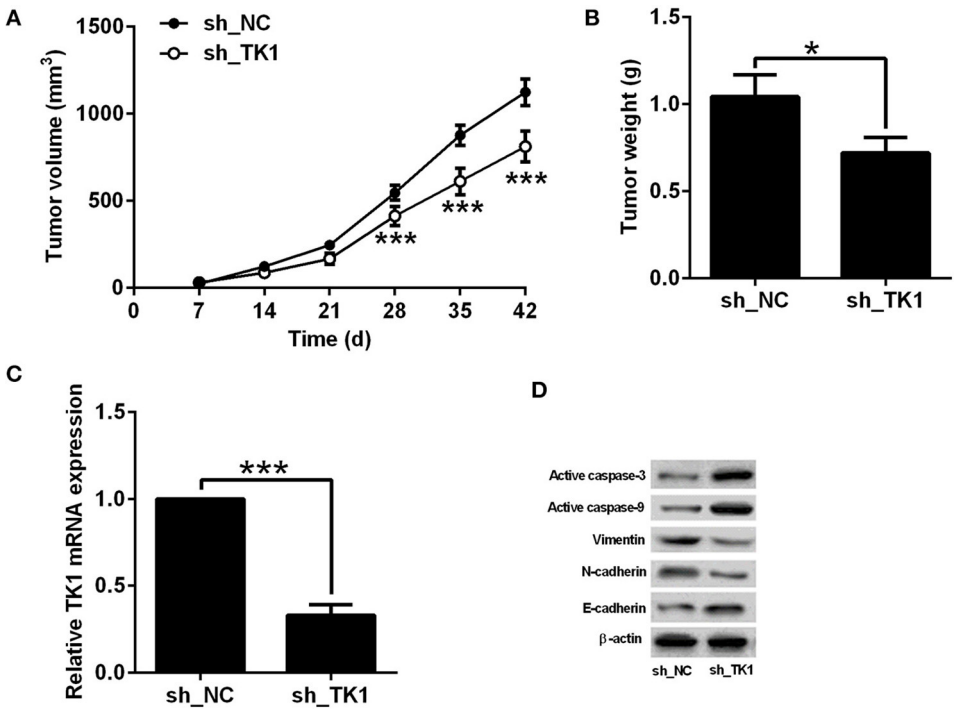

FIGURE 4 | Thymidine kinase 1 (TK1) knockdown suppressed *in vivo* tumor growth of thyroid carcinoma cells. **(A)** *In vivo* tumor growth of TPC-1 cells from sh_NC group and sh_TK1 group. **(B)** Weight of the tumor tissues from sh_NC and sh_TK1 group. **(C)** qRT-PCR analysis of TK1 mRNA expression levels in tumor tissues from sh_NC and sh_TK1 groups. **(D)** Western blot analysis of active caspase-3, caspase-9, vimentin, N-cadherin, and E-cadherin protein expression levels of the tumor tissues from sh_NC and sh_TK1. $N = 6$; $^{*}P < 0.05$ and $^{***}P < 0.001$.

TK1 Knockdown Suppressed *in vivo* Tumor Growth of Thyroid Carcinoma Cells

The effects of TK1 knockdown on the *in vivo* tumor growth of TPC-1 were evaluated in nude mice xenografts model. As shown in **Figure 4A**, TK1 knockdown reduced the tumor volume in the nude mice; consistently, the weight of dissected tumor tissue was significantly lower in the h_TK1 group when compared to the sh_NC group (**Figure 4B**). The quantitative real-time PCR analysis showed that TK1 was downregulated in the tumor tissues from the sh_TK1 group when compared to the sh_NC group (**Figure 4C**). In addition, TK1 knockdown increased the protein levels of active caspase-3, caspase-9, and E-cadherin, but decreased the protein levels of vimentin and N-cadherin (**Figure 4D**).

TK1 Expression Was Regulated by miR-34a-5p in Thyroid Carcinoma Cells

To determine the factors that contribute to the upregulation of TK1 in thyroid carcinoma, the StarBase tool (http://starbase.sysu.edu.cn/index.php) was used to predict miRNAs that could regulate TK1 expression. Among the predicted miRNAs, miR-34a-5p was selected for examination, and it was downregulated in the TPC-1 and BC-PAP cells when compared to normal thyroid follicular epithelial cells (**Figure 5A**). The overexpression of miR-34a-5p was achieved by transfecting TPC-1 and BC-PAP cells with miR-34a-5p mimics (**Figures 5B,C**). Furthermore, the luciferase reporter assay was performed to determine the interaction between miR-34a-5p and TK1. The putative binding sites between TK1 3′UTR and miR-34a-5p are shown in **Figure 5D**. Overexpression of miR-34a-5p significantly suppressed the luciferase activity of the wild-type luciferase constructs but not the mutant ones in TPC-1 and BC-PAP cells (**Figures 5E,F**). Consistently, miR-34a-5p overexpression markedly repressed the mRNA and protein expression levels of TK1 in both TPC-1 and BC-PAP cells (**Figures 5G–J**).

DISCUSSION

Patients with advanced thyroid carcinoma had poor prognosis with low overall survival (13, 14). Unfortunately, the

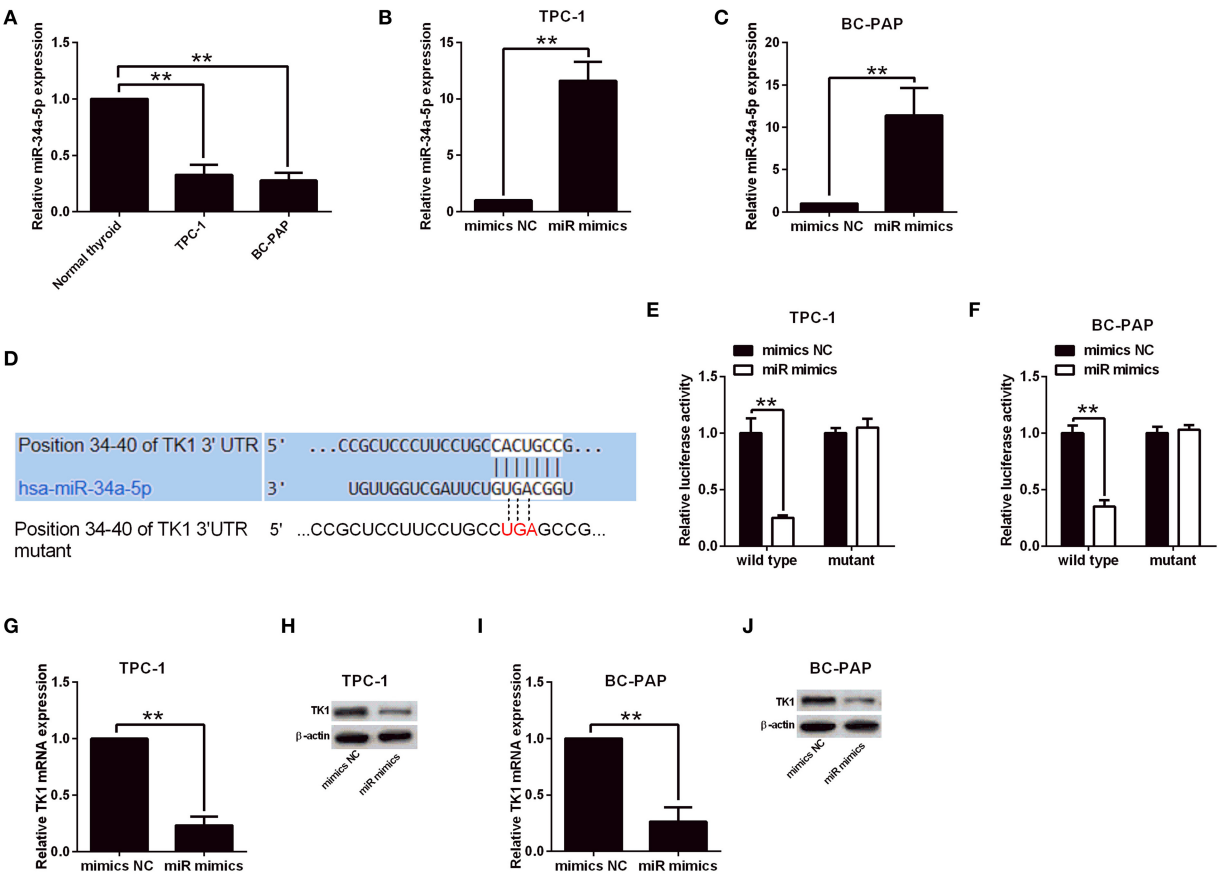

FIGURE 5 | Thymidine kinase 1 (TK1) expression was regulated by miR-34a-5p in thyroid carcinoma cells. **(A)** Quantitative real-time PCR (qRT-PCR) analysis of miR-34a-5p expression level in normal thyroid follicular epithelial cells, TPC-1 and BC-PAP cells. **(B,C)** MiR-34a-5p expression in TPC-1 and BC-PAP cells with mimics NC or miR mimics transfection, respectively, by qRT-PCR analysis. **(D)** Predicted binding sites between TK1 3′UTR and miR-34a-5p by TargetScan tool. **(E,F)** Luciferase reporter assay was used to investigate luciferase activity of wild and mutant TPC-1 and BC-PAP cells with miRNAs and luciferase reporter vectors cotransfection, respectively. **(G–J)** qRT-PCR and Western blot were used to detect TK1 mRNA and protein expression levels in TPC-1 and BC-PAP cells with mimics NC or miR mimics transfection, respectively. $N = 3$; $^{**}P < 0.01$.

underlying mechanisms of thyroid carcinoma progression remain unclear. The elevated expression of TK1 has been implicated in the progression of thyroid carcinoma (11), while the role of TK1 in thyroid carcinoma progression has not been explored. In this study, we found that serum TK1 levels were markedly increased in the patients with thyroid nodules. Further online data mining showed that TK1 expression was upregulated in thyroid carcinoma tissues, and higher expression of TK1 was correlated with shorter DFS of patients with thyroid carcinoma. Silencing of TK1 suppressed cell proliferation, invasion, migration, and EMT and also induced cell apoptosis in the thyroid carcinoma cell lines. *In vivo* data showed that TK1 knockdown inhibited *in vivo* tumor growth of thyroid carcinoma cells. Moreover, the upregulated TK1 in the thyroid carcinoma cells was associated with the downregulation of miR-34a-5p.

The prognostic role of TK1 has been widely studied in the cancer studies (5, 6, 15, 16). The increased Tk1 mRNA levels in the plasma-derived exosomes are associated with clinical resistance to CDK4/6 inhibitors in metastatic breast cancer patients (17). Using immunohistochemistry, TK1 was found to be located on the cellular membrane of the colorectal, lung, and breast cancer cells. The upregulation of TK1 in these malignant tissues indicated the potential prognostic role of TK1 (18). Serum detection of TK1 is sensitive and specific for the prediction of early stage and advanced lung cancer (19). In this study, it was showed that serum TK1 levels were upregulated in patients with thyroid nodules, suggesting that TK1 might be involved in the development of thyroid cancer. Our findings were in accordance with the previous studies that thyroid carcinoma tissues were accompanied with higher expression levels of TK1 (20). Besides, the i*n vitro* studies showed the consistent upregulation of TK1 in thyroid carcinoma cells.

In this study, it was the first time to show that TK1 knockdown suppressed *in vitro* and *in vivo* carcinoma cell progression. It was reported in pancreatic cancer the silencing of TK1 suppressed cancer cell proliferation via inducing S phase arrest by P21 upregulation. P21was an inhibitor of the cyclin-dependent kinase and could inhibit the activation of CDK1, CDK2, and CDK4. TK1 might interact with P21 by combining with the C-terminal domain of P21, and promote the proliferation of cancer cells (21). In addition, growth and differentiation factor 15 was considered to be the main downstream mediator of TK1 function, which induced the metastatic attributes of lung cancer cells (22). Taken together, the results in this study might imply that TK1 promoted thyroid carcinoma progression via P21 or growth and differentiation factor 15 by increasing cell proliferation, invasion, and migration.

The bioinformatic prediction results revealed that TK1 could be potentially regulated by miRNAs. MiR-34a-5p was found to be upregulated in the thyroid carcinoma cell lines. Further studies showed that miR-34a-5p repressed TK1 expression in thyroid carcinoma cells via targeting the 3′UTR of TK1. Previously, miR-34a-5p was shown to be downregulated in the thyroid carcinoma tissues and played a tumor-suppressive role in the thyroid carcinoma cells (23). In addition, miR-34a-5p also functioned as tumor-suppressive factor in esophageal squamous cell carcinoma (24), non-small cell lung cancer (25), and breast cancer (26). Collectively, the upregulation of TK1 may be related to downregulated miR-34a-5p expression, which contributed to the enhanced progression of thyroid carcinoma.

In summary, the results in this study demonstrated the upregulation of TK1 in thyroid nodules as well as thyroid carcinoma tissues. The downregulated miR-34a-5p in thyroid carcinoma resulted in higher TK1 level, which promoted thyroid carcinoma cell proliferation, invasion, and migration. This study may provide novel insights into the role TK1 played in regulating thyroid carcinoma progression. However, there are still some limitations in this study. For example, although higher level of TK1 was confirmed in thyroid cancer patients, the lower expression level of miR-34a-5p was not detected. In addition, the upregulated TK1 in thyroid cancer patient may be resulted from the downregulated miR-34a-5p, but the upstream and downstream molecular mechanisms were still unclear. To further investigate and elucidate the role of TK1 in thyroid carcinoma progression, future studies are necessary.

DATA AVAILABILITY STATEMENT

The raw data supporting the conclusions of this article will be made available by the authors, without undue reservation, to any qualified researcher.

ETHICS STATEMENT

The studies involving human participants were reviewed and approved, and all the experimental protocols were approved by the Ethics Committee of the First Affiliated Hospital of Southern University of Science and Technology. The patients/participants provided their written informed consent to participate in this study. The animal study was reviewed and approved by All the animal experiments were approved by the Animal Ethics Committee of First Affiliated Hospital of Southern University of Science and Technology.

AUTHOR CONTRIBUTIONS

WW, GW, and FD designed and supervised the whole study. CL, JW, and LZ performed the experiments. HH, PZ, and ZP collected the serum samples. FL and JC performed the data analysis. WW wrote the manuscript. All authors approved the manuscript for submission.

FUNDING

The study was supported by the First Affiliated Hospital of Southern University of Science and Technology, Second Clinical College of Jinan University.

REFERENCES

1. Sanabria A, Kowalski LP, Shah JP, Nixon IJ, Angelos P, Williams MD, et al. Growing incidence of thyroid carcinoma in recent years: factors underlying overdiagnosis. *Head Neck.* (2018) 40:855–66. doi: 10.1002/hed.25029
2. Cabanillas ME, McFadden DG, Durante C. Thyroid cancer. *Lancet.* (2016) 388:2783–95. doi: 10.1016/S0140-6736(16)30172-6
3. Leboulleux S, Tuttle RM, Pacini F, Schlumberger M. Papillary thyroid microcarcinoma: time to shift from surgery to active surveillance? *Lancet Diabetes Endocrinol.* (2016) 4:933–42. doi: 10.1016/S2213-8587(16)30180-2
4. Grani G, Lamartina L, Durante C, Filetti S, Cooper DS. Follicular thyroid cancer and Hurthle cell carcinoma: challenges in diagnosis, treatment, and clinical management. *Lancet Diabetes Endocrinol.* (2018) 6:500–14. doi: 10.1016/S2213-8587(17)30325-X
5. Zhou J, He E, Skog S. The proliferation marker thymidine kinase 1 in clinical use. *Mol Clin Oncol.* (2013) 1:18–28. doi: 10.3892/mco.2012.19
6. Jagarlamudi KK, Shaw M. Thymidine kinase 1 as a tumor biomarker: technical advances offer new potential to an old biomarker. *Biomark Med.* (2018) 12:1035–48. doi: 10.2217/bmm-2018-0157
7. Wang Y, Jiang X, Wang S, Yu H, Zhang T, Xu S, et al. Serological TK1 predict pre-cancer in routine health screenings of 56,178 people. *Cancer Biomark.* (2018) 22:237–47. doi: 10.3233/CBM-170846
8. Wei YT, Luo YZ, Feng ZQ, Huang QX, Mo AS, Mo SX. TK1 overexpression is associated with the poor outcomes of lung cancer patients: a systematic review and meta-analysis. *Biomark Med.* (2018) 12:403–13. doi: 10.2217/bmm-2017-0249
9. Wang J, Liu Q, Zhou X, He Y, Guo Q, Shi Q, et al. Thymidine kinase 1 expression in ovarian serous adenocarcinoma is superior to Ki-67: a new prognostic biomarker. *Tumour Biol.* (2017) 39:1010428317706479. doi: 10.1177/1010428317706479
10. Zhu X, Shi C, Peng Y, Yin L, Tu M, Chen Q, et al. Thymidine kinase 1 silencing retards proliferative activity of pancreatic cancer cell via E2F1-TK1-P21 axis. *Cell Prolif.* (2018) 51:e12428. doi: 10.1111/cpr.12428
11. Chen Y, Ying M, Chen Y, Hu M, Lin Y, Chen D, et al. Serum thymidine kinase 1 correlates to clinical stages and clinical reactions and monitors the outcome of therapy of 1,247 cancer patients in routine clinical settings. *Int J Clin Oncol.* (2010) 15:359–68. doi: 10.1007/s10147-010-0067-4
12. Wang Z, Lv J, Zou X, Huang Z, Zhang H, Liu Q, et al. A three plasma microRNA signature for papillary thyroid carcinoma diagnosis in Chinese patients. *Gene.* (2019) 693:37–45. doi: 10.1016/j.gene.2019.01.016
13. Henke LE, Pfeifer JD, Baranski TJ, DeWees T, Grigsby PW. Long-term outcomes of follicular variant vs. classic papillary thyroid carcinoma. *Endocr Connect.* (2018) 7:1226–35. doi: 10.1530/EC-18-0264
14. Cho SG, Kwon SY, Kim J, Cho DH, Na MH, Kang SR, et al. Risk factors of malignant fluorodeoxyglucose-avid lymph node on preablation positron emission tomography in patients with papillary thyroid cancer undergoing radioiodine ablation therapy. *Medicine.* (2019) 98:e14858. doi: 10.1097/MD.0000000000014858
15. von Euler H, Eriksson S. Comparative aspects of the proliferation marker thymidine kinase 1 in human and canine tumour diseases. *Vet Comp Oncol.* (2011) 9:1–15. doi: 10.1111/j.1476-5829.2010.00238.x
16. Aufderklamm S, Todenhofer T, Gakis G, Kruck S, Hennenlotter J, Stenzl A, et al. Thymidine kinase and cancer monitoring. *Cancer Lett.* (2012) 316:6–10. doi: 10.1016/j.canlet.2011.10.025
17. Del Re M, Bertolini I, Crucitta S, Fontanelli L, Rofi E, De Angelis C, et al. Overexpression of TK1 and CDK9 in plasma-derived exosomes is associated with clinical resistance to CDK4/6 inhibitors in metastatic breast cancer patients. *Breast Cancer Res Treat.* (2019) 178:57–62. doi: 10.1007/s10549-019-05365-y
18. Weagel EG, Burrup W, Kovtun R, Velazquez EJ, Felsted AM, Townsend MH, et al. Membrane expression of thymidine kinase 1 and potential clinical relevance in lung, breast, and colorectal malignancies. *Cancer Cell Int.* (2018) 18:135. doi: 10.1186/s12935-018-0633-9
19. Alegre MM, Weyant MJ, Bennett DT, Yu JA, Ramsden MK, Elnaggar A, et al. Serum detection of thymidine kinase 1 as a means of early detection of lung cancer. *Anticancer Res.* (2014) 34:2145–51.
20. Karbownik M, Brzezianska E, Lewinski A. Increased expression of mRNA specific for thymidine kinase, deoxycytidine kinase or thymidine phosphorylase in human papillary thyroid carcinoma. *Cancer Lett.* (2005) 225:267–73. doi: 10.1016/j.canlet.2004.10.044
21. Park JJ, Park MH, Oh EH, Soung NK, Lee SJ, Jung JK, et al. The p21-activated kinase 4-Slug transcription factor axis promotes epithelial-mesenchymal transition and worsens prognosis in prostate cancer. *Oncogene.* (2018) 37:5147–59. doi: 10.1038/s41388-018-0327-8
22. Malvi P, Janostiak R, Nagarajan A, Cai G, Wajapeyee N. Loss of thymidine kinase 1 inhibits lung cancer growth and metastatic attributes by reducing GDF15 expression. *PLoS Genet.* (2019) 15:e1008439. doi: 10.1371/journal.pgen.1008439
23. Liu H, Deng H, Zhao Y, Li C, Liang Y. LncRNA XIST/miR-34a axis modulates the cell proliferation and tumor growth of thyroid cancer through MET-PI3K-AKT signaling. *J Exp Clin Cancer Res.* (2018) 37:279. doi: 10.1186/s13046-018-0950-9
24. Zhou H, Yang L, Xu X, Lu M, Guo R, Li D, et al. miR-34a inhibits esophageal squamous cell carcinoma progression via regulation of FOXM1. *Oncol Lett.* (2019) 17:706–12. doi: 10.3892/ol.2018.9593
25. Wang F, Li Z, Xu L, Li Y, Li Y, Zhang X, et al. LIMD2 targeted by miR34a promotes the proliferation and invasion of nonsmall cell lung cancer cells. *Mol Med Rep.* (2018) 18:4760–6. doi: 10.3892/mmr.2018.9464
26. Rui X, Zhao H, Xiao X, Wang L, Mo L, Yao Y. MicroRNA-34a suppresses breast cancer cell proliferation and invasion by targeting Notch1. *Exp Ther Med.* (2018) 16:4387–92. doi: 10.3892/etm.2018.6744

Conflict of Interest: The authors declare that the research was conducted in the absence of any commercial or financial relationships that could be construed as a potential conflict of interest.

frontiers in Oncology

ORIGINAL RESEARCH
published: 04 February 2020
doi: 10.3389/fonc.2020.00060

miR-936 Suppresses Cell Proliferation, Invasion, and Drug Resistance of Laryngeal Squamous Cell Carcinoma and Targets GPR78

Xi-Jun Lin[1†], Hui Liu[2†], Pei Li[1†], Hai-Feng Wang[1†], An-Kui Yang[3,4,5], Jin-Ming Di[6], Qi-Wei Jiang[7], Yang Yang[7], Jia-Rong Huang[7], Meng-Ling Yuan[7], Zi-Hao Xing[7], Meng-Ning Wei[7], Yao Li[7], Zhi Shi[7] and Jin Ye[1]**

[1] Department of Otolaryngology-Head and Neck Surgery, The Third Affiliated Hospital, Sun Yat-sen University, Guangzhou, China, [2] Division of Pulmonary and Critical Care, Department of Internal Medicine, The Third Affiliated Hospital, Sun Yat-sen University, Guangzhou, China, [3] Department of Head and Neck, Sun Yat-sen University Cancer Center, Guangzhou, China, [4] State Key Laboratory of Oncology in South China, Guangzhou, China, [5] Collaborative Innovation Center for Cancer Medicine, Guangzhou, China, [6] Department of Urology, The Third Affiliated Hospital, Sun Yat-sen University, Guangzhou, China, [7] Department of Cell Biology & Institute of Biomedicine, National Engineering Research Center of Genetic Medicine, Guangdong Provincial Key Laboratory of Bioengineering Medicine, College of Life Science and Technology, Jinan University, Guangzhou, China

MicroRNAs (miRs) play important roles in tumor progression. miR-936 has been reported to suppress cell invasion and proliferation of glioma and non-small cell lung cancer. Nevertheless, the function of miR-936 in laryngeal squamous cell carcinoma (LSCC) remains undiscovered. Hence, our study was to investigate the role of miR-936 in LSCC. In our present research, we have testified that miR-936 was substantially downregulated in LSCC tissues compared with adjacent normal tissues. Furthermore, miR-936 could inhibit proliferation, migration and invasion, and improve the sensitivity to doxorubicin and cisplatin of LSCC cells. Additionally, luciferase reporter assays were performed to confirm that GPR78 was a novel target of miR-936, and the protein expression of GPR78 was obviously inhibited by miR-936 in LSCC cells. In summary, our study indicates that the miR-936/GPR78 axis could be both a diagnostic marker and a therapeutic target for LSCC.

Keywords: laryngeal squamous cell carcinoma, miR-936, GPR78, proliferation, invasion, drug resistance

OPEN ACCESS

Edited by:
Chang Zou,
Jinan University, China

Reviewed by:
Xuerong Wang,
Nanjing Medical University, China
Hui Zhang,
Shandong University, China

****Correspondence:***
Zhi Shi
tshizhi@jnu.edu.cn
Jin Ye
yejin@mail.sysu.eud.cn

† These authors have contributed equally to this work

Specialty section:
This article was submitted to Molecular and Cellular Oncology, a section of the journal Frontiers in Oncology

Received: *27 June 2019*
Accepted: *14 January 2020*
Published: *04 February 2020*

Citation:
Lin X-J, Liu H, Li P, Wang H-F, Yang A-K, Di J-M, Jiang Q-W, Yang Y, Huang J-R, Yuan M-L, Xing Z-H, Wei M-N, Li Y, Shi Z and Ye J (2020) miR-936 Suppresses Cell Proliferation, Invasion, and Drug Resistance of Laryngeal Squamous Cell Carcinoma and Targets GPR78. Front. Oncol. 10:60. doi: 10.3389/fonc.2020.00060

INTRODUCTION

Laryngeal cancer ranks at the fourteenth most universal type of cancer in the world (1). It is estimated there over 13,000 new laryngeal cancer cases and 3,000 death cases took place in the United States, while 26,000 new cases and 14,000 deaths in China (1–3). Laryngeal squamous cell carcinoma (LSCC) occupies 85–90% of total malignant tumors in the larynx (4, 5). Despite advances in diagnosis and treatment, the long-term prognosis of LSCC patients has not been satisfactory in the past 20 years (6–8). Accordingly, a profound apprehension of the molecular biological mechanisms involving in LSCC tumorigenesis and development is imminently needed.

MicroRNAs (miRs) are a classical non-coding small RNA playing crucial regulatory roles in diverse pathological and physiological progresses by a posttranscriptional mechanism through binding the 3′-untranslated regions (3′-UTR) of target genes (9–12). And miRs can act as tumor oncogenes or suppressors through regulating their target genes that are usually dysregulated

in cancer (13–15). In our current study, we have proven that miR-936 expression profile is meaningfully reduced in LSCC specimens, and overexpression of miR-936 suppresses LSCC cells proliferation migration and invasion. Moreover, our results have further exhibited that GPR78 is a direct target of miR-936.

MATERIALS AND METHODS

Patients and Specimens

Twenty-five cases of LSCC and matching normal tissues were acquired from patients at the Department of Otolaryngology-Head and Neck Surgery, the Third Affiliated Hospital, Sun Yat-sen University and the Department of Head and Neck, Cancer Center, Sun Yat-sen University between December 2013 and February 2017. All patients were diagnosed as LSCC for the first time who underwent total or partial laryngectomy without chemical therapy or neoadjuvant radical before and after surgery. Signed informed approvals were acquired from patients, and the study was approved by the ethics committee of the Third Affiliated Hospital, Sun Yat-sen University.

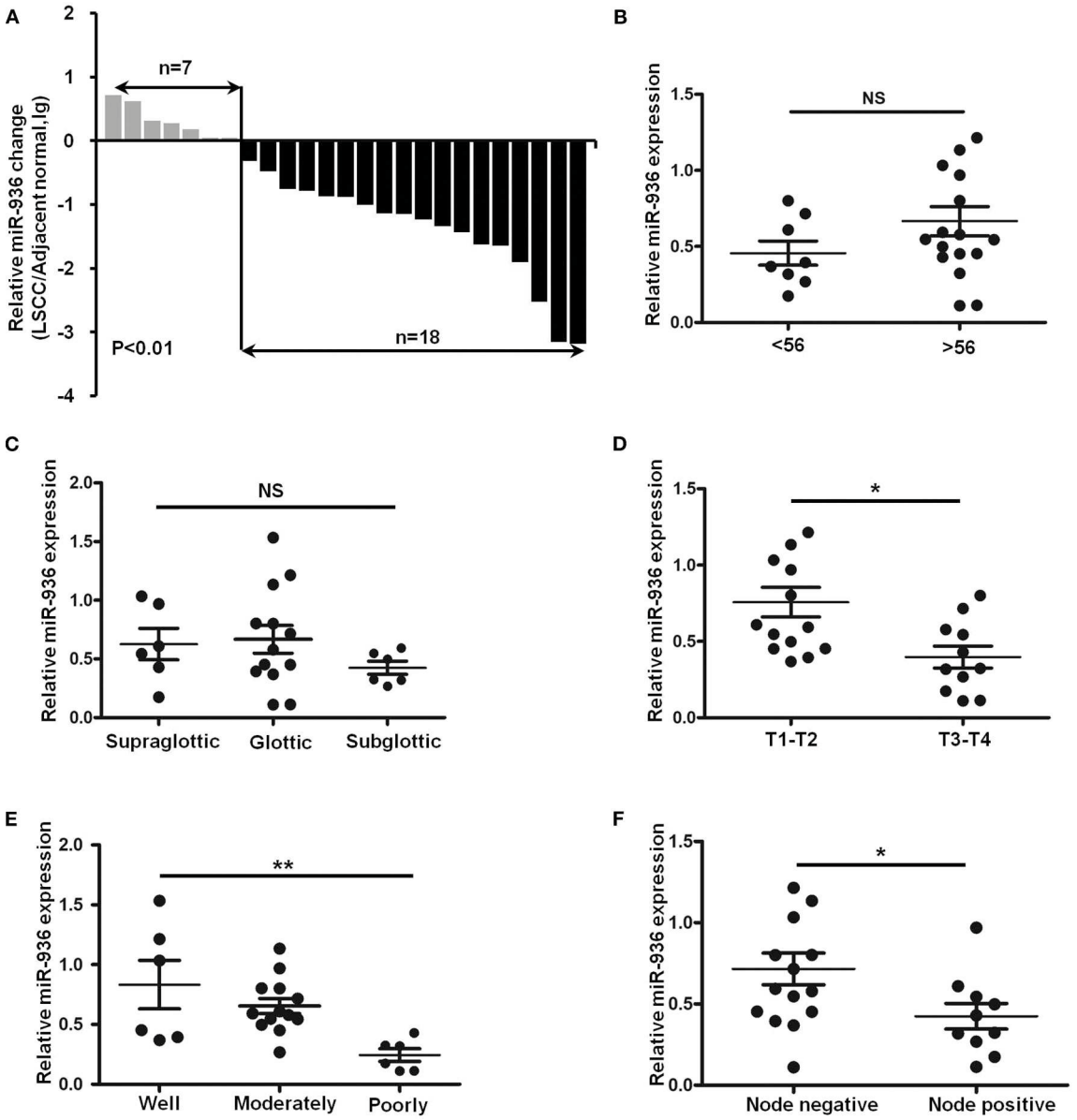

FIGURE 1 | Downregulation of miR-936 in LSCC is correlated with T stages, differentiation and lymph node metastasis. **(A)** Expression of miR-936 in 25 pairs of LSCC tissues and adjacent normal tissues was detected using RT-qPCR. The relative miR-936 expression in two groups of LSCC tissues classified by age **(B)**, T stage **(D)**, and lymph node metastasis **(F)** were analyzed with Mann-Whitney *U*-test. The relative miR-936 expression in three groups of LSCC tissues classified by differentiation **(C)** and primary location **(E)** were analyzed with Kruskal-Wallis test. Data are presented as mean ± SD or median with the interquartile range. $^{*}p < 0.05$; $^{**}p < 0.01$; NS, no statistical significance.

Cell Culture and Reagents

The human LSCC cell line Hep-2, the normal bronchial epithelium cell line 16HBE and the HEK293T were ordered from China Center for Type Culture Collection (CCTCC). The human LSCC cell line KB-3-1 was kindly provided by Dr. Zhesheng Chen (St. John's University, USA). The cells were cultured at 37°C with 5% CO_2 in a humidified atmosphere in Dulbecco's modified Eagle's medium (DMEM) containing 100 Unit/ml penicillin, 100 ng/ml streptomycin and 10% fetal bovine serum (FBS). Cell lines applied in this project were authenticated by short tandem repeat fingerprinting <3 months when this study was started. Anti-GPR78 (AB61731a) was from Sangon Biotech. The antibody of anti-GAPDH (KM9002) was purchased from Tianjin Sungene Biotech.

TABLE 1 | Relationship between miR-936 expression level and clinicopathologic parameters.

Characteristics (*n*)	miR-936 level[a]	*P*-value[b]
Age		0.0857
<56 (8)	0.4560 ± 0.2251	
≥56 (17)	0.6663 ± 0.3930	
T classification		0.0092
T1-2 (14)	0.7573 ± 0.3623	
T3-4 (11)	0.3976 ± 0.2368	
Primary location		0.3969
Supraglottic (6)	0.6266 ± 0.3269	
Glottic (13)	0.6668 ± 0.4270	
Subglottic (6)	0.4246 ± 0.1377	
Differentiation		0.0066
Well (6)	0.8329 ± 0.4957	
Moderately (6)	0.6546 ± 0.2286	
Poorly (13)	0.2446 ± 0.1313	
Lymph node metastasis		0.0315
Negative (14)	0.7273 ± 0.3892	
Positive (11)	0.4357± 0.2389	

[a]*Scores determined by qRT-PCR in mean ± SD.*
[b]*Student's T- test (for 2 groups) or one way ANOVA (for > 2 groups).*

Plasmid

The synthesized precursor hsa-miR-936 was cloned into lentiviral vector pLKO.1-GFP to generate the hsa-miR-936 lentivirus construct. The GPR78 3′UTR fragment was cloned into a psiCHECK-2 dual luciferase reporter construct. Lentivirus was packaged with HEK293T cells and harvested from the supernatant of medium. Stable cell line was obtained through infecting lentivirus in Hep-2 or KB-3-1 cells and selecting with puromycin.

RNA Extraction and Real-Time Quantitative PCR (RT-qPCR)

Total RNAs were extracted from cells and tissues by applying HiPure Total RNA Mini Kit (Magen). Reverse transcription was performed with HiFi-script cDNA kit (Cwbio) according to the instruction. The Bestar™ Real time PCR Master Mix was applied for RT-qPCR by SYER Green Method. All reactions were carried out in triplicate and repeated at least three independent times. The results of RT-qPCR were normalized to U6 by applying the $2^{-\Delta\Delta Ct}$ method. The following primers were ordered from Sangon Biotech:

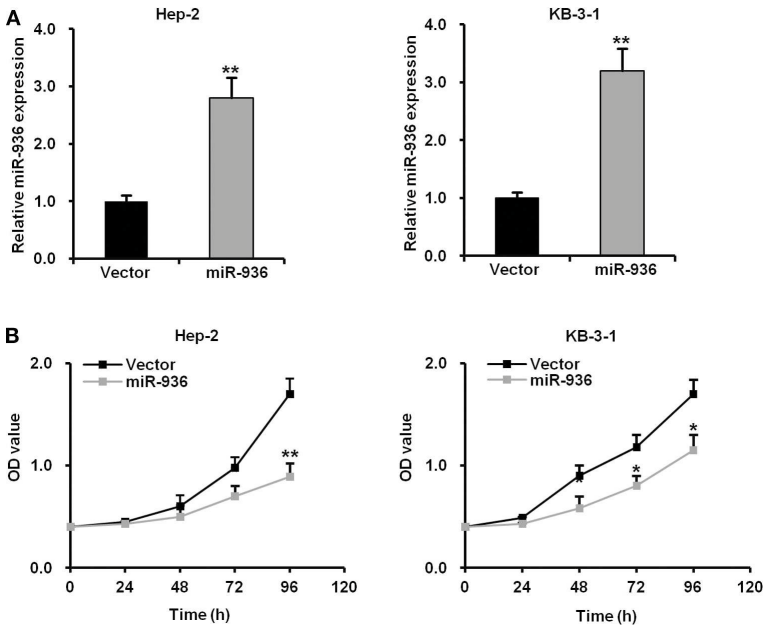

FIGURE 2 | Overexpression of miR-936 suppresses the proliferation of LSCC cells. **(A)** RT-qPCR analysis of the relative miR-936 expression in Hep-2 and KB-3-1 cells expressed vector control and miR-936. **(B)** Cell proliferation of the two LSCC cell lines was measured using the MTT assay. OD values were measured every 24 h for 96 h with or without miR-936 transfection. Data are presented as mean ± SD. Student's *t*-test was used for statistical analysis. $^*p < 0.05$; $^{**}p < 0.01$.

miR-936 forward: 5′-AACGAGACGACGACAGAC-3′; miR-936 reverse: 5′-ACAGTAGAGGGAGGAATCGCAG-3′; U6 forward: 5′- GCGCGTCGTGAAGCGTTC-3′; U6 reverse: 5′-GTGCAGGGTCCGAGGT-3′ (16).

Western Blot Analysis

Cells were washed with PBS, resuspended and lysed in RIPA buffer containing protease inhibitors (0.03% aprotinin, 10 ng/ml PMSF, 1 μM sodium orthovanadate, 1% NP-40, 0.1% SDS and 0.5% sodium deoxycholate,) at 4°C for 30 min. After centrifuging at 14,000 × g for 10 min, lysate supernatants were collected and stored at −80°C. Proteins were isolated by 12% SDS-PAGE gels and transferred to the membrane of polyvinylidene difluoride. After that, membrane was blocked by 5% BSA for 1 h, then incubated with the primary antibody and secondary antibody, successively. According to instruction, signal was measured through the chemiluminescent gel imaging system of ChemiDoc XRS (Bio-RAD) (17, 18).

MTT Assay

Cells plated in 96-well plate were incubated for 0, 1, 2, 3 days, then add MTT 0.5 mg/ml. After 4 h incubation at 37°C, carefully

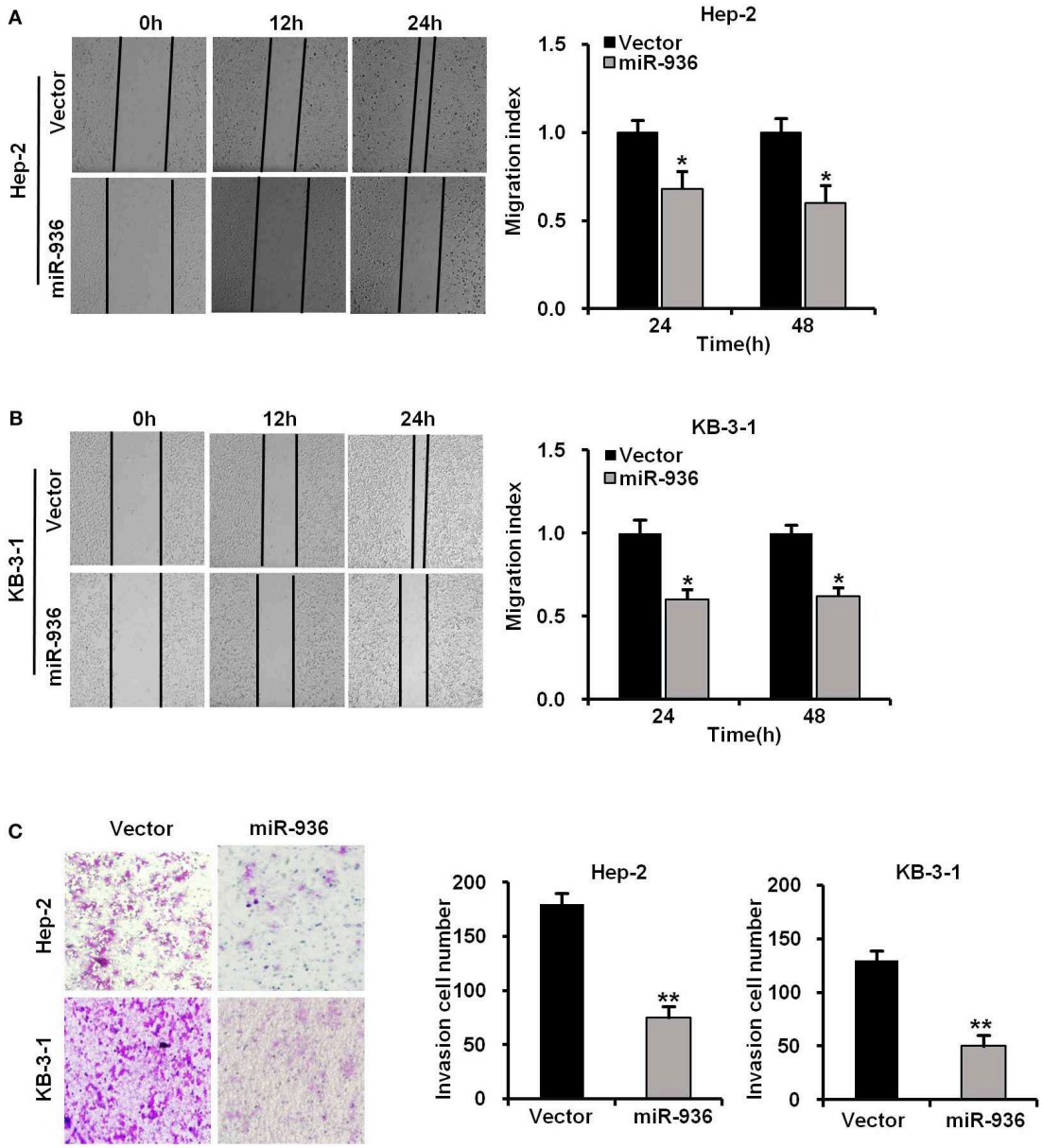

FIGURE 3 | Overexpression of miR-936 suppresses the migration and invasion of LSCC cells. **(A,B)** Representative images and quantification of the indicated cells migration as determined with wound healing assay. **(C)** Representative images and quantification of the indicated cells invasion as determined with Transwell assay. Data are presented as mean ± SD. Student's *t*-test was used for statistical analysis. $^{*}p < 0.05$; $^{**}p < 0.01$.

absorb the culture medium in the well to prevent the cells from taking away formazan crystals, and dissolved crystals with 100 μl of DMSO. Multiscan Spectrum (Thermofisher) was used to measure the absorbance at 570 nm (19, 20).

Wound Healing Assay

Cells were cultured in 6-well plate. Until the cells reached 80–90% confluence, using a sterile 10 μl pipette tip to draw a straight mark on the cell monolayer. After drawing, the delineated cells were washed and incubated in serum-free medium. The gap of wounds were measured by microscopic photograph at a certain time (21).

Transwell Assay

Cells were plated in the upper compartment containing matrigel-coated polycarbonate membrane filter of a modified Boyden chamber (Corning), and the lower chamber was plated complete medium, and allowed to migrate for 24 h. Wiped the cells on the upper surface of membrane and fixed the cells on the lower surface of membrane by 4% paraformaldehyde and stained by 0.1% crystal violet staining solution (22).

Luciferase Reporter Assay

The GPR78 mutated and wild-type (WT) 3′-UTR fragments were cloned into psiCHECK-2 reporter. HEK293T cells were plated in 24-well plates and co-transfected with mutated or WT 3′-UTR luciferase reporter and pLKO.1-GFP-miR-936. After 24 h, according to a protocol, cell lysates were obtain, and Firefly/Renilla luciferases ratios were measured with the Dual Luciferase Reporter Assay Kit (Promega) (23).

Statistical Analysis

All statistics were analyzed by SPSS 20.0, and the results were shown as mean ± SD or median with the interquartile range. The Student's *t*-test and Mann–Whitney U-test were applied to analyze comparisons of two groups, and one-way ANOVA and Kruskal-Wallis test were applied to analyze comparisons of multiple groups. The $P < 0.05$ were considered statistically significant.

RESULTS

Downregulation of miR-936 in LSCC Is Correlated With Differentiation, Lymph Node Metastasis and T Stages

To explore miR-936 expression in the LSCC tissues, RT-qPCR was used to check with 25 pairs of laryngeal cancer and normal tissue. Results suggested that miR-936 expression was meaningfully downregulated in LSCC, with 72% (18/25) of

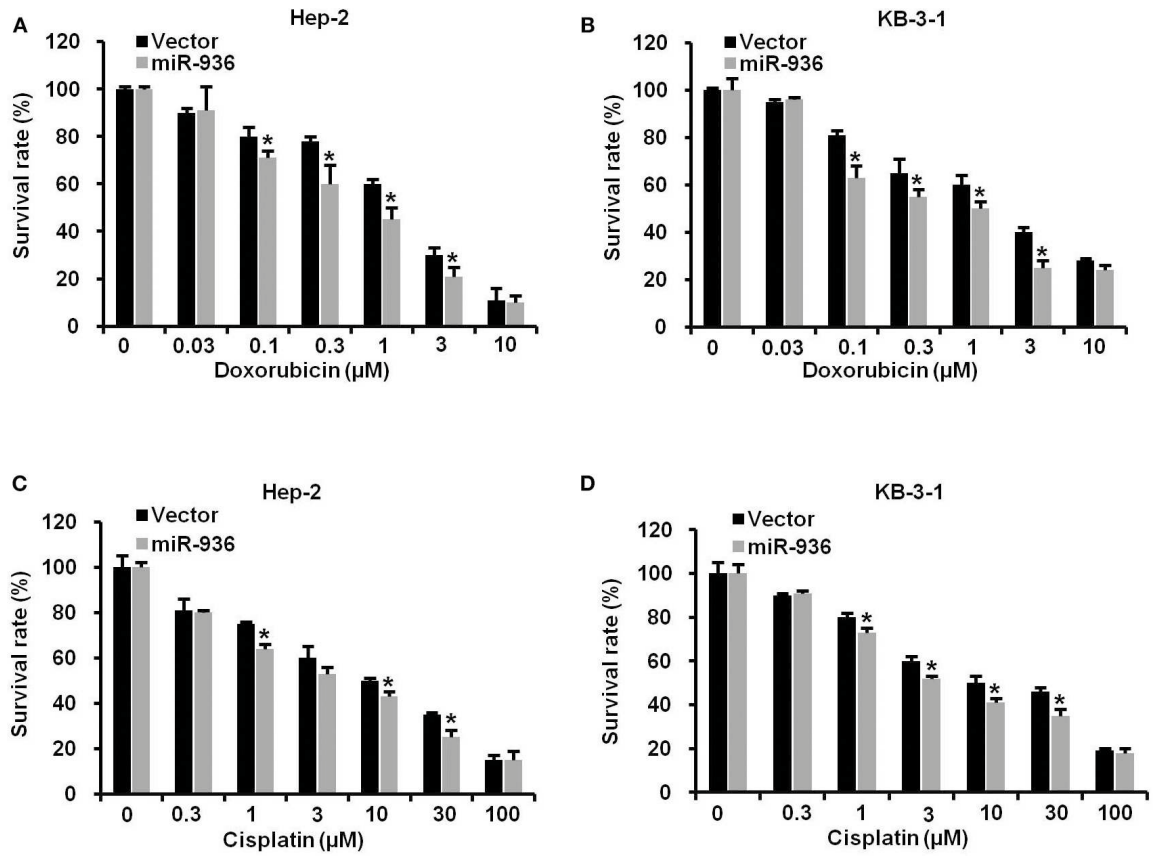

FIGURE 4 | Overexpression of miR-936 improves the drug sensitivity of LSCC cells to doxorubicin and cisplatin. **(A–D)** Cell survival of the indicated cells treated with doxorubicin and cisplatin as determined with MTT assay. Data are presented as mean ± SD. Student's *t*-test was used for statistical analysis. $^*P < 0.05$.

the tumor tissues showing reduced expression compared to matched normal controls (**Figure 1A**). Further, we found that miR-936 expression was correlated with tumor grade, lymph node metastasis and T Stages, but not correlated with tumor primary locations and age. The expression of miR-936 in negative lymph node metastasis, well-differentiation and T1-2 groups were higher than that in positive lymph node metastasis, poor differentiation, and T3-4 groups respectively (**Table 1** and **Figures 1B–F**). According to these data, the progression of LSCC may be associated with miR-936 expression.

Overexpression of miR-936 Suppresses the Proliferation of LSCC Cells

To investigate the function of miR-936 in LSCC, Hep-2 and KB-3-1 cells were infected with lentivirus expressing precursor miR-936, which successfully upregulated miR-936 in the cells (**Figure 2A**). The growth curves determined by MTT assay indicates that the proliferation abilities of Hep-2 and KB-3-1 cells were significantly attenuated when miR-936 was overexpressed (**Figure 2B**).

Overexpression of miR-936 Suppresses the Migration and Invasion of LSCC Cells

To further verify whether miR-936 has an influence on the migration and invasion of LSCC cells, we performed wound healing and transwell assays in Hep-2 and KB-3-1 cells with miR-936 overexpression. The outcomes revealed that the migration and invasion of miR-936 overexpressing cells were importantly decreased when compared with control cells (**Figures 3A–C**).

Overexpression of miR-936 Improves the Drug Sensitivity of LSCC Cells to Doxorubicin and Cisplatin

To verify the effect of miR-936 on LSCC cells treated with chemotherapy drugs, we treated indicated cells with doxorubicin or cisplatin in different concentrations. As shown in **Figures 4A–D**, the drug resistance to doxorubicin or cisplatin was significantly lower in cells overexpressing miR-936 in comparison with control groups in Hep-2 and KB-3-1 cells. These data suggested that increasing miR-936 expression could improve the drug sensitivity of LSCC cells to chemotherapeutic drugs.

miR-936 Directly Targets GPR78

To understand the mechanism of miR-936 as a tumor suppressor in LSCC, we combined RNAhybird and PITA to search the new potential targets of miR-936. Both algorithms reveal that GPR78 was a downstream gene of miR-936. We then performed western blot analysis and found that overexpressing miR-936 in Hep-2 and KB-3-1 cells could decrease GPR78 protein levels notably (**Figure 5A**). The interaction between miR-936 and the 3′-UTR of GPR78 was illustrated in **Figure 5B**. And luciferase reporter assays were used in HEK293T cells to test whether miR-936 could directly interact with the 3′-UTR of GPR78. The ratio of

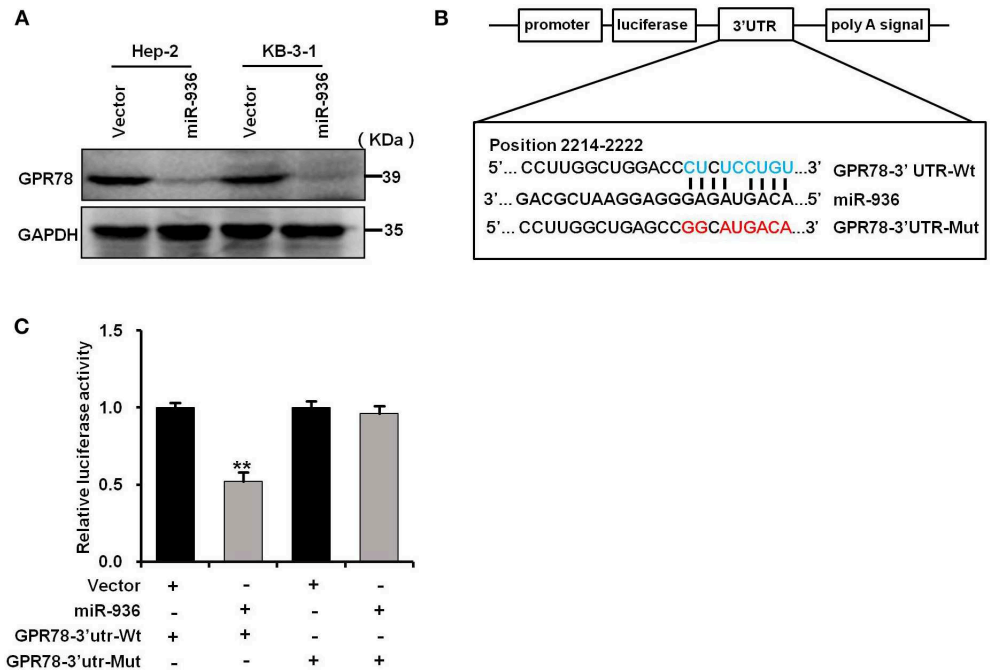

FIGURE 5 | miR-936 directly targets GPR78. **(A)** Western blot analysis of GPR78 protein expressions in the indicated cells. GAPDH is the loading control. **(B)** A schematic diagram of the reporter constructs showed the wild type (Wt) and mutant (Mut) sequences of the miR-936 binding sites within human GPR78 3′-UTR. **(C)** Luciferase activity of reporters with GPR78 Wt or Mut 3′-UTR in the HEK293T cells. Data are presented as mean ± SD. Student's *t*-test was used for statistical analysis. $^{**}p < 0.01$.

fluorescence activity indicates the inhibitory effect of miR-936 on GPR78 in wild or mutant 3′-UTR. As exhibited in **Figure 5C**, overexpression of miR-936 markedly suppressed the luciferase activity of GPR78 WT 3′-UTR compared to mutant 3′-UTR. The result above indicated that miR-936 directly suppresses GPR78 expression through binding its 3′-UTR (2214nt∼2222nt).

DISCUSSION

The development of tumors is a synergistic process of tumor-associated activation and inhibition genes. A growing number of studies have shown that abnormal expression of miRs happened in most types of human malignancies, including LSCC (24). In our present study, miR-936 was downregulated in LSCC tissues in comparison with matching normal tissues, and correlated with poor clinical features, suggesting that miR-936 might be associated with tumor progression in LSCC. Biological function experiments indicated that overexpression of miR-936 meaningfully inhibited the proliferation, migration, and invasion of LSCC cells. Furthermore, overexpression of miR-936 improved the drug sensitivity of LSCC cells to doxorubicin and cisplatin which currently are used for LSCC chemotherapy in clinic, indicating the significance of the findings that miR-936 sensitized the anticancer effects of doxorubicin and cisplatin in LSCC. Moreover, computerized algorithm predicted that GPR78 was a direct downstream target of miR-936, and that overexpression of miR-936 can effectively reduce GPR78 protein expression in LSCC cells. Previous researches have manifested that down-regulated miRs are often described as biomarkers or therapeutic targets in laryngeal squamous cell carcinoma. For instance, we recently reported t miR-194 works as a tumor suppressor in LSCC through targeting Wee1 (23). The expression of miR-375 is also reduced in LSCC tissues, and overexpression of miR-375 could reduce LSCC cell proliferation, motility and invasion by targeting IGF1R (25). In addition, miR-34a/c is also downregulated in LSCC tissues and inhibits LSCC cells proliferation by inducing cell cycle arrest through directly suppressing GALNT7 (26). While miR-27a is upregulated in LSCC specimens, and overexpression of miR-27a enhances LSCC cells proliferation by targeting PLK2 (27). MiR-93 is also upregulated in LSCC tissues and promotes the proliferation, migration, and invasion by inhibiting cyclin G2 (28).

Previous studies have been reported that miR-936 were down-regulated in glioma and induced cell cycle arrest via targeting CKS1 (29). Another report has also demonstrated that miR-936 could directly target E2F2 to inhibit the invasion and proliferation of non-small cell lung cancer cell (30). However, the biological functions of miR-936 have not been described in other tumors, including LSCC. Our study confirmed that miR-936 expression profile was downregulated in LSCC tissues, which indicates that miR-936 may be related to the progression of LSCC. Searching miRNA target genes is fundamental to understanding its carcinogenic regulatory mechanism and the effective molecular therapeutic targets. By bioinformatics algorithm and experiment validation, we testified that GPR78 was a direct target of miR-936. GPR78, an orphan G-protein coupled receptor, is situated in an area of chromosome 4p where have been shown connection to schizophrenia and bipolar affective dysfunction (31). Recently, GPR78 was testified highly expressed in lung cancer cell, and knockdown of GPR78 prominently suppressed cell migration and metastasis (32). However, the expression and function of GPR78 in LSCC need to be further investigated in the future.

In conclusion, our results proved that miR-936 attenuated the proliferation, migration and invasion of LSCC cells and targeted GPR78. Moreover, high level of miR-936 could improve the sensitivity of LSCC cells to doxorubicin and cisplatin. The results manifests that the miR-936/GPR78 axis could play as a novel biomarker and a therapeutic target of LSCC.

DATA AVAILABILITY STATEMENT

The datasets generated for this study are available on request to the corresponding author.

ETHICS STATEMENT

The studies involving human participants were reviewed and approved by the ethics committee of The Third Affiliated Hospital, Sun Yat-sen University. The patients/participants provided their written informed consent to participate in this study.

AUTHOR CONTRIBUTIONS

X-JL, HL, PL, H-FW, ZS, and JY designed the projects, conducted the experiments, analyzed the results, and wrote the manuscript. A-KY, J-MD, Q-WJ, YY, J-RH, M-LY, Z-HX, M-NW, and YL conducted the experiments. All authors read and agreed the final manuscript.

FUNDING

This work was funded by grants from the National Natural Science Foundation of China Nos. 81772540 (ZS), 81772752 (J-MD), 81472760 (HL), and 81902771 (PL), the Science and Technology Program of Guangdong Nos. 2019A050510023 (ZS), 2017A020215122 (J-MD), 2014A030313057 (JY), and 2014A020212078 (HL), the Medical Scientific Research Foundation of Guangdong Province No. 2018118215914106 (PL), the Science and Technology Program of Guangzhou No 201709010038 (J-MD).

REFERENCES

1. Siegel RL, Miller KD, Jemal A. Cancer statistics, 2019. *CA Cancer J Clin.* (2019) 69:7–34. doi: 10.3322/caac.21551
2. Feng RM, Zong YN, Cao SM, Xu RH. Current cancer situation in China: good or bad news from the 2018 Global Cancer Statistics? *Cancer Commun.* (2019) 39:22. doi: 10.1186/s40880-019-0368-6

3. Chen W, Zheng R, Baade PD, Zhang S, Zeng H, Bray F, et al. Cancer statistics in China, 2015. *CA Cancer J Clin.* (2016) 66:115–32. doi: 10.3322/caac.21338
4. Thompson LD. Laryngeal dysplasia, squamous cell carcinoma, and variants. *Surg Pathol Clin.* (2017) 10:15–33. doi: 10.1016/j.path.2016.10.003
5. Baugnon KL, Beitler JJ. Pitfalls in the staging of cancer of the laryngeal squamous cell carcinoma. *Neuroimaging Clin N Am.* (2013) 23:81–105. doi: 10.1016/j.nic.2012.08.008
6. Kolator M, Kolator P, Zatonski T. Assessment of quality of life in patients with laryngeal cancer: a review of articles. *Adv Clin Exp Med.* (2018) 27:711–5. doi: 10.17219/acem/69693
7. Garcia-Leon FJ, Garcia-Estepa R, Romero-Tabares A, Gomez-Millan Borrachina J. Treatment of advanced laryngeal cancer and quality of life. Systematic review. *Acta Otorrinolaringol Esp.* (2017) 68:212–9. doi: 10.1016/j.otoeng.2017.06.010
8. Obid R, Redlich M, Tomeh C. The treatment of laryngeal cancer. *Oral Maxillofac Surg Clin North Am.* (2019) 31:1–11. doi: 10.1016/j.coms.2018.09.001
9. Quevillon Huberdeau M, Simard MJ. A guide to microRNA-mediated gene silencing. *FEBS J.* (2019) 286:642–52. doi: 10.1111/febs.14666
10. Treiber T, Treiber N, Meister G. Regulation of microRNA biogenesis and its crosstalk with other cellular pathways. *Nat Rev Mol Cell Biol.* (2019) 20:5–20. doi: 10.1038/s41580-018-0059-1
11. Gebert LFR, MacRae IJ. Regulation of microRNA function in animals. *Nat Rev Mol Cell Biol.* (2019) 20:21–37. doi: 10.1038/s41580-018-0045-7
12. Duchaine TF, Fabian MR. Mechanistic Insights into MicroRNA-Mediated Gene Silencing. *Cold Spring Harb Perspect Biol.* (2019) 11:a032771. doi: 10.1101/cshperspect.a032771
13. Setijono SR, Kwon HY, Song SJ. MicroRNA, an antisense RNA, in sensing myeloid malignancies. *Front Oncol.* (2017) 7:331. doi: 10.3389/fonc.2017.00331
14. Kuninty PR, Schnittert J, Storm G, Prakash J. MicroRNA targeting to modulate tumor microenvironment. *Front Oncol.* (2016) 6:3. doi: 10.3389/fonc.2016.00003
15. Huang JT, Wang J, Srivastava V, Sen S, Liu SM. MicroRNA machinery genes as novel biomarkers for cancer. *Front Oncol.* (2014) 4:113. doi: 10.3389/fonc.2014.00113
16. Ye J, Zou MM, Li P, Lin XJ, Jiang QW, Yang Y, et al. Oxymatrine and cisplatin synergistically enhance anti-tumor immunity of CD8(+) T cells in Non-small cell lung cancer. *Front Oncol.* (2018) 8:631. doi: 10.3389/fonc.2018.00631
17. Huang JR, Qin WM, Wang K, Fu DR, Zhang WJ, Jiang QW, et al. Cyclin-dependent kinase 7 inhibitor THZ2 inhibits the growth of human gastric cancer *in vitro* and *in vivo*. *Am J Transl Res.* (2018) 10:3664–76.
18. Mei XL, Yang Y, Zhang YJ, Li Y, Zhao JM, Qiu JG, et al. Sildenafil inhibits the growth of human colorectal cancer *in vitro* and *in vivo*. *Am J Cancer Res.* (2015) 5:3311–24.
19. Yuan ML, Li P, Xing ZH, Di JM, Liu H, Yang AK, et al. Inhibition of WEE1 suppresses the tumor growth in laryngeal squamous cell carcinoma. *Front Pharmacol.* (2018) 9:1041. doi: 10.3389/fphar.2018.01041
20. Yang Y, Qiu JG, Li Y, Di JM, Zhang WJ, Jiang QW, et al. Targeting ABCB1-mediated tumor multidrug resistance by CRISPR/Cas9-based genome editing. *Am J Transl Res.* (2016) 8:3986–94.
21. Luo Y, Wu JY, Hou GL, Lu MH, Shi Z, Di JM. ODAM is a predictor for biomedical recurrence and inhibits the migration and invasion of prostate cancer. *Am J Transl Res.* (2016) 8:670–9.
22. Luo Y, Jiang QW, Wu JY, Qiu JG, Zhang WJ, Mei XL, et al. Regulation of migration and invasion by Toll-like receptor-9 signaling network in prostate cancer. *Oncotarget.* (2015) 6:22564–74. doi: 10.18632/oncotarget.4197
23. Li P, Yang Y, Liu H, Yang AK, Di JM, Tan GM, et al. MiR-194 functions as a tumor suppressor in laryngeal squamous cell carcinoma by targeting Wee1. *J Hematol Oncol.* (2017) 10:32. doi: 10.1186/s13045-017-0402-6
24. Li P, Liu H, Wang Z, He F, Wang H, Shi Z, et al. MicroRNAs in laryngeal cancer: implications for diagnosis, prognosis and therapy. *Am J Transl Res.* (2016) 8:1935–44.
25. Luo J, Wu J, Li Z, Qin H, Wang B, Wong TS, et al. miR-375 suppresses IGF1R expression and contributes to inhibition of cell progression in laryngeal squamous cell carcinoma. *Biomed Res Int.* (2014) 2014:374598. doi: 10.1155/2014/374598
26. Li W, Ma H, Sun J. MicroRNA34a/c function as tumor suppressors in Hep2 laryngeal carcinoma cells and may reduce GALNT7 expression. *Mol Med Rep.* (2014) 9:1293–8. doi: 10.3892/mmr.2014.1929
27. Tian Y, Fu S, Qiu GB, Xu ZM, Liu N, Zhang XW, et al. MicroRNA-27a promotes proliferation and suppresses apoptosis by targeting PLK2 in laryngeal carcinoma. *BMC Cancer.* (2014) 14:678. doi: 10.1186/1471-2407-14-678
28. Xiao X, Zhou L, Cao P, Gong H, Zhang Y. MicroRNA-93 regulates cyclin G2 expression and plays an oncogenic role in laryngeal squamous cell carcinoma. *Int J Oncol.* (2015) 46:161–74. doi: 10.3892/ijo.2014.2704
29. Wang D, Zhi T, Xu X, Bao Z, Fan L, Li Z, et al. MicroRNA-936 induces cell cycle arrest and inhibits glioma cell proliferation by targeting CKS1. *Am J Cancer Res.* (2017) 7:2131–43.
30. Zhou X, Tao H. Overexpression of microRNA-936 suppresses non-small cell lung cancer cell proliferation and invasion via targeting E2F2. *Exp Ther Med.* (2018) 16:2696–702. doi: 10.3892/etm.2018.6490
31. Underwood SL, Christoforou A, Thomson PA, Wray NR, Tenesa A, Whittaker J, et al. Association analysis of the chromosome 4p-located G protein-coupled receptor 78 (GPR78) gene in bipolar affective disorder and schizophrenia. *Mol Psychiatry.* (2006) 11:384–94. doi: 10.1038/sj.mp.4001786
32. Dong DD, Zhou H, Li G. GPR78 promotes lung cancer cell migration and metastasis by activation of Galphaq-Rho GTPase pathway. *BMB Rep.* (2016) 49:623–8. doi: 10.5483/BMBRep.2016.49.11.133

Conflict of Interest: The authors declare that the research was conducted in the absence of any commercial or financial relationships that could be construed as a potential conflict of interest.

frontiers in Oncology

ORIGINAL RESEARCH
published: 07 February 2020
doi: 10.3389/fonc.2020.00058

7-Methoxy-1-Tetralone Induces Apoptosis, Suppresses Cell Proliferation and Migration in Hepatocellular Carcinoma via Regulating c-Met, p-AKT, NF-κB, MMP2, and MMP9 Expression

*Ying Wen[1,2], Xiaoyan Cai[2], Shaolian Chen[3], Wei Fu[1,2], Dong Chai[1,2], Huainian Zhang[1,2] and Yongli Zhang[1,2]**

[1] Guangzhou Key Laboratory of Construction and Application of New Drug Screening Model Systems, Guangdong Pharmaceutical University, Guangzhou, China, [2] Department of Cell Biology and Medical Genetics, School of Life Sciences and Biopharmaceutics, Guangdong Pharmaceutical University, Guangzhou, China, [3] Department of Clinical Laboratory, The First Affiliated Hospital, Guangdong Pharmaceutical University, Guangzhou, China

OPEN ACCESS

Edited by:
Chang Zou,
Shenzhen People's Hospital, Jinan University, China

Reviewed by:
Sabarish Ramachandran,
Texas Tech University Health Sciences Center, United States
Yuan Ye,
Affiliated Hospital of Guilin Medical University, China
Juan Cen,
Henan University, China

***Correspondence:**
Yongli Zhang
zyl28_gdpu@163.com

Specialty section:
This article was submitted to Molecular and Cellular Oncology, a section of the journal Frontiers in Oncology

Received: 27 October 2019
Accepted: 13 January 2020
Published: 07 February 2020

Citation:
Wen Y, Cai X, Chen S, Fu W, Chai D, Zhang H and Zhang Y (2020) 7-Methoxy-1-Tetralone Induces Apoptosis, Suppresses Cell Proliferation and Migration in Hepatocellular Carcinoma via Regulating c-Met, p-AKT, NF-κB, MMP2, and MMP9 Expression. Front. Oncol. 10:58. doi: 10.3389/fonc.2020.00058

This study aimed to determine the anti-proliferative and anti-migratory effects of 7-methoxy-1-tetralone (MT) in hepatocellular carcinoma (HCC) cells. MTT assay assessed HCC cell viability; cell apoptosis of HCC cells was determined by flow cytometry; wound healing assay evaluated HCC cell migratory ability; protein expression levels were assessed using western blot assay; the *in vivo* antitumor effects of MT were tested in BALB/c nude mice and the pathological changes within the tumor tissues were evaluated by immunohistochemistry. MT treatment significantly suppressed the cell proliferative and migratory potentials of HepG2 cells, and induced HepG2 cell apoptosis. The western blot assay showed that MT treatment caused a suppression on c-Met, phosphorylated AKT (p-AKT), NF-κB, matrix metallopeptidase 2 (MMP2)/MMP9 protein levels in HepG2 cells. Further *in vivo* animal studies deciphered that MT treatment suppressed tumor growth of HepG2 cells in the nude mice, but had no effect on the body weight and the organ index of liver and spleen. Further immunohistochemistry analysis of the dissected tumor tissues showed that MT treatment significantly suppressed the protein expression levels of NF-κB, MMP9, MMP2, and p-AKT. In summary, the present study demonstrated the anti-tumor effects of MT on the HCC, and MT suppressed HCC progression possibly via regulating proliferation- and migration-related mediators including c-Met, p-AKT, NF-κB, MMP2, and MMP9 in HepG2 cells.

Keywords: 7-methoxy-1-tetralone, hepatocellular carcinoma, cell proliferation, cell apoptosis, cell migration

INTRODUCTION

Hepatocellular carcinoma (HCC) represents one of the most severe human malignancies with a high mortality (1). High risk factors such as hepatitis B virus (HBV) or hepatitis C virus (HCV) infection, alcohol abuse, hemochromatosis psychosis, and so on, may lead to a chronic liver disease, then with progression to cirrhosis, eventually leading to the occurrence of HCC (2–4).

Surgical interventions (surgical resection, liver transplantation, and locoregional therapies) have been playing important roles in the treatment of HCC (5, 6). However, only 15% patients are eligible for the potentially curative treatments since a majority of patients diagnosed with HCC already have liver dysfunction and/or are at advanced stages (III or IV), and these patients cannot benefit from these interventions (7, 8). Sorafenib is the only FDA-approved medication for the management of advanced HCC (9, 10). However, a large percentage of patients still experience disease progression after sorafenib treatment (11). Therefore, there is still a large unmet medical need to develop new therapeutic strategies to treat HCC.

7-methoxy-1-tetralone (MT) is mainly used as the organic material or intermediate in chemical engineering currently (12–15). Our research group revealed that wild Juglansshurica leather has strong anti-tumor effects through the long-term study, while MT may be one of the effective components. Sun et al. (16) revealed that the compounds extracted from green peel of *Juglans mandshurica* possessed the insecticidal activities, further investigation deciphered that MT is one of the major active components (the relative content: 6.81%). Recently, studies showed that extracts from green peel of *J. mandshurica* exhibited moderate inhibitory effects on the lung cancer cells (17) Nevertheless, systematic study of MT's potential to repress human hepatoma cell growth has not been documented.

This study was undertaken to gain deeper insights into the anti-hepatocellular carcinoma activities and anti-neoplastic molecular mechanisms of MT. Changes to cell proliferation, apoptosis and migration and AKT, phosphorylated AKT (p-AKT), NF-κB, and matrix metallopeptidase 2 (MMP2)/MMP9 protein expression following application of MT are defined in this study using *in vitro* cell culture and *in vivo* animal experiments, in order to provide the experimental basis for its future clinical application.

MATERIALS AND METHODS

Cell Culture and Chemical Reagents

The two human hepatoma cell lines (HepG2 and LO2) were a generous gift from Sun Yat-sen University. HepG2 and LO2 cells were kept in DMEM (Thermo Fisher Scientific, Waltham, USA) supplemented with 10% fetal bovine serum (FBS; Thermo Fisher Scientific) in a humidified incubator (Sanyong, Tokyo, Japan) with 5% CO_2 at 37°C. Dimethyl sulfoxide (DMSO) was used to dissolve MT (purity > 98%; Sigma-Aldrich, St. Louis, USA) to prepare the stock solution, and the stock solution was diluted with cell culture medium as the respective working concentrations, and the concentration of DMSO in the working solution was <0.1% (18).

Cell Viability Assay

The anti-proliferative effects of MT were evaluated by MTT assay. LO2 and HepG2 (1×10^5 cells/well) were seeded at 96-well plates. The seeded cells were subjected to incubate with different concentrations of MT (31.25, 62.5, 125, 250, 500, and 1,000 μM) for 24, 48, and 72 h, respectively. Fluorouracil (5-FU, 50 μM) served as a positive control. After 4 h incubation with MTT (5 mg/ml) at 37°C. Cell viability was evaluated by measuring the absorbance at 570 nm.

Flow Cytometry Analysis of Cell Apoptosis

Apoptosis was determined using flow cytometer with a commercial Annexin V-FITC Apoptosis Detection Kit (KaiJi, Nanjing, China) by following the manufacture's protocol. In brief, HepG2 cells were subjected to treatment with different concentrations of drugs for 48 h after plating as a monolayer. Cells were rinsed twice with cold phosphate buffered saline (PBS) and trypsinized gently using the trypsin reagent, then cells were re-suspended in 1× binding buffer and were incubated FITC Annexin V and propidium iodide (PI) for 15 min at room temperature in the dark. A BD FACSCalibur flow cytometer (BD Biosciences, Franklin Lakes, USA) was used to identify the different subpopulations of apoptotic cells.

Wound Healing Assay

HepG2 cells after different treatments were allowed to grow in 6-well plates until ∼90% confluence. A sterile 200 μL pipette tip was used to create a wound in the HepG2 cell monolayer. HepG2 cells were rinsed twice with PBS to remove debris, and HepG2 cells were incubated with serum-free medium for indicated time durations. At indicated time points, images of the plates were acquired under a microscope and the migrating distances were analyzed by Image-Pro-Plus software (19).

Western Blot Analysis

Total proteins were obtained by lysing the cells or tissues using RIPA buffer (Beyotime). The BCA quantitative analysis kit was used to measure concentrations of protein samples (Beyotime). Equal aliquots of protein samples were separated by sodium dodecyl sulfate-polyacrylamide gel electrophoresis and the proteins were electro-transferred onto a PVDF membrane (Millipore, Burlington, USA). The PVDF membrane was probed with different primary antibodies, and protein bands were visualized by an enhanced chemiluminescence method (Thermo Fisher Scientific). Antibodies for c-Met (Cat. #4560), Akt (Cat. #4685) p-Akt (Cat. #4060), NF-κB (Cat. #8242), MMP2 (Cat. #40944), MMP9 (Cat. #13667), β-actin (Cat. #8457) and the corresponding secondary antibodies were obtained from Cell Signal Technology Inc. (Danvers, USA).

In vivo Animal Studies to Assess Tumor Growth

Five-week-old BALB/c nude mice ($n = 25$) used for *in vivo* experiments were purchased from the Guangdong Laboratory Animal Center. HepG2 cells (7×10^6 cells/ml) were subcutaneously administered into the right sub-axillary region of the mice. When the diameters reached a length >3 mm, mice were randomly assigned to five groups and administered with different drugs by the intraperitoneal injection. Mice from the control group mice received saline, mice from the positive control group mice received 5-FU (15 mg/kg/d) and mice from the experimental group received MT (80, 120, or 160 mg/kg/d). Subcutaneous tumors were measured using calipers, and tumor volume was assessed using the following formula: $width^2 \times$

length × 0.5 (20). Body weight was measured every day. Mice received 19 doses in total and were sacrificed for harvesting tumors at 24 h after the last dose. The organ index for liver and spleen was determined as organ weight (g)/body weight (g). All the experimental procedures of the animal studies were under the approval by the Animal Ethics Committee of Guangdong Pharmaceutical University.

Hematoxylin and Eosin (HE) Staining Assay

HE staining assay was used to observe pathological changes within the tumor tissues. Tumor tissues were embedded in paraffin, sectioned into 4 μm slices and deparaffinized in xylene for 15 min followed by re-hydration in the graded ethanol. After staining with hematoxylin for 5–10 min, the slides were incubated with 1% hydrochloride alcohol for 20 s. Following 5–10 min running water washing, the slides were stained with 0.5% eosin for 3 min. The morphology of the HE-stained tumor tissues were evaluated using a light microscope.

Immunohistochemical Analysis of Tumor Tissues

The paraffin sections were deparaffinized using xylene and hydrated through graded ethanol. After antigen retrieval, 3% H_2O_2 was used to quench endogenous peroxidase. After PBS washing, slides were incubated with 10% bovine serum albumin (BSA) for 10 min, and then primary antibodies including MMP2 (1:200), MMP9 (1:200), p-Akt (1:500) and NF-κB (1:100) were added to incubate with the slices overnight at 4°C. After that, slides were incubated with secondary antibodies for 30 min at room temperature. 3,3′- diaminobenzidine (DAB) as a chromogen was used to visualize the antigens. After counterstaining with hematoxylin, the slides were dehydrated and mounted for viewing. For the negative control, primary antibody was replaced by BSA. The percentage of positive staining area was measured by Image J.

Statistical Analysis

A SPSS statistical software package (IBM, Armonk, USA) was used for performing data analysis. Results data are presented as the mean ± standard deviation. Differences between the mean values for the different groups were determined using one-way ANOVA followed by Dunnett's multiple comparison test. A *P*-value less than 0.05 was defined to be statistically significant.

RESULTS

MT Inhibited Proliferation of HepG2 Cells but Has Little Cytotoxic Effects on Normal LO2 Cells

The cytotoxic effects of MT on LO2 cells were determined by treating cells with different concentrations of MT (0–1,000 μM) for 24, 48, 72 h, respectively. In addition, HepG2 cells were subjected to incubate with elevated MT concentrations (0–500 μM) for 48 h. 5-Fluorouracil (5-Fu, 50 μM) was used as a positive control in this investigation. As shown in **Figure 1A**, increasing concentrations of MT exhibited anti-proliferative actions in LO2 cells in a time- and concentration-dependent way. Nevertheless, the 48 h treatment duration was selected for our follow-up study because MT had the greatest dose-dependent effect on LO2 cells at 48 h after treatment. The results in **Figure 1B** indicated that MT was more effective to inhibit the proliferation of HepG2 cells when compared with LO2 cells. For subsequent experiments three different concentrations for MT (40,100, 250 μM) were used.

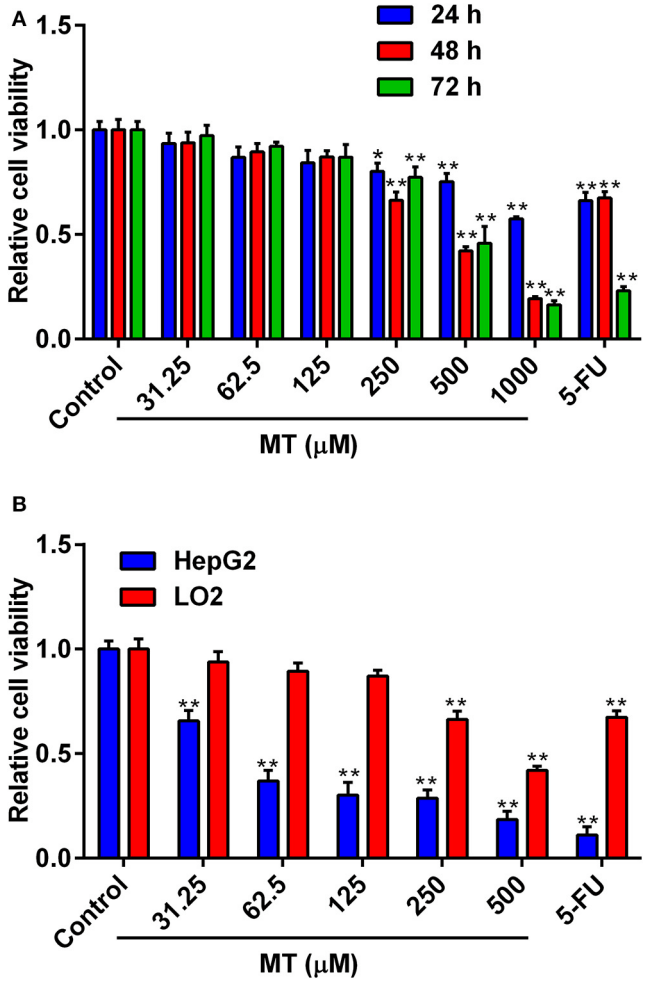

FIGURE 1 | Anti-proliferative activity of MT on LO2 and HepG2 cells. **(A)** Effects of MT and 5-FU on the proliferation of LO2 cells were determined by MTT assay. **(B)** Effects of MT and 5-FU on the proliferation of HepG2 cells and LO2 cells at after 48 h treatment with MT were determined by MTT assay. Data from at least three independent experiments performed in triplicates are presented; $^{*}P < 0.05$ and $^{**}P < 0.01$ compared to the corresponding control groups.

Effects of MT on the Cell Apoptosis of HepG2 Cells

To validate the effects of MT on HepG2 cell apoptosis, flow cytometry was performed to analyze Annexin V-FITC/PI stained HepG2 cells. MT treatment mildly increased the number of apoptotic cells (AV+PI+ and AV+PI- cells) compared to the control group (**Figure 2**). The percentage of apoptotic HepG2

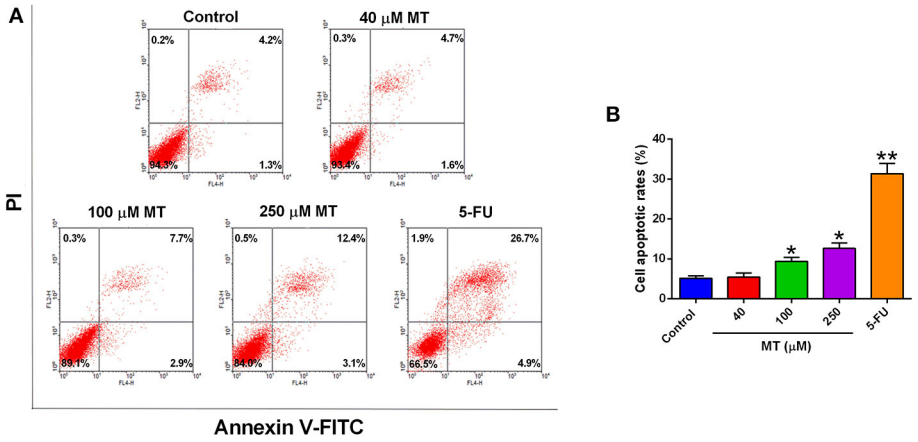

FIGURE 2 | Effects of MT treatment on the cell apoptosis of HepG2 cells. **(A)** HepG2 cells were incubated with different concentrations of MT for 48 h and analyzed by flow cytometry. Histograms showed that distribution of apoptotic cells after different treatment. **(B)** Quantification of cell apoptosis from the histograms. Data from at least three independent experiments performed in triplicates are presented; $^{*}P < 0.05$ and $^{**}P < 0.01$ compared to the corresponding control groups.

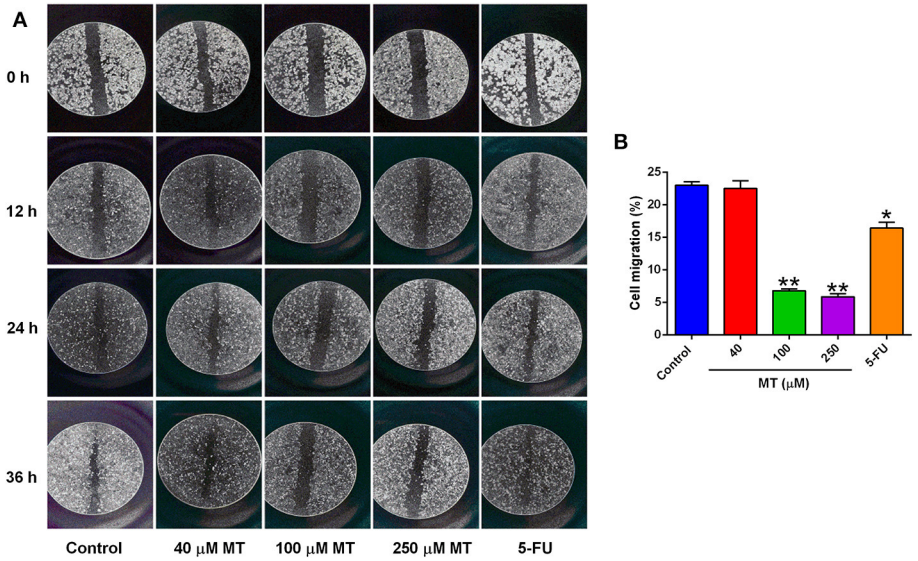

FIGURE 3 | Effects of MT on HepG2 cell migration was determined by wound-healing test. **(A)** Representative images (at a magnification of 5×) of the wound healing of HepG2 cells after different drug treatments. **(B)** Quantification of cell migration of HepG2 cells after different treatments. Data from at least three independent experiments performed in triplicates are presented; $^{*}P < 0.05$ and $^{**}P < 0.01$ compared to the corresponding control groups.

cells following treatment with 0, 40, 100, or 250 μM MT for 48 h were 5.44 ± 0.84, 5.07 ± 1.22, 7.15 ±1.92, and 11.45 ±1.11%, respectively (**Figure 2**). On the other hand, 5-FU induced much more HepG2 apoptotic cells than that treated with MT (**Figure 2**).

MT Suppressed Migration in HepG2 Cells

Wound healing assay was undertaken to evaluate the effect of MT on HepG2 cell migration. As demonstrated in **Figure 3**, the cells of different concentration group were tightly connected at 0 h. The scratch of the control group, 40 μM low dose group and 5-FU group was significantly prolonged at 12, 24, and 36 h after drug treatment, while 100 and 250 μM groups were not obvious, indicated that the healing of the scratch was significantly reduced following treatment with 100 and 250 μM MT (**Figure 3**).

Effects of MT on c-Met, NF-κB, p-Akt, Akt, and MMP2/MMP9 Protein Expression in HepG2 Cells

To assess the significance of the expression patterns of proliferation and migration-related proteins in response to MT, HepG2 cells were subjected to treatment with elevated MT concentrations (0, 40, 100, and 250 μM) for 48 h, and expression levels of c-Met, AKT, p-AKT, NF-κB, and MMP2/9, which closely

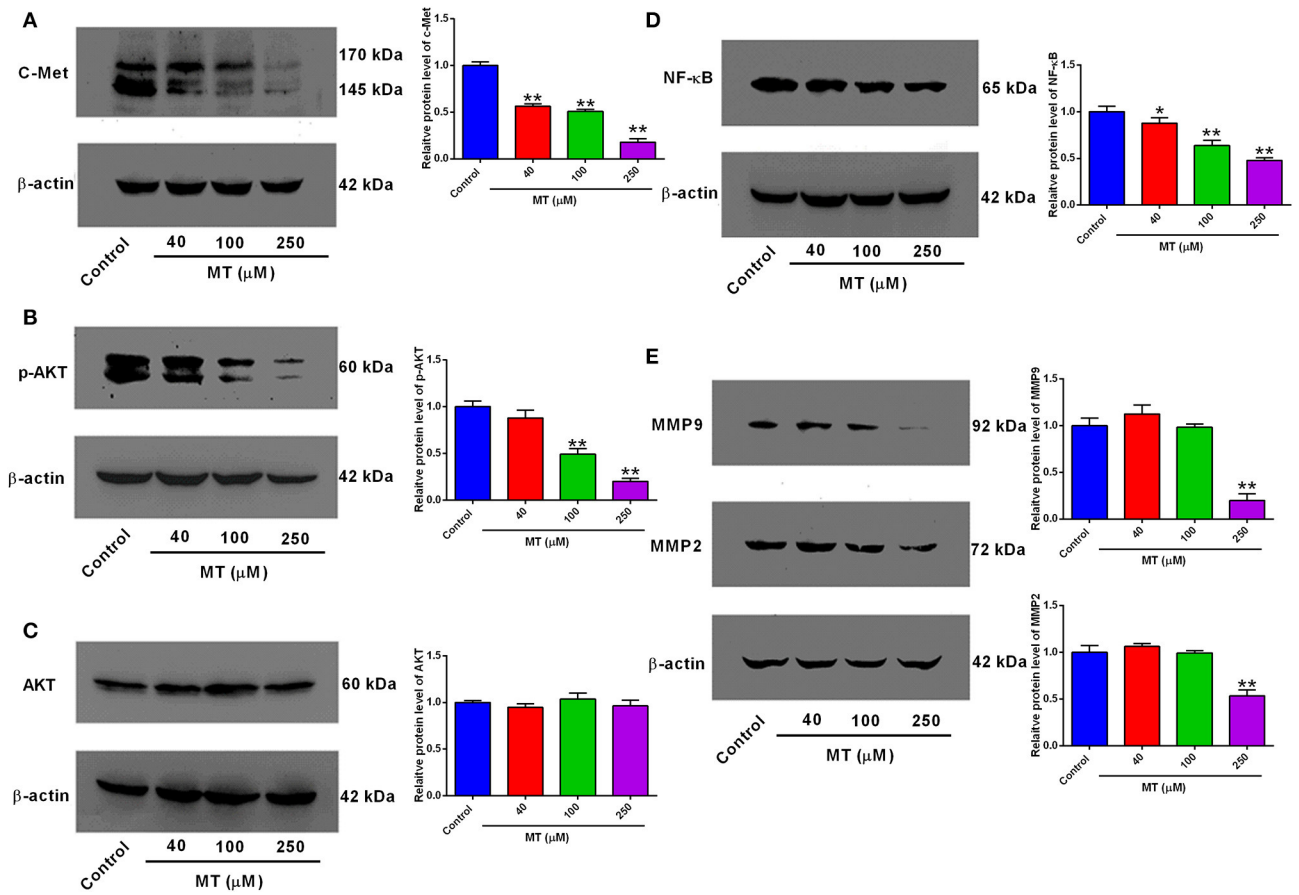

FIGURE 4 | Effects of MT treatment on the protein expression levels of c-Met, p-AKT, AKT, NF-κB, MMP2, and MMP9 in HepG2 cells. **(A)** c-Met, **(B)** p-AKT, **(C)** AKT, **(D)** NF-κB, **(E)** MMP9 and MMP2 in MT-treated HepG2 cells were assessed by Western Blot analysis and were quantified using ImageJ software. Data from at least three independent experiments performed in triplicates are presented; $^{*}P < 0.05$ and $^{**}P < 0.01$ compared to the corresponding control groups.

involved in the regulation of proliferation and migration were demonstrated in **Figure 4**. The expression of c-Met, p-Akt, NF-κB, and MMP2/9 significantly decreased compared with control group after 48 h of treatment with HepG2 cells with 40, 100, and 250 μM MT (**Figure 5B**), while the expression change of Akt protein was not obvious. MT at concentration of 40 μM significantly repressed c-Met and NF-κB protein expression levels (**Figure 4**); MT at a concentration of 100 μM significantly down-regulated p-AKT, NF-κB protein expression (**Figure 4**); MT at a concentration of 250 μM inhibited c-Met, p-AKT, NF-κB, and MMP2/MMP9 protein expression levels (**Figure 4**); while the AKT protein levels were not affected by MT treatment in HepG2 cells (**Figure 4**).

MT Inhibits Tumor Growth *in vivo*

BALB/c nude mice were sacrificed after 19 days receiving MT, 5-FU, or saline by intraperitoneal injection. MT treatment failed to affect mice body weight, while 5-FU treatment reduce the mice body weight (**Figure 5A**). The photos of representative tumor images from different treatment groups are demonstrated in **Figure 5B**. Tumor volume and tumor weight were significantly reduced by MT and 5-FU treatment when compared to the control group (**Figures 5C,D**). The tumor inhibition rates were 40.57% (80 mg/kg MT group), 51.43% (120 mg/kg MT group), 79.43% (160 mg/kg MT group), and 89.71% (5-FU group). MT and 5-FU had no effects on the organ indexes of liver or spleen (**Figures 5E,F**).

Pathological Morphology and Relative Protein Expressions *in vivo*

Pathological morphology of tumor tissues was detected in saline group, MT (80, 120, 160 mg/kg) groups and 5-FU group and were presented in **Figures 6A,B**. In the saline control group, tumor cells were mainly intact. While, in the MT and 5-FU group, some of tumor cells in the exposed area were characterized with necrosis and cell fragmentation. These observations suggested that the cells were in a vigorous growth stage. However, in different dose of MT and 5-Fu groups, the typical increased nuclei volume and shrunken intercellular space were considerably reduced, and some chromosome fractures and integrated nuclear membranes were observed. Immunohistochemistry staining (**Figure 6C**) presents the four proteins (p-Akt, NF- κB, MMP9, and MMP2) expressions in saline group, 160 mg/ml MT group and 5-FU group, respectively. The percent of positive staining in

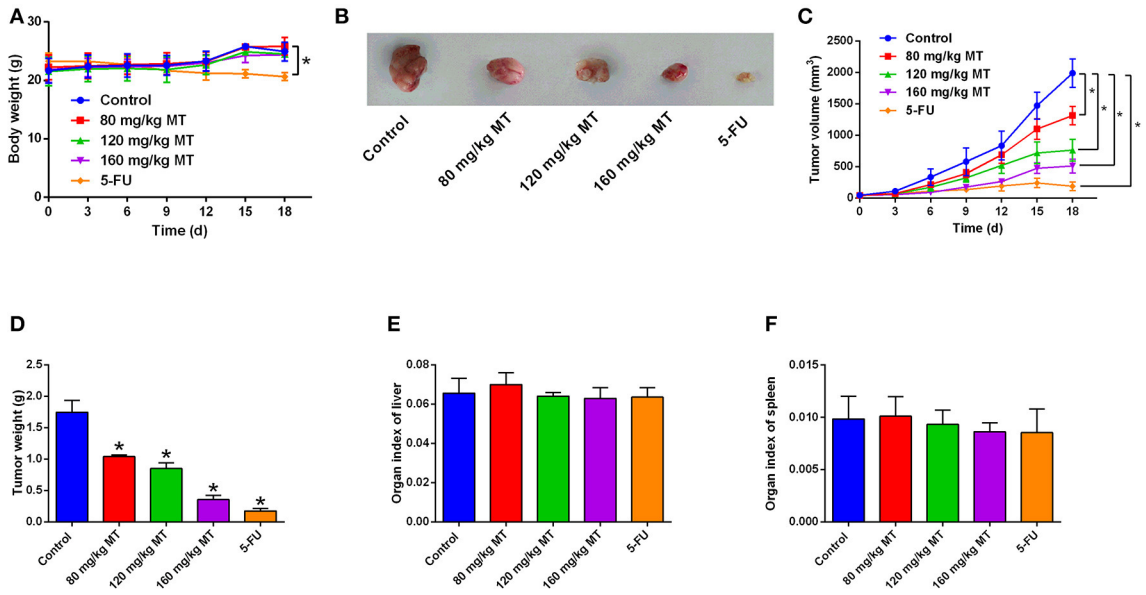

FIGURE 5 | MT inhibits tumor growth *in vivo*. **(A)** Body weight of mice after different treatments were determined every day. **(B)** Representative images of tumor tissues dissected from mice after different treatments. **(C)** The tumor volumes were measured every 3 days for 19 days in different treatment groups. **(D)** The tumor weight was measured after all nude mice were sacrificed. **(E,F)** Organ index of liver **(E)** and spleen **(F)** in the nude mice after different treatments were determined. $N = 5$. $^*P < 0.05$ compared to the corresponding control groups.

saline group are: p-Akt (2.91 ± 0.96%), NF-κB (35.47 ± 1.78%), MMP9 (7.64 ± 1.27%), and MMP2 (9.69 ± 1.34%). The positive staining ratio of the four proteins in MT (160 mg/kg) group were all significantly lower; the positive expression of the four proteins in 5-FU group was also remarkably repressed (**Figures 6D–G**).

DISCUSSION

In the current investigation, we demonstrated the antitumor effects of MT against HCC progression and deciphered the underlying molecular mechanisms. Our results illustrated that MT treatment concentration-dependently repressed HCC cell viability. Mechanistically, MT downregulated NF-κB, Akt, p-Akt, MMP2/MMP9 expression levels in HCC cells. This inhibitory effect was further verified in a BALB/c nude mouse tumor-hypodermic transplantation model. Thus, MT requires further assessment as an effective strategy for the HCC treatment.

HCC metastasis largely contributed to the recurrence of this human malignancy (21). The key process for tumor metastases involves the dissolved surrounding tumor matrix and basement membrane caused by tumor-associated proteases (22). Therefore, MTT assay and wound healing assay was carried out to detect the HepG2 cell growth and migratory abilities, respectively, after treatment with MT in our study. Our results elucidated that MT remarkably repressed the proliferation and migration of HepG2.

Potential molecular mediators that were involved in the inhibitory actions of MT on HepG2 cell proliferation and migration were analyzed. MMPs has been well-documented for their regulatory actions on tumor metastasis. Studies found that dysregulated MMP2/9 in the solid tumors largely contributed to the tumor metastasis including HCC (23, 24). Additionally, the cell growth inhibitory effect could also attributed to the inhibition of MMPs (25). C-Met is a high-affinity receptor and can be targeted activated by hepatocyte growth factor (HGF). The activation of c-Met involves various signaling pathways including PI3K/Akt and MAPK/Erk signaling pathways, which are key mediators in HCC cell proliferation and metastasis (26–28). Moreover, studies also illustrated that deregulated c-Met is associated with the invasiveness and progression of HCC (29–31) and anti-tumor mechanisms of many components extracted from Chinese herbal medicine and plants were related to the expression level of HGF/c-Met (31–38). MT showed moderate enhancing effects on the HepG2 cells apoptosis, but remarkably inhibited the migratory potential of HepG2 cells, suggesting that the inhibitory actions of MT may be more relevant to the tumor metastasis. In this study, we further investigated into the PI3K/AKT/NF-κB signaling pathway, which represents a key pathway in regulating HCC progression. Activation of PI3K/AKT/NF-κB signaling pathway is effective to enhance HCC cell proliferative, invasive and migratory potentials. Activation of NF-κB requires the Akt phosphorylation, which stimulates the IκB kinase complex, phosphorylates and inactivates IκB (39–42). There is evidence showing that NF-κB up-regulated MMP-9 expression (43–45), while the NF-κB inhibition could downregulate MMP-2 expression (46). In current investigation, MT treatment remarkably repressed Akt phosphorylation and NF-κB activation, which may lead to the suppressed MMP2/9 expression in HepG2 cells. Collectively, our results revealed a potential mechanism of MT-mediated tumor-suppressive actions in HCC.

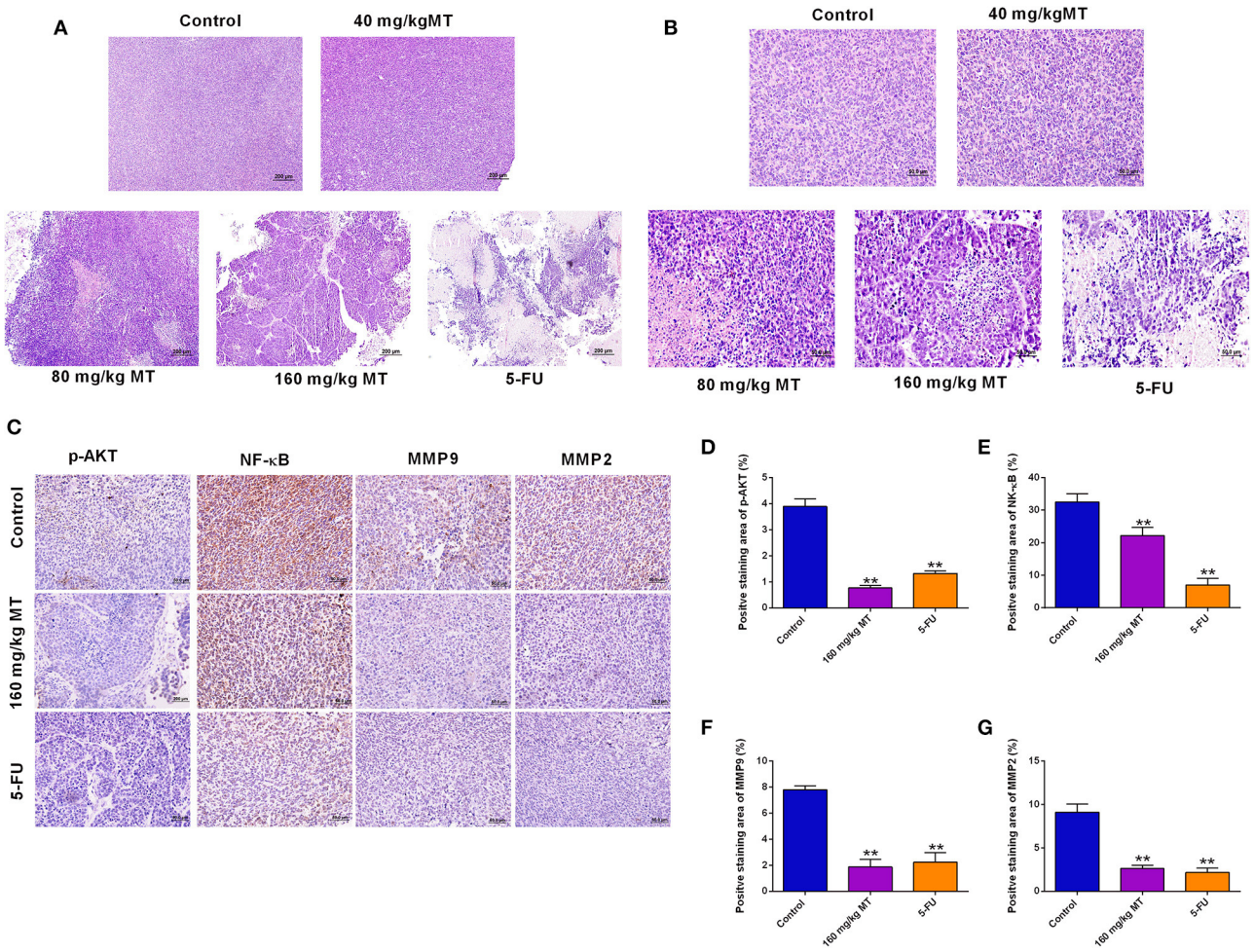

FIGURE 6 | Pathological morphology and relative protein expressions in the tumor tissues. **(A,B)** HE staining of tumor of nude mice from different treatment groups, original magnification: **(A)** 10× **(B)** 40×. **(C)** Immunohistochemistry for p-Akt, NF-κB, MMP9, and MMP2 in tumors of nude mice in different groups, original magnification: 40×. **(D–G)** The results of the ratio of positive staining of p-Akt **(D)**, NF-κB **(E)**, MMP9 **(F)** and MMP2 **(G)** are analyzed and Quantified by ImageJ. $N = 5$. $^{**}P < 0.01$ compared to the corresponding control groups.

From a clinical perspective, evaluation of chemotherapeutics should consider their antitumor effects as well as financial cost and adverse effects. In the current investigation, we revealed that MT did not affect mice body weight in comparison with 5-Fu treatment, which may suggest the potential application of MT in antitumor therapy with limited adverse effects. In addition, our data implied that MT treatment of HCC may be acted via repressing c-Met/PI3K/AKT pathway, thereby inhibited MMP2/9.

There are several study limitations for the current work. MT induced moderate apoptosis in the HepG2 cells, and the molecular mechanisms underlying MT-mediated HCC cell apoptosis require further examination. The anti-tumor effects of MT were determined in one HCC cell line, and other types of HCC cell lines should be employed to confirm the anti-tumor effects of HCC. The expression levels of p-AKT, NF-κB, MMP9/2 were only quantified by IHC in the tumor tissues, and further studies may employ western blot assay to determine the levels of these proteins in the tumor tissues.

In summary, the present study demonstrated the anti-tumor effects of MT on the HCC, and MT suppressed HCC progression possibly via regulating proliferation and migration-related mediators including c-Met, p-AKT, NF-κB, MMP2, and MMP9 in HepG2 cells. However, further examination is required to assess the therapeutic potential of MT in HCC.

DATA AVAILABILITY STATEMENT

The raw data supporting the conclusions of this article will be made available by the authors, without undue reservation, to any qualified researcher.

ETHICS STATEMENT

The animal study was reviewed and approved by Animal Ethics Committee of Guangdong Pharmaceutical University.

AUTHOR CONTRIBUTIONS

YZ and YW designed the study and wrote the manuscript. YW, XC, and SC performed the experiments and collected data. WF and DC performed statistical analysis. HZ performed the animal studies. All authors read and revised the manuscript before submission.

FUNDING

This study was supported by the projects of Guangzhou Key Laboratory of Construction and Application of New Drug Screening Model Systems (No. 201805010006) and Key Laboratory of New Drug Discovery and Evaluation of Ordinary Universities of Guangdong province (No. 2017KSYS002).

REFERENCES

1. Ferlay J, Soerjomataram I, Dikshit R, Eser S, Mathers C, Rebelo M, et al. Cancer incidence and mortality worldwide, sources, methods and major patterns in GLOBOCAN 2012. *Int J Cancer*. (2015) 136:E359–86. doi: 10.1002/ijc.29210
2. Xu J, Li J, Liu ZJ. MicroRNAs in the occurrence and development of primary hepatocellular carcinoma. *Adv Clin Exp Med*. (2016) 25:971–5. doi: 10.17219/acem/36460
3. Puppala S, Patel R, Yap KS, Patel J, Wah T, Snoddon A. Hepatocellular carcinoma: modern image-guided therapies. *Postgrad Med J*. (2016) 92:165–71. doi: 10.1136/postgradmedj-2014-132923
4. Wang FS, Fan JG, Zhang Z, Gao B, Wang HY. The global burden of liver disease: the major impact of China. *Hepatology*. (2014) 60:2099–108. doi: 10.1002/hep.27406
5. Gbolahan OB, Schacht MA, Beckley EW, LaRoche TP, O'Neil BH, Pyko M. Locoregional and systemic therapy for hepatocellular carcinoma. *J Gastrointest Oncol*. (2017) 8:215–28. doi: 10.21037/jgo.2017.03.13
6. Donadon M, Solbiati L, Dawson L, Barry A, Sapisochin G, Greig PD, et al. Hepatocellular carcinoma: the role of interventional oncology. *Liver Cancer*. (2016) 6:34–43. doi: 10.1159/000449346
7. Kim DW, Talati C, Kim R. Hepatocellular carcinoma (HCC): beyond sorafenib-chemotherapy. *J Gastrointest Oncol*. (2017) 8:256–65. doi: 10.21037/jgo.2016.09.07
8. Roxburgh P, Evans TR. Systemic therapy of hepatocellular carcinoma, are we making progress? *Adv Ther*. (2008) 25:1089–104. doi: 10.1007/s12325-008-0113-z
9. Desai J R, Ochoa S, Prins PA, He AR. Systemic therapy for advanced hepatocellular carcinoma: an update. *J Gastrointest Oncol*. (2017) 8:243–55. doi: 10.21037/jgo.2017.02.01
10. Keating GM. Sorafenib: a review in hepatocellular carcinoma. *Target Oncol*. (2017) 12:243–53. doi: 10.1007/s11523-017-0484-7
11. He AR, Goldenberg AS. Treating hepatocellular carcinoma progression following first-line sorafenib: therapeutic options and clinical observations. *Therapeutic Adv Gastroenterol*. (2013) 6:447–58. doi: 10.1177/1756283X13498540
12. Suzuki R, Takizawa T, Kuwata Y, Mutoh M, Ishiguro N, Utoguchi N, et al. Effective anti-tumor activity of oxaliplatin encapsulated in transferrin-PEG-liposome. *Int J Pharm*. (2008) 346:143–50. doi: 10.1016/j.ijpharm.2007.06.010
13. Cabrera EV, Gil AC, Ortega JG, Bedoya L, Sánchez J, Banerjee AK. A one-pot synthesis of 6-Isopropyl-7-methoxy-1-tetralone and 6-Isopropyl-7-methoxy-2-tetralone. *Org Prep Proc Int*. (2014) 46:272–6. doi: 10.1080/00304948.2014.903146
14. Stathakis CI, Neokosmidis E, Koftis TV. A scalable synthesis of the antidepressant agomelatine by a tandem allylic chlorination–isomerization process. *Annalen Der Chemie Und Pharmacie*. (2015) 46:6376–9. doi: 10.1002/ejoc.201402886
15. Reddy PA, Rao GSK. Vilsmeier reaction on some 6- and 7-methoxy-1- and 2-tetralones. *J Chem Sci*. (1980) 89:435–9.
16. Sun ML, Song ZQ, Fang GZ. [Insecticidal activity and active components of alcohol extract from *Juglans mandshurica* Maxim leaves]. *Ying Yong Sheng Tai Xue Bao*. (2007) 18:2910.
17. Li J, Xu KP, Zou ZX, Zou H, Long HP, Tan LH, et al. Two new compounds from the green peel of Juglans mandshurica. *J Asian Nat Prod Res*. (2017) 19:1087–92. doi: 10.1080/10286020.2017.1295228
18. Chen J, Teng J, Ma L, Tong H, Ren B, Wang L, et al. Flavonoids isolated from the flowers of limonium bicolor and their *in vitro* antitumor evaluation. *Pharmacogn Mag*. (2017) 13:222–5. doi: 10.4103/0973-1296.204566
19. Wang L, Wu X, Wang R, Yang C, Li Z, Wang C, et al. BRD4 inhibition suppresses cell growth, migration and invasion of salivary adenoid cystic carcinoma. *Biol Res*. (2017) 50:19. doi: 10.1186/s40659-017-0124-9
20. Liu Y, Murray-Stewart T, Casero RA Jr, Kagiampakis I, Jin L, Zhang J, et al. Targeting hexokinase 2 inhibition promotes radiosensitization in HPV16 E7-induced cervical cancer and suppresses tumor growth. *Int J Oncol*. (2017) 50:2011–23. doi: 10.3892/ijo.2017.3979
21. Tao YM, Liu Z, Liu HL. Dickkopf-1 (DKK1) promotes invasion and metastasis of hepatocellular carcinoma. *Dig Liver Dis*. (2013) 45:251–7. doi: 10.1016/j.dld.2012.10.020
22. Korpi JT, Hagström J, Lehtonen N. Expression of matrix metalloproteinases-2,−8,−13,−26, and tissue inhibitors of metalloproteinase-1 in human osteosarcoma. *Surg Oncol*. (2011) 20:18–22. doi: 10.1016/j.suronc.2010.08.004
23. Tang Y, Lv P, Sun Z, Han L, Zhou W. 14-3-3beta promotes migration and invasion of human hepatocellular carcinoma cells by modulating expression of MMP2 and MMP9 through PI3K/Akt/NF-kappaB pathway. *PLoS ONE*. (2016) 11:e0146070. doi: 10.1371/journal.pone.0146070
24. Bartels RH. Spinal extradural metastasis: review of current treatment options. *Ca A Cancer J Clin*. (2008) 58:245–59. doi: 10.3322/CA.2007.0016
25. Zhang Y, Wang L, Zi Y, Zhang L, Guo Y, Huang Y. Oridonin effectively reverses the drug resistance of cisplatin involving induction of cell apoptosis and inhibition of MMP expression in human acute myeloid leukemia cells. *Saudi J Biol Sci*. (2017) 24:678–86. doi: 10.1016/j.sjbs.2017.01.042
26. Graziani A, Gramaglia D, Cantley LC, Comoglio PM. The tyrosine-phosphorylated hepatocyte growth factor/scatter factor receptor associates with phosphatidylinositol 3-kinase. *J Biol Chem*. (1991) 266:22087–90.
27. Ponzetto C, Bardelli A, Zhen Z, Maina F, Zonca PD, Giordano S, et al. A multifunctional docking site mediates signaling and transformation by the hepatocyte growth factor/scatter factor receptor family. *Cell*. (1994) 77:261–71. doi: 10.1016/0092-8674(94)90318-2
28. Fixman ED, Naujokas MA, Rodrigues GA, Moran MF, Park M. Efficient cell transformation by the Tpr-Met oncoprotein is dependent upon tyrosine 489 in the carboxy-terminus. *Oncogene*. (1995) 10:237–49.
29. Gao F, Deng G, Liu W, Zhou K, Li M. Resveratrol suppresses human hepatocellular carcinoma via targeting HGF-c-Met signaling pathway. *Oncol Rep*. (2017) 37:1203–11. doi: 10.3892/or.2017.5347
30. You H, Ding W, Dang H, Jiang Y, Rountree CB. c-Met represents a potential therapeutic target for personalized treatment in hepatocellular carcinoma. *Hepatology*. (2011) 54:879–89. doi: 10.1002/hep.24450
31. Shi MD, Liao YC, Shih YW, Tsai LY. Nobiletin attenuates metastasis via both ERK and PI3K/Akt pathways in HGF-treated liver cancer HepG2 cells. *Phytomedicine*. (2013) 20:743–52. doi: 10.1016/j.phymed.2013.02.004
32. Cao HH, Cheng CY, Su T, Fu XQ, Guo H, Li T, et al. Quercetin inhibits HGF/c-Met signaling and HGF-stimulated melanoma cell migration and invasion. *Mol Cancer*. (2015) 14:103. doi: 10.1186/s12943-015-0367-4
33. Garcia-Vilas JA, Quesada AR, Medina MA. Damnacanthal, a noni anthraquinone, inhibits c-Met and is a potent antitumor compound against Hep G2 human hepatocellular carcinoma cells. *Sci Rep*. (2015) 5:8021. doi: 10.1038/srep08021
34. Hyuga S. The pharmacological actions of ephedrine alkaloids-free ephreda herb extract and preparation for clinical application. *Yakugaku Zasshi*. (2017) 137:179–86. doi: 10.1248/yakushi.16-00233-4
35. Li Z, You K, Li J, Wang Y, Xu H, Gao B, Wang J. Madecassoside suppresses proliferation and invasiveness of HGF-induced human hepatocellular

carcinoma cells via PKC-cMET-ERK1/2-COX-2-PGE2 pathway. *Int Immunopharmacol*. (2016) 33:24–32. doi: 10.1016/j.intimp.2016.01.027
36. Yang X, Yang Y, Tang S, Tang H, Yang G, Xu Q, et al. Anti-tumor effect of polysaccharides from *Scutellaria barbata* D. Don on the 95-D xenograft model via inhibition of the C-met pathway. *J Pharmacol Sci*. (2014) 125:255–63. doi: 10.1254/jphs.13276FP
37. Mehta R, Katta H, Alimirah F, Patel R, Murillo G, Peng X, et al. Deguelin action involves c-Met and EGFR signaling pathways in triple negative breast cancer cells. *PLoS ONE*. (2013) 8:e65113. doi: 10.1371/journal.pone.0065113
38. Hong SW, Jung KH, Lee HS, Son MK, Yan HH, Kang NS, et al. SB365, Pulsatilla saponin D, targets c-Met and exerts antiangiogenic and antitumor activities. *Carcinogenesis*. (2013) 34:2156–69. doi: 10.1093/carcin/bgt159
39. Wu L, Zheng J, Chen P, Liu Q, Yuan Y. Small nucleolar RNA ACA11 promotes proliferation, migration and invasion in hepatocellular carcinoma by targeting the PI3K/AKT signaling pathway. *Biomed Pharmacother*. (2017) 90:705–12. doi: 10.1016/j.biopha.2017.04.014
40. Shan RF, Zhou YF, Peng AF, Jie ZG. Inhibition of Aurora-B suppresses HepG2 cell invasion and migration via the PI3K/Akt/NF-kappaB signaling pathway *in vitro*. *Exp Ther Med*. (2014) 8:1005–9. doi: 10.3892/etm.2014.1844
41. Huang S, Pettaway CA, Uehara H, Bucana CD, Fidler IJ. Blockade of NF-kappaB activity in human prostate cancer cells is associated with suppression of angiogenesis, invasion, and metastasis. *Oncogene*. (2001) 20:4188–97. doi: 10.1038/sj.onc.1204535
42. Graham TR, Odero-Marah VA, Chung LW, Agrawal KC, Davis R, Abdel-Mageed AB. PI3K/Akt-dependent transcriptional regulation and activation of BMP-2-Smad signaling by NF-κB in metastatic prostate cancer cells. *Prostate*. (2009) 69:168–80. doi: 10.1002/pros.20870
43. Andela VB, Gordon AH, Zotalis G, Rosier RN, Goater JJ, Lewis GD, et al. NFκB: a pivotal transcription factor in prostate cancer metastasis to bone 1. *Clin Ortho Relat Res*. (2004) 22:81–2. doi: 10.1016/j.urolonc.2003.12.011
44. Kim D, Kim S, Koh H, Yoon SO, Chung AS, Cho KS, et al. Akt/PKB promotes cancer cell invasion via increased motility and metalloproteinase production. *FASEB J*. (2001) 15:1953. doi: 10.1096/fj.01-0198com
45. Chandrasekar B, Mummidi S, Mahimainathan L, Patel DN, Bailey SR, Imam SZ, et al. Interleukin-18-induced human coronary artery smooth muscle cell migration is dependent on NF-kappaB- and AP-1-mediated matrix metalloproteinase-9 expression and is inhibited by atorvastatin. *J Biol Chem*. (2006) 281:15099. doi: 10.1074/jbc.M600200200
46. Felx M, Guyot MC, Isler M, Turcotte RE, Doyon J, Khatib AM, et al. Endothelin-1 (ET-1) promotes MMP-2 and MMP-9 induction involving the transcription factor NF-kappaB in human osteosarcoma. *Clin Sci*. (2006) 110:645–54. doi: 10.1042/CS20050286

Conflict of Interest: The authors declare that the research was conducted in the absence of any commercial or financial relationships that could be construed as a potential conflict of interest.

frontiers in Oncology

CASE REPORT
published: 25 February 2020
doi: 10.3389/fonc.2020.00032

Change of Pathological Type to Metaplastic Squamous Cell Carcinoma of the Breast During Disease Recurrence: Case Report and Literature Review

Tianhui Guo[1], *Zhiying Chen*[2], *Jinpeng Xu*[2] *and Yongchun Zhang*[2*]

[1] *Department of Radiation Oncology, Laoshan Branch of Affiliated Hospital of Qingdao University, Qingdao, China,*
[2] *Department of Radiation Oncology, The Affiliated Hospital of Qingdao University, Qingdao, China*

Background: Metaplastic squamous cell carcinoma (SCC) of the breast is a rare and heterogeneous group of primary breast malignancies. The etiology, pathogenesis, and proper treatment for this kind rare breast cancer are still unclear.

Case presentation: We reported a case of a 55-year-old woman with a palpable lump in the inner quadrant of the right breast. She underwent a right breast mass resection and sentinel lymph node biopsy, which revealed that the tumor was an invasive ductal carcinoma, followed by four cycles of doxorubicin plus cyclophosphamide and four cycles of docetaxel as adjuvant chemotherapy, and then simultaneous integrated boost intensity modulated radiotherapy to the whole right breast. After 2 years' follow-up, she had biopsy-proven disease recurrence in the right breast, which revealed SCC, and a mammogram showed abnormalities in the lower inner quadrant of the right breast and left axillary lymph nodes. Then we performed bilateral breast modified radical mastectomy, which confirmed that the recurrent tumors were metaplastic SCC, followed by adjuvant chemotherapy and adjuvant radiotherapy of the left supraclavicular and apical axillary regions. There has been no recurrent or metastatic evidence in the 16 months' follow-up since the second surgery.

Conclusion: This case report shows that evolution of pathology type in recurrent breast cancer after initial treatment is possible. Detailed pathologic and immunohistochemical analyses are needed for identification of this change. Surgery and adjuvant radiation and chemotherapy are appropriate treatments for recurrent primary SCC of the breast.

Keywords: breast cancer, recurrence, metaplastic squamous cell carcinoma, treatment, case report

OPEN ACCESS

Edited by:
Pascale Cohen,
Université Claude Bernard Lyon 1, France

Reviewed by:
Daniele Vergara,
University of Salento, Italy
Shiyu Song,
Virginia Commonwealth University Health System, United States

***Correspondence:**
Yongchun Zhang
zyc18661805058@163.com

Specialty section:
This article was submitted to Molecular and Cellular Oncology, a section of the journal Frontiers in Oncology

Received: *26 September 2019*
Accepted: *09 January 2020*
Published: *25 February 2020*

Citation:
Guo T, Chen Z, Xu J and Zhang Y (2020) Change of Pathological Type to Metaplastic Squamous Cell Carcinoma of the Breast During Disease Recurrence: Case Report and Literature Review. Front. Oncol. 10:32. doi: 10.3389/fonc.2020.00032

BACKGROUND

Breast cancer is the most common cancer of women in China and the United States, for which the clinical manifestation and the biological behavior are heterogeneous (1, 2). The most common pathological types of the breast cancer are ductal carcinoma and lobular carcinoma, which account for more than 70% of breast carcinoma. Metaplastic breast carcinoma, however, is a rare and heterogeneous group of primary breast malignancies accounting for $< 1\%$ of invasive breast

cancer (3). These tumors including the type of squamous cell carcinoma (SCC) are non-glandular differentiation. The etiology and nosogenesis of metaplastic breast carcinoma are still uncertain. There are several hypotheses for the pathogenesis of breast SCC. One theory is that the lesion is adenocarcinoma with an excessive form of squamous metaplasia (4). Another one is that it is straightly developed from the epithelium of the mammary ducts; moreover, an alternate theory is that the tumor arises from foci of squamous metaplasia within a pre-existing adenocarcinoma of the breast (5).

Because primary breast SCC is rare, a detailed metastatic workup is needed to rule out the possibility of metastatic disease. There are no characteristic clinical and imaging manifestations for SCC of the breast. Hence, the nature of the lesion needs to be determined by the pathology (4). In this paper, we presented a report of recurrent breast cancer of which the pathological type changed from the ductal carcinoma to metaplastic SCC.

CASE PRESENTATION

In 2015, a 55-year-old woman with a palpable lump in the inner quadrant of the right breast presented to the Breast Center in our hospital. She had no other clinical symptoms such as pain, skin change, nipple retraction, or nipple discharge. She was a non-smoker and denied having any systemic diseases or any family history of breast or ovary cancer, but her father died of gastric adenocarcinoma, and her mother died of lung

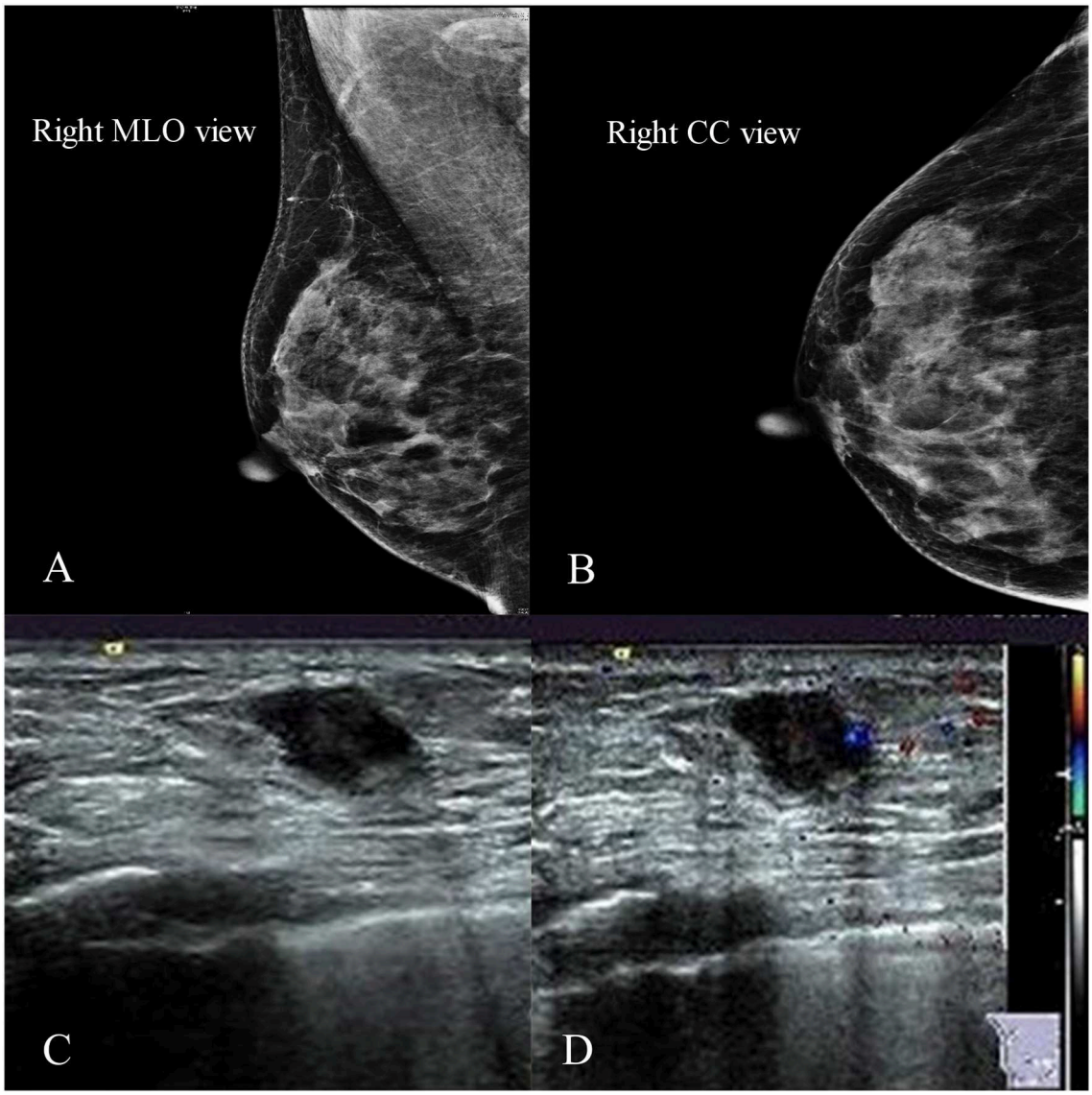

FIGURE 1 | Imaging of the primary tumor. **(A,B)** Right mammogram showed that the local structure of the inner quadrant of the right breast was crowding. **(C,D)** Ultrasound showed an irregular hypoechoic mass of 1.2 × 0.8 cm located at 3–4 o'clock.

cancer. On physical examination, there was a 2 × 1 cm mass at 3 o'clock in the right breast, 2 cm away from the nipple. The lump was firm, border unclear, moveable, irregular, and not fixed to the skin or chest wall. No abnormality was found in the axillary or supraclavicular lymph nodes. A mammogram showed a lesion classified as Breast Imaging Reporting and Data System 4B in the inner quadrant of the right breast (**Figures 1A,B**). The ultrasound showed an irregular hypoechoic mass of 1.2 × 0.8 cm located at 3–4 o'clock, and no positive lymph node was detected (**Figures 1C,D**).

We performed an ultrasound-guided core needle biopsy, which confirmed the diagnosis of invasive ductal carcinoma (IDC). After detailed discussion with the surgeon, the patient chose to preserve her breast. So we performed a right breast mass resection and sentinel lymph node biopsy on December 14, 2015. An invasive carcinoma in the mammary gland was localized in the lower inner quadrant with a maximum diameter of 0.6 cm. Histologically, the tumor was predominantly grade 2 IDC (about 60%), partial invasive micropapillary carcinoma (about 20%), and partial ductal carcinoma *in situ* (about

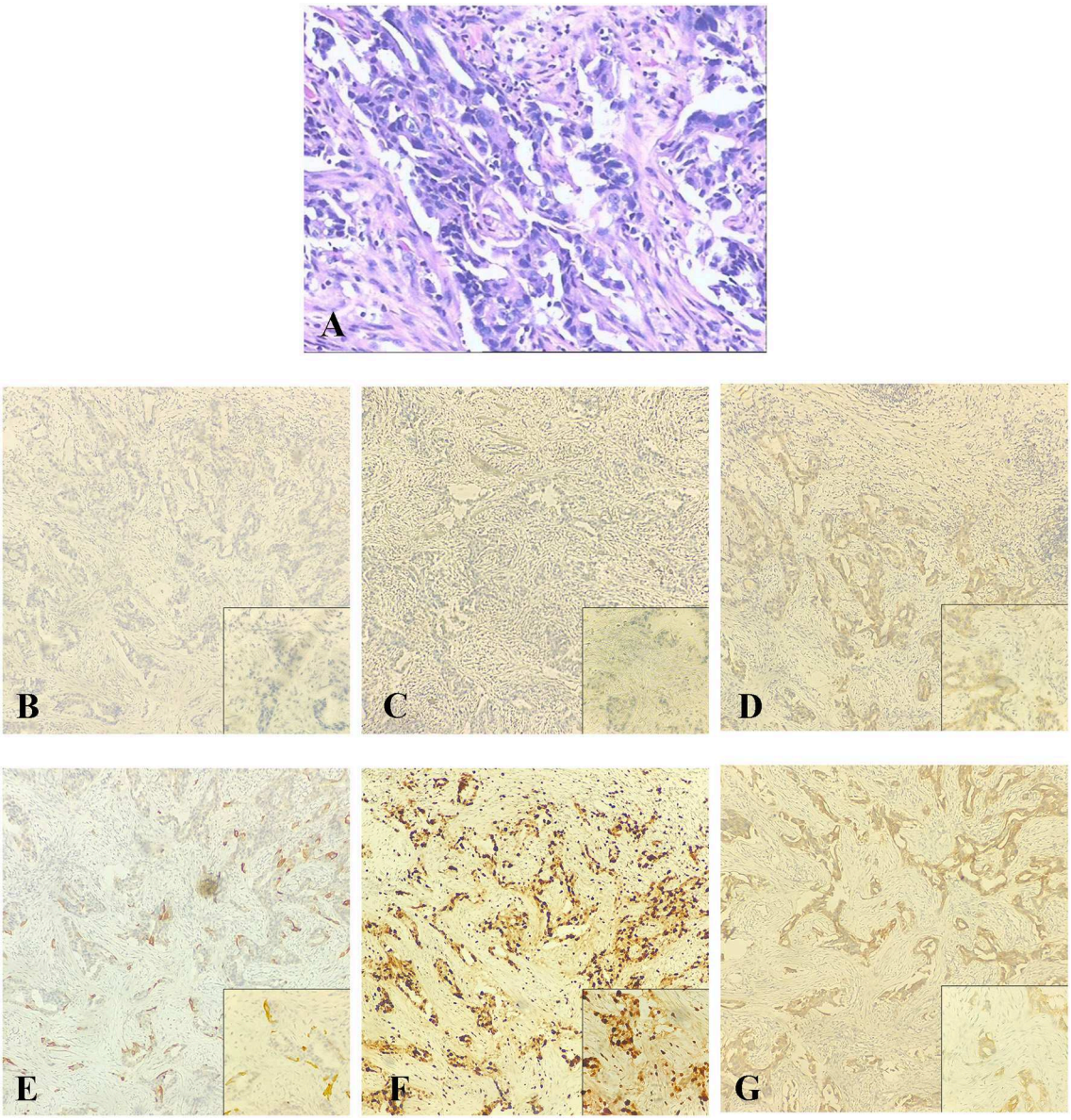

FIGURE 2 | The postoperative pathological examination with hematoxylin and eosin (HE) staining and immunohistochemical (IHC) staining of the primary tumor in 2015. **(A)** Histological findings with HE staining at high magnification (40×) showed that the tumor was an invasive ductal carcinoma. **(B–G)** IHC staining was used to detect the expressions of ER, PR, HER-2, CK5/6, Ki-67, and EGFR at original magnification (10×). **(B)** ER negative. **(C)** PR negative. **(D)** HER-2 weakly positive. **(E)** CK5/6 negative. **(F)** Ki-67 positive (80%). **(G)** EGFR focal positive.

TABLE 1 | The patient's characteristics and treatment process.

Gender		**Female**	
Age, year		55	
Process	Primary diagnosis	November, 2015 3 o'clock of the right breast	
	Primary pathology	Predominant invasive ductal carcinoma	
		Immunohisto-chemistry	ER(–), PR(–), HER-2(1+), CK5/6(–), Ki-67(+,80%), EGFR(focal+), E-Cadherin(+)
	Treatments	Surgery	Mass enlargement resection Sentinel lymph node biopsy
		Adjuvant chemotherapy	4 × AC→ 4 × T
		Adjuvant radiotherapy	SIB-IMRT to the whole right breast (whole-50.4Gy, high-risk area-60.2Gy)
	DFS	24 months	
	Recurrent diagnosis	March, 2018 4 o'clock of the right breast	
	Recurrent pathology	Metaplastic squamous cell carcinoma	
		Immunohisto-chemistry	ER(–), PR(–), Her-2(–), CK5/6(+), Ki-67(+,70%), EGFR(+), E-Cadherin(+)
	Treatments	Surgery	Breast modified radical mastectomy
		Adjuvant chemotherapy	3 × TP→ 3 × docetaxel+capcitabine
		Adjuvant radiotherapy	IMRT to the left supraclavicular and apical axillary regions (50Gy)
	DFS	16 months (last follow-up time: August, 2019)	

(–): Negative expression; (+): Positive expression.
4 × AC→ 4 × T: four cycles chemotherapy of doxorubicin and cyclophosphamide followed by four cycles of docetaxel.
SIB-IMRT: simultaneous integrated boost intensity modulated radiotherapy.
6 × TP: Six cycles chemotherapy of docetaxel and cisplatin.
DFS, disease-free survival.

20%) with focal dysplasia in the upper resection margin (**Figure 2**). There was no metastasis in the sentinel lymph nodes (0/6). Immunohistochemical staining showed that the tumor was ER-negative, PR-negative, CerbB-2–positive (intensity 1), CK5/6-negative, P53-positive 70%, EGFR-focal positive, and Ki-67–positive 80%, and a FISH test demonstrated negative Her-2 gene amplification (**Table 1**). Thus, the tumor was pT1N0M0, equivalent to stage Ia.

After surgery, the patient received adjuvant chemotherapy with four cycles of doxorubicin and cyclophosphamide followed by four cycles of docetaxel every 3 weeks. She then underwent adjuvant radiation with simultaneous integrated boost intensity modulated radiotherapy (SIB-IMRT) to the whole right breast to a total dose of 50.4 Gy in 28 fractions and to the high-risk area for recurrence to a total dose of 60.2 Gy in 28 fractions (**Supplementary Figure 1**). Since the surgery, there had been no evidence of recurrence or metastasis for 24 months' follow-up.

Then the patient felt a nodule in the right breast again, and the size of this nodule gradually increased. Four months later, she received an ultrasound examination, which found that there was an irregular non-homogeneous-echo mass in the lower inner quadrant of the right breast below the surgical incision and had biopsy-proven disease recurrence in the right breast which revealed SCC. A mammogram showed an abnormal density shadow in the lower inner quadrant of the right breast, which lead to suspicion of malignant lesions, and enlarged left axillary lymph nodes (**Figure 3**), which biopsy indicated to be invasive carcinoma. The multidisciplinary team (MDT) conference board recommended bilateral breast modified radical mastectomy on March 15, 2018. An invasive carcinoma in the right mammary gland was localized in the lower inner quadrant, measuring 1.6 × 1.5 × 1.3 cm, and 1 of the 15 left axillary lymph nodes removed was malignant. No abnormality was found in the left breast or right axillary lymph nodes. Microscopic examination of the tumors revealed metaplastic SCC with an ER-negative, PR-negative, Her-2–negative, CK5/6-positive, P53-positive 50%, EGFR-positive, and Ki-67–positive 70% phenotype detected by immunohistochemical staining (**Figure 4**; **Table 1**).

Following surgery, the case was then discussed in an MDT conference because of the change of pathological type. Adjuvant chemotherapy with six cycles of docetaxel and cisplatin was planned (TP chemotherapy). But after three cycles, the TP chemotherapy was stopped because of severe drug-related gastrointestinal adverse events. The patient then accepted docetaxel and capecitabine for another three cycles. From October 10, 2018, to November 15, 2018, she underwent adjuvant radiotherapy with intensity modulated radiotherapy (IMRT) to the left supraclavicular and apical axillary regions with a total dose of 50 Gy in 25 fractions (**Supplementary Figure 2**). There has been no recurrent or metastatic evidence in the 16 months' follow-up since the second surgery.

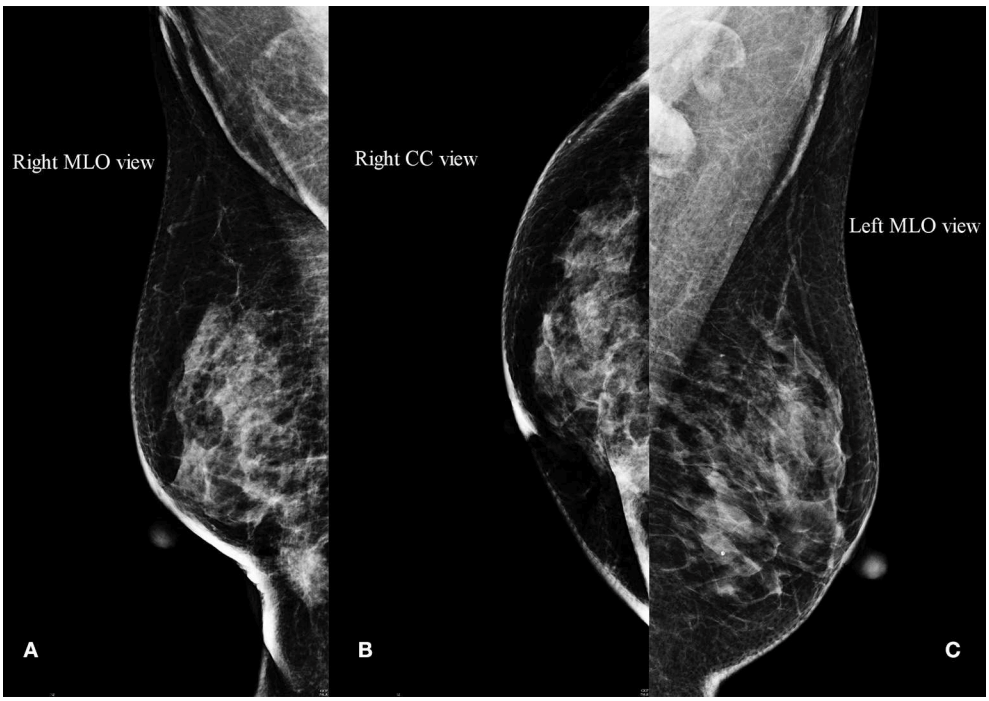

FIGURE 3 | Mammogram. **(A,B)** An abnormal density shadow in the lower inner quadrant of the right breast suspected to be malignant lesions. **(C)** Enlarged left axillary lymph nodes.

DISCUSSION

SCC of the breast was first reported by Troell in 1908 (6). Because SCC of the breast was a very rare type of malignancy, no large prospective randomized clinical trials have been performed to study its pathogenesis, specific radiologic characteristics, effective treatment management, and prognosis. As a metaplastic carcinoma, SCC also shows heterogeneous characteristic features. The question of the origin of metaplastic breast cancers is still unclear. Behranwala et al. proposed two theories explaining the development mechanism of SCC of the breast: (1) arising from benign breast disease and (2) arising from invasive duct carcinoma (7). However, van Deurzen et al. demonstrated that the phenotypic changes of breast cancer are the result of malignant transformation of breast cancer stem/progenitor cells (histogenesis) or specific genetic mutations taking place at early or late stages of carcinogenesis (dedifferentiation) (8). Furthermore, Avigdor et al. performed whole exome sequencing for eight patients containing both conventional *in situ* or IDC and metaplastic components, which showed that the genomic landscape of an intertwined metaplastic breast tumor may generally be the same as the non-metaplastic component, and the different histologies of these cancers may be driven mainly by epigenetic or non-coding changes (9). As for our patient, her recurrent pathological histology was a pure metaplastic SCC, which is classified as pure epithelial type according to the World Health Organization (WHO), (3) indicating that her phenotypic change was more likely the result of malignant transformation of breast cancer stem/progenitor cells.

SCC may have some common clinicopathological features, such as the larger tumor size and larger proportion of T3–4, grade III, and triple-negative (lack of expression of ER, PR, and HER2) tumors than IDC (10). It presents less frequent lymphovascular invasion, but there is no difference in occurrence of positive lymph nodes between SCC and IDC patients (10). According to previous studies, 3–4% of SCC patients develop distant metastases (7, 10). However, there are no specific imaging characteristics for the metaplastic SCC patients. The pathological criteria for the diagnosis of SCC of the breast are as follows: (a) nipple, skin, or its appendages are not the sources of the tumor; (b) over 90% of tumor areas must be squamous cells; (c) other invasive components (ductal or mesenchymal) do not exist in the whole tumor; and (d) other sites of primary SCC (PSCC) are excluded (11). The recurrent tumor in this case satisfied all of these conditions. Significantly, the pathological type of the first resected malignant tumor in the right breast was IDC, but after adjuvant chemotherapy and radiotherapy, the type of the recurrent mass changed to metaplastic SCC This indicated that pathological phenotypes of tumors could transform one type to another, especially for those with metaplastic components (6). Graziano et al. (12) reported that IDC of the breast could progress to metaplastic SCC after induction chemotherapy. Previous research revealed that long-standing breast implants and acute unilateral breast pain and enlargement might also cause secondary PSCC of the breast (13, 14). Furthermore, PSCC of the breast possibly arises from previous radiation (15). Above all, metaplastic SCC of the breast can be induced by a breast implant, chemotherapy, or radiation.

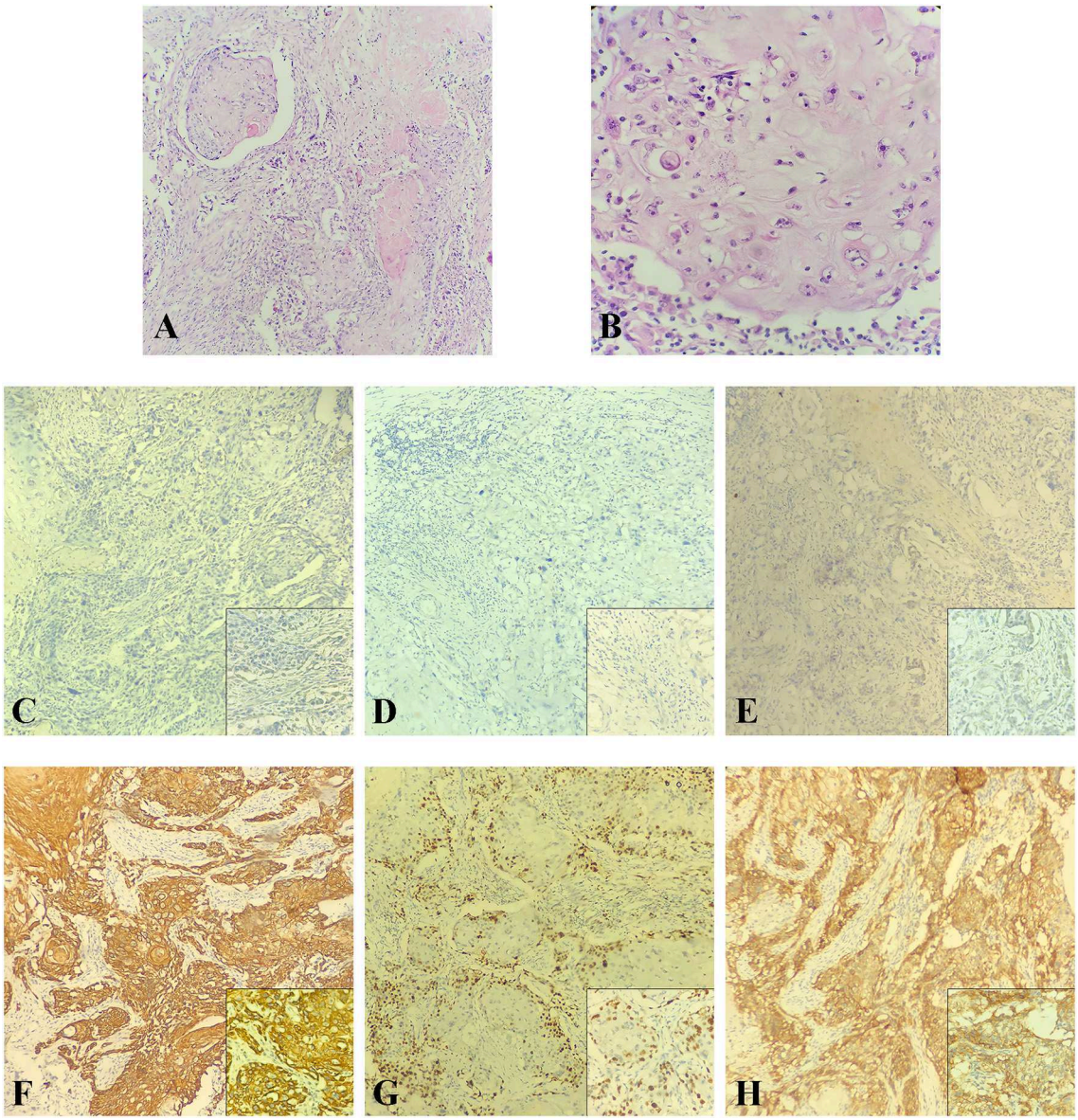

FIGURE 4 | The postoperative pathological examination with HE staining and IHC staining of the recurrent tumor in 2018. **(A,B)** Histological findings with HE staining showed that the recurrent tumor was a metaplastic squamous cell carcinoma with prominent keratinization that exhibited an infiltrative growth pattern. **(A)** Original magnification (10×). **(B)** High magnification (40×). **(C–H)** IHC staining was used to detect the expressions of ER, PR, HER-2, CK5/6, Ki-67, and EGFR at original magnification (10×). **(C)** ER negative. **(D)** PR negative. **(E)** HER-2 negative. **(F)** CK5/6 positive. **(G)** Ki-67 positive (70%). **(H)** EGFR positive.

PSCC of the breast is usually a highly malignant and hormone receptor–negative tumor, which indicates that hormone-based therapy may not have an effect on these tumors. Besides, HER2-targeted therapy is not greatly effective either for negative Her-2 gene amplification. Treatment strategies of PSCC are not different from those of other triple-negative histologic types of breast tumors, which include neoadjuvant therapy, surgery, chemotherapy, hormonal therapy, and radiotherapy. Liu et al. (6) found that TP as neoadjuvant therapy may be effective for those breast PSCC patients. Several studies revealed that compared with IDC, the PSCC patients of the breast have more rapid progression, shorter overall survival, and poorer prognosis (6, 7, 10). For this patient, the second surgery was decided to perform bilateral breast modified radical mastectomy because we are not sure about the origin of the left metastatic axillary lymph node. It may be metastasized from the tumor of the right breast or from an occult cancer of the left breast. Then we used TP chemotherapy as the second adjuvant chemotherapy and adjuvant radiotherapy in the left supraclavicular and apical axillary regions. There has been no recurrent or metastatic evidence till now. Some researchers studied the landscape of somatic genetic alterations of breast PSCC patients, which

demonstrated that TP53 and PI3KCA gene mutation might be caused by the activation of the Wnt and PI3K/AKT/mTOR pathway, (16) and this may provide us a new treatment strategy for breast SCC patients. Besides, epigenetic therapies may be effective treatments for metaplastic breast carcinomas (9). But the most therapeutic regimen for this rare disease still remains unclear. Therefore, knowing its pathogenesis, clinical features, and specific imaging characteristics is crucial to choose the optimal treatment for such a rare and aggressive disease.

In conclusion, this case report shows that evolution of pathology type in recurrent breast cancer after initial treatment is possible. Detailed pathologic and immunohistochemical analyses are needed for identification of this change. Surgery and adjuvant radiation and chemotherapy are appropriate treatments for recurrent PSCC of the breast.

DATA AVAILABILITY STATEMENT

All data sets generated for this study are included in the article/**Supplementary Material**.

ETHICS STATEMENT

The authors of this manuscript obtained patient consent for publication of clinical data and images. The patient's details were anonymized, and the patient signed the consent form for the publication. Due to the retrospective and non-interventional nature of the study, permission by the local ethics committee was not required.

AUTHOR CONTRIBUTIONS

TG, ZC, JX, and YZ collected the patient's data and provided the figures. TG designed the study and finished the original manuscript. JX revised the manuscript and provided the immunohistochemical figures. YZ provided final approval for the version to be published. The final version of the manuscript was read and approved by all authors.

ACKNOWLEDGMENTS

We thank Girish Talakatta, Ph.D., a postdoc of Sun Yat-Sen University Cancer Center, for providing professional medical writing assistance.

SUPPLEMENTARY MATERIAL

The Supplementary Material for this article can be found online at: https://www.frontiersin.org/articles/10.3389/fonc.2020.00032/full#supplementary-material

REFERENCES

1. Chen W, Zheng R, Baade PD, Zhang S, Zeng H, Bray F, et al. Cancer statistics in China, 2015. *CA Cancer J Clin*. (2016) 66:115–32. doi: 10.3322/caac.21338
2. Siegel RL, Miller KD, Jemal A. Cancer statistics, 2019. *CA Cancer J Clin*. (2019) 69:7–34. doi: 10.3322/caac.21551
3. Eble JN, Tavassoli FA, Devilee P. *Pathology and Genetics of Tumours of the Breast and Female Genital Organs*. Lyon: Iarc (2003). p. 37–41.
4. Guerriero G, Zagami MG, Montesano M, Primavera A, Carino R, Battista C, et al. Squamous cell carcinoma of the breast diagnosis by vacuum-assisted core biopsy. *Tumor*. (2005) 91:418–20. doi: 10.1177/030089160509100507
5. Hennessy BT, Krishnamurthy S, Giordano S, Buchholz TA, Kau SW, Duan Z, et al. Squamous cell carcinoma of the breast. *J Clin Oncol*. (2005) 23:7827–35. doi: 10.1200/JCO.2004.00.9589
6. Liu J, Yu Y, Sun JY, He SS, Wang X, Yin J, et al. Clinicopathologic characteristics and prognosis of primary squamous cell carcinoma of the breast. *Breast Cancer Res Treat*. (2015) 149:133–40. doi: 10.1007/s10549-014-3224-z
7. Behranwala KA, Nasiri N, Abdullah N, Trott PA, Gui GP. Squamous cell carcinoma of the breast: clinico-pathologic implications and outcome. *Eur J Surg Oncol*. (2003) 29:386–9. doi: 10.1053/ejso.2002.1422
8. van Deurzen CH, Lee AH, Gill MS, Menke-Pluijmers MB, Jager A, Ellis IO, et al. Metaplastic breast carcinoma: tumour histogenesis or dedifferentiation? *J Pathol*. (2011) 224:434–7. doi: 10.1002/path.2872
9. Avigdor BE, Beierl K, Gocke CD, Zabransky DJ, Cravero K, Kyker-Snowman K, et al. Whole-exome sequencing of metaplastic breast carcinoma indicates monoclonality with associated ductal carcinoma component. *Clin Cancer Res*. (2017) 23:4875–84. doi: 10.1158/1078-0432.CCR-17-0108
10. Zhu L, Chen K. Clinicopathological features, treatment patterns, and prognosis of squamous cell carcinoma of the breast: an NCDB analysis. *BMC Cancer*. (2019) 19:26. doi: 10.1186/s12885-018-5212-x
11. Rosen PP. *Rosen's Breast Pathology*. Philadelphia, PA: Lippincott Williams & Wilkins (2001).
12. Graziano L, Graziano PF, Bitencourt AG, Soto DB, Hiro A, Nunes CC. Metaplastic squamous cell carcinoma of the breast: a case report and literature review. *Rev Assoc Med Bras (1992)*. (2016) 62:618–21. doi: 10.1590/1806-9282.62.07.618
13. Olsen DL, Keeney GL, Chen B, Visscher DW, Carter JM. Breast implant capsule-associated squamous cell carcinoma: a report of 2 cases. *Hum Pathol*. (2017) 67:94–100. doi: 10.1016/j.humpath.2017.07.011
14. Buchanan PJ, Chopra VK, Walker KL, Rudolph R, Greco RJ. Primary squamous cell carcinoma arising from a breast implant capsule: a case report and review of the literature. *Aesthet Surg J*. (2018) 38:NP97–NP102. doi: 10.1093/asj/sjy092
15. Singh H, Williams SP, Kinsella V, Lynch GR. Postradiation squamous cell cancer of the breast. *Cancer Invest*. (2000) 18:343–6. doi: 10.3109/07357900009012177
16. Ng CKY, Piscuoglio S, Geyer FC, Burke KA, Pareja F, Eberle CA, et al. The landscape of somatic genetic alterations in metaplastic breast carcinomas. *Clin Cancer Res*. (2017) 23:3859–70. doi: 10.1158/1078-0432.CCR-16-2857

Conflict of Interest: The authors declare that the research was conducted in the absence of any commercial or financial relationships that could be construed as a potential conflict of interest.

frontiers in Oncology

ORIGINAL RESEARCH
published: 27 February 2020
doi: 10.3389/fonc.2020.00228

Reversal Effect of ALK Inhibitor NVP-TAE684 on ABCG2-Overexpressing Cancer Cells

Jingqiu Wang[1,2], Jing-Quan Wang[1], Chao-Yun Cai[1], Qingbin Cui[1,3], Yuqi Yang[1], Zhuo-Xun Wu[1], Xingduo Dong[1], Leli Zeng[1,4], Linguo Zhao[2], Dong-Hua Yang[1] and Zhe-Sheng Chen[1]**

[1] Department of Pharmaceutical Sciences, College of Pharmacy and Health Sciences, St. John's University, Queens, NY, United States, [2] College of Chemical Engineering, Nanjing Forestry University, Nanjing, China, [3] School of Public Health, Guangzhou Medical University, Guangzhou, China, [4] Tomas Lindahl Nobel Laureate Laboratory, Research Centre, The Seventh Affiliated Hospital, Sun Yat-sen University, Shenzhen, China

OPEN ACCESS

Edited by:
Amit K. Tiwari,
University of Toledo, United States

Reviewed by:
Hua Zhu,
The Ohio State University,
United States
Shikha Kumari,
University of Nebraska Medical
Center, United States

***Correspondence:**
Dong-Hua Yang
yangd1@stjohns.edu
Zhe-Sheng Chen
chenz@stjohns.edu

Specialty section:
This article was submitted to
Molecular and Cellular Oncology,
a section of the journal
Frontiers in Oncology

Received: 16 November 2019
Accepted: 10 February 2020
Published: 27 February 2020

Citation:
Wang J, Wang J-Q, Cai C-Y, Cui Q,
Yang Y, Wu Z-X, Dong X, Zeng L,
Zhao L, Yang D-H and Chen Z-S
(2020) Reversal Effect of ALK Inhibitor
NVP-TAE684 on
ABCG2-Overexpressing Cancer Cells.
Front. Oncol. 10:228.
doi: 10.3389/fonc.2020.00228

Failure of cancer chemotherapy is mostly due to multidrug resistance (MDR). Overcoming MDR mediated by overexpression of ATP binding cassette (ABC) transporters in cancer cells remains a big challenge. In this study, we explore whether NVP-TAE684, a novel ALK inhibitor which has the potential to inhibit the function of ABC transport, could reverse ABC transporter-mediated MDR. MTT assay was carried out to determine cell viability and reversal effect of NVP-TAE684 in parental and drug resistant cells. Drug accumulation and efflux assay was performed to examine the effect of NVP-TAE684 on the cellular accumulation and efflux of chemotherapeutic drugs. The ATPase activity of ABCG2 transporter in the presence or absence of NVP-TAE684 was conducted to determine the impact of NVP-TAE684 on ATP hydrolysis. Western blot analysis and immunofluorescence assay were used to investigate protein molecules related to MDR. In addition, the interaction between NVP-TAE684 and ABCG2 transporter was investigated via *in silico* analysis. MTT assay showed that NVP-TAE684 significantly decreased MDR caused byABCG2-, but not ABCC1-transporter. Drug accumulation and efflux tests indicated that the effect of NVP-TAE684 in decreasing MDR was due to the inhibition of efflux function of ABCG2 transporter. However, NVP-TAE684 did not alter the expression or change the subcellular localization of ABCG2 protein. Furthermore, ATPase activity analysis indicated that NVP-TAE684 could stimulate ABCG2 ATPase activity. Molecular *in silico* analysis showed that NVP-TAE684 interacts with the substrate binding sites of the ABCG2 transporter. Taken together, our study indicates that NVP-TAE684 could reduce the resistance of MDR cells to chemotherapeutic agents, which provides a promising strategy to overcome MDR.

Keywords: NVP-TAE684, ATP-binding cassette (ABC) transporter, ABCG2, ALK inhibitor, multidrug resistance (MDR)

INTRODUCTION

Antineoplastic drugs can induce cancer cells resistant to treatment which makes the therapeutic effect of anti-cancer drugs greatly reduced and leads to multidrug resistance (MDR) (1). Classical MDR are mainly involved in drug-resistant proteins, which include the permeability-glycoprotein (P-gp/ABCB1) (2), multidrug resistance proteins (MRPs/ABCCs) (3), and breast cancer resistance protein (BCRP/MXR/ABCP/ABCG2) (4, 5).

P-gp, also known as MDR1 or ABCB1, is one of the most representative protein of ABC transporters (6–8). ABCB1 can identify various anti-cancer chemotherapeutic drugs, such as taxanes, camptothecins, anthracyclines, et al. (9). ATP hydrolysis provides energy for ABC transporters to extrude substrates out of tumor cells and lower the intracellular concentration of anticancer drugs, which results in weakening of the efficacy of chemotherapeutic drugs and eventually produces MDR (10).

The sub-family of MRPs/ABCCs is the C subgroup of ABC transporters. At present, nine MRPs with transport function have been found, ranging from MRP1 to MRP9 (11–13). Some of their structures (MRPs 4, 5, 7, 8, and 9) are similar to that of ABCB1. They contain two transmembrane regions and two ATP binding domains (14). But some of them have three transmembrane domains such as MRPs 1, 2, 3, and 6. MRP1/ABCC1 mediates the transport of anticancer drugs, including anthracyclines, methotrexate and doxorubicin (15–17).

ABCG2 is the first ABC semi-transporter found on cell membrane (18–20). Overexpression of ABCG2 can lead cancer cells resistant to various chemotherapeutic drugs. There are many overlaps between ABCG2, ABCB1, and ABCC1 in chemotherapeutic substrates, such as doxorubicin, epirubicin and mitoxantrone (21–23). However, the efflux capacity of ABCG2 for some chemotherapeutic drugs, such as vincristine and paclitaxel, is significantly lower than that of the other two drug-resistant proteins. In addition to chemotherapeutic drugs, ABCG2 has strong efflux ability to tyrosine kinase inhibitors, which can cause drug resistance in molecular targeted therapy. For example, imatinib and nilotinib for leukemia, sorafenib for liver cancer, erlotinib for NSCLC and lapatinib for HER2-positive breast cancer are substrates of ABCG2 (24–26). Therefore, screening the inhibitors of these three drug-resistant proteins is one of the effective methods to reverse MDR and improve efficacy of chemotherapy.

NVP-TAE684 is a selective ALK inhibitor which inhibits different downstream signaling transduction molecules in cancer cells, thereby down-regulating cell cycle and cell proliferation regulatory genes, resulting in arresting cell cycle, inhibiting cell proliferation and inducing cell apoptosis. NVP-TAE684 shows good anti-tumor effects to some mutant cells that are resistant to other ALK inhibitors (27–29). It was reported that NVP-TAE684 reverses MDR in human osteosarcoma by inhibiting ABCB1 function (30). However, whether NVP-TAE684 could affect other ABC transports has not been reported. In this study, we evaluate whether NVP-TAE684 can improve anticancer efficacy of drugs in ABCG2 or ABCC1 overexpressing MDR cells.

MATERIALS AND METHODS

Chemicals

NVP-TAE684 was acquired from Chemie Tek (Indianapolis, IN). Fetal bovine serum (FBS), penicillin/streptomycin (P/S), Dulbecco's modified Eagle's Medium (DMEM), 0.25% trypsin and bovine serum albumin (BSA) were obtained from Corning Incorporated (Corning, NY). The GAPDH loading control monoclonal antibody (GA1R) (1 mg/mL, Cat # MA5-15738, lot #: SA247966), Alexa Fluor 488 conjugated goat anti-mouse IgG cross-adsorbed secondary antibody (2 mg/mL, Cat # A32723) were obtained from Thermo Fisher Scientific Inc (Rockford, IL). The anti-ABCG2 antibody, clone BXP-21 (Cat # MAB4146, lot #: 3026758) was obtained from Millipore (Billerica, MA). Horseradish peroxidase (HRP)-conjugated rabbit anti-mouse IgG secondary antibody (Cat # 7076S, lot #: 32) was obtained from Cell Signaling Technology Inc (Danvers, MA). Mitoxantrone, SN-38, topotecan, cisplatin, dimethylsulfoxide (DMSO), 3-(4,5-dimethylthiazolyl)-2,5-diphenyltetrazolium bromide (MTT), 4′,6-diamidino-2-phenylindole (DAPI), paraformaldehyde, Triton X-100 and other chemicals were purchased from Sigma Chemical Co (St. Louis, MO). Ko143 was purchased from Enzo Life Sciences (Farmingdale, NY). [^{3}H]-Mitoxantrone (2.5 Ci/mmol) was purchased from Moravek Biochemicals, Inc (Brea, CA).

Cell Lines and Cell Culture

The non-small cell lung cancer (NSCLC) NCI-H460 and its mitoxantrone-selected NCI-H460/MX20 cell line withABCG2 overexpression were used. NCI-H460/MX20 cell line was maintained in medium with 20 ng/mL mitoxantrone (31). The ABCG2-transfected HEK293 cell lines (HEK293/ABCG2-482-G2, HEK293/ABCG2-482-R2, and HEK293/ABCG2-482-T7) were transfected with full length ABCG2 coding arginine (R), glycine (G) or threonine (T) at 482 position, respectively. Its corresponding parental cell line, HEK293/pcDNA3.1, was transfected with an empty vector pcDNA3.1. All transfected cells were cultured with G418 at the concentration of 2 mg/mL. The human epidermal carcinoma cell line KB-3-1 and its ABCC1-overexpressing KB-CV60 cell line, were maintained in medium with 1 mg/mL of cepharanthine and 60 ng/mL of vincristine (32). Cells were grown in DMEM medium containing 10% FBS and 1% P/S, and kept in a 37°C humidified incubator supplied with 5% CO_2. All drug-resistant cells were cultured in drug-free medium for more than 2 weeks before use.

Cell Viability Examined by MTT Assay

MTT assay was used to measure the cell viability for the ABCG2 and ABCC1 reversal study as previously described (33). NCI-H460 and NCI-H460/MX20 cells, HEK293/pcDNA3.1 and HEK293/ABCG2 cells, KB-3-1 and KB-CV60 cells were used for the study. A total of 5×10^3 cells were seeded into each well of a 96-well plate. On the next day, cells were treated with a serial concentrations of NVP-TAE684 for the toxicity test. For the reversal study, different concentrations of substrates were added 2 h after cells were pre-treated with NVP-TAE684, Ko143 (a positive reversal agent of ABCG2) or MK571(a positive

reversal agent of ABCC1) at non-toxic concentrations. After 72 h treatment, MTT solution at 4 mg/mL was added and further incubated for 4 h. Finally, DMSO was added to each well after discarding the MTT solution. The OD values at 570 nm was determined with an accuSkan™ GO UV/Vis Microplate Spectrophotometer (Fisher Sci., Fair Lawn, NJ).

Western Blotting

NCI-H460/MX20 cells were incubated with or without NVP-TAE684 (0.5 μM) for 0, 24, 48, and 72 h. Total protein was obtained by lysing cells on ice with lysis buffer (20 mM Tris-HCl pH 7.5, 150 mM NaCl, 1 mM Na_2EDTA, 1 mM EGTA, 1% Triton, 2.5 mM sodium pyrophosphate, 1 mm β–glycerophosphate, 1 mM Na_3VO_4, and 1 μg/mL leupeptin). The protein concentrations of the cell lysates were determined using Pierce™ BCA Protein Assay Kit (Thermo Scientific, Rockford, IL) to ensure equal protein loading. SDS-polyacrylamide gel electrophoresis was used to separate the protein and then transferred onto the PVDF membrane. After 2 h blocking with non-fat milk, the membrane was incubated with primary antibody against ABCG2 or GAPDH (1:1000) at 4°C. On the next day, the membrane was incubated with HRP-labeled secondary antibody (1:1000) at room temperature for 2 h and detected by electrochemiluminescence. Photographs were taken and the relative band density was analyzed by Image J.

Immunofluorescence Assay

NCI-H460 and NCI-H460/MX20 cells (2×10^4 cells per well) were seeded into 24-well plates. Then NCI-H460/MX20 cells were incubated with 0.5 μM NVP-TAE684 for 0, 24, 48, and 72 h. After treatment with NVP-TAE684, cells were fixed in 4% polyformaldehyde, permeated with 0.25% Triton X-100. Then, 6% BSA was used to block the non-specific reaction. After incubation with antibody against ABCG2 (1:1000) overnight at 4°C. Cells were incubated with fluorescent IgG antibody (1:1000) in the dark for 2 h. DAPI (1 μg/mL) was used to stain nuclei of cells. A Nikon TE-2000S fluorescence microscopy (Nikon Instruments Inc., Melville, NY) was used to collect immunofluorescence images.

ATPase Assay

As previously described (34), the ABCG2 membrane vesicles that overexpressed ABCG2 were from the protein extraction kit (Qproteome Plasma Membrane Protein Kit, Qiagen). Briefly, 20 μg ABCG2 membrane vesicles were incubated in assay buffer (containing pH 6.8 50 mM MES, 50 mM KCl, 5 mM sodium azide, 2 mM EGTA, 2 mM DTT, 1 mM ouabain, and 10 mM $MgCl_2$). Then 0-40 μM NVP-TAE684 was incubated with these membrane vesicles for 3 min. The ATP hydrolysis was initialized by 5 mM of Mg-ATP, while 5% SDS solution was used to terminate the reaction. Subsequently, the light

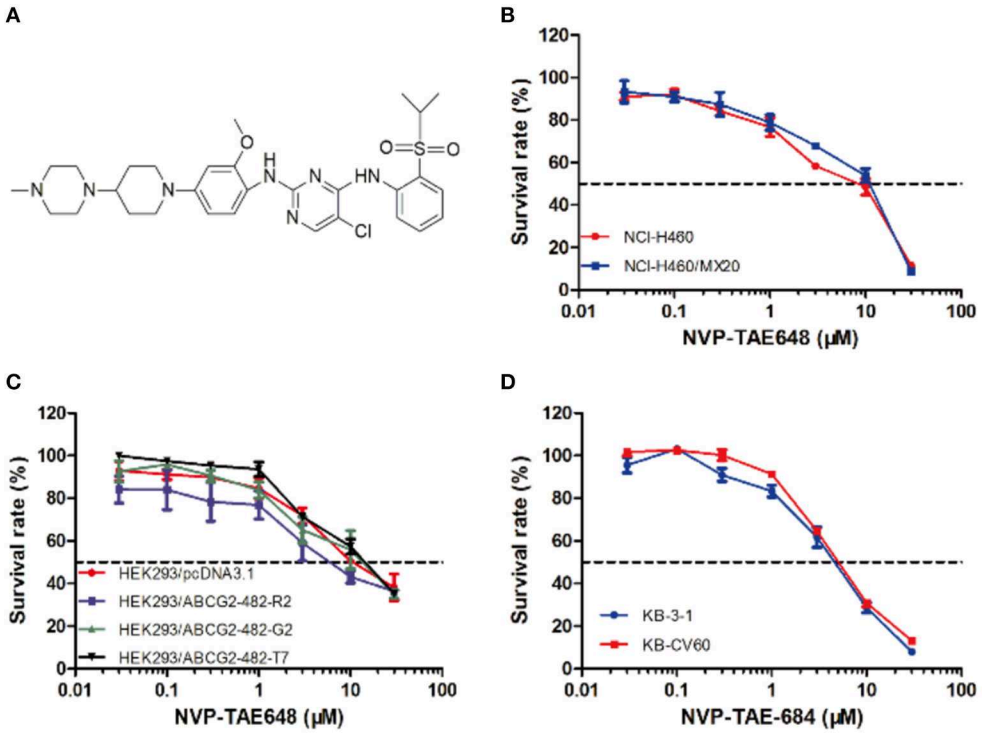

FIGURE 1 | Structure of NVP-TAE684 and its cytotoxicity in sensitive, ABCG2-, and ABCC1-mediated MDR cells. **(A)** Chemical structure of NVP-TAE684. **(B)** Survival rate of mitoxantrone-selected NCI-H460/MX20 and its parental cells treated with NVP-TAE684 for 72 h. **(C)** Survival rate of empty vector or full length ABCG2-transfected HEK293 cells after 72 h treatment with NVP-TAE684. **(D)** Survival rate of KB-3-1 and KB-CV60 cells treated with NVP-TAE684 for 72 h.

TABLE 1 | NVP-TAE684 lowered the IC_{50} values of anticancer agents in NCI-H460/MX20 cells.

Treatment	IC_{50} ± SD[a] (RF[b]) (μM)	
	NCI-H460	NCI-H460/MX20
Mitoxantrone	0.026 ± 0.009 (1.00)	2.783 ± 0.047 (105.40)
+NVP-TAE684 (0.2 μM)	0.023 ± 0.018 (0.88)	0.227 ± 0.057 (8.61)*
+NVP-TAE684 (0.5 μM)	0.019 ± 0.002 (0.73)	0.115 ± 0.056 (4.34)*
+Ko 143 (0.5 μM)	0.026 ±0.012 (0.99)	0.123 ±0.041 (4.67)*
SN-38	0.039 ± 0.020 (1.00)	2.547 ± 0.138 (67.29)
+NVP-TAE684 (0.2 μM)	0.025 ± 0.021 (0.65)	0.113 ± 0.091 (2.98)*
+NVP-TAE684 (0.5 μM)	0.022 ± 0.013 (0.59)	0.089 ± 0.010 (2.35)*
+Ko 143 (0.5 μM)	0.032 ± 0.022 (0.85)	0.090 ± 0.010 (2.38)*
Topotecan	0.042 ± 0.006 (1.00)	3.486 ± 0.110 (83.66)
+NVP-TAE684 (0.2 μM)	0.037 ± 0.009 (0.88)	0.186 ± 0.099 (4.45)*
+NVP-TAE684 (0.5 μM)	0.030 ± 0.009 (0.71)	0.108 ±0.079 (2.60)*
+Ko 143 (0.5 μM)	0.062 ± 0.010 (1.49)	0.119 ± 0.068 (3.85)*
Cisplatin	2.155 ± 0.075 (1.00)	2.704 ± 0.068 (1.25)
+NVP-TAE684 (0.2 μM)	2.573 ± 0.063 (1.19)	2.703 ± 0.046 (1.25)
+NVP-TAE684 (0.5 μM)	2.673 ± 0.067 (1.24)	2.907 ± 0.088 (1.35)
+Ko 143 (0.5 μM)	2.931 ± 0.066 (1.36)	2.636 ± 0.090 (1.22)

[a] *IC_{50} values represent the mean ± SD obtained from three independent experiments.*
[b] *Resistance fold (RF) was calculated by dividing the IC_{50} values of NCI-H460/MX20 cell by the IC_{50} of NCI-H460 cell in the presence or absence of NVP-TAE684 or positive control inhibitor. *Indicates $p < 0.05$ vs. cells treated with antineoplastic drug only.*

absorption at 880 nm was measured by the accuSkan GO UV/Vis Microplate Spectrophotometer.

Accumulation and Efflux Assay

To determine the intracellular [^{3}H]-mitoxantrone accumulation, 1×10^5 NCI-H460 and NCI-H460/MX20 cells were inoculated into 24-well plates. On the next day, 0.2 and 0.5 μM NVP-TAE684 or 0.5 μM Ko143 were added 2 h before adding [^{3}H]-mitoxantrone. After that, the cells were digested with trypsin to dissociate the cells into 5 mL scintillation solution. For [^{3}H]-mitoxantrone efflux determination, 0.2 and 0.5 μM NVP-TAE684 or 0.5 μM Ko143 were added 2 h before adding [^{3}H]-mitoxantrone. After that, the supernatant was discarded and medium was added with the absence or presence of inhibitor. Finally, cells were collected at 0, 30, 60, and 120 min. Packard TRICARB 1900CA liquid scintillation analyzer (Downers Grove, IL) was used to measure the radioactivity.

Molecular Docking Analysis

The molecular docking analysis was conducted in Maestro v11.1 (Schrödinger, LLC) by the default protocols (35). The ligand NVP-TAE684 was prepared, then ABCG2 protein (Protein Data Bank ID: 6FFC) (36) was prepared. The ABCG2 protein obtained was bound to a synthetic derivative of ABCG2 inhibitor Ko143 (36). The docking grid was generated based on the position of the Ko143 derivative with the default protocol. Subsequently, glide docking was performed and induce-fit docking was conducted based on the results of glide docking.

Statistical Analysis

All data were presented as the mean ± SD. All experiments were done independently at least three times. One-way ANOVA was used to analyze the difference between control and experimental group. It was considered as significant when p-value is < 0.05.

RESULTS

Reversal Effect of NVP-TAE684 on the ABCG2-Mediated Drug-Resistant Cells

We examined the cytotoxicity of NVP-TAE684 on cells overexpressed ABCG2 or ABCC1. As shown in **Figure 1**, NVP-TAE684 showed non-toxicity at low concentrations. Therefore, based on this result, we selected non-toxic concentrations of NVP-TAE684, which are 0.2 μM and 0.5 μM, for the following studies.

As shown in **Table 1**, the IC_{50} values of several known ABCG2 substrates (mitoxantrone, SN-38 and topotecan) in NCI-H460/MX20 cells was concentration-dependently decreased by NVP-TAE684 compared with their control cells. Also, the efficacy of above substrates in ABCG2-gene-transfected cells compared with that in empty vector transfectant cells was significantly increased after co-cultured with NVP-TAE684 (**Table 2**). However, the cytotoxicity of cisplatin, which is not a substrate of ABCG2, was not significantly affected by NVP-TAE684. These results indicated that NVP-TAE684 could antagonize MDR mediated by ABCG2-overexpression. As shown in **Table 3**, the IC_{50} value of vincristine in KB-CV60 cells was not significantly reduced by NVP-TAE684, which indicated that NVP-TAE684 could not reverse MDR mediated by ABCC1.

NVP-TAE684 Does Not Change the Protein Expression or Localization of ABCG2

Western blotting and immunofluorescence analysis were performed to examine the expression and subcellular localization of ABCG2. According to the results in **Figure 2**, after incubation with 0.5 μM NVP-TAE684 for 24, 48, and 72 h, the expression of ABCG2 (72 kDa) was not altered. In addition, the ABCG2 expression remained unchanged after incubation with 0.2, 0.5, and 1 μM of NVP-TAE684 for up to 72 h. Furthermore, as shown in **Figure 3**, the localization of ABCG2 transporter was remained on cell membrane after treated with NVP-TAE684 at indicated concentration for 0, 24, 48, 72 h.

NVP-TAE684 Increased the [^{3}H]-Mitoxantrone Intracellular Accumulation in NCI-H460/MX20 Cells

To understand the mechanism of action of NVP-TAE684 for reversal activity, drug accumulation assay was conducted to evaluate the effect of NVP-TAE684 on the [^{3}H]-mitoxantrone accumulation in sensitive and drug-resistant cells. It was found that NVP-TAE684 had the ability to significantly increase the intracellular concentration of [^{3}H]-mitoxantrone in ABCG2 overexpression cells, while NVP-TAE684 did not have impact on

TABLE 2 | NVP-TAE684 lowered the IC_{50} values of anticancer drugs in ABCG2-gene-transfected cells.

Treatment	IC_{50} ± SD[a] (RF[b]) (μM)			
	HEK293/pcDNA3.1	HEK293/ABCG2-482-G2	HEK293/ABCG2-482-R2	HEK293/ABCG2-482-T7
Mitoxantrone	0.053 ± 0.014 (1.00)	0.928 ± 0.199 (17.36)	1.077 ± 0.340 (20.15)	1.197 ± 0.098 (22.40)
+NVP-TAE684 (0.2 μM)	0.080 ± 0.011 (1.49)	0.440 ± 0.082 (8.23)*	0.416 ± 0.164 (7.79)*	0.548 ± 0.042 (10.25)*
+NVP-TAE684 (0.5 μM)	0.060 ± 0.007 (1.12)	0.099 ± 0.018 (1.87)*	0.221 ± 0.016 (4.13)*	0.329 ± 0.118 (6.15)*
+Ko 143 (0.5 μM)	0.072 ± 0.010 (1.35)	0.110 ± 0.069 (2.20)*	0.171 ± 0.024 (3.20)*	0.351 ± 0.052 (6.57)*
SN-38	0.072 ± 0.012 (1.00)	1.577 ± 0.152 (21.82)	1.590 ± 0.119 (22.00)	1.600 ± 0.131 (22.14)
+NVP-TAE684 (0.2 μM)	0.085 ± 0.013 (1.18)	0.604 ± 0.163 (8.35)*	0.477 ± 0.115 (6.60)*	0.583 ± 0.153 (8.07)*
+NVP-TAE684 (0.5 μM)	0.068 ± 0.012 (0.94)	0.117 ± 0.011 (1.16)*	0.138 ± 0.054 (1.91)*	0.267 ± 0.152 (3.70)*
+Ko 143 (0.5 μM)	0.089 ± 0.011 (1.24)	0.387 ± 0.018 (5.36)*	0.397 ± 0.083 (5.49)*	0.469 ± 0.164 (6.49)*
Topotecan	0.032 ± 0.01 (1.00)	0.858 ± 0.142 (26.40)	0.659 ± 0.116 (20.28)	0.966 ± 0.158 (29.73)
+NVP-TAE684 (0.2 μM)	0.026 ± 0.012 (0.84)	0.232 ± 0.187 (7.16)*	0.110 ± 0.016 (3.40)*	0.281 ± 0.024 (8.64)*
+NVP-TAE684 (0.5 μM)	0.023 ± 0.008 (0.71)	0.058 ± 0.031 (1.79)*	0.055 ± 0.011 (1.68)*	0.142 ± 0.044 (4.37)*
+Ko 143 (0.5 μM)	0.022 ± 0.012 (0.69)	0.114 ± 0.089 (3.52)*	0.059 ± 0.012 (1.81)*	0.170 ± 0.160 (5.23)*
Cisplatin	1.616 ± 0.750 (1.00)	1.768 ± 0.751 (1.09)	2.086 ± 1.147 (1.29)	1.547 ± 0.876 (0.96)
+NVP-TAE684 (0.2 μM)	1.915 ± 0.487 (1.18)	1.712 ± 0.897 (1.06)	2.312 ± 1.426 (1.43)	1.557 ± 0.984 (0.93)
+NVP-TAE684 (0.5 μM)	2.009 ± 0.669 (1.24)	2.107 ± 0.715 (1.30)	1.987 ± 1.359 (1.23)	1.408 ± 0.781 (0.87)
+Ko 143 (0.5 μM)	2.191 ± 0.55 (1.35)	1.926 ± 0.542 (1.19)	1.868 ± 1.186 (1.16)	1.668 ± 1.072 (1.03)

[a] *IC_{50} values represent the mean ± SD obtained from three independent experiments.*
[b] *Resistance fold (RF) was calculated from dividing the IC_{50} values of HEK293/ABCG2 cells by the IC_{50} of HEK293/pcDNA3.1 cells in the presence or absence of NVP-TAE684 or positive control inhibitor. *Indicates $p < 0.05$ vs. cells treated with antineoplastic drug only.*

the [^{3}H]-mitoxantrone accumulation in its parental NCI-H460 cells (**Figure 4A**).

The Efflux Activity of ABCG2 Was Inhibited by NVP-TAE684 in NCI-H460/MX20 Cells

Since ABCG2 transporter can pump out drugs, drug efflux assay was used to evaluate whether NVP-TAE684 can affect the efflux function of ABCG2 transporter. It was found that NVP-TAE684 significantly reduced the extrusion of [^{3}H]-mitoxantrone in NCI-H460/MX20 cells, but it had no significant effect on the efflux function mediated by ABCG2 in corresponding parental cells. These data demonstrated that NVP-TAE684 can impede the efflux activity of ABCG2 transporter which resulted in increasing the intracellular accumulation of anticancer drugs (**Figures 4B,C**).

NVP-TAE684 Stimulated the ABCG2 ATPase Activity

To determine the effect of NVP-TAE684 on ABCG2 ATPase activity, an ATPase assay kit was used to measure the ABCG2-mediated ATP hydrolysis in membrane vesicles after incubation with a serial concentrations of NVP-TAE684. According to **Figure 5**, the ATPase activity of ABCG2 transporter was stimulated by NVP-TAE684 in a concentration-dependent pattern. ATPase activity reached a maximum of 211.6% of the basal activity for ABCG2. The stimulatory effect of NVP-TAE684 reached 50% maximal (EC_{50}) at 0.091 μM for ABCG2.

TABLE 3 | NVP-TAE684 does not reverse MDR mediated by ABCC1.

Treatment	IC_{50} ± SD[a] (RF[b]) (μM)	
	KB-3-1	KB-CV60
Vincristine	0.075 ± 0.019 (1.00)	1.383 ± 0.060 (18.44)
+NVP-TAE684 (0.2 μM)	0.085 ± 0.013 (1.14)	1.447 ± 0.066 (19.30)
+NVP-TAE684 (0.5 μM)	0.063 ± 0.017 (0.82)	1.168 ± 0.078 (15.58)
+MK571 (25 μM)	0.067 ± 0.015 (0.90)	0.347 ± 0.121 (4.63)*
Cisplatin	1.398 ± 0.120 (1.00)	1.457 ± 0.093 (1.04)
+NVP-TAE684 (0.2 μM)	1.475 ± 0.150 (1.06)	1.568 ± 0.071 (1.12)
+NVP-TAE684 (0.5 μM)	1.175 ± 0.081 (0.84)	1.287 ± 0.141 (0.92)
+MK571 (25 μM)	1.327 ± 0.084 (0.95)	1.437 ± 0.072 (1.03)

[a] *IC_{50} values represent the mean ± SD obtained from three independent experiments.*
[b] *Resistance fold (RF) was calculated from dividing the IC_{50} values of KB-CV60 cells by the IC_{50} of KB-3-1 cell line in the presence or absence of NVP-TAE684 or positive control inhibitor. *Indicates $p < 0.05$ vs. group treated with antineoplastic drug only.*

Molecular Docking Analysis on the Interaction of NVP-TAE684 and ABCG2

To explore the interaction between NVP-TAE684 and ABCG2, a molecular docking analysis was performed. The docked position of NVP-TAE684 and ABCG2 protein with highest docking score (-12.929 kcal/mol) was shown in **Figure 6**. Both hydrogen bonds and π-π interaction are included in the interaction of NVP-TAE684 and ABCG2 protein: π-π interaction between the methoxy phenyl group of NVP-TAE684 and the residue Phe439; hydrogen bonds formed between the residue Asn436 and the sulfonylphenyl or methoxy groups of NVP-TAE684.

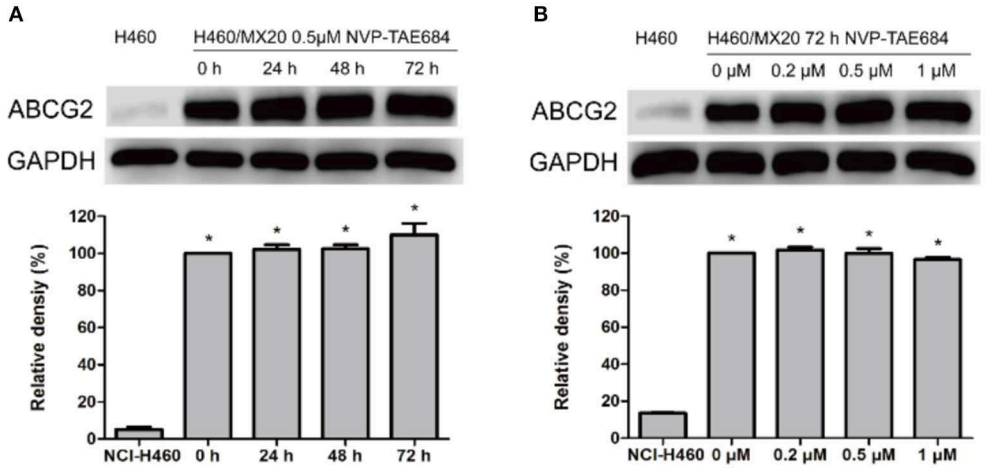

FIGURE 2 | The protein expression of ABCG2 was not changed after co-incubation with NVP-TAE684. **(A)** ABCG2 expression after treatment with 0.5 μM NVP-TAE684 for 0, 24, 48, and 72 h. **(B)** ABCG2 protein expression after treatment with 0.2, 0.5, 1 μM NVP-TAE684 for 72 h. Image J was used to quantify the relative band density. *$p < 0.05$, compared with control group.

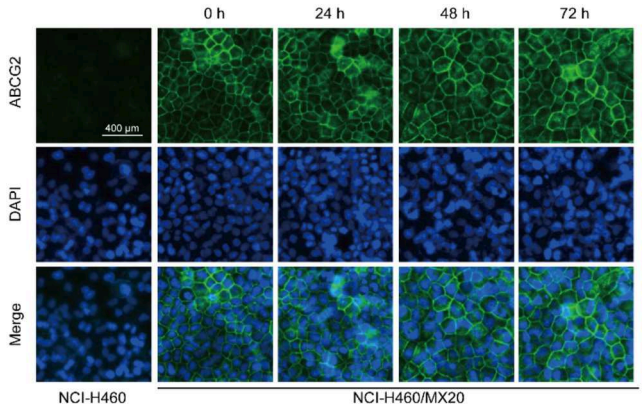

FIGURE 3 | Subcellular localization of ABCG2 was not changed after treatment with NVP-TAE684 at 0.5 μM.

DISCUSSION

ABCG2 protein is a member of ABC transporters (37). ABCG2 overexpression can lead to MDR. Substrates of ABCG2 include anthracyclines, camptothecins and methotrexate (38). Since ABCG2 is an important contributor to MDR, inhibiting ABCG2 activity may help improve the efficacy of chemotherapeutic drugs. At present, various specific and non-specific inhibitors of ABCG2 have been found. FTC is a mycotoxin isolated from Aspergillus fumigatus (39, 40). It can specifically sensitize chemotherapeutic agents to MDR mediated by ABCG2. However, its use *in vivo* is limited due to its neurotoxic effect. FTC tetracyclic analog Ko143 could interrupt the efflux activity of ABCG2 transporter (41), which has no toxicity in mice with high oral dose. Ko143 is the first specific ABCG2 inhibitor suitable for use *in vivo* (42). However, Ko143 is rapidly metabolized into a compound that is ineffective for clinical use (35). Thus, it is important to find more effective and non-toxic ABCG2 reversal agents. Recent research reported that some ALK inhibitors could sensitize chemotherapeutic drugs to ABC-mediated MDR (7, 43, 44). NVP-TAE684 is an ALK inhibitor which was reported that it could inhibit ABCB1 transporter function, but whether NVP-TAE684 could inhibit ABCG2 or ABCC1 transporter has not been reported. In this study, we explore whether NVP-TAE684 could reverse ABCG2- or ABCC1-mediated MDR and the results showed that NVP-TAE684 had reversal effects on ABCG2-mediated drug-resistant cells but showed no reversal effect on ABCC1-mediated MDR.

First, we tested the cytotoxicity of NVP-TAE684 and we found that NVP-TAE684 showed low toxicity at low concentrations. We selected two non-toxic concentrations for reversal study. MTT results showed that IC_{50} values of several known ABCG2 substrates, including mitoxantrone, SN-38 and topotecan, in mitoxantrone-selected NCI-H460/MX20 cells reduced upon the treatment by NVP-TAE684 at non-toxicity concentrations. To confirm that the reversal effect was related to ABCG2, we determined the effect of NVP-TAE684 on ABCG2-gene-transfected HEK293 cells. We found that NVP-TAE684 showed reversal effect on HEK293/ABCG2 cells. However, the cytotoxicity of cisplatin, which is a non-substrate of ABCG2 (45), was not altered by NVP-TAE684. Moreover, we evaluated the reversal effect of NVP-TAE684 on ABCC1-overexpressing KB-CV60 cells and found that NVP-TAE684 had no significant reversal effect on KB-CV60 cells. These results indicated that NVP-TAE684 was specific to the substrates of the ABCG2 transporter.

Downregulating ABCG2 expression may lead to reversing MDR. In order to understand whether NVP-TAE684 affects either protein expression or localization of ABCG2, immunofluorescence and Western blotting experiments were

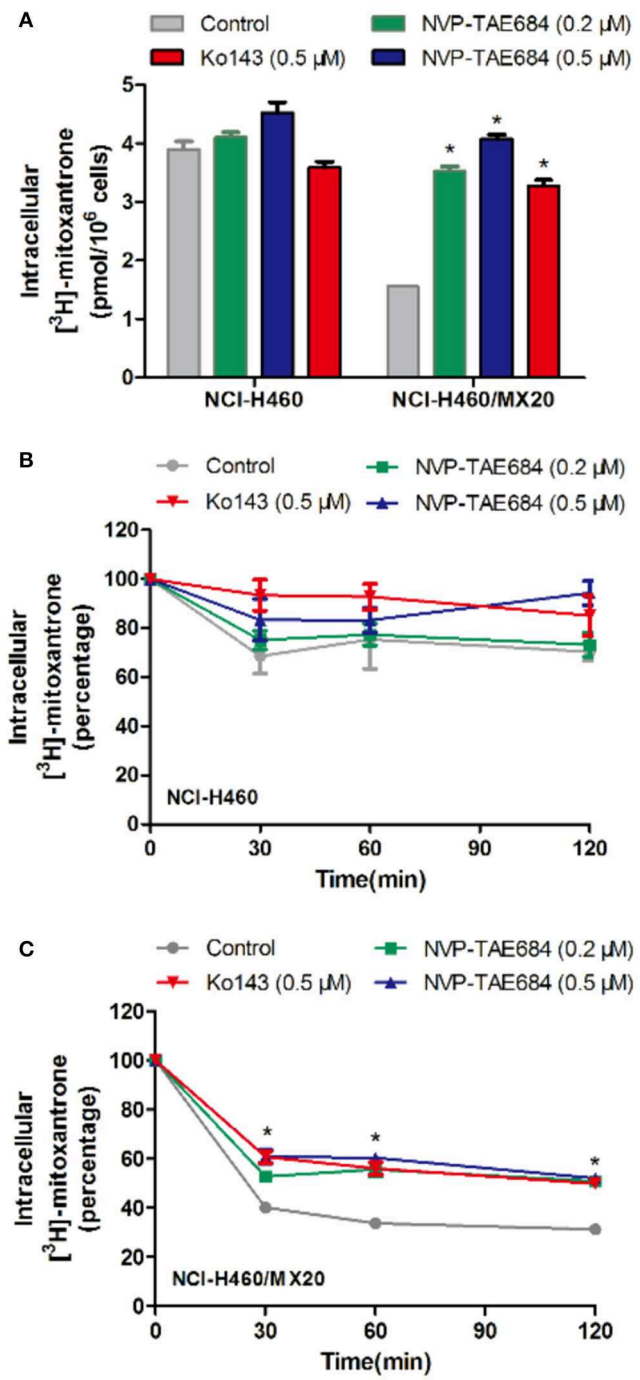

FIGURE 4 | NVP-TAE684 inhibited the efflux function of ABCG2 which resulted in increasing intracellular concentration of [^{3}H]-mitoxantrone. **(A)** The effect of NVP-TAE684 on the [^{3}H]-mitoxantrone accumulation in MDR cells. **(B,C)** The effects of NVP-TAE684 on the efflux activity mediated by ABCG2 in NCI- H460/MX20 and NCI-H460 cells. Ko143 served as a reference inhibitor of ABCG2. *$p < 0.05$, compared with control group.

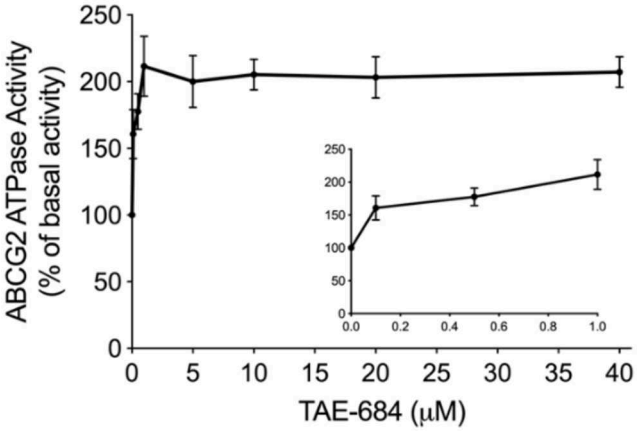

FIGURE 5 | NVP-TAE684 stimulates the activity of ABCG2 ATPase. Data are mean ± SD, representatives of three independent experiments.

carried out. Immunofluorescence results showed that the subcellular localization of ABCG2 transporter was unchanged when the cells were cultured with NVP-TAE684. In addition, immunoblotting results indicated that NVP-TAE684 did not downregulate the expression of ABCG2 transporter after up to 72 h treatment. Therefore, NVP-TAE684 did not change the expression of ABCG2 transporter and its subcellular localization.

It has been found that cancer cells can pump antineoplastic drugs out of cells through a complicated efflux pump system, thereby reducing intracellular concentration of many structurally unrelated anticancer drugs and leading to MDR (46, 47). According to our results, the intracellular concentration of tritium-labeled antineoplastic drug in MDR cells was significantly increased by NVP-TAE684 treatment, while no change was found in corresponding parental cells. Further assay suggested that NVP-TAE684 significantly reduced the efflux of tritium-labeled chemotherapeutic agent in drug resistant cells. These results showed that NVP-TAE684 has inhibitory activity on efflux activity of ABCG2 transporter and it resulted in increasing the accumulation of antineoplastic agents. Since ABCG2 has an ATP-binding region that is essential for substrate transport, and the function of ABCG2 transporter relies on the energy from the hydrolysis of ATP by the transporter, which can be modulated by the presence of substrates or inhibitors. Thus, monitoring ATPase activity allows for identification of those compounds that interact with ABCG2. ABCG2 exhibits a drug-dependent ATP hydrolysis activity, and a variety of ABCG2 inhibitors, as well as ABCG2 substrates, can either stimulate or inhibit ATPase activity (48). The results showed that the activity of ABCG2 ATPase was stimulated by NVP-TAE684, suggesting that NVP-TAE684 could act as a substrate, which may competitively occupy the drug binding site of ABCG2 transporter. Molecular docking study showed that NVP-TAE684 can interact with the transmembrane domain of ABCG2 with a docking score of−12.929 kcal/mol, and the interaction between NVP-TAE684 and ABCG2 proteins includes π-π interaction and hydrogen bond. This indicates that NVP-TAE684 has a strong direct interaction with ABCG2. Therefore, the reversal effect of ALK

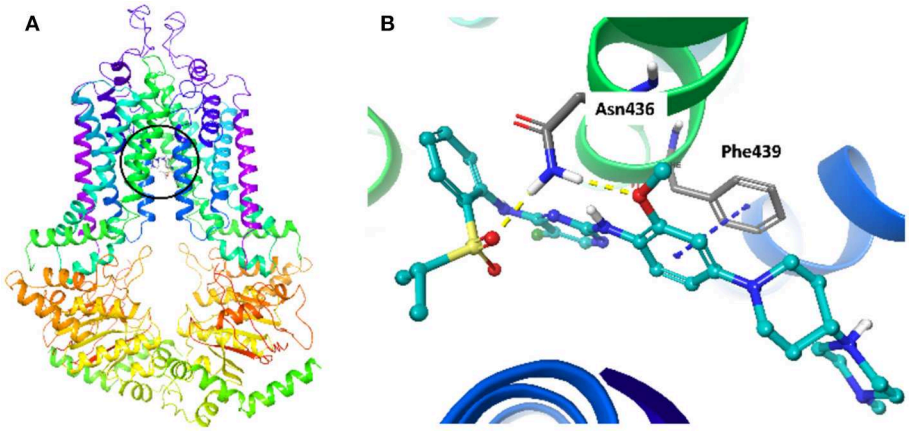

FIGURE 6 | The induced fit docking analysis of NVP-TAE684 and ABCG2 protein (PDB: 6FFC). **(A)** The binding site of NVP-TAE684 with ABCG2 protein was indicated with a circle. The ABCG2 protein was shown as ribbons. **(B)** The predicted binding mode of NVP-TAE684 and ABCG2 protein. Hydrogen bonds and π-π stacking were indicated with yellow and blue dot line, respectively. The atoms of NVP-TAE684 was colored as follows: carbon-cyan, hydrogen-white, oxygen-red, nitrogen-blue, fluoride-green, sulfur-yellow.

inhibitor NVP-TAE684 was related to its inhibition on drug efflux function probably by competitively occupy the substrate binding site of ABCG2 transporter.

CONCLUSION

This study suggests that NVP-TAE684 reverses ABCG2-mediated MDR by inhibiting the efflux activity of cancer cells, therefore increasing intracellular concentration of chemotherapeutic drugs. Our study provides a rationale for the combinational use of NVP-TAE684 and ABCG2-substrate drugs to circumvent ABCG2-mediated MDR.

DATA AVAILABILITY STATEMENT

All datasets generated for this study are included in the article/supplementary material.

AUTHOR CONTRIBUTIONS

Conceptualization: D-HY and Z-SC. Methodology: JW, C-YC, QC, J-QW, YY, Z-XW, XD, and LZe. Writing—original draft preparation: JW. Writing, review, and editing: JW, D-HY, Z-SC, and LZh. Supervision: Z-SC and D-HY. Funding acquisition: Z-SC and LZh.

FUNDING

This work was supported by the College of Pharmacy and Health Sciences, St. John's University.

ACKNOWLEDGMENTS

The authors would like to thank Drs. Robert W. Robey and Susan E. Bates (NCI, NIH, Bethesda, MD) for providing the NCI-H460 and NCI-H460/MX20 cell lines. We thank Dr. Shin-Ichi Akiyama for providing KB-3-1 and KB-CV60 cell lines. Thanks are also given to Dr. Stephen Aller (The University of Alabama at Birmingham, Birmingham, AL) for the human ABCG2 homology model. The authors are thankful to Dr. Tanaji T. Talele (St. John's University, New York, NY) for providing the computing resources for the docking study. JW would like to thank the Project Funded by the National First-class Disciplines (PNFD), and the Project Funded by the Priority Academic Program Development of Jiangsu Higher Education Institutions (PAPD) for supporting his study at St. John's university.

REFERENCES

1. Ye Q, Liu K, Shen Q, Li Q, Hao J, Han F, et al. Reversal of multidrug resistance in cancer by multi-functional flavonoids. *Front Oncol*. (2019) 9:487. doi: 10.3389/fonc.2019.00487
2. Alfarouk KO, Stock C-M, Taylor S, Walsh M, Muddathir AK, Verduzco D, et al. Resistance to cancer chemotherapy: failure in drug response from ADME to P-gp. *Cancer Cell Int*. (2015) 15:71. doi: 10.1186/s12935-015-0221-1
3. Berger W, Hauptmann E, Elbling L, Vetterlein M, Kokoschka EM, Micksche M. Possible role of the multidrug resistance-associated protein (MRP) in chemoresistance of human melanoma cells. *Int J Cancer*. (1997) 71:108–15.
4. Bircsak KM, Moscovitz JE, Wen X, Archer F, Yuen PYS, Mohammed M, et al. Interindividual regulation of the breast cancer resistance protein ABCG2 transporter in term human placentas. *Drug Metab Disposit*. (2018) 46:619–27. doi: 10.1124/dmd.117.079228
5. Alamolhodaei NS, Tsatsakis AM, Ramezani M, Hayes AW, Karimi G. Resveratrol as MDR reversion molecule in breast cancer: an overview. *Food Chem Toxicol*. (2017) 103:223–32. doi: 10.1016/j.fct.2017.03.024
6. Vaidyanathan A, Sawers L, Gannon A-L, Chakravarty P, Scott AL, Bray SE, et al. ABCB1 (MDR1) induction defines a common resistance mechanism in paclitaxel- and olaparib-resistant ovarian cancer cells. *Br J Cancer*. (2016) 115:431. doi: 10.1038/bjc.2016.203

7. Yang L, Li M, Wang F, Zhen C, Luo M, Fang X, et al. Ceritinib enhances the efficacy of substrate chemotherapeutic agent in human ABCB1-Overexpressing leukemia cells *in vitro*, *in vivo* and *ex-vivo*. *Cell Physiol Biochem*. (2018) 46:2487–99. doi: 10.1159/000489655
8. Alam A, Küng R, Kowal J, McLeod RA, Tremp N, Broude EV, et al. Structure of a zosuquidar and UIC2-bound human-mouse chimeric ABCB1. *Proc Natl Acad Sci USA*. (2018) 115:E1973–82. doi: 10.1073/pnas.1717044115
9. Morad SAF, Davis TS, MacDougall MR, Tan S-F, Feith DJ, Desai DH, et al. Role of P-glycoprotein inhibitors in ceramide-based therapeutics for treatment of cancer. *Biochem Pharmacol*. (2017) 130:21–33. doi: 10.1016/j.bcp.2017.02.002
10. Bernstein H-G, Hildebrandt J, Dobrowolny H, Steiner J, Bogerts B, Pahnke J. Morphometric analysis of the cerebral expression of ATP-binding cassette transporter protein ABCB1 in chronic schizophrenia: circumscribed deficits in the habenula. *Schizophrenia Res*. (2016) 177:52–8. doi: 10.1016/j.schres.2016.02.036
11. Dhasmana D, Singh A, Shukla R, Tripathi T, Garg N. Targeting nucleotide binding domain of Multidrug Resistance-associated Protein-1 (MRP1) for the reversal of multi drug resistance in cancer. *Sci Rep*. (2018) 8:11973. doi: 10.1038/s41598-018-30420-x
12. Johnson ZL, Chen J. Structural basis of substrate recognition by the multidrug resistance protein MRP1. *Cell*. (2017) 168:1075–85.e9. doi: 10.1016/j.cell.2017.01.041
13. Peterson BG, Tan KW, Osa-Andrews B, Iram SH. High-content screening of clinically tested anticancer drugs identifies novel inhibitors of human MRP1 (ABCC1). *Pharmacol Res*. (2017) 119:313–26. doi: 10.1016/j.phrs.2017.02.024
14. Renes J, De Vries EGE, Nienhuis EF, Jansen PLM, Müller M. ATP- and glutathione-dependent transport of chemotherapeutic drugs by the multidrug resistance protein MRP1. *Br J Pharmacol*. (1999) 126:681–8. doi: 10.1038/sj.bjp.0702360
15. Banerjee M, Kaur G, Whitlock BD, Carew MW, Le XC, Leslie EM. Multidrug Resistance Protein 1 (MRP1/ABCC1)-mediated cellular protection and transport of methylated arsenic metabolites differs between human cell lines. *Drug Metab Disposit*. (2018) 46:1096–5. doi: 10.1124/dmd.117.079640
16. Lee YH, Kang H-M, Kim M-S, Lee J-S, Jeong C-B, Lee J-S. The protective role of multixenobiotic resistance (MXR)-mediated ATP-binding cassette (ABC) transporters in biocides-exposed rotifer *Brachionus koreanus*. *Aqua Toxicol*. (2018) 195:129–36. doi: 10.1016/j.aquatox.2017.12.016
17. Wong ILK, Zhu X, Chan K-F, Law MC, Lo AMY, Hu X, et al. Discovery of Novel Flavonoid Dimers To Reverse Multidrug Resistance Protein 1 (MRP1, ABCC1) mediated drug resistance in cancers using a high throughput platform with "Click Chemistry". *J Med Chem*. (2018) 61:9931–51. doi: 10.1021/acs.jmedchem.8b00834
18. van Hoppe S, Sparidans RW, Wagenaar E, Beijnen JH, Schinkel AH. Breast cancer resistance protein (BCRP/ABCG2) and P-glycoprotein (P-gp/ABCB1) transport afatinib and restrict its oral availability and brain accumulation. *Pharmacol Res*. (2017) 120:43–50. doi: 10.1016/j.phrs.2017.01.035
19. Ripperger A, Krischer A, Robaa D, Sippl W, Benndorf RA. Pharmacogenetic aspects of the interaction of AT1 receptor antagonists With ATP-binding cassette transporter ABCG2. *Front Pharmacol*. (2018) 9:463. doi: 10.3389/fphar.2018.00463
20. Khunweeraphong N, Stockner T, Kuchler K. The structure of the human ABC transporter ABCG2 reveals a novel mechanism for drug extrusion. *Sci Rep*. (2017) 7:13767. doi: 10.1038/s41598-017-11794-w
21. Pedersen JM, Khan EK, Bergström CAS, Palm J, Hoogstraate J, Artursson P. Substrate and method dependent inhibition of three ABC-transporters (MDR1, BCRP, and MRP2). *Eur J Pharm Sci*. (2017) 103:70–6. doi: 10.1016/j.ejps.2017.03.002
22. Krapf MK, Gallus J, Wiese M. 4-Anilino-2-pyridylquinazolines and -pyrimidines as highly potent and nontoxic inhibitors of breast cancer resistance protein (ABCG2). *J Med Chem*. (2017) 60:4474–95. doi: 10.1021/acs.jmedchem.7b00441
23. Mirzaei SA, Gholamian Dehkordi N, Ghamghami M, Amiri AH, Dalir Abdolahinia E, Elahian F. ABC-transporter blockage mediated by xanthotoxin and bergapten is the major pathway for chemosensitization of multidrug-resistant cancer cells. *Toxicol Appl Pharmacol*. (2017) 337:22–9. doi: 10.1016/j.taap.2017.10.018
24. Hira D, Terada T. BCRP/ABCG2 and high-alert medications: Biochemical, pharmacokinetic, pharmacogenetic, and clinical implications. *Biochem Pharmacol*. (2018) 147:201–10. doi: 10.1016/j.bcp.2017.10.004
25. Docquier J-D, Mangani S. An update on β-lactamase inhibitor discovery and development. *Drug Resist Updates*. (2018) 36:13–29. doi: 10.1016/j.drup.2017.11.002
26. Bagal SK, Omoto K, Blakemore DC, Bungay PJ, Bilsland JG, Clarke PJ, et al. discovery of allosteric, potent, subtype selective, and peripherally restricted TrkA kinase inhibitors. *J Med Chem*. (2019) 62:247–65. doi: 10.1021/acs.jmedchem.8b00280
27. Galkin AV, Melnick JS, Kim S, Hood TL, Li N, Li L, et al. Identification of NVP-TAE684, a potent, selective, and efficacious inhibitor of NPM-ALK. *Proc Natl Acad Sci USA*. (2007) 104:270–5. doi: 10.1073/pnas.0609412103
28. Schönherr C, Ruuth K, Yamazaki Y, Eriksson T, Christensen J, Palmer Ruth H, et al. Activating ALK mutations found in neuroblastoma are inhibited by Crizotinib and NVP-TAE684. *Biochem J*. (2011) 440:405–14. doi: 10.1042/BJ20101796
29. Ceccon M, Mologni L, Bisson W, Scapozza L, Gambacorti-Passerini C. Crizotinib-resistant NPM-ALK mutants confer differential sensitivity to unrelated Alk inhibitors. *Mol Cancer Res*. (2013) 11:122–32. doi: 10.1158/1541-7786.MCR-12-0569
30. Ye S, Zhang J, Shen J, Gao Y, Li Y, Choy E, et al. NVP-TAE684 reverses multidrug resistance (MDR) in human osteosarcoma by inhibiting P-glycoprotein (PGP1) function. *Br J Pharmacol*. (2016) 173:613–26. doi: 10.1111/bph.13395
31. Robey RW, Honjo Y, van de Laar A, Miyake K, Regis JT, Litman T, et al. A functional assay for detection of the mitoxantrone resistance protein, MXR (ABCG2). *Biochim Biophys Acta*. (2001) 1512:171–82. doi: 10.1016/S0005-2736(01)00308-X
32. Aoki S, Chen Z-S, Higasiyama K, Setiawan I, Akiyama S-i, Kobayashi M. Reversing effect of agosterol a, a spongean sterol acetate, on multidrug resistance in human carcinoma cells. *Jpn J Cancer Res*. (2001) 92:886–95. doi: 10.1111/j.1349-7006.2001.tb01177.x
33. Mirzaei SA, Reiisi S, Ghiasi Tabari P, Shekari A, Aliakbari F, Azadfallah E, et al. Broad blocking of MDR efflux pumps by acetylshikonin and acetoxyisovalerylshikonin to generate hypersensitive phenotype of malignant carcinoma cells. *Sci Rep*. (2018) 8:3446. doi: 10.1038/s41598-018-21710-5
34. Zhang X-Y, Zhang Y-K, Wang Y-J, Gupta P, Zeng L, Xu M, et al. Osimertinib (AZD9291), a Mutant-selective EGFR inhibitor, reverses ABCB1-mediated drug resistance in cancer cells. *Molecules*. (2016) 21:1236. doi: 10.3390/molecules21091236
35. Cai C-Y, Zhai H, Lei Z-N, Tan C-P, Chen B-L, Du Z-Y, et al. Benzoyl indoles with metabolic stability as reversal agents for ABCG2-mediated multidrug resistance. *Eur J Med Chem*. (2019) 179:849–62. doi: 10.1016/j.ejmech.2019.06.066
36. Jackson SM, Manolaridis I, Kowal J, Zechner M, Taylor NMI, Bause M, et al. Structural basis of small-molecule inhibition of human multidrug transporter ABCG2. *Nat Struct Mol Biol*. (2018) 25:333–40. doi: 10.1038/s41594-018-0049-1
37. Ji N, Yang Y, Cai C-Y, Lei Z-N, Wang J-Q, Gupta P, et al. VS-4718 antagonizes multidrug resistance in ABCB1- and ABCG2-overexpressing cancer cells by inhibiting the efflux function of ABC transporters. *Front Pharmacol*. (2018) 9:1236. doi: 10.3389/fphar.2018.01236
38. Yokoyama S, Tamaru S, Tamaki S, Nakanishi D, Mori A, Yamakawa T, et al. Genetic risk factors associated with antiemetic efficacy of palonosetron, aprepitant, and dexamethasone in Japanese breast cancer patients treated with anthracycline-based chemotherapy. *Clin Breast Cancer*. (2018) 18:e157–65. doi: 10.1016/j.clbc.2017.05.013
39. Robinson AN, Tebase BG, Francone SC, Huff LM, Kozlowski H, Cossari D, et al. Coexpression of ABCB1 and ABCG2 in a cell line model reveals both independent and additive transporter function. *Drug Metab Disposit*. (2019) 47:715–23. doi: 10.1124/dmd.118.086181
40. Zhao R-Q, Wen Y, Gupta P, Lei Z-N, Cai C-Y, Liang G, et al. Y6, an epigallocatechin gallate derivative, reverses abcg2-mediated mitoxantrone resistance. *Front Pharmacol*. (2019) 9:1545. doi: 10.3389/fphar.2018.01545
41. Abdel Gaber SA, Müller P, Zimmermann W, Hüttenberger D, Wittig R, Abdel Kader MH, et al. ABCG2-mediated suppression of chlorin e6 accumulation and photodynamic therapy efficiency in glioblastoma cell lines

can be reversed by KO143. *J Photochem Photobiol B Biol*. (2018) 178:182–91. doi: 10.1016/j.jphotobiol.2017.10.035
42. Mendoza C, Perez-Urrutia N, Alvarez-Ricartes N, Barreto GE, Pérez-Ordás R, Iarkov A, et al. cotinine plus krill oil decreased depressive behavior, and increased astrocytes survival in the hippocampus of mice subjected to restraint stress. *Front Neurosci*. (2018) 12:952. doi: 10.3389/fnins.2018.00952
43. Zhou W-j, Zhang X, Cheng C, Wang F, Wang X-k, Liang Y-j, et al. Crizotinib (PF-02341066) reverses multidrug resistance in cancer cells by inhibiting the function of P-glycoprotein. *Br J Pharmacol*. (2012) 166:1669–83. doi: 10.1111/j.1476-5381.2012.01849.x
44. Yang K, Chen Y, To KKW, Wang F, Li D, Chen L, et al. Alectinib (CH5424802) antagonizes ABCB1- and ABCG2-mediated multidrug resistance *in vitro*, *in vivo* and *ex vivo*. *Exp Mol Med*. (2017) 49:e303-e. doi: 10.1038/emm.2016.168
45. Wu Y, Jin D, Wang X, Du J, Di W, An J, et al. UBE2C induces cisplatin resistance via ZEB1/2-dependent upregulation of ABCG2 and ERCC1 in NSCLC cells. *J Oncol*. (2019) 2019:15. doi: 10.1155/2019/8607859
46. Wang Z, Lu W, Rajapaksha P, Wilkop T, Cai Y, Wei Y. Comparison of *in vitro* and *in vivo* oligomeric states of a wild type and mutant trimeric inner membrane multidrug transporter. *Biochem Biophys Rep*. (2018) 16:122–9. doi: 10.1016/j.bbrep.2018.10.006
47. Yang H-B, Hou W-T, Cheng M-T, Jiang Y-L, Chen Y, Zhou C-Z. Structure of a MacAB-like efflux pump from Streptococcus pneumoniae. *Nat Commun*. (2018) 9:196. doi: 10.1038/s41467-017-02741-4
48. Prieß M, Göddeke H, Groenhof G, Schäfer LV. Molecular mechanism of ATP hydrolysis in an ABC transporter. *ACS Central Sci*. (2018) 4:1334–43. doi: 10.1021/acscentsci.8b00369

Conflict of Interest: The authors declare that the research was conducted in the absence of any commercial or financial relationships that could be construed as a potential conflict of interest.

frontiers in Oncology

REVIEW
published: 06 March 2020
doi: 10.3389/fonc.2020.00317

Glucose Metabolism on Tumor Plasticity, Diagnosis, and Treatment

Xiaoping Lin [1,2,3], Zizheng Xiao [1,2], Tao Chen [1,2], Steven H. Liang [3] and Huiqin Guo [4]**

[1] Department of Nuclear Medicine, Sun Yat-sen University Cancer Center, Guangzhou, China, [2] State Key Laboratory of Oncology in South China, Collaborative Innovation Center for Cancer Medicine, Sun Yat-sen University Cancer Center, Guangzhou, China, [3] Division of Nuclear Medicine and Molecular Imaging, Department of Radiology, Harvard Medical School, Massachusetts General Hospital, Boston, MA, United States, [4] Department of Thoracic Surgery, Beijing Sijitan Hospital, Capital Medical University, Beijing, China

Malignant cells support tumor proliferation and progression by adopting to metabolic changes. Tumor cells altered metabolism by increasing glucose uptake and fermentation of glucose to lactate, even in the aerobic state and the presence of functioning mitochondria. Glucose metabolism in tumor plasticity has attracted great interests by clinicians and scientists in the past decades. This review discusses the previous and emerging researches on the tumor plasticity altered by changing glucose metabolism in different cancer cells, including cancer stem cells (CSCs). In addition, we summarize the rising applications of glucose metabolism in tumor diagnosis and treatment. Our objective is to direct future investigation on this altered metabolic phenotype and its application in patient care.

Keywords: metabolism, tumor, plasticity, glucose, Warburg effect, diagnosis, treatment

OPEN ACCESS

Edited by:
Dong-Hua Yang,
St. John's University, United States

Reviewed by:
Yi Li,
Fox Chase Cancer Center,
United States
Zhiyi Zhang,
Jinan University, China

****Correspondence:***
Xiaoping Lin
guohuiqin2@163.com
Huiqin Guo
linxp@sysucc.org.cn

Specialty section:
This article was submitted to Molecular and Cellular Oncology, a section of the journal Frontiers in Oncology

Received: *27 December 2019*
Accepted: *21 February 2020*
Published: *06 March 2020*

Citation:
Lin X, Xiao Z, Chen T, Liang SH and Guo H (2020) Glucose Metabolism on Tumor Plasticity, Diagnosis, and Treatment. Front. Oncol. 10:317. doi: 10.3389/fonc.2020.00317

INTRODUCTION

The characteristics of malignant cells, including sustaining cell proliferation, escaping cell death, attaining immortality by inducing new blood vessel formation and promoting tumor cell invasion and metastasis, were summarized in the year 2000 (1). After one decade of conceptual advance, two emerging traits were added—altering energy metabolism and evading immune demolition (2). In recent years, increasing number of studies focus on the alteration of energy metabolism, that allows tumor cells to survive and spread even in challenging conditions. However, a paradigm shift has occurred adding to our knowledge of the function of glycolysis in glucose metabolism over the last decade (3). In this review, we attempt to provide a better understanding of glucose metabolism in tumor plasticity which may contribute to the design and outcome of novel diagnostics and treatment strategies.

GLUCOSE METABOLISM AND THE WARBURG EFFECT IN TUMORS

Normally, glucose is processed by glycolysis to generate ATP and pyruvate. Then the ribose 5-phosphate and NADPH were produced through the pentose phosphate pathway (PPP), or enter into the tricarboxylic acid (TCA) cycle in mitochondrion. Glucose-derived citrate is converted to acetyl-CoA, oxaloacetate (OAA), or a-ketoglutarate (a-KG). Glutamine is deaminated to form glutamate, which is processed to produce a-KG for use in the TCA cycle.

The main pathway of glucose metabolism in cancer cells is aerobic glycolysis, termed Warburg effect (4). In cancer cells, glucose uptake and the production of lactate was dramatically increased, even in the presence of oxygen and fully functioning mitochondria (5). This classic type of metabolic change provides substrates required for cancer cell proliferation and division, which is involved in tumor growth, metastatic progression and long-term survival (5–8). It must be emphasized that both glycolysis and mitochondrial metabolism are crucial to cancer cells in the Warburg Effect (5).

Glucose metabolism in tumor is governed by both oncogenes and cancer-producing factors (6). Metabolic reprogramming of cancer cells is regulated by transcription factors that include c-*Myc*, *p53* and hypoxia-inducible factor (HIF) 1α (9). The reprogramming is a complex interaction of various signaling pathways, such as Notch, Akt, phosphoinositide-3-kinase (PI3K), PTEN, mammalian target of rapamycin (mTOR), and AMP-activated protein kinase (AMPK) (10, 11).

c-*Myc* can stimulate glycolysis, glutaminolysis, and nucleotide synthesis (12). c-*Myc* mediated glucose metabolic reprogramming primarily on mitochondrial aerobic metabolism (13). Glycolysis can be promoted by c-*Myc* through direct induction of glycolytic-associated enzymes (14). Besides, mitochondrial biogenesis can be promoted by c-*Myc* with stable function and the number of mitochondria in tumor cells.

p53 is the main adverse regulator during tumor metabolic reprogramming (15). *p53* inhibits glycolysis by inducing glycolysis and apoptosis regulator (TIGAR), inhibiting phosphoglycerate mutase (PGM) to upregulate expression of TP53, and repressing glucose transporter (GLUT)-1 and GLUT -4 (6, 16–18). Also, *p53* can alter oxygen consumption and the synthesis of cytochrome c oxidase 2 (SCO2) protein, which is critical for regulating the cytochrome c oxidase(COX) complex (19). Moreover, *p53* promotes mitochondrial glutaminase (GLS2) and limits glutaminolysis in response to oxidative stress or DNA damage (20).

HIF-1 is a heterodimeric protein that could alter various genes coded for enzymes involved in glucose metabolism. The phosphatidylinositol 3-kinase (PI3K) and ERK mitogen-activated protein kinase (MAPK) pathways affect HIF-1α protein synthesis. In glucose metabolism, glyceraldehyde-3-P-dehydrogenase (GAPDH), GLUT-1, hexokinase (including HK1 and HK2), autocrine motility factor/ (AMF/GPI), enolase 1(ENO1), plasminogen activator receptor (TPI), Pyruvate kinase(PKM), 6-phosphofructo-2-kinase/fructose-2,6-biphosphatase-3(PFKBF3, PFKL, PGK1), and LDHA can be transcriptionally activated by HIF-1 (21).

THE IMPACT OF GLUCOSE METABOLISM ON TUMOR PLASTICITY

Tumor cells need to survive drastic changes in the microenvironment such as hypoxia, nutrient storage, and acidic pH (22). A huge number of cancer cells show remarkable plasticity in metabolic adaptation. The reprogrammed glucose metabolism allows cancer cells to satisfy high proliferation requests. In addition, it provides some survival and growth advantages, including high carbon source for anabolism, rapid ATP availability to supply the energy, abundant lactic acid to increase the redox status (NADPH) via the glycine–serine pathway (6–8). Lactic acid induces metabolic "dormancy" and is involved in EMT and tumor immune response by reducing pH in the tumor environment (5, 8, 23–25). To manage all the situations above, cancer cells must maintain a balance to deliver adequate energy with constrained resources and to meet the biosynthetic demands of proliferation. Though oxidative phosphorylation(OXPHOS) would be the best energy provider, the physiological reality is that both OXPHOS and glycolysis collaborate to produce ATP under the local oxygen concentration. Coordinate results are net increments in glucose utilization and lactic acid secretions. This process is known as the glycolytic switch, which is corresponding to uncoupling glycolysis from OXPHOS (26).

Glucose Metabolism and Cancer Cell Proliferation

Cell proliferation requires expanded uptake of supplements, lifted flux through biosynthetic pathways, support of metabolic intermediates, and proceeded recovery of cofactors required to supply energy or reducing equivalents for reactions. Cancer cells preferred aerobic glycolysis for cell proliferation. In addition, aerobic glycolysis produces metabolic precursors that are essential for rapid cell proliferation (25). As proliferation is the key feature of cancer cells, aerobic glycolysis allows cancer cells to meet the requirements of generating enough ATP and biosynthetic precursors. The goal of aerobic glycolysis is to preserve high levels of glycolytic intermediates to maintain anabolic reactions in cells instead of generating lactate and ATP. Thus, it may explain why increased glucose metabolism happens in proliferating cancer cells (26).

The biosynthesis in proliferating cells requires building blocks for the synthesis of nucleotides, lipids, and non-essential amino acids—those that glycolytic intermediates can supply (27). The PPP can produce the reducing equivalents in the form of NADPH molecules and generates nucleotide and lipid precursors. The TCA cycle can generate acetyl-CoA and glutamine and drive them into the cytosol. As a result, the anabolic metabolism of amino acids and lipids is supplied by both glycolysis and the TCA cycle within mitochondria (27). NAD+ is an essential cofactor of nucleotide and amino acid biosynthesis. The maintenance of biosynthesis in proliferating cells demands the regeneration of NAD+. The conversion of pyruvate to lactate can partially produce NAD+ (28). Because cells use as much as 10% of their entire proteome and half of all of their metabolic genes to produce proteins involved in glycolysis, the cost of using Warburg Effect in aerobic glycolysis as a tradeoff to promote biosynthesis is vast (29). Mitochondrial functions occur concomitantly with the aerobic glycolysis and limiting mitochondrial activity may not occur during the Warburg Effect (5). Under energy stress conditions, the apparent shift from glycolysis to OXPHOS by mitochondrial elongation contribute

to tumor survival. Remodeling of mitochondrial morphology is a remarkable protection of tumor cells from stress (30).

Glucose Metabolism and EMT

EMT is a process that involves a high level of cellular plasticity. EMT is often activated during cancer cell invasion, systemic dissemination, and metastasis (31, 32). EMT is an important step preceding to invasion and metastasis in tumor cells. Epithelial cells lose the junctions among cells and their polarized organization during EMT. They change cytoskeletal organization, transform the shape, and acquire mesenchymal characteristics, such as fibroblast-like cell morphology and increased capability of invasion and migration (32, 33).

The plasticity of glucose metabolism is important in EMT (34). The genes and biochemical mechanisms impact glucose metabolism during EMT of cancer cells. Crosstalk network has been explored between EMT and cancer metabolism (35). PI3K-AKT-mTOR, EGFR-RAS-MAPKs, and JAK2-STAT3 signaling pathways can mediate EMT (36). HIF1α, Myc and FOXM1 regulate both metabolism and EMT (37). LKB1 / AMPK (Liver kinase B1/AMP-activated protein kinase) downregulates SNAIL and ZEB1and inhibits the invasion and migration of tumor cells, by regulating FOXO3, TGF- β, NF-κB, AKT, and mTOR signaling pathways (34).

Glucose transporters, especially GLUT-1 and GLUT-3, promote tumor progression by increasing glucose influx and activating downstream molecular pathways (38). GLUT-1 increases matrix metalloproteinase 2 (MMP-2) *in vitro* and *in vivo*, which contributes to EMT and cellular invasiveness (34, 39). GLUT-3 gene could be activated by ZEB1, which is an EMT marker (34). HK2 is a well-known hypoxia-inducible gene that can induce EMT (34). PFK increases glycolytic flux and EMT by maintaining this glycolytic phenotype in cancer cells *in vitro*. Pyruvate kinase M2 (PKM2) can prompt EMT both by metabolic and non-metabolic mechanisms (40). PKM2 increases glucose uptake and lactate production to support cell survival and invasion (41).

Besides the enzymes involved glucose metabolism, altered mitochondrial function also contributes to EMT induction (34). Tumor cell migration and metastasis was stimulated by abnormal TCA cycling coupled with mitochondrial superoxide production (42).

Glucose Metabolism and Cancer Stem Cells

Cancer consists of mainly stem cells (CSCs) and non-CSCs (2). CSCs have the potentials of self-renew and tumor initiation (43, 44). CSCs adapt to metabolic plasticity, which is determined by the factors present in the tumor microenvironment (TME). Metabolic plasticity allows these cancer stem cells to switch between OXPHOS and glycolysis (45). Only complete oxidation through the TCA cycle cannot supply enough anabolic precursors such as pyruvate and glutamine. CSCs prefer to rely on glycolysis and the PPP and devolve mitochondrial infrastructure and function. This predominantly glycolytic metabolism offers sufficient energy to support the basic needs of CSCs. The maturation of metabolic network matches the increasing energy demands of specialized progeny cells. The oxidative metabolism infrastructure contains mitochondrial biogenesis and maturation, and networks of the TCA cycle and electron transport chain. A concurrent rise in mitochondrial ROS may prime CSCs for lineage differentiation (46). The main difference between cancer cells and CSCs is the metabolic shift and mitochondrial resetting. CSCs display the metabolic change and mitochondrial resetting into precise bioenergetic states and lose the unique metabolic phenotypes after differentiation. Compared with differentiated neoplastic cells, CSCs exhibit a more prominent Warburg effect. Aerobic glycolysis may produce enough glycolytic intermediates into the PPP to supply molecules that are necessary for anabolic metabolism and growth of CSCs (47). In CSCs, the oxidative metabolism and mitochondrial structure are altered to commit glycolysis (48). Aerobic glycolysis is one of the important aspects in maintaining CSCs and inducing their differentiation. Specifically, aerobic glycolysis is critical in preserving the stemness of CSCs, while switching to oxidative metabolism is the characteristic of stem cell differentiation. Besides, aerobic glycolysis is essential to the properties of CSCs (46). Multiple regulatory factors including metabolic enzymes promoted the metabolic plasticity of stem cells in breast cancers. The metabolism-regulating genes and epigenetic factors that regulate glucose metabolism might also regulate the expression of EMT (49). An enhanced Warburg effect was observed in metastatic prostate cancers (44).

Moreover, metabolic flexibility diverge the fates CSCs, which include dormancy to minimize stress damage, proliferation and self-renewal to preserve progenitor pools, and pedigree specification for tissue regeneration (48). Depending on the metabolic characteristics of the tumor cells of origin, isogenic glioma stem cells (GSCs) exhibits heterogeneity in metabolic characteristics. They can be divided into mitochondrial and glycolytic phenotypes. Cells of the mitochondrial type consume more oxygen and maintain a higher ATP content; those of the glycolytic type consume more glucose and produce more lactate. Both metabolic phenotypes are independent and stable. They can coexist within a given tumor. The environmental factors further influence the metabolic preferences of these cells. For example, CSCs that rely on OXPHOS can switch to aerobic glycolysis in response to metabolic stress (50).

Glucose Metabolism and Tumor Microenvironment (TME)

In addition to the inherent alterations in the tumor cells, the metabolic competition and cooperation among the TME components support tumor proliferation, progression, and therapeutic resistance (9). TME consist of different types of cells, that include cancer associated fibroblasts (CAFs), non-cancer cell stroma, immune cells, and endothelial cells (51). The TME forms a pro-tumorigenic cocoon around the tumor cells. Intrinsic traits (e.g., genetic programs in cancer cells) and extrinsic factors (e.g., nutrient availability, oxygen tension, pH) contribute to the deregulated metabolism in TME. TME enforces metabolic plasticity to adapt to hypoxic and acidic environment, nutrient deprivation and competition, oxidative stress, and

immune surveillance (52). Reprogramming of the metabolism occurs in tumor and non-tumor cells. The interactions and competitions in TME components guarantee the steady supply of nutrients and molecules for tumor growth even under hypoxic conditions. Metabolic reprogramming also affects TME. Hypoxia inhibits this process by upregulating PDK1 and LDHA (53, 54). When HIF1α is activated in CAFs, the activity of mitochondria drops and lactate production increases. This is consistent with a glycolytic phenotype. It leads to slow down metabolism in the microenvironment (55). Lactate accumulation resulted from continuous activation of glycolytic and LDHA enzymes leads to a low-pH microenvironment during tumor progression. Nutrient deficiency is another microenvironment stress that cancer cell often encounters. Numerous studies have shown that reprogramming of glucose metabolism upon nutrient starvation in tumor cells occurs in order to use energy to support their growth (56–61).

The reverse Warburg Effect was proposed in the last decade (62). The energy-rich metabolites of aerobic glycolysis, such as lactate and pyruvate, are generated by cancer associated fibroblasts and taken up and used in the TCA cycle in mitochondria of epithelial cancer cells. Thus, efficient energy production such as ATP generation, which leads to increase cell proliferation and reduce cell death (62). The reverse Warburg effect can benefit tumor cells by cooperative utilization of oxygen between stromal cells and tumor cells (55). Cancer cells induce stromal cells to undergo "aerobic glycolysis." Their products are returned to the cancer cells to be used for mitochondrial OXPHOS (63). The metabolic heterogeneity in TME allows cancer and stromal cells to exchange metabolites between them to maintain maximal cellular growth (18).

The immune system plays an important role in TME. The immune cells in the TME can detect and eliminate the abnormal cells or tumor cells and protect the body from damage caused by tumor cells (64). Tumor cells activate immune cells, and the activated innate or adaptive immune cells can maintain homeostasis (9, 65). The immune system affects cancer survival and progression (23, 66). Tumor cells develop different mechanisms to escape the immune response. They include strategies at the genetic, epigenetic and metabolic levels. It implements to resist immune recognition and decrease apoptosis (67).

There is a complex interaction between malignant cells and immune cells in the tumor stroma (66). Metabolism regulates tumor cells to escape immune surveillance and to coexist with stroma cells. Tumor and other different types of cells in the TME compete for nutrient. Inflammation induced by oncogene in the tumors promotes adaptive metabolic changes in the surrounding non-tumor cells to secrete metabolites. Tumors use these metabolites as alternative nutrient sources to meet their increasing demands for anabolic function (68).

Metabolism is essential to lymphocyte for its development, function and inducing tolerance (69). T cells prefer glycolysis upon activation, though they had lower glycolytic flux when resting. Activated by TCR- and CD28-mediated co-stimulation, T cells switch to a rapid increase in glucose uptake and glycolysis (69–71), as well as glutaminolysis (69, 72, 73). In contrast, the activation of T cells and dendritic cells can be inhabited by lactate accumulation (74, 75). Lactate prevents cytokine release and monocyte migration, while promotes the formation of tumor-associated macrophage 2 (TAM2) phenotype. It leads to upregulate the expression of arginase 1, promote immune escape and tumor progression (25, 76–78). Lactate reduces the production of IFN-γ from T cells and NK cells, and decreases the level of nuclear factor of activated T cells (NFAT), which also contributes to immune escape and tumor progression (79, 80). As antigen presenting cells and a source of cytokines, B lymphocytes also have a critical role in antitumor immunity (81, 82). B cells upon activation use both glycolysis and OXPHOS, which is different from T cells. However, the deletion of GLUT-1 or inhibition of glycolysis in B cells suppresses antibody production *in vivo* (69, 70).

CLINICAL APPLICATION OF TARGETING GLUCOSE METABOLISM IN TUMOR

Attempts to target the glucose metabolism, especially on Warburg effect, for cancer diagnosis and therapy emerges in the past decades and is still in developing.

Application of Glucose Metabolism in Cancer Diagnosis

Many different types of human tumors dramatically enhanced uptake and use of glucose. Since 1976, positron emission tomography (PET) with a radiolabeled analog of glucose (^{18}F-fluorodeoxyglucose, FDG) was applied to non-invasively visualize glucose uptake in human body. This tracer is the most impressively clinical utility of the Warburg effect (2, 6). Increased FDG implies high glucose uptake which is an indication of the glycolytic switch. It provides information about the pathologic differentiation and precise stageing of tumors, predicts treatment response and gives an indication of overall prognosis (83). The positron-emitting radionuclide fluorine-18 replaces the normal hydroxyl group at the C-2 position in the glucose molecule. After injection into the body, the tracer is transported into cells by glucose transporters, especially GLUT-1 and GLUT-3, followed by phosphorylation with the hexokinase, especially HK2, to produce ^{18}F-FDG-6-phosphate (^{18}F-FDG-6-p). ^{18}F-FDG-6-p cannot be released from the cell and is trapped in the cytoplasm. Because of the lack of the 2'hydroxyl group, ^{18}F-FDG-6-p cannot further proceed to glycolytic pathway (84). PET scanner detects the radioactive decay of ^{18}F-FDG-6-p and form the body images of the distribution of ^{18}F-FDG. Thus, the presence of living malignance can be identified by the accumulated amounts of ^{18}F-FDG-6-p (84, 85). The sites and the semi-quantitative analysis of high glucose uptake (e.g., standard uptake value, SUV) in the whole body can be identified. In the vast majority of malignance, glucose is trapped in cancer cells more than normal tissues with the exception of the brain and brown fat. It relates to the metabolic characteristics at the tumor site (42). Owing to the limitation of spatial resolution and some particular pathology subtypes(e.g., signet ring cell carcinoma, well-differentiated cancer), the sensitivity

and specificity varied across different applications using ^{18}F-FDG–PET (26, 85).

PET imaging tracers are able to detect the PKM2, such as N,N-diarylsulfonamide (DASA) compounds bind to PKM2. ^{11}C-labeled analog of DASA-23 was applied to the orthotopic U87 and GBM39 patient-derived tumors in preclinical models of glioblastoma multiforme and to monitor the response of the PKM2 activator TEPP-46 in GBM39 tumors (86).

An analog of glutamine, 4-^{18}F-(2S,4R)-fluoroglutamine (^{18}F-FGln), is taken up by cancer cells *in vitro* and its specific uptake can be detected on PET imaging in mouse xenograft model *in vivo*. Thus, the glutamine metabolism in gliomas and its uptake can be evaluated (87). Other investigational PET agent, such as 5-^{11}C-(2S)-glutamine (87, 88), was also exploited for its ability to take up and retain glutamine in some tumors (87).

As another device in molecular imaging, a few agents have been developed to detect the glucose metabolism in magnetic resonance (MR). The hyperpolarized agents can form the better imaging for remarkable enhancement compared to conventional MR imaging. Magnetic resonance spectroscopy(MRS) can image the conversion of ^{13}C-labeled pyruvate to lactate in patients (83). It is possible to identify malignance and monitor treatment response by evaluating the distribution of ^{13}C-pyruvate and the altered ^{13}C -lactate/^{13}C -pyruvate in preclinical MRS study in prostate cancer and glioma (83, 89). Some other targetable processes in glucose metabolism, such as the detection of 2HG, can also be used for new imaging technology (90, 91).

Application of Glucose Metabolism in Cancer Treatment

To date, various agents involved in glucose metabolism are actively investigated as novel targets with therapeutic potential (**Table 1**). It helps to overcome drug resistance or increase the efficacy of current combination therapy (88, 109). Compared to diagnosis, targeting glucose metabolism in treatment seems faint due to their efficacy or safety concern. Several drugs with efficacy confirmed and multi-targets, as well as some old non-chemotherapeutic drugs with new aspects of inhabiting tumor glucose metabolism will be discussed below.

GLUTs control the influx of glucose, especially GLUT-1. Several GLUT-1 inhibitory agents, including WZB117 and STF-31 have been tested (94, 105). STF-31 was effective in decreasing glucose uptake, inducing cell apoptosis and inhibiting tumor progression. However, STF-31 has a narrow therapeutic potential due to its molecular restriction (110, 111). WZB117 can effectively inhibit glucose uptake, cell proliferation, and tumor progression both *in vivo* and *in vitro*. However, its efficacy remains in doubt (105). A glucose-conjugated LDH inhibitor, glucose-conjugated methyl ester (NHI-Glc-2), is a promising compound. It is a weaker inhibitor than the N-OH methyl ester (NHI-2) on the isolated enzyme. It can increase the glucose uptake by exploiting the GLUT-1 overexpression,

TABLE 1 | Metabolic modulators arising from the metabolic theory of cancer.

Target	Therapy	Reference
Glucose transporters (GLUTs)	2-deoxyglucose (2DG)	(92, 93)
	Phloretin	(49, 71)
	Silybin	(26, 94)
	Glutor	(95)
	STF-31	(94, 96)
	WZB117	(94, 96)
	Fasentin	(97, 98)
Hexokinase (HK)	2-deoxyglucose (2DG)	(92, 93)
	3- bromopyruvate (3BP)	(26, 96)
	Lonidamine(LND)	(99, 100)
	Methyl jasmonate	(94, 97)
Glyceraldehyde 3-phosphate dehydrogenase(GAPDH)	3- bromopyruvate (3BP)	(26, 96)
	Ornidazole, a-chlorohydrin	(24)
Phosphofructokinase (PFK)	3-(3-pyridinyl)-1-(4-pyridinyl)-2-propen-1-one (3PO)	(26, 93)
Pyruvate kinase-M2 (PK-M2)	TLN-232/CAP-23	(26, 92, 94)
	Shikonin	(24, 26)
	Alkannin	(24, 26)
	TEPP-46	(24, 86)
	DASA-58	(24, 101)
	ML-265	(17, 102)
	Oleanolic acid (OA)	(103)
	dimethylaminomicheliolide (DMAMCL)	(104)
Lactate dehydrogenase (LDH)	2,3-dihydroxynaphtalen-1-carboxylic acid (FX11)	(24, 94)
	N-hydroxy-2-carboxy-substituted indoles (NHI)	(24, 105)
	Oxamate	(24)
	R-(-)-gossypol / AT101	(24)
	3-hydroxyisoxazole-4-carboxylic acid (HICA)	(26, 34)
	Gossypol/Galloflavin	(52)
	5 designed peptides(QLYNL, LIYNLL, IYNLLK,KVVYNVA, and KVVYNV)	(52)
	1-(Phenylseleno)-4-(Trifluoromethyl)	(52)
	Benzene(PSTMB)	(24, 105)
	Oxamate(siRNA LDHA gene, Galloflavin)	(92, 96)
	FK866	(26, 52)
	AZD3965	(24, 52)

(Continued)

TABLE 1 | Continued

Target	Therapy	Reference
	AR-C155858	(95, 106)
	a-cyano-4-hydroxycinnamic acid (CHC), 4,4-diisothiocyanatostilbene-2,2′ -disulphonic acid(DIDS), Quercetin	(52, 106)
	BAY-8002	(52)
	Syrosingopine	(52)
Isocitrate dehydrogenase (IDH)	AGI-5198	(102, 107)
	AGI-6780	(102, 108)
PDK	TKIS	(52, 102)
	Dichloroacetate (DCA)	(14, 49)

reduce lactate production and decrease proliferation of cancer cells (105).

Currently, inhibition of lactate transport is being tested as an alternative approach. But LDHA inhibitors had some limitations, such as high toxicity, low drug exposure or a lack of LDHA dependence in human tumor inhibitors (112). Nevertheless, an inhibitor of human LDH isoforms, Galloflavin is a natural phenol derivative and a product of gallic acid oxidation (105, 113). The analogs of Gossypol, a natural component extracted from the cotton seeds has been screened for small molecular inhibitors specific for LDHA. 3-dihydroxy-6-methyl-7-(phenylmethyl)-4-propylnaphthalene-1-carboxylic acid (FX11) was proved to effectively inhibit proliferation of cancer cells *in vitro* and *in vivo* by enhancing the levels of oxidative stress. Another isoform-specific inhibitors of LDHA, N-hydroxyindole-based compounds, can compete with its substrate pyruvate and the cofactor, NADH (92, 97).

The reversal reprogramming in IDH mutant tumors seems more successful (114, 115). The mechanism of 2HG-mediated transformation may vary in different kinds of tumors. It may inhibit the dual metabolic flux of glycolysis and oxidative PPP (88, 116). In preclinical studies, the inhibition of mutant IDH has been shown to dramatically decrease the generation of 2HG and cause cancer cells to differentiate into normal cells (107, 108). An inhibitor of mutant IDH2, AG-221, has been put forward in early phase clinical trials (113).

New compounds also target dual inhibition, such as the inhibition of metabolic plasticity and metabolic rescue in cancer cells. Compounds targeting glucose, glutamine and lactate metabolism have been found to exert anticancer effects by inhibiting growth of tumor-associated endothelial cells (24). A new glucose uptake inhibitor, Glutor, targets GLUTs (GLUT-1, -2, and -3), diminishes glycolytic flux and selectively suppresses growth of a variety of cancer cells. Glutor combined with glutaminase inhibitor CB-839 synergistically inhibits the proliferation of colon cancer cells (95).

Compared to conventional cytotoxic therapy, modulation of particular targets with altered glycolytic metabolism would reduce treatment toxicity. A number of studies show that treatment combined with vitamin C leads to interfering with glycolysis and the TCA cycle and inhibits ATP and NADPH production. It can kill cancer cells by increasing oxidative stress and further inhibition in cancer cell survival and invasion. (117–122). Preclinical studies have shown that vitamin C at the concentration below 5 mM could prevent proliferation of cancer cells (123–125). Because of the anti-oxidant capacity, vitamin C can prevent the growth of circulating tumor cells (CTCs). Vitamin C also reduces pyruvate and glutathione (GSH). Extracellular matrix remodeling and cancer cell motility were reduced by vitamin C by boosting ROS levels. It can increase expression of E-cadherin, decrease expression of Snail and inhibit matrix metalloproteinases (MMPs) (105, 126, 127).

Metformin is a common drug for diabetes. The metformin/hypoglycemia combination has synergistic anti-neoplastic effects to decrease the pro-survival protein MCL-1 and cause cell death (128). Metformin combined with ritonavir targets OXPHOS, in particular, GLUT-4. It can effectively inhibit the AKT and mTORC1 phosphorylation and pro-survival mitochondrial complex I (MCL1) (116, 129).

Aspirin is a common pain reliever and anti-inflammatory drug. It also inhibits MCL1 activity (130). In the past two decades, its anti-neoplastic action has been investigated against different malignancies and tumor cell lines. Dalton's lymphoma (T-cell lymphoma) cells obtained from tumor-bearing mice treated by aspirin showed a change of expression of pH regulators MCT-1 and V-ATPase, as well as change in cell survival regulatory molecules including GLUT-1 (131). Aspirin can also modulate glucose uptake by depressing GLUT-1 through targeting NF-κB or NF κB/HIF1α signaling to inhibit proliferation (132).

CONCLUSION

Despite the extensive study on cancer metabolism with interesting results accumulated in the last decades, questions are still arising. The key process of balance among glycolysis, TCA and other pathways of the glucose metabolism in tumor remains unclear, as it is the essential mechanism of Warburg effect. In addition, it should be considered to develop more tumor-specific tracers and drugs based on the metabolic switch in tumor cells, cancer stem cells or the interaction with immune system. The ideal drugs should only applied in tumor by blocking specific pathway(s) for its metabolic plasticity but not in normal tissues. Despite the emerging of metabolic enzymes or transporters inhibitors, the efficiency of targeting tumor glucose metabolism is being challenged. To explore the metabolic plasticity in cancer under intrinsic and extrinsic influences, tumorous glucose metabolism should be addressed. Nevertheless,

with technological advances, it is expected that we will uncover many other unknown aspects of glucose metabolism in cancer and use them to benefit patient care.

AUTHOR CONTRIBUTIONS

XL and HG conceived and designed the study. XL wrote the first draft. ZX, TC, and SL wrote some sections of the article. HG edited the article. All authors read and approved the final version of submission.

FUNDING

This work was supported by the Fund of Natural Science Foundation of Guangdong Province, China, No. 2018A030310239.

REFERENCES

1. Hanahan D, Weinberg RA. The hallmarks of cancer. *Cell.* (2000) 100:57–70. doi: 10.1016/S0092-8674(00)81683-9
2. Hanahan D, Weinberg RA. Hallmarks of cancer: the next generation. *Cell.* (2011) 144:646–74. doi: 10.1016/j.cell.2011.02.013
3. Semenza GL. Hypoxia-inducible factors: coupling glucose metabolism and redox regulation with induction of the breast cancer stem cell phenotype. *EMBO J.* (2017) 36:252–9. doi: 10.15252/embj.201695204
4. Warburg O. On the origin of cancer cells. *Science.* (1956) 123:309–14. doi: 10.1126/science.123.3191.309
5. Liberti MV, Locasale JW. The Warburg effect: how does it benefit cancer cells? *Trends Biochem Sci.* (2016) 41:211–8. doi: 10.1016/j.tibs.2015.12.001
6. Levine AJ, Puzio-Kuter AM. The control of the metabolic switch in cancers by oncogenes and tumor suppressor genes. *Science.* (2010) 330:1340–4. doi: 10.1126/science.1193494
7. Locasale JW. Serine, glycine and one-carbon units: cancer metabolism in full circle. *Nat Rev Cancer.* (2013) 13:572–83. doi: 10.1038/nrc3557
8. Zdralevic M, Vucetic M, Daher B, Marchiq I, Parks SK, Pouyssegur J. Disrupting the 'Warburg effect' re-routes cancer cells to OXPHOS offering a vulnerability point via 'ferroptosis'-induced cell death. *Adv Biol Regul.* (2018) 68:55–63. doi: 10.1016/j.jbior.2017.12.002
9. Gupta S, Roy A, Dwarakanath BS. Metabolic cooperation and competition in the tumor microenvironment: implications for therapy. *Front Oncol.* (2017) 7:68. doi: 10.3389/fonc.2017.00068
10. Masui K, Tanaka K, Ikegami S, Villa GR, Yang H, Yong WH, et al. Glucose-dependent acetylation of Rictor promotes targeted cancer therapy resistance. *Proc Natl Acad Sci USA.* (2015) 112:9406–11. doi: 10.1073/pnas.1511759112
11. Koczula KM, Ludwig C, Hayden R, Cronin L, Pratt G, Parry H, et al. Metabolic plasticity in CLL: adaptation to the hypoxic niche. *Leukemia.* (2016) 30:65–73. doi: 10.1038/leu.2015.187
12. Maher EA, Marin-Valencia I, Bachoo RM, Mashimo T, Raisanen J, Hatanpaa KJ, et al. Metabolism of [U-13 C]glucose in human brain tumors *in vivo*. *NMR Biomed.* (2012) 25:1234–44. doi: 10.1002/nbm.2794
13. Murphy TA, Dang CV, Young JD. Isotopically nonstationary 13C flux analysis of Myc-induced metabolic reprogramming in B-cells. *Metab Eng.* (2013) 15:206–17. doi: 10.1016/j.ymben.2012.07.008
14. Kim JW, Gao P, Liu YC, Semenza GL, Dang CV. Hypoxia-inducible factor 1 and dysregulated c-Myc cooperatively induce vascular endothelial growth factor and metabolic switches hexokinase 2 and pyruvate dehydrogenase kinase 1. *Mol Cell Biol.* (2007) 27:7381–93. doi: 10.1128/MCB.00440-07
15. Shi L, Jackstadt R, Siemens H, Li H, Kirchner T, Hermeking H. p53-induced miR-15a/16-1 and AP4 form a double-negative feedback loop to regulate epithelial-mesenchymal transition and metastasis in colorectal cancer. *Cancer Res.* (2014) 74:532–42. doi: 10.1158/0008-5472.CAN-13-2203
16. Yang X, Ye H, He M, Zhou X, Sun N, Guo W, et al. LncRNA PDIA3P interacts with c-Myc to regulate cell proliferation via induction of pentose phosphate pathway in multiple myeloma. *Biochem Biophys Res Commun.* (2018) 498:207–213. doi: 10.1016/j.bbrc.2018.02.211
17. Mendez-Lucas A, Li X, Hu J, Che L, Song X, Jia J, et al. Glucose catabolism in liver tumors induced by c-MYC can be sustained by various PKM1/PKM2 ratios and pyruvate kinase activities. *Cancer Res.* (2017) 77:4355–4364. doi: 10.1158/0008-5472.CAN-17-0498
18. Wilde L, Roche M, Domingo-Vidal M, Tanson K, Philp N, Curry J, et al. Metabolic coupling and the Reverse Warburg Effect in cancer: Implications for novel biomarker and anticancer agent development. *Semin Oncol.* (2017) 44:198–203. doi: 10.1053/j.seminoncol.2017.10.004
19. Kondoh H, Lleonart ME, Gil J, Wang J, Degan P, Peters G, et al. Glycolytic enzymes can modulate cellular life span. *Cancer Res.* (2005) 65:177–85.
20. Wegiel B, Vuerich M, Daneshmandi S, Seth P. Metabolic switch in the tumor microenvironment determines immune responses to anti-cancer therapy. *Front Oncol.* (2018) 8:284. doi: 10.3389/fonc.2018.00284
21. Semenza GL. Targeting HIF-1 for cancer therapy. *Nat Rev Cancer.* (2003) 3:721–32. doi: 10.1038/nrc1187
22. Oizel K, Chauvin C, Oliver L, Gratas C, Geraldo F, Jarry U, et al. Efficient mitochondrial glutamine targeting prevails over glioblastoma metabolic plasticity. *Clin Cancer Res.* (2017) 23:6292–304. doi: 10.1158/1078-0432.CCR-16-3102
23. Damgaci S, Ibrahim-Hashim A, Enriquez-Navas PM, Pilon-Thomas S, Guvenis A, Gillies RJ. Hypoxia and acidosis: immune suppressors and therapeutic targets. *Immunology.* (2018) 154:354–62. doi: 10.1111/imm.12917
24. Polet F, Feron O. Endothelial cell metabolism and tumour angiogenesis: glucose and glutamine as essential fuels and lactate as the driving force. *J Intern Med.* (2013) 273:156–65. doi: 10.1111/joim.12016
25. Colegio OR, Chu NQ, Szabo AL, Chu T, Rhebergen AM, Jairam V, et al. Functional polarization of tumour-associated macrophages by tumour-derived lactic acid. *Nature.* (2014) 513:559–63. doi: 10.1038/nature13490
26. Porporato PE, Dhup S, Dadhich RK, Copetti T, Sonveaux P. Anticancer targets in the glycolytic metabolism of tumors: a comprehensive review. *Front Pharmacol.* (2011) 2:49. doi: 10.3389/fphar.2011.00049
27. Lunt SY, Vander Heiden MG. Aerobic glycolysis: meeting the metabolic requirements of cell proliferation. *Annu Rev Cell Dev Biol.* (2011) 27:441–64. doi: 10.1146/annurev-cellbio-092910-154237
28. Harris RA, Tindale L, Cumming RC. Age-dependent metabolic dysregulation in cancer and Alzheimer's disease. *Biogerontology.* (2014) 15:559–77. doi: 10.1007/s10522-014-9534-z
29. Madhukar NS, Warmoes MO, Locasale JW. Organization of enzyme concentration across the metabolic network in cancer cells. *PLoS ONE.* (2015) 10:e0117131. doi: 10.1371/journal.pone.0117131
30. Li J, Huang Q, Long X, Guo X, Sun X, Jin X, et al. Mitochondrial elongation-mediated glucose metabolism reprogramming is essential for tumour cell survival during energy stress. *Oncogene.* (2017) 36:4901–12. doi: 10.1038/onc.2017.98
31. Tiwari N, Gheldof A, Tatari M, Christofori G. EMT as the ultimate survival mechanism of cancer cells. *Semin Cancer Biol.* (2012) 22:194–207. doi: 10.1016/j.semcancer.2012.02.013
32. Mani SA, Guo W, Liao MJ, Eaton EN, Ayyanan A, Zhou AY, et al. The epithelial-mesenchymal transition generates cells with properties of stem cells. *Cell.* (2008) 133:704–15. doi: 10.1016/j.cell.2008.03.027
33. Payen VL, Porporato PE, Baselet B, Sonveaux P. Metabolic changes associated with tumor metastasis, part 1: tumor pH, glycolysis and the pentose phosphate pathway. *Cell Mol Life Sci.* (2016) 73:1333–48. doi: 10.1007/s00018-015-2098-5
34. Kang H, Kim H, Lee S, Youn H, Youn B. Role of metabolic reprogramming in Epithelial? Mesenchymal Transition (EMT). *Int J Mol Sci.* (2019) 20:E2042. doi: 10.3390/ijms20082042

35. Thiery JP, Sleeman JP. Complex networks orchestrate epithelial-mesenchymal transitions. *Nat Rev Mol Cell Biol.* (2006) 7:131–42. doi: 10.1038/nrm1835
36. Xu W, Yang Z, Lu N. A new role for the PI3K/Akt signaling pathway in the epithelial-mesenchymal transition. *Cell Adh Migr.* (2015) 9:317–24. doi: 10.1080/19336918.2015.1016686
37. Huang R, Zong X. Aberrant cancer metabolism in epithelial-mesenchymal transition and cancer metastasis: Mechanisms in cancer progression. *Crit Rev Oncol Hematol.* (2017) 115:13–22. doi: 10.1016/j.critrevonc.2017.04.005
38. Macheda ML, Rogers S, Best JD. Molecular and cellular regulation of glucose transporter (GLUT) proteins in cancer. *J Cell Physiol.* (2005) 202:654–62. doi: 10.1002/jcp.20166
39. Phillips RM, Lam C, Wang H, Tran PT. Bittersweet tumor development and progression: emerging roles of epithelial plasticity glycosylations. *Adv Cancer Res.* (2019) 142:23–62. doi: 10.1016/bs.acr.2019.01.002
40. Hamabe A, Konno M, Tanuma N, Shima H, Tsunekuni K, Kawamoto K, et al. Role of pyruvate kinase M2 in transcriptional regulation leading to epithelial-mesenchymal transition. *Proc Natl Acad Sci USA.* (2014) 111:15526–31. doi: 10.1073/pnas.1407717111
41. Li C, Zhao Z, Zhou Z, Liu R. PKM2 promotes cell survival and invasion under metabolic stress by enhancing warburg effect in pancreatic ductal adenocarcinoma. *Dig Dis Sci.* (2016) 61:767–73. doi: 10.1007/s10620-015-3931-2
42. Porporato PE, Payen VL, Perez-Escuredo J, De Saedeleer CJ, Danhier P, Copetti T, et al. A mitochondrial switch promotes tumor metastasis. *Cell Rep.* (2014) 8:754–66. doi: 10.1016/j.celrep.2014.06.043
43. Park CY, Tseng D, Weissman IL. Cancer stem cell-directed therapies: recent data from the laboratory and clinic. *Mol Ther.* (2009) 17:219–30. doi: 10.1038/mt.2008.254
44. Aguilar E, Marin de Mas I, Zodda E, Marin S, Morrish F, Selivanov V, et al. Metabolic reprogramming and dependencies associated with epithelial cancer stem cells independent of the epithelial-mesenchymal transition program. *Stem Cells.* (2016) 34:1163–76. doi: 10.1002/stem.2286
45. Sancho P, Barneda D, Heeschen C. Hallmarks of cancer stem cell metabolism. *Br J Cancer.* (2016) 114:1305–12. doi: 10.1038/bjc.2016.152
46. Jang H, Yang J, Lee E, Cheong JH. Metabolism in embryonic and cancer stemness. *Arch Pharm Res.* (2015) 38:381–8. doi: 10.1007/s12272-015-0558-y
47. Shen YA, Wang CY, Hsieh YT, Chen YJ, Wei YH. Metabolic reprogramming orchestrates cancer stem cell properties in nasopharyngeal carcinoma. *Cell Cycle.* (2015) 14:86–98. doi: 10.4161/15384101.2014.974419
48. Folmes CD, Dzeja PP, Nelson TJ, Terzic A. Metabolic plasticity in stem cell homeostasis and differentiation. *Cell Stem Cell.* (2012) 11:596–606. doi: 10.1016/j.stem.2012.10.002
49. Walsh HR, Cruickshank BM, Brown JM, Marcato P. The flick of a switch: conferring survival advantage to breast cancer stem cells through metabolic plasticity. *Front Oncol.* (2019) 9:753. doi: 10.3389/fonc.2019.00753
50. Shibao S, Minami N, Koike N, Fukui N, Yoshida K, Saya H, et al. Metabolic heterogeneity and plasticity of glioma stem cells in a mouse glioblastoma model. *Neuro Oncol.* (2018) 20:343–54. doi: 10.1093/neuonc/nox170
51. Lyssiotis CA, Kimmelman AC. Metabolic interactions in the tumor microenvironment. *Trends Cell Biol.* (2017) 27:863–75. doi: 10.1016/j.tcb.2017.06.003
52. de la Cruz-López KG, Castro-Muñoz LJ, Reyes-Hernández DO, García-Carranca A, Manzo-Merino J. Lactate in the regulation of tumor microenvironment and therapeutic approaches. *Front Oncol.* (2019) 9:1143. doi: 10.3389/fonc.2019.01143
53. Kim JW, Tchernyshyov I, Semenza GL, Dang CV. HIF-1-mediated expression of pyruvate dehydrogenase kinase: a metabolic switch required for cellular adaptation to hypoxia. *Cell Metab.* (2006) 3:177–85. doi: 10.1016/j.cmet.2006.02.002
54. Semenza GL, Roth PH, Fang HM, Wang GL. Transcriptional regulation of genes encoding glycolytic enzymes by hypoxia-inducible factor 1. *J Biol Chem.* (1994) 269:23757–63.
55. Shan M, Dai D, Vudem A, Varner JD, Stroock AD. Multi-scale computational study of the Warburg effect, reverse Warburg effect and glutamine addiction in solid tumors. *PLoS Comput Biol.* (2018) 14:e1006584. doi: 10.1371/journal.pcbi.1006584
56. Huang, Li T, Wang L, Zhang L, Yan R, Li K, et al. Hepatocellular carcinoma redirects to ketolysis for progression under nutrition deprivation stress. *Cell Res.* (2016) 26:1112–30. doi: 10.1038/cr.2016.109
57. Sun L, Song L, Wan Q, Wu G, Li X, Wang Y, et al. cMyc-mediated activation of serine biosynthesis pathway is critical for cancer progression under nutrient deprivation conditions. *Cell Res.* (2015) 25:429–44. doi: 10.1038/cr.2015.33
58. Ma L, Tao Y, Duran A, Llado V, Galvez A, Barger JF, et al. Control of nutrient stress-induced metabolic reprogramming by PKCzeta in tumorigenesis. *Cell.* (2013) 152:599–611. doi: 10.1016/j.cell.2012.12.028
59. Daye D, Wellen KE. Metabolic reprogramming in cancer: unraveling the role of glutamine in tumorigenesis. *Semin Cell Dev Biol.* (2012) 23:362–9. doi: 10.1016/j.semcdb.2012.02.002
60. Boroughs LK, DeBerardinis RJ. Metabolic pathways promoting cancer cell survival and growth. *Nat Cell Biol.* (2015) 17:351–9. doi: 10.1038/ncb3124
61. Valencia T, Kim JY, Abu-Baker S, Moscat-Pardos J, Ahn CS, Reina-Campos M, et al. Metabolic reprogramming of stromal fibroblasts through p62-mTORC1 signaling promotes inflammation and tumorigenesis. *Cancer Cell.* (2014) 26:121–35. doi: 10.1016/j.ccr.2014.05.004
62. Pavlides S, Whitaker-Menezes D, Castello-Cros R, Flomenberg N, Witkiewicz AK, Frank PG, et al. The reverse Warburg effect: aerobic glycolysis in cancer associated fibroblasts and the tumor stroma. *Cell Cycle.* (2009) 8:3984–4001. doi: 10.4161/cc.8.23.10238
63. Xu XD, Shao SX, Jiang HP, Cao YW, Wang YH, Yang XC, et al. Warburg effect or reverse Warburg effect? A review of cancer metabolism. *Oncol Res Treat.* (2015) 38:117–22. doi: 10.1159/000375435
64. Davies M. New modalities of cancer treatment for NSCLC: focus on immunotherapy. *Cancer Manag Res.* (2014) 6:63–75. doi: 10.2147/CMAR.S57550
65. Gonzalez H, Hagerling C, Werb Z. Roles of the immune system in cancer: from tumor initiation to metastatic progression. *Genes Dev.* (2018) 32:1267–84. doi: 10.1101/gad.314617.118
66. Bremnes RM, Al-Shibli K, Donnem T, Sirera R, Al-Saad S, Andersen S, et al. The role of tumor-infiltrating immune cells and chronic inflammation at the tumor site on cancer development, progression, and prognosis: emphasis on non-small cell lung cancer. *J Thorac Oncol.* (2011) 6:824–33. doi: 10.1097/JTO.0b013e3182037b76
67. Liu Y, Cao X. Immunosuppressive cells in tumor immune escape and metastasis. *J Mol Med.* (2016) 94:509–22. doi: 10.1007/s00109-015-1376-x
68. Ahmed N, Escalona R, Leung D, Chan E, Kannourakis G. Tumour microenvironment and metabolic plasticity in cancer and cancer stem cells: Perspectives on metabolic and immune regulatory signatures in chemoresistant ovarian cancer stem cells. *Semin Cancer Biol.* (2018) 53:265–81. doi: 10.1016/j.semcancer.2018.10.002
69. Caro-Maldonado A, Wang R, Nichols AG, Kuraoka M, Milasta S, Sun LD, et al. Metabolic reprogramming is required for antibody production that is suppressed in anergic but exaggerated in chronically BAFF-exposed B cells. *J Immunol.* (2014) 192:3626–36. doi: 10.4049/jimmunol.1302062
70. Romero-Garcia S, Moreno-Altamirano MMB, Prado-Garcia H, Sánchez-García FJ. Lactate contribution to the tumor microenvironment: mechanisms, effects on immune cells and therapeutic relevance. *Front Immunol.* (2016) 7:52. doi: 10.3389/fimmu.2016.00052
71. Jacobs SR, Herman CE, Maciver NJ, Wofford JA, Wieman HL, Hammen JJ, et al. Glucose uptake is limiting in T cell activation and requires CD28-mediated Akt-dependent and independent pathways. *J Immunol.* (2008) 180:4476–86. doi: 10.4049/jimmunol.180.7.4476
72. Wang R, Dillon CP, Shi LZ, Milasta S, Carter R, Finkelstein D, et al. The transcription factor Myc controls metabolic reprogramming upon T lymphocyte activation. *Immunity.* (2011) 35:871–82. doi: 10.1016/j.immuni.2011.09.021
73. Wang R, Green DR. Metabolic reprogramming and metabolic dependency in T cells. *Immunol Rev.* (2012) 249:14–26. doi: 10.1111/j.1600-065X.2012.01155.x
74. Gottfried E, Kunz-Schughart LA, Ebner S, Mueller-Klieser W, Hoves S, Andreesen R, et al. Tumor-derived lactic acid modulates dendritic cell activation and antigen expression. *Blood.* (2006) 107:2013–21. doi: 10.1182/blood-2005-05-1795

75. Fischer K, Hoffmann P, Voelkl S, Meidenbauer N, Ammer J, Edinger M, et al. Inhibitory effect of tumor cell-derived lactic acid on human T cells. *Blood.* (2007) 109:3812–9. doi: 10.1182/blood-2006-07-035972
76. Goetze K, Walenta S, Ksiazkiewicz M, Kunz-Schughart LA, Mueller-Klieser W. Lactate enhances motility of tumor cells and inhibits monocyte migration and cytokine release. *Int J Oncol.* (2011) 39:453–63. doi: 10.3892/ijo.2011.1055
77. Carmona-Fontaine C, Bucci V, Akkari L, Deforet M, Joyce JA, Xavier JB. Emergence of spatial structure in the tumor microenvironment due to the Warburg effect. *Proc Natl Acad Sci USA.* (2013) 110:19402–7. doi: 10.1073/pnas.1311939110
78. Ohashi T, Aoki M, Tomita H, Akazawa T, Sato K, Kuze B, et al. M2-like macrophage polarization in high lactic acid-producing head and neck cancer. *Cancer Sci.* (2017) 108:1128–34. doi: 10.1111/cas.13244
79. Brand A, Singer K, Koehl GE, Kolitzus M, Schoenhammer G, Thiel A, et al. LDHA-associated lactic acid production blunts tumor immunosurveillance by T and NK cells. *Cell Metab.* (2016) 24:657–71. doi: 10.1016/j.cmet.2016.08.011
80. Sun L, Suo C, Li ST, Zhang H, Gao P. Metabolic reprogramming for cancer cells and their microenvironment: beyond the Warburg Effect. *Biochim Biophys Acta Rev Cancer.* (2018) 1870:51–66. doi: 10.1016/j.bbcan.2018.06.005
81. Nelson BH. CD20+ B cells: the other tumor-infiltrating lymphocytes. *J Immunol.* (2010) 185:4977–82. doi: 10.4049/jimmunol.1001323
82. Linnebacher M, Maletzki C. Tumor-infiltrating B cells: the ignored players in tumor immunology. *Oncoimmunology.* (2012) 1:1186–8. doi: 10.4161/onci.20641
83. Bohndiek SE, Brindle KM. Imaging and 'omic' methods for the molecular diagnosis of cancer. *Expert Rev Mol Diagn.* (2010) 10:417–34. doi: 10.1586/erm.10.20
84. Wadsak W, Mitterhauser M. Basics and principles of radiopharmaceuticals for PET/CT. *Eur J Radiol.* (2010) 73:461–9. doi: 10.1016/j.ejrad.2009.12.022
85. Gambhir SS. Molecular imaging of cancer with positron emission tomography. *Nat Rev Cancer.* (2002) 2:683–93. doi: 10.1038/nrc882
86. Witney TH, James ML, Shen B, Chang E, Pohling C, Arksey N, et al. PET imaging of tumor glycolysis downstream of hexokinase through noninvasive measurement of pyruvate kinase M2. *Sci Transl Med.* (2015) 7:310ra169. doi: 10.1126/scitranslmed.aac6117
87. Venneti S, Dunphy M, Zhang H, Pitter KL, Zanzonico P, Campos C, et al. Glutamine-based PET imaging facilitates enhanced metabolic evaluation of gliomas *in vivo*. *Sci Transl Med.* (2015) 7:274ra217. doi: 10.1126/scitranslmed.aaa1009
88. Vander Heiden MG, DeBerardinis RJ. Understanding the intersections between metabolism and cancer biology. *Cell.* (2017) 168:657–669. doi: 10.1016/j.cell.2016.12.039
89. Nelson SJ, Kurhanewicz J, Vigneron DB, Larson PE, Harzstark AL, Ferrone M, et al. Metabolic imaging of patients with prostate cancer using hyperpolarized [1-^{13}C]pyruvate. *Sci Transl Med.* (2013) 5:198ra108. doi: 10.1126/scitranslmed.3006070
90. Andronesi OC, Kim GS, Gerstner E, Batchelor T, Tzika AA, Fantin VR, et al. Detection of 2-hydroxyglutarate in IDH-mutated glioma patients by *in vivo* spectral-editing and 2D correlation magnetic resonance spectroscopy. *Sci Transl Med.* (2012) 4:116ra114. doi: 10.1126/scitranslmed.3002693
91. Choi C, Ganji SK, DeBerardinis RJ, Hatanpaa KJ, Rakheja D, Kovacs Z, et al. 2-hydroxyglutarate detection by magnetic resonance spectroscopy in IDH-mutated patients with gliomas. *Nat Med.* (2012) 18:624–9. doi: 10.1038/nm.2682
92. Cheong H, Lu C, Lindsten T, Thompson CB. Therapeutic targets in cancer cell metabolism and autophagy. *Nat Biotechnol.* (2012) 30:671–8. doi: 10.1038/nbt.2285
93. Veys K, Alvarado-Diaz A, De Bock K. Measuring glycolytic and mitochondrial fluxes in endothelial cells using radioactive tracers. *Methods Mol Biol.* (2019) 1862:121–36. doi: 10.1007/978-1-4939-8769-6_9
94. Granja S PC, Reis RM, Martinho O, Baltazar F. Glucose addiction in cancer therapy advances and drawbacks. *Curr Drug Metab.* (2015) 16:221–42. doi: 10.2174/1389200216666150602145145
95. Reckzeh ES, Karageorgis G, Schwalfenberg M, Ceballos J, Nowacki J, Stroet MCM, et al. Inhibition of glucose transporters and glutaminase synergistically impairs tumor cell growth. *Cell Chem Biol.* (2019) 26:1214–28.e25. doi: 10.1016/j.chembiol.2019.06.005
96. Muschen M. Metabolic gatekeepers to safeguard against autoimmunity and oncogenic B cell transformation. *Nat Rev Immunol.* (2019) 19:337–48. doi: 10.1038/s41577-019-0154-3
97. Talekar M, Boreddy SR, Singh A, Amiji M. Tumor aerobic glycolysis: new insights into therapeutic strategies with targeted delivery. *Expert Opin Biol Ther.* (2014) 14:1145–59. doi: 10.1517/14712598.2014.912270
98. Sabnis HS, Somasagara RR, Bunting KD. Targeting MYC dependence by metabolic inhibitors in cancer. *Genes.* (2017) 8:114. doi: 10.3390/genes8040114
99. Fang J, Quinones QJ, Holman TL, Morowitz MJ, Wang Q, Zhao H, et al. The H+-linked monocarboxylate transporter (MCT1/SLC16A1): a potential therapeutic target for high-risk neuroblastoma. *Mol Pharmacol.* (2006) 70:2108–15. doi: 10.1124/mol.106.026245
100. Goldman A, Khiste S, Freinkman E, Dhawan A, Majumder B, Mondal J, et al. Targeting tumor phenotypic plasticity and metabolic remodeling in adaptive cross-drug tolerance. *Sci Signal.* (2019) 12:eaas8779. doi: 10.1126/scisignal.aas8779
101. Chen TJ, Wang HJ, Liu JS, Cheng HH, Hsu SC, Wu MC, et al. Mutations in the PKM2 exon-10 region are associated with reduced allostery and increased nuclear translocation. *Commun Biol.* (2019) 2:105. doi: 10.1038/s42003-019-0343-4
102. Kinnaird A, Michelakis ED. Metabolic modulation of cancer: a new frontier with great translational potential. *J Mol Med.* (2015) 93:127–42. doi: 10.1007/s00109-014-1250-2
103. Guerra F, Arbini AA, Moro L. Mitochondria and cancer chemoresistance. *Biochim Biophys Acta Bioenerg.* (2017) 1858:686–99. doi: 10.1016/j.bbabio.2017.01.012
104. Guo J, Xue Q, Liu K, Ge W, Liu W, Wang J, et al. Dimethylaminomicheliolide (DMAMCL) suppresses the proliferation of glioblastoma cells via targeting pyruvate kinase 2 (PKM2) and rewiring aerobic glycolysis. *Front Oncol.* (2019) 9:993. doi: 10.3389/fonc.2019.00993
105. El Hassouni B, Granchi C, Vallés-Marti A, Supadmanaba IGP, Bononi G, Tuccinardi T, et al. The dichotomous role of the glycolytic metabolism pathway in cancer metastasis: interplay with the complex tumor microenvironment and novel therapeutic strategies. *Semin Cancer Biol.* (2019):S1044-579X(19)30180-4. doi: 10.1016/j.semcancer.2019.08.025
106. Colen CB, Seraji-Bozorgzad N, Marples B, Galloway MP, Sloan AE, Mathupala SP. Metabolic remodeling of malignant gliomas for enhanced sensitization during radiotherapy: an *in vitro* study. *Neurosurgery.* (2006) 59:1313–23; discussion 1323–4. doi: 10.1227/01.NEU.0000249218.65332.BF
107. Rohle D, Popovici-Muller J, Palaskas N, Turcan S, Grommes C, Campos C, et al. An inhibitor of mutant IDH1 delays growth and promotes differentiation of glioma cells. *Science.* (2013) 340:626–30. doi: 10.1126/science.1236062
108. Wang F, Travins J, DeLaBarre B, Penard-Lacronique V, Schalm S, Hansen E, et al. Targeted inhibition of mutant IDH2 in leukemia cells induces cellular differentiation. *Science.* (2013) 340:622–6. doi: 10.1126/science.1234769
109. Martinez-Outschoorn UE, Peiris-Pages M, Pestell RG, Sotgia F, Lisanti MP. Cancer metabolism: a therapeutic perspective. *Nat Rev Clin Oncol.* (2017) 14:11–31. doi: 10.1038/nrclinonc.2016.60
110. Liu Y, Cao Y, Zhang W, Bergmeier S, Qian Y, Akbar H, et al. A small-molecule inhibitor of glucose transporter 1 downregulates glycolysis, induces cell-cycle arrest, and inhibits cancer cell growth *in vitro* and *in vivo*. *Mol Cancer Ther.* (2012) 11:1672–82. doi: 10.1158/1535-7163.MCT-12-0131
111. Chan DA, Sutphin PD, Nguyen P, Turcotte S, Lai EW, Banh A, et al. Targeting GLUT1 and the Warburg effect in renal cell carcinoma by chemical synthetic lethality. *Sci Transl Med.* (2011) 3:94ra70. doi: 10.1126/scitranslmed.3002394
112. Boudreau A, Purkey HE, Hitz A, Robarge K, Peterson D, Labadie S, et al. Metabolic plasticity underpins innate and acquired resistance to LDHA inhibition. *Nat Chem Biol.* (2016) 12:779–86. doi: 10.1038/nchembio.2143
113. Kishton RJ, Rathmell JC. Novel therapeutic targets of tumor metabolism. *Cancer J.* (2015) 21:62–9. doi: 10.1097/PPO.0000000000000099
114. Losman JA, Kaelin WG Jr. What a difference a hydroxyl makes: mutant IDH, (R)-2-hydroxyglutarate, and cancer. *Genes Dev.* (2013) 27:836–52. doi: 10.1101/gad.217406.113

115. Tateishi K, Wakimoto H, Iafrate AJ, Tanaka S, Loebel F, Lelic N, et al. Extreme vulnerability of IDH1 mutant cancers to NAD+ depletion. *Cancer Cell.* (2015) 28:773–84. doi: 10.1016/j.ccell.2015.11.006
116. de Padua MC, Delodi G, Vučetić M, Durivault J, Vial V, Bayer P, et al. Disrupting glucose-6-phosphate isomerase fully suppresses the "Warburg effect" and activates OXPHOS with minimal impact on tumor growth except in hypoxia. *Oncotarget.* (2017) 8:87623–37. doi: 10.18632/oncotarget.21007
117. Ngo B, Van Riper JM, Cantley LC, Yun J. Targeting cancer vulnerabilities with high-dose vitamin C. *Nat Rev Cancer.* (2019) 19:271–82. doi: 10.1038/s41568-019-0135-7
118. Park S, Ahn S, Shin Y, Yang Y, Yeom CH. Vitamin C in cancer: a metabolomics perspective. *Front Physiol.* (2018) 9:762. doi: 10.3389/fphys.2018.00762
119. Polireddy K, Dong R, Reed G, Yu J, Chen P, Williamson S, et al. High dose parenteral ascorbate inhibited pancreatic cancer growth and metastasis: mechanisms and a phase I/IIa study. *Sci Rep.* (2017) 7:17188. doi: 10.1038/s41598-017-17568-8
120. Schoenfeld JD, Sibenaller ZA, Mapuskar KA, Wagner BA, Cramer-Morales KL, Furqan M, et al. $O_{2\cdot-}$ and H_2O_2-mediated disruption of Fe metabolism causes the differential susceptibility of NSCLC and GBM cancer cells to pharmacological ascorbate. *Cancer Cell.* (2017) 31:487–500.e8. doi: 10.1016/j.ccell.2017.07.008
121. Yun J, Mullarky E, Lu C, Bosch KN, Kavalier A, Rivera K, et al. Vitamin C selectively kills KRAS and BRAF mutant colorectal cancer cells by targeting GAPDH. *Science.* (2015) 350:1391–6. doi: 10.1126/science.aaa5004
122. Uetaki M, Tabata S, Nakasuka F, Soga T, Tomita M. Metabolomic alterations in human cancer cells by vitamin C-induced oxidative stress. *Sci Rep.* (2015) 5:13896. doi: 10.1038/srep13896
123. Chen Q, Espey MG, Sun AY, Pooput C, Kirk KL, Krishna MC, et al. Pharmacologic doses of ascorbate act as a prooxidant and decrease growth of aggressive tumor xenografts in mice. *Proc Natl Acad Sci USA.* (2008) 105:11105–9. doi: 10.1073/pnas.0804226105
124. Shenoy N, Creagan E, Witzig T, Levine M. Ascorbic acid in cancer treatment: let the phoenix fly. *Cancer Cell.* (2018) 34:700–6. doi: 10.1016/j.ccell.2018.07.014
125. Mikirova N, Casciari J, Riordan N, Hunninghake R. Clinical experience with intravenous administration of ascorbic acid: achievable levels in blood for different states of inflammation and disease in cancer patients. *J Transl Med.* (2013) 11:191. doi: 10.1186/1479-5876-11-191
126. Cha J, Roomi MW, Ivanov V, Kalinovsky T, Niedzwiecki A, Rath M. Ascorbate supplementation inhibits growth and metastasis of B16FO melanoma and 4T1 breast cancer cells in vitamin C-deficient mice. *Int J Oncol.* (2013) 42:55–64. doi: 10.3892/ijo.2012.1712
127. Sajadian SO, Tripura C, Samani FS, Ruoss M, Dooley S, Baharvand H, et al. Vitamin C enhances epigenetic modifications induced by 5-azacytidine and cell cycle arrest in the hepatocellular carcinoma cell lines HLE and Huh7. *Clin Epigenetics.* (2016) 8:46. doi: 10.1186/s13148-016-0213-6
128. Elgendy M, Ciro M, Hosseini A, Weiszmann J, Mazzarella L, Ferrari E, et al. Combination of hypoglycemia and metformin impairs tumor metabolic plasticity and growth by modulating the PP2A-GSK3β-MCL-1 axis. *Cancer Cell.* (2019) 35:798–815.e5. doi: 10.1016/j.ccell.2019.03.007
129. Dalva-Aydemir S, Bajpai R, Martinez M, Adekola KU, Kandela I, Wei C, et al. Targeting the metabolic plasticity of multiple myeloma with FDA-approved ritonavir and metformin. *Clin Cancer Res.* (2015) 21:1161–71. doi: 10.1158/1078-0432.CCR-14-1088
130. Dang CV. Links between metabolism and cancer. *Genes Dev.* (2012) 26:877–90. doi: 10.1101/gad.189365.112
131. Kumar A, Vishvakarma NK, Tyagi A, Bharti AC, Singh SM. Anti-neoplastic action of aspirin against a T-cell lymphoma involves an alteration in the tumour microenvironment and regulation of tumour cell survival. *Biosci Rep.* (2012) 32:91–104. doi: 10.1042/BSR20110027
132. Liu YX, Feng JY, Sun MM, Liu BW, Yang G, Bu YN, et al. Aspirin inhibits the proliferation of hepatoma cells through controlling GLUT1-mediated glucose metabolism. *Acta Pharmacol Sin.* (2019) 40:122–32. doi: 10.1038/s41401-018-0014-x

Conflict of Interest: The authors declare that the research was conducted in the absence of any commercial or financial relationships that could be construed as a potential conflict of interest.

frontiers in Oncology

REVIEW
published: 07 April 2020
doi: 10.3389/fonc.2020.00472

The Role of Exosomal microRNA in Cancer Drug Resistance

Qiao-ru Guo[1,2†], Hui Wang[3†], Ying-da Yan[1†], Yun Liu[1], Chao-yue Su[1], Hu-biao Chen[4], Yan-yan Yan[5], Rameshwar Adhikari[6], Qiang Wu[2,7] and Jian-ye Zhang[1,2*]*

[1] Guangdong Provincial Key Laboratory of Molecular Target & Clinical Pharmacology, School of Pharmaceutical Sciences and the Fifth Affiliated Hospital, Guangzhou Medical University, Guangzhou, China, [2] Key Laboratory of Tropical Translational Medicine of Ministry of Education, Hainan Medical University, Haikou, China, [3] Guangzhou Institute of Pediatrics/Guangzhou Women and Children's Medical Center, Guangzhou Medical University, Guangzhou, China, [4] School of Chinese Medicine, Hong Kong Baptist University, Hong Kong, China, [5] Collaborative Innovation Center for Cancer, Institute of Respiratory and Occupational Diseases, Medical College, Shanxi Datong University, Datong, China, [6] Research Centre for Applied Science and Technology, Tribhuvan University, Kirtipur, Nepal, [7] Key Laboratory of Emergency and Trauma of Ministry of Education, School of Tropical Medicine and Laboratory Medicine, Hainan Medical University, Haikou, China

OPEN ACCESS

Edited by:
Dong-Hua Yang,
St. John's University, United States

Reviewed by:
Xiumei Huang,
Indiana University Bloomington,
United States
Bethany Hannafon,
University of Oklahoma Health
Sciences Center, United States

***Correspondence:**
Qiang Wu
wuqiang001001@aliyun.com
Jian-ye Zhang
jianyez@163.com

† These authors have contributed equally to this work

Specialty section:
This article was submitted to Molecular and Cellular Oncology, a section of the journal Frontiers in Oncology

Received: 14 January 2020
Accepted: 16 March 2020
Published: 07 April 2020

Citation:
Guo Q, Wang H, Yan Y, Liu Y, Su C, Chen H, Yan Y, Adhikari R, Wu Q and Zhang J (2020) The Role of Exosomal microRNA in Cancer Drug Resistance. Front. Oncol. 10:472. doi: 10.3389/fonc.2020.00472

Exosomes affect the initiation and progression of cancers. In the tumor microenvironment, not only cancer cells, but also fibroblasts and immunocytes secrete exosomes. Exosomes act as a communicator between cells by transferring different cargos and microRNAs (miRNAs). Drug resistance is one of the critical factors affecting therapeutic effect in the course of cancer treatment. The currently known mechanisms of drug resistance include drug efflux, alterations in drug metabolism, DNA damage repair, alterations of energy programming, cancer stem cells and epigenetic changes. Many studies have shown that miRNA carried by exosomes is closely associated with the development of drug resistance mediated by the above-mentioned mechanisms. This review article will discuss how exosomal miRNAs regulate the drug resistance.

Keywords: exosome, miRNA, cancer, drug resistance, mechanism

INTRODUCTION

Chemotherapy, radiotherapy, surgery, and targeted therapy are important modalities of cancer treatment. However, the emergence of drug resistance leads to dismal prognosis in cancer patients. As an emerging therapeutic target and diagnostic biomarker, exosomal miRNAs play vital roles in tumor invasion, metastasis and progression. Studies have found that the occurrence and development of drug resistance is closely related to miRNA carried by exosomes (1–5). In this review article we discuss several classic mechanisms that exosomal miRNA involves in drug resistance. Also, we summarize the role of exosomal miRNA mediated drug resistance in different types of cancers.

THE BIOGENESIS OF EXOSOME AND miRNA

Exosomes are extracellular vesicles (EV) with the size ranges between 30 and 100 nm. Exosomes are released to the extracellular environment after the fusion of the multivesicular body (MVB) or late endosomes with the plasma membrane (6). It was first described in 1983 as "seems to be akin to reverse endocytosis" (7), and has gradually recognized an important factor in oncology research (8). Many studies have shown that exosome can promote the intercellular communication (9) by transferring varieties of cargos, such as nucleic acid, proteins and metabolites (10–16).

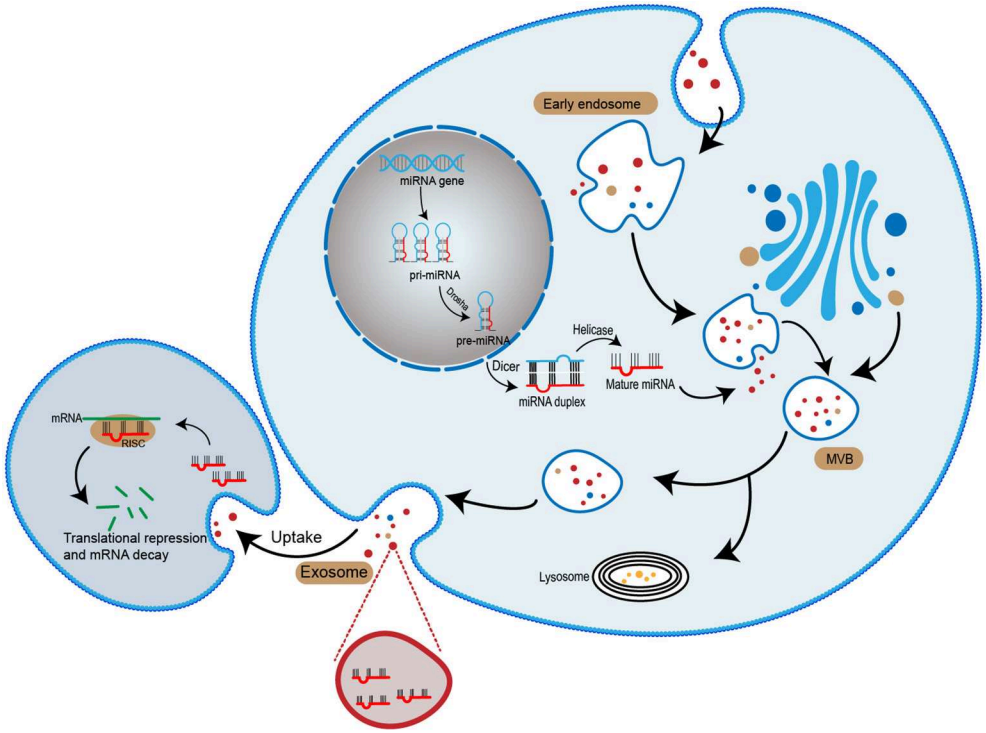

FIGURE 1 | The biogenesis of exosomal miRNA. miRNA genes are transcribed into primary miRNA (pri-miRNA). The pri-miRNA is cleaved by Dorsha complex to produce precursor miRNA (pre-miRNA) and exported into the cytoplasma. Subsequently, pre-miRNA is processed by Dicer complex to become mature miRNA. Mature miRNA is sorted into exosomes and released to the extracellular space. With the recipient cell uptake exosomes, the miRNA entered the cell and mediates gene suppression by targeted translational repression and mRNA degradation.

microRNA (miRNA) is an important cargo that delivered by exosomes (17). miRNAs usually consist of 19–25 nucleotides. It can regulate post-transcriptional silence of target genes. Following the transcription of miRNA gene, a small hairpin-shaped RNA called pre-miRNA is generated. The pre-miRNA is exported into cytoplasm and processed by Dicer, a kind of RNase III-type endonuclease, and subsequently releases a small RNA duplex (18, 19). The RNA duplex will unwind after loading onto an Argonaute (AGO) protein and forming RNA-induced silencing complex (RISC) (20). Once binding to a RISC, the miRNA is complementary pairing with the mRNA. Depending on whether miRNA and mRNA are fully bind, two different mechanisms occur: (1) mRNA specifies cleavage if miRNA is sufficiently complementary to mRNA; (2) the productive translation is inhibited when miRNA is insufficiently complementary to mRNA (21, 22). Therefore, miRNA can regulate various physiological and pathological activities (**Figure 1**).

THE CURRENT UNDERSTANDING OF CANCER DRUG RESISTANCE

Cancer drug resistance can be divided into intrinsic and acquired resistance. Intrinsic resistance occurs before receiving therapy, which limits the use of anticancer drugs. Acquired resistance may develop during treatment even if some drugs have anticancer effects at the early stage (23). Drug resistance seriously impacts the effectiveness of chemotherapy and molecular targeted therapies, ultimately leading dismal prognosis and tumor relapse.

Because of genomic instability, tumors may include a diverse collection of cells that possess different sensitivity to treatment (24). The positive selection of drug-resistant tumor subpopulation causes drug resistance. Therefore, accurate assessment of tumor heterogeneity is important to address drug resistance (25). The application of high-throughput screening technology facilitates the identification of genotype and helps predict drug response, providing convenience to individual therapy. In the past few years, microfluidic chips show tremendous promise in the study of tumor heterogeneity and the establishment of preclinical models (26). Grosselin et al. (27) set up a high-throughput droplet microfluidics platform. On this platform, the single cell chromatin landscapes of thousand cells can be profiled. They used the patient-derived xenograft models of acquired resistance to chemotherapy and target therapies in breast cancer and found a common chromatin signature between drug-sensitive and resistant cells (27). This technique paves the way to study the role of chromatin heterogeneity.

The limited cancer models hinder the clinical prediction of drug efficacy. Therefore, it is urgent to establish more reasonable, advanced and high-throughput cancer models to

deal with drug resistance and explore the underlying factor of heterogeneous patient responses. Gao et al. (28) established about 1,000 patient-derived tumor xenograft models (PDXs) with a diverse set of driver mutation using high-throughput screening technology. It has been demonstrated that these PDXs have the potential to predict patient response to targeted therapies and perform *in vivo* compound screens (28). Furthermore, a 3D model of tumor tissue made up of numerous different cell types can better mimic tumor microenvironment and provide the similar information about clinical response. Kather et al. developed a 3D model of tumor tissue which reproduced key features of colorectal cancer (CRC) and based on the individual patient data, yielding *in silico* tumor explant (29).

Combinations of drugs are also the effective way to overcome or bypass drug resistance (30). Epidermal growth factor receptor tyrosine kinase inhibitor (EGFR TKI) is beneficial for the treatment of non-small cell lung cancer with EGFR mutation (31). However, after treatment with EGFR TKI for 10–14 months, the efficacy declines (32), the primary and acquired drug resistance limits their clinical benefit (33). To combat resistance, in addition to developing new drugs, drugs combinations through a so-called bypass signaling mechanism, is an excellent choice (34). In addition, nanomedicine approach can be used to encapsulate and co-delivery drugs in specific materials to improve their bioavailability and thus overcome drug resistance (35, 36). The application of high-throughput drug screening can identify the effective drug combination regimens. Using high-throughput screening technology, researchers identified that potassium antimony tartrate in combination with topotecan can significantly enhance the sensitivity of non-small cell lung cancer and colorectal cancer to *cis*-diamminedichloroplatinum/cisplatin (CDDP). It was found that topotecan impairs the ability to repair CDDP-induced DNA damage (37). DNA damage repair is a classic mechanism by which cells develop drug resistance, as detailed later in this article.

Cancer biomarkers are present in tumor tissue or serum that help to detect cancers in their early stage, simplified the prognosis of cancer development (38). Cancer biomarkers help stratify patients to receive specific therapeutics. Biomarker could be DNA, mRNA, protein and various cellular metabolites (39). Over the past years, many advances have been made in the detection and evaluation of cancer biomarkers (40–44). In the next section, we will detail the development of exosomal miRNA as cancer biomarkers.

EXOSOMAL miRNA AS A REGULATOR AND BIOMARKER IN CANCER

Exosomal miRNA is involved in the proliferation, invasion, migration and drug resistance of various cancers. Therefore, exosomal miRNA has the potential to be the biomarkers for cancer diagnosis and treatment. In **Table 1**, we summarize some recent researches on various exosomal miRNA as regulators and biomarkers in various cancers.

TABLE 1 | Exosomal miRNA as regulators and biomarkers in different cancers.

Cancer type	Exosomal miRNA	References
Breast cancer	miR-9; miR-222; miR-105; miR-10b; miR-122; miR-1246	(45–50)
Colon cancer	miR-146a-5p; miR-200b; miR-193a; miR-125-3p; miR-25-3p; miR-27a; miR-130a	(14, 51–55)
Gastric cancer	miR-139; miR-130a; miR-21; miR-423-5p; miR-451; miR-10b-5p; miR-195-5p; miR-20a-3p; miR-296-5p	(4, 16, 56–59)
Lung cancer	miR-23a; miR-126; miR-96; miR-222-3p; let-7a-5p; miR16; miR-322; miR-497; miR-17	(60–65)
Liver cancer	miR-1237-3p; miR-335; miR-320a; miR-103; miR-18a; miR-221; miR-222; miR-224; miR-101; miR-106b; miR-122; miR-195	(66–70)
Ovarian cancer	Let-7; miR-200; miR-29a-3p; miR-21-5p; miR-205; miR-145; miR-200c; miR-940; miR-6126; miR-1246; miR-100; miR-320; miR-23a	(12, 71–77)
Pancreatic cancer	miR-21; miR-155; miR-365; miR-1231; miR-155; miR-301a; miR-1246; miR-4644; miR-3976; miR-4306	(78–83)
Prostate cancer	miR-1290; miR-375; miR-21-5p; miR-196a-5p; miR-501-3p; miR-1246	(84–87)
Oral cancer	miR-382-5p; miR-1246; miR-21; miR-34a-5p	(88–91)
Nasopharynx cancer	miR-23a; miR-24-3p; miR-9	(92–94)

Breast cancer (BC) is a highly prevalent cancer and the second leading cause of cancer-related death among women (95, 96). MiR-9 is a classic miRNA in cancer development. Baroni et al. indicated that exosomal miR-9 has the ability to induce human breast fibroblasts to have cancer associated fibroblasts (CAFs)-like properties (45). Exosome transferring miR-222 can promote BC cells migration and invasion by activating Nuclear factor-κB (NF-κB) (46). Exosomal miRNA also regulate tumor growth by influencing the metabolic reprogramming of BC cells. Yan et al. suggested that BC cells secrete exosomal miR-105 to promote tumor growth through the regulation of metabolic reprogramming in stromal cells (47).

Exosomal miRNA regulates tumor growth in other cancers as well. In colorectal cancer (CRC), transforming growth factor-beta (TGF-β) significantly contributes to the upregulation of exosome-meditated miR-200b, which promotes colorectal cancer cell proliferation by suppressing the expression of p27 in target cells. (51). Li et al. demonstrated that the absence of exosomal miR-148b derived from CAFs is the cause of invasion and metastasis in endometrial cancer (97). In lung cancer, Wu et al. indicated that exosomal miR-96 is associated with proliferation, migration and drug resistance by directly binding to wild-type LMO7 gene (60).

The expression of some exosomal miRNA in cancers is specific. The specificity enables exosomal miRNA to become cancer biomarkers. Sohn et al. proposed that serum exosomal miRNAs have the potential to become novel biomarkers for hepatocellular carcinoma (66). Moreover, Huang et al.

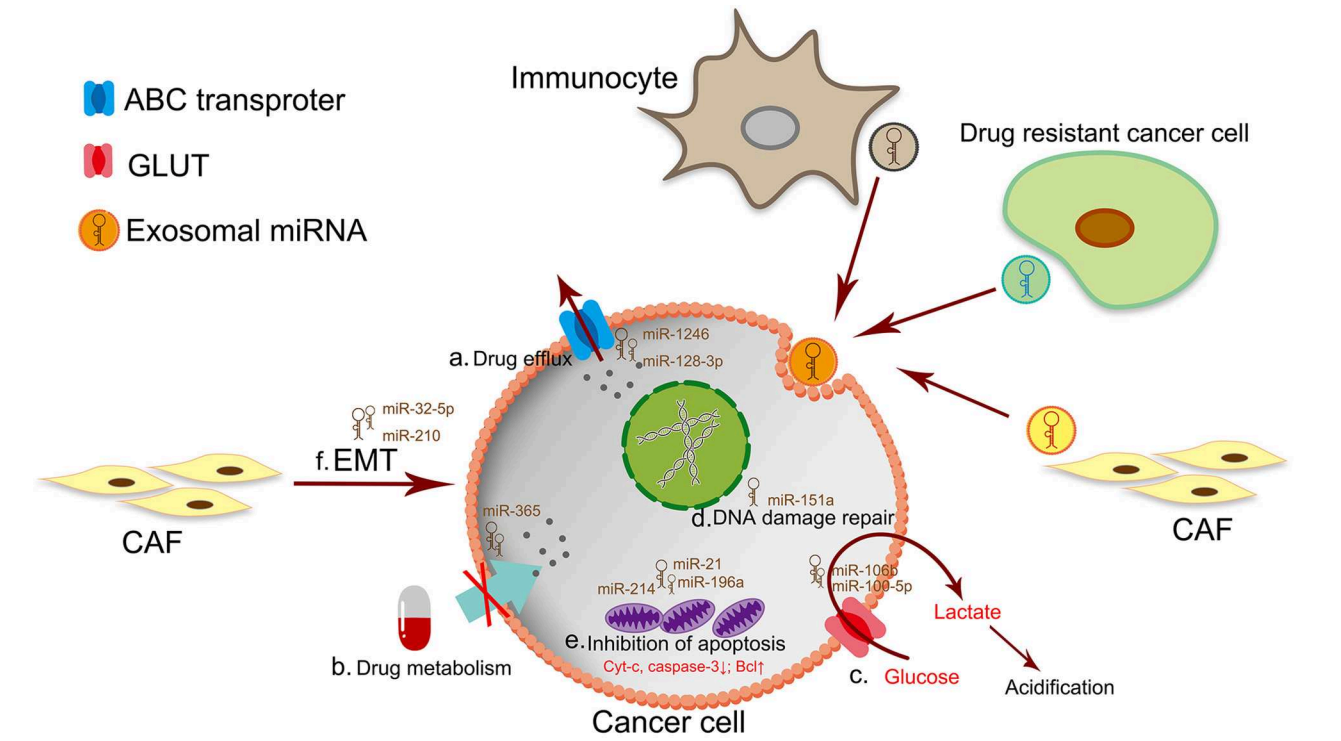

FIGURE 2 | The mechanism of drug resistance in cancer cells. a. Drug efflux by the ATP-binding cassette (ABC) transporter superfamily. b. The dysfunction of drug metabolism by drug inactivation or lack of drug activation. c. The excessive production of lactate leads to TME acidosis. The acidic TME makes cancer cells a strong survival advantage and drug resistance. d. DNA damage repair is a classic mechanism for drug resistant. e. Drug resistant-cancer cells are often accompanied by downregulation of intracellular apoptotic proteins or up-regulation of anti-apoptotic proteins. f. Targeting therapy of CSCs by inhibiting EMT has become an effective way to anticancer and prevent drug resistance.

extracted serum-derived exosome from patients with gastric non-cardia adenocarcinoma and detected the expression of miRNA. They identified the expression of miR-195-5p, miR-20a-3p, and miR-196-5p in exosomes and found that these miRNAs significantly increased. This finding provided a reference for clinical application and diagnosis using exosomal miRNAs (56).

THE MECHANISM OF CANCER DRUG RESISTANCE WITH EXOSOMAL miRNA

The mechanism of drug resistance is complex, the currently known mechanisms of drug resistance include drug efflux (98), mutation of drug target (99, 100), alterations in drug metabolism (101), DNA damage repair (102, 103), alterations of energy programming, cancer stem cells and epigenetic changes (104, 105). Most of these processes were regulated by exosomal miRNA (**Figure 2**). Different treatments have been developed to circumvent these resistance mechanisms (106–112). In this section we associate several mechanisms of drug resistance with miRNAs.

Drug Efflux and Metabolism in Cancers

Drug resistance is always accompanied by the dysfunction of pharmacokinetic factors, that are absorption, distribution, metabolism and elimination (ADME) of drugs. Exosomal miRNA participate drug resistance by interfering drug efflux and metabolism as well.

The excessive drug efflux is a classic mechanism of drug resistance. The human ATP-binding cassette (ABC) transporter superfamily is closely associated with the excessive efflux of drug. In the ABC transporter superfamily, several ATP-driven efflux transporters are the classic regulator of drug efflux: ABCB1 (P-gp/MDR1), ABCC1 (MRP1), ABCG2 (BCRP), ABCC2, MDR4 and MDR5 (113–118). The efficacy of drugs is closely related to the concentration of the drug inside the cells. In drug resistant-tumor cells, overexpression of these ABC transporters pumps anticancer drug out of cells, decreasing the concentration of drugs.

Tumor-derived exosomal miRNA cargo regulates the expression of ABC transporters and facilitates drug resistance in tumor cells. ABCB1 is one of the ABC transporters, some researchers reported that ABCB1 enriched in microvesicles and exosomes shed by drug-resistant cells (119). These EVs transfer ABCB1 to drug-sensitive cells, making the recipient cells express functional ABCB1 and acquiring drug resistance. However, the half-life of ABCB1 is shorter than 24 h and the transfer of ABCB1 is unstable (120). The resistant mechanism of drug-sensitive cells cannot be merely explained by the transfer of ABCB1. Sousa conjectured in his review that ABCB1 may co-transport with miRNA so that ABCB1 can be

expressed stably for a long time (121). After that, exosomal miRNA modulates transcripts in recipient cells to acquire resistance phenotype (122). For example, exosomal miR-1246 secreted by ovarian cancer (OC) cells inhibits the expression of Cav1 and upregulates ABCB1 expression to induce tumor-promoting phenotype and drug resistance. Based on the preclinical experiments *in vivo*, miR-1246 inhibitor treatment in combination with chemotherapy shows great potential in the treatment of OC (12). Exosomal miRNA is a double-edged sword in the occurrence and development of drug resistance. Some miRNAs have positive effects in drug resistance, while some can enhance the chemosensitivity of cancer cells. Liu et al. found that exosome-transmitted miR-128-3p down-regulates the expression of MDR5, decreasing oxaliplatin efflux and improving chemosensitivity of oxaliplatin-resist cells in colorectal cancer (123).

The activation of drug is related to the corresponding enzymes in body. The prodrug is activated by enzyme action, or the drug is metabolized into an inactive form due to some enzymes *in vivo*. For example, gemcitabine is metabolized by deoxycytidine kinase (dCK) and incorporate with nucleosides in DNA and RNA, preventing DNA from replicating properly. Cytidine deaminase (CDA) is an enzyme that metabolizes gemcitabine to become an inactive form. When the tumor emerges drug resistance, it is often accompanied by the inactivation of dCK or activation of CDA, leading to gemcitabine degradation or inactivation and eventually causing drug resistance (78, 124, 125). Exosomal miRNA is involved in drug metabolism. In pancreatic adenocarcinoma, tumor associated macrophages secrete exosomes that transferring miR-365 to induce gemcitabine-resistance (79). The specific mechanism is that macrophage-derived exosomes (MDE) transfer miR-365 into pancreatic ductal adenocarcinoma (PDAC) cells. Once miR-365 entered PDAC cells, the concentration of triphosphate-nucleotide (NTP) is increasing. NTP can compete with phosphorylated gemcitabine for DNA incorporation, so that it prevents activation of gemcitabine. Moreover, exosomal miR-365 upregulates the expression of CDA and promotes the inactivation of gemcitabine leading to gemcitabine resistance (79).

Metabolic Reprogramming and TME Acidosis

Energy reprogramming has been accepted as a hallmark of cancer (126). In order to maintain survival, proliferation and dissemination, cancer cells need to reprogram their metabolism to ensure the increasing energy demand (127–129). Mitochondrial oxidative phosphorylation (OXPHOS) and glycolysis are two major metabolic pathways to generate adenosine triphosphate (ATP) to support physiological activities in our daily life. A common characteristic in primary and metastatic cancer is the upregulation of glycolysis (130). Glycolysis usually occurs in an anoxic condition. However, even in aerobic conditions, cancer cells undergo aerobic glycolysis by reprogramming the glucose metabolism and glycolysis is still widespread in TME. This phenomenon is called Warburg Effect. An important reason of this effect is that during glycolysis, glucose is metabolized into pyruvate and lactate. In cancer cells, excessive production of lactate leads to TME acidosis (131). The acidic TME largely contributes to the immunologic escape, because the decrease in extracellular pH leads to the reduction of cytotoxic T- cell function, thus the cancer cells can acquire a strong survival advantage which promotes cancer metastasis, invasion and drug resistance (132–134).

Regulation of glycolysis is one of the ways to inhibit cancer drug resistance (134). The GLUT family is closely related to glucose transport into cells. GLUT1, one of the family members in GLUT, is upregulated in many malignant tumors (135). The upregulation of GLUT1 is associated with mammalian target of rapamycin (mTOR) and the activation of mTOR increases glycolysis and promotes drug resistance (132). The decreased expression of miR-100 is involved in drug resistance in several cancer. mTOR is a target gene of miR-100-5p which binds to the 3′UTR directly and decreases the expression of mTOR and enhances chemo-sensitive of cancer cells. Qin et al. (136) indicated in their study that the expressing of miR-100-5p is not only related to the cell itself, but also to the extracellular microenvironment. Exosome as a messenger for intracellular communication, the concentration of miR-100-5p in exosomes is reflected the content in surrounding microenvironment. The downregulation of miR-100-5p in microenvironment leads to cisplatin resistance in lung cancer cells (136). In addition, TP53INP1 is also a stress protein, which has been indicated to play a tumor suppressive role by regulating metabolic homeostasis (137). Fang et al. showed that CAF derives exosomal miR-106b, which promotes gemcitabine resistance by directly targeting TP53INP1 (138).

DNA Damage Repair

As a target of anticancer drugs, DNA damage induces cancer cell death. Genotoxic agents are designed for damaging DNA or preventing the synthesis of new DNA to inhibit cell proliferation. Genotoxic agents are classified as direct damage, such as cisplatin; and indirect damage, such as topoisomerase inhibitors (24). However, in addition to cell death, DNA damage response (DDR) includes the DNA damage repair (139).

DNA damage repair is originally a way to maintain genomic stability in cells. However, DNA damage repair has also been found to be a resistance mechanism because of the widespread use of genotoxic agents (140). DNA repair mechanisms can be briefly divided into the following four categories: (a) Nucleotide excision repair (NER): NER works in a way that is suitable for repairing bulky DNA lesions by using DNA ligase to attach repair patch to the damage DNA regions, which is associated with platinum agent resistance. (b) Base excision repair (BER): BER works through repairing a small number of bases and performing some modification, such as alkylation and oxidative lesions. This repair mechanism is related to the resistance of genotoxic agents nitrosoureas. (c) Mismatch repair (MMR): MMR participates in the modification of oxidation and methylation by bypassing the lesions to replicate. (d) DNA double-strand break repair: Double-strand break (DSB): DSB is the most toxic form of DNA damage. Two main repair pathways of DSB are non-homologous end joining (NHEJ) and homologous recombination (HR) (139, 141). Briefly, these two repair pathways have their own characteristics. NHEJ is more rapid, while HR is more complex and accurate. This mechanism is applicable to the damage

induced by topoisomerase inhibitors, temozolomide (TMZ) and some alkylating agents (142).

Exosomal miRNA is a regulator to inhibit DNA damage repair. XRCC4 is a major participator of NHEJ, which forms a heterodimer with DNA ligase IV and covalently joins the broken DNA (143). There have been reports of XRCC4 linked to TMZ resistance in earlier years. XRCC4 is a direct target of miR-151a, the low expression of which leads to the upregulation of XRCC4 and triggers the DNA repair that makes cell resistant to TMZ. To investigate the effects of exosomal miR-151a on cancer cells, researchers incubated glioblastoma multiforme (GBM) receptor cells with exosomes secreted by TMZ-resistant cells and TMZ-sensitive cells. The result shows that GBM receptor cells co-cultured with TMZ-resistant exosomes have stronger resistance to TMZ. However, when researchers restore miR-151a in TMZ-resistant exosomes, the TMZ resistance of GBM recipient cells is significantly decreases (144). This study shows that exosomes have the ability to transfer chemoresistance to sensitive cancer cells and exosomal miR-151a has the potential to become a prognostic factor in GBM treatment.

Deregulation of Apoptosis

Resisting cell death is a characteristic of cancers, which leads the unlimited proliferation of cancer cells and the development of drug resistance (145, 146). Drug resistant-cancer cells are often accompanied by downregulation of intracellular apoptotic proteins or up-regulation of anti-apoptotic proteins.

Exosome secreted by drug-resistant cells can transmit the resistance to neighboring cells. Zhang et al. (147) indicated that exosomal miR-214 mediates gefitinib resistance in non-small cell lung cancer (NSCLC). Compared with sensitive cancer cells, the miR-214 in exosomes secreted by gefitinib resistant-cells is significantly increased. Gefitinib resistant-cells secreted exosomal miR-214 could confer gefitinib resistance in NSCLC by suppressing cell apoptosis (147). In addition to cancer cells, exosomes secreted by stroma cells also act on resistant targets by transferring miRNA, making cancer cells to acquire drug resistance. Paclitaxel is a common agent for the treatment of ovarian cancer. However, the efficacy of paclitaxel treatment is greatly reduced if the ovarian cancer cells develop resistance to paclitaxel. By using sequencing technology, Au Yeung et al. (148) identified that miR-21 isomiRNAs have higher expression level in the exosomes of cancer-associated adipocytes (CAAs) and CAFs than in those from ovarian cancer cells. After exosomal miR-21 transship to ovarian cancer cells, miR-21 binds to apoptotic protease activating factor 1 (APAF1) and the expression of APAF1 is downregulated (148). APAF1 combined with cytochrome c (Cyt-c) and dATP to form apoptosomes, increasing caspase-9 and caspase-3, leading to massive mitochondrial damage and finally inducing cell apoptosis (149). Therefore, the decrease of APAF1 has the ability to suppress apoptosis and eventually cause drug resistance in cancer cells. This result showed that in omental tumor microenvironment, cancer cells have a negative effect on neighboring stromal-derived exosomal miR-21 and acquire malignant phenotype, including drug resistance (148). Moreover, exosomal miR-196a derived from CAFs confers cisplatin resistance in head and neck cancer (HNC). In order to explore the mechanism of exosomal miR-196a in HNC cells, Qin et al. (150) used miRecords algorithm and finally found the target of exosomal miR-196a: CDKN1B and ING5. CDKN1B and ING5 exhibit different functions in miR-196a-mediated cisplatin resistance. ING5 gene is a major gene to regulate apoptosis. Therefore, they proposed that exosomal miR-196a promote cisplatin-resistance in HNC cells by suppressing apoptosis of cancer cells (150).

Epithelial-to-Mesenchymal Transition (EMT) and Cancer Stem Cells (CSCs)

In the process of cancer growth, genetic and non-genetic factors induce biological heterogeneity, resulting in phenotypic difference of tumors. The phenotypic diversity of malignant cancers is considered as a significant driver that induces drug resistance.

The cancer stem cells (CSCs) concept provides a good explanation for the association between heterogeneity and the resistance of cancer cells. Because of the renewal properties and genomic instability, CSCs are closely related to the proliferation, metastasis, and recurrence of cancer (151). Epigenetic regulation has a great contribution to the behaviors of cancer cells. Epigenetic differences between CSCs and non-CSCs have a great possibility that caused by epithelial-to-mesenchymal transition (EMT) (152). When epithelial cells transform into mesenchymal cells, cancer cells acquire the properties of migration and invasion and even drug resistance (153–155). What's interesting lies on the study that shows that EMT only occurs in tumors with CSCs (156–158). In tumor microenvironment, CSCs comprise a small proportion of total cells in tumor, most of the cancer cells are non-CSCs (157). However, the traditional cancer treatment merely kills most of the non-CSCs and the CSCs are retained. These residual CSCs eventually induce tumor recurrence and drug resistance through differentiation (159–162).

In recent years, targeting therapy of CSCs by inhibiting EMT has become an effective way to treat cancers and prevent drug resistance (163–167). EMT is an effective target to affect drug resistance. Exosomal miR-32-5p is proved to induce multidrug resistance in hepatocellular carcinoma via the PI3K/AKT pathway to promote EMT and angiogenesis (168). CSCs themselves also secret exosomes to induce drug resistance. MiR-155 is a classic and multifunctional modulating miRNA which is overexpressed in multiple malignant cancers (169). Santos et al. (170) carried out a study which supports a putative mechanism of exosomal miRNA transmission between cancer cells: miR-155 is enriched in exosomes secreted by CSCs and drug resistant cells. In addition, they observed the downregulation of E-Cadherin (E-Cad) and upregulation of mesenchymal biomarkers, which demonstrated that CSCs and drug resistant cells have the ability to trigger the EMT process in recipient cells by transferring exosomal miR-155 and eventually lead to the recipient cells possess resistance (170). In pancreatic cancer cells, the gemcitabine-resistant CSCs can secret miR-210 enriched

TABLE 2 | Summary of common anticancer drugs and exosomal miRNA involved in drug resistance.

Anticancer drug type	Agents	Cancer type	Exosomal miRNA	Resistance mechanism	References
Antimetabolites	5-FU	Hepatocellular Carcinoma	miR-32-5p	Promote angiogenesis and EMT	(168)
	Gemcitabine	Pancreatic Cancer	miR-365	Prevent gemcitabine activation and promote gemcitabine inactivation	(79)
		Non-small Cell Lung Cancer	miR-222-3p	Directly target the promoter of SOCS3 to transfer malignant phenotypic trait	(63)
		Pancreatic Cancer	miR-210	Inhibit GEM-induced cell cycle arrest, antagonize GEM-induced apoptosis, and promote tube formation and cell migration	(171)
		Pancreatic Cancer	miR-155	Suppressing the key gemcitabine-metabolizing enzyme, DCK	(78)
		Pancreatic Cancer	miR-106b	Promote GEM resistance of cancer cells by directly targeting TP53INP1	(138)
Platinum compounds	Cisplatin	Head and Neck Cancer	miR-196a	Exosomal miR-196a derives from CAFs binds novel targets, CDKN1B and ING5, to endow HNC cells with cisplatin resistance	(150)
		Gastric Cancer	miR-21	Suppress cell apoptosis and enhance activation of PI3K/AKT signaling pathway by down-regulation of PTEN	(16)
		Lung Cancer	miR-100-5p	Exosomes confer recipient cells' resistance to cisplatin in an exosomal miR-100-5p-dependent manner with mTOR as its potential target both *in vitro* and *in vivo*	(136)
		Non-small Cell Lung Cancer	miR-425-3p	Exosomal miR-425-3p facilitated autophagic activation in the recipient cells by targeting AKT1, eventually leading to chemoresistance	(172)
	Carboplatin	Breast Cancer	miR-222/223	Exosomal miR-222/223 promote quiescence in a subset of cancer cells and confers drug resistance	(173)
	Oxaliplatin	Colorectal Cancer	miR-128-3p	miR-128-3p suppress EMT and increased intracellular oxaliplatin accumulation	(123)
		Colorectal Cancer	miR-46146	Directly target PDCD10 and induce oxaliplatin chemoresistance	(174)
Topoisomerase inhibitor	Doxorubicin	Gastric Cancer	miR-501	Downregulate BLID, inactivate caspase-9/-3 and phosphorylate Akt	(175)
Microtubule poisons	Paclitaxel	Ovarian Cancer	miR-21	Target APAF1 and confer chemoresistance	(148)
		Ovarian Cancer	miR-1246	Target Cav1/p-gp/M2-type Macrophage Axis	(12)
		Gastric Cancer	miR-155-5p	Induce EMT and chemoresistant phenotypes	(176)
Molecular targets agents	Imatinib	Chronic Myeloid Leukemia	miR-365	Inhibit expression of pro-apoptosis protein in sensitive CML cells	(177)
	Trastuzumab	Breast Cancer	miR-567	Suppress autophagy and reverse chemoresistance by targeting ATG5	(178)
	Gefitinib	Non-small Cell Lung Cancer	miR-214	–	(147)

exosomes. Gemcitabine-resistant CSCs enhance drug resistant by transferring exosomal miR-210 to gemcitabine-sensitive cells (171).

During these years, more and more studies have revealed that different types of cells secrete exosomal miRNA in tumor microenvironment and participate in the process of drug resistance. The drug resistant mechanism of exosomal miRNA on several common anticancer chemotherapeutic agents and molecular targeted agents are summarized in **Table 2**.

CONCLUSIONS

Drug resistance is an eternal topic in cancer treatment. In this article, we discussed the role of exosomal miRNA in different mechanisms of drug resistance. Some of them act as "communicators" and some of them "biomarkers" that facilitate communication between cancer cells with other cancer cells or cancer cells with tumor microenvironment, enriching the knowledge background about the diagnosis of cancer. However, drug resistance in cancer is not caused by only one or several mechanisms, it is the combined action of the intrinsic (such as mutation) and extrinsic (such as drug inactivation) factors. Although progress has been made in suppressing the emergence of drug resistance, there is still a long way to go to eradicate the problem of drug resistance. Nevertheless, the knowledge of exosomal miRNA will provide some clues to help exploring the secret of cancer drug resistance.

AUTHOR CONTRIBUTIONS

QG, QW, and JZ conceived the review. QG, YL, and CS searched the literature and drafted the manuscript. YaY, RA, and HC critically appraised the literature. YiY, HW, and CS edited the manuscript. All authors approved the final version of the manuscript.

FUNDING

This work was supported by National Natural Science Foundation of China (81773888, U1903126 and 81902152), Guangdong Basic and Applied Basic Research Foundation (2020A1515010005, 2020A1515010605), Fund from Guangzhou Institute of Pediatrics/Guangzhou Women and Children's Medical Center (No: IP-2018-012).

REFERENCES

1. Gao D, Jiang L. Exosomes in cancer therapy: a novel experimental strategy. *Am J Cancer Res.* (2018) 8:2165—75.
2. Ha D, Yang N, Nadithe V. Exosomes as therapeutic drug carriers and delivery vehicles across biological membranes: current perspectives and future challenges. *Acta Pharm Sin B.* (2016) 6:287–96. doi: 10.1016/j.apsb.2016.02.001
3. Huang W, Yan Y, Liu Y, Lin M, Ma J, Zhang W, et al. Exosomes with low miR-34c-3p expression promote invasion and migration of non-small cell lung cancer by upregulating integrin α2β1. *Signal Transduct Target Ther.* (2020).
4. Liu F, Bu Z, Zhao F, Xiao D. Increased T-helper 17 cell differentiation mediated by exosome-mediated microRNA-451 redistribution in gastric cancer infiltrated T cells. *Cancer Sci.* (2018) 109:65–73. doi: 10.1111/cas.13429
5. Yousafzai NA, Wang H, Wang Z, Zhu Y, Zhu L, Jin H, et al. Exosome mediated multidrug resistance in cancer. *Am J Cancer Res.* (2018) 8:2210–26.
6. Hessvik NP Llorente A. Current knowledge on exosome biogenesis and release. *Cell Mol Life Sci.* (2018) 75:193–208. doi: 10.1007/s00018-017-2595-9
7. Johnstone RM, Adam M, Hammond JR, Orr L, Turbide C. Vesicle formation during reticulocyte maturation. Association of plasma membrane activities with released vesicles (exosomes). *J Biol Chem.* (1987) 262:9412–20.
8. Harding C, Heuser J, Stahl P. Receptor-mediated endocytosis of transferrin and recycling of the transferrin receptor in rat reticulocytes. *J Cell Biol.* (1983) 97:329–39. doi: 10.1083/jcb.97.2.329
9. Wan Z, Gao X, Dong Y, Zhao Y, Chen X, Yang G, et al. Exosome-mediated cell-cell communication in tumor progression. *Am J Cancer Res.* (2018) 8:1661—73.
10. Bayraktar R, Van Roosbroeck K, Calin GA. Cell-to-cell communication: microRNAs as hormones. *Mol Oncol.* (2017) 11:1673–86. doi: 10.1002/1878-0261.12144
11. Devhare PB, Sasaki R, Shrivastava S, Di Bisceglie AM, Ray R, Ray RB. Exosome-mediated intercellular communication between hepatitis c virus-infected hepatocytes and hepatic stellate cells. *J Virol.* (2017) 91:e02225–16. doi: 10.1128/JVI.00349-17
12. Kanlikilicer P, Bayraktar R, Denizli M, Rashed MH, Ivan C, Aslan B, et al. Exosomal miRNA confers chemo resistance via targeting Cav1/p-gp/M2-type macrophage axis in ovarian cancer. *EBioMed.* (2018) 38:100–12. doi: 10.1016/j.ebiom.2018.11.004
13. Qin Y, Peng Y, Zhao W, Pan J, Ksiezak-Reding H, Cardozo C, et al. Myostatin inhibits osteoblastic differentiation by suppressing osteocyte-derived exosomal microRNA-218: a novel mechanism in muscle-bone communication. *J Biol Chem.* (2017) 292:11021–33. doi: 10.1074/jbc.M116.770941
14. Teng Y, Ren Y, Hu X, Mu J, Samykutty A, Zhuang X, et al. MVP-mediated exosomal sorting of miR-193a promotes colon cancer progression. *Nat Commun.* (2017) 8:14448. doi: 10.1038/ncomms14448
15. Yang F, Ning Z, Ma L, Liu W, Shao C, Shu Y, et al. Exosomal miRNAs and miRNA dysregulation in cancer-associated fibroblasts. *Mol Cancer.* (2017) 16:148. doi: 10.1186/s12943-017-0718-4
16. Zheng P, Chen L, Yuan X, Luo Q, Liu Y, Xie G, et al. Exosomal transfer of tumor-associated macrophage-derived miR-21 confers cisplatin resistance in gastric cancer cells. *J Exp Clin Cancer Res.* (2017) 36:53. doi: 10.1186/s13046-017-0528-y
17. Li Y, Yin Z, Fan J, Zhang S, Yang W. The roles of exosomal miRNAs and lncRNAs in lung diseases. *Signal Transduct Target Ther.* (2019) 4:47. doi: 10.1038/s41392-019-0080-7
18. Achkar NP, Cambiagno DA, Manavella PA. miRNA biogenesis: a dynamic pathway. *Trends Plant Sci.* (2016) 21:1034–44. doi: 10.1016/j.tplants.2016.09.003
19. Lee Y, Ahn C, Han J, Choi H, Kim J, Yim J, et al. The nuclear RNase III Drosha initiates microRNA processing. *Nature.* (2003) 425:415–9. doi: 10.1038/nature01957
20. Ha M, Kim VN. Regulation of microRNA biogenesis. *Nat Rev Mol Cell Biol.* (2014) 15:509–24. doi: 10.1038/nrm3838
21. Bartel DP. microRNAs: genomics, biogenesis, mechanism, and function. *Cell.* (2004) 116:281–97. doi: 10.1016/S0092-8674(04)00045-5
22. Zeng Y, Cullen BR. Sequence requirements for micro RNA processing and function in human cells. *RNA.* (2003) 9:112–23. doi: 10.1261/rna.2780503
23. Zahreddine H, Borden KLB. Mechanisms and insights into drug resistance in cancer. *Front Pharmacol.* (2013) 4:28. doi: 10.3389/fphar.2013.00028
24. Holohan C, Van Schaeybroeck S, Longley DB, Johnston PG. Cancer drug resistance: an evolving paradigm. *Nat Rev Cancer.* (2013) 13:714–26. doi: 10.1038/nrc3599
25. Dagogo-Jack I, Shaw AT. Tumour heterogeneity and resistance to cancer therapies. *Nat Rev Clin Oncol.* (2018) 15:81–94. doi: 10.1038/nrclinonc.2017.166
26. Dhiman N, Kingshott P, Sumer H, Sharma CS, Rath SN. On-chip anticancer drug screening - recent progress in microfluidic platforms to address challenges in chemotherapy. *Biosens Bioelectron.* (2019) 137:236–54. doi: 10.1016/j.bios.2019.02.070
27. Grosselin K, Durand A, Marsolier J, Poitou A, Marangoni E, Nemati F, et al. High-throughput single-cell ChIP-seq identifies heterogeneity of chromatin states in breast cancer. *Nat Genet.* (2019) 51:1060–6. doi: 10.1038/s41588-019-0424-9
28. Gao H, Korn JM, Ferretti S, Monahan JE, Wang Y, Singh M, et al. High-throughput screening using patient-derived tumor xenografts to predict clinical trial drug response. *Nat Med.* (2015) 21:1318–25. doi: 10.1038/nm.3954

29. Kather JN, Charoentong P, Suarez-Carmona M, Herpel E, Klupp F, Ulrich A, et al. High-throughput screening of combinatorial immunotherapies with patient-specific *in silico* models of metastatic colorectal cancer. *Cancer Res Cell Death Dis.* (2018) 78:5155–63. doi: 10.1158/0008-5472.CAN-18-1126
30. Yuan M, Huang L-L, Chen J-H, Wu J, Xu Q. The emerging treatment landscape of targeted therapy in non-small-cell lung cancer. *Signal Transduct Target Ther.* (2019) 4:61. doi: 10.1038/s41392-019-0099-9
31. Vyse S, Huang PH. Targeting EGFR exon 20 insertion mutations in non-small cell lung cancer. *Signal Transduct Target Ther.* (2019) 4:5. doi: 10.1038/s41392-019-0038-9
32. Wu S, Shih J. Management of acquired resistance to EGFR TKI-targeted therapy in advanced non-small cell lung cancer. *Mol Cancer.* (2018) 17:38. doi: 10.1186/s12943-018-0777-1
33. Yang L, Ying S, Hu S, Zhao X, Li M, Chen M, et al. EGFR TKIs impair lysosome-dependent degradation of SQSTM1 to compromise the effectiveness in lung cancer. *Signal Transduct Target Ther.* (2019) 4:25. doi: 10.1038/s41392-019-0059-4
34. Tong CWS, Wu WKK, Loong HHF, Cho WCS, To KKW. Drug combination approach to overcome resistance to EGFR tyrosine kinase inhibitors in lung cancer. *Cancer Lett Cancer Res.* (2017) 405:100–10. doi: 10.1016/j.canlet.2017.07.023
35. Han W, Shi L, Ren L, Zhou L, Li T, Qiao Y, et al. A nanomedicine approach enables co-delivery of cyclosporin A and gefitinib to potentiate the therapeutic efficacy in drug-resistant lung cancer. *Signal Transduct Target Ther.* (2018) 3:16. doi: 10.1038/s41392-018-0019-4
36. Senapati S, Mahanta AK, Kumar S, Maiti P. Controlled drug delivery vehicles for cancer treatment and their performance. *Signal Transduct Target Ther.* (2018) 3:7. doi: 10.1038/s41392-017-0004-3
37. Sun Y, Jiang W, Lu W, Song M, Liu K, Chen P, et al. Identification of cisplatin sensitizers through high-throughput combinatorial screening. *Int J Oncol.* (2018) 53:1237–46. doi: 10.3892/ijo.2018.4447
38. Sharma AK. Emerging trends in biomarker discovery: ease of prognosis and prediction in cancer. *Semin Cancer Biol.* (2018) 52:iii–iv. doi: 10.1016/j.semcancer.2018.05.008
39. Wu L, Qu X. Cancer biomarker detection: recent achievements and challenges. *Chem Soc Rev.* (2015) 44:2963–97. doi: 10.1039/C4CS00370E
40. Bhoola NH, Mbita Z, Hull R, Dlamini Z. Translocator protein (TSPO) as a potential biomarker in human cancers. *Int J Mol Sci.* (2018) 19:2176. doi: 10.3390/ijms19082176
41. Folprecht G. Tumor mutational burden as a new biomarker for PD-1 antibody treatment in gastric cancer. *Cancer Commun.* (2019) 39:74–74. doi: 10.1186/s40880-019-0417-1
42. Han X, Wang J, Sun Y. Circulating tumor DNA as biomarkers for cancer detection. *Genomics Proteomics Bioinformatics.* (2017) 15:59–72. doi: 10.1016/j.gpb.2016.12.004
43. Patel SP, Kurzrock R. PD-L1 expression as a predictive biomarker in cancer immunotherapy. *Mol Cancer Ther.* (2015) 14:847–56. doi: 10.1158/1535-7163.MCT-14-0983
44. Wang H, Peng R, Wang J, Qin Z, Xue L. Circulating microRNAs as potential cancer biomarkers: the advantage and disadvantage. *Clin Epigenet.* (2018) 10:59. doi: 10.1186/s13148-018-0492-1
45. Baroni S, Romero-Cordoba S, Plantamura I, Dugo M, D'Ippolito E, Cataldo A, et al. Exosome-mediated delivery of miR-9 induces cancer-associated fibroblast-like properties in human breast fibroblasts. *Cell Death Dis.* (2016) 7:e2312. doi: 10.1038/cddis.2016.224
46. Ding J, Xu Z, Zhang Y, Tan C, Hu W, Wang M, et al. Exosome-mediated miR-222 transferring: An insight into NF-κB-mediated breast cancer metastasis. *Exp Cell Res.* (2018) 369:129–38. doi: 10.1016/j.yexcr.2018.05.014
47. Yan W, Wu X, Zhou W, Fong MY, Cao M, Liu J, et al. Cancer-cell-secreted exosomal miR-105 promotes tumour growth through the MYC-dependent metabolic reprogramming of stromal cells. *Nat Cell Biol.* (2018) 20:597–609. doi: 10.1038/s41556-018-0083-6
48. Singh R, Pochampally R, Watabe K, Lu Z, Mo Y-Y. Exosome-mediated transfer of miR-10b promotes cell invasion in breast cancer. *Mol Cancer.* (2014) 13:256. doi: 10.1186/1476-4598-13-256
49. Fong MY, Zhou W, Liu L, Alontaga AY, Chandra M, Ashby J, et al. Breast-cancer-secreted miR-122 reprograms glucose metabolism in premetastatic niche to promote metastasis. *Nat Cell Biol.* (2015) 17:183–94. doi: 10.1038/ncb3094
50. Zhai L, Li M, Pan W, Chen Y, Li M, Pang J, et al. *In situ* detection of plasma exosomal microRNA-1246 for breast cancer diagnostics by a Au nanoflare probe. *ACS Appl Mater Interfaces.* (2018) 10:39478–86. doi: 10.1021/acsami.8b12725
51. Zhang Z, Xing T, Chen Y, Xiao J. Exosome-mediated miR-200b promotes colorectal cancer proliferation upon TGF-β1 exposure. *Biomed Pharmacother.* (2018) 106:1135–43. doi: 10.1016/j.biopha.2018.07.042
52. Cheng W, Liao T, Lin C, Yuan LE, Lan H, Lin H, et al. RAB27B-activated secretion of stem-like tumor exosomes delivers the biomarker microRNA-146a-5p, which promotes tumorigenesis and associates with an immunosuppressive tumor microenvironment in colorectal cancer. *Int J Cancer.* (2019) 145:2209–24. doi: 10.1002/ijc.32338
53. Wang J, Yan F, Zhao Q, Zhan F, Wang R, Wang L, et al. Circulating exosomal miR-125a-3p as a novel biomarker for early-stage colon cancer. *Sci Rep.* (2017) 7:4150. doi: 10.1038/s41598-017-04386-1
54. Zeng Z, Li Y, Pan Y, Lan X, Song F, Sun J, et al. Cancer-derived exosomal miR-25-3p promotes pre-metastatic niche formation by inducing vascular permeability and angiogenesis. *Nat Commun.* (2018) 9:5395. doi: 10.1038/s41467-018-07810-w
55. Liu X, Pan B, Sun L, Chen X, Zeng K, Hu X, et al. Circulating exosomal miR-27a and miR-130a act as novel diagnostic and prognostic biomarkers of colorectal cancer. *Cancer Epidemiol Biomark Prev.* (2018) 27:746–54. doi: 10.1158/1055-9965.EPI-18-0067
56. Huang Z, Zhu D, Wu L, He M, Zhou X, Zhang L, et al. Six serum-based miRNAs as potential diagnostic biomarkers for gastric cancer. *Cancer Epidemiol Biomark Prev.* (2017) 26:188–96. doi: 10.1158/1055-9965.EPI-16-0607
57. Xu G, Zhang B, Ye J, Cao S, Shi J, Zhao Y, et al. Exosomal miRNA-139 in cancer-associated fibroblasts inhibits gastric cancer progression by repressing MMP11 expression. *Int J Biol Sci.* (2019) 15:2320–9. doi: 10.7150/ijbs.33750
58. Yang H, Zhang H, Ge S, Ning T, Bai M, Li J, et al. Exosome-Derived miR-130a activates angiogenesis in gastric cancer by targeting C-MYB in vascular endothelial cells. *Mol Ther.* (2018) 26:2466–75. doi: 10.1016/j.ymthe.2018.07.023
59. Yang H, Fu H, Wang B, Zhang X, Mao J, Li X, et al. Exosomal miR-423-5p targets SUFU to promote cancer growth and metastasis and serves as a novel marker for gastric cancer. *Mol Carcinogenesis.* (2018) 57:1223–36. doi: 10.1002/mc.22838
60. Wu H, Zhou J, Mei S, Wu D, Mu Z, Chen B, et al. Circulating exosomal microRNA-96 promotes cell proliferation, migration and drug resistance by targeting LMO7. *J Cell Mol Med.* (2017) 21:1228–36. doi: 10.1111/jcmm.13056
61. Hsu YL, Hung JY, Chang WA, Lin YS, Pan YC, Tsai PH, et al. Hypoxic lung cancer-secreted exosomal miR-23a increased angiogenesis and vascular permeability by targeting prolyl hydroxylase and tight junction protein ZO-1. *Oncogene.* (2017) 36:4929–42. doi: 10.1038/onc.2017.105
62. Grimolizzi F, Monaco F, Leoni F, Bracci M, Staffolani S, Bersaglieri C, et al. Exosomal miR-126 as a circulating biomarker in non-small-cell lung cancer regulating cancer progression. *Sci Rep.* (2017) 7:15277. doi: 10.1038/s41598-017-15475-6
63. Wei F, Ma C, Zhou T, Dong X, Luo Q, Geng L, et al. Exosomes derived from gemcitabine-resistant cells transfer malignant phenotypic traits via delivery of miRNA-222-3p. *Mol Cancer.* (2017) 16:132. doi: 10.1186/s12943-017-0694-8
64. Zhang L, Hao C, Zhai R, Wang D, Zhang J, Bao L, et al. Downregulation of exosomal let-7a-5p in dust exposed- workers contributes to lung cancer development. *Respir Res.* (2018) 19:235. doi: 10.1186/s12931-018-0949-y
65. Yang Y, Liu Q, Lu J, Adah D, Yu S, Zhao S, et al. Exosomes from Plasmodium-infected hosts inhibit tumor angiogenesis in a murine Lewis lung cancer model. *Oncogenesis.* (2017) 6:e351. doi: 10.1038/oncsis.2017.52
66. Sohn W, Kim J, Kang SH, Yang SR, Cho J-Y, Cho HC, et al. Serum exosomal microRNAs as novel biomarkers for hepatocellular carcinoma. *Exp Mol Med.* (2015) 47:e184. doi: 10.1038/emm.2015.68
67. Fang T, Lv H, Lv G, Li T, Wang C, Han Q, et al. Tumor-derived exosomal miR-1247-3p induces cancer-associated fibroblast activation

to foster lung metastasis of liver cancer. *Nat Commun.* (2018) 9:191. doi: 10.1038/s41467-017-02583-0
68. Wang F, Li L, Piontek K, Sakaguchi M, Selaru FM. Exosome miR-335 as a novel therapeutic strategy in hepatocellular carcinoma. *Hepatology.* (2018) 67:940–54. doi: 10.1002/hep.29586
69. Zhang Z, Li X, Sun W, Yue S, Yang J, Li J, et al. Loss of exosomal miR-320a from cancer-associated fibroblasts contributes to HCC proliferation and metastasis. *Cancer Lett.* (2017) 397:33–42. doi: 10.1016/j.canlet.2017.03.004
70. Fang J, Zhang Z, Shang L, Luo Y, Lin Y, Yuan Y, et al. Hepatoma cell-secreted exosomal microRNA-103 increases vascular permeability and promotes metastasis by targeting junction proteins. *Hepatology.* (2018) 68:1459–75. doi: 10.1002/hep.29920
71. Kobayashi M, Salomon C, Tapia J, Illanes SE, Mitchell MD, Rice GE. Ovarian cancer cell invasiveness is associated with discordant exosomal sequestration of Let-7 miRNA and miR-200. *J Transl Med.* (2014) 12:4. doi: 10.1186/1479-5876-12-4
72. Zhou J, Li X, Wu X, Zhang T, Zhu Q, Wang X, et al. Exosomes released from tumor-associated macrophages transfer miRNAs that induce a Treg/Th17 cell imbalance in epithelial ovarian cancer. *Cancer Immunol Res.* (2018) 6:1578–92. doi: 10.1158/2326-6066.CIR-17-0479
73. He L, Zhu W, Chen Q, Yuan Y, Wang Y, Wang J, et al. Ovarian cancer cell-secreted exosomal miR-205 promotes metastasis by inducing angiogenesis. *Theranostics.* (2019) 9:8206–20. doi: 10.7150/thno.37455
74. Kim S, Choi MC, Jeong J-Y, Hwang S, Jung SG, Joo WD, et al. Serum exosomal miRNA-145 and miRNA-200c as promising biomarkers for preoperative diagnosis of ovarian carcinomas. *J Cancer.* (2019) 10:1958–67. doi: 10.7150/jca.30231
75. Chen X, Ying X, Wang X, Wu X, Zhu Q, Wang X. Exosomes derived from hypoxic epithelial ovarian cancer deliver microRNA-940 to induce macrophage M2 polarization. *Oncol Rep.* (2017) 38:522–8. doi: 10.3892/or.2017.5697
76. Kanlikilicer P, Rashed MH, Bayraktar R, Mitra R, Ivan C, Aslan B, et al. Ubiquitous release of exosomal tumor suppressor miR-6126 from ovarian cancer cells. *Cancer Res.* (2016) 76:7194–207. doi: 10.1158/0008-5472.CAN-16-0714
77. Pan C, Stevic I, Müller V, Ni Q, Oliveira-Ferrer L, Pantel K, et al. Exosomal microRNAs as tumor markers in epithelial ovarian cancer. *Mol Oncol.* (2018) 12:1935–48. doi: 10.1002/1878-0261.12371
78. Patel GK, Khan MA, Bhardwaj A, Srivastava SK, Zubair H, Patton MC, et al. Exosomes confer chemoresistance to pancreatic cancer cells by promoting ROS detoxification and miR-155-mediated suppression of key gemcitabine-metabolising enzyme, DCK. *Br J Cancer.* (2017) 116:609–19. doi: 10.1038/bjc.2017.18
79. Binenbaum Y, Fridman E, Yaari Z, Milman N, Schroeder A, Ben David G, et al. Transfer of miRNA in macrophage-derived exosomes induces drug resistance in pancreatic adenocarcinoma. *Cancer Res.* (2018) 78:5287–99. doi: 10.1158/0008-5472.CAN-18-0124
80. Nakamura S, Sadakari Y, Ohtsuka T, Okayama T, Nakashima Y, Gotoh Y, et al. Pancreatic juice exosomal microRNAs as Biomarkers for detection of pancreatic ductal adenocarcinoma. *Ann Surg Oncol.* (2019) 26:2104–11. doi: 10.1245/s10434-019-07269-z
81. Shang S, Wang J, Chen S, Tian R, Zeng H, Wang L, et al. Exosomal miRNA-1231 derived from bone marrow mesenchymal stem cells inhibits the activity of pancreatic cancer. *Cancer Med.* (2019) 8:7728–40. doi: 10.1002/cam4.2633
82. Madhavan B, Yue S, Galli U, Rana S, Gross W, Müller M, et al. Combined evaluation of a panel of protein and miRNA serum-exosome biomarkers for pancreatic cancer diagnosis increases sensitivity and specificity. *Int J Cancer.* (2015) 136:2616–27. doi: 10.1002/ijc.29324
83. Wang X, Luo G, Zhang K, Cao J, Huang C, Jiang T, et al. Hypoxic tumor-derived exosomal miR-301a mediates M2 macrophage polarization via PTEN/PI3Kγ to promote pancreatic cancer metastasis. *Cancer Res.* (2018) 78:4586–98. doi: 10.1158/0008-5472.CAN-17-3841
84. Huang X, Yuan T, Liang M, Du M, Xia S, Dittmar R, et al. Exosomal miR-1290 and miR-375 as prognostic markers in castration-resistant prostate cancer. *Eur Urol.* (2015) 67:33–41. doi: 10.1016/j.eururo.2014.07.035
85. Malla B, Aebersold DM, Dal Pra A. Protocol for serum exosomal miRNAs analysis in prostate cancer patients treated with radiotherapy. *J Transl Med.* (2018) 16:223. doi: 10.1186/s12967-018-1592-6
86. Rodríguez M, Bajo-Santos C, Hessvik NP, Lorenz S, Fromm B, Berge V, et al. Identification of non-invasive miRNAs biomarkers for prostate cancer by deep sequencing analysis of urinary exosomes. *Mol Cancer.* (2017) 16:156. doi: 10.1186/s12943-017-0726-4
87. Bhagirath D, Yang TL, Bucay N, Sekhon K, Majid S, Shahryari V, et al. microRNA-1246 is an exosomal biomarker for aggressive prostate cancer. *Cancer Res.* (2018) 78:1833–44. doi: 10.1158/0008-5472.CAN-17-2069
88. Sun L, Xu K, Cui J, Yuan D, Zou B, Li J, et al. Cancer-associated fibroblast-derived exosomal miR-382-5p promotes the migration and invasion of oral squamous cell carcinoma. *Oncol Rep.* (2019) 42:1319–28. doi: 10.3892/or.2019.7255
89. Sakha S, Muramatsu T, Ueda K, Inazawa J. Exosomal microRNA miR-1246 induces cell motility and invasion through the regulation of DENND2D in oral squamous cell carcinoma. *Sci Rep.* (2016) 6:38750. doi: 10.1038/srep38750
90. Li L, Li C, Wang S, Wang Z, Jiang J, Wang W, et al. Exosomes derived from hypoxic oral squamous cell carcinoma cells deliver miR-21 to normoxic cells to elicit a prometastatic phenotype. *Cancer Res.* (2016) 76:1770–80. doi: 10.1158/0008-5472.CAN-15-1625
91. Li Y, Tao Y, Gao S, Li P, Zheng J, Zhang S, et al. Cancer-associated fibroblasts contribute to oral cancer cells proliferation and metastasis via exosome-mediated paracrine miR-34a-5p. *EBioMedicine.* (2018) 36:209–20. doi: 10.1016/j.ebiom.2018.09.006
92. Bao L, You B, Shi S, Shan Y, Zhang Q, Yue H, et al. Metastasis-associated miR-23a from nasopharyngeal carcinoma-derived exosomes mediates angiogenesis by repressing a novel target gene TSGA10. *Oncogene.* (2018) 37:2873–89. doi: 10.1038/s41388-018-0183-6
93. Ye S, Zhang H, Cai T, Liu Y, Ni J, He J, et al. Exosomal miR-24-3p impedes T-cell function by targeting FGF11 and serves as a potential prognostic biomarker for nasopharyngeal carcinoma. *J Pathol.* (2016) 240:329–40. doi: 10.1002/path.4781
94. Lu J, Liu Q, Wang F, Tan J, Deng Y, Peng X, et al. Exosomal miR-9 inhibits angiogenesis by targeting MDK and regulating PDK/AKT pathway in nasopharyngeal carcinoma. *J Exp Clin Cancer Res.* (2018) 37:147. doi: 10.1186/s13046-018-0814-3
95. Siegel RL, Miller KD, Jemal A. Cancer statistics, 2017. *CA Cancer J Clin.* (2017) 67:7–30. doi: 10.3322/caac.21387
96. Tong CWS, Wu M, Cho WCS, To KKW. Recent advances in the treatment of breast cancer. *Front Oncol.* (2018) 8:227. doi: 10.3389/fonc.2018.00227
97. Li B, Lu W, Qu J, Ye L, Du G, Wan X. Loss of exosomal miR-148b from cancer-associated fibroblasts promotes endometrial cancer cell invasion and cancer metastasis. *J Cell Physiol.* (2019) 234:2943–53. doi: 10.1002/jcp.27111
98. Fletcher JI, Williams RT, Henderson MJ, Norris MD, Haber M. ABC transporters as mediators of drug resistance and contributors to cancer cell biology. *Drug Resist Updat.* (2016) 26:1–9. doi: 10.1016/j.drup.2016.03.001
99. Alsop K, Fereday S, Meldrum C, deFazio A, Emmanuel C, George J, et al. BRCA mutation frequency and patterns of treatment response in BRCA mutation-positive women with ovarian cancer: a report from the Australian Ovarian Cancer Study Group. *J Clin Oncol.* (2012) 30:2654–63. doi: 10.1200/JCO.2011.39.8545
100. Cardona AF, Arrieta O, Zapata MI, Rojas L, Wills B, Reguart N, et al. Acquired resistance to Erlotinib in EGFR mutation-positive lung adenocarcinoma among hispanics (CLICaP). *Target Oncol.* (2017) 12:513–23. doi: 10.1007/s11523-017-0497-2
101. Mazerska Z, Mróz A, Pawłowska M, Augustin E. The role of glucuronidation in drug resistance. *Pharmacol Ther.* (2016) 159:35–55. doi: 10.1016/j.pharmthera.2016.01.009
102. Nientiedt C, Heller M, Endris V, Volckmar A-L, Zschäbitz S, Tapia-Laliena MA, et al. Mutations in BRCA2 and taxane resistance in prostate cancer. *Sci Rep.* (2017) 7:4574. doi: 10.1038/s41598-017-04897-x
103. Sakai W, Swisher EM, Karlan BY, Agarwal MK, Higgins J, Friedman C, et al. Secondary mutations as a mechanism of cisplatin resistance in BRCA2-mutated cancers. *Nature.* (2008) 451:1116–20. doi: 10.1038/nature06633
104. Leon G, MacDonagh L, Finn SP, Cuffe S, Barr MP. Cancer stem cells in drug resistant lung cancer: targeting cell surface markers and signaling pathways. *Pharmacol Ther.* (2016) 158:71–90. doi: 10.1016/j.pharmthera.2015.12.001
105. Lytle NK, Barber AG, Reya T. Stem cell fate in cancer growth, progression and therapy resistance. *Nat*

Rev Cancer. (2018) 18:669–80. doi: 10.1038/s41568-018-0056-x
106. Fumarola C, Bonelli MA, Petronini PG, Alfieri RR. Targeting PI3K/AKT/mTOR pathway in non small cell lung cancer. *Biochem Pharmacol*. (2014) 90:197–207. doi: 10.1016/j.bcp.2014.05.011
107. Li L, Han R, Xiao H, Lin C, Wang Y, Liu H, et al. Metformin sensitizes EGFR-TKI-resistant human lung cancer cells *in vitro* and *in vivo* through inhibition of IL-6 signaling and EMT reversal. *Clin Cancer Res*. (2014) 20:2714–26. doi: 10.1158/1078-0432.CCR-13-2613
108. Mitchell R, Hopcroft LEM, Baquero P, Allan EK, Hewit K, James D, et al. Targeting BCR-ABL-independent TKI resistance in chronic myeloid leukemia by mTOR and autophagy inhibition. *J Natl Cancer Inst*. (2018) 110:467–78. doi: 10.1093/jnci/djx236
109. Rodrik-Outmezguine VS, Okaniwa M, Yao Z, Novotny CJ, McWhirter C, Banaji A, et al. Overcoming mTOR resistance mutations with a new-generation mTOR inhibitor. *Nature*. (2016) 534:272–6. doi: 10.1038/nature17963
110. Wang L, Dong X, Ren Y, Luo J, Liu P, Su D, et al. Targeting EHMT2 reverses EGFR-TKI resistance in NSCLC by epigenetically regulating the PTEN/AKT signaling pathway. *Cell Death Dis*. (2018) 9:129. doi: 10.1038/s41419-017-0120-6
111. Xiao B, Zhang M, Viennois E, Zhang Y, Wei N, Baker MT, et al. Inhibition of MDR1 gene expression and enhancing cellular uptake for effective colon cancer treatment using dual-surface-functionalized nanoparticles. *Biomaterials*. (2015) 48:147–60. doi: 10.1016/j.biomaterials.2015.01.014
112. Zhang S, Anjum R, Squillace R, Nadworny S, Zhou T, Keats J, et al. The Potent ALK inhibitor Brigatinib (AP26113) overcomes mechanisms of resistance to first- and second-generation ALK inhibitors in preclinical models. *Clin Cancer Res*. (2016) 22:5527–38. doi: 10.1158/1078-0432.CCR-16-0569
113. Chen L, Manautou JE, Rasmussen TP, Zhong X-B. Development of precision medicine approaches based on inter-individual variability of BCRP/ABCG2. *Acta Pharm Sin B*. (2019) 9:659–74. doi: 10.1016/j.apsb.2019.01.007
114. Chen Z, Shi T, Zhang L, Zhu P, Deng M, Huang C, et al. Mammalian drug efflux transporters of the ATP binding cassette (ABC) family in multidrug resistance: A review of the past decade. *Cancer Lett*. (2016) 370:153–64. doi: 10.1016/j.canlet.2015.10.010
115. Valinezhad Sani F, Palizban A, Mosaffa F, Jamialahmadi K. Glucosamine reverses drug resistance in MRP2 overexpressing ovarian cancer cells. *Eur J Pharmacol*. (2020) 868:172883. doi: 10.1016/j.ejphar.2019.172883
116. Toyoda Y, Takada T, Suzuki H. Inhibitors of human ABCG2: from technical background to recent updates with clinical implications. *Front Pharmacol*. (2019) 10:208. doi: 10.3389/fphar.2019.00208
117. Reid G, Wielinga P, Zelcer N, De Haas M, Van Deemter L, Wijnholds J, et al. Characterization of the transport of nucleoside analog drugs by the human multidrug resistance proteins MRP4 and MRP5. *Mol Pharmacol*. (2003) 63:1094–103. doi: 10.1124/mol.63.5.1094
118. Němcová-Fürstová V, Kopperová D, Balušíková K, Ehrlichová M, Brynychová V, Václavíková R, et al. Characterization of acquired paclitaxel resistance of breast cancer cells and involvement of ABC transporters. *Toxicol Appl Pharmacol*. (2016) 310:215–28. doi: 10.1016/j.taap.2016.09.020
119. Lopes-Rodrigues V, Seca H, Sousa D, Sousa E, Lima RT, Vasconcelos MH. The network of P-glycoprotein and microRNAs interactions. *Int J Cancer*. (2014) 135:253–63. doi: 10.1002/ijc.28500
120. Levchenko A, Mehta BM, Niu X, Kang G, Villafania L, Way D, et al. Intercellular transfer of P-glycoprotein mediates acquired multidrug resistance in tumor cells. *Proc Natl Acad Sci USA*. (2005) 102:1933–8. doi: 10.1073/pnas.0401851102
121. Sousa D, Lima RT, Vasconcelos MH. Intercellular transfer of cancer drug resistance traits by extracellular vesicles. *Trends Mol Med*. (2015) 21:595–608. doi: 10.1016/j.molmed.2015.08.002
122. Bebawy M, Combes V, Lee E, Jaiswal R, Gong J, Bonhoure A, et al. Membrane microparticles mediate transfer of P-glycoprotein to drug sensitive cancer cells. *Leukemia*. (2009) 23:1643–9. doi: 10.1038/leu.2009.76
123. Liu T, Zhang X, Du L, Wang Y, Liu X, Tian H, et al. Exosome-transmitted miR-128-3p increase chemosensitivity of oxaliplatin-resistant colorectal cancer. *Mol Cancer*. (2019) 18:43. doi: 10.1186/s12943-019-0981-7
124. Gebregiworgis T, Bhinderwala F, Purohit V, Chaika NV, Singh PK, Powers R. Insights into gemcitabine resistance and the potential for therapeutic monitoring. *Metabolomics*. (2018) 14:156. doi: 10.1007/s11306-018-1452-7
125. Nakano Y, Tanno S, Koizumi K, Nishikawa T, Nakamura K, Minoguchi M, et al. Gemcitabine chemoresistance and molecular markers associated with gemcitabine transport and metabolism in human pancreatic cancer cells. *Br J Cancer*. (2007) 96:457–63. doi: 10.1038/sj.bjc.6603559
126. Hanahan D Weinberg RA. Hallmarks of cancer: the next generation. *Cell*. (2011) 144:646–74. doi: 10.1016/j.cell.2011.02.013
127. Sancho P, Barneda D, Heeschen C. Hallmarks of cancer stem cell metabolism. *Br J Cancer*. (2016) 114:1305–12. doi: 10.1038/bjc.2016.152
128. Yang Z, Cappello T, Wang L. Emerging role of microRNAs in lipid metabolism. *Acta Pharm Sin B*. (2015) 5:145–50. doi: 10.1016/j.apsb.2015.01.002
129. Yoshida GJ. Metabolic reprogramming: the emerging concept and associated therapeutic strategies. *J Exp Clin Cancer Res*. (2015) 34:111. doi: 10.1186/s13046-015-0221-y
130. Gatenby RA Gillies RJ. Why do cancers have high aerobic glycolysis? *Nat Rev Cancer*. (2004) 4:891–9. doi: 10.1038/nrc1478
131. Hirschhaeuser F, Sattler UGA, Mueller-Klieser W. Lactate: a metabolic key player in cancer. *Cancer Res*. (2011) 71:6921–5. doi: 10.1158/0008-5472.CAN-11-1457
132. Bhattacharya B, Low SHH, Soh C, Kamal Mustapa N, Beloueche-Babari M, Koh KX, et al. Increased drug resistance is associated with reduced glucose levels and an enhanced glycolysis phenotype. *Br J Pharmacol*. (2014) 171:3255–67. doi: 10.1111/bph.12668
133. Fischer K, Hoffmann P, Voelkl S, Meidenbauer N, Ammer J, Edinger M, et al. Inhibitory effect of tumor cell-derived lactic acid on human T cells. *Blood*. (2007) 109:3812–9. doi: 10.1182/blood-2006-07-035972
134. Morandi A Indraccolo S. Linking metabolic reprogramming to therapy resistance in cancer. *Biochim Biophys Acta Rev Cancer*. (2017) 1868:1–6. doi: 10.1016/j.bbcan.2016.12.004
135. Guo Q, Li C, Zhou W, Chen X, Zhang Y, Lu Y, et al. GLUT1-mediated effective anti-miRNA21 pompon for cancer therapy. *Acta Pharm Sin B*. (2019) 9:832–42. doi: 10.1016/j.apsb.2019.01.012
136. Qin X, Yu S, Zhou L, Shi M, Hu Y, Xu X, et al. Cisplatin-resistant lung cancer cell-derived exosomes increase cisplatin resistance of recipient cells in exosomal miR-100-5p-dependent manner. *Int J Nanomed*. (2017) 12:3721–33. doi: 10.2147/IJN.S131516
137. Saadi H, Seillier M, Carrier A. The stress protein TP53INP1 plays a tumor suppressive role by regulating metabolic homeostasis. *Biochimie*. (2015) 118:44–50. doi: 10.1016/j.biochi.2015.07.024
138. Fang Y, Zhou W, Rong Y, Kuang T, Xu X, Wu W, et al. Exosomal miRNA-106b from cancer-associated fibroblast promotes gemcitabine resistance in pancreatic cancer. *Exp Cell Res*. (2019) 383:111543. doi: 10.1016/j.yexcr.2019.111543
139. Goldstein M Kastan MB. The DNA damage response: implications for tumor responses to radiation and chemotherapy. *Ann Rev Med*. (2015) 66:129–43. doi: 10.1146/annurev-med-081313-121208
140. Jackson SP Bartek J. The DNA-damage response in human biology and disease. *Nature*. (2009) 461:1071–8. doi: 10.1038/nature08467
141. Hnízda A Blundell TL. Multicomponent assemblies in DNA-double-strand break repair by NHEJ. *Curr Opin Struct Biol*. (2019) 55:154–60. doi: 10.1016/j.sbi.2019.03.026
142. Salehan MR Morse HR. DNA damage repair and tolerance: a role in chemotherapeutic drug resistance. *Br J Biomed Sci*. (2013) 70:31–40. doi: 10.1080/09674845.2013.11669927
143. Kang Y Yan CT. Regulation of DNA repair in the absence of classical non-homologous end joining. *DNA Repair*. (2018) 68:34–40. doi: 10.1016/j.dnarep.2018.06.001
144. Zeng A, Wei Z, Yan W, Yin J, Huang X, Zhou X, et al. Exosomal transfer of miR-151a enhances chemosensitivity to temozolomide in drug-resistant glioblastoma. *Cancer Lett*. (2018) 436:10–21. doi: 10.1016/j.canlet.2018.08.004
145. Lin M, Tang S, Zhang C, Chen H, Huang W, Liu Y, et al. Euphorbia factor L2 induces apoptosis in A549 cells through the mitochondrial pathway. *Acta Pharm Sin B*. (2017) 7:59–64. doi: 10.1016/j.apsb.2016.06.008

146. Pistritto G, Trisciuoglio D, Ceci C, Garufi A, D'Orazi G. Apoptosis as anticancer mechanism: function and dysfunction of its modulators and targeted therapeutic strategies. *Aging.* (2016) 8:603–19. doi: 10.18632/aging.100934
147. Zhang Y, Li M, Hu C. Exosomal transfer of miR-214 mediates gefitinib resistance in non-small cell lung cancer. *Biochem Biophys Res Commun.* (2018) 507:457–64. doi: 10.1016/j.bbrc.2018.11.061
148. Au Yeung CL, Co N-N, Tsuruga T, Yeung T-L, Kwan S-Y, Leung CS, et al. Exosomal transfer of stroma-derived miR21 confers paclitaxel resistance in ovarian cancer cells through targeting APAF1. *Nat Commun.* (2016) 7:11150. doi: 10.1038/ncomms11150
149. Gortat A, Sancho M, Mondragón L, Messeguer À, Pérez-Payá E, Orzáez M. Apaf1 inhibition promotes cell recovery from apoptosis. *Protein Cell.* (2015) 6:833–43. doi: 10.1007/s13238-015-0200-2
150. Qin X, Guo H, Wang X, Zhu X, Yan M, Wang X, et al. Exosomal miR-196a derived from cancer-associated fibroblasts confers cisplatin resistance in head and neck cancer through targeting CDKN1B and ING5. *Genome Biol.* (2019) 20:12. doi: 10.1186/s13059-018-1604-0
151. Dawson MA Kouzarides T. Cancer epigenetics: from mechanism to therapy. *Cell.* (2012) 150:12–27. doi: 10.1016/j.cell.2012.06.013
152. Polyak K Weinberg RA. Transitions between epithelial and mesenchymal states: acquisition of malignant and stem cell traits. *Nat Rev Cancer.* (2009) 9:265–73. doi: 10.1038/nrc2620
153. Aiello NM, Maddipati R, Norgard RJ, Balli D, Li J, Yuan S, et al. EMT subtype influences epithelial plasticity and mode of cell migration. *Dev Cell.* (2018) 45:681–95.e4. doi: 10.1016/j.devcel.2018.05.027
154. Pearson G W. Control of invasion by epithelial-to-mesenchymal transition programs during metastasis. *J Clin Med.* (2019) 8:646. doi: 10.3390/jcm8050646
155. Wang J, Zhang Z, Li R, Mao F, Sun W, Chen J, et al. ADAM12 induces EMT and promotes cell migration, invasion and proliferation in pituitary adenomas via EGFR/ERK signaling pathway. *Biomed Pharmacother.* (2018) 97:1066–77. doi: 10.1016/j.biopha.2017.11.034
156. Chen L, Li Y, Wu L, Yu G, Zhang W, Huang C, et al. TRAF6 regulates tumour metastasis through EMT and CSC phenotypes in head and neck squamous cell carcinoma. *J Cell Mol Med.* (2018) 22:1337–49. doi: 10.1111/jcmm.13439
157. Shibue T Weinberg RA. EMT, CSCs, drug resistance: the mechanistic link and clinical implications. *Nat Rev Clin Oncol.* (2017) 14:611–29. doi: 10.1038/nrclinonc.2017.44
158. Xu M, Wang S, Wang Y, Wu H, Frank JA, Zhang Z, et al. Role of p38γ MAPK in regulation of EMT and cancer stem cells. *Biochim Biophys Acta Mol Basis Dis.* (2018) 1864:3605–17. doi: 10.1016/j.bbadis.2018.08.024
159. Eyler CE Rich JN. Survival of the fittest: cancer stem cells in therapeutic resistance and angiogenesis. *J Clin Oncol.* (2008) 26:2839–45. doi: 10.1200/JCO.2007.15.1829
160. Heng WS, Gosens R, Kruyt FAE. Lung cancer stem cells: origin, features, maintenance mechanisms and therapeutic targeting. *Biochem Pharmacol.* (2019) 160:121–33. doi: 10.1016/j.bcp.2018.12.010
161. Steinbichler TB, Dudás J, Skvortsov S, Ganswindt U, Riechelmann H, Skvortsova I-I. Therapy resistance mediated by cancer stem cells. *Semin Cancer Biol.* (2018) 53:156–67. doi: 10.1016/j.semcancer.2018.11.006
162. Vander Linden C Corbet C. Therapeutic targeting of cancer stem cells: integrating and exploiting the acidic niche. *Front Oncol.* (2019) 9:159. doi: 10.3389/fonc.2019.00159
163. Bekaii-Saab T El-Rayes B. Identifying and targeting cancer stem cells in the treatment of gastric cancer. *Cancer.* (2017) 123:1303–12. doi: 10.1002/cncr.30538
164. Ghasemi F, Sarabi PZ, Athari SS, Esmaeilzadeh A. Therapeutics strategies against cancer stem cell in breast cancer. *Int J Biochem Cell Biol.* (2019) 109:76–81. doi: 10.1016/j.biocel.2019.01.015
165. Rosa R, D'Amato V, De Placido S, Bianco R. Approaches for targeting cancer stem cells drug resistance. *Exp Opin Drug Discov.* (2016) 11:1201–12. doi: 10.1080/17460441.2016.1243525
166. Talukdar S, Emdad L, Das SK, Sarkar D, Fisher PB. Evolving strategies for therapeutically targeting cancer stem cells. *Adv Cancer Res.* (2016) 131:159–91. doi: 10.1016/bs.acr.2016.04.003
167. Teeuwssen M, Fodde R. Wnt signaling in ovarian cancer stemness, EMT, and therapy resistance. *J Clin Med.* (2019) 8:1658. doi: 10.3390/jcm8101658
168. Fu X, Liu M, Qu S, Ma J, Zhang Y, Shi T, et al. Exosomal microRNA-32-5p induces multidrug resistance in hepatocellular carcinoma via the PI3K/Akt pathway. *J Exp Clin Cancer Res.* (2018) 37:52–52. doi: 10.1186/s13046-018-0677-7
169. Bayraktar R, Van Roosbroeck K. miR-155 in cancer drug resistance and as target for miRNA-based therapeutics. *Cancer Metastasis Rev.* (2018) 37:33–44. doi: 10.1007/s10555-017-9724-7
170. Santos JC, Lima N d S, Sarian LO, Matheu A, Ribeiro ML, Derchain SFM. Exosome-mediated breast cancer chemoresistance via miR-155 transfer. *Sci Rep.* (2018) 8:829–9. doi: 10.1038/s41598-018-19339-5
171. Yang Z, Zhao N, Cui J, Wu H, Xiong J, Peng T. Exosomes derived from cancer stem cells of gemcitabine-resistant pancreatic cancer cells enhance drug resistance by delivering miR-210. *Cell Oncol.* (2019) 43:123–36. doi: 10.1007/s13402-019-00476-6
172. Ma Y, Yuwen D, Chen J, Zheng B, Gao J, Fan M, et al. Exosomal transfer of cisplatin-induced miR-425-3p confers cisplatin resistance in NSCLC through activating autophagy. *Int J Nanomed.* (2019) 14:8121–32. doi: 10.2147/IJN.S221383
173. Bliss SA, Sinha G, Sandiford OA, Williams LM, Engelberth DJ, Guiro K, et al. Mesenchymal stem cell-derived exosomes stimulate cycling quiescence and early breast cancer dormancy in bone marrow. *Cancer Res.* (2016) 76:5832–44. doi: 10.1158/0008-5472.CAN-16-1092
174. Xu Y, Zhu M. Novel exosomal miR-46146 transfer oxaliplatin chemoresistance in colorectal cancer. *Clin Transl Oncol.* (2019). doi: 10.1007/s12094-019-02237-1. [Epub ahead of print].
175. Liu X, Lu Y, Xu Y, Hou S, Huang J, Wang B, et al. Exosomal transfer of miR-501 confers doxorubicin resistance and tumorigenesis via targeting of BLID in gastric cancer. *Cancer Lett.* (2019) 459:122–34. doi: 10.1016/j.canlet.2019.05.035
176. Wang M, Qiu R, Yu S, Xu X, Li G, Gu R, et al. Paclitaxel-resistant gastric cancer MGC-803 cells promote epithelial-to-mesenchymal transition and chemoresistance in paclitaxel-sensitive cells via exosomal delivery of miR-155-5p. *Int J Oncol.* (2019) 54:326–38. doi: 10.3892/ijo.2018.4601
177. Min Q, Wang X, Zhang J, Chen Q, Li S, Liu X, et al. Exosomes derived from imatinib-resistant chronic myeloid leukemia cells mediate a horizontal transfer of drug-resistant trait by delivering miR-365. *Exp Cell Res.* (2018) 362:386–93. doi: 10.1016/j.yexcr.2017.12.001
178. Han M, Hu J, Lu P, Cao H, Yu C, Li X, et al. Exosome-transmitted miR-567 reverses trastuzumab resistance by inhibiting ATG5 in breast cancer. *Cell Death Dis.* (2020) 11:43. doi: 10.1038/s41419-020-2250-5

Conflict of Interest: The authors declare that the research was conducted in the absence of any commercial or financial relationships that could be construed as a potential conflict of interest.

frontiers in Oncology

ORIGINAL RESEARCH
published: 07 April 2020
doi: 10.3389/fonc.2020.00466

Circulating Tumor DNA Is Capable of Monitoring the Therapeutic Response and Resistance in Advanced Colorectal Cancer Patients Undergoing Combined Target and Chemotherapy

Hua Cao[1†], Xinyi Liu[2†], Yixin Chen[1], Pan Yang[2], Tanxiao Huang[2], Lele Song[2†] and Ruilian Xu[1]*

[1] Department of Oncology, Shenzhen People's Hospital, The 2nd Clinical Medical School of Ji'nan University, The First Affiliated Hospital of Southern University of Science and Technology, Shenzhen, China, [2] HaploX Biotechnology, Co., Ltd., Shenzhen, China

OPEN ACCESS

Edited by:
Dong-Hua Yang,
St. John's University, United States

Reviewed by:
Jigang Wang,
China Academy of Chinese Medical Sciences, China
Francesco Grignani,
University of Perugia, Italy

***Correspondence:**
Ruilian Xu
xuruilian@126.com

[†] These authors have contributed equally to this work

Specialty section:
This article was submitted to Molecular and Cellular Oncology, a section of the journal Frontiers in Oncology

Received: 30 November 2019
Accepted: 16 March 2020
Published: 07 April 2020

Citation:
Cao H, Liu X, Chen Y, Yang P, Huang T, Song L and Xu R (2020) Circulating Tumor DNA Is Capable of Monitoring the Therapeutic Response and Resistance in Advanced Colorectal Cancer Patients Undergoing Combined Target and Chemotherapy. Front. Oncol. 10:466. doi: 10.3389/fonc.2020.00466

Colorectal cancer (CRC) is a highly lethal disease worldwide. The majority of patients receiving targeted therapy or chemotherapy develop drug resistance, while its molecular mechanism remains to be elucidated. The plasma circulating tumor DNA (ctDNA) exhibited the potential in identifying gene variations and monitoring drug resistance in CRC treatment. In this study, we monitored the ctDNA mutational changes in advanced CRC patients underwent first-line therapy with bevacizumab and cetuximab combined with chemotherapy. The mutation spectrum of 43 patients was established by a 605-gene next-generation sequencing (NGS) panel. The baseline measurement shows that genes with the highest mutation frequency were TP53 (74%), APC (58%), KRAS (40%), SYNE1 (33%), LRP1B (23%), TOP1 (23%), and PIK3CA (21%). Mutations in TP53, APC, and KRAS were detected in 29 paired plasma and tissue samples with the consistency of 81, 67, and 42%, respectively. Clinically targetable gene mutations, such as APC, RNF43, SMAD4, BRAD1, KRAS, RAF1, and TP53, were also identified in ctDNA. The overall consistency between ctDNA and tissue samples was 54.6%. Alleviation of mutational burden in BRAF, KRAS, AMER1, and other major driving genes was observed following the first-line therapy. Patients with KRAS and TP53 mutations in tissues appeared to benefit more than the wild-type counterpart. The dynamic change of plasma mutation status was consistent with the tissue tumor burden and was closely correlated with disease progression. In conclusion, ctDNA monitoring is a useful method for molecular genotyping of colorectal cancer patients. Dynamic changes in resistance can be sensitively monitored by gene variation status, which potentially helps to develop treatment strategy.

Keywords: colorectal cancer, ctDNA, NGS, sequencing, bevacizumab, cetuximab, monitoring, resistance

INTRODUCTION

Colorectal cancer is one of the most common malignant tumors worldwide, responsible for the second and fourth highest mortality among men and women, respectively (1, 2). Standard therapies, including chemotherapy, radiotherapy, targeted therapy, and surgery, are frequently used for colorectal cancer treatment. However, tumor cells can evolve under the pressure of treatment selectivity. Therefore, elucidating the genetic alterations that may potentially drive tumor cell resilience is crucial to advance the knowledge in cancer therapy (2).

Liquid biopsy has been widely recognized as a real time monitoring method to detect tumor-related genetic alterations (3). In fact, liquid biopsy has been largely used to analyze circulating tumor DNA (ctDNA), circulating tumor cells (CTC) and exosomes isolated from peripheral blood. This method can potentially recognize, at the genomic level, tumors associated with lower invasiveness (4). CTC, exosomes, and ctDNAs are widely used in clinical diagnosis and in treatment monitoring, however, there are still some limitations that deserve improvement. Among these three types of biological materials, ctDNA has unique advantage in monitoring the tumor genotype with the development of next generation sequencing (NGS). It is recognized as a method to reveal tumor genome information and can be used to discover cancer evolution and clonal heterogeneity. Therefore, it can be used as a tumor biomarker to evaluate treatment efficiency and drug resistance (5–9).

The NGS technology has been used to monitor changes on ctDNA levels in peripheral blood and in the dynamic change of drug-resistant genes, therefore allowing the selection of novel therapeutic approaches and drug strategies. Due to its effectiveness and fast accessibility, NGS has been widely used in liquid biopsies to analyze genomic alterations in the peripheral blood of cancer patients. In the present study, we used an established sequencing workflow to detect genomic alterations in tumor tissues and peripheral blood from CRC patients who have received first-line therapy with bevacizumab and cetuximab combined with chemotherapy. The NGS panel containing 605 tumor-associated genes was used to detect the main driver gene mutations, resistance-related mutations, and to track dynamic changes of tumor ctDNA during treatment. Our observation suggests that it is vital to identify CRC patients with drug resistance during treatment and adapt the treatment strategy accordingly.

METHODS AND MATERIALS

Patients and Samples

A prospective cohort study was designed and implemented in the Shenzhen People's Hospital (Shenzhen, China). Blood samples and intestinal tumor tissues were collected at the Shenzhen People's Hospital. This research was approved by the Shenzhen People's Hospital Ethics Committee and conducted in accordance with its guiding principles. All patients received written informed consent for the use of clinical samples. Patient information was kept anonymous for confidentiality. The main inclusion criteria include adults over 18 years old and those have complete clinicopathological information and confirmed diagnosis of CRC by imaging examination (including endoscopy, ultrasound, MRI, CT, etc.) and/or subsequent pathological examination. Subjects were included for those who have the indications for adjuvant chemotherapy, neoadjuvant chemotherapy, or chemotherapy combined with target therapy (target therapy includes but is not limited to cetuximab, apatinib, bevacizumab, and trastuzumab) based on current condition. Patients were also included for those with blood samples and/or tissue samples available before the start of the current therapy, and those who can be followed up and agree to provide the subsequent blood samples during and after therapy. The main exclusion criteria include pregnant woman, and those who have history of cancers other than CRC, or history of therapy on other cancers. Subjects were excluded for those with no blood and/or tissue samples available before the start of therapy or those not available for follow-up or cannot provide blood samples during and after therapy. Patients with incomplete information were also excluded. As a result, a cohort of 41 patients with advanced CRC (excluding two patients with stage I CRC), treated with cetuximab, apatinib, bevacizumab, trastuzumab, neoadjuvant, adjuvant chemotherapy, or any combination, was enrolled into the study. Tissue samples were prepared from formalin-fixed and paraffin-embedded (FFPE) samples and 10 ml peripheral blood samples were collected with anticoagulant tubes. The patient clinical information related to each sample is shown in **Table 1**. Progression free survival (PFS) was used to assess the effectiveness of therapy.

DNA Extraction and Quantification

For the FFPE samples, ten 5 μm tumor slices were used for DNA extraction using the QIAamp DNA FFPE Kit (QIAGEN, Valencia, CA, USA) following the manufacturer's instructions. DNA from fresh tissue samples was extracted using the EasyPure® Genomic DNA Kit (Beijing TransGen Biotech, Beijing, China). Blood samples from patients were collected in Ethylene Diamine Tetraacetic Acid (EDTA) tubes and centrifuged at 1,600 g for 10 min and at 4°C. The supernatants were further centrifuged at 10,000 × g for 10 min at 4°C, and plasma was harvested and stored at −80°C until further use. ctDNA was extracted from 3 to 3.5 ml plasma using the QIAamp Circulating Nucleic Acid kit (Qiagen, Inc., Valencia, CA, USA) according to the manufacturers' instructions. Blood cell fragments (including peripheral blood lymphocytes and red cells) were preserved at −20°C for further study. We applied the RelaxGene blood DNA system (Tiangen Biotech) to extract genomic DNA from peripheral blood lymphocytes (PBLs) as the normal control for mutation calling from cancer tissues and ctDNA. The quality control of the DNA was achieved using Qubit 2.0 (Thermo Fisher Scientific), in accordance with manufacturer's instructions.

Library Construction and Sequencing

DNA from blood samples was cleaved using a double-stranded DNA Fragmentase (Roche Sequencing and Life Science, Indianapolis, IL 46250, USA). The construction of the ctDNA library was performed using a KAPA Library preparation kit

TABLE 1 | Demographic and clinical characteristics of study participants.

Characteristics	Patients
Age, year, median (range)	43 (25–84)
Sex, *n* (%)	
Male	31 (72.1%)
Female	12 (27.9%)
Anatomical position of primary lesion, *n* (%)	
Transverse colon	1 (2.33%)
Cecum	1 (2.33%)
Sigmoid colon	10 (23.26%)
Left colon	5 (11.63%)
Right colon	9 (20.93%)
Rectum	15 (34.88%)
The junction of rectum and sigmoid colon	2 (4.65%)
Stage, *n* (%)	
1	2 (4.65%)
3A	2 (4.65%)
3B	3 (6.98%)
3C	1 (2.33%)
4	35 (81.4%)
Resection of primary tumor, *n* (%)	
Yes	27 (62.79%)
No	16 (37.21%)
Metastatic site, *n* (%)	
Lung	6 (13.95%)
Liver	11 (25.58%)
Lymph gland	7 (16.28%)
Peritoneum	3 (6.98%)
Multi-organ	8 (18.6%)
Others	2 (4.65%)
None	6 (13.95%)
Treatment line at the time of baseline sampling, *n* (%)	
1st line	5 (11.63%)
2nd line	2 (4.65%)
3rd line	2 (4.65%)
Adjuvant chemotherapy	2 (4.65%)
Neoadjuvant chemotherapy	8 (18.6%)
None	24 (55.81%)
Baseline sample, *n* (%)	
Blood	4 (9.3%)
Tissue	20 (46.51%)
Tissue+blood	19 (44.19%)
Number of blood samples at monitoring points, *n* (%)	
0	24 (55.81%)
1	12 (27.91%)
2	6 (13.95%)
4	1 (2.33%)
RAS status in tissue, *n* (%)	
Wild	26 (60.47%)
Mut	17 (39.53%)

(KAPA Biosystems, Wilmington, MA 01887, USA). Sequencing was performed to an average depth of 5,000 × on Illumina Novaseq6000. A sequencing panel of 605 genes targeting the exome regions was used to identify mutations. The logarithmic ratio of each gene region was properly computed. WESPlus gene panel (an upgraded version of the standard whole-exome sequencing (WES) (HaploX Biotechnology) for cancer tissue sequencing. Seven to eight polymerase chain reaction (PCR) cycles, depending on the amount of DNA input, were performed on Pre-LM-PCR Oligos (Kapa Biosystems, Inc.) in 50 μl reactions. DNA sequencing was then performed on the Illumina Novaseq 6000 system according to the manufacturer's instructions. Data which meet the following criteria were chosen for subsequent analysis: the ratio of remaining data filtered by fastq in raw data is ≥85%; the proportion of Q30 bases is ≥85%; the ratio of reads on the reference genome is ≥85%; target region coverage ≥98%; average sequencing depth in tissues is ≥500×; average sequencing depth in blood cfDNA is ≥1,500×. The called somatic variants need to meet the following criteria: the read depth at a position is ≥20×; the variant allele frequency (VAF) is ≥2% for tissue DNA and ≥0.05% for cfDNA from blood; somatic-$P \leq 0.01$; strand filter ≥1. Allele frequencies were calculated for Q30 bases. The copy number variation was detected by CNVkit version 0.9.3 (https://github.com/etal/cnvkit). Further analyses of genomic alterations were also performed, including single nucleotide variants (SNVs), copy number variations (CNVs), insertion/deletion (Indels), fusions, and structural variation. Tumor mutation burden (TMB) was referred as the total number of incorrect coding, base substitution, insertion, and deletion in somatic cells per million bases.

Statistical Analysis

All charts and data analyses were performed using R statistical software package (https://www.r-project.org/). The significant difference of TMB in tumor tissues was determined by Student's *t*-test. According to the type of *KRAS* and *TP53* mutation identified (i.e., common or non-common). Survival curves were compared by Log-rank (Mantel-Cox) test. $P < 0.05$ was considered statistically significant. Data was represented with 95% confidence interval. Several packages of the R software were used to plot some figures, including the "ComplexHeatmaps" package (**Figures 1**, **2B**, **3**, **4**), the "ggplot2" package (**Figures 2C,D**), and the "survival" package (**Figure 5**).

RESULTS

Mutation Profiling of CRC Patients Before Therapy in Tissue and Blood

In order to verify the feasibility of ctDNA in peripheral blood by NGS, we first recruited 43 CRC patients (including 41 stage III-IV and 2 stage I patients) undergoing chemotherapy combined with target therapy agents (cetuximab, apatinib, trastuzumab) in neoadjuvant and/or adjuvant therapy. The baseline clinical characteristics of these patients are shown in **Table 1**. Their median age was 53 years old (ranged from 25 to 84 years old). The majority of the CRC patients were male ($n = 31$, 72.1%). The most frequent site of metastasis was the liver ($n = 11$, 25.58%), followed by lymph node ($n = 7$, 16.28%), lungs ($n = 6$, 13.95%), and peritoneum ($n = 3$, 6.98%). Among all patients, a total of 26 (60.47%) presented wild-type RAS. The number of patients

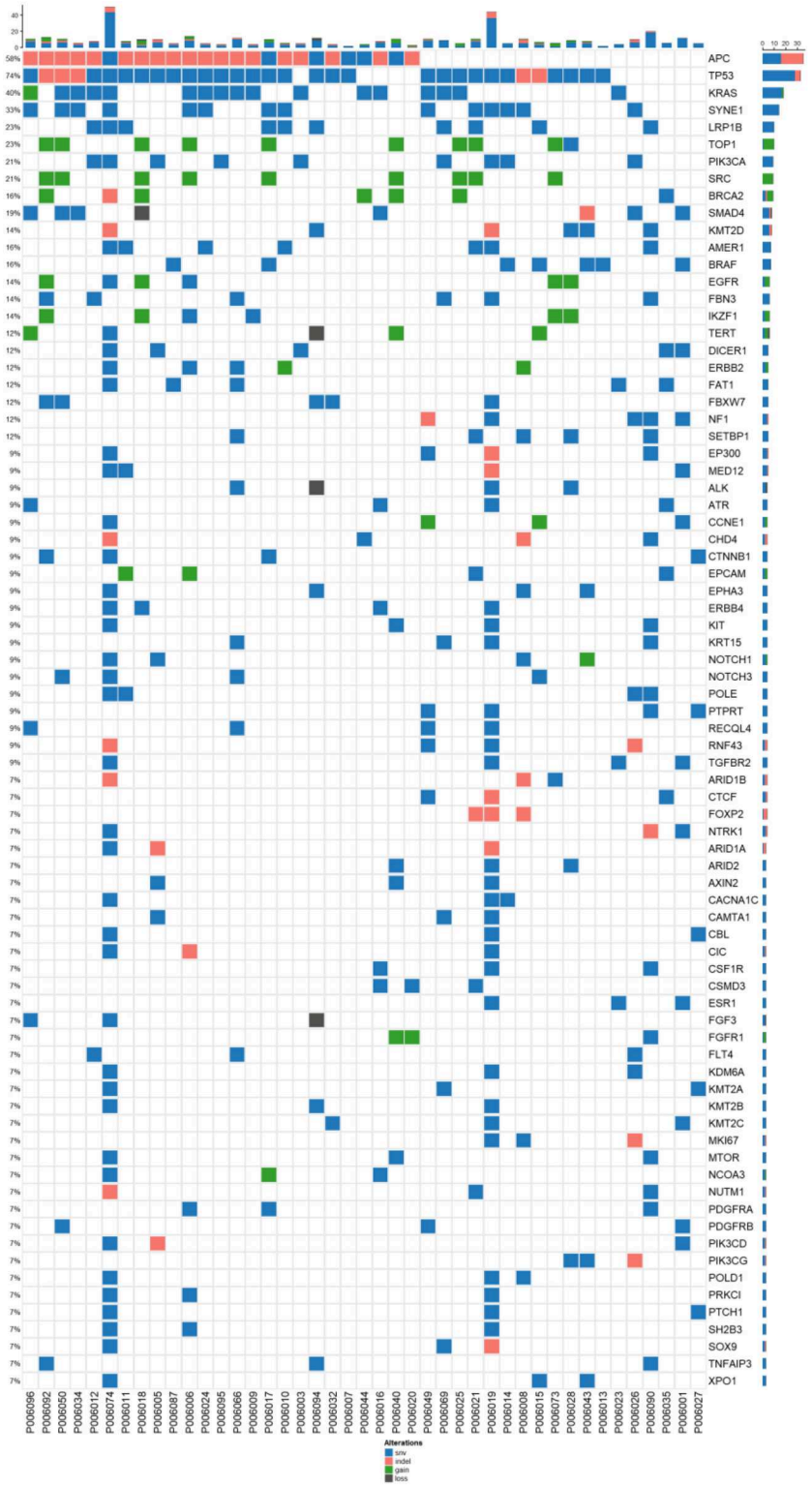

FIGURE 1 | Mutation spectrum of baseline plasma and tissue samples from 43 patients CRC. The genes with a high mutation frequency among all patients are listed on the left and individual patients are represented by the columns. Mutation types of non-synonymous single nucleotide variant, SNV (single nucleotide variant), indel (insertion-deletion), gain(stop gain, non-sense mutation), and loss(stop loss, missense mutation) are represented by blue, orange, and dark, respectively.

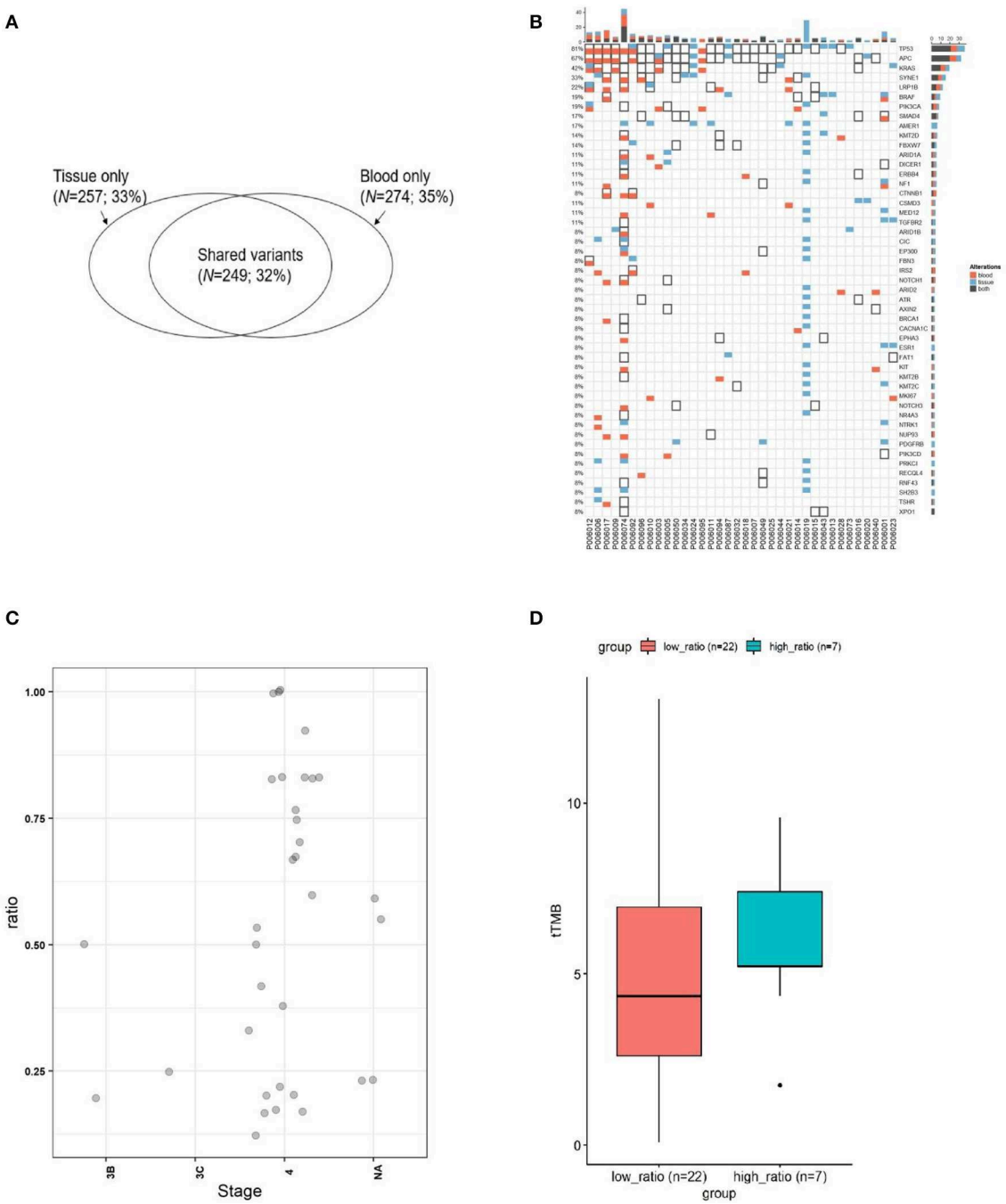

FIGURE 2 | The concordance of mutation between ctDNA and the corresponding tumor tissues from CRC. **(A)** Wenn diagram shows the number and percentage of overlapped and unique mutations between the tissue DNA and the corresponding blood ctDNA samples. **(B)** Mutation spectrum of baseline plasma and the corresponding tumor tissues from 35 subjects. **(C)** The mutation concordance ratio for different stages between blood ctDNA samples and tumor tissue samples from 28 patients. **(D)** Comparison of tumor mutation burden (TMB) in low consistency (<75%) and high consistency (>75%) groups.

with stage I, III, and IV was 2 (4.65%), 6 (13.96%), and 35 (81.4%), respectively. Two patients were treated with adjuvant chemotherapy (4.65%), while 8 were treated with neoadjuvant chemotherapy (18.6%), 5 patients were at the first-line therapy (11.63%), and 2 patients at the second-line therapy (4.65%), and 2 patients at the third-line therapy (4.65%). A total of 24 patients were solely treated with chemotherapy (55.81%).

Among 41 advanced colorectal cancers, 78 genes with high frequency mutations were identified. The top ten highly mutated genes were *TP53* (74%), *APC* (58%),

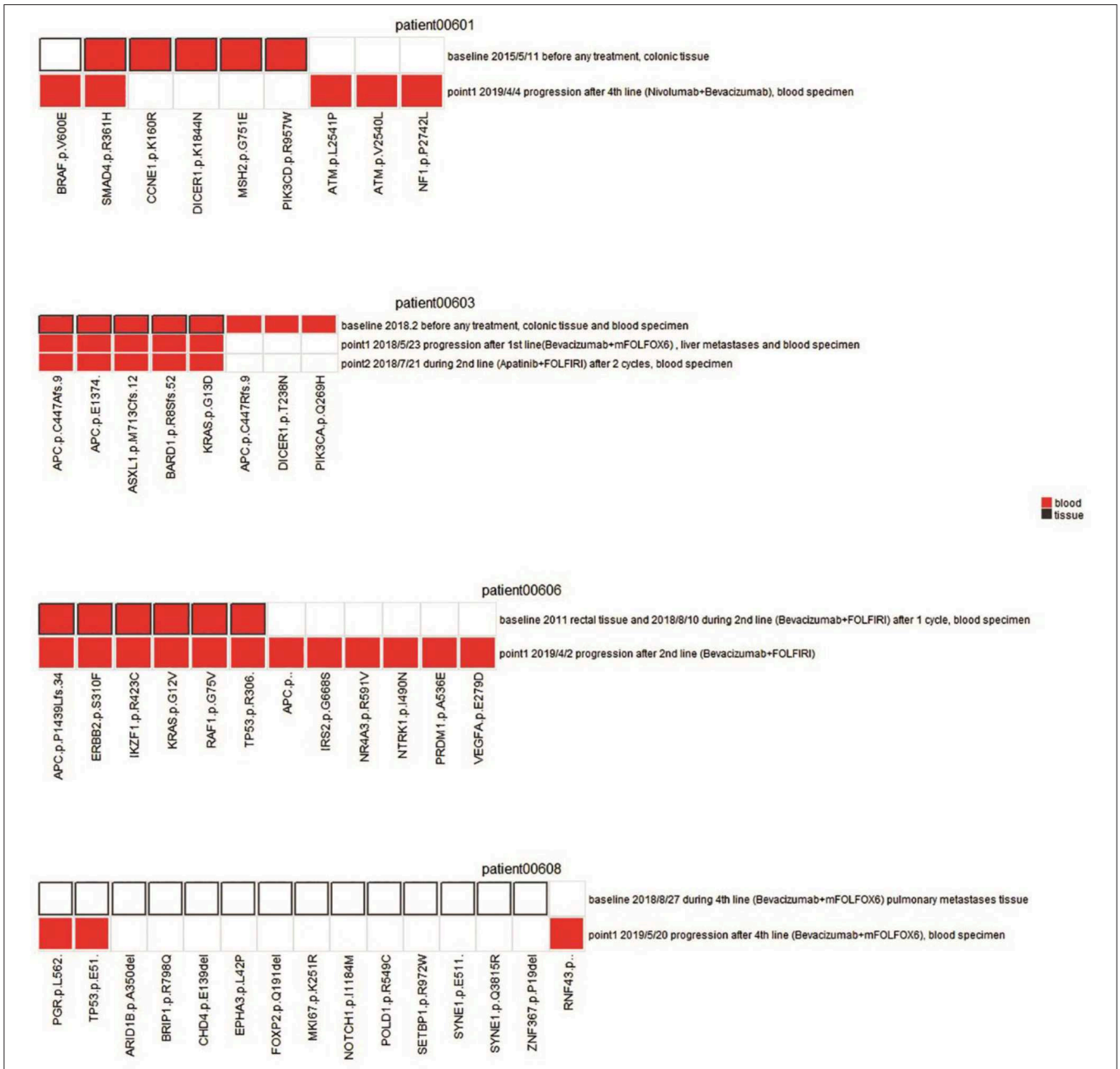

FIGURE 3 | Comparison of mutation status between plasma and tissues in four patients. Mutations for both pre-therapeutic tissue or blood samples and post-therapeutic blood samples were compared. Red squares indicate mutations from blood, and white squares with black solid border indicate mutations from tissue. Red squares with black solid border indicate mutations found in both blood and tissue. White squares with light gray border indicate no mutations.

KRAS (40%), *SYNE1* (33%), *LRP1B* (23%), *TOP1* (23%), *PIK3CA* (21%), *SRC* (21%), *BRCA2* (16%), and *SMAD4* (19%) (**Figure 1**). The most frequent SNV mutations were observed in *KRAS* (n = 32, 74.4%), *TP53* (n = 18, 41.8%), and *SYNE1* (n = 23, 53.5%). The most frequent Indel mutations were observed in APC3 gene in 25 of 43 patients (58.1%). The most frequent CNVs occurred in *TOP1* and *SRC* (**Figure 1**).

Blood and tissue samples were collected from all patients before receiving any therapy. By comparing the mutational rates (and their consistency) in tissues and plasma, we found that 249 out of 506 mutations detected in tissue samples were also found in the corresponding ctDNA samples (**Figure 2A**). The consistency calculated on mutational sites between tissue and blood samples was 32%. Our sequencing strategy enabled the detection of SNVs, indels, CNVs, and gene fusions in DNA

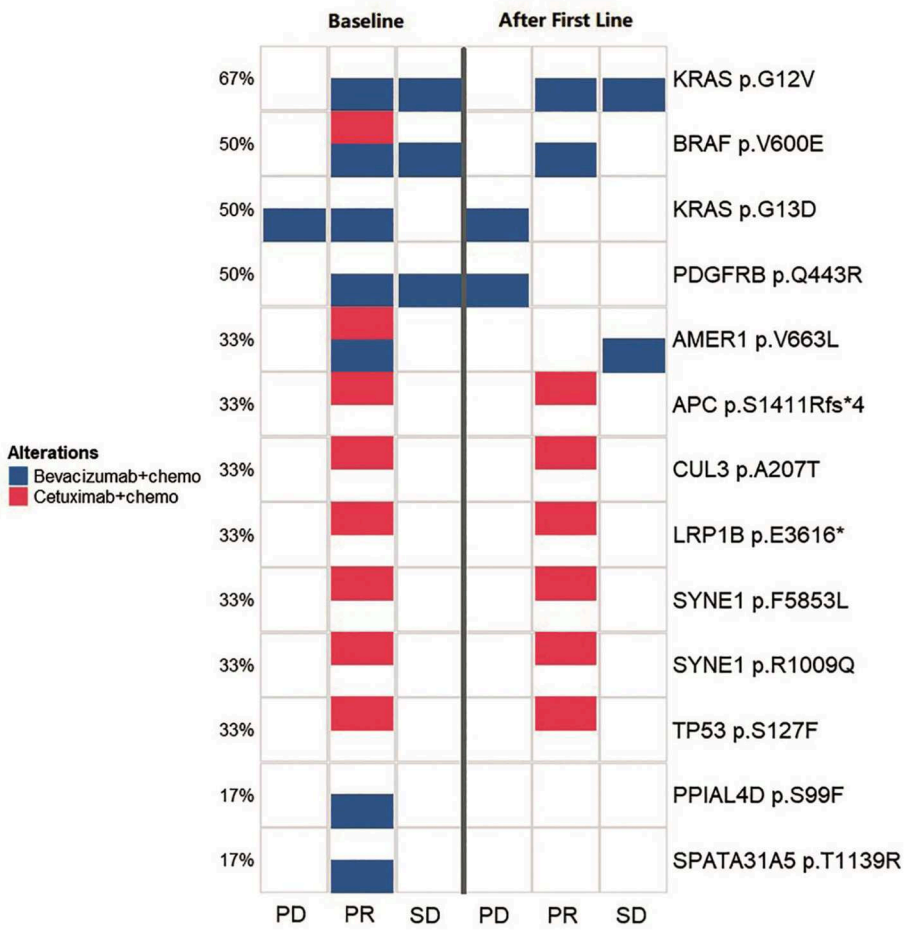

FIGURE 4 | Comparison of the spectrum of key mutations before and after the first-line therapy. The left three lanes (baseline group) and the right three lanes (after first line group) indicate the high-frequency mutational status for baseline (before the first-line therapy) and after the first-line therapy. Annotations to the right of the panel show the exact mutations and the percentage to the left of the panel shows the frequency for a certain mutation. The three lanes in both group illustrates the mutational status for PD, PR, and SD groups, respectively. Blue squares indicates cases with bevacizumab/chemotherapy that carried corresponding labeled mutations and red squares indicates cases with cetuximab/chemotherapy that carried corresponding labeled mutations.

derived from tumor tissues and ctDNA. In patients with paired tissue and blood samples, a total of 206 SNVs and 43 short Indels were detected (**Figure 2B**). The frequency of mutations and the consistency between tissue and blood samples are shown in **Figure 2B**. The most consistent gene was *TP53* (81%), followed by *APC* (67%) and *KRAS* (42%).

The consistency at individual CRC stages was determined by comparing the detection of mutations in ctDNA and corresponding tumor tissues for each patient (**Figure 2C**). It can be observed that the consistency for stage IV patients distributed in a wide range, and 24% of patients exhibited a consistency >0.75 (7/29), while 76% of patients exhibited a consistency <0.75 (22/29). The tTMB (tissue TMB) between those with a consistency >0.75 and those <0.75 was not statistically different (**Figure 2D**), although the trend showed that the group with lower consistency (< 0.75) had a lower tTMB.

Treatment Significantly Altered Mutational Landscape in ctDNA

A NGS panel containing 605 genes was used to monitor the genetic alterations following the therapy. Here we compared the alterations of gene mutations at different time points following treatment to assess the potential effect of therapy and to find any potential instruction on therapeutic strategy. Four specific cases were presented to illustrate the significance of NGS assay in clinical treatment.

Patient 00601 first presented adenocarcinoma (stage IV), and bilateral lung metastasis were found 6 months after surgery. The patient was treated with Bevacizumab and Nivolumab, and blood samples were collected 1 year after treatment. *BRAF* V600E and *SMAD4* R361H were still detected after a series of therapies compared with previously surgical resected samples. Although mutations in some genes (such as *CCNE1, DICER1, MSH2,* and *PIK3CD*) were altered, new mutations (*ATM* p.L2541P, *ATM*

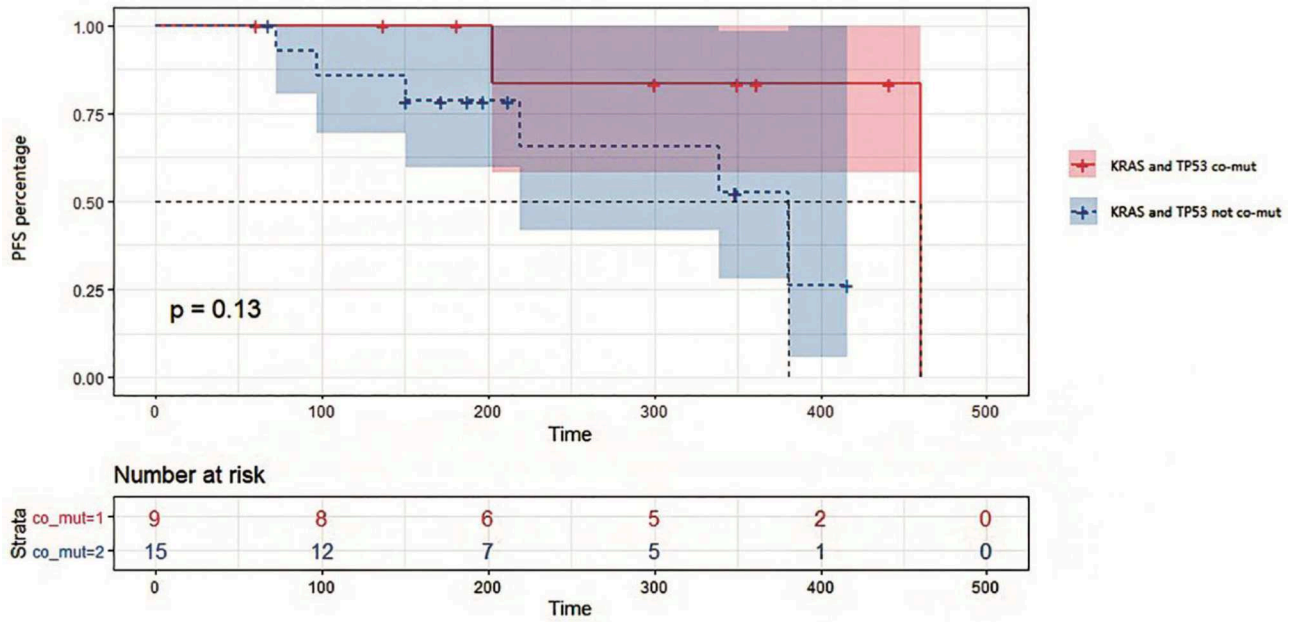

FIGURE 5 | Kaplan-Meier survival analysis on progression-free survival in patients with or without KRAS and TP53 co-mutations in tissues. Survival curves were compared by Log-rank (Mantel-Cox) test. $P = 0.13$ for statistical comparison between the two groups. Data was represented with 95% confidence interval.

p.V2540L, and *NF1* p.P2742L) were identified (**Figure 3**). We speculate that these new mutations, combined with those that still existed, may suggest the development of drug resistance or metastasis.

Patient 00603 presented sigmoid adenocarcinoma (T4aN0M1), and metastasis was found in the liver, lung, and lymph nodes. A combined treatment of Bevacizumab and Apatinib with FOLFIRI was applied but did not substantially alter the key driver gene mutations in *APC*, *ASXL1*, *BARD1*, and *KRAS* (**Figure 3**). These mutations could correlate with disease progression and poor overall prognosis of the patient, as he only survived 194 days after confirmation of diagnosis.

Patient 00606 presented rectal cancer (stage IV) with lung and brain metastasis. Blood samples were collected after 1 week treatment with Bevacizumab and FOLFIRI (second-line treatment). However, gene mutations of *APC, ERBB2, IKZF1, KRAS, and RAF1* were still detected after treatment compared with pre-therapeutic results. Moreover, new mutations of *APC, IRS2, NR4A3, NTRK1, PRDM1,* and *VEGFA* were detected. Discover of these new mutation normally suggest disease progression or new metastasis, which was proved by the clinical status of PD of the patient (**Figure 3**).

Patient 00608 presented rectal cancer (stage IV) and lung metastasis. Blood sampling was also performed to investigate the disease progression following Bevacizumab and FOLFOX6 treatment. The genetic variation from needle biopsy samples of pulmonary metastases greatly differed from that of the blood detection (**Figure 3**). Novel *RNF43* mutation sites in ctDNA were identified, supporting previous observation showing that *RNF43* frameshift mutation may contribute to tumorigenesis (6).

Comparison of Key Mutations in Baseline and After First-Line Therapy

We monitored key mutation changes of 13 patients between baseline and after the first-line therapy of bevacizumab, cetuximab with chemotherapy and grouped the patients by response [progressed diseases (PD), partial response (PR), and stable disease (SD)]. The key mutations were different between baseline tissues and progressive ctDNA samples in all three groups (**Figure 4**). Most of the genes were reported to contribute to the carcinogenesis of CRC. Compared with baseline, a new mutation (*PDGFRB* p.Q443R) was observed during disease progression. More importantly, the combination of bevacizumab/chemotherapy or cetuximab/chemotherapy was able to alleviate the mutation of the driving gene, such as *BRAF*, *KRAS*, *AMER1*. Mutations in *PPIAL4D* p.S99F and *SPATA31A5* p.T1139R were not observed after therapy. The above observations suggest that mutational profile of ctDNA may help to determine the response of patients to treatment.

TP53/KRAS Mutations in Tumor Tissue Are Potential Predictive Factors for Treatment Response

In this study, 18 patients were treated with bevacizumab combined with chemotherapy, while 4 patients were treated with cetuximab combined with chemotherapy, and 2 with chemotherapy alone. We divided these patients into two groups by *TP53/KRAS* co-mutation. It can be seen from the survival analysis in **Figure 5** that PFS appeared to be shorter for patients with no *TP53/KRAS* co-mutation, with a median PFS of 381 days for no co-mutation group compared with 460 days in

TP53/KRAS co-mutation group ($p = 0.13$). Patients with *KRAS* and *TP53* co-mutations in tissues exhibited a potentially better response to treatment than those containing the respective wild type genes. The relationship between the prognosis of first-line therapy and the *TP53/KRAS* co-mutations is worth more investigation.

DISCUSSION

In this study, we explored the practicability and clinical value of ctDNA in CRC therapy using paired blood and tissue biopsy samples. To clarify the correlation between drug efficacy and mutations, we built up mutational profiles for 43 CRC patients. We dynamically monitored the mutation status of each patient and investigated its relationship with therapeutic response, including drug resistance (10). Our study revealed many gene mutations with the 605-gene panel. Apart from previously reported mutations in *APC, TP53, KRAS, SYNE1, PI3KCA, SMAD4,* and *BRAF*, some other mutations may also potentially be used as biomarkers for CRC prognosis. We also showed that ctDNA may be used to analyze TMB, which is an effective method to monitor the burden of mutations following therapy. The consistency between ctDNA and tissue biopsy was 32%.

We collected plasma ctDNA and tumor tissues in CRC patients following cetuximab, apatinib, trastuzumab, neoadjuvant, adjuvant chemotherapy, or any combination of them to track tumor dynamics, including therapeutic response, metastasis, and drug resistance. Despite the limited cohort ($n = 41$), the samples represented patients of advanced CRC with integrated clinical information. Four representative patients with treatment plans and mutational changes were presented and analyzed in detail (**Figure 3**). Although the mutational profile of each patient was distinct, our results indicated that the mutation of driver genes dynamically changed in different patients and treatment plans. Therefore, it is vital to detect these gene mutations in an individualized manner. We believe this strategy can support the establishment of reasonable treatment plan for each patient (11–14).

After comparing key mutation profiles between baseline and after first-line therapy (**Figure 4**), a new mutation (*PDGFRB* p.Q443R) was observed during disease progression. Consistent with previously observations, *PDGFRB* appeared to promote the development of CRC (15, 16). Moreover, combinations including bevacizumab-chemotherapy and cetuximab-chemotherapy could diminish the mutations of driving genes, such as *BRAF, KRAS, AMER1*, and therefore potentially prevent disease progression. *BRAF* and *KRAS* are driver genes of CRC, while *AMER1* is a frequently mutated gene in this condition (17). Mutations in two other genes (*PPIAL4D* p.S99F and *SPATA31A5* p.T1139R) were previously rarely reported, which may constitute alternate mutation sites that deserve more in-depth investigation. Since gene mutations typically accumulate over time, CRC with distinct heterogeneity may exhibit different genetic characteristics. The mutational information from a single tissue biopsy is limited by space and time, and may be biased in accessing the therapeutic effect or monitoring cancer progression. Ideally, multiple biopsies may be obtained to avoid this bias. Although we did not achieve ideal condition, our study improved the understanding in the roles of ctDNA in CRC monitoring and response assessment in the practice of precision medicine.

TP53 mutations in early CRC have been considered a poor prognostic factor. However, the function of mutated TP53 has not been fully characterized (18). In our study, *TP53* and *KRAS* mutations were considered favorable factors for overall survival and disease progression of CRC. PFS was potentially shorter for patients without *TP53/KRAS* co-mutations compared with *TP53/KRAS* mutated patients and therefore might have more treatment benefit (**Figure 5**). Indeed, these two genes were often found co-mutated in our sequencing results. Therefore, although some potential interesting findings were revealed in the current study, it requires further validation using a larger number of patients. In this study, we confirmed the roles of ctDNA in dynamic monitoring of CRC therapy, which supports more extensive use of the method in future therapy.

In this study, we monitored the mutational changes and therapeutic response of late-stage CRC patients following chemotherapy combined with bevacizumab and/or cetuximab. It appeared that high frequency mutations of key driver gene, such as APC, TP53, and KRAS, were the markers that sensitively reflected the therapeutic response, while alleviation of mutations in BRAF, AMER1, and other major driver genes was also observed following the therapy. The dynamic change of plasma mutation status following the combined therapy was consistent with the tissue tumor burden and was closely correlated with disease progression. Therefore, ctDNA detection appeared to be a useful method for the molecular genotyping and sensitive for monitoring mutational status, which potentially helps to develop treatment strategy targeting actionable variations. Our observations were supported by several previous reports focusing on the monitoring capability of NGS-based liquid biopsy in late-stage CRC therapy (4, 19–24). However, the regimes used in these studies varied according to different situation. Some studies focused on the monitoring of cetuximab-based therapy for RAS wild type patients (19–21), while others emphasize the monitoring of multiple targets, including EGFR, HER2, SMAD4, and NF1 (4, 21–23). Interestingly, one study investigated the ability of both mutation and methylation markers in monitoring (24). Although the therapeutic regimes and targets varied, the observations from these studies all support the use of NGS-based liquid biopsy for therapeutic response monitoring and target identification, which endorsed our conclusions.

There were some limitations in this study. Firstly, the sample size was still small. Although 43 patients were included, only 35 patients had paired baseline plasma and corresponding tumor tissues, and key mutation changes between baseline and after the first-line therapy were obtained from 13 patients. Therefore, incomplete paired samples and loss of follow-up were key issues in the study, which increased the difficulties in analysis and making solid conclusion. These issues can be solved by increasing the number of total subjects and patients with complete information may increase accordingly.

Meanwhile, strict fulfillment of inclusion and exclusion criteria may also increase the ratio of patients with complete information. Secondly, the therapeutic strategy in this study varied among different patients. Therefore, studies on mutational changes may be differentially affected by various chemotherapy drugs, and conclusions based on mixed therapies may be compromised. It would be nice to study the mutational changes with patients from homogeneous treatment, however, this was difficult operationally, as late-stage CRC patients from multiple lines of therapy generally have diversified conditions and will adopt different therapies in the real world.

DATA AVAILABILITY STATEMENT

The datasets generated for this study can be found in the Genome Sequence Archive for Human (GSA-Human) (Accession: PRJCA002282).

ETHICS STATEMENT

The studies involving human participants were reviewed and approved by Shenzhen People's Hospital. The patients/participants provided their written informed consent to participate in this study.

AUTHOR CONTRIBUTIONS

RX designed the study. HC and XL performed the sample collection, data collection, and manuscript writing. YC, PY, and TH performed the sequencing and data analysis. XL, PY, and LS wrote the manuscript. LS and RX proof read the manuscript.

FUNDING

This study was supported by the project Monitoring the efficacy of chemotherapy and evaluation of drug resistance in digestive tract tumors based on liquid biopsy and project Head-to-head comparison of apatinib mesylate combined with chemotherapy: a randomized study of bevacizumab combined with chemotherapy as second-line therapy for advanced intestinal cancer patients (SYLY201725), supported by Sanming project of Shenzhen People's Hospital.

REFERENCES

1. Wang B, Wu S, Huang F, Shen M, Jiang H, Yu Y, et al. Analytical and clinical validation of a novel amplicon-based NGS assay for the evaluation of circulating tumor DNA in metastatic colorectal cancer patients. *Clin Chem Lab Med*. (2019) 57:1501–10. doi: 10.1200/JCO.2019.37.15_suppl.e15084
2. Onidani K, Shoji H, Kakizaki T, Yoshimoto S, Okaya S, Miura N, et al. Monitoring of cancer patients via next-generation sequencing of patient-derived circulating tumor cells and tumor DNA. *Cancer Sci*. (2019) 110:2590–9. doi: 10.1111/cas.14092
3. Osumi H, Shinozaki E, Takeda Y, Wakatsuki T, Ichimura T, Saiura A, et al. Clinical relevance of circulating tumor DNA assessed through deep sequencing in patients with metastatic colorectal cancer. *Cancer Med*. (2019) 8:408–17. doi: 10.1002/cam4.1913
4. Zhang H, Liu R, Yan C, Liu L, Tong Z, Jiang W, et al. Advantage of next-generation sequencing in dynamic monitoring of circulating tumor DNA over droplet digital PCR in cetuximab treated colorectal cancer patients. *Transl Oncol*. (2019) 12:426–31. doi: 10.1016/j.tranon.2018.11.015
5. Xu R, Zhong G, Huang T, He W, Kong C, Zhang X, et al. Sequencing of circulating tumor DNA for dynamic monitoring of gene mutations in advanced non-small cell lung cancer. *Oncol Lett*. (2018) 15:3726–34. doi: 10.3892/ol.2018.7808
6. Lai C, Sun W, Wang X, Xu X, Li M, Huang D, et al. RNF43 frameshift mutations contribute to tumourigenesis in right-sided colon cancer. *Pathol Res Pract*. (2019) 215:152453. doi: 10.1016/j.prp.2019.152453
7. Lyskjær I, Kronborg CS, Rasmussen MH, Sørensen BS, Demuth C, Rosenkilde M, et al. Correlation between early dynamics in circulating tumour DNA and outcome from FOLFIRI treatment in metastatic colorectal cancer. *Sci Rep*. (2019) 9:11542. doi: 10.1038/s41598-019-47708-1
8. Yang N, Li Y, Liu Z, Qin H, Du D, Cao X, et al. The characteristics of ctDNA reveal the high complexity in matching the corresponding tumor tissues. *BMC Cancer*. (2018) 18:319. doi: 10.1186/s12885-018-4199-7
9. Baltruskeviciene E, Mickys U, Zvirblis T, Stulpinas R, Pipiriene Zelviene T, Aleknavicius E. Significance of KRAS, NRAS, BRAF and PIK3CA mutations in metastatic colorectal cancer patients receiving Bevacizumab: a single institution experience. *Acta Med Litu*. (2016) 23:24–34. doi: 10.6001/actamedica.v23i1.3267
10. Benson AB, Venook AP, Cederquist L, Chan E, Chen Y-J, Cooper HS, et al. Colon cancer, version 1. 2017, NCCN clinical practice guidelines in oncology. *J Natl Comprehens Cancer Netw*. (2017) 15:370–98. doi: 10.6004/jnccn.2017.0036
11. Liebs S, Keilholz U, Kehler I, Schweiger C, Haybäck J, Nonnenmacher A, et al. Detection of mutations in circulating cell-free DNA in relation to disease stage in colorectal cancer. *Cancer Med*. (2019) 8:3761–9. doi: 10.1002/cam4.2219
12. Parseghian CM, Napolitano S, Loree JM, Kopetz S. Mechanisms of innate and acquired resistance to Anti-EGFR therapy: a review of current knowledge with a focus on rechallenge therapies. *Clin Cancer Res*. (2019) 25:6899–908. doi: 10.1158/1078-0432.CCR-19-0823
13. Marcuello M, Vymetalkova V, Neves RPL, Duran-Sanchon S, Vedeld HM, Tham E, et al. Circulating biomarkers for early detection and clinical management of colorectal cancer. *Mol Aspects Med*. (2019) 69:107–22. doi: 10.1016/j.mam.2019.06.002
14. Hamfjord J, Guren TK, Dajani O, Johansen JS, Glimelius B, Sorbye H, et al. Total circulating cell-free DNA as a prognostic biomarker in metastatic colorectal cancer before first-line oxaliplatin-based chemotherapy. *Ann Oncol*. (2019) 30:1088–95. doi: 10.1093/annonc/mdz139
15. Cai H, Shi Q, Tang Y, Chen L, Chen Y, Tao Z, et al. Positron emission tomography imaging of platelet-derived growth factor receptor β in colorectal tumor xenograft using zirconium-89 labeled dimeric affibody molecule. *Mol Pharm*. (2019) 16:1950–7. doi: 10.1021/acs.molpharmaceut.8b01317
16. Olsen RS, Dimberg J, Geffers R, Wågsäter D. Possible role and therapeutic target of PDGF-D signalling in colorectal cancer. *Cancer Invest*. (2019) 37:99–112. doi: 10.1080/07357907.2019.1576191
17. Sanz-Pamplona R, Lopez-Doriga A, Paré-Brunet L, Lázaro K, Bellido F, Alonso MH, et al. Exome sequencing reveals AMER1 as a frequently mutated gene in colorectal cancer. *Clin Cancer Res*. (2015) 21:4709–18. doi: 10.1158/1078-0432.CCR-15-0159
18. Papaxoinis G, Kotoula V, Giannoulatou E, Koliou GA, Karavasilis V, Lakis S, et al. Phase II study of panitumumab combined with capecitabine and oxaliplatin as first-line treatment in metastatic colorectal cancer patients: clinical results including extended tumor genotyping. *Med Oncol*. (2018) 35:101. doi: 10.1007/s12032-018-1160-1
19. Toledo RA, Cubillo A, Vega E, Garralda E, Alvarez R, de la Varga LU, et al. Clinical validation of prospective liquid biopsy monitoring in patients with wild-type RAS metastatic colorectal cancer treated with FOLFIRI-cetuximab. *Oncotarget*. (2017) 8:35289–300. doi: 10.18632/oncotarget.13311
20. Goldberg RM, Montagut C, Wainberg ZA, Ronga P, Audhuy F, Taieb J, et al. Optimising the use of cetuximab in the continuum of care for

patients with metastatic colorectal cancer. *ESMO Open*. (2018) 3:e000353. doi: 10.1136/esmoopen-2018-000353

21. Mei Z, Shao YW, Lin P, Cai X, Wang B, Ding Y, et al. SMAD4 and NF1 mutations as potential biomarkers for poor prognosis to cetuximab-based therapy in Chinese metastatic colorectal cancer patients. *BMC Cancer*. (2018) 18:479. doi: 10.1186/s12885-018-4298-5
22. Knebel FH, Bettoni F, da Fonseca LG, Camargo AA, Sabbaga J, Jardim DL. Circulating tumor DNA detection in the management of anti-EGFR therapy for advanced colorectal cancer. *Front Oncol*. (2019) 9:170. doi: 10.3389/fonc.2019.00170
23. Liu R, Zhao X, Guo W, Huang M, Qiu L, Zhang W, et al. Dynamic monitoring of HER2 amplification in circulating DNA of patients with metastatic colorectal cancer treated with cetuximab. *Clin Transl Oncol*. (2019). doi: 10.1007/s12094-019-02215-7. [Epub ahead of print].
24. Boeckx N, Op de Beeck K, Beyens M, Deschoolmeester V, Hermans C, De Clercq P, et al. Mutation and methylation analysis of circulating tumor DNA can be used for follow-up of metastatic colorectal cancer patients. *Clin Colorectal Cancer*. (2018) 17:e369–79. doi: 10.1016/j.clcc.2018.02.006

Conflict of Interest: XL, PY, TH, and LS are currently employed by HaploX Biotechnology. HaploX provided the next generation sequencing service for this study.

The remaining authors declare that the research was conducted in the absence of any commercial or financial relationships that could be construed as a potential conflict of interest.

frontiers in Oncology

MINI REVIEW
published: 22 April 2020
doi: 10.3389/fonc.2020.00569

Recent Advances in Cancer Plasticity: Cellular Mechanisms, Surveillance Strategies, and Therapeutic Optimization

*Giuseppe Nicolò Fanelli, Antonio Giuseppe Naccarato and Cristian Scatena**

Division of Pathology, Department of Translational Research and New Technologies in Medicine and Surgery, University of Pisa, Pisa, Italy

The processes of recurrence and metastasis, through which cancer relapses locally or spreads to distant sites in the body, accounts for more than 90% of cancer-related deaths. At present there are very few treatment options for patients at this stage of their disease. The main obstacle to successfully treat advanced cancer is the cells' ability to change in ways that make them resistant to treatment. Understanding the cellular mechanisms that mediate this cancer cell plasticity may lead to improved patient survival. Epigenetic reprogramming, together with tumor microenvironment, drives such dynamic mechanisms favoring tumor heterogeneity, and cancer cell plasticity. In addition, the development of new approaches that can report on cancer plasticity in their native environment have profound implications for studying cancer biology and monitoring tumor progression. We herein provide an overview of recent advancements in understanding the mechanisms regulating cell plasticity and current strategies for their monitoring and therapy management.

Keywords: cancer plasticity, stem cell, heterogeneity, recurrence, liquid biopsy

OPEN ACCESS

Edited by:
Dong-Hua Yang,
St. John's University, United States

Reviewed by:
Andreas Stylianou,
University of Cyprus, Cyprus
Pei-Wen Hsiao,
Academia Sinica, Taiwan

****Correspondence:***
Cristian Scatena
cristian.scatena@unipi.it

Specialty section:
This article was submitted to Molecular and Cellular Oncology, a section of the journal Frontiers in Oncology

Received: *30 November 2019*
Accepted: *30 March 2020*
Published: *22 April 2020*

Citation:
Fanelli GN, Naccarato AG and Scatena C (2020) Recent Advances in Cancer Plasticity: Cellular Mechanisms, Surveillance Strategies, and Therapeutic Optimization. Front. Oncol. 10:569. doi: 10.3389/fonc.2020.00569

CANCER CELL PLASTICITY: A NEW LEVEL OF HETEROGENEITY IN A TUMOR

Tumor heterogeneity can be inter-tumoral, if genetic variations are found among different patients with tumors of the same type, or intra-tumoral, involving different cancer cells in the same tumor. In particular, intra-tumor heterogeneity can be caused by genetic variation, modulation in the expression of a gene, transition among cellular states or environmental changes (1). Thus, it is easy to understand that intra-tumor heterogeneity drives cancer progression and represents the main cause of treatment failure (2).

Initially, two models were proposed to justify intra-tumor heterogeneity: the "clonal evolution" model and the "cancer stem-like cell" (CSC) model. The first contemplates differences among cancer cells due to stochastic alterations in genes; according to this theory, clones which gain a growth advantage are selected over time (3, 4). The second involves CSCs, a minority population of cancer cells with self-renewing capacity that initiates and maintains tumor growth, in contrast with the majority of the cancer cells which show a more differentiated phenotype (5–7). Lately, a third model has been proposed: the "CSC plasticity" model, where CSCs possess the capacity to move between stem and differentiated states. This shift may be caused by intrinsic cues such as

genetic mutations and/or epigenetic modifications but also by extrinsic cues from the tumor microenvironment (inflammation, injury, senescence). In addition, the tumor-initiating potential is enhanced by the overexpression of transcription factors involved in the process of epithelial-to-mesenchymal transition (EMT) (8–10) and CSCs exhibit an induced EMT program (11). These data suggest that EMT is strictly linked to CSC features. Indeed, CSCs switch between epithelial and mesenchymal states and this process depends on both genetic mutations, epigenetic modifications and transcriptional modulation of cancer cells and signals provided by the tumor microenvironment through the mediation of growth factors, cytokines, cancer-associated fibroblasts (CAFs), tumor associated macrophages (TAMs) and hypoxia (12, 13) (**Figure 1**). These transitions promote metastasis at distant sites as well as drug resistance and, therefore, disease recurrence (14–16). In breast cancer cells co-expression of epithelial and mesenchymal genes promotes stemness inducing the formation of 3D-spheroid structures named "tumor-spheres" (17). Moreover, cells with intermediate state of EMT showed similar tumor-initiating potential when compared with fully differentiated mesenchymal cells in a mouse model of prostate cancer (18). Thus, we suppose that cancer cell stemness may be associated with a partial EMT phenotype and, indeed, cells which exhibit this intermediate EMT state possess a much more pronounced plasticity (19). According to this definition, the CSC plasticity model suggests that the two historical models of cancer heterogeneity, i.e., the clonal evolution model and the CSC model, are not mutually exclusive (1, 20–22). We believe that this third model suggests a new level of complexity in tumor heterogeneity concept.

NOVEL APPROACHES FOR MONITORING TUMOR CELL PLASTICITY AND PROGRESSION

Solid tumors are consisted of several sub-clonal cells populations, which compete in a Darwinian manner under the selective pressures of endogenous and exogenous factors, leading to the

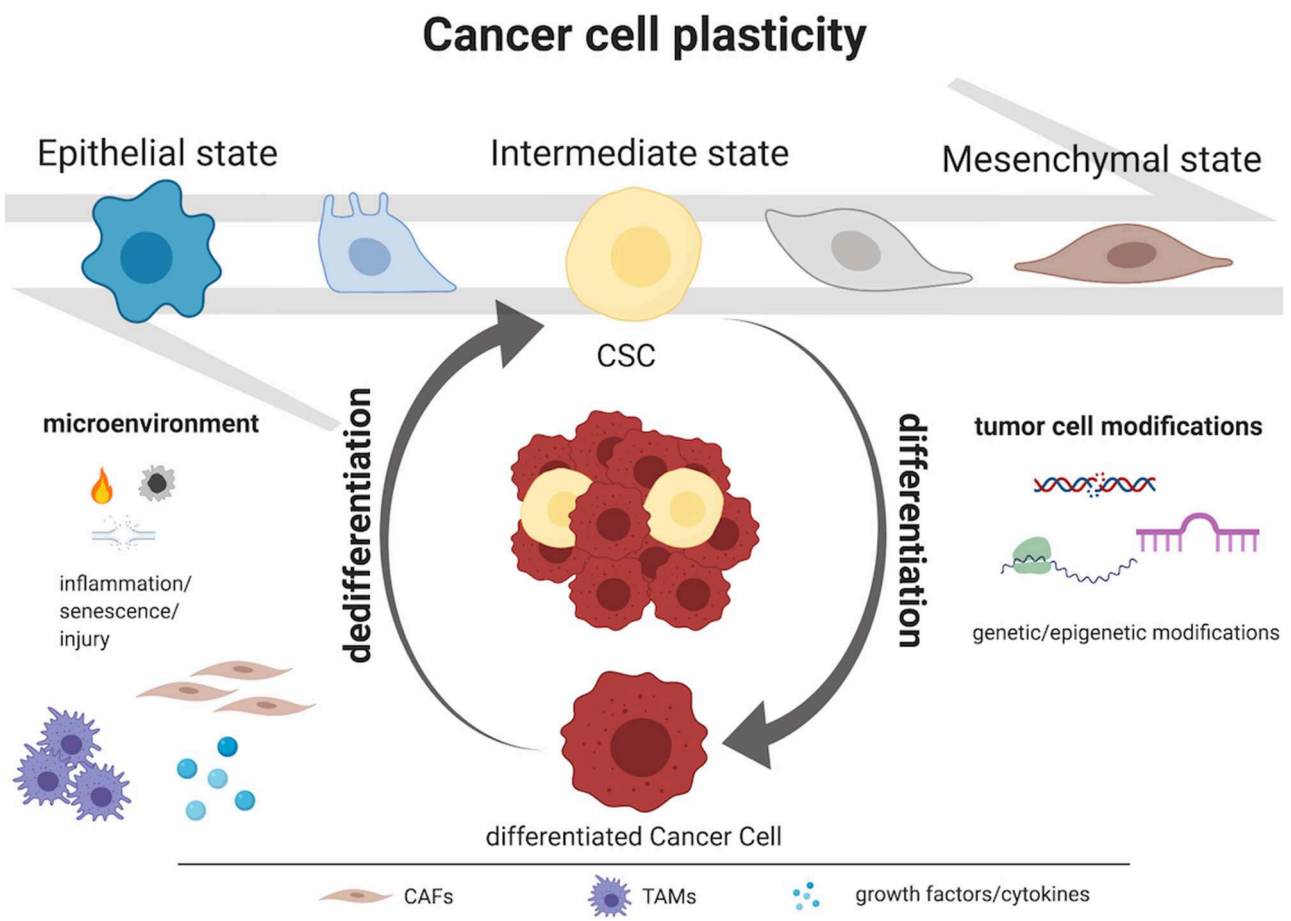

FIGURE 1 | Mechanisms governing CSC plasticity model. Intra-tumor heterogeneity relies on the capacity to shift dynamically and reversibly between CSC and non-CSC/differentiated state. Tumor cell modifications as genetic and epigenetic alterations and microenvironment perturbations as inflammation, injury, and senescence represent the major causes of cancer cells plasticity. Moreover, CSCs exhibit an induced epithelial-to-mesenchymal transition (EMT) program and, particularly, they display an intermediate state of EMT. This process depends on both genetic mutations, epigenetic modifications and transcriptional modulation of cancer cells and signals provided by the tumor microenvironment (i.e., growth factors, cytokines, CAFs or TAMs). Created with BioRender.com.

clonal evolution of a dominant subclone that will characterize the tumor's molecular landscape. Hence, it will be highly heterogeneous and will dynamically change during the disease progression, so longitudinal sampling is essential to define therapeutic strategies.

Currently, cancer molecular profile is evaluated through "solid biopsies" from primary tumor or metastatic nodule; however, this approach has several issues: (i) biopsies are not representative of the whole tumor mass; (ii) often tumor site is not accessible; (iii) frequently, biopsies cannot be serially performed; (iv) each metastasis could have a different genomic landscape; (v) finally, therapeutic selective pressure has to be considered too (23–28). To overcome these limitations the novel approach of "liquid biopsy" is gaining attention.

The rapid turnover of cancer cells results in the constant release into the bloodstream of: (i) cell-free circulating tumor DNA (ctDNA); (ii) tumor derived RNA (predominantly micro-RNAs and long-non-coding-RNA) (29); (iii) circulating tumor cells (CTCs); and (iv) extracellular vesicles (EVs) (sub-cellular structures with a membrane that contain nucleic acids and/or proteins) (30–33). This enables clinicians to repeatedly and non-invasively interrogate the dynamic evolution of human cancers.

CTCs are (probably) intravasated or passively spread from the primary and/or secondary tumor sites into the bloodstream, and could be responsible for the beginning of distant metastases.

In cancer patients CTCs can be isolated single or in clusters with other CTCs or with endothelial cells, platelets, leukocytes and fibroblasts, conferring them resistance to oxidative stress, and protection from the immune system (34). Their absolute number is really low ($\sim$1 CTC per 1×10^9 blood cells), especially in early cancer stage, and can vary between cancer types (34–36).

CTCs detection and isolation challenges are related to the high sensitivity and specificity required, and several factors still hamper standardized clinical application. Different approaches have been extensively investigated to isolate CTCs: (i) technologies such as density gradient stratification, membrane filtration, photoacoustic detection, dielectric mobility, and microfluidic separation are based on CTCs physical properties (density, size, mechanical plasticity, and dielectric mobility) that are different from those of other blood cells (37, 38). However, these techniques have low specificity (39), so new antibody-based functional assays have been developed: (ii) cytometric high-throughput imaging which provides the scanning of cells on slides; (iii) negative depletion of leucocytes and erythrocytes (Batch cell lysis, Microfluidic CTC-iChip, Immunomagnetic separation) (40) using specific antigens such as CD45 for leucocytes and glycophorin for erythrocytes; (iv) positive CTC enrichment by specific markers expressed on the cell surface (CellSearch, Magsweeper, Microfluidic CTC-Chip) such as epithelial cell adhesion molecule (EpCAM) (41) cytokeratins (CK8, CK18, CK19) (42) or tumor specific markers (TTF-1, PSA, HER-2 etc.) (43, 44). Nevertheless, no agreement has been reached on the specific antibodies to test. Indeed, EpCAM is usually lost during EMT, that sustains CTC migration, extravasation and apoptosis/anoikis resistance (45). Additionally, CTCs may develop a stem-like phenotype (46, 47). Hence, it is possible to find "commingling" CTCs that express epithelial, EMT or cancer stem cells phenotype; these CTCs have the highest plasticity potential and thus may represent CSCs (48). Different expression levels of stem cell markers such as CD24, CD44, CD133, ALDH, NANOG, OCT4, were found in ovarian (49), breast (50), and prostate CTCs (51). Remarkably, CTCs differentially express genes involved in oncogenic signaling pathways depending on their plasticity or stemness levels (52–54).

Finally, innovative developed approaches to CTCs/CSCs isolation are based on: (v) CTCs functional features such as protein secretion and cell migration (Epispot assay, Invasion assay) that allow the attachment of these cells to synthetic substrates co-treated with specific matching molecules (55); (vi) nanotechnology (Immunomagnetic nanobeads, Nanostructures substrates in microchip) (56, 57); (vii) the combination of surface/cytoplasmic markers, size and dielectrophoretic migration properties (DEPArray) (58).

Despite different approaches, in our opinion none of them completely satisfy the necessary requirements since low purity, loss of CTCs, and a narrow detection range still need to be tackled.

Finally, an additional central aspect to consider in the cancer plasticity is the complex network of epithelial-stromal cells interactions. Stroma undergoes, in parallel with the epithelial compartment, in a dynamic remodeling that may predict and explain several clinico-pathological features (59–63). To date, several *in-vitro* and in *in-vivo* models have been created and novel approaches have been used to study this interaction and its remodeling (64–66): genomic (scRNA-seq); protein translation and secretion (serial analysis of gene expression, antibody arrays and bead-based arrays, mass spectrometry and yeast, bacterial and mammalian secretion traps); autocrine, paracrine and long distance (cells co-culture, proximal culture); and directly in human tissue (multispectral imaging analysis). However, stroma characterization is still incomplete and fragmentary, also because of the difficulty to perform an "evolution tracking" of the whole stromal compartment.

Since malignancies development and progression are the result of these complex interactions, we believe that the treatment with chemotherapeutic agents against the cancer epithelial compartment combined with novel stroma-targeted therapies, may efficiently reduce cancer recurrence, also thank to the targeting and eradication of CSCs.

CLINICAL RELEVANCE OF CANCER CELL PLASTICITY: LIMITATIONS AND NEW OPPORTUNITIES

Though the presence of CTCs has been known since the 1869 (67), their clinical relevance was demonstrated only in 1994 (68). Despite their low number in the blood stream, they are related to clinical outcomes (34–36). In our opinion CTCs and CSCs may represent the key for early diagnosis, better prognostic stratification and a more accurate therapeutic response prediction; in addition, their concentration and pheno/genotyping could be easily measured and repeated

over time. To date, however, only few authors tried to demonstrate advantages of liquid biopsy over the solid biopsies in cancer surveillance and follow-up (69, 70); this is also due to the important technical issues still to be overcome. In addition, according to recent insights, CSCs do not constitute an autonomous compartment; rather, they play an active role in the microsystem, constituted both by the epithelial and the stromal compartments; indeed several authors have demonstrated the mutual influences between CSCs and their microenvironment (71–74).

We think that one promising approach to eradicate CSCs may be to target the EMT (75): inhibitors of TGFβ-induced EMT as well as SRC, MEK, or ALK5 inhibitors have been tested (76, 77). Interestingly, also inflammatory cytokines—IL6 and IL8 in particular—may represent potential therapeutic targets of EMT: IL-6 acts as a direct regulator of breast CSCs (BCSCs) self-renewal (78) and high levels of IL-6 are demonstrated to be associated to poor clinical outcome (79); on the other hand, BCSCs have been successfully eradicated both *in vitro* and in animal models by blocking the IL-8 receptor CXCR1 (80). In addition, in patients with HER2 positive breast cancer, treatment with HER2 inhibitors decreased the content of BCSCs (81), suggesting that combination therapies that include HER2 targeting agents may overcome BCSCs resistance. Based on this knowledge, we believe that therapies targeting BCSCs represent an urgent need to prevent recurrence. Other authors have suggested to target also Notch, Hedgehog, Wnt and PI3K/Akt/mTOR pathways (82). Intriguingly recent evidences demonstrate that CSCs rely on mitochondrial biogenesis for their propagation (83). Lamb et al. previously demonstrated that the antibiotic doxycycline, in a known inhibitor of the 28S mitochondrial ribosome subunit, inhibits CSC propagation *in vitro* (84). In 2018 we performed a pilot clinical trial and demonstrated that doxycycline treatment decreases the expression of CSC markers in breast cancer tumor samples (85). We thus propose that selected antibiotics, in monotherapy or in combination, may be further studied as interesting drugs for the eradication of CSCs.

From now on, this review concentrates on specific issues concerning cancer cell plasticity in breast cancer, glioblastoma, and melanoma, which represent our expertise and, in our opinion, the most challenging models in this field. A detailed table is then provided reporting the latest knowledge in other tumor models.

CSC PLASTICITY IN BREAST CANCER

Breast cancer has been largely investigated in terms of its etiology (86–89) and still little is known on the mechanisms of its progression. Breast cancer cells commonly gain genetic and epigenetic modifications in their genome (90), contributing to its characteristic intra-tumor heterogeneity (91–96). Intra-tumor heterogeneity is strongly influenced by numerous factors from the tumor microenvironment: breast cancer cells are indeed under continuous selective pressure due to attacks by the immune system or administered therapies (97, 98). This supports breast cancer progression, conferring a competitive advantage to specific subclones (92).

In recent decades, a hierarchical organization has been proposed, where cancer cells with self-renew capacity, the so-called BCSCs, are postulated to be at the top of the tumor pyramid. Al-Hajj et al. in 2003 first isolated a population of BCSCs expressing high levels of CD44 and low levels of CD24 ($CD44^{+}CD24^{-/low}$) and capable to form tumors when injected into immune deficient mice (99). Since then, numerous studies have tested other biomarkers to sort BCSCs: among all, aldehyde dehydrogenase 1 (ALDH1) resulted to be a potentially useful alternative or complement to the $CD44^{+}CD24^{-/low}$ phenotype, particularly in high grade and HER2 positive tumors (100). BCSCs not only possess high tumorigenic properties but represent the cells that mediate tumor metastasis. Indeed, the $CD44^{+}/CD24^{-/low}$ phenotype is highly expressed in triple negative breast cancers (101, 102) and is associated to poor overall survival (103, 104); moreover, it has been reported among cancer cells spread into the bone marrow (105) or to the lung (106) of patients with breast cancer. At present, BCSCs are believed to enter the circulation and become CTCs: indeed, high expression levels of BCSC markers have been found in CTCs (107). Thanks to their capacity of anoikis resistance, CTCs with BCSC phenotype have the potential to seed metastatic lesions (108). Studies from liquid biopsy samples demonstrate that CTCs with a BCSC phenotype are enriched in the group with clinical disease progression (107).

A large number of studies also suggest that BCSCs display resistance to traditional cancer therapies (109–116). Cytotoxic chemotherapies target the bulk of the tumor composed of highly proliferative breast cancer cells and does not affect BCSCs that, over time, cause tumor relapse (81). In addition, genetic alterations may confer to BCSCs intrinsic chemoresistance, including modifications in proteins involved in the detoxification of chemotherapy agents (117). As reported above, BCSCs express high levels of ALDH1, that metabolizes cyclophosphamide, thus minimize its toxic effects (101). Also, tumor microenvironment plays a crucial role in BCSC chemoresistance: in hypoxic conditions, activation of hypoxia induced factors not only promotes the formation of new blood vessel but also a BCSCs quiescent phenotype (118, 119).

CSC PLASTICITY IN GLIOBLASTOMA

Glioblastoma (GBM) is the most frequent and deadly glial tumor (120); it is morphologically (121) and molecularly (97, 122, 123) characterized by high intra- and inter- tumor heterogeneity, which may play a pivotal role in recurrence and therapy resistance (124, 125).

The Cancer Genome Atlas has identified four GBM molecular subtypes: proneural, neural, classical, and mesenchymal (126). However, it has been demonstrated how multiple molecular subtypes may co-exist in the same tumor mass (122) or how GBM presents hybrid states with the expression of a peculiar signature overlapping two molecular subtypes (127). The establishment and the constant evolution of this heterogeneity equilibrium are

due to glioma stem cells (GSCs) (128) and can be influenced by cytotoxic therapies and other endogenous factors (129, 130). However, how GSC heterogeneity is determined still remains unclear; *in-vitro* studies have shown that GSCs preserve their capability for recapitulating their primary heterogeneity also after many cell divisions, and temozolomide (TMZ) does not influence this capacity (131, 132); though, the same cytotoxic drug is able to drive GSCs heterogeneity and further drug resistance (133).

GSCs' isolation and characterization are based on stem markers expression; therefore, their choice is fundamental. One of the first discovered marker was CD133 (134); however, its expression is highly variable (∼20–60%) (135), and also CD133– cells have a clonogenic potential. Indeed, Chen et al. (136) divided GSCs into three subtypes based on malignant potential (MP): type 1 (high MP) and type 3 (mild MP) were CD133−; whereas, type 2 GSCs (moderate MP) were CD133+. An additional marker is CD15, which is more frequently expressed in GBM than CD133; CD15+ GSCs are more clonogenic, proliferative and tumorigenic (137). CD44 represents another reliable marker: indeed, CD44+ GSCs present high tumor-sphere forming and tumorigenic potential, and have the capability to restore the heterogeneity of the parental GBM (138). Furthermore, ALDH1A3+ GSCs, besides having the above mentioned features, express other stem cell markers, such as musashi and nestin, and are able to differentiate into several neural lineages (139, 140), and promote TMZ resistance (141).

Nevertheless, a clear-cut segregation of GBM cells between CSCs and non-CSCs is not possible yet; instead, it is more conceivable the ability of GBM cells to transit among states or the acquisition of intermediate or metastable cellular state, exhibiting a wide and continuous range of CSC signature (142, 143).

CSC PLASTICITY IN MELANOMA

Melanoma represents a significant challenge, with low curative rates (<10%) and poor prognosis (median survival: 6–9 months) in the metastatic stage (144–146). Aggressive melanoma has revealed to co-express specific genes and proteins of multiple cellular types, including embryonic stem cells and endothelial cells, underlying cell plasticity.

3D *in vitro* models demonstrated that melanoma cells are able to form perfusable, vasculogenic-like channels, a biological phenomenon called vasculogenic mimicry (VM) (147). The treatment with endostatin has proved no effect on the inhibition of melanoma VM (148), thus portraying aggressive melanoma as being able to survive by its own perfusion network (149).

On the other hand, a large number of molecular studies jointly revealed a strong stem signature in aggressive melanoma, with still unknown practical significance (150–152). In particular, Nodal, a signaling pathway active in embryonic development, was notably upregulated in more aggressive melanoma (153). The nodal family of proteins, are a subset of the TGFβ superfamily and cooperate to the pluripotency of human embryonic stem cells (154). This observation led researchers to recognize a commonality in the phenotype of aggressive melanoma, linking vascular, embryonic and cancer stem cell properties.

CSC PLASTICITY IN OTHER SOLID TUMORS

Several authors have demonstrated how it is possible to isolate CSCs in most solid malignancies. However, several aspects and molecular features regarding cell stemness still remain uncovered; this means that even if most markers across different cancer are the same (**Table 1**), a common and reliable signature is still lacking, due to technical issues mostly. Nevertheless, in our opinion, a change in clinical trials approach may be of help to overcome this limitation. Indeed, the implementation of biobanks of fresh tissues and biological fluids may represent a precious source for the next future when new techniques and novel approaches will be introduced.

TABLE 1 | CSCs markers in other solid tumors.

Type of cancer	CSCs Markers	References
Head and neck squamous cell carcinoma	ALDH1, BMI1, c-MET, CD44, CD133	(155–159)
Lung cancer	ALDH1A1, ABCG2, BMI1, CD44, CD133, CD87, CD90, CD166, EpCAM, NANOG, NUCLEOSTEMIN, OCT4, PODXL-1, SOX2	(117, 160–163)
Esophageal carcinoma	ALDH1, ABCG2, CD13, CD44, CD90, CD271, INTEGRIN7, ICAM1, LGR5, SOX9	(164)
Gastric cancer	BMI1, CD44, CD54, CD71, CD90, CD133, CD166, LGR5, MUSASHI-1, OCT4, SOX2	(165)
Hepatocellular carcinoma	CD13, CD24, CD34, CD90, CD133, EpCAM, OV-6, SOX9, SOX12	(166–169)
Pancreatic cancer	ALDH1, c-MET, CD24, CD44, CD133, CXCR4, DCLK1, EpCAM, Lgr5	(170)
Colon cancer	ALDH1, CD26, CD29, CD44S, CD166, CXCR4	(171, 172)
Prostate cancer	ALDH7A1, ATXN1, CD24, CD44, PTEN, CD133, GATA3, KLF4, MYC, NKX3-1, TACSTD2, TNFSF11, TNFRSF11B	(50, 52, 173)
Ovarian cancer	ALDH1A1, c-MYC, CD24, CD44, CD117, CD133, CD243, CD338, EpCAM, IL-17R, LIN28, NANOG, OCT4, ROR1, SOX2	(49, 174–180)

Most stemness markers are the same but a universal signature is still lacking.

CONCLUSIONS AND FUTURE DIRECTIONS

Future research studies will be needed in order to improve our understanding of the complex phenomenon of cancer cell plasticity. The recent insights on the role of plasticity in cancer progression and relapse highlights the need to develop new and combinatorial therapies, that aim to: (i) inhibit specific cell markers; (ii) interfere with stemness and EMT signaling pathways; (iii) affect also components of the tumor microenvironment.

AUTHOR CONTRIBUTIONS

GF and AN wrote the paper. CS conceived the idea, supervised, and edited the manuscript. All authors discussed and commented on the manuscript.

REFERENCES

1. Meacham CE, Morrison SJ. Tumour heterogeneity and cancer cell plasticity. *Nature*. (2013) 501:328–37. doi: 10.1038/nature12624
2. Bedard PL, Hansen AR, Ratain MJ, Siu LL. Tumour heterogeneity in the clinic. *Nature*. (2013) 501:355–64. doi: 10.1038/nature12627
3. Nowell P. The clonal evolution of tumor cell populations. *Science*. (1976) 194:23–8. doi: 10.1126/science.959840
4. Baylin SB, Jones PA. A decade of exploring the cancer epigenome — biological and translational implications. *Nat Rev Cancer*. (2011) 11:726–34. doi: 10.1038/nrc3130
5. Easwaran H, Tsai H-C, Baylin Stephen B. Cancer epigenetics: tumor heterogeneity, plasticity of stem-like states, and drug resistance. *Mol. Cell*. (2014) 54:716–27. doi: 10.1016/j.molcel.2014.05.015
6. Xin H, Kong Y, Jiang X, Wang K, Qin X, Miao Z-H, et al. Multiz-drug–resistant cells enriched from chronic myeloid leukemia cells by doxorubicin possess tumor-initiating–cell properties. *J Pharm Sci*. (2013) 122:299–304. doi: 10.1254/jphs.13025FP
7. Duggal R, Minev B, Vescovi A, Szalay A. *Cancer Stem Cell Models and Role in Drug Discovery*. *Stem Cells and Human Diseases*. Dordrecht: Springer. (2011) p. 217–28. doi: 10.1007/978-94-007-2801-1_10
8. Mani SA, Guo W, Liao M-J, Eaton EN, Ayyanan A, Zhou AY, et al. The epithelial-mesenchymal transition generates cells with properties of stem cells. *Cell*. (2008) 133:704–15. doi: 10.1016/j.cell.2008.03.027
9. Morel A-P, Lièvre M, Thomas C, Hinkal G, Ansieau S, Puisieux A. Generation of breast cancer stem cells through epithelial-mesenchymal transition. *PLoS ONE*. (2008) 3:e2888. doi: 10.1371/journal.pone.0002888
10. Wellner U, Schubert J, Burk UC, Schmalhofer O, Zhu F, Sonntag A, et al. The EMT-activator ZEB1 promotes tumorigenicity by repressing stemness-inhibiting microRNAs. *Nat Cell Biol*. (2009) 11:1487–95. doi: 10.1038/ncb1998
11. Gupta PB, Chaffer CL, Weinberg RA. Cancer stem cells: mirage or reality? *Nat Med*. (2009) 15:1010–2. doi: 10.1038/nm0909-1010
12. Liu S, Cong Y, Wang D, Sun Y, Deng L, Liu Y, et al. Breast cancer stem cells transition between epithelial and mesenchymal states reflective of their normal counterparts. *Stem Cell Rep*. (2014) 2:78–91. doi: 10.1016/j.stemcr.2013.11.009
13. Beerling E, Seinstra D, de Wit E, Kester L, van der Velden D, Maynard C, et al. Plasticity between epithelial and mesenchymal states unlinks EMT from metastasis-enhancing stem cell capacity. *Cell Rep*. (2016) 14:2281–8. doi: 10.1016/j.celrep.2016.02.034
14. Ye X, Brabletz T, Kang Y, Longmore GD, Nieto MA, Stanger BZ, et al. Upholding a role for EMT in breast cancer metastasis. *Nature*. (2017) 547:E1–3. doi: 10.1038/nature22816
15. Scheel C, Weinberg RA. Cancer stem cells and epithelial–mesenchymal transition: concepts and molecular links. *Semin Cancer Biol*. (2012) 22:396–403. doi: 10.1016/j.semcancer.2012.04.001
16. La Ferla M, Lessi F, Aretini P, Pellegrini D, Franceschi S, Tantillo E, et al. ANKRD44 gene silencing: a putative role in trastuzumab resistance in Her2-like breast cancer. *Front Oncol*. (2019) 9:547. doi: 10.3389/fonc.2019.00547
17. Grosse-Wilde A, Fouquier d'Hérouël A, McIntosh E, Ertaylan G, Skupin A, Kuestner RE, et al. Stemness of the hybrid epithelial/mesenchymal state in breast cancer and its association with poor survival. *PLoS ONE*. (2015) 10:e0126522. doi: 10.1371/journal.pone.0126522
18. Ruscetti M, Quach B, Dadashian EL, Mulholland DJ, Wu H. Tracking and functional characterization of epithelial-mesenchymal transition and mesenchymal tumor cells during prostate cancer metastasis. *Cancer Res*. (2015) 75:2749–59. doi: 10.1158/0008-5472.CAN-14-3476
19. Pastushenko I, Brisebarre A, Sifrim A, Fioramonti M, Revenco T, Boumahdi S, et al. Identification of the tumour transition states occurring during EMT. *Nature*. (2018) 556:463–8. doi: 10.1038/s41586-018-0040-3
20. Rompolas P, Mesa KR, Greco V. Spatial organization within a niche as a determinant of stem-cell fate. *Nature*. (2013) 502:513–8. doi: 10.1038/nature12602
21. Merrell AJ, Stanger BZ. Adult cell plasticity *in vivo*: de-differentiation and transdifferentiation are back in style. *Nat Rev Mol Cell Biol*. (2016) 17:413–25. doi: 10.1038/nrm.2016.24
22. Ge Y, Fuchs E. Stretching the limits: from homeostasis to stem cell plasticity in wound healing and cancer. *Nat Rev Genetics*. (2018) 19:311–25. doi: 10.1038/nrg.2018.9
23. Siravegna G, Mussolin B, Buscarino M, Corti G, Cassingena A, Crisafulli G, et al. Clonal evolution and resistance to EGFR blockade in the blood of colorectal cancer patients. *Nat Med*. (2015) 795–801. doi: 10.1038/nm.3870
24. Diaz LA, Williams RT, Wu J, Kinde I, Hecht JR, Berlin J., et al. The molecular evolution of acquired resistance to targeted EGFR blockade in colorectal cancers. *Nature*. (2012) 486:537–40. doi: 10.1038/nature11219
25. Russo M, Siravegna G, Blaszkowsky LS, Corti G, Crisafulli G, Ahronian LG., et al. Tumor heterogeneity and lesion-specific response to targeted therapy in colorectal cancer. *Cancer Discov*. (2015) 6:147–53. doi: 10.1158/2159-8290.CD-15-1283
26. Murtaza M, Dawson SJ, Pogrebniak K, Rueda OM, Provenzano E, Grant J., et al. Multifocal clonal evolution characterized using circulating tumour DNA in a case of metastatic breast cancer. *Nat Commun*. (2015) 6:8760. doi: 10.1038/ncomms9760
27. Morelli MP, Overman MJ, Dasari A, Kazmi SM, Mazard T, Vilar E., et al. Characterizing the patterns of clonal selection in circulating tumor DNA from patients with colorectal cancer refractory to anti- EGFR treatment. *Ann Oncol*. (2015) 26:731–6. doi: 10.1093/annonc/mdv005
28. Indraccolo S, Lombardi G, Fassan M, Pasqualini L, Giunco S, Marcato R., et al. Genetic, epigenetic, and immunologic profiling of MMR-deficient relapsed glioblastoma. *Clin Cancer Res*. (2019) 25:1828–37. doi: 10.1158/1078-0432.CCR-18-1892
29. Salvianti F, Canu L, Poli G, Armignacco R, Scatena C, Cantini G, et al. New insights in the clinical and translational relevance of miR483-5p in adrenocortical cancer. *Oncotarget*. (2017) 8:65525–33. doi: 10.18632/oncotarget.19118
30. Fanelli GN, Gasparini P, Coati I, Cui R, Pakula H, Chowdhury B, et al. LONG-NONCODING RNAs in gastroesophageal cancers. *Noncoding RNA Res*. (2018) 3:195–212. doi: 10.1016/j.ncrna.2018.10.001
31. Del Re M, Bertolini I, Crucitta S, Fontanelli L, Rofi E, De Angelis C, et al. Overexpression of TK1 and CDK9 in plasma-derived exosomes is associated with clinical resistance to CDK4/6 inhibitors in metastatic breast cancer patients. *Breast Cancer Res Treat*. (2019) 178:57–62. doi: 10.1007/s10549-019-05365-y
32. Saraggi D, Galuppini F, Fanelli GN, Remo A, Urso EDL, Bao RQ, et al. MiR-21 up-regulation in ampullary adenocarcinoma and its pre-invasive lesions. *Pathol Res Pract*. (2018) 214:835–9. doi: 10.1016/j.prp.2018.04.018
33. Fassan M, Facchin S, Munari G, Fanelli GN, Lorenzon G, Savarino E. Noncoding RNAs as drivers of the phenotypic plasticity of

oesophageal mucosa. *World J Gastroenterol*. (2017) 23:7653–6. doi: 10.3748/wjg.v23.i43.7653
34. Palmirotta R, Lovero D, Cafforio P, Felici C, Mannavola F, Pelle E, et al. Liquid biopsy of cancer: a multimodal diagnostic tool in clinical oncology. *Ther Adv Med Oncol*. (2018) doi: 10.1177/1758835918794630
35. Krebs MG, Metcalf RL, Carter L, Brady G, Blackhall FH, Dive C. Molecular analysis of circulating tumour cells — biology and biomarkers. *Nat Rev Clin Oncol*. (2014) 11:129–144. doi: 10.1038/nrclinonc.2013.253
36. Cristofanilli M, Budd GT, Ellis MJ, Stopeck A, Matera J, Miller MC., et al. Circulating tumor cells, disease progression, and survival in metastatic breast cancer. *N Engl J Med*. (2004) 351:781–91. doi: 10.1056/NEJMoa040766
37. Mazzini C, Pinzani P, Salvianti F, Scatena C, Paglierani M, Ucci F, et al. Circulating tumor cells detection and counting in uveal melanomas by a filtration-based method. *Cancers*. (2014) 6:323–32. doi: 10.3390/cancers6010323
38. Pinzani P, Scatena C, Salvianti F, Corsini E, Canu L, Poli G, et al. Detection of circulating tumor cells in patients with adrenocortical carcinoma: a monocentric preliminary study. *J Clin Endocrinol Metab*. (2013) 98:3731–8. doi: 10.1210/jc.2013-1396
39. Arya SK, Lim B, Rahman ARA. Enrichment, detection and clinical significance of circulating tumor cells. *Lab Chip*. (2013) 13:1995. doi: 10.1039/c3lc00009e
40. van der Toom EE, Verdone JE, Gorin MA, Pienta KJ. Technical challenges in the isolation and analysis of circulating tumor cells. *Oncotarget*. (2016) 7:62754–66. doi: 10.18632/oncotarget.11191
41. Alix-Panabières C, Pantel K. Challenges in circulating tumour cell research. *Nat Rev Cancer*. (2014) 14:623–31. doi: 10.1038/nrc3820
42. Schneck H, Gierke B, Uppenkamp F, Behrens B, Niederacher D, Stoecklein NH, et al. EpCAM-independent enrichment of circulating tumor cells in metastatic breast cancer. *PLoS ONE*. (2015) 10:e0144535. doi: 10.1371/journal.pone.0144535
43. Messaritakis I, Stoltidis D, Kotsakis A, Dermitzaki E-K, Koinis F, Lagoudaki E, et al. TTF-1- and/or CD56-positive circulating tumor cells in patients with small cell lung cancer (SCLC). *Sci Rep*. (2017) 7:45351. doi: 10.1038/srep45351
44. Beije N, Onstenk W, Kraan J, Sieuwerts AM, Hamberg P, Dirix LY, et al. Prognostic impact of HER2 and ER status of circulating tumor cells in metastatic breast cancer patients with a HER2-negative primary tumor. *Neoplasia*. (2016) 18:647–53. doi: 10.1016/j.neo.2016.08.007
45. Yadavalli S, Jayaram S, Manda SS, Madugundu AK, Nayakanti DS, Tan TZ, et al. Data-driven discovery of extravasation pathway in circulating tumor cells. *Sci Rep*. (2017) 7:43710. doi: 10.1038/srep43710
46. Correnti M, Raggi C. Stem-like plasticity and heterogeneity of circulating tumor cells: current status and prospect challenges in liver cancer. *Oncotarget*. (2016) 8:7094–115. doi: 10.18632/oncotarget.12569
47. Aktas B, Tewes M, Fehm T, Hauch S, Kimmig R, Kasimir-Bauer S. Stem cell and epithelial-mesenchymal transition markers are frequently overexpressed in circulating tumor cells of metastatic breast cancer patients. *Breast Cancer Res*. (2009) 11:R46. doi: 10.1186/bcr2333
48. Tam WL, Weinberg RA. The epigenetics of epithelial-mesenchymal plasticity in cancer. *Nat Med*. (2013) 19:1438–49. doi: 10.1038/nm.3336
49. Blassl C, Kuhlmann JD, Webers A, Wimberger P, Fehm T, Neubauer H. Gene expression profiling of single circulating tumor cells in ovarian cancer—establishment of a multi-marker gene panel. *Mol Oncol*. (2016) 10:1030–42. doi: 10.1016/j.molonc.2016.04.002
50. Powell AA, Talasaz AH, Zhang H, Coram MA, Reddy A, Deng G., et al. Single cell profiling of circulating tumor cells: transcriptional heterogeneity and diversity from breast cancer cell lines. *PLoS ONE*. (2012) 7: e33788. doi: 10.1371/journal.pone.0033788
51. Miyamoto DT, Lee RJ, Kalinich M, LiCausi JA, Zheng Y, Chen T., et al. An RNA-based digital circulating tumor cell signature is predictive of drug response and early dissemination in prostate cancer. *Cancer Discov*. (2018) 8:288–303. doi: 10.1158/2159-8290.CD-16-1406
52. Gorges TM, Kuske A, Röck K, Mauermann O, Müller V, Peine S., et al. Accession of tumor heterogeneity by multiplex transcriptome profiling of single circulating tumor cells. *Clin Chem*. (2016) 62:1504–1515. doi: 10.1373/clinchem.2016.260299
53. LoPiccolo J, Blumenthal GM, Bernstein WB, Dennis PA. Targeting the PI3K/Akt/mTOR pathway: effective combinations and clinical considerations. *Drug Resist Updat*. (2008) 11:32–50. doi: 10.1016/j.drup.2007.11.003
54. Yeung TM, Gandhi SC, Wilding JL, Muschel R, Bodmer WF. Cancer stem cells from colorectal cancer-derived cell lines. *Proc Natl Acad Sci USA*. (2010) 107:3722–7. doi: 10.1073/pnas.0915135107
55. Alix-Panabières C, Pantel K. Clinical applications of circulating tumor cells and circulating tumor dna as liquid biopsy. *Cancer Discovery*. (2016) 6:479–91. doi: 10.1158/2159-8290.CD-15-1483
56. Lin M, Chen J-F, Lu Y-T, Zhang Y, Song J, Hou S, et al. Nanostructure embedded microchips for detection, isolation, and characterization of circulating tumor cells. *Acc Chem Res*. (2014) 47:2941–50. doi: 10.1021/ar5001617
57. Ming Y, Li Y, Xing H, Luo M, Li Z, Chen J, et al. Circulating tumor cells: from theory to nanotechnology-based detection. *Front Pharmacol*. (2017) 8:35. doi: 10.3389/fphar.2017.00035
58. Abonnenc M, Manaresi N, Borgatti M, Medoro G, Fabbri E, Romani A, et al. Programmable interactions of functionalized single bioparticles in a dielectrophoresis-based microarray chip. *Anal Chem*. (2013) 85:8219–24. doi: 10.1021/ac401296m
59. Ting DT, Wittner BS, Ligorio M, Vincent Jordan N, Shah AM, Miyamoto DT., et al. Single-cell RNA sequencing identifies extracellular matrix gene expression by pancreatic circulating tumor cells. *Cell Rep*. (2014) 8:1905–18. doi: 10.1016/j.celrep.2014.08.029
60. Giuliano M, Shaikh A, Lo HC, Arpino G, De Placido S, Zhang XH, et al. Perspective on circulating tumor cell clusters: why it takes a village to metastasize. *Cancer Res*. (2018) 78:845–52. doi: 10.1158/0008-5472.CAN-17-2748
61. Li L, Cole J, Margolin DA. Cancer stem cell and stromal microenvironment. *Ochsner J*. (2013) 13:109–18. doi: 10.1002/9781118356203.ch21
62. Cazet AS, Hui MN, Elsworth BL, Wu SZ, Roden D, Chan CL, et al. Targeting stromal remodeling and cancer stem cell plasticity overcomes chemoresistance in triple negative breast cancer. *Nat Commun*. (2018) 9:2897. doi: 10.1038/s41467-018-05220-6
63. Park TS, Donnenberg VS, Donnenberg AD, Zambidis ET, Zimmerlin L. Dynamic interactions between cancer stem cells and their stromal partners. *Curr Pathobiol Rep*. (2014) 2:41–52. doi: 10.1007/s40139-013-0036-5
64. Krause S, Maffini MV, Soto AM, Sonnenschein C. A novel 3D *in vitro* culture model to study stromal-epithelial interactions in the mammary gland. *Tissue Eng Part C Methods*. (2008) 14:261–71. doi: 10.1089/ten.tec.2008.0030
65. Fang X, Sittadjody S, Gyabaah K, Opara EC, Balaji KC. Novel 3D co-culture model for epithelial-stromal cells interaction in prostate cancer. *PLoS ONE*. (2013) 8:e75187. doi: 10.1371/journal.pone.0075187
66. Lang SH, Stower M, Maitland NJ. *In vitro* modelling of epithelial and stromal interactions in non-malignant and malignant prostates. *Br J Cancer*. (2000) 82:990–7. doi: 10.1054/bjoc.1999.1029
67. Ashworth TR. A case of cancer in which cells similar to those in the tumours where seen in the blood after death. *Australian Med J*. (1869) 14:146–7.
68. Krebs MG, Hou JM, Ward TH, Blackhall FH, Dive C. Circulating tumour cells: their utility in cancer management and predicting outcomes. *Ther Adv Med Oncol*. (2010) 2:351–65. doi: 10.1177/1758834010378414
69. Sprenger T, Conradi LC, Beissbarth T, Ermert H, Homayounfar K, Middel P, et al. Enrichment of CD133-expressing cells in rectal cancers treated with preoperative radiochemotherapy is an independent marker for metastasis and survival. *Cancer*. (2013) 119:26–35. doi: 10.1002/cncr.27703
70. Lin S, Xu Y, Gan Z, Han K, Hu H, Yao Y, et al. Monitoring cancer stem cells: insights into clinical oncology. *Onco Targets Ther*. (2016) 9:731–40. doi: 10.2147/OTT.S96645
71. Alvarado AG, Thiagarajan PS, Mulkearns-Hubert EE, Silver DJ, Hale JS, Alban TJ, et al. Glioblastoma cancer stem cells evade innate immune suppression of self-renewal through reduced TLR4 expression. *Cell Stem Cell*. (2017) 20:450–61.e4. doi: 10.1016/j.stem.2016.12.001
72. Lathia JD, Mack SC, Mulkearns-Hubert EE, Valentim CL, Rich JN. Cancer stem cells in glioblastoma. *Genes Dev*. (2015) 29:1203–17. doi: 10.1101/gad.261982.115

73. Sundar SJ, Hsieh JK, Manjila S, Lathia JD, Sloan A. The role of cancer stem cells in glioblastoma. *Neurosurg Focus*. (2014) 37:E6. doi: 10.3171/2014.9.FOCUS14494
74. Turaga SM, Lathia JD. Adhering towards tumorigenicity: altered adhesion mechanisms in glioblastoma cancer stem cells. *CNS Oncol*. (2016) 5:251–9. doi: 10.2217/cns-2016-0015
75. Tsai JH, Yang J. Epithelial-mesenchymal plasticity in carcinoma metastasis. *Genes Dev*. (2013) 27:2192–206. doi: 10.1101/gad.225334.113
76. Reka AK, Kuick R, Kurapati H, Standiford TJ, Omenn GS, Keshamouni VG. Identifying inhibitors of epithelial-mesenchymal transition by connectivity map–based systems approach. *J Thorac Oncol*. (2011) 6:1784–92. doi: 10.1097/JTO.0b013e31822adfb0
77. Chua K-N, Sim W-J, Racine V, Lee S-Y, Goh BC, Thiery JP. A cell-based small molecule screening method for identifying inhibitors of epithelial-mesenchymal transition in carcinoma. *PLoS ONE*. (2012) 7:e33183. doi: 10.1371/journal.pone.0033183
78. Sansone P, Storci G, Tavolari S, Guarnieri T, Giovannini C, Taffurelli M, et al. IL-6 triggers malignant features in mammospheres from human ductal breast carcinoma and normal mammary gland. *J Clin Invest*. (2007) 117:3988–4002. doi: 10.1172/JCI32533
79. Korkaya H, Liu S, Wicha MS. Regulation of cancer stem cells by cytokine networks: attacking cancer's inflammatory roots. *Clin Cancer Res*. (2011) 17:6125–9. doi: 10.1158/1078-0432.CCR-10-2743
80. Ginestier C, Liu S, Diebel ME, Korkaya H, Luo M, Brown M, et al. CXCR1 blockade selectively targets human breast cancer stem cells *in vitro* and in xenografts. *J Clin Invest*. (2010) 120:485–97. doi: 10.1172/JCI39397
81. Li X, Lewis MT, Huang J, Gutierrez C, Osborne CK, Wu MF, et al. Intrinsic resistance of tumorigenic breast cancer cells to chemotherapy. *J Natl Cancer Inst*. (2008) 100:672–9. doi: 10.1093/jnci/djn123
82. Chiotaki R, Polioudaki H, Theodoropoulos PA. Cancer stem cells in solid and liquid tissues of breast cancer patients: characterization and therapeutic perspectives. *Curr Cancer Drug Targets*. (2015) 15:256–69. doi: 10.2174/1568009615666150211102503
83. Peiris-Pagès M, Martinez-Outschoorn UE, Pestell RG, Sotgia F, Lisanti MP. Cancer stem cell metabolism. *Breast Cancer Res*. (2016) 18:55. doi: 10.1186/s13058-016-0712-6
84. Lamb R, Ozsvari B, Lisanti CL, Tanowitz HB, Howell A, Martinez-Outschoorn UE, et al. Antibiotics that target mitochondria effectively eradicate cancer stem cells, across multiple tumor types: treating cancer like an infectious disease. *Oncotarget*. (2015) 6:4569–84. doi: 10.18632/oncotarget.3174
85. Scatena C, Roncella M, Di Paolo A, Aretini P, Menicagli M, Fanelli G, et al. Doxycycline, an inhibitor of mitochondrial biogenesis, effectively reduces cancer stem cells (CSCs) in early breast cancer patients: a clinical pilot study. *Front Oncol*. (2018) 8:452. doi: 10.3389/fonc.2018.00452
86. Fernandez SV, Russo J. Estrogen and xenoestrogens in breast cancer. *Toxicol Pathol*. (2009) 38:110–22. doi: 10.1177/0192623309354108
87. Naccarato AG, Lessi F, Zavaglia K, Scatena C, Hamad MAA, Aretini P, et al. Mouse mammary tumor virus (MMTV) - like exogenous sequences are associated with sporadic but not hereditary human breast carcinoma. *Aging*. (2019) 11:7236–41. doi: 10.18632/aging.102252
88. Mazzanti CM, Lessi F, Armogida I, Zavaglia K, Franceschi S, Hamad MAL, et al. Human saliva as route of inter-human infection for mouse mammary tumor virus. *Oncotarget*. (2015) 6:18355–63. doi: 10.18632/oncotarget.4567
89. Mazzanti CM, Al Hamad M, Fanelli G, Scatena C, Zammarchi F, Zavaglia K, et al. A mouse mammary tumor virus env-like exogenous sequence is strictly related to progression of human sporadic breast carcinoma. *Am J Pathol*. (2011) 179:2083–90. doi: 10.1016/j.ajpath.2011.06.046
90. Vogelstein B, Papadopoulos N, Velculescu VE, Zhou S, Diaz LA, Kinzler KW. Cancer genome landscapes. *Science*. (2013) 339:1546–58. doi: 10.1126/science.1235122
91. Marjanovic ND, Weinberg RA, Chaffer CL. Cell plasticity and heterogeneity in cancer. *Clin Chem*. (2012) 59:168–79. doi: 10.1373/clinchem.2012.184655
92. Prasetyanti PR, Medema JP. Intra-tumor heterogeneity from a cancer stem cell perspective. *Mol Cancer*. (2017) 16:41. doi: 10.1186/s12943-017-0600-4
93. Medema JP, Vermeulen L. Microenvironmental regulation of stem cells in intestinal homeostasis and cancer. *Nature*. (2011) 474:318–26. doi: 10.1038/nature10212
94. Junttila MR, de Sauvage FJ. Influence of tumour micro-environment heterogeneity on therapeutic response. *Nature*. (2013) 501:346–54. doi: 10.1038/nature12626
95. Lu P, Weaver VM, Werb Z. The extracellular matrix: a dynamic niche in cancer progression. *J Cell Biol*. (2012) 196:395–406. doi: 10.1083/jcb.201102147
96. Lessi F, Scatena C, Aretini P, Menicagli M, Franceschi S, Naccarato AG, et al. Molecular profiling of microinvasive breast cancer microenvironment progression. *J Transl Med*. (2019) 17:187. doi: 10.1186/s12967-019-1936-x
97. McGranahan N, Swanton C. Clonal heterogeneity and tumor evolution: past, present, and the future. *Cell*. (2017) 168:613–28. doi: 10.1016/j.cell.2017.01.018
98. Colak S, Medema JP. Cancer stem cells - important players in tumor therapy resistance. *FEBS J*. (2014) 281:4779–91. doi: 10.1111/febs.13023
99. Al-Hajj M, Wicha MS, Benito-Hernandez A, Morrison SJ, Clarke MF. Prospective identification of tumorigenic breast cancer cells. *Proc Natl Acad Sci USA*. (2003) 100:3983–8. doi: 10.1073/pnas.0530291100
100. Ricardo S, Vieira AF, Gerhard R, Leitao D, Pinto R, Cameselle-Teijeiro JF, et al. Breast cancer stem cell markers CD44, CD24 and ALDH1: expression distribution within intrinsic molecular subtype. *J Clin Pathol*. (2011) 64:937–46. doi: 10.1136/jcp.2011.090456
101. Croker AK, Allan AL. Inhibition of aldehyde dehydrogenase (ALDH) activity reduces chemotherapy and radiation resistance of stem-like ALDHhiCD44+ human breast cancer cells. *Breast Cancer Res Treat*. (2011) 133:75–87. doi: 10.1007/s10549-011-1692-y
102. Croker AK, Goodale D, Chu J, Postenka C, Hedley BD, Hess DA, et al. High aldehyde dehydrogenase and expression of cancer stem cell markers selects for breast cancer cells with enhanced malignant and metastatic ability. *J Cell Mol Med*. (2008) 13:2236–52. doi: 10.1111/j.1582-4934.2008.00455.x
103. Liu R, Wang X, Chen GY, Dalerba P, Gurney A, Hoey T, et al. The prognostic role of a gene signature from tumorigenic breast-cancer cells. *N Engl J Med*. (2007) 356:217–26. doi: 10.1056/NEJMoa063994
104. Honeth G, Bendahl P-O, Ringnér M, Saal LH, Gruvberger-Saal SK, Lövgren K, et al. The CD44+/CD24-phenotype is enriched in basal-like breast tumors. *Breast Cancer Res*. (2008) 10:R53. doi: 10.1186/bcr2108
105. Balic M, Lin H, Young L, Hawes D, Giuliano A, McNamara G, et al. Most early disseminated cancer cells detected in bone marrow of breast cancer patients have a putative breast cancer stem cell phenotype. *Clin Cancer Res*. (2006) 12:5615–21. doi: 10.1158/1078-0432.CCR-06-0169
106. Liu H, Patel MR, Prescher JA, Patsialou A, Qian D, Lin J, et al. Cancer stem cells from human breast tumors are involved in spontaneous metastases in orthotopic mouse models. *Proc Natl Acad Sci USA*. (2010) 107:18115–20. doi: 10.1073/pnas.1006732107
107. Baccelli I, Schneeweiss A, Riethdorf S, Stenzinger A, Schillert A, Vogel V., et al. Identification of a population of blood circulating tumor cells from breast cancer patients that initiates metastasis in a xenograft assay. *Nat Biotechnol*. (2013) 31:539–44. doi: 10.1038/nbt.2576
108. Batlle E, Clevers H. Cancer stem cells revisited. *Nat Med*. (2017) 23:1124–34. doi: 10.1038/nm.4409
109. Phillips HS, Kharbanda S, Chen R, Forrest WF, Soriano RH, Wu TD, et al. Molecular subclasses of high-grade glioma predict prognosis, delineate a pattern of disease progression, and resemble stages in neurogenesis. *Cancer Cell*. (2006) 9:157–73. doi: 10.1016/j.ccr.2006.02.019
110. Lagadec C, Vlashi E, Della Donna L, Meng Y, Dekmezian C, Kim K, et al. Survival and self-renewing capacity of breast cancer initiating cells during fractionated radiation treatment. *Breast Cancer Res*. (2010) 12:R13. doi: 10.1186/bcr2479
111. Karimi-Busheri F, Rasouli-Nia A, Mackey JR, Weinfeld M. Senescence evasion by MCF-7 human breast tumor-initiating cells. *Breast Cancer Res*. (2010) 12:R31. doi: 10.1186/bcr2583
112. Fillmore CM, Kuperwasser C. Human breast cancer cell lines contain stem-like cells that self-renew, give rise to phenotypically diverse progeny and survive chemotherapy. *Breast Cancer Res*. (2008) 10:R25. doi: 10.1186/bcr1982
113. Shafee N, Smith CR, Wei S, Kim Y, Mills GB, Hortobagyi GN, et al. Cancer stem cells contribute to cisplatin resistance in Brca1/p53-mediated mouse mammary tumors. *Cancer Res*. (2008) 68:3243–50. doi: 10.1158/0008-5472.CAN-07-5480

114. Diehn M, Cho RW, Lobo NA, Kalisky T, Dorie MJ, Kulp AN, et al. Association of reactive oxygen species levels and radioresistance in cancer stem cells. *Nature*. (2009) 458:780–3. doi: 10.1038/nature07733
115. Yu F, Yao H, Zhu P, Zhang X, Pan Q, Gong C, et al. let-7 regulates self-renewal and tumorigenicity of breast cancer cells. *Cell*. (2007) 131:1109–23. doi: 10.1016/j.cell.2007.10.054
116. Zielske SP, Spalding AC, Wicha MS, Lawrence TS. Ablation of breast cancer stem cells with radiation. *Transl Oncol*. (2011) 4:227–33. doi: 10.1593/tlo.10247
117. Hirschmann-Jax C, Foster AE, Wulf GG, Nuchtern JG, Jax TW, Gobel U, et al. A distinct "side population" of cells with high drug efflux capacity in human tumor cells. *Proc Natl Acad Sci USA*. (2004) 101:14228–33. doi: 10.1073/pnas.0400067101
118. Crowder SW, Balikov DA, Hwang Y-S, Sung H-J. Cancer stem cells under hypoxia as a chemoresistance factor in the breast and brain. *Curr Pathobiol Rep*. (2014) 2:33–40. doi: 10.1007/s40139-013-0035-6
119. Mimeault M, Batra SK. Hypoxia-inducing factors as master regulators of stemness properties and altered metabolism of cancer- and metastasis-initiating cells. *J Cell Mol Med*. (2013) 17:30–54. doi: 10.1111/jcmm.12004
120. Kirkpatrick JP, Laack NN, Shih HA, Gondi V. Management of GBM: a problem of local recurrence. *J Neuro Oncol*. (2017) 134:487–93. doi: 10.1007/s11060-016-2347-y
121. Jung CS, Unterberg AW, Hartmann C. Diagnostic markers for glioblastoma. *Histol Histopathol*. (2011) 26:1327–41. doi: 10.14670/HH-26.1327
122. Sottoriva A, Spiteri I, Piccirillo SGM, Touloumis A, Collins VP, Marioni JC, et al. Intratumor heterogeneity in human glioblastoma reflects cancer evolutionary dynamics. *Proc Natl Acad Sci USA*. (2013) 110:4009–14. doi: 10.1073/pnas.1219747110
123. Turtoi A, Musmeci D, Naccarato AG, Scatena C, Ortenzi V, Kiss R, et al. Sparc-like protein 1 is a new marker of human glioma progression. *J Proteome Res*. (2012) 11:5011–21. doi: 10.1021/pr3005698
124. Franceschi S, Lessi F, Aretini P, Ortenzi V, Scatena C, Menicagli M, et al. Cancer astrocytes have a more conserved molecular status in long recurrence free survival (RFS) IDH1 wild-type glioblastoma patients: new emerging cancer players. *Oncotarget*. (2018) 9:24014–27. doi: 10.18632/oncotarget.25265
125. Franceschi S, Mazzanti CM, Lessi F, Aretini P, Carbone FG, La Ferla M, et al. Investigating molecular alterations to profile short- and long-term recurrence-free survival in patients with primary glioblastoma. *Oncol Lett*. (2015) 10:3599–606. doi: 10.3892/ol.2015.3738
126. Verhaak RG, Hoadley KA, Purdom E, Wang V, Qi Y, Wilkerson MD, et al. Integrated genomic analysis identifies clinically relevant subtypes of glioblastoma characterized by abnormalities in PDGFRA, IDH1, EGFR, and NF1. *Cancer Cell*. (2010) 17:98–110. doi: 10.1016/j.ccr.2009.12.020
127. Meyer M, Reimand J, Lan X, Head R, Zhu X, Kushida M, et al. Single cell-derived clonal analysis of human glioblastoma links functional and genomic heterogeneity. *Proc Natl Acad Sci USA*. (2015) 112:851–6. doi: 10.1073/pnas.1320611111
128. Singh SK, Clarke ID, Hide T, Dirks PB. Cancer stem cells in nervous system tumors. *Oncogene*. (2004) 23:7267–73. doi: 10.1038/sj.onc.1207946
129. Baysan M, Woolard K, Bozdag S, Riddick G, Kotliarova S, Cam MC, et al. Micro-environment causes reversible changes in DNA methylation and mRNA expression profiles in patient-derived glioma stem cells. *PLoS ONE*. (2014) 9:e94045. doi: 10.1371/journal.pone.0094045
130. Bhat Krishna PL, Balasubramaniyan V, Vaillant B, Ezhilarasan R, Hummelink K, Hollingsworth F, et al. Mesenchymal differentiation mediated by NF-κB promotes radiation resistance in glioblastoma. *Cancer Cell*. (2013) 24:331–46. doi: 10.1016/j.ccr.2013.08.001
131. Brown DV, Filiz G, Daniel PM, Hollande F, Dworkin S, Amiridis S, et al. Expression of CD133 and CD44 in glioblastoma stem cells correlates with cell proliferation, phenotype stability and intra-tumor heterogeneity. *PLOS ONE*. (2017) 12:e0172791. doi: 10.1371/journal.pone.0172791
132. Sugimori M, Hayakawa Y, Boman BM, Fields JZ, Awaji M, Kozano H, et al. Discovery of power-law growth in the self-renewal of heterogeneous glioma stem cell populations. *PLoS ONE*. (2015) 10:e0135760. doi: 10.1371/journal.pone.0135760
133. Welker AM, Jaros BD, An M, Beattie CE. Changes in tumor cell heterogeneity after chemotherapy treatment in a xenograft model of glioblastoma. *Neuroscience*. (2017) 356:35–43. doi: 10.1016/j.neuroscience.2017.05.010
134. Uchida N, Buck DW, He D, Reitsma MJ, Masek M, Phan TV, et al. Direct isolation of human central nervous system stem cells. *Proc Natl Acad Sci USA*. (2000) 97:14720–5. doi: 10.1073/pnas.97.26.14720
135. Holmberg Olausson K, Maire CL, Haidar S, Ling J, Learner E, Nistér M, et al. Prominin-1 (CD133) defines both stem and non-stem cell populations in CNS development and gliomas. *PLoS ONE*. (2014) 9:e106694. doi: 10.1371/journal.pone.0106694
136. Chen R, Nishimura MC, Bumbaca SM, Kharbanda S, Forrest WF, Kasman IM, et al. A hierarchy of self-renewing tumor-initiating cell types in glioblastoma. *Cancer Cell*. (2010) 17:362–75. doi: 10.1016/j.ccr.2009.12.049
137. Son MJ, Woolard K, Nam D-H, Lee J, Fine HA. SSEA-1 is an enrichment marker for tumor-initiating cells in human glioblastoma. *Cell Stem Cell*. (2009) 4:440–52. doi: 10.1016/j.stem.2009.03.003
138. Jijiwa M, Demir H, Gupta S, Leung C, Joshi K, Orozco N, et al. CD44v6 regulates growth of brain tumor stem cells partially through the AKT-mediated pathway. *PLoS ONE*. (2011) 6:e24217. doi: 10.1371/journal.pone.0024217
139. Choi SA, Lee JY, Phi JH, Wang K-C, Park C-K, Park S-H, et al. Identification of brain tumour initiating cells using the stem cell marker aldehyde dehydrogenase. *Eur J Cancer*. (2014) 50:137–49. doi: 10.1016/j.ejca.2013.09.004
140. Rasper M, Schafer A, Piontek G, Teufel J, Brockhoff G, Ringel F, et al. Aldehyde dehydrogenase 1 positive glioblastoma cells show brain tumor stem cell capacity. *Neuro Oncol*. (2010) 12:1024–33. doi: 10.1093/neuonc/noq070
141. Schafer A, Teufel J, Ringel F, Bettstetter M, Hoepner I, Rasper M, et al. Aldehyde dehydrogenase 1A1–a new mediator of resistance to temozolomide in glioblastoma. *Neuro Oncol*. (2012) 14:1452–64. doi: 10.1093/neuonc/nos270
142. Chambers I, Silva J, Colby D, Nichols J, Nijmeijer B, Robertson M, et al. Nanog safeguards pluripotency and mediates germline development. *Nature*. (2007) 450:1230–4. doi: 10.1038/nature06403
143. Hayashi K, Lopes SMCdS, Tang F, Surani MA. Dynamic equilibrium and heterogeneity of mouse pluripotent stem cells with distinct functional and epigenetic states. *Cell Stem Cell*. (2008) 3:391–401. doi: 10.1016/j.stem.2008.07.027
144. Song X, Zhao Z, Barber B, Farr AM, Ivanov B, Novich M. Overall survival in patients with metastatic melanoma. *Curr Med Res Opin*. (2015) 31:987–91. doi: 10.1185/03007995.2015.1021904
145. Falanga A, Marchetti M, Massi D, Merelli B, Verzeroli C, Russo L, et al. Thrombophilic status may predict prognosis in patients with metastatic BRAFV600-mutated melanoma who are receiving BRAF inhibitors. *J Am Acad Dermatol*. (2016) 74:1254–6.e4. doi: 10.1016/j.jaad.2015.11.006
146. Massi D, Simi L, Sensi E, Baroni G, Xue G, Scatena C, et al. Immunohistochemistry is highly sensitive and specific for the detection of NRASQ61R mutation in melanoma. *Mod Pathol*. (2014) 28:487–97. doi: 10.1038/modpathol.2014.137
147. Maniotis AJ, Folberg R, Hess A, Seftor EA, Gardner LMG, Pe'er J, et al. Vascular channel formation by human melanoma cells *in vivo* and *in vitro*: vasculogenic mimicry. *Am J Pathol*. (1999) 155:739–52. doi: 10.1016/S0002-9440(10)65173-5
148. van der Schaft DWJ, Seftor REB, Seftor EA, Hess AR, Gruman LM, Kirschmann DA, et al. Effects of angiogenesis inhibitors on vascular network formation by human endothelial and melanoma cells. *JNCI J Natl Cancer Inst*. (2004) 96:1473–7. doi: 10.1093/jnci/djh267
149. Hendrix MJC, Seftor EA, Hess AR, Seftor REB. Vasculogenic mimicry and tumour-cell plasticity: lessons from melanoma. *Nat Rev Cancer*. (2003) 3:411–21. doi: 10.1038/nrc1092
150. Bittner M, Meltzer P, Chen Y, Jiang Y, Seftor E, Hendrix M, et al. Molecular classification of cutaneous malignant melanoma by gene expression profiling. *Nature*. (2000) 406:536–40. doi: 10.1038/35020115
151. Carr KM, Bittner M, Trent JM. Gene-expression profiling in human cutaneous melanoma. *Oncogene*. (2003) 22:3076–80. doi: 10.1038/sj.onc.1206448

152. Demou ZN, Hendrix MJC. Microgenomics profile the endogenous angiogenic phenotype in subpopulations of aggressive melanoma. *J Cell Biochem*. (2008) 105:562–73. doi: 10.1002/jcb.21855
153. Topczewska JM, Postovit L-M, Margaryan NV, Sam A, Hess AR, Wheaton WW, et al. Embryonic and tumorigenic pathways converge via nodal signaling: role in melanoma aggressiveness. *Nat Med*. (2006) 12:925–32. doi: 10.1038/nm1448
154. Schier AF, Shen MM. Nodal signalling in vertebrate development. *Nature*. (2000) 403:385–9. doi: 10.1038/35000126
155. Sun S, Wang Z. Head neck squamous cell carcinoma c-Met(+) cells display cancer stem cell properties and are responsible for cisplatin-resistance and metastasis. *Int J Cancer*. (2011) 129:2337–48. doi: 10.1002/ijc.25927
156. Rothenberger N, Stabile L. Hepatocyte growth factor/c-met signaling in head and neck cancer and implications for treatment. *Cancers*. (2017) 9:39. doi: 10.3390/cancers9040039
157. Chen C, Wei Y, Hummel M, Hoffmann TK, Gross M, Kaufmann AM, et al. Evidence for epithelial-mesenchymal transition in cancer stem cells of head and neck squamous cell carcinoma. *PLoS ONE*. (2011) 6:e16466. doi: 10.1371/journal.pone.0016466
158. Chen D, Wu M, Li Y, Chang I, Yuan Q, Ekimyan-Salvo M, et al. Targeting BMI1 + cancer stem cells overcomes chemoresistance and inhibits metastases in squamous cell carcinoma. *Cell Stem Cell*. (2017) 20:621–34.e6. doi: 10.1016/j.stem.2017.02.003
159. Ricci-Vitiani L, Lombardi DG, Pilozzi E, Biffoni M, Todaro M, Peschle C, et al. Identification and expansion of human colon-cancer-initiating cells. *Nature*. (2006) 445:111–5. doi: 10.1038/nature05384
160. Wang T, Lv M, Shen S, Zhou S, Wang P, Chen Y., et al. Cell-free microRNA expression profiles in malignant effusion associated with patient survival in non-small cell lung cancer. *PLoS ONE*. (2012) 7:e43268. doi: 10.1371/journal.pone.0043268
161. Maheswaran S, Sequist LV, Nagrath S, Ulkus L, Brannigan B, Collura CV, et al. Detection of mutations inEGFRin circulating lung-cancer cells. *N Engl J Med*. (2008) 359:366–77. doi: 10.1056/NEJMoa0800668
162. Chiou SH, Wang ML, Chou YT, Chen CJ, Hong CF, Hsieh WJ, et al. Coexpression of oct4 and nanog enhances malignancy in lung adenocarcinoma by inducing cancer stem cell-like properties and epithelial-mesenchymal transdifferentiation. *Cancer Res*. (2010) 70:10433–44. doi: 10.1158/0008-5472.CAN-10-2638
163. Dhar M, Wong J, Che J, Matsumoto M, Grogan T, Elashoff D, et al. Evaluation of PD-L1 expression on vortex-isolated circulating tumor cells in metastatic lung cancer. *Sci Rep*. (2018) 8:2592. doi: 10.1038/s41598-018-19245-w
164. Harada K, Pool Pizzi M, Baba H, Shanbhag ND, Song S, Ajani JA. Cancer stem cells in esophageal cancer and response to therapy. *Cancer*. (2018) 124:3962–4. doi: 10.1002/cncr.31697
165. Bekaii-Saab T, El-Rayes B. Identifying and targeting cancer stem cells in the treatment of gastric cancer. *Cancer*. (2017) 123:1303–12. doi: 10.1002/cncr.30538
166. Yin S, Li J, Hu C, Chen X, Yao M, Yan M, et al. CD133 positive hepatocellular carcinoma cells possess high capacity for tumorigenicity. *Int J Cancer*. (2007) 120:1444–50. doi: 10.1002/ijc.22476
167. Zhu Z, Hao X, Yan M, Yao M, Ge C, Gu J., et al. Cancer stem/progenitor cells are highly enriched in CD133+CD44+population in hepatocellular carcinoma. *Int J Cancer*. (2009) 126:2067–78. doi: 10.1002/ijc.24868
168. Yang ZF, Ngai P, Ho DW, Yu WC, Ng MNP, Lau CK, et al. Identification of local and circulating cancer stem cells in human liver cancer. *Hepatology*. (2008) 47:919–28. doi: 10.1002/hep.22082
169. Yang ZF, Ho DW, Ng MN, Lau CK, Yu WC, Ngai P, et al. Significance of CD90+ cancer stem cells in human liver cancer. *Cancer Cell*. (2008) 13:153–66. doi: 10.1016/j.ccr.2008.01.013
170. Di Carlo C, Brandi J, Cecconi D. Pancreatic cancer stem cells: perspectives on potential therapeutic approaches of pancreatic ductal adenocarcinoma. *World J Stem Cells*. (2018) 10:172–82. doi: 10.4252/wjsc.v10.i11.172
171. Steinert G, Schölch S, Niemietz T, Iwata N, García SA, Behrens B., et al. Immune escape and survival mechanisms in circulating tumor cells of colorectal cancer. *Cancer Res*. (2014) 74:1694–704. doi: 10.1158/0008-5472.CAN-13-1885
172. Huang EH, Hynes MJ, Zhang T, Ginestier C, Dontu G, Appelman H, et al. Aldehyde dehydrogenase 1 is a marker for normal and malignant human colonic Stem Cells (SC) and tracks SC overpopulation during colon tumorigenesis. *Cancer Res*. (2009) 69:3382–9. doi: 10.1158/0008-5472.CAN-08-4418
173. Miyamoto DT. RNA-Seq of single prostate CTCs implicates noncanonical Wnt signaling in antiandrogen resistance. *Science*. (2015) 349:1351–6. doi: 10.1126/science.aab0917
174. Peng S, Maihle NJ, Huang Y. Pluripotency factors Lin28 and oct4 identify a sub-population of stem cell-like cells in ovarian cancer. *Oncogene*. (2010) 29:2153–9. doi: 10.1038/onc.2009.500
175. Meirelles K, Benedict LA, Dombkowski D, Pepin D, Preffer FI, Teixeira J, et al. Human ovarian cancer stem/progenitor cells are stimulated by doxorubicin but inhibited by Mullerian inhibiting substance. *Proc Natl Acad Sci USA*. (2012) 109:2358–63. doi: 10.1073/pnas.1120733109
176. Siu MKY, Wong ESY, Kong DSH, Chan HY, Jiang L, Wong OGW, et al. Stem cell transcription factor NANOG controls cell migration and invasion via dysregulation of E-cadherin and FoxJ1 and contributes to adverse clinical outcome in ovarian cancers. *Oncogene*. (2012) 32:3500–9. doi: 10.1038/onc.2012.363
177. Di J, Duiveman-de Boer T, Zusterzeel PLM, Figdor CG, Massuger LFAG, Torensma R. The stem cell markers oct4a, Nanog and c-Myc are expressed in ascites cells and tumor tissue of ovarian cancer patients. *Cell Oncol*. (2013) 36:363–74. doi: 10.1007/s13402-013-0142-8
178. Belotte J, Fletcher NM, Alexis M, Morris RT, Munkarah AR, Diamond MP, et al. Sox2 gene amplification significantly impacts overall survival in serous epithelial Ovarian cancer. *Reprod Sci*. (2014) 22:38–46. doi: 10.1177/1933719114542021
179. Yan HC, Xu JUN, Fang LS, Qiu YY, Lin XM, Huang HX, et al. Ectopic expression of the WWOX gene suppresses stemness of human ovarian cancer stem cells. *Oncol Lett*. (2015) 9:1614–20. doi: 10.3892/ol.2015.2971
180. Wen Y, Hou Y, Huang Z, Cai J, Wang Z. SOX2 is required to maintain cancer stem cells in ovarian cancer. *Cancer Sci*. (2017) 108:719–31. doi: 10.1111/cas.13186

Conflict of Interest: The authors declare that the research was conducted in the absence of any commercial or financial relationships that could be construed as a potential conflict of interest.

frontiers in Oncology

ORIGINAL RESEARCH
published: 29 May 2020
doi: 10.3389/fonc.2020.00712

Long-Term Exposure of Early-Transformed Human Mammary Cells to Low Doses of Benzo[a]pyrene and/or Bisphenol A Enhances Their Cancerous Phenotype via an AhR/GPR30 Interplay

Caterina F. Donini[1,2,3†], Myriam El Helou[1,2,4†], Anne Wierinckx[1,2,5], Balázs Győrffy[6], Sophie Aires[1,2], Aurélie Escande[7], Séverine Croze[1,5], Philippe Clezardin[1,8], Joël Lachuer[1,2,5], Mona Diab-Assaf[4], Sandra E. Ghayad[4], Béatrice Fervers[1,2,3†], Vincent Cavaillès[9†], Véronique Maguer-Satta[2†] and Pascale A. Cohen[1,2,3,5,8]*

[1] Université Lyon 1, Lyon, France, [2] CRCL-Centre de Recherche en Cancérologie de Lyon-Inserm U1052-CNRS U5286, Lyon, France, [3] Département Cancer et Environnement, Centre Léon Bérard, Lyon, France, [4] Faculty of sciences II, Lebanese University, Fanar, Lebanon, [5] ProfileXpert, SFR-Est, CNRS UMR-S3453, INSERM US7, Lyon, France, [6] Department of Bioinformatics, Semmelweis University and TTK Lendület Cancer Biomarker Research Group, Budapest, Hungary, [7] UMR5569 (UM IRD CNRS), Montpellier, France, [8] INSERM, UMR1033 LYOS, Lyon, France, [9] IRCM - Institut de Recherche en Cancérologie de Montpellier, INSERM U1194, Université de Montpellier, Institut régional du Cancer de Montpellier, CNRS, Montpellier, France

It is of utmost importance to decipher the role of chronic exposure to low doses of environmental carcinogens on breast cancer progression. The early-transformed triple-negative human mammary MCF10AT1 cells were chronically (60 days) exposed to low doses (10^{-10} M) of Benzo[a]pyrene (B[a]P), a genotoxic agent, and/or Bisphenol A (BPA), an endocrine disruptor. Our study revealed that exposed MCF10AT1 cells developed, in a time-dependent manner, an acquired phenotype characterized by an increase in cancerous properties (anchorage independent growth and stem-like phenotype). Co-exposure of MCF10AT1 cells to B[a]P and BPA led to a significantly greater aggressive phenotype compared to B[a]P or BPA alone. This study provided new insights into the existence of a functional interplay between the aryl hydrocarbon receptor (AhR) and the G protein-coupled receptor 30 (GPR30) by which chronic and low-dose exposure of B[a]P and/or BPA fosters the progression of MCF10AT1 cells into a more aggressive substage. Experiments using AhR or GPR30 antagonists, siRNA strategies, and RNAseq analysis led us to propose a model in which AhR signaling plays a "driver role" in the AhR/GPR30 cross-talk in mediating long-term and low-dose exposure of B[a]P and/or BPA. Retrospective analysis of two independent breast cancer cohorts revealed that the *AhR/GPR30* mRNA expression signature resulted in poor breast cancer prognosis, in particular in the ER-negative and the triple-negative subtypes. Finally, the study identified targeting AhR and/or GPR30 with specific antagonists as a strategy

OPEN ACCESS

Edited by:
Hamid Morjani,
Université de Reims
Champagne-Ardenne, France

Reviewed by:
Christos Roussakis,
Université de Nantes, France
Fabrice Fleury,
UMR6286 Unité de fonctionnalité et
Ingénierie des Protéines
(UFIP), France

***Correspondence:**
Pascale A. Cohen
pascale.cohen@univ-lyon1.fr

† These authors have contributed equally to this work

Specialty section:
This article was submitted to Molecular and Cellular Oncology, a section of the journal Frontiers in Oncology

Received: 29 November 2019
Accepted: 15 April 2020
Published: 29 May 2020

Citation:
Donini CF, El Helou M, Wierinckx A, Győrffy B, Aires S, Escande A, Croze S, Clezardin P, Lachuer J, Diab-Assaf M, Ghayad SE, Fervers B, Cavaillès V, Maguer-Satta V and Cohen PA (2020) Long-Term Exposure of Early-Transformed Human Mammary Cells to Low Doses of Benzo[a]pyrene and/or Bisphenol A Enhances Their Cancerous Phenotype via an AhR/GPR30 Interplay. Front. Oncol. 10:712. doi: 10.3389/fonc.2020.00712

capable of inhibiting carcinogenesis associated with chronic exposure to low doses of B[a]P and BPA in MCF10AT1 cells. Altogether, our results indicate that the engagement of both AhR and GPR30 functions, in particular in an ER-negative/triple-negative context of breast cells, favors tumor progression and leads to poor prognosis.

Keywords: environmental factors, Benzo[a]pyrene, Bisphenol-A, breast cancer, tumor progression, AhR, GPR30

INTRODUCTION

Progression of human breast epithelial cells from non-cancerous to pre-malignant and of early-transformed mammary cells to malignant stages is a multiyear, multistep, multiscale, and multipath disease process. More than 85% of breast cancers are sporadic and potentially attributable to long-term exposure to environmental factors, such as chemical carcinogens (1–5). Given the increasing evidence that common environmental carcinogens play a significant role in breast cancer, increased attention has been paid to molecular mechanisms through which pollutants affect breast tumor formation, progression, and/or invasion (6–8). The identification of such molecular mechanisms could have several societal and environmental consequences, and may lead to the discovery of human biomarkers of exposure to environmental carcinogens exploitable for breast cancer prevention.

Previous *in vitro* investigations have mainly been conducted on human mammary epithelial cells or on human breast cancer cells, reflecting the impact of environmental factors on the earlier and later stages of carcinogenesis (9–13). However, little is known on the impact of exposure to pollutants on the breast early-transformed stage. Short-term exposure of cells to carcinogens at micro- to millimolar concentrations was previously typically investigated (1, 2, 14–16) which, while informative, is not optimal in mimicking natural chronic exposure to low doses of environmental carcinogens and to reflect physiologically-achievable levels of environmental mammary carcinogens. Additionally, few studies have attempted to mimic natural environmental exposure by assessing the impact of exposure to a combination of several pollutants with distinct mechanisms of action that may interact or induce a greater adverse effect than the use of individual compounds.

Benzo[a]pyrene (B[a]P), a family member of poly-cyclic aromatic hydrocarbons, is considered to be a tobacco, environmental, and dietary chemical carcinogen classified as Group 1 carcinogen by the IARC (17). B[a]P is a tumor initiator that binds and forms a complex with the aryl hydrocarbon receptor (AhR) (18–20). Upon such activation, the AhR-transcriptional complex activates specific DNA-recognition elements, such as xenobiotic response elements (XREs), and upregulates the expression of genes such as cytochrome P450 isoforms (including *CYP1A1*). These latter are involved in the metabolic activation of B[a]P in genotoxic metabolites forming DNA adducts relevant for carcinogenesis [for review, (21, 22)]. A growing body of evidence is accumulating implicating the B[a]P/AhR/CYP1A1 pathway in carcinogenesis (23–25). At early stages of carcinogenesis, short-term and millimolar B[a]P doses were shown to induce aggressiveness and transformation of non-cancerous human mammary epithelial cells (26–28). The impact of chronic and low-dose exposure of these cells to B[a]P was scarcely investigated, but seems to foster progression toward the early-transformed stage by favoring increased mesenchymal, stem-like, and anchorage-independent growth properties (9–13, 29).

Bisphenol-A (BPA) is a monomer of polycarbonate plastics and human exposure to BPA mainly occurs through the oral route due to the leaching of BPA in food and beverage containers, but non-dietary sources such as dust, air and cosmetics are also relevant (30). BPA has been the focus of widespread concern due to the fact that it interferes with endocrine signaling pathways even at extremely low doses, and thus belongs to the endocrine-disrupting compounds (EDC) (31, 32). BPA is known to bind to estrogen receptors alpha and beta (ERα and ERβ), to the G protein-coupled receptor 30 (GPR30) but also to the pregnane X receptor (PXR) (31, 33). Although several *in vivo* studies reported a carcinogenic potential of BPA [reviewed in (32)], the World Health Organization (WHO) indicated that there is currently insufficient evidence on which to base this carcinogenic potential (34). *In vitro* studies have however revealed that BPA causes adverse effects in non-cancerous mammary epithelial cells or in breast cancer cell lines, including increased cell proliferation, cell stemness, oxidative stress, and alterations of cell signaling pathways involved in carcinogenesis (13, 29, 35–38).

The MCF10 unique model of breast cancer progression comprises a series of isogenic triple-negative cell lines derived from MCF10A cells (MCF10A, MCF10AT1 and MCF10CA1a.cl1 cells). The parental cell line (MCF10A) having been originally isolated from a woman with fibrocystic change (39), the members of the MCF10 series belong to the triple negative/basal-like subtype (ER-negative, progesterone receptor (PR)-negative, HER2-negative) (40–42). These cell lines thus recapitulate the stages of mammary carcinogenesis (43), making this a valuable *in vitro* model for studying the progression of triple-negative breast cancer (44–46). In the present study, we used MCF10AT1 breast cells which represent the transformed early stage in the MCF10 unique model of breast cancer progression (43, 44) to further characterize the carcinogenic potential of B[a]P and BPA. To our knowledge, these cells have never been used to test the impact of chronic and low-dose exposure to environmental pollutants.

Abbreviations: B[a]P, benzo[a]pyrene; AhR, aryl hydrocarbon receptor; XRE, xenobiotic response element; BPA, bisphenol-A; EDC, endocrine-disrupting compound; ERα, estrogen receptor alpha; ERβ, estrogen receptor beta; GPR30, G protein-coupled receptor 30; PXR, pregnane X receptor; PR, progesterone receptor; AIG, anchorage-independent growth; MFE, mammosphere formation efficiency; RT-qPCR, real-time quantitative polymerase chain reaction; TCDD, 2,3,7,8-Tetrachlorodibenzo-p-dioxin; OS, overall survival.

The main objectives of this work were to newly investigate: (i) whether long-term and low-dose exposure to B[a]P and/or BPA triggers the progression of early-transformed mammary cells to a more aggressive stage; (ii) whether their combination enhances the effect of each compound tested individually, in particular whether BPA facilitates the pro-carcinogenic activity of B[a]P; and (iii) to identify candidate strategies capable of inhibiting mammary carcinogenesis linked to chronic exposure to the environmental pollutants B[a]P and/or BPA.

Our data reveal that long-term and low-dose exposure to B[a]P and BPA increases cancerous properties of the MCF10AT1 cell line. Importantly exposure to the two pollutants leads to a greater deleterious impact than the compounds tested individually, and our data highlight the existence of a unique functional cross-talk between AhR and GPR30 in mediating those effects. The clinical relevance of the AhR/GPR30 interplay is validated by the observation of high mRNA expression levels of these two receptors in breast cancer patients as markers of poor prognosis. Finally, this study identified AhR and GPR30 as novel targets for strategies inhibiting the development of cancer-associated properties (AIG and MFE) in early-transformed human mammary cells following long-term and low-dose exposure to B[a]P and BPA.

MATERIALS AND METHODS

Cell Culture

Early-transformed human mammary MCF10AT1 cells and the MCF10AT1-derived cancerous MCF10CA1a.cl1 cells (Karmanos Institute, Detroit, USA) were purchased from Karmanos Institute (Detroit, USA) and maintained in complete DMEM/Ham's F12 medium with 5% horse serum (Thermo Fisher Scientific, Waltham, USA) and additional supplements: 100 ng/mL cholera enterotoxin, 10 mg/mL insulin, 0.5 mg/mL hydrocortisol, 20 ng/mL epidermal growth factor (Sigma, Saint Louis, USA) 100 units/mL penicillin and 100 mg/mL streptomycin. MCF-7 cells were purchased from ATCC (Teddington, UK) and grown according to the manufacturer's recommendations. HG5LN PXR cells stably expressing PXR (47), were grown in DMEM containing phenol red and 1 g/L glucose with 5% fetal calf serum (FCS) and additional supplements: 1 mg/mL G418 and 0.5 μg/mL puromycin.

Reagents

B[a]P and BPA were purchased from Sigma (Saint Louis, USA). 2,3,7,8-Tetrachlorodibenzo-p-dioxin (TCDD), used as a control, was purchased from LGC Standard (Molsheim, France). The GPR30 agonist G1, the GPR30 antagonist G15, and the AhR agonist ITE were from TOCRIS Bioscience (Bristol, UK); the AhR antagonist GNF351 from Calbiochem (Billerica, USA).

Establishment and Maintenance of the Chronically Exposed Cellular Model

MCF10AT1 cells were chronically exposed or not to 10^{-10} M of B[a]P or to 10^{-10} M BPA, alone or in combination, during 60 days (≈20 passages) in phenol red-free DMEM/Ham's F12 medium with 5% steroid-depleted, dextran-coated and charcoal-treated horse serum, containing the above-mentioned supplements (further referred to as DCC medium). Unexposed MCF10CA1a.cl1 cells were grown concomitantly in the same medium for 60 days and named MCF10CA1a.cl1_{60d}. Media and treatments were changed every 2 days. Cells were frozen every 2 weeks.

Anchorage-Independent Growth (AIG)

Anchorage-independent growth was assessed by soft agar assay as previously described (48). Single-cell suspensions (75×10^3) were seeded onto soft agar, and colonies were counted after 3 weeks of incubation.

Mammosphere Formation Efficiency (MFE)

Single-cell suspensions were seeded using non-adherent mammosphere culture conditions (49). After 7 days, primary mammospheres (first generation) were counted, collected, trypsinized, and replated for 10 days in non-adherent culture conditions to generate second-generation mammospheres. The culture media were replenished every 2–3 days.

RNA Extraction and Real-Time Quantitative Polymerase Chain Reaction (RT-qPCR)

Total RNA extraction, reverse transcription and RT-qPCR measurements were performed as described previously (29, 48). RNA lysates were extracted after exposure to the different molecules tested, untreated cells were used as controls in the presence of the corresponding volume of solvent. One microgram of total RNA from each sample was reverse-transcribed as previously described (48). RT-qPCR measurements were performed using a CFX96 with the SsoAdvanced Universal SYBR green supermix (BioRad, Hercules, USA), according to the manufacturer's recommendations. The primers used to explore the expression of the *ERα, ERβ, PXR, AhR, GPR30, CYP1A1,* and *28S* genes are listed in the **Supplementary Table 1**.

Western Blot

Western blot experiments were performed as previously described (48) using the following antibodies: AhR (1:1,000, ab2770; Abcam, Paris, France), GPR30 (1:1,000, NBP1-31239; Novus Biologicals, Littleton, USA), α-tubulin (1:10,000, T5168; Sigma), phospho-p42/44 MAPK (1:1,000, 9106; Cell Signaling), p42/44 MAPK (1:1,000, 9102; Cell Signaling, Danvers, USA).

GPR30 or *AhR Silencing*

Stealth™ siRNAs siRNA-GPR30 and Stealth™ siRNAs siRNA-AhR and their corresponding scrambled control RNA (scrambled) were obtained from Ambion (Carlsbad, USA,4390825) and Invitrogen (Carlsbad, USA, AHRHSS100337/336), respectively. Fifty nM of siRNA-GPR30, 5 nM of siRNA-AhR or corresponding scrambled RNA were transfected into MCF10AT1 cells with lipofectamine RNAimax (Invitrogen). Transfections were performed directly at the time of cell seeding. Western blots were performed 48 h post-transfection. Exposure to G1, TCDD, or ITE for RNA collection or luciferase assay was performed 24 h post-transfection.

Luciferase Assay

Cells were plated and then transfected with 150 ng XRE-firefly luciferase reporter plasmid (XRE-luc) (50) and 10 ng Renilla luciferase plasmid (pTK-RL). Twenty-four hours after transfection cells were grown for 8 h in the presence of the indicated treatment, and luciferase activity was then assessed as previously described (48).

Short-Term Exposure Experiments

In AIG experiments, MCF10AT1 cells were exposed to BPA and/or B[a]P 10^{-10} M, ITE 10^{-10} M, or G1 10^{-10} M for 72 h in the presence or the absence of a 2 h pre-treatment with the AhR antagonist GNF351 10^{-7} M or the GPR30 antagonist G15 10^{-8} M. Exposure was maintained throughout the course of the experiments. In MFE assays, MCF10AT1 cells were exposed to BPA and/or B[a]P 10^{-10} M, ITE 10^{-10} M, or G1 10^{-10} M in the presence or the absence of GNF351 10^{-7} M or G15 10^{-8} M only during the time-course of the experiments.

RNA-Seq Experiments and Analyses

RNA isolation, library preparation, and RNA-Seq were performed by the core facility ProfileXpert (Lyon, France) from three independent cell-culture replicates of each tested cell line (unexposed $MCF10AT1_{60d}$ cells, B[a]P 10^{-10} M exposed $MCF10AT1_{60d}$, BPA 10^{-10} M exposed $MCF10AT1_{60d}$ cells, B[a]P+BPA 10^{-10} M exposed $MCF10AT1_{60d}$). The resulting RNA were isolated using the RNeasy mini kit (Qiagen) according to the manufacturer's protocol and ribosomal depletion was performed with the Ribo-zero gold kit (Epicentre). Libraries were performed from 20 ng ribosomal depleted RNA with the NEXTFLEX® Rapid Directional RNA-Seq Library Prep Kit (BIOO-Scientific). Libraries were sequenced using an Illumina NextSeq 500 platform (flow cell highoutput V2) and a 75 bp paired-end sequencing with ∼30–35 million reads per sample. After trimming, reads were aligned to the human genome (hg19) using TopHat-2 v. 2.1.0 and data normalization (FPKM) was performed with Cufflinks software v.2.1.1. Data were logged on the NCBI Gene Expression Omnibus (GEO) website (http://www.ncbi.nlm.nih.gov/geo/) and are available as a GSE142073 dataset. Transcripts were considered as differentially expressed when the p-value of a student non-parametric t-test was ≤ 0.05. The Aryl Hydrocarbon Receptor Signaling Canonical Pathway was evaluated with a functional analysis created with Ingenuity Pathway Analysis software (IPA®, QIAGEN Redwood City, www.qiagen.com/ingenuity). The GPR30 gene expression signature described by Pandey and collaborators (51) was introduced in the Ingenuity Pathway Analysis software to assess the GPR30 signaling pathway.

Cell Proliferation

A total of 4×10^4 cells/well were seeded onto and cultured in 24-well plates. Proliferating cells were analyzed using the Scepter™ 2.0 Cell Counter (Merck Millipore, Billerica, USA).

Cell Viability Assay

A total of 10^4 cells/well were plated onto a 96-well plate and treated for 4 days as indicated. Cell viability was assessed as previously described (52).

Breast Tumor Cohorts

Women with primary breast tumors ($n = 113$) and known clinical follow-up who had not received any therapy before surgery and who relapsed, or not, while receiving endocrine therapy and/or chemotherapy were recruited from the BB-0033-00050, Biological Resources Center (CRB) Centre Léon Bérard, Lyon France (CLB cohort, **Supplementary Table 2**) (53). This study has been approved by the local ethics committee (CRB Centre Léon Bérard, France). The CRB Centre Léon Bérard is quality certified according NFS96-900 French standard and, ISO 9001 for clinical trials, ensuring scientific rigor for sample conservation, traceability and quality, as well as ethical rules observance and defined rules for transferring samples for research purposes (Ministry of Health for activities authorization n° AC-2019-3426 and DC-2008-99). The material used in the study has been collected in agreement with all applicable laws, rules, and requests of French and European government authorities, including the patients' informed written consents. Extraction of total RNA from frozen tumor samples and RT-qPCR measurements were performed as previously described (52, 53). Univariate analyses were performed using the SPSS™ Software (IBM, USA). The IBM SPSS software (IBM) was used for all statistical analyses in which the prognostic value of *AhR* and *GPR30* mRNA levels was analyzed. The data were divided at the median value of *AhR* or *GPR30* mRNA expression into two groups with either high or low expression levels. The Kaplan-Meier plotter (KMP) cohort was established from a meta-analysis of the gene-expression profiles of 1,877 primary breast cancer samples from patients who had not received any therapy prior to surgery (54). A $p < 0.05$ was considered statistically significant.

Long-Term Inhibitory Strategies

MCF10AT1 cells were chronically (60 days) exposed or not to (B[a]P + BPA) 10^{-10} M, alone or in combination with GNF351 10^{-7} M and/or G15 10^{-8} M. Control experiments were performed in MCF10AT1 cells exposed for 60 days to GNF351 10^{-7} M and/or G15 10^{-8} M. The resulting established cells were then tested for AIG and MFE as described above.

RESULTS

Chronic and Low-Dose Exposure to B[a]P and/or BPA of Early-Transformed MCF10AT1 Cells Leads to an Enhanced and Acquired Aggressive Phenotype

The MCF10AT1 cells and the MCF10AT1-derived MCF10CA1a.cl1 respectively represent the early-transformed and cancerous stages in the unique MCF10 model of triple negative breast cancer progression (43, 44). Validation of progression to malignancy of MCF10AT1 cells was investigated by assessing: (i) anchorage-independent growth (AIG), a

hallmark of carcinogenesis associated with aggressiveness and metastasis in malignant cells; (ii) cancer stem-like and self-renewing properties by assessing first and second generation mammosphere-forming efficiency (MFE), as a growing body of evidence suggests that cancer stem-like cells are involved in generating and maintaining pre-malignant and malignant lesions (55–57). Consistent with the substage of breast cancer progression displayed by each cell line, MCF10AT1 cells formed significantly fewer and smaller colonies in soft agar (AIG) and significantly fewer mammospheres than the cancerous MCF10CA1a.cl1 cells (**Supplementary Figures 1A,B**).

In order to identify the impact of B[a]P and BPA on progression to malignancy in conditions mimicking environmental exposure, the MCF10AT1 cells were chronically (60 days) exposed or not to physiologically-relevant concentrations (10^{-10} M) of B[a]P and/or BPA (58–62) ($MCF10AT1_{60d}$). Unexposed $MCF10AT1_{60d}$ and $MCF10CA1a.cl1_{60d}$ cells displayed unmodified AIG and MFE phenotypes (**Figures 1A,B** and **Supplementary Figure 1C**) compared to the corresponding parental cells (**Supplementary Figures 1A,B**). $MCF10AT1_{60d}$ cells exposed to the carcinogenic B[a]P pollutant at a concentration as low as 10^{-10} M exhibited significantly increased AIG (**Figure 1A**), increased colony size (**Supplementary Figure 1C**) and higher MFE (**Figure 1B**) compared to the unexposed $MCF10AT1_{60d}$ cells. The EDC BPA (10^{-10} M, 60 days exposure) also enhanced the cancerous properties of the exposed $MCF10AT1_{60d}$ cells (significant increase in AIG, in colony size and in MFE), while that impact was always significantly lower than that of 60-days exposure to 10^{-10} M B[a]P (**Figures 1A,B**, **Supplementary Figure 1C**). Of utmost interest, the combination of B[a]P with BPA (10^{-10} M) had a significantly greater effect than B[a]P (10^{-10} M) tested individually (**Figures 1A,B**, **Supplementary Figure 1C**). The cancerous features displayed by the $MCF10AT1_{60d}$ cells exposed to the B[a]P + BPA (10^{-10} M) combination was at least equivalent (**Figure 1A** and **Supplementary Figure 1C**) if not greater (second generation of mammospheres, **Figure 1B**) than those displayed by the unexposed cancerous $MCF10CA1a.cl1_{60d}$ cells. **Supplementary Figure 2** eliminated the possibility that the aggressive phenotypes observed in the different exposed $MCF10AT1_{60d}$ cells were the consequence of an increase in cell proliferation (compared to unexposed $MF10AT1_{60d}$).

Unexposed or exposed $MCF10AT1_{60d}$ cells were grown for a further 30 days in the absence of any treatment ($MCF10AT1_{60+30d}$ cells), and then tested for AIG and MFE. The number and size of colonies in soft agar (**Figure 1C** and **Supplementary Figure 1D**) and the number of mammospheres (**Figure 1D**) were similar between $MCF10AT1_{60d}$ and $MCF10AT1_{60+30d}$ cells, thus demonstrating that the aggressive phenotype induced by chronic exposure of MCF10AT1 cells to low-doses of B[a]P and/or BPA is an acquired phenotype.

Taking advantage of the systematic freezing of exposed cells over the experimental time-course, AIG and MFE were retrospectively tested after 23 and 48 days of exposure and compared to 60 days of exposure (**Figures 1E,F**). The number of colonies in soft agar and mammospheres significantly increased between 23–48 and 48–60 days of chronic exposure, thus demonstrating that the longer MCF10AT1 cells are exposed to low doses of B[a]P and/or BPA, the more aggressive is their resulting phenotype. Once again, the combined exposure to B[a]P + BPA (10^{-10} M) caused more deleterious effects than those of B[a]P or BPA individually, irrespective of the exposure time.

Collectively, our results suggest that: (i) chronic, low-dose exposure to B[a]P or BPA enhances the cancerous properties of MCF10AT1 cells, with exposure to B[a]P being the most effective; (ii) the resulting aggressive phenotype was acquired and not reversed or softened when exposure was stopped; (iii) the duration of the exposure to pollutants impacted the magnitude of the aggressiveness developed by the exposed cells; (iv) combining BPA to B[a]P had more impact than exposure to B[a]P alone and was at least equivalent or higher than that of cancerous MCF10Ca1a.cl1 cells, supporting progression toward the cancerous substage.

AhR and GPR30 are Both Expressed and Functional in MCF10AT1 Cells

As AhR is the main target of B[a]P and BPA is known to bind to ERα, ERβ, GPR30, and PXR, we investigated the presence of these receptors in MCF10AT1 cells. **Supplementary Figure 3** validated that *ERα, ERβ,* and *PXR* were not or scarcely expressed in MCF10AT1 and MCF10CA1a.cl1 cells. Conversely, we newly reported that AhR and GPR30 receptors are concomitantly expressed at the mRNA and protein levels in MCF10AT1 and MCF10CA1.cl1 cells (**Figures 2A,B**). Of interest, AhR expression levels are higher both at the mRNA and protein levels in the MCF10AT1 cells compared to MCF10ACA1a.cl1.

Gene reporter experiments performed in MCF10AT1 cells demonstrated that TCDD, a well-known AhR ligand and activator of AhR-direct transcriptional activity (50), led to an increase in XRE-luciferase activity (**Figure 2C**). The selective AhR agonist ITE (63) also led to a stronger and dose-dependent activation of AhR-driven transcriptional activity in MCF10AT1 cells (**Figure 2C**). A concentration as low as 10^{-11} M of ITE was sufficient to give rise to a significant increase in XRE-luc activity (**Figure 2C**) and the effect of ITE was prevented (**Figure 2D**) by a 100-fold excess of the AhR antagonist GNF351 (64).

Rapid phosphorylation of MAPK is one of the main downstream effects of GPR30 activation (65). In MCF10AT1 cells, the MAPK pathway is rapidly activated (increase in the phospho-p42/p44 MAPK/MAPK ratio) in the presence of the selective GPR30 agonist G1 (66) and this activation is impaired in the presence of the GPR30 antagonist G15 (67) (**Figure 2E**), newly revealing the presence of functional GPR30 in MCF10AT1 cells.

The MFE and AIG Responses Triggered by B[a]P and/or BPA Occur Through a Functional Cross-Talk Between AhR and GPR30 in MCF10AT1 Cells

We then aimed at investigating the possible involvement of the AhR and/or GPR30 receptors in mediating the

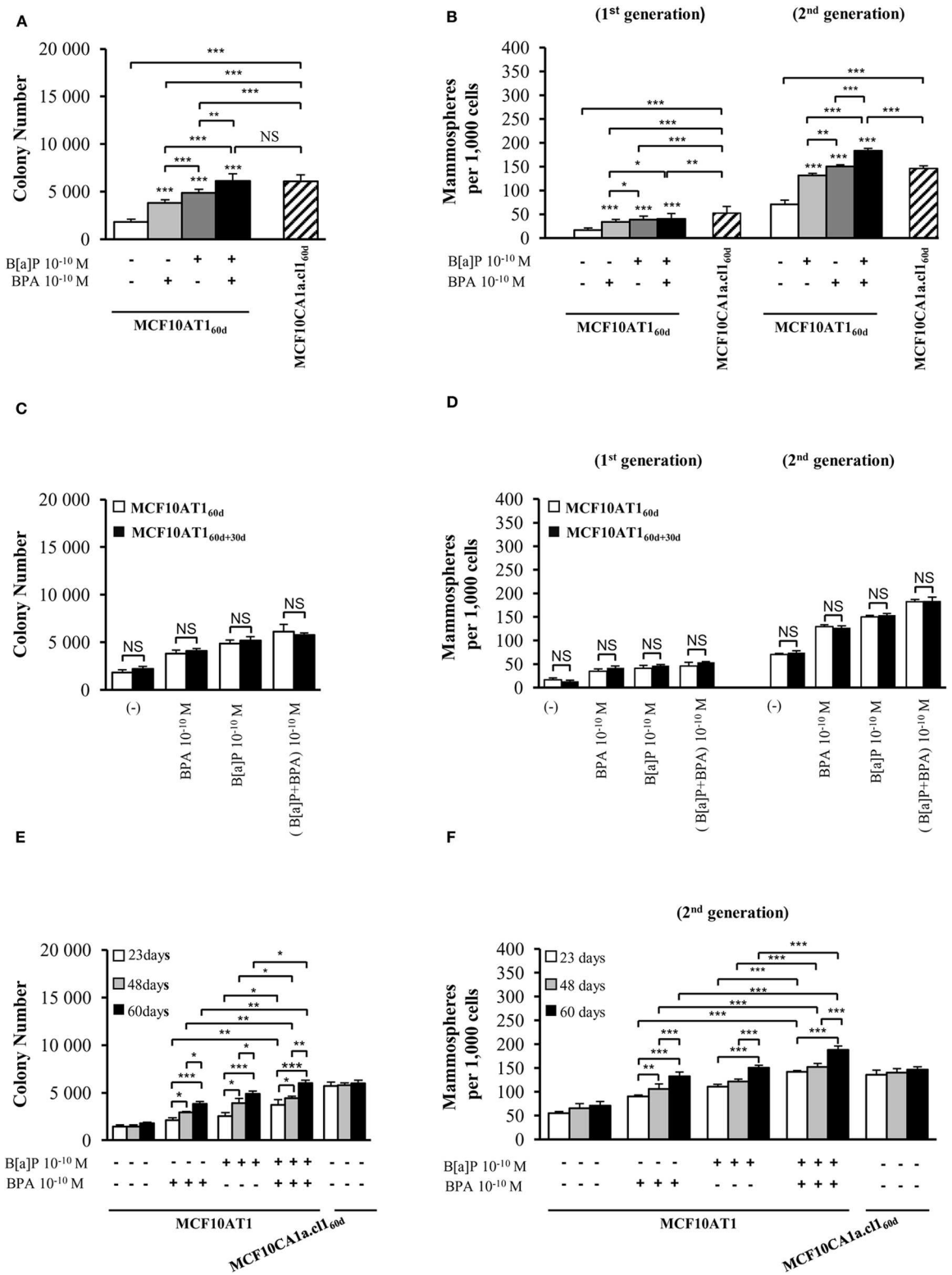

FIGURE 1 | Cumulative and low-dose exposure of BPA and/or B[a]P increases MCF10AT1 cancerous properties (AIG and MFE assays). **(A)** Average number of MCF10AT1$_{60d}$ colonies in soft agar after 60 days of chronic exposure to B[a]P and/or BPA (10^{-10} M). **(B)** Average number of primary and secondary MCF10AT1$_{60d}$

(Continued)

FIGURE 1 | mammospheres formed after 60 days of chronic exposure to B[a]P and/or BPA (10^{-10} M). In **(A,B)**, exposure was maintained throughout the course of the experiments. **(C,D)** After 60 days of chronic exposure to B[a]P and/or BPA (10^{-10} M), MCF10AT1 cells were grown for a further 30 days without any exposure, and single-cell suspensions of cells were seeded in soft agar **(C)** or in non-adherent mammosphere culturing conditions **(D)**. **(E,F)** Time-dependent acquisition of the aggressive phenotype: average number of colonies in soft agar **(E)** and of secondary mammospheres **(F)** following 23, 48, or 60 days of chronic exposure to B[a]P and/or BPA (10^{-10} M). Data illustrated in **(A–F)** represent mean ± SD of at least three independent experiments, in triplicate. $^{***}p < 0.001$, $^{**}p < 0.01$, $^{*}p < 0.05$ or NS (not significant) in Student *t*-test.

tumorigenic effects of exposure to B[a]P and/or BPA 10^{-10} M in short-term experiments. This was tested in the presence or absence of selective antagonists of AhR or GPR30 (GNF351 and G15, respectively) at non-toxic concentrations (**Supplementary Figures 4A,B**).

Figure 3A demonstrates that short-term (72 h) exposure to 10^{-10} M BPA and/or 10^{-10} M B[a]P were sufficient to generate increased colony numbers in AIG assays. GNF351 and G15 were able to completely inhibit the effects of B[a]P and/or BPA on AIG (**Figure 3A**). This result was, at least to some extent, expected with the B[a]P/GNF351 and the BPA/G15 combinations, but was totally surprising concerning the BPA/GNF351 and the B[a]P/G15 combinations. In MFE assays conducted with MCF10AT1 cells exposed only during the time-course of the experiments (**Figure 3B**), the increased number of mammospheres induced by 10^{-10} M BPA was totally blocked in the presence of G15, as expected, but also in the presence of GNF351. Conversely, B[a]P-induced MFE was completely inhibited by GNF351, while the GPR30 antagonist G15, surprisingly resulted in a partial but significant inhibition. The impact of the G15 or GNF351 on the combination B[a]P+BPA was similar to that observed with B[a]P alone.

We then performed the same experiments using G1 and ITE agonists, at 10^{-10} M non-toxic concentrations (**Supplementary Figures 4C,D**). **Figures 3C,D** show similar data as those obtained with B[a]P and/or BPA in **Figures 3A,B**, namely that: (i) low-dose exposure of MCF10AT1 cells to 10^{-10} M G1 or 10^{-10} M ITE gives rise to significantly increased colony number (AIG) or increased MFE in the same range as that observed with 10^{-10} M BPA or 10^{-10} M B[a]P, respectively; (ii) G15 and GNF351 were both able to totally inhibit G1-dependent AIG or MFE; (iii) the impact of ITE on MFE was totally blocked in the presence of GNF351, while only partially inhibited by G15.

To confirm the above data supporting the involvement of both GPR30 and AhR receptors in mediating the effects of low dose (10^{-10} M) BPA, B[a]P, G1, or ITE, we used a siRNA strategy silencing either AhR or GPR30 (**Figures 4A,B**). We verified that siRNA-AhR or siRNA-GPR30 had, however, no impact on GPR30 or AhR expression, respectively (**Figures 4A,B**), nor on MCF10AT1 cell viability (**Supplementary Figures 4E,F**).

Findings from AIG and MFE experiments conducted in MCF10AT1 exposed to BPA, B[a]P, G1, or ITE 10^{-10} M in the presence of siRNA-AhR or of siRNA-GPR30 (**Figures 4C–F**) corroborated those obtained using the AhR- or GPR30-antagonists (GNF351 and G15, respectively) (**Figures 3A–D**). Indeed, AhR knock-out resulted in a total inhibition of BPA-, B[a]P-, G1-, or ITE-mediated effects (**Figures 4C,E**). GPR30 silencing, while totally inhibiting BPA- or G1-mediated effects (**Figures 4D,F**), was slightly less effective in inhibiting MFE or AIG assays when cells were exposed to B[a]P (**Figures 4D,F**) or ITE (**Figure 4D**). The impact of siRNA-AhR or siRNA-GPR30 on the combination B[a]P+BPA was similar to that observed with B[a]P alone (**Figures 4C–F**).

Altogether these results support the idea that both AhR and GPR30 receptors play a role in mediating the deleterious effects exerted by BPA, G1, B[a]P, or ITE on the MCF10AT1 early-transformed cells. More importantly, our data highlight a functional cross-talk between GPR30 and AhR.

GPR30-Dependent Mechanisms are Correlated With Enhanced AhR Transcriptional Activity

To further decipher the interplay between AhR and GPR30, we performed XRE-luciferase reporter assays. As anticipated, AhR-driven transcriptional activity in MCF10AT1 cells was fostered by TCDD 10^{-7} M or ITE 10^{-10} M and lost following AhR silencing (**Figure 5A**). Very interestingly, the GPR30 agonist G1 was also able to significantly increase XRE-luciferase activity in a dose-dependent manner, as illustrated by its effect at 10^{-7} M and 10^{-6} M, which is, to our knowledge, the first such report in the literature (**Figure 5B**). The G1-induced XRE-luciferase signal was totally inhibited in the presence of GNF351 (**Figure 5C**) and also in the presence of siRNA-AhR (**Figure 5D**). Silencing GPR30 by a siRNA-GPR30 strategy gave rise to a partial but significant decrease in G1- (10^{-6} M) (**Figure 5E**), TCDD- (10^{-7} M), and ITE- (10^{-10} M) (**Figure 5F**) -dependent activation of XRE-luciferase activity. Altogether, these data recapitulate the cross-talk between AhR and GPR30 on a simplified XRE-luciferase response.

As *CYP1A1* is amongst the canonical genes regulated by AhR with a promoter containing typical XRE, we further investigated endogenous *CYP1A1* mRNA levels in MCF10AT1 cells upon ITE and G1 treatment. Consistent with **Figures 5**, **6** revealed that: (i) *CYP1A1* mRNA levels significantly increased upon treatment with TCDD 10^{-7} M and ITE 10^{-7} M (**Figure 6A**); (ii) the impact of ITE 10^{-7} M was completely impaired in the presence of siRNA-AhR (**Figure 6A**) or GNF351 10^{-6} M (**Figure 6B**), and significantly decreased in the presence of siRNA-GPR30 (**Figure 6C**). **Figures 6D–F** highlight that G1 10^{-6} M resulted in a significant increase in *CYP1A1* mRNA levels, and that this was totally impeded in the presence of siRNA-AhR (**Figure 6D**), GNF351 10^{-6} M (**Figure 6E**) and significantly decreased in the presence of siRNA-GPR30 (**Figure 6F**). Altogether, our XRE-luciferase experiments and RT-qPCR experiments confirmed, at the transcriptional

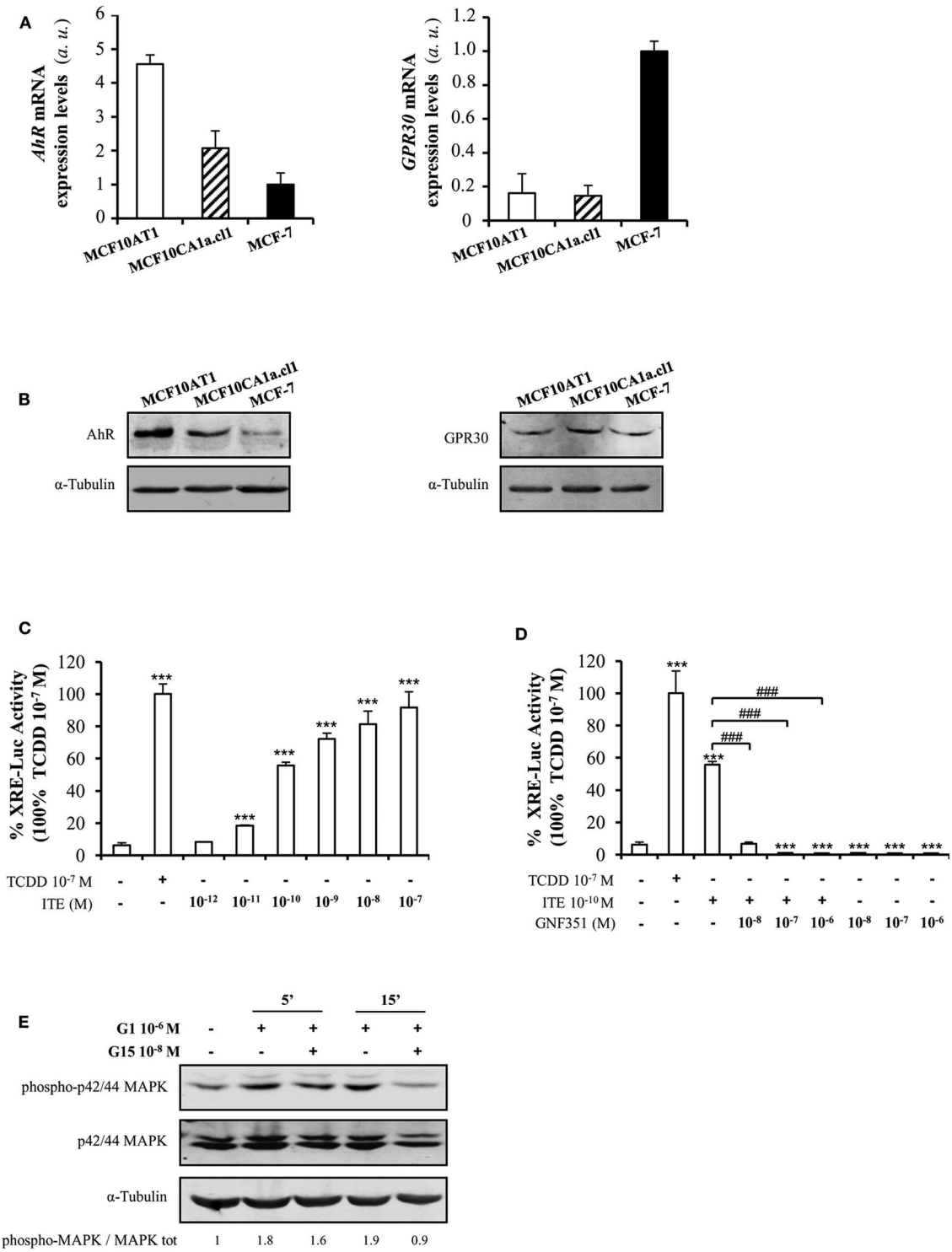

FIGURE 2 | AhR and GPR30 receptors are present and functional in the MCF10AT1 cells. **(A)** RT-qPCR analysis of *AhR* and *GPR30* mRNA expression levels represented in arbitrary units *(a.u.)* in the MCF10AT1 and MCF10CA1a.cl1 cells. MCF-7 cells were used as a control. Values represent mean ± SD of three

(Continued)

FIGURE 2 | independent experiments conducted in triplicate. **(B)** Representative Western blot analyses from three independent experiments of AhR and GPR30 protein expression in MCF10AT1 and MCF10CA1a.cl1 cells. MCF-7 cells were used as a control. **(C)** XRE-luciferase activity following 8 h exposure of MCF10AT1 cells to ITE at the indicated concentrations. TCDD 10^{-7} M was used as a control and results were expressed as % of TCDD 10^{-7} M activity. $^{***}p < 0.001$ in Student *t*-test. **(D)** XRE-luciferase activity upon 8 h of exposure to ITE 10^{-10} M alone or in combination with GNF351 at the indicated concentrations. TCDD 10^{-7} M was used as a control, and results were expressed as % of TCDD 10^{-7} M activity. Student *t*-tests revealed the statistically significant differences between unexposed and exposed cells: $^{***}p < 0.001$; and between ITE and ITE+GNF351: $^{\#\#\#}p < 0.001$. Values in **(C,D)** represent mean ± SD of three independent experiments. **(E)** Representative Western blot analyses from three independent experiments of the phospho-MAPK/MAPK ratio upon exposure of MCF10AT1 cells to G1 (GPR30 agonist) for the times indicated, in the presence or absence of a 2 h pre-treatment with G15 (GPR30 antagonist).

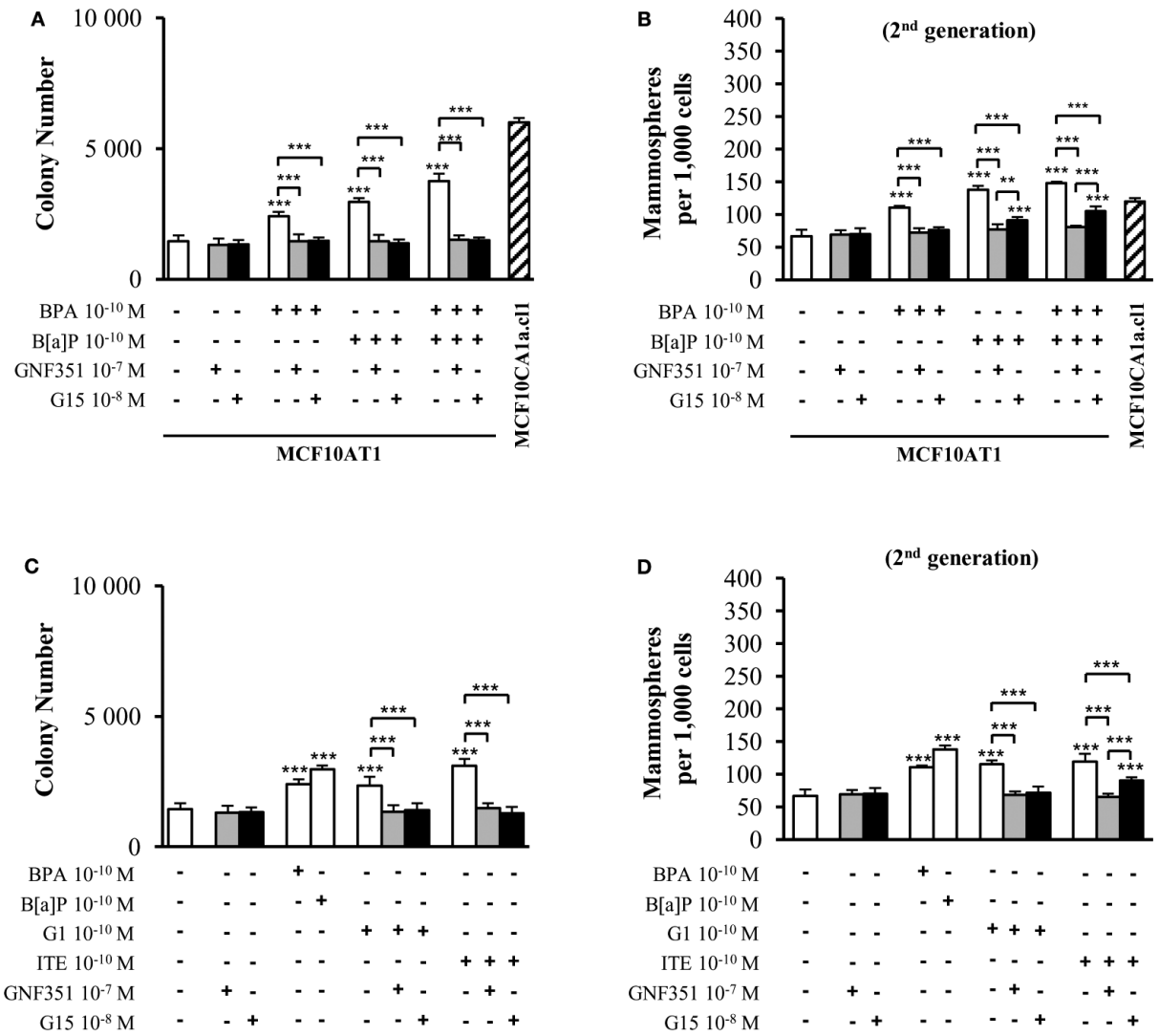

FIGURE 3 | Effects of short-term exposure of MCF10AT1 cells by BPA, B[a]P, ITE, and G1 on AIG and MFE are inhibited by GPR30 and AhR antagonists. Average number of colonies in soft agar **(A)** or of secondary mammospheres **(B)** upon exposure to B[a]P and/or BPA 10^{-10} M for 72 h in the presence or absence of a 2 h pre-treatment with GNF351 10^{-7} M or G15 10^{-8} M. Exposure was maintained throughout the course of the experiments. Unexposed MCF10CA1a.cl1 cells were used as a control. **(C)** Average number of colonies in soft agar or **(D)** secondary mammospheres formed after 72 h exposure with ITE 10^{-10} M or G1 10^{-10} M in the presence or the absence of a 2 h pre-treatment with GNF351 10^{-7} M or G15 10^{-8} M. Exposure to BPA 10^{-10} M or B[a]P 10^{-10} M was used as controls. Exposure was maintained throughout the course of the experiments. Data illustrated in **(A–D)** represent mean ± SD of at least three independent experiments, in triplicate. $^{***}p < 0.001$, $^{**}p < 0.01$ in Student *t*-test.

level, that GPR30-dependent mechanisms significantly impact and favor, directly or indirectly, AhR-driven transcriptional-dependent events.

Having verified that protein expression levels of AhR and of GPR30 were similar in both the unexposed and the pollutants-exposed $MCF10AT1_{60d}$ cells (**Supplementary Figure 5A**), the

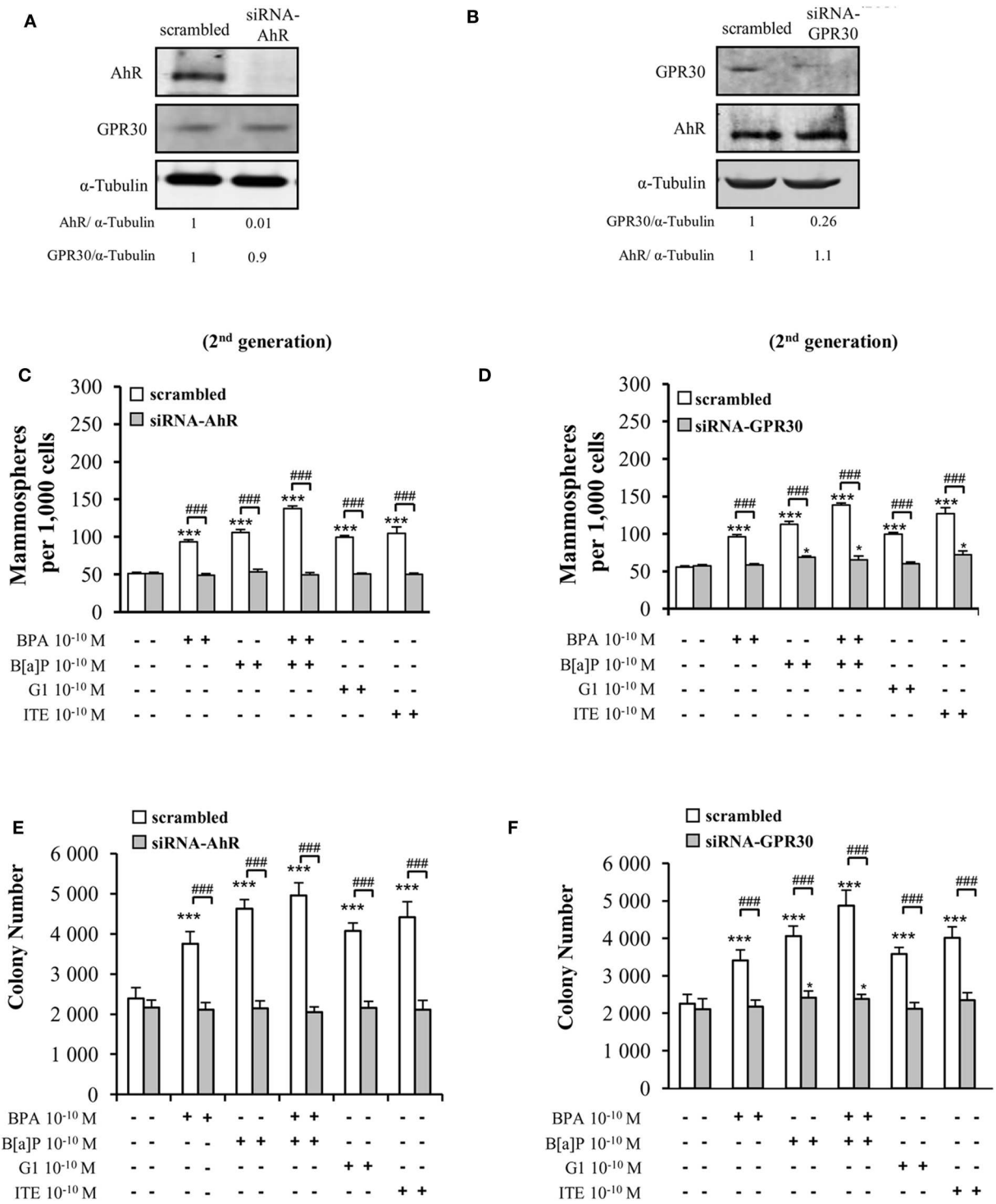

FIGURE 4 | Effects of short-term exposure of BPA, B[a]P, ITE and G1 10^{-10} M on AIG and MFE are inhibited by siRNA-AhR and siRNA-GPR30. Representative Western blot analysis from three independent experiments of AhR and GPR30 expression in transfected MCF10AT1 cells with **(A)** siRNA-AhR, **(B)** siRNA-GPR30 or their scrambled controls. Quantification of protein expression levels was normalized against tubulin expression. **(C,D)** Secondary mammospheres formation and **(E,F)** average number of colonies in soft agar, with the following treatments: BPA and/or B[a]P, G1, or ITE, 10^{-10} M. Cells were transfected with either siRNA-AhR, siRNA-GPR30 or their scrambled controls before being subjected to the treatments. Treatments were maintained throughout the course of experiments. (mean ± SD of 2 independent experiments, in triplicate). ***$p < 0.001$, *$p < 0.05$ vs. their respective unexposed; ###$p < 0.001$ siRNA vs. scrambled in Student *t*-test.

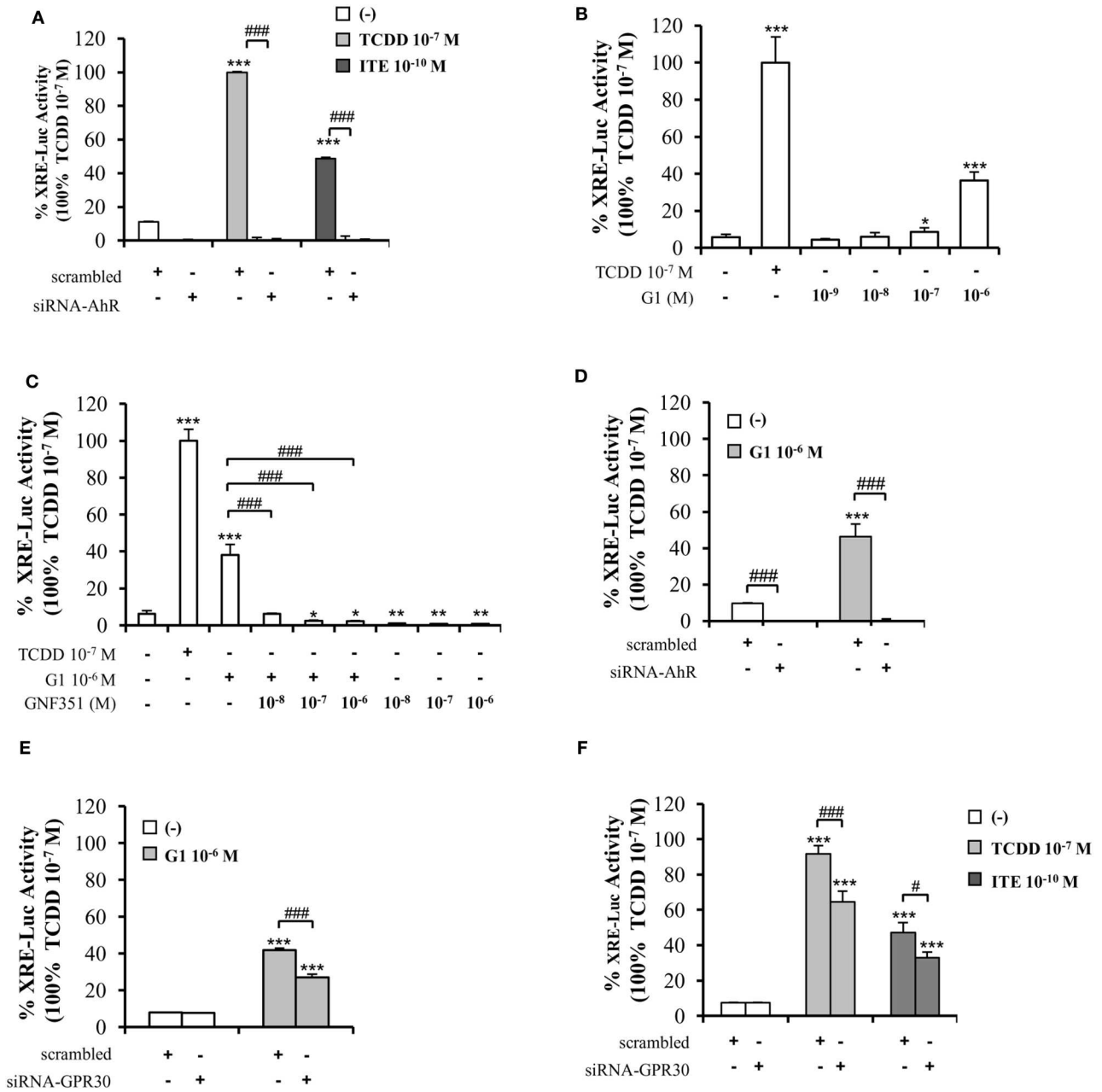

FIGURE 5 | Involvement of GPR30 in AhR transcriptional activity using XRE-luciferase assays. XRE-luciferase activity following 8 h exposure of MCF10AT1 cells to **(A)** ITE at the indicated concentrations, TCDD 10^{-7} M was used as a control and results were expressed as % of TCDD 10^{-7} M activity; in the presence or absence of siRNA-AhR **(B)** G1 at the indicated concentrations. TCDD 10^{-7} M was used as a control; **(C)** G1 10^{-6} M alone or in combination with GNF351 at the indicated concentrations; TCDD 10^{-7} M was used as a control. **(D,E)** XRE-luciferase activity in MCF10AT1 cells transfected with **(D)** siRNA-AhR, **(E)** siRNA-GPR30 or their respective scrambled and treated 48 h after siRNA transfection for 8 h with G1 10^{-6} M. **(F)** XRE-luciferase activity in MCF10AT1 cells transfected with either scrambled RNA or siRNA-GPR30 and treated for 8 h with TCDD 10^{-7} M or ITE 10^{-10} M after 48 h of siRNA transfection. All data represent mean ± SD of three independent experiments conducted in triplicate. $^{*}p < 0.05$, $^{**}p < 0.01$, $^{***}p < 0.001$; $^{\#}p < 0.05$; $^{\#\#\#}p < 0.001$ in Student *t*-test.

RNAseq data of each cell line were analyzed using the Ingenuity Pathway Analysis software. AhR core signaling was identified as significantly dysregulated in the $MCF10AT1_{60d}$ exposed cells compared to unexposed control $MCF10AT1_{60d}$ cells. Indeed, the significant enrichment of this canonical pathway was observed both in the B[a]P-exposed $MCF10AT1_{60d}$ cells ($p = 9.39\ 10^{-3}$), in the B[a]P + BPA exposed $MCF10AT1_{60d}$ cells ($p = 7.56\ 10^{-3}$), but also in the BPA-exposed $MCF10AT1_{60d}$ cells ($p = 1.26\ 10^{-2}$) (data not shown). Conversely, assessing the GPR30 signature previously described by Pandey and

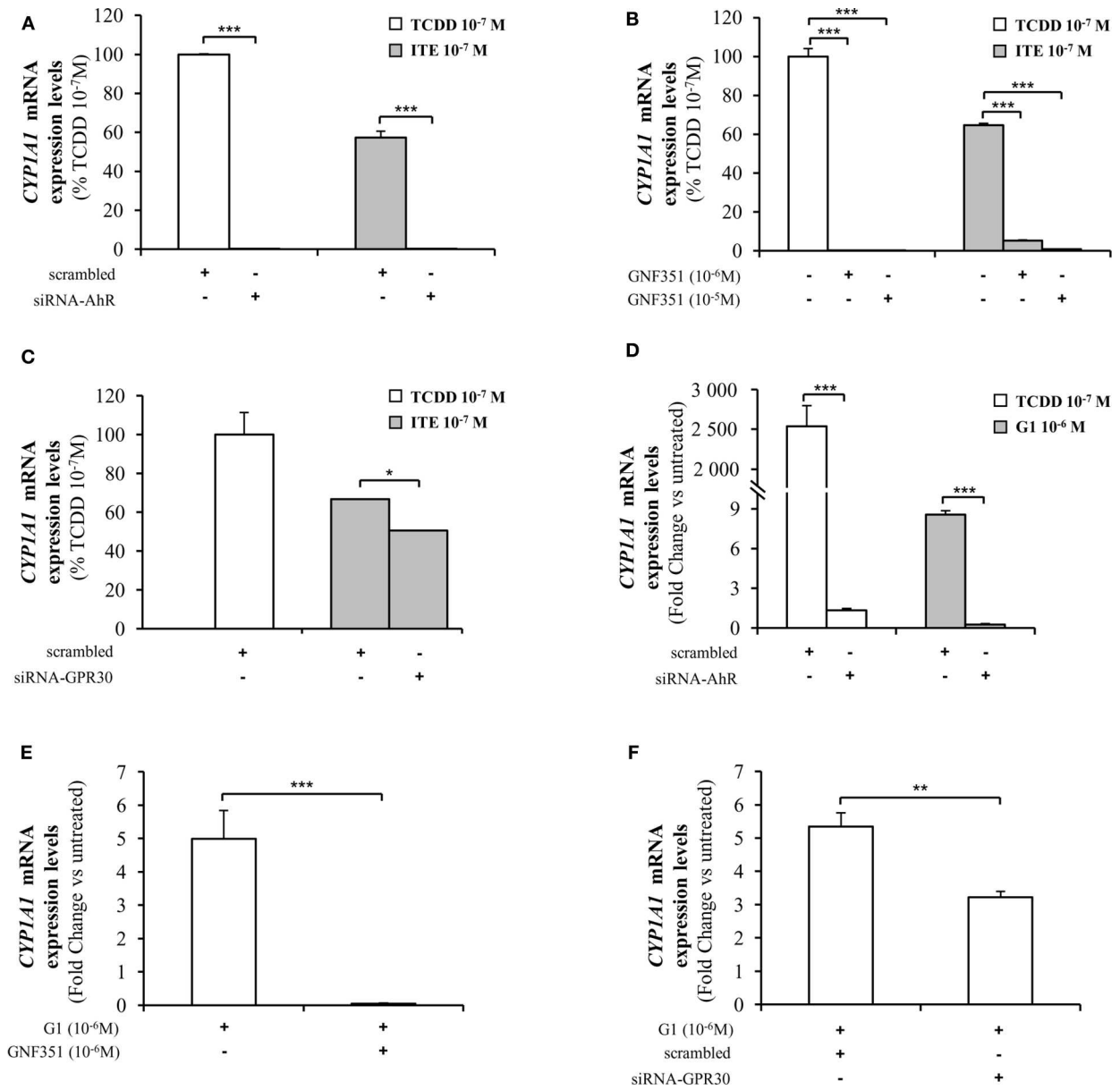

FIGURE 6 | Analysis of *CYP1A1* mRNA levels by quantitative RT-qPCR in MCF10AT1 cells. **(A)** *CYP1A1* expression levels in cells transfected with either siRNA-AhR or scrambled RNA after 4 h of exposure to ITE 10^{-7} M. TCDD 10^{-7} M was used as a control and results are expressed as % of TCDD 10^{-7} M activity. **(B)** *CYP1A1* mRNA expression levels in cells treated with GNF351 alone at indicated concentrations or in combination with ITE 10^{-7} M or TCDD 10^{-7} M. TCDD 10^{-7} M was used as a control and results are expressed as % of TCDD 10^{-7} M activity. **(C)** *CYP1A1* mRNA expression levels in cells transfected with either siRNA-GPR30 or scrambled RNA and exposed to ITE 10^{-7} M for 4 h. TCDD 10^{-7} M was used as a control and results are expressed as % of TCDD 10^{-7} M activity. **(D)** *CYP1A1* mRNA expression levels in cells transfected with either siRNA-AhR or scrambled RNA and exposed to G1 10^{-6} M or TCDD 10^{-7} M for 24 h. TCDD 10^{-7} M was used as a control. **(E)** *CYP1A1* mRNA expression levels in cells treated with G1 10^{-6} M in the presence or absence of GNF351 10^{-6} M. **(F)** *CYP1A1* mRNA expression levels in cells transfected with either siRNA-GPR30 or scrambled RNA and exposed to G1 10^{-6} M for 24 h. Data represent mean ± SD of 3 independent experiments conducted in triplicate. **(A–F)** The Student *t*-test was applied to reveal statistically significant differences between treatments: $^{*}p < 0.05$, $^{**}p < 0.01$, $^{***}p < 0.001$.

collaborators (51) in the Ingenuity Pathway Analysis software did not reveal any dysregulation in GPR30 signaling when the exposed $MCF10AT1_{60d}$ cells were compared with the unexposed control $MCF10AT1_{60d}$ cells (data not shown). As rapid phosphorylation of MAPK is one of the main downstream effects of GPR30 activation (65), we assessed the activation status of the MAPK pathway in the unexposed and exposed $MCF10AT1_{60d}$ cells. **Supplementary Figure 5B** demonstrated that chronic and low-dose-exposure of MCF10AT1 cells to B[a]P and/or BPA at 10^{-10} M did not lead to any activation of p42/p44MAPK ($MCF1Ca1.cl1_{60d}$ cells were used as controls). Altogether, our data suggest that AhR signaling is constitutively

TABLE 1 | Univariate analysis of the *GPR30* mRNA expression levels, the *AhR* mRNA expression levels and the *GPR30/AhR* mRNA expression signature with regards to overall survival (OS) in different subclasses of the 113 breast cancer samples of the CLB cohort.

	n	***GPR30* mRNA levels**			***AhR* mRNA levels**			***AhR/GPR30* signature**		
		HR[a]	**95% CI[b]**	***p*[c]**	**HR[a]**	**95% CI[b]**	***p*[c]**	**HR[a]**	**95% CI[b]**	***p*[c]**
All breast tumor samples	113	2.78	0.8 to 4.1	NS (0.09)	0.68	0.6 to 3.4	NS (0.41)	6.15	1.1 to 5.6	**0.01**
ER+ subclass	68	0.66	0.4 to 9.2	NS (0.42)	0.10	0.2 to 3.1	NS (0.75)	0.67	0.4 to 6.5	NS (0.41)
ER- subclass	45	5.39	1.1 to 13.3	**0.02**	2.08	0.7 to 9.7	NS (0.15)	10.25	1.7 to 20.1	**0.001**
Luminal subclass (ER+/PR+)[d]	62	0.03	0.2 to 6.3	NS (0.87)	0.11	0.2 to 3.8	NS (0.74)	0.45	0.4 to 8.5	NS (0.50)
HER2- enriched subclass (ER-/PR-/HER2+)[d]	16	2.56	0.5 to 63.1	NS (0.11)	0.17	0.2 to 18.2	NS (0.68)	4.47	0.8 to 96.6	**0.03**
Triple negative subclass (ER-/PR-/HER2-)[d]	21	-	NA[e]	–	0.005	0.1 to 12.1	NS (0.94)	-	N/A[f]	-

[a]*HR, Hazard ratio.*
[b]*95% CI, 95% confidence interval.*
[c]*p was considered significant when p < 0.05 (bold values). NS, not significant.*
[d]*subclasses of breast cancer were determined using immunohistology (ER, PR, HER2) according to the St Gallen recommendation (68).*
[e]*N/A, not applicable as all the cases are censored in the high GPR30 mRNA level group.*
[f]*N/A, not applicable as all the cases are censored in the high GPR30 and/or AhR mRNA level group.*

activated in the $MCF10AT1_{60d}$ exposed to pollutants vs. unexposed cells.

The *GPR30/AhR* Gene Expression Signature Indicates Poor Prognosis

To investigate the clinical relevance of AhR and GPR30, we performed RT-qPCR analyses to explore *GPR30* and *AhR* mRNA expression levels in a cohort of 113 human primary breast tumor samples (**Table 1**) (53). The resulting Kaplan-Meier curves are shown in **Figure 7**. By univariate analysis, we found that neither *GPR30* nor *AhR* mRNA levels were informative ($p = 0.09$ and $p = 0.41$, **Figures 7A,B**, respectively), while an *AhR/GPR30* gene expression signature based on high expression levels of both *GPR30* and *AhR* was significantly associated with shorter overall survival (OS) ($p = 0.01$, **Table 1** and **Figure 7C**). Regarding breast cancer subclasses, the *AhR/GPR30* gene expression signature was more informative in the ER-negative ($p = 0.001$) than in the ER-positive ($p = 0.41$) (**Table 1**, **Figures 7D,E**) or luminal subclasses and ($p = 0.50$) (**Table 1**). The situation was less clear for the HER2-enriched and triple-negative subclasses, considering the limited size of available samples ($n = 16$ and $n = 21$, respectively). We thus performed retrospective analysis of gene-expression array data using the KMP cohort, which contains a sizeable number of breast cancer patients (1,308 ER-positive, 569 ER-negative, 1,055 luminal, 419 HER2-enriched, and 403 triple-negative/basal-like). The most striking results (**Table 2**, univariate analysis) indicated that the *AhR/GPR30* signature was again more informative than *GPR30* mRNA or *AhR* mRNA levels alone and was associated with shorter OS in the ER-negative subclass ($p = 0.005$), but not in the ER-positive or the luminal subclasses (**Table 2**). The "all breast tumor samples" univariate analysis of the KMP cohort did not validate what was observed in the CLB cohort, but this discrepancy might reflect the difference in proportion of the ER-positive and ER-negative subclasses in the two cohorts. Finally, the KMP cohort revealed that the *AhR/GPR30* signature was associated with shorter OS in the triple-negative subclass ($p = 0.033$). Altogether, our data reveal a new/original signature based on a combination of high *AhR* mRNA expression levels and high *GPR30* mRNA expression levels that represents a novel marker for poor prognosis in breast cancer, especially in ER-negative or triple-negative subclasses.

Strategies Inhibiting the Impact of Chronic and Low-Dose Exposure to B[a]P and BPA in Early-Transformed MCF10AT1 Cells

To identify candidate strategies capable of blocking mammary carcinogenesis associated with chronic exposure to low doses (10^{-10}M) of the environmental pollutants B[a]P and BPA, MCF10AT1 cells were exposed for 60 days, in the presence or the absence of the AhR antagonist GNF351 10^{-7} M and/or the GPR30 antagonist G15 10^{-8} M (**Figures 8A,B**). Exposure for 60 days to the two antagonists, alone or in combination, had no impact on MFE and AIG. Strikingly, co-exposure for 60 days to B[a]P + BPA 10^{-10} M with GNF351 10^{-7} M and/or G15 10^{-8} M was sufficient to inhibit the development of pollutants-driven enhancement of cancerous properties (AIG and MFE) in MCF10AT1 cells (**Figures 8A,B**).

DISCUSSION

A growing body of *in vitro* and *in vivo* experimental evidence suggests the implication of environmental factors in the development and progression of breast cancer. People are chronically exposed to a mixture of environmental factors, usually present at low-dose concentrations, constituting a complex exposome. B[a]P is detected at picomolar concentrations in body fluids and tissues of cancer patients (58–60). BPA is detected at nanomolar concentrations in human samples such as serum, urine and maternal milk (61, 62). The major obstacles in studying the impact of these two pollutants *in vitro* on breast tumorigenesis are thus the choice

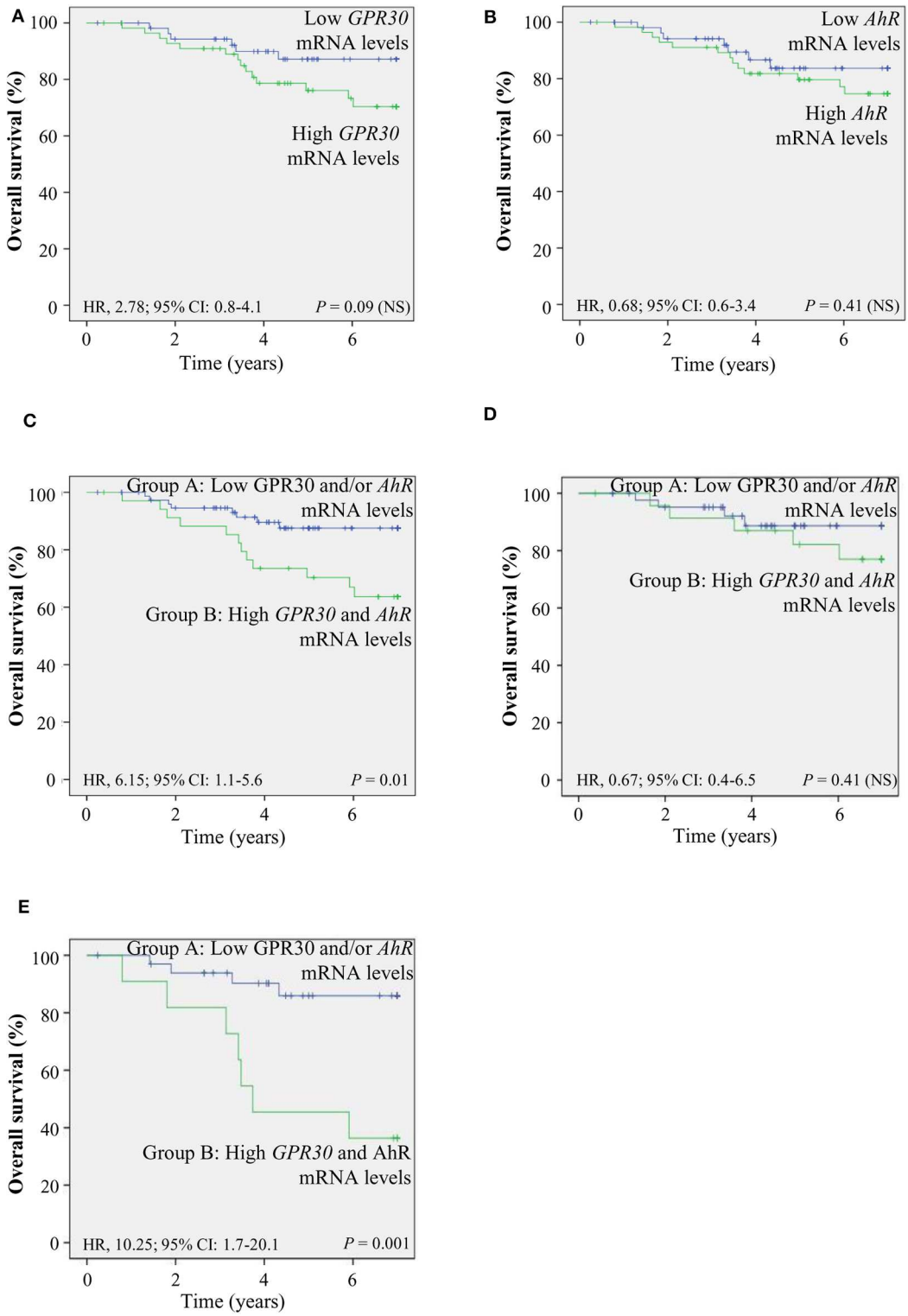

FIGURE 7 | The *AhR/GPR30* mRNA expression signature is of poor prognosis and is associated with shorter overall survival (OS). Kaplan-Meier analysis (univariate analysis) of OS in the CLB breast cancer cohort of: **(A)** *GPR30* mRNA expression levels; **(B)** *AhR* mRNA expression levels; **(C–E)** Patients were divided into two groups: patients expressing low *GPR30* mRNA levels and/or low levels of *AhR* mRNA (group A) and patients expressing high mRNA levels of *GPR30* and *AhR* (group B). **(C)** *AhR/GPR30* gene expression signature in all breast tumor samples. **(D)** *GPR30/AhR* gene expression signature in the ER-positive subclass. **(E)** *GPR30/AhR* mRNA expression signature in the ER-negative subclass. NS, not significant.

TABLE 2 | Univariate analysis of the *GPR30* mRNA expression levels, the *AhR* mRNA expression levels and the *GPR30/AhR* mRNA expression signature with regards to overall survival (OS) in different subclasses of the 1,877 breast cancer samples of the Kaplan-Meier plotter (KMP) cohort.

	n	***GPR30* mRNA levels**			***AhR* mRNA levels**			***AhR/GPR30* signature**		
		HR[a]	**95% CI[b]**	***p*[c]**	**HR[a]**	**95% CI[b]**	***p*[c]**	**HR[a]**	**95% CI[b]**	***p*[c]**
All breast tumor samples	1,877	0.83	0.68 to 1.01	NS (0.06)	0.91	0.73 to 1.15	NS (0.4)	0.78	0.46 to 1.10	NS (0.14)
ER+ subclass	1,308	0.82	0.62 to 1.08	NS (0.15)	0.83	0.63 to 1.1	NS (0.2)	0.67	0.26 to 1.08	NS (0.06)
ER- subclass	569	1.46	1.06 to 2.02	**0.02**	1.24	0.89 to 1.73	NS (0.2)	1.88	1.43 to 2.33	**0.005**
Luminal subclass	1,055	1.2	0.88 to 1.64	NS (0.24)	0.8	0.58 to 1.11	NS (0.18)	0.95	0.5 to 1.4	NS (0.82)
HER2- enriched subclass	419	1.22	0.84 to 1.77	NS (0.29)	0.79	0.54 to 1.16	NS (0.23)	0.99	0.45 to 1.53	NS (0.99)
Triple negative / Basal-like subclass	403	1.44	0.97 to 2.13	NS (0.06)	1.22	0.79 to 1.88	NS (0.36)	1.85	1.28 to 2.41	**0.033**

[a]*HR, Hazard ratio.*
[b]*95% CI, 95% confidence interval.*
[c]*p was considered significant when p < 0.05 (bold values). NS, not significant.*
[d]*breast cancer subclasses were based on the St Gallen recommendation (68) according to Gyorffy et al. (69).*

of a relevant cellular model and the use of relevant exposure conditions (long-term and low-dose exposure) mimicking natural exposure. The few studies having investigated the impact of chronic and low-dose exposure of B[a]P or BAP on tumor progression have focused on the early stage of carcinogenesis (non-transformed epithelial cells) (9–13, 29) MCF10AT1 breast cells (representing the early-transformed stage of the unique MCF10 model of mammary progression from normal epithelium to triple negative breast cancer (43, 44) have, to our knowledge, never been used to test the impact of chronic and low-dose exposure to environmental pollutants. While the genotoxic and pro-carcinogenic B[a]P and the EDC BPA are two of the most studied pollutants, no previous studies, to our knowledge, have investigated whether the combination of BPA and B[a]P, each compound possessing distinct mechanisms of action, induces potentiating effects on tumor progression.

The present study aimed at addressing: (i) the effects of long-term, cumulative exposure to low doses of B[a]P or BPA on the mammary early-transformed substage; (ii) whether the combination of BPA with B[a]P, each compound possessing distinct mechanisms of action, impacts breast tumor progression differently from what might be observed with each compound tested alone. Our study reveals that long term and low dose (10^{-10} M) exposure to B[a]P and/or BPA increases the cancerous properties (AIG and cancer stem-like properties) of the early-transformed MCF10AT1 cells, and the longer the cells were exposed, the greater was the impact. Co-exposure of MCF10AT1 cells with the B[a]P and BPA led to a significantly greater aggressive phenotype compared to B[a]P alone, suggesting that BPA facilitates the pro-carcinogenic activity of B[a]P and supporting the potentiating effects of distinct pollutants present in the exposome. Importantly, the aggressiveness developed by the exposed $MCF10AT1_{60d}$ cells was acquired and not softened or reverted after stopping B[a]P and/or BPA exposure. Altogether, our data reveal that long-term and low dose exposure to B[a]P and/or BPA irreversibly favors the evolution of early-transformed human mammary cells toward breast tumor progression.

Mechanistically, while B[a]P and BPA are well-known activators of AhR and GPR30, respectively, our short-term exposure experiments highlight that the MFE and AIG response triggered by exposure of MCF10AT1 cells to B[a]P and/or BPA occurs through a functional cross-talk between AhR and GPR30. Regarding the impact of inactivating AhR or GPR30 by two different strategies (using an antagonist molecule or a siRNA strategy), the BPA, BPA+B[a]P, or G1 impact on AIG and MFE was totally reversed when AhR was inhibited, while the GPR30 inactivation globally seemed to lead to a significant but not total, reversion of B[a]P, BPA+B[a]P, or ITE impact (in particular in MFE experiments). Finally, this study provided evidence that long-term (60 days) co-exposure to B[a]P + BPA 10^{-10} M with the AhR antagonist GNF351 10^{-7} M and/or the GPR30 antagonist G15 10^{-8} M inhibited the development of pollutants-driven enhancement of cancerous properties in MCF10AT1 cells.

The AhR/CYP1A1 pathway participates in carcinogenesis by mediating stem properties, the formation of mammospheres, expansion of breast cancer stem cells, and the transcriptional activity of AhR is mainly implicated in such effects (24). Our study also reveals that GPR30 participates and favors AhR-dependent transcriptional activity in early-transformed breast cells. Indeed, the GPR30 agonist G1 was able to stimulate AhR-dependent driven activity and *CYP1A1* gene transcription. GPR30 silencing by a siRNA strategy led to a significant, yet moderate, decrease in ITE-, G1-, or TCDD-mediated activation of AhR-driven transcriptional activity or *CYP1A1* transcription. This suggests that GPR30-dependent mechanisms other than those influencing the AhR-driven transcriptional mechanisms might be involved in the AhR/GPR30 cross-talk impacting AIG and MFE. Altogether, our *in vitro* data support a model in which GPR30 is involved in an AhR-dependent network leading to increased cancerous properties of early-transformed mammary cells.

We thus propose a model (**Figure 8C**) in which AhR signaling plays a "driving role" in the AhR/GPR30 cross-talk

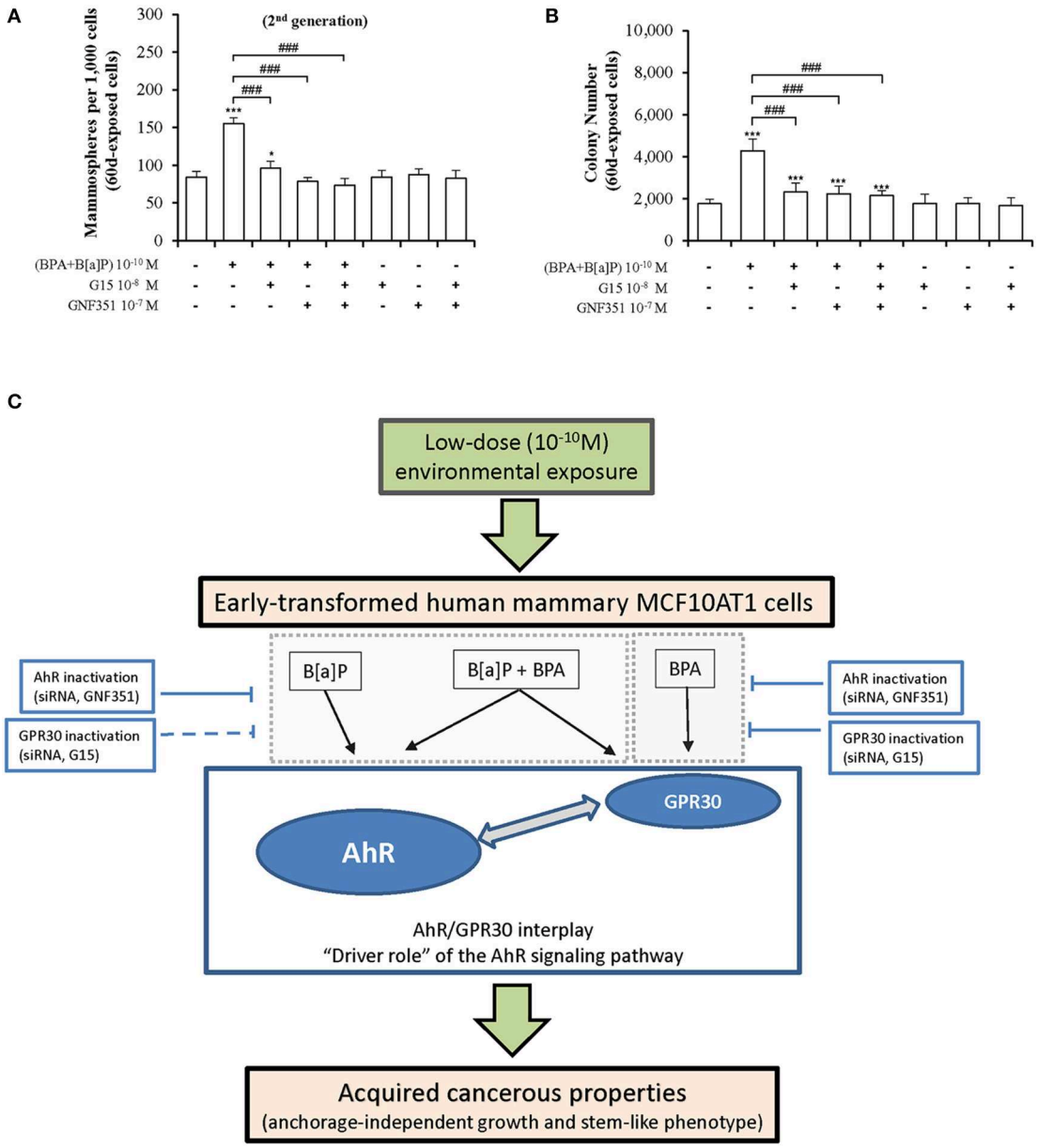

FIGURE 8 | Long-term and low-dose exposure to B[a]P and/or BPA in promoting cancerous properties of early-transformed human mammary cells is driven by AhR/GPR30 cross-talk. Inhibition of the effects due to chronic and low-dose exposure of MCF10AT1 cells to BPA+B[a]P (10^{-10} M), using AhR and/or GPR30 antagonists: **(A)** formation of secondary mammospheres, **(B)** AIG. The MCF10AT1 cells were chronically (60 days) unexposed or exposed to B[a]P + BPA 10^{-10} M, alone or in combination with GNF351 10^{-7} M and/or G15 10^{-8} M. Control experiments were performed in MCF10AT1 cells exposed for 60 days to GNF351 10^{-7} M and/or G15 10^{-8} M (mean ± SD of 3 independent experiments, in triplicate). $^{*}p < 0.05$, $^{***}p < 0.001$ vs. unexposed; $^{\#\#\#}p < 0.001$ vs. BPA+B[a]P (10^{-10} M); **(C)** Diagram summarizing our findings.

in mediating the effects of long-term and low dose exposure of B[a]P and/or BPA on AIG and MFE in MCF10AT1 cells. The relevance of our model was supported by our RNAseq data demonstrating that the canonical AhR signaling pathway was significantly enriched in the B[a]P-exposed $MCF10AT1_{60d}$ cells, in the B[a]P + BPA exposed MCF10AT160d cells, but also in the BPA-exposed $MCF10AT1_{60d}$ cells. Strengthening our findings, previous studies support a role for AhR and breast tumor progression: (i) AhR expression levels were significantly up-regulated in human breast ductal carcinoma *in situ* and breast cancer tissues compared to normal/benign breast tissues (70, 71); (ii) an *in vivo* model of breast tumorigenesis suggests that AhR is constitutively activated at early stages of mammary tumorigenesis (72); (iii) the prognostic value of AhR seems to be dependent on the activation/inactivation of metastatic processes (73).

While this research was ongoing, a study was published supporting our data by demonstrating in the ERα-negative SKBR3 breast cancer cells that the environmental pollutant 3-methylcholantrene, mainly known to exert its carcinogenic effects through AhR, stimulates cell growth response through a functional interaction between AhR and GPR30 (74). However, in the ERα-positive MCF-7 breast cancer cell line, possessing the well-identified close cross-talk between AhR and ERα [for review (75)], 10^{-5} M G1 was demonstrated to increase transcription of *CYP1A1* mRNA in AhR-dependent, but GPR30-independent, mechanisms (76). As MCF10AT1 cells used in this study are triple-negative cells and the SKBR3 cells are ERα-negative, one cannot exclude that the detrimental functional cross-talk between AhR and GPR30 might be exacerbated in such a specific cellular breast context. Supporting previous data highlighted that in the ERα-negative/triple negative context, an AhR-signaling reinforces cell aggressiveness and induces breast cancer stem cells (77–80).

Altogether, our *in vitro* data thus demonstrated the role of the AhR/GPR30 cross-talk in favoring tumor progression, at least in a triple-negative breast context. Previous controversial studies emerged regarding the prognostic value of AhR or GPR30 expression levels in breast cancers (71, 73, 80–84), and these discrepancies have been suggested as possibly related to the breast cancer subgroup or the substage considered. In the present study, the clinical relevance of our *in vitro* findings was further reinforced by retrospective analysis of two independent breast cancer cohorts, showing that in only ER-negative or triple-negative breast cancer subclasses, the gene signature involving both *AhR* and *GPR30* mRNA levels were of poor prognosis.

Hence, we have provided novel insights into the progression of early-transformed human mammary cells upon long-term and low-dose exposure to B[a]P and/or BPA and deciphered the involvement of the functional crosstalk occurring between AhR and GPR30 leading to an exacerbated AhR-driven network. Our *in vitro* and retrospective data analyses further support the idea that the deleterious impact of this cross-talk might be of utmost importance in the progression of ER-negative or triple-negative breast cancers. More importantly, strategies targeting AhR and/or GPR30 were demonstrated to be efficient in inhibiting the deleterious impact of cumulative and low-dose exposure to B[a]P and/or BPA in early-transformed MCF10AT1 cells. The identification of such molecular mechanisms may help in the discovery of human biomarkers of environmental carcinogen exposure and the development of preventive strategies.

DATA AVAILABILITY STATEMENT

The datasets generated from this study can be found in the NCBI Gene Expression Omnibus (GEO) [http://www.ncbi.nlm.nih.gov/geo/ (GSE142073)].

ETHICS STATEMENT

This study has been approved by the local ethics committee (CRB Centre Léon Bérard, France). All subjects gave written informed consent.

AUTHOR CONTRIBUTIONS

PAC, VM-S, VC, and BF participated in the design of the study. CD, ME, SG, and SA performed the *in vitro* data. PAC and CD performed the biostatistical analysis on the CLB cohort. BG performed the biostatistical analysis on the KMP cohort. AW, SC, and JL performed and analyzed the RNAseq data. SG, MD-A, AE, and PC participated in scientific discussions. PAC, CD, and ME wrote the manuscript. BG, AW, PC, JL, VC, VM-S, BF, CD, SG, and ME participated in the scientific revisions of the manuscript. PAC supervised the study.

FUNDING

CD was funded by the ANR (2011 ANR-CESA-018-01, Agence Nationale de la Recherche, France) and the University of Lyon 1. ME was funded by a PhD grant from the Lebanese University. This work was funded by the ANR (2011 ANR-CESA-018-01), Lyon Biopôle, and supported by grants from the Ligue nationale contre le cancer LNCC (committees 42 and 71).

ACKNOWLEDGMENTS

The authors thank the Centre de Ressources Biologiques (CRB) of the Centre Léon Bérard (BB-0033-00050). We are grateful to B. Manship for editing. We thank Dr. Balaguer for providing the HG5LN PXR cell line and the XRE-luc plasmid. Some of the work performed by ME during her thesis has been partly included in this article (85).

SUPPLEMENTARY MATERIAL

The Supplementary Material for this article can be found online at: https://www.frontiersin.org/articles/10.3389/fonc.2020.00712/full#supplementary-material

REFERENCES

1. Guengerich FP. Metabolism of chemical carcinogens. *Carcinogenesis.* (2000) 21:345–51. doi: 10.1093/carcin/21.3.345
2. DeBruin LS, Josephy PD. Perspectives on the chemical etiology of breast cancer. *Environ Health Perspect.* (2002) 110(Suppl.1):119–28. doi: 10.1002/sc271_5_1835
3. Hecht SS. Tobacco smoke carcinogens and breast cancer. *Environ Mol Mutagen.* (2002) 39:119–26. doi: 10.1002/em.10071
4. Roukos DH, Murray S, Briasoulis E. Molecular genetic tools shape a roadmap towards a more accurate prognostic prediction and personalized management of cancer. *Cancer Biol Ther.* (2007) 6:308–12. doi: 10.4161/cbt.6.3.3994
5. Kelloff GJ. *Cancer Chemoprevention* Totowa, NJ: Humana Press Inc. (2005). doi: 10.1007/978-1-59259-768-0

6. Benigni R, Bossa C. Mechanisms of chemical carcinogenicity and mutagenicity: a review with implications for predictive toxicology. *Chem Rev.* (2011) 111:2507–36. doi: 10.1021/cr100222q
7. Rudel RA, Fenton SE, Ackerman JM, Euling SY, Makris SL. Environmental exposures and mammary gland development: state of the science, public health implications, and research recommendations. *Environ Health Perspect.* (2011) 119:1053–61. doi: 10.1289/ehp.1002864
8. Koual M, Cano-Sancho G, Bats AS, Tomkiewicz C, Kaddouch-Amar Y, Douay-Hauser N, et al. Associations between persistent organic pollutants and risk of breast cancer metastasis. *Environ Int.* (2019) 132:105028. doi: 10.1016/j.envint.2019.105028
9. Siriwardhana N, Wang HC. Precancerous carcinogenesis of human breast epithelial cells by chronic exposure to benzo[a]pyrene. *Mol Carcinog.* (2008) 47:338–48. doi: 10.1002/mc.20392
10. Rathore K, Wang HC. Green tea catechin extract in intervention of chronic breast cell carcinogenesis induced by environmental carcinogens. *Mol Carcinog.* (2012) 51:280–9. doi: 10.1002/mc.20844
11. Rathore K, Wang HC. Mesenchymal and stem-like cell properties targeted in suppression of chronically-induced breast cell carcinogenesis. *Cancer Lett.* (2013) 333:113–23. doi: 10.1016/j.canlet.2013.01.030
12. Pluchino LA, Wang HC. Chronic exposure to combined carcinogens enhances breast cell carcinogenesis with mesenchymal and stem-like cell properties. *PLoS ONE.* (2014) 9:e108698. doi: 10.1371/journal.pone.0108698
13. Clement F, Xu X, Donini CF, Clement A, Omarjee S, Delay E, et al. Long-term exposure to bisphenol A or benzo(a)pyrene alters the fate of human mammary epithelial stem cells in response to BMP2 and BMP4, by pre-activating BMP signaling. *Cell Death Differ.* (2017) 24:155–66. doi: 10.1038/cdd.2016.107
14. Mehta RG. Experimental basis for the prevention of breast cancer. *Eur J Cancer.* (2000) 36:1275–82. doi: 10.1002/S0959-804900100-3
15. Caruso JA, Reiners JJJr, Emond J, Shultz T, Tainsky MA, Alaoui-Jamali M, et al. Genetic alteration of chromosome 8 is a common feature of human mammary epithelial cell lines transformed *in vitro* with benzo[a]pyrene. *Mutat Res.* (2001) 473:85–99. doi: 10.1016/s0027-5107(00)00140-8
16. Jaiswal AS, Panda H, Pampo CA, Siemann DW, Gairola CG, Hromas R, et al. Adenomatous polyposis coli-mediated accumulation of abasic DNA lesions lead to cigarette smoke condensate-induced neoplastic transformation of normal breast epithelial cells. *Neoplasia.* (2013) 15:454–60. doi: 10.1593/neo.13176
17. IARC. Chemical agents and related occupations. *IARC Monogr Eval Carcinog Risks Hum.* (2012) 100:9–562.
18. Rundle A, Tang D, Hibshoosh H, Estabrook A, Schnabel F, Cao W, et al. The relationship between genetic damage from polycyclic aromatic hydrocarbons in breast tissue and breast cancer. *Carcinogenesis.* (2000) 21:1281–9.
19. Shi S, Yoon DY, Hodge-Bell KC, Bebenek IG, Whitekus MJ, Zhang R, et al. The aryl hydrocarbon receptor nuclear translocator (Arnt) is required for tumor initiation by benzo[a]pyrene. *Carcinogenesis.* (2009) 30:1957–61. doi: 10.1093/carcin/bgp201
20. Kasala ER, Bodduluru LN, Barua CC, Sriram CS, Gogoi R. Benzo(a)pyrene induced lung cancer: role of dietary phytochemicals in chemoprevention. *Pharmacol Rep.* (2015) 67:996–1009. doi: 10.1016/j.pharep.2015.03.004
21. Keshava C, Divi RL, Whipkey DL, Frye BL, McCanlies E, Kuo M, et al. Induction of CYP1A1 and CYP1B1 and formation of carcinogen-DNA adducts in normal human mammary epithelial cells treated with benzo[a]pyrene. *Cancer Lett.* (2005) 221:213–24. doi: 10.1016/j.canlet.2004.08.038
22. Shi Q, Godschalk RWL, van Schooten FJ. Inflammation and the chemical carcinogen benzo[a]pyrene: partners in crime. *Mutat Res.* (2017) 774:12–24. doi: 10.1016/j.mrrev.2017.08.003
23. Divi RL, Lindeman TL, Shockley ME, Keshava C, Weston A, Poirier MC. Correlation between CYP1A1 transcript, protein level, enzyme activity and DNA adduct formation in normal human mammary epithelial cell strains exposed to benzo[a]pyrene. *Mutagenesis.* (2014) 29:409–17. doi: 10.1093/mutage/geu049
24. Al-Dhfyan A, Alhoshani A, Korashy HM. Aryl hydrocarbon receptor/cytochrome P450 1A1 pathway mediates breast cancer stem cells expansion through PTEN inhibition and beta-Catenin and Akt activation. *Mol Cancer.* (2017) 16:14. doi: 10.1186/s12943-016-0570-y
25. Vazquez-Gomez G, Rocha-Zavaleta L, Rodriguez-Sosa M, Petrosyan P, Rubio-Lightbourn J. Benzo[a]pyrene activates an AhR/Src/ERK axis that contributes to CYP1A1 induction and stable DNA adducts formation in lung cells. *Toxicol Lett.* (2018) 289:54–62. doi: 10.1016/j.toxlet.2018.03.012
26. Calaf G, Russo J. Transformation of human breast epithelial cells by chemical carcinogens. *Carcinogenesis.* (1993) 14:483–92.
27. Russo J, Tahin Q, Lareef MH, Hu YF, Russo IH. Neoplastic transformation of human breast epithelial cells by estrogens and chemical carcinogens. *Environ Mol Mutagen.* (2002) 39:254–63. doi: 10.1002/em.10052
28. Guo J, Xu Y, Ji W, Song L, Dai C, Zhan L. Effects of exposure to benzo[a]pyrene on metastasis of breast cancer are mediated through ROS-ERK-MMP9 axis signaling. *Toxicol Lett.* (2015) 234:201–10. doi: 10.1016/j.toxlet.2015.02.016
29. Chapellier M, Bachelard-Cascales E, Schmidt X, Clement F, Treilleux I, Delay E, et al. Disequilibrium of BMP2 levels in the breast stem cell niche launches epithelial transformation by overamplifying BMPR1B cell response. *Stem Cell Reports.* (2015) 4:239–54. doi: 10.1016/j.stemcr.2014.12.007
30. Giulivo M, Lopez de Alda M, Capri E, Barcelo D. Human exposure to endocrine disrupting compounds: their role in reproductive systems, metabolic syndrome and breast cancer. A review. *Environ Res.* (2016) 151:251–64. doi: 10.1016/j.envres.2016.07.011
31. Delfosse V, Grimaldi M, le Maire A, Bourguet W, Balaguer P. (Nuclear receptor profiling of bisphenol-A and its halogenated analogues. *Vitam Horm.* 2014) 94:229–51. doi: 10.1016/B978-0-12-800095-3
32. Seachrist DD, Bonk KW, Ho SM, Prins GS, Soto AM, Keri RA. A review of the carcinogenic potential of bisphenol A. *Reprod Toxicol.* (2016) 59:167–82. doi: 10.1016/j.reprotox.2015.09.006
33. Thomas P, Dong J. Binding and activation of the seven-transmembrane estrogen receptor GPR30 by environmental estrogens: a potential novel mechanism of endocrine disruption. *J Steroid Biochem Mol Biol.* (2006) 102:175–9. doi: 10.1016/j.jsbmb.2006.09.017
34. FAO/WHO, J. F. W. E. M., t.R.T.a.H.A.o,.B. A. O. O., Organization, W. H., Nations, F.a.A.O.o.t.U., and, F. A. O./W. H. O., et al. *Toxicological and health aspects of Bisphenol A : report of Joint FAO/WHO Expert Meeting 2-5 November 2010 and report of Stakeholder Meeting on Bisphenol A, 1 November 2010 Ottawa, Canada / Food and Agriculture Organization of the United Nations, World Health Organization.* Geneva: World Health Organization (2011).
35. Wetherill YB, Akingbemi BT, Kanno J, McLachlan JA, Nadal A, Sonnenschein C, et al. *In vitro* molecular mechanisms of bisphenol A action. *Reprod Toxicol.* (2007) 24:178–98. doi: 10.1016/j.reprotox.2007.05.010
36. Fernandez SV, Russo J. Estrogen and xenoestrogens in breast cancer. *Toxicol Pathol.* (2010) 38:110–22. doi: 10.1177/0192623309354108
37. Jenkins S, Betancourt AM, Wang J, Lamartiniere CA. Endocrine-active chemicals in mammary cancer causation and prevention. *J Steroid Biochem Mol Biol.* (2012) 129:191–200. doi: 10.1016/j.jsbmb.2011.06.003
38. Marchese S, Silva E. Disruption of 3D MCF-12A breast cell cultures by estrogens–an *in vitro* model for ER-mediated changes indicative of hormonal carcinogenesis. *PLoS ONE.* (2012) 7:e45767. doi: 10.1371/journal.pone.0045767
39. Soule HD, Maloney TM, Wolman SR, Peterson WDJr, Brenz R, McGrath CM, et al. Isolation and characterization of a spontaneously immortalized human breast epithelial cell line, MCF-10. *Cancer Res.* (1990) 50:6075–86.
40. Neve RM, Chin K, Fridlyand J, Yeh J, Baehner FL, Fevr T, et al. A collection of breast cancer cell lines for the study of functionally distinct cancer subtypes. *Cancer Cell.* (2006) 10:515–27. doi: 10.1016/j.ccr.2006.10.008
41. Sarrio D, Rodriguez-Pinilla SM, Hardisson D, Cano A, Moreno-Bueno G, Palacios J. Epithelial-mesenchymal transition in breast cancer relates to the basal-like phenotype. *Cancer Res.* (2008) 68:989–97. doi: 10.1158/0008-5472.CAN-07-2017
42. Kadota M, Yang HH, Gomez B, Sato M, Clifford RJ, Meerzaman D, et al. Delineating genetic alterations for tumor progression in the MCF10A series of breast cancer cell lines. *PLoS ONE.* (2010) 5:e9201. doi: 10.1371/journal.pone.0009201
43. Miller FR. Xenograft models of premalignant breast disease. *J Mammary Gland Biol Neoplasia.* (2000) 5:379–91. doi: 10.1023/a:1009577811584

44. Dawson PJ, Wolman SR, Tait L, Heppner GH, Miller FR. MCF10AT: a model for the evolution of cancer from proliferative breast disease. *Am J Pathol.* (1996) 148:313–9.
45. Li Q, Mullins SR, Sloane BF, Mattingly RR. p21-Activated kinase 1 coordinates aberrant cell survival and pericellular proteolysis in a three-dimensional culture model for premalignant progression of human breast cancer. *Neoplasia.* (2008) 10:314–29. doi: 10.1593/neo.07970
46. Banda M, Speyer CL, Semma SN, Osuala KO, Kounalakis N, Torres Torres KE, et al. Metabotropic glutamate receptor-1 contributes to progression in triple negative breast cancer. *PLoS ONE.* (2014) 9:e81126. doi: 10.1371/journal.pone.0081126
47. Lemaire G, Benod C, Nahoum V, Pillon A, Boussioux AM, Guichou JF, et al. Discovery of a highly active ligand of human pregnane x receptor: a case study from pharmacophore modeling and virtual screening to "*in vivo*" biological activity. *Mol Pharmacol.* (2007) 72:572–81. doi: 10.1124/mol.106.033415
48. Vendrell JA, Thollet A, Nguyen NT, Ghayad SE, Vinot S, Bieche I, et al. ZNF217 is a marker of poor prognosis in breast cancer that drives epithelial-mesenchymal transition and invasion. *Cancer Res.* (2012) 72:3593–606. doi: 10.1158/0008-5472.CAN-11-3095
49. Dontu G, Abdallah WM, Foley JM, Jackson KW, Clarke MF, Kawamura MJ, et al. *In vitro* propagation and transcriptional profiling of human mammary stem/progenitor cells. *Genes Dev.* (2003) 17:1253–70. doi: 10.1101/gad.1061803
50. Rasmussen MK, Balaguer P, Ekstrand B, Daujat-Chavanieu M, Gerbal-Chaloin S. Skatole (3-Methylindole) is a partial aryl hydrocarbon receptor agonist and induces CYP1A1/2 and CYP1B1 expression in primary human hepatocytes. *PLoS ONE.* (2016) 11:e0154629. doi: 10.1371/journal.pone.0154629
51. Pandey DP, Lappano R, Albanito L, Madeo A, Maggiolini M, Picard D. Estrogenic GPR30 signalling induces proliferation and migration of breast cancer cells through CTGF. *EMBO J.* (2009) 28:523–32. doi: 10.1038/emboj.2008.304
52. Thollet A, Vendrell JA, Payen L, Ghayad SE, Ben Larbi S, Grisard E, et al. ZNF217 confers resistance to the pro-apoptotic signals of paclitaxel and aberrant expression of Aurora-A in breast cancer cells. *Mol Cancer.* (2010) 9:291. doi: 10.1186/1476-4598-9-291
53. Nguyen NT, Vendrell JA, Poulard C, Gyorffy B, Goddard-Leon S, Bieche I, et al. A functional interplay between ZNF217 and estrogen receptor alpha exists in luminal breast cancers. *Mol Oncol.* (2014) 8:1441–57. doi: 10.1016/j.molonc.2014.05.013
54. Mihaly Z, Kormos M, Lanczky A, Dank M, Budczies J, Szasz MA, et al. A meta-analysis of gene expression-based biomarkers predicting outcome after tamoxifen treatment in breast cancer. *Breast Cancer Res Treat.* (2013) 140:219–32. doi: 10.1007/s10549-013-2622-y
55. Farnie G, Clarke RB. Mammary stem cells and breast cancer–role of Notch signalling. *Stem Cell Rev.* (2007) 3:169–75. doi: 10.1007/s12015-007-0023-5
56. Charafe-Jauffret E, Monville F, Ginestier C, Dontu G, Birnbaum D, Wicha MS. Cancer stem cells in breast: current opinion and future challenges. *Pathobiology.* (2008) 75:75–84. doi: 10.1159/000123845000123845
57. Kakarala M, Wicha MS. Implications of the cancer stem-cell hypothesis for breast cancer prevention and therapy. *J Clin Oncol.* (2008) 26:2813–20. doi: 10.1200/JCO.2008.16.3931
58. Obana H, Hori S, Kashimoto T, Kunita N. Polycyclic aromatic hydrocarbons in human fat and liver. *Bull Environ Contam Toxicol.* (1981) 27:23–7.
59. Hecht SS, Carmella SG, Chen M, Dor Koch JF, Miller AT, Murphy SE, et al. Quantitation of urinary metabolites of a tobacco-specific lung carcinogen after smoking cessation. *Cancer Res.* (1999) 59:590–6.
60. Besaratinia A, Maas LM, Brouwer EMC, Moonen EJC, De Kok TMCM, Wesseling GJ, et al. A molecular dosimetry approach to assess human exposure to environmental tobacco smoke in pubs. *Carcinogenesis.* (2002) 23:1171–6. doi: 10.1093/carcin/23.7.1171
61. Vandenberg LN, Chahoud I, Heindel JJ, Padmanabhan V, Paumgartten FJ, Schoenfelder G. Urinary, circulating, and tissue biomonitoring studies indicate widespread exposure to bisphenol A. *Environ Health Perspect.* (2010) 118:1055–70. doi: 10.1289/ehp.0901716
62. Teeguarden JG, Twaddle NC, Churchwell MI, Yang X, Fisher JW, Seryak LM, et al. 24-hour human urine and serum profiles of bisphenol A: evidence against sublingual absorption following ingestion in soup. *Toxicol Appl Pharmacol.* (2015) 288:131–42. doi: 10.1016/j.taap.2015.01.009
63. Song Z, Pollenz RS. Ligand-dependent and independent modulation of aryl hydrocarbon receptor localization, degradation, and gene regulation. *Mol Pharmacol.* (2002) 62:806–16. doi: 10.1124/mol.62.4.806
64. Smith KJ, Murray IA, Tanos R, Tellew J, Boitano AE, Bisson WH, et al. Identification of a high-affinity ligand that exhibits complete aryl hydrocarbon receptor antagonism. *J Pharmacol Exp Ther.* (2011) 338:318–27. doi: 10.1124/jpet.110.178392
65. Filardo EJ, Quinn JA, Bland KI, Frackelton ARJr. Estrogen-induced activation of Erk-1 and Erk-2 requires the G protein-coupled receptor homolog, GPR30, and occurs via trans-activation of the epidermal growth factor receptor through release of HB-EGF. *Mol Endocrinol.* (2000) 14:1649–60. doi: 10.1210/mend.14.10.0532
66. Bologa CG, Revankar CM, Young SM, Edwards BS, Arterburn JB, Kiselyov AS, et al. Virtual and biomolecular screening converge on a selective agonist for GPR30. *Nat Chem Biol.* (2006) 2:207–12. doi: 10.1038/nchembio775
67. Dennis MK, Burai R, Ramesh C, Petrie WK, Alcon SN, Nayak TK, et al. *In vivo* effects of a GPR30 antagonist. *Nat Chem Biol.* (2009) 5:421–7. doi: 10.1038/nchembio.168
68. Goldhirsch A, Winer EP, Coates AS, Gelber RD, Piccart-Gebhart M, Thurlimann B, et al. Personalizing the treatment of women with early breast cancer: highlights of the St Gallen International Expert Consensus on the Primary Therapy of Early Breast Cancer 2013. *Ann Oncol.* (2013) 24:2206–23. doi: 10.1093/annonc/mdt303
69. Gyorffy B, Benke Z, Lanczky A, Balazs B, Szallasi Z, Timar J, et al. RecurrenceOnline: an online analysis tool to determine breast cancer recurrence and hormone receptor status using microarray data. *Breast Cancer Res Treat.* (2012) 132:1025–34. doi: 10.1007/s10549-011-1676-y
70. Li ZD, Wang K, Yang XW, Zhuang ZG, Wang JJ, Tong XW. Expression of aryl hydrocarbon receptor in relation to p53 status and clinicopathological parameters in breast cancer. *Int J Clin Exp Pathol.* (2014) 7:7931–7.
71. Saito R, Miki Y, Hata S, Takagi K, Iida S, Oba Y, et al. Aryl hydrocarbon receptor in breast cancer-a newly defined prognostic marker. *Horm Cancer.* (2014) 5:11–21. doi: 10.1007/s12672-013-0160-z
72. Trombino AF, Near RI, Matulka RA, Yang S, Hafer LJ, Toselli PA, et al. Expression of the aryl hydrocarbon receptor/transcription factor (AhR) and AhR-regulated CYP1 gene transcripts in a rat model of mammary tumorigenesis. *Breast Cancer Res Treat.* (2000) 63:117–31. doi: 10.1023/a:1006443104670
73. Jeschke U, Zhang X, Kuhn C, Jalaguier S, Colinge J, Pfender K, et al. The prognostic impact of the Aryl Hydrocarbon Receptor (AhR) in primary breast cancer depends on the lymph node status. *Int J Mol Sci.* (2019) 20. doi: 10.3390/ijms20051016
74. Cirillo F, Lappano R, Bruno L, Rizzuti B, Grande F, Guzzi R, et al. AHR and GPER mediate the stimulatory effects induced by 3-methylcholanthrene in breast cancer cells and cancer-associated fibroblasts (CAFs). *J Exp Clin Cancer Res.* (2019) 38:335. doi: 10.1186/s13046-019-1337-2
75. Tarnow P, Tralau T, Luch A. Chemical activation of estrogen and aryl hydrocarbon receptor signaling pathways and their interaction in toxicology and metabolism. *Expert Opin Drug Metab Toxicol.* (2019) 15:219–29. doi: 10.1080/17425255.2019.1569627
76. Tarnow P, Tralau T, Luch A. G protein-coupled receptor 30 ligand G-1 increases aryl hydrocarbon receptor signalling by inhibition of tubulin assembly and cell cycle arrest in human MCF-7 cells. *Arch Toxicol.* (2016) 90:1939–48. doi: 10.1007/s00204-015-1615-5
77. Romagnolo DF, Papoutsis AJ, Laukaitis C, Selmin OI. Constitutive expression of AhR and BRCA-1 promoter CpG hypermethylation as biomarkers of ERalpha-negative breast tumorigenesis. *BMC Cancer.* (2015) 15:1026. doi: 10.1186/s12885-015-2044-9
78. Novikov O, Wang Z, Stanford EA, Parks AJ, Ramirez-Cardenas A, Landesman E, et al. An aryl hydrocarbon receptor-mediated amplification loop that enforces cell migration in ER-/PR-/Her2- human breast cancer cells. *Mol Pharmacol.* (2016) 90:674–88. doi: 10.1124/mol.116.105361
79. Stanford EA, Wang Z, Novikov O, Mulas F, Landesman-Bollag E, Monti S, et al. The role of the aryl hydrocarbon receptor in the development of cells with the molecular and functional characteristics of cancer stem-like cells. *BMC Biol.* (2016) 14:20. doi: 10.1186/s12915-016-0240-y

80. Mohamed HT, Gadalla R, El-Husseiny N, Hassan H, Wang Z, Ibrahim SA, et al. Inflammatory breast cancer: Activation of the aryl hydrocarbon receptor and its target CYP1B1 correlates closely with Wnt5a/b-beta-catenin signalling, the stem cell phenotype and disease progression. *J Adv Res.* (2019) 16:75–86. doi: 10.1016/j.jare.2018.11.006
81. Lappano R, Pisano A, Maggiolini M. GPER function in breast cancer: an overview. *Front Endocrinol.* (2014) 5:66. doi: 10.3389/fendo.2014.00066
82. O'Donnell EF, Koch DC, Bisson WH, Jang HS, Kolluri SK. The aryl hydrocarbon receptor mediates raloxifene-induced apoptosis in estrogen receptor-negative hepatoma and breast cancer cells. *Cell Death Dis.* (2014) 5:e1038. doi: 10.1038/cddis.2013.549
83. Vacher S, Castagnet P, Chemlali W, Lallemand F, Meseure D, Pocard M, et al. High AHR expression in breast tumors correlates with expression of genes from several signaling pathways namely inflammation and endogenous tryptophan metabolism. *PLoS ONE.* (2018) 13:e0190619. doi: 10.1371/journal.pone.0190619
84. Hsu LH, Chu NM, Lin YF, Kao SH. G-protein coupled estrogen receptor in breast cancer. *Int J Mol Sci.* (2019) 20:e20306. doi: 10.3390/ijms20020306
85. El Helou M. *Exploration of the Impact of Chronic and Low Doses Exposure of Environmental Factors on the Pre-cancerous Mammary Cells MCF10AT1.* (dissertation/PhD's thesis). Lyon, University Claude Bernard Lyon 1, Beirut, Lebanese University (2017).

Conflict of Interest: The authors declare that the research was conducted in the absence of any commercial or financial relationships that could be construed as a potential conflict of interest.

frontiers in Oncology

REVIEW
published: 05 August 2020
doi: 10.3389/fonc.2020.01358

Proteoglycans as Therapeutic Targets in Brain Cancer

Zoya Yan[1] *and Shanzhi Wang*[2]*

[1] Horace Greeley High School, Chappaqua, NY, United States, [2] Chemistry Department, University of Arkansas at Little Rock, Little Rock, AR, United States

Proteoglycans (PGs) are heavily glycosylated diverse proteins consisting of a "core protein" covalently attached to glycosaminoglycans (GAGs) and present on the cell surface, extracellular matrix, and intracellular milieu. Extracellular proteoglycans play crucial roles in facilitating cell signaling and migration, interacting with growth factor receptors, intracellular enzymes, extracellular ligands, and matrix components, as well as structural proteins and promoting significant tumor-microenvironment interactions in cancerous settings. As a result of their highly regulated expression patterns, recent research has focused on the role of proteoglycans in the development of nervous tissue, such as their effect on neurite outgrowth, participation in the development of precursor cell types, and regulation of cell behaviors. The present review summarizes current progress for the studies of proteoglycan function in brain cancer and explains recent research involving brain glycoproteins as modulators of migration, cell adhesion, glial tumor invasion, and neurite outgrowth. Furthermore, we highlight the correlations between specific proteoglycan alterations and the suggested cancer-associated proteoglycans as novel biomarkers for therapeutic targets.

Keywords: proteoglycan, glycosaminoglycan, glioblastoma, brain cancer, biomarker, inflammation

OPEN ACCESS

Edited by:
Chang Zou,
Shenzhen People's Hospital, Jinan University, China

Reviewed by:
Joseph Zaia,
Boston University, United States
Yongwei Zhang,
Albert Einstein College of Medicine, United States

***Correspondence:**
Shanzhi Wang
sxwang2@ualr.edu

Specialty section:
This article was submitted to Molecular and Cellular Oncology, a section of the journal Frontiers in Oncology

Received: *01 December 2019*
Accepted: *29 June 2020*
Published: *05 August 2020*

Citation:
Yan Z and Wang S (2020) Proteoglycans as Therapeutic Targets in Brain Cancer. Front. Oncol. 10:1358. doi: 10.3389/fonc.2020.01358

INTRODUCTION OF BRAIN CANCER

Brain tumors are abnormal cell growths in the brain, though only malignant tumors are cancerous. There are two types of brain tumors: the primary brain tumor, which originates from and resides within the brain, and the secondary (metastatic) brain tumor, which originates from cancer outside of the central nervous system (CNS) then spreads into the brain. While primary tumors are the more frequent solid tumors in children, metastatic tumors are more commonly diagnosed in adult patients (1).

In recent decades, the worldwide brain tumor incidence rate has increased across all ages. The standardization of age in varying countries is between 0.01–12.7 in males and 0.01–10.7 in females per 100,000 people, with the highest incidence in northern Europe and the lowest in Africa (2). According to the Central Brain Tumor Registry of the United States (CBTRUS), the incidence rate of CNS tumors in the United States (23.03 per 100,000 cases for a total count of 392,982) incident tumors, of which 121,277 cases

are malignant and 271,705 non-malignant) is lower in males (20.59 per 100,000 for 165,148 total cases) than in females (25.31 per 100,000 for 227,834 total cases) (3). In addition, in the United States, the 5-years survival rate following the diagnosis of a primary malignant CNS tumor is about 35% (2008–2014 data)[1]. The mortality rate of CNS cancers is estimated at about 3.4 per 100,000 in the world (2).

Across all age groups, the most common brain tumors develop from glial cells, which are gliomas that encompass a large scope of tumors and can be classified into four grades as follows: grade I (pilocytic astrocytoma), grade II (diffuse astrocytoma), grade III (anaplastic astrocytoma), and grade IV (glioblastoma multiforme) (4). Grade III and IV are categorized as high-grade or malignant gliomas with extremely poor prognosis, with grade IV diagnoses (which account for half of primary brain tumors) seeing a 5-years survival rate of <10% (5). The most common intracranial tumors in adults are brain metastases, with over 150,000 cases in the United States alone. Despite the considerable effect of varying primary tumor types on the incidence of metastases, 8–10% of adults diagnosed with cancer will develop brain metastases (6).

Developing treatment for CNS cancer is one of the most exigent branches of study in oncology. Although therapeutic approaches that exploit the immune system are a promising alternative strategy to surgery, radiotherapy, and anticancer drug therapy, multidrug resistance is a substantial obstacle restricting the success of conventional chemotherapy (7). The innate chemoresistance of many primary brain tumors and insufficient penetration of cytotoxic drugs across the blood-brain barrier (BBB) are also both responsible for the unsuccessful response of brain tumors to chemotherapy (8). Due to the urgency for novel therapies that combat these occurrences, researchers have emphasized and prioritized the development of anticancer drugs.

Using *in vitro* methods, Kwon et al. directly tested the effects of sialic acid glycan and glycosylation on BBB influx and efflux of IgG, specifically the influx and efflux processes for BBB endothelial cells, and facilitated "direct measurement of the Permeability Coefficient in each direction" (9, 10). In the study, BBB pharmacokinetics were found to be considerably affected by modest changes of IgG glycan profiles with sialylated glycans, suggesting that modifying IgG glycan could become an effective technique in increasing the concentration of the brain's therapeutic antibodies. Because immune pathways induced by sialylated IgG cause little inflammation, sialylation may therefore suggest beneficial clinical possibilities and further implications for patients with other CNS diseases such as Alzheimer's disease (11–13).

Abbreviations: BBB, blood-brain barrier; CS, chondroitin sulfate; CNS, central nervous system; DS, dermatan sulfate; ECM, extracellular matrix; GAGs, glycosaminoglycans; GBM, glioblastoma; HS, heparan sulfate; HP, heparin; HA, hyaluronic acid; KS, keratan sulfate; NG2, neuron-glial antigen 2; PG, proteoglycan.

[1]Available online at: https://www.cancer.org/content/dam/cancer-org/research/cancer-facts-and-statistics/annual-cancer-facts-and-figures/2019/cancer-facts-and-figures-2019.pdf

ROLES OF PROTEOGLYCANS IN BRAIN CANCER

Proteoglycans (PGs) are heavily glycosylated proteins and present on the cell surface, extracellular matrix (ECM), and intracellular milieu (14). The basic PG unit consists of a "core protein" covalently attached to glycosaminoglycans (GAGs), which are long chains consisting of linear or branched carbohydrate polymers that are negatively charged under certain physiological conditions, expressed on most mammalian cells. The six known GAGs are heparin (HP), hyaluronic acid (HA), heparan sulfate (HS), chondroitin sulfate (CS), keratan sulfate (KS), and dermatan sulfate (DS). These GAGs' respective disaccharide units contain different uronic and amino sugars (15). Their structure is demonstrated in **Figure 1**. GAGs are considerably linked to several diseases, including cancer, inflammation, bacterial infections, multiple sclerosis, viral infections, and Alzheimer's disease, as they interact with ligands to modulate physiological and pathological processes. Given such active involvement, GAG-based drugs are of considerable interest to researchers and have yielded promising outcomes in both animal and clinical trials, suggesting prospective development in therapeutics (16).

GAG to PG linkage is crucial to establishing and maintaining the fundamental functions of CNS, such as migration, cellular proliferation, specification, plasticity, synaptogenesis, and regeneration. Their mechanisms and functions have been summarized in many reviews (17–20). PG diversity depends on differential expression of protein sequences, variations in the length, and profile of GAG modifications. PGs regulate growth factors that affect cell adhesion, neurite outgrowth (21), ECM assembly, and tumor cell invasion (22, 23). Syndecans and glypicans are the two main transmembrane PGs containing HS chains in the CNS. Heparan sulfate PGs directly influence the aggregation and activity of AMPA receptors, which hinders cognitive functions by inducing or maintaining long-term potentiation (LTP) (24). Chondroitin sulfate PG, which is expressed abundantly in the cerebellum and hippocampus but decreases significantly postnatally, affects the stabilization of synapses and axonal sprouting (25). **Figure 2** demonstrates the selected cellular localization and significance for tumor development of the PGs discussed.

Chondroitin Sulfate Proteoglycan

Chondroitin sulfate PG 4, commonly referred to as neuron-glial antigen 2 (NG2), contributes to the stabilization of interaction between cell and substratum on endothelial basement membranes, especially at the early spreading stage of melanoma cells (26) In addition, CS PG 4 is a suggested biomarker in glioblastoma (GBM) (27). NG2-expressing oligodendrocyte precursor cells support neurons and synaptic signaling physiologically and carry out these functions in both brains that are healthy and those in the process of injury repair and regeneration. Moreover, NG2 protein facilitates tumorigenesis and tumor progression (28). In the previous study of human GBM cells, more cells survived under NG2-mediated

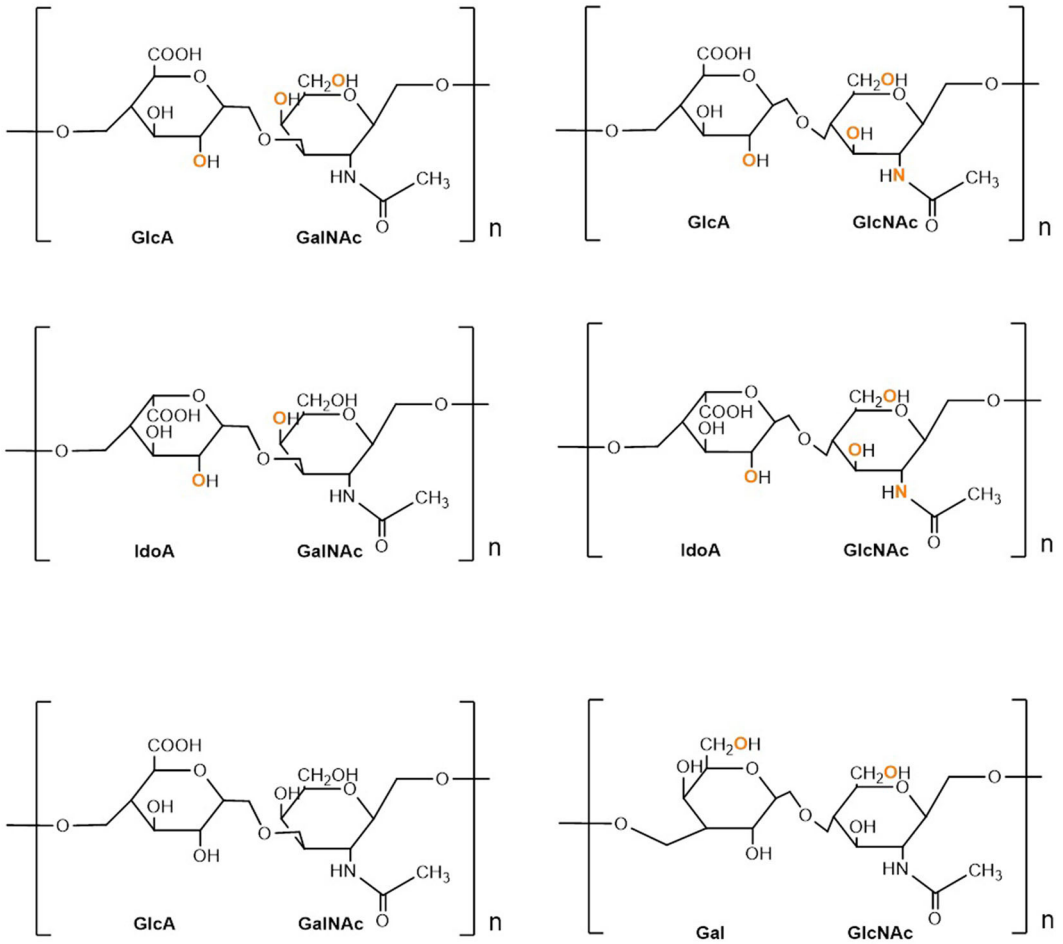

FIGURE 1 | Structure and composition of GAGs. Sulphation sites are shown in orange.

activation (29) and chemoresistance through integrin-dependent PI3K/Akt signaling (30).

Gliomagenesis is induced by unusual expression of neuron-glial antigen 2 endocytosis *in vivo* murine oligodendrocyte precursor cells, which provides another mechanism through which benign precursor cells can be converted into cancer stem cells (31). Additionally, NG2-expressing precursor cells demonstrate significant developmental plasticity. For instance, activating Notch signaling induced pericyte-like differentiation in NG2-positive GBM cancer stem cells, which during tumor angiogenesis contributed to vessel stabilization (32). Although these results suggest that NG2 plays a role in cancer stem cells, it is still uncertain whether the GAG moieties or the PG's other functional domains are responsible for the stemness-related functions.

Lam et al. reported an efficient and effective "glial progenitor cell-based therapy" for congenital myelin CNS disorders (33). From bone marrow stromal cells, they produced glial progenitor cells in a 14-days CS PG 4-based induction protocol. The generated cells were highly enriched in oligodendrocyte precursor cell marker expression. After being transplanted into the myelin-deficient mice, the cells differentiated successfully into myelinogenic oligodendrocytes. Both lifespan and motor function were improved significantly by remyelination of the shiverer mouse. Their study demonstrated the feasibility of human bone marrow stromal cells as a source of glial progenitor cells for attaining such myelinogenic oligodendrocytes (33). The novel induction protocol overcame existing hurdles of cell source restriction and timeframe requirements, providing a method for efficient myelin disorder glial therapy.

In addition, lecticans were also investigated as a group of chondroitin sulfate PGs due to their role in linking ECM molecules (34). The unique composition of brain ECM causes brain tissue to resist invasion by non-neuronal tumors (35). Due to its moderate plasticity, CNS has a considerable capacity for regeneration, although changes in ECM have been observed after trauma and throughout the development of CNS disease. The modification of PGs in ECM is shown as one of the factors leading to change in CNS plasticity. Through control of neurotransmission and synaptic connections, the scaffold of proteins and sugars in the ECM changes the functionality of surrounding tissue (36).

To activate immune cells, CS PGs generally collect the microenvironment's signals and bind immunological receptors,

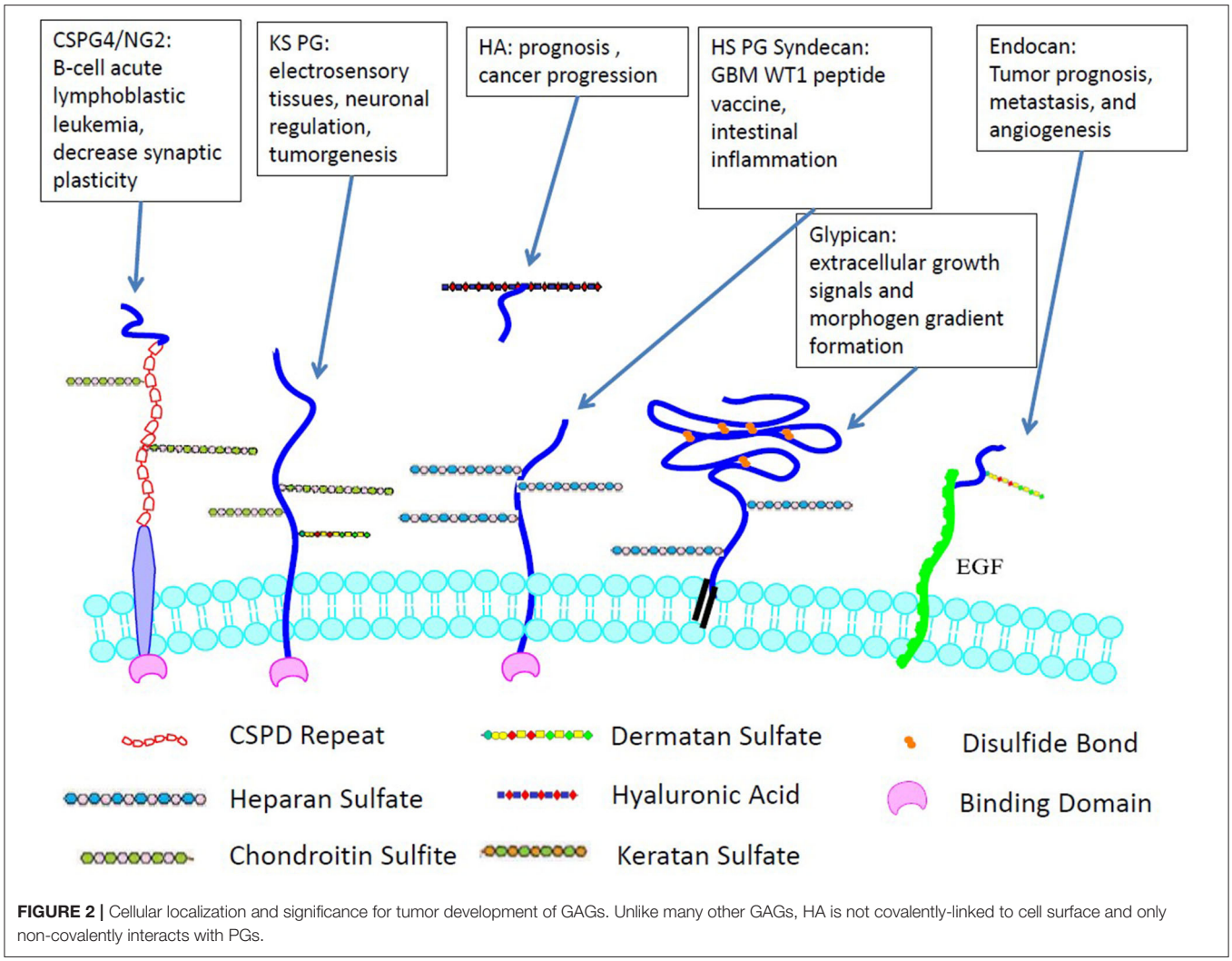

FIGURE 2 | Cellular localization and significance for tumor development of GAGs. Unlike many other GAGs, HA is not covalently-linked to cell surface and only non-covalently interacts with PGs.

thus boosting inflammatory responses. CS PGs also stimulate matrix-degrading enzymes and bind signaling molecules in immune cells such as chemokines and cytokines (37).

Heparan Sulfate Proteoglycans

Heparin has anticoagulant activity and can only be produced by mast cells. Heparan sulfate also functions as an anticoagulant, though on a lower level than heparin, and is generated by nearly all cell types. Present both in the ECM and on the cell surface, heparan sulfate PGs (HSPG) facilitate cell-microenvironment interactions and cell signaling pathways. In GBM, HS glycosaminoglycans expression and their regulating enzymes are changed, but the structure and content of the HS itself remain unknown. For example, glypicans of the HS PG families [See review: Wang et al. (38)] are proteins that are membrane-bound and that modulate morphogen gradient formation and extracellular growth signals to engage in organ development (39). Crucially, some studies reported an increased level of glypicans in the peripheral blood of patients, holding glypicans as a promising new biomarker in the cancer field (40). Tran et al. used LC-MS analysis to portray the differences in both HS disaccharide content and structure. As a result, they suggested inter-tumoral differences in PG expression and function have potential implications for therapeutic stratification (41).

Spyrou studied the inhibition of heparanase in brain tumor cells of children and subsequently reduced their invasive capacity, proliferation, and tumor growth *in vivo*. The results suggest that heparanase affects both tumor cells and their ECM in cases of malignant brain tumors. However, the inhibitor (PG545) failed to pass the BBB due to its size, and thus direct injection or a new drug delivery system is required (42).

Hyaluronic Acid

Hyaluronan (or hyaluronic acid) is a "multifunctional GAG synthesized as a large negatively charged linear polymer by distinct hyaluronan synthases" (43). While aggrecan-related components generally result in clear regional distribution patterns, hyaluronan is widely distributed in the white and gray matter (44). HA interacts with several cell membrane receptors, including CD44 and Lymphatic vessel endothelial hyaluronan

receptor 1, the former being the more thoroughly studied receptor for HA-mediated motility in cancer progression. In addition, certain PGs use link modules to form supramolecular complexes with HA. Generally, high levels of HA and HA receptors are correlated with poor prognosis in cancer patients.

Using pluripotent stem cells-derived and primary brain microvascular endothelial cells, Al-Ahmad et al. tested the effect of HA on BBB properties. The impact of HA signaling on developmental and mature brain microvascular endothelial cells was assessed by measuring changes in transendothelial electrical resistance, permeability, brain microvascular endothelial cells markers localization, and expression, CD44 expression, and hyaluronan levels. HA treatment generally reduced barrier function and P-glycoprotein activity. The effects were more evident with treatment using oligomeric forms of HA and exacerbated when the treatment was applied during the brain microvascular endothelial cells differentiation phase (considered developmental BBB). The hyaluronidase activity, as well as an increase in CD44 expression during prolonged oxygen-glucose deprivation stress, were also observed. Inhibiting HA signaling by the antibody blockade of CD44 reversed the treatment's adverse effects, thus conveying the significance of HA signaling through CD44 on BBB properties (45). Moreover, Hartheimer et al. determined how hyaluronidases can sensitize GBM stem cells to chemotherapy drugs by disrupting the HA-CD44 signaling, with which they further developed a combined treatment of hyaluronidases and chemotherapy drugs by disrupting the stemness-promoting HA to target GBM stem cells. This combination therapy shows promise even when temozolomide treatment alone causes resistance (46).

Dermatan Sulfate PG—Endocan: A New Biomarker and Therapeutic Target

Endocan is a novel endothelial cell-specific molecule with 50 kDa molecular weight and high solubility in water. As a proteoglycan, endocan is secreted into the blood and formed in the presence of CS. In normal tissues, CS and DS PGs are expressed in endothelial cells but are overexpressed in certain tumor endothelial cells. Unsurprisingly, abnormal expression levels of endocan were observed in tumor prognosis, angiogenesis, and metastasis. Researchers believe that the role of endocan is to regulate the tumor by tumor-related angiogenesis, cell inflammation, lymphangiogenesis, and other aspects (47). Accordingly, Kijima et al. studied surface marks from patient derived xenografts and cell lines based on array comparative genomic hybridization to investigate the early stages of GBM tumorigenesis (48). In additional to research that found raised levels of systemic inflammatory markers to be correlated with cardiovascular disease (49), a recent study revealed that the specific sulfation level of DS is crucial in synaptic plasticity and is related to changes in the expression of glutamate receptors and other associated synaptic proteins (50). As such, endocan became a valuable target for GBM diagnosis and therapy.

As another interesting target, dermatan sulfate epimerase 1 is overexpressed in many types of cancer as a tumor-rejection antigen. The CS/DS chains mediate several growth factor signals. However, investigating their roles in gliomas involves less work. Liao et al. examined the expression of Dermatan sulfate epimerase 1 in gliomas by utilizing a public database and conducting immunohistochemistry on a tissue array. Their investigation revealed that Dermatan sulfate epimerase 1 regulates the HB-EGF/ErbB pathway, which participates in GBM cells' malignant behavior. Treating epidermal growth factor receptor and ErbB2 with selected inhibitors thus suppressed malignant phenotypes, demonstrating that the upregulation of Dermatan sulfate epimerase in gliomas contributes to controlling malignant behavior in cancer cells (51).

Keratan Sulfate (KS)

Keratan sulfate (KS) is a sulfated GAG, which contains structurally unique characteristics of diversity in the linker oligosaccharides connecting to the core protein. The repeating disaccharide unit in KS contains one galactose and one N-acetylglucosamine and is linked to core proteins via either N-linked or O-linked glycosylation of the PGs. KS is most abundant in the cornea, and second abundant in the brain (52). Negatively charged KS modifications of synaptic vesicle protein 2 interacted with both Ca^{2+} ions and other neurotransmitters such as dopamine, establishing the PG delivery complex (53). Furthermore, high sulfation level KS PGs are commonly found in the brain. For example, synaptic vesicle proteins 2 played significant neuronal and synaptic regulatory roles (54).

An earlier study reported that highly sulfated KS was overexpressed in malignant astrocytic tumors (55). It has also been found that the interruption of Synaptic vesicle proteins 2 functionality is associated with epilepsy (56). These results were confirmed by the subsequent research of the interactivity of KS with nerve growth factor and receptor proteins, neuroregulatory proteins, synaptic proteins and neurotransmitters (57). In addition, abnormal sulfation degrees of KS are observed in the brains of Alzheimer's patients (58). Tsidulko's work demonstrated that PG composition and ECM structure in normal brain tissue were affected during temozolomide induced chemotherapy. These changes were believed to participate in the development of the tumorigenic niche for the expansion of the residual glioma cells and the disease progression (59). Recently, researchers have reviewed the influences of KS sulfation on electrosensory tissues and neuronal regulation. KS with overexpressed sulfation level interacts with neuroregulatory proteins. Hence, actin and tubulin cytoskeletal development was stabilized by KS PG microtubule-associated proteins during neuritogenesis (60).

THE ROLE OF PGs IN BRAIN INFLAMMATION AND PLASTICITY

In general, PGs have influenced several aspects of tumor biology such as tumor cell adhesion and migration, cell proliferation, angiogenesis, and inflammation. Up- and down-regulated expression in PG core proteins is observed in many cancers and usually related to changes in cell signaling and invasion (19, 61). Jang et al. found that the interaction between the intracellular domain of some transmembrane PGs with the

cytoplasmic domain of proteins promoted the signaling (62). In an earlier review, the cytoplasmic domain of syndecan-1 was found to have interaction with talin to modulate integrin signaling via a syndecan-1-integrin-insulin-like complex (63). Likewise, the cytoplasmic tail of transmembrane heparan sulfate PG syndecan-4 interacts with α-actinin regulating cytoskeletal organization. Fröhling et al.' recent research suggested that the loss of syndecan-4 expression is correlated with the increase if intestinal inflammation. While primarily expressed in the colonic epithelium, syndecan-4 accumulated the deficiency during the growth of susceptibility regarding the intestinal inflammation. Mechanisms were proposed that syndecan-4 played a role in protecting against inflammation, keeping the epithelial gut barrier's unity and regeneration (64). When using anti-syndecan-4 antibodies as a therapeutic approach to treat patients with inflammatory disorders, researchers must carefully evaluate patients who have inflammatory diseases associated with an epithelial barrier function.

Many PGs were proposed as markers for therapy evaluation. For example, syndecan-4 mRNA expression was specified as the unique marker to predict the GBM multiforme patient's response during the WT1 peptide vaccine treatment (65). Letoha et al. reported that syndecan-4 bound and mediated the transfer of a cell-penetrating short peptide with 17 amino acids into the cells (66). Roy et al. then demonstrated a positive correlation between glioma grade and serglycin expression level in GBM progression (67).

There is significant evidence showing that the sulfate composition of CS GAG chains changes with age. As a result of aging and aggregation of proteins, the deposition of HS PGs and CS PGs results in the injury of protective perineuronal nets with increased cell death (60). Dying neurons then induce inflammation, ECM degrades through the proteolytic activity of enzymes, inducing responses that amplify neuronal death and neuroinflammation (68). Simultaneously, overexpression of chondroitin 6-*O*-sulfotransferase 1 may decrease the ratio of 4–6S in perineuronal nets and increase seizure susceptibility (69). This is supported by Foscarin's work that the age-associated rise in the ratio of 4–6S GAG in perineuronal nets may decrease synaptic plasticity (70). Their studies highlighted the necessity for genetic manipulation of other enzymes such as chondroitin sulfotransferases to discover their biological functions and generate the profile of sulfation's role in development and aging.

Recent preclinical research demonstrated the antitumoral effects of chondroitin sulfate PG 4. The NG2-directed chimeric antigen receptor T-cells were proved to efficiently target GBM cancer stem cells (71). The combination of anti-NG2 antibodies was induced in chemotherapy in B-cell acute lymphoblastic leukemia (72).

CONCLUSION

In summary, adjustments in PG core proteins, biosynthetic enzymes, and extracellular regulating enzymes are correlated with many developmental anomalies and overgrowth or tumor predisposition syndromes. PGs facilitate the activity of various signaling pathways and stimulate cell-microenvironment interactions in tumors. Due to such a diverse range of functions, PGs and their modifying enzymes are an imperative area of study that may potentially uncover therapeutic targets and biomarkers of GBM. In the damaged CNS, PGs accumulate during traumatic brain injuries, multiple sclerosis, and spinal cord injuries, driving pathogenesis and neuroinflammation. It should be noted that compared to the *in vitro* examination, more complex factors may interfere with the regulated expression of PGs in ECM *in vivo*. When assessing experiment data for therapeutic targets and treatment strategies, researchers should carefully consider adverse side effects that can be avoided in advance.

AUTHOR CONTRIBUTIONS

All authors participated in writing and revising the manuscript.

FUNDING

This work has been supported by UA Little Rock Startup Grant.

ACKNOWLEDGMENTS

We wish to acknowledge the support of UA Little Rock for the Startup Package.

REFERENCES

1. Louis DN, Ohgaki H, Wiestler OD, Cavenee WK, Burger PC, Jouvet A, et al. The WHO classification of tumours of the central nervous system. *Acta Neuropathol.* (2007) 114:97–109. doi: 10.1007/s00401-007-0243-4
2. Kalan Farmanfarma KH, Mohammadian M, Shahabinia Z, Hassanipour S, Salehiniya H. Brain cancer in the world: an epidemiological review. *World Cancer Res J.* (2019) 6:E1356. doi: 10.32113/wcrj_20197_1356
3. Ostrom QT, Gittleman H, Truitt G, Boscia A, Kruchko C, Barnholtz-Sloan JS. CBTRUS statistical report: primary brain and other central nervous system tumors diagnosed in the United States in 2011–2015. *Neuro Oncol.* (2018) 20(suppl.4):iv1–86. doi: 10.1093/neuonc/noy131
4. Wesseling P, Capper D. WHO (2016) classification of gliomas. *Neuropathol Appl Neurobiol.* (2018) 44:139–50. doi: 10.1111/nan.12432
5. Wilson TA, Karajannis MA, Harter DH. Glioblastoma multiforme: state of the art and future therapeutics. *Surg Neurol Int.* (2014) 5:64. doi: 10.4103/2152-7806.132138
6. Ferguson SD, Everson RG, Wagner KM, Yeboa DN, McCutcheon IE, Sawaya R. Neurosurgical 31 brain metastases. *Adult CNS Radiat Oncol.* (2018) 27:431. doi: 10.1007/978-3-319-42878-9_31
7. Liu C, Zong H. Developmental origins of brain tumors. *Curr Opin Neurobiol.* (2012) 22:844–9. doi: 10.1016/j.conb.2012.04.012
8. Regina A, Demeule M, Laplante A, Jodoin J, Dagenais C, Berthelet F, et al. Multidrug resistance in brain tumors: roles of the blood-brain barrier. *Cancer Metastasis Rev.* (2001) 20:13–25. doi: 10.1023/a:1013104423154
9. Kwon H, Crisostomo AC, Smalls HM, Finke JM. Anti-αβ oligomer IgG and surface sialic acid in intravenous immunoglobulin: measurement and correlation with clinical outcomes in Alzheimer's disease treatment. *PLoS ONE.* (2015) 10:e0120420. doi: 10.1371/journal.pone.0120420

10. Finke JM, Ayres KR, Brisbin RP, Hill HA, Wing EE, Banks WA. Antibody blood-brain barrier efflux is modulated by glycan modification. *Biochim Biophys Acta*. (2017) 1861:2228–39. doi: 10.1016/j.bbagen.2017.06.008
11. Alter G, Ottenhoff TH, Joosten SA. Antibody glycosylation in inflammation, disease and vaccination. *InSeminars Immunol*. (2018) 39:102–10. doi: 10.1016/j.smim.2018.05.003
12. Ravetch JV, Kaneko Y, Nimmerjahn F. *Polypeptides With Enhanced Anti-Inflammatory And Decreased Cytotoxic Properties And Relating Methods. United States patent application US 16/150,058*. New York, NY: US patent (2019).
13. Zhou X, Kinlough CL, Hughey RP, Jin M, Inoue H, Etling E, et al. Sialylation of MUC4β N-glycans by ST6GAL1 orchestrates human airway epithelial cell differentiation associated with type-2 inflammation. *JCI insight*. (2019) 4:e122475. doi: 10.1172/jci.insight.122475
14. Bedini E, Corsaro MM, Fernández-Mayoralas A, Iadonisi A. Chondroitin, dermatan, heparan, and keratan sulfate: structure and functions. In: E Cohen, H Merzendorfer, editors. *Extracellular Sugar-Based Biopolymers Matrices. Biologically-Inspired Systems*. Cham: Springer (2019).
15. Aquino RS, Park PW. Glycosaminoglycans and infection. *Front Biosci*. (2016) 21:1260–77. doi: 10.2741/4455
16. Morla S. Glycosaminoglycans and glycosaminoglycan mimetics in cancer and inflammation. *Int J Mol Sci*. (2019) 20:1963. doi: 10.3390/ijms20081963
17. Vitale D, Kumar Katakam S, Greve B, Jang B, Oh E-S, Alaniz L, et al. Proteoglycans and glycosaminoglycans as regulators of cancer stem cell function and therapeutic resistance. *FEBS J*. (2019) 286:2870–82. doi: 10.1111/febs.14967
18. Karamanos NK, Piperigkou Z, Theocharis AD, Watanabe H, Franchi M, Baud S, et al. Proteoglycan chemical diversity drives multifunctional cell regulation and therapeutics. *Chem Rev*. (2018) 118:9152–232. doi: 10.1021/acs.chemrev.8b00354
19. Wade A, Robinson AE, Engler JR, Petritsch C, David James C, Phillips JJ. Proteoglycans and their roles in brain cancer. *FEBS J*. (2013) 280:2399–417. doi: 10.1111/febs.12109
20. Quirico-Santos T, Fonseca CO, Lagrota-Candido L. Brain sweet brain: importance of sugars for the cerebral microenvironment and tumor development. *Arq Neuropsiquiatr*. (2010) 68:799–803. doi: 10.1590/S0004-282X2010000500024
21. Kanai MI, Kim MJ, Akiyama T, Takemura M, Wharton K, O'Connor MB, et al. Regulation of neuroblast proliferation by surface glia in the Drosophila larval brain. *Sci Rep*. (2018) 8:3730. doi: 10.1038/s41598-018-22028-y
22. Walker C, Mojares E, del Río Hernández A. Role of extracellular matrix in development and cancer progression. *Int J Mol Sci*. (2018) 19:3028. doi: 10.3390/ijms19103028
23. Ferrer VP, Moura Neto V, Mentlein R. Glioma infiltration and extracellular matrix: key players and modulators. *Glia*. (2018) 66:1542–65. doi: 10.1002/glia.23309
24. Holmes BB, DeVos SL, Kfoury N, Li M, Jacks R, Yanamandra K, et al. Heparan sulfate proteoglycans mediate internalization and propagation of specific proteopathic seeds. *Proc Natl Acad Sci USA*. (2013) 110:E3138–47. doi: 10.1073/pnas.1301440110
25. Sim H, Hu B, Viapiano MS. Reduced expression of the hyaluronan and proteoglycan link proteins in malignant gliomas. *J Biol Chem*. (2009) 284:26547–56. doi: 10.1074/jbc.M109.013185
26. Finocchiaro G, Pellegatta S. NG2/CSPG4 in glioblastoma: about flexibility, *Neuro-Oncology*. (2019) 21:697–8. doi: 10.1093/neuonc/noz055
27. Svendsen A, Verhoeff JJ, Immervoll H, Brøgger JC, Kmiecik J, Poli A, et al. Expression of the progenitor marker NG2/CSPG4 predicts poor survival and resistance to ionising radiation in glioblastoma. *Acta Neuropathol*. (2011) 122:495–510. doi: 10.1007/s00401-011-0867-2
28. Yadavilli S, Hwang EI, Packer RJ, Nazarian J. The role of NG2 proteoglycan in glioma. *Transl Oncol*. (2016) 9:57–63. doi: 10.1016/j.tranon.2015.12.005
29. Downward J. PI 3-kinase, Akt and cell survival. *Semin Cell Dev Biol*. (2004) 15:177–82. doi: 10.1016/j.semcdb.2004.01.002
30. Chekenya M, Krakstad C, Svendsen A, Netland IA, Staalesen V, Tysnes BB, et al. The progenitor cell marker NG2/MPG promotes chemoresistance by activation of integrin-dependent PI3K/Akt signaling. *Oncogene*. (2008) 27:5182–94. doi: 10.1038/onc.2008.157
31. Daynac M, Chouchane M, Collins HY, Murphy NE, Andor N, Niu J, et al. Lgl1 controls NG2 endocytic pathway to regulate oligodendrocyte differentiation and asymmetric cell division and gliomagenesis. *Nat Commun*. (2018) 9:2862. doi: 10.1038/s41467-018-05099-3
32. Guichet PO, Guelfi S, Teigell M, Hoppe L, Bakalara N, Bauchet L, et al. Notch1 stimulation induces a vascularization switch with pericyte-like cell differentiation of glioblastoma stem cells. *Stem Cells*. (2015) 33:21–34. doi: 10.1002/stem.1767
33. Lam G, Shea GK, Wu LK, Sui LMT, Hei KC, Yin YWC, et al. Neuron-Glial Antigen 2 (NG2)-based Glial Induction of Human BMSCs: a fast & safe glial progenitor cell-based therapy for congenital myelin disorders of the central nervous system. *bioRxiv*. (2019) 658997. doi: 10.1101/658997
34. Yamaguchi Y. Lecticans: organizers of the brain extracellular matrix. *Cell Mol Life Sci*. (2000) 57:276–89. doi: 10.1007/PL00000690
35. Veillon L, Fakih C, Abou-El-Hassan H, Kobeissy F, Mechref Y. Glycosylation changes in brain cancer. *ACS Chem Neurosci*. (2017) 9:51–72. doi: 10.1021/acschemneuro.7b00271
36. Warren PM, Dickens SM, Gigout S, Fawcett JW, Kwok JC. Regulation of CNS plasticity through the extracellular matrix. In: *The Oxford Handbook of Developmental Neural Plasticity*. New York, NY: Oxford University Press (2018). doi: 10.1093/oxfordhb/9780190635374.013.11
37. Stephenson EL, Yong VW. Pro-inflammatory roles of chondroitin sulfate proteoglycans in disorders of the central nervous system. *Matrix Biol*. (2018) 71:432–42. doi: 10.1016/j.matbio.2018.04.010
38. Qiao D, Meyer K, Mundhenke C, Drew SA, Friedl A. Heparan sulfate proteoglycans as regulators of fibroblast growth Factor-2 signaling in brain endothelial cells. *J Biol Chem*. (2003) 278:16045–53. doi: 10.1074/jbc.M211259200
39. Sarrazin S, Lamanna WC, Esko JD. Heparan sulfate proteoglycans. *Cold Spring Harbor Perspectiv Biol*. (2011) 3:a004952. doi: 10.1101/cshperspect.a004952
40. Nagarajan A, Malvi P, Wajapeyee N. Heparan sulfate and heparan sulfate proteoglycans in cancer initiation and progression. *Front Endocrinol*. (2018) 9:483. doi: 10.3389/fendo.2018.00483
41. Tran VM, Wade A, McKinney A, Chen K, Lindberg OR, Engler JR, et al. Heparan sulfate glycosaminoglycans in glioblastoma promote tumor invasion. *Mol Cancer Res*. (2017) 15:1623–33. doi: 10.1158/1541-7786.MCR-17-0352
42. Spyrou A, Kundu S, Haseeb L, Yu D, Olofsson T, Dredge K, et al. Inhibition of heparanase in pediatric brain tumor cells attenuates their proliferation, invasive capacity, and *in vivo* tumor growth. *Mol Cancer Therapeutics*. (2017) 16:1705–16. doi: 10.1158/1535-7163.MCT-16-0900
43. Park JB, Kwak HJ, Lee SH. Role of hyaluronan in glioma invasion. *Cell Adh Migr*. (2008) 2:202–7. doi: 10.4161/cam.2.3.6320
44. Bonneh-Barkay D, Wiley CA. Brain extracellular matrix in neurodegeneration. *Brain Pathol*. (2009) 19:573–85. doi: 10.1111/j.1750-3639.2008.00195.x
45. Al-Ahmad AJ, Patel R, Palecek SP, Shusta EV. Hyaluronan impairs the barrier integrity of brain microvascular endothelial cells through a CD44-dependent pathway. *J Cerebral Blood Flow Metab*. (2019) 39:1759–75. doi: 10.1177/0271678X18767748
46. Hartheimer JS, Park S, Rao SS, Kim Y. Targeting hyaluronan interactions for glioblastoma stem cell therapy. *Cancer Microenvironment*. (2019) 12:47–56. doi: 10.1007/s12307-019-00224-2
47. Yang J, Yang Q, Yu S, Zhang X. Endocan: a new marker for cancer and a target for cancer therapy. *Biomed Rep*. (2015) 3:279–83. doi: 10.3892/br.2015.438
48. Kijima N, Kanematsu D, Shofuda T, Nonaka M, Iwata R, Fukai J, et al. TMOD-01 characterization of patient-derived primary cell lines and xenografts for glioblastoma. *Neuro-Oncology*. (2019) 21(Suppl.6):vi262. doi: 10.1093/neuonc/noz175.1100
49. Zhao T, Kecheng Y, Zhao X, Hu X, Zhu J, Wang Y, et al. The higher serum endocan levels may be a risk factor for the onset of cardiovascular disease: a meta-analysis. *Medicine*. (2018) 97:e13407. doi: 10.1097/MD.0000000000013407
50. Li Q, Wu X, Wu Q, Ge B, Guo X, Ntim M, et al. Impaired cognitive function and altered hippocampal synaptic plasticity in mice lacking dermatan sulfotransferase Chst14/D4st1. *Front Mol Neurosci*. (2019) 12:26. doi: 10.3389/fnmol.2019.00026

51. Liao WC, Liao CK, Tsai YH, Tseng T-J, Chuang L-C, Lan C-T, et al. DSE promotes aggressive glioma cell phenotypes by enhancing HB-EGF/ErbB signaling. *PLoS ONE*. (2018) 13:e0198364. doi: 10.1371/journal.pone.0198364
52. Ohmae M, Yamazaki Y, Sezukuri K, Takada J. Keratan sulfate, a "unique" sulfo-sugar: structures, functions, and synthesis. *Trends Glycosci Glycotechnol.* (2019) 31:E129–36. doi: 10.4052/tigg.1830.1E
53. Caterson B, Melrose J. Keratan sulfate, a complex glycosaminoglycan with unique functional capability. *Glycobiology*. (2018) 28:182–206. doi: 10.1093/glycob/cwy003
54. Jia M, Travaglia A, Pollonini G, Fedele G, Alberini CM. Developmental changes in plasticity, synaptic, glia, and connectivity protein levels in rat medial prefrontal cortex. *Learning Memory*. (2018) 25:533–43. doi: 10.1101/lm.047753.118
55. Kato Y, Hayatsu N, Kaneko MK, Ogasawara S, Hamano T, Takahashi S, et al. Increased expression of highly sulfated keratan sulfate synthesized in malignant astrocytic tumors. *Biochem Biophys Res Commun*. (2008) 369:1041–6. doi: 10.1016/j.bbrc.2008.02.130
56. Wan QF, Zhou ZY, Thakur P, Vila A, Sherry DM, Janz R, et al. SV2 acts via presynaptic calcium to regulate neurotransmitter release. *Neuron.* (2010) 66:884–95. doi: 10.1016/j.neuron.2010.05.010
57. Conrad AH, Zhang Y, Tasheva ES, Conrad GW. Proteomic analysis of potential keratan sulfate, chondroitin sulfate, A., and hyaluronic acid molecular interactions. *Invest Ophthalmol Vis Sci*. (2010) 51:4500–15. doi: 10.1167/iovs.09-4914
58. Zhang Z, Takeda-Uchimura Y, Foyez T, Ohtake-Niimi S, Narentuya Akatsu H, Nishitsuji K, et al. Deficiency of a sulfotransferase for sialic acid-modified glycans mitigates Alzheimer's pathology. *Proc Natl Acad Sci USA*. (2017) 114:E2947–54. doi: 10.1073/pnas.1615036114
59. Tsidulko AY, Bezier C, de La Bourdonnaye G, Suhovskih AV, Pankova TM, Kazanskaya GM, et al. Conventional anti-glioblastoma chemotherapy affects proteoglycan composition of brain extracellular matrix in rat experimental model *in vivo*. *Front Pharmacol*. (2018) 9:1104. doi: 10.3389/fphar.2018.01104
60. Melrose J. Functional consequences of keratan sulfate sulfation in electrosensory tissues and in neuronal regulation. *Adv Biosystems*. (2019) 3:1800327. doi: 10.1002/adbi.201800327
61. Nikitovic D, Berdiaki A, Spyridaki I, Krasanakis T, Tsatsakis A, Tzanakakis GN. Proteoglycans—biomarkers and targets in cancer therapy. *Front Endocrinol*. (2018) 9:69. doi: 10.3389/fendo.2018.00069
62. Jang B, Jung H, Hong H, Oh ES. Syndecan transmembrane domain modulates intracellular signalling by regulating the oligomeric status of the cytoplasmic domain. *Cell Signalling*. (2018) 52:121–6. doi: 10.1016/j.cellsig.2018.09.003
63. Stepp MA, Pal-Ghosh S, Tadvalkar G, Pajoohesh-Ganji A. Syndecan-1 and its expanding list of contacts. *Adv Wound Care*. (2015) 4:235–49. doi: 10.1089/wound.2014.0555
64. Fröhling M, Tepasse P, Intemann J, Sambale M, Sherwood J, Paruzel P, et al. Syndecan-4 modulates epithelial gut barrier function and epithelial regeneration in experimental colitis. *Inflamm Bowel Dis*. (2018) 24:2579–89. doi: 10.1093/ibd/izy248
65. Takashima S, Oka Y, Fujiki F, Morimoto S, Nakajima H, Nakae Y, et al. Syndecan-4 as a biomarker to predict clinical outcome for glioblastoma multiforme treated with WT1 peptide vaccine. *Future Sci.* (2016) 2:FSO96. doi: 10.4155/fsoa-2015-0008
66. Letoha T, Keller-Pintér A, Kusz E, Kolozsi C, Bozsó Z, Tóth G, et al. Cell-penetrating peptide exploited syndecans. *Biochim Biophys Acta*. (2010) 1798:2258–65. doi: 10.1016/j.bbamem.2010.01.022
67. Roy A, Attarha S, Weishaupt H, Edqvist PH, Swartling FJ, Bergqvist M, et al. Serglycin as a potential biomarker for glioma: association of serglycin expression, extent of mast cell recruitment and glioblastoma progression. *Oncotarget*. (2017) 8:24815. doi: 10.18632/oncotarget.15820
68. Candelario-Jalil E, Yang Y, Rosenberg GA. Diverse roles of matrix metalloproteinases and tissue inhibitors of metalloproteinases in neuroinflammation and cerebral ischemia. *Neuroscience.* (2009) 158:983–94. doi: 10.1016/j.neuroscience.2008.06.025
69. Yutsudo N, Kitagawa H. Involvement of chondroitin 6-sulfation in temporal lobe epilepsy. *Exp Neurol*. (2015) 274:126–33. doi: 10.1016/j.expneurol.2015.07.009
70. Foscarin S, Raha-Chowdhury R, Fawcett JW, Kwok JC. Brain ageing changes proteoglycan sulfation, rendering perineuronal nets more inhibitory. *Aging*. (2017) 9:1607. doi: 10.18632/aging.101256
71. Beard RE, Zheng Z, Lagisetty KH, Burns WR, Tran E, Hewitt SM, et al. Multiple chimeric antigen receptors successfully target chondroitin sulfate proteoglycan 4 in several different cancer histologies and cancer stem cells. *J Immunother Cancer.* (2014) 2:25. doi: 10.1186/2051-1426-2-25
72. Lopez-Millan B, Sanchez-Martinez D, Roca-Ho H, Gutierrez-Aguera F, Molina O, Diaz de la Guardia R, et al. NG2 antigen is a therapeutic target for MLL-rearranged B-cell acute lymphoblastic leukemia. *Leukemia*. (2019) 33:1557–69. doi: 10.1038/s41375-018-0353-0

Conflict of Interest: The authors declare that the research was conducted in the absence of any commercial or financial relationships that could be construed as a potential conflict of interest.

frontiers in Oncology

ORIGINAL RESEARCH
published: 01 October 2020
doi: 10.3389/fonc.2020.01784

Effects of the Oncoprotein PAX3-FOXO1 on Modulation of Exosomes Function and Protein Content: Implications on Oxidative Stress Protection and Enhanced Plasticity

Assil Fahs[1,2], Farah Ramadan[1], Farah Ghamloush[3], Abeer J. Ayoub[1,2], Fatima Ali Ahmad[1], Firas Kobeissy[4], Yehia Mechref[5], Jingfu Zhao[5], Rui Zhu[5], Nader Hussein[6], Raya Saab[2,3] and Sandra E. Ghayad[1]**

[1] Department of Biology, Faculty of Science II, Lebanese University, Fanar, Lebanon, [2] Department of Anatomy, Cell Biology and Physiology, American University of Beirut, Beirut, Lebanon, [3] Department of Pediatrics and Adolescent Medicine, Children's Cancer Institute, American University of Beirut, Beirut, Lebanon, [4] Department of Biochemistry and Molecular Genetics, Faculty of Medicine, American University of Beirut, Beirut, Lebanon, [5] Department of Chemistry and Biochemistry, Texas Tech University, Lubbock, TX, United States, [6] Cancer Biology Stem Cells and Molecular Immunology Laboratory, Faculty of Sciences, Lebanese University, Beirut, Lebanon

OPEN ACCESS

Edited by:
Boris Zhivotovsky,
Karolinska Institutet (KI), Sweden

Reviewed by:
Francesco Marampon,
Sapienza University of Rome, Italy
Luisa Lanfrancone,
European Institute of Oncology (IEO), Italy

***Correspondence:**
Sandra E. Ghayad
sandra.ghayad@ul.edu.lb
Raya Saab
rs88@aub.edu.lb

Specialty section:
This article was submitted to Molecular and Cellular Oncology, a section of the journal Frontiers in Oncology

Received: 15 February 2020
Accepted: 11 August 2020
Published: 01 October 2020

Citation:
Fahs A, Ramadan F, Ghamloush F, Ayoub AJ, Ahmad FA, Kobeissy F, Mechref Y, Zhao J, Zhu R, Hussein N, Saab R and Ghayad SE (2020) Effects of the Oncoprotein PAX3-FOXO1 on Modulation of Exosomes Function and Protein Content: Implications on Oxidative Stress Protection and Enhanced Plasticity. Front. Oncol. 10:1784. doi: 10.3389/fonc.2020.01784

Rhabdomyosarcoma (RMS) is a highly malignant soft tissue sarcoma classified into two major histologic subtypes: embryonal (ERMS) and alveolar (ARMS). ARMS subtype is clinically more aggressive, and characterized by an oncogenic fusion protein PAX3-FOXO1 (P3F) that drives oncogenic cellular properties. To understand the role of the fusion oncoprotein in paracrine signaling, we focused on secreted exosomes, which have been demonstrated to contribute to metastasis in multiple tumor types. Advanced Proteomics-bioinformatics analysis of the protein cargo of exosomes isolated from C2C12 myoblasts transduced with P3F fusion gene revealed 52 deregulated proteins compared to control cells, with 26 enriched and 26 depleted proteins. Using both PANTHER gene classification and Ingenuity Pathway Analysis (IPA) software, we found that the main biological processes in which the 52 deregulated proteins are involved, include "catalytic activity," "binding," "metabolic process," and "cellular process." The pathways engaging the 26 enriched proteins include the "14-3-3 mediated signaling," "cell cycle," and "ERK5, VEGF, IGF1,and p70S6K signaling." Furthermore, the main nodes in which deregulated exosome proteins and miRNAs intersected revealed pathways conferring protection from stress and promoting plasticity. Based on the bioinformatics analysis and the altered exosome proteome profile, we performed biochemical functional analysis to study the diverse properties of these exosomes where angiogenesis, stemness, and anti-oxidative stress properties were validated using different platforms. P3F-modulated exosomes activated ERK, 4-EBP1, and MMP-2 in recipient cells, and enhanced angiogenesis and stemness. In addition, P3F led to lower

cellular reactive oxygen species levels and enhanced resistance against oxidative stress; and treatment of stromal cells with P3F-modulated exosomes also conferred protection against exogenous oxidative stress. Our findings highlight the role of P3F fusion protein in modulating exosome cargo to confer a protective effect on recipient cells against oxidative stress and to promote plasticity and survival, potentially contributing to the known aggressive phenotype of the fusion gene-positive subtype of RMS.

Keywords: Rhabdomyosarcoma, PAX3-FOXO1, exosomes, oxidative stress, plasticity

INTRODUCTION

Rhabdomyosarcoma (RMS) is an aggressive soft tissue sarcoma of the skeletal muscle generally affecting children and adolescents (1). It is currently classified, according to the World Health Organization (WHO), into four histological subtypes with embryonal (ERMS), and alveolar (ARMS) being the two most frequent subtypes (2). ARMS has been described as more aggressive having a prognostic disadvantage compared to ERMS, specifically in the majority subset expressing the fusion oncoprotein PAX3-FOXO1 (or less commonly PAX7-FOXO1) (3). In fact, fusion status which divides RMS cases into fusion positive (FPRMS) and fusion negative (FNRMS) allows a better classification and determination of prognostic features (4). Common translocations involve the DNA binding domain of either PAX3 or PAX7 with the transactivation domain of FOXO1 resulting in PAX3/7-FOXO1 fusion oncoprotein that enhances RMS growth and metastasis by acting at target genes involved in proliferation, migration and invasion (5). RMS cells can modulate the tumor microenvironment to enhance both cancer cell and recipient cell motility favoring metastatic disease (6). For instance, MMP (matrix metalloproteinase) production by RMS cells, and to a higher propensity by ARMS cells, has been found to induce extracellular matrix remodeling and enhance invasiveness (7).

Exosomes are extracellular vesicles with a diameter ranging between 20–150 nm secreted under both physiological and pathological conditions and their cargo modulates signaling pathways in recipient cells (8). They have been demonstrated to promote tumor growth in a variety of cancer types including Ewing sarcoma, osteosarcoma and melanoma by promoting metastasis (9–11). In fact, different proteins and nucleic acids are enriched or depleted within cancer cell-derived exosomes, an indication that their sorting into exosomes is a selective process and that cancer cells can influence recipient cell behavior through the release of exosomes with modulated cargo. Functional changes induced by cancer cell-derived exosomes include the activation of angiogenesis and enhancement of recipient cell migration and invasion (6, 12–15). Proteomic profiling of RMS-derived exosomes revealed the presence of proteins such as integrins and annexins in both FPRMS and FNRMS-derived exosomes which have been implicated in tumor metastasis (12, 13, 16, 17). Selective miRNA enrichment has also been demonstrated in RMS-derived exosomes and in P3F transduced myoblasts which were found to enhance recipient fibroblast migration and invasion (6, 18).

Cellular plasticity involves adaptation to changes in the microenvironment and physiological conditions that would allow cell survival and growth (19). In cancer, plasticity involves the acquisition of characteristics favoring tumor progression and cancer cell survival under stress conditions. For instance, Ewing sarcoma and melanoma cells were found to express the TGFβ co-receptor endoglin correlating with cell plasticity, enhanced survival and invasion (20). Plasticity also involves the attainment of stem cell characteristics that include an ability to invade and disseminate into surrounding tissue (21). Cancer stem cell (CSC) features have been observed in ERMS cells that express markers such as CD133, exhibit chemoresistance and can form rhabdomyospheres, all of which are stem cell characteristics (22, 23). Moreover, aspects of plasticity that sustain cancer cell survival include acquiring resistance to and protection from oxidative stress. Oxidative stress results from an imbalance between pro-oxidative and anti-oxidative cellular pathways. Reactive oxygen species (ROS) including hydrogen peroxide (H_2O_2), are required for physiological signal transduction, but their levels are elevated in cancer cells as a result of augmented metabolic rates (24, 25). While ROS can enhance cancer proliferation and metastasis, an over-accumulation of ROS creates oxidative stress that can threaten cell survival. Therefore, cancer cells exhibit resistance to oxidative damage by the activation of alternate signaling pathways with lower ROS production and increased induction of antioxidant enzymes (26). Of note, oxidative stress can also enhance exosomes production with altered nucleic acid content that can confer changes in recipient cells and sustain their survival against stress (27, 28). In this study, we demonstrate that the *P3F* fusion gene modulates exosomes to promote recipient cell plasticity and response to oxidative stress that may favor tumor growth and metastasis.

MATERIALS AND METHODS

Cell Lines and Viruses

C2C12 mouse myoblasts were purchased from the ATCC (Virginia, United States) and cultured in Dulbecco's modified Eagle's medium AQ (DMEM AQ, Sigma, Setagaya, Japan) supplemented with 20% fetal bovine serum (FBS, Sigma) and 1% penicillin (100 units/ml) – streptomycin (100 μg/ml) antibiotics (Sigma). MSCV-IRES-GFP-PAX3-FOXO1 (MSCV-P3F) and MSCV-IRES-GFP (MSCV-GFP) plasmids were a kind gift from Dr. Gerard Grosveld (St. Jude Children's Research Hospital, Memphis, United States). The human ERMS cell lines

JR1 and the ARMS cell lines Rh30, were generously donated by Dr. Peter Houghton (Columbus, OH, United States), and have been previously described [reviewed in (29)]. HUVEC (human umbilical vein endothelial cells) and HEK293T (human embryonic kidney) cells were also purchased from ATCC. As described previously, viral supernatants were produced by transfecting 293T cells with MSCV-P3F or MSCV-GFP vectors using calcium phosphate (18). C2C12 cells were then transduced in suspension with either MSCV-GFP viruses (forming Ctrl-C2C12 cells) or MSCV-P3F (forming P3F-C2C12 cells) at 32°C, 1250 × *g* for 1 h with 8 μg/ml Polybrene (hexadimethrine bromide; Sigma), and sorted using FACS Aria SORP cell sorter (BD, New Jersey, United States) after selection with 2 μg/ml Puromycin (Abcam). Wild-type mouse embryonic fibroblasts (MEFs) and *p53*−/− (FVB.129-*Trp53*^{tm1Brn}) MEFs were isolated from E13.5 embryos of mixed C57BL/6 × 129/Sv 77 background (Jackson Laboratory, Maine, United States) using the procedure approved by the Institutional Care and Use Committee (IACUC) at the American University of Beirut, and following the IACUC-approved guidelines. MEFs are cultured in DMEM AQ, media supplemented with 10% fetal bovine serum (FBS, Sigma), 1% penicillin (100 units/ml) – streptomycin (100 μg/ml) antibiotics (Sigma), 1% sodium pyruvate, and 1% non-essential amino acids. All cells were maintained under standard conditions (humidified atmosphere, 95% air, 5% CO2, 37°C).

Exosome Isolation

Exosomes were isolated as previously described (6). Briefly, Ctrl-C2C12 cells, P3F-C2C12 cells, JR1 and Rh30 cells were incubated in exosome-free medium prepared by ultracentrifugation at 100,000 × *g*, overnight at 4°C. Exosomes were then isolated from the conditioned media by differential ultracentrifugations (18): 300 × *g* for 10-min 2,000 × *g* for 20-min centrifugation, and then 10,000 × *g* for 30 min. Finally, ExoQuick Exosome Precipitation Solution (System Biosciences, mountainite, CA, United States) was added to the resulting supernatant, and stored overnight at 4°C to allow exosome precipitation. The following day, the condensed medium was ultracentrifuged at 100,000 × *g* for 70 min, the pellet resuspended in PBS 1X, and ultracentrifuged at 110,000 × *g* for 70 min to remove any contaminating element. The final pellet was resuspended in 300 μL of PBS for functional assays and stored at −80°C. All centrifugations were done at 4°C. Recipient cells were treated with exosomes at 1X and 10X concentration, where 1X corresponds to exosomes isolated from an equivalent number of cells to those treated and 10X is 10 times this value.

Protein Extraction, and Western Blot

Proteins were extracted from 3 independently transduced cells and their respective exosomes using CHAPS lysis buffer (30 mM Tris–Cl, pH 7.5; 150 mM NaCl; and 1% CHAPS) mixed with 25X protease inhibitor (Roche, Basel, Switzerland). After adding the appropriate volume of lysis buffer, the mixture was sonicated for 20 min, centrifuged for 30 min at 13,000 × *g* at 4°C, then the supernatant containing the proteins was collected (12) and quantified using Bradford protein assay. Equal amounts of proteins were loaded and separated using 10% or 12% acrylamide gels, then transfered to a polyvinylidene difluoride (PVDF, Bio-Rad, CA, United States) membrane or nitrocellulose membrane (Santa Cruz, Heidelberg, Germany) in TGS1X-10% methanol transfer buffer. Membranes were blocked to prevent non-specific binding with 3% BSA-TBS1X-0.001% Tween [Tris (hydroxymethyl); NaCl; KCl and Tween 20; pH = 7.5] or 5% milk-TBS1X-0.001% Tween for 1 h, and then probed with primary antibodies (listed below) at 4°C overnight where they were washed 3 times by TBS1X-0.001% Tween for 5 min before adding the corresponding species-specific Horseradish Peroxidase (HRP)-conjugated secondary antibodies (Santa Cruz) for 2 h. Results were then detected on ChemiDoc machine (Bio-Rad) using Clarity Western ECL reagent (Bio-Rad) as a substrate.

The primary antibodies used were: anti-Hsc70, anti-GAPDH, anti-Vimentin, anti-Fibronectin, anti-Actin, anti-Basigin, anti-Calnexin (Santa Cruz), anti-phospho-ERK, anti-phospho-4EBP1, anti-ERK, anti-4EBP1 (Cell signaling, Danvers, United States), anti-TSG101 (Abcam, Cambridge, United Kingdom), anti-gp47, and anti-gp91, and anti-NOX1 (Upstate, NY, United States).

LC-MS/MS Analysis

Extracted proteins from Ctrl-C2C12- and P3F-C2C12-derived exosomes were subjected to sample clean-up and tryptic digestion as described previously (12). The LC-MS analysis of the tryptic digested proteins was performed using a 3000 Ultimate nano-LC system (Dionex, CA, United States) interfaced to an electrospray ionization (ESI) source equipped LTQ Orbitrap Velos mass spectrometer (Thermo Scientific, CA, United States). Aliquots of 1 μg of tryptic digests were injected and initially desalted on-line using an Acclaim PepMap100 C18 pre-column (75 μm I.D. 20 mm length, 3 μm particle sizes, 100Å particle size, Thermo Scientific) at a flow rate of 3 μL/min. The purified peptides were separated using an Acclaim PepMap100 C18 capillary column (75 μm I.D., 150 mm length, 2 μm, 100Å, Thermo Scientific) at a flow rate of 0.35 μL/min. The gradient applied to achieve separation was as follow: solvent B (99.9% ACN with 0.1% formic acid) was maintained at 5% from 0 to 10 min, increased to 20% over 55 min, 20–30% over 25 min, 30–50% over 20 min, 50–80% over 1 min, 80% over 4 min, decreased to 5% over 1 min, and finally was maintained at 5% for 4 min. Solvent A was 98% HPLC water, 1.9% ACN, and 0.1% FA. The LTQ Orbitrap Velos was operated in a data-dependent acquisition mode with 2 scan events. The first scan was a full MS scan of m/z 400-2000 with a mass resolution of 15,000. The second scan event was a CID MS/MS repeated on top 10 intense ions selected from the previous scan event with an isolation window of m/z 3.0. The mass spectrometry proteomics data have been deposited to the ProteomeXchange Consortium via the PRIDE partner repository.

LC-MS Data Processing

Proteome Discover version m1.2 (Thermo Scientific) was used to convert raw files acquired from LC-MS analysis to mascot generic format (*.mgf) files. The *.mgf files were subjected to MASCOT version 2.4 (Matrix Science Inc., Boston, United States) to search against protein database. The carbamidomethylation of cysteine was a fixed modification and the oxidation of

methionine was considered as a variable modification. The mass shift tolerance for matching peptide precursors and fragments was 6 ppm and 0.8 Da, respectively. Enzyme was specified as trypsin. A maximum of 2 miscleavage was allowed. MASCOT searching results were then exported to Scaffold (version 3.6.3, Proteome Software, Portland, OR, United States) for further processing and quantification. Identified proteins were filtered using the following criteria: Peptide threshold = 95%, protein thresholds = 99%, with a minimum of 2 peptides identified. The quantification was based on spectral counting. The quantitative proteomic results were further subjected to statistical analysis.

Bioinformatic Analysis

For gene ontology analysis, including differential molecular function and biological processes, PANTHER software (Protein Analysis Through Evolutionary Relationships; http://www.pantherdb.org/genes/batchIdSearch.jsp) was used to classify genes into distinct categories of molecular functions and biological processes. Genes were classified into families and subfamilies of shared function, which were then categorized using a highly controlled vocabulary (ontology terms) by the biological process and molecular function. Functional pathways and protein association were examined using the computational bioinformatics program, Pathway Studio software (v.11.4.0.8; Elsevier) as previously described (30, 31). This bioinformatics platform enables the analysis and visualization of altered pathways and protein network association needed to construct and recognize altered cellular processes and involved molecular functional pathways.

The identified proteins were analyzed using Ingenuity Pathway Analysis (IPA) software (Ingenuity® Systems, www.ingenuity.com), to find diseases, functions, and networks in which the identified proteins are implicated; the analysis was done for the deregulated proteins with their fold changes. The analysis was also done by PANTHER Software[1], which was used to identify the molecular processes and biological pathways linked to these proteins.

Gelatin Zymography Assay

Proteins were extracted from culture supernatant of MEF cells treated with 10X exosomes for 72 h and run along with FBS (positive control) on 0.75 mm SDS-PAGE gel, containing gelatin (Bio-Rad) as a substrate, washed twice and incubated overnight in substrate buffer at 37°C with shaking. Gels were then stained with coomassie blue (Thermo Scientific) for 1 h at RT, de-stained with ethanol, acetic acid and water solution. Results were detected on ChemiDoc machine. Band staining intensity was determined by densitometry, using ImageJ software (32).

Tube Formation Assay

Matrigel (Corning, NY, United States) was diluted 1:1 by HUVEC cell medium and added very carefully into a 96-well plate, avoiding bubbles. The plate was placed in the incubator at 37°C for 30 min to solidify, after which HUVEC cells (15,000 cells/well) were plated on top and treated with either Ctrl-C2C12-derived exosomes or P3F-C2C12-derived exosomes at1X and 10X concentrations then left for 2 h to form tubes. Images were taken by light transmission microscopy and analyzed by ImageJ software (angiogenesis analyzer) as previously performed (6).

Sphere Formation Assay

p53−/− MEFs and C2C12 cells (2×10^3/well) suspended in Matrigel™:serum-free media (1:1) were uniformly plated around the bottom rim of 24-well plates with 3% serum-containing media supplemented with 20 ng/mL epidermal growth factor (EGF, R&D Systems, Minnesota, United States) and 2% B27 (Invitrogen, CA, United States). The medium was replenished every 72 h. Micrographs of the spheres formed after 5 days were taken and counted (33).

MTT Proliferation Assay

Transduced C2C12 cells (8000 cell/well) were plated in 96-well plates. The following day, they were treated with different concentrations of H_2O_2 (Sigma) ranging from 0 to 500 μM. MTT (Roche) was added according to the manufacturer's instructions after 24 h. The absorbance was measured by ELISA reader (at a 595 nm wavelength). Results were computed as the mean percent absorbance of H_2O_2-treated condition relative to control (untreated). Each experiment was repeated at least 3 times, each performed in triplicate.

Trypan Blue Exclusion Assay

C2C12 cells were seeded in 24-well plates at a density of 10,000 cells/well. After 5 h of incubation at 37°C, Ctrl-C2C12-, or P3F-C2C12-derived exosomes (at 10X concentration) were added to the cells. Then 40 h later, cells were treated simultaneously with 60 μM H_2O_2 and Ctrl-C2C12 or P3F-C2C12 exosomes at 10X concentration. Cells were counted using trypan blue (Sigma) at 8 and 24 h following H_2O_2 treatment. Each experiment was repeated at least 3 times, each performed in triplicate.

Flow Cytometry for ROS Production Evaluation

Reactive oxygen species levels were evaluated for Ctrl-C2C12 and P3F-C2C12, or C2C12 cells treated with Ctrl-C2C12-derived exosomes or P3F-C2C12-derived exosomes at a 10X concentration. In summary, 30,000 cells were seeded in 6-well plates, and incubated at 37°C for 48 h. When needed, exosomes were added 5 h post plating. On the day of the experiment, control wells were incubated for 1 h with either H_2O_2 (positive control) or 10 mM N-Acetyl-Cysteine (NAC), negative control, which is a ROS inhibitor (Sigma). ROS was detected by incubating cells for 30 min with the cell permanent reagent 2', 7'–dichlorofluorescin diacetate (DCF-DA; 1 mg/ml, Sigma), a fluorogenic dye that measures hydroxyl, peroxyl, and other ROS activity within the cell. After diffusion into the cell, DCF-DA is deacetylated by cellular esterases to a non-fluorescent compound, which is later oxidized by ROS into 2', 7' –dichlorofluorescein (DCF). DCF is a highly fluorescent compound, which can be

[1]http://pantherdb.org

detected by fluorescence spectroscopy with maximum excitation and emission spectra of 495 nm and 529 nm, respectively. Cells were then trypsinized, centrifuged at 1500 rpm for 7 min, and the pellet was resuspended with 300 μL of PBS. Finally, cells were analyzed by the Guava EasyCyte8 flow cytometer.

Statistical Analysis

Statistical comparisons were made between the control and treatment groups using Student's *t*-test. A p-value < 0.05 was considered to indicate a statistically significant difference. The PCA analysis for LC-MS results was performed by MarkerView 1.1 (AB Sciex, Framingham, United States).

RESULTS

PAX3-FOXO1 Alters Protein Cargo of C2C12 Derived Exosomes

The myogenic background of the murine C2C12 myoblasts is the ideal system to evaluate cellular effects of *P3F* (18, 34). As previously published, C2C12 cells transduced with P3F-expressing vector (P3F-C2C12) show features of transformation, including enhanced anchorage-independent growth when compared to cells transduced with empty vector (Ctrl-C2C12) (18). Analysis of this system previously showed that *P3F* alters the miRNA content of exosomes, leading to over-expression of *miR-486-5p*, in turn promoting pro-tumorigenic cellular properties (18). However, the effect of possible changes in the protein content of exosomes in response to P3F has not been characterized to date. In this study, we interrogated the proteomic content of C2C12 exosomes in response to P3F expression. We extracted exosomal proteins and subjected them to LC-MS/MS proteomics analysis (**Supplementary Figure 1**). The results showed excellent reproducibility within each cell line (**Figure 1A**). Principal components analysis (PCA) shows that the protein content of 3 independent extractions from Ctrl-C2C12 exosomes clustered together and separately from the 3 independent protein extractions from P3F-C2C12 exosomes, meaning that there is a difference between the protein cargo of Ctrl-C2C12 and P3F-C2C12 exosomes (**Figure 1A**). LC-MS/MS results were validated by western blot for a subset of proteins identified to be common among Ctrl-C2C12 and P3F-C2C12 exosomes, showing excellent concordance of results. Along with the common exosomal protein markers, TSG101, Hsc70, and GAPDH, we detected the presence of Vimentin, Basigin, Fibronectin, and Actin. The negative control Calnexin, a cellular protein that is localized to the endoplasmic reticulum was, as expected, excluded from exosomes (**Figure 1B**).

By comparing the expression levels of the proteins found within P3F-C2C12-derived exosomes to those within Ctrl-C2C12-derived exosomes revealed by LC-MS/MS analysis, we identified 52 proteins differentially expressed; 26 proteins were significantly enriched in P3F-C2C12-derived exosomes among which 7 were exclusively present within these exosomes and 26 were significantly down-regulated proteins among which 13 were excluded from these exosomes (**Table 1**).

PAX3-FOXO1 Fusion Protein Modifies the Exosomal Protein Cargo in Favor of Processes and Pathways Implicated in Cancer Progression

Bioinformatics analysis was performed in order to unravel the possible effects that the 52 deregulated proteins can impose on recipient cells, using the two software: Panther classification system and IPA. Panther software highlighted the molecular functions and the biological processes in which these 52 deregulated proteins were implicated (**Figures 2A,B**). "Catalytic activity" and "binding" were the top molecular functions for both enriched and down-regulated proteins (**Figure 2A**). It is important to note that "antioxidant activity" is the only molecular function exclusively found in the exosomes derived from P3F-C2C12 cells with 4% of the enriched proteins implicated (**Figure 2A**). Furthermore, "metabolic process," and "cellular process" were the top biological processes in which both enriched and down-regulated proteins are implicated (**Figure 2B**). "Apoptotic process" appears to be the only biological process eliminated from the exosomes after P3F transduction (**Figure 2B**). These processes underline the implication of the P3F-C2C12-derived exosomes in tumor progression.

Ingenuity Pathway Analysis software was used to assess the canonical pathways implicated and the downstream diseases and functions in which the 26 significantly enriched proteins are involved (**Figures 2C,D**). The enrichment of the identified proteins seem to implicate "14-3-3 mediated signaling," "cell cycle: G2/M DNA damage checkpoint regulation," and "ERK5, VEGF, IGF1, and p70S6K signaling," all of which are important in cell plasticity and cancer progression (**Figure 2C**). Moreover, "cellular movement" and "cell death and survival" appear in the top 10 diseases and functions where these deregulated proteins are implicated (**Figure 2D**). IPA software allows for identification of common networks in which the deregulated proteins may be intersecting. Three networks resulted from this analysis with all three having more than one identified deregulated focus molecule (**Figures 2E–G**). In these networks, we could identify important nodes previously implicated in RMS biology and progression such as: FAK, PKC, MEK, PI3K/AKT/ERK/MAPK, NFkB, TP53, HRAS, as well as proteins involved in cellular signaling and angiogenesis such as VEGF.

PAX3-FOXO1-Deregulated Proteins and miRNA in Exosomes Are Involved in Cell Survival and Cellular Plasticity

We had previously characterized the miRNA cargo modulated by P3F in C2C12-derived exosomes (18). We now paired both the deregulated 111 miRNA and the 52 proteins using IPA, and found largely common functions where these molecules are implicated, specifically down-regulating apoptosis, cell death and necrosis, and inducing cell proliferation, invasion, and metastasis (**Figure 3A**). This result is in line with the functional effect of P3F-C2C12 exosomes presented in our previous work (18), where these exosomes were found to promote viability, invasion, and migration of recipient cells. Comparing the

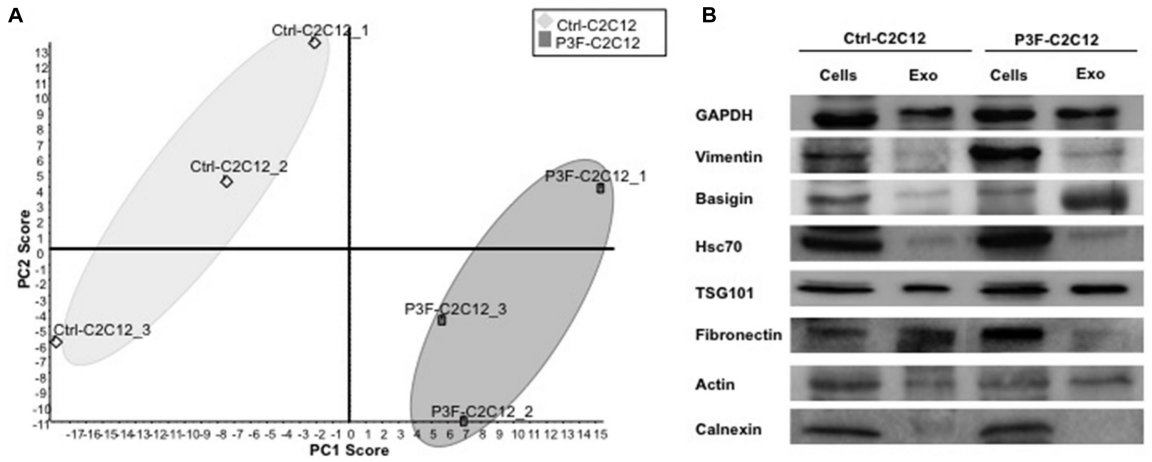

Proteins	Ratio Exo-P3F vs Exo-Ctrl	*p-value*
GAPDH	0.32	**0.02**
Vimentin	2.18	**0.03**
Basigin	5.88	**0.03**
Hsc70	1.78	0.18
TSG101	0.23	0.12
Fibronectin	0.07	0.10
Actin	1.35	0.26

FIGURE 1 | LC-MS/MS protein profiling of C2C12-derived exosomes. **(A)** Score plot obtained by Principal Component analysis (PCA) for LC–MS/MS results of 3 independently transduced preparations of Ctrl-C2C12 and P3F-C2C12 exosomes. **(B)** Western Blot analysis of the indicated proteins in exosomes and respective cell lysates. The table represents the expression level of the represented proteins in P3F-C2C12 exosomes compared to Ctrl-C2C12 exosomes as quantified by LC-MS/MS with their respective *p*-values.

generated networks by IPA from miRNA and proteins separately, we identified 3 common nodes focusing on Insulin, Follicle-stimulating hormone (FSH), and TP53. **Figures 3B–D** clarify the upstream and downstream deregulated miRNA and proteins identified within the exosomes that are regulated by or regulate these three nodal proteins.

PAX3-FOXO1-Modulated Exosomes Induce Cell Survival Pathways, Angiogenesis and Stemness in Recipient Cells

We have previously shown that exosomes isolated from P3F-C2C12 cells were able to induce proliferation, invasion and migration of recipient cells (MEFs and C2C12) compared to cells treated with Ctrl-C2C12-derived exosomes (18). In line with the pathways identified by network analysis in **Figures 2C,E,F**, we verified that treatment with P3F-C2C12-derived exosomes leads to increased phosphorylation (and therefore activation) of ERK and 4-EBP1 (**Figure 4A**), which are essential mediators of cancer cell survival and proliferation (35, 36).

In view of the nodal proteins identified to be involved in cytoskeletal organization and matrix degradation, such as Basigin, Filamin A, and others (**Figure 2E**), we examined the functional effects of the modulated exosomes on collagenase activity using zymography assay. Indeed, P3F-modulated exosomes led to higher MMP-2 activity in treated MEFs, as compared to cells treated with Ctrl-C2C12-derived exosomes evident by the increase in gelatinolytic bands (digested regions; **Figure 4B**).

Since the identified networks also involved angiogenic proteins such as VEGF and TNF (**Figures 2C,G**), we investigated the effect of P3F-C2C12-derived exosomes on angiogenesis by conducting a matrigel tube formation assay that evaluates the ability of HUVECs to differentiate into capillary-like structures when plated on matrigel (6). Counting the nodes, which are defined as the intersection of 3 or more branches of tubular connections, the total length which is the sum of length of segments, isolated elements and branches in the analyzed area and the total mesh area, which represents the area occupied by the primary capillary-like tubes, we found a significant increase when HUVECs were treated with P3F-C2C12-derived exosomes compared to control, at 10X but not 1X concentration (**Figure 4C**).

Exosomes can reprogram transcription within recipient cancer cells allowing their dedifferentiation into CSC with sphere-forming capacities (37). To examine whether P3F-modulated exosomes would enhance their ability to confer stem-like properties to recipient cells, we examined their effects on sphere-forming capacity of MEFs and C2C12 cells. We used *p53*−/− MEFs for this assay, as wild-type MEFs were not prone to forming spheres in culture. For both *p53*−/− MEFs and C2C12 cells, we found that treatment with P3F-modulated exosomes led to a significant increase in the number of formed spheres 5 days post treatment, relative to the control-derived exosomes (**Figures 4D,E**).

TABLE 1 | List of the 26 significantly enriched and 26 significantly down-regulated proteins in P3F-C2C12-derived exosomes compared to those in Ctrl-C2C12-derived exosomes with their fold changes and *p*-value.

		Expression level Exo-P3F *versus* Exo-Ctrl	*p*-value
	Enriched proteins		
1	Leukocyte elastase inhibitor (Serpinb1a)	Infinity	6.3.E-06
2	Lymphocyte antigen 6C1 (Ly6c1)	Infinity	7.5.E-04
3	Lymphocyte antigen 6D (Ly6d)	Infinity	2.6.E-03
4	Histone H1.5 (Hist1h1b)	Infinity	7.0.E-03
5	Calreticulin (Calr)	Infinity	8.9.E-03
6	Retinoic acid-induced protein 3 (Gprc5a)	Infinity	2.8.E-02
7	Rho GDP-dissociation inhibitor 2 (Arhgdib)	Infinity	3.7.E-02
8	Prostaglandin reductase 1 (Ptgr1)	28.2	2.9.E-03
9	Embigin (Emb)	15.47	2.0.E-02
10	Basigin (Bsg)	5.88	3.3.E-02
11	Hsc70-interacting protein (St13)	3.74	2.3.E-02
12	Glutathione S-transferase P 1 (Gstp1)	3.65	2.2.E-02
13	Nucleoside diphosphate kinase B (Nme2)	3.56	3.8.E-02
14	Annexin A1 (Anxa1)	3.49	4.6.E-03
15	Superoxide dismutase (Sod1)	3.45	3.4.E-04
16	Monocarboxylate transporter 1 (Slc16a1)	3.41	2.3.E-02
17	Granulins (Grn)	2.94	3.3.E-02
18	Fatty acid-binding protein, epidermal (Fabp5)	2.76	7.4.E-03
19	Alpha-actinin-1 (Actn1)	2.68	1.7.E-02
20	14-3-3 protein zeta/delta (Ywhaz)	2.2	9.1.E-04
21	Vimentin (Vim)	2.18	3.5.E-02
22	CD82 antigen (Cd82)	2.06	9.7.E-03
23	Major vault protein (Mvp)	2.01	9.0.E-03
24	Malate dehydrogenase, cytoplasmic (Mdh1)	1.84	3.9.E-02
25	14-3-3 protein epsilon (Ywhae)	1.82	4.7.E-02
26	Sodium/potassium-transporting ATPase subunit alpha-1 (Atp1a1)	1.7	3.2.E-02
	Down-regulated proteins		
1	Alpha-enolase (Eno1)	0.67	4.5.E-02
2	Glyceraldehyde-3-phosphate dehydrogenase (Gapdh)	0.32	1.5.E-02
3	Adenosylhomocysteinase (Ahcy)	0.28	4.8.E-02
4	T-complex protein 1 subunit theta (Cct8)	0.23	4.9.E-02
5	T-complex protein 1 subunit zeta (Cct6a)	0.21	2.7.E-02
6	Integrin alpha-5 (Itga5)	0.2	2.2.E-02
7	Serine protease HTRA1 (Htra1)	0.19	4.0.E-02
8	Myosin-9 (Myh9)	0.18	2.8.E-02
9	Voltage-dependent calcium channel subunit alpha-2/delta-1 (Cacna2d1)	0.14	3.9.E-02
10	Transitional endoplasmic reticulum ATPase (Vcp)	0.13	2.8.E-02
11	Talin-1 (Tln1)	0.13	5.7.E-03
12	Peptidyl-prolyl *cis*-trans isomerase C (Ppic)	0.08	7.2.E-03
13	Filamin-A (Flna)	0.02	1.0.E-03
14	Sorcin (Sri)	0	4.3.E-06
15	Serine protease 23 (Prss23)	0	4.7.E-04
16	Ras-related protein Rab-5C (Rab5c)	0	4.7.E-04
17	N(G),N(G)-dimethylarginine dimethylaminohydrolase 2 (Ddah2)	0	9.5.E-04
18	Mimecan (Ogn)	0	4.7.E-03
19	Band 4.1-like protein 2 (Epb41l2)	0	1.1.E-02
20	Ras-related protein R-Ras2 (Rras2)	0	1.4.E-02
21	EGF-like repeat and discoidin I-like domain-containing protein 3 (Edil3)	0	2.4.E-02
22	Inter-alpha-trypsin inhibitor heavy chain H3 (Itih3)	0	2.4.E-02
23	DnaJ homolog subfamily A member 2 (Dnaja2)	0	2.9.E-02
24	LIM and senescent cell antigen-like-containing domain protein 1 (Lims1)	0	3.4.E-02
25	Large neutral amino acids transporter small subunit 1 (Slc7a5)	0	3.4.E-02
26	Integrin-linked protein kinase (Ilk)	0	3.8.E-02

The expression levels presented are the ratio of the level of the indicated proteins found by LC-MS/MS within the P3F-C2C12 exosomes compared to Ctrl-C2C12 exosomes.

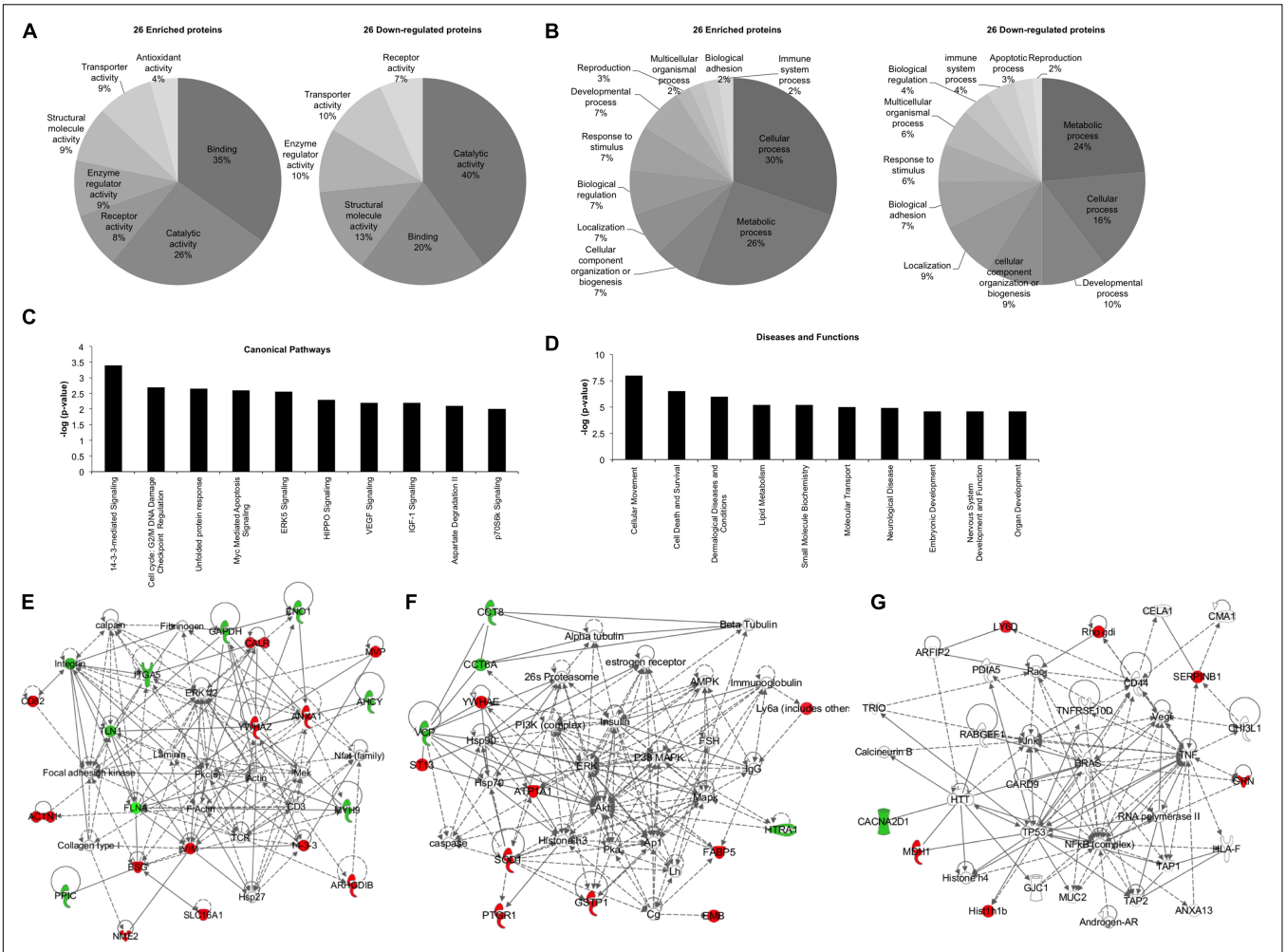

FIGURE 2 | Bioinformatics analysis of the deregulated proteins between Ctrl-C2C12 and P3F-C2C12 exosomes. **(A,B)** Pie charts determined by Panther analysis presenting the molecular functions **(A)**, and the biological processes **(B)** for the 26 enriched and 26 down-regulated proteins. **(C,D)** histograms from IPA analysis of the 26 enriched proteins showing the top 10 canonical pathways **(C)** and the top 10 diseases and functions **(D)**. **(E–G)** Generated networks by IPA analysis of the deregulated proteins in C2C12-P3F-derived exosomes compared to Ctrl-C2C12-derived exosomes. Proteins colored in red are enriched and those colored in green are down-regulated. The higher the level of enrichment or down-regulation, the more intense the color is presented. Edges (lines and arrows between nodes) represent direct (solid lines) and indirect (dashed lines) interactions between molecules as supported by information in the Ingenuity knowledge base.

These results highlight the ability of the P3F fusion protein to promote cellular plasticity and tumorigenic aspects through exosomes.

PAX3-FOXO1 Fusion Protein Is Implicated in Redox Homeostasis and Tolerance/Protection From Oxidative Stress by Decreasing ROS Levels in Both Transduced and Recipient Cells

Of the 26 enriched proteins in P3F-C2C12-derived exosomes, we found that 4 proteins are implicated in the ROS pathway. These proteins include prostaglandin reductase 1 (PtgR1), which has an oxidoreductase activity that can reduce cytotoxic unsaturated aldehydes and ketones produced by lipid peroxidation during oxidative stress (38); glutathione S-transferase (GST), which detoxifies secondary metabolites produced by interaction between ROS and cellular components (39); superoxide dismutase (SOD1), which is an antioxidant enzyme that reduces superoxide (O_2^-) and prevents its accumulation (40); and malate dehydrogenase, which is activated by ROS and seems to act as a redox regulator in response to environmental changes (41). These 4 enzymes mainly act by decreasing ROS levels. Since ROS contributes to oxidative stress, we hypothesized that the P3F fusion protein may be influencing redox homeostasis and response to oxidative stress. Indeed, the expression levels of the 3 main subunits of the NADPH oxidase complex, which is a main enzymatic producer of ROS: gp91, gp47, and Nox1 were decreased in P3F-transduced C2C12 cells compared to control cells (**Figure 5A**). Several bands appear for Nox1 protein due to different glycosylation sites (42). This result was confirmed by flow cytometry analysis using the DCF-DA dye to detect ROS levels, where we found that P3F-C2C12 cells have markedly decreased

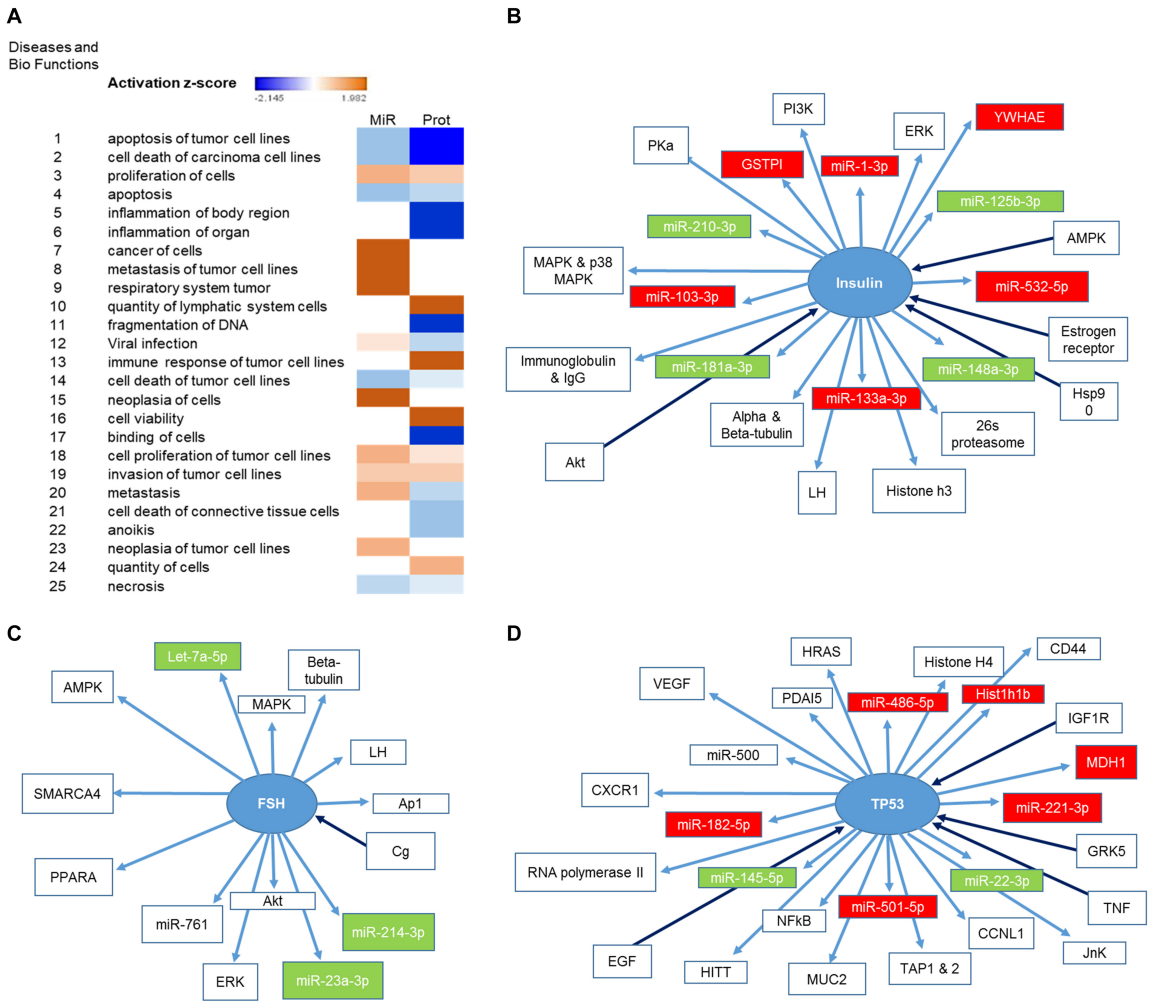

FIGURE 3 | Identification of the pathways in which both deregulated miRNA and proteins are implicated. **(A)** Heat map representing the diseases and bio functions in which both deregulated miRNA and proteins are implicated and their corresponding activation score. **(B,D)** Representation of the upstream and downstream miRNA and proteins in pathways centering on **(B)** Insulin, **(C)** FSH, and **(D)** TP53. Proteins and miRNAs colored in red are enriched and those colored in green are down-regulated.

proportion of DCF-positive cells as compared to Ctrl-C2C12 cells, demonstrating lower ROS levels in response to P3F expression (**Figure 5B**).

Next, we subjected the transduced cells to oxidative stress in order to test the protective effect of the fusion protein. After treating the cells with different concentrations of H_2O_2 (0 to 500 μM) for 24 h, P3F-C2C12 cells showed a higher IC_{50} (68 μM) than Ctrl-C2C12 cells (36.8 μM; **Figure 5C**). Thus, P3F-C2C12 cells are more tolerant to endogenous and exogenous oxidative stress than control cells. These results show that the PAX3-FOXO1 fusion protein can decrease ROS levels in host cells, likely contributing to cell survival.

Since P3F-C2C12 cells were found to be tolerant to H_2O_2-induced oxidative stress, we next investigated whether this resistance is provided to recipient cells through exosome cargo. Treating C2C12 myoblasts with a combination of H_2O_2 and P3F-C2C12-derived exosomes at 10X concentration showed significantly higher viability in comparison to cells treated with H_2O_2 and Ctrl-C2C12-derived exosomes (1.88 *versus* 1.05 at 8 h; and 1.27 *versus* 0.88 at 24 h; **Figures 6A,B**). Interestingly, this protective effect was also observed when treating human ERMS JR1 cells with a combination of H_2O_2 and ARMS Rh30-derived exosomes showing a significantly higher viability when compared to cells treated with H_2O_2 and JR1-derived exosomes (**Figure 6C**). This confirms a protection conferred by FPRMS-derived exosomes to recipient cells in conditions of oxidative stress.

To clarify whether this protection was related to decreased levels of ROS in cells treated with P3F-modulated exosomes as opposed to control exosomes, we pretreated C2C12 cells with exosomes for 48 h, and then exposed them to H_2O_2, and evaluated ROS levels by DCF-DA.

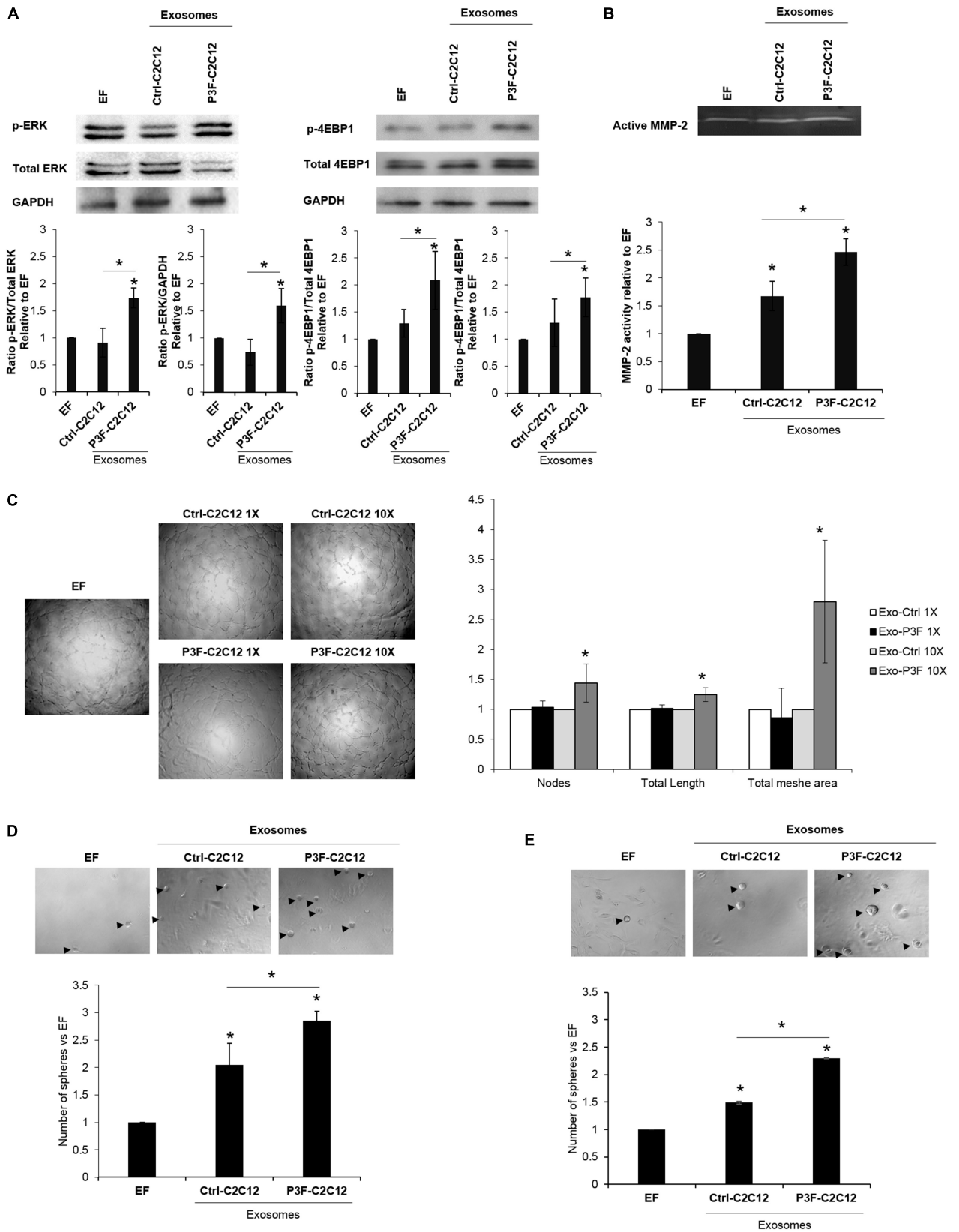

FIGURE 4 | Continued

FIGURE 4 | C2C12-P3F-derived exosomes promote angiogenesis and induce stemness of recipient cells. **(A)** Western blot for the indicated proteins in MEFs treated with Exo-free (EF) media, 10X Ctrl-C2C12-derived exosomes, and 10X P3F-C2C12-derived exosomes. GAPDH is used as a loading control. Histograms presenting the levels of phosphorylation of ERK and 4EBP1 compared to Exo-free condition, quantified by ImageJ software from $n = 3$ different western blots. **(B)** Zymography image of digested regions showing MMP2 activity in MEFs treated with either Ctrl-C2C12-derived exosomes or P3F-C2C12-derived exosomes for 72 h. Relative MMP-2 activity from 3 independent experiments was quantified by ImageJ software and presented by a histogram. **(C)** Representative phase contrast photomicrographs of endothelial tube formation of HUVECs cultured on Matrigel with either Exo-Free medium (EF), 1X, or 10X C2C12-MSCV-derived exosomes or C2C12-P3F-derived exosomes, as specified. Quantitation of the total number of nodes, total length and total mesh area of the different conditions are shown in the histogram, which represent the mean of 3 independent experiments, each performed in triplicate. **(D,E)** Representative phase contrast photomicrographs and histograms showing the ratio of the spheres formed by p53−/− MEFs **(D)** or C2C12 cells **(E)** treated with either Exo-Free medium (EF) or 10X C2C12-MSCV-derived exosomes or C2C12-P3F-derived exosomes, as specified. All data are reported as means of at least three independent experiments ± SD. Asterisks (*) denote a statistically significant difference (p-value < 0.05).

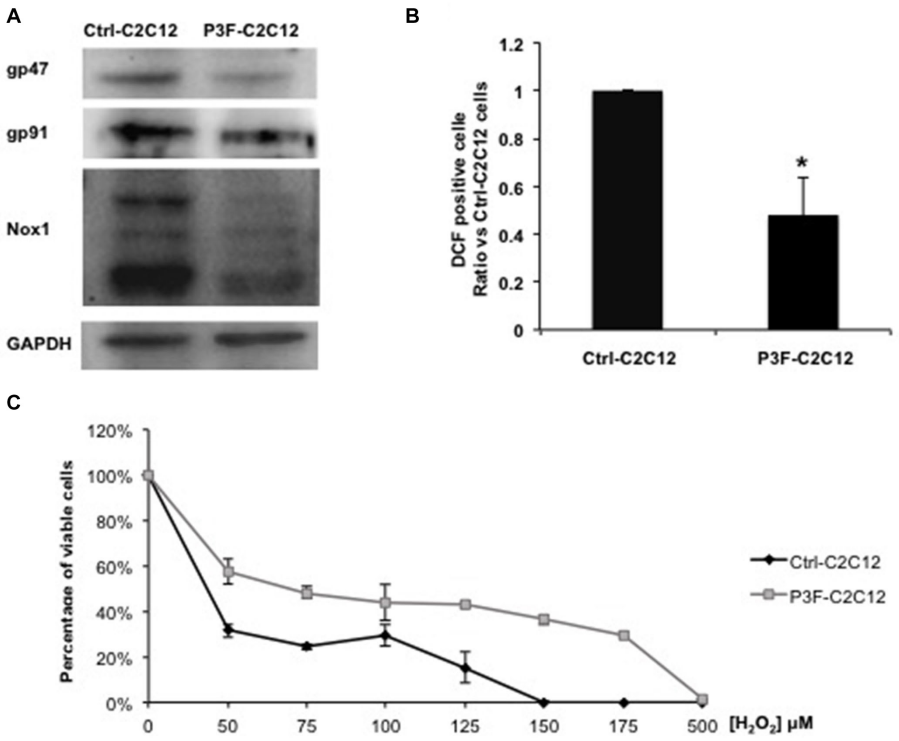

FIGURE 5 | P3F decreases ROS levels in transduced cells. **(A)** Western blot analysis of gp47, gp91, and Nox1 protein levels; subunits of the NADPH oxidase complex. GAPDH is used as a loading control. **(B)** Histogram representing the percentage ± SD of DCF-DA positive cells, relative to control Ctrl-C2C12 cells; numbers shown are average of three independent experiments. **(C)** MTT assay determining the IC50 of Ctrl-C2C12 and P3F-C2C12 cells treated with ascending concentrations of H_2O_2 for 24 h. Data are reported as mean of three independent experiments ± SD. Asterisks denote a statistically significant difference (p-value < 0.05); (*) compared to control Exo-free treated cells.

Treatment with exosomes, whether control or PAX3-FOXO1-modulated, both had an inhibitory effect on ROS production (**Figure 6D**). The induction of ROS observed by treating the recipient cells with H_2O_2 was significantly decreased when co-treated with either exosome type, but to a much higher extent when treated with P3F-C2C12-derived exosomes. Indeed, P3F-C2C12-derived exosomes were able to decrease ROS levels by 6.6 fold whereas Ctrl-C2C12-derived exosomes decreased it only by 2.4 fold when compared to H_2O_2 treatment alone (**Figure 6D**). These observations define a clear role of P3F-modulated exosomes in protecting recipient cells, even in the presence of oxidative stress, from elevated intracellular ROS levels.

DISCUSSION

Rhabdomyosarcoma is an aggressive pediatric cancer with limited improvement in overall survival outcomes in patients with aggressive subtypes and advanced stages (1). Presence of the P3F or the less common PAX7-FOXO1 fusion oncoprotein is associated with increased incidence of metastasis and disease aggressiveness (43, 44). There is therefore a pressing need for identifying effective therapeutic targets and biomarkers for these fusion gene positive (FP) RMS.

Exosomes can act *via* paracrine signaling on neighboring stromal cells altering their behavior and enhancing tumor growth (9, 15, 45). Both FPRMS and FNRMS cells secrete quantifiable amounts of exosomes with specific cargo that can influence

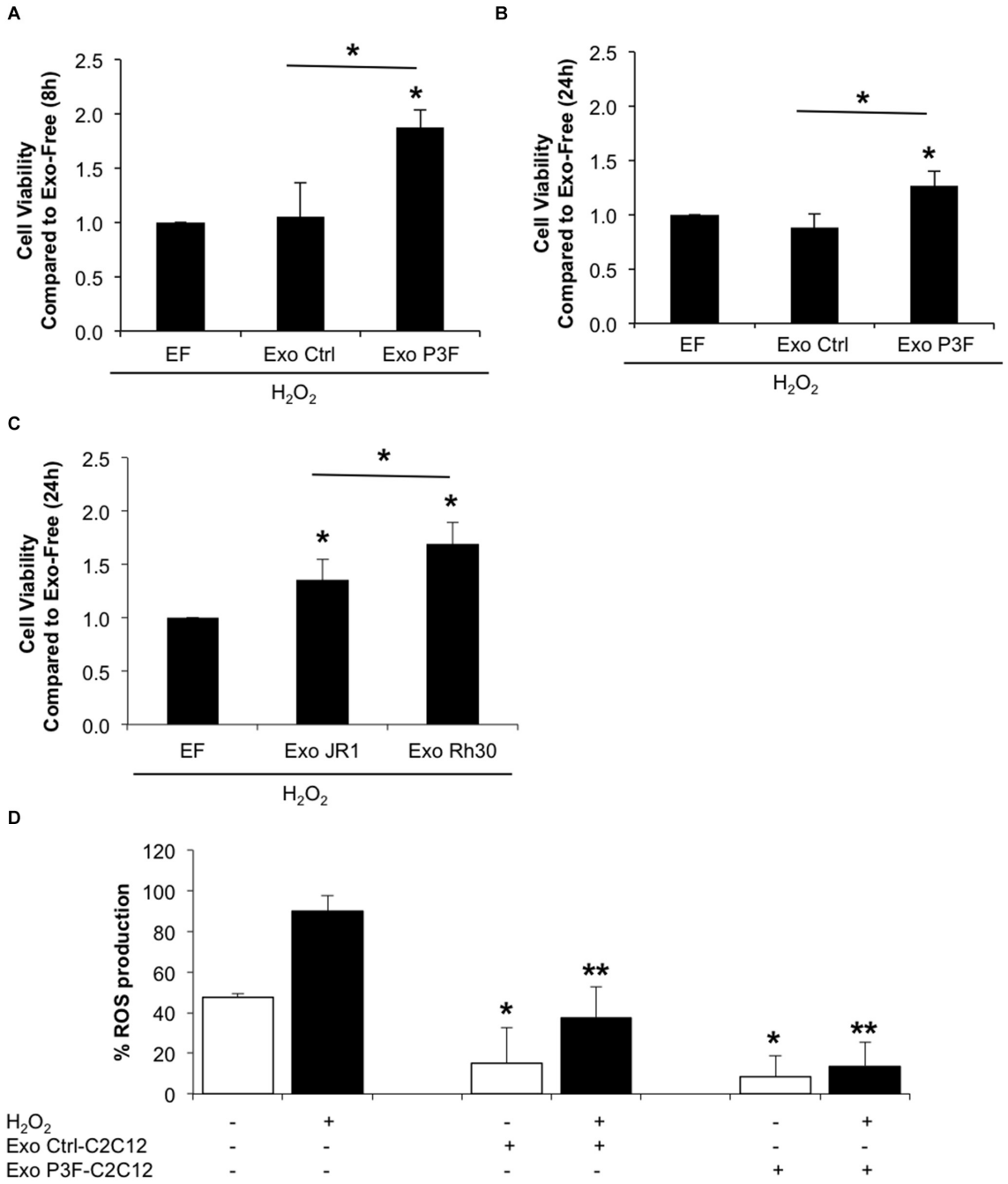

FIGURE 6 | P3F confers protection from oxidative stress in both autocrine and paracrine manner through exosomes. **(A,B)** Histograms representing the ratio of living cells in each condition relative to the exo-free control, after 8 h **(A)** and 24 h **(B)** of H_2O_2 treatment assessed by Trypan blue exclusion assay. **(C)** Histogram representing the ratio of living cells in each condition relative to the exo-free control, after 24 h of H_2O_2 treatment assessed by Trypan blue exclusion assay. Data are reported as mean of three independent experiments ± SD. Asterisks denote a statistically significant difference (p-value < 0.05). **(D)** Histogram displaying the percentage of DCF positive cells in each condition. Data are reported as mean of three independent experiments ± SD. Asterisks denote a statistically significant difference (p-value < 0.05); (*) compared to control Exo-free treated cells and (**) compared to H_2O_2 treated cells.

cancer-related processes including cell motility and angiogenesis (6), and fusion status plays a role in modulating exosome cargo to favor tumor invasion (6, 12, 18).

In this study, we investigated the effects of P3F on myoblasts using C2C12 cells, and studied its role in modulation of exosome protein content and paracrine signaling. Both the previously

identified deregulated miRNA revealed by microarray profiling (18) and the deregulated exosomal proteins identified in this study were associated with pathways important in cell plasticity including cellular motility, cell survival, and protection from oxidative stress. The networks identified centered on insulin, FSH and TP53, all of which have previously been associated with the expression of P3F or implicated in RMS tumor progression. For instance, both insulin, and insulin-like growth factors (IGF) regulate skeletal muscle differentiation, and their pathways are deregulated in RMS (46, 47). Using C2C12 myoblasts, Wang et al. showed that P3F and IGF2 cooperate to induce cell proliferation and invasion (48). Additionally, P3F has been shown to up-regulate the expression of IGF1 receptor and IGF2, both contributing to FPRMS proliferation (49). P3F also induces aberrant and elevated expression of GLUT4, enhancing cellular response to insulin (50). As for FSH, its receptors are expressed in both FPRMS and FNRMS human cell lines, as well as in primary tumor samples. Stimulation of RMS cells with FSH results in enhanced proliferation and chemotaxis, indicating a role in promoting RMS progression (51). FSH down-regulates FOXO1 mRNA levels, and FSH receptor activation results in FOXO1 phosphorylation, which inhibits FOXO1-mediated repression of apoptosis and promotes cell survival (52, 53). However, whether P3F contributes to FSH-mediated repression of wild type FOXO1 is yet to be determined. Finally, p53 pathway deregulation has been observed in RMS and contributes to tumor progression and relapse (54–56). While p53 pathway deregulation in FNRMS is mainly via inactivation mutations in *TP53*, in FPRMS its deregulation is likely mediated by the fusion oncoprotein, as PAX proteins have been shown to transcriptionally inhibit p53 (57). Moreover, *TP53* loss markedly increases the progression of P3F-driven tumors in mice (58). Indeed, 85% of human tumors harboring P3F fusion were associated with *p53* inactivation, suggesting a cooperativity between the fusion protein and p53 pathway deregulation in driving tumorigenesis (59). In concordance, our results further reveal that P3F expression leads to exosomal-mediated deregulation of these signaling pathways, likely contributing to their deregulation in recipient cells.

Functionally, exosomes of P3F-transduced cells modulated recipient cell plasticity to favor proliferation, invasion, angiogenesis and stemness, as well as protect them from the hostile conditions of the tumor microenvironment (TME). Angiogenesis and neovascularization are indicative of cell plasticity that allows tumor growth and cell survival in hypoxic conditions of the TME (19, 60). Ploeger et al. showed that fibroblasts exhibit a high dynamic plasticity in wound healing resulting from a combination of recruitment and cell proliferation, a plasticity that seems to be regulated by the micro-environment (61). P3F-modulated exosomes were able to induce tube formation and migration of recipient HUVECs, as well as induce degradation of matrix via activation of MMPs, indicating a role for these exosomes in inducing angiogenesis and alteration of the stromal matrix.

Escaping cell death is another indication of cellular plasticity in response to change in physiological conditions (21, 62). Pathway analysis by IPA of the proteins and miRNA modulated in exosomes by P3F showed a common impact on reducing apoptosis and increasing cell viability (see **Figure 3A**: 10 out of 25 pathways are implicated in death pathways). This is further evidenced by the observed resistance of cells treated with P3F-modulated exosomes to apoptosis in response to exogenous oxidative stress, which may be impacted by both modulation of oxidative stress pathway, as well as resistance to apoptosis in general. Of note, elevated ROS levels are detected in almost all cancers, due at least in part to the high metabolic activity and mitochondrial dysfunction of cancer cells. In comparison, normal cells exhibit moderate levels of ROS, enough for them to act as second messengers in signal transduction, and contribute to physiological processes within these cells (63). To cope with the ever-present state of oxidative stress, cancer cells up-regulate their antioxidant pathways to escape cell death (64). For instance, in RMS, elevated ROS levels are compensated by an up-regulation of ROS-scavenging pathways, thus conferring resistance to ROS-induced stress (65). Moreover, up-regulation of ROS production in RMS cells following radiation therapy was rapidly compensated by an up-regulation of nuclear factor erythroid 2-related factor (NRF2) levels which, in turn, promotes the expression of antioxidant enzymes and miRNA that protected RMS cells from ROS-induced DNA damage (66). This has been suggested as a possible Achilles' heel of cancer cells, as they may be susceptible to treatments that can alter their redox homeostasis, either by further increasing intracellular ROS levels or by targeting antioxidant abilities (64, 67). RMS might be particularly vulnerable to this pathway, as demonstrated by Chen et al. using a high-throughput screen. They reasoned that this sensitivity may be especially applicable to RMS, as it derives from a skeletal muscle cell lineage, since skeletal muscle cells have unique metabolic properties including a high aerobic activity and a robust antioxidant defense system against excessive ROS, which make them particularly sensitive to redox-altering agents (55). In fact, analysis of RMS samples revealed oxidative stress-induced genomic mutations that enhance RMS cell survival against oxidative damage whereas combinational targeting of the major antioxidative pathways up-regulated in RMS, the thioredoxin (TRX) and glutathione (GSH) synthesis pathways, using GSH-depleting agents and TRX-reductase inhibitors seems to induce cancer cell death (55, 64). Therapeutic interventions using agents that can increase ROS production also offer promising therapeutic results. For instance, carfilzomib and alvocidib, in addition to synthetic statins, where shown to act in synergism with HDAC inhibitors by increasing oxidative stress showing effective activity against ERMS xenografts (55). Erastin, another GSH-depleting agent that subsequently up-regulates ROS production, also induces RMS cell death (67). Notably, following ROS-inducing radiation therapy, FPRMS cells were found to produce higher levels of antioxidant miRNA including *miR-22*, *miR-210,* and *miR-375* compared to FNRMS, where the expression of *miR-375* was only observed in FPRMS, and certain antioxidant enzymes including catalase and glutathione peroxidase 4 (66). Moreover, Martin et al. demonstrated that FPRMS treatment with fenretinide induces ROS production accompanied by a reduction in P3F transcriptional activity. ROS-induction in FPRMS using Triterpenoid down-regulated the expression of transcription factors including P3F suggesting

the need to determine the link between oxidative stress and P3F in RMS (68, 69). Altogether, RMS cells have been shown to modulate intracellular signaling pathways to maintain redox homeostasis, an aspect of cellular plasticity that protects against oxidative damage and highlights the importance of using redox-based therapeutic strategies in combination with conventional chemotherapeutic treatments against RMS. Our results further underline this finding, and specifically implicate the P3F protein in modulating oxidative stress response, not only in an autocrine manner in RMS cells, but also through paracrine effects on stromal cells *via* exosomes. We observed lower ROS levels within the P3F transduced C2C12 cells, with enhanced survival upon treatment with H_2O_2. We identified an enrichment of 4 REDOX proteins in exosomes in response to P3F that may be contributing to the observed decrease in intracellular ROS levels in recipient cells, confirming paracrine protective effects of the fusion oncoprotein via exosomes. Indeed, previous studies have implicated exosomes in modulating response to oxidative stress and conferring antioxidant resistance in several settings (27, 70), and our results now demonstrate the additional effect of oncoproteins such as P3F in further augmenting this response.

Altogether, our results indicate that the P3F oncoprotein down-regulates ROS levels, exerting a protective effect against oxidative stress-induced cell death in an autocrine manner. This effect can also be transferred to stromal and other cells through secreted exosomes that also affect recipient cell invasion, migration, and pro-angiogenic properties. We have shown that the P3F fusion protein is able to modulate the content of exosomes secreted by fusion-positive cells and that these exosomes seem to confer cellular plasticity and invasive properties, including augmentation of pro-angiogenic signaling. Detailed understanding of the pathways through which P3F alters the metabolic response of cells may uncover novel therapeutic targets for enhancing cell death in response to metabolic stress in this setting, and should be the focus of future studies.

DATA AVAILABILITY STATEMENT

The original contributions presented in the study are publicly available. This data can be found here: ProteomeXchange Consortium via the PRIDE partner repository (Accession Number: PXD017543).

AUTHOR CONTRIBUTIONS

AF, FG, AA, and FA conducted most of the experiments and data analysis. AF, FR, and FG helped in drafting the manuscript. FK, YM, JZ, and RZ performed and analyzed the LC-MS/MS experiments. NH helped in the design of the flow cytometry experiments and their analysis. SG and RS oversaw the design and coordination of the studies, and drafted the manuscript. All authors read and approved the final manuscript.

FUNDING

This work was funded by an MPP grant from the American University of Beirut Medical Center, Faculty of Medicine and with support from the Lebanese University.

ACKNOWLEDGMENTS

The authors thank shared core facilities at the American University of Beirut Faculty of Medicine (AUBFM).

SUPPLEMENTARY MATERIAL

The Supplementary Material for this article can be found online at: https://www.frontiersin.org/articles/10.3389/fonc.2020.01784/full#supplementary-material

REFERENCES

1. Breneman JC, Lyden E, Pappo AS, Link MP, Anderson JR, Parham DM, et al. Prognostic factors and clinical outcomes in children and adolescents with metastatic rhabdomyosarcoma-a report from the intergroup rhabdomyosarcoma study IV. *J Clin Oncol*. (2003) 21:78–84. doi: 10.1200/JCO.2003.06.129
2. Rudzinski ER, Anderson JR, Hawkins DS, Skapek SX, Parham DM, Teot LA. The world health organization classification of skeletal muscle tumors in pediatric rhabdomyosarcoma a report from the children's oncology group. *Arch Pathol Lab Med*. (2015) 139:1281–7. doi: 10.5858/arpa.2014-0475-OA
3. Williamson D, Missiaglia E, De Reyniès A, Pierron G, Thuille B, Palenzuela G, et al. Fusion gene-negative alveolar rhabdomyosarcoma is clinically and molecularly indistinguishable from embryonal rhabdomyosarcoma. *J Clin Oncol*. (2010) 28:2151–8. doi: 10.1200/JCO.2009.26.3814
4. Rudzinski ER, Anderson JR, Chi YY, Gastier-Foster JM, Astbury C, Barr FG, et al. Histology, fusion status, and outcome in metastatic rhabdomyosarcoma: a report from the children's oncology group. *Pediatr Blood Cancer*. (2017) 64:e26645. doi: 10.1002/pbc.26645
5. Shern JF, Chen L, Chmielecki J, Wei JS, Patidar R, Rosenberg M, et al. Comprehensive genomic analysis of rhabdomyosarcoma reveals a landscape of alterations affecting a common genetic axis in fusion-positive and fusion-negative tumors. *Cancer Discov*. (2014) 4:216–31. doi: 10.1158/2159-8290.CD-13-0639
6. Ghayad SE, Rammal G, Ghamloush F, Basma H, Nasr R, Diab-Assaf M, et al. Exosomes derived from embryonal and alveolar rhabdomyosarcoma carry differential miRNA cargo and promote invasion of recipient fibroblasts. *Sci Rep*. (2016) 6:37088. doi: 10.1038/srep37088
7. Diomedi-Camassei F, Boldrini R, Ravà L, Donfrancesco A, Boglino C, Messina E, et al. Different pattern of matrix metalloproteinases expression in alveolar versus embryonal rhabdomyosarcoma. *J Pediatr Surg*. (2004) 39:1673–9. doi: 10.1016/j.jpedsurg.2004.07.014
8. Théry C, Zitvogel L, Amigorena S. Exosomes: composition, biogenesis and function. *Nat Rev Immunol*. (2002) 2:569–79. doi: 10.1038/nri855
9. Miller IV, Raposo G, Welsch U, Prazeres da Costa O, Thiel U, Lebar M, et al. First identification of Ewing's sarcoma-derived extracellular vesicles and exploration of their biological and potential diagnostic implications. *Biol Cell*. (2013) 105:289–303. doi: 10.1111/boc.201200086
10. Raimondi L, De Luca A, Gallo A, Costa V, Russelli G, Cuscino N, et al. Osteosarcoma cell-derived exosomes affect tumor microenvironment by specific packaging of microRNAs. *Carcinogenesis*. (2019) 41:666–77. doi: 10.1093/carcin/bgz130

11. Peinado H, Alečković M, Lavotshkin S, Matei I, Costa-Silva B, Moreno-Bueno G, et al. Melanoma exosomes educate bone marrow progenitor cells toward a pro-metastatic phenotype through MET. *Nat Med*. (2012) 18:883–91. doi: 10.1038/nm.2753
12. Rammal G, Fahs A, Kobeissy F, Mechref Y, Zhao J, Zhu R, et al. Proteomic profiling of rhabdomyosarcoma-derived exosomes yield insights into their functional role in paracrine signaling. *J Proteome Res*. (2019) 18:3567–79. doi: 10.1021/acs.jproteome.9b00157
13. Hoshino A, Costa-Silva B, Shen TL, Rodrigues G, Hashimoto A, Tesic Mark M, et al. Tumour exosome integrins determine organotropic metastasis. *Nature*. (2015) 527:329–35. doi: 10.1038/nature15756
14. Zhang Y, Wang XF. A niche role for cancer exosomes in metastasis. *Nat Cell Biol*. (2015) 17:709–11. doi: 10.1038/ncb3181
15. Lobb RJ, Lima LG, Möller A. Exosomes: key mediators of metastasis and pre-metastatic niche formation. *Semin Cell Dev Biol*. (2017) 67:3–10. doi: 10.1016/j.semcdb.2017.01.004
16. Paolillo M, Schinelli S. Integrins and exosomes, a dangerous liaison in cancer progression. *Cancers*. (2017) 9:95. doi: 10.3390/cancers9080095
17. Maji S, Chaudhary P, Akopova I, Nguyen PM, Hare RJ, Gryczynski I, et al. Exosomal annexin II promotes angiogenesis and breast cancer metastasis. *Mol Cancer Res*. (2017) 15:93–105. doi: 10.1158/1541-7786.MCR-16-0163
18. Ghamloush F, Ghayad SE, Rammal G, Fahs A, Ayoub AJ, Merabi Z, et al. The PAX3-FOXO1 oncogene alters exosome miRNA content and leads to paracrine effects mediated by exosomal miR-486. *Sci Rep*. (2019) 9:14242. doi: 10.1038/s41598-019-50592-4
19. Yuan S, Norgard RJ, Stanger BZ. Cellular plasticity in cancer. *Cancer Discov*. (2019) 9:837–51. doi: 10.1158/2159-8290.cd-19-0015
20. Pardali E, Van Der Schaft DWJ, Wiercinska E, Gorter A, Hogendoorn PCW, Griffioen AW, et al. Critical role of endoglin in tumor cell plasticity of Ewing sarcoma and melanoma. *Oncogene*. (2011) 30:334–45. doi: 10.1038/onc.2010.418
21. da Silva-Diz V, Lorenzo-Sanz L, Bernat-Peguera A, Lopez-Cerda M, Muñoz P. Cancer cell plasticity: impact on tumor progression and therapy response. *Semin Cancer Biol*. (2018) 53:48–58. doi: 10.1016/j.semcancer.2018.08.009
22. Nakahata K, Uehara S, Nishikawa S, Kawatsu M, Zenitani M, Oue T, et al. Aldehyde dehydrogenase 1 (ALDH1) is a potential marker for cancer stem cells in embryonal rhabdomyosarcoma. *PLoS One*. (2015) 10:e0125454. doi: 10.1371/journal.pone.0125454
23. Walter D, Satheesha S, Albrecht P, Bornhauser BC, D'Alessandro V, Oesch SM, et al. CD133 positive embryonal rhabdomyosarcoma stem-like cell population is enriched in rhabdospheres. *PLoS One*. (2011) 6:e19506. doi: 10.1371/journal.pone.0019506
24. Sosa V, Moliné T, Somoza R, Paciucci R, Kondoh H, LLeonart ME. Oxidative stress and cancer: an overview. *Ageing Res Rev*. (2013) 12:376–90. doi: 10.1016/j.arr.2012.10.004
25. Nisimoto Y, Diebold BA, Constentino-Gomes D, Lambeth JD. Nox4: a hydrogen peroxide-generating oxygen sensor. *Biochemistry*. (2014) 53:5111–20. doi: 10.1021/bi500331y
26. Kumari S, Badana AK, Murali Mohan G, Shailender G, Malla RR. Reactive oxygen species: a key constituent in cancer survival. *Biomark Insights*. (2018) 13:1177271918755391. doi: 10.1177/1177271918755391
27. Eldh M, Ekström K, Valadi H, Sjöstrand M, Olsson B, Jernås M, et al. Exosomes communicate protective messages during oxidative stress; possible role of exosomal shuttle RNA. *PLoS One*. (2010) 5:e15353. doi: 10.1371/journal.pone.0015353
28. Chettimada S, Lorenz DR, Misra V, Dillon ST, Reeves RK, Manickam C, et al. Exosome markers associated with immune activation and oxidative stress in HIV patients on antiretroviral therapy. *Sci Rep*. (2018) 8:7227. doi: 10.1038/s41598-018-25515-4
29. Hinson ARP, Jones R, Lisa LE, Belyea BC, Barr FG, Linardic CM. Human rhabdomyosarcoma cell lines for rhabdomyosarcoma research: utility and pitfalls. *Front Oncol*. (2013) 3:183. doi: 10.3389/fonc.2013.00183
30. Bonnet A, Lagarrigue S, Liaubet L, Robert-Granié C, SanCristobal M, Tosser-Klopp G. Pathway results from the chicken data set using GOTM, pathway studio and ingenuity softwares. *BMC Proc*. (2009) 3(Suppl. 4):S11. doi: 10.1186/1753-6561-3-s4-s11
31. Yuryev A, Kotelnikova E, Daraselia N. Ariadne's chemeffect and pathway studio knowledge base. *Expert Opin Drug Discov*. (2009) 4:1307–18. doi: 10.1517/17460440903413488
32. Toth M, Sohail A, Fridman R. Assessment of gelatinases (MMP-2 and MMP-9) by gelatin zymography. *Methods Mol Biol*. (2012) 878:121–35. doi: 10.1007/978-1-61779-854-2_8
33. Kitajima S, Kohno S, Kondoh A, Sasaki N, Nishimoto Y, Li F, et al. Undifferentiated state induced by Rb-p53 double inactivation in mouse thyroid neuroendocrine cells and embryonic fibroblasts. *Stem Cells*. (2015) 33:1657–69. doi: 10.1002/stem.1971
34. Marshall AD, Lagutina I, Grosveld GC. PAX3-FOXO1 induces cannabinoid receptor 1 to enhance cell invasion and metastasis. *Cancer Res*. (2011) 71:7471–80. doi: 10.1158/0008-5472.CAN-11-0924
35. Deschênes-Simard X, Kottakis F, Meloche S, Ferbeyre G. ERKs in cancer: friends or foes? *Cancer Res*. (2014) 74:412–9. doi: 10.1158/0008-5472.CAN-13-2381
36. Ma XM, Blenis J. Molecular mechanisms of mTOR-mediated translational control. *Nat Rev Mol Cell Biol*. (2009) 10:307–18. doi: 10.1038/nrm2672
37. Hu Y, Yan C, Mu L, Huang K, Li X, Tao D, et al. Fibroblast-derived exosomes contribute to chemoresistance through priming cancer stem cells in colorectal cancer. *PLoS One*. (2015) 10:e0125625. doi: 10.1371/journal.pone.0125625
38. Dick RA, Kwak MK, Sutter TR, Kensler TW. Antioxidative function and substrate specificity of NAD(P)H-dependent alkenal/one oxidoreductase. A new role for leukotriene B4 12-hydroxydehydrogenase/15-oxoprostaglandin 13-reductase. *J Biol Chem*. (2001) 276:40803–10. doi: 10.1074/jbc.M105487200
39. Hayes JD, Pulford DJ. The glut athione s-transferase supergene family: regulation of GST and the contribution of the lsoenzymes to cancer chemoprotection and drug resistance part II. *Crit Rev Biochem Mol Biol*. (1995) 30:445–600. doi: 10.3109/10409239509083492
40. Fukai T, Ushio-Fukai M. Superoxide dismutases: role in redox signaling, vascular function, and diseases. *Antioxidants Redox Signal*. (2011) 15:1583–606. doi: 10.1089/ars.2011.3999
41. Scheibe R, Backhausen JE, Emmerlich V, Holtgrefe S. Strategies to maintain redox homeostasis during photosynthesis under changing conditions. *J Exp Bot*. (2005) 56:1481–9. doi: 10.1093/jxb/eri181
42. Matsumoto M, Katsuyama M, Iwata K, Ibi M, Zhang J, Zhu K, et al. Characterization of N-glycosylation sites on the extracellular domain of NOX1/NADPH oxidase. *Free Radic Biol Med*. (2014) 68:196–204. doi: 10.1016/j.freeradbiomed.2013.12.013
43. Parham DM, Barr FG. Classification of rhabdomyosarcoma and its molecular basis. *Adv Anat Pathol*. (2013) 20:387–97. doi: 10.1097/PAP.0b013e3182a92d0d
44. Hawkins DS, Gupta AA, Rudzinski ER. What is new in the biology and treatment of pediatric rhabdomyosarcoma? *Curr Opin Pediatr*. (2014) 26:50–6. doi: 10.1097/MOP.0000000000000041
45. Tai YL, Chen KC, Hsieh JT, Shen TL. Exosomes in cancer development and clinical applications. *Cancer Sci*. (2018) 109:2364–74. doi: 10.1111/cas.13697
46. Blandford MC, Barr FG, Lynch JC, Randall RL, Qualman SJ, Keller C. Rhabdomyosarcomas utilize developmental, myogenic growth factors for disease advantage: a report from the children's oncology group. *Pediatr Blood Cancer*. (2006) 46:329–38. doi: 10.1002/pbc.20466
47. Tarnowski M, Tkacz M, Zgutka K, Bujak J, Kopytko P, Pawlik A. Picropodophyllin (PPP) is a potent rhabdomyosarcoma growth inhibitor both in vitro and in vivo. *BMC Cancer*. (2017) 17:532. doi: 10.1186/s12885-017-3495-y
48. Wang W, Kumar P, Wang W, Epstein J, Helman L, Moore JV, et al. Insulin-like growth factor II and PAX3-FKHR cooperate in the oncogenesis of rhabdomyosarcoma. *Cancer Res*. (1998) 58:4426–33.
49. Ayalon D, Glaser T, Werner H. Transcriptional regulation of IGF-I receptor gene expression by the PAX3-FKHR oncoprotein. *Growth Horm IGF Res*. (2001) 11:289–97. doi: 10.1054/ghir.2001.0244
50. Armoni M, Quon MJ, Maor G, Avigad S, Shapiro DN, Harel C, et al. PAX3/forkhead homolog in rhabdomyosarcoma oncoprotein activates glucose transporter 4 gene expression in vivo and in vitro. *J Clin Endocrinol Metab*. (2002) 87:5312–24. doi: 10.1210/jc.2002-020318

51. Poniewierska-Baran A, Schneider G, Sun W, Abdelbaset-Ismail A, Barr FG, Ratajczak MZ. Human rhabdomyosarcoma cells express functional pituitary and gonadal sex hormone receptors: therapeutic implications. *Int J Oncol*. (2016) 48:1815–24. doi: 10.3892/ijo.2016.3439
52. Nechamen CA, Thomas RM, Cohen BD, Acevedo G, Poulikakos PI, Testa JR, et al. Human follicle-stimulating hormone (FSH) receptor interacts with the adaptor protein APPL1 in HEK 293 Cells: potential involvement of the PI3K pathway in FSH signaling1. *Biol Reprod*. (2004) 71:629–36. doi: 10.1095/biolreprod.103.025833
53. Rosairo D, Kuyznierewicz I, Findlay J, Drummond A. Transforming growth factor-β: its role in ovarian follicle development. *Reproduction*. (2008) 136:799–809. doi: 10.1530/REP-08-0310
54. Taylor AC, Shu L, Danks MK, Poquette CA, Shetty S, Thayer MJ, et al. p53 mutation and MDM2 amplification frequency in pediatric rhabdomyosarcoma tumors and cell lines. *Med Pediatr Oncol*. (2000) 35:96–103. doi: 10.1002/1096-911X(200008)35:23.0.CO;2-Z
55. Chen X, Stewart E, Shelat AA, Qu C, Bahrami A, Hatley M, et al. Targeting oxidative stress in embryonal rhabdomyosarcoma. *Cancer Cell*. (2013) 24:710–24. doi: 10.1016/j.ccr.2013.11.002
56. Mai PL, Best AF, Peters JA, DeCastro RM, Khincha PP, Loud JT, et al. Risks of first and subsequent cancers among TP53 mutation carriers in the National Cancer Institute Li-Fraumeni syndrome cohort. *Cancer*. (2016) 122:3673–81. doi: 10.1002/cncr.30248
57. Stuart ET, Haffner R, Oren M, Gruss P. Loss of p53 function through PAX-mediated transcriptional repression. *EMBO J*. (1995) 14:5638–45. doi: 10.1002/j.1460-2075.1995.tb00251.x
58. Keller C, Arenkiel BR, Coffin CM, El-Bardeesy N, DePinho RA, Capecchi MR. Alveolar rhabdomyosarcomas in conditional Pax3:Fkhr mice: cooperativity of Ink4a/ARF and Trp53 loss of function. *Genes Dev*. (2004) 18:2614–26. doi: 10.1101/gad.1244004
59. Abraham J, Nuñez-Álvarez Y, Hettmer S, Carrió E, Chen HIH, Nishijo K, et al. Lineage of origin in rhabdomyosarcoma informs pharmacological response. *Genes Dev*. (2014) 28:1578–91. doi: 10.1101/gad.238733.114
60. Mihic-Probst D, Ikenberg K, Tinguely M, Schraml P, Behnke S, Seifert B, et al. Tumor cell plasticity and angiogenesis in human melanomas. *PLoS One*. (2012) 7:e33571. doi: 10.1371/journal.pone.0033571
61. Ploeger DT, Hosper NA, Schipper M, Koerts JA, De Rond S, Bank RA. Cell plasticity in wound healing: paracrine factors of M1/ M2 polarized macrophages influence the phenotypical state of dermal fibroblasts. *Cell Commun Signal*. (2013) 11:29. doi: 10.1186/1478-811X-11-29
62. Taddei ML, Giannoni E, Comito G, Chiarugi P. Microenvironment and tumor cell plasticity: an easy way out. *Cancer Lett*. (2013) 341:80–96. doi: 10.1016/j.canlet.2013.01.042
63. Liou GY, Storz P. Reactive oxygen species in cancer. *Free Radic Res*. (2010) 44:479–96. doi: 10.3109/10715761003667554
64. Habermann KJ, Grünewald L, van Wijk S, Fulda S. Targeting redox homeostasis in rhabdomyosarcoma cells: GSH-depleting agents enhance auranofin-induced cell death. *Cell Death Dis*. (2017) 8:e3067. doi: 10.1038/cddis.2017.412
65. Fan TWM, Kucia M, Jankowski K, Higashi RM, Ratajczak J, Ratajczak MZ, et al. Rhabdomyosarcoma cells show an energy producing anabolic metabolic phenotype compared with primary myocytes. *Mol Cancer*. (2008) 7:79. doi: 10.1186/1476-4598-7-79
66. Marampon F, Codenotti S, Megiorni F, Del Fattore A, Camero S, Gravina GL, et al. NRF2 orchestrates the redox regulation induced by radiation therapy, sustaining embryonal and alveolar rhabdomyosarcoma cells radioresistance. *J Cancer Res Clin Oncol*. (2019) 145:881–93. doi: 10.1007/s00432-019-02851-0
67. Dächert J, Ehrenfeld V, Habermann K, Dolgikh N, Fulda S. Targeting ferroptosis in rhabdomyosarcoma cells. *Int J Cancer*. (2020) 146:510–20. doi: 10.1002/ijc.32496
68. Herrero Martín D, Boro A, Schäfer BW. Cell-based small-molecule compound screen identifies fenretinide as potential therapeutic for translocation-positive rhabdomyosarcoma. *PLoS One*. (2013) 8:e55072. doi: 10.1371/journal.pone.0055072
69. Kasiappan R, Jutooru I, Mohankumar K, Karki K, Lacey A, Safe S. Reactive oxygen species (ROS)-inducing triterpenoid inhibits rhabdomyosarcoma cell and tumor growth through targeting SP transcription factors. *Mol Cancer Res*. (2019) 17:794–805. doi: 10.1158/1541-7786.MCR-18-1071
70. Saeed-Zidane M, Linden L, Salilew-Wondim D, Held E, Neuhoff C, Tholen E, et al. Cellular and exosome mediated molecular defense mechanism in bovine granulosa cells exposed to oxidative stress. *PLoS One*. (2017) 12:e0187569. doi: 10.1371/journal.pone.0187569

Conflict of Interest: The authors declare that the research was conducted in the absence of any commercial or financial relationships that could be construed as a potential conflict of interest.

Advantages of publishing in Frontiers

OPEN ACCESS
Articles are free to read for greatest visibility and readership

FAST PUBLICATION
Around 90 days from submission to decision

HIGH QUALITY PEER-REVIEW
Rigorous, collaborative, and constructive peer-review

TRANSPARENT PEER-REVIEW
Editors and reviewers acknowledged by name on published articles

Frontiers
Avenue du Tribunal-Fédéral 34
1005 Lausanne | Switzerland

Visit us: www.frontiersin.org
Contact us: info@frontiersin.org | +41 21 510 17 00

REPRODUCIBILITY OF RESEARCH
Support open data and methods to enhance research reproducibility

DIGITAL PUBLISHING
Articles designed for optimal readership across devices

FOLLOW US
@frontiersin

IMPACT METRICS
Advanced article metrics track visibility across digital media

EXTENSIVE PROMOTION
Marketing and promotion of impactful research

LOOP RESEARCH NETWORK
Our network increases your article's readership